Wind and Seismic Effects

NIST SP 871

PROCEEDINGS OF
THE 26TH JOINT
MEETING OF
THE U.S.-JAPAN
COOPERATIVE PROGRAM
IN NATURAL RESOURCES
PANEL ON WIND AND
SEISMIC EFFECTS

Issued September 1994

Noel J. Raufaste,
EDITOR

Building and Fire Research Laboratory
National Institute of Standards and Technology
Gaithersburg, MD 20899

U.S. DEPARTMENT OF COMMERCE
Ronald H. Brown, Secretary

TECHNOLOGY ADMINISTRATION
Mary L. Good, Under Secretary for Technology

National Institute of Standards and Technology
Arati Prabhakar, Director

PREFACE

This publication is Proceedings of the 26th Joint Meeting of the U.S.-Japan Panel on Wind and Seismic Effects. The meeting was held at the National Institute of Standards and Technology, Gaithersburg, Maryland during 17-20 May 1994. Forty-five papers were authored--23 by U.S. members and 22 by Japanese. Thirty-four papers were presented orally. The papers were organized into six themes: Wind Engineering; Earthquake Engineering; Storm Surge and Tsunamis; Northridge Southern California and Hokkaido Nansei-Oki Japan Earthquakes; Summary of Joint Cooperative Research Programs; and Report of Task Committee Workshops conducted during the past year.

BACKGROUND

Responding to the need for improved engineering and scientific practices through exchange of technical data and information, research personnel, and research equipment, the United States and Japan in 1961 created the U.S.-Japan Cooperative Science Program. Three collateral programs comprise the Cooperative Science Program. The U.S.-Japan Cooperative Program in Natural Resources (UJNR), one of the three, was created in January 1964. The objective of UJNR is to exchange information on research results and exchange scientists and engineers in the area of natural resources for the benefit of both countries. UJNR is composed of 16 Panels each responsible for specific technical subjects.

The Panel on Wind and Seismic Effects was established in 1969. Seventeen U.S. and six Japanese agencies participate with representatives of private sector organizations to develop and exchange technologies aimed at reducing damages from high winds, earthquakes, storm surge, and tsunamis. This work is produced through collaboration between U.S. and Japanese member researchers working in 10 task committees. Each committee focuses on specific technical issues, e.g., earthquake strong motion data. The Panel provides the vehicle to exchange technical data and information on design and construction of civil engineering lifelines, buildings, and waterfront structures, and to exchange high wind and seismic measurement records. Annual meetings alternate between Japan and the United States (odd numbered years in Japan; even numbered years in the United States). These one-week technical meetings provide the forum to discuss ongoing research and research results; one-week technical study tours follow the meetings.

The National Institute of Standards and Technology (NIST) provides the U.S.-side chair and secretariat. The Public Works Research Institute (PWRI), Japan, provides the Japan side chair and secretariat.

Cooperative research is performed through formal Panel Programs. In 1981, cooperative research in Large-Scale Testing was started under the auspices of the Panel. Also in 1981, joint research on Reinforced Concrete Structures was initiated. Full-scale testing was performed at the Building Research Institute (BRI), one of the six Japanese member organizations, with supporting tests in Japan and in the United States. Two years later, a joint research program on Steel Structures was initiated. Full-scale testing again was led by BRI with supporting tests in the United States and Japan. The U.S.-Japan coordinated

program for Masonry Building Research was started in 1985. A U.S.-Japan coordinated program on Precast Seismic Structural Systems was initiated in 1991. A joint program on Seismic Performance of Composite and Hybrid Structures was initiated in 1993. In 1994, a joint program was initiated on Physical and Numerical Simulation of Structural Damages Due to Liquefaction and Development of Countermeasure Techniques.

Task Committee meetings, exchanges of data and information through technical presentations at annual Panel meetings, exchanges of guest researchers, visits to respective research laboratories and informal interactions between Panel meetings, joint workshops and seminars, and joint cooperative research programs all contribute to the development and effective delivery of knowledge that has influenced design and construction practices in both countries. Guest research exchanges have advanced the state of technology in areas of steel, concrete, and masonry structures under seismic forces; developed techniques to analyze risks from liquefaction; modeled water seepage in dam foundations; performed comparative analyses of seismic design of U.S. and Japanese bridges.

Direct communication between counterpart country organizations is the cornerstone of the Panel. Effective information exchanges and exchanges of personnel and equipment have strengthened domestic programs of both countries. There are opportunities for experts in various technical fields to get to know their foreign counterparts, conduct informal exchanges, bring their respective views to the frontiers of knowledge, and advance knowledge of their specialties.

The Panel's activities resulted in improved building and bridge standards and codes and design and construction practices in hydraulic structures in both countries, for example:

- created and exchanged digitized earthquake records used as the basis of design and research for Japan and the United States;
- transferred earthquake engineering information and strong-motion measurement techniques for use by seismically active countries, e.g., Australia, Canada, Italy, Mexico, Peru, Taiwan, Turkey, and North Africa;
- produced data that advanced retrofit techniques for bridge structures;
- developed field test data for use in aerodynamic retrofit of bridge structures;
- produced full-scale test data that advanced seismic design standards for buildings;
- advanced technology for repairing and strengthening reinforced concrete, steel, and masonry structures;
- improved in-situ measurement methods for soil liquefaction and stability under seismic loads;
- created a database comparing Japanese and U.S. standard penetration tests to improve prediction of soil liquefaction;
- created database on storm surge and tsunamis and verified mathematical models of tsunami and storm surge warning systems;
- established a library resource of current research on wind and earthquake engineering and on storm surge and tsunamis;
- published proceedings of Panel meetings, Task Committee Workshops, and special publications such as List of Panel Publications and translated two-volume series on

earthquake resistant construction using base isolation systems;

- gained better knowledge of both countries' research, design, and construction capabilities from indepth visits to host country's laboratories and building and public works projects. Results of such visits contribute to creation of new Task Committees, agendas for Joint Panel meetings and task committee workshops, special visits of U.S.-Japan researchers, and joint collaborative research.

HIGHLIGHTS OF THE TECHNICAL SITE VISITS

Eight technical sites were visited at five locations. A summary of the visits follow.

GAITHERSBURG, MD

1. National Institute of Standards and Technology (NIST)[1]. The delegation was provided an overview of the Building and Fire Research Laboratory (BFRL); tours of BFRL's structures, materials, environmental, and fire facilities; NIST's Research Reactor and its Cold Neutron Source of the NIST Materials and Engineering Laboratory; and an overview of the NIST Advanced Technology Program.

The mission of NIST is to promote U.S. economic growth by working with industry to develop and apply technology, measurements, and standards. BFRL, one of eight Laboratories making up NIST, increases the competitiveness of industry and public safety through performance prediction and measurement technologies and technical advances that improve the life cycle quality of constructed facilities. BFRL's efforts are closely coordinated with complementary activities of industry, professional and trade organizations, academe, and other agencies of government. The vision for BFRL, the structure of its technical programs, and the determination and timing of its technical products are based on analyses of industry needs and BFRL's own unique resources and capabilities.

Annually, BFRL publishes over 200 reports describing research findings from its over 150 research projects. Its projects, list of publications, impacts of its research, and examples of how BFRL serves its customers are summarized in four companion reports *Projects '94*; *Publications '93*; *Impacts*; and *NIST Building and Fire Research Laboratory -- Collaborating With Our Customers*.

BFRL's laboratory facilities include: six-degree-of-freedom structural testing facility; large-scale structural testing facility with the 53 MN (12-million pound) universal structural testing machine; environmental chambers; guarded hot-plate; calibrated hot-box; plumbing tower; building materials imaging and modeling laboratory; large burn facility for conducting experimental fires in full-scale and related combustion toxicity facility, large industrial fire test facilities, fire suppression test facilities; and a fire simulation laboratory.

---

[1] For further information about NIST's work, contact Noel Raufaste, Secretary-General UJNR Panel on Wind and Seismic Effects and Head, Cooperative Research Programs, NIST on facsimile 301-975-4032 or e-mail, raufaste@micf.nist.gov.

In the Structures Division, the delegation was provided a summary of BFRL's research on earthquake hazards reduction. Analytical and experimental studies are performed on seismic behavior of masonry structures, seismic resistance of precast structures, residual strength and energy absorbing resistance of precast concrete structures, strengthening methodologies for buildings and bridge substructures, and performance requirements for passive and active energy dissipation systems for buildings and lifeline structures. BFRL is mandated to perform post-disaster investigations; the findings are used to develop the most probable technical causes of failures and to improve seismic design and construction of buildings and structures against future earthquakes.

In the Building Materials Division, the delegation was provided a summary of work on the development of methods to determine the quality and prediction of service lives of organic building materials. Research includes identifying degradation mechanisms, improving characterizing methods, and developing mathematical models of the degradation processes. Research was discussed on developing computer models that simulate the development of the microstructure of concrete during the setting process. Such models are used to predict concrete performance, strength, and durability. The delegation discussed BFRL work in developing prototype expert systems such as HWYCON, an interactive expert system designed to help highway inspectors and engineers diagnose problems, select materials for construction, and repair highways and highway structures.

In the Building Environment Division, green technologies research was highlighted. BFRL is exploring the use of refrigerant mixtures to improve the efficiency of refrigeration cycles and to replace harmful chlorofluorocarbon refrigerants that damage the ozone layer of the upper atmosphere. In a related area, the delegation toured BFRL's controls laboratory. With the aid of a computerized energy monitoring and control system, this laboratory performs fundamental research on heating, ventilating, and air conditioning (HVAC) control systems, on control dynamics, and on adaptive optimization techniques. It uses a computerized energy monitoring and control system with BFRL software, which controls an air handler, a building, a heating/cooling plant, and a laboratory test facility for evaluating the performance of conventional and advanced HVAC/control systems. BFRL is fostering the development of more intelligent, integrated, and optimized building mechanical systems. A dynamic building/heating, ventilating, and air-conditioning control system simulation program is used to study HVAC/control system dynamics and interactions. Research addresses the development, evaluation, and testing of communication protocol standards for the open exchange of information between equipment from different vendors and between different control levels in hierarchical and distributed building management systems. Results from this research serve as a basis for HVAC standards to assist the control system manufacturers to develop interoperable systems and methods for testing conformance to the standards.

In the Fire Safety Engineering Division, the delegation was exposed to its experimental research on pool burning. This research addresses the characterization of the physical and chemical properties of pool-burning flames as a function of pool diameter and liquid-fuel molecular structure. The experimental program consists of measurements of flame temperature, velocities, chemical-species composition, particulate characteristics, radiative-

transfer characteristics, and energy feedback from the flame to the liquid fuel. A demonstration was provided featuring a turbulent spray burner used to determine the fire suppression capabilities of different gaseous agents, considered for possible halon replacement (known to deplete stratospheric ozone).

The delegation visited NIST's 20-MW research reactor -- a national center for the application of reactor radiation to a variety of problems. Each year, over 700 people from industry, universities, and other government agencies use the experimental facilities at the reactor to perform collaborative and independent research projects. For example, researchers are using neutrons produced by the reactor to study the structural properties of the new high-temperature superconductors and to determine how these properties are changed and related to material processing. The Cold Neutron Facility makes a world-class, fully instrumented laboratory for cold neutron research easily available for the first time to U.S. scientists working in advanced materials science, chemistry, and biology. The measurement capabilities of this facility are being used in a NIST Advanced Technology Program project which aims to improve the properties while reducing the cost of finished ceramics. These parts have a range of applications in a variety of industries, from high heat load engines to electronic components.

At the end of the day, NIST's Advanced Technology Program (ATP) was presented to the delegation. ATP promotes rapid commercialization of new scientific discoveries. ATP provides technology development funding for high risk technologies through cooperative research agreements to single businesses or industry joint ventures. ATP supports development of laboratory prototypes and proof of technical feasibility but not project development or proof of commercial feasibility. ATP provides matching funds annually for up to 5 years, not to exceed 50% of the total research.

BOSTON, MA

2. Massachusetts Institute of Technology, Center for Construction Research and Education (CCRE)[2]. CCRE performs nonclassical civil engineering classwork and contracted research directed at helping construction firms identify barriers to improving their construction practices and recommending methods to resolve barriers. Examples of work include developing procedures that forecast size of construction markets, identify pitfalls to performing successful construction practices, predict liability issues, develop construction management techniques and environmental technologies such as hazardous waste reduction including management of solid waste reduction, waste water treatments and airborne pollution. Work in geotechnical engineering addresses fluid transport of toxic materials in water, earth, and rock, and work in structures and materials include composites, fiber reinforced ceramics, NDEs for remote sensing of bridge decks and leaks in piping. CCRE's work in intelligent highway vehicle systems (IHVS) Traffic Management Systems centers on integrating those advanced technologies, developed for other industry applications, that have potential to improve design and construction practices.

---

[2] Dr. Fred Moavenzadeh, Director, Center for Construction Research and Education hosted the delegation.

CCRE is developing a Consortium for Infrastructure Development composed of 10 U.S. firms to understand how different technologies interact within the infrastructure. CCRE predicts infrastructure will be the next major U.S. design and construction challenge.

CCRE is part of the Pierce Laboratory, one of two Laboratories of the Department of Civil and Environmental Engineering. It annually perform $10 million of contract research mostly from the Federal Government. Their links with design and construction experts domestically and internationally are strong and effective. Their outreach includes planning seminars and conferences with domestic and foreign public and private construction organizations, hosting foreign students and faculty and industry professionals to work on specific projects, sending MIT students and faculty to U.S. construction firms and to other country laboratories, and publishing a quarterly newsletter, *Construction*.

3. Central Artery (I-93)/ Tunnel (I-90) Project (CA/T)[3]. This construction project will replace Boston's 40 year old elevated Central Artery with a widened and mostly underground 8-10 lane interstate highway through downtown Boston and an east/west Seaport Access Road (tunnel) through South Boston to Logan Airport in the Third Boston Harbor Tunnel. CA/T is under the direction of the Massachusetts Highway Department. Bechtel/Parsons Brinckeroff are prime contractors managing CA/T's design and construction. Boston designed their expressways in the 1950s to serve 75 K vehicles per day. Today it is overloaded and inefficiently serves 190 K vehicles daily. The new expressway is expected to accommodate 240 K vehicles daily. CA/T is the last link in the U.S. interstate highway system; 12 km of urban highway, about 1/2 (5.6 km) in cut-and-cover tunnels. The overall project is expected to cost $7.7 billion; 85% paid by Federal funds and 15% by State monies derived from gasoline taxes and bonds.

The delegation visited the site of the 3rd Boston Harbor Tunnel. The actual construction for this part of the CA/T Project began in September 1991 with the arrival of the huge Harbor dredge "superscoop." The Boston Harbor crossing consisted of placing 12 double-boxed immersed tubes in a 15 m deep by 30 m wide by 1.2 km long trench under Boston Harbor. The associated east and south Boston land based cut and cover tunnel approaches to these tubes will be completed at the end of 1995 in time for the Project's first phase opening in December 1995.

Modern Continental/Obayashi[4], the subcontractors to the Logan Airport end of the Third Boston Harbor Tunnel, hosted this portion of the visit. The exit ramp required over 370 000 m^3 of concrete and 900 000 m^3 of material were excavated. The cut walls were stabilized using a Japanese technique of soil/concrete mix of compressive strength about 300 Pa. Tie-backs range from 24 to 35 m in length. Soil from this site and other construction sites are transported to several islands in the Boston Harbor for future use as parks. Boston citizens hope the largest Island, Spectacle Island, when completed will be designated a National Park. The construction cost for this section is about $246 million.

---

[3] Richard A. Jarvis, Public Outreach Coordinator hosted the delegation.

[4] John Pastore, Assistant Project Manager hosted the delegation.

The South Boston tunnel approaches, constructed by the joint venture of Kiewit/Perini/Atkinson/Cashman, is 1.2 km in length; construction costs are about $180 million. A parking garage will be constructed on top of the south approach. While at the Logan Airport approach, the covered space will revert back to the airport as tarmac and for sound barrier buffer space. Caissons were driven to bed rock to prevent the roadway from heaving. Slurry walls were placed to bedrock 37 m down. At each end of the approach, a 77 m diameter circular cofferdam was excavated to bedrock, 37 m down and concrete was placed in eight lifts. The circular cofferdam is the meeting place for the East/South tubes and will also serve as the foundation for Vent Building #6 in South Boston. Work is performed in 2 shifts of 10 hours each, 6-days per week.

The highway approaches at Logan Airport and South Boston enter into an immersed binocular tube tunnel made up of 12 concrete-lined steel tubes each measuring 98 m x 24 m x 12 m high and weighing 2.3×10^6 kg. A third tube, northbound from Boston to Logan Airport, will serve as an HOV lane. A 30 m wide by 15 m deep trench was dredged to accommodate the submerged tunnel. The deepest section is 20 m below the harbor bottom. Over 680,000 m^3 of rock and sediment were removed. Bethlehem Steel in Baltimore fabricated the 12-section 2-tube tunnels, floated them to Boston and placed them using an electronic positioning system by gantry cranes installed on two barges. The tunnel rests on 0.9 m bed of coarse gravel with 2 m ballast on top. Six meters of backfill line the sides of the tunnel. Each tube was joined to its adjoining one by the pressure of the water compressing its end gaskets. Workers inside the tube opened valves to drain water between the end of the tubes. Watertight doors were removed and concrete cast around the inside of the tubes. The outer steel walls include a 1.5 m by 2.1 m thick layer of reinforced concrete. Tunnel concrete strength is 41 MPa. The road slab is 3 m thick with air ducts imbedded in the slab. Fire detection systems are installed and emergency stairs are constructed into the barrier walls separating the tunnels for driver/passenger egress into passageways.

A four-year environmental analysis was performed to consider appropriate methods for transporting excavated materials to locations to dispose of the construction wastes. Over 9.2M m^3 of earth will be moved; some temporarily stored for later use as backfill; the majority for permanent placement. About half of the 1.5M m^3 dredged material will be dumped in the ocean 40 km offshore; excavated earth will be used as fill on several islands as noted before. CAD designs were used to help designers view the approaches and tunnel through the perspective of the drivers.

The city center's new artery construction will be mostly underground (ranging from 24 m to 37 m deep) replacing the elevated I-93 central artery. Work is expected to start in mid-1994. Reinforced concrete walls of the cut and cover highway tunnel with a temporary steel structural system will support the elevated highway during construction of the underground artery. Green space will cover the construction and help visually link neighborhoods that were separated by the elevated highway.

CAD designs simulated views of the project and showed relationships to adjoining neighborhoods. Co-integration of the design and construction was performed with professional societies such as AASHTO, ACI, ASCE, AISC. As there are no

design/construction standards for underground highways, a modified AASHTO Standard was used. Utility lines are now being relocated in Downtown Boston.

Working with the Federal Highway Administration and MIT, CA/T planners developed an intelligent highway vehicle system (IHVS) to manage traffic by using techniques such as closed circuit television of traffic flow, CO_2 monitoring, loop detection, electronic toll collection, randomly monitoring vehicles every 60 m to predict traffic delays, and ramp signal traffic information. Traffic information will be displayed electronically at selected shopping centers and broadcast on radio and television. An advanced public transportation system will be installed at bus stops to display location of buses and a central control system will manage transportation on the central artery.

CA/T management meets with citizen activist groups informing them about proposed design and construction schemes and requesting their comments. CA/T's present plan reflects reductions from potential vehicle pollution and improvements in highway/bridge architectural appearances from such meetings. For example, the delegation was told about Scheme Z, a 37 m high six loop $350 million highway interchange. Citizens voiced concern about expected air and noise pollution from the many vehicles and about the unsightly 12 story highway ramps. After much public discussion, the interchange design was modified to a 12 m high two loop highway interchange above ground with other loops underground. The revised costs, however, were three times the original cost, now totaling $1.2 billion.

The Massachusetts Highway Department highlighted some "innovated" design and construction practices used on this project:

- a soil/concrete mix was used to stabilize earth serving as retaining walls to the 3rd Harbor Tunnel resulting in economy over the traditional steel shoring procedures,
- caissons stabilizing entry roads permitted use of thinner slab thicknesses which reduced project costs,
- micro tunnel jacking to install utility systems permitted installations at shallower depths resulting in less excavation and a lower cost,
- cofferdams at tunnel ends facilitated highway connections at the tunnel,
- temporary beam structural system used to support existing elevated highways over new cut and cover tunnel construction permits normal traffic flow during period of the construction,
- adaptive reuse by capping 27 landfills and islands in Boston Harbor with excavated soil will result in new public parks,
- rodent control officials are educating citizens about controlling displaced rodents during construction,
- discussions with citizen interest groups resulted in revised CA/T design and construction plans by incorporating citizens' recommendations.

4. The Boston Harbor Project Deer Island Treatment Plant[5].

In the 1980's Boston Harbor was one of the most polluted in the United States. Covering nearly 130×10^6 m^2, the harbor has been a dumping ground for all sorts of waste. In 1985, the Massachusetts Legislature created the Massachusetts Water Resource Authority (MWRA) to supply water and sewerage services to 61 Boston-area cities and towns (more than 2 million people) and to improve the water quality of Boston Harbor. Interim improvements have included the cessation of scum discharges (1989) and sludge discharges (1991) from the existing treatment plant at Deer Island. MWRA is in the process of upgrading its sewage treatment operations. This facility on Deer Island, at the mouth of Boston Harbor, will be replaced by a 4.81 million m^3 per day plant, the 2nd largest facility in the United States. A new secondary sewerage treatment facility will be completed in 1994. Eight sludge digesters have been constructed to come on-line with the primary plant; one will be used for methane gas. Eight additional digesters will be installed from 1994-1999 to service the secondary plant. Each egg-shaped digester will control 11 400 m^3 of sludge.

Instead of discharging effluent into the Harbor, it will be transported through a 7.5 m wide outfall tunnel drilled in rock 133 m below the sea bed and connected to 55 diffusers at the end of the tunnel 15.2 km out into the Massachusetts Bay. Tunneling proceeds at about 37 m per day performed in three, 8-hour shifts. About 6.5 km of tunneling have been completed towards a planned completion in July 1996. The $200-million tunnel is a joint venture of Kiewit, Atkinson, and Kenny Construction Companies.

BLACKSBURG, VA

5. Virginia Polytechnic Institute and State University, Center for Intelligent Material Systems and Structures, Fiber and Electro-Optics Center, and Center for Construction Engineering.

In the Intelligent Material Systems and Structures Laboratory[6] the delegation discussed several projects:

- Determining phase transfer characteristics of Shape Memory Alloys (SMA) to improve impact tolerance of SMA hybrid composites. By embedding small amounts of fibrous SMA materials into brittle composite materials, greater composite impact damage toughness can be achieved. Impact strain energy is more readily absorbed by their high-strain-to-failure two-phase SMA materials than by the brittle host composites and is not available to initiate damage in the host composite material.
- Detecting damage in structures using direct and converse electromechanical properties of piezoelectric materials. This approach provides opportunities for the simultaneous actuation and sensing of structures (e.g., collocated actuator/sensor). The variation in the electrical impedance of a piezoelectric patch bonded to a structure, while driven

---

5 Tim Watkins, Public Information Coordinator, hosted the delegation.

6 Dr. Zaffir A. Choudhry, Center for Intelligent Material Systems and Structures, hosted the delegation.

by a fixed alternating electric field over a frequency range, provides valuable information about the structural dynamic behavior. This information, which is analogous to the frequency response and easily obtainable, can use vibration signatures-based non-destructive evaluation. This work is expected to have utility in damping antennae and controlling vibrations and noise in robotic systems, space platforms, and machinery.

- Developing vibration signature based damage detection techniques which allow for the localization of the actuation and sensing area. In experiments with a truss structure, and using a single piezoelectric patch for actuation and sensing, localization was shown to be possible at higher frequencies typically from 20 to 100 kHz.
- Developing low-cost variable friction electrostatic damper for active/passive vibration control.
- Developing active and passive material tagging concepts for health monitoring of structures. Tagging involves adding a small amount of micron-sized "tagging" sensor particles to the host material and using them to determine the state-of-the-material. Active tagging involves exciting the sensing particles and measuring the response of the host material. Passive tagging involves sensing the distribution of the particles. An example of a passive technique is adding magnetic particles to an adhesive and using an eddy current probe to detect voids in a tagged adhesive bond. Applications of passive and active tagging techniques include characterization of adhesive bonds, cure monitoring, intelligent processing, nondestructive materials evaluation, damage detection, and in-service health monitoring.

At the Fiber and Optical Research Center[7] the delegation discussed work in:

- Monitoring building system's temperature and state-of-health using embedded optical fiber sensors. Impact monitoring using time of flight signal processing was demonstrated to determine when and where a structure is impacted. Acoustic waves are measured using the optical fiber sensors embedded in the structure. Measurements also are being performed to determine a structure's plastic deformation, elongation, etc. This work involves post processing of the data; research is underway toward real time processing.
- Detecting corrosion on aluminum substrates under coatings using optical fiber sensing. This work focuses on monitoring corrosion on aircraft parts to reduce failure probability and downtime for inspection and repair.
- Performing experiments using sapphire fiber with coatings such as titanium oxide as a tool for high temperatures (i.e. greater than 1000 °C).

At the Center for Construction Engineering[8], the delegation was shown a demonstration of their Laser Based Digital Positioning System, a metrology based technology. The system makes 3-D measurements digitally in real time with accuracy of 1 mm at 100 m. The system must use at least two fixed laser transmitters whose signals are recorded by a survey

---

7 Mr. Mark Miller, Research Associate hosted the delegation.

8 Dr. Yvan Beliveau, hosted the delegation.

rod equipped with a receiver and processor. The information is processed and analyzed to provide the dimensional location of the desired point. The digital positioning data is entered to CAD systems to create real time as-built models. The reverse permits locating or laying out points in space. The system can be configured to self-calibrate.

The positioning system is being tested to measure pavement leveling, curb lanes, fine grading for slopes, and equipment automation. It is claimed to have applications to model full vibrations of bridges or other structures such as space stations, controlling automated work systems such as heavy equipment operation for earthwork operation, and used for just-in-time fabrication.

This technology is being coordinated with the Civil Engineering Research Foundation and the CORPS through a Cooperative Research Development Agreement (CRADA) program. A consortium has been formed to bring together this CRADA; members include Spatial Positioning Systems (a spin-off business), Bechtel Corporation, Jacobus Technologies, National Science Foundation, Intergraph, and DuPont.

VICKSBURG, MS

6. Waterways Experiment Station

The delegation was hosted by the U.S. Army Corps of Engineers' Waterways Experiment Station[9] (WES). Located in Vicksburg, Mississippi, WES is an Army research and development facility, comprised of five laboratories and a center. WES was established by the U.S. Army in 1929. It's annual budget is over $360 million. It's staff includes about 1500 civilian employees and several members of the armed forces.

The program at WES included a mini-symposium and visits to the Geotechnical Laboratory, the Structures Laboratory, and the Information Technology Laboratory (ITL). The symposium included presentations by Mr. Vincent Chiarito on *Seismic Evaluation of Reinforced Concrete Intake Structures*; by Dr. Takashi Iijima on *Overview of Research Performed by the Public Works Research Institute*, and by Dr. Kazuhiko Kawashima on *Ground Motion Characteristics Based on Analysis of Strong Motion Records*. WES staff learned that a number of PWRI's research programs are similar to theirs, and showed strong interest in collaborative research with PWRI.

The world's largest centrifuge is under construction at the Geotechnical Laboratory. It has a radius of 6.5 m, a maximum payload at 350 g of 2000 kg, and a maximum g-force of 1,144,000 kg. It is scheduled to be in operation in early 1995. ITL is designated as DoD High Performance Computing Center. One of the highlights of the visit was a demonstration of a virtual reality walk through the ITL. In the Structures Laboratory, computer-based analytical modeling is extensively used to solve many of the solution-oriented tasks. It also provided technical expertise in the Corps-wide effort to evaluate, rehabilitate, and maintain

---

9 Dr. A.G. Franklin, Chief Earthquake Engineering and Geophysics Division, WES scheduled the visit.

many aging hydraulic structures operated by the Corps.

LOS ANGELES, CA

7. Damage sites from Northridge Earthquake.

At the California Department of Transportation's (CALTRANS) District 7 Office,[10] the delegation was briefed on the status of CALTRANS repairs to damaged bridges and highways from the Northridge Earthquake. Following the briefing, CALTRANS hosted a visit to three bridge sites. Within days after the earthquake, CALTRANS estimated highway and bridge repairs would cost more than $670 million. In May 1994, these estimates were revised to $308 million because many bridges and highways only required repairs, not full demolition and rebuilding, and there was less roadway damage than originally estimated. The Governor of California enacted emergency procurement permitting CALTRANS to award contracts after the lowest bid was accepted for repairs, demolition and construction of highways and bridges to minimize down time. Generally, a short list of five bidders having proved experience with CALTRANS and the ability to finance portions of the job (would be later reimbursed) were accepted. CALTRANS incorporated bonuses and penalties in many of these contracts; some bonuses and penalties were as large as $200 thousand per day. One contractor saved many days of proposed construction schedule by renting a train to haul construction equipment and materials from the source to Los Angeles.

Immediately after the earthquake, CALTRANS began identifying alternative traffic routes around damaged highways and bridges. CALTRANS daily adjusted traffic routings as debris was cleared and repairs completed. Citizens also offered recommendations to speed traffic flow, which CALTRANS implemented.

The status of the three bridges the delegation visited are:

- Interchange I-5/Route 14 (Golden State/Antelope Freeway) now accommodates all vehicle traffic on its truck bypass. Two contracts were let for the demolition of the three most seriously damaged overhead ramps. Work is expected to be completed in July 1994. The five other damaged bridge superstructures (less severely damaged than the first three) will be destroyed and rebuilt one at a time permitting vehicle traffic use of the others.
- Eastbound spans of Route 118 (Simi Valley Freeway) at Mission Boulevard and Gothic Avenue and at Bull Creek Canyon have been replaced. The eastbound structure is in the process of being replaced. These bridges were designed to a site specific earthquake spectra based on a maximum magnitude of 7.5. The maximum credible earthquake for this specific area has not been adjusted due to the Northridge Earthquake; however, the new structures are designed to meet present seismic criteria. The bridge decks were widened to accommodate a future HOV lane.
- I-10 and LaCienega bridge is open. The bridge was designed with shear keys to

---

[10] Mr. Vincent Moreno, Public Affairs Office, District 7, hosted the delegation.

reduce lateral movement; lack of adequate confinement was a major factor in its extensive damage.

Other bridge repairs are based on their original design specifications; however, footings are being strengthened by increasing their size and adding additional reinforcement.

8. Seven Oaks Dam Project.

The U.S. Army Corps of Engineers[11] hosted the delegation to this earth/rock fill dam site that will control the flood plain downstream of the Santa Ana River. Flood water will be diverted, as needed, into an open space below the dam to provide a natural floodway and into a wildlife habitat corridor. Fourteen floods occurred in this region during the 1900s. In the past, they flooded over 44,500 ha of land to an average depth of 1 m. The dam when completed will be 192 m high (167 m above and 24 m feet below ground), its crest length is 914 m and 13 m wide at the top. Its detached spillway will be located about 0.5 km east of the dam; water will drain into a neighboring valley. The dam's reservoir is designed for about 60,000 ha. The inlet structure will screen sediment before traveling through the 61 m high, 500 m outlet tunnel, the intake tower, air shaft, exit tunnel, and finally the plunge pool. The project's cost is $1.4 billion; $460 million for the dam and $940 million to improve the channel to the Pacific Ocean and raise the Pravo Dam and enlarge its Reservoir located downstream of the Seven Oaks Dam.

The delegation visited the dam construction site. Some construction has started in preparation for the actual dam. The coffer dam is under construction, pilot holes were drilled for the air shaft, the spillway's foundation was grouted, the intake structure is nearing completion.

Forty workers are now involved in the construction; they will increase to 300 as work on the dam itself is started. Estimated date of project completion is between 1998 and 2000.

Noel J. Raufaste, Secretary-General
U.S.-Side Panel on Wind and Seismic Effects

---

[11] Dr. William Roper, Assistant Director R&D (Civil Works) Corps of Engineers scheduled the visit.

ABSTRACT

This publication is the Proceedings of the 26th Joint Meeting of the U.S.-Japan Panel on Wind and Seismic Effects. The meeting was held at the National Institute of Standards and Technology, Gaithersburg, Maryland, during May 17-20, 1994. The Proceedings include the program, list of members, panel resolutions, task committee reports, and 45 technical papers.

The papers were presented under six themes: (I) - Wind Engineering, (II) - Earthquake Engineering, (III) - Storm Surge and Tsunamis, (IV) - Joint Cooperative Research Program, (V) - Northridge Southern California and Hokkaido Nansei-Oki Earthquakes and (VI) - Summaries of Task Committee Workshop Reports (oral presentations only).

KEYWORDS: accelerograph; bridges; building technology; disaster reduction; earthquakes; geotechnical engineering; ground failures; lifelines; liquefaction; masonry; repair and retrofit; risk assessment; seismic; soils; standards; storm surge; structural engineering; tsunamis; and wind loads.

CONTENTS

PAGE

PREFACE III

ABSTRACT XVI

AGENDA FOR 26TH JOINT UJNR MEETING XXIII

LIST OF PANEL MEMBERS XXXIII

LIST OF TASK COMMITTEE MEMBERS XLIX

RESOLUTIONS LIII

THEME: WIND ENGINEERING

Wind Tunnel Experiment for a Super Long-Span Cable-Stayed Bridge in Smooth Flow
Hiroshi Sato, Ryuichi Toriumi, Makoto Kitagawa, and Hiroshi Katsuchi 3

Wind Tunnel Tests on Tapered Cylinders for Highway Support Structures
Harold R. Bosch 17

Standards to Resist Hurricane Wind Forces
G. Robert Fuller and R. D. Marshall 31

Inauguration of International Wind Engineering Forum and New U.S.-Japan Cooperative Research Program
Hisashi Okada and Hiroyuki Yamanouchi 39

THEME: EARTHQUAKE ENGINEERING

A Seismic Retrofitting Manual for Highway Bridges
Ian G. Buckle, Ian M. Friedland, and James D. Cooper 47

Development of Innovative Seismic Response Control of Bridges
Kazuhiko Kawashima, Shigeki Unjoh, and Hidetoshi Mukai 59

Innovative Seismic Testing Procedures
Stephen A. Mahin and S. C. Liu 81

Standard Test Procedures for Seismic Isolation Systems
Harry W. Shenton, III 97

State of the Arts in Japan Concerned With Application of Carbon Fiber for Rehabilitation and Strengthening for Concrete Bridges
Nishikawa Kazuhiro, and Koga Masajiro 109

Construction Automation Research
K. P. Chong and S. C. Liu 123

Design Guidelines for Precast Reinforced Concrete Buildings
Shinsuke Nakata, Masaomi Teshigawara
Takashi Kaminosono, and Hitoshi Shiohara 133

A Post-Earthquake System for Estimating Seismic Damage to Road Facilities by a Strong Motion Observation Network
Hisanori Otsuka, Ryoji Hagiwara and Yoshio Ninomiya 139

Use of Probabilistic Earthquake Models for Design and Evaluation
Jeffrey K. Kimball and Ann Bieniawski 151

Structural Model of Functional Damage Due to an Earthquake in Urban Area
Kazuhiko Kawashima, Hideki Sugita,
Tomoru Nakajima, and Takashi Sato 175

Dynamic Behavior of Pile Foundation in Liquefaction Process
T. Kagawa, C. Minowa, and H. Mizuno 187

Suitability of SASW Method in Complex Geosystems
D. W. Sykora, J. M. Roesset, and K. H. Stokoe II 199

Effectiveness of Measures Against Liquefaction Confirmed at a Recent Earthquake—A Case History During 1993 Kushiro-Oki Earthquake
S. Iai, Y. Matsunaga, T. Morita, and H. Sakurai 213

Review of Progress in Dynamic Geotechnical Centrifuge Research
Ronald F. Scott 227

Shaking Table Failure Tests of Actual Size RC Structures
Chikahiro Minowams, Keiichi Ohtani, Nobuyuki Ogawa,
Tadashi Mikoshiba, Toshihiro Hayashida, and Tsuneo Okada 247

Response of a Mid-Water Depth Platform Subject to Earthquakes
Charles E. Smith 267

Uplift of Sewage Manholes During 1993 Kushiro-Oki Earthquake
Osamu Matsuo, Hisanori Otsuka, Yoshio Ninomiya, and Junichi Koseki 285

Survey of Research in the Area of Seismic Response of Concrete Dams
Robert L. Hall, and William E. Roper, ... 297

Damage and Behavior of Dams During the 1993 Kushiro Oki Earthquake and the 1993 Hokkaido Nansei Oki Earthquake
Akira Nakamura, Nario Yasuda, and Tomoya Iwashita 305

THEME: STORM SURGE AND TSUNAMIS

Evaluation of Seismic and Flood Hazards Potential for a Large Earth-Filled Dam
N. Simon, M. Reich, P. C. Wang, R. Khanbilvardi, and T. McSpadden 329

Tsunami Runup Distribution Generated by the July 12, 1993, Hokkaido-Nansei-Oki Earthquake
E. N. Bernard and F. I. González 335

Propagation of Hokkaido-Nansei-Oki Earthquake Tsunami Around Cape Aonae
Shigenobu Tanaka, Shinji Sato, and Kenji Noguchi 345

Numerical Modeling Tsunamis
Philip L.-F. Liu 357

THEME: SUMMARY OF JOINT COOPERATIVE RESEARCH PROGRAMS

The Status of the U.S. Precast Seismic Structural Systems (PRESSS) Program
M. J. N. Priestly and H. S. Lew 365

The Present and Future of the United States-Japan Cooperative Earthquake Research Program Utilizing Large-Scale Testing Facilities
Hiroyuki Yamanouchi 369

THEME: NORTHRIDGE SOUTHERN CALIFORNIA AND HOKKAIDO NANSEI-OKI EARTHQUAKES

The January 17, 1994, Northridge Earthquake, California
H. S. Lew, Jim Cooper, Sam Hacopian, Walter Hays, and Mike Mahoney 375

Summary Report on the Northridge, South California, U.S.A., Earthquake of January, 1994
Yukihiko Sumiyoshi, Tomomitsu Fujii, Kazuhiko Kawashima, Tatsuo Uwabe, Kouichi Koshiumi, Eiichi Itoigawa, Yoshiaki Nakamura, Kimihiko Izumi, and Hideki Sugita 427

The M8.1 Guam Earthquake of August 8, 1993
A. Gerald Brady 461

Infrastructure Damage by 1993 Hokkaido-Nansei-Oki Earthquake
Takashi Iijima, Yutaka Iida, Kazuhiko Kawashima, Hisanori Otsuka, Osamu Matsuo, Shigenobu Tanaka, Akira Nakamura, Masanori Nakano, and Ryosuke Tsunaki 467

12 July 1993 Hokkaido-Nansei-Oki Earthquake
Riley M. Chung 499

MANUSCRIPTS AUTHORED FOR PANEL MEETING BUT NOT PRESENTED ORALLY

Technological Development for Automatic Construction Methods of Caissons
Masanori Nakano, Jiro Fukui, and Shigeru Takagi 529

Strong-Motion Records on the Hokkaido-Nansei-Oki Earthquake in 1993
Masashi Satoh, Yuji Ono, Toshio Yamauchi, and Hiroaki Nishi 541

Development of Integrated Numerical Research System for Prevention and Estimation of Coastal Disaster
Tomotsuka Takayama, Chiaki Goto, Hidenori Shibaki, and Toshio Aono 555

Structural Testing of Confined Masonry for the Third World Housing
Hatsukazu Mizuno, Tetsuro Goto, Masanori Iiba, Hiroto Kato, and Yutaka Yamazaki 569

Guideline for Safety Evaluation of Structural Response-Control Building (Tentative)
Kitagawa Yoshikazu, Midorikawa Mitsumasa, Iiba Masanori, Fujitani Hideo, and Kashima Toshihide 581

Tsunami Disaster Caused by Hokkaido-Nansei-Oki Earthquake in 1993
Shunji Niwa, Takekazu Akagiri, Masakatsu Horino, and Masaharu Tsuzawa 591

The Dam Safety Program
William S. Bivins and Harold W. Andress 601

Multi-Hazard Mitigation for Non-Engineered Structures
Michael Mahoney 607

Use of Structural Response Data from Small Earthquakes and Aftershocks
Erdal Şafak 613

Three Recent Tsunamis—Warning System Response
Michael E. Blackford 625

Hurricane Storm Surge Analysis for the Coast of Delaware
David J. Mark, Norman W. Scheffner, and Keith D. Watson 629

APPENDIX: TASK COMMITTEE REPORTS 649

Agenda
26th Technical Panel Meeting on Wind and Seismic Effects
16–20 May 1994

Monday 16 May

0930 Welcome and Overview of BFRL
Richard N. Wright, Director, BFRL

1005 Overview Structures Division - H.S. Lew, Chief
Laboratory B-135

1020 Overview Building Materials Division - Geoffrey Frohnsdorff, Chief
Quality Control/Quality Assurance (B-213)
Expert Systems and Materials Reference Laboratory
Image Processing and Modeling (B-337)

1115 Overview Fire Research - Ken Steckler, Physicist
Discuss Pool Fires, Other Topics

1135 Discuss Fire Suppression - Anthony Hamins, Mechanical Engineer

1150 Lunch

1330 Cold Neutron Research Facility - Michael Rowe, Chief, Reactor Radiation Division
Neutron Nondestructive Evaluation
Polymer Measurements, Other Topics

1410 NIST's Advanced Technology Program - James Hill, Head, ATP's Construction Program

1435 Green Technologies - James Hill, Chief, Building Environment Division
Refrigerant Laboratory (B-129)
Building Controls Laboratory (B-121)

1500 Wrap-Up - Noel Raufaste, Head, Cooperative Research Programs
BFRL Conference Room (B-221)

Tuesday 17 May

1000 **OPENING CEREMONIES**
(Lecture Room B, Administration Building)

Call to order by Noel RAUFASTE, Secretary-General US Side, UJNR Panel

Opening remarks by Raymond KAMMER, Deputy Director, National Institute of Standards and Technology

Remarks by Yukihide HAYASHI, Counsellor for Science and Technology, Embassy of Japan

Remarks by Richard N. WRIGHT, Chairman US-Side, Panel on Wind and Seismic Effects, Director, Building and Fire Research Laboratory

Remarks by Takashi IIJIMA, Chairman Japan-Side, Panel on Wind and Seismic Effects, Director-General, Public Works Research Institute

Introduction of U.S. Members by U.S. Panel Chairman

Introduction of Japan Members by Japan Panel Chairman

Elect Joint Meeting Chairman

Adopt Agenda

Adjourn

1115 Group Photograph

1130 **Lunch**: Hosted by the National Institute of Standards and Technology, Raymond KAMMER, Deputy Director

THEME - WIND ENGINEERING

1230-1410 **Technical Session - Wind Engineering**
Chairman: Dr. Takashi IIJIMA

1230 Wind Tunnel Experiment for a Super Long-Span Cable-Stayed Bridge in Smooth Flow, Hiroshi SATO*, Ryuichi TORIUMI, Makoto KITAGAWA, PWRI, and Hiroshi KATSUCHI, HSBA

1250 Wind Tunnel Tests on Tapered Cylinders for Highway Support Structures, Harold R. BOSCH, FHWA

1310 Standards to Better Resist the Effects of Hurricanes and Tornadoes, Richard MARSHALL*, NIST and Robert FULLER, HUD

1330 Inauguration of International Wind Engineering Forum and New U.S.-Japan Cooperative Research Program, Hisashi OKADA* and Hiroyuki YAMANOUCHI, BRI

1350 Discussion

1410 Break

TASK COMMITTEE MEETINGS

1430-1650 Task Committee Meetings

T/C A Strong Motion Data and Applications (G. Brady/S. Iai, Chairmen)
Room B111 Administration Building

T/C C Evaluation and Improvement of Structures (K. Chong/Okada, Chairmen)
Lecture Room B Administration Building

T/C D Dam Earthquake Engineering (W. Roper/K. Nishikawa, Chairmen)
Room B113 Administration Building

T/C H Soil Behavior and Stability During Earthquakes (G. Franklin/K. Kawashima, Chairmen)
Room A369/Building 224

T/C I Storm Surge and Tsunami (H. Meyers/H. Sato, Chairmen)
Room B221/Building 226

1650 **Adjourn for day**

*Presenter

Wednesday 18 May

THEME - EARTHQUAKE ENGINEERING

0830-1130 Technical Session - Earthquake Engineering Part 1

Chairman: Dr. Richard WRIGHT

0830 A Seismic Retrofitting Manual for Highway Bridges, Ian G. BUCKLE, Ian M. FRIEDLAND (NCEER), and James D. COOPER, FHWA

0850 Development of Innovative Response Control of Bridges, Kazuhiko KAWASHIMA*, Shigeki UNJOH, and Hidetoshi MUKAI, PWRI

0910 Innovative Seismic Experimental Methods, Steve MAHIN*, UC Berkeley and S.C. LIU, NSF

0930 Discussion

0950 Break

1010 Standard Test Procedures for Seismic Isolation Systems, Harry SHENTON, III, NIST

1030 State-of-the-Art in Japan Concerning the Application of Carbon Fiber for the Rehabilitation and Strengthening of Concrete Bridges, Kazuhiro NISHIKAWA*, PWRI and Masajiro KOGA, Obayashi Corporation

1050 Construction Automation Research, Ken P. CHONG* and S.C. LIU, NSF

1110 Discussion

1130 Adjourn for Lunch

1130 Lunch: Hosted by Federal Emergency Management Agency, Richard Moore, Associate Director for Mitigation

1230-1410 **Technical Session - Earthquake Engineering**
Chairman: Dr. Richard WRIGHT

1230 Design Guidelines for Precast Reinforced Concrete Buildings, Shinsuke NAKATA, Masaomi TESHIGAWARA, Takashi KAMINOSONO, and Hitoshi SHIOBARA*, BRI

1250 A Predicting System for the Seismic Damage of Road Facilities by a Strong Motion Observation Network, Hisanori OTSUKA and Yoshio NINOMIYA, PWRI (presented by Koichi YOKOYAMA*)

1310 Use of Probabilistic Earthquake Models for Design and Evaluation, Jeffrey K. KIMBALL* and Ann BIENIAWSKI, DOE/DP

1330 Structural Model on Functional Damage Due to an Earthquake in Urban Area, Kazuhiko KAWASHIMA, Hideki SUGITA*, Tomoru NAKAJIMA, and Takashi SATO, PWRI

1350 Discussion

1410 Break

TASK COMMITTEE MEETINGS

1430-1700 Task Committee Meetings

T/C B Testing and Evaluation Procedures for Building Systems (H.S. Lew/K. Ohtani, Chairmen)
Room B111 Administration Building

T/C F Disaster Prevention Methods for Lifeline Systems (R. Chung/K. Kawashima, Chairmen)
Room B113 Administration Building

T/C G Structural Control and Intelligent Material Systems (S.C. Liu/Shiohara, Chairmen)
Room A369/Building 224

T/C J Wind and Earthquake Engineering for Transportation Systems (J. Cooper/K. Yokoyama, Chairmen)
Lecture Room B, Administration Building

T/C K Wind and Earthquake Engineering for Offshore and Coastal Facilities (C. Smith/S. Iai, Chairmen)
Room B221/Building 226

1700 **Adjourn for day**

Thursday 19 May

THEME - EARTHQUAKE ENGINEERING - PART II

0830-1130 **Technical Session - Earthquake Engineering-Part II**
Chairman: Dr. Takashi IIJIMA

0830 Dynamic Behavior of Pile Foundation in Liquefaction Process, Chikahiro MINOWA*, Hatsukazu MIZUNO, and Takaaki KAGAWA, NIED

0850 Suitability of SASW Method in Complex Geosystems, David W. SYKORA, Woodward-Clyde Consultants, Jose M. ROESSET, and Kenneth H. STOKOE II, WES

0910 Effectiveness of Measures Against Liquefaction Confirmed at a Recent Earthquake - A Case History During 1993 Kushiro-Oki Earthquake, Susumu IAI*, Yasuo MATSUNAGA, Toshikazu MORITA, and Hirotaka SAKURAI, PHRI

0930 Discussion

0950 Break

1010 Review of Progress in Dynamic Geotechnical Centrifuge Research, Ronald F. SCOTT, California Institute of Technology

1030 Failure Tests of Actual Size RC Structures, Keiichi OHTANI*, Nobuyuki OGAWA, Tadashi MIKOSHIBA, Chikahiro MINOWA, Toshihiro HAYASHIDA, and Tsuneo OKADA, NIED

1050 Response of Mid-Water Platforms Subjected to Earthquakes, Charles SMITH, MMS

1110 Discussion

1130 Adjourn for lunch

1130 Lunch: Hosted by U.S. Geological Survey, Robert L. Wesson, Chief, Office of Earthquakes, Volcanoes, and Engineering

1230-1410 **Earthquake Engineering (Continued)**

Chairman: Dr. Takashi IIJIMA

1230 Uplift of Sewage Manholes During 1993 Kushiro-oki Earthquake, Osamu MATSUO, Junichi KOSEKI, Hisanori OTSUKA, and Yoshio Ninomiya, PWRI (presented by Masayuki KANDA)

1250 Survey of Research in the Area of Seismic Response of Concrete Dams, Robert L. HALL, WES and William E. ROPER*, CORPS

1310 Behaviours and Damages of Dams During 1993 Kushiro Oki Earthquake and 1993 Hokkaido Nansei Oki Earthquake, Akira NAKAMURA, Nario YASUDA, and Tomoya IWASHITA, PWRI (presented by Shigetoshi KOBAYASHI)

1330 Evaluation of Seismic and Flood Hazards Potential for a Large Earth-Filled Dam, Nick SIMOS, BNL, Morris REICH, BNL, Ping WENG, BNL, Reza KHANBILVARD, BNL, and Tom MCSPADDEN, DOE/EH

1350 Discussion

1410 Break

THEME - STORM SURGE AND TSUNAMIS

Chairman: Dr. Takashi IIJIMA

1430-1550 **Technical Session - Storm Surge and Tsunamis**

1430 Tsunami Runup Distribution Generated by the July 12, 1993, Hokkaido-Nansei-Oki Earthquake, Eddie N. BERNARD and Frank I. GONZALEZ, NOAA (presented by Michael BLACKFORD)

1450 Propagation of Hokkaido-Nansei-Oki Earthquake Tsunami Around Cape Aonae, Shigenobu TANAKA and Kenji NOGUCHI, PWRI (presented by Takashi IIJIMA)

1510 Numerical Modeling of Tsunamis, Philip LIU, Cornell University

1530 Discussion

1550 Break

THEME - SUMMARY OF JOINT COOPERATIVE RESEARCH PROGRAMS

Chairman: Dr. Takashi IIJIMA

1610-1710 **Technical Session - Joint Cooperative Research Programs**

1610 U.S.-Japan Cooperative Research in Precast Seismic Structural Systems (PRESSS) Program--Status Report, Nigel PRIESTLY, UCSD and H.S. LEW*, NIST

1630 The Present and Future of the U.S.-Japan Cooperative Earthquake Research Program Utilizing Large-Scale Testing Facilities, Hiroyuki YAMANOUCHI, BRI (presented by Hisashi OKADA)

1650 Discussions

1710 **Adjourn for day**

Friday 20 May

THEME - NORTHRIDGE SOUTHERN CALIFORNIA AND HOKKAIDO NANSEI-OKI EARTHQUAKES
Chairman: Dr. Richard WRIGHT

0815-1030 **Technical Session - Northridge Southern California and Hokkaido Nansei-Oki Earthquakes**

0815 Summary U.S.-Side Investigation of Damages from Northridge Southern California Earthquake, H.S. LEW, NIST

0835 Summary Japan-Side Investigation of Damages from Northridge Southern California Earthquake, Yukihiko SUMIYOSHI, Tomomitsu FUJII, Kazuhiko KAWASHIMA*, Tatsuo UWABE, Kouichi TORIUMI, Eiichi ITOIGAWA, Yoshiaki NAKAMURA, Kimihiko IZUMI, and Hideki SUGITA, PWRI

0855 Discussion

0910 The M8.1 Guam Earthquake of 8 August 1993, Gerald BRADY, USGS

0930 Infrastructures Damage by 1993 Hokkaido-Nansei-Oki Earthquake, Takashi IIJIMA*, Yutaka IIDA, Kazuhiko KAWASHIMA, Hisanori OTSUKA, Osamu MATSUO, Shigenobu TANAKA, Akira NAKAMURA, and Masanori NAKANO, PWRI

0950 12 July 1993, Hokkaido Earthquake, Riley CHUNG, NIST

1010 Discussion

1030 Break

THEME - REPORT OF TASK COMMITTEE WORKSHOPS

Chairman: Dr. Richard WRIGHT

1045-1145 **Technical Session - Report of Workshops**

1045	T/C "A"	Strong Motion Data (Presented by S. Iai)
1055	T/C "G&J"	3rd Workshop on Earthquake Protective Systems of Bridges (Presented by K. Kawashima)
1105	T/C "I"	3rd Workshop on Tsunamis (Presented by H. Meyers)
1115	T/C "J"	2nd Workshop on Seismic Retrofit of Bridges (Presented by S. Mahin)
1125	T/C "J"	10th Workshop on Bridge Engineering (Presented by J. Cooper)

1135 Discussion

1145 Adjourn for Lunch

1145 Lunch: Hosted by the National Science Foundation, William W. HAKALA, Director for Mechanical and Structural Systems Division

1230-1415 **TASK COMMITTEE REPORTS AND RESOLUTIONS**

Report of Task Committees
Chairman: Dr. Richard WRIGHT

T/C A	Strong-Motion Data and Applications
T/C B	Testing and Evaluation Procedures for Building Systems
T/C C	Evaluation and Improvement of Structures
T/C D	Dam Earthquake Engineering
T/C F	Disaster Prevention Methods for Lifeline Systems
T/C G	Structural Control and Intelligent Materials Systems
T/C H	Soil Behavior and Stability During Earthquakes
T/C I	Storm Surge and Tsunami
T/C J	Wind and Earthquake Engineering for Transportation Systems
T/C K	Wind and Earthquake Engineering for Offshore and Coastal Facilities

1415-1430 Break

1430-1530 **Adoption of Final Resolutions**

1530-1540 Break

CLOSING CEREMONIES

1540 Call to Order by Noel J. RAUFASTE, Secretary-General, US-Side Panel

Closing Remarks by Takashi IIJIMA, Chairman Japan-Side Panel

Closing Remarks by Richard N. WRIGHT, Chairman US-Side Panel

1600 **Conclusion of Joint Meeting**

United States-Side Panel on Wind and Seismic Effects
Membership List
May 1994

Dr. Richard N. Wright
Chairman
Director, Building and Fire Research Laboratory
National Institute of Standards and Technology
U.S. Department of Commerce
Gaithersburg, MD 20899
301-975-5900 FAX 301-975-4032 wright@micf.nist.gov

Mr. Noel J. Raufaste
Secretary-General
Head, Cooperative Research Programs
Building and Fire Research Laboratory
National Institute of Standards and Technology
U.S. Department of Commerce
Gaithersburg, MD 20899
301-975-5905 FAX 301-975-4032 raufaste@micf.nist.gov

Dr. Kharaiti L. Abrol
Acting Director
Structural Engineering Service (088475)
Department of Veterans Affairs
810 Vermont Avenue, NW
Washington, DC 20420
202-233-7379 FAX 202-233-2115

Dr. John Ake
Geophysicist
Seismotectonics and Geophysics Section
P.O. Box 25007
Bureau of Reclamation
U.S. Department of the Interior
Denver, CO 80225
303-236-4195 FAX 303-236-6763

Dr. S. T. Algermissen
Deputy for Geologic Hazard & Risk Assessment
Office of International Geology
U.S. Geological Survey
917 National Center
12201 Sunrise Valley Drive
U.S. Department of the Interior
Reston, VA 22092
703-648-6051 FAX 703-648-4227

Mr. Charles E. Anderson
Seismic Safety Coordinator
P.O. Box 25007 (D-3130)
Bureau of Reclamation
U.S. Department of the Interior
Denver, CO 80225
303-236-9114 FAX 303-236-6763

Dr. Celso S. Barrientos
Supervisory Physical Scientist
National Environmental Satelite Data
Information Service - Code E/RA28
National Oceanic and Atmospheric Administration
U.S. Department of Commerce
5200 Auth Road
Camp Springs, MD 20746
301-763-8102 FAX 301-763-8108

Dr. Eddie N. Bernard
Director, Pacific Marine Environmental Laboratory
National Oceanic and Atmospheric Administration
U.S. Department of Commerce
7600 Sand Point Way, NE
BIN C15700/Building 3
Seattle, WA 98115-0070
206-526-6800 FAX 206-526-6815

Dr. Roger D. Borcherdt
Branch of Seismology
U.S. Geological Survey
U.S. Department of the Interior
345 Middlefield Road, MS 977
Menlo Park, CA 94025
415-329-5619 FAX 415-329-5163

Dr. A. Gerald Brady
Research Civil Engineer
Branch of Earthquake and Geomagnetic Information
U.S. Geological Survey
U.S. Department of the Interior
345 Middlefield Road, MS 977
Menlo Park, CA 94025
415-329-5664 FAX 415-329-5163

Mr. H. Lee Butler
Chief, Research Division
Coastal Engineering Research Center
U.S. Army Engineer Waterways Experiment Station
Office CEWES-CR
3909 Halls Ferry Road
Vicksburg, MS 39180-6199
601-634-2405 FAX 601-634-4314

Dr. Ken P. Chong
Program Director, Mechanical & Structural Systems
National Science Foundation
4201 Wilson Boulevard - Room 545
Arlington, VA 22230
703-306-1361 FAX 703-306-0291

Dr. Riley Chung
Group Leader, Earthquake Engineering
Structures Division
Building and Fire Research Laboratory
National Institute of Standards and Technology
U.S. Department of Commerce
Gaithersburg, MD 20899
301-975-6056 FAX 301-869-6275

Mr. James D. Cooper
Deputy Chief, Structures Division, HNR-10
Federal Highway Administration
U.S. Department of Transportation
6300 Georgetown Pike
McLean, VA 22101
703-285-2060 FAX 703-285-2766

Dr. A. G. Franklin
Chief, Earthquake Engineering & Geophysics Division
CEWES-GH Geotechnical Laboratory
U.S. Army Engineer Waterways Experiment Station
3909 Halls Ferry Road
Vicksburg, MS 39180-6199
601-634-2658 FAX 601-634-4134

Mr. G. Robert Fuller
Special Assistant
Office of Single Family Housing
Room 9184 HS
U.S. Department of Housing and Urban Development
Washington, DC 20410-8000
202-708-4549 FAX 202-708-5966

Mr. James H. Gates
Caltrans - Structures
P. O. Box 942874
Sacramento, CA 94274
916-227-8773 FAX 916-227-8174

Mr. Peter E. Gurvin
Director, Building Design and Engineering Division
Foreign Building Operations
Building SA-6, Room 335
U.S. Department of State
Washington, DC 20520
703-875-6117 FAX 703-875-6204

Dr. Walter W. Hays
Deputy for Research Applications
Office of Earthquake, Volcanoes and Engineering
905 National Center
U.S. Geological Survey
U.S. Department of the Interior
Reston, VA 22092
703-648-6711 FAX 703-648-6717

Mr. James R. Hill
Manager, Natural Hazards Mitigation Programs
Office of Safety, Health and Quality Assurance
U.S. Department of Energy
Washington, DC 20545
301-903-4508 FAX 301-903-8585 Jim.Hill@HQ.DOE.gov

Mr. Larry C. Hultengren
Senior Structural Engineer
Office of Civil/Structural Engineering
Foreign Building Operations
U.S. Department of State
Washington, DC 20520
703-875-6194 FAX 703-875-6204

Dr. William B. Joyner
Geophysicist
Branch of Seismology
U.S. Geological Survey
U.S. Department of the Interior
345 Middlefield Road, MS 977
Menlo Park, CA 94025
415-329-5640 FAX 415-329-5163

Mr. Roger M. Kenneally
Structural Engineer
Structural and Seismic Engineering Branch
Mail Stop NL/S - 217A
U.S. Nuclear Regulatory Commission
Washington, DC 20555
301-492-3893 FAX 301-492-3696

Dr. H. S. Lew
Chief, Structures Division
Building and Fire Research Laboratory
National Institute of Standards and Technology
U.S. Department of Commerce
Gaithersburg, MD 20899
301-975-6061 FAX 301-869-6275

Dr. Shih-Chi Liu
Program Director, Structural Systems
Division of Biological and Critical Systems
National Science Foundation
4201 Wilson Boulevard - Room 545
Arlington, VA 22230
703-306-1362 FAX 703-306-0291

Dr. Stephen Markwell
Chief, Geotechnical and Geology Division
Code D-3600 - P.O. Box 25007
Bureau of Reclamation
U.S. Department of the Interior
Denver, CO 80225
303-236-9329 FAX 303-236-6763

Dr. Francis G. McLean
Chief, Geotechnical Engineering and Embankment
Dams Branch
P.O. Box 25007
Bureau of Reclamation
U.S. Department of the Interior
Denver, CO 80225
303-236-3854 FAX 303-236-6763

Dr. Raymond E. Meyer
Senior Program Manager
Office of Foreign Disaster Assistance
N/S Room 1262A
Department of State
320 21st Street, NW
Washington, DC 20523-0008
202-647-7530 FAX 202-647-4036

Mr. Herbert Meyers
Chief, Earth Geophysics
National Geophysical Data Center
National Oceanic and Atmospheric Administration
U.S. Department of Commerce
325 Broadway
Boulder, CO 80303-3328
303-497-6521 FAX 303-497-6513

Mr. Ugo Morelli
Policy Manager for Seismology
Federal Emergency Management Agency
500 C Street, SW
Washington, DC 20472
202-646-2810 FAX 202-646-3104

Mr. Howard D. Nickerson
Earthquake Engineering and Weapons Specialist
Naval Facilities Engineering Command
Hoffman Building #2, Room 12S63, Code 04B2
200 Stovall Street
Alexandria, VA 22332
202-433-8599 FAX 202-433-8777

Dr. William E. Roper
Assistant Director
Research and Development (Civil Works)
U.S. Army Corps of Engineers
20 Massachusetts Avenue, N.W
Washington, DC 20314-1000
202-272-0257 FAX 202-272-0907

Dr. John B. Scalzi
Program Director, Structures and Building Systems
National Science Foundation
4201 Wilson Boulevard - Room 545
Arlinton, VA 22230
703-306-1361 FAX 703-306-0291

Dr. Charles E. Smith
Research Program Manager
Offshore Minerals Management
Technology Assessment and Research Branch
Minerals Management Service
U.S. Department of the Interior
381 Elden Street, MS 4800
Herndon, VA 22070-4817
703-787-1559 FAX 703-787-1010

Dr. T. T. Soong
Samuel P. Capen Professor
Department of Civil Engineering
National Center for Earthquake Engineering Research
State University of New York at Buffalo
212 Ketter Hall
Buffalo, NY 14260
716-645-2469 FAX 716-645-3733

Mr. Stan Strickland
Chief, Air Base Systems Branch
Stop 37, WL/FIVC/OL, Bldg. 1120
139 Barnes Drive, STE 2
Tyndall AFB, FL 32403-6001
904-283-3707 FAX 904-283-3722

ALTERNATE MEMBERS

Dr. Clifford J. Astill
Program Director
Division of Biological and Critical Systems
National Science Foundation
4201 Wilson Boulevard - Room 545
Arlington, VA 22230
703-306-1361 FAX 703-306-0291

Dr. Mehmet K. Celebi
Research Civil Engineer
Branch of Earthquake and Geomagnetic Information
U.S. Geological Survey
U.S. Department of the Interior
345 Middlefield Road, MS 977
Menlo Park, CA 94025
415-329-5623 FAX 415-329-5163

Mr. Michael Changery
Chief, Global Analysis Branch
National Climatic Data Center
National Oceanic and Atmospheric Administration
U. S. Department of Commerce
Federal Building
Ashville, NC 28801
704-271-4765 FAX 704-271-4246

Mr. C. Y. Chen
Senior Civil/Geotechnical Engineer
Office of Foreign Buildings
Department of State
Code SA-6, Rm. 327
Washington, DC 20520
703-875-6207 FAX 703-875-6204

Mr. Vincent P. Chiarito
Research Structural Engineer
Structural Mechanics Division
Structures Laboratory
U.S. Army Engineer Waterways Experiment Station
3909 Halls Ferry Road
Vicksburg, MS 39180-6199
601-634-2714 FAX 601-634-3412

Dr. James F. Costello
Senior Structural Engineer
Structural and Seismic Engineering Branch
Structural Section
Office of Nuclear Regulatory Research
U.S. Nuclear Regulatory Commission
Mail Stop 007NL
Washington, DC 20555
301-492-3818 FAX 301-492-3696

Mr. Lucian G. Guthrie
Structural Engineer
Office of Chief of Engineers
Headquarters U.S. Army Corps of Engineers
Corps of Engineers Civil Works Engineering Div.
U.S. Department of the Army
20 Massachusetts Avenue, N.W.
Washington, DC 20314-1000
202-272-8673 FAX 202-272-1485

Dr. Robert L. Hall
Chief, Structural Analysis Group
U.S. Army Engineer Waterways Experiment Station
3909 Halls Ferry Road
Vicksburg, MS 39180-6199
601-634-2567 FAX 601-634-3412

Dr. James R. Houston
Chief, Coastal Engineering Research Center
U.S. Army Engineer Waterways Experiment Station
3909 Halls Ferry Road
Vicksburg, MS 39180-6199
601-634-2000 FAX 601-634-2055

Mr. James Lander
Geophysicist
Cooperative Institute for Research in
Environmental Sciences
University of Colorado
Campus Box 449, Room 152 RL3
3100 Marine Street
Boulder, CO 80309
303-497-6446 FAX 303-497-6513

Mr. Robert R. Ledzian
Senior Staff Assistant for Research
Office of Liaison - Engineering Research, Code 3020
Bureau of Reclamation
U.S. Department of the Interior
1849 C Street, N.W.
Washington, DC 20240
202-208-3432 FAX 202-208-6252

Mr. Tingley K. Lew
Research Structural Engineer
Structures Division
Naval Facilities Engineering Service Center - ESC 62
560 Center Drive
Port Hueneme, CA 93043-4328
805-982-1234 FAX 805-982-1418

Mr. Michael Mahoney
Physical Scientist
Federal Emergency Management Agency
500 C Street, SW
Washington, DC 20472
202-646-2810 FAX 202-646-3104

Dr. J. Eleonora Sabadell
Director, Natural and Manmade Hazards Mitigation Program
Directorate of Engineering
National Science Foundation
4201 Wilson Boulevard - Room 545-03
Arlington, VA 22230
703-306-1361 FAX 703-306-0291

Dr. Erdal Safak
Research Structural Engineer
U.S. Geological Survey
U.S. Department of the Interior
922 National Center
Reston, VA 22092
703-648-6534 FAX 703-648-6717

Japan-Side Panel on Wind and Seismic Effects
Membership List
May 1994

Dr. Takashi Iijima
Chairman, Japan-side Panel on Wind & Seismic Effects
Director-General
Public Works Research Institute
Ministry of Construction
1, Asahi, Tsukuba-shi,
Ibaraki-ken 305
Tel. 298-64-2821 Fax. 298-64-2148

Dr. Kazuhiko Kawashima
Secretary, Japan-side Panel on Wind & Seismic Effects
Research Coordinator for Underground Development
Department of Planning and Administration
Public Works Research Institute
Ministry of Construction
1, Asahi, Tsukuba-shi,
Ibaraki-ken 305
Tel. 298-64-2473 Fax. 298-64-1527

Dr. Hiroshi Sato
Secretary, Japan-side Panel on Wind & Seismic Effects
Head, Structures Division
Public Works Research Institute
Ministry of Construction
1, Asahi, Tsukuba-shi,
Ibaraki-ken 305
Tel. 298-64-2874 Fax. 298-64-0565

Dr. Tokunosuke Fujitani
Chief, The Second Research Laboratory
Applied Meteorology Research Division
Meteorological Research Institute
Japan Meteorological Agency
1-1 Nagamine, Tsukuba-shi,
Ibaraki-ken 305
Tel. 298-53-8620 Fax. 298-55-7240

Mr. Ryoji Hagiwara
Head, Ground Vibration Division
Director, Earthquake Disaster
Prevention Department
Public Works Research Institute
Ministry of Construction
1, Asahi, Tsukuba-shi,
Ibaraki-ken 305
Tel. 298-64-2926 Fax. 298-64-0598

Dr. Hisahiro Hiraishi
Associate Director for Composite
Structures Research
Structural Engineering Department
Building Research Institute
Ministry of Construction
1, Tatehara, Tsukuba-shi,
Ibaraki-ken 305
Tel. 298-64-6639 Fax. 298-64-6773

Dr. Kiichi Horai
Head, Seismology and Volcanology
Research Division
Meteorological Research Institute
Japan Meteorological Agency
1-1, Nagamine, Tsukuba-shi,
Ibaraki-ken 305
Tel. 298-53-8675 Fax. 298-51-3730

Dr. Susumu Iai
Chief, Geotechnical Earthquake
Engineering Laboratory
Port and Harbour Research Institute
Ministry of Transport
3-1-1, Nagase, Yokosuka
Kanagawa-ken 239
Tel. 298-53-8675 Fax. 298-51-3730

Dr. Takamasa Inatomi
Director, Structural Engineering Division
Port and Harbour Research Institute
Ministry of Transport
3-1-1, Nagase, Yokosuka
Kanagawa-ken, 239
Tel. 468-44-5027 Fax. 468-44-4095

Dr. Yoshikazu Kitagawa
Director, International Institute of
Seismology and Earthquake Engineering
Building Research Institute
Ministry of Construction
1, Tatehara, Tsukuba-shi,
Ibaraki-ken 305
Tel. 298-64-6677 Fax. 298-64-6777

Dr. Yasuyuki Koga
Director, Earthquake Disaster
Prevention Department
Public Works Research Institute
Ministry of Construction
1, Asahi, Tsukuba-shi,
Ibaraki-ken 305
Tel. 298-64-2829 Fax. 298-64-0598

Mr. Osamu Matsuo
Head, Soil Dynamics Division
Earthquake Disaster Prevention Department
Public Works Research Institute
Ministry of Construction
1, Asahi, Tsukuba-shi,
Ibaraki-ken 305
Tel. 298-64-2933 Fax. 298-64-2576

Mr. Kiyoshi Mimura
Director, Geographic Department
Geographical Survey Institute
Ministry of Construction
1, Kitazato, Tsukuba-shi,
Ibaraki-ken 305
Tel. 298-64-2667 Fax. 298-64-1804

Mr. Chikahiro Minowa
Cooperative Research Officer
National Research Institute for
Earth Science and Disaster Prevention
3-1, Tennodai, Tsukuba-shi,
Ibaraki-ken, 305
Tel. 298-51-1611 Fax. 298-51-1622

Mr. Hatsukazu Mizuno
Special Researcher for International
Standards, Planning Department
Building Research Institute
Ministry of Construction
1, Tatehara, Tsukuba-shi,
Ibaraki-ken 305
Tel. 298-64-6760 Fax. 298-64-2989

Mr. Akira Nakamura
Head, Fill Type Dam Division
Public Works Research Institute
Ministry of Construction
1, Asahi, Tsukuba-shi,
Ibaraki-ken 305
Tel. 298-64-2413 Fax. 298-64-0164

Mr. Masanori Nakano
Head, Foundation Engineering Division
Structure and Bridge Department
Public Works Research Institute
Ministry of Construction
1, Asahi, Tsukuba-shi,
Ibaraki-ken 305
Tel. 298-64-2873 Fax. 298-64-0565

Dr. Shinsuke Nakata
Director, Production Department
Building Research Institute
Ministry of Construction
1, Tatehara, Tsukuba-shi,
Ibaraki-ken 305
Tel. 298-64-6644 Fax. 298-64-6774

Mr. Kazuhiro Nishikawa
Head, Bridge Division
Structure and Bridge Department
Public Works Research Institute
Ministry of Construction
1, Asahi, Tsukuba-shi,
Ibaraki-ken 305
Tel. 298-64-2905 Fax. 298-64-0565

Dr. Setuo Noda
Deputy Director General
Port and Harbour Research Institute
Ministry of Transport
3-1-1, Nagase, Yokosuka
Kanagawa-ken 239
Tel. 468-44-5000 Fax. 468-42-9265

Dr. Shigeyuki Noto
Director, Structures Division
Civil Engineering Research Institute
Hokkaido Development Agency
1-3, Hiragisi, Toyohira-ku
Sapporo, Hokkaido, 062
Tel. 11-841-1111 Fax. 11-824-1226

Dr. Nobuyuki Ogawa
Head, Earthquake Engineering Laboratory
National Research Institute for Earth
Science and Disaster Prevention
Science and Technology Agency
3-1, Tennodai, Tsukuba-shi,
Ibaraki-ken 305
Tel. 298-51-1611 Fax. 298-51-5658

Mr. Keiichi Ohtani
Director, Disaster Prevention Research Division
National Research Institute for Earth
Science and Disaster Prevention
Science and Technology Agency
3-1, Tennodai, Tsukuba-shi,
Ibaraki-ken 305
Tel. 298-51-1611 Fax. 298-51-1622

Dr. Hisashi Okada
Head, Aerodynamics Division
Structural Engineering Department
Building Research Institute
Ministry of Construction
1, Tatehara, Tsukuba-shi,
Ibaraki-ken 305
Tel. 298-64-6641 Fax. 298-64-6773

Dr. Izuru Okawa
Head, Geotechnical Engineering Division
Structural Engineering Department
Building Research Institute
Ministry of Construction
1, Tatehara, Tsukuba-shi,
Ibaraki-ken 305
Tel. 298-64-6642 Fax. 298-64-6773

Mr. Shin Ootsuka
Head, Typhoon Research Division
Meteorological Research Institute
Japan Meteorological Agency
1-1, Nagamine, Tsukuba-shi,
Ibaraki-ken 305
Tel. 298-53-8663 Fax. 298-55-2683

Dr. Hisanori Otsuka
Head, Earthquake Engineering Division
Earthquake Disaster Prevention Department
Public Works Research Institute
Ministry of Construction
1, Asahi, Tsukuba-shi,
Ibaraki-ken 305
Tel. 298-64-2932 Fax. 298-64-0598

Mr. Masashi Satou
Head, Structures Section
Civil Engineering Research Institute
Hokkaido Development Bureau
Hokkaido Development Agency
1-3, Hiragishi, Toyohira-ku
Sapporo, Hokkaido, 062
Tel. 11-841-1111 Fax. 11-824-1226

Dr. Tomotsuka Takayama
Director, Hydraulic Engineering Division
Port and Harbour Research Institute
Ministry of Transport
3-1-1, Nagase, Yokosuka
Kanagawa-ken 239
Tel. 468-44-5009 Fax. 468-44-3888

Mr. Shigenobu Tanaka
Head, Coastal Engineering Division
River Department
Public Works Research Institute
Ministry of Construction
1, Asahi, Tsukuba-shi,
Ibaraki-ken 305
Tel. 298-64-2327 Fax. 298-64-1168

Dr. Tatsuo Uwabe
Chief, Earthquake Disaster Prevention Laboratory
Structural Engineering Division
Port and Harbour Research Institute
Ministry of Transport
3-1-1, Nagase, Yokosuka
Kanagawa-ken 239
Tel. 468-44-5030 Fax. 468-44-0839

Dr. Hiroyuki Yamanouchi
Director, Structural Engineering Department
Building Research Institute
Ministry of Construction
1, Tatehara, Tsukuba-shi,
Ibaraki-ken 305
Tel. 298-64-6633 Fax. 298-64-6773

Dr. Koichi Yokoyama
Director, Structure and Bridge Department
Public Works Research Institute
Ministry of Construction
1, Asahi, Tsukuba-shi,
Ibaraki-ken 305
Tel. 298-64-2835 Fax. 298-64-0565

May 1994

List of Task Committee Members

Task Committee	US Side	Japanese Side
A. Strong-Motion Data and Applications	A.G. Brady* C.J. Astill R.D. Borcherdt M.K. Celebi A.G. Franklin W.B. Joyner R.B. MacDonald F.G. McLean H. Meyers S.T. Algermissen C.S. Barrientos G.R. Fuller T.K. Lew E. Safak	S. Noda* Y. Kitagawa R. Hagiwara K. Horai K. Mimura S. Iai H. Mizuno K. Ohtani
B. Testing and Evaluation Procedures for Building Systems	H.S. Lew* V.P. Chiarito J.E. Sabadell C.E. Smith K. Abrol S. Sweeney A. Bieniawski	K.Ohtani* O. Matsuo H. Mizuno S. Noda I. Okawa H. Sato
C. Evaluation and Improvement of Structures	K.P. Chong* P.A. Brady C. Mutreja J.O. Jirsa H.S. Lew T.K. Lew H.D. Nickerson D.H. Oh M.A. Phipps J.B. Scalzi S. Woodson S.A. Asar M.K. Celebi G.R. Fuller K.L. Abrol R.L. Hall D. Ellsworth	H. Yamanouchi* H. Hiraishi K. Yokoyama Y. Koga M. Nakano T. Fujitani S. Nakata S. Otsuka I. Okawa H. Sato

D.	Earthquake Engineering for Dams	W.E. Roper* R.L. Hall L.G. Guthrie R. Davidson M.E. Hynes A.G. Franklin R. Navidi L. Von Thun W. Allerton F.G. McLean J.R. Hill	A. Nakamura* R. Hagiwara K. Kawashima H. Otsuka
E.	OPEN		
F.	Disaster Prevention Methods for Lifeline Systems	R.M. Chung* C.J. Astill M.K. Celebi J.D. Cooper G. Al-Chaar T.K. Lew J.B. Scalzi J.S. Spencer S. Wu J.R. Hill S. Sommer	Y. Koga* K. Kawashima R. Hagiwara N. Ogawa H. Otsuka T. Uwabe S. Noto M. Sato
G.	Structural Control and Intelligent Material Systems	S.C. Liu* V.P. Chiarito K.P. Chong J.R. Hayes L.C. Hultengren T.T. Soong	Y. Kitagawa* K. Kawashima N. Ogawa H. Yamanouchi H. Sato C. Minowa H. Otsuka
H.	Soil Behavior and Stability During Earthquakes	A.G. Franklin* C.J. Astill R.D. Borcherdt C.Y. Chen F.G. McLean C.E. Smith R.M. Chung	R. Hagiwara A. Nakamura O. Matsuo H. Mizuno S. Iai Y. Koga S. Noto T. Inatomi M. Nakano
I.	Storm Surge and Tsunami	H. Meyers* C.J. Astill C.S. Barrientos E.N. Bernard L. Butler J. Lander W.E. Roper	S. Tanaka* S. Otsuka T. Takayama S. Otsuka

J. Wind and Earthquake Engineering for Transportation Systems	J.D. Cooper* A.G. Franklin J.H. Gates J.B. Scalzi H.S. Lew P. Yen H.R. Bosch	K. Yokoyama* T. Fujitani R. Hagiwara K. Nishikawa K. Kazuhiko H. Otsuka H. Sato M. Nakano Y. Koga M. Sato
K. Wind and Earthquake Engineering for Offshore and Coastal Facilities	C.E. Smith* C.S. Barrientos W.E. Roper J.E. Sabadell M.C. Miller M.K. Celebi	T. Uwabe* T. Fujitani M. Nakano S. Noda T. Inatomi S. Iai

*Chairman

RESOLUTIONS

Resolutions of the Twenty-Sixth Joint Meeting U.S.-Japan Panel on Wind and Seismic Effects (UJNR)

National Institute of Standards and Technology
Gaithersburg, Maryland
May 17–20, 1994

The following resolutions are hereby adopted:

1. The Twenty-Sixth Joint Panel Meeting provided the forum to exchange valuable technical information which was beneficial to both countries. In view of the importance of cooperative programs on the subject of wind and seismic effects, the continuation of Joint Panel Meetings is considered essential.

2. The following activities have been conducted since the Twenty-Fifth Joint Meeting:

a. Seven Japan researchers performed earthquake engineering assignments as guest researchers in the U.S.: C. Minowa and N. Ogawa from NIED worked at Wayne State University; H. Sugita and M. Kanda from PWRI worked at the University of California (Berkeley) and Virginia Polytechnic Institute; M. Iiba and H. Fujitani from BRI worked at the National Center for Earthquake Engineering Research (SUNY) and H. Shiohara also from BRI worked at Virginia Polytechnic Institute. N. Yasuda from PWRI visited the Headquarters U. S. Army Corps of Engineers for exchange of technical information.

   Four U.S. researchers performed earthquake engineering assignments as guest researchers in Japan: A. Taylor, NIST, D. Norman, WES, and M. Yashinsky, Caltrans worked at PWRI; and M.A. Riley from NCEER worked at BRI.

b. Technical documents, research reports, and proceedings of workshops have been exchanged. These contributed to the development of research programs and enhanced on-going research in both countries.

c. Seven workshops and conferences were held:

   (1) Workshop on Strong Motion Data, Task Committee (A), Menlo Park, CA, 10-17 December 1993.

   (2) The 1st U.S.-Japan Joint Technical Coordinating Committee on Composite and Hybrid Structures Program, Task Committee (B), Tsukuba, Japan, 8-9 November 1993.

   (3) The Fourth U.S.-Japan Joint Technical Coordinating Committee on Precast Seismic Structural Systems Program, Task Committee (B), Tsukuba, Japan, 16-19 May 1994.

   (4) The Third Workshop on Earthquake Protective Systems of Bridges, Task Committees (G&J), Berkeley, CA, 24-27 January 1994.

(5) The Third Workshop on Tsunamis, Task Committee (I), Osaka, Japan, 28 August 1993.

(6) The Tenth Bridge Workshop, Task Committee (J), Lake Tahoe, NV, 10-14 May 1994.

(7) The 2nd Workshop on Seismic Retrofit of Bridges, Task Committee (J), Berkeley, CA, January 20-21, 1994.

3. The Panel, in celebration of the 25th Anniversary of its creation and in remembrance of the 70 year anniversary of the Kanto Earthquake, jointly conducted with the International Decade for Natural Disaster Reduction (IDNDR) Promotion Section of the Ministry of Construction, a one-day Symposium on the (IDNDR), in Tokyo on May 21, 1993. The Symposium increased the awareness of Japanese disaster relief and mitigation decision-makers about the disastrous effects from strong winds and earthquakes. MOC's IDNDR Promotion Section and PWRI published the Proceedings of the Symposium and distributed copies to the U.S.-side and to the Japan earthquake disaster prevention community.

4. The Panel will continue to seek methods to contribute to the IDNDR such as exchanging Proceedings of Joint Panel Meetings and of Task Committee Workshops with their respective country's National Committees for the IDNDR.

5. Japanese and U.S. members performed joint investigations of damage of the 12 July 1993 Hokkaido-nansei-oki Earthquake and the 17 January 1994 Northridge California Earthquake. Experiences from these disaster investigations were reported at the 26th Joint Panel Meeting. The Panel recognizes the importance of using these findings in its on-going work, and of the need to continue performing future joint post-disaster investigations to improve engineering and construction practices. Information from these natural disasters will be transferred to Panel members and to others in the engineering and construction communities through Panel reports and presentations. Special Panel Theme Sessions, such as featured at the 26th Joint Panel Meeting, are encouraged for dissemination of timely information.

6. The Panel approved the Task Committee reports developed and presented during the Twenty-Sixth Joint Panel Meeting. Each report includes objectives and scope of work, accomplishments, future plans, and other information.

7. The Panel endorsed the following proposed Task Committee Workshops during the coming year.

a. Task Committee (B) plans its 2nd Joint Technical Coordinating Committee Meeting on Composite and Hybrid Structural Systems, July 1994, Chicago, IL, USA.

b. Task Committees (C&G) plan their 2nd Workshop on Structural Control and Intelligent Material Systems, May 1995, Tsukuba, Japan.

c. Task Committee (F) plans its 6th Joint Workshop on Disaster Prevention for Lifeline Systems December 1994, Los Angeles, CA, USA.

d. Task Committee (H) plans its 4th Joint Workshop on Remedial Treatment of Potentially Liquefiable Soils, July 4-8, 1994, Tsukuba, Japan.

e. Task Committee (J) plans its 11th Bridge Workshop, May 1995, Tsukuba, Japan.

f. Task Committees (K&I) plan a Second Workshop on Wind and Earthquake Engineering for Offshore and Coastal Facilities, January 1995, Berkeley, CA, USA.

Scheduling for the Workshops shall be performed by the U.S. and Japan Chairmen of the respective Task Committees with concurrence of the Joint Panel Chairmen. Results of each activity conducted before the 27th Joint Meeting shall be presented at the 27th Joint Panel Meeting.

8. The Panel recognizes the importance of collaborative joint research programs. The Panel endorses the initiation of joint research programs on Composite and Hybrid Structures and on Soil Liquefaction and Countermeasures.

9. The Panel, in December 1993, published its first issue of *Wind and Seismic Effects Newsletter*. The newsletter summarized the Panel's activities and accomplishments. The second newsletter (to include a report on the 26th Joint Panel Meeting) will be published during the summer of 1994.

10. The Panel recognizes the importance of continued exchange of personnel, technical information, research results, and recorded data that lead to mitigating losses from strong winds and earthquakes. The Panel also recognizes the importance of using available large-scale testing facilities in both countries. Thus, these activities should be continued, strengthened, and expanded. The Panel will provide official endorsement to facilitate these exchanges.

11. The Twenty-Seventh Joint Panel Meeting of the UJNR Panel on Wind and Seismic Effects will be held at PWRI, Tsukuba, Japan, May 1995. Specific dates, program, and itinerary will be proposed by the Japan-Side with concurrence of the U.S.-Side Panel.

WIND ENGINEERING

Wind Tunnel Experiment for a Super Long-Span Cable-Stayed Bridge in Smooth Flow

by

Hiroshi Sato[1], Ryuichi Toriumi[2], Makoto Kitagawa[3] and Hiroshi Katsuchi[4]

ABSTRACT

Aerodynamic stability of the Tatara bridge, which is a super long-span cable-stayed bridge whose center span length is 890m, was investigated through wind tunnel test using full aeroelastic model in smooth flow. The geometric scale of the model was 1/70. The stiffness, mass and geometric shape of girder and tower were simulated by stiffening bars, additional mass and exterior wooden forms. Each cable was designed and adjusted so that they had proper mass distribution and tensile force. The drag force acting on each cable was also simulated. From the wind tunnel experiment, it was found that the flutter speed of the bridge was high enough. The wind induced vibration observed was vortex-induced vibration with small amplitude only. The vortex-induced vibration will be evaluated considering the results of wind tunnel test in turbulent flow. As for the aerodynamic stability of the bridge in turbulent flow and at erection stage, wind tunnel tests are in progress. The topographical effects are also planned to be studied.

KEYWORDS
Aerodynamic stability, Super long-span cable-stayed bridge, Full aeroelastic model test, Wind tunnel test

1.INTRODUCTION

The Tatara Bridge, which is under construction in Japan, is a super long-span cable-stayed bridge (Figure-1, Photo-1). The center span length of the bridge will be 890m, which is almost 300m longer than that of the Yan-pu Bridge in China, the world's longest cable-stayed bridge at present. For such a long span bridge, it is very important to evaluate the aerodynamic stability of the bridge before its construction. Usually, the aerodynamic stability of bridges in Japan is evaluated by spring mounted rigid model wind tunnel tests. However, as the Tatara bridge has such a long span, it was thought that wind tunnel test using a full aeroelastic model should be conducted in the Large Boundary Layer Wind Tunnel

1)Head, Structure Div., Structure and Bridge Dept., PWRI
2)Senior Research Engineer, ditto
3)Manager, First Design Div., Design Dept., Honshu-Shikoku Bridge Authority
4)First Design Div., ditto

in PWRI. The Tatara bridge will be surrounded by islands as shown in Figure-2. Some of the islands have high mountains up to 400m above the sea level. Therefore, it was considered that topographical effect should be studied using topographical model.

This paper reports the design and characteristics of full aeroelastic model of the Tatara bridge, and the wind tunnel test result in smooth flow. The test results of the wind tunnel test in turbulent flow, and the topographical effects on aerodynamic response of the bridge will be reported in other opportunity.

2.PURPOSE OF THE STUDY

The purpose of this study is to make clear the aerodynamic characteristics of a super long-span cable-stayed bridge, the Tatara bridge. The wind tunnel test in smooth flow gives us fundamental data to evaluate the aerodynamic stability of the Tatara bridge.

3.AEROELASTIC FULL MODEL OF THE TATARA BRIDGE

The model was fabricated with a geometric scale of 1/70. Except for the cables, the model was designed by well known methods, i.e. steel frame was designed to achieve proper stiffness, additional mass was installed to simulate mass and polar moment of inertia, and the frame and additional mass were covered with exterior wooden forms to simulate geometrical shape.

Froude number similitude was adopted to the design of the model. This means wind speed ratio was 8.4 .

Table-1 shows the required and designed mass and stiffness of girder, tower and cable.

Attention was paid to the design of the cables. As well as the number of the cable, mass and tensile force of each cable was simulated. The drag force acting on each cable was also similar to the prototype bridge. Piano wires were used to simulate axial stiffness. In order to give proper mass to each cable, cylindrical mass pieces were placed at a certain interval. The mass pieces were so designed that the cables might have proper mass and drag force. For the similarity of drag force, the difference in Reynolds number were taken into account. Similar method was used for the design of cables in the model of Akashi Kaikyo Bridge[1]. Tensile force in each cable was measured from its natural frequency, and adjusted by turning turnbuckle installed at the end of cable. Figure-3 shows the final error of the tensile force in each cable.

During the preliminary wind tunnel test, it was found that the stay cables of the model vibrated in wind. At certain wind speed, the vibrational amplitude became so large that stay cables might touch each other. In the real bridge, the wind-induced vibration of stay cables will be eliminated by installing dampers or by some other

methods. Therefore the vibration of each cable in the model was eliminated by installing thin extra cables as shown in Figure-4. Through preliminary wind tunnel study, it was found that the thin extra cables would not affect aerodynamic characteristics of the model so significantly.

Photo-2 shows the model of the Tatara bridge in the Large Boundary Layer Wind Tunnel. The structural characteristis of the model were as follows.

(1)STATIC CHARACTERISTICS

Static loading tests were carried out in order to check the static characteristic of the model. Figure-5 show the results. Either in holizontal, vertical and torsional loading, the results shows good agreement with calculated results.

(2)DYNAMIC CHARACTERISTICS

Free vibration tests in windless condition were carried out to check the dynamic characteristics of the model. Table-2 shows the calculated and measured natural frequency of the model. Figure-6 shows the vibrational mode shape. Because of the good agreement between calculated and measured results, it was confirmed that the model represented the prototype bridge well. Table-2 also shows the logarithmic damping decrement observed. The damping observed was a little larger than the target value of 0.02. The difference between target damping and observed one should be considered.

4.EXPERIMENTS IN SMOOTH FLOW

The followings are results of the wind tunnel tests in smooth flow with the angle of attack 0 deg.

(1)Vibrational Amplitude

Figure-7 shows the relationship between vibrational amplitude and wind speed. No divergent vibration such as flutter was observed up to the reference wind speed of flutter. When the reduced wind speed was about 1.0, small vertical bending vortex-induced vibration was observed. The vibrational mode was 1st symmetric one. Usually, when 1st symmetric vortex-induced vibration is observed, vortex-induced vibration of higher modes are expected in higher wind speeds. However, in this case, no higher modes vibration was observed.

(2) Change of Damping

Relationship between wind speed and logarithmic decrement is shown in Figure-8. The decrease of damping at the reduced wind speed of 1.0 is coincident with the appearance of vortex-induced vibration. At higher wind speed, the damping increased with the wind speed.

(3)Change of Frequency

Change of the frequency with the wind speed is shown in Figure-9. The frequency of torsion, vertical and horizontal bending scarcely

changed.

5.DISCUSSION

Through the full model wind tunnel test, it was verified that the critical wind speed for flutter of the Tatara bridge is high enough.

Relationship between wind speed and logarithmic decrement from the flutter analysis of the Tatara bridge is shown in Figure-10. This result shows the reduced onset wind speed of flutter is about 7.5. In the section model tests conducted in advance, no flutter was observed up to the reduced wind speed of 5. In the present full model wind tunnel test, no flutter was observed up to the reduced wind speed of 4. As far as the wind speed range where full model test was conducted is concerned, all the three results show stable characteristics of the bridge to flutter. Although the Tatara bridge is a super long-span cable-stayed bridge, no unfamiliar flutter characteristics was observed so far.

The only wind induced vibration observed was vortex-induced vibration with small amplitude. In the section model tests, no vortex-induced vibration was observed as shown in Figure-7. The vortex-induced vibration will be evaluated considering its characteristics in turbulent flow.

6.CONCLUSION

Through the full aeroelastic model wind tunnel test, the aerodynamic stability of the Tatara bridge was investigated. No divergent vibration such as flutter was observed. This means the Tatara bridge is aerodynamically stable. The only wind induced vibration observed was vortex-induced vibration with small amplitude. The vibration will be evaluated considering its characteristics in turbulent flow.

7.FUTURE STUDY

The wind tunnel test for erection stage of the Tatara bridge and wind tunnel test in turbulent flow are in progress. Wind tunnel study for the topographical effect on the Tatara bridge is scheduled. The results will be reported in other opportunity.

REFERENCES

1)Yokoyama K., Kanazaki T. and Yasuda M., Boundary Layer Wind Tunnel Study on Full Model Aeroelastic Long Span Bridge Model, Proc. of 23rd. Joint Panel Meeting on Wind and Seismic Effects, UJNR, 1991.

2)Sumiyoshi Y., Endo T., Miyata T., Sato H. and Kitagawa M., Experiments for the Akashi Kaikyo Bridge in a Large Boundary Layer Wind Tunnel, Proc. of International Seminar on Utilization of Large Boundary Layer Wind Tunnel, Tsukuba, Japan, 1993.

Table-1 Similarity of the Model

	Unit	Required	Designed
Girder(Center of Center Span)			
Axial Stiffness (E*A)	N	456.5	475,808
Bending Stiffness			
Vertical (E*Iv)	N·cm²	17,368	17,375
Horizontal (E*Ih)	N·cm²	730,168	729,654
Torsional Stiffness (G*J)	N·cm²	14,638	16,352
Mass	g/cm	38.4	40.3
Polar Moment of Inertia	g·cm²/cm	5,543.5	5,421.6
Tower(Average)			
Stiffness		See below	See below
Mass(Average: each shaft)	g/cm	25.8	25.8
Cable(Uppermost Cable of Center Span)			
Axial Stiffness (E*A)	N	63.28	64.11
Mass	g/cm	0.22815	0.22794

Deformation of Tower by specified load

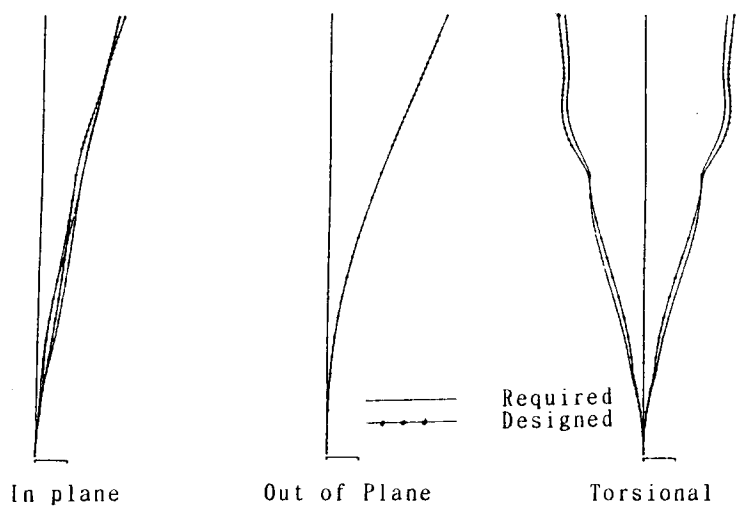

Table-2 Natural Frequency and Damping

Vibrational Mode	Natural Frequency (Hz)		Logarithmic Damping Decrement
	Required	Measured	
Vertical			
1st symmetric	1.883	2.014	0.0429
1st anti-symmetric	2.252	2.407	0.0408
2nd symmetric	2.757	2.959	(0.0238)*
Torsional			
1st symmetric	3.987	4.326	(0.0180)*
Horizontal			
1st symmetric	0.684	0.725	0.0130

*:Measured without extra cables

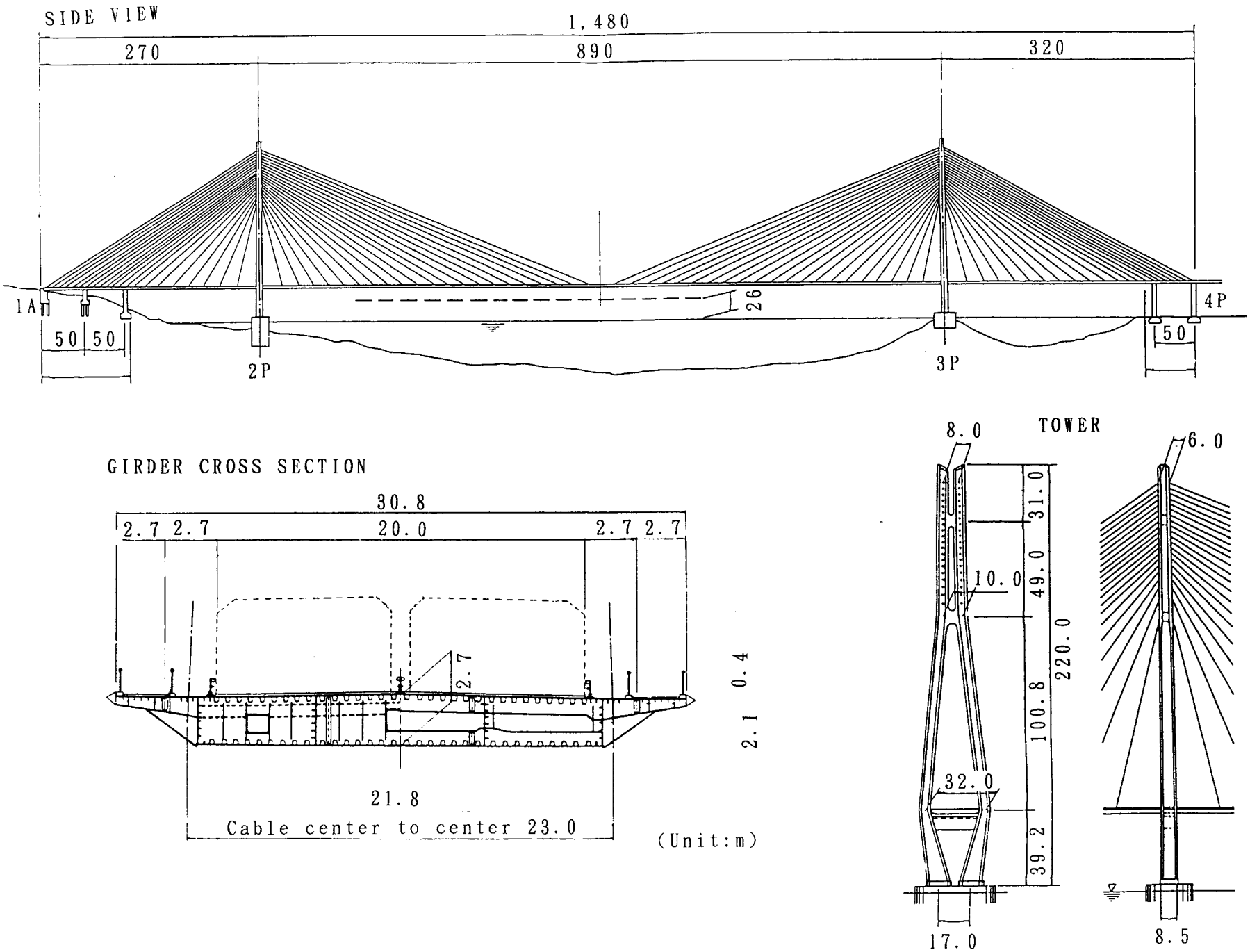

Figuer-1 Tatara Bridge

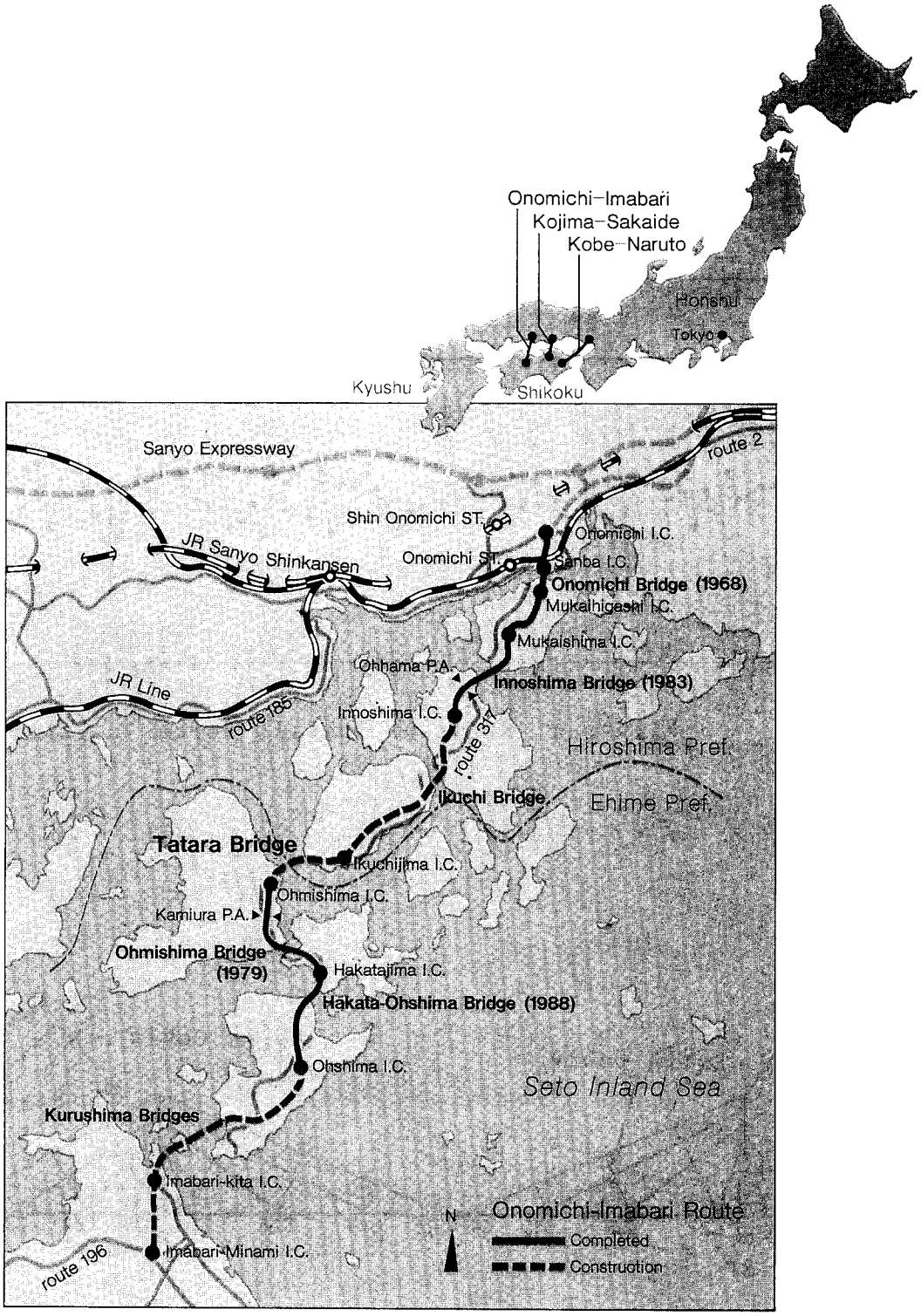

Figure-2 Location of the Tatara Bridge

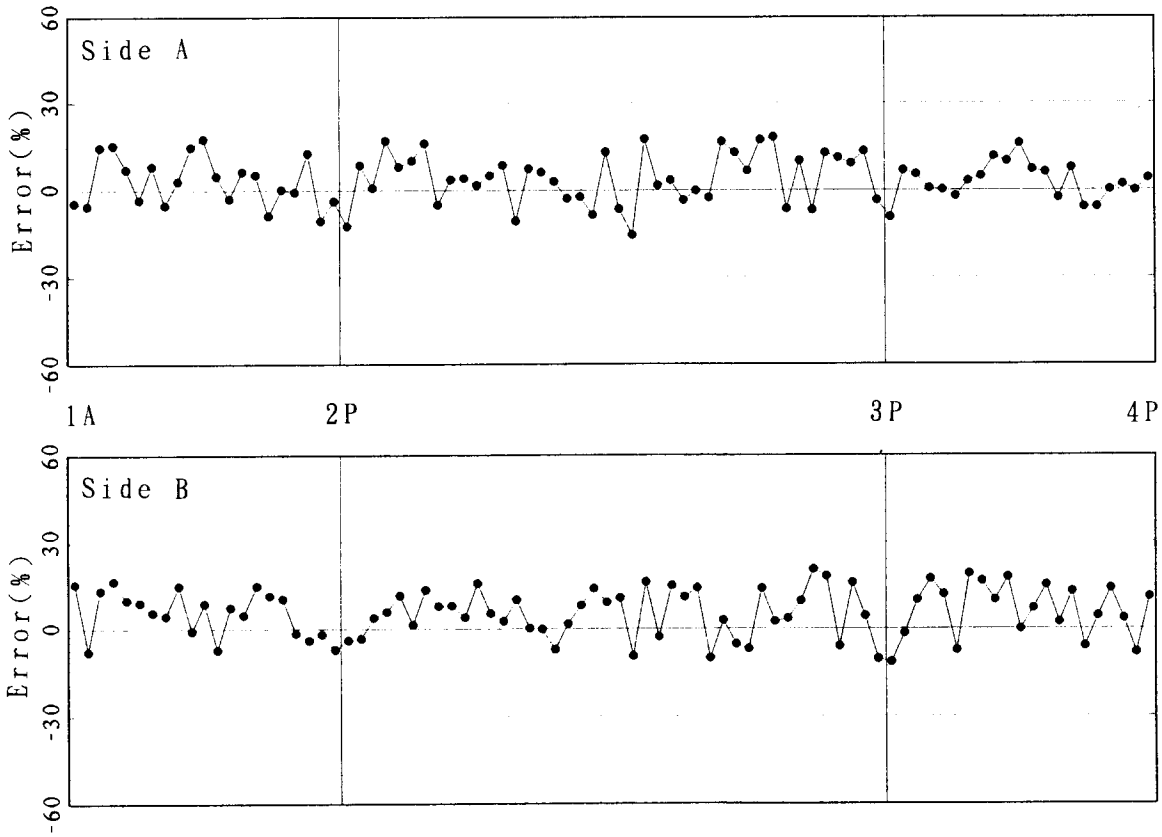

Figure-3 Error of Tensile Force in Cable

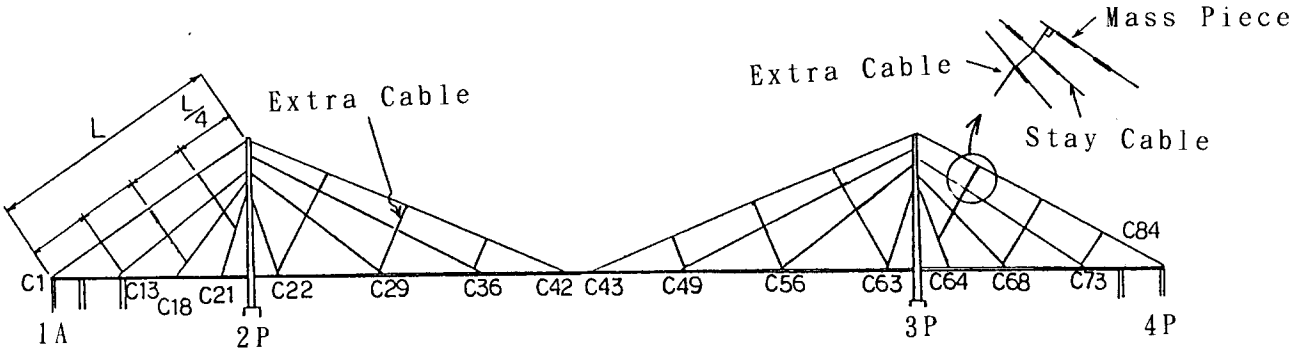

Figure-4 Extra Cable Arrangement

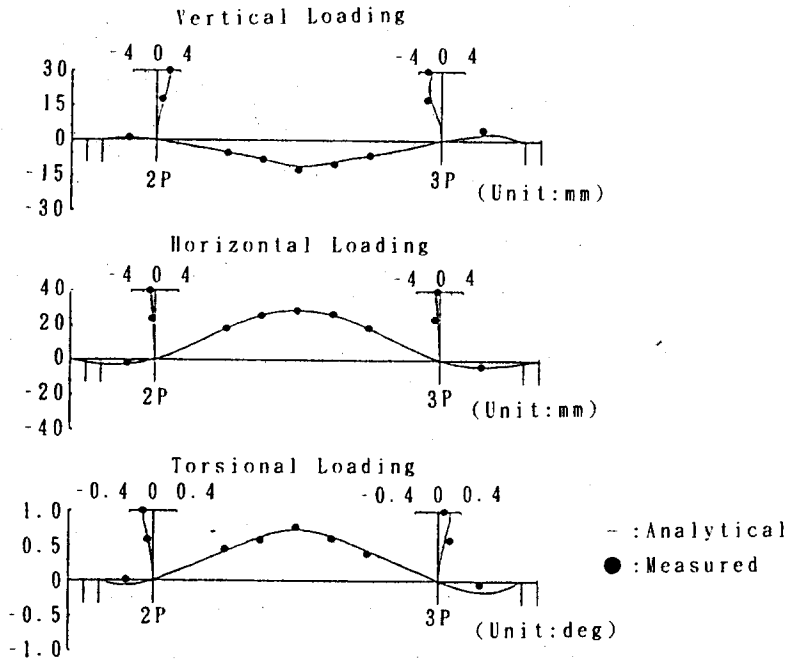

Figure-5 Static Loading Test Results

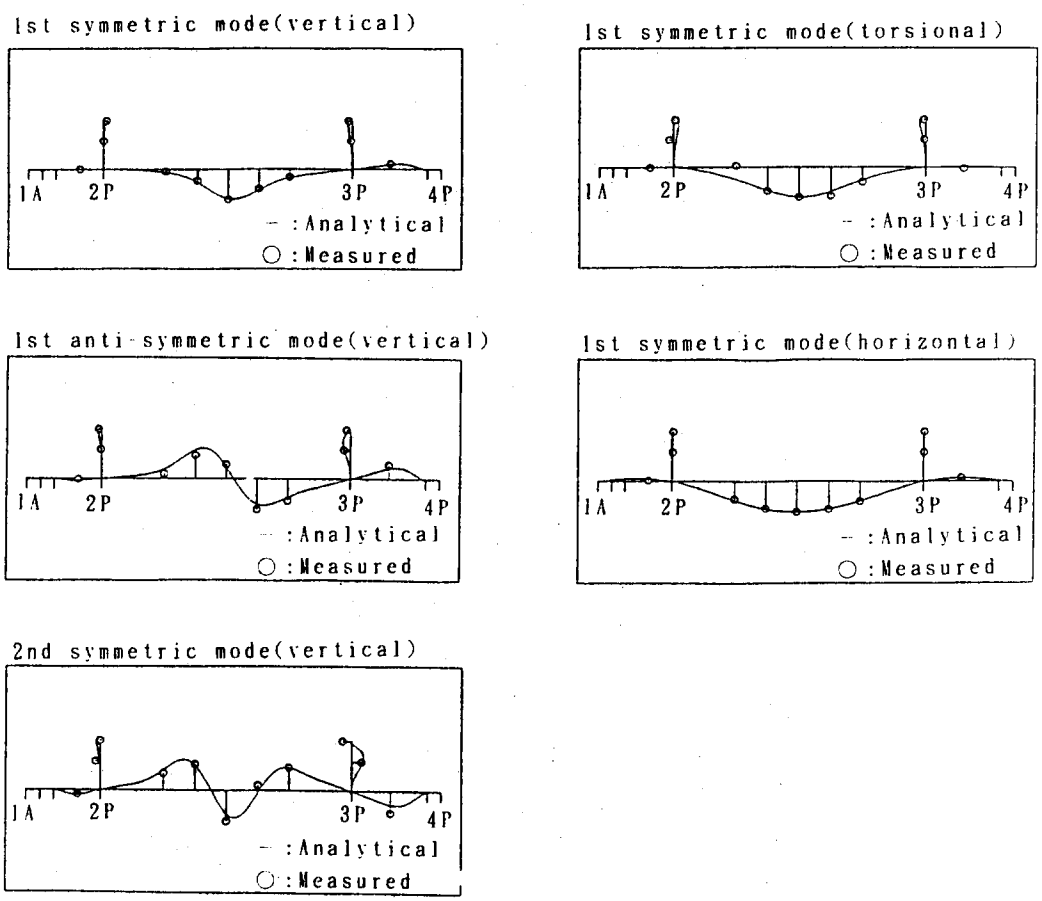

Figure-6 Natural Vibrational Mode Shape

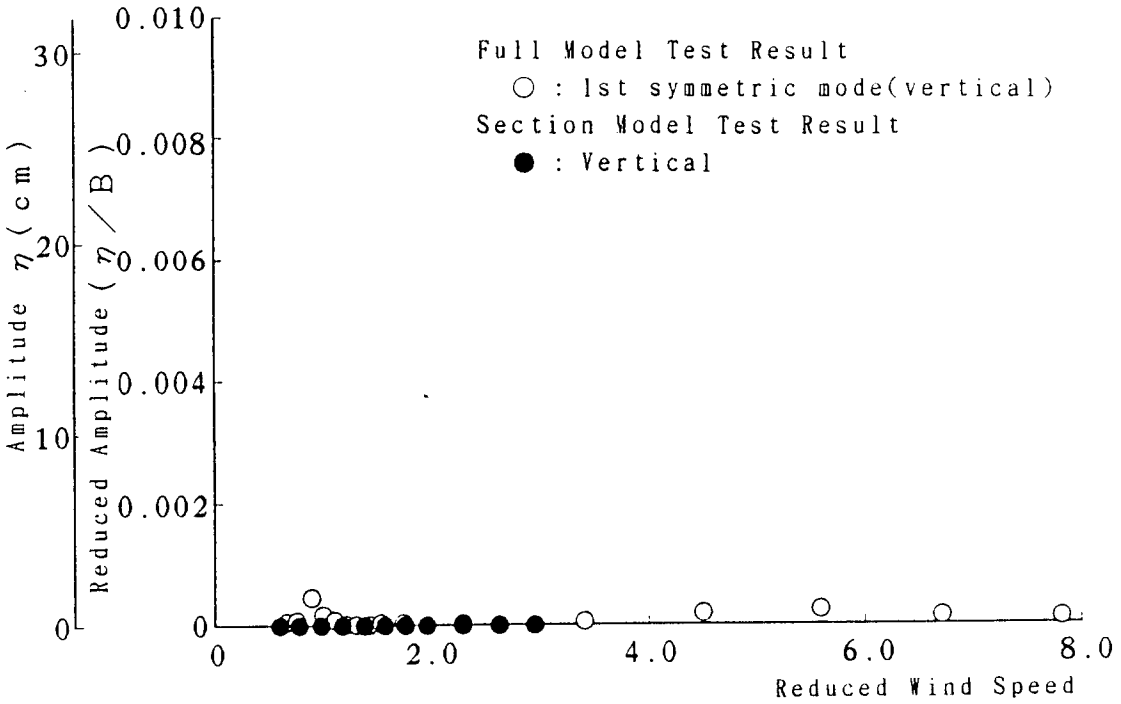

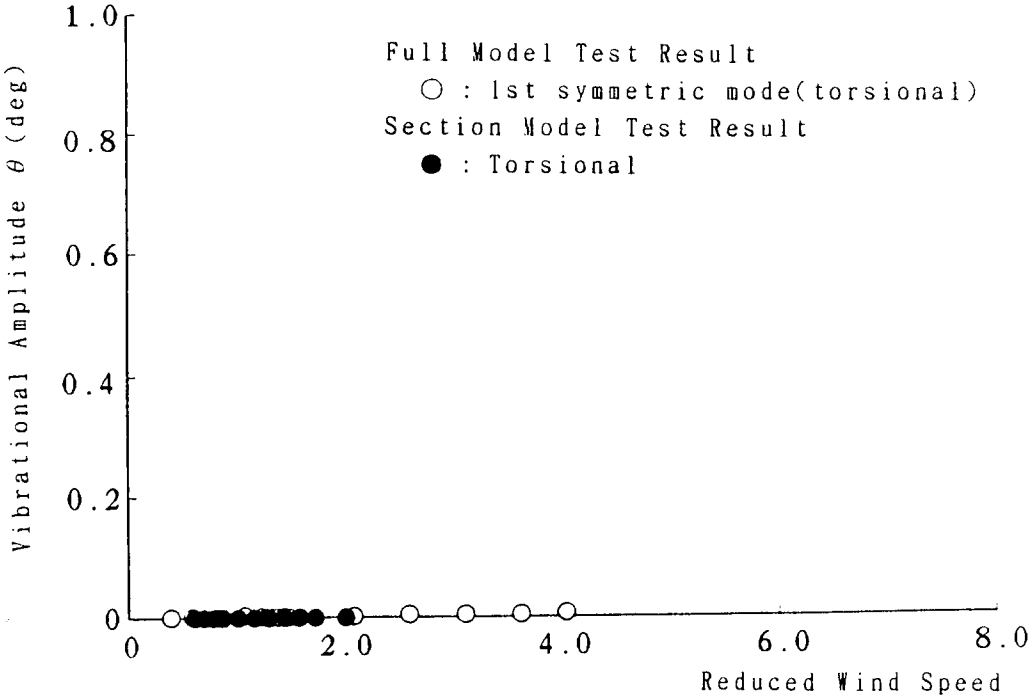

Figure-7 Reduced Wind Speed - Vibrational Amplitude

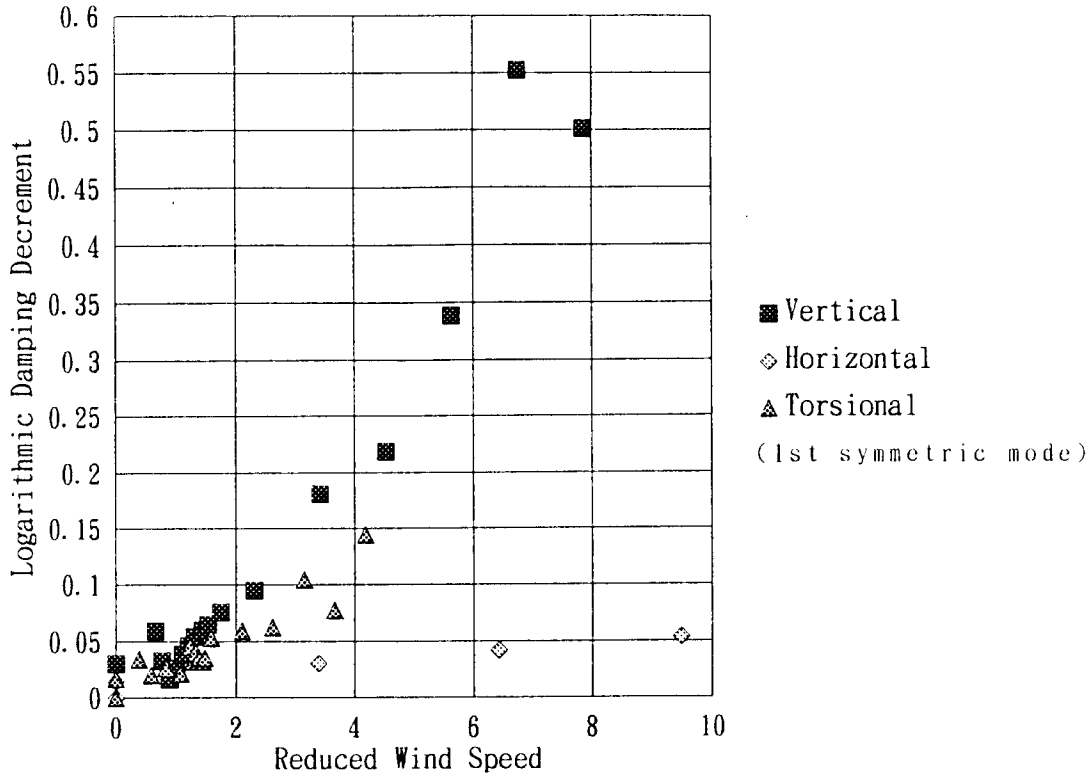

Figure-8 Reduced Wind Speed - Logarithmic Damping Decrement

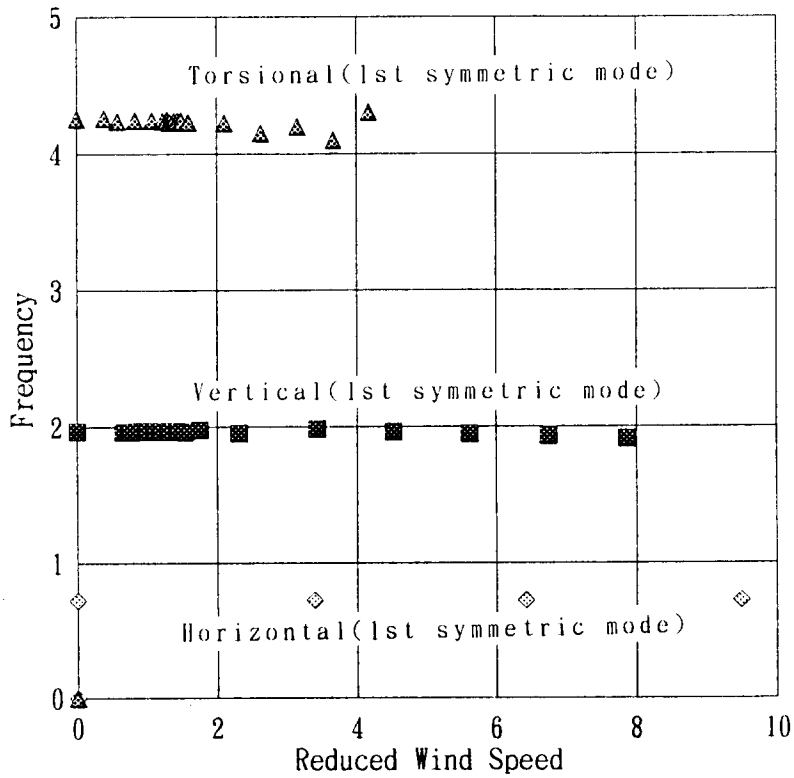

Figure-9 Reduced Wind Speed - Frequency

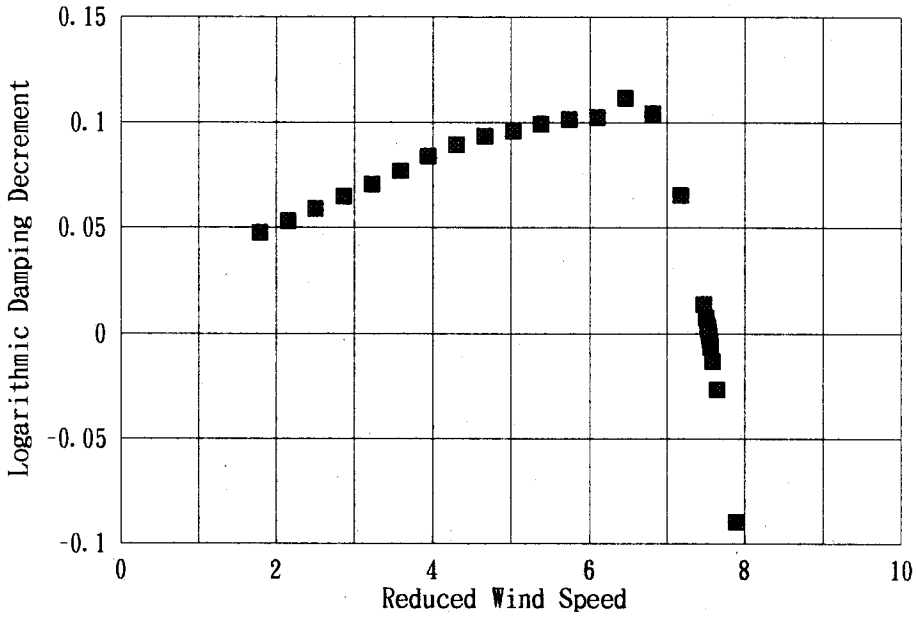

Figure-10 Reduced Wind Speed - Damping (Analytical)

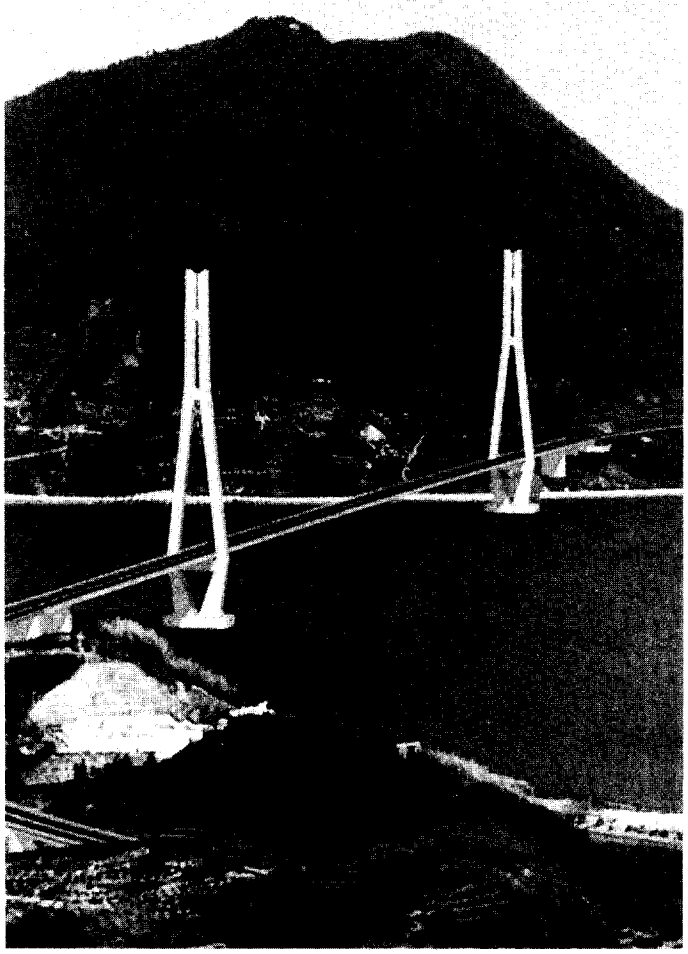

Photo-1 Tatara Bridge

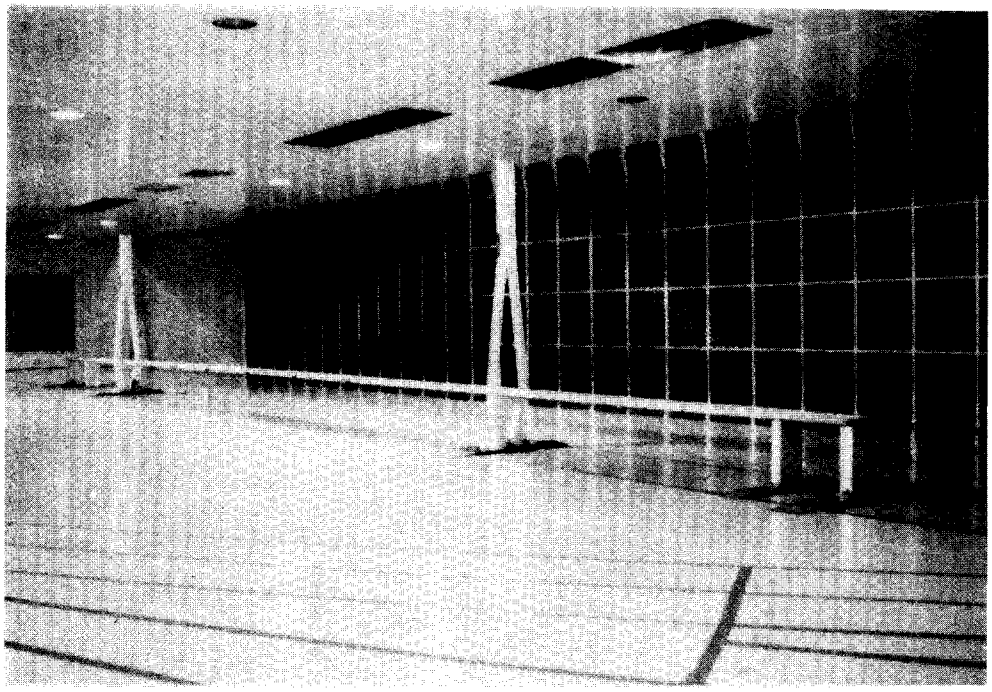

Photo-2 Model of the Tatara Bridge

Wind Tunnel Tests on Tapered Cylinders for Highway Support Structures

by

Harold R. Bosch*

ABSTRACT

Highway support structures are an important component of the nation's highway system. Over the years, wind-induced vibration of these structures has been observed throughout the country under a variety of conditions. A number of recent major failures, some resulting in deaths, has sparked interest in the wind loads on and fatigue design of highway support structures. Design is currently guided by the AASHTO specifications. Although the design codes received major revision in 1985, there is concern that they still do not adequately address the effects of wind on these structures. To gain better understanding of the problem and to develop recommendations for code revisions, several projects have been initiated at the State and Federal levels. One of these studies is being conducted by the Federal Highway Administration's research staff located in McLean, Virginia. A portion of this project involves wind tunnel testing to establish the effects of wind on tapered cylinders. The test program and some of its early results will be the topic of this paper.

KEYWORDS: cylinders; drag; highway signs; luminaires; traffic signals; wind loads.

1. INTRODUCTION

Along the nation's highways and within its cities, there is a vast array of highway support structures such as overhead or roadside signs, high light towers, light poles, and signal standards. These structures and the hardware they support are essential for the safe and efficient movement of vehicles, passengers, and goods throughout the highway system. They provide the means for illuminating the right-of-way, directing the traveller through signing, and regulating traffic flow at intersections. Highway appurtenances, as they are sometimes called, consist mainly of circular or multi-sided cylindrical components which are interconnected through welded and/or bolted joints. Frequently, the components are uniformly tapered along their length to optimize the design, reduce cost, and improve aesthetics. Most structures rest on concrete footings or foundations and are attached using an anchor bolt arrangement. For safety reasons, the bolt or base assembly is often designed to breakaway easily under impact loading.

Over the years, wind-induced vibration of highway support structures has been observed throughout the country under a variety of conditions. While random, small amplitude motions are seldom of concern, some types of vibration can and have lead to failures due to fatigue. These failures may be of the nuisance type requiring maintenance and repairs or, in some cases, catastrophic resulting in collapse and deaths. Structural vibrations can result from slow steady winds, strong turbulent winds, and/or gust loads from trucks. The nature and significance of the vibrations depends upon wind conditions, structural dynamic properties, and stress levels within critical components. The design of these structures to resist wind and other loads is currently guided by the American Association of State Highway and Transportation Officials (AASHTO) Standard Specifications for Structural Supports for Highway Signs, Luminaires, and Traffic Signals [1].

Although the design codes received a major revision in 1985, there is concern that they still do not adequately address the effects of wind on

* Research Structural Engineer, FHWA Turner-Fairbank Highway Research Center, 6300 Georgetown Pike, Mclean, Virginia 22101.

modern highway support structures. Since 1985, significant changes have occurred in design philosophies, material choices, and manufacturing processes. Several recent structural failures underscore the need for improved design procedures and revised specifications to ensure more fatigue-resistant structures. To gain a better understanding of how wind affects these structures and to develop recommendations for code revisions, several projects have been initiated at both the State and Federal levels.

The Federal Highway Administration's (FHWA's) Aerodynamics Laboratory at the Turner-Fairbank Highway Research Center (TFHRC) has long been involved in the study of wind effects on transportation structures. To address the problem of wind-induced vibration of highway support structures, the Aerodynamics Laboratory staff have conducted a comprehensive literature search. Although significant data exists regarding basic wind forces on uniform (non-tapered) structural sections, little or no detailed information could be found for the wide variety of tapered, cross-sectional shapes employed in these structures. Several studies have been conducted to investigate local problems, specific structures, or structural details; however, no comprehensive investigations were identified.

Recently, the FHWA has initiated research to improve our understanding of this problem and to establish detailed wind load data which is not presently available. The first phase of this work will involve wind tunnel testing of scaled section models to establish wind forces on and response behavior of structural components as well as attached hardware such as signal heads, luminaires, and sign panels. For the second phase, wind tunnel tests will be performed using full aeroelastic models to characterize the dynamic response of highway support structures under a variety of wind conditions. These laboratory tests will be complemented by full scale wind and response measurements on existing structures wherever possible. The third and final phase will concentrate on developing new or improved methods for predicting the response of these structures to wind.

Phase one of the research is well underway and progress on wind tunnel testing of tapered cylinders will reported in what follows. This paper will describe the laboratory, model design, and test methods. The results of force measurements on a representative sample of tapered and non-tapered cylinders will be presented. These results will be discussed and conclusions will be drawn.

2. AERODYNAMICS LABORATORY

The research is being conducted in the Aerodynamics Laboratory at TFHRC. Established in the late 1950's, the Laboratory has been used primarily to ensure the aerodynamic stability of long span bridges. The facility includes a large lab area containing a wind tunnel, several unique test fixtures, instrumentation systems, and lab test equipment as well as an adjacent office area housing staff, computer systems, reference materials, and records. The wind tunnel is a low velocity, open-circuit, laminar flow design. Air enters a double inlet section, passes through a diffusing section containing a series of 8 screens, and exits a 6 by 6-ft nozzle into the test area (see Figure 1). The air flow is quite laminar and well controlled at speeds up to 50-ft/s. For experiments where turbulent flow is desired, an active turbulence generator is inserted into the circuit between the wind tunnel nozzle and the test area. With this system, large scale turbulence can be simulated in the vertical and along-wind directions, independently. The vertical angle of the wind can be changed by rotating the wind tunnel nozzle up and down or by rotating the model around its longitudinal axis as needed.

Section models are used for most experiments. These models are designed to relatively large scale ratios (1:25 to 1:100) to ensure adequate reproduction of geometric details. To measure wind forces, the section model in mounted in a force-balance assembly and placed in the test area. For dynamic response measurements, the models are mounted on a spring suspension

system in a rigid frame surrounding the test area. Air flow studies are accomplished by installing velocity probes on a 3-D, motorized traverse system and surveying the flow field around the section model.

3. MODEL DESIGN

A series of rigid, lightweight section models has been designed for the static and dynamic wind tunnel tests. These models comprise a range of cross-sections and taper ratios which are intended to be representative of those commonly found in highway support structures. Model diameters were selected to provide a suitable Reynolds number (Re) range for testing (see Figure 2). So far, 53 models have been fabricated with either circular, octagonal, or hexagonal cross-sections. All sections were carefully machined from wood, aluminum, or steel to ensure crisp details, proper surface roughness, adequate rigidity, and low total weight. Initially, sharp corners have been specified for the octagonal and hexagonal sections. Later in the research program, models with a range of corner radii will be fabricated and tested. All models are 60 inches long with rigid force-balance adaptor plates mounted on each end. For each of the 3 shapes, there is a set of 5 uniform (non-tapered) section models with diameters of 2, 3, 4, 5, and 6 inches. Tapered sections have 3 equivalent (central) diameters of 3, 4, and 5 inches each with taper ratios (in/ft) of 5, 10, 14, 20, 25, and 30 percent. In addition to the manufactured shapes, two tapered models were fabricated using sections of actual poles. The first is a circular aluminum specimen with a central diameter of 5 inches and a taper ratio of 26.6 percent. The other is an octagonal steel specimen with a central diameter of 4.5 inches, taper ratio of 13.4 percent, and corner radius of 5.6 percent.

4. TEST PROCEDURE

To measure wind forces on the cylindrical sections, each model was prepared and carefully mounted in the force-balance. This force-balance system supports the section model in a horizontal orientation and measures the 3 force components of lift, drag, and pitching moment (see Figure 3). Although not used during this testing, it is capable of rotating the model about its longitudinal axis to vary the angle of attack. Since the force-balance is actually two separate balance mechanisms, it is capable of measuring unbalanced loads on models. This feature has proved to be extremely useful for this study. All models were thoroughly inspected for surface defects and weighed prior to testing. For tapered models, a tuning weight was installed inside the small end to establish a perfectly balanced section prior to testing. Each section model was tested at 31 different wind speeds and all tests were performed twice to ensure repeatability of the results. Wind speeds were carefully chosen to provide the maximum range of Reynolds number possible and to avoid regions where undesirable vibrations would develop in the model. In general, speeds ranged from 5 to 30 ft/s and the same speed settings were not necessarily selected for each model. Multi-sided sections were tested in two primary orientations -- corner and face (see Figure 4). At a later time, tests will be conducted over a range of wind angles. During each test, readings from the balance, pitot tubes, barometer, and temperature sensors were continuously sampled at a rate of 100 Hz for a period of at least 90 seconds. Each of the 6 force components were low-pass filtered at 30 Hz prior to recording.

5. TEST RESULTS

At this point in the test program, force measurements have been completed in laminar flow on all of the 53 models available. This represents more than 82 separate setups and 164 total tests. Mean and root-mean-square (RMS) values have been computed for all 6 of the model end forces at each wind speed tested. These "end" forces have been combined into 3 "model" forces (lift, drag, and moment) for computing MEAN and RMS force coefficients. Only the results obtained for mean axial (drag) forces will be presented here.

5.1 Circular Cylinders

For the uniform (non-tapered) circular cylinders tested, the drag forces are very consistent. When model end forces are compared, it is clear that the wind load on the cylinders is perfectly balanced as expected (see Figure 5). The measured drag coefficients range from 1.21 to 1.23. These measurements correspond well with values found in published data [3].

The influence of taper was evaluated using "equivalent" cylinder diameters of 3, 4, and 5 inches. For the tapered circular cylinders tested, the total drag on the model generally decreases with increasing taper ratio. It is interesting to note that most of the reduction in force results from the first 5 percent of tapering (see Figures 6-7). The difference (unbalance) between model end forces becomes larger with increasing taper ratio as expected. The magnitude of the unbalance seems to decrease, however, as the equivalent cylinder diameter increases (see Figures 8-9). For the 3-inch cylinders, the measured drag coefficients range from 1.22 to 1.17 over the 30 percent range of tapers. The 4 and 5-inch cylinders produce drag coefficients which range from 1.23 to 1.16 and 1.22 to 1.12, respectively. Generally, results indicate that tapering of circular cylinders has a positive influence on drag by reducing forces as much as 8 percent in some cases.

To determine the adequacy of the fabricated section models, tests were also performed on a section removed from an actual luminaire pole. The section selected was aluminum with an equivalent diameter of 5.065 inches and a taper ratio of 26.6 percent. The member end forces and drag coefficients obtained for the prototype specimen correspond very well with those obtained for Model CC5.25 (see Figures 10-11). This indicates that model details faithfully reproduce the prototype conditions.

5.2 Octagonal Cylinders

For the uniform (non-tapered) octagonal cylinders, the drag forces were also quite consistent. The end drag forces for each model were equal, indicating balanced load conditions. Model drag forces were higher for the face orientation than the corner orientation (see Figure 12). Measured drag coefficients range from 1.60 to 1.67 and 1.30 to 1.35 for the face and corner orientations, respectively. These values compare very well with those obtained in other laminar flow wind tunnel and tow tank tests on octagonal cylinders [4-5].

As before, the influence of taper was evaluated using 3 equivalent diameters of 3, 4, and 5 inches. The diameter referenced here is that of the inscribed circle. For the tapered octagonal cylinders tested, the total drag force also tends to decrease with increasing taper ratio. The amount of force reduction, however, does not appear to be as great as for the circular cylinders (see Figure 13). The unbalance between model end forces tends to increase with increasing taper ratio and decrease with increasing equivalent diameter.

For 3-inch octagonal cylinders tested in the corner orientation, the measured drag coefficients range from 1.43 to 1.34 over the 30 percent range of tapers tested. The 4 and 5-inch cylinders produce drag coefficients which range from 1.41 to 1.29 and 1.36 to 1.25, respectively.

As found in the uniform cylinder tests, significantly higher drag forces and coefficients were measured for tapered octagonal cylinders in the face orientation. For the 3 and 4-inch cylinders, measured drag coefficients range from 1.72 to 1.58 and 1.65 to 1.55, respectively. Problems were encountered when processing data from the 5-inch cylinders in face orientation and the results of those tests will not be reported here.

To assess the adequacy of the fabricated octagonal models, a comparison was also made using a prototype specimen. The section selected was galvanized steel with an equivalent diameter of 4.468 inches and a taper ratio of 13.4 percent. The model end forces and drag coefficients obtained for the prototype specimen correspond reasonably well with those obtained for Model OC4.14 (see Figures 14-15). The small differences found are likely due to the

larger diameter and corner radius which are not replicated in this particular model.

5.3 Hexagonal Cylinders

For the uniform (non-tapered) hexagonal cylinders, only 3 of the 5 section models have been tested. Tests on cylinders with diameters of 2, 3, and 4 inches have been completed for both face and corner orientations. As for the other uniform cylinders, the end drag forces were found to be equal, indicating balanced loading on the section. In contrast with the octagonal cylinders, drag forces on the hexagonal sections were larger for models in corner orientation than in face orientation (see Figure 16). Measured drag coefficients range from 1.99 to 1.89 and 1.66 to 1.51 for the corner and face orientations, respectively. Since no tapered sections have been tested yet, results for these sections cannot be presented here.

6. CONCLUSIONS

Although the research reported herein is continuing and is only part of a larger investigation, some interim conclusions may be drawn. For all of the circular cylinders tested, including the tapered ones, drag coefficients ranging from 1.12 to 1.23 have been obtained, with an average value of about 1.17. While these values are in excellent agreement with published data, they are 2 to 12 percent higher than the 1.1 recommended in the AASHTO code specifications. Generally, tapering is beneficial and reduces the drag force on these cylinders. Design calculations based upon code values would seem to be more applicable to tapered sections than uniform ones.

For octagonal cylinders, the AASHTO specifications recommend a drag coefficient of 1.2 for design. Tests on cylinders with a corner orientation, produced drag coefficients ranging from 1.25 to 1.43 with an average of about 1.34. A comparable range of 1.55 to 1.72 and average of 1.62 were obtained for face orientation. Again, these values compare very well with other research findings; however, they are 4 to 44 percent higher than code values. Test results indicate that tapering may not be as beneficial for the octagonal cylinders.

For the 3 non-tapered hexagonal cylinders tested, average drag coefficients of 1.60 and 1.94 have been obtained for the face and corner orientations, respectively. It is interesting to note here that the corner orientation results in the larger forces on the section. These limited results appear to be reasonable. The AASHTO specifications do not specifically address hexagonal members.

The reader is reminded that the tests reported on here were conducted using laminar approach flows and were confined to the subcritical flow regime with Reynolds numbers ranging from about 3×10^3 to 1×10^5. Additionally, all multi-sided models were designed and fabricated with sharp corners. The results presented are applicable only to these conditions.

As mentioned earlier, this is one of several studies underway to improve our understanding of how wind affects highway support structures. In the months and years ahead, these on-going investigations should provide the detailed information necessary for recommending code revisions.

7. ACKNOWLEDGEMENTS

A portion of the work reported here was accomplished by Ms. Anna M. Chesnul under a Research Fellowship sponsored by the National Highway Institute. The author would like to express his appreciation to Ms. Chesnul as well as her academic advisor, Dr. Ahmad H. Namini, for their significant contributions.

8. REFERENCES

[1] AASHTO, Standard Specifications for Structural Supports for Highway Signs, Luminaires, and Traffic Signals, 1985.

[2] ASCE Task Committee on Wind Forces, "Wind Forces on Structures," Transactions, ASCE, Volume 126, 1961.

[3] Hoerner, Sighard F., Fluid-Dynamic Drag, published by the author, 1965.

[4] James, W.D., Effects of Reynolds Number and Corner Radius on Two-Dimensional Flow Around Octagonal, Dodecagonal, and Hexdecagonal Cylinders, PhD Dissertation, University of Iowa, 1976.

[5] Mehta, Kishor C., et al, Wind Drag Coefficients for Octagonal Cylinders, report to Texas Department of Highways and Public Transportation, Texas Tech University, 1990.

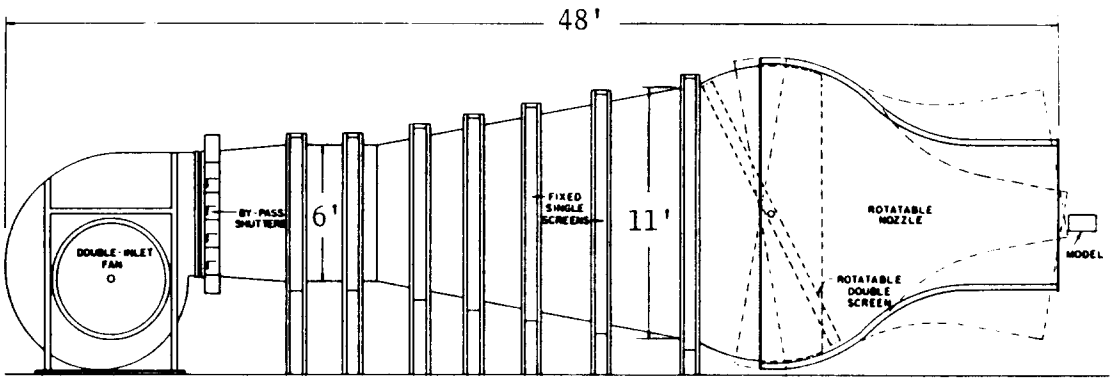

Figure 1. FHWA Vincent Memorial Wind Tunnel

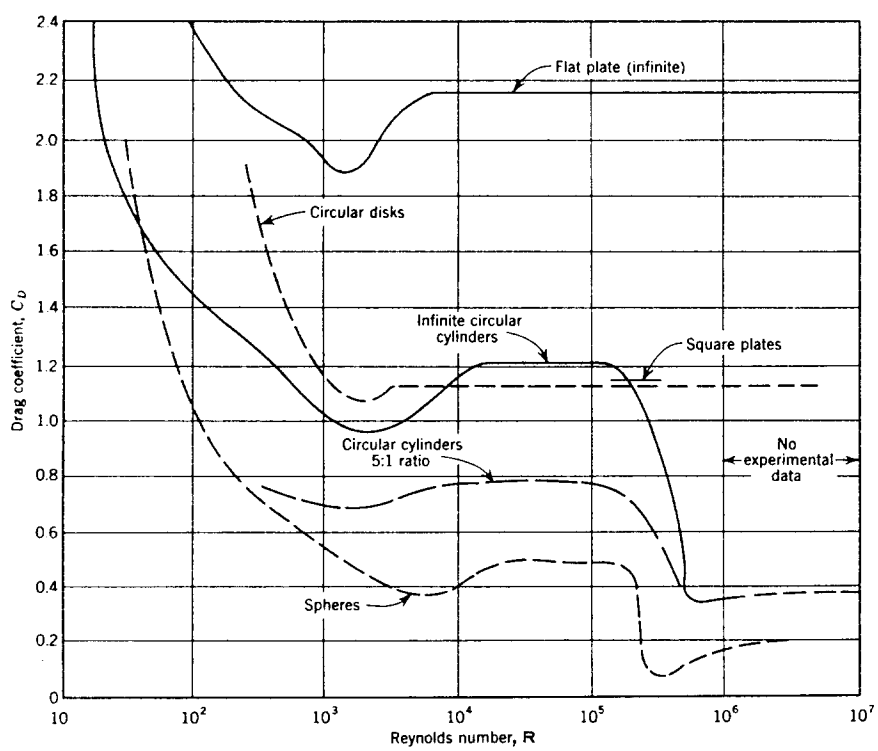

Figure 2. Drag Coefficients for Spheres and Long Cylinders [2]

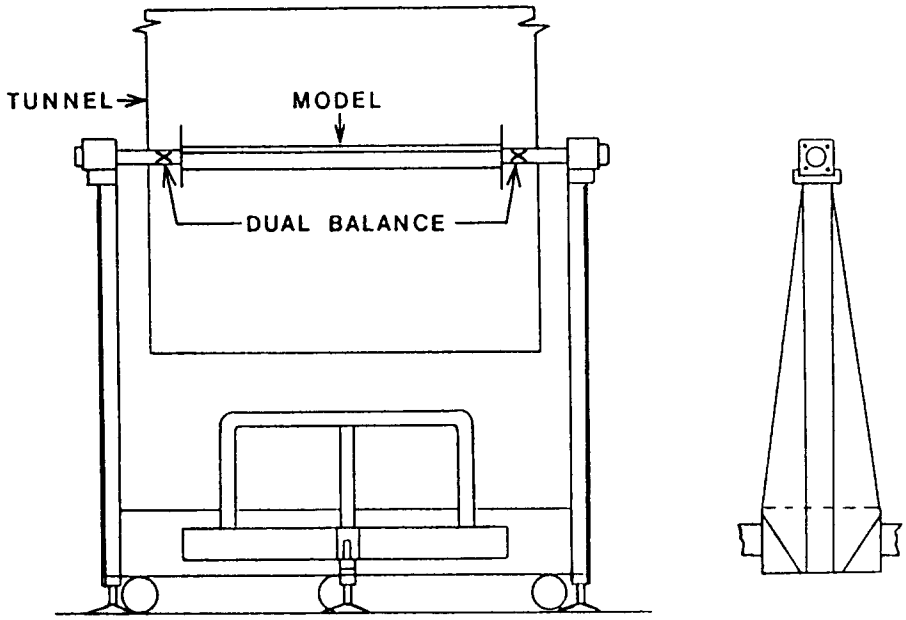

Figure 3. FHWA Dual Force-Balance System

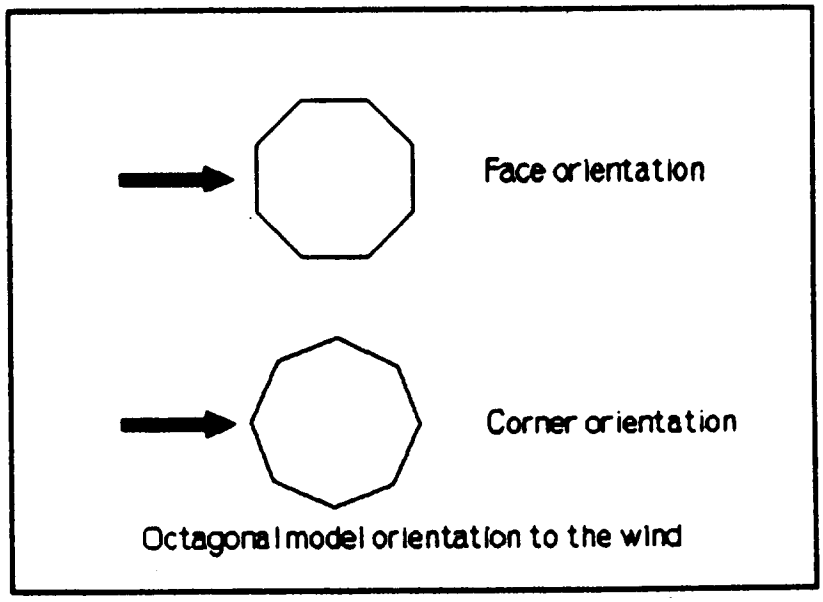

Figure 4. Orientation of Multi-Sided Models in Wind Flow

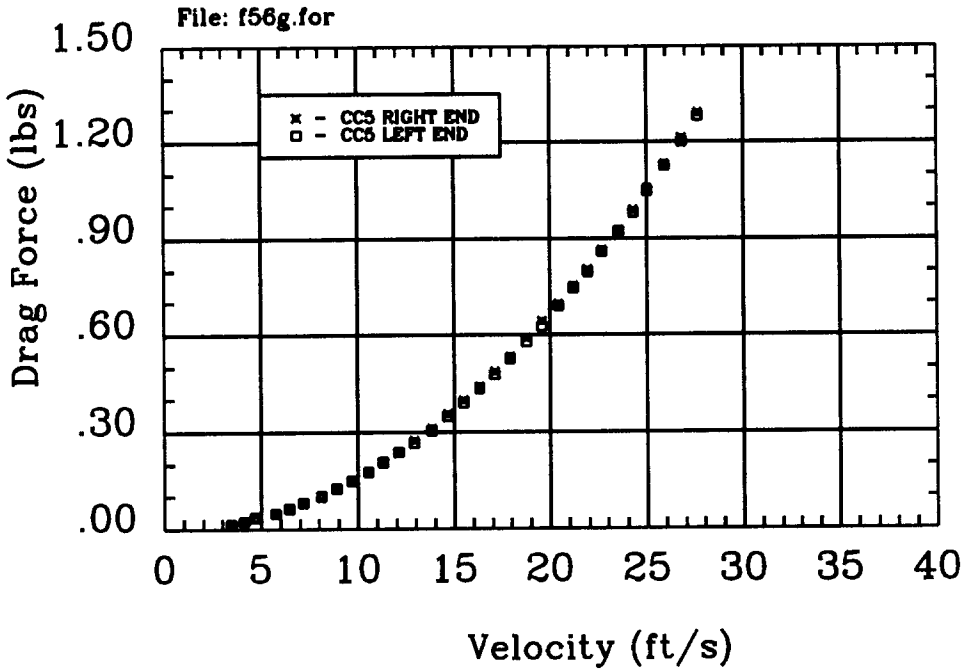

Figure 5. Drag Force at Ends of Model CC5.00

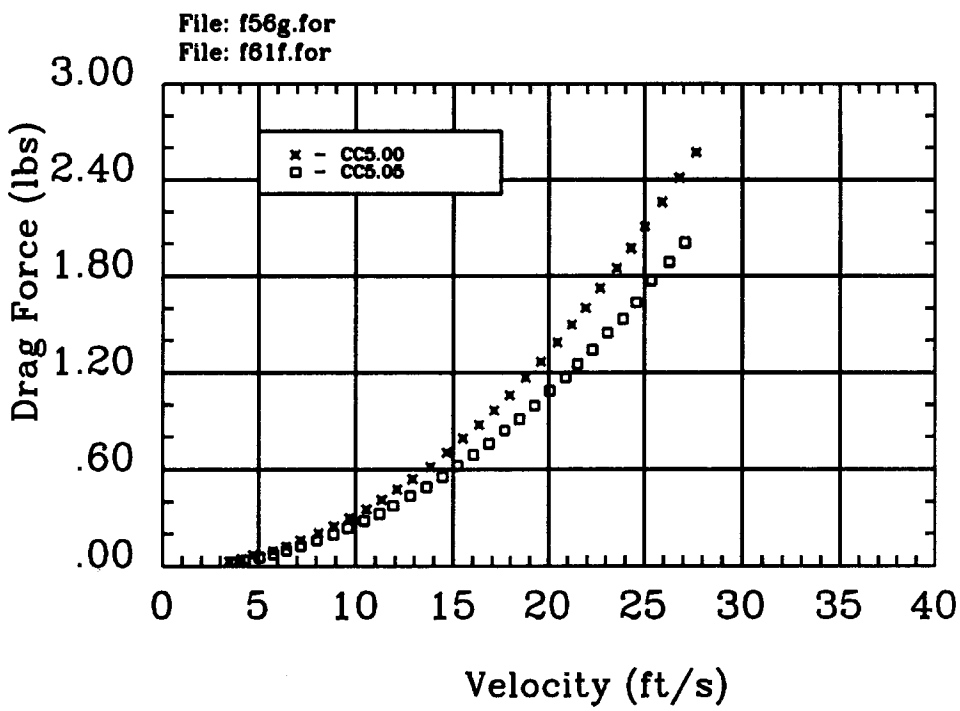

Figure 6. Drag Force on Models CC5.00 and CC5.05

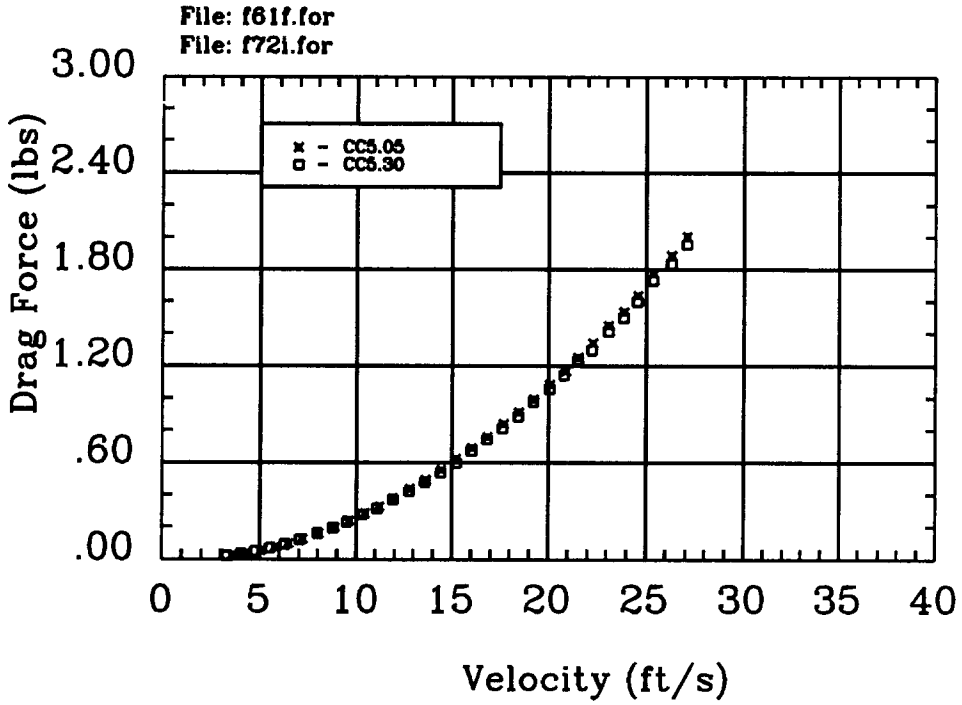

Figure 7. Drag Force on Models CC5.05 and CC5.30

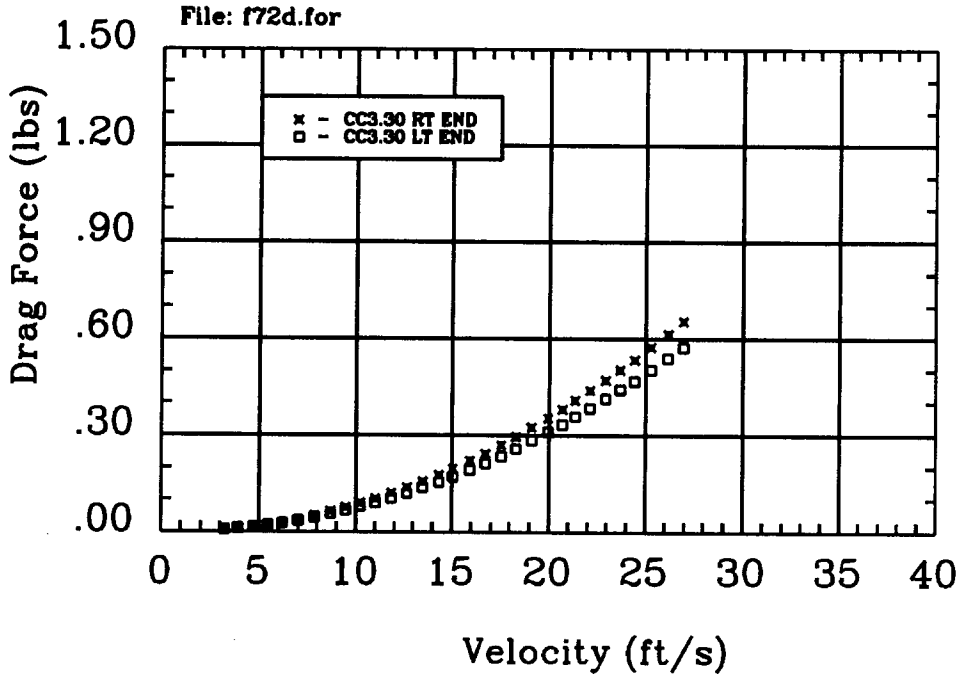

Figure 8. Drag Force at Ends of Model CC3.30

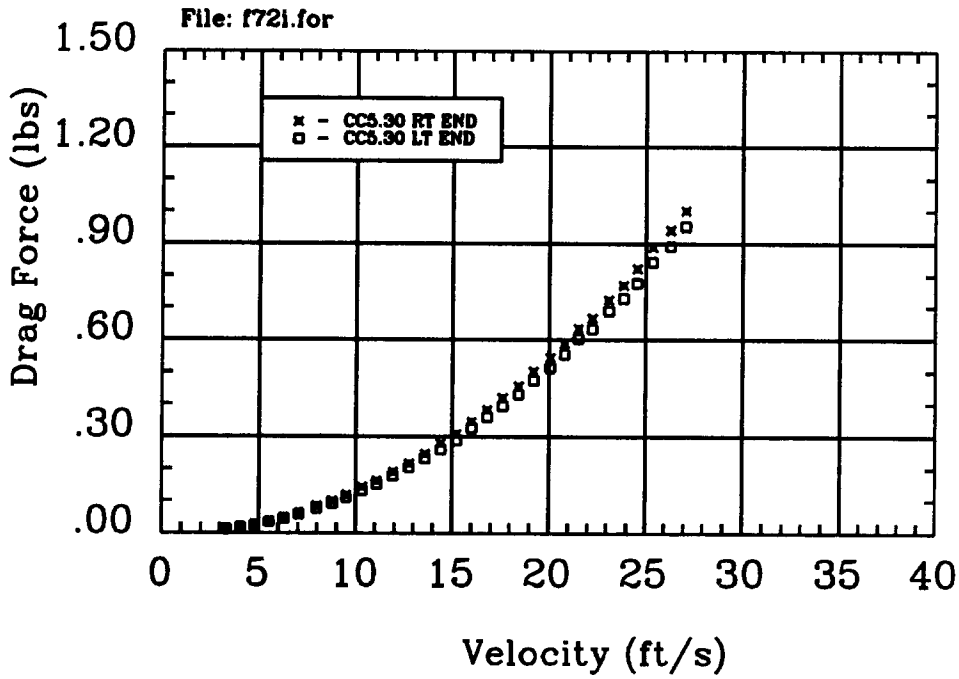

Figure 9. Drag Force at Ends of Model CC5.30

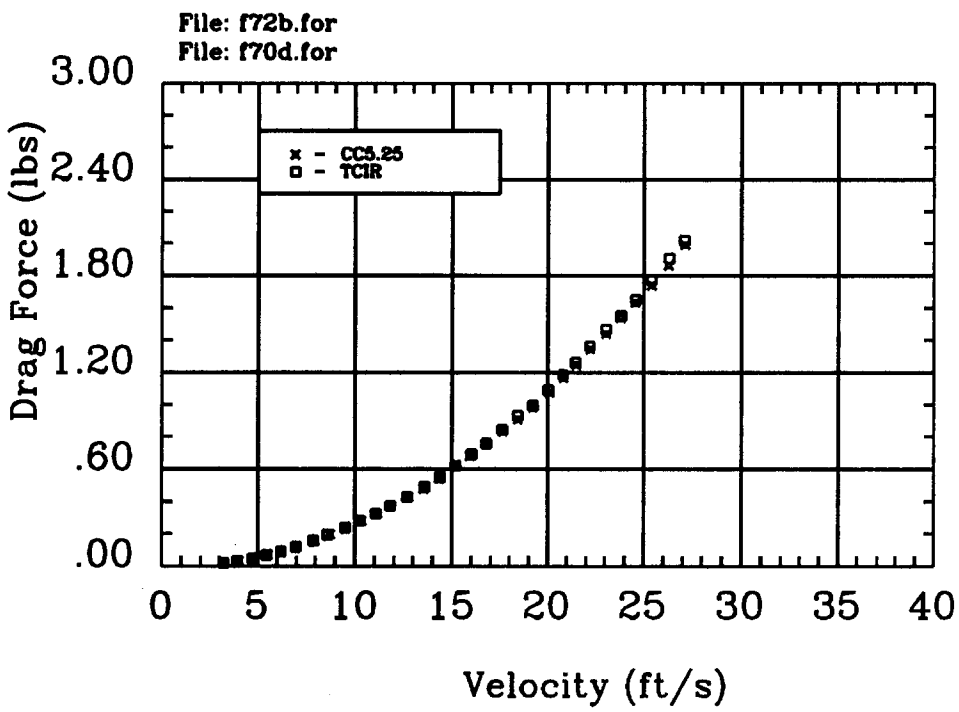

Figure 10. Drag Force on Models CC5.25 and TCIR

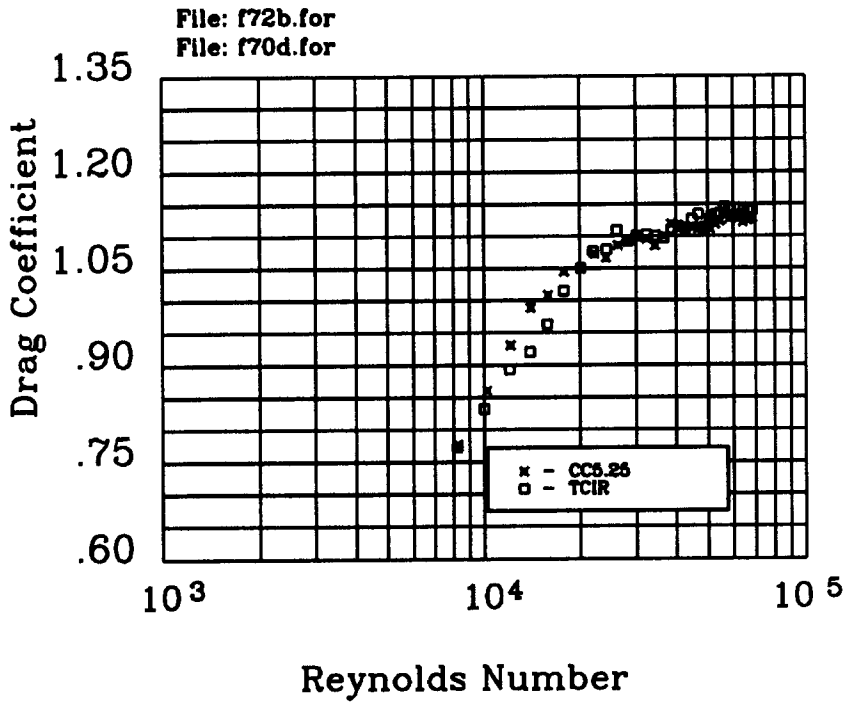

Figure 11. Drag Coefficients for Models CC5.25 and TCIR

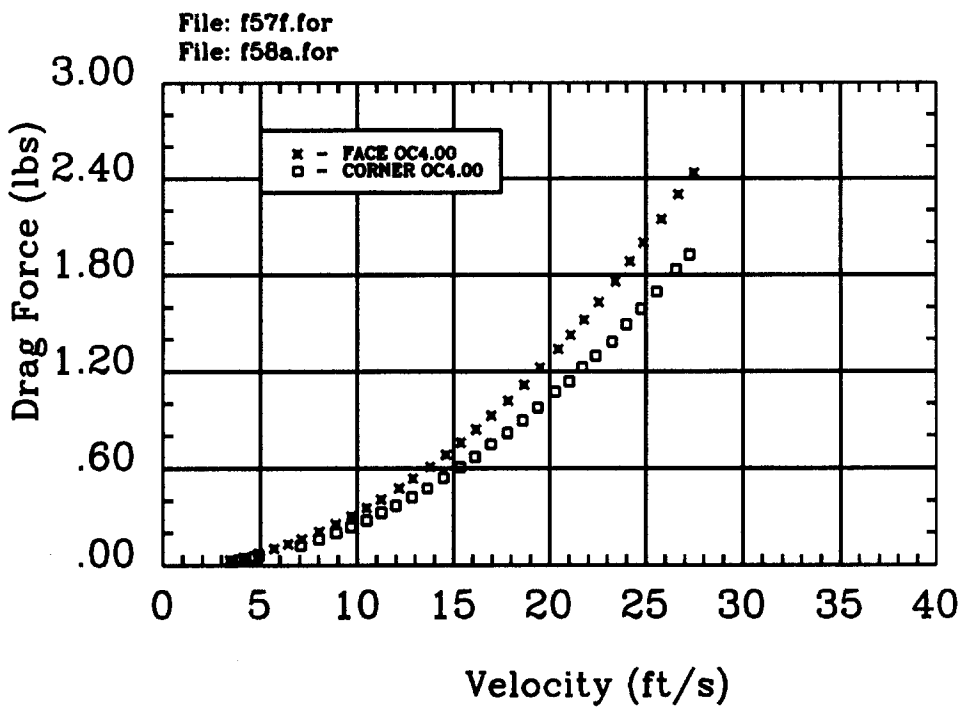

Figure 12. Drag Force on Model OC4.00 - Face/Corner Orientation

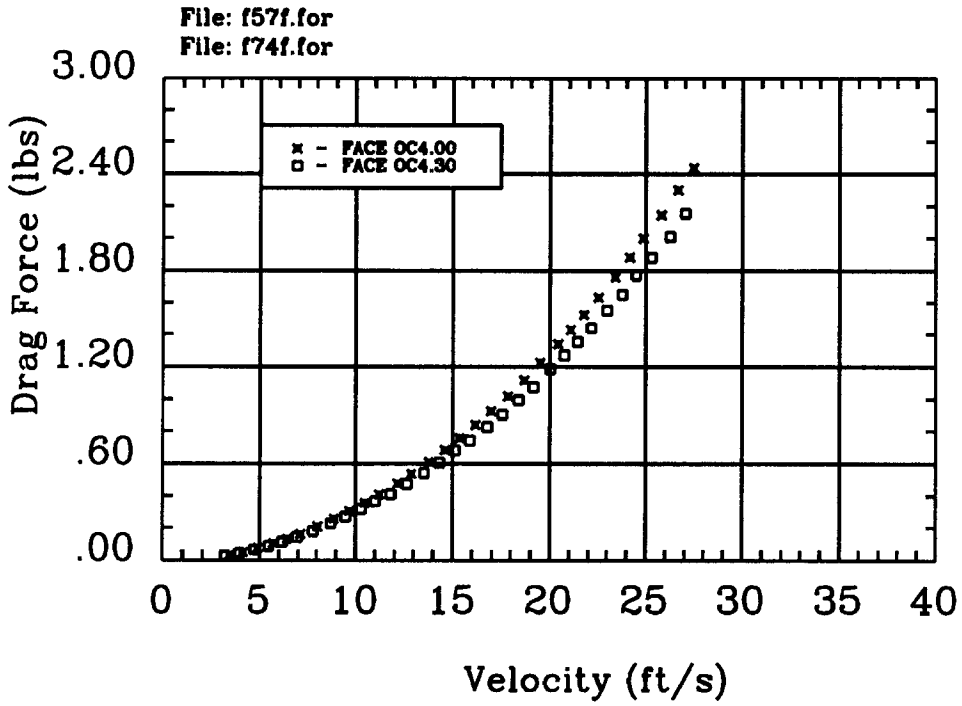

Figure 13. Drag Force on Models OC4.00 and OC4.30 - Face

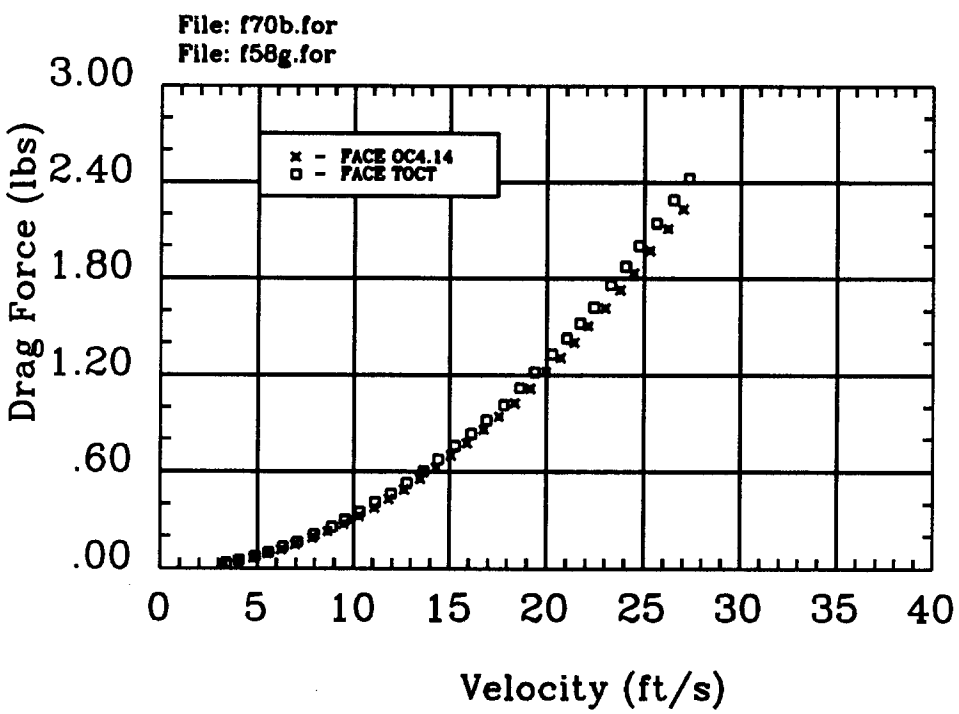

Figure 14. Drag Force on Models OC4.14 and TOCT - Face

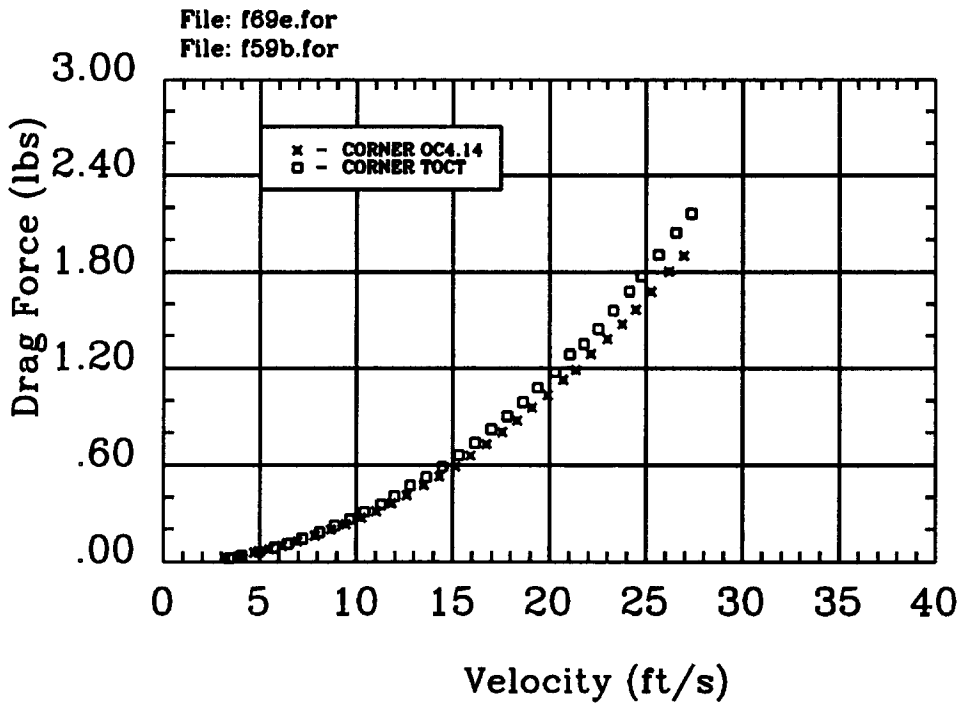

Figure 15. Drag Force on Models OC4.14 and TOCT - Corner

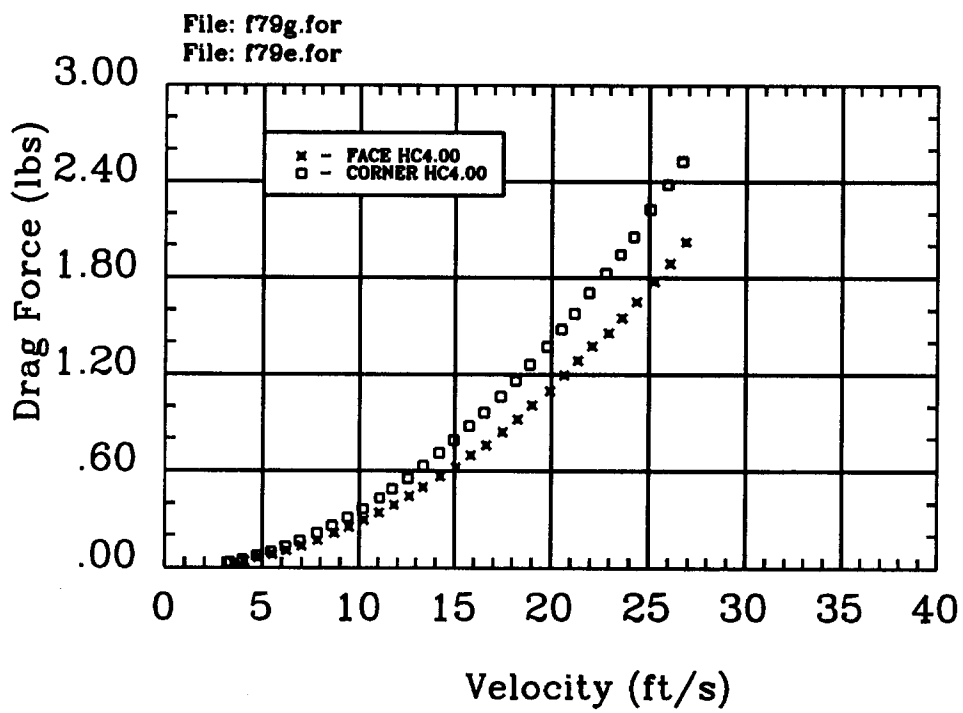

Figure 16. Drag Force on Model HC4.00 - Face/Corner Orientation

Standards to Resist Hurricane Wind Forces

by

G. Robert Fuller[1] and R. D. Marshall[2]

ABSTRACT

On August 24, 1992, Hurricane Andrew struck the coast of south Florida, and then proceeded across the Florida peninsula and the Gulf of Mexico before hitting Louisiana on August 26. Damages of over $30 billion, deaths exceeding 55, and over 200,000 people left homeless prompted the Department of Housing and Urban Development (HUD) to examine its wind design standards for manufactured housing and other residential construction. To review the adequacy of HUD's wind standards, the Department contracted for a study by the National Institute of Standards and Technology (NIST). Based on this study, a wind design and construction standard for manufactured housing, referencing the American Society of Civil Engineers (ASCE) Standard 7-88 was developed and published on January 14, 1994. Research is now being conducted by NIST to provide information so that HUD can further develop standards for wind and tornado resistant construction in other areas of the U.S.

KEYWORDS: anchorage, building codes, damage assessment, design standards, hazard mitigation, hurricane, manufactured housing, residential construction, structural engineering, tornado, wind, wind speed.

1. INTRODUCTION

The purpose of the National Manufactured Housing Construction and Safety Standards Act of 1974 is to reduce the number of personal injuries and deaths, and the insurance costs and property damage resulting from manufactured home failures, and to improve the quality and durability of manufactured homes. In 1993, manufactured housing accounted for approximately 25 percent of all new single-family homes sold in the U.S. Design and construction of this type of housing is covered by the Manufactured Home Construction and Safety Standards (MHCSS), administered by HUD. The MHCSS, which became effective in 1976, prescribes minimum loads for design against wind and snow.

Based on the performance of manufactured housing in Hurricane Hugo in 1989 and in Hurricane Andrew in 1992, it became apparent that the current provisions of the MHCSS were inadequate to ensure satisfactory performance under extreme wind conditions, and the Department undertook a comprehensive review of the requirements in 1992. This paper describes the current wind load requirements, the general types of failures experienced in south Florida during Hurricane Andrew, and amendments to the wind load provisions which are to become effective in July of 1994. Additional problems with ensuring the satisfactory performance of this type of construction in extreme winds are described in this paper.

Following Hurricane Andrew, HUD conducted field investigations of the damage experienced in the hurricane by manufactured housing, as well as other residences constructed under HUD subsidized or mortgage insurance programs. The primary goal of these investigations was to ensure that Federal standards provide adequate protection to manufactured home occupants during high wind conditions. In addition, damage surveys and assessments of single- and

[1] U.S. Department of Housing and Urban Development, Washington, DC 20410-8000

[2] National Institute of Standards and Technology, Gaithersburg, MD 20899

multi-family housing construction were made to evaluate the adequacy of building codes and HUD's Minimum Property Standards.

2. WIND SPEEDS IN HURRICANE ANDREW

The number of reliable wind speed records in a landfalling hurricane usually is quite limited, and Hurricane Andrew was no exception. In fact, no anemometers exposed to winds in the eyewall of Andrew survived long enough or had the recording capability to register the maximum wind speeds. In the months following Andrew, considerable effort was expended in locating records of wind speed and/or barometric pressure from which to reconstruct the wind field over the area of heaviest damage. The highest recorded gust speed, corrected for anemometer error, was 79 m/s (177 mph) at Perrine. There were no confirmed sightings of tornadoes in Dade County and subsequent aerial surveys did not show any evidence of tornado damage.

Reinhold et al. (1993) used a computer-based model that makes use of information on the storm track, barometric pressure data, and the radius of maximum winds. The transition from over-water to over-land exposure and reductions in speed as the storm moves inland are accounted for by an empirical decay model. The model was calibrated against partial records obtained inside the eyewall and complete records obtained outside the eyewall. Results of the analysis are shown in Figure 1 as fastest-mile isotachs. Estimates of fastest-mile wind speeds for standard conditions (10 m (32.8 ft) height in flat, open country) in the area of heaviest damage range from 55 m/s (122 mph) at Florida City to 65 m/s (145 mph) north of Perrine where the northern sector of the eyewall crossed the coastline. The upper-bound estimate of the fastest-mile wind speed in the Tamiami Airport/Country Walk area is 60 m/s (135 mph). A map of the affected area is shown in Figure 2 (Marshall 1993). The maximum recorded gust speeds at selected locations are given in the original units of knots.

3. PERFORMANCE OF MANUFACTURED HOMES IN HURRICANE ANDREW

Damage to manufactured homes in Hurricane Andrew ranged from minor loss of roofing materials to total destruction. In general, those units manufactured after the adoption of the MHCSS in 1976 suffered less damage than did those units manufactured prior to 1976. However, conventional residential construction located adjacent to manufactured home parks performed better, in some instances significantly better, than did manufactured homes, including HUD-labeled units. Based on damage surveys and a reconstruction of wind speeds over the affected area, it appears that HUD-labeled units began to experience damage to roof and wall coverings at fastest-mile speeds of up to 42 m/s (95 mph) and significant structural damage at wind speeds of from 45 to 54 m/s (100 to 120 mph). At wind speeds ranging from 54 to 60 m/s (120 to 135 mph), there were numerous instances of HUD-labeled units suffering total destruction.

Commonly observed failures included loss of roof membranes and failure of roof sheathing, failure of uplift straps at truss-to-wall connections where staple crowns pulled through the strap material, loss of cladding on endwalls and near corners where large negative (suction) pressures develop, loss of add-on construction such as expanded rooms or porches with resulting missile damage and damage to the parent unit at points of attachment, complete separation of superstructure from floor and underframe, and loss of the complete unit due to failure of tiedown straps or withdrawal of soil anchors. In Florida, some form of anchorage system had been installed in almost every case. The anchor failures that were observed involved helical anchors or rock anchors installed in the local coral which is covered by 150 to 300 mm (6 to 12 inches) of sand.

4. CURRENT WIND LOAD REQUIREMENTS OF THE MHCSS

The MHCSS wind load requirements in effect at the time of Hurricane Andrew identified two

wind zones for the United States. Zone II (hurricane) included the Gulf and Atlantic Coast region, the coastal regions of Alaska, and Puerto Rico. All other regions of the United States were designated as Zone I (non-hurricane). Approximately, the boundary between the two zones followed the 40 m/s (90 mph) wind-speed contour of an early version of American National Standard A58.1 (Now ASCE 7 - Minimum Design Loads for Buildings and Other Structures). The basic wind load requirements of the MHCSS were as follows:

	Horizontal Load	Uplift
Zone I	718 Pa (15 psf)	431 Pa (9 psf)
Zone II	1,197 Pa (25 psf)	718 Pa (15 psf)

For the design of components/elements such as eaves and cornices, the MHCSS required uplift loads equal to 2.5 times the uplift loads listed above. For wind exposures in coastal and other areas where wind records indicated significantly higher wind speeds than are implied by the loads listed above, the Department could establish more stringent requirements for homes known to be destined for such areas.

There were no requirement in the MHCSS for permanent foundations, but it was recommended that windstorm protection in the form of soil anchors and tiedown hardware be designed to resist horizontal and uplift loads equal to 1.5 times the values listed above. However, specific requirements for windstorm protection devices and the enforcement of these requirements are left to the individual States. Recommendations for the design and installation of such devices are addressed in American National Standard A225.1 - Manufactured Home Installations.

5. REVIEW OF BUILDING CODES AND STANDARDS

Following Hurricane Andrew, the wind load provisions of selected codes and standards were compared. For Dade County, Florida, the basic wind speed (fastest-mile speed at 10 m (32.8 ft) in exposure category C) specified by ASCE 7-88 is 49 m/s (110 mph), and the corresponding design speed is 52 m/s (116 mph). In general, the wind load requirements of ASCE 7-88 exceed those of the other codes and standards included in this comparison.

Based on the requirements for structural stability (sliding and uplift), the design loads required by the MHCSS at the time of Hurricane Andrew corresponded to a basic wind speed of from 36 to 38 m/s (80 to 85 mph). A similar analysis of the South Florida Building Code (SFBC-88) provisions indicates that the specified design speed of 54 m/s (120 mph) was, in effect, a gust speed. The drag and uplift loads required by the SFBC-88 corresponded to basic wind speeds of 41 and 44 m/s (91 and 98 mph), respectively.

Although ASCE 7-88 and the Standard Building Code (SBC-91) reference the same basic wind speed of 49 m/s (110 mph) and the same source of pressure coefficient data, SBC-91 requires average drag and uplift loads that are approximately 75 percent of the values required by ASCE 7-88. The major reasons for this difference in design loads are a reduction factor of 0.8 applied to the pressure coefficients used in SBC-91 and disregard for the fact that the wind speed probability distributions for hurricanes and for extra-tropical storms are different.

6. PROBABILITIES OF FAILURE

Design wind speeds should reflect the local wind climate (distribution of extremes) and the consequences of structural failure. For ordinary buildings and structures it is generally accepted that the design wind loads should have as their basis the wind speeds associated with a mean recurrence interval (MRI) of about 50 years. Although the probability that these speeds will be exceeded in a 50-yr period is relatively high (64 percent), the use of load factors or allowable stresses in the design process reduces the risk of a structural failure to about 5 percent over the same interval (Gupta and Moss 1993). Generally, the available information from which to estimate the probability of failure of a building or other structure is very limited.

Nevertheless, it is useful to examine the relative risk associated with various design requirements and extreme wind environments. In the following, probabilities of failure implicit in the MHCSS wind load requirements in effect at the time of Hurricane Andrew are compared with those of ASCE 7-88 (Minimum Design Loads for Buildings and Other Structures) for Dade County, Florida; Omaha, Nebraska; and Tucson, Arizona. Extreme wind speeds for Dade County are due to hurricanes while the extremes for the other two locations are governed by extra-tropical wind events.

Implicit in the MHCSS wind load requirements in effect at the time of Hurricane Andrew are basic wind speeds (50-yr MRI) of 29 and 36 m/s (65 and 80 mph) for Zone I (non-hurricane) and Zone II (hurricane), respectively. According to ASCE 7-88, the basic wind speeds for Dade County, Omaha and Tucson are 49, 37 and 34 m/s (110, 83 and 75 mph), respectively. The ultimate load capacity or strength of the structure can be estimated from the design equation

$$\phi R \geq \gamma L \qquad (1)$$

in which R is the nominal resistance of the material or component under consideration, ϕ is the resistance factor, L is the nominal (code-specified) load or load combination, and γ is the load factor. If typical values of 0.8 for the resistance factor and 1.3 for the wind load factor are selected, the reference wind speed at or near the ultimate strength of the structure (ultimate limit state) will be $(1.3/0.8)^{1/2} = 1.275$ times the basic wind speed. In the case of Dade County, Florida, for example, the wind speed at failure should correspond to (49)(1.05)(1.275) = 66 m/s (147 mph). Note that the factor of 1.05 is a structure importance factor required by ASCE 7-88 for design in hurricane-prone regions. If it is further assumed that the coefficient of variation (COV) of structural strength is 0.1, then the distribution functions for load and ultimate strength can be plotted against a reference dynamic pressure, q, as is shown in Figure 3 for Dade County, Florida. By integrating the product of the load function, $Q_L(q)$, and resistance function, $p_R(q)$, it is possible to estimate the probabilities of failure with the results as shown in Table 1. The load function, $Q_L(q)$, for Dade County is based on the wind speed distributions developed by Georgiou et al. (1983), and for Omaha and Tucson on the distributions developed by Simiu et al. (1979).

Although the absolute values of the probabilities listed in Table 1 are reliable only to the extent that the simplifying assumptions represent the true relationship between load and resistance, it is their relative values (MHCSS/ASCE 7) that are of primary interest. It can be seen from Table 1 that, at the time of Hurricane Andrew, manufactured homes sited in Dade County had a risk of failure during a 10-yr exposure that was of the order of 10 times the risk of ordinary buildings designed in accordance with the wind load provisions of ASCE 7-88. This same ratio is seen to apply for Omaha, even though the corresponding probabilities are only about half those for Dade County. For Tucson, the probability of failure for manufactured homes during a 10-yr exposure is about 5 times that of ordinary buildings and structures designed in accordance with ASCE 7-88 and about 1/5 that of manufactured homes sited in Dade County. Not shown in Table 1 are the effects of variability of resistance on the calculated probabilities. In general, increasing the coefficient of variation of resistance will increase the probability of failure, particularly for lower mean values of resistance as is the case for the MHCSS wind load criteria. For example, the probability of failure during a 10-yr exposure at Tucson ranges from 0.27 to 0.42 for a corresponding range in COV of 0.05 to 0.20 in the case of the MHCSS design criteria.

7. REVISED STANDARDS

Based on the experience gained from Hurricanes Hugo and Andrew, on a comprehensive review of the wind load provisions of the model codes and of ASCE 7-88, and on the results of economic impact studies, an amended rule was published in the *Federal Register* in January, 1994. This amended rule is to become effective

on July 13, 1994. The new wind zones are shown in Figure 4 with Zones II and III corresponding to basic wind speeds of 45 and 49 m/s (100 and 110 mph), respectively. Zone I retains the current MHCSS wind load requirements for non-hurricane regions. The new design wind load requirements for Zones II and III are summarized in Table 2.

8. FUTURE WORK

The MHCSS rule change is considered to be an interim measure as it is limited to the design and construction of manufactured housing units destined for hurricane-prone areas for which the basic wind speed is 45 m/s (100 mph) or higher. The rule change does not address construction in non-hurricane areas for which the current requirements still apply. As is indicated by the failure probabilities in Table 1, there are areas in the non-hurricane region for which the probabilities of failure remain unacceptably high. Specifically, improvements in the provisions for the design of cladding are required for wall corner zones, roof edge zones, and roof overhangs. In addition, it is doubtful that traditional approaches to windstorm protection (shallow soil anchors, tiedown straps and dry-stacked concrete block piers) will prove to be adequate or cost-effective in hurricane-prone regions. Alternative approaches using permanent foundation systems are being investigated. Finally, the significance of tornadoes as a design consideration is being examined.

9. REFERENCES

ASCE (1990). *Minimum Design Loads for Buildings and Other Structures,* ASCE 7-88, American Society of Civil Engineers, New York, NY, 94 pp.

Georgiou, P.N., Davenport, A.G. and Vickery, B.J. (1983). "Design Wind Speeds for Regions Dominated by Tropical Cyclones." *Journal of Wind Engineering and Industrial Aerodynamics,* Vol. 13, 139-152.

Gupta, A.K. and Moss, P.J. (Eds.) (1993). *Design of Low-Rise Buildings Subjected to Lateral Forces.* CRC Press, Boca Raton, FL, 286 pp.

HUD (1994). Final Rule - Manufactured Home Construction and Safety Standards on Wind Standards, *Federal Register,* Vol. 59, No. 10, January 14, Office of the Assistant Secretary for Housing, Dept. of Housing and Urban Development, Washington, DC, pp 2456-2474.

Marshall, R.D. (1993). "Wind Load Provisions of the Manufactured Home Construction and Safety Standards - A Review and Recommendations for Improvement." NISTIR 5189, National Institute of Standards and Technology, Gaithersburg, MD, 90 pp.

MHCSS (1992). *Federal Manufactured Home Construction and Safety Standards,* 24 CFR, Part 3280, U.S. Dept. of Housing and Urban Development, Washington, DC, pp 196-223.

NCSBCS (1987). "NCSBCS Standard for Manufactured Home Installations (Manufactured Home Sites, Communities, and Set-ups) - ANSI A225.1-1992." National Conference of States on Building Codes and Standards, Herndon, VA, 49 pp.

Reinhold, T.A., Vickery, P.J. and Powell, M.D. (1993). "Wind Speeds in Hurricane Andrew: Myths and Reality." *Proceedings,* 7th U.S. National Conference on Wind Engineering, UCLA, Los Angeles, CA, Vol. 2, pp 563-577.

Simiu, E., Changery, M.J. and Filliben, J.J. (1979). "Extreme Wind Speeds at 139 Stations in the Contiguous United States." NBS Building Science Series 142, National Bureau of Standards, Washington, DC, 147 pp.

Table 1. Probability of Attaining Ultimate Limit State
$\phi = 0.8$ $\gamma = 1.3$ COV (R) = 0.1

Location	Design Criteria	Probability			
Exposure Period		1 yr	10 yrs	25 yrs	50 yrs
Dade County, Florida	MHCSS	0.037	0.313	0.609	0.847
U_{50} = 49 m/s (110 mph)	ASCE 7	0.003	0.033	0.081	0.155
Omaha, Nebraska	MHCSS	0.018	0.165	0.362	0.594
U_{50} = 37 m/s (83 mph)	ASCE 7	0.002	0.016	0.039	0.077
Tucson, Arizona	MHCSS	0.007	0.067	0.160	0.295
U_{50} = 34 m/s (75 mph)	ASCE 7	0.001	0.014	0.034	0.066

Table 2. MHCSS Revised Design Wind Pressures, January 14, 1994

ELEMENT	ZONE II (psf)	ZONE III (psf)
Anchorage for Lateral and Vertical Stability:		
Net horizontal drag	±39	±47
Uplift	−27	−32
Main Wind Force Resisting System:		
Shearwalls, diaphragms and their fastening and anchorage systems	±39	±47
Ridge beams and other main roof support beams	−30	−36
Components and Cladding:		
Roof trusses in all areas; trusses shall be doubled within 3'-0" from each end of roof	−39	−47
Exterior roof coverings, sheathing & fastenings; all areas except following	−39	−47
Within 3"-0" of gable end or endwall if no overhang is provided	−73	−89
Within 3'-0" of ridge or sidewall if no eave is provided	−51	−62
Eaves (Overhangs at sidewalls)	−51	−62
Gables (Overhangs at endwalls)	−73	−89
Wall studs in sidewalls and endwalls, exterior windows & sliding glass doors, exterior coverings, sheathing & fastenings:		
Within 3'-0" from each corner of sidewall and endwall	±48	±58
All other areas	±38	±46

Note: 1 ft = 0.3048 m 1 psf = 47.88 Pa

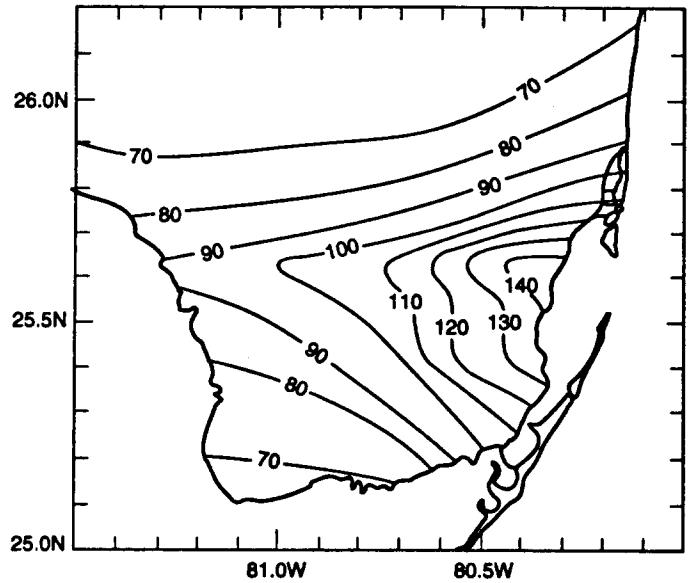

Figure 1. Isotachs of estimated maximum fastest-mile wind speeds (mph) in Hurricane Andrew. (Reinhold et al. 1993). Note: 1 mph = 0.447 m/s.

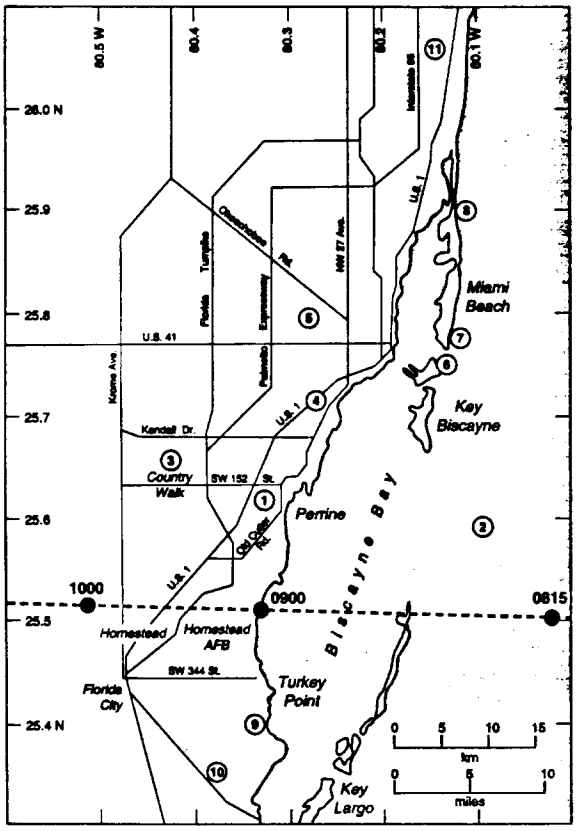

	LOCATION	Pk. Gust (knots)
1	Perrine*	154
2	Fowey Rocks C-MAN	147
3	Tamiami Airport*	108
4	Miami WSFO/NHC	142
5	Miami International	81
6	Virginia Key	98
7	Miami Beach DARDC	92
8	Haulover NOS	85
9	Turkey Point (10 m)*	85
10	Turkey Point (60 m)*	83
11	Fort Lauderdale	76

* Anemometer failed
1 kt = 0.514 m/s = 1.151 mph

Figure 2. Area map showing approximate storm track and key locations, Hurricane Andrew.

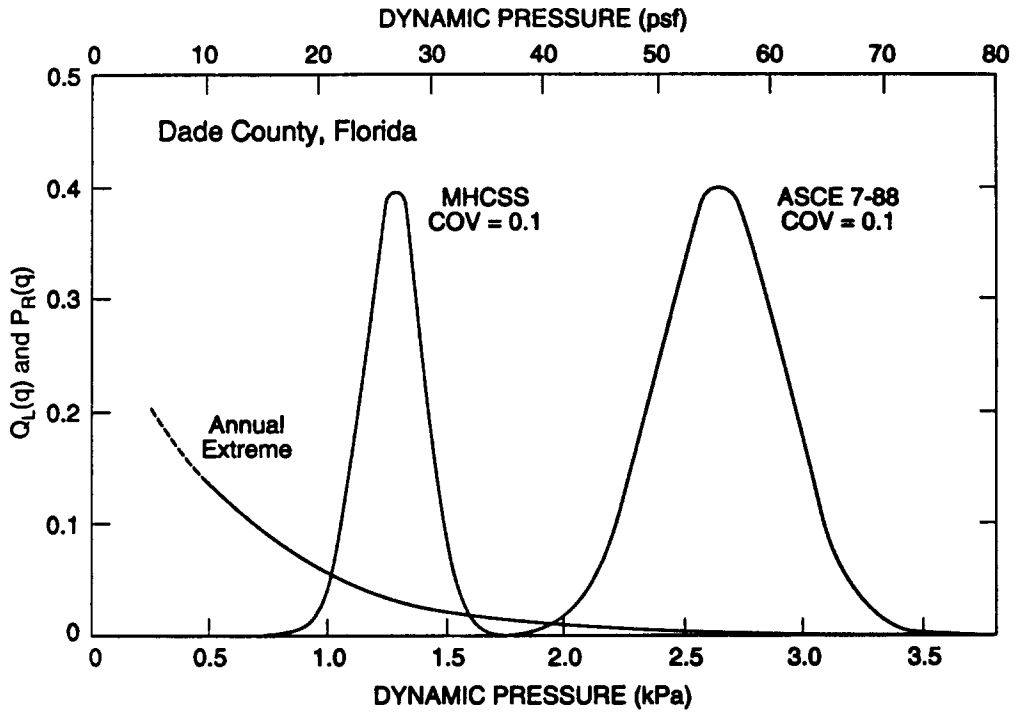

Figure 3. Probability functions for load and resistance, Dade County, Florida.
(Based on MHCSS wind load provisions in effect at time of Hurricane Andrew)

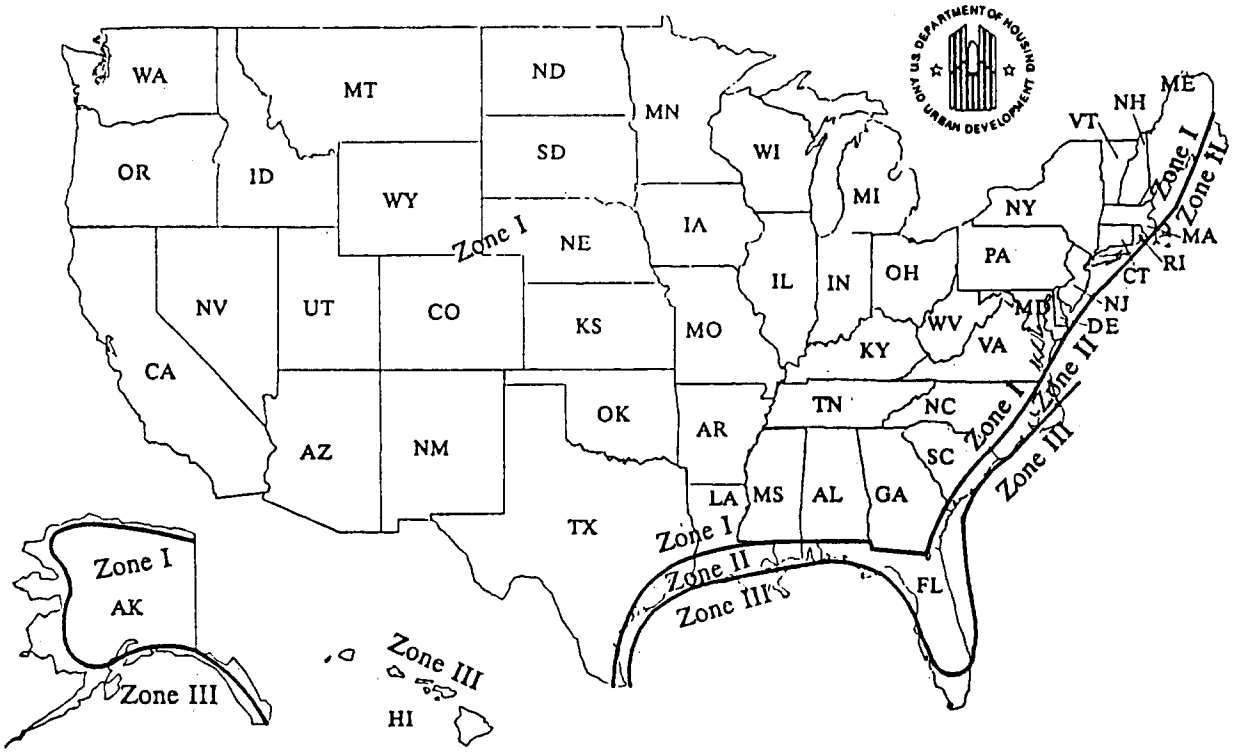

Figure 4. Basic wind zone map for manufactured housing, based on ASCE 7-88.
(Revised Manufactured Home Construction and Safety Standard, January 14, 1994)

Inauguration of International Wind Engineering Forum and New U.S.-Japan Cooperative Research Program

by

Hisashi Okada[1] and Hiroyuki Yamanouchi[2]

Abstract
Interest in wind engineering are recently growing. Many researchers and engineers have become to seek much information and to wish information exchange on wind engineering in the wide of the world. But it is rather difficult because of language barrier and etc. Responding to the request, the International Wind Engineering Forum (IWEF) was established in Japan and the US, where information exchange can be carried out without strict limitations but somewhat systematically. The inaugural meeting of the forum was held in Tokyo on March 17, 1994. Tentative activities of the Forum in Japan side will be establishment of data banks of research information on wind engineering, despatching the information in English and Japanese, publishing news letters and etc.

Key Words:
wind engineering, information exchange, cooperative activities between the US and Japan

1. INTRODUCTION

Japan is well known as one of the most active seismic countries. Attentions of the most people gather fairly less to wind engineering than to earthquake engineering. But a little change in this situation is occurring these days. Topics on wind engineering are more often heard than before. Domestic and International symposiums in wind engineering are called more frequently. The number of researchers is increasing. Figure 1 shows the number of papers in World Conference of Wind Engineering [1]. The Number of papers has been increasing steadily. It is remarkable thing that the papers of Japanese has occupied about 25% of the total since 6th conference.

The reasons why the change mentioned above is occurring are considered to come from the constructions of high-rise buildings of which design wind loads are greater than the design seismic loads and etc. Figure 2 shows the comparison of seismic and wind design loads in Japan.

Under these situations, wishes for the international exchange of information have been raised up. Remarkable increase of Japanese papers in international conference is one of the evidences. Many researchers want to exchange information more actively but some of them cannot find the ways. There are also language barrier and etc.

There is the background which we could not miss on the way to esablishment of the IWEF. New research cooperation in construction technology is required under the New US-Japan Economic Partnership Framework. Disaster prevention/ Building safety is one of the important items in the research cooperation. Wind engineering researches on mitigation of disaster coused by strong winds, control of response of tall buildings due to strong winds and etc. are expected to have much weight in the item.

Responding to the wishes under the background, we made the International Wind Engineering Forum (= IWEF) where international exchange of information can be carried out without strict limitation but somewhat systematically.

Authors have participated in the action for the establishment as originators and made a great role on the way. Having meetings with professors of TTU and CSU and program directors of NSF were some of the actions to

(1) Head, Aerodynamics Division, Structural Engineering Department, Building Research Institute, Ministry of Construction
(2) Director of Structural Engineering Department, ditto

make up the Forum.
The inaugural meeting of the IWEF was held at Toranomon Pastoral Hotel , Tokyo Japan, on March 17, 1994. The number of participants including person from Korea were more than 100. Four person including Prof. Bienkiewicz, one of the originator of the IWEF, CSU, were invited from the US and one person from Taiwan as the speakers. They and Japanese originators presented proposal of the IWEF, present states of wind engineering in Taiwan, US and Japan, cooperative research activities on wind engineering which had produced fruitful results, and etc. in the meeting. The program is shown in Figure 2. Enthusiastic discussion on the gist, management and goal of the IWEF followed the presentations.
In this paper, the gist, tentative activities, management and etc. of the IWEF which were presented in the meeting are described [2].

2. PROPOSAL OF THE IWEF

Inaugural Meeting of the IWEF was opened with opening address and proposal of the IWEF by Dr. Fujii, president of Wind Engineering Research Institute Co., Ltd. In the proposal, he explained motive and gist for the establishment, intended tentative activities management and etc. of the IWEF. The details will be introduced in the following sections.

3. MOTIVE FOR THE ESTABLISHMENT

Things relevant to wind such as wind resistant design, wind response evaluation and wind environmental evaluation is recently raising the practical importance. Many related domestic and international symposiums has been held. The international information exchange has been extensively carried out. State of the international information exchange and collaboration has been improved. But the present state is not sufficient. One of the reasons is a language barrier between Japan and English language countries. Some exchanges and collaborations have been carried out on personal relationship. Many things cannot be expected from such exchanges and collaborations. The idea regarding the forum, where international information exchange can be carried out somewhat systematically without severe restriction, has come from the background.

4. ACTIVITIES OF THE IWEF

Tentative activities which are carried out in Japan side are as follows:

(1) Collection of publications, information of research facilities on wind engineering in Japan, establishment of these data base and despatching the information in English to foreign countries.
(2) Collection of information relative to wind engineering in overseas and preparation of the data base.
(3) Collection of information on strong wind disaster, establishment of the data base and giving support to surveys in damage sites.
(4) Planning and holding lecture meetings and seminars regarding to wind resistance design of building construction, offer of the useful information and promotion of the spread of wind engineering information.
(5) Planning and promotion of advanced research projects relative to wind engineering.
(6) Support to the human exchange both in Japan and between foreign countries and Japan.
(7) Publishing news letters (2 times a year) on which activities of the IWEF, information on the data base established in the IWEF and etc. are informed.

5. MANAGEMENT OF THE IWEF

The organization of the IWEF will be tentatively be placed in Japan and the US. on equal terms. Fig. 1 shows the organization. The headquarters are positioned in the followings.

Japan side : Kenchiku Kenkyu Shinko Kyokai (Japan Association for Building Research Promotion)
US. side : Colorado State University

The organization is expected to expand to the other countries. The organization in the both countries intends to organize respective branches. The branches are expected to support the IWEF activities from various

aspects. The constituent members are composed of the following originators.

Co. - Chairman :
Japan side :
T. Ohkuma
(Kanagawa University)
US. side :
B. Bienkiewicz
(Colorado State University)

Advisory Board :
Japan side :
H. Okada
(Building Research Institute, Ministry of Construction)
K. Fujii
(Wind Engineering Research Institute Co., Ltd.)
Y. Tamura
(Tokyo Polytechnic Institute)
H. Yamanouchi
(Building Research Institute, Ministry of Construction)
US. side :
Four People are supposed to be the Advisory Board members.

One of the most important problem is how to secure funds for the management of the IWEF. In the meantime, the management will be carried out by the donations and compensation for the information given by the IWEF. The volunteer activities by the people who understand the gist of the IWEF are expected and welcomed. It is required for the IWEF to make much effort on getting understanding of many people. The efforts surely produce cooperation of many people with founds and/or supporting activities for the IWEF. Applications for the public financial supports are also very important to secure the founds.

6. FUTURE PROSPECTIVE

After the proposal of the IWEF, states of wind engineering research in Taiwan, the US. and Japan were introduced. The issues of wind engineering we face are presented. Cooperative research activities between the US and Japan and the Universities in the US which have been carried out and produced fruitful results were also introduced. These presentation are very references on consideration of what and how to do in the IWEF.

Following the presentations, enthusiastic discussions were exchanged on the activities, perspective, management, goal and etc. of the IWEF among participants in the meeting.

In the concluding remarks of the meeting, Prof. Ohkuma, chairman of the Japan side, presented history of wind engineering in Japan, contribution which Japan should render in the wind engineering area and etc. And he said he wished that many countries join into the circles for information exchange and cooperative research activities which the IWEF was going to promote and many people support the activities of IWEF.

Actual activities will be decided with reference to questionnaires which were offered from participants after the meeting. The first action will be publication of the first news letter.

LATEST NEWS

(1) BRI will invite Prof. Bienkiewicz for the promotion of the IWEF activities in this summer.

(2) List of research papers in domestic conferences in 1993 and 1994 will be made in English and delivered people who want to receive this fall.

(3) Seminar on the wind resistance design on roof will be held in this summer.

Reference

[1] T. Ohkuma," Concluding/ Philosophical Remarks - Japanese wind engineering is expected to contribute to the world", Inaugural Meeting of the International Wind Engineering Forum, 1994

[2] K. Fujii ,"Proposal of the International Wind Engineering Forum", Inaugural Meeting of the International Wind Engineering Forum, 1994

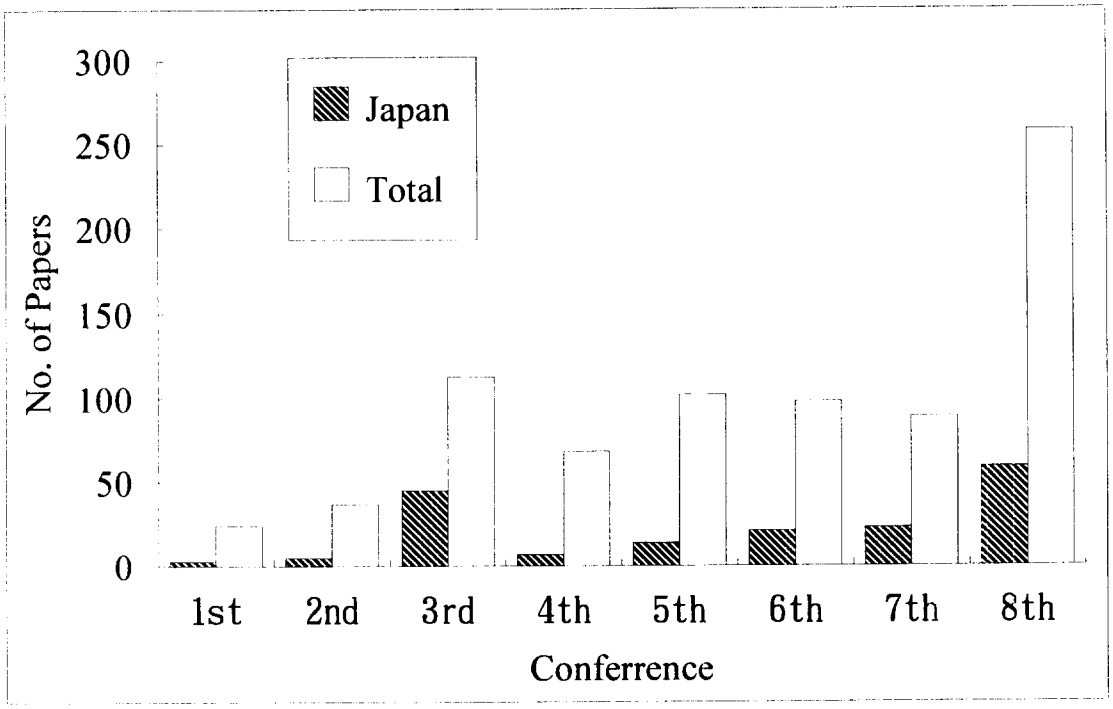

Fig. 1 The Number of Papers presented at the International Conference of Wind Engineering

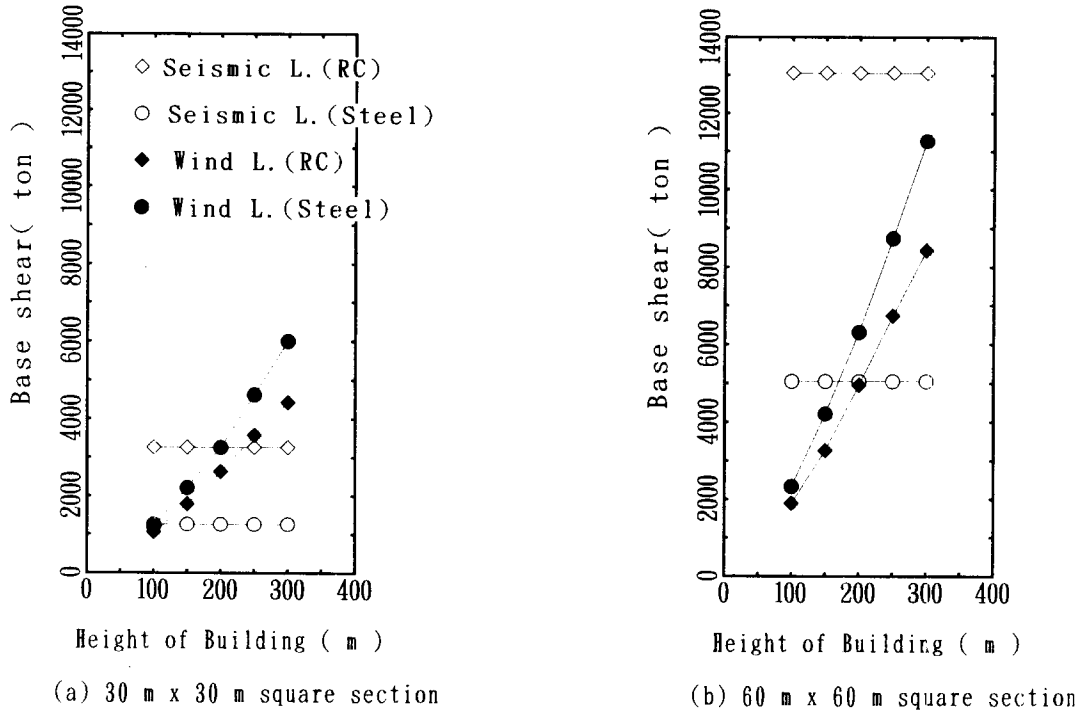

Fig.2 Comparison of seismic and wind design loads in Japan

INAUGURAL MEETING

OF

THE INTERNATIONALWIND ENGINEERING FORUM

Toranomon Pastoral Hotel, Tokyo, Japan

March 17, 1994

Presiding: Prof. J.Kanda (University of Tokyo)

9:00- 9:30	**Opening Address / Proposal of the International Wind Engineering Forum**	Dr. Fujii (Wind Engineering Institute Co. Ltd.)
8:30-10:15	**Wind Engineering Research in USA**	Prof. A. Kareem (University of Notre Dame)
10:15-10:30	Coffee Break	

Presiding: Prof. J.R. McDonald (Texas Tech University)

10:30-11:15	**Wind Engineering Activities in Taiwan**	Prof. CM. Cheng (Tamkang University)
11:15-12:00	**Wind Engineering Activities in Japan**	Prof. Y. Tamura(Tokyo Institute of Polytechnics)
12:00-13:30	Lunch	

Presiding: Prof. H.Kawai (Tokyo Denki University)

13:30-14:15	**US-Japan Activities in Wind Engineering**	Prof. B.Bienkiewicz (Colorado State University)
14:15-15:00	**US-Japan Governmental Organizations Cooperative Activities**	Dr. H. Okada (Building Research Institute)
15:0-15:15	Coffee Break	

Presiding: Prof.A.Kareem(University of Notre Dame)

15:15:-16:00	**Wind Engineering Research: Status and Issues**	Dr. J. E. Sabadell (National Science Foundation)
16:00-16:45	**CSU/TTU Cooperation Program in Wind Engineering**	Prof. J. R. McDonald (Texas Tech University)
16:45-17:00	**Concluding/Philosophical Remarks**	Prof. T. Ohkuma (Kanagawa University)
18:00-20:30	**Party**	

Fig.3 Program of the Inaugural Meeting of the IWEF

Organization of IWEF

	US side	*Japan side*
Headquaters	Colorado State University	Japan Association for Building Research Promotion (K.K.S.K.)
Co-chairman	Prof.B.Bienkiewicz	Prof.T.Ohkuma
Advisory Board	IWEF has commenced with four members in the US and Japan respectively.	

Branches

- US side
- Japan side
- Other Contry

Fig. 4 View of Organization of the IWEF

EARTHQUAKE ENGINEERING

A Seismic Retrofitting Manual for Highway Bridges

by

Ian G. Buckle[1], Ian M. Friedland[1], and James D. Cooper[2]

ABSTRACT

In 1983, the Federal Highway Administration (FHWA) published a set of guidelines for seismic retrofitting of highway bridges. These guidelines presented what was then considered to be the state-of-the-art for screening, evaluating, and retrofitting of seismically deficient bridges. In the 10 years since publication of the FHWA guidelines, there has been significant progress in understanding the response of bridges and in the development of new and improved retrofit technologies. As a consequence, the 1983 guidelines have recently been updated and reissued as a retrofit manual. This paper describes this revision, which was performed by the National Center for Earthquake Engineering Research under contract to the FHWA, and discusses a number of significant changes made in the new manual.

KEYWORDS: bridges; earthquake; seismic design; seismic retrofit.

1. BACKGROUND

Of all the components of a typical highway system, the highway bridge has been the most closely studied for seismic vulnerability. As a consequence, standards have been developed and adopted nationwide for the seismic design of new bridges. By comparison, the seismic retrofitting of existing bridges is a relatively new endeavor. Only a few retrofitting schemes have been used in practice and, given the present state of knowledge, retrofitting is still somewhat of an art requiring considerable engineering judgement.

The San Fernando, California, earthquake of 1971 caused a significant amount of bridge damage and, as a result, initiated a large research effort into seismic bridge design and behavior in the mid- to late 1970s. The majority of this work was jointly sponsored by the California Department of Transportation (CALTRANS), the FHWA, and the National Science Foundation. The primary goal of this effort was to *minimize* the risk of unacceptable damage during a design earthquake. One result of this effort was the publication by the American Association of State Highway and Transportation Officials (AASHTO) of the first comprehensive national highway bridge seismic design guide, the AASHTO "Guide Specification for Seismic Design of Highway Bridges," in 1983.

The San Fernando earthquake also provided the impetus for the FHWA and CALTRANS to address the seismic retrofitting of existing bridges to withstand earthquake forces and movements. The culmination of this effort was the publication of the 1983 FHWA report "Seismic Retrofitting Guidelines for Highway Bridges" (Report No. FHWA/RD-83/007) which was based primarily on research results and information available in the late 1970s. At the time the guidelines were issued, the existing technology for highway bridge retrofitting was limited and many of the proposed techniques had not been field demonstrated. In the 10 or so years since, new and improved technologies for retrofitting bridge columns and footings have been developed and implemented, together with methods to stabilize soils to prevent liquefaction, and to ensure adequate connections between the

[1]National Center for Earthquake Engineering Research, State University of New York at Buffalo, Buffalo, NY 14261

[2]Federal Highway Administration, Turner-Fairbank Highway Research Center, 6300 Georgetown Pike, McLean, VA 22101

bridge superstructure and substructure. Many of these advances in the state-of-the-art are the result of an aggressive research program which was begun by CALTRANS following the Loma Prieta earthquake which occurred near San Francisco in October 1989.

2. THE SEISMIC RETROFITTING MANUAL FOR HIGHWAY BRIDGES

In order to capture these advances in seismic retrofitting and to make the current state-of-the-art available to bridge owners and engineers, the FHWA initiated a project to update the 1983 guidelines. This effort has resulted in a new document titled the "Seismic Retrofitting Manual for Highway Bridges" (hereafter referred to as the Retrofitting Manual) which was completed near the end of 1993 by the National Center for Earthquake Engineering Research (NCEER), under contract to the FHWA.

The new Retrofitting Manual offers procedures for evaluating and upgrading the seismic resistance of existing highway bridges. Specifically it contains:

- A preliminary screening process to identify and prioritize bridges that need to be evaluated for seismic retrofitting;
- A methodology for quantitatively evaluating the seismic capacity of an existing bridge and determining the overall effectiveness of alternative seismic retrofitting measures; and
- Retrofit measures and design requirements for increasing the seismic resistance of existing bridges.

The Retrofitting Manual does not prescribe requirements dictating when and how bridges are to be retrofitted. The decision to retrofit a bridge depends on a number of factors, several of which are outside the scope of the Manual. These include, but are not limited to, the availability of funding, as well as political, social, and economic considerations. The primary focus of the Retrofitting Manual is directed towards the engineering factors.

3. MAJOR CHANGES

The Retrofitting Manual is based in large part on the 1983 guidelines. In some cases, existing material was updated as appropriate. In other cases, completely new material has been added. One notable editorial change is the format of the new document: the 1983 guidelines used a specification–language format followed by a commentary; the new Retrofitting Manual presents guidelines, recommendations, and commentary in one combined section. This shift in style, from a specification to a technical report, led to the change in title from "Guidelines" to "Manual," and it is believed that this improves overall readability. In addition, the Manual format reflects the fact that the state-of-practice in bridge seismic retrofitting is changing rapidly at this time, and that it is premature to prepare specifications at a time when new insight and experience is an almost daily occurrence.

Major technical changes in the Retrofitting Manual include the following:

- An increased emphasis is placed on bridge importance, and the minimum requirements for retrofitting "essential" bridges have been increased, even in low seismic zones. This has been achieved by redefining the Seismic Performance Categories (SPC) so that, for example, an essential bridge that was previously in SPC A is now classified as SPC B with more rigorous retrofitting requirements as a consequence.
- A new preliminary screening algorithm has been introduced which separates the quantitative evaluation of structure vulnerability and seismic hazard from the subjective assessment of importance and other societal issues. A two-part

procedure is thus proposed which first involves the ordering of all bridges based on a numerical rating of structure vulnerability and seismic hazard. A prioritized list is then obtained by reordering this first list to include such judgmental issues as importance, non-seismic deficiencies, remaining useful life, network redundancy, and economic and political factors. A new Priority Index is then defined which is a mix of engineering and societal factors.

- In addition to the capacity/demand (C/D) ratio method for detailed bridge evaluation, a second method based on equivalent lateral strength is now included. This method avoids some of the conservatism in the C/D method which can lead to unnecessarily expensive retrofit schemes. The new equivalent lateral strength method does require more effort to understand and apply; however, it's use is expected to result in lower retrofit costs.

- Expanded sections on retrofit measures are included, reflecting recent progress in the development of practical field techniques. These sections cover column strengthening using jackets, footing upgrades using overlays, and seismic isolation using elastomeric bearings. An expanded section on cable restrainers is also included. It is interesting to note that at the time the 1983 guidelines were issued, most of the retrofitting techniques described therein were identified as *potential* retrofit measures since few, if any, had actually been implemented in the field at that time. In the intervening ten years, this situation has changed and most of the measures described in the new Manual are based on field experience.

Some of these technical changes are discussed in more detail below.

4. RETROFITTING PHILOSOPHY

The underlying philosophy in the new Retrofitting Manual is that, whenever practical, deficient components be strengthened to new design standards. At first sight this may appear to be inconsistent with the overall goals of retrofitting, and not economically justifiable if the structure as a whole will perform below the standards for new construction. There are two reasons that the Retrofitting Manual makes this recommendation. One is that the cost to strengthen a component to new design standards is usually not that much greater than the cost of partial strengthening. The second reason is that it is possible that retrofitting will be a phased operation that takes place over the life of the structure. Changes in construction technologies and economic situations may make it feasible to strengthen some components in the future even though it is not economical to do so now. If component retrofitting were performed to standards below those for new construction, it could become necessary to restrengthen these components during a second phase of retrofitting, resulting in a higher total cost.

There may be cases, however, where it is not feasible to strengthen components to new standards. In these cases, the Retrofitting Manual recommends a preference to at least strengthen such components to lower standards rather than to reject retrofitting altogether. The Retrofitting Manual provides guidance on the selection of acceptable levels of strengthening, but notes that this still requires the judgement of the engineer, taking into consideration the performance of the remainder of the structure.

The Retrofitting Manual also discusses a number of secondary factors that must be considered when retrofitting. One of these is the repairability of the structure following an earthquake. If possible, component strengthening should not be done at the risk of forcing damage to other components that are more difficult to inspect and repair. For example, it is undesirable to strengthen a ductile component if load would then be transferred to

a nonductile or brittle component. This may be the case even if calculations indicated an overall increase in seismic capacity.

Maintenance and inspection of retrofitted components are also discussed in the Retrofitting Manual, as they should also be considered during the retrofit design stage. Many years may pass before a structure is subjected to an earthquake. The retrofit measure must be designed so that it can be maintained to function as planned when and if an earthquake does occur.

5. BRIDGE CLASSIFICATION

Before seismic retrofitting can be undertaken for a group of bridges, they must first be classified according to their Seismic Performance Category (SPC). The SPC is determined by a combination of seismic hazard and structure importance.

Seismic hazard is reflected in the Acceleration Coefficient, A, which is assigned to all locations covered by Division I-A of the AASHTO *Standard Specifications for Highway Bridges*. When multiplied by the acceleration due to gravity, g, the product, $A \cdot g$, represents the likely peak horizontal ground acceleration that will occur due to an earthquake sometime within a 475 year period. More rigorously, this acceleration has a 10 percent probability of being exceeded within a 50 year time frame.

Bridge importance is not so readily quantified. Two Importance Classifications (I) are specified in the Retrofitting Manual: essential and standard. "Essential" bridges are those which must continue to function after an earthquake or which cross routes that must continue to operate immediately following an earthquake. All other bridges are classified as "standard." The determination of the Importance Classification of a bridge is necessarily subjective and consideration should be given to societal/survival and security/defense requirements.

The societal/survival evaluation addresses a number of socio-economic needs and includes, for example, the need for access for emergency relief and recovery operations immediately following an earthquake.

Security/defense requirements may be evaluated using the 1973 Federal-Aid Highway Act, which required that a plan for defense highways be developed by each state. The defense highway network provides connecting routes to military installations, industries, and resources not covered by the Federal-Aid primary routes.

An "essential" bridge is therefore one that satisfies one or more of the following conditions:

- ❒ a bridge that is required to provide secondary life safety; e.g., a bridge that provides access to local emergency services such as hospitals. This category also includes those bridges that cross routes which provide secondary life safety, and bridges that carry lifelines such as electric power and water supply pipelines;

- ❒ a bridge whose loss would create a major economic impact; e.g., a bridge that serves as a major link in a transportation system;

- ❒ a bridge that is formally defined by a local emergency plan as critical; e.g., a bridge that enables civil defense, fire departments, and public health agencies to respond immediately to disaster situations. This category also includes those bridges that cross routes which are defined as critical in a local emergency response plan and those that are located on identified evacuation routes; or

- ❒ a bridge that serves as a critical link in the security/defense roadway network.

Based on the above considerations for seismic hazard and importance, four Seismic Performance Categories are defined in the Retrofitting Manual as shown in Table 1.

These SPC's are assigned differently from those in the AASHTO specifications for new design, where no allowance for structure importance is made in seismic zones with acceleration coefficients less than 0.29. In view of the high cost of retrofitting, it is important to be able to distinguish between "essential" and "standard" structures and especially so in low to moderate seismic zones. Such a distinction also enables a more rational allowance to be made for the nature of the seismic hazard in the central and eastern U.S. where the maximum credible earthquake is expected to be significantly larger than the "design" earthquake (475 year-event). This implies that if an essential bridge in the east is to remain fully operational following a large earthquake, it will need to be retrofitted to a standard higher than that required by the current specification for new construction. This observation is reflected in the assignment of SPC's for essential bridges in Table 1.

6. THE RETROFITTING PROCESS

Seismic retrofitting is one solution for minimizing the hazard of existing bridges that are vulnerable to serious damage during an earthquake. Because not all bridges in the highway system can be retrofitted simultaneously, the most critical bridges should be retrofitted first. The selection of bridges for retrofitting requires an appreciation for the economic, social, administrative, and practical aspects of the problem, as well as the engineering aspects. Seismic retrofitting is only one of several possible courses of action; others include bridge closure, bridge replacement, or acceptance of the risk of seismic damage. Bridge closure or replacement is usually not justified by seismic deficiency alone and will generally only be considered when other deficiencies exist. Therefore, for all practical purposes, a choice must be made between retrofitting or accepting the seismic risk. This choice will depend on the importance of the bridge and on the cost and effectiveness of retrofitting.

The process of retrofitting bridges involves an assessment of a multitude of variables and requires the use of considerable judgement. It is therefore helpful to divide the process into three major stages. These are:

- preliminary screening;
- detailed evaluation; and
- design of retrofit measures.

Each of these stages is outlined below and described in further detail in the Retrofitting Manual. Figure 1 is a flow chart which illustrates the retrofitting process for each SPC.

7. PRELIMINARY SCREENING

Preliminary screening of an inventory of bridges is recommended to identify those bridges which are seismically deficient and those in the greatest need of retrofitting. This is particularly useful when a comprehensive retrofitting program is to be implemented.

The Retrofitting Manual describes a method for developing a Seismic Rating System which may be used to prioritize bridges on a highway system according to their need for seismic hazard reduction. Factors considered in the seismic rating process include structural vulnerabilities, seismic and geotechnical hazards, and bridge importance or criticality. In this way, the most hazardous bridges are identified. Bridges high on the list should be investigated further to determine the benefits of retrofitting. Because the decision to retrofit depends on political, social, and economic factors as well as engineering issues, high priority bridges may not necessarily be retrofitted. On the other hand, bridges with a lower priority may need to be retrofitted immediately.

One very important consideration that is not adequately reflected in the Seismic Rating System is the relationship of the bridge to other bridges on the system that may also be damaged during an earthquake. These types of considerations should be made prior to making a

detailed evaluation of the seismic capacity of the bridge.

A further consideration when deciding if retrofitting is warranted is the age and condition of the bridge. It would not be rational to spend a large amount to retrofit a bridge with only five years of service life remaining. An unusually high seismic vulnerability may, however, be a justification to accelerate closure or replacement of such a bridge.

A bridge in poor physical condition that is scheduled for nonseismic rehabilitation should be given a higher priority for seismic retrofitting, since construction savings can be realized by performing both the nonseismic and seismic work simultaneously.

The above examples do not represent all possible cases, but they do illustrate some of the principles involved in a retrofitting decision. In most cases, the Seismic Rating System is used as a guide to making retrofitting decisions, but not as the final word. Common sense and engineering judgement will be necessary in weighing the actual costs and benefits of retrofitting, against the risks of doing nothing. Also, the effect on the entire highway system must be kept in mind.

The preliminary screening process recommended in the new Retrofitting Manual is demonstrated in Figure 2, where the terms are defined as follows: A is the acceleration coefficient for the bridge site; I is the bridge importance; V is the vulnerability rating of the bridge; S is the soil site coefficient; and E is the seismic hazard rating, which is based on the acceleration and site coefficients.

8. DETAILED EVALUATION

Two alternative methods for the detailed evaluation of existing bridges are currently available. One is based on a quantitative assessment of the "capacities" and "demands" of individual components of a bridge structure. The other evaluates the lateral strength of the bridge as a new structure.

8.1 Capacity/Demand Method

The first method was proposed in the 1983 FHWA Retrofit Guide and has been used in a modified form by CALTRANS since the early 1980's. In this method, the results from an elastic spectral analysis are used to calculate the force and displacement "demands" which are then compared with the "capacities" of each of the components to resist these forces and displacements. In the case of reinforced concrete columns, ultimate capacities are modified to reflect the ability of the column to resist post-elastic deformations. Capacity/ Demand (C/D) ratios are intended to represent the decimal fraction of the design earthquake at which a local failure of the components is likely to occur. Therefore, a C/D ratio less than 1.0 indicates that component failure may occur during the design earthquake and retrofitting may be appropriate.

An overall assessment of the consequences of local component failure is necessary to determine the need for retrofitting. Retrofitting should be considered when an assessment indicates that local component failure will result in unacceptable overall performance. The effect of potential retrofitting may be assessed by performing a detailed re-evaluation of the retrofitted bridge.

The determination of what constitutes a serious consequence of component failure will depend on the importance of the bridge. Collapse of the structure is serious in almost all cases since there is always a potential for loss of life in such an occurrence. In other cases, severe distortions or critical loss of strength will impair the ability of the bridge to carry emergency traffic which is unacceptable for certain important bridges. Repairability of seismic damage is also a consideration. If repairs can be made quickly without serious delays to traffic, damage may be acceptable. This is another area in which engineering judgement is required.

Once it has been determined to consider retrofitting, acceptable methods may be selected from among a number of those suggested in the

Retrofitting Manual. If the seismic response of the structure is affected, then a reanalysis should be performed and new set of component C/D ratios calculated. The new C/D ratios will reflect a change in the size of the earthquake that will cause serious damage. A decision to use any retrofitting method will be based on a relative benefit-to-cost analysis. Hypothetically, this benefit-to-cost analysis may be objective and rigorous, but it is more likely that it will be subjective and based, in large part, on judgement.

8.2 Lateral Strength Method

The Retrofitting Manual also provides an alternative analysis approach which examines the lateral strength of the bridge as a system, or at least individual segments of the bridge as a system, and determines, through an incremental collapse analysis, the load-deformation characteristics of the bridge up to collapse. The fraction of the design earthquake that can be resisted without collapse is then an indicator of the need for retrofitting and the extent of strengthening required. This procedure therefore determines the strength and ductility of the critical collapse mechanism but it can also be used to identify the onset of damage when serviceability criteria may be important. The method emphasizes deformation capacity rather than strength since, although strength is important, it is less important than the ability to sustain substantial deformations without collapse. It is believed that fewer bridges assessed under this procedure will be found in need of retrofit than by the C/D ratio method. When retrofit is required, it should be less extensive. The increased level of effort required of the designer will then be offset by reduced retrofit costs in the field.

9. RETROFIT MEASURES

There are two alternative strategies that a designer may adopt when faced with retrofitting a bridge. One is based on conventional strengthening techniques which increase the capacity of the structure to meet the likely demand. This is the most common approach used in the United States at this time. The second strategy is based on reducing the demand on the structure such that its existing capacity is sufficient to withstand the given earthquake. This latter approach involved the use of an earthquake protective system, such as seismic isolation or the addition of a mechanical energy dissipation device. Both strategies are described and detailed in the Retrofitting Manual.

9.1 Conventional Retrofit Measures

The new Retrofit Manual describes conventional retrofit measures for bearings, seats, and expansion joints, including joint and bearing restrainers, bearing seat extensions, and overall bearing replacement. The Manual also discusses techniques for strengthening reinforced concrete substructures through column jacketing and wrapping, cap/column and column/footing joint strengthening, and cap beam retrofitting. Retrofit measures for foundations include strengthening footings for flexural and shear strength, ensuring adequate reinforcement anchorage, and sufficient strength in the pile/footing connection to resist overturning or uplift, along with problems related to abutments and approach slabs. Finally, the Manual also discusses problems associated with hazardous sites, including sites with liquefiable soils, bridges on or near unstable slopes, and bridges crossing or near active faults. These techniques represent the current state-of-the-art; however, the art is changing rapidly at this time.

9.2 Earthquake Protective Systems

The term "earthquake protective system" includes passive and active devices which can be installed in a bridge to minimize the seismic demand on the members of the structure. Active systems are considered outside the scope of the Manual but passive devices are being used in several states as a cost-effective retrofit measure for many bridge types. Passive systems discussed in the Manual include mechanical systems, which simply dissipate energy and thus reduce response, and seismic isolation systems, which

change the natural period of a bridge so that earthquake loads are significantly reduced. The Manual provides a discussion on seismic isolation concepts and on some of the options available at this time for design and implementation.

10. SUMMARY

The new "Seismic Retrofitting Manual for Highway Bridges" contains detailed information about each of the major steps in the bridge seismic retrofit process, as shown in Figure 1. It describes procedures for preliminary screening of bridges along with two alternate procedures for the detailed evaluation of them. These evaluation methods include a quantitative evaluation of the C/D ratios for individual bridge components, and an alternative method based on assessment of a structure's lateral strength.

The procedures for evaluating bridges for retrofitting also include the identification and assessment of retrofit measures. A number of potential retrofitting measures and retrofit design requirements are discussed in the Manual. Specifically, retrofit measures for the types of bridge components which have performed poorly during past earthquakes are discussed in detail. Retrofitting by these or other equivalent methods should be considered when components are identified by a detailed evaluation as being deficient. The decision to use a retrofitting scheme will be based on an assessment of its effectiveness in preventing unacceptable overall performance, the cost of retrofitting, and the remaining service life of the bridge. The Retrofitting Manual also includes several worked example problems intended to help illustrate the process of planning the retrofitting of a typical highway bridge.

Detailed design of retrofit measures should be performed using the guidelines contained in the Retrofitting Manual in conjunction with the current AASHTO bridge design specifications. If possible, components which are selected for retrofitting should generally be strengthened to conform to the specifications for new construction, even though the structure may otherwise be seismically deficient.

11. ACKNOWLEDGEMENTS

The "Seismic Retrofitting Manual for Highway Bridges" was developed under the FHWA-sponsored project titled "Seismic Vulnerability of Existing Highway Construction, FHWA Contract DTFH61-92-C-00106, by the National Center for Earthquake Engineering Research. The authors acknowledge the assistance of Dr. John Kulicki of Modjeski and Masters Inc., and Dr. Roy A. Imbsen of Imbsen & Associates Inc., in the review phases of the Manual. Any opinions, findings, and conclusions or recommendations expressed in the Retrofitting Manual or this paper are those of the authors and do not necessarily reflect the view of NCEER, the FHWA, or the U.S. Department of Transportation.

Table 1. Seismic Performance Category

Acceleration Coefficient	Importance Classification	
	Essential	Standard
$A \leq 0.09$	B	A
$0.09 < A \leq 0.19$	C	B
$0.19 < A \leq 0.29$	C	C
$0.29 < A$	D	C

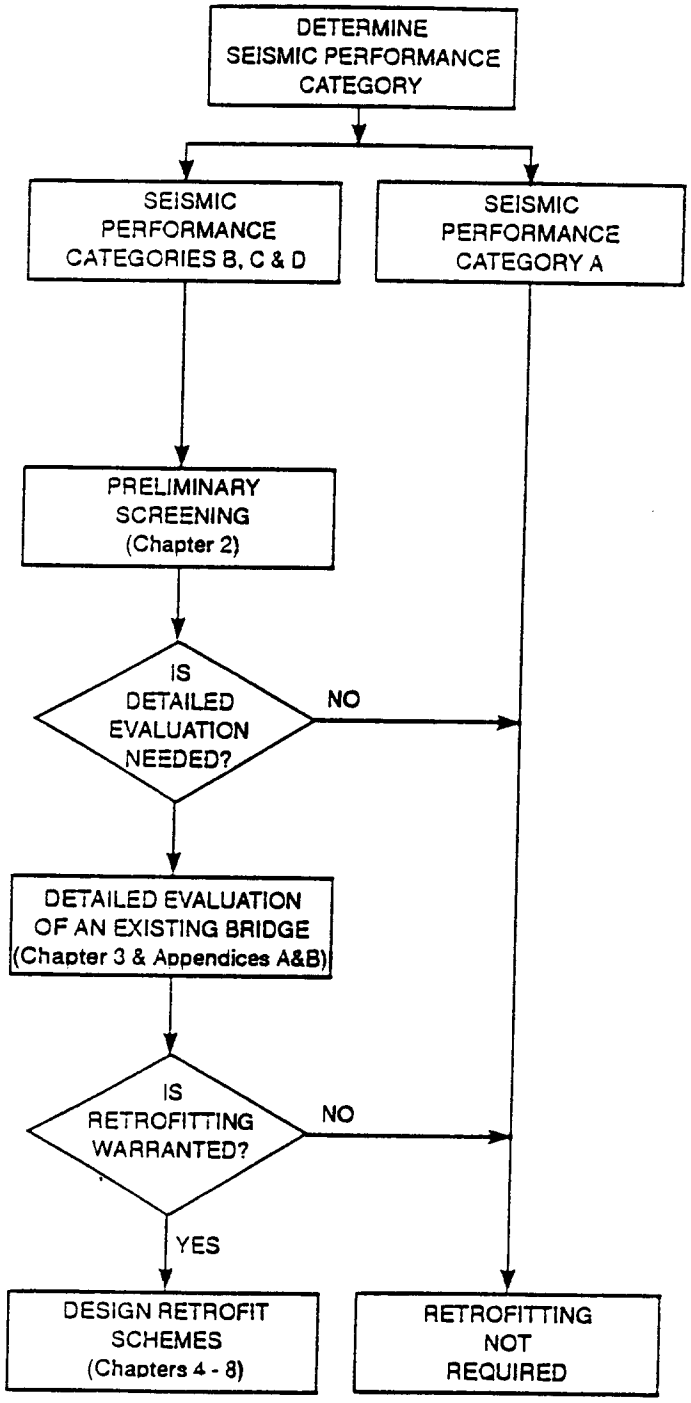

Figure 1. The Seismic Retrofitting Process

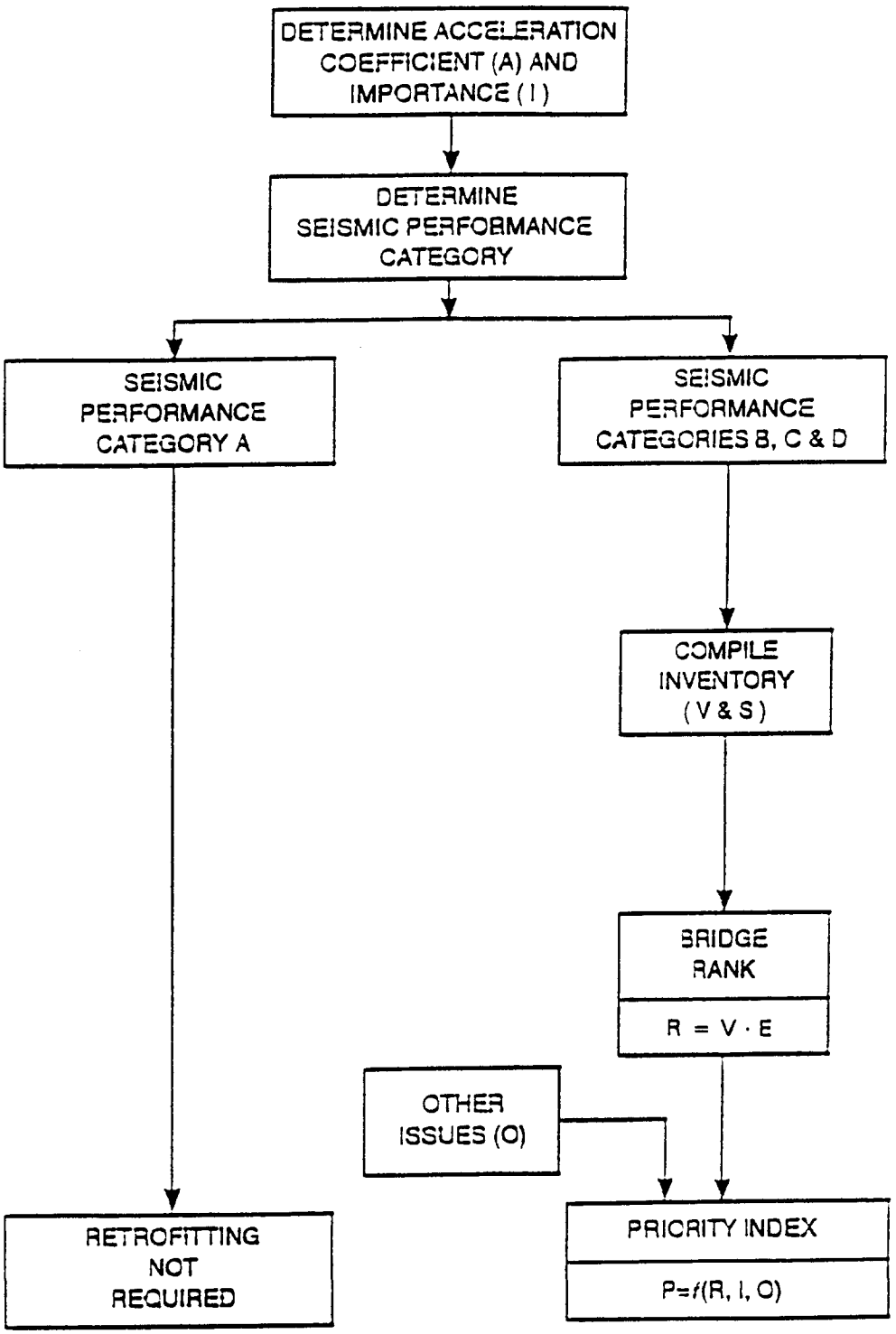

Figure 2. The Preliminary Screening Process

Development of Innovative Seismic Response Control of Bridges

by

Kazuhiko Kawashima[1], Shigeki Unjoh[2] and Hidetoshi Mukai[3]

ABSTRACT

This paper presents variable dampers in which the damping force can be changed depending on the structural response, and the variable stiffness control in which the instantaneous natural period of structures can be changed so that the resonance with the predominant ground motion be avoided. A cylinder/piston type model of the variable damper was developed, and the effectiveness of the variable dampers was verified by a shaking table test. An experimental model of the electro-rheological (ER) fluid damper is also being developed, and its performance is being studied by a series of dynamic loading test.

Key Words :Variable Damper,
Variable Stiffness Control,
Electro Rheological Fluid,
ER Damper, Damper, Bridges,
Seismic Response Control

1. INTRODUCTION

Variable damper, in which damping coefficient can be variable dependent on structural response, for structural response control against an earthquake was proposed by the authors in 1989 (Kawashima and Unjoh 1989, Taguchi et al 1990), and various studies have been made at the Public Works Research Institute. This investigation was initiated to develop an appropriate seismic control algorithm for bridges. Because the active control requires a lot of energy to control the bridge seismic response in a satisfactory level, an alternative approach was required.

The concept of variable dampers is very unique. The variable damper works as a load transmitting member as well as a usual energy dissipator. The variable damper has been effectively adopted in a field of mechanical engineering, in particular in a suspension system for an aircraft and an automobile. An active suspension for improving driving comfortableness and stability of automobiles is one of such examples (Sugawara 1986, Millikan 1987). However, it is a new idea to apply the variable damper for structural response control against an earthquake. Two variable dampers were developed at the Public Works research Institute. One adopts a cylinder/piston type, and the other uses the electro-rheological (ER) fluid.

Variable stiffness is an interesting field of extension of the variable damper. If one shifts the natural period of structures, the structural response may be significantly reduced by avoiding the resonance with the ground motion.

This paper presents the current studies for the variable dampers and variable stiffness for response control of bridges against an earthquake.

2. VARIABLE DAMPER

2.1 Concept of a Variable Damper

A unique technic in application of dampers to bridges is to distribute the seismic lateral force to as many piers as possible. By

1) Research Coordinator for Underground Development, Planning and Research Administration Department, Public Works research Institute, Ministry of Construction, Tsukuba Science City, 305 Japan
2) Senior Research Engineer, Earthquake Engineering Division, Earthquake Disaster Prevention Department, ditto
3) Assistant Research Engineer, ditto

using the dampers in an over-damped zone, the dampers work as force transmitting members from deck to piers. The dampers used for such purpose are called as the damper stoppers. It should be noted that by adopting the damper stoppers, thermal force induced in substructures due to elongation/shrinkage of deck associated with the temperature change can be reduced because the damper stoppers do not resist for the low-rate movement. The damper stoppers have been successfully implemented in many bridges (Izeki 1980).

Because few energy dissipation is made in the damper stopper, it is effective to decrease the damping ratio so that energy dissipation can be maximum when the bridge is subjected to a ground motion caused by a large earthquake. Because the damper stopper is effective for preventing a small deck vibration associated with breaking loads and wind effects, the function as the damper stopper is effective at small deck displacement. On the other hand when the deck response becomes excessive during an earthquake, the stopper is required to present further build up of the deck response.

Thus, the variable dampers with the following requirements may be superior to the existing dampers and damper stoppers:

1) Damping coefficient is very large during a small deck vibration for preventing the deck vibration due to breaking loads of vehicles and wind effects. It is movable against the low rate motions such as the elongation of deck by temperature change.

2) Against the seismic response with the deck response over a certain value, the damping coefficient is set so as to make energy dissipation maximum.

3) Against excessive deck response during an earthquake, high damping coefficient is required to function as a stopper. Smooth and gradual increase of the damping force may be effective for preventing shocks.

Although various types of the variable damper can be made, the simplest structure may be an piston-cylinder viscous damper as shown in **Fig. 1**. A by-pass is installed between the cylinder-cells divided by the piston. Damping coefficient of the damper can be controlled by varying an amount of viscous flow of the by-pass. Various technologies for controlling such flow are available. External energy required for such control is generally much smaller than that required for the active control.

2.2 Effectiveness of Variable Dampers

Fig. 2 shows the deck displacement dependent damping ratio of the variable damper proposed for bridges (Kawashima, Unjoh and Shimizu 1991, Kawashima, Unjoh, Nagashima and Shimizu 1991, Kawashima, Unjoh and Shimizu 1992). Various control algorithm may be used such as to vary h_1, h_2 and h_3 in time depending on bridge response for optimizing the deck response. The damping ratio can be varied depending on both/either the deck velocity and/or the deck displacement (Kawashima, Unjoh and Shimizu 1991). Partial control in which the control is made only partially in time can be made (Kawashima, Unjoh and Shimizu 1991). For simplicity, the damping ratios h_1, h_2 and h_3 are assumed here to be constant during an earthquake. It should be however noted that any relation between the damping ratio vs. the relative displacement and/or relative velocity can be incorporated in the analysis. In fact, various control algorithm is being developed. Ban-Ban control algorithm (Feng and Shinozuka 1990) and more sophisticated time dependent algorithm is also being developed (Yang, Li and Wu 1994, Sun and Goto 1994).

For studying the effectiveness of the variable damper, a simple span girder bridge, as shown in Fig. 3, with a span length of 30m was analyzed. The response in longitudinal direction was considered. Although the variable damper has better implementation for multi-span continuous bridges, a simple span bridge was considered for analysis for simplicity. The deck was assumed to be supported by elastic bearings, and two variable dampers were installed between the deck and the piers.

The weight of superstructure and stiffness

of a pier were assumed as 2368 KN and 17350 KN/m so that the fundamental natural period of the bridge is 0.5 second if the both bearings are hinged. The lateral stiffness of rubber bearings per pier is assumed as 6276 KN/m so that the fundamental natural period of the bridge supported by the rubber bearings be 1.0 second. Damping ratio of the bridge was assumed as 0.02.

The bridge response with and without control by the variable dampers was computed. The damping ratios in Fig. 2 were assumed as $h_1 = 0.5$ and $h_2 = h_3 = 3$. As shown in Table 1, the peak deck displacement and the peak deck acceleration decrease to 26% and 44% of those without control, respectively.

The damping force and stroke required for the variable dampers are 632 KN$\times$2 = 1264 KN and 5.78 cm, respectively. Because the weight of deck is 2368 KN, the damping force is 53 % of the deck weight. The variable dampers with this specification can be designed and fabricated within the current scope of dampers technology.

2.3 Verification of Variable Dampers through Shake Table Tests

For verifying the feasibility of the variable dampers, a prototype variable damper was developed as shown in Photo 1 (Kawashima, Unjoh and Mukai 1993). It is a piston-cylinder type viscous damper with a by-pass installed between two cylinder-cells divided by the piston. The model was designed so that the maximum damping force is 200 KN and the stroke is $\pm$13 cm. Damping force can be controlled by a personal computer depending on a relative displacement and/or a velocity between a deck and a pier. The electricity required for control is only 50 W. This is extremely small as compared with the energy required for the active control.

A series of dynamic loading tests was made for the model. Fig. 4 shows a hysteresis loop of the damping force vs. stroke. Both command signal and actual data are presented. The hysteresis loop obtained by the loading test is very close with the command.

For verifying the effectiveness of the variable damper, a series of shake table tests was made. A simple span bridge model was fabricated on a shake table as shown in Fig. 5. The deck is 7.6 m long and 390 KN in weight. The piers are 1.6 m long. The deck is supported by four rubber bearings, and the prototype variable damper was installed between the deck and the pier as shown in Photo 2.

The model bridge was excited by a ground acceleration. The peak table acceleration was set as about 180 cm/sec^2 and 413 cm/sec^2. The excitation by the table motion with peak acceleration of 413 cm/sec^2 was not made for the model without control, because the deck response became excessive.

Figs. 6 and 7 compares the deck displacement of the model bridge, with and without control by the variable damper, subjected to the table acceleration with peak acceleration of about 180 cm/sec^2. Predicted response by the analysis which will be described later is also presented. The deck responses are 376 cm/sec^2 and 9.2 cm for no control, and they are decreased to 203 cm/sec^2 and 1.3 cm by the variable damper. The maximum damping force required for this control is 71 KN, which corresponds to 18% of the deck weight.

A simulation of the experiments by the analytical method presented in the previous chapter was made. The deck, piers and rubber bearings were idealized by a discrete linear frame. Figs. 6 and 7 compare the deck displacement and the damping force developed in the variable damper between the experiments and analyses. The predicted responses are quite close with the measured responses.

3. VARIABLE STIFFNESS CONTROL

3.1 Concept

Most of bridges with usual size have the natural period ranging from 0.3 to 1.5 second, and this range corresponds to the predominant period of earthquake-induced ground motions.

Thus the resonance of the bridges response with the ground motion tends to be developed during an earthquake. The bridge response could be reduced provided the resonance of bridge response with the ground motion could be avoided.

Although it is hard to predict the predominant period of ground motion prior to an earthquake, it can be evaluated time by time basis during an earthquake. The moving window analysis may be used for evaluating the instantaneous predominant period of ground motion T^*. The resonance of bridge response with the ground motion may be avoided if the instantaneous natural period of bridges T be shifted from the instantaneous predominant period of ground motion T^* during an earthquake.

There are various methods to shift the instantaneous natural period of bridges during an earthquake. Flexibility of bearings may be changed, and active tendons/bracings may be adopted.

If one provides the variable dampers for a bridge which is elastically supported by rubber bearings, the natural period of the bridge can be varied by changing the damping coefficient of the variable dampers. If one makes the damping ratio of the variable damper very large, the variable dampers would acts as the damper stoppers. In another word, they work as force transmitting members. On the other hand, if one makes the damping ratio small, the natural period of the bridge takes the value computed from the stiffness of the rubber bearings and piers. Thus although the variable dampers are essentially dampers, they can be used in an over-damped range as force transmitting members to change the natural period of structures. The variable dampers have various advantage for controlling the instantaneous natural period of bridges because it is more stable for long term use than the active tendons/bracing systems. The energy required is also much less.

Fig. 8 shows the algorithm of the variable stiffness control. The instantaneous predominant period of ground motion T^* at time t_i is computed by the moving window Fourier spectrum. The damping coefficient of variable dampers is varied so that the instantaneous natural period of the bridge T be shifted to prevent the resonance with the ground motion.

Although several algorithm can be considered, the period shift is assumed here as

$$T = \alpha T \qquad (1)$$

where,

T : instantaneous natural period of a bridge at time t_i

T^*: instantaneous predominant period of an earthquake ground motion at time t_i

α : control coefficient

The coefficient α has to be determined depending on the undamped natural period of the bridge T_0 and the instantaneous predominant period T^* of an ground motion.

3.2 Effectiveness of Variable Stiffness Control

To study the effectiveness of the variable stiffness control, a three-span continuous girder bridge, as shown in Fig. 9, with a span length of 90m is analyzed. The response in longitudinal direction is considered. The superstructure of the model is supported by elastic bearings, and four variable dampers with the same characteristics are installed between the deck and the piers. The weight of the superstructure and spring stiffness of the rubber bearings are assumed as 4719 KN and 6247 KN/m, respectively. The stiffness of piers is assumed so that the fundamental natural period of the bridge is 0.5 sec when the deck is supported by hinges. The stiffness of rubber bearings is set so that the fundamental natural period of bridge is 1 sec when the deck is supported by the elastic bearings. The damping ratio of the bridge without control is assumed as 0.02.

An acceleration ground motion as shown in Fig. 10 is used as an input acceleration. The instantaneous predominant frequency ($1/T^*$) of the input acceleration is also shown in Fig. 10.

Because the predominant period of ground motion is about 1 sec., α in Eq. (1) was assumed as 1/2.

Fig 11 shows how the natural period of the bridge change depending on the damping coefficient of the variable dampers. At the damping coefficient C of about 4200 KN•sec/m, the fundamental natural period of bridge becomes very large, because this corresponds to the critical damping of the structure. Although the period shift may be made in the damping coefficient range of 0 to over 8000 KN•sec/m, it is assumed here that the period shift be made in the over-damped range(damping coefficient $C \geqq$ 4200 KN•sec/m).

Fig. 12 compares the deck acceleration and displacement of the bridge with and without control. The peak displacement and peak acceleration of deck decreases to 17% and 50% of those without control. The bending moment of pier bottom decreases to 52% of the one without control. The peak damping force required for the four variable dampers is 761 KN$\times$4 = 3040 KN and peak stroke is 3.1cm.

3.3 Development of a Variable Damper for Variable Stiffness Control

For verifying the variable stiffness control, a variable damper is being developed. Although Eq. (1) was originally proposed, some modifications are required for making the control simple and effective. Firstly it is modified so that the control is made only when the instantaneous natural period T of the structure at time t is between $\beta_1 T^*$ and $\beta_2 T^*$. The coefficients β_1 and β_2 are tentatively proposed to set as 3/4 and 5/4, respectively. Secondly, it is modified so that T increases to 1.5 times as large as T^*.

In this modification, Eq. (1) is written as

$$T = 1.5T^* \leqq T_F \qquad (2)$$
$$(\beta_1 T^* \leqq T \leqq \beta_2 T^*)$$

With use of the variable damper being developed, a shake table test similar with the one presented in 2.3 is planned to verify the effectiveness of variable stiffness control algorithm.

At this moment, an algorithm to detect the predominant period T^* is being studied. Some time delay associated with the time required for AD conversion, a computation of running Fourier spectrum and DA conversion at each time step requires to be shorten.

5. DEVELOPMENT OF A VARIABLE DAMPER USING ER FLUID

5.1 Design and Development of a ER Damper

Electro-rheological (ER) fluid is an innovative material which has a potential application for a wide range of engineering fields. The viscosity of ER fluid can be changed depending on the electric field applied. Because reliable ER fluid with high application to practical use was recently developed, various application has been initiated especially in mechanical systems (Sasada et al 1975A, Sasada et al 1975B, Ushijima et al 1988, Duclos 1988, Ehrgott and Masri 1992).

In a cylinder-type damper system with an orifice and a piston as shown in Fig. 13, the damping force of the ER damper may be given as

$$F = F_V + F_E \qquad (3)$$

$$F_V = \frac{12 \cdot L \cdot A^2 \cdot v}{B \cdot H^3} \eta \qquad (4)$$

$$F_E = \frac{3 \cdot L \cdot A}{H} \tau_y(E) \qquad (5)$$

where,

F : damping force developed by an ER damper

F_V :damping force developed by fluid viscosity through an orifice

F_E :damping force developed by ER effects

A : pressure area of a piston

v : velocity of a piston

L, B, H : length, width and distance of electrodes

η : viscosity of ER fluid

$\tau_y(E)$: shear stress developed by ER effects

E : applied electric field strength

Shear stress developed by the ER effects $\tau_y(E)$ is controlled by the applied electric field strength E between the electrodes, and is written as

$$\tau_y(E) = a \cdot E^{\beta} \qquad (6)$$

where

a , β : coefficients dependent on the material

According to the dynamic loading tests for an ER fluid used in this study, which will be described later, they are

$$\left.\begin{aligned} a &= 2.06\times10^{-4} \\ \beta &= 1.7 \end{aligned}\right\} \qquad (7)$$

It should be noted in Eq. (3) that only *FE* can be changed by controlling the applied electric field strength. Fig. 14 shows an illustration of Eq. (3) for a steady state constant displacement loading. The damping force due to ER effect is frequency independent while the damping force due to fluid viscosity is frequency dependent. Therefore, it is required that the damping force developed by the ER effect be much larger than the damping force developed by the fluid viscosity to control structural response in a wide range by varying the applied electric field strength.

5.2 Development of ER Damper and a Dynamic Loading Test

An experimental model of ER damper is being developed. It was designed so that the maximum damping force and the maximum stroke of the piston are 20 kgf and $\pm$40 mm, respectively. Fig. 15 and Photo 3 show the model. The damper is 521 mm long, and has a orifice (electrodes) of 134 mm long and 3 mm wide. Pressure area of the piston is 2,089 mm^2. Rubber sleeve is used to enclose the ER fluid. Colloidal solution which includes silicon oil with mixing carbon powder is used as the ER fluid. The initial viscosity of the ER fluid is 1.3 $\times10^{-8}$ kgf•s/mm^2, and the shear stress τ_y at 2 kV/mm is 68.0×10^{-6} kgf/mm^2. The voltage of the electrodes is controlled between DC 0 and 6kV.

The performance of the model ER damper is being studied through a series of dynamic loading tests. Tests were made for the displacement, velocity and electric field dependency of the damping force.

Fig. 16 shows the force vs. displacement hysteresis loops. With the loading displacement being $\pm$20 mm, the loading frequency was varied from 0.5 to 10 Hz. It is seen in Fig. 16 that because there is a static friction of about 10 kgf between the piston and the cylinder, accuracy of control with small damping force is poor. It is also seen in Fig. 16 that there is a phase lag. This is caused by the compressibility of ER fluid and deformation of the rubber sleeve.

Fig. 17 shows the voltage vs. the damping force relation. The damping force at zero voltage represents the damping force due to fluid viscosity. The damping force increases as the voltage increases due to the ER effect. However, the damping force due to ER effect is smaller than the damping force due to fluid viscosity. An improvement for making ER effect larger is required.

6. CONCLUDING REMARKS

The variable dampers and variable stiffness control which are being developed at the Public Works Research Institute was described. Because the variable damper is a simple extension of the damper stopper technology which has been used in Japan for long time, it is expected that the variable dampers be implemented in the near future. Various research on the variable stiffness including development of the prototype model and shake table tests are currently being made.

An experimental model of ER damper is being developed, and a series of dynamic loading tests are being made. Although it was developed as designed, it was found that the damping force developed by the ER effect is smaller that the damping force developed by the fluid viscosity. It is required to modify the damping force due to ER effect large enough so that the control by ER effect can be made in a

wide range of damping force.

ACKNOWLEDGMENTS

The research presented herein is being made as a part of the U.S.-Japan Cooperative Research on Hybrid Control of Bridges under auspices of the Panel on Wind and Seismic Effects, UJNR. The authors extend their sincere appreciation to the strong support of Dr. S. C. Liu, NSF, Dr. H. S. Lew, NIST, Mr. J. D. Cooper, FHWA, Professor M. Shinozuka, Princeton University, Professor J. N. Yang and Professor M. Feng, University of California at Irvine.

REFERENCES

1) Duclos, T., G. (1988) "Design of devices using electro rheological fluids," SAE Technical Paper No. 881134
2) Ehrgott, R., C. and Masri, S., F. (1992) "Modeling the oscillatory dynamic behavior of electro rheological materials in shear," Smart, Mater. Struct. 1
3) Feng, Q. and Shinozuka, M. (1990) "Use of a variable damper for hybrid control of bridge response under earthquake, U.S. National Workshop on Structural Control Research, University of Southern California, CA, U.S.A.
4) For example, Izeki, H. (1980) " Viscous shear stopper, proposal to the multi-continuous girder bridge," Bridges and Foundations, pp. 30-33 (in Japanese)
5) Kawashima, K. and Unjoh, S. (1989). "Development of Hybrid Control Technology." Civil Engineering Journal, Tokyo, Japan, pp. 2-5, Vol. 32-6 (in Japanese).
6) Kawashima, K., Unjoh, S., Nagashima, H. and Shimizu, H. (1991). "Current research efforts in Japan for passive and active control of highway bridges against earthquakes." Proc. 23rd Joint Meeting, U.S.-Japan Panel on Wind and Seismic Effects, UJNR, Tsukuba, Japan, 187-209.
7) Kawashima, K., Unjoh, S. and Shimizu, H. (1991). "Earthquake response control of highway bridges by variable damper." Proc. of Colloquium on Control of Structures, Japan Society of Civil Engineers, Part. B, pp.221-224, July, 1991 (in Japanese)
8) Kawashima, K., Unjoh, S. and Shimizu, H. (1992). "Seismic response control of highway bridges by variable damper." 24th Joint Meeting, U.S.-Japan Panel on Wind and Seismic Effects, UJNR, Gaithersburg, May, 1992, NIST Special Publication 843
9) Kawashima, K., Unjoh, S., Iida, H. and Mukai, H. (1992). "Effectiveness of the variable damper for reducing seismic response of highway bridges, Proc. of 2nd U.S.-Japan Workshop on Earthquake Protective Systems for Bridges, Tsukuba, Dec. 7-8, 1992, Technical Note of the Public Works Research Institute, No. 3196.
10) Kawashima, K., Unjoh, S. and Mukai, H. (1993). "Seismic response control of highway bridges by variable dampers." 25th Joint Meeting, Panel on Wind and Seismic Effects, UJNR, Tsukuba, Japan, Technical Note of Public Works Research Institute.
11) Kawashima, K., Unjoh, S. and Mukai, H. (1994) "Seismic response control of highway bridges by variable stiffness control," The 3rd US-Japan Workshop on Earthquake Protective Systems fro Bridges, Berkeley, CA, U.S.A.
12) Kawashima, K., Unjoh, S., Suzuki, S. and Endoh, S. (1994) "Application of electro-rheological fluid for variable damper", The 3rd US-Japan Workshop on Earthquake Protective Systems for Bridges, Berkeley, CA, U.S.A.
13) Milliken, Jr., W., F. (1987). "Lotus active suspension system." Proc. 11th International Conference on Experimental Safety Vehicles, Washington D.C., U.S.A., 467-475.
14) Sasada, T., Kishi, T. and Kamijo, K. (1975A) "Electro viscous effects of

polymer and solid particle solutions," Proc. Japan Society of Mechanical Engineers, Vol.41, No.342

15) Sasada, T., Kamijo, K. and Kishi, T. (1975B) "Electro viscous effects of uni-phase liquid," Proc. Japan Society of Mechanical Engineers, Vol.41, No.343

16) Edited by Scott, D. and Yamagichi, J. (1983) "Solidifying fluid transforms clutches and flow valves," Automotive Engineering, Vol.91, No.11

17) Sugawara, F. (1986). "Electronically controlled shock absorber system used as a road sensor which utilizes super sonic waves." Proc. Society of Automotive Engineers, Milwaukee, Wisconsin, U.S.A., 6.15-6.25.

18) Sun, L. and Goto, Y. (1994) "Fuzzy control of bridge vibration by using variable dampers, " The 3rd US-Japan Workshop on Earthquake Protective Systems for Bridges, Berkeley, CA, U.S.A.

19) Taguchi, J., Iwasaki, T., Adachi, Y., Sasaki, Y. and Kawashima, K. (1990). " U.S.-Japan cooperative research program on hybrid control of seismic response of bridge structures." 22nd Joint Meeting, U.S.-Japan Panel on Wind and Seismic Effects, UJNR, Gaithersburg, Maryland, USA, May, 1990, NIST Special Publication.

20) Ushijima, T, Takano, K. and Noguchi, T.(1988) "Rheological characteristics of ER fluids and their application to anti-vibration devices with control mechanism for automobiles," SAE paper #881787

21) Yang, J. N., Li, Z. and Wu, J., C. (1994) "Hybrid protective systems for seismic-excited bridges," The 3rd US-Japan Workshop on Earthquake Protective Systems for Bridges, Berkeley, CA, U.S.A.

Table 1 Peak Responses

Analytical Cases	Deck			Pier		Variable Damper		
	Displace-ment (cm)	Velocity (cm/s)	Accele-ration (cm/s ^{2})	Shear Force (KN)	Bending Moment (KN·m)	Damping Force (KN)	Relative Displacement (cm)	Relative Velocity (cm/s)
NO CONTROL	33.00	189.0	1,300	1,637	32,333	———	———	———
WITH CONTROL	8.46	48.4	567	786	15,102	614	5.78	60.7

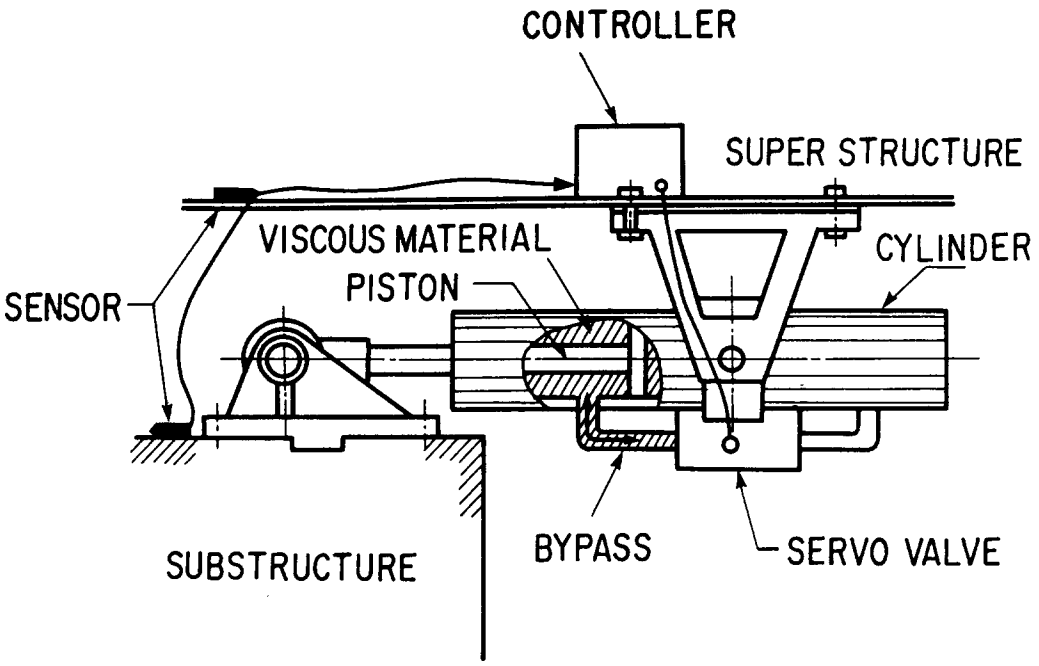

Fig. 1 Variable Damper

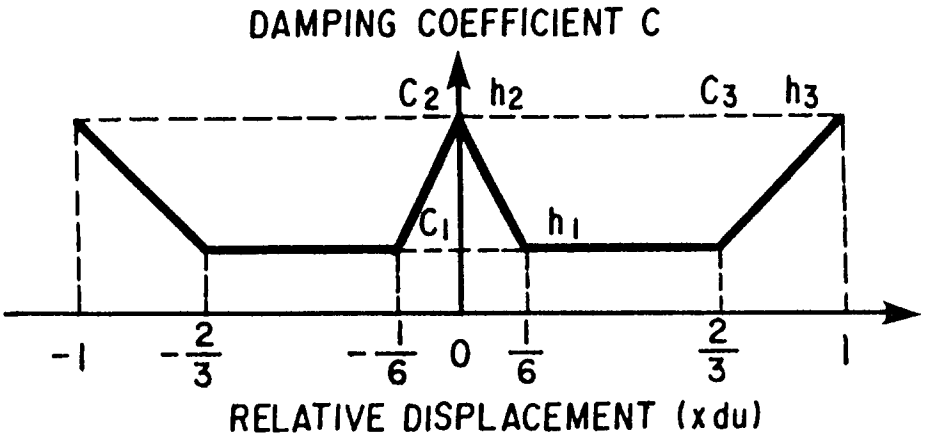

Fig. 2 Analytical Idealization of Damping Force vs. Relative Displacement Relation

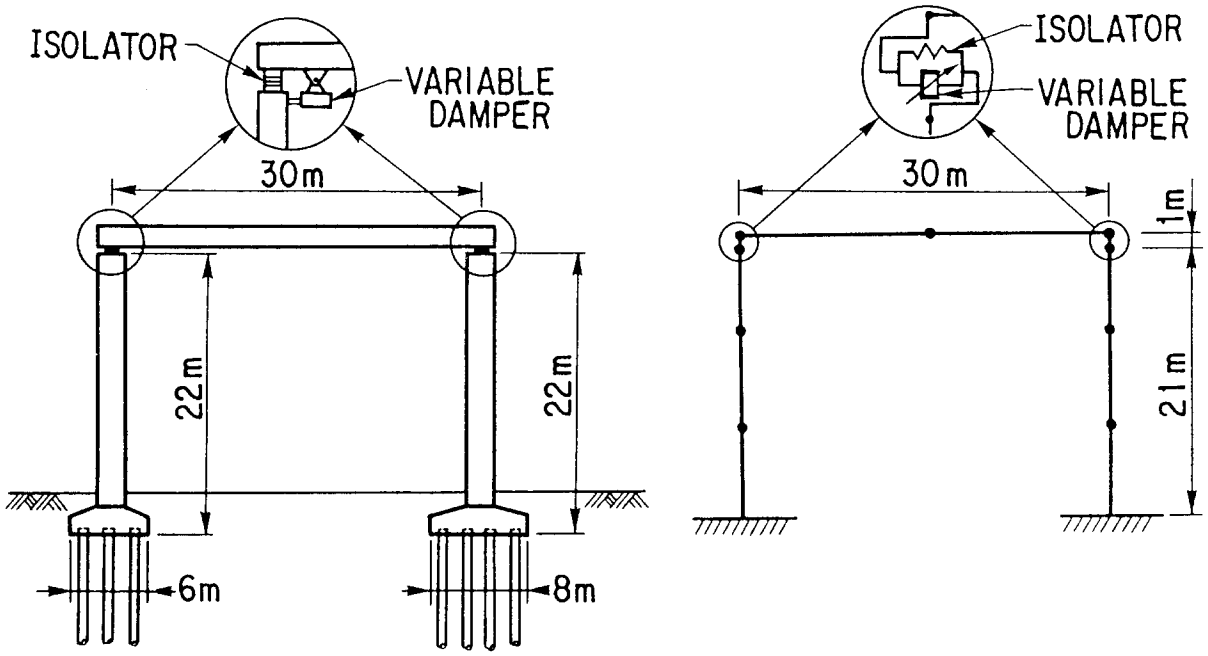

Fig. 3 Bridge Analyzed and Analytical Idealization

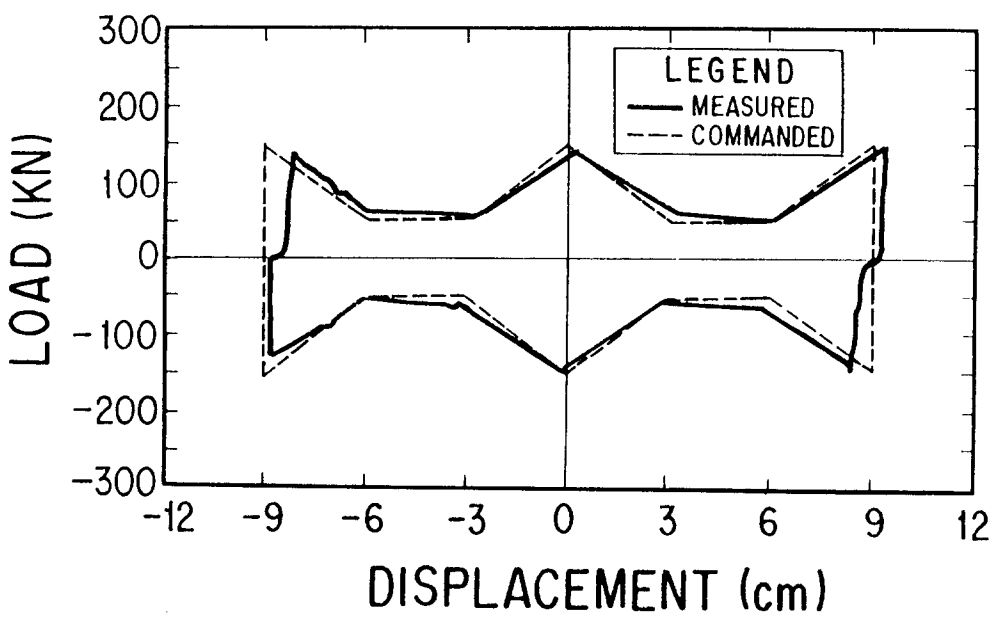

Fig. 4 Damping Force vs. Relative Displacement Relation from Dynamic Loading Test of Variable Damper

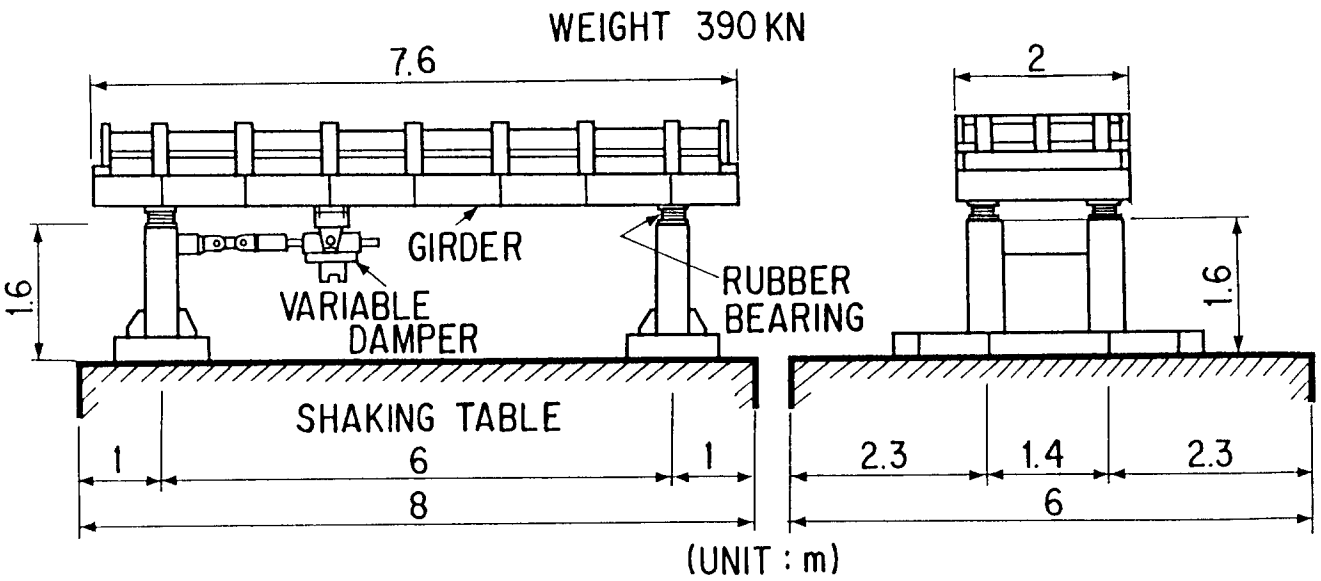

Fig. 5 Shake Table Test of a Model Bridge with a Variable Damper

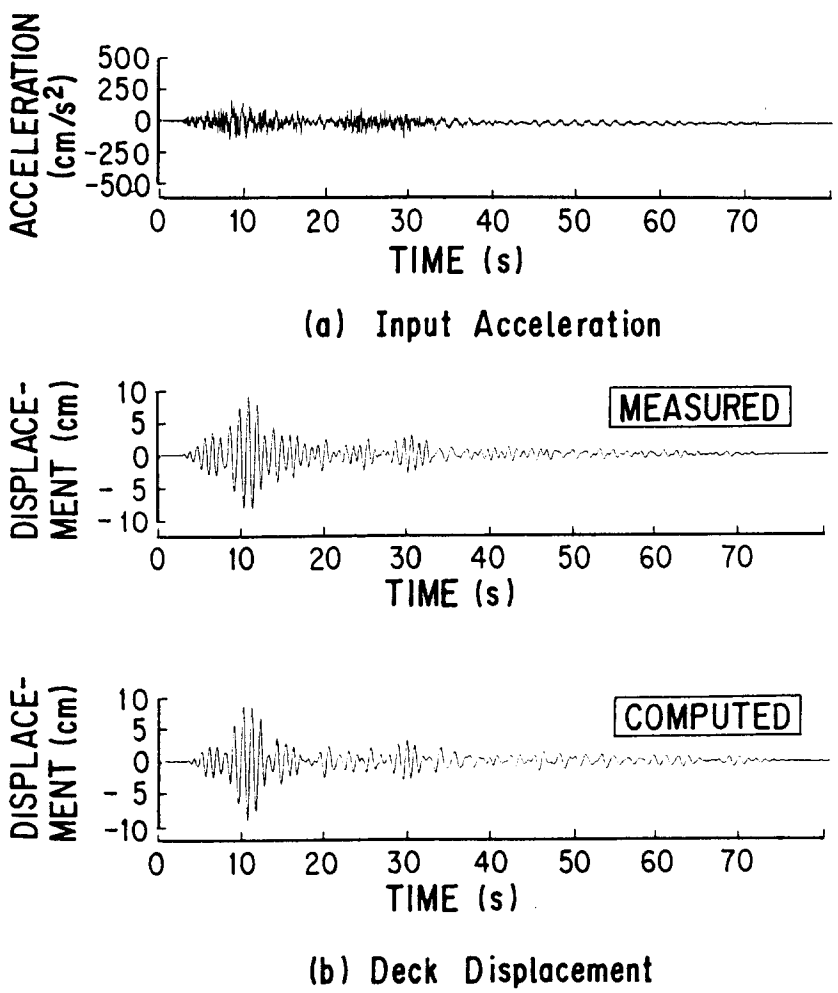

Fig. 6 Measured and Predicted Response of a Model Bridge without Control, subjected to a Table Motion with Peak Acceleration of 172 cm/sec^2

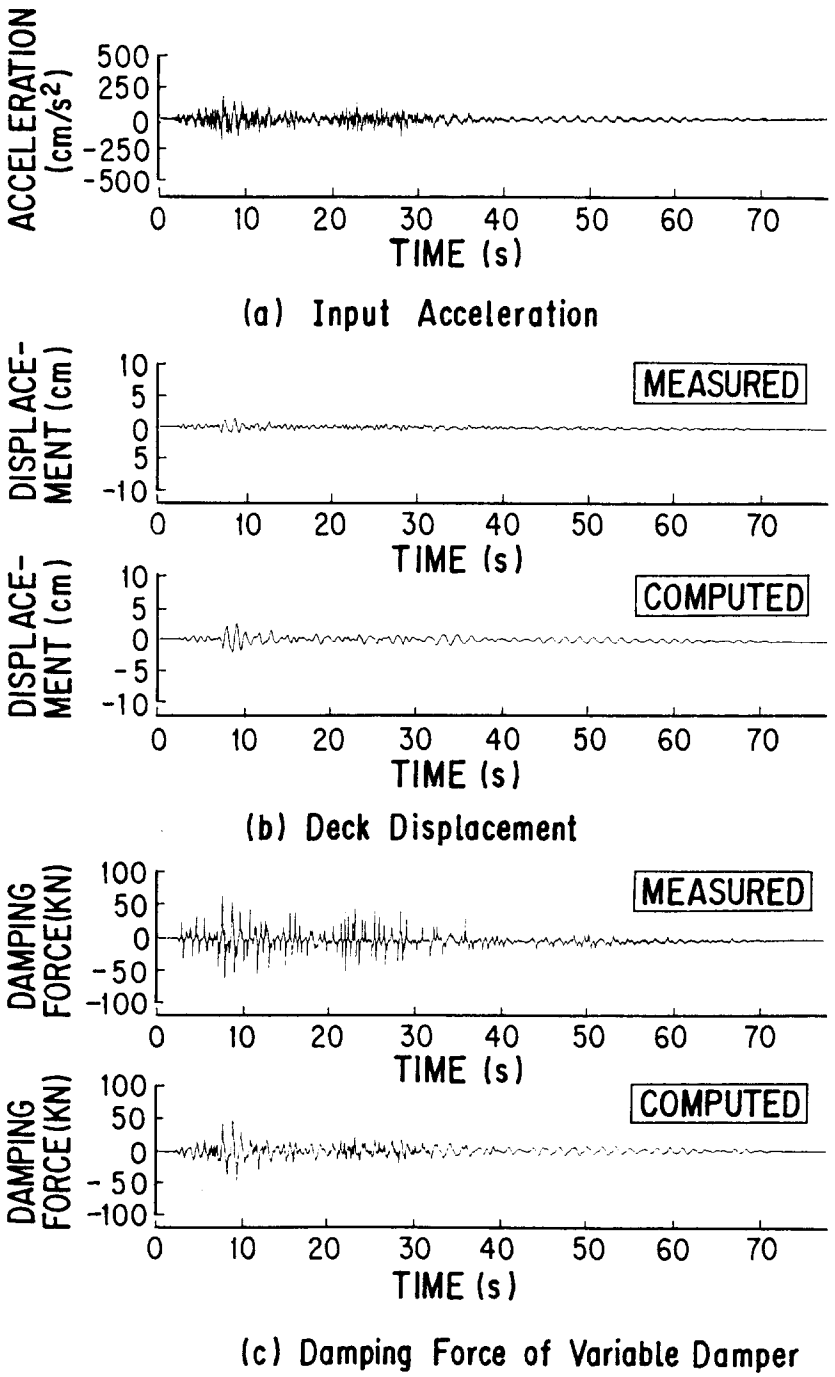

Fig. 7 Measured and Predicted Response of a Model Bridge with Control, subjected to a Table Motion with Peak Acceleration of 185 cm/sec^2

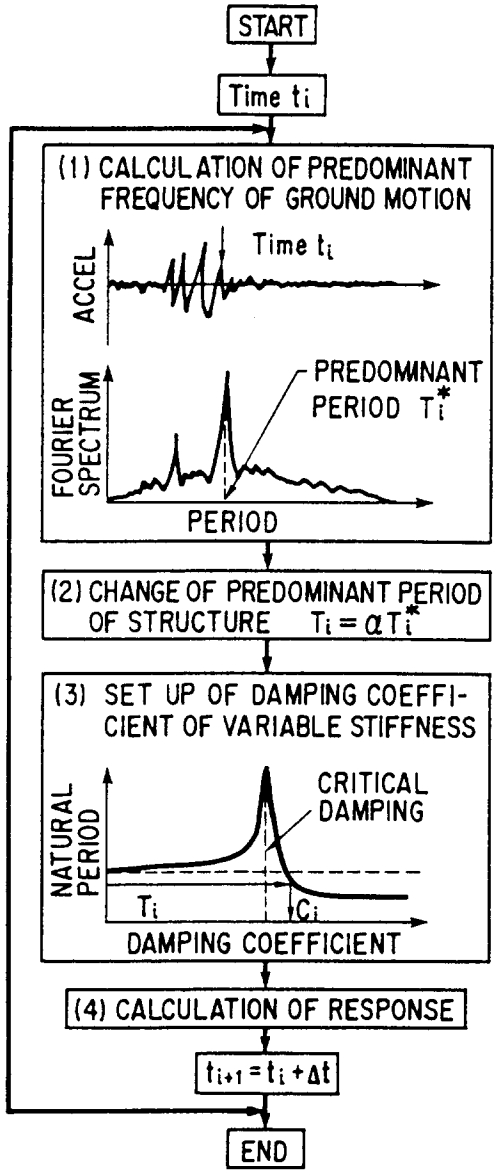

Fig. 8 Control Algorithm of Variable Stiffness

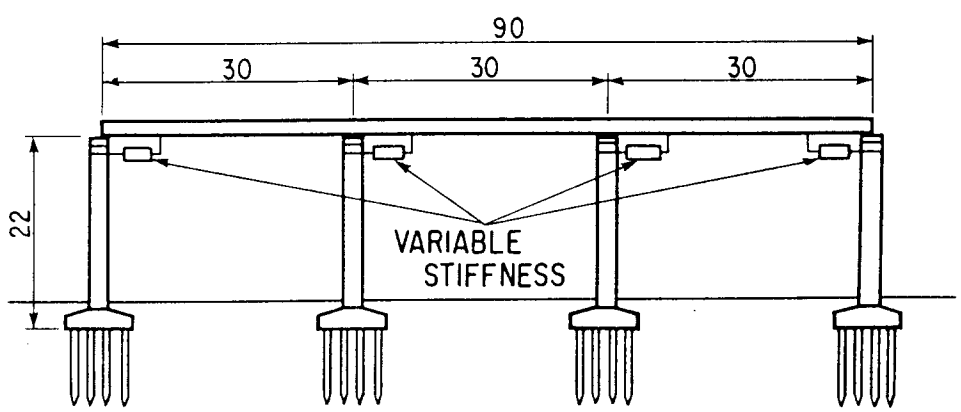

Fig. 9 Model Bridge Analysed

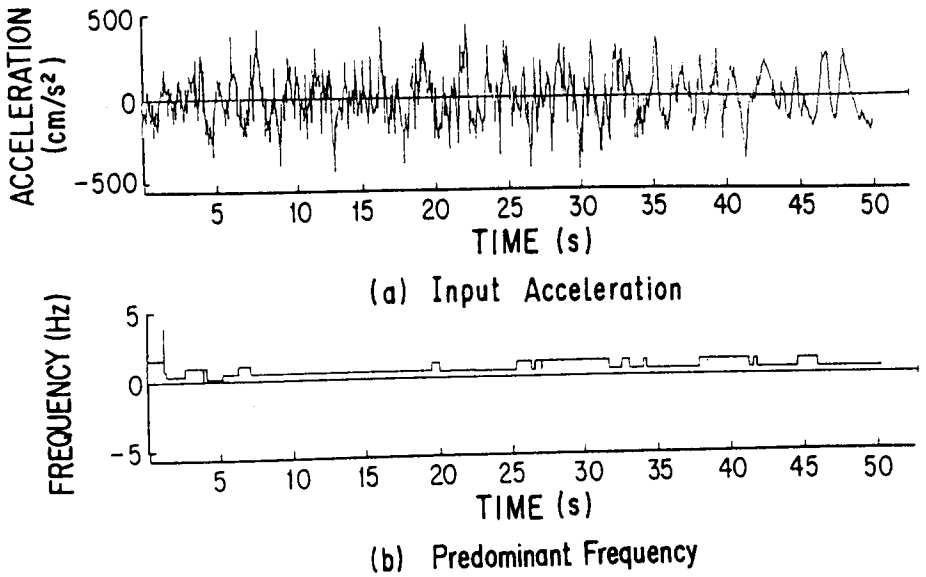

Fig. 10 Input Acceleration and the Predominant Period

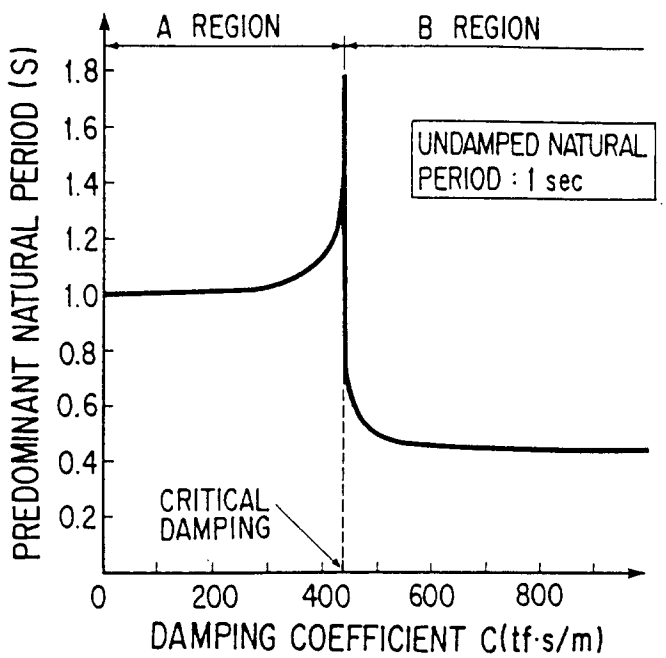

Fig. 11 Dependence of Natural Period of the Bridge on Damping Ratio of Variable Dampers

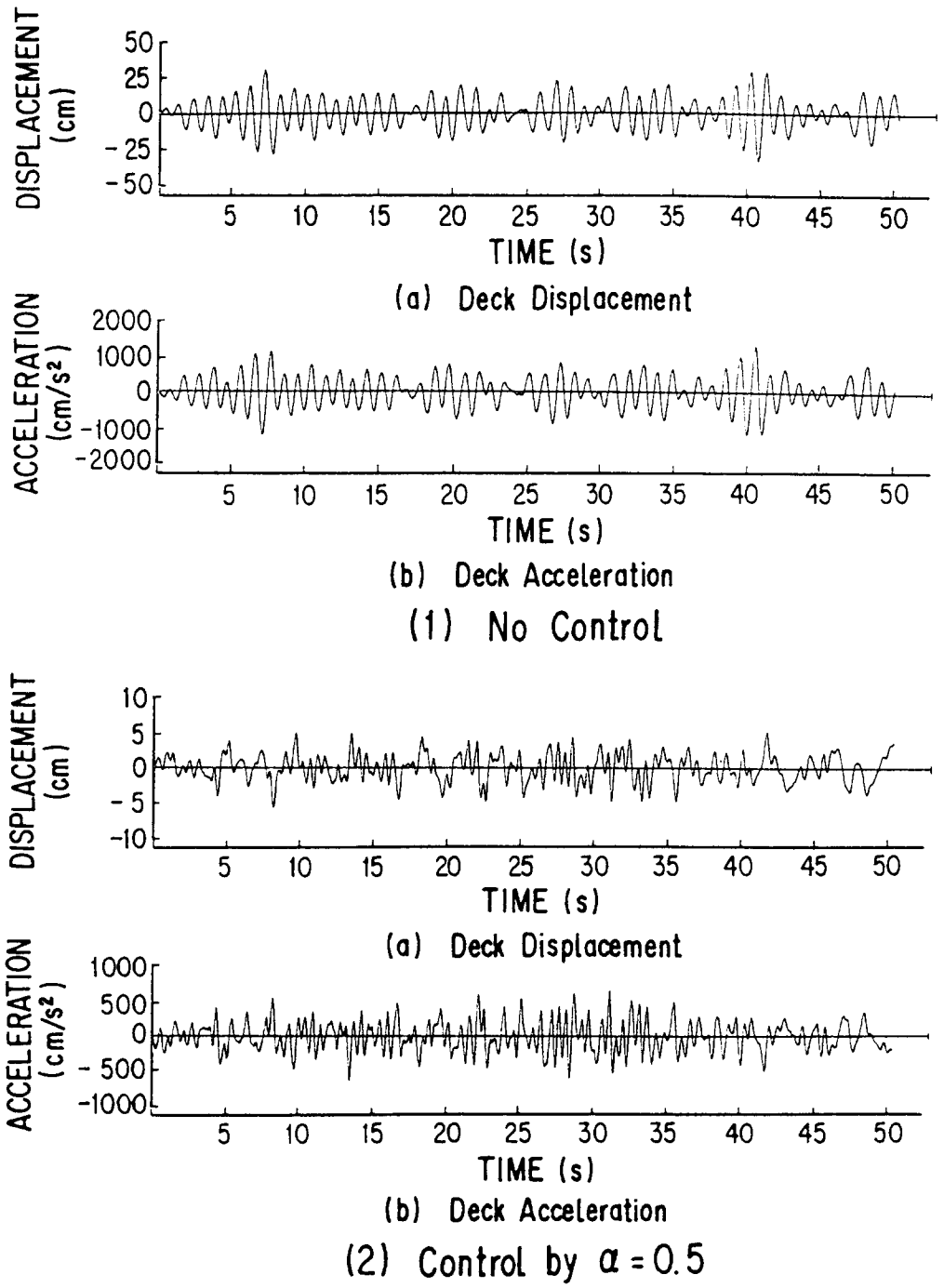

Fig. 12 Effectiveness of Variable Stiffness Control

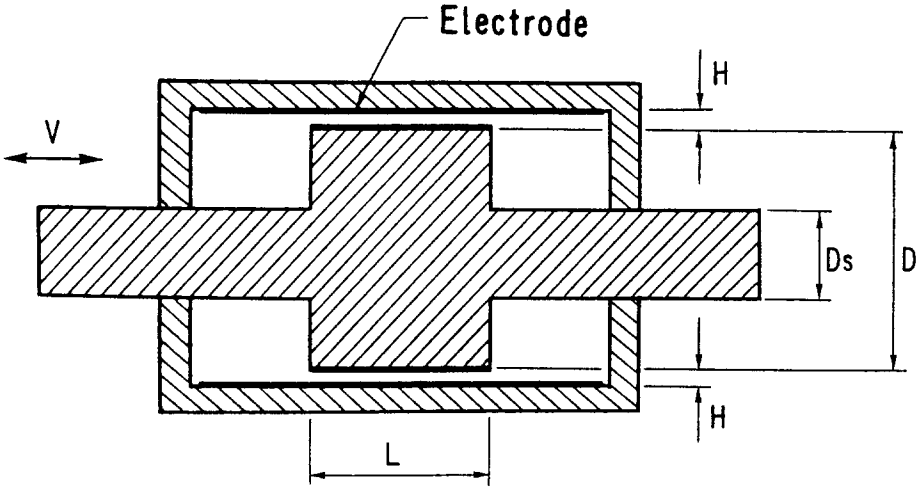

Pressure Area of Piston : $A = \frac{\pi}{4}(D^2 - D_s^2)$

Width of Electrode : $B = \pi(D + H)$

Fig. 13 Cylinder Type ER Damper

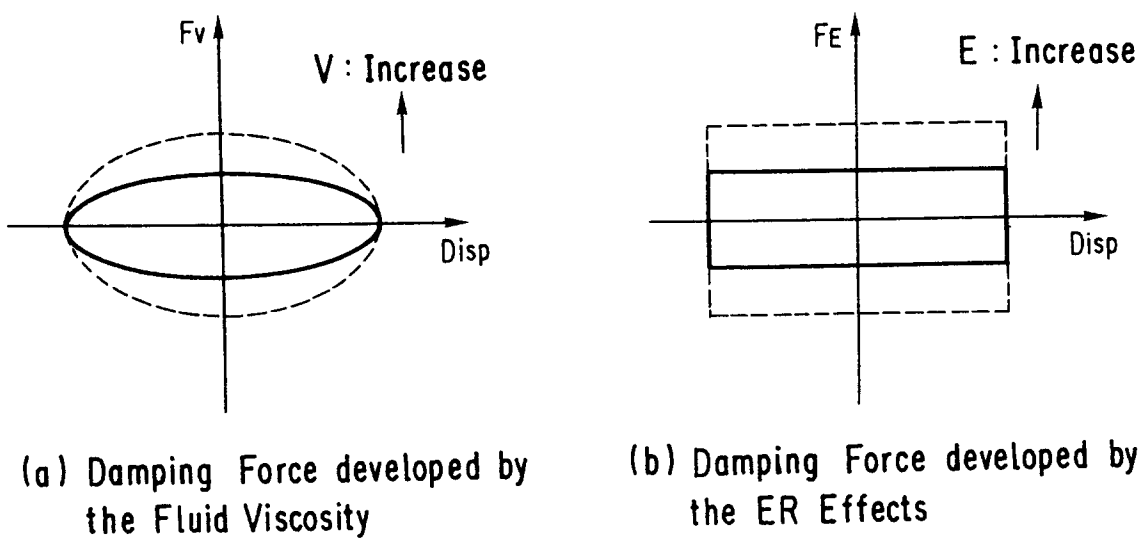

Fig. 14 Illustration of the Damping Force developed by the ER Damper

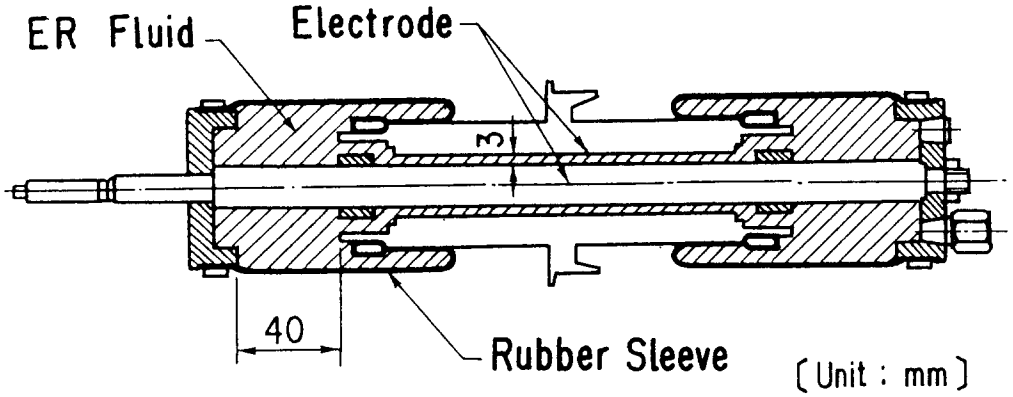

Fig. 15 Experimental ER Damper Developed

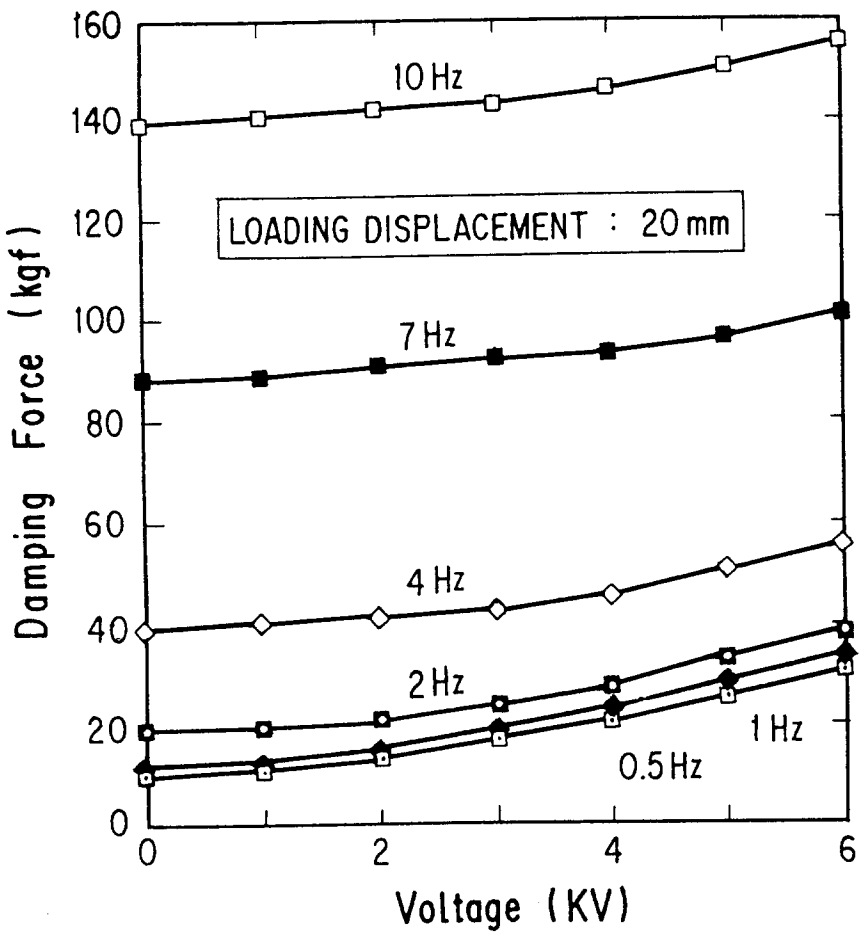

Fig. 17 Relation between Damping Force and Applied Voltage

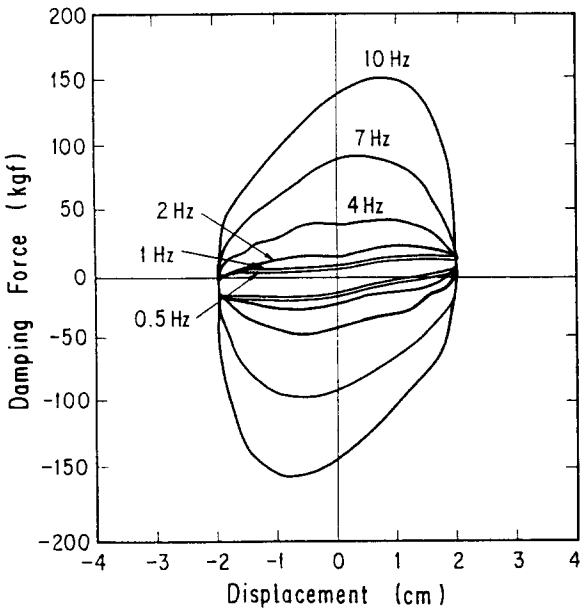

(1) Applied Voltage = 0kV

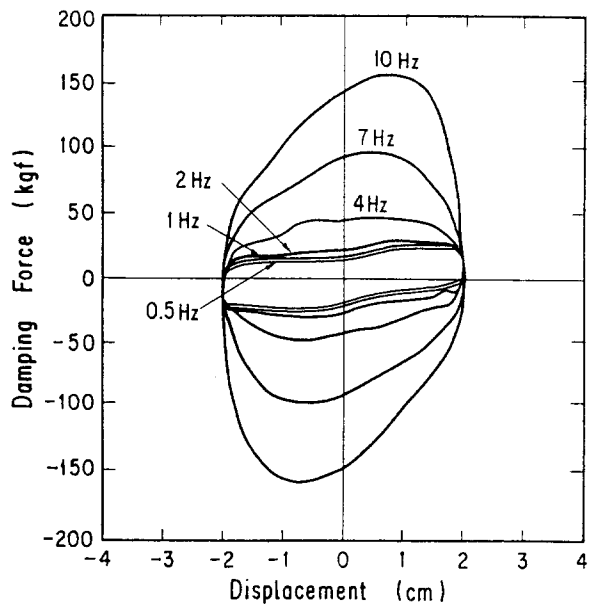

(2) Applied Voltage = 3kV

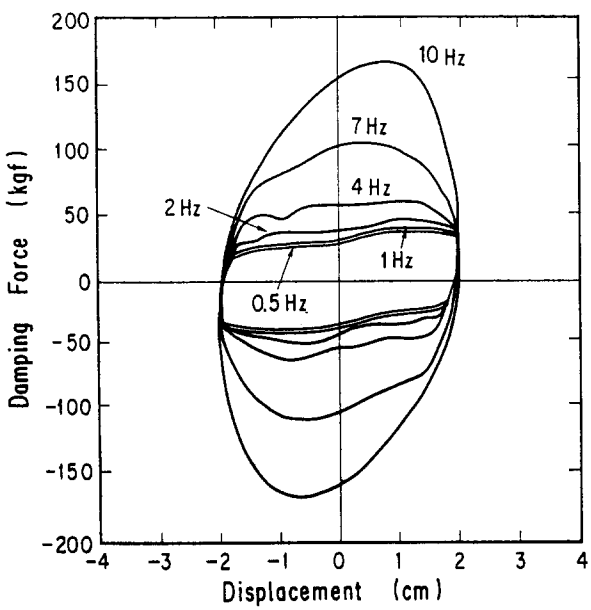

(3) Applied Voltage = 6kV

Fig. 16 Hysteresis Loops of Force–Displacement Relation

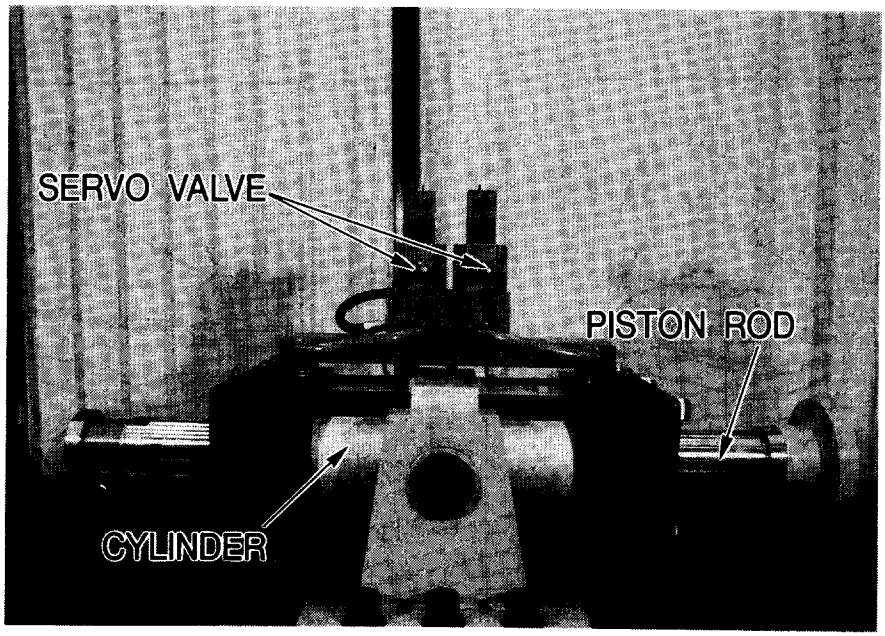

Photo 1 Prototype Model of Variable Damper

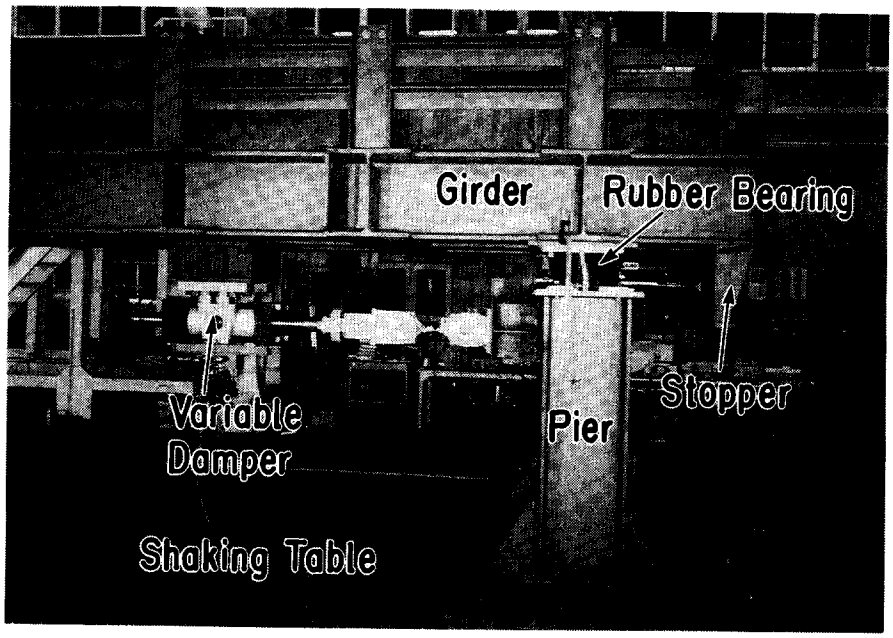

Photo 2 Model Bridge and Prototype Variable Damper Model

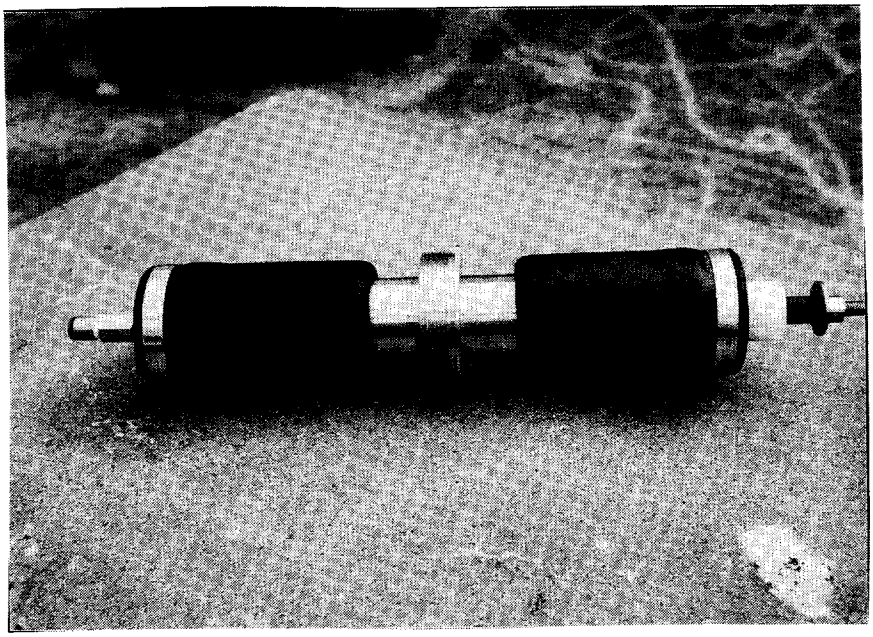

Photo 3 Experimental Model of ER Damper

Innovative Seismic Testing Procedures

by

Stephen A. Mahin* and S. C. Liu*

ABSTRACT

Experimental methods remain a key factor in developing and verifying seismic-resistant design and analysis methods. The need for experimental research is likely to increase in the coming years as engineers develop innovative structural systems utilizing high performance materials, active and passive control systems and special structural systems. Moreover, experimental results are needed to develop and validate numerical models that can take advantage of high performance workstations and other advanced computer capabilities becoming available within the design industry. Recent experiences with earthquakes also suggests that greater emphasis will be placed in the years to come on more quantitative prediction and control of damage, leading to increased needs for verified design and analysis methods.

As attention is turned to more complex and larger structural systems, especially those comprising the civil infra-structure, researchers are challenged to develop increasingly complex experimental test methods. In this paper, a brief overview of available experimental methods is presented and future directions are examined. Several recent examples of special testing arrangements used for infrastructure elements will used to highlight the paper. The first of these relate to simple tests of large single degree-of-systems requiring the cyclic application of large lateral loads. Other tests requiring refined three-dimensional control of the forces and displacements applied to multiple degree of freedom specimens are then presented. Extension of on-line computer control techniques to the realistic simulation of dynamic aspects of seismic structural response are then briefly described.

KEYWORDS: experimental methods, earthquakes; seismic-resistant design; infra-structure; buildings.

INTRODUCTION

The ease with which experimental research may be performed has improved markedly in recent years with the increased availability of electro-hydraulic actuator systems to impose forces and displacements, the greater reliability and accuracy of instrumentation and, most significantly, the development of high speed, relatively low cost digital data acquisition and control systems. In most instances, experiments used to assess the quasi-static inelastic cyclic behavior of structures and structural components remain relatively simple. In fact, the increasing need to carry out field tests on very large components of infrastructure systems results for practical and economical reasons in the use of very simple, low tech approaches to loading. However, complications can arise due to the magnitude of the required loads and the need to investigate the three dimensional response characteristics of specimens. In other cases, quasi-static loading is not sufficient and loading histories more representative of the response of the specimen to actual earthquake ground motions are required.

Shaking tables enable the researcher to simulate within the laboratory the dynamic motion of the ground supporting a structure during an earthquake. These simulators remain the most realistic seismic test procedures. None the less, available shaking tables significant place significant limitations on the weight, strength and size of specimens that can be tested. In the U.S. several moderate sizedables are available with sizes up to 20 ft (6.1 m) square. The largest of these earthquake

* Nishkian Professor of Structural Engineering, Dept. of Civil Engineering, University of California, Berkeley, CA

** Program Manager, Earthquake Hazards Mitigation, National Science Foundation, Arlington, VA

t simulators, located at the University of California at Berkeley, is being upgraded with funding from the National Science Foundation to subject specimens weighing up to 70 tons to full three-dimensional seismic excitations. Several groups in the U.S. are currently considering the technical and economic feasibility of large shaking tables.

In addition, many infrastructure elements, like bridges and pipelines, are supported at points not expected to have the same ground motion. Several laboratories in the U.S. (e.g., the University of Southern California, Energy Technology Research Center, University of California at Berkeley, etc.) have developed several relatively small shaking tables capable of subjecting such spatially distributed systems to multiple support excitations.

Dynamic loading can be also imposed on a structure by means of underground explosions, and by a variety of mechanical vibration generators. Often vibration generators utilize reciprocating masses and can only develop simple harmonic excitations in the structure. Recent efforts have been under taken to utilize controllable gas jets or mechanical extruding devices to impose variable force excitations of short duration.

Because of the need to test large structures under dynamic excitations several efforts have been carried out to develop on-line computer control procedures. These experiments outwardly resemble typical quasi-static tests, but a computer is used during the test to monitor the specimen and determine its deformation response. Ideally, the specimen undergoes the same displacement history as if it were subjected to a particular ground motion. These procedures are similar to typical computer programs except that the restoring force characteristics of the test structure are measured experimentally, rather than computed analytically. The procedures have been shown to produce accurate results on large structures and have a great deal of flexibility to carry out innovative tests. Typically, tests are carried out slowly, but recent efforts have focused on developing real time loading capabilities. A full scale, five story masonry structure was recently tested using such techniques at the University of California at San Diego.

CYCLIC PLANAR LOADING OF LARGE STRUCTURAL SYSTEMS

In most cases, planar tests of structural components and systems can be carried out in a simple manner. The specimen and actuator can be attached to a suitable reaction floor or frame, and the actuator can be used to impose the appropriate load or displacement history. However, in some cases the loads required becomes so large that the size (and cost) of the required reaction frame and actuators become excessive. While it is possible to build larger reaction and loading facilities, structural test demands can always exceed capacity.

A special case requiring the test of a large and strong structure arose following the 1989 Loma Prieta earthquake. It was desirable to test a portion of the I-880 Cypress viaduct that partially collapsed in Oakland. This two level reinforced concrete structure utilized multi-celled box girders to support the upper and lower level roadways, and a two level, single span beam-column framework to support the box girders and to provide lateral resistance in the transverse direction. Tests were desired to assess the precise causes of the observed collapse of the upper level of the structure and to determine the efficacy of various retrofit schemes suggested for other double deck viaducts damaged in the San Francisco bay area.

Some of the methods considered for loading the viaduct are schematically illustrated in Fig. 1. These included the attachment of post-tensioning tendons to the deck levels and using post-tensioning jacks to apply the lateral loads. Because cyclic loading was desired, tendons would have to be installed on both sides of the viaduct. Problems associated with this scheme relate to the need for piles or other types of (costly) foundations to transmit the tendon force to the ground, and the need to anchor the tendons relatively far from the structure in order to minimize the vertical component of the tendon force on the structure. The congested urban setting of this structure precluded this simple approach.

Another approach considered the construction of a reaction frame as shown in the center portion of Fig. 1. This would allow the use of double acting electro-hydraulic actuators. However, the tests were estimated to require upwards of 4 million pounds of lateral force. The design of the foundations for the external reaction frame in this case became very difficult. In particular, uplift forces were very large because of the desire to minimize the width of the reaction frame. Because of the poor soil at the site, the reaction frame scheme was considered prohibitively expensive.

The strategy eventually selected for these tests is shown on the right hand side of Fig. 1. Because the failure occurred in the upper level, it was not viewed as essential to apply lateral loads directly at the lower level. Similarly, it was not necessary to assess the contribution of the soil-foundation system to the lateral response. As a result, it was possible to devise a self-equilibrating steel reaction frame within the structure. Large steel collars were attached around the base of the lower columns. Diagonal steel braces extended upwards from these collars (through holes punched in the lower deck) and joined just below the upper deck at a reaction block. Pairs of simple, single acting (compression) oil jacks were installed on both sides of the reaction block. These transmitted force to loading blocks that were post-tensioned to the upper deck of the viaduct. Braces and oil jacks were installed in pairs on each side of a frame to preserve symmetry of loading. Three sets of transverse frames were introduced into the test specimen, resulting in six diagonal braced bents and a total of twelve hydraulic jacks.

Simple oil jacks were utilized instead of double acting actuators in this case because of the time (and expense) required to special order the large number of relatively high capacity actuators needed to develop the loads anticipated in this test. The oil jacks were easily available from local prestressing supply companies.

The oil jack arrangement could produce the cyclic loading required. For specimen motion to the left, the left jacks would be extended (with the right jacks retracted). For motion to the right, the jacks on the right were extended. Relatively simple, manually operated hydraulic equipment was effectively employed to carry out the tests.

In another similar situation, a retrofit strategy for a telecommunications center was to be evaluated. The existing structure contained a composite concrete/structural steel shear wall. A structural steel frame was provided in the existing structure to help carry gravity loads and seismic overturning forces, and the concrete infill and encasement was utilized to resist shear. Retrofit of the structure included thickening the concrete walls, filling in the numerous openings located in the existing walls, adding shear transfer studs to the existing steel framing to enhance shear transfer between the steel frame and the new concrete, and the addition of partial transverse confinement. Because of the complex stress transfer mechanism between the steel frame and the concrete and between the new and old concrete, it was desired to employ a large scale test specimen to verify the retrofit concept. Similarly, it was desirable to include as many bays and stories in the model as possible to minimize boundary condition effects where the specimen were attached to actuators and the reaction floor. It was, of course, not economically possible to test a model of the entire 15 story building. Thus, a portion of the structure was selected incorporating as many of the salient features as possible.

Several alternatives for specimen configuration and loading were considered. Ideally, a model would have been constructed and attached with double acting actuators to an existing strong floor and reaction wall. This approach is shown in the left hand illustration of Fig. 2. The minimum one-third scale considered acceptable for these tests resulted in a very large lateral load resistance. This load (in excess of 3,000 kips) could be developed by available laboratory actuators; however, the overturning moment developed resulted in excessively complex and expensive details for attaching the specimen to the reaction floor.

Another option considered for loading the specimen was to utilize a large capacity (4,000 kips) universal testing machine. In this case, the problem of resisting wall overturning

moments could be resolved by doubling the size (height) of the specimen. In this fashion, the wall would be tested as a simply supported beam, with its midspan representing the base of the wall in the prototype. While this option solved most of the problems encountered with the previous approach, it resulted in a specimen with twice the size, but without any apparent gain in useful information. In addition, for cyclic loading, it would be necessary to remove the specimen from the testing machine and invert it. Because instrumentation would have to be repeatedly removed and re-installed each time the wall was flipped, the time and effort required for testing made this option impracticable..

The option eventually employed for this test was adapted from the testing approach used for the Cypress viaduct (Fig. 1). A self-equilibrating frame was attached directly to the wall test specimen. The specimen selected was three bays wide and two stories tall, and constructed at one-third scale. Large composite steel and reinforced concrete load transfer girders were attached monolithically to the top and bottom of the test panels. Pairs of steel diagonal braces were attached externally to the lower transfer girder on each face of the test specimen. Pairs of single acting oil jacks were attached to the reaction block at the top of the braces . These jacks transferred load to each side of the specimen by means of a reaction block attached to the upper distribution beam. Operation of this test under cyclic loading was similar to that described previously for the Cypress viaduct.

Another interesting example involves field testing of a seismically isolated bridge located in Walnut Creek, California. Since this was the first totally new bridge to be isolated in the U.S., it was desirable to assess the ability of design and analysis assumptions to capture its dynamic response characteristics, especially in the nonlinear range. In this case a series of tests were undertaken at different times during construction. First, the individual columns were tested to determine their dynamic characteristics. This was done by pulling pairs of columns together using wire rope and a long stroke hydraulic jack. An explosive bolt, used to connect segments of the wire rope, was detonated to release the applied loads. This procedure proved to be extremely effective in achieving the quick release vibratory response of the columns.

Once the isolators and deck were installed on top of the columns, ambient and forced vibration tests were carried out. A pair of reciprocating mass vibration generators were used to induce forces along the longitudinal and transverse axes of the deck, as well as torsion action about a vertical axis. These test produced information regarding the period, mode shapes and damping characteristics of the bridge in the elastic range. Because of the nonperfect symmetry of the bridge, modes were highly cross coupled. The resulting modal beating phenomenon complicated interpretation of results.

While of great importance, the forced vibration tests provide little insight into the inelastic response of the system. Because the base isolation system would permit the structure to be deformed into the inelastic range with little permanent damage, a series of quick release tests were carried out with laterally imposed displacements approaching the maximum displacements anticipated during the design earthquake. In this case, time and financial constraints prevented the use of loading apparatus shown in Figure 1. It was decided to load the bridge along its longitudinal axis and utilize the abutment or adjacent frame as the reaction frame. The seismic isolation system resulted in relatively low loads being transferred to the abutment. Consequently, the capacity of the abutment was insufficient to resist the loads required to load the entire bridge. As a result, hydraulic actuators were placed between the isolated section of the bridge and an adjacent non-isolated cast-in-place reinforced concrete bridge. This is schematically illustrated in Fig. 4.

It was estimated that it would be necessary to displace the bridge about 6 inches (15 cm) to allow the deck to spring back to zero permanent displacement following the test. This displacement also corresponded to that anticipated during the design level earthquake. Loading was again achieved using hydraulic actuators. Initially, it was anticipated that the rapid release of load would be achieved by installing gas springs on the compression side

of the jacks. When the oil pressure used to load the jacks was quickly released, the pressurized gas on the opposite side of the jack piston would force the jack to retract quickly. Such tests have been successfully carried out in Japan by the Public Works Research Institute. Unfortunately, the available construction time schedule did not permit construction and verification of this system. In stead a simpler system was developed. This is schematically shown in Fig. 5. In this case, simple oil jacks were used to push the seismically isolated portion of the bridge away from the adjacent cast in place bridge. When the desired displacement of the isolated bridge was reached, a displacement restraining wedge was inserted in the gap between the two bridges and the oil jacks were removed. The displacement restraints were diamond shaped with loading applied along one of the diagonals. Stability was maintained by a large tension bolt installed along the other diagonal. An explosive charge was placed in the bolt and detonated to achieve the quick release. Four sets of these oil jacks and displacement restrain devices were used at the interface between the two bridges. These simple tests worked well and provided useful information on the nonlinear dynamic response of the isolated bridge. Primary difficulties were associated with coordinating test and construction schedules, practical issues of instrumenting a 700 ft long structure (more than 5 miles (8.3 km) of wire was needed for the instrumentation), and weather.

CYCLIC LOAD TESTS IN MULTIPLE DEGREE OF FREEDOM SPECIMENS

In multiple degree of freedom systems, additional complexity is introduced because of the need to determine the distribution of forces or displacements applied at each actuator. As a means of simplifying this problem, it is common to make the imposed loads or displacements a function of parameters measured at other locations during the test; thus, an invariant relative distribution of displacements or forces is often imposed.. In the case of inelastic response, it is usually preferable to control the force distribution, as localized damage to the structure could substantially alter the structure's deformed shape (e.g., by the formation of weak stories). This test procedure can be implemented easily with conventional electro-hydraulic actuators by identifying one actuator as the master and setting the command signal for the other (slave) actuators to be a proportion of the force measured in the master actuator. Because of the possible instability of a structure tested into the inelastic range using force control only, most tests of this type would specify the displacement at the master actuator. The force in the master actuator would still be used to control the forces in the remaining actuators even though the master actuator is under displacement control. This arrangement is shown schematically in Fig. 6.

When specimens are loaded in two or three dimensions, other complications arise. For example, consider the simple floor diaphragm in Fig. 7. Three actuators are attached to control the in-plane transverse, longitudinal and rotational motion of the diaphragm. If only longitudinal motion is required, elongation of only the longitudinal actuator will not produce the desired result. This is because of the arching action of the typically short length actuators. The in-plane rotation of the transverse actuators due to longitudinal actuator motion causes transverse motion of the specimen as shown in Fig. 7, along with transverse forces in the specimen. In addition, the displacement and forces measured in the longitudinal actuator will differ from those developed in the specimen in the undistorted longitudinal direction. These undesirable effects must be corrected for by lengthening of the transverse actuators.

Under displacement control, the command displacement of an actuator in the above test setup should thus depend on the command displacement of the other actuators. The geometric corrections will depend on the test setup, and are usually straight foreword to derive. However, they have in general a nonlinear form which is difficult to implement by simple analog manipulation of the control signals.

This nonlinearity does not introduce any special complication when the specimen will be subjected to predetermined displacement histories. Appropriate geometric manipulation of the displacement command signals can be

made by digital computer (e.g., using a simple spreadsheet program) prior to the test.

Force readings in actuator load cells, must be processed following a test to correct for the rotation of the actuators relative to the initial coordinate system of the specimen (see Fig. 8). The measured (or commanded) displacements are used (along with information on the actuator and structural configuration) to compute the forces along the structure's principal axes. At large displacements (and/or short actuator lengths) an actuator can induce significant forces along both of the principal axes of the specimen (P_x and P_y in the figure) and correction of the measured load cell force becomes essential.

An example of such a test is that shown in Fig. 9. The prototype bridge structure supports an elevated roadway and an extended "outrigger" beam is required to contribute to the transverse load resisting system through bending, shear and axial load. In the longitudinal direction of the roadway, the beam is also required to develop torsion when contributing to the lateral load resisting system. Testing of this outrigger was carried out considering horizontal motions of the deck in the transverse and longitudinal directions. The simplified test specimen used is shown in Fig. 9. A "cloverleaf" displacement pattern was specified at the tip of the column in the test specimen which results in simultaneous displacements in both principal directions. The ideal displacements were modified prior to the test to obtain command displacements corrected for geometric effects. A computer based function generator is used to send the corrected command signals (as voltages) to conventional analog servo-controllers.

An interesting feature of this test is that, in the transverse direction, the axial load in the column depends not only on initial gravity loads, but also varies due to overturning moment effects as a function of the transverse load applied. Simple considerations of statics were used to determine the appropriate axial load as a fixed fraction of the applied transverse lateral load (plus the initial gravity loading). This was implemented in the tests using simple analog summing amplifiers and analog circuitry.

This situation becomes more complex, if mixed force and displacement modes of actuator control are used. While the displacements in master actuators can still be pre-computed based on the desired specimen displacements at these locations, the corrections for the forces must be performed on-line during the test so that they can be used to specify the forces to be imposed at other levels. The transformation functions relating forces measured in the load cell and along the specimen's principal axes can be derived prior to the test, but they will change throughout the test as the displacements vary. More significantly, the displacements at the degrees of freedom under force control will not be known prior to the test, so measured displacements must be used during the test to determine the appropriate transformations between the desired force in a particular direction and the force measured in the load cell.

For reasonably small displacements and simple test configurations, it may be possible to utilize analog techniques to modify the loads to be applied to actuators in three dimensional tests. In other cases, the required transformations may be come sufficiently complex, and the displacements sufficiently large that digital procedures are necessary (or preferred). Relatively simple and low cost micro-computer based, control processors are available for single and multiple axis control. This may be implemented in such a manner that the digital controller makes the various transformations and carries out the appropriate electronic control functions for the servo-control system. It can also be implemented in a more conventional analog control situation. In this case, the micro-processor repeatedly reads the displacements and forces at the actuators, makes the appropriate transformations and sends the command displacements or forces to conventional analog controllers.

PROOF TEST OF A DOUBLE LEVEL VIADUCT

An example of a test in which such digital control is used is shown if Fig. 10. In

this case the lateral load resistance of a double deck viaduct was investigated. Earthquake-like motion in each principal plan direction was imposed quasi-statically using hydraulic actuators attached to rigid reaction frames post-tensioned to the laboratory strong floor. The columns in the prototype structure were assumed in design to be pinned at the base of the lower column and at the tip of the upper column. Considerations of asymmetry under lateral loading were used to isolate the test specimen from the remainder of the structure along the midspan of the deck in each direction. Roller supports were desired at these locations; they were implemented using vertical pin ended steel struts because of the significant uplift forces that could be developed.

A total of 10 hydraulic actuators were employed in the test. Lateral loads were applied to the top of the upper column and to the lower deck. Gravity loads were simulated in this one-third scale model using a combination of concrete and lead weights as well as vertically oriented hydraulic actuators. Because the finite length of the vertical support struts resulted in small vertical motions of the support points under lateral displacements, a specially designed vertical actuator was provided under the column to maintain the axial load in the column at a proper level. This actuator also compensated for inelastic elongation of the plastic hinge region in the lower column, and overturning moment effects due to transverse loading. A post-tensioning rod also extended up through the center of the column and was loaded with a hydraulic actuator at its top in order to maintain the column axial load at the proper level.

Because of the desire to simulate realistically the distribution of gravity moment and shear in the transverse bent cap, two vertical actuators were used to load the bent cap at the interior webs of the box girder used for the bridge deck. In addition, to replicate the positive moment at the midspan of the bent cap due to dead load, a steel outrigger was cantilevered from the edge of the specimen and a constant vertical upward force was applied during the test.

At the lower deck level two actuators were used to impose specified displacements in the transverse direction and to limit torsion. A single displacement controlled actuator was used in the longitudinal direction at the deck level.

Two actuators were connected in a horizontal plane to the top of the column. The forces in these actuators were controlled rather than displacement as done at the lower level. If displacements were controlled at both levels, changes in deflected shape (that might occur as a result of concentrated yielding in one of the columns) could not be detected. In this case, the force in the upper level actuators was based on an assumed triangular mode shape, the ideal mass distribution at the two levels, and the column heights. For the test specimen, the force at the top level was 1.25 times the force applied at the lower level in the same direction. This actual force in the actuators were computed on-line during the test.

Because the actuators at the upper level were rotated with respect to the principal axes of the structure, a geometric correction was also applied. Since the top of the column displaces during the test, the geometric correction depended on the displaced configuration of the specimen at each step in the test. Furthermore, the forces measured in the load cells of the actuators attached to the lower deck were not oriented in the principal direction of the deck once the structure was subjected to large bi-directional motions. Thus, these forces were also corrected prior to being used to determine the lateral forces to be imposed at the top of the columns. The horizontal components of the forces imposed by the initially vertical actuators were also computed and used in the derivation of the forces to be applied at the upper level.

A dedicated high speed PC-based microprocessor was used to make these coordinate transformations and to control the specimen during the test. The microprocessor required continual input of the measured deck level actuator loads, the measured column top and deck level displacements. The control process was repeated approximately 7000 times per second. The microprocessor provided the actuator control apparatus with analog output signals for controlling the force at the top of the column.

A wide variety of loading histories were considered for the test. These included simple diagonal load paths, cloverleaf patterns and other sequences that would help identify the mechanical characteristics of the structure. The loading history selected is shown in Fig. 11.

Each step of loading was divided into three phases. In the first phase, the structure was subjected to a simple displacement cycle in the transverse direction (longitudinal displacement at the lower deck is restrained during this excursion) followed by a simple cyclic excursion in the longitudinal direction. The second phase involved two cycles of bi-directional loading in a square pattern; one clockwise and one counter clockwise. The maximum amplitude of the bi-directional excursion was the same as that for the uni-directional excursions; i.e., the projected displacement in the transverse direction was reduced to about 70% of that imposed during the unidirectional excursions. The third phase repeated the first phase so that deterioration of mechanical properties may be easily detected. This loading history was found to be very effective in assessing the effect of bidirectional loading histories. In more recent tests, the square pattern has been replaced with a circular pattern. This appears to be more realistic and not to have as severe effects on the specimen as the square pattern.

The displacement history shown relates only to the lower level. The forces applied to the top of the column corresponded to those associated with the triangular mode shape and the forces required at the lower level to develop the specified displacements. Because of the complexity of bi-directional response, the upper column moved bi-directionally even under uni-directional displacements at the lower level.

PSEUDO-DYNAMIC TESTING

These on-line computer controlled test procedures can be extended to include hybrid analysis. The most common form of this type of testing in earthquake engineering is the so-called pseudo-dynamic test. In most current applications, the actuators are under displacement control. The control computer, in addition to making the various required geometric and other corrections, uses data obtained regarding the restoring force characteristics of the specimen at a particular instant in time to solve the governing differential equations of motion of the test specimen for a numerically specified ground motion. In this manner the dynamic response of the specimen can be simulated quasi-statically using conventional electro-hydraulic loading systems. Dynamic effects are simulated in the computer by the governing differential equations, and the nonlinear restoring forces are determined 'continuously' from the specimen during the test.

Detailed discussion of these procedures, and their advantages and limitations, are beyond the scope of this paper. More complete description of these procedures may be found citations listed in references by Thewalt (1991a and b).

Important extensions to the pseudo-dynamic test method include:

- Real-time or near real-time testing of structures exhibiting rate sensitivity, such as the seismic response of structures containing visco-elastic dampers.

- Development of new "implicit" algorithms that allow the use of time integration intervals that do not depend on the shortest natural period of the entire system. These algorithms will substantially accelerate testing of large complex systems with numerous degrees of freedom, and will improve accuracy by reducing numerical error propagation effects.

- Development of reliable methods for on-line diagnosis of the accuracy of pseudo-dynamic test results. Assessing the accuracy of pseudo-dynamic test results is difficult, and reliable methods to identify and eliminate spurious results are required. Issues related to identifying deleterious effects associated with stress relaxation and strain rate effects for yielding structures need especially to be addressed. Methods for certifying pseudo-dynamic test results or facilities should be developed and adopted.

- Development of new algorithms are needed that can exploit the abilities of digital (rather than analog) controllers. For instance, it is theoretically possible to develop test procedures in which the specimen's motion is continuous. That is, the need to repeatedly stop for the measurements and calculations to take place at each step would be eliminated. This feature would make the tests more realistic, and significantly reduce error propagation effects due to stress relaxation in the inelastic range.

- A key feature of pseudo-dynamic testing is the ability to test a part of the structural system while analytically representing the remaining portions. Substantial additional work needs to be carried out to explore fully the limitations and capabilities of this substructuring approach.

  - ✔ The deformations at rotational degrees of freedom at the intersection of the analytical and experimental substructures are difficult to predict and control. Such difficulties should be explored and refined solutions developed.

  - ✔ Better methods for assessing the error propagation characteristics of substructuring approaches needs to be developed.

  - ✔ Methods for mixed displacement and force control need to be developed. For example, if a column (or base isolator) at the base of a structure is to be tested, the axial load in the specimen is likely to be an important parameter. However, it may be very difficult to control this axial force using the axial deformation degree of freedom of the test specimen because the required accuracy of displacement control may exceed the ability of most available hydraulic equipment. In addition, the high stiffness (and therefore frequencies) associated with this vertical response mode may likely result in significant numerical difficulties. Direct computation and control of the axial force in the specimen would be preferable. For practical and safety reasons, it is desirable to continue to control the more flexible lateral motion of the specimen using displacement command signals. Additional information on numerical procedures to implement such mixed force/displacement algorithms is presented by Thewalt (1991 b).

  - ✔ In large structures, it may be desirable to test several major components simultaneously. Such "distributed" pseudo-dynamic tests may be desirable in bridge structures where the bridge deck is expected to remain essentially elastic, whereas columns, piers, abutments and restraining or energy dissipation devices may undergo significant yielding. Substructuring techniques may be effectively used in such situations to obviate the need to construct those large portions of the structure which under-go well understood behavior. Details on methods to implement such procedures are discussed by Thewalt and Mahin (1994).

- Pseudo-dynamic tests also may have difficulties where the specimen to be tested is especially stiff. In such situations, very small displacements may have to be controlled. Because of imprecision in displacement transducers, friction and other mechanical errors associated with electro-hydraulic actuators, and so on, such tests are likely to result in spurious results. In some cases, the use of ***very*** precise instrumentation has produced satisfactory results. However, in other cases, dynamic interaction between the electronic control system and the test specimen can occur. This can lead to unstable tests. Various approaches to this have been attempted (e.g., detuning the control system, artificially softening the system through use of elastomeric bearings between the actuators and the specimen, adding virtual mass to the specimen, etc.) and in some instances these have been

successful. However, the ability to specify force as the control parameter, rather than displacement, would seem to be desirable in such situations. Algorithms to implement such tests are described by Thewalt and Mahin (1994).

- While some significant testing has been done to account for soil-structure interaction effects, more effort should be carried out on this topic for different types of situations and foundations. The ability of testing structures in the field using pseudo-dynamic methods would be a significant advance. This would be particularly useful in the assessment of as-built seismic characteristics of existing structures and in evaluating the efficacy of seismic retrofits. The theoretical and practical issues related to performing pseudo-dynamic tests where the structure is founded on soil, rather than on a *rigid* laboratory floor, need to be resolved, however.

Additional experience with pseudo-dynamic tests is required, especially with structures subjected to multiple components of excitation. Special emphasis is required to validate the method through matched shaking table and pseudo-dynamic tests.

Extension of the pseudo-dynamic test method to non-seismic problems should also be explored. For example, collision problems (ice impact on offshore structures, for instance) or dynamic aspects of moving loads (vehicles moving over a bridge) appear to be logical and useful extensions of the method.

CONCLUDING REMARKS

A wide variety of loading procedures are available for assessing the cyclic inelastic behavior of structures. Usual concerns relate to instrumentation, data acquisition and load/stroke capacity. In some tests special loading systems are required to develop and react the large forces required. In other cases, accurate measurement and control of structural response requires a variety of geometric and other corrections. Modern microprocessors make the execution of such tests relatively simple, and allow for even more complex hybrid experimental analysis procedures, such as the pseudo-dynamic test method.

Often practical considerations place the main restrictions on laboratory testing. As testing is applied to larger and more complex systems, costs of testing increases accordingly. Efforts are needed to upgrade experimental facilities and equipment to facilitate the types of tests described in this paper. Field testing is often difficult, but provides important real world conditions not possible to simulate in the laboratory.

ACKNOWLEDGMENTS

The authors are especially indebted to Professors Christopher Thewalt and Jack Moehle at the University of California at Berkeley who participated significantly in some of the test programs discussed in this paper. The tests described in this paper were funded by the California Department of Transportation, the National Science Foundation, and EQE International. The authors gratefully acknowledge this support. It must be recognized that the views expressed in this paper are those of the author alone. They do not necessarily reflect the policies or opinions of the of the research sponsors, the National Science Foundation, or the University of California at Berkeley.

REFERENCES

1. Thewalt, C. and Mahin, S. " The Pseudo-dynamic Test Method: Numerical Aspects," ***Experimental and Numerical Methods in Earthquake Engineering***, Ed. Donea, J. and Jones, P., Kluwer Academic Publishers, Boston, 1991.

2. Thewalt, C. and Mahin, S. " The Pseudo-dynamic Test Method: Verification and Extensions," ***Experimental and Numerical Methods in Earthquake Engineering***, Ed. Donea, J. and Jones, P., Kluwer Academic Publishers, Boston, 1991.

3. Thewalt, C. and Mahin, S., "An Unconditionally Stable Hybrid Pseudodynamic Algorithm," submitted to ***International Journal of Earthquake Engineering and Structural Dynamics***, 1994.

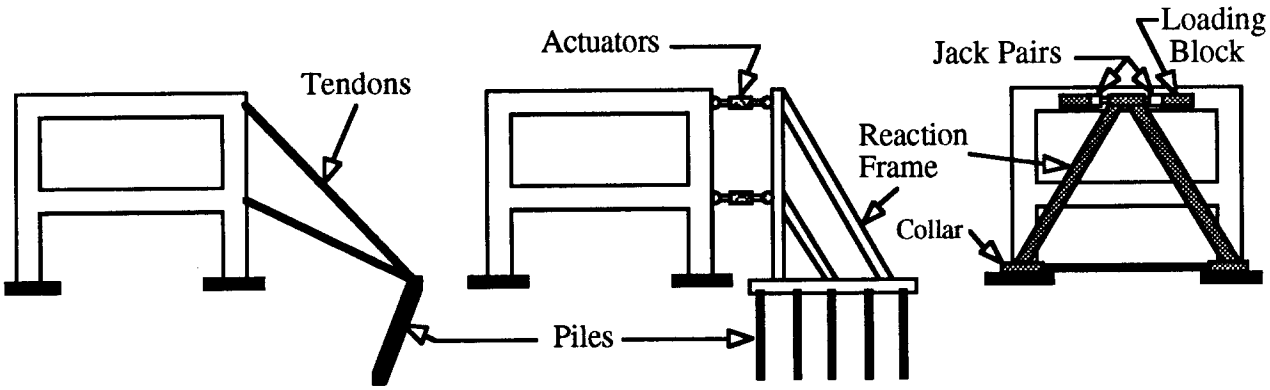

Fig. 1 Alternative Methods Considered for Field Testing of Viaduct

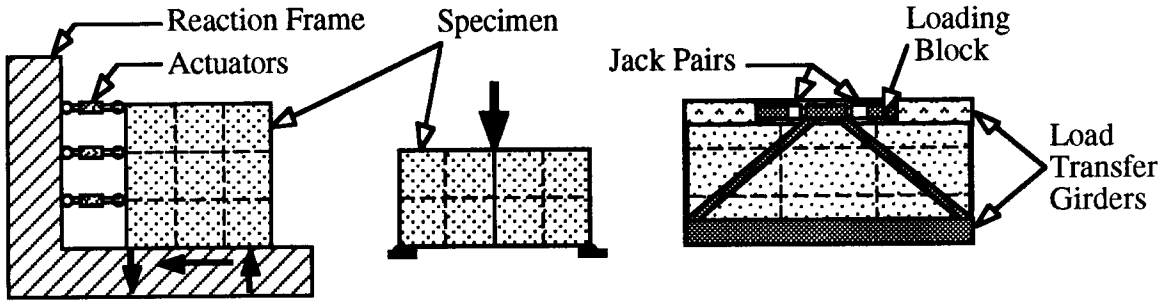

Fig2 Alternative Loading Arrangements Considered for Composite Wall Tests

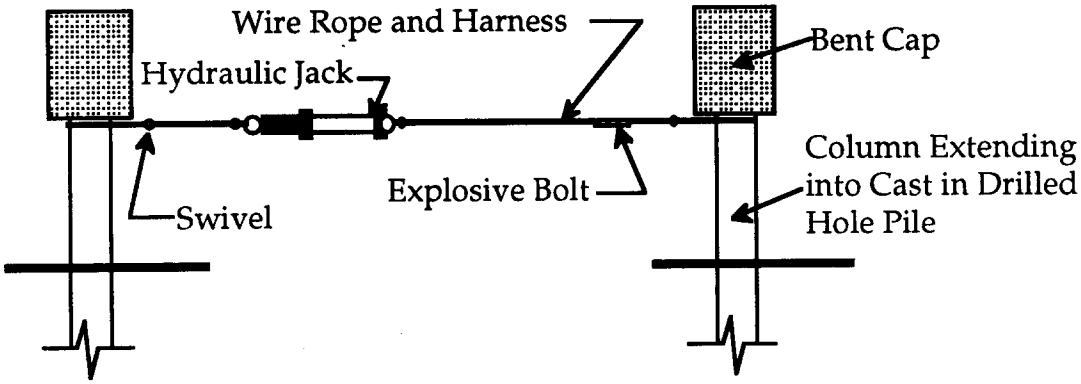

Fig. 3 Mechanism Used to Achieve Snap Back Vibration Experiment for Bridge Columns

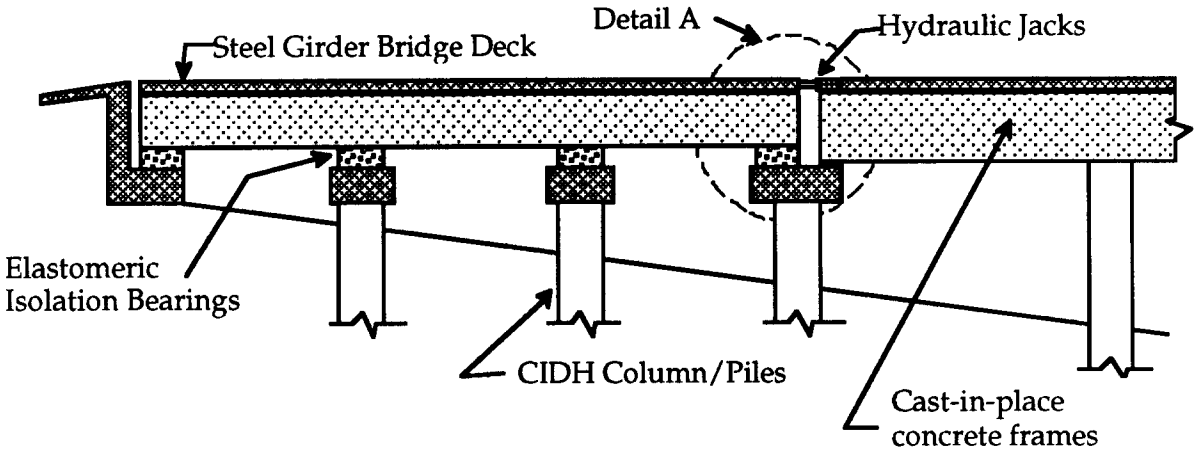

Fig. 4 Schematic Drawing of Walnut Creek Seismically Isolated Bridge Showing Placement of Hydraulic Jacks Used in Quick Release Tests

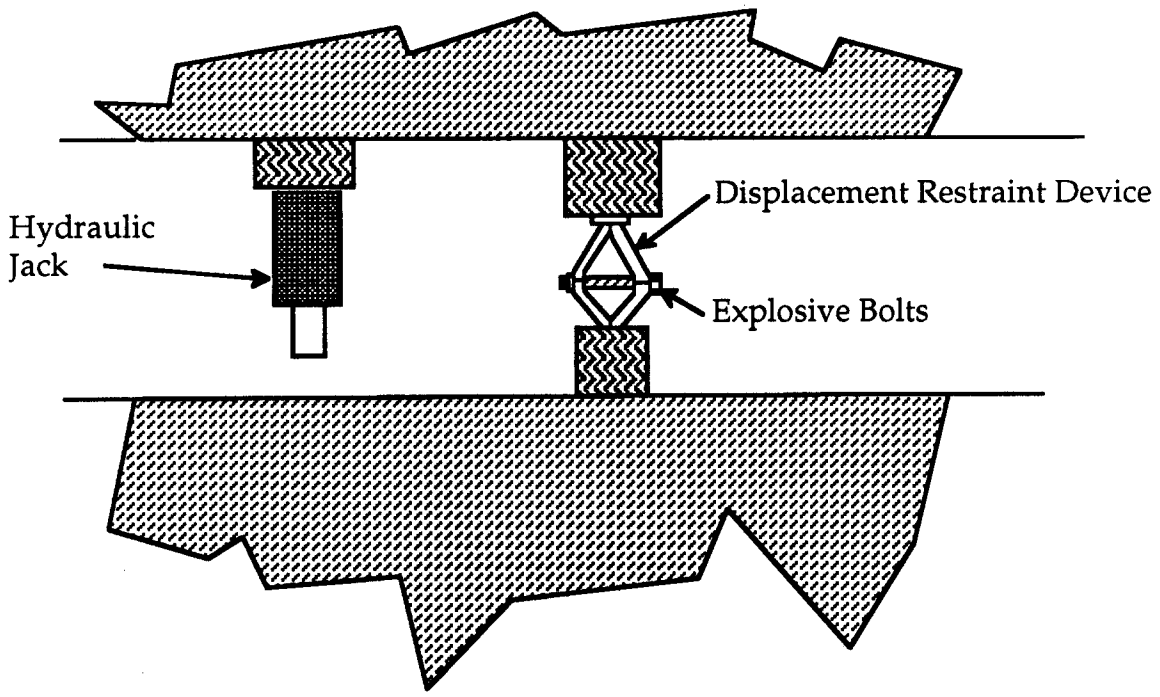

Fig. 5. Schematic Detail "A" Showing Hydraulic Jack and Displacement Restraint Device Used to Achieve Quick Release Test of Walnut Creek Isolated Bridge

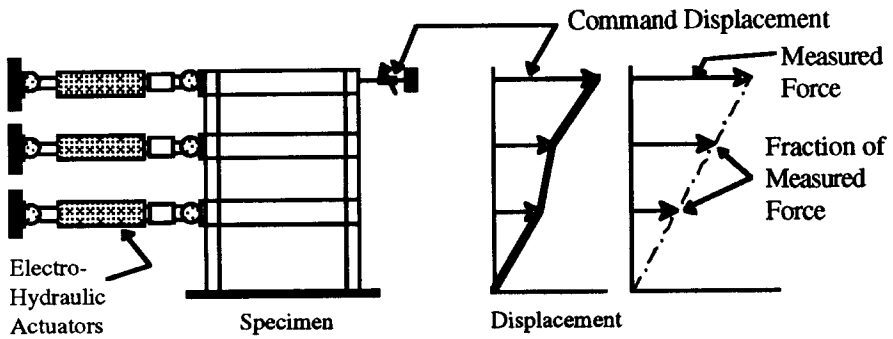

Fig. 6 Typical Planar Test of Multi-degree of Freedom System

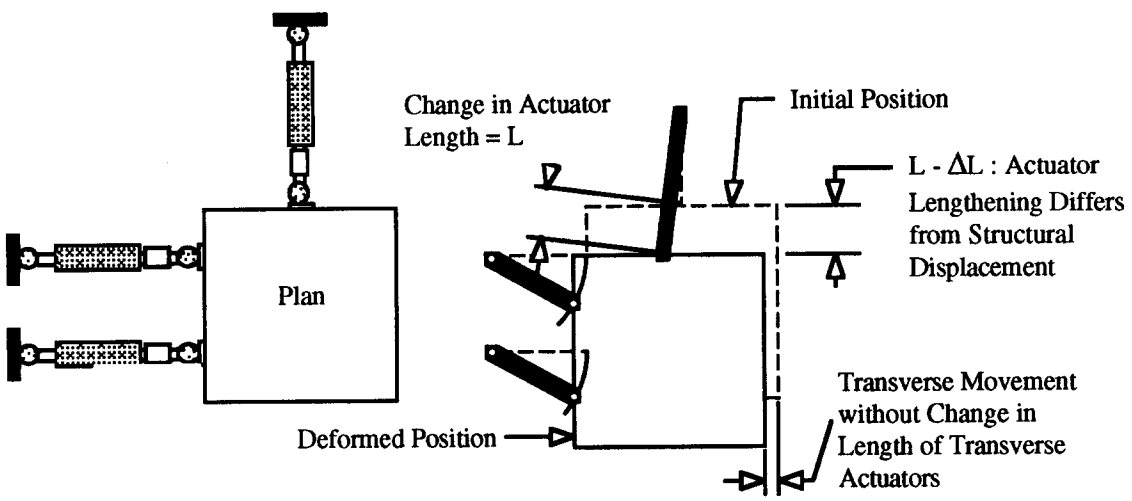

Fig. 7 Interaction of Actuator Displacements in Three Dimensional Tests

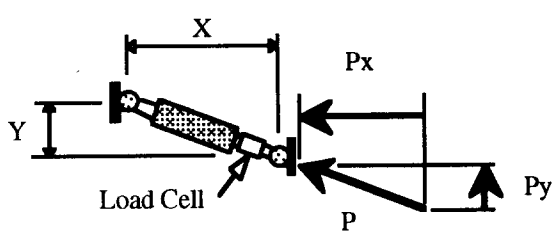

Fig. 8 Differences Between Forces Measured by Load Cell and Those Applied Along Specimen's Principal Axes

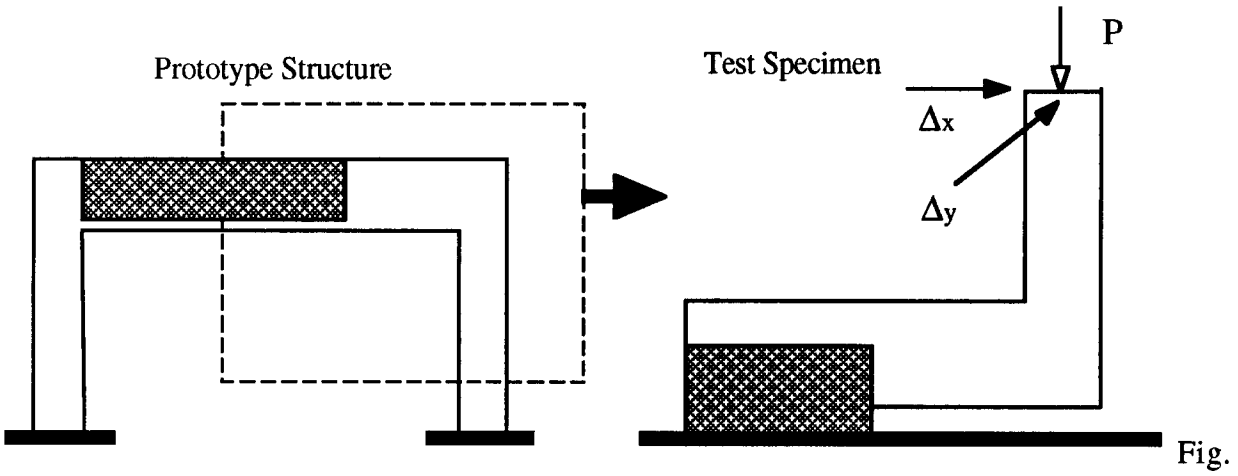

Fig. 9 Bi-directional testing of an Outrigger Bent Cap

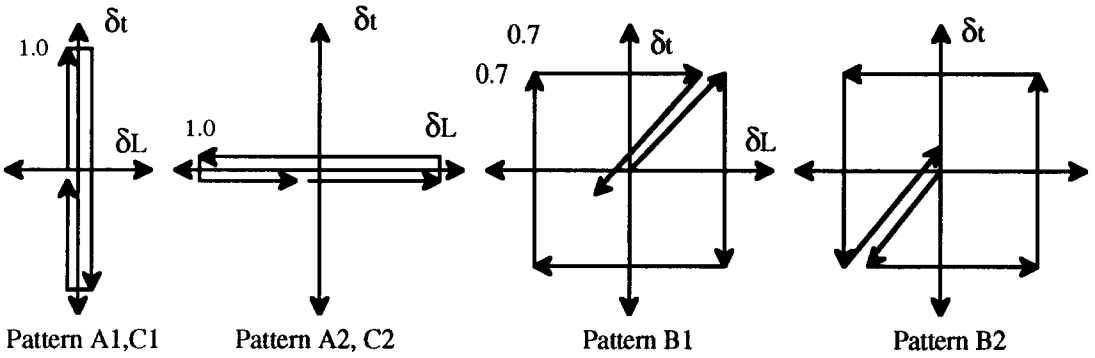

Fig. 10 Displacement History for Proof Test Specimen

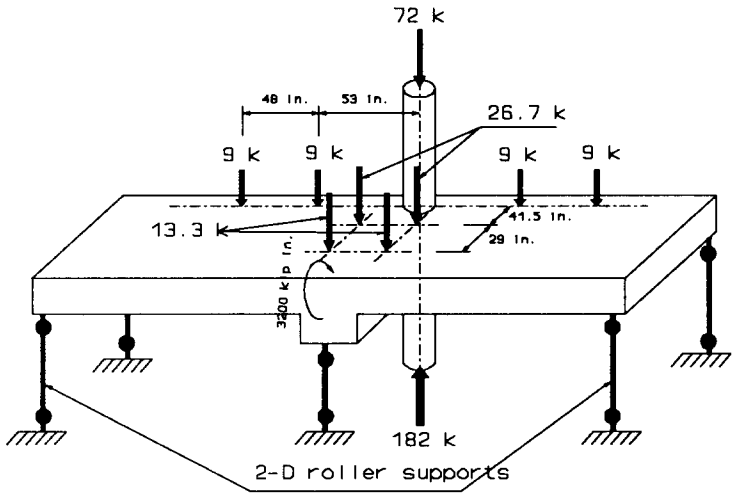

Simulation of dead loads

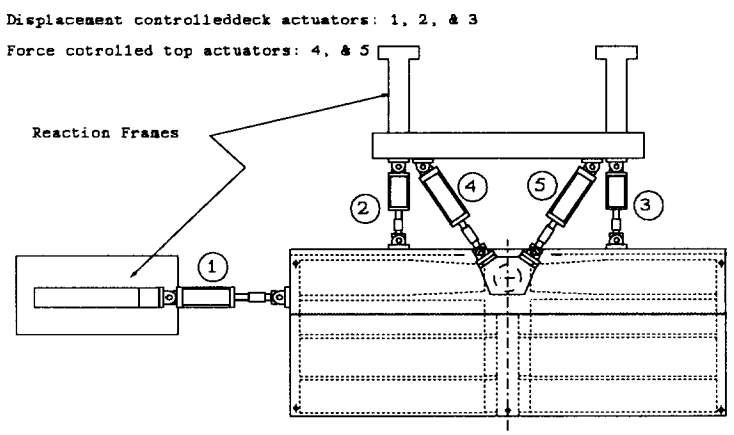

Lateral Load Acluators

Fig. 11 Test Setup for Proof Test of Double Deck Viaduct

Standard Test Procedures for Seismic Isolation Systems

by

Harry W. Shenton, III*

ABSTRACT

The Building and Fire Research Laboratory of the National Institute of Standards and Technology is currently engaged in an effort to develop guidelines for testing of seismic isolation systems. A comprehensive set of draft guidelines for testing has been developed and are available for use. The guidelines were developed to be independent of the type of superstructure, and generally independent of the type of isolation system. Three classes of tests are addressed in the guidelines: pre-qualification, prototype and quality control testing. The final guidelines for testing will be developed from the draft guidelines, based on industry feedback of the draft guidelines, and a test program to assess and evaluate the draft guidelines.

KEYWORDS: base isolation; building code; experimental; guidelines; seismic isolation; standard; testing.

1. INTRODUCTION

Seismic isolation is now generally accepted as a proven technology in earthquake hazard mitigation. A testimony to this fact is the increasing number of structures to be isolated in the United States and around the world (Kelly, 1993). One factor that has most certainly fostered confidence in the technology is the heavy reliance placed on testing to verify the performance and quality of manufacture of the isolation system.

Testing is currently required by the two major building codes that have adopted guidelines for design of isolated structures: for buildings, the 1991 *Uniform Building Code* (*Uniform*, 1991), and for bridges, the 1991 AASHTO *Guide Specifications for Seismic Isolation Design* (*Guide*, 1991). And although each requires an extensive series of tests, there currently do not exist standards for conducting these tests. As a result, test requirements are freely interpreted, leading to variability in the test procedures and subsequent test results from one supplier to the next. Furthermore, the lack of standard test procedures precludes an easy comparison of the performance of different isolation systems.

The Building and Fire Research Laboratory of the National Institute of Standards and Technology (NIST) is currently engaged in an effort to develop guidelines (i.e., a pre-standard) for testing of seismic isolation systems. The first phase of this effort is complete, as signified by the publication of *draft guidelines* for testing of seismic isolation systems (Shenton, 1994a; Shenton, 1994b; Shenton, 1994c). The final guidelines for testing will be developed from the draft guidelines, based on industry feedback and a testing program. Presented in the paper is a brief summary and overview of the draft guidelines and a discussion of the plans for developing the final guidelines for testing.

2. OVERVIEW OF THE DRAFT GUIDELINES

2.1 Scope

Rather than focus on a particular isolation system and application, e.g., seismic isolation of bridges using elastomeric bearings, the guidelines were developed to be comprehensive and broad in scope. The guidelines were developed to be independent of the type of superstructure, and therefore, are applicable to a broad range of projects, e.g., buildings, bridges, water towers,

* Research Structural Engineer
National Institute of Standards and Technology, Gaithersburg, Maryland 20899

etc. The guidelines are also generally independent of the type of isolation system, i.e., the test procedures are applicable to elastomeric, sliding, or hybrid isolation systems.

Three basic classes of tests are covered by the guidelines: pre-qualification, prototype and quality control testing. These are defined as follows:

> **Pre-Qualification tests** need not be project specific and are conducted in order to establish the fundamental properties and characteristics of the isolation system, and to determine the extent to which these properties are dependent on load and environmental factors.
>
> **Prototype tests** are project specific and are conducted to verify the design properties of the isolation system prior to construction.
>
> **Quality Control (QC) tests** are project specific and are conducted to verify the quality of manufacture and as-built properties of the isolation system prior to installation.

The guidelines are intended for *passive* systems that isolate in the *horizontal* plane only. Although some of the test procedures may be applicable to active systems, or systems that isolate in the vertical plane, the procedures were not developed with the latter in mind.

2.2 Rated Capacity

Fundamental to the guidelines is the concept of rated capacity. The onus is on the supplier of the isolation system to report certain fundamental properties of the isolation system, prior to testing. The properties to be reported include such things as seismic design displacement, thermal design displacement, effective horizontal stiffness at the design displacement, and energy dissipated per cycle at the design displacement. The complete list of properties to be rated is presented in Table 1.

Conditions under which the tests are conducted as outlined in the guidelines are based on the rated capacity of the system. For example, in a typical cyclic lateral load test, the vertical load and lateral displacement of the test are based on the suppliers rated capacity of the isolation system. In this way the test procedures are independent of the type of superstructure and autonomous of existing design guidelines and building codes for isolated structures. The standard list of rated properties should also facilitate the comparison of isolation systems from different suppliers and assist the designer in selecting the most appropriate system for the application.

2.3 General Requirements

The majority of the tests found in the guidelines are of a compression/shear type, i.e., a constant vertical load is maintained while the specimen is deformed laterally in shear. Many of the tests are, therefore, very similar in terms of the test set-up and test requirements. Consequently, general requirements are outlined in the guidelines for a typical compression/shear test, and exceptions or special requirements are noted in the test description.

General requirements address most of the issues related to test setup and instrumentation. Minimum requirements of the test facility, instrumentation, instrumentation calibration, data acquisition, and data analysis are discussed. This includes, for example, the number, type and positioning of displacement transducers; load capacity and calibration of the test facility, and a detailed description of the procedure for determining the effective stiffness and energy dissipation from a typical compression/shear test.

2.4 Pre-qualification Tests

Pre-qualification tests are formally not required by the codes today; nevertheless, tests of this type are usually conducted in one form or another as a new isolation system is developed. The purpose of the test series is to establish the

fundamental properties of the system and to characterize the response. The tests are designed to determine such things as the dependence on frequency of loading, vertical load, load direction and temperature, to name just a few. Tests are also outlined for establishing the ultimate or reserve capacity under load conditions likely to be encountered during an earthquake, and under normal operating conditions. The pre-qualification series is the most extensive and comprehensive of the three class of tests: pre-qualification tests are to be conducted only once, for any given system of a particular design, material and construction. Conceivably, in the future, a supplier may be required to submit the results of their pre-qualification test series as part of the bid package in order to be considered for a job.

Briefly, a complete series of pre-qualification tests is to include all tests listed in Table 2, a full series of prototype tests (Table 3) and applicable quality control tests (Table 4). Each pre-qualification test is to be performed separately on two specimens. Whenever possible, tests are to be conducted on full scale specimens; however, recognizing the limitations of existing test facilities, scale model specimens are acceptable, provided they are not less than 1/4 full scale and are representative of the full scale prototype.

Performance criteria, or a framework for specifying the criteria in the final guidelines, have been established for all test in the draft guidelines. Some of the criterion for the pre-qualification series are simply "benchmarks" for classifying the response of the isolation system. Others are measures of performance and the quality of manufacture: systems that do not meet or exceed these criteria may not perform adequately in service.

An example test description from the pre-qualification series is presented in Figure 1.

2.5 Prototype Tests

The prototype test series is intended to verify the principal design properties of the isolation system, namely, effective stiffness and energy dissipation. Other tests are included to verify reserve capacity or satisfactory performance under simulated seismic and non-seismic loads. The prototype series outlined in the guidelines is similar to, and in part based on, the test requirements given in the 1991 UBC (*Uniform*, 1991) and the 1991 AASHTO *Guide* (*Guide*, 1991).

A complete series of prototype tests is to include all tests listed in Table 3, and applicable quality control tests listed in Table 4. Each prototype test is to be performed on two full scale specimens. Properly documented prototype tests previously conducted on a unit of similar size may be used to satisfy the requirements of prototype testing, provided:

- the unit to be tested is similar in design, materials and construction;
- the largest dimension of the unit to be tested is within $\pm 10\%$ of the same dimension of the unit previously tested;
- most other critical dimensions are within $\pm 15\%$ of the size previously tested.

The latter is intended to provide relief from testing units that are identical in all respects, from one project to the next.

The most important test of the prototype series is the test to determine effective stiffness and energy dissipation. The basic test requires three fully reversed cycles at $\pm 0.25D$, $\pm 0.50D$, $\pm 0.75D$ and $\pm 1.0D$, at the design temperature and under the design vertical load, where D is the design lateral displacement. The full extent of testing, however, is in part based on the outcome of the pre-qualification test series: systems that are found to be dependent on vertical load, frequency of load, bilateral load or temperature are required to undergo additional tests, over and above the basic sequence described above.

2.6 Quality Control Tests

Quality control is an essential and integral element of any manufacturing process. It includes, among other things, proper documenta-

tion, material traceability, manufacturing instruction, inspection, part identification and testing. The quality control tests described in the guidelines are intended to be included *as part of* the supplier's overall quality control/quality assurance program, and are not to be construed as a comprehensive quality control program.

Two types of QC tests are discussed in the guidelines, production tests and completed unit tests. Production tests are conducted during fabrication, on the materials or parts that go into fabrication of a unit or device. Tests are then conducted on completed units, generally to verify the properties and manufacturing consistencies of the production units.

Pre-qualification and prototype tests can and should be independent of the type of isolation system; however, because of the nature of production tests and some of the completed unit tests, QC tests tend to be system specific. For this reason, the QC tests are contained in separate reports (Shenton, 1994b; Shenton, 1994c). Presented below is a brief overview of recommended QC tests for elastomeric and sliding isolation systems.

2.6.1 Elastomeric Systems

The guidelines outline a number of production tests for elastomeric systems. These tests are to be conducted on representative samples of the elastomer used in fabrication of the isolation unit. The recommended tests include hardness, tensile strength and elongation at break, bond strength, compression set, low temperature properties, high temperature aging and ozone resistance. A performance criterion is established for each production test that is based on a design specified value. Materials that do not meet or exceed these criteria should not be used in fabrication of isolation units.

Three completed unit tests are outlined for elastomeric systems: sustained compression, compression stiffness, and effective stiffness and energy dissipation (Table 4a). The sustained compression test was developed years ago as a means of testing the strength of the elastomer and steel bond. In this test the unit is subject to a vertical load equal to 1.5 times the nominal vertical load capacity, for a duration of not less than twelve hours. An exception is provided in the guidelines to reduce the time to three hours if a minimum number of consecutive tests have been conducted without failure.

It should be noted here that there is considerable debate within the community regarding the scope of quality control testing required. Since QC tests can be very expensive and time consuming, the debate centers around the number of completed unit tests to be conducted as part of the QC program. One position advocates testing every unit that comes out of the plant, while another would permit testing a percentage of the units produced, provided the results proved satisfactory based on a specified performance or acceptance criterion. Both options are communicated in the draft guidelines in a special "draft option" box. This is one example of an issue that must be, and will be resolved in the process of developing the final "Guidelines for Testing ...".

2.6.2 Sliding Systems

A series of production tests are outlined in the guidelines for a generic sliding device. The recommended tests include surface roughness, trueness of surface, interface material properties, backing material properties, bearing pad attachment and sliding interface attachment. Again, performance criteria are outlined that are based on a design specified value: materials that do not meet or exceed the minimum values should not be used in the fabrication of units or devices.

Two completed unit tests are included for sliding systems: sustained compression and effective stiffness and energy dissipation (Table 4b). The sustained compression test is similar to the sustained compression test for elastomeric systems, but is intended only for systems that are susceptible to creep.

3. PLANS FOR DEVELOPING THE FINAL GUIDELINES FOR TESTING

The draft guidelines are extremely comprehensive and fairly complete, nevertheless, they are still considered draft and are likely to undergo modest revision before the final "Guidelines for Testing..." are published. Over the next twelve to eighteen months efforts will be focused on developing the final guidelines for testing. The final guidelines are to be based on industry review of the draft guidelines, and a testing program. These steps will provide important feedback for developing the final guidelines.

The industry review of the draft guidelines will be carried out on several fronts. The draft guidelines are to be distributed to various individuals and organizations over the next several months. Individuals will be encouraged to provide written comments on the guidelines, and to provide reference to evidence or documentation that supports any suggested changes. The draft guidelines will also be submitted to various working groups or committees of selected code writing organizations for formal review and comment. Finally, a one day workshop is scheduled to be held that will provide a forum for review and discussion of the draft guidelines. The workshop will bring together individuals from private industry, research and government, with experience and interest in the design, fabrication and construction of seismic isolation systems and isolated structures. Participants will be charged with addressing some of the more important and unresolved issues related to testing. Feedback from these different avenues of review will be taken under consideration as the draft guidelines are revised and brought into final form.

A limited test program is to be undertaken at NIST over the next year, for the purpose of assessing and evaluating the procedures outlined in the draft guidelines. A selected number of isolation units will be tested that are representative of hardware available today. Tests will be conducted in strict accordance with the draft guidelines, with the objective of uncovering problems or inconsistencies in the procedures. Note that although different isolation systems will be tested, the purpose here is not to conduct a rigorous study to compare the relative performance of various isolation systems.

In a related effort, HITEC, the Highway Innovative Technology Evaluation Center of the Civil Engineering Research Foundation (CERF) is presently collaborating with the California Department of Transportation, and the Federal Highway Administration, to test and evaluate market ready seismic isolation systems for bridges. Organizers of the HITEC program are currently reviewing the NIST draft guidelines; in all probability the draft guidelines will be adopted for use in the HITEC test program. The results of the HITEC program should be extremely valuable, and will provide additional input in the effort to develop the final guidelines for testing.

4. SUMMARY

The Building and Fire Research Laboratory of the National Institute of Standards and Technology is presently engaged in an effort to develop guidelines for testing seismic isolation systems, i.e., a precursor to a standard for testing. The first phase of the effort is complete, as signified by the publishing of *draft* guidelines for testing.

The draft guidelines are extremely comprehensive and broad in scope. The guidelines are independent of the type of superstructure and generally independent of the type of isolation system. Therefore, the guidelines are applicable to seismic isolation of buildings, bridges, etc. Three classes of tests are covered by the guidelines, pre-qualification, prototype and quality control testing. The pre-qualification series is the first and most extensive of the three, but would only be required once for any system of a given design, material and construction.

The effort to develop the final guidelines will be carried out over the next year; however, the draft guidelines are sufficiently complete that they can be used effectively in their present form. The effort to develop the final guidelines

is to be based on industry review of the draft guidelines and a testing program. The adoption of these guidelines for testing should facilitate and further promote the use of seismic isolation as a viable means for earthquake hazard mitigation.

5. ACKNOWLEDGEMENTS

The draft guidelines were developed with the assistance of an Oversight Committee of experts from the field of seismic isolation, this included: Dr. Ian Buckle, Dr. Ron Mayes, Dr. Charles Kircher, Dr. Victor Zayas and Professor James M. Kelly. The author gratefully acknowledges the committees assistance and support in this effort.

6. REFERENCES

Guide Specifications for Seismic Isolation Design (1991), American Association of State Highway and Transportation Officials, Washington, D.C.

Kelly, J.M., (1993), "State-of-the-Art and State-of-the Practice in Base Isolation", Proceedings of ATC 17-1 Seminar on Seismic Isolation, Passive Energy Dissipation, and Active Control, Applied Technology Council, Redwood City, California.

Shenton III, H.W. (1994a), **Draft Guidelines for Pre-Qualification and Prototype Testing of Seismic Isolation Systems**, NISTIR 5359, National Institute of Standards and Technology, Gaithersburg, Maryland.

Shenton III, H.W. (1994b), **Draft Guidelines for Quality Control Testing of Elastomeric Seismic Isolation Systems**, NISTIR 5345, National Institute of Standards and Technology, Gaithersburg, Maryland.

Shenton III, H.W. (1994c), **Draft Guidelines for Quality Control Testing of Sliding Seismic Isolation Systems**, NISTIR 5371, National Institute of Standards and Technology, Gaithersburg, Maryland.

Uniform Building Code (1991), International Conference of Building Officials, Whittier, Calif.

Table 1. Standard Rated Capacity List

Parameter	Notation	Description
Stiffness:		
Horizontal	K_H	Effective horizontal stiffness at the Design Displacement and Design Vertical Load.
Horizontal under Wind	K_W	Effective horizontal stiffness at the Design Wind Load and Design Vertical Load.
Vertical	K_V	Effective vertical stiffness at the Design Vertical Load.
Energy Dissipation	E_H	Energy dissipated per cycle at the Design Displacement and Design Vertical Load.
Lateral Deformation:		
Design Displacement	D	Nominal displacement capacity, including that resulting from torsion, Draft Option corresponding to a level of ground motion that has a 10 percent probability of being exceeded in a 50 year period.
Maximum Displacement	D_{TM}	Total maximum displacement capacity, including that resulting from torsion, Draft Option corresponding to a level of ground motion that has a 10 percent probability of being exceeded in a 100 year period.
Thermal Displacement	D_t	Nominal thermal displacement capacity.
Vertical Deformation:		
Design Displacement	D_V	Nominal vertical displacement under the Design Vertical Load.
Creep Displacement	D_c	Creep displacement under the Design Vertical Load.
Rotation	θ	Nominal rotation capacity about an axis in the horizontal plane, and perpendicular to the direction of lateral loading under the Design Vertical load.
Compression:		
Low	P_L	Lower limit of load range of satisfactory seismic performance, includes the effect of vertical ground motion and overturning.

Table 1. (cont'd) Standard Rated Capacity List

Parameter	Notation	Description
Design Vertical Load	P_D	Nominal capacity in compression for dead and live load.
High	P_U	Upper limit of load range of satisfactory seismic performance, includes the effect of vertical ground motion and overturning.
Tension	P_T	Nominal capacity in tension.
Lateral Load:		
Wind	F_W	Nominal wind load capacity.
Braking/Centrifugal load	F_b	Nominal braking/centrifugal load capacity.
Degradation Cycle Limit	N_D	Number of cycles to $\pm D$ with a vertical load of P_D corresponding to a $\pm 15\%$ change in Effective Stiffness, or a $\pm 30\%$ change in Energy Dissipation relative to the first complete cycle Effective Stiffness or Energy Dissipation, respectively.
Thermal Cycle Limit	N_t	Number of cycles to $\pm D_t$ with a vertical load of P_D corresponding to a $\pm 15\%$ change in Effective Stiffness, or a $\pm 30\%$ change in Energy Dissipation relative to the first complete cycle Effective Stiffness or Energy Dissipation, respectively.
Temperature:		
Low	T_L	Lower limit of operating temperature.
Design	T_D	Nominal design temperature.
High	T_U	Upper limit of operating temperature.

Table 2. Schedule of Pre-Qualification Tests[1]

Category	Test	Title/Purpose
I	I.1	Establish dependence on virgin loading
	I.2	Establish dependence on frequency of load
	I.3	Establish dependence on load cycle history
	I.4	Establish dependence on load cycling
	I.5	Establish dependence on vertical load
	I.6	Establish dependence on load direction
	I.7	Establish dependence on load plane rotation
	I.8	Establish dependence on bilateral load
	I.9	Establish dependence on temperature
	I.10	Establish dependence on creep
	I.11	Establish dependence on aging
II	II.1	Ultimate compression under zero lateral load
	II.2	Compression in displaced position
	II.3	Ultimate Tension under zero lateral load
	II.4	Tension in displaced position
	II.5	Lateral load and displacement capacity under design vertical load

[1]Pre-qualification shall also include a complete series of prototype tests (Table 3) and quality control tests (Table 4).

Table 3. Schedule of Prototype Tests[1]

Category	Test	Title/Purpose
III	III.1	Effective Stiffness and Energy Dissipation
	III.2	Stability against degradation
	III.3	Stability at Maximum Lateral Displacement
IV	IV.1	Wind load
	IV.2	Thermal displacement
	IV.3	Stability with thermal cycling
	IV.4	Braking/Centrifugal force

[1]Prototype shall also include a complete series of quality control tests (Table 4).

Table 4. Schedule of Quality Control Tests

(a.) QC Tests for Elastomeric Systems

Test	Title/Purpose
1	Sustained Compression
2	Compression Stiffness
3	Effective Stiffness and Energy Dissipation

(b.) QC Tests for Sliding Systems

Test	Title/Purpose
1	Sustained Compression
2	Effective Stiffness and Energy Dissipation

Test Designation: I.5

Purpose: Establish dependence on vertical load.

Sequence: Three fully reversed cycles to peak displacements of $\pm D$. Tests shall be conducted for vertical loads corresponding to P_L, P_D, P_U. The frequency of loading shall be not less than f_L or 0.004 cyc/sec.

Procedure: Place the specimen in the test machine and secure to the supports and loading plate. Apply the full vertical load to the specimen and allow the load to stabilize. Apply the cyclic lateral load to the specimen for the required 3 fully reversed cycles of the test. Remove the vertical load. The test shall be run continuously without pause between cycles. The test shall be conducted at the vertical loads specified in the order P_L, P_D and P_U. Sufficient time shall be allowed between tests at the different vertical loads to dissipate any heat developed during the previous test.

Criteria: The System, Unit or Component response is considered to be independent of vertical load if:

(1.) the Average Effective Stiffnesses measured at vertical loads corresponding to P_L and P_U are within $\pm\alpha\%$ of the Average Effective Stiffness measured at the vertical load corresponding to P_D, i.e.,

$$\frac{\left| K_H^P - K_H \right|}{K_H} \leq 0.01\alpha$$

where K_H is the reference Average Effective Stiffness measured at a vertical load corresponding to P_D, and K_H^P denotes the Average Effective Stiffness measured at vertical loads corresponding to P_L and P_U.

(2.) the Average Energy Dissipation measured at vertical loads corresponding to P_L and P_U are within $\pm\beta\%$ of the Average Energy Dissipation measured at the vertical load corresponding to P_D, i.e.,

$$\frac{\left| E_H^P - E_H \right|}{E_H} \leq 0.01\beta$$

where E_H is the reference Average Energy Dissipation measured at a vertical load corresponding to P_D, and E_H^P denotes the Average Energy Dissipation measured at vertical loads corresponding to P_L and P_U.

Figure 1. Example Test Description (Shenton, 1994a; see original reference for details and symbol definitions)

State of the Arts in Japan Concerned With Application of Carbon Fiber for Rehabilitation and Strengthening for Concrete Bridges

by

Nishikawa Kazuhiro[1], and Koga Masajiro[2]

ABSTRACT

Currently, some rehabilitation and strengthening methods (retrofitting methods) are employed for concrete structures. But these methods have many problems such as reliability, weight increase and existing member deterioration. Recently, Carbon Fiber Sheet Glueing Method or Carbon Fiber Strand Winding Method are employed, because of easy execution, no weight increase and no deteriorate influence to existing members. In this report, fundamental properties of carbon fiber products and verification tests for application to concrete structures are briefly described.

KEYWORDS: Retrofitting, Seismic retrofitting, Carbon fiber, CFRP Strand, CFRP Sheet

REQUIREMENT FOR REHABILITATION AND STRENGTHENING OF CONCRETE STRUCTURES

1. Current Situations On Concrete Structures In JAPAN

Current situations on concrete structures, which were constructed in 1950's as infrastructures in Japan with careful attensions toward the concrete material selection and the construction management, is faced to rehabilitate oneself because of a shortage of serviceability instead of a life-span of used materials.

Concrete structures, constructed in 1970's, are heavily damaged like surface cracks of concrete and rusts of reinforcing steel by the reason that we could not help from employment of undesireble materials such as alkali-active aggregate and sea-sand, because of the shortage of good materials for concrete under construction fevers in Japan's drastically expanded economy.

Concrete structures came after expansion of basic infrastructure, which were constructed in severe cir cumstances, for example under salty atmosphere in seaside or under attack of de-icing agent in cold district, are now facing with the area-decreases or breakes of reinforcing steels because of own corrosion.

1) Head, Bridge Division, Structure and Bridge Department, Public Works Research Institute, Ministry of Construction,
Tsukuba Science City, JAPAN

2) Secretary of Carbon Fiber Retrofitting System's Technical Research Association,
Chiyodaku, Tokyo, JAPAN

2. Increase Of Design Load

Concrete structures, constructed in 1980's, are not allowed to increase working load additionally, because these were desired to design a smart structures by the economic reason, and which was reallized by the development of design technique.

From end of 1980's to beginning of 1990's, it was realized that the bearing forces of members in the structures were not enough against the increase of traffic capacity and load, and sometimes occured the damages of it. In 1993, the design load for bridges has changed from 20 Tons to 25 Tons.

By the reason of above mentioned, the rehabilitation and strengthening of concrete structures is urgently required, today.

3. Outline Of Rehabilitation And Strengthening Methods For Concrete Structures

Currently, some rehabilitation and strengthening methods (shortly named in this report; retrofitting methods) are employed for concrete structures, for example;

① Repair of members by resin based cohesive-aid injection

② Retrofitting of members by concrete placing with reinforcement; namely, concrete thickness increasing method

③ Retrofitting of members by steel plate glued; namely, steel jacketing method.

But these methods have many problems such as executive reliabilities, increase of member weight and deterioration to existing member.

Recently,

④ Carbon-Fiber-Sheet Glueing Method or Carbon-Fiber-Strand Winding Method; namely, Carbon-Fiber method, has been employed, because that this method has easy executive process, no weight increase, no deteriorate influence to existing members and high retrofitting effect.

The comparison between method ②, ③, ④ is shown in Table 1.

Table 1 Comparison between Retrofitting methods

Items	④ Carbon Fiber Method	③ Steel Jacket Method	② Concrete Placing Meth.
I Structure			
1. Weight Increase	non	increase	heavy
2. Influence to exist. Structure	non	drilling for Anchor	surface-Chipping
3. Durability	long term	short term	long term
II Construction			
1. Applicable Place	narrow & wide	flat place	wide
2. Workability	simple & fast	complex	long curing
3. Work Circumstance	noiseless	loud	loud
III Liability Problems	surfacing. resin cohesion crush resist.	injection-aid effect	combined-ability
IV Economy; Cost			
1. Material	high	high	low
2. Construction	low	high	high
3. Maintenance	low	high	low

CARBON FIBERS FOR RETROFITTING

1. Carbon Fiber Production

High Performance Carbon Fiber (shortly named; H.P.C.F.) is manufactured by following methods;

① Chemical made from continued organic compound "Molecule-Fiber"

② Chemical made from "Pitch"

③ Chemical made by "Chemical Vapour Deposition Method"

Highly continued Organic moleculefiber, which is mainly used as a raw materials for HPCF. under industrial production, is Rayon or Poly-Acrylic-Nitrile (PAN). The raw material is carbonized under stretched and stabilized condition to make a carbon fiber structure having selectional fiber alignment. Through these procedure, HPCF.is manufactured, which has anisotropy, high density, high tensile strength and high modulus characteristics.

Pitch, which is used as a raw materials for HPCF. under industrial production, is petroleum pitch or liquified coke pitch. Manufacturing procedure for HPCF. made from pitch is same as that from PAN, but "Mesophase-Pitch" is used to make easily a carbon fiber structure having selectional fiber alignment.

HPCF., as above mentioned, has superior mechanical and chemical characteristics than that of steel and in same time has lightweight, no magnetic, no rust, no corrosion and high durability.

Toray Industries Inc. developed carbonizing technology for Filament-Yarn produced from PAN in 1969.

Tonen Corporation, petroleum refining company, have been developing to product a Carbon-Fiber from oil type Mesophese-Pitch from 1970'.

Mitsubishi-Kasei Corporation is continueing to accumulate the coal chemical technology for half a century and succeeded to industrialize a coal pitch based Carbon-Fiber production in 1978.

2. Carbon Fiber Strand

Carbon Fiber Strand, consisted of about 12,000 filaments of HPCF., can be employed to retrofit by winding onto the surface of concrete and steel structures because of superior mechanical and chemical characteristics and flexibility carried from HP CF.. External view of carbon fiber strand is shown in Photo 1.

3. Carbon Fiber Sheet

(1) Torayca-Cloth is a textile material fabricated from HPCF."Toray ca" produced by Toray. Torayca-Cloth can retrofit the concrete structure by glueing onto concrete surface with epoxy resin, which can be hardened under atmospheric temperature.

(2) Forca-Tow-Sheet is a dry uni-directional fiber fabric made up of HPCF.. The fibers are attached to a netted thin glass fabric with a layer of resin adhesive which is easily dissolved into resin.

(3) Replark is a sheet of HPCF ."Dialead" produced by Mitsubishi-Ka sei, which is impregnated with epoxy resin under stretching to uni-direction. Replark can be applicable onto surface of various structures because of high realization of full tensile strength of HPCF. and superior workability.

External view of these carbon fiber sheets are shown in Photo 2 to 4, respectively.

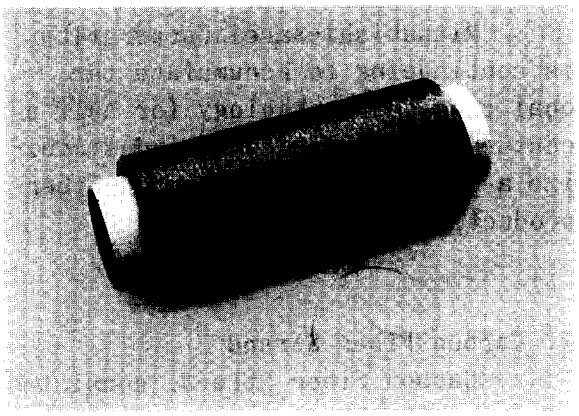

Photo 1 Carbon Fiber Strand

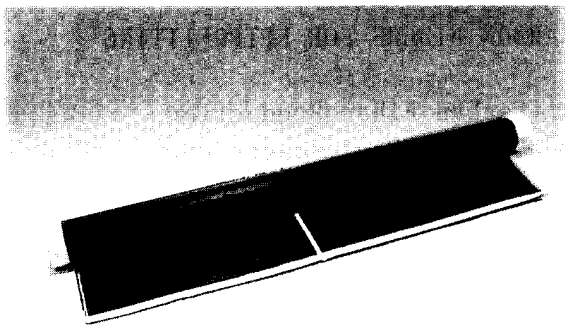

Photo 2 Torayca-Cloth

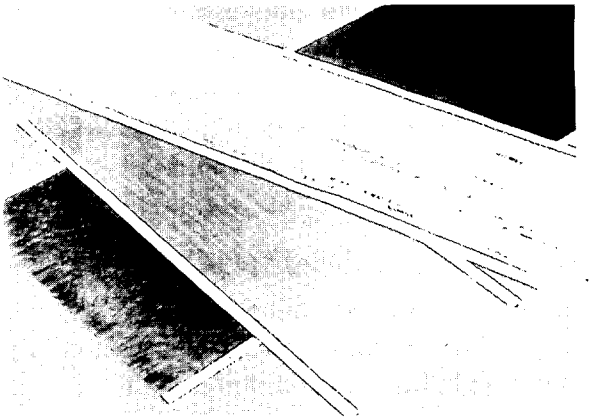

Photo 3 Forca-Tow-Sheet

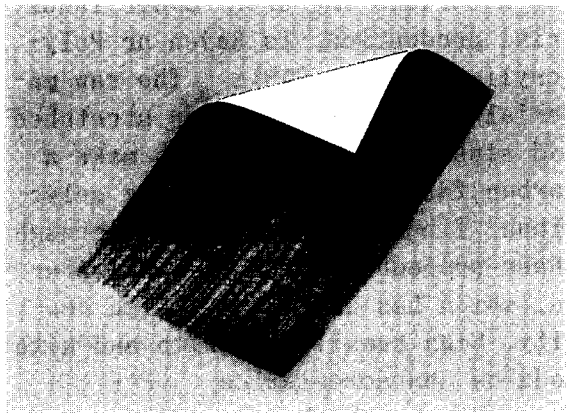

Photo 4 Replark

(4) Design Standards employed by CRS Research Association:
Now, under the activity of "Carbon Fiber Retrofitting System's (CRS) Technical Research Association", which was established and has been managed by the co-operation with Oba yashi, Toray, Tonen and Mitsubishi-Kasei and has been researching the application of HPCF. to the concrete structure, following data is used as specific values on design work;

Tensile Strength	: 250	kgf/mm2
Elastic Modulus	: 25,000	kgf/mm2
Elongation	: over 1.0	%

RETROFITTING METHOD WITH CARBON FIBER STRAND FOR EXISTING REINFORCED CONCRETE COLUMNS AGAINST SEISMIC LOAD

1. Application Research On Carbon Fiber

It is noted that the research activities on Carbon Fiber need to fully employ the merits of that, such as high strength and durability, because unit-weight price of Carbon Fiber is 100 to 200 times of that of steel. It is also necessary to develop the applications under special conditions, in which the current construction procedures are not available nor effective. From these views, the employment of carbon fiber for retrofitting of existing reinforced concrete structures is considered to be technically and economically promising or not.

For retrofitting of existing reinforced concrete structures, two types of carbon fiber products; Carbon-Fiber Strand and Carbon-Fiber Sheet, are employed. The aimes of retrofitting techniques employed these products are as follows;

1) Shear retrofitting by winding with Carbon Fiber Strand or Sheet.
2) Flexural retrofitting by glueing with Carbon Fiber Sheet.
3) Combination of the above technique 1) and 2).

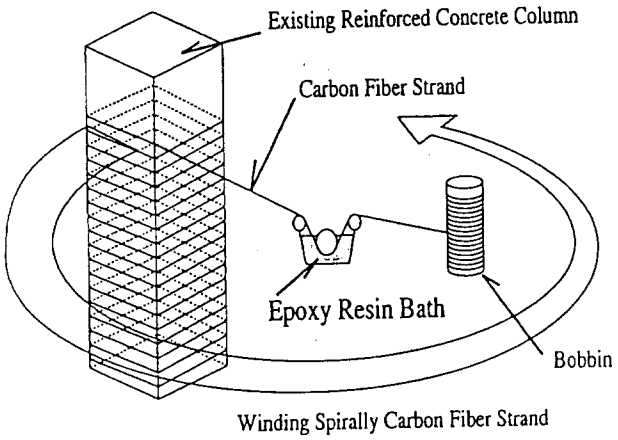

Fig. 2 **Shear Retrofitting for Columns**

2. Fundamental Properties Of Carbon Fiber Strand

The high strength and high modulus type of Carbon-Fiber (HPCF.) can be employed for the structural engineering applications, and to realize full strength of Carbon-Fiber, Carbon-Fiber Reinforced Plastics (CFRP), in which Epoxy Resin is impregnated and hardened, is usually carried out.

Stress-strain relationship of CFRP Strand is as shown in Fig.4, comparing other materials, and fundamental properties are as follows;

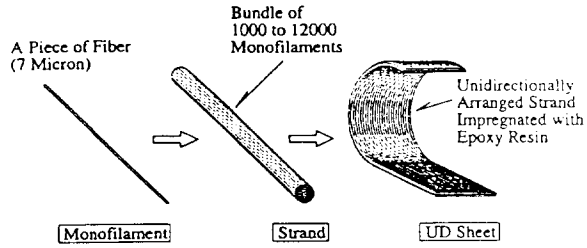

Fig. 1 **Products of Carbon Fiber**

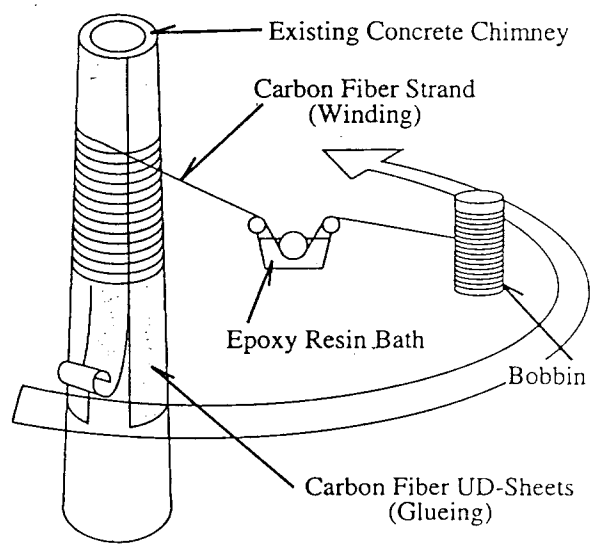

Fig. 3 **Flexural Retrofitting for Chimneys**

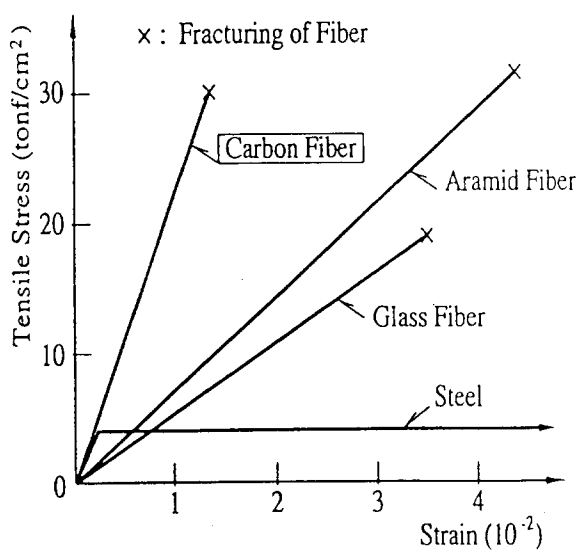

Fig. 4 **Comparison of Stress Strain Relationship**

Tensile strength: 300 kgf/mm2, 10 times of that of steel
Elastic modulus : 2,4000 kgf/mm2, almost equal to that of steel
Elongation : 1.2%, much smaller than that of steel, Yielding does not appear
Weight density : 1.8 gw/cm3, one-forth of that of steel
Durability : Excellent, rust does not appear

The tensile test results of the CFRP Strands manufactured by Mit subishi-Kasei, which is the only one currentry employed for this retrofitting method in Japan, are shown in Fig.5.

In usual, because of the nominal tensile strength of CFRP Strand is defined to 95% of passing rate within test pieces through the material test, the value of specified tensile strength of CFRP Strand is adopted to be 270 kgf/mm2. If 99% of passing rate is necessary, then the value of that is adopted to be 250 kgf/mm2.

Carbon Fiber Strand has superior properties than steel, such as high strength, high durability, and light weight, however, brittleness should be noted for application of Carbon Fiber.

For retrofitting material, Carbon Fiber, which has higher elastic modulus than that of Aramid or Glass Fibers, is chosen by the reason that confinement of concrete is increased by employing higher modulus materials.

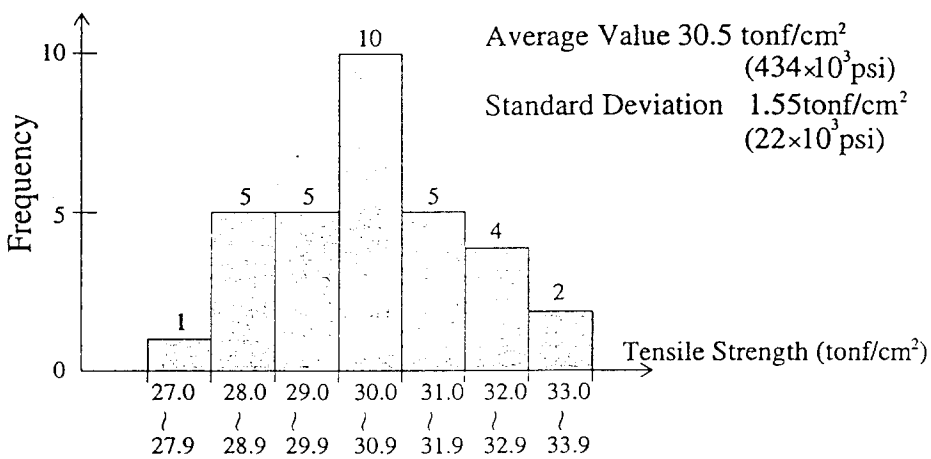

Fig. 5 **Tensile Test Result of CFRP strands**

3. Seismic Retrofitting Method For Existing Concrete Columns

(1) Outline of CFRP Strand Winding Method

There are some existing reinforced concrete columns, which have not enough shear strength and ductility against a severe earthquake shock. For these occasion, a new seismic retrofitting method for such columns has developed by Obayashi Corp. and Mitsubishi-Kasei Corp.. In this method, Carbon Fiber Strand is wound onto the surface of the existing column. This technique can improve easily the earthquake resistant capacity of columns as follows:

1) Increase of shear strength
2) Improvement of ductility
3) Increase of compressive capacity

Various tests, described in the following chapters, were carried out to discuss the above mentioned retrofitting performance.
From these result, it is recognized that this retrofitting method is effective for improving shear strength and ductility,and quantitative evaluations of retrofitting performances were established, and design procedures of this technique were proposed.

The winding work of Carbon Fibers in this retrofitting method is carried out by an automatic winding machine, by the reason of expensive Carbon-Fiber is employed, therefore, machine-based construction procedure is necessary to save labors and costs. The automatic winding machine for chimney is shown in photo 5 and for building in Photo 6.

This machine is also applicable to retrofitting for bridge columns.

(2) Advantages of CFRP Strand Winding Method

This method has the following advantages, comparing with others.

1) easy realization for required shear and ductile capacities.

2) no deteriorate influence to stiffness of the existing columns.

3) minimum weight increase by retrofitting.

4) no skillful workers for construction.

5) easy quality control for construction.

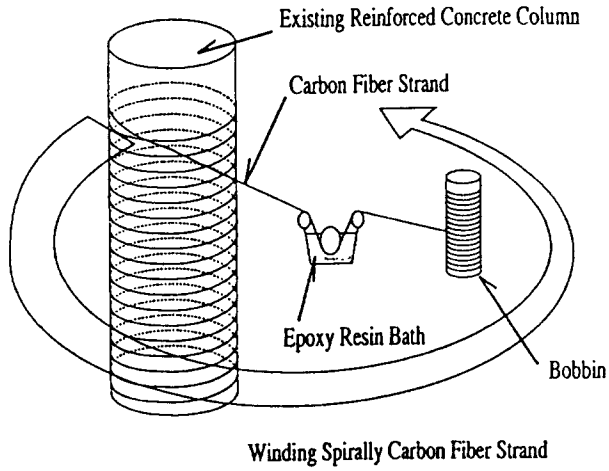

Fig. 6 **Seismic Retrofitting for Columns**

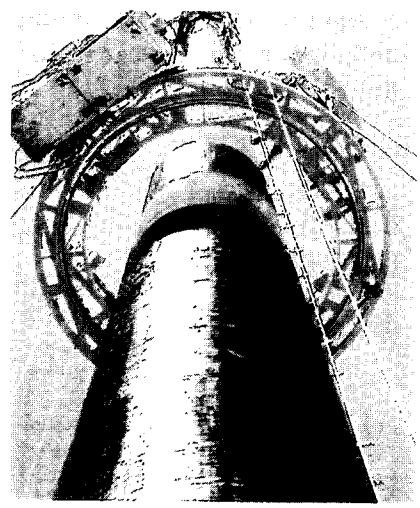

Photo 5 **Winding Machine for Chimneys**

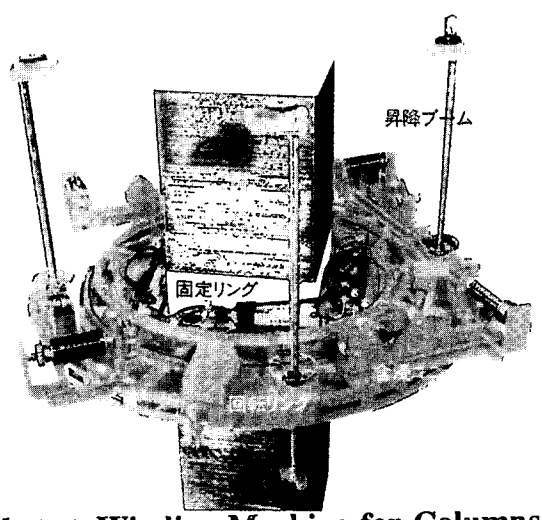

Photo 6 **Winding Machine for Columns**

4. Structural Performance Of Columns Retrofitted By CFRP Strand Winding Method

(1) Lateral loading test against retrofitted columns with circular cross section

The aim of this test was to verify the influence on strength and ductility of retrofitted columns with CFRP Strand. The employed specimens, as shown in Fig.7, were 5 reinforced concrete columns, which were 1/4 scaled models with circular cross section.

Test variables were ① retrofitting quantity of CFRP Strand and ② substrate treatment (Bond treatment and Unbond treatment) between CFRP Strand and concrete surface as shown in Fig.8.

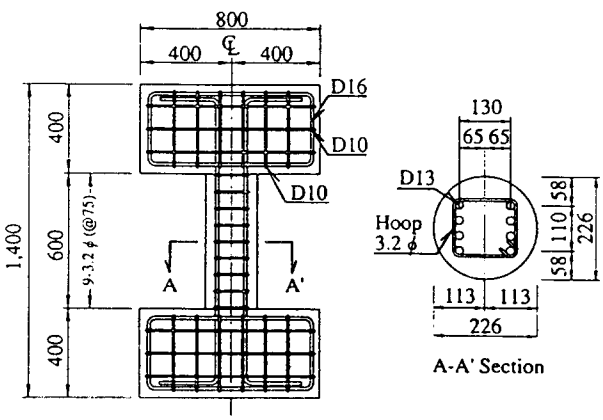

Fig. 7 **Column Specimen**

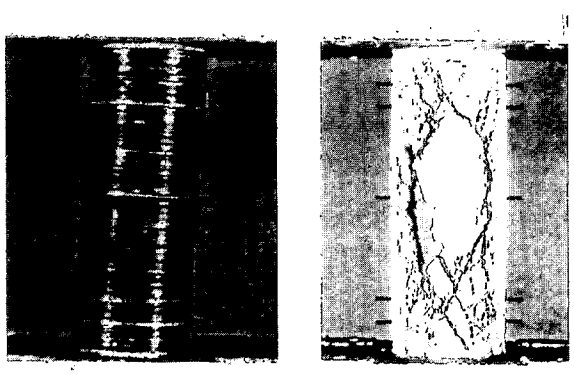

(a) Retrofitted (b) Unretrofitted

***Photo* 7 Columns after Testing**

The findings from this test are as follows;

1) The CFRP Strand Winding Method improves strength and ductility of columns.

2) The CFRP retrofitting can change the failure mode of columns from bond splitting type to flexural type.

3) Heavy CFRP retrofitting is quite effective for strength increase.

4) The Bond treatment is effective for strength increase and the Unbond treatment is effective for ductility improvement.

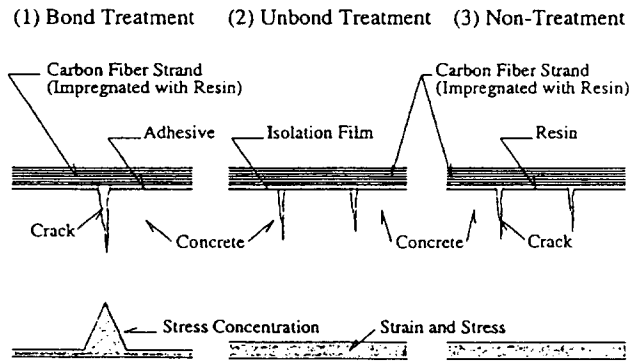

Strain and Stress Distribution of CFRP Strand

***Fig. 8* Substrate Treatment of Concrete Surface**

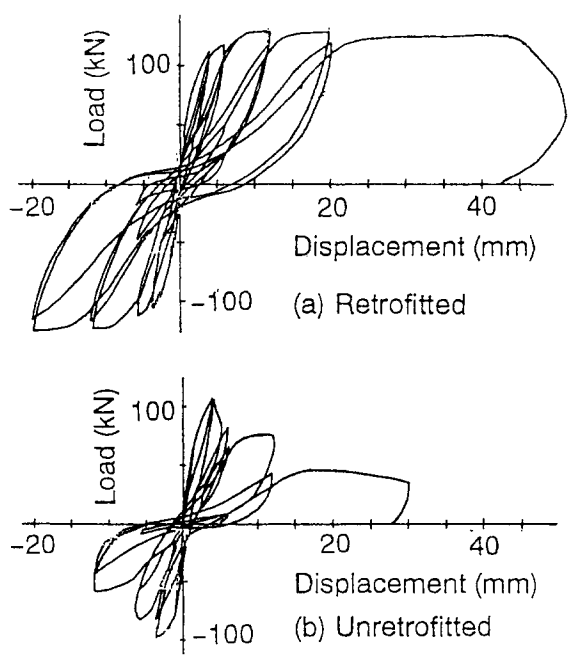

***Fig.* 9 Load displacement Relationship**

(2) Lateral loading test against retrofitted columns with square cross section

The aim of this test was to discuss the performance of the CFRP retrofitting method for columns with square cross section. The employed specimens, as shown in Fig.10, were 10 reinforced concrete columns, which were 1/4 scaled models with square cross section.

Test variables were ① retrofitting quantity of CFRP Strand and ② substrate treatment (Unbond treatment and Non-treatment) between CFRP Strand and the concrete surface.

The failure modes are shown in photo 8, comparing the retrofitted specimens with the non-retrofitted ones.

The findings from this test are as follows;

1) For the columns with square cross section, the CFRP retrofitting is as effective as for the circular cross section.

2) Diffrence between the Unbond treatment and the Non-treatment is negligibly small. The Non-treatment is preferred, because it saves one process of construction.

3) The reinforcing performance of CFRP Strand can be evaluate as that of ordinary steel bars.

In this procedure, the strength ratio between CFRP and steel can convert the CFRP quantity into the steel reinforcement quantity.

(3) Flexural shear loading test against retrofitted beam

The aim of this test was to propose a quantitative evaluation for shear strength of columns retrofitted by CFRP Strand Winding Method. The employed specimens, as shown in

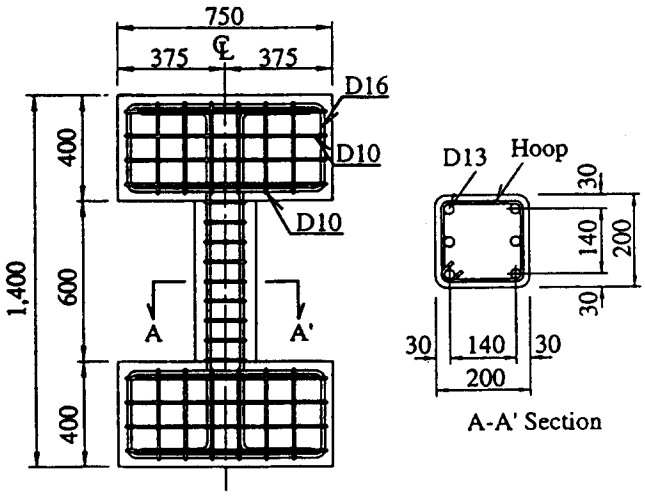

*Fig.*10 **Column Specimen**

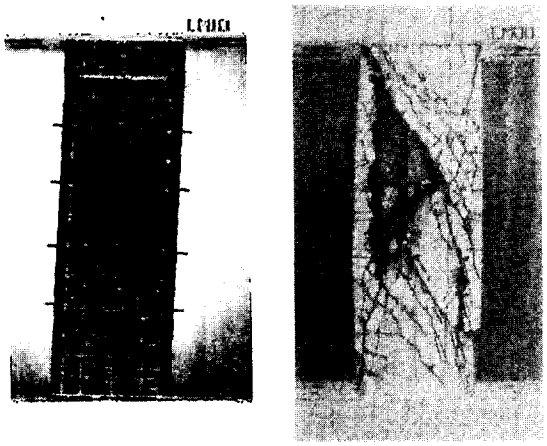

(a) Retrofitted (b) Unretrofitted

Photo 8 **Failure mode of Tested Columns**

Fig.11, were 15 reinforced concrete beams with rectangular cross section.

Test variables were ① shear reinforcing quantity of CFRP Strand, ② shear span ratio (= Depth/Shear span) and ③ compressive strength of concrete.

The failure patterns and shear & deflection relationship are shown in Fig.12 and Fig.13, respectively.

The findings from this test are a s follows;

1) CFRP Strand Winding is quite effective for shear reinforcement.

2) Increase in CFRP Strand improves maximam shear bearing force of the specimen.

3) The shear strength of the members retrofitted by CFRP Strand can be calculated by the application of the current design equation for ordinary steel reinforcing bars. In the equation, the design tensile strength of CFRP Strand is defined to be 2/3 of the full of that.

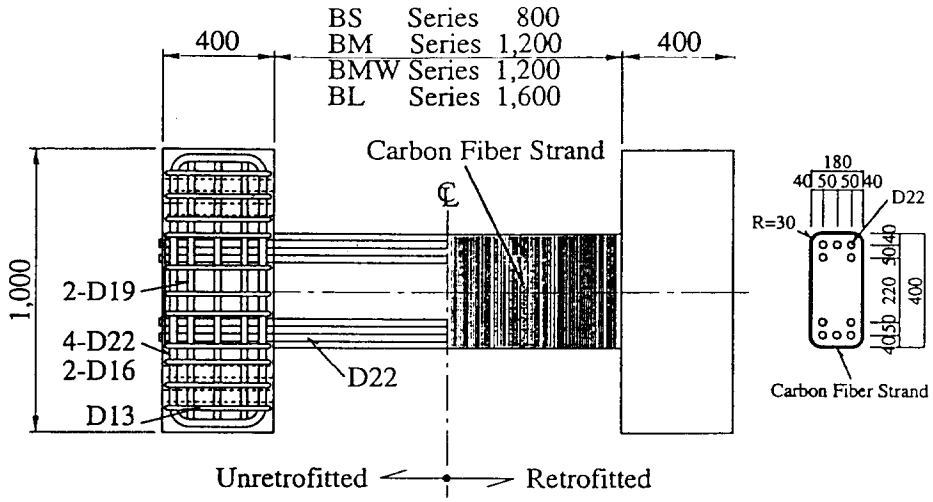

Fig. 11 **Specimen of Shear Strength Test**

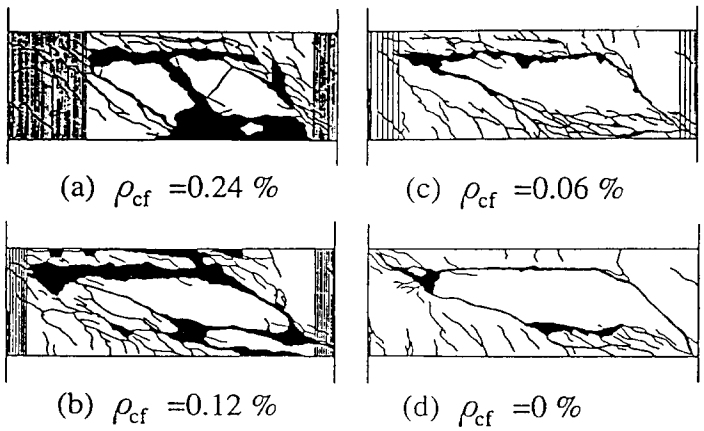

Fig. 12 **Failure Patterns (BMW Series)**

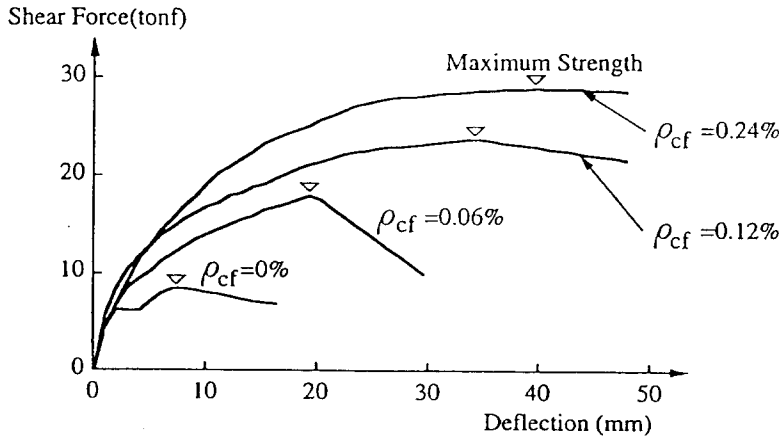

Fig. 13 **Shear Force - Deflection Relationship**

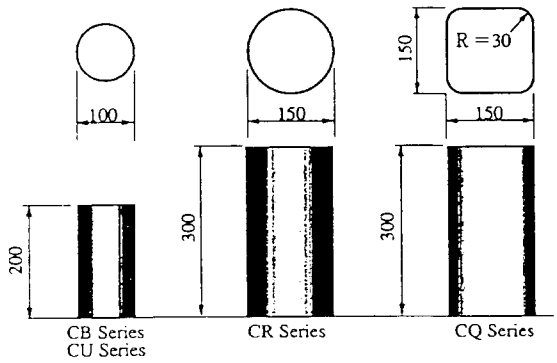

Fig. 14 Specimens

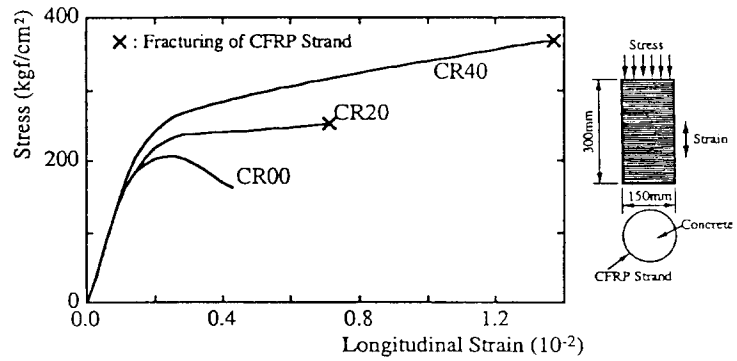

Fig. 15 Stress - Strain Relationship (CR Series)

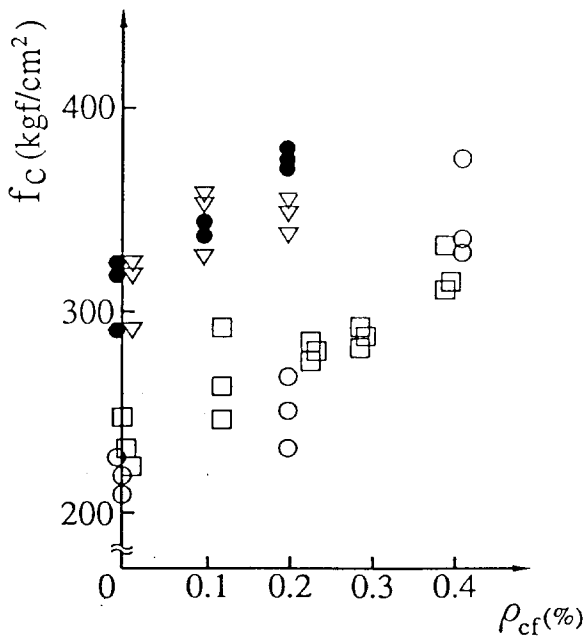

$$\rho_{cf} = \frac{A_{cf} \cdot \ell}{A_c \cdot S}$$

ρ_{cf}: Ratio of CFRP Strand
A_{cf}: Area of CFRP Strand
A_c: Area of Concrete Section
ℓ : Perimeter of Specimen
S : Spacing of CFRP Strand

● : CB Series
▽ : CU Series
○ : CR Series
□ : CQ Series

Fig. 16 Compressive Strength of Confined Concrete

(4) Compression test of concrete cylinders confined by CFRP Strand Winding

The aim of this test was to evaluate confinement effect on compressive strength and ductility of concrete confined by CFRP Strand Winding. Test variables were ① quantity of CFRP Strand, ② type of cross section of the specimen, and so on.

The examples of Stress-Strain relationship of concrete is shown in Fig.15, and the relationship between compressive strength and CFRP quantity is shown in Fig.16. The findings from this test are as follows;

1) The CFRP Strand retrofitting improves the compressive strength and ductility of the concrete specimen. This effect grows when the quantity of CFRP Strands is increased.

2) The confinement effect is more evident for the cylinders than for the rectangulars.

(5) Lateral loading test against retrofitted bridge columns with rectangular cross section

The aim of this test was to

discuss the performance of bridge columns with rectangular cross section retrofitted by CFRP Strand Winding method against shear failure and buckling of existing longitudinal reinforcing bars. The employed specimens were 11 reinforced cncrete bridge columns, which were 1/3 scaled models with rectangular cross section. Test variable were ① quantity of CFRP Strand, ② shear span ratio, and so on.

The failure pattern and load & displacement relationship for shear failure type of the specimen are shown in Photo 9 and Fig.17, respectively. Others for Re-bar buckling type of the specimen are shown in Photo 10 and Fig.18, respectively.

These test results lead the following conclusions for the appropriate retrofitting with CFRP Strand ; 1) Shear failure of the bridge columns can be avoided, so that a required level of ductility can be provided.

2) Buckling of longitudinal reinforcement in flexural failure can be avoided, so that a required level of ductility can be provided.

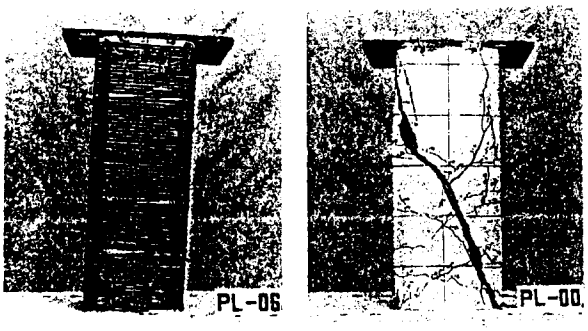

(a) Retrofitted (b) Unretrofitted

***Photo* 9 Failure Mode**

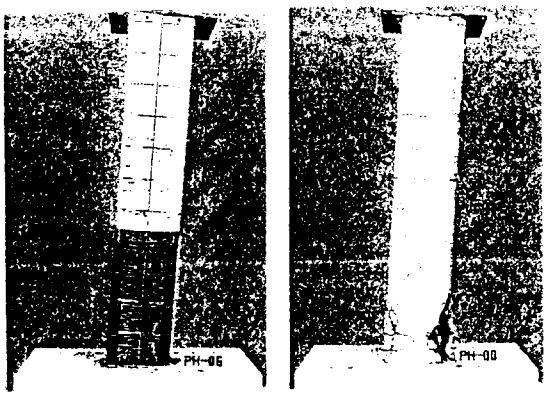

(a) Retrofitted (b) Unretrofitted

***Photo*10 Failure Mode**

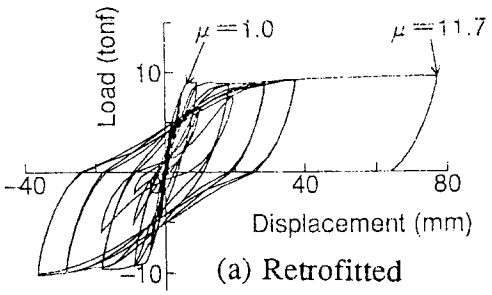

(a) Retrofitted

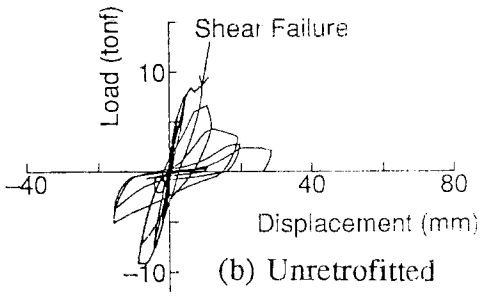

(b) Unretrofitted

***Fig.*17 Load - Displacement Relationship (Shear Failure Type)**

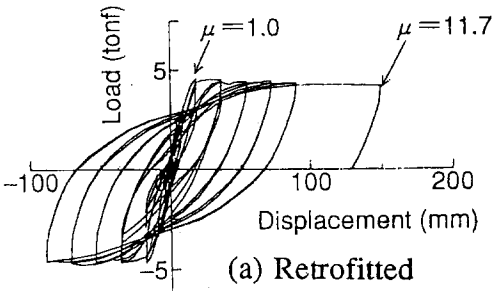

(a) Retrofitted

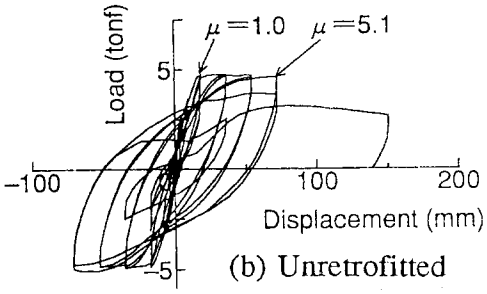

(b) Unretrofitted

***Fig.*18 Load - Displacement Relationship (Re-bar Buckling Type)**

5. Durability of CFRP Strand

To verify long-term effects of the retrofitting by CFRP Strand Winding Method, the following tests have been carrying out.

① An accelerated weathering test of CFRP Strand.

② An out-door exposure test of CFRP Strand.

③ A chemical resistance test of CFRP Strand.

The result of the accelerated exposure test is shown in Fig.19. In usual, this retrofitting method employs some finishings over the wound CFRP Strands around the column surface, therefore, durability problem of CFRP Strand does not seem to rise. Even if there is no finishing, durability of the CFRP Strand is almost perfect.

RETROFITTING WITH CARBON-FIBER SHEET GLUEING METHOD FOR CONCRETE STRUCTURE

1. Application To Concrete Beam Retrofitting

Carbon-Fiber Sheet has a wide application area by the reason of its speciality; mechanical and chemical superior characteristics, and easy employment in the narrow and broad space or at the small and wide area of structure without machinery but with only man-power because of light weight of that.

In the application to beam retrofitting, as shown in Fig.20,

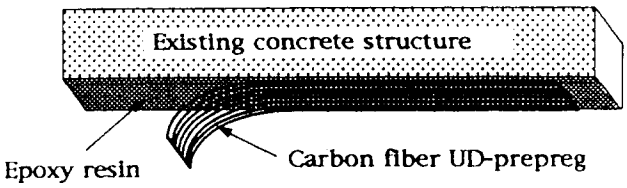

Fig.20 Glueing of carbon fiber

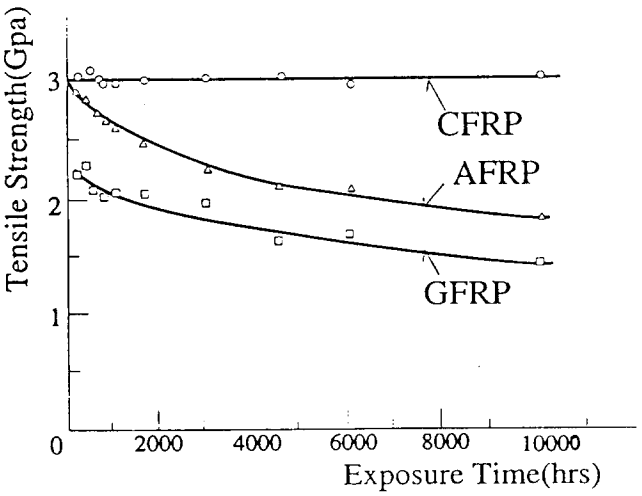

*Fig.*19 **Tensile Strength - Exposure Time Relationship**

Carbon Fiber Sheet is glued onto the surface along to the member axis direction of existing beam, with the epoxy resin. After resin impregnated into Carbon Fiber Sheet and hardened, Sheet type Carbon Fiber Reinforced Pastics(CFRP Sheet) works for flexural retrofitting.

On this retrofitting method, as shown in Fig.21, CFRP Sheet,which is glued onto face of concrete, can work as same as Re-Bar and co-operated with Re-Bar.

CFRP Sheet,consisted of Carbon Fiber volume 175～300 gw/m2, has about 0.1 mm converted thickness and has about 250 kgf/cm permissible force per each ply,so that equals to 13 mm diameter Re-Ber arranged about 150 mm spacing. The number of glueing plies of CFRP Sheet would be determined by the condition of working load.

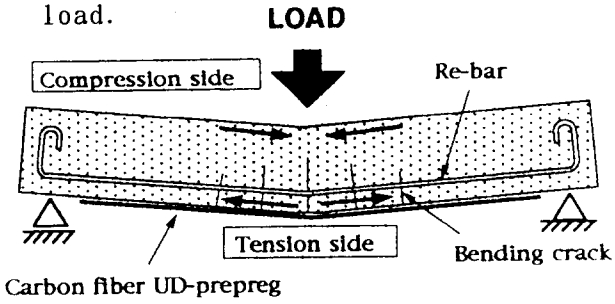

Fig.21 Retrofitting for bending moment

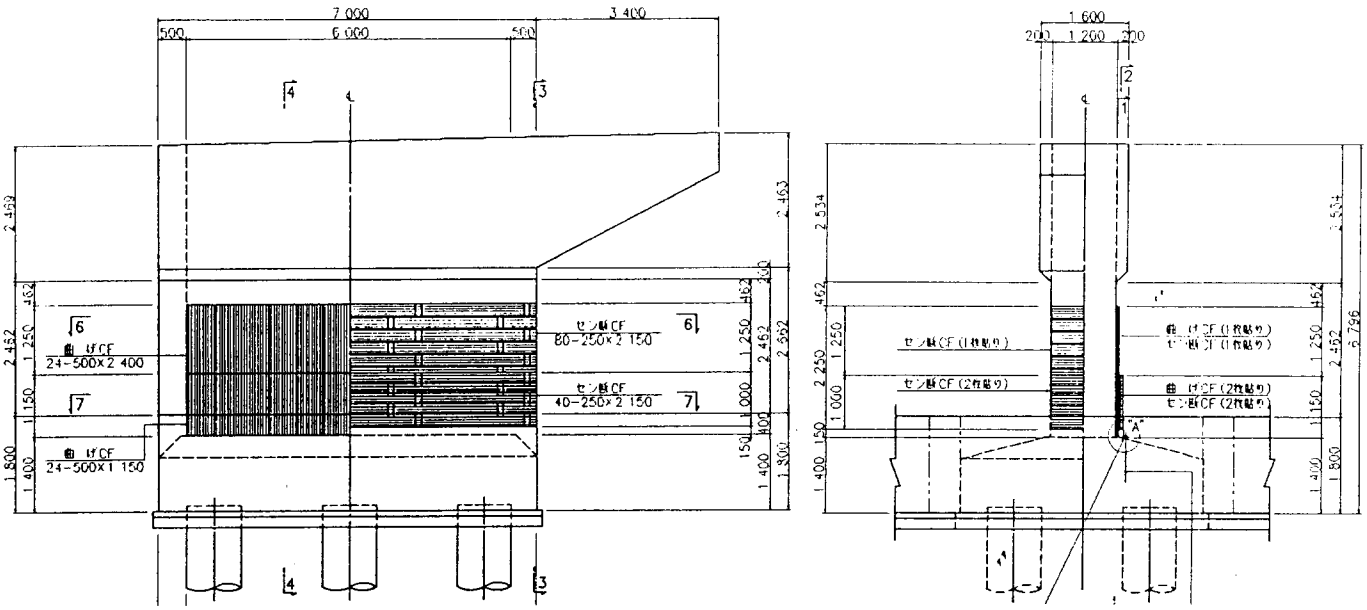

Fig. 22 Pier's Column Retrofitting by Carbor Fiber Sheet

2. Application To Pier's Column Retrofitting

As shown in Fig.22, Carbon Fiber Sheet is glued along to the member axis direction of existing pier with epoxy resin. CFRP Sheet can resist against working moment, as same as beam. And in the case that CFRP Sheet is added to horizontal direction, that Sheet can work for shear force resistance and also have the confinement effect for the vertical CFRP Sheet.

REFERENCES

1) Y.KOBATAKE:「A RESEARCH FOR SEISMIC RETROFITTED REINFORCED CONCRETE COLUMN BY NEW MATERIALS(No.1 ～3)」、Obayashi Corp.Technical Research Institute's Report No.33 ～38、1986～89

2) Y.KOBATAKE:「A STUDY ON THE STRENGTHENING WITH CARBON FIBER FOR EARTHQUAKE RESISTANT CAPACITY OF EXISTING REINFORCED CONCRETE COLUMNS」、Workshop on Repair and Retrofit of Existing Structures UJNR Tukuba、Japan May 8-9, 1987

3) Y.KOBATAKE:「APPLICATIONS OF RETROFIT METHOD WITH CARBON FIBER FOR EXISTING REINFORCED CONCRETE STRUCTURE」、The 22nd Joint UJNR Panel Meeting、Japan、May 12-14, 1990

4) Moto.OKANO:「The Strengthening Methods of Existing Road Bridge with Carbon Fiber Reinforced Plastics」、Fire Resistant Materials、No.45[5]、p332～339、1993

5) Masaj.KOGA:「Rehabilitation and Strengthening for Structures with Carbon Fibers」、No.5、Technical Research Report of N.S.I.and T. Association、p37～43、1993.11

6) T.HOSHIJIMA:「Strengthening of Reinforced Concrete Chimneys, Columns and Beams with Carbon Fiber Reinforced Plastics」、FRP Reinforcement for Concrete Structure -International Symposium- ACI.SP-138、1993

7) Y.KOBATAKE:「Seismic Retrofitting of Existing Reinforced Concrete Bridge Columns by Carbon Fiber Strand Winding Method」、Obayashi Technical Presentation Report、March 1994

Construction Automation Research

by

K. P. Chong and S. C. Liu
National Science Foundation

ABSTRACT

Construction processes are behind the state-of-the-art of manufacturing as well as computer sciences and control. Successful and efficient construction automation require robust, effective and flexible material handling, system integration, sensing and control, etc. A survey of mainly NSF supported research in construction is presented in this paper.

KEYWORDS: Construction automation; material handling; computer-integrated methods; robotics; sensing and control.

1. INTRODUCTION

Construction is one of the largest industry in the U.S.(Chong, et al, 1993; NCR, 1988), amounting to about 8% of the GNP and employing six million people (Rossow and Moavenqadeh, 1974). A bottleneck of construction research, development, and competitiveness is automation. Constructed systems include the traditional civil engineering structures (such as, buildings, bridges, tunnels, railways, airports and harbors), demolished constructed systems due to earthquakes, hurricanes, blasting and other natural/man-made hazards. In both cases there are mismatches between manufacturing know-how and construction; between computer science/control know-how and construction. Successful and efficient construction automation require robust and effective: material handling; data capture; artificial intelligence; system integration; operation research; computational mechanics in structured and unstructured (demolished) structures; sensing, pattern recognition, and control; qualitative vision analysis; prefabrication; intelligent and flexible robots, etc. The end product should be safe, durable, environmentally friendly and intelligent civil infrastructure systems (Chong, et al 1992; 1993). These techniques and research findings can also be applied to mining, ship construction and air-plane manufacturing.

Major objectives of the research in construction automation are:

1. To investigate construction dynamics of both structured and unstructured facilities.

2. Continue to develop a better understanding of analysis, design and construction processes, leading to basic principles and methods for robust automation.

3. Continue to support research efforts in computer integrated construction for the competitiveness of the construction industry and to build up the technology base.

4. Encourage multidisciplinary research collaborations among groups of academic, industry and government agencies.

5. Encourage knowledge and technology transfer to industry and users.

In a recent paper (Lewis, 1993+) the inclusion of various structures to automate was addressed. In buildings, the primary needs for automation occur in structure,

enclosure skin, interior finishes. In light industrial the primary needs are structure, piping, electrical. In heavy industrial the needs are piping, electrical, mechanical equipment. Finally, in power, chief requirements are in piping, mechanical equipment and electrical.

The Construction Industry Institute (CII) has studied what makes sense to automate (Tucker et al. 1990); the answers depend on the type of construction application(Business Roundtable Report 1982).

According to Hendrickson and Au (1989) construction automation makes sense in the following situations:

* in hazardous environments - e.g. outer space, nuclear reactors and undersea construction

* robotics permit broader use of non-human senses and constrained spaces

* robots are tireless

* to achieve improved quality, greater consistency and precision

* cost savings

Examples of existing construction robots have been documented by various researchers (e.g. Oppenheim and Skibniewski, 1988; Paulson, 1985; and Whittaker, 1986).

2. WORKSHOPS AND SYMPOSIA

Numerous workshop related to construction automation have been held. The following is a summary of three of the workshops sponsored by NSF.

o NSF workshop on "Construction Automation: Computer-Integrated Construction", April, 1987; John L. Wilson (Lehigh University).

The commonalty of directions is discussed under six headings (Wilson, 1987):

(a) System Architecture and Organizational Structure - an architecture is needed for open, interactive environment for computer applications in engineering, design, construction and facilities management.

(b) Structure, Formalization and Classification of Knowledge - research includes data requirements in each discipline and sharing between disciplines.

(c) New Languages and Representation Techniques - to provide unified, timely and accurate two-way communication among all parties.

(d) Intelligent Interfaces - to interface computer applications and databases intelligently with knowledge-based components.

(e) Designing for Automation - new design that recognizes the characteristics of construction machinery, including material handling, maintenance.

(f) Sensing and Monitoring - for dimensional/configuration control, materials/components identification, location and control, etc.

o "Technological Innovation in Construction", April, 1991; Dan Halpin (Purdue University)/R. Fechtig (ETH, Zurich).

Subjects considered as major activities are:

(a) Organizational structure and its impact on innovation and competitiveness

(b) Management of technological innovation in construction

(c) The influence of contracting forms on technological innovation and transfer

(d) Means of evaluating risks and potential returns on investments in advance technology

(e) Identification of major needs for advanced technology in individual countries

(f) Analysis of the process by which technologies have been successfully transferred

o "Research Needs in Automated Excavation and Material handling", April, 1993; B. Dendrou (ZEi/Mi Inc.) / R.Sterling (University of Minnesota) / M. Gaus (University at Buffalo).

Excavation technology is a key component in many publicworks activities and services which affect the national health and safety, standard of living and economic competitiveness. Furthermore, the relative importance of underground construction in infrastructure will increase drastically in the near future, as environmental and living standards rise. However, the U.S. underground construction industry at present is weak. The Directorate of Engineering at NSF recognizing the importance of this industrial basis has recently supported a review of excavation and underground technology in Europe and Japan. The results of this review clearly demonstrate the both the Japanese and Europeans are moving ahead of the U.S. in Research an Development, and innovation in automated excavation technology, which will position them to capture a potential world market worth 100 billion dollars over the next 10 years (this estimate reflects the findings of two recent surveys conducted for the directorate for Engineering at NSF).

Topics that are being addressed are the following:

* New developments of the Underground and Surface Space

* Automated Excavation and Materials Handling

* Site characterization and Modeling

Other Major symposia include the annual "International Symposium on Automation and Robotics in Construction(ISARC), the most recent one (10th Symposium) was held in Houston, Texas in May, 1993 (Watson, et al, 1993)

3. EXAMPLES OF RESEARCH AREAS AND PROJECTS

In 1987, NSF issued a "Construction Automation Research" Initiative, which was well received by the community. The following examples listed in the initiative are purely illustrative. The computer is expected to play a central role in all of these areas, in terms of modeling, analysis, representation, and control. The close coupling of the design process with construction via computerization will enhance constructability, functionality, flexibility, and maintainability of the end product.

* coupling of design and construction through project databases and knowledge bases

* design integration with construction process planning and control, end use, and maintenance

* computer models of the whole construction process (e.g., incorporating geometric and functional relationships in large spatial assemblies)

* methodologies for planning and scheduling of the whole construction process

* knowledge management (computer-based deployment and use of knowledge among interacting processes)

* adaptable construction systems (analogous to flexible manufacturing systems)

* logistics of parts, materials, and information

While robotics, sensing, metrology, materials handling, and other specific technologies may be included in the scope of proposed projects, the work supported by this initiative will focus on computer integration, and will be expected to produce new engineering knowledge relating to the systems integration of construction rather than to any individual operation or component of the process. Proposals may involve real systems and processes as well as more theoretical or simulation-based investigations. The research emphasis is on technical rather then management issues.

Strong involvement of industry in the proposed research is particularly encouraged. This may take several forms, such as establishment of a research advisory board including members from industry, or actual research collaboration between academic and industry engineers.

In the U.S., most of the basic physical systems research is carried out by materials and equipment manufacturers (e.g. W.R. Grace, Caterpillar Tractor, etc.). This is strictly product oriented research (Halpin, et al, 1991). Recent studies indicate that the U.S. has not been aggressive in transforming basic research in the construction area into marketable products (Gerwick, 1990). The Japanese excel in taking existing research and coverting it into market ready construction technology. In 1990, the senior author organized a panel of experts to visit strongholds and sites in Japan to assess its construction technologies. According to this report(Tucker, et al, 1991) Japanese companies have invested heavily in developing automated equipment, although they have produced very few practical pieces to date. Much of their motivation to automate stems from their desire to improve the unsafe, dirty, and unsophisticated reputation construction has among workers. A poor safety record can be cause for an owner to exclude a contractor from bidding his projects for a period ranging from 30 days to several months. Nevertheless, very few young workers are entering construction, leaving companies with an aging work force. The companies believe that automating construction equipment will make construction safer and give it a more technical aura.

Additionally, technological innovation can be used to help sell both existing customers and new prospects. Despite their push toward automation of construction equipment, Japanese companies do not use computers as widely as U.S. companies for schedule or cost control, relying instead on manual methods for the most part. However,

Table 1. Relative Status of Construction R&D in the U.S. and Japan.

CATEGORY	R & D		IMPLEMENTATION	
	STATUS	TREND	STATUS	TREND
Structural Steel	+	↑	+	↑
High-Performance Concrete	+	↑	-	↑
High-Performance Composites	+	↑	+	↑
Geotechnical Materials	+	↑	O	↑
Construction Contractors	+	↑		
Construction Suppliers	O	↑		
Universities	-	↓		
Government	O	→		

Coding System Japan Compared to the U.S.	
Status	**Trend**
< Far Behind	⇑ Pulling Ahead Strongly
- Behind	↑ Gaining Ground
O Even	→ Holding Constant
+ Ahead	↓ Falling Behind
> Far Ahead	⇓ Losing Quickly

Japanese companies are actively exploring ways to transfer information form CAD models to field equipment, including manipulation of that information and data from the surrounding environment using artificial intelligence. The reduced incidence of claims in Japanese construction may partially explain the less frequent use of computers in project controls. The following Table summarizes the relative status of construction R & D in the U.S. and Japan (Tucker, et al, 1991):

Initiatives such as the Civil Infrastructure Systems Research of NSF (Chong, et al, 1993; Lepkowski, 1993) and the Construction Productivity Advancement Research (CPAR) program of the U.S. Army Corps of Engineers are attempting to rectify this shortcoming by funding and/or encouraging technology transfer of construction technology.

In order to focus resources and accelerate technology development in architectural, engineering and construction related areas, research centers have grown up within the past decade to link industry and universities in cooperative efforts (Halpin, et al. 1991). Among these centers are:

(1) The Construction Industry Institute (CII) at University of Texas, Austin, TX

(2) NSF-ATLSS Engineering Research Center (ERC) on Large Structural Systems, Lehigh University, Bethlehem, Pennsylvania.

(3) Center for Integrated Facilities Engineering (CIFE), Stanford University, Stanford, California

(4) NSF-National Center for Earthquake Engineering Research, Sunny-Buffalo, NY

(5) NSF - ERC for Offshore Technology Research Center, Texas A&M University and University of Texas at Austin

(6) NSF - Science & Technology Center (STC) for Advanced Cement-Based Materials

(7) NSF - STC for Southern California earthquake Center, University of Southern California

(8) National Institute of Standards and Technology (NIST), Robot Systems Division (see Albus, et al 1992)

(9) U.S. Army Corps of Engineers Construction Engineering Research Laboratory (CERL)

(10) Factory-Built Housing Research Center Tennesse Technological University, Cookville, TN

The following are examples of NSF sponsored construction automation research projects related to civil infrastructure systems.

*Bob Tatum, Stanford University: "Mechanism and Strategies for Technological Innovation in Construction." For fundamental understanding of construction technology and to provide mechanisms/strategies for more rapid technical advancement.

*Chris Hendrickson/Dan Rehak, Carnegie Mellon University: "KBES Construction Planning Process." For the selection of construction technology, work tasks definition, costs/time/resources estimation and scheduling.

*Jeffrey Ullman, et al, Stanford University: "Integrated Data Exchange and Concurrent Design for Engineered Facilities." An integrating compute environment to support concurrent design with fast data exchange and powerful change management capabilities, and improve life-cycle facility management.

*Owen R. Mitchell, et al, University of Texas, Arlington: "Integrated Modeling and Control for Intelligent Material Handling." Intelligent Material handling systems approach for rapid deployment and automation of new material handling requirements in environments with uncertainties and minimal structure.

*Gerhard Fischer et al, University of Colorado at Boulder: "Supporting Collaborative Design with Integrated Knowledge-based Design Environments." Conceptual framework and prototype system for collaboration among members of design teams.

*Raymond Levitt, Stanford University: "The virtual Design Team: Simulation, Decision-making, and Information Flow in Concurrent, Multidisciplinary Design." Integration of AI and coordination theory to develop a virtual design team, which is an object-oriented, discrete event computer simulation model of the flow of decisions and information among participants in complex, multidisciplinary design projects.

* J.M. De La Garza, VPI: "Methods for Expediting the Transfer of Construction Technology." KBES and CAD are used in design/construction integration. Life-cycle applications and technology transfer are also investigated.

Yvan J. Beliveau, VPI: "Dynamic Damping of Payload Motion for Cranes." Develop a strategy for damping of payload motion for various kinds of cranes used in construction.

*J. Vanegas, Georgia Tech: "Integrated Design/Construction." For conceptual framework and model for infrastructure rehiblitation.

*J.S. Russell, University of Wisconsin-Madision: "Computer-Integrated Concrete Placement Systems." Built with existing pumped-concrete equipment.

*O.R. Mitchell, F.L. Lewis, University of Texas at Arlington: "Integrated Modeling and Control for Intelligent Material Handling." Allows rapid automation of any material handling requirements including uncertainties in the environment.

*M. J. Skibniewski, Purdue University: "Computerized Robotics Management for Construction Sites." A system to manage diverse robots on construction sites (Skibniewski, 1992; Russell, et al, 1990).

*William L. Whittaker, et al, Carnegie Mellon University: "Autonomous Retrieval of Buried Objects." To develop and integrate the perception, planning, and manipulation technologies needed for autonomously detecting, uncovering, and retrieving fragile buried objects, e.g. waste containers, munitions, and cables exposure.

*Boyd C. Paulson, Stanford University: "An object-Oriented Approach for integrated Project Management Software." To construct systems that offer greater flexibility, higher intelligence and better integration, using "building block"

*Victor E. Sanvido, Pennsylvania State Univeristy: "Applying Computer-Integrated Manufacturing Concepts to Construction." Identifies activites in construciton (in relationship to integrated Identifies activities in construction(in relationship to integrated manufacturing), techniques nad tools for construction automation.

*Carl Haas, et al, University of Texas-Austin:"Large Scale Manipulator Technology for Construction." Automation in piping construction, e.g. in power plants, petro-chemical and chilling plants

4. SUMMARY AND CONCLUSION

An overview of the state of the art and NSF projects in construction automation are presented. The authors hope that this paper will act as a catalyst, generating interest and further research in these areas. This paper reflects the personal views of the authors, not necessarily those of the National Science Foundation.

BIBLIOGRAPHY

Albus, J.S., Bostelman, R.V. and Dagalakis, N.G., "The NIST SPIDER, a Robot Crane," J. of Robotic Systems, October 1992.

Business Roundtable Report (BRR) B-3, Construction Technology Needs and Priorities, August 1982.

Chong, K.P., Liu, S.C., et al Civil Infrastructure Systems Research: Strategic Issues, NSF 93-5, Jan. 1993.

Chong, K.P., and Liu, S.C., "Engineering Research on Smart Materials," NSF Directions, Vol. 5, No. 5, 1992.

Halpin, D.W., et al, Technological Innovation in Construction, Purdue University, April 1991.

Halpin, D.W., "Automated Construction Technology: Background and Barriers," IABSE Proceedings P-147/90, August 1990.

Hendrickson, C., and Au, T., Project Management of Construction, Prentice Hall, 1989.

Lepkowski, W., "NSF Proposes New Infrastructure Research Unit," Chemical and Engineering News, P.27, June 7, 1993.

Lewis, F.L., "Robotics, Automation, and Machine Intelligence in Construction," J. American Institute of Constructors, to appear (1993+).

NRC (National Research Council), Building for Tomorrow - Global Enterprise and the U.S. Construction Industry National Academy Press, 1988.

Oppenheim, I.J., and Skibniewski, M.J., "Robots in Construction," Encyclopedia of Robotics, John Wiley & Sons, 1988.

Paulson, B.C., "Automation and Robotics for Construction," ASCE J. of Construction Engineering & Management, Vol. 111, No, 3, pp. 190-207, 1985.

Rossow, J.K., and Moavenzadeh, F., The Construction Industry, Department of Civil Engineering, MIT, 1974.

Russell, J. Skibniewski, M., and Vanegas, J., "Framework for Construction Robot Fleet Management System," ASCE Journal of Construction Engineering and Management, Vol. 116, No. 3, September, pp. 448-462, 1990.

Skibniewski, M. "Robot Implementation Issues for the Construction Industry," in Human Robot Interaction, Rahimi, M. and Karwowski, W., eds., Taylor & Francis Publishers, London, U.K., -Washington, D.C., ISBN 0-85066-809-3, pp.347-366, 1992

Tucker, R.L., et al, Construction Technologies in Japan Japanese Technology Evaluation Center (JTEC), Loyola College, Baltimore, MD, June, 1991.

Tucker, R.L., et al, CII Task Force, "Needs Assessment for Construction Automation," Construction Industry Institute, University of Texas-Austin, September 1990.

Watson, G.H., Tucker, R.L. and Walters, J.K. (eds), Automation and Robotics in Construction X, Elsevier, Amsterdam, 1993.

Whittaker, W.L., "Cognitive Robots for Construction," Annual Research Review, The Robotics Institute, Carnegie Mellon University, Pittsburgh, pp. 6-17, 1986.

Wilson, J.L., NSF Workshop on Construction Automation: Computer-Integrated Construction, Lehigh University, April, 1987.

Design Guidelines for Precast Reinforced Concrete Buildings

by

Shinsuke Nakata*, Masaomi Teshigawara*
Takashi Kaminosono* and Hitoshi Shiohara*

ABSTRACT

This paper introduces "Design Guidelines for Reinforced Concrete Buildings (draft)," under development as a part of Japanese PRESSS project. The guidelines has been drafted by Guidelines Drafting Working Group, and discussed in Design Guidelines Committee of Japanese PRESSS. Values of some design coefficients have not been finalized. Extensive commentary will accompany the guidelines to explain the concept behind requirements and to suggest methods of calculation.

1. INTRODUCTION

Japanese side PRESSS project team has already reported three research results; "Design Guidelines", "Construction Guidelines" and "Design Manual for Precast Connections".This introduces only seismic design concept from "Design Guidelines". This guidelines were completed by PRESSS Guidelines Drafting Group ; S.Otani, Chairman, University of Tokyo, M.Teshigawara, Secretary, Building Research Institute ,Y.Inoue, Housing and Urban Development Corporation , M. Hayashi, P.S. Corporation , T.Kaminosono, Building Research Institute, I.Kawabata Taisei Corporation , M.Kimizuka, Tokyu Corporation ,S.Nakata, Building Research Institute ,K.Yagishita, Toda Corporation ,K.Yoshioka, Ohbayashi Coporation .

2. SCOPE

The total height of a building shall be not more than 60 m. A structure, in each principal direction, shall consists of ductile moment-resisting frames, or ductile moment-resisting frames with continuous structural walls, or independent structural walls. The structural wall shall be continuous from the foundation to the roof level. Mass, stiffness and strength in a structure shall be arranged uniformly in plan and along elevation. Eccentricity ratio and rigidity ratio of a structure, specified in Building Standard Law Enforcement Order,Japan shall be not more than 0.15 and not less than 0.6, respectively. Height-to-width ratio of a building shall be not more than 4. The structure of a building shall be clearly planned to form a specified total yield mechanism, in which flexural yield hinges shall develop, as a general rule, at the ends of all floor beams and at the base of the first story columns and walls.

A building, designed and constructed under the guidelines, shall resist gravity loads and medium intensity ground motions to ensure serviceability, and shall not collapse during an intense ground motion. The building shall maintain serviceability during a strong wind and snow loading.

Precast connection (denoted as PCa connection) of PCa members shall be provided with strength sufficient to transfer member actions caused by specified design loads. The strength deterioration and slippage deformation at PCa connections shall meet "Evaluation Criteria for PCa Connection Performance".

PCa members and connections shall satisfy required serviceability, durability and fire resistance.

3. MATERIALS

Quality, mix, production, materials of concrete and precast concrete specified for RC members shall meet the provisions of Japan Architectural Standard Specification JASS-5

* Building Research Institute
Ministry of Construction ,Japan

"Reinforced Concrete Work".

Quality and types of concrete for PCa connection shall be as good as or superior to those of concrete specified for RC members. Quality, mix, production and materials shall meet the provisions of "PRESSS PCa Construction Guidelines." Grade and quality of reinforcing bars shall meet Japan Industrial Standards (JIS) G-3112 "Steel Bars for Concrete Reinforced." Compressive strength of mortar used in PCa connection shall be not less than that of concrete specified for RC and PCa members. Types, quality, mix, production and materials shall meet the provisions of "PRESSS PCa Construction Guidelines."

Reinforcing bars can be jointed by gas pressured welding, flare welding, lap splicing and other joints specially approved by Minister of Construction.

Work of gas pressured welding shall meet "Guidelines for Gas Pressured Welding for Reinforcing Bars" issued by Japan Gas Pressured Welding Institute.

Steel plates can be jointed by welding or high tension bolts. Work of welding and high tension bolt friction joint of steel plates and work of flare welding of reinforcing bars shall meet the provisions of JASS-10 "Precast Concrete Work" and JASS-6 "Steel Work".

Table 1 : Types and nominal strength of concrete specified for RC and PCa members

Type of Concrete	Specified Concrete Strength (kgf/cm2)
Normal Concrete	210 - 360
Light-weight concrete	210 - 270

4 .EARTHQUAKE RESISTANT DESIGN (NONLINEAR ANALYSIS PROCEDURE)

4.1 Outline of Structural Design

This section defines the structural design method for structural members. Structural design of PCa members may follow the methods for RC members.

Design for Gravity Loads

Stress in every part of structural members under dead load, live load, and snow load, specified in Building Standard Law Enforcement Order, shall not exceed allowable stresses for long-term loading . Design of structural members in the super-structure under earthquake loads shall conform to two cases provisions ; nonlinear analysis or linear analysis . However,design of a building of more than 31 meters in height shall conform to the provisions of nonlinear analysis .

The performance of super-structure, basement and foundation structure of a building shall be examined for serviceability limit state under medium intensity earthquake motions and for ultimate limit state under an intense earthquake motion.

4.2 Method of Earthquake Resistant Design

(1) Earthquake resistant design shall be based on a static nonlinear analysis of a building under monotonically increasing lateral loading taking into account realistic elastic and inelastic characteristics of constituent structural members.

(2) The analysis may be carried out in the longitudinal and transverse directions, separately.

(3) Lateral load shall be increased monotonically in the analysis under dead loads, specified in Article 84 of Building Standard Law Enforcement Order, and live load for earthquake load calculation.

4.2.1 Serviceability Limit State

Design story shear Qi at story i for the serviceability limit state design under the action of an earthquake motion shall be

$$Qi = Ci\ Wi \qquad (4.1)$$

$$Ci = Z\ Rt\ Ai\ CB \qquad (4.2)$$

where,Ci: story shear coefficient, Wi: sum of dead and live loads above the i-th story, Z: seismic zone coefficient, Rt: vibration characteristic coefficient, Ai: coefficient for story shear distribution, CB: standard base shear coefficient of 0.2. Coefficients Z, Rt, and Ai are defined in Notification No. 1793 of Ministry of Construction, 1980.

4.2.2 Ultimate Limit State

Required lateral load resisting capacity Quni of story i for the ultimate limit state design shall be

$$Quni = Cuni\ Wi \quad (4.3)$$
$$Cuni = Z\ Rt\ Ai\ CunB \quad (4.4)$$

where,Cuni: story shear coefficient for ultimate limit state design, Z, Rt, Wi, and Ai are defined in Section 4.2.1, CunB: standard base shear coefficient of 0.3 for moment-resisting frame structures, and 0.3, 0.35, and 0.4 for wall-frame structures in which structural walls resist up to 30%, 30 to 70%, and over 70% of the base overturning moment at design limit deflection Ru1, respectively. Fig.1 shows the outline of this design criteria.

4.3 Nonlinear Incremental Lateral Load Analysis

4.3.1 Modeling of Building

(1) A building structure may be idealized as a series of plane frames in a principal direction if the effect of torsion and transverse frames can be neglected.

(2) If the effect of torsion and transverse frames cannot be neglected, a building must be analyzed as a three dimensional structure.

(3) The lateral displacement of the parallel frames at each floor level may be assumed to be equal.

(4) A structure shall be analyzed including super-structure and sub-structure.

4.3.2 Lateral Force Distribution

The distribution of lateral loads shall be the same as the one assumed in the serviceability limit state design

4.3.3 Lateral Loading Analysis

(1) Horizontal loads shall be assumed to act at the floor level of each floor.

(2) The analysis may terminated when the maximum story drift angle of a story reaches a design proof drift angle of Ru2.

4.3.4 Modeling of Structural Members

(1) A column and beam shall be represented by a line member considering the following deformations:

Column: Bending, shear and elastic axial deformations,

Beam: Bending and shear deformations.

(2) A beam-column connection may be assumed to deform in shear, or to be rigid in a region specified in Commentary of Article 8.2 in "Standard of Structural Calculation for Reinforced Concrete Structures" of Architectural Institute of Japan.

(3) Inelastic deflection of a column and beam may be assumed to concentrate at the member end, represented by rotation of a rigid-plastic rotational spring.

(4) Shear, flexural and axial deformations at section centroid of a structural wall shall be included in the model.

(5) The deformation of soil and piles shall be considered in the analysis if appropriate.

4.4 Stiffness and Strength of Structural Members

4.4.1 Elastic Stiffness

(1) The effect of reinforcing bars and orthogonal members shall be included in the flexural stiffness of a member.

(2) Shape factor for shear deformation may be taken to be 1.2 as a rectangular section.

4.4.2 Hysteresis Model

(1) The stiffness characteristics of a column and beam under monotonically increasing load may be assumed to be of trilinear type with stiffness changes at flexural cracking of concrete and tensile yielding of longitudinal reinforcement.

(2) Axial stiffness of a column may be assumed to be proportional to axial load.

(3) Stiffness characteristics of a structural wall shall be evaluated separately for shear and flexure. Stiffness in shear shall be assumed to change at shear cracking and shear strength, represented by a trilinear relation. Stiffness in flexure shall be assumed to change at flexural cracking and yielding, represented by a trilinear relation.

4.4.3 Yield Resistance of Structural Members

Yield resistance of structural members shall be evaluate using material strength specified in Chapter 3.

4.5 Performance Criteria at Serviceability Limit State

The building shall satisfy the followings at design earthquake load for serviceability limit state specified in Section 4.2.1;
(1) No flexural yielding shall occur in structural members, and
(2) Story drift angle at each story shall be less than 1/200 rad.

4.6 Performance Criteria at Ultimate Limit State

4.6.1 Performance Criteria at Design Limit Deflection

At the maximum story drift angle of a story reaching design limit deflection of Ru1 rad, the story shear at each story shall exceed 0.9 times the required lateral load resisting capacity. The design limit deflection, Ru1, shall be as follows:

Frame structure: 1/100 rad.,
Wall-frame structure: 1/100. 1/120, or 1/150 rad.,

in which structural walls resist up to 30%, 30 to 70%, and over 70% of the base overturning moment at design limit deflection Ru1, respectively. (refer to Fig.1)

4.6.2 Performance Criteria at Design Proof Deflection

At the maximum story drift angle of a story reaching a design proof deflection of Ru2 rad., the structure and structural members shall satisfy the followings; where, the design proof deflection in terms of story drift angle shall be given below:

Frame structure: 1/50 rad.,
Wall-frame structure: 1/50, 1/60, and 1/75 rad.,

in which structural walls resist up to 30%, 30 to 70%, and over 70% of the base overturning moment at design proof deflection Ru2, respectively.
(1) The story shear at each story shall exceed the required lateral load carrying capacity specified in Section 4.2.2,
(2) The deformation at a specified yield hinge of each structural member shall not exceed the deformation capacity, and
(3) The resistance other than the specified yield hinges in each structural member shall be greater than the design force amplification factors a times the stress calculated at the design proof deflection. The design force amplification factors shall be as follows;

a) a_1 for shear and bond stress of girders,
b) a_2 for flexural moment of columns,
c) a_3 for shear and bond stress of columns,
d) a_4 for flexural moment of walls,
e) a_5 for shear of walls,
f) a_6 for shear in beam-column connections,

(4) Axial force in columns shall be less than 2/3 Nu and 3/4 Nt, where Nu: ultimate compressive strength of the column, and Nt: ultimate tensile strength.

4.6.3 Limit of Axial Stress in Exterior Columns

Axial force in corner columns under bi-direction earthquake loading shall be less than 2/3 Nu and 3/4 Nt.

4.6.4 Design of PCa Connections

Design stresses for PCa connections shall be equal to the stress developed at the connections calculated at the design proof deflection Ru2 multiplied by amplification coefficients specified in 4.6.2. Design of PCa connections shall conform to the provisions of "PRESSS Design Manuals for PCa Connections."

5 DEMAND TO CONNECTION PERFORMANCE

The equivalent monolithic connection has three subcategories including
(1) equivalent monolithic strong connection (EMSC),
(2) equivalent monolithic ductile connection (EMDC),
(3) equivalent monolithic extensible connection (EMEC).

These are sumarized as shown in Table 2. The object of this chapter is to give quantitative definition to the performance of good connection designed by emulation approach.

The demand of equivalent monolithic connection is summarized as follows;

a) Design moment and/or forces for connections and precast elements can be predicted by the structural analysis generally used for monolithic system.

b) Connections are strong enough to transfer the design moment and/or forces. If the connection failure or yielding occurred in early stage of loading, unexpected failure or yielding mode of precast system will take place. To avoid such change of structural performance of precast system, connections should have at least comparable strength to equivalent monolithic system.

c) Serviceability, durability and fire resistance are as same as in monolithic system.

Specified conditions for monolithic system are also applied to precast system. Items to be considered are deflection, crack width, creep and shrinkage of concrete and mortar, concrete cover thickness, corrosion protection, fire protection, mechanical properties of connection materials under high temperature

d) Structural performance of precast system under earthquake loading is comparable to that of monolithic system. Precast system should have at least comparable deformation capability and same collapse mechanism to equivalent monolithic system for lateral loading. Maximum inter story drift angle of precast system during an earthquake should be within the limit specified for monolithic system even if some slip deformation take place at connection interface. Allowable limit of ship deformation is given in terms of the ratio of the additional inter story drift angle due to slip to the total inter story drift angle .

6. CONCLUSION

As a Japanese side for U.S. - Japan Cooperative Research Program on Precast Seismic Structural System (PRESSS) , the research results were completed ; "Design Guidelines for Monolithic Reinforced Concrete Buildings" "Construction Guidelines" and "Design Manual for Precast Connections". Since 1989, we ,U.S.-Japan PRESSS Project Team aimed most advanced methodology for the targets of this project. That lead to really fruitful discussion from the viewpoint of research methodology.

Table 2 : Classification of Connection Performance for equivalent monolithic connection

Construction Method	Type of Connection	Description
	strong connection (EMSC)	rigid connection for non-yield part
equivalent monolithic	ductile connection (EMDC)	rigid connection for yield part
	extensible connection (EMEC)	connection for non-yield part

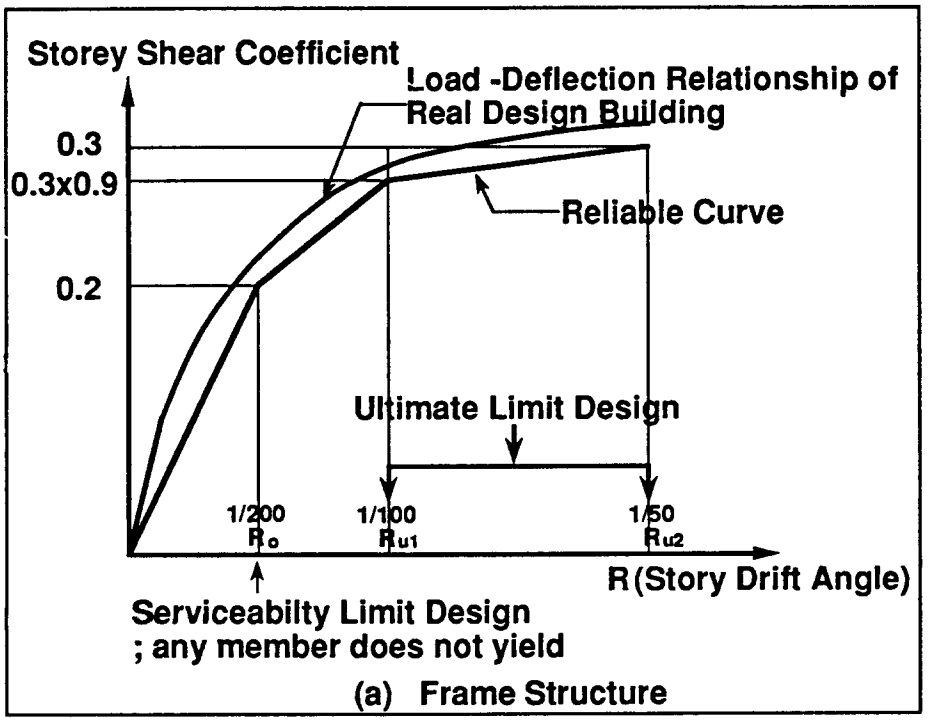

(a) Frame Structure

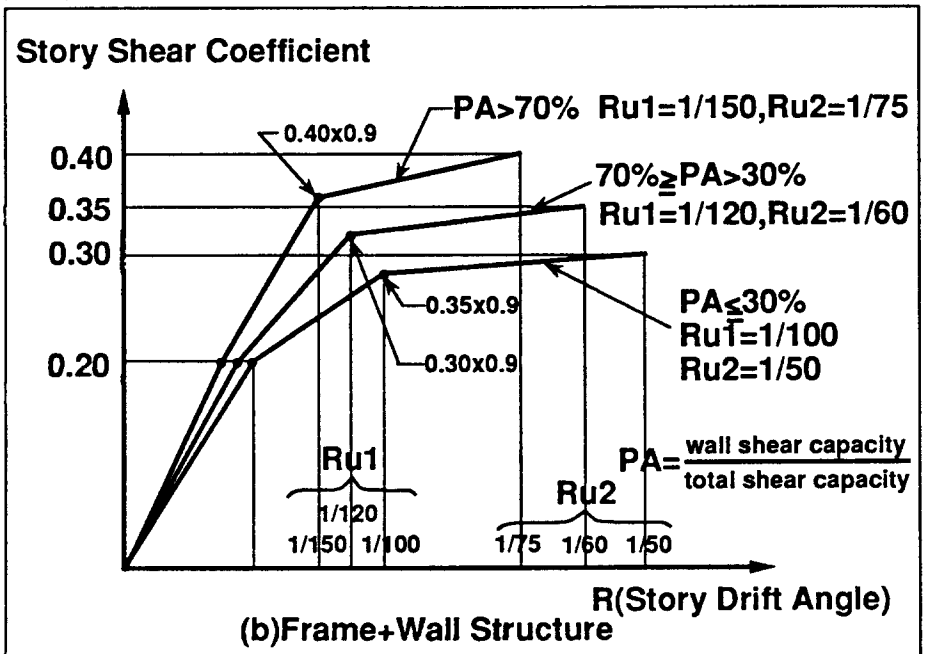

(b)Frame+Wall Structure

Fig.1 OUTLINE OF PRESSS SEISMIC DESIGN

A Post-Earthquake System for Estimating Seismic Damage to Road Facilities by a Strong Motion Observation Network

by

Hisanori Otsuka[1], Ryoji Hagiwara[2] and Yoshio Ninomiya[3]

ABSTRACT

The Ground Vibration Division of the Public Works Research Institute studies procedures for efficiently inspecting road facilities immediately after an earthquake. This paper presents a system for estimating seismic damage to bridges using data from real-time-transmitting accelerographs stationed in a strong motion observation network.

KEYWORDS: Strong Motion Observation Network, Seismic Damage, Spectrum Intensity, Earthquake Hazard Information

1. INTRODUCTION

Japan largely depends on road traffic for transportation of people and commodities. Roads also play an important role in providing lifelines and supporting urban activity.

Thus, after an earthquake, immediate repair and restoration are required. In the aftermath of an earthquake, many road administrators such as the Ministry of Construction, local governments and so forth, require employees and contractors to inspect road facilities, direct traffic, establish detours and restore damaged facilities.

Earthquakes in large cities pose special problems since roads are congested and roadsides are densely built-up. Therefore, immediate traffic recovery and restoration of road facilities are of special concern there. This requires a reasonable number of accelerographs to be taken. Estimating seismic damage to road facilities immediately after an earthquake would allow inspection of road facilities to be conducted efficiently. The Work Office of the Regional Construction Bureau, Ministry of Construction plans to install about 10 accelerographs and establish the first phase of a Strong Motion Observation Network in this fiscal year.

This paper will discuss a system for estimating both ground vibration characteristics at random points and seismic damage to reinforced concrete piers.

Both recorded accelerograms and observed damage to road bridge piers, which occurred during the 1993 Kushiro-Oki Earthquake are used to check the validity of this system.

2. SYSTEM FOR ESTIMATING SEISMIC DAMAGE

Figure 1 shows flow of information. When an earthquake occurs, real-time-transmitting accelerographs record strong motion and transmit the data to a Work Office immediately. The Work Office measures ground vibration characteristics such as maximum acceleration and Spectrum Intensity from all administered accelerographs, and estimates seismic

1) Head, Earthquake Engineering Division, Public Works Research Institute, Ministry of Construction, Tsukuba City, Japan
2) Head, Ground Vibration Division, ditto
3) Senior Research Engineer, ditto

damage with an Engineering Work Station (EWS). The estimated results are shown in the EWS at the Work Office and used for the inspection and so forth. The allowable timelag from occurrence of an earthquake to display of estimated seismic damage is considered to be only several minutes.

Figures 2, 3 and 4 show examples of display in the EWS, i.e., epicenter, locations of seismic-damaged road facilities and a liquefaction hazard map, respectively.

To establish a system based on strong-motion data, map data, road facility data and ground data, we designed a program to calculate the following and display the results at the EWS:

(1) Epicenter location
(2) Horizontal maximum acceleration and Spectrum Intensity at each mesh in a map and important road facilities
(3) Liquefaction potential of meshes in a map
(4) Seismic damage to road facilities

This paper presents methods to calculate both Spectrum Intensity at random points, and the degree of seismic damage to reinforced concrete piers of bridges.

3. ESTIMATION OF GROUND VIBRATION CHARACTERISTICS AT RANDOM POINTS

Strong motion data in the estimation system is transmitted immediately from accelerographs to an EWS at a Work Office. To produce useful information from these data, we need to estimate ground vibration values which can estimate the seismic damage to each type of road facility. Since it is well known that Spectrum Intensity (SI)[1] has a high correlation to damage to road bridge piers, the authors adopted SI to estimate such damage. Three methods to calculate SI are presented and observed SI values are compared. Strong motion data observed at 12 points in the 1993 Kushiro-Oki Earthquake are used to calculate the observed SI values.

Table 1 and Figure 5 show observed SI and strong motion observation points[2], respectively.

Three different methods to calculate SI are as follows.

3.1 A method based on attenuation formulae using a strong motion data base

SI can be represented by the following formula according to the definition proposed by Housner[3] :

$$SI=\int_{0.1}^{2.5} Sv\ (T,\ h=0.2)\ dT \cdots\cdots\cdots\cdots (1)$$

where SI : spectrum intensity (cm)
Sv : velocity spectrum (cm/sec)
T : natural period (sec)
h : damping factor

SI Attenuation formulae are obtained using 394 components of horizontal strong motion shown in the Seismic Design of Specification for Highway Bridges[4] . When ground classification and formula patterns are the same as those used in the specifications[5], the following formula can be obtained:

$$\{SI(M,\ \Delta,\ GCi)\}=\begin{Bmatrix} 65.056\times 10^{0.2557M} \\ 7.181\times 10^{0.4398M} \\ 11.341\times 10^{0.4241M} \end{Bmatrix}\times\left(\Delta+30\right)^{-1.224} \cdots (2)$$

where M : magnitude of an earthquake
Δ: distance from the epicenter
GCi : ground type (i=1,2,3) indicated in Specifications for Highway Bridges

SI at a random point is calculated by the formula (2) for the ground type at the point.

3.2 A method based on attenuation formulae using observed strong motion data

Since the formula in 3.1 are based on data from all of Japan, the dispersion of data

is large. Therefore, SI should be calculated by a method considering characteristics of both the earthquake and the local ground conditions. Thus SI attenuation relationships are formulated based on the data obtained in the Strong Motion Observation Network. The procedure to derive the new formulae is the same as 3.1.

3.3 A method for calculating directly from observed strong motion data

When the epicenter and the magnitude of an earthquake are known, the methods presented in 3.1 and 3.2 can be used. But SI at any point can be directly calculated without those methods from strong motion data from observation points. SI is calculated considering the distances from the calculation point to observation points, based on the following formula :

$$SIp = \overline{SI} + \frac{1}{n}\sum\left\{\left(SIi - \overline{SI}\right)\frac{\overline{L}}{Li}\right\} \cdots \quad (3)$$

where SIp : SI at the point concerned (cm)
SI : The average SI of all observation points (cm)
n : The number of observation points used in the calculation
SIi : SI at observation point i
L : The average distance from all observation points to each calculation point
Li : Distances from all observation points to one particular point

In this paper, n equals 11, SI and L are the average value of 11 points excluding the point concerned. Since the number of observation points is relatively small, the values obtained using formula (3) are multiplied by 0.76 for ground types II and III. Here, 0.76 was derived from the relation between the attenuation formulae in (2). Thus in this paper, the third method had to use information concerning the epicenter and the magnitude of the earthquake. If we have enough observation points for each ground type, we do not need such information.

3.4 Comparison of 3 methods

Figure 6 shows observed SI and the results calculated by the methods proposed in 3.1, 3.2 and 3.3.

Where (a): observed values and attenuation curves
(b): points plotted in coordinates of observed values and calculated values, and lines drawn as observed value = calculated value.

Figure 6 (a) indicates that the attenuation curve of (1) in 3.1 for the ground type III is the largest, following by II and I (I < II < III). However the difference between II and III is small. Major observation values are plotted above those curves.

Because the curves of 3.2 consider characteristics of the earthquake and the local ground conditions, it is clear that the attenuation curves coincide with observation values.

In Fig.6(b), almost all points due to 3.1 are below the solid line: i.e. the calculated value is smaller than the observed value shown in Fig.6(a). The solid line is located in roughly the center of the points derived in methods of 3.2 and 3.3. Calculated systematic error and dispersion are small. In method 3.3 only distance from an observation point to a point concerned is considered, but in method 3.2, the direction to the epicenter is also considered, thus it can be said that the latter is better than the former. However, it is difficult to evaluate characteristics of the local seismic amplification at any ground in the method of 3.2. On the other hand, the method of 3.3 can calculate automatically the ground vibration characteristics of the observation point; accordingly, SI can be accurately calculated when the point concerned is

similar to neighboring observation points in ground seismic amplification. This method can be improved to reflect more local characteristics based on the accumulation of strong motion data and ground seismic amplification data. In addition, the fact that this method does not require the information of the epicenter and magnitude of the earthquake is a great advantage, because this system must automatically calculate SI values immediately after an earthquake.

4.CALCULATION OF SEISMIC DAMAGE TO ROAD BRIDGE PIERS

The authors estimated seismic damage to 10 road bridge piers using strong motion characteristics (SI) calculated by the method proposed in 3.3. Road bridges damaged by the 1993 Kushiro-Oki earthquake are used. The difference between the degree of actual damage to piers due to the Kushiro-Oki Earthquake and the degree of estimated damage is considered.

4.1 Seismic damage and characteristics of objective bridges

10 bridges were selected considering degree of damage (3 class) and ground type (3 types) among damaged bridges located on national highways and prefectural roads. Figure 7 and Table 2 represent structural characteristics and degree of seismic damage of these bridge piers, respectively.

As shown in Figure 7, severe damage was caused by shear cracking at the ends of reinforced bars in reinforced concrete circular-column piers.

4.2 A method for earthquake response analysis

Table 2 also shows estimated SI and estimated ductility factor μ. Ductility factor μ is defined as the ratio ($\delta/\delta y$) of response displacement at the top of the pier δ to the yield displacement at the same point δy. An Analytical model of a reinforced concrete pier is assumed to be a 1-mass system (see Fig.8). Subjecting this model to earthquake motions of 3 different SI values (30, 60 and 150 cm), provided the ductility factors are shown in Fig.9. Input motions for earthquake response analysis were adjusted in amplitude to attain the target values of SI. Estimated μ values in Table 2 were thus obtained for each pier.

4.3 Comparison of actual damage and estimated damage for study bridges

Figure 10 shows analytical results as components of both ductility factors and allowable ductility factors. This figure indicates that wall-type piers were not damaged when μ was less than 4, but circular-column piers were damaged even at a μ value of 1.5. Theoretically, circular column piers are supposed to be more resistant to earthquake-induced damage, but this not actually the case. According to this figure, circular-column piers were damaged at $\mu/\mu a \geqq 0.7$ (solid line), in which μa is the allowable ductility factor.

5.CONCLUSION

We have examined system for estimating seismic damage to road facilities by a strong motion observation network. In this paper, methods for both calculating spectrum intensity at any point and evaluating the degree of seismic damage to reinforced concrete piers were considered. The following results were obtained:

(1)The methods of estimating SI at random points using attenuation formulae based on observed strong motion data and considering the weighted distances show a good coincidence of observed values.

(2)For damage to piers, earthquake response analysis using SI-adjusting input motion was conducted. As a result of these calculations, the relationship between

SI and the ductility factor is clarified. Therefore, if estimated SI values are known after the earthquake, ductility factors can be obtained without complicated response analysis.

(3)Wall-type piers are damaged when μ is more than around 4 and circular-column piers are damaged when $\mu/\mu a \geqq 0.7$.

6. ACKNOWLEDGEMENTS

This study was conducted by PWRI and Kanto Regional Construction Bureau. The authors wish to express their thanks to the Hokkaido Development Bureau and the Hokkaido prefectural government for collecting the material.

[1] Ninomiya Y. Tokida K, Otsuka H: Response Analysis for Ground Vibration Characteristics and Damage to Structures The 22nd JSCE Earthquake Engineering Symposium, 1993.6 (in Japanese)

[2] Otsuka H, Yoshimi S: Chap.1 Earthquake and Ground Vibration, Report on the Disaster Caused by the 1993 Kushiro-Oki Earthquake, PWRI, 1994.6 (in Japanese)

[3] G.W. Housner: Behavior of Structures During Earthquakes ASCE, 1959.10

[4] Japan Road Assosiation: Specifications for Highway Bridges part V : Seismic Design, 1990.2

[5] Kawashima.K, Aizawa.K, Takahashi.K: Attenuation of Peak Ground Motions and Absolute Acceleration Response Spectra, Report of The Public Works Research Institute, Ministry of Construction, Vol.166, 1985.9 (in Japanese)

Table-1 Observation SI

No.	Observation Point	Ground Type	Distance from the epicenter Δ (km)	S I Observation (cm)
1	Chiyoda Bridge	I	81	62.9
2	Horoman Bridge	I	141	12.5
3	Otanoshike Bridge	II	20	92.6
4	Ishikari-kako Bridge	III	251	19.2
5	Shari Bridge	II	119	74.4
6	On-netoh Bridge	II	101	91.2
7	Hiroo Bridge	I	108	40.6
8	Shimamatsuzawa Bridge	II	231	15.6
9	Sapporo IC Viaduct	II	241	42.7
10	Ohtsu Bank	III	63	135.8
11	Sarukawa Bank	II	197	66.5
12	Mukawa Bank	III	200	62.4

Table-2 Specification and damages of the study bridges

Degree of Damage	No.	High Way Route Town	Bridge	Foundation Type	Objective pier		Ground Type	Distance from the epicenter Δ (km)	Estimated S I (cm)	Estimated μ	Damage
Severe Damage	1	Prefectural Road Taiki-machi	Yoda Bridge	Pile	P_3	Circular column	II	82	93.1	4.66	Fracture of Reinforcement (Cut-off Point)
	2	National High Way 240 Akan-machi	Matsunoe Bridge	Caisson	P_3	Circular column	I	39	70.2	1.40	Buckling of Reinforcement (Cut-off Point)
	3	Prefectural Road Onbetsu-machi	Hatsune Bridge	Pile	P_4	Circular column	II	42	91.7	1.83	Shear Cracking (Cut-off Point)
Minor Damage	4	Main Prefectural Road Shibecha-machi	Shintawa Bridge	Spread	P_1	Wall type	I	56	62.5	4.38	Cracking
No-Damage	5	National High Way 391 Shibecha-machi	Gozikkoku Bridge	Caisson	P_2	Circular column	II	46	84.2	2.11	No-Damage
	6	Prefectural Road Akan-machi	Assamugawa Bridge	Spread	P_1	Circular column	I	36	72.1	1.44	No-Damage
	7	National High Way 38 Shiranuka-machi	Koitoi Bridge	Spread	P_2	Wall type	I	23	85.5	3.42	No-Damage
	8	National High Way 44 Nemuro-city	On-netoh Bridge	Caisson	P_8	Wall type	II	101	69.1	1.38	No-Damage
	9	National High Way 44 Kushiro-machi	Takadai Bridge	Pile	P_1	Wall type	III	18	95.2	2.38	No-Damage
	10	National High Way 38 Kushiro-city	Otanoshike Bridge	Pile	P_1	Wall type	II	20	75.6	3.40	No-Damage

Table-3 Input motion used for analysis

Ground Type	Observation Values			Input Motion		
	Name Distance from the epicenter	Amax (gal)	SI (cm)	No.	Amax (gal)	SI (cm)
I	Chiyoda Bridge LG Δ =81km	345	62.9	I - 1	159.7	30
				I - 2	493.4	90
				I - 3	822.3	150
II	Otanoshike Bridge LG Δ =20km	456	92.6	II - 1	147.8	30
				II - 2	443.4	90
				II - 3	739.0	150
III	Ohtsu Bridge TR Δ =83km	314	135.8	III - 1	63.3	30
				III - 2	207.9	90
				III - 3	346.5	150

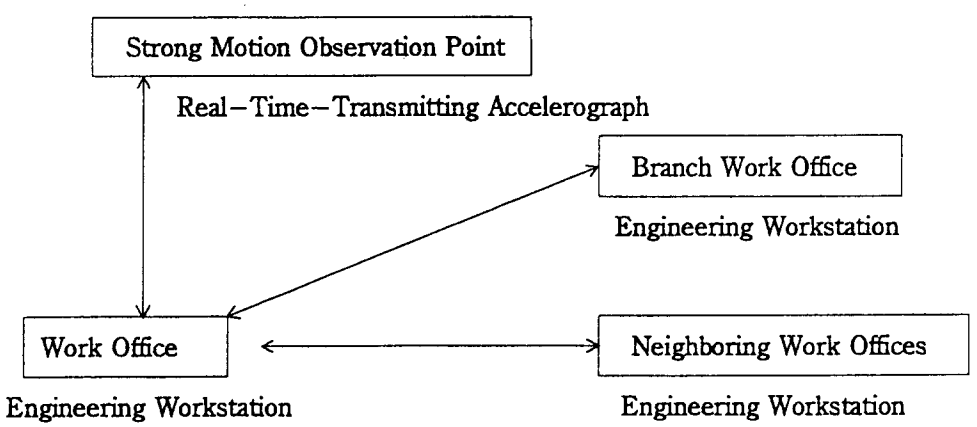

Fig-1 Flow of Information

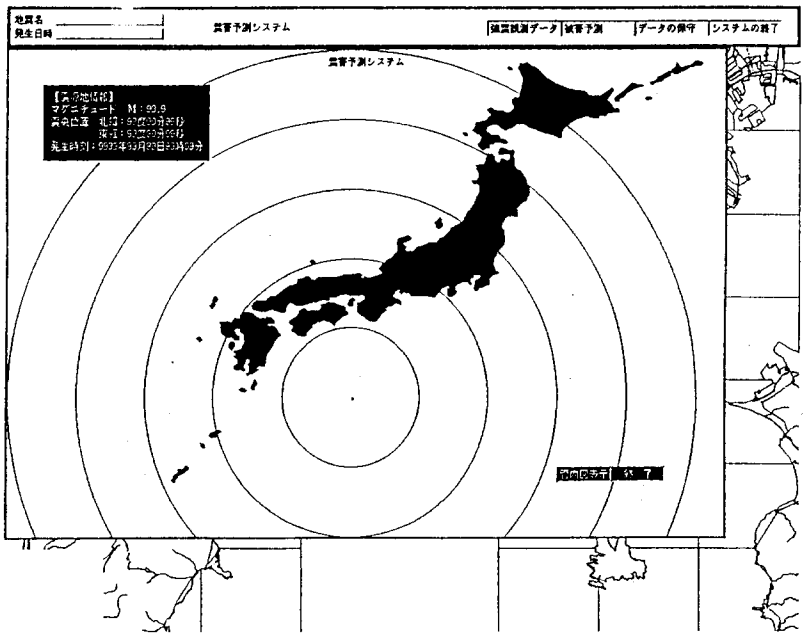

Fig-2 Calculation of location of an epicenter

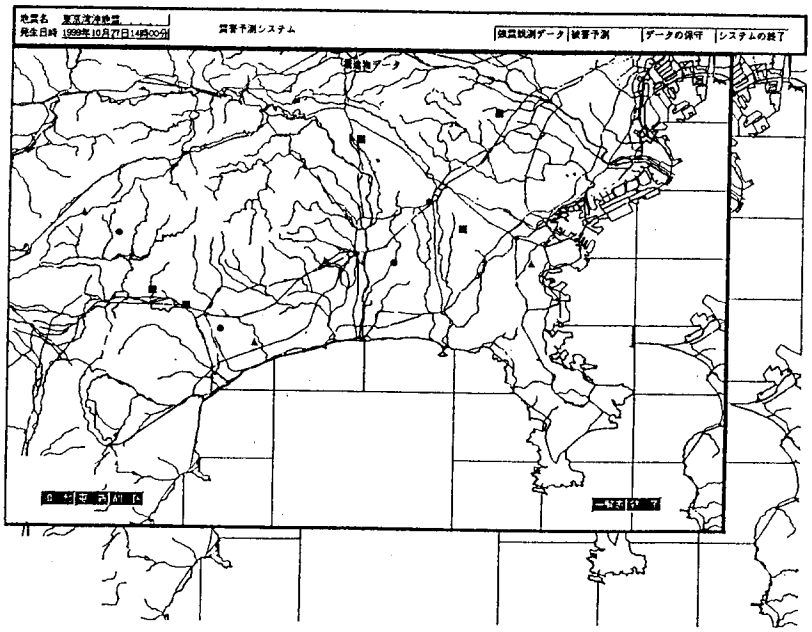

Degrees of seismic damage

Fig-3 Locations of seismic-damaged road facilities

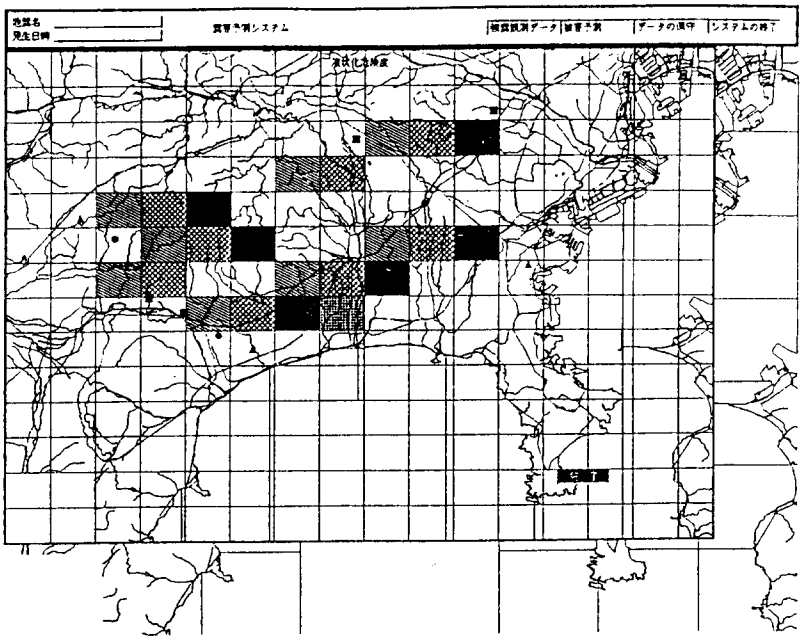

Fig-4 Liquefaction hazard map

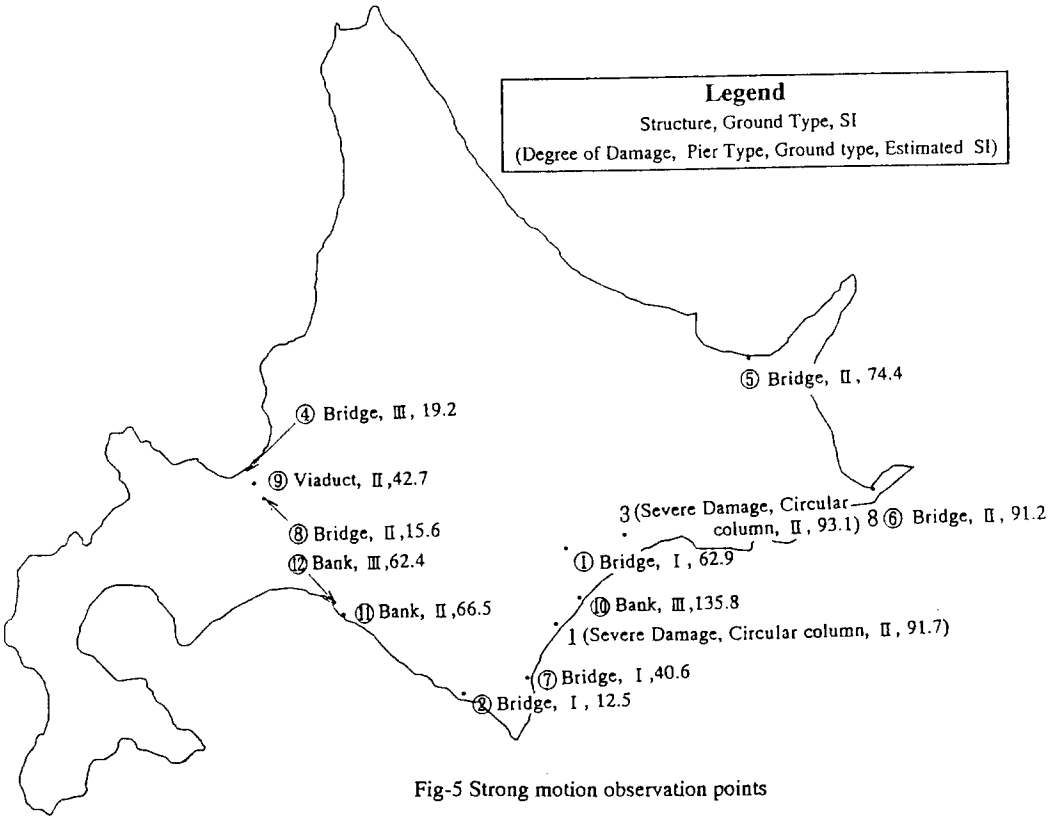

Fig-5 Strong motion observation points

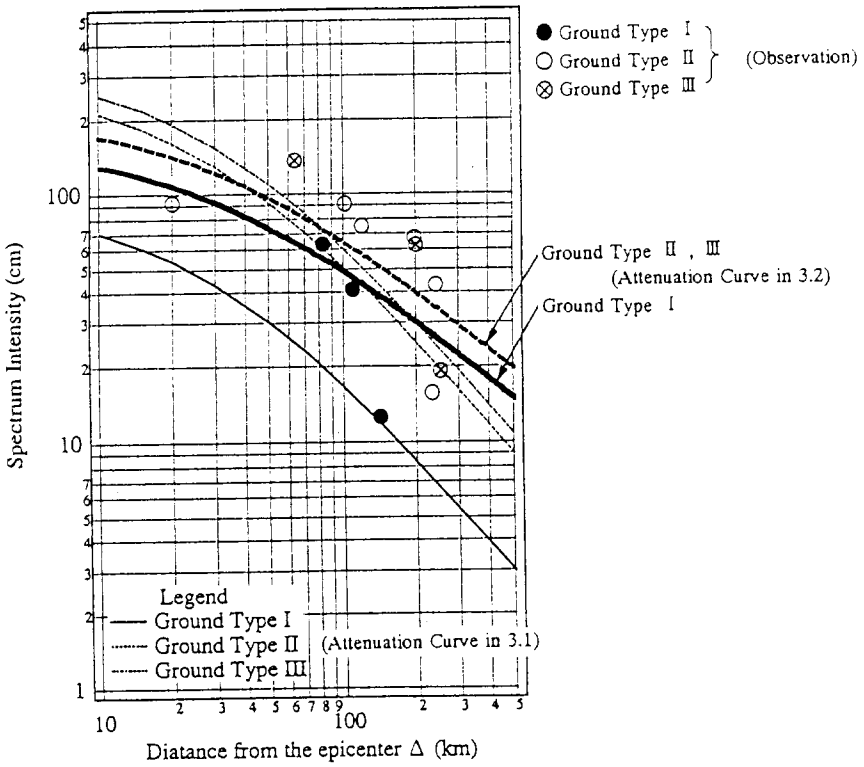

(a) The comparison between observed SI and predicted SI

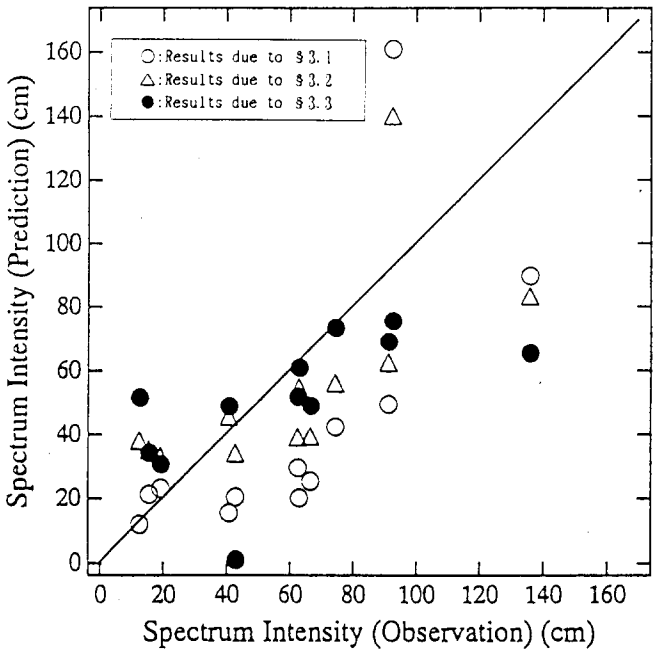

(b) The relationship of observed SI and estimated SI

Fig-6 The comparison of observed SI to estimated SI

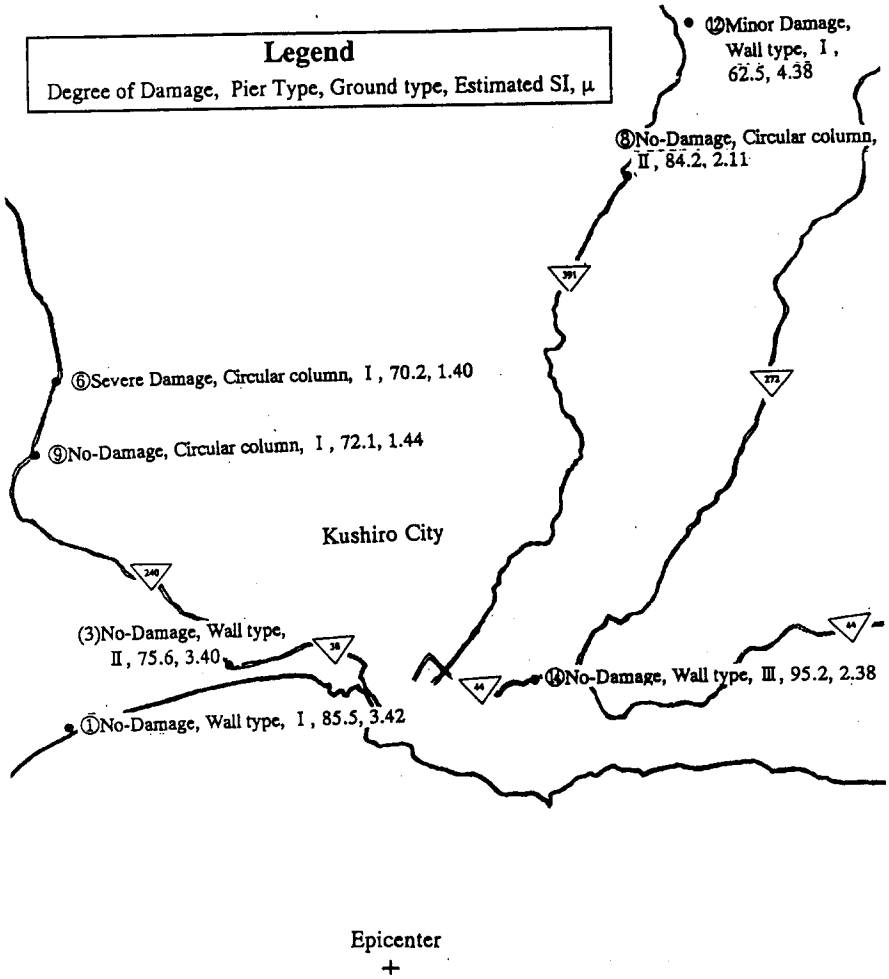

Fig-7 Road bridge points for seismic response analysis

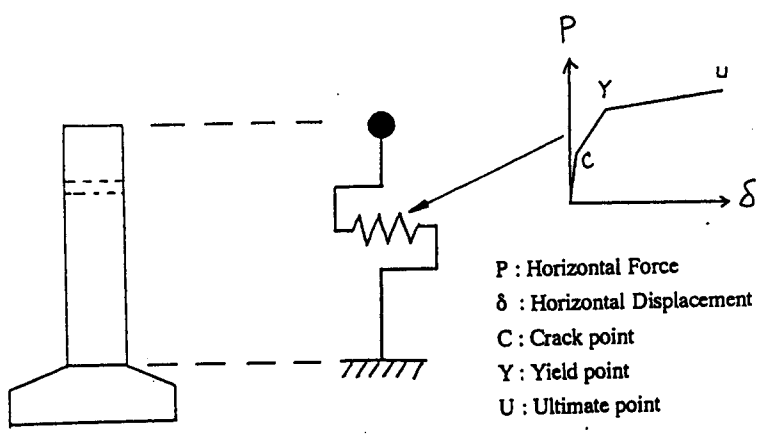

Fig-8 Analysis model

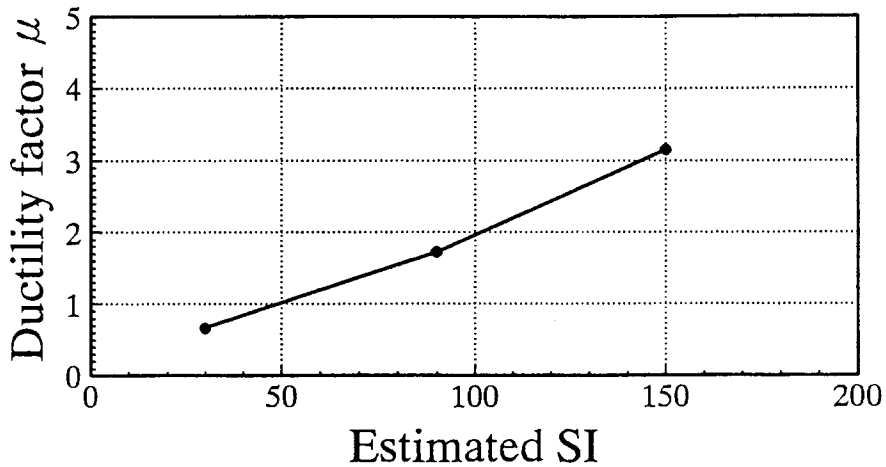

Fig-9 Relation between ductility factor and Spectrum Intensity (Hatsune bridge)

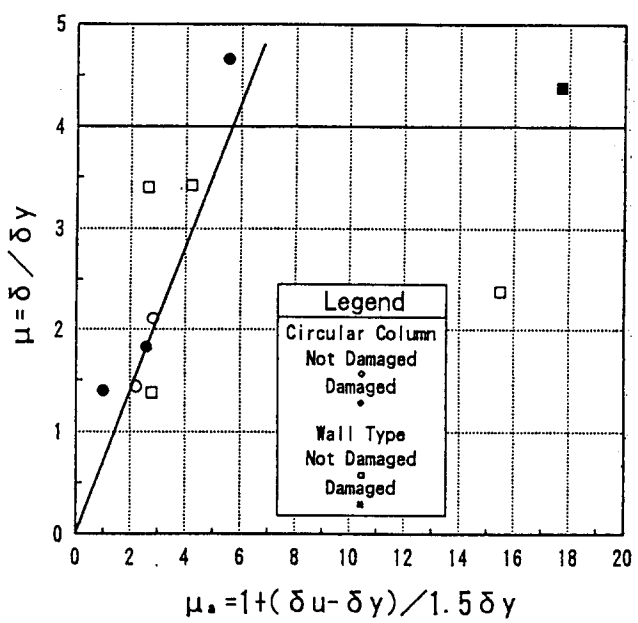

Fig-10 The relation between real and analytical damage

Use of Probabilistic Earthquake Models for Design and Evaluation

by

Jeffrey K. Kimball* and Ann Bieniawski*

ABSTRACT

This paper outlines the use of probabilistic seismic hazard models to establish seismic design and evaluation requirements consistent with the earthquakes which control the seismic hazard. Current probabilistic seismic hazard curves for the Eastern United States indicate that the size of the controlling earthquake(s) is generally less than magnitude 6 at a distance within 50 kilometers of the site. This information has implications regarding the response spectral shape which should be used for the design of new facilities and the evaluation of existing facilities. For the majority of Eastern United States sites with rock site conditions the use of the NEHRP (1991) design spectral shape will overpredict ground motion for frequencies less than about 5 Hertz. This paper suggests that a separate design earthquake spectral shape should be developed for the Eastern United States that is consistent with the magnitudes and distances which control the seismic hazard.

KEYWORDS: seismic hazard; spectral shape; response spectra; controlling earthquakes; seismic design.

1. INTRODUCTION

The purpose of this paper is to outline how probabilistic seismic hazard models can be used to establish seismic design and evaluation requirements consistent with the earthquakes which control the seismic hazard. The Department of Energy (DOE) has established seismic design requirements based on the use of target performance goals which are expressed as the mean annual probability of exceedance of acceptable behavior limits of structures and equipment due to the effects of earthquakes. The overall DOE approach is described in the proceedings for the 25th Joint Meeting on Wind and Seismic Effects in the paper of Hill and Murray (1993). The seismic criteria utilize probabilistic seismic hazard curves for specification of earthquake loading combined with deterministic response evaluation methods and permissible behavior limits. As discussed in Hill and Murray (1993), the Design Basis Earthquake (DBE) is established by selecting a probabilistic mean peak ground acceleration used to scale a median deterministic response spectrum shape. One reason for this choice is the controversy that exists regarding the shape and amplitude of the probabilistic Uniform Hazard Spectra for all spectral frequencies.

The median deterministic DBE response spectrum shape should be consistent with the expected earthquake magnitudes, distances and the site conditions for the site in question. Current DOE seismic design requirements, as discussed in Hill and Murray (1993), specify two available choices in the selection of the response spectrum: The first choice involves the use of standard spectral shapes such as that

* U.S. Department of Energy
Washington, DC 20585

developed by Newmark and Hall (1978); the second and more preferred choice involves the development of a site-specific spectral shape. The impact of the choice of spectral shape on design and evaluation is not trivial. The spectral shape, along with the peak acceleration, can determine how a structure is designed and can impact decisions regarding which existing structures require strengthening to meet modern seismic design requirements. The probabilistic seismic hazard curve can be used to aid in making the selection of the spectral shape to be used for design and evaluation. The discussion below describes one approach for using probabilistic seismic hazard information to assist in selecting the spectral shape for Eastern United States rock sites.

2. PROBABILISTIC SEISMIC HAZARD: CONTROLLING EARTHQUAKES

As discussed in Kimball (1992), the general purpose of a probabilistic seismic hazard analysis is to evaluate the vibratory ground shaking at a particular site by considering the viable sources of earthquakes, the likelihood of earthquake occurrences for each source, an estimate of the particular ground motion parameter of interest, and an analytical model for estimating the probability of exceeding the ground motion parameter. State-of-the-art probabilistic seismic hazard analysis allows the use of multi-valued models and alternative hypotheses, with the results displaying both the central value and the full distribution of hazard results. The probabilistic seismic hazard analysis can be used to perform sensitivity studies which determine the significance of the various input parameters. Additionally, the identification of the significant seismic sources in terms of magnitude and distance can be quantified.

Comprehensive probabilistic seismic hazard studies have been completed by Lawrence Livermore National Laboratory (LLNL) for the Department of Energy and the United States Nuclear Regulatory Commission. Figure 1 displays the peak ground acceleration mean seismic hazard curve for a DOE site near Kansas City, Missouri, using the LLNL methodology. Figure 1 shows the total seismic hazard, and the contribution to the seismic hazard for earthquakes between magnitude 5 and 6, and above magnitude 6. Figure 1 shows that the peak acceleration seismic hazard is based on about equal contributions from earthquakes above and below magnitude 6.

The probabilistic seismic hazard result can also be displayed by magnitude and distance bins. Figure 2A shows the seismic hazard results for peak ground acceleration using the Electric Power Research Institute (EPRI) seismic hazard methodology for a site in South Carolina, for five magnitude and six distance bins with the percent of seismic hazard contribution shown for each bin. The total for all of the bins would sum to one. Figure 2A shows that the peak acceleration is dominated by magnitudes less than 6 at distance less than about 50 kilometers. Figure 2B shows a similar plot in terms of 1 Hertz spectral acceleration. In this case the seismic hazard is dominated by magnitudes 6 to 7 at distances between 50 and 200 kilometers.

The seismic hazard results can also be used to derive the average magnitude(s) and distance(s) which controls the seismic hazard curve. The average magnitude(s) and

distance(s) can be considered as defining the probabilistic controlling earthquakes; those earthquakes that have the greatest influence on the ground motion at the site in question. Given the fact that different magnitude(s) and distance(s) may control the high and low frequency content of the probabilistic seismic hazard estimate (as shown by Figures 1 and 2), the assessment of controlling earthquakes should be completed for both high and low ground motion frequencies. The discussion below shows how the probabilistic derived average magnitude(s) and distances(s) can be used to estimate design spectra for frequencies greater than 1 Hertz.

A compilation of average magnitudes and distances is available from LLNL for the location of 69 commercial nuclear power plants in the Eastern United States. These estimates were completed by determining the average magnitude and distance which controls the probabilistic seismic hazard curve for the average of 5 and 10 Hertz spectral acceleration (the high frequency portion of the spectra), and the average of 1 and 2.5 Hertz spectral acceleration (the low frequency portion of the spectra). Summary results from this compilation are shown on Tables 1 and 2, which display the number of reactor sites which fall within each magnitude/distance bin, with the first number being associated with the average of 5 and 10 Hertz and the second number being associated with the average of 1 and 2.5 Hertz. Table 1 shows the dominant magnitudes and distances for the LLNL mean seismic hazard data while Table 2 is based on the LLNL median seismic hazard data. Table 1 shows that 15 of 69 reactor sites had a dominant magnitude of 5.5 with 7 of the 15 being in the distance range of 35 to 39.9 kilometers for the high frequency (average of 5 and 10 Hertz) portion of the hazard curve. The information contained on these tables can be visualized using the magnitude/distance bin graphs shown on Figures 3A through 3D.

Tables 1 and 2 and Figures 3A through 3D can be used to reach the following conclusions. Generally magnitudes less than about 6 dominate the seismic hazard at the reactor sites for frequencies greater than 1 Hertz. There is a slight shift towards larger magnitudes and greater distances controlling the lower frequency portion of the ground motion but this shift does not appear to be very significant. In reviewing the individual reactor sites the shift towards larger magnitudes at greater distance dominating the lower frequencies is most significant when the site is within about 100 to 200 kilometers of larger (M>6.5) historic earthquakes such as the 1886 Charleston, South Carolina event or the 1811-1812 New Madrid, Missouri events. This trend is evident on Figure 2 with the EPRI mean seismic hazard curve as well. The result shown on Figure 2 is for a site that is about 145 kilometers from the 1886 Charleston South Carolina earthquake. In terms of determining the dominant distances, the seismic hazard appears to be controlled by earthquakes within 45 kilometers for the mean hazard and about 25 kilometers for the median hazard.

3. CONTROLLING EARTHQUAKES: IMPLICATIONS FOR THE DESIGN

As indicated above for the Eastern United States the controlling earthquakes are generally less than magnitude 6, for distances less than about 25 to 45 kilometers. With respect to seismic design implications it is instructive to

compare the response spectra from the controlling earthquakes to the response spectra typically used for design. Figure 4 displays two typical design earthquake response spectra based on the 1991 National Earthquake Hazards Reduction Program (NEHRP) Recommended Provisions (NEHRP, 1991) and Newmark and Hall (1978) for rock site conditions. The median and one standard deviation spectral shapes are shown for the Newmark and Hall (1978) response spectra. As Figure 4 shows, the NEHRP (1991) rock spectral shape, which is also the spectral shape utilized in the 1991 Uniform Building Code (UBC, 1991), is between the median and one standard deviation Newmark and Hall (1978) rock spectra for frequencies above 2 Hertz and about equal to the median Newmark and Hall spectra for lower frequencies. Figure 4 also shows that the 1 Hertz spectral acceleration is equal to the peak ground acceleration for the NEHRP spectral shape and the median Newmark and Hall spectral shape, and about 1.35 times the peak acceleration for the one standard deviation Newmark and Hall spectral shape.

How do the NEHRP (1991) and Newmark and Hall (1978) spectral shapes compare to the spectral shapes from the controlling earthquakes? Tables 1 and 2 can be used to select magnitude/distance pairs to compare to standard design spectral shapes. Table 3 displays eight sets of magnitude/distance pairs that represent the information displayed in Tables 1 and 2. Table 3 also lists three Eastern United States and three Western United States ground motion attenuation models to derive the spectral shapes for the 8 magnitude/distance pairs. The primary reason to use both Eastern and Western United States attenuation models is to quantify the relative difference in spectral shape between the two geographic regions, recognizing that the data base on which the NEHRP (1991) and Newmark and Hall (1978) spectral shapes were based is exclusively Western United States data. The spectral shape for each of the magnitude/distance pairs will be quantified using each of the attenuation models, with the results being normalized to a peak ground acceleration of 1g to compare with the NEHRP (1991) and Newmark and Hall (1978) spectral shapes. The normalized spectral shapes for the eight magnitude/distance pairs for the Eastern and Western United States attenuation models are shown on Table 4 in terms of relative acceleration amplification factors at seven ground motion frequencies.

The results shown on Table 4 can be used to derive a spectral shape for both the East and West. Figure 5 shows the envelope of the data from Table 4 for the two geographic regions. From a relative spectral shape perspective, the Eastern United States spectral shape is enriched in the high frequency region when compared to the Western United States. Considering the uncertainties in characterizing Eastern United States earthquake source spectra and ground motion, an approach would be to develop a "composite" spectra based on the two individual spectra shown on Figure 5. In developing the "composite" spectra the following considerations were utilized. First, an attempt was made to maintain the broadness of the spectral shapes shown on Figure 4, with the maximum spectral acceleration occurring over about a factor of four in frequency. Second, an attempt was made to maintain the general spectral shapes shown on Figure 5 recognizing that to match the Eastern United States spectral shape a shift in frequency

would be necessary. Finally, an attempt was made to conservatively reflect the values for the maximum spectral acceleration based on the data shown on Table 4.

The "composite" spectral shape derived from Table 4 is shown on Figure 6 compared to the NEHRP (1991) spectral shape and the median Newmark and Hall (1978) spectral shape. The "composite" spectral shape has a maximum spectral acceleration of 2.4 between frequencies of 5 to 20 Hertz, retaining the broadness shown in Figure 5, shifted to higher frequencies to reflect Eastern United States earthquake source characteristics. For frequencies less than 4 to 5 Hertz the "composite" spectra is significantly less than the NEHRP (1991) and Newmark and Hall (1978) spectral shapes. The primary reason for this discrepancy pertains to the magnitudes of the earthquakes used in this analysis compared to those that were used to derive the standard spectral shapes shown on Figure 4.

In an attempt to explore the differences between the "composite" spectra and the Newmark and Hall (1978) spectra, the actual data base that was used to develop the Newmark and Hall spectral shape was reviewed (see Newmark 1973, Newmark et al 1973 and Hall et al 1976). Newmark and Hall (1978) compiled a set of representative strong motion data which was normalized to 1g peak ground acceleration, and statistical analyses were performed to derive the spectral amplification functions. Retrospectively looking at the data base used, the majority of data pertains to soil sites which recorded strong motion from earthquakes in the magnitude range 5.3 to 7.7, with about two thirds of the data from earthquakes larger than magnitude 6. Data was from soil sites because Newmark and Hall recognized that the rock data was very limited and could represent biased statistical results.

Newmark and Hall (1978) also developed recommendations for the ratio of velocity to acceleration (V/A) for both rock and soil. In general the peak velocity region of the response spectra is associated with frequencies of about .5 Hertz to 5 Hertz, while the peak acceleration is associated with the high frequency portion of the response spectra.

The velocity to acceleration ratio for the strong motion data from soil sites from Newmark (1973) are shown on Figure 7A as a function of earthquake magnitude, along with the best fit correlation between magnitude and V/A. Figure 7A also lists the recommended value for V/A of 121.9 cm/sec/g from Newmark and Hall (1978) which intersects the best fit line at about magnitude 6.5. Figure 7A indicates that the ratio of V/A is a function of earthquake magnitude, with larger earthquakes providing more lower frequency energy relative to smaller earthquakes.

While the Newmark (1973) data base was not sufficient to make a similar plot for rock sites, the strong motion data base for pre-1972 has been searched to identify all rock records within 100 kilometers of earthquakes above magnitude 5. The rationale for selecting pre-1972 data was to keep the data as close to that available in defining the original Newmark and Hall (1978) spectra as possible. Figure 7B shows the V/A for all rock records above magnitude 5 plotted as a function of magnitude. Figure 7B also plots the V/A derived from the Campbell (1990) attenuation model

for rock like sites for distances of 5 and 100 kilometers. The Campbell V/A lines tend to bracket the pre-1972 recorded rock data and show a similar magnitude dependent trend when compared to Figure 7A. However, the V/A for rock sites is substantially lower than soil sites reflecting the general trend that soil sites amplify ground motion in the peak velocity region compared to the peak acceleration region (see Borcherdt 1994).

Given the fact that the controlling earthquakes for the Eastern United States are generally lower than magnitude 6, Figure 7B can be used to justify a lower spectral shape compared to either the NEHRP (1991) or Newmark and Hall (1978) response spectra for frequencies less than about 5 Hertz for use in the Eastern United States. It is beneficial to point out that the relative underconservatism of the NEHRP (1991) spectral shape in relation to the composite spectral shape for frequencies greater than 10 Hertz does not actually exist in design. The NEHRP Recommended Provisions uses a normalized lateral design force coefficient which utilizes the maximum spectral acceleration value for the very low period portion of the spectra instead of the actual value. For controlling earthquakes between magnitude 5.3 and 6 from Tables 1 and 2, the rock V/A from Figure 7B ranges from about 20 cm/sec/g to 80 cm/sec/g, substantially less than the 91 cm/sec/g implied by the NEHRP (1991) or Newmark and Hall (1978) response spectra. The composite spectra shown on Figure 5 has an implied V/A of about 60 cm/sec/g which is consistent with the empirical trend shown on Figure 7B. A similar conclusion would be applicable for soil sites for earthquakes less than magnitude 6 based on the data shown on Figure 7A.

4. DISCUSSION

The above discussion indicates that the design earthquake response spectra shape referenced in the 1991 version of the NEHRP Recommended Provisions may not be appropriate for the Eastern United States between frequencies of 1 and 5 Hertz, primarily because the magnitudes of the earthquakes which dominate the seismic hazard in the east are smaller compared to the magnitudes used to develop the NEHRP (1991) design spectra.

The choice of design earthquake spectral shape has implications for the seismic design of both new and existing facilities. If the goal of the NEHRP Recommended Provisions is to develop a consistent seismic design process for the entire United States, the basic seismic design input must recognize differences in the size of the earthquakes which dominate the seismic hazard. For new buildings which have fundamental frequencies between 1 and 5 Hertz, the design of a building in the East, on rock, will be more conservative than the design of a building in the West, on comparable rock, due to the inherent conservatism in the NEHRP (1991) spectral shape. As the NEHRP Recommended Provisions are revised, an attempt should be made to determine if this current practice should be continued, or as this paper suggests, a separate design earthquake response spectra be developed for the east. Additional work should also be completed to determine if the trend identified in this paper extends to frequencies less than 1 Hertz.

The shape of the design earthquake response spectra also has implications for the seismic assessment of existing facilities. The United States Federal Government

will soon be assessing the seismic safety of all existing Federally owned and leased buildings. Because seismic retrofit can be expensive and because the Federal inventory is quite large, this process must include some type of prioritization process for both the evaluation and potential seismic strengthening for existing Federal facilities. If the design earthquake spectral shape provides an inconsistent measure of earthquake likelihood, then the prioritization and mitigation process may not identify or retrofit the facilities with the highest seismic risk.

5. CONCLUSIONS

The assessment of the probabilistic seismic hazard can be used to determine the magnitudes and distances of the earthquakes which dominate the probabilistic seismic hazard. This information has implications regarding the response spectral shape which should be used for the design of new facilities and the evaluation of existing facilities. Current probabilistic seismic hazard curves for the Eastern United States indicate that the size of the controlling earthquake is generally less than magnitude 6 at a distance within 50 kilometers of the site. The spectral shape from magnitudes less than about 6 will not be the same as the spectral shape included in the 1991 NEHRP Recommended Provisions.

A separate design earthquake spectral shape should be developed for the Eastern United States that is consistent with the magnitudes and distances which control the seismic hazard. Figure 6 shows one possible spectral shape developed from both Eastern and Western attenuation models for magnitudes between 5 and 6 at distances less than about 50 kilometers for frequencies greater than 1 Hertz. For the majority of Eastern United States sites with rock site conditions the use of the NEHRP (1991) design spectral shape will overpredict ground motion for frequencies less than about 5 Hertz. Additional work should also be completed to determine if the trend identified in this paper extends to frequencies less than 1 Hertz.

6. REFERENCES

1. Atkinson, G.M., and Boore, D.M. (1990). "Recent Trends in Ground Motion and Spectral Response Relations for North America," Earthquake Spectra, Vol. 6, #1, pg. 15.

2. Boore, D.M., et al (1993). "Estimation of Response Spectra and Peak Acceleration from Western North American Earthquakes: An Interim Report," U.S. Geological Survey Open File Report 93-509, 72 pgs.

3. Campbell, K.W., (1990). "Empirical Prediction of Near-Source Soil and Soft-Rock Ground Motion for the Diablo Canyon Power Plant Site, San Luis Obispo County, California," Dames and Moore letter report to Lawrence Livermore National Laboratory.

4. EPRI, (1993). "Guidelines for Determining Design Basis Ground Motions," Electric Power Research Institute, TR-102293, 4 Volumes.

5. Geomatrix, (1992). "Seismic Ground Motion Study for West San Francisco Bay Bridge," Final report to Caltrans, Division of Structures, Sacramento, California.

6. Hall, W.J., et al (1976). "Statistical Studies of Vertical and Horizontal Earthquake Spectra," Report for U.S. Nuclear Regulatory Commission, NUREG-0003, 140 pages.

7. Hill, J.R., and Murray, R.C. (1993). "DOE NPH Mitigation Policy and Standards Program," Proceedings of the 25th Joint Meeting, UJNR, Wind and Seismic Effects, ISSN 0386-5878, pg. 655.

8. Kimball, J.K. (1992). "Resolving Uncertainties in Seismic Hazard Models," Proceedings of the 24th Joint Meeting, UJNR, Wind and Seismic Effects, NIST SP843, pg. 115.

9. McGuire, R.K., et al (1988). "Engineering Model of Earthquake Ground Motion for Eastern North America," Electric Power Research Institute Report, NP-6074.

10. NEHRP (1991). "NEHRP Recommended Provisions for the Development of Seismic Regulations for New Buildings," FEMA 222.

11. Newmark, N.M., (1973). "A Study of Vertical and Horizontal Earthquake Spectra," Report for U.S. Atomic Energy Commission, WASH-1255, 151 pages.

12. Newmark, N.M., et al (1973). "Seismic Design Spectra for Nuclear Power Plants," ASCE Journal of the Power Division, Vol. 99, No. PO2, pg. 287.

13. Newmark, N.M., and Hall, W.J., (1978). "Development of Criteria for Seismic Review of Selected Nuclear Power Plants," Report for U.S. Nuclear Regulatory Commission, NUREG/CR-0098, 49 pages.

14. Uniform Building Code (UBC), (1991 Edition), International Conference of Building Officials, Whittier California.

TABLE 1

LLNL MEAN SEISMIC HAZARD - DOMINANT EARTHQUAKES

Summary of deaggregated magnitudes and distances using the 1993 LLNL mean seismic hazard curves. The deaggregated magnitudes and distances represent the dominant magnitude and distance.

		DISTANCE (Km)					
Magnitude	# of Sites	20-24.9	25-29.9	30-34.9	35-39.9	40-44.9	45+
5.5	15/17		1/0	2/2	7/1	5/8	0/6
5.6	21/21	1/0	5/3	10/4	3/5	2/4	0/5
5.7	16/18		11/3	2/5	3/6	0/3	0/1
5.8	12/9		6/0	2/3	3/4	1/1	0/1
5.9	2/2		0/1	1/0		1/0	0/1
6.0	2/2	1/0		1/0	0/1		0/1
6.1	1/0					1/0	
	# of Sites	2/0	23/7	18/14	16/17	10/16	0/15

2 Numbers Provided - 1st is # of Avg. 5/10 Hz while the 2nd is # of Avg. 1/2.5 Hz

TABLE 2

LLNL MEDIAN SEISMIC HAZARD - DOMINANT EARTHQUAKES

Summary of deaggregated magnitudes and distances using the 1993 LLNL mean seismic hazard curves. The deaggregated magnitudes and distances represent the dominant magnitude and distance.

		DISTANCE (Km)				
Magnitude	# of Sites	13-14.9	15-16.9	17-19.9	20-24.9	25+
5.3	10/3		4/0	6/3		
5.4	16/11	1/0	4/1	11/5	0/5	
5.5	20/18	8/0	7/5	3/5	2/8	
5.6	14/9	8/0	4/1	2/3	0/5	
5.7	8/14	7/0	1/2	0/2	0/6	0/4
5.8	0/11		0/3	0/5	0/2	0/1
5.9				0/1		
	# of Sites	24/0	20/12	22/24	2/26	0/5

2 Numbers Provided - 1st is # of Avg. 5/10 Hz while the 2nd is # of Avg. 1/2.5 Hz

TABLE 3

Representative controlling magnitudes and distances that will be used to assess spectral shape using several Eastern U.S. and Western U.S. attenuation models.

For LLNL Mean Model Ground Motion For:

Mb	M	R (Km)
5.5	5.0	37.5
5.7	5.25	27.5
6	5.5	22.5
6.1	5.6	41

For LLNL Median Model Ground Motion For:

Mb	M	R (Km)
5.3	4.8	16.0
5.5	5	15
5.7	5.25	14
5.8	5.3	22

GROUND MOTION ATTENUATION MODELS

Rock Site Conditions

Eastern U.S.	Western U.S.
McGuire et al., 1988	Geomatrix, 1992
Atkinson/Boore, 1990	Boore, et al 1993
EPRI, 1993	Campbell, 1990

TABLE 4

Normalized spectral acceleration values using Eastern and Western Attenuation Models and representative controlling magnitudes and distances using LLNL 1993 mean results.

LLNL Mean Results

Eastern United States							Western United States				
25	20	10	5	2.5	2	1	20	10	5	2	1
2.1	2.5	1.4	.94	.78	.32	.10	1.3	2	2.2	.78	.3
2.1	2.5	1.4	.97	.80	.36	.13	1.3	2	2.2	.87	.38
2.1	2.6	1.4	1.0	.83	.43	.17	1.3	2	2.2	.95	.42
2.06	2.5	1.5	1.1	.99	.48	.20	1.2	1.9	2.2	1.1	.50
2.26		1.9	.94		.44	.15	1.05	1.3	1.5	.62	.24
2.34		1.8	.94		.48	.18	1.05	1.6	1.8	.72	.27
2.38		1.8	.95		.53	.22	1.05	1.9	2.0	.82	.32
2.22		1.9	1.0		.60	.26	1.05	1.8	2.0	.82	.33
		2.1	1.6			.21		1.6	2.2	1.4	.53
		2.0	1.5			.25		1.6	2.2	1.5	.61
		2.0	1.5			.29		1.6	2.2	1.6	.74
		2.1	1.6			.37		1.6	2.2	1.7	.78

LLNL Median Results

Eastern United States							Western United States				
25	20	10	5	2.5	2	1	20	10	5	2	1
2.1	2.6	1.8	.88	.77	.36	.10	1.4	2.2	2.1	.61	.22
2.1	2.6	1.8	.90	.70	.40	.13	1.4	2.1	2.1	.69	.26
2.1	2.6	1.8	.92	.64	.46	.17	1.4	2.1	2.2	.81	.32
2.1	2.6	1.8	.94	.59	.48	.18	1.3	2.0	2.2	.88	.36
2.4		1.4	.88		.28	.08	1.05	1.3	1.4	.59	.22
2.5		1.4	.91		.31	.10	1.05	1.5	1.7	.67	.25
2.5		1.4	.95		.35	.12	1.05	1.8	1.9	.77	.29
2.47		1.4	.98		.38	.14	1.05	1.7	1.9	.75	.29
		2	1.5			.24		1.6	2.2	1.3	.45
		1.9	1.4			.21		1.6	2.2	1.4	.53
		1.9	1.4			.17		1.6	2.2	1.5	.61
		1.9	1.4			.14		1.6	2.2	1.5	.66

KANSAS CITY PROBABILISTIC SEISMIC HAZARD CURVE
FIGURE 1

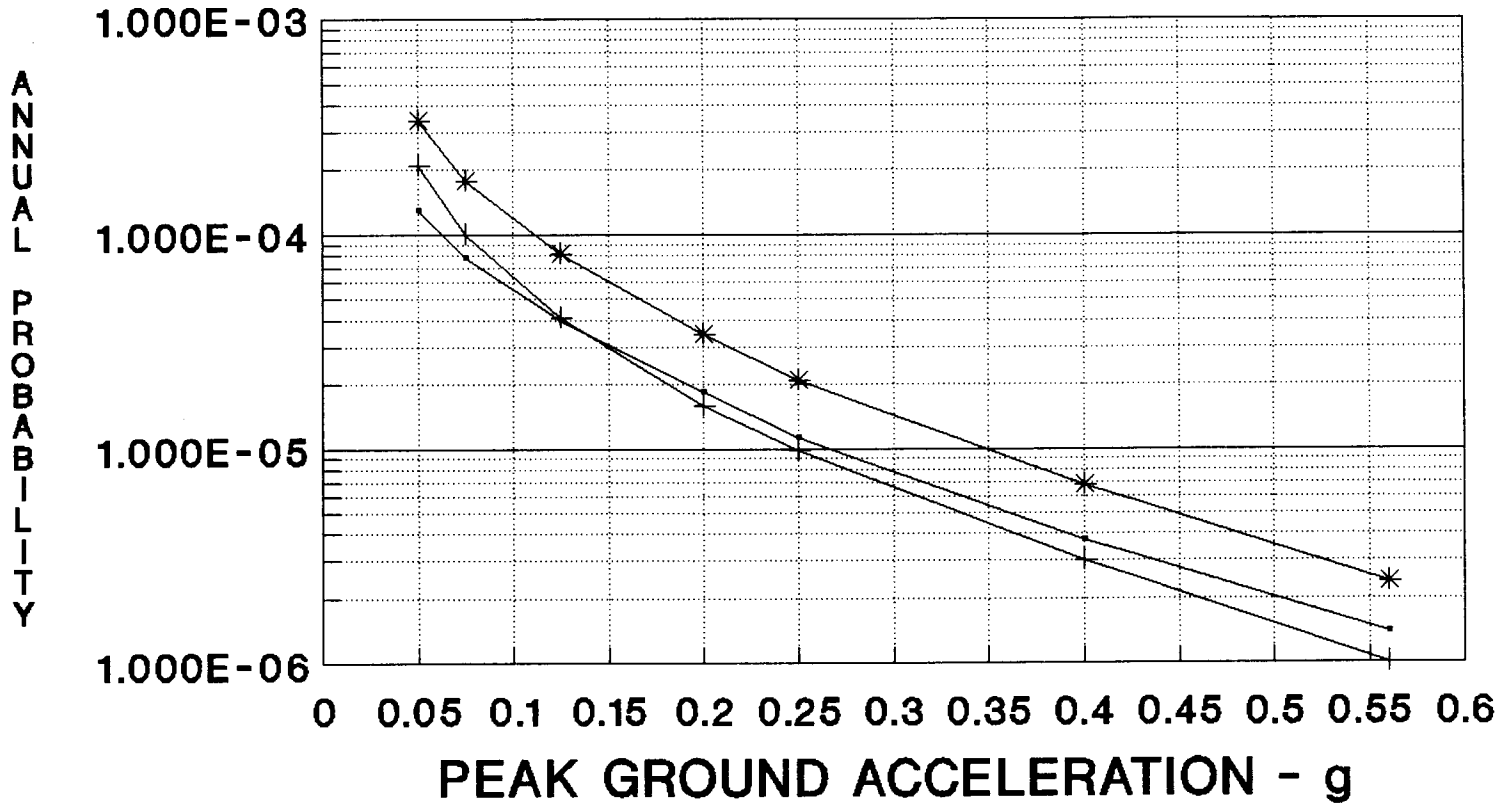

MAG 5 - 6 MAG 6+ TOTAL HAZARD

PROBABILISTIC SEISMIC HAZARD CURVE FOR KANSAS CITY MISSOURI SHOWING THE TOTAL SEISMIC HAZARD AND THE BREAKDOWN OF THE TOTAL HAZARD INTO MAGNITUDE 5 TO 6 AND LARGER THAN 6

EPRI MEAN PROBABILISTIC SEISMIC HAZARD
PEAK GROUND ACCELERATION
FIGURE 2A

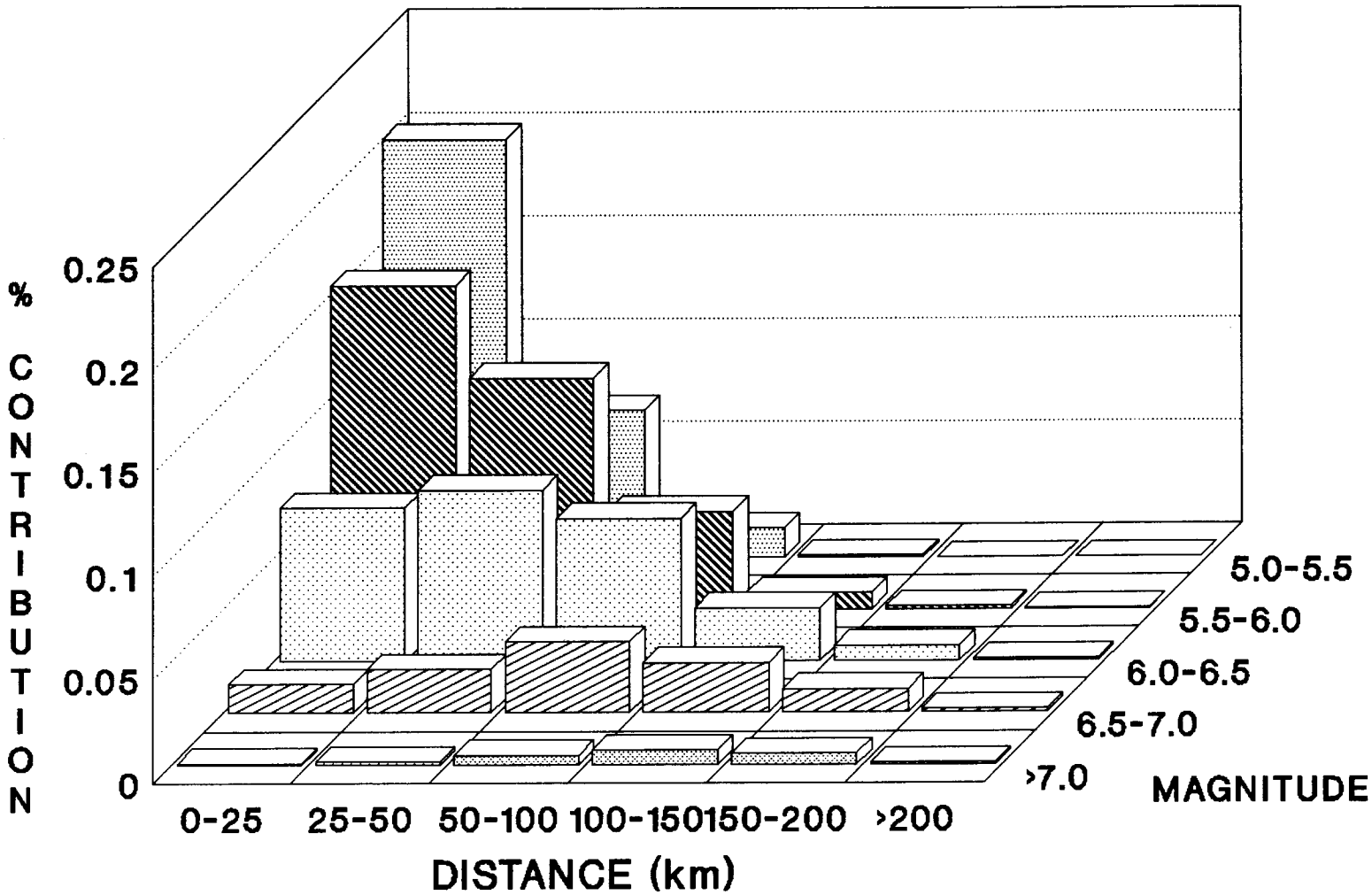

EPRI MEAN PROBABILISTIC SEISMIC HAZARD
1 HERTZ SPECTRAL ACCELERATION
FIGURE 2B

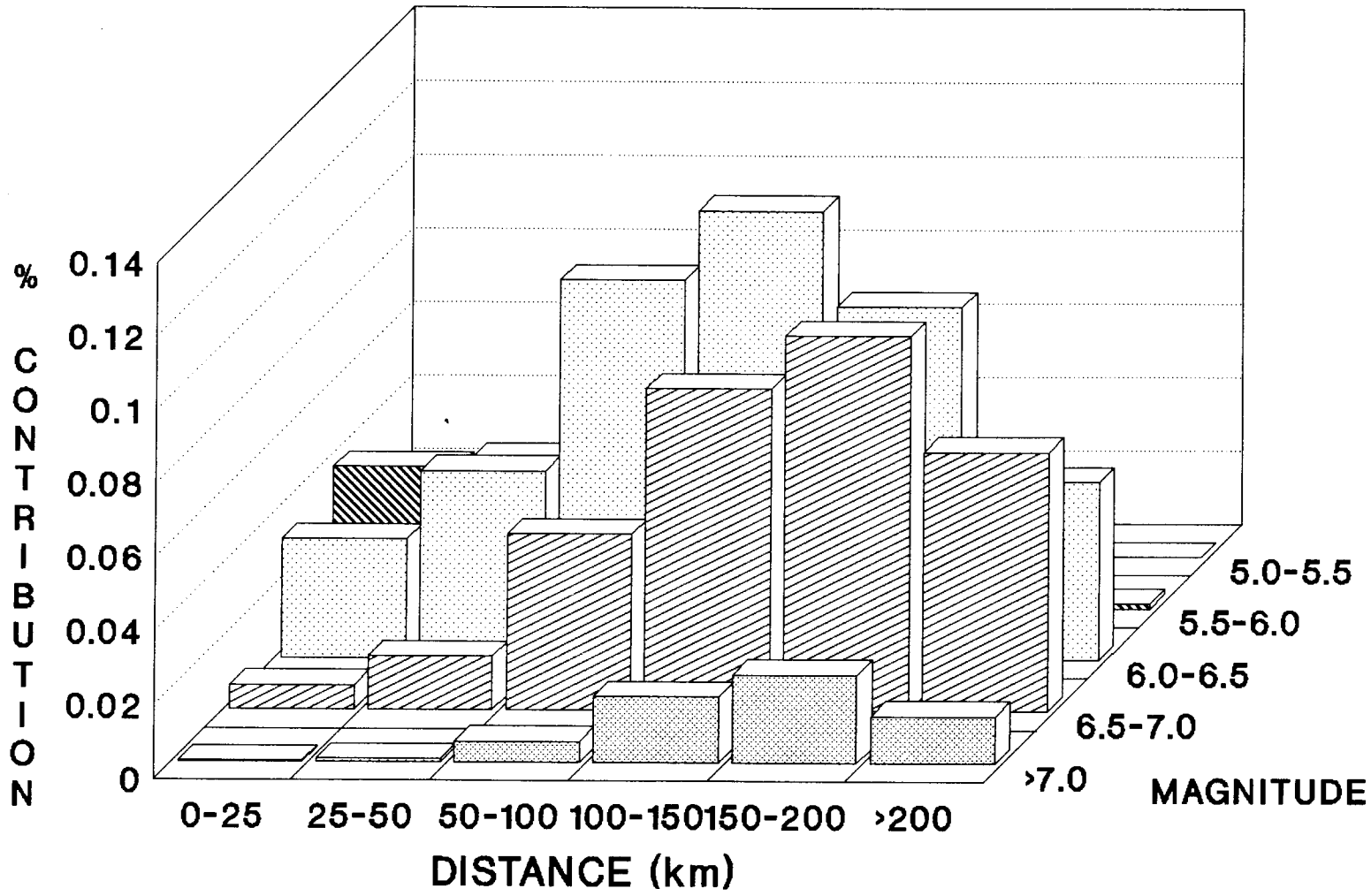

LLNL MEAN SEISMIC HAZARD
DOMINANT EARTHQUAKES
FIGURE 3A

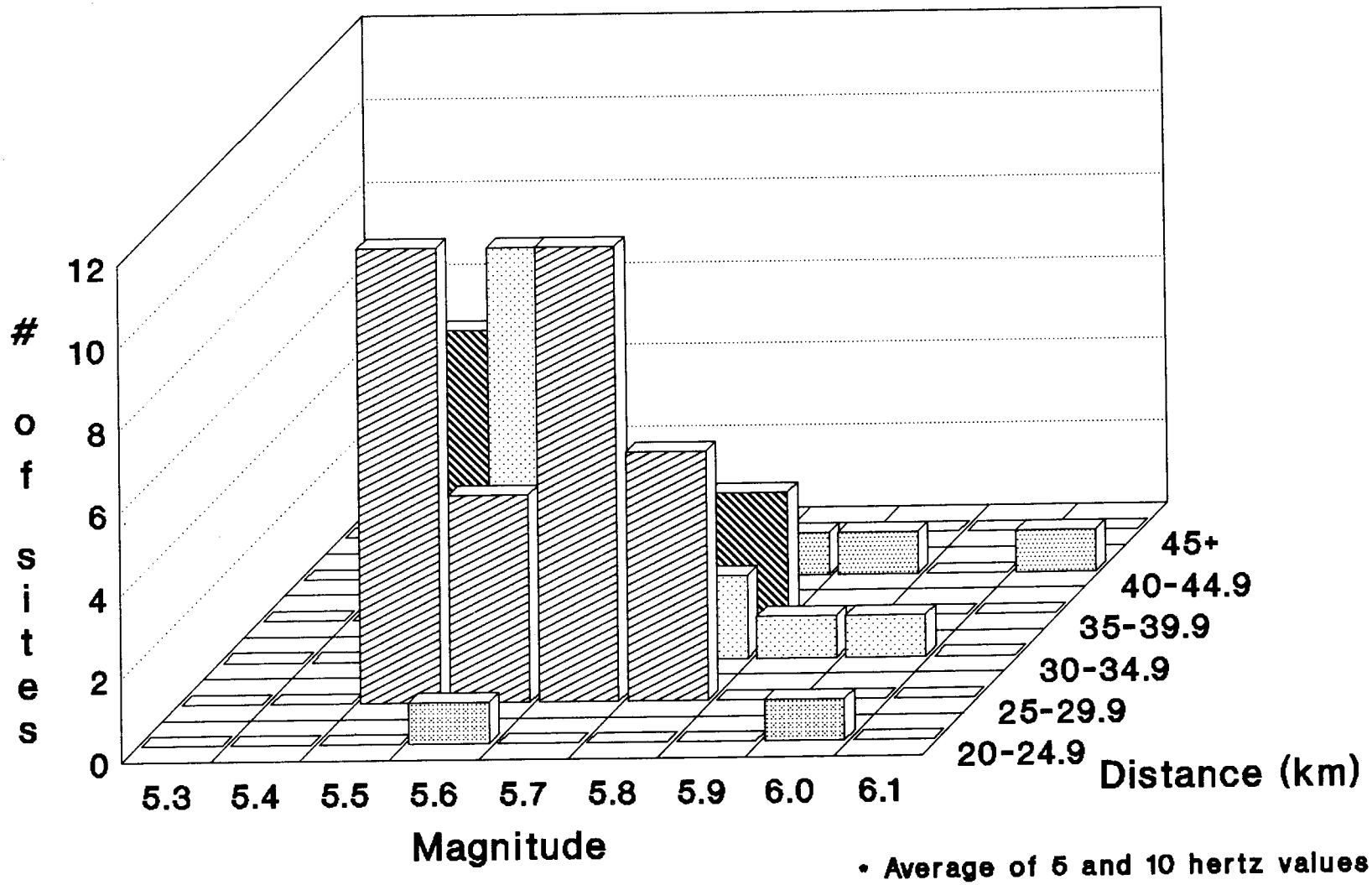

• Average of 5 and 10 hertz values

LLNL MEAN SEISMIC HAZARD
DOMINANT EARTHQUAKES
FIGURE 3B

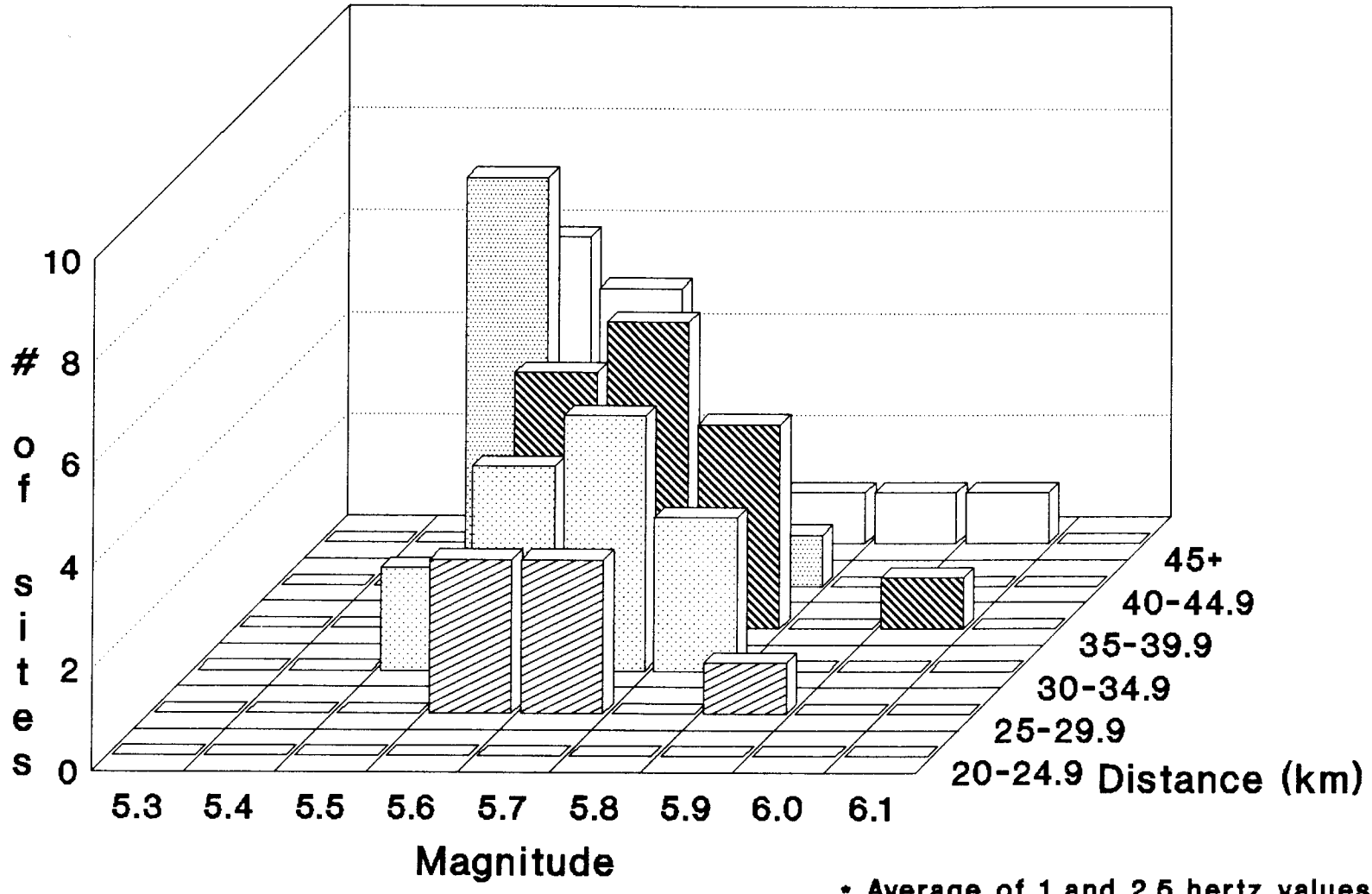

* Average of 1 and 2.5 hertz values

LLNL MEDIAN SEISMIC HAZARD
DOMINANT EARTHQUAKES
FIGURE 3C

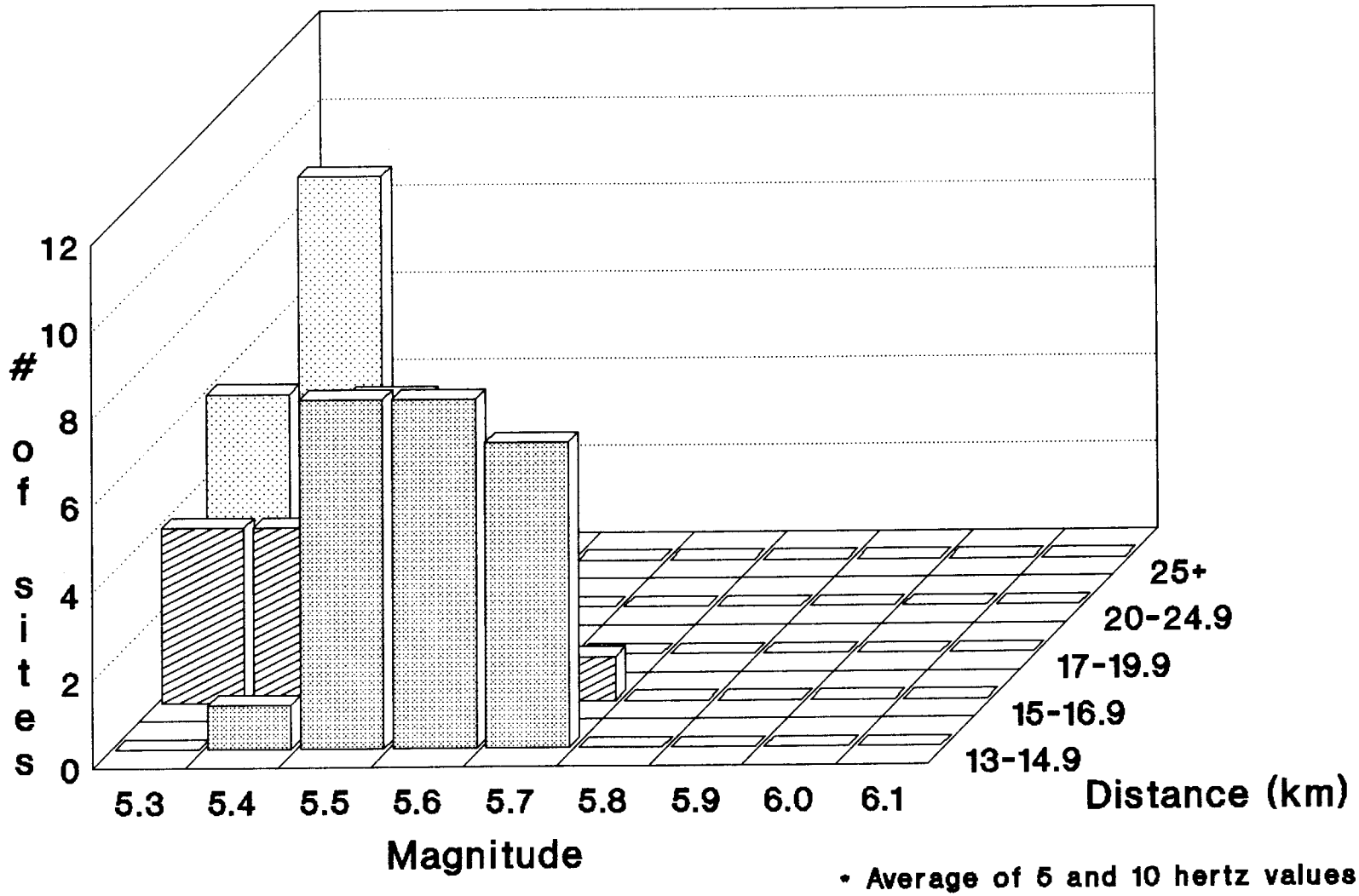

* Average of 5 and 10 hertz values

LLNL MEDIAN SEISMIC HAZARD
DOMINANT EARTHQUAKES
FIGURE 3D

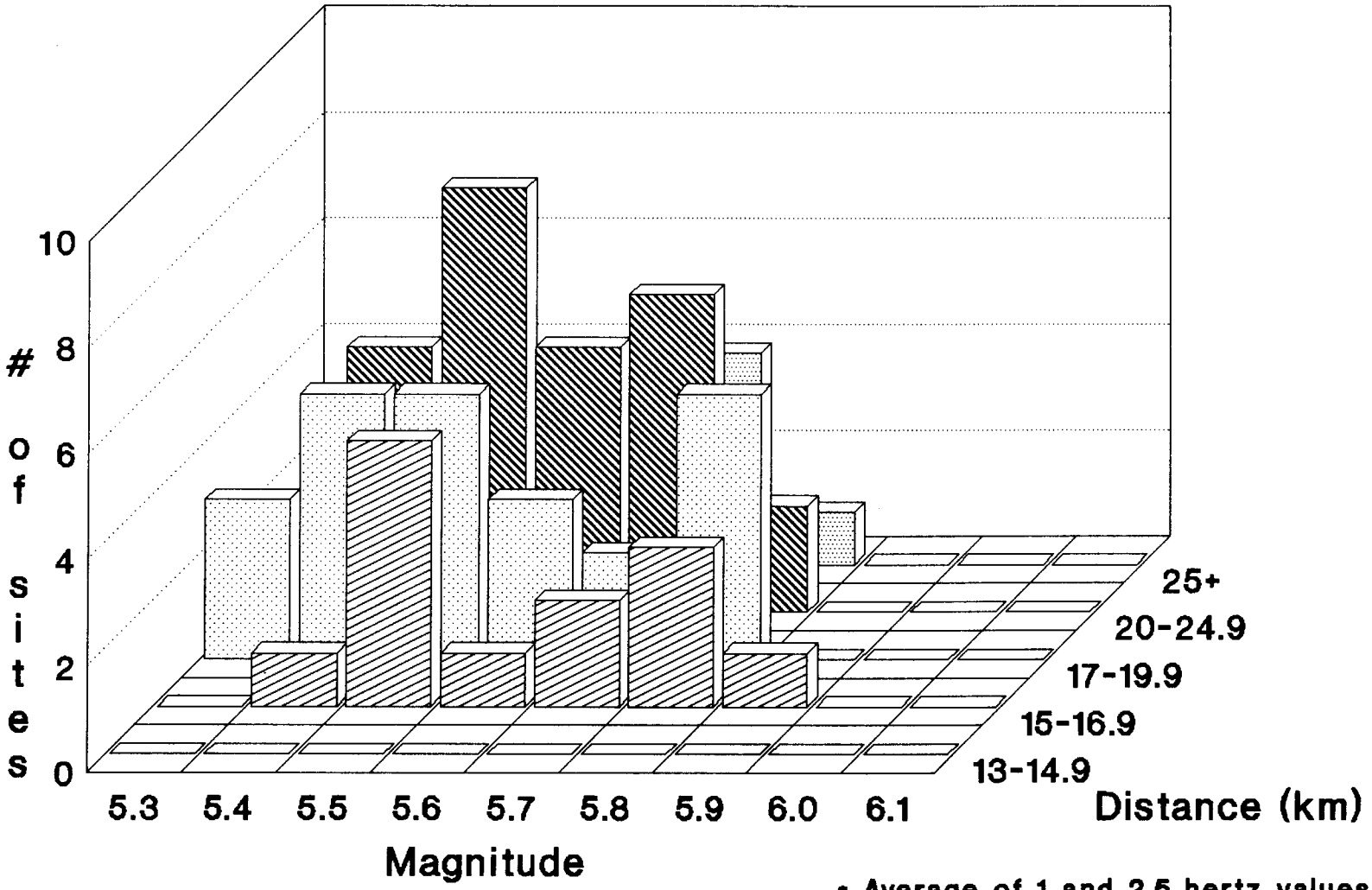

• Average of 1 and 2.5 hertz values

RESPONSE SPECTRA COMPARISONS NEWMARK AND HALL VERSUS NEHRP

FIGURE 4

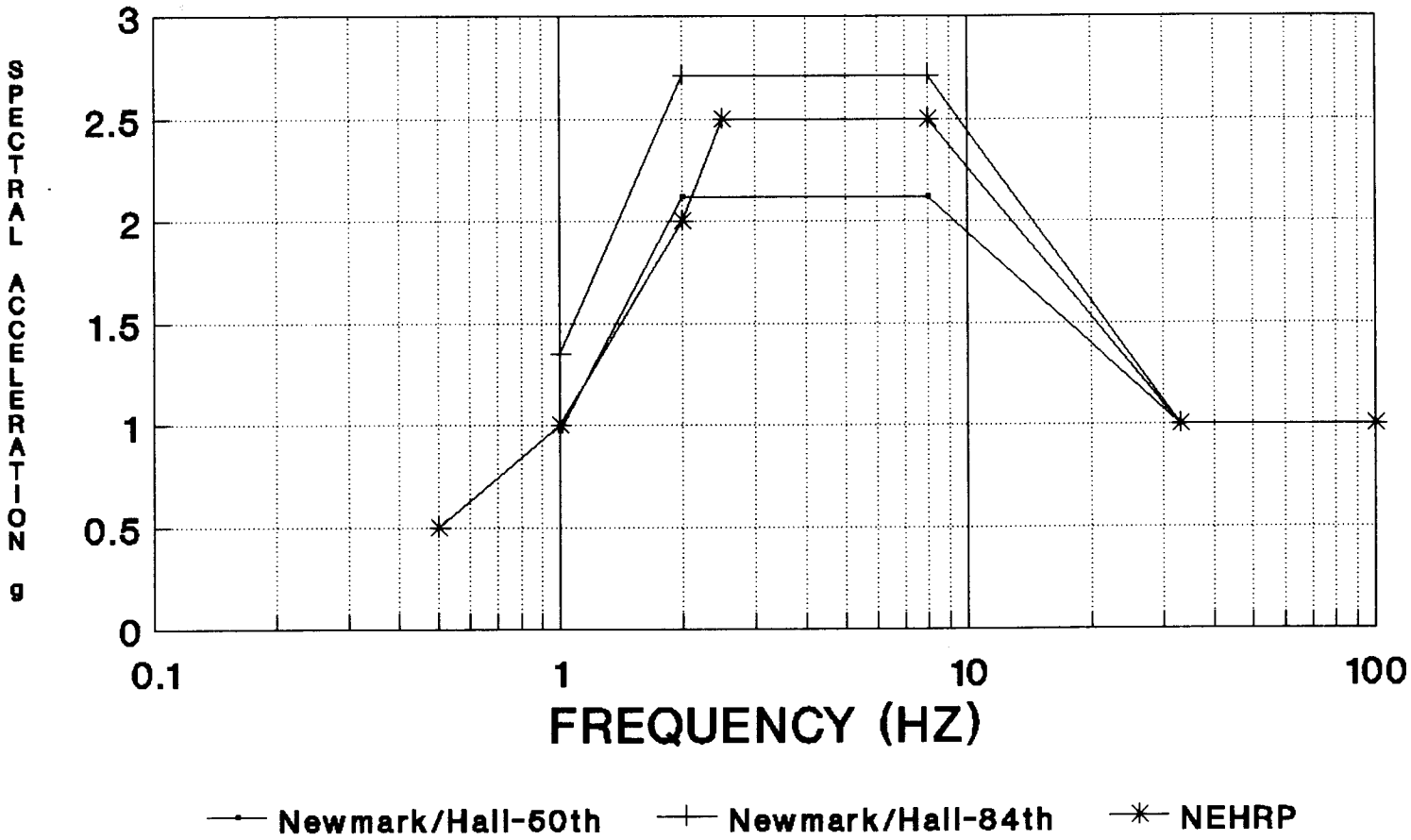

RESPONSE SPECTRA SHAPES BASED ON NEWMARK AND HALL (1978) AND NEHRP (1991) FOR ROCK SITE CONDITIONS

RESPONSE SPECTRA COMPARISONS USING DEAGGREGATED HAZARD CURVES

FIGURE 5

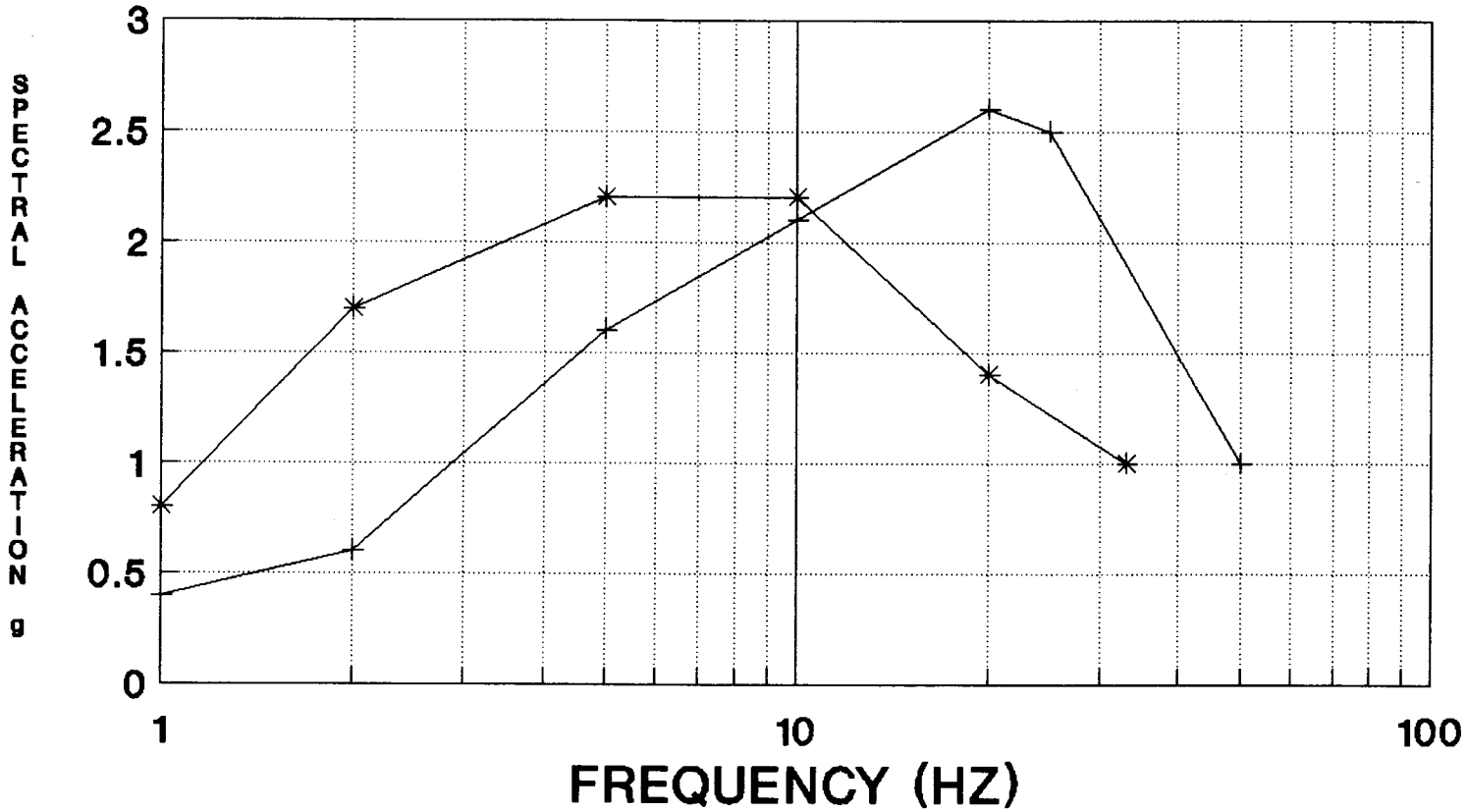

EUS WUS

ENVELOPE OF THE NORMALIZED SPECTRAL SHAPES FOR THE EASTERN AND WESTERN UNITED STATES SHOWN ON TABLE 4. THE EASTERN SHAPE IS ENRICHED IN THE HIGH FREQUENCIES.

RESPONSE SPECTRA COMPARISONS
COMPOSITE SPECTRAL SHAPE
FIGURE 6

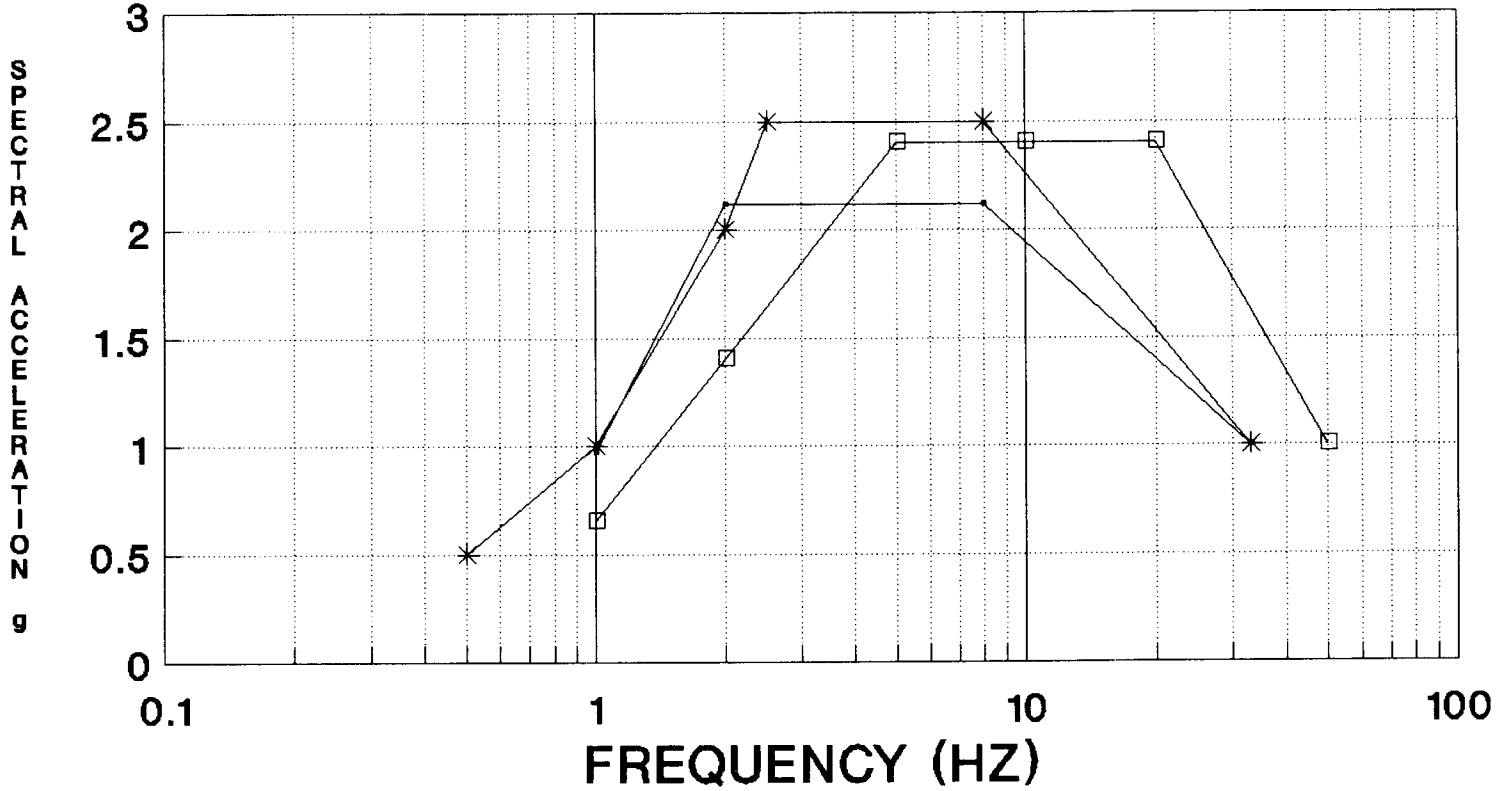

Newmark/Hall-50th NEHRP COMPOSITE

COMPOSITE RESPONSE SPECTRA DERIVED FROM FIGURE 5 AND TABLE 4 COMPARED TO THE NEHRP 1991 SPECTRAL SHAPE AND THE MEDIAN NEWMARK AND HALL 1978 SPECTRAL SHAPE

NEWMARK (1973) STRONG MOTION DATA
VELOCITY/ACCELERATION RATIO
FIGURE 7A

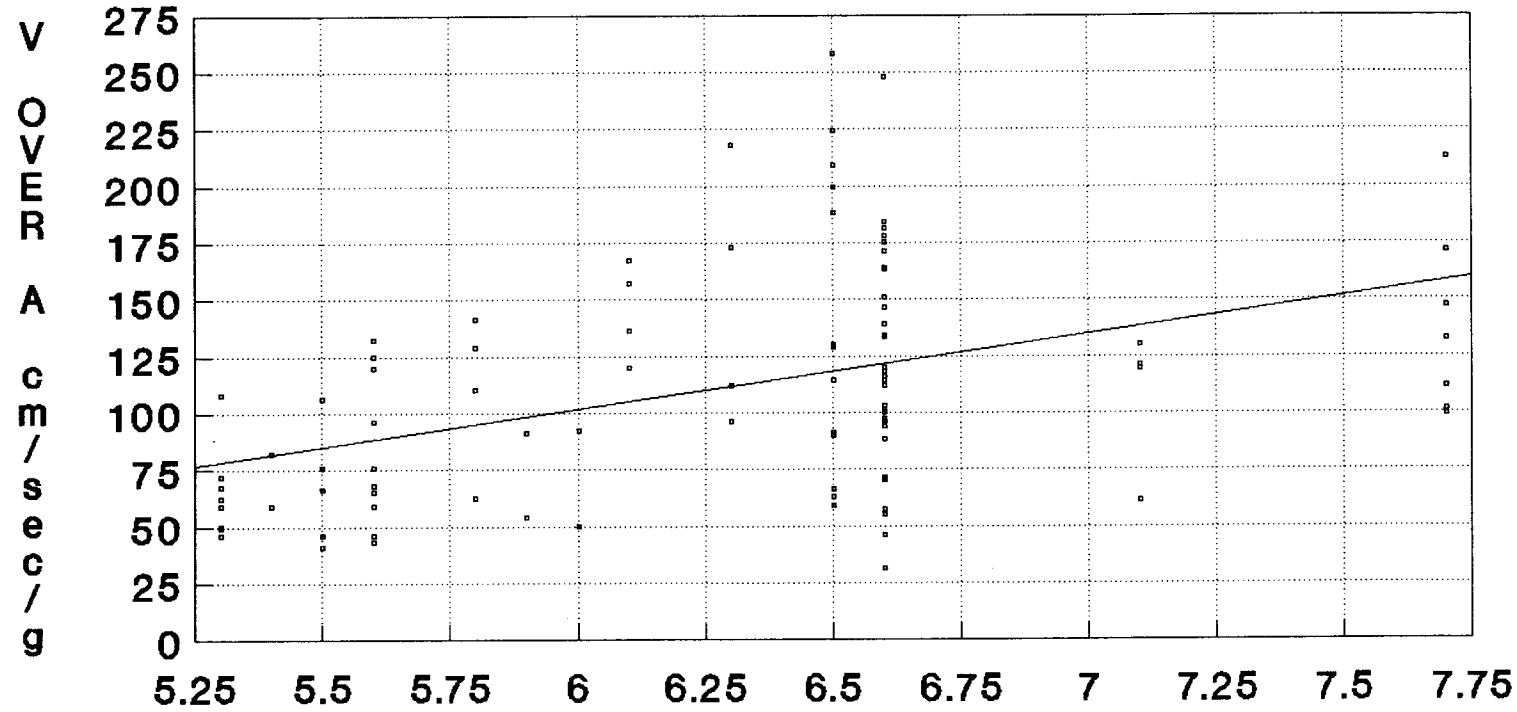

NEWMARK/HALL (1978)

121 CM/SEC/g FOR SOIL

Newmark Data

PLOT OF INDIVIDUAL DATA POINTS FOR SOIL SITES USING NEWMARK (1973) DATA SET ALONG WITH THE BEST FIT LINEAR RELATIONSHIP SHOWING MAGNITUDE DEPENDENT V/A

VELOCITY/ACCELERATION RATIO'S FROM ROCK PRE-1972 DATA (NEWMARK/HALL LIKE DATA)

FIGURE 7B

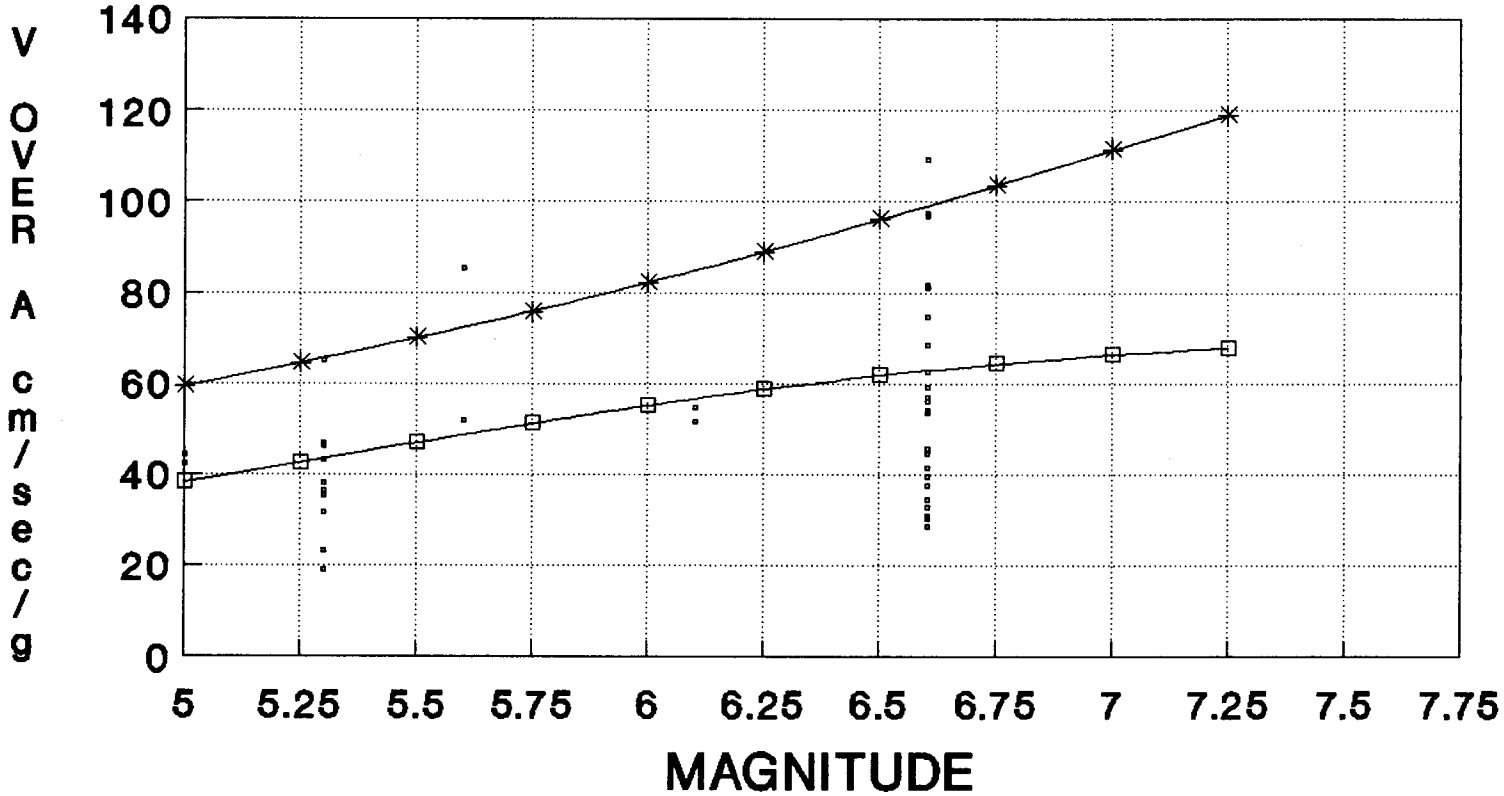

· ROCK DATA —✳— CAMP 100 KM —⊡— CAMP 5 KM

PLOT OF INDIVIDUAL DATA POINTS FOR ROCK SITES FOR PRE 1972 STRONG MOTION DATA COMPARED TO V/A BASED ON CAMPBELL 1990 ATTENUATION MODEL - SHOWING MAGNITUDE DEPENDENT V/A

Structural Model of Functional Damage Due to an Earthquake in Urban Area

by

Kazuhiko Kawashima[1], Hideki Sugita[2], Tomoru Nakajima[3] and Takashi Sato[4]

ABSTRACT

In urban area, functions of various facilities are closely related. Once a physical damage is developed to a facility due to an earthquake, this would cause loss or decrease of functions of the other facilities which are related with the facility directly damaged by the earthquake. The propagation of functional damage is developed in this way, and this would be considered as a new type of earthquake disaster especially in urban area.

This paper presents the structural model of functional damage due to an earthquake in urban area. The structural model is formulated for analyzing how the interaction between functions of various facilities can be developed. Nineteen functions including road, railway, water, electricity and telephone are considered in the analysis. Based on the analysis, it is pointed out that the facility most influential to the propagation of functional damage is road.

KEY WORDS: Earthquake Disaster, Functional Damage, Physical Damage, Propagation Path, Structural Model

1. INTRODUCTION

In urban area of Japan, large scale earthquake has not been occurred since 1923 Kanto Earthquake of magnitude 7.9. The metropolis in urban area has been developed based on the highly growth of economy after this event. Although the metropolis has not experienced large scale earthquake, once it occurs, new type of earthquake disaster which is completely different from the disaster shown in Kanto Earthquake would be developed. For upgrading the seismic safety of urban area, it is quite important to figure out the outline of new type earthquake disaster considering with the configuration of metropolis.

Following facts can be pointed out as the features of metropolis.

(1) Transportation systems and mass-communication systems have been highly developed. Based on these developments, urban area has been much enlarged. Breakdown of these systems will make it impossible to maintain the activity of whole urban area.

(2) Computer systems for transmitting and analyzing information have been highly developed. Dependency on computer systems has been increased in almost all industries. Breakdown of these systems will make it impossible to maintain the industrial activities.

(3) Lifeline systems such as road, railway, electricity, gas, water and telephone have been highly developed. Breakdown of these systems will make it impossible to maintain the life activities.

(4) Those systems described above have highly dependency on each other. Due to the interaction of systems, function of facilities becomes possible to be affected by the earthquake damage of the other facilities.

(5) Propagation of functional damage can be developed simultaneously in whole urban area. Because of the complexity of propagation paths, it becomes difficult to evaluate the total loss or

1) Planning Division, Public Works Research Institute (Head, Earthquake Engineering Division)
2) Research Engineer, Earthquake Engineering Division, Public Works Research Institute
3) Kita-sorachi Construction Office, Hokkaido Development Bureau (Earthquake Engineering Division, Public Works Research Institute)
4) Earthquake Engineering Division, Public Works Research Institute

decrease of functions due to an earthquake.

Structural model of functional damage which represents the propagation of functional damage among fundamental facilities in urban area was studied. Because the structural model can be varied with the scale of earthquake, the scale of metropolis and the configuration of industries, it was assumed as a premise that Tokyo metropolis was attacked by Kanto Earthquake. Because emphasis of the study was placed on the propagation paths of earthquake disaster, brainstorming method was adopted to figure out the interaction among fundamental facilities qualitatively.

2. FUNCTIONAL DAMAGE DUE TO AN EARTHQUAKE IN URBAN AREA

Fig. 1 shows the classification of fundamental facilities of which industries of a metropolis are consists. Fundamental facilities were classified by modifying the industrial classification which has been used for the input-output analysis of industries. Because the damage of [Electricity, Gas and Water], [Transportation and Communication] and [Public Service] facilities were supposed to have much influence on the propagation of functional damage, they were classified into more precise facilities so that propagation paths from each facilities could be shown in the structural model. On the contrary, [Agriculture], [Forestry], [Marine Products], [Mining], [Manufacture] and [Construction] facilities were summarized into [Production] because they were not supposed to have much influence on propagation of functional damage. And because the facilities associated with life activities were not shown in the industrial classification, [Residence] facilities were newly added to the fundamental facilities for taking account the damage of residential activity into the structural model.

As a result, nineteen facilities were determined as the fundamental facilities in urban area. And for making the expression easier, nineteen facilities were classified into five groups, such as [Transportation Facilities], [Lifeline Facilities], [wholesale/ Financial Facilities], [Service/ Public Facilities] and [Others].

Concerned with each nineteen fundamental facilities, seismic damage which can be expected to be developed by an earthquake was studied by brainstorming method. Brainstorming was carried out by 4-6 persons who were specialists on earthquake engineering. Associated with [Lifeline Facilities] and [Wholesale/ Financial Facilities], interviews to administrators were carried out in addition to the results of brainstorming.

On the brainstorming, seismic damage was classified into physical damage, direct functional damage, primary functional damage and secondary functional damage in accordance with the propagation stages of earthquake disaster. Physical damage means the damage of structures and equipments. Direct functional damage means the loss or decrease of functions developed in the facility due to physical damage. Primary functional damage means the loss or decrease of functions developed in the facility as a result of the primary propagation from direct functional damage. Secondary functional damage means the loss or decrease of functions developed in the facility as a result of the secondary propagation from primary functional damage.

Based on the brainstorming and interview, 527 items of seismic damage which include 148 items of physical damage, 121 items of direct functional damage, 138 items of primary functional damage and 120 items of secondary functional damage were extracted. **Table 1** shows the seismic damage of road facilities and financial facilities which are expected to be developed by an earthquake. Associated with road facilities, typical propagation paths are estimated as follows;

(1) [Subsidence on Road] and [Slope Failure] as physical damage will cause [Passing Prohibition] and [Passing restriction] as direct functional damage.

(2) [Passing Prohibition] and [Passing Restriction] as direct functional damage will cause

[Passing Trouble of Vehicles] as primary functional damage.
(3) Passing trouble of emergency vehicles, such as fire engines and ambulances, cause [Spread of Fire] and [Casualties] as secondary functional damage.

Associated with financial facilities, typical propagation paths of functional damage are estimated as follows;
(1) [Collapse of Bank Building] as physical damage cause [Trouble of Service at Counter] as direct functional damage.
(2) [Trouble of Service at Counter] as direct functional damage cause [Restriction of Payment] and [Psychological Confusion] as primary functional damage.
(3) [Restriction of Payment] as primary functional damage cause [Bankruptcy of Companies] as secondary functional damage.

As was mentioned before, emphasis of this study was placed on clarifying the outline of disaster propagation rather than the detail of functional interaction. Because it was difficult to express 527 items of seismic damage in a structural model, before the formulation of structural model, it was required to summarize all these items into fewer representative seismic damage. Therefore 527 items of seismic damage were summarized by VE (Value Engineering) method. Fundamental policy of summarization was as follows;
(1) Physical damage and direct functional damage are closely related each other. Because direct functional damage could be represented by physical damage, direct functional damage was neglected in the structural model.
(2) Physical damage was represented by nineteen seismic damage for each nineteen fundamental facilities. For example, all physical damage of [Road] facilities such as [Subsidence in Road] and [Slope Failure] were represented by [Physical Damage of Road Facilities].
(3) Primary functional damage was also represented by seismic damage for each nineteen fundamental facilities. Primary functional damage of [Road] facilities such as [Passing Trouble of Fire Engines] and [Passing Trouble of Ambulances] were represented by [Trouble of Road Transportation]. Associated with [Wholesale/ Financial], [Service/ Public] and [Others] facilities, functional damage ought to be represented by [Restriction of Commerce], [Restriction of Finance] and [Restriction of Service] alternatively. But they were defined as secondary functional damage because they could be also considered as the damage due to primary functional damage of [Transportation] and [Lifeline] facilities.
(4) Secondary functional damage was classified based on the fundamental functions of metropolis, i.e. economy, residence and public service. Functional damage associated with economy was represented by [Restriction of Production], [Restriction of Commerce], [Restriction of Finance] and [Restriction of Service]. Functional damage associated with residence was represented by [Restriction of Residence], [Restriction of Materials], [Restriction of Behavior] and [Restriction of Information]. And functional damage associated with public service was represented by [Restriction of Medication], [Restriction of Education], [Restriction of Administration] and [Restriction of Mass Communication].

Although seismic damage was summarized into fewer representative damage to make the structural model clear, 527 items of seismic damage was reflected in evaluating the interaction between representative damage.

3. STRUCTURAL MODEL OF FUNCTIONAL DAMAGE DUE TO AN EARTHQUAKE IN URBAN AREA

Fig. 2 shows the structural model formulated by brainstorming method. It represents the basic interaction between functional damage developed by an earthquake. Based on this model, several features of the earthquake disaster propagation can be deduced.
(1) As shown in **Fig. 3**, two types of disaster propagation can be observed. Associated with the first type of disaster propagation (designated

hereinafter as forward propagation), seismic damage propagate from physical damage to secondary functional damage via primary functional damage. Associated with the second type of disaster propagation (designated hereinafter as same stage propagation), several seismic damage which belong to the same stage cause each other. For example, [Damage of Road Facilities] cause [Damage of Gas Facilities] in the stage of physical damage. Also, [Trouble of Electricity Supply] cause [Trouble of Road Transportation] in the stage of primary functional damage.

(2) In the stage of physical damage, [Damage of Road Facilities], [Damage of Harbor Facilities], [Damage of River Facilities] and [Damage of Water Supply Facilities] cause the same stage propagation. [Damage of Road Facilities] causes physical damage of lifeline facilities such as electricity, gas, water, sewerage and communication which are embedded in the road embankment. Associated with [Damage of Harbor Facilities], [Damage of River Facilities] and [Damage of Water Supply Facilities], flood developed by these damage cause physical damage of road facilities and railroad facilities.

(3) In the stage of primary functional damage, [Trouble of Electricity Supply] causes the same stage propagation. [Trouble of Electricity Supply] causes the primary functional damage of transportation facilities and lifeline facilities due to their highly dependency on electricity.

Because the structural model represents the outline of disaster propagation qualitatively, quantitative effects such as the strength of interaction and the rapidity of propagation are not considered at this time. Therefore, It is required to improve the structural model for taking account these quantitative effects into analysis in the future.

4. FUNDAMENTAL FACILITIES MOST INFLUENTIAL TO EARTHQUAKE DISASTER PROPAGATION

Fig. 4 shows the comparison of total number of propagation paths starting from each physical damage of nineteen fundamental facilities. Because the quantitative effects was not expressed in the structural model, the influence of physical damage was evaluated by counting the number of propagation paths for each nineteen fundamental facilities. From this study, following points can be deduced.

(1) Most of all the propagation paths are developed by physical damage of [Transportation Facilities] and [Lifeline Facilities]. Propagation paths developed by physical damage of [Wholesale/ Finance Facilities], [Service/ Public Facilities] and [Others] are quite few. This is because [Transportation Facilities] and [Lifeline Facilities] are used for various industries depending on the characteristics of users. On the contrary, [Wholesale/ Finance Facilities], [Service/ Public Facilities] and [Others] are used by limited users in specific industry. Therefore it is pointed out that physical damage of facilities with highly publicity, such as [Transportation Facilities] and [Lifeline Facilities], is more influential to the earthquake disaster propagation.

(2) Among [Transportation Facilities] and [Lifeline Facilities], [Road], [Electricity Supply] and [River] facilities produce more propagation paths than the other facilities. The number of propagation paths is increasing in the order of [Road], [Electricity Supply], [River] facilities. If physical damage of [Road] facilities can be prevented by conducting appropriate seismic countermeasures, about 36 % of all the propagation paths in the structural model can be interrupted. And if physical damage of these three facilities can be prevented, about 62 % of all the propagation paths can be interrupted.

For studying the difference of disaster propagation characteristics among [Transportation Facilities], **Fig.5** and **Fig.6** show the number of propagation paths starting from [Road] facilities and [Airport] facilities alternatively. Although both of these facilities have highly publicity, the number of propagation paths starting from [Airport] Facilities is much less than that of [Road] facilities. This is because physical damage of [Road] facilities develop the same stage propagation,

and physical damage of [Airport] facilities does not develop the same stage propagation. Therefore it is pointed out that fundamental facilities which develop the same stage propagation are more influential to the earthquake disaster propagation.

5. FUNCTIONS OF METROPOLIS MOST VULNERABLE AGAINST EARTHQUAKE DISASTER

Fig.7 shows the comparison of total number of propagation paths getting to each secondary functional damage of metropolis. Because propagation paths getting to the secondary functional damage represent the factors causing each damage, the vulnerability of metropolitan functions can be evaluated by counting the number of propagation paths for each metropolitan functions. Based on this study, the number of propagation paths is largest in [Restriction of Production], [Restriction of Commerce], and [Restriction of Service] among all functional damage. [Restriction of Education], [Restriction of Medication] and [Restriction of Administration] are following above-mentioned functional damage. Therefore, for increasing the seismic safety of metropolis, appropriate seismic countermeasures which interrupt the propagation paths getting to these vulnerable functions are required to be conducted.

For studying the factors which develop [Restriction of Production], **Fig.8** shows the number of propagation paths from each physical damage of nineteen fundamental facilities. Associated with [Restriction of Commerce] and [Restriction of Service], the tendency is almost same with [Restriction of Production]. From this figure, it is pointed out to be effective to prevent the physical damage of [Road] facilities for reducing [Restriction of Production].

CONCLUDING REMARKS

For studying the interaction of functional damage due to earthquake in urban area, structural model of earthquake disaster propagation was formulated by brainstorming method. Associated with the disaster propagation characteristics, fundamental facilities most influential to disaster propagation and metropolitan functions most vulnerable against earthquake disaster, following conclusions were deduced with use of the structural model.

(1) Two types of disaster propagation were observed. In the forward propagation, seismic damage propagate from physical damage to secondary functional damage via primary functional damage. In the same stage propagation, several seismic damage which belongs to the same stage cause each other. Physical damage of road facilities, harbor facilities, river facilities, water supply facilities and primary functional damage of electricity supply facilities cause the same stage propagation.

(2) Physical damage of road facilities, electricity supply facilities and river facilities are most influential to the disaster propagation. If physical damage of road facilities can be prevented, about 36% of all the propagation paths can be interrupted. If physical damage of three facilities can be prevented, about 62% of all propagation paths can be interrupted.

(3) Among the functions of metropolis, production, commerce and service are most vulnerable against earthquake disaster. Because the major factor causing restrictions of these functions is the physical damage of road facilities, it is important to prevent the physical damage of road facilities for increasing the seismic safety in urban area.

REFERENCES

(1) Kazuhiko KAWASHIMA and Takashi KANOH: Evaluation of Indirect Economic Effects Caused by The 1983 Nihonkai-chubu, Japan, Earthquake, Earthquake Spectra, Vol.6, No.4, November 1990

(2) Public Works Research Institute: Evaluation of Economical Indirect Damage Caused by Earthquakes, Report of PWRI, Vol.186-1, Dec. 1991

Table 1 Damage Expected to be Developed on Fundamental Facilities

(a) Road Facilities

PHYSICAL DAMAGE	PROPAGATE TO	DIRECT FUNCTIONAL DAMAGE	PROPAGATE TO	PRIMARY FUNCTIONAL DAMAGE	PROPAGATE TO	SECONDARY FUNCTIONAL DAMAGE
a) SUBSIDENCE	a), b)	a) PASSING PROTECTION	a)~l)	a) PASSING TROUBLE OF FIRE ENGINE	a), b)	a) SPREAD OF FIRE
b) SLOPE FAILURE	a), b)	b) TRAFFIC CONTROL	a)~l)	b) PASSING TROUBLE OF AMBULANCE	b), f)	b) CASUALTIES
c) DAMAGE OF BRIDGE	a), b)	c) TROUBLE IN INTERRUPTING FIRE		c) PASSING TROUBLE OF PATROL CAR	c)	c) RESTRICTION OF POLICE ACTIVITY
d) BLOCKADE OF TUNNEL	a), b)	d) TROUBLE IN TRAFFIC MANAGEMENT	a)~m)	d) PASSING TROUBLE OF TRUCK	d), j)	d) SHORTAGE OF DAILY GOODS
e) DAMAGE OF TRAFFIC SIGNAL	d), g)	e) TROUBLE IN FLOWING SEWAGE		e) PASSING TROUBLE OF PASSENGER CAR	k), l), m)	e) SHORTAGE OF RELIEF GOODS
f) DAMAGE OF CROSSWALK	f), i)	f) TROUBLE IN SIDEWALK PROTECTION	i), j), m)	f) PASSING TROUBLE OF BUS	k), l), n)	f) DELAY OF FIRST AID
g) DAMAGE OF SIDEWALK PROTECTION	f), i)	g) TROUBLE IN PREVENTING ACCIDENT	m)	PASSING TROUBLE OF CAB		g) DELAY OF RESTORATION
h) DAMAGE OF LIGHTNING	g)	h) TROUBLE IN PARKING	l)	PASSING TROUBLE OF MOTORCYCLE		h) INCREACE OF TIME FOR COMMUNICATION
i) DAMAGE OF PARKING METER	h), k)	i) TROUBLE IN SIDEWALK	i), j)	PASSING TROUBLE OF BYCYCLE		i) DECREACE OF INFORMATION AMOUNT
j) DAMAGE OF TRAFFIC SIGN	d), g)	j) TROUBLE IN TAKING REST	k)	g) PASSING TROUBLE OF VEHICLE FOR RESTORATION	b), e), g)	j) STAGNATION OF INDUSTRY STAGNATION OF COMMERCE
k) FALLING DOWN OF TREE	c)	k) TROUBLE IN COLLECTING MONEY		h) PASSING TROUBLE OF VEHICLE FOR MEDIA	h), i)	k) INCREACE OF TIME FOR GOING HOME
l) DAMAGE OF GUTTER	e)			PASSING TROUBLE OF VEHICLE FOR ADMINISTRATION		l) INCREACE OF TIME FOR GOING OFFICE/SCHOOL
m) DAMAGE OF UNDERGROUND PATH	i)			i) PASSING TROUBLE FOR EVACUATION	b), o)	m) INCREACE OF VEHICLE LEFT ON LOAD
n) DAMAGE OF TALL GATE	k)			j) PASSING TROUBLE FOR GOING HOME	k)	n) DELAY OF DESTRIBUTION OF MAIL/PAPER
o) DAMAGE OF FOOTBRIDGE	f), i)			PASSING TROUBLE FOR GOING OFFICE/SCHOOL		o) INCREACE OF TIME FOR EVACUATION
q) DAMAGE OF SIDEWALK	f), i)			k) PASSING TROUBLE FOR LEISURE		
r) DAMAGE OF SERVICE AREA	h), j), k)			l) TROUBLE IN GETTING ON/OFF	j), n)	
				m) TRAFFIC ACCIDENT	a), b)	

(b) Financial Facilities

PHYSICAL DAMAGE	PROPAGATE TO	DIRECT FUNCTIONAL DAMAGE	PROPAGATE TO	PRIMARY FUNCTIONAL DAMAGE	PROPAGATE TO	SECONDARY FUNCTIONAL DAMAGE
a) DAMAGE OF BANK BUILDING	a), c), d)	a) TROUBLE IN COUNTER SERVICE	c), e)	a) TROUBLE ON INPUT/OUTPUT OF DEPOSIT/SAVINGS DATA	a), b)	a) COUNTER SERVICE BY LABOR
b) DAMAGE OF ON-LINE SYSTEM	b)	b) TROUBLE IN ON-LINE SYSTEM	a), b), d)	b) TROUBLE ON GETTING DEPOSIT	c)	b) DELAY OF SERVICE
		c) TROUBLE IN CD SERVICE	a), b)	c) PSYCOLOGICAL CONFUSION	b)	c) BUNKRUPTCY OF COMPANIES
		d) TROUBLE IN ATM SERVICE	d)	d) SHORTAGE OF PREPARING CASH	b), c)	
				e) OFFICIAL ANNOUNCEMENT ON RESTRICTION OF PAYMENT	c)	

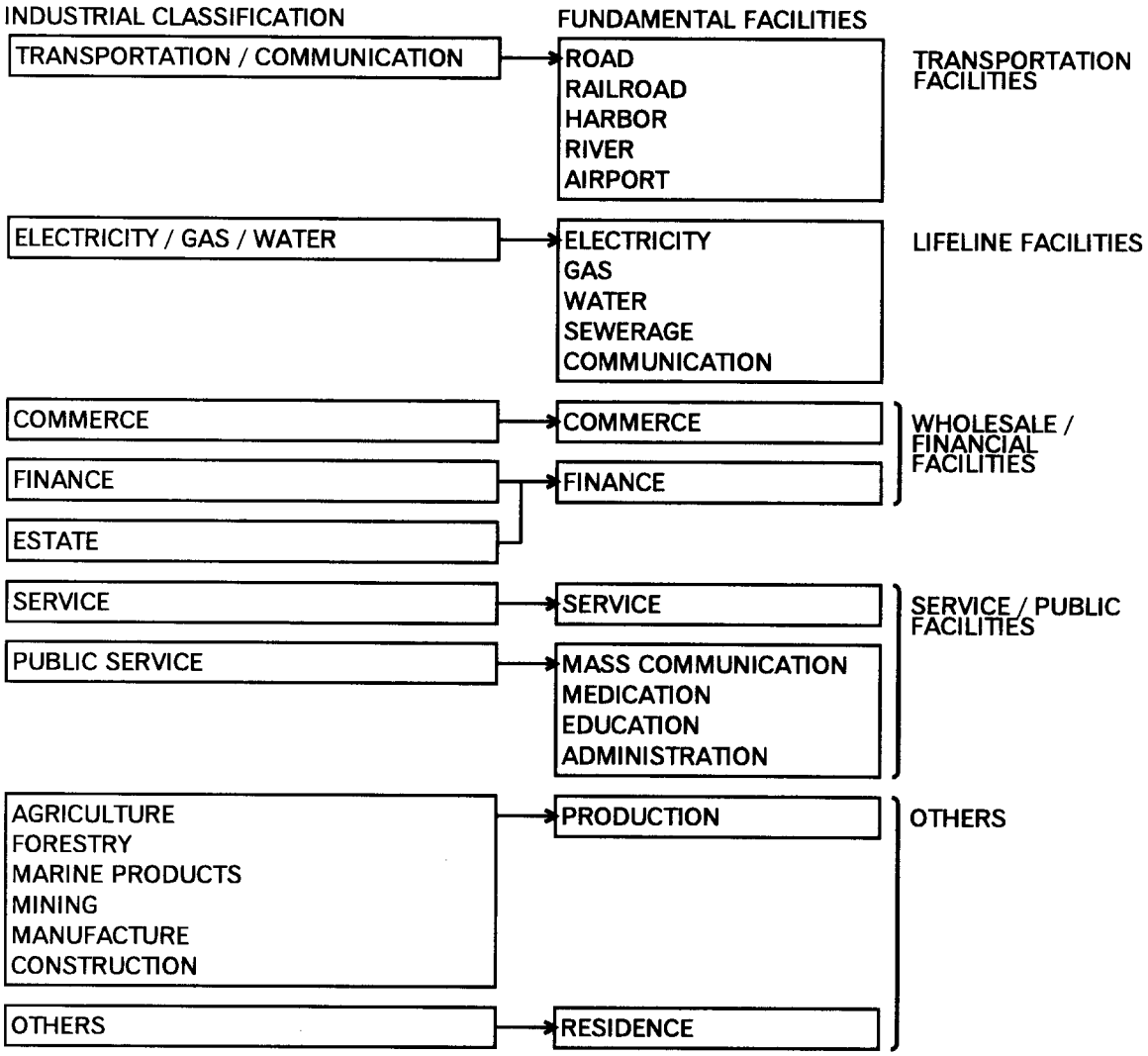

Fig. 1 Classification of Fundamental Facilities in Urban Area

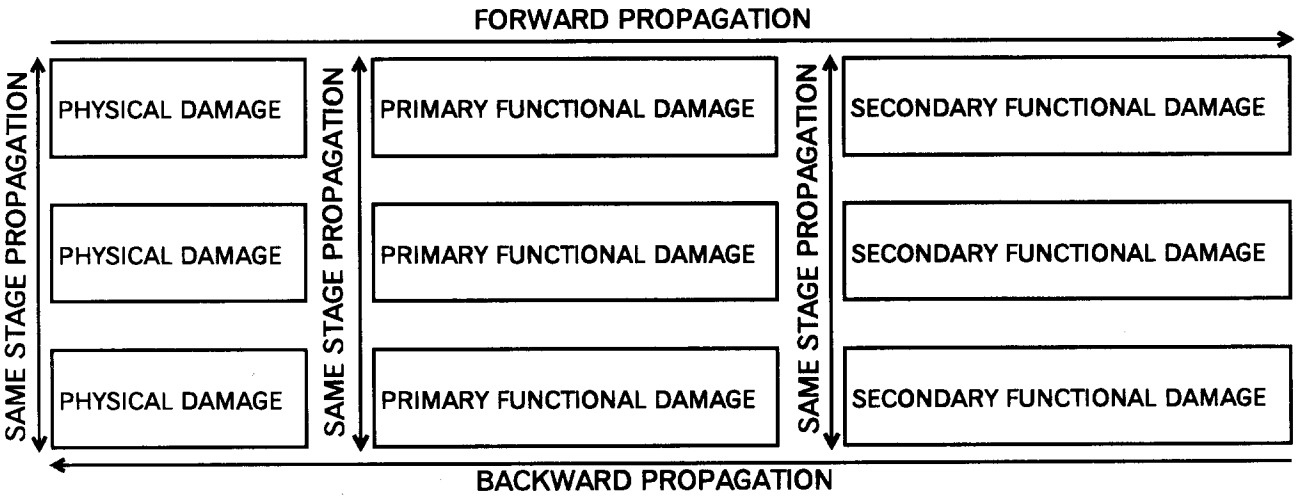

Fig. 3 Direction of Disaster Propagation

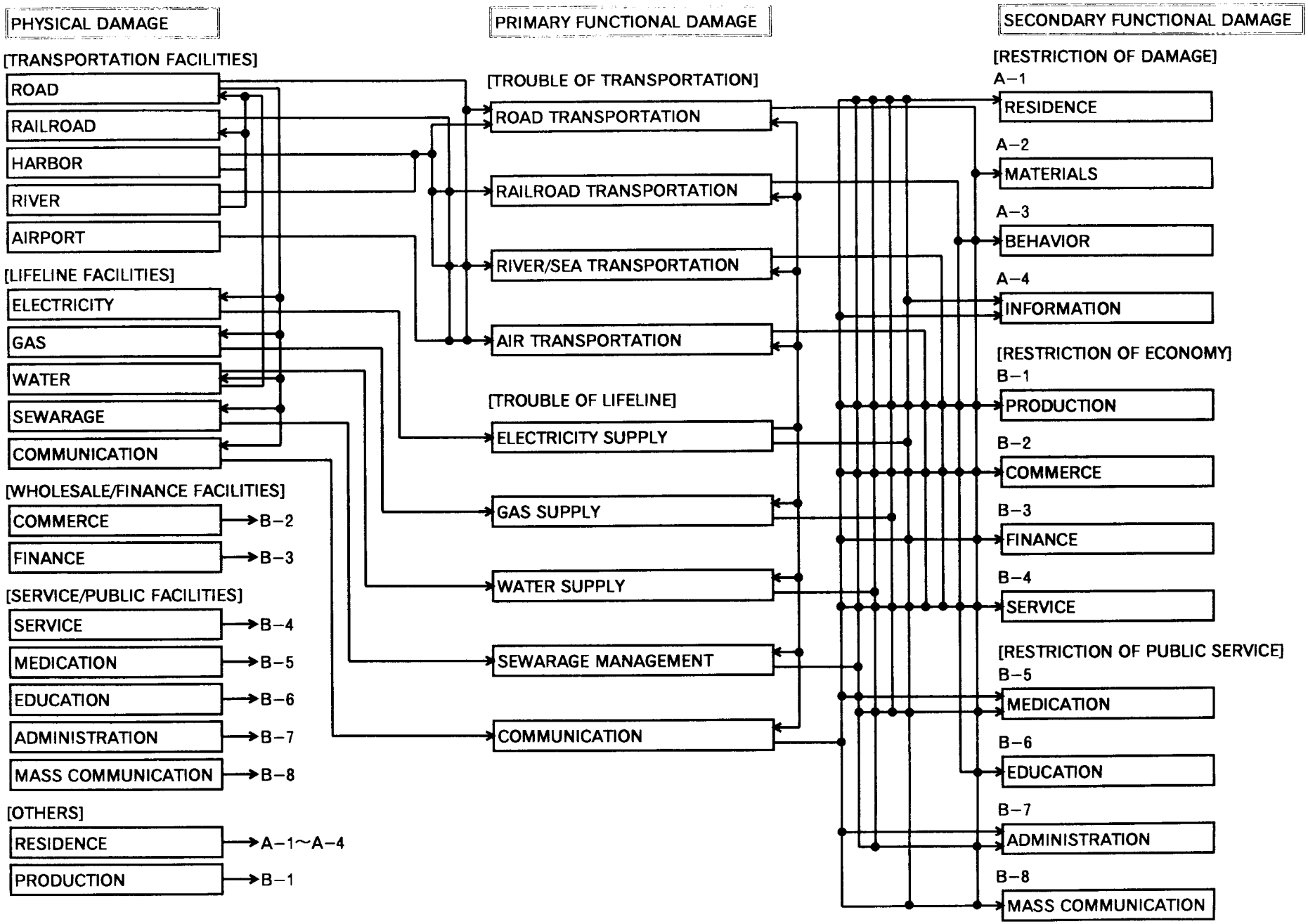

Fig. 2 Structural Model of Earthquake Disaster Propagation in Urban Area

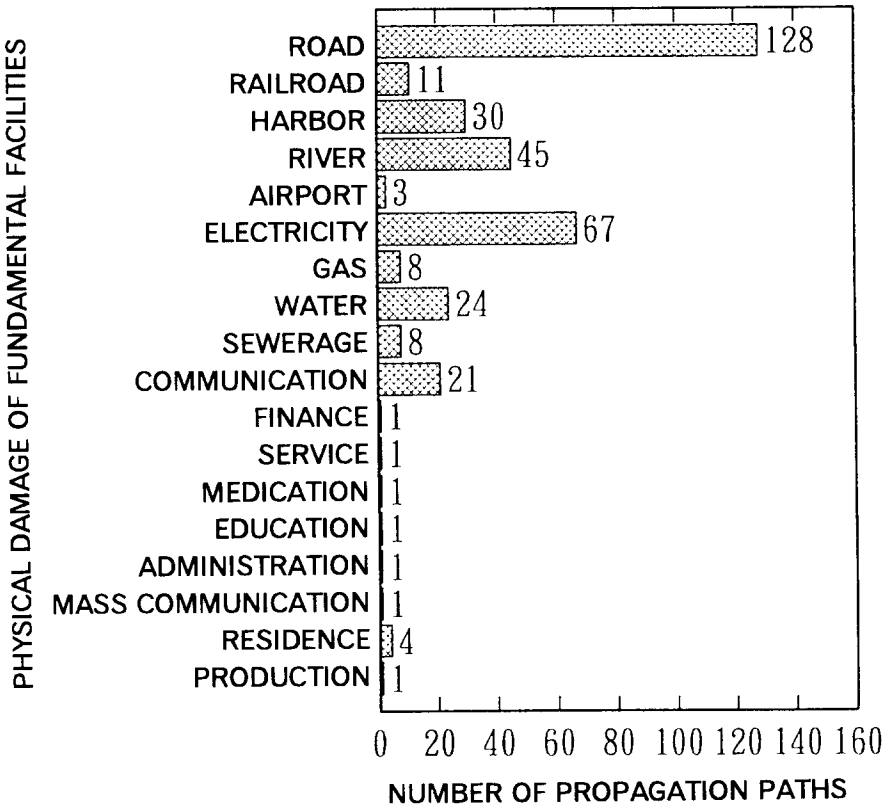

Fig. 4 Fundamental Facilities Most Influential to Disaster Propagation

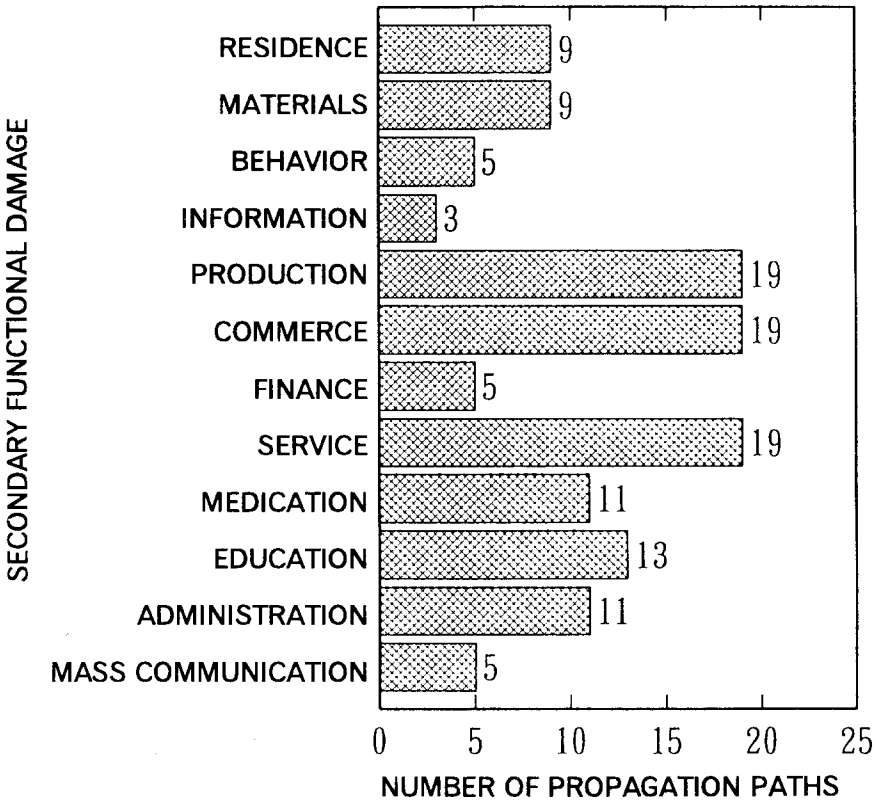

Fig. 5 Influence of Physical Damage of Road Facilities

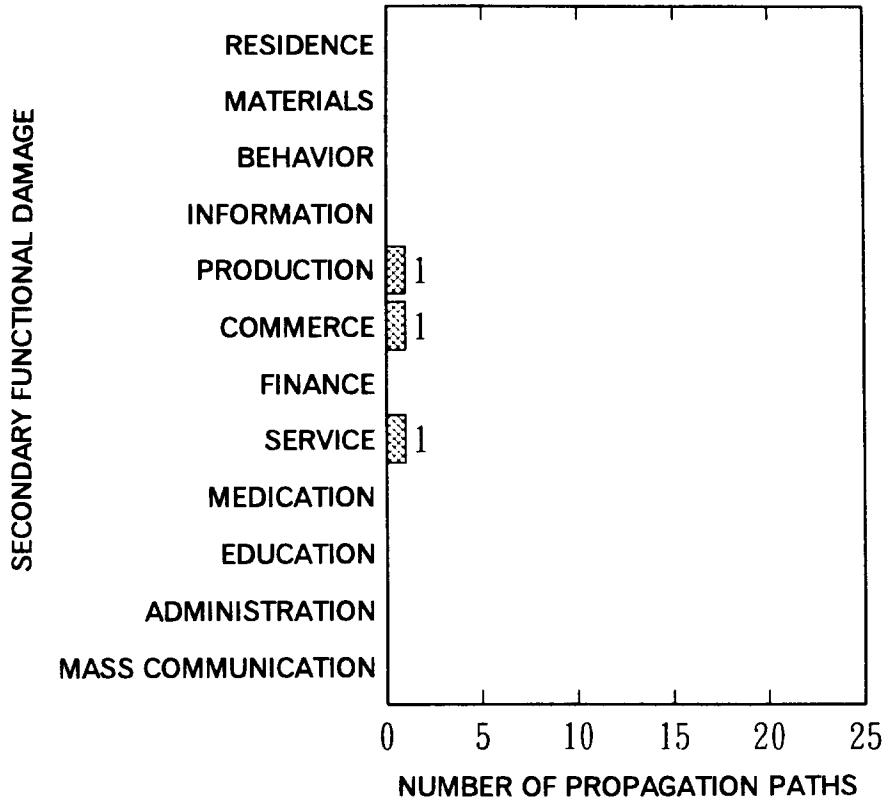

Fig. 6 Influence of Physical Damage of Airport Facilities

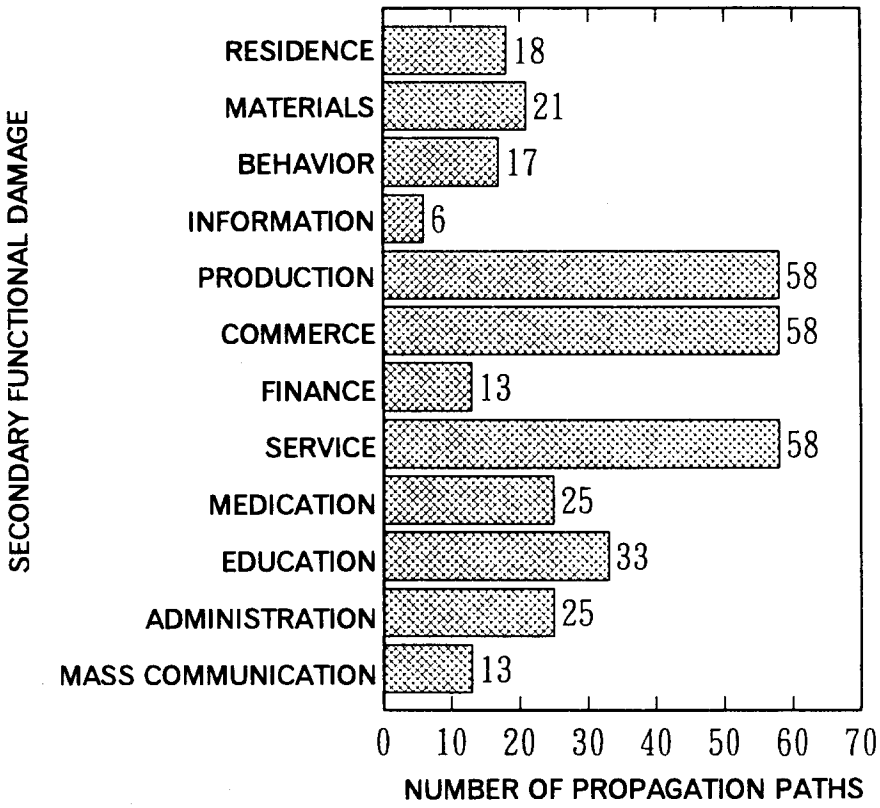

Fig. 7 Metropolitan Functions Most Vulnerable against Disaster Propagation

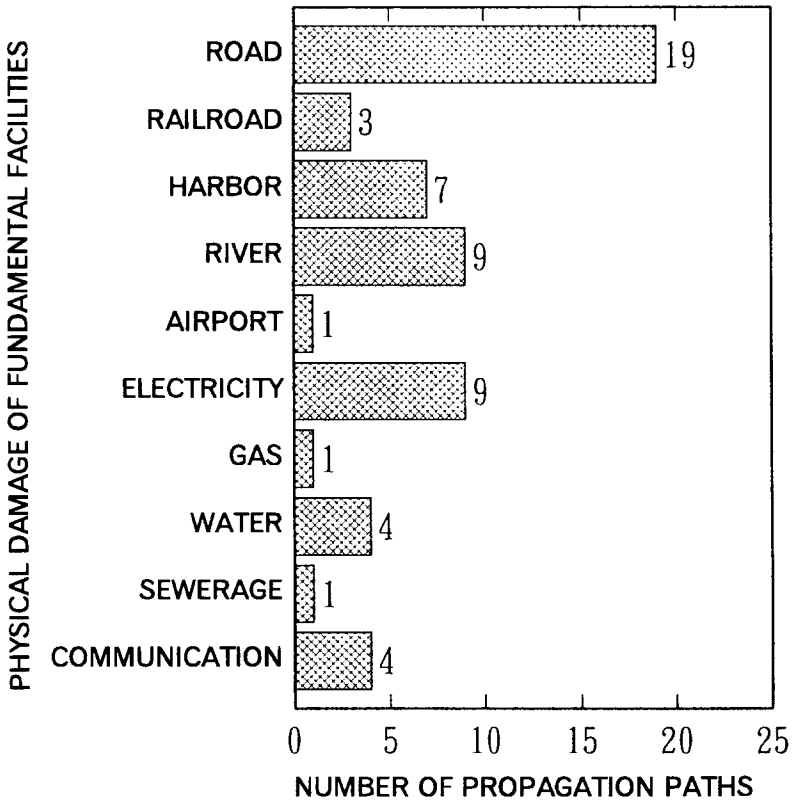

Fig. 8 Factors Causing Restriction of Production

Dynamic Behavior of Pile Foundation in Liquefaction Process

by

T. Kagawa[1], C. Minowa[2] and H. Mizuno[3]

ABSTRACT

This paper highlights results and a preliminary analysis of a series of shaking-table tests on model pile-foundation systems in loose saturated sand. The ultimate objective of this research is to develop numerical methods and design guidelines for pile foundations in potentially liquefiable sand deposits. This study, although preliminary in nature, demonstrated the significance of liquefaction on pile responses and provided an improved understanding of the soil-pile interaction in liquefying sand.

INTRODUCTION

Pile foundations are common at potentially liquefiable sites, and they have experienced damage and failures during major earthquakes. A number of studies have been made in recent years on dynamic and seismic behavior of isolated piles and of groups of piles, to increase our understanding of seismic soil-pile-structure interaction. The state of the art in this field, however, has not advanced to a point where we can predict the performance of pile foundations when the surrounding soils undergo liquefaction during an earthquake.

A joint research was initiated in 1992 between the National Research Institute for Earth Science and Disaster Prevention (NIED), Science and Technology Agency of Japan and Wayne State University to study the response of pile foundations in liquefying sand. As an initial step toward establishing rational analysis procedures and design guidelines for pile foundations at potentially liquefiable soil deposits, this joint research attempts to quantify the lateral soil-reaction response of piles when the surrounding soils undergo liquefaction. To accomplish this objective, the first and the second series of shaking-table tests were already conducted, respectively, in April, 1992 and July, 1993 at NIED. Also model pile-section tests are being conducted at Wayne State University to obtain an improved insight into the results from the shaking-table tests.

This paper highlights the first series of the shaking-table tests on model piles in loose saturated sand and the major findings from the tests. This is followed by a summary of results from our preliminary

---

1) Professor, Department of Civil Engineering, College of Engineering, Wayne State University, Detroit, Michigan, U.S.A.
2) Cooperative Research Officer, National Research Institute for Earth Science and Disaster Prevention. Science and Technology Agency, Tsukuba-City, Japan
3) International Codes and Standards Research, Building Research Institute, Ministry of Construction, Tsukuba-City, Japan

numerical analyses using existing nonlinear soil-pile-structure interaction methods.

DESCRIPTION OF SHAKING-TABLE TESTS

Background

No field observations on the response of pile foundations in liquefying sand layers are available at present. Therefore, one of the major tasks of this research is to obtain reliable experimental data on the lateral soil reaction responses of piles when the surrounding soils undergo liquefaction and flow through the piles. Such data may be obtained by two experimental methods, centrifuge tests and 1-g model tests. The similitude requirements for these types of tests were summarized by several investigators; i.e., Kagawa (1978), Iai (1989), etc. Centrifuge tests involve large geometrical scaling, typically on the order of 50 to 100. Therefore, it becomes difficult to satisfy the geometrical similarity on soil particle size. This may result in incorrect representation of the failure strength of the sand mass around the model pile. Also, small-scale tests require large reduction in the rate of pore pressure redistribution. For these reasons, the authors prefer 1-g model tests with reasonably large models.

However, the size of the model pile-foundation system in this research is rather small to reduce experimental cost and to serve as the preliminary tests to the large-scale tests, which are scheduled to be performed in 1996 through 1998. A large-scale laminar shear box with a height exceeding five meters is being designed at NIED. Pile foundations with nearly prototype scales will be installed in this shear box, and the effects of liquefaction and lateral flow of liquefied soils on piles will be studied.

Sand Layer

The saturated sand layers for the tests were prepared in a laminated shear box with a plan dimension of 2 by 2 meters and a height of 1 meter. The shear box consisted of twelve independent rectangular steel frames with a height of 10 cm, stacked on top of each other with bearings between the frames to force the sand layer to deform in one-dimensional shear deformation. The laminated shear box with sand and the model pile foundation is shown in Fig. 1.

The test sand was the Kasumigaura sand taken from the bed of the Kasumigaura Lake near the city of Tsuchiura, Japan. The physical characteristics of the Kasumigaura sand have been studied reasonably well by various researchers in Japan. The sand is well graded with a moderate amount of fines. The specific gravity of the sand was 2.71; the percent weight of fines (silts and clays) was 3.4 %; the mean particle diameter (D_{50}) was 0.0885 cm; the uniformity coefficient was 5.62; the maximum and minimum dry densities were 1.76 and 1.36 g/cm^3; and the coefficient of permeability was 3.1 x 10^{-2} cm/sec..

For each shaking-table test, a fresh sand layer was prepared by pouring the wet test sand into the shear box, which was partially filled with water. The density, water content, and the shear-wave velocity of the sand layer thus prepared were measured before and after shaking. Results are summarized in Table. 1.

Model Pile Foundation

The model pile foundation system consisted of two steel strips, placed in line with the direction of shaking with a clear distance of 18 cm, and a steel box filled with

lead shots. The length, width, and thickness of the steel strips (model piles) were 91.7 cm, 5 cm, and 0.6 cm. The plan dimension of the steel box was 27.8 by 17.3 cm with a height of 8.3 cm. The steel box with lead shots represented a structure with a translational degree-of-freedom only. The total weight of the steel box and the lead shots was 12.4 kgf. The steel strips were rigidly bolted to the steel box, to reproduce the fixed-head condition for the model piles. The tips of the model piles were pinned at the base of the shear box. Therefore, they were free to rotate.

Instrumentation

Figure 2 shows a schematic view of the cross section of the sand layer-model pile foundation system and of the layout of various instrumentation devices. For the sand layer, acceleration responses were measured at four levels, A-1, A-2, A-3 and A-5; and the excess pore-water pressures were measured also at four levels, P-1 through P-4, and P-5. For the model pile foundation system, six pairs of strain gages were attached to the model pile, 1-1 through 6-1 and 1-2 through 6-2; the soil stresses on the model pile were measured at three levels, F-1 through F-3; and the acceleration and the displacement responses of the structural mass were measured, A-5 and D-4. In addition, the displacement responses of the frames were monitored at three levels, D-1 through D-3 to estimate free-field soil movements.

Shaking-Table Input

The large-scale shaking table at the National Research Institute for Earth Science and Disaster Prevention has a table dimension of 15 by 14.5 meters with a maximum model weight of 500 tons. The table is excited by four synchronized actuators in a fixed horizontal direction with a maximum displacement amplitude of 22 cm.

In the first series of the shaking-table tests conducted in 1992, a random wave with uniform power amplitudes over the frequency range up to about 25 Hz was used as input to the shaking table. The peak table acceleration was about 100, 140, 140, 160, and 160 gals respectively for Test Nos. 2 through 6. These acceleration levels were considered to be consistent with the typical acceleration levels associated with historical liquefaction events and sufficiently large to produce liquefaction over the entire depth of the sand layers on the shaking table.

SUMMARY OF TEST RESULTS

Pore Pressure Responses

Figure 3 shows the time histories of measured responses from Test 3. Results from the other tests are similar to those in this figure. Several important observations may be made. For example, acceleration at shallow depths decreases dramatically as pore pressures build up, and it tends to increase again with time. Excess pore pressures at deeper depths increase first and then decrease steadily with time, while those at shallower depths tend to be constant or even increase during shaking. These responses are due to the upward redistribution of excess pore pressures. The excess pore pressures at P-5 are difficult to dissipate, due mainly to its long drainage path.

Table 2 summarizes the peak excess pore-water pressure ratios within the sand layers. Except Test 2, the sand layers liquefied almost throughout their entire

depths. It should be noted that larger pore pressure ratios were recorded at shallower depths and that excess pore pressure ratios exceeded unity by large margins at locations P-4 and P-5. The latter observation is due to the upward flow of the excess pore pressures developed at deeper depths. Also it should be noted that the excess pore pressures measured at P-5 (at 10-cm depth and between the model piles) are different from the readings at P-4, which was located at the same depth but in the free field. These seemingly inconsistent and complex observations are related closely to the relative speed of pore pressure buildup and of pore pressure redistribution and dissipation.

Acceleration Responses

The peak acceleration within the sand layers are summarized in Table 3. Except Test 4, the peak acceleration is larger at shallower depths. The peak accelerations of the structural mass are higher than those at A-3, except Test 5. These observations could be explained by carefully examining how excess pore pressures developed and redistributed within the sand layers, and they demonstrate the importance of the effect of liquefaction on the responses of the sand layer and the model pile.

p-y Relations

A preliminary analysis has been completed on the data obtained from the strain-gage pairs attached to the model pile. Figure 4 shows the typical results from this analysis.

The analysis yielded the following tentative conclusions on the lateral soil reaction versus pile deflection (p-y) relation of the model pile. The p-y relation for the initial stage of shaking appears to be a softening type; the p-y relation becomes mainly of a viscous type when the surrounding sands undergo liquefaction; and the p-y relation gradually transforms back to the initial softening type as excess pore pressures dissipate from the sand layer. Also the dilatancy tendency of liquefied sands is seen in the p-y relations.

Another analysis yielded the simple results on the change of lateral soil reaction coefficient versus pile, and reduction of the shear velocity of sand layer during the excitation. Fig. 5 shows the reductions which were brought by excess pore pressure increase. In the estimation of lateral soil reaction coefficients, the deformations of pile were assumed the fifth polynomials of height positions.

NUMERICAL ANALYSIS METHODS

Response of the model pile-foundation system to shaking-table excitation was computed in two steps; computation of the response of the sand layer and computation of the response of the model piles. The sand layer was assumed to deform in one-dimensional shear, and the response of the sand layer was obtained by a nonlinear site-response method SRANG2. The response of the model piles was computed by a nonlinear soil-pile-structure interaction method NONSPS2. These programs were documented by Kagawa (1992a and 1992b). Therefore, the key features of these methods are highlighted below.

Response of Sand Layer

It was reasonable to assume that the sand layer in the laminated shear box deformed in one-dimensional shear. Therefore, the response of the sand layer

was obtained by the one-dimensional wave-propagation theory that has been the most common tool for site-response analyses. Computed responses of the sand layer were then used in a subsequent soil-pile-structure interaction analysis as multiple soil-support input motions. The stress-strain relation of the sand was represented by a multiple, elastic-plastic spring model, which may be considered a simplified version of the multi-surface plasticity model. Excess pore pressures developed in the sand layers during shaking and they redistributed during and after shaking. The simple pore pressure model by Kagawa and Kraft (1981) was used to evaluate the pore pressure development aspect, and a standard one-dimensional consolidation model was used to compute redistribution and dissipation of excess pore pressures.

In the present analysis, the sand layer was divided into eighteen horizontal layers with an equal thickness of 5 cm. The small-strain shear moduli at the mid heights of the layers were computed from the experimental equation proposed by Iwasaki, Tatsuoka and Takagi (1978). The backbone curve of the shear stress versus shear strain relation was determined from an average trend of the shear-modulus reduction curves obtained by various investigators for cohesionless soils. The computed shear-wave velocity was about 60 m/sec. at 5-cm depth and 150 m/sec. at 85-cm depth. These agree well with the measured shear-wave velocities in Table 1, which range from 80 to 118 m/sec..

Response of Model Pile-Foundation System

The numerical method used to obtain the response of the model pile-foundation system was based on a beam-on-Winkler foundation model, which is similar to the one reported by Kagawa and Kraft (1981). In this method, a pile-supported structure is represented by a single-pile system; the superstructure is represented by a series of lumped masses, connected by beams; the pile is divided into segments; and each pile segment is connected to free-field soil through soil-pile elements. The numerical method is capable of representing complex soil-pile conditions such as; 1) nonlinear stress-strain behavior of soils around a pile, 2) excess pore pressure buildup in the free-field and around a pile, and 3) excess pore pressure redistribution and dissipation in the radial direction away from the pile and in the vertical direction. The EI of the model pile was estimated to be 1.9×10^5 kgf-cm^2.

SUMMARY OF RESULTS FROM NUMERICAL RESPONSE ANALYSIS

Figure 6 shows typical comparisons between measured and computed responses of the model pile-foundation system. Acceleration responses at A-4 (structural mass), A-3 (10-cm depth), A-2 (35-cm depth), and P-3 (25-cm depth) are shown in Fig. 6. Meassured accelerations and pore pressures agree reasonably well with measured responses. However, computed acceleration responses tend to include larger amplitudes than those from computations. Also computed sand displacements were generally less than those from the tests. These results appear to suggest the importance of dilatancy tendency of liquefied sand in controlling the responses of the sand layer and the model pile. In addition, dissipation of excess pore pressures had a significant impact on computed pore pressure responses. Bending moment in the model pile was controlled mainly by the deformation of the sand layer except near the structural model, and liquefaction of the sand layer increased

considerably the magnitude of the bending moment in the model pile.

SUMMARY COMMENTS

This study yielded several important conclusions and observations itemized below:

1. Excess pore pressure responses in the sand layer are affected significantly by their redistribution and dissipation.
2. The excess pore pressures in sand beneath the structural model appear to be "trapped," and they are slow to dissipate compared to those in the free field at the same elevation.
3. The sand layers in liquefied conditions exhibit dilatancy. This was indicated in the responses of the sand layers and in the lateral soil reaction versus pile displacement (p-y) relations of the model piles.
4. The lateral soil reaction versus pile displacement relations exhibit complex behavior during shaking. The lateral soil reaction to the model pile does not vanish even after the liquefaction of surrounding sand.
5. Bending moment in the model pile increased significantly due to liquefaction of the sand layer.

The experiment and the analysis presented in this paper could not answer all the questions that we wanted to resolve. We expect that these questions will be answered from ongoing experimental and analytical efforts.

ACKNOWLEDGMENT

The authors appreciate encourage -ment provided by Dr. N. Ogawa, the National Research Institute for Earth Science and Disaster Prevention and technical supports provided by Mr. A. Abe, Tokyo Soil Research Co., Ltd., and Dr. M. Yoshikawa, Tsukuba Research Institute, Okumura Corporation.

REFERENCES

Iai, S. "Similitude for Shaking Table Tests on Soil-Structure-Fluid Model in 1g Gravitational Field." Soils and Foundations, Vol.29, No.1 (1989): 105-118.

Iwasaki, T., Tatsuoka, F., and Takagi, Y. "Shear Moduli of Sands under Cyclic Torsional Shear Loading." Soils and Foundations, Vol.20, No.1 (1978): 45-59.

Kagawa, T. "On the Similitude in Model Vibration Tests of Earth Structure." Proceedings, Japan Society of Civil Engineers, No.275 (1978): 57-67 (in Japanese).

Kagawa, T. and Kraft, L.M., Jr. "Lateral Pile Response during Earthquake." Journal, Geotechnical Engineering Division, ASCE, Vol.107, No.12 (1981): 1713-1731.

Kagawa, T. SRANG2 and NONSPS2 - Numerical Methods for Nonlinear Earthquake Response of Soil-Pile System, Geotechnical Engineering Report, Department of Civil Engineering, Wayne State University, Detroit, Michigan, 1992a.

Kagawa, T. "Effects of Liquefaction on Lateral Pile Responses." Geotechnical Special Publication, No.34, ASCE (1992b): 207-223.

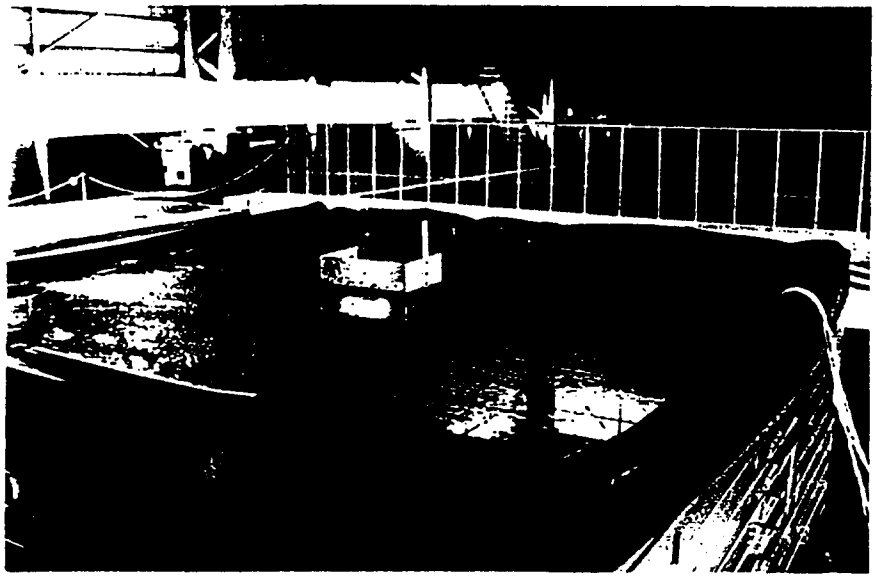

Fig. 1 Photo of Shaking-Table Model

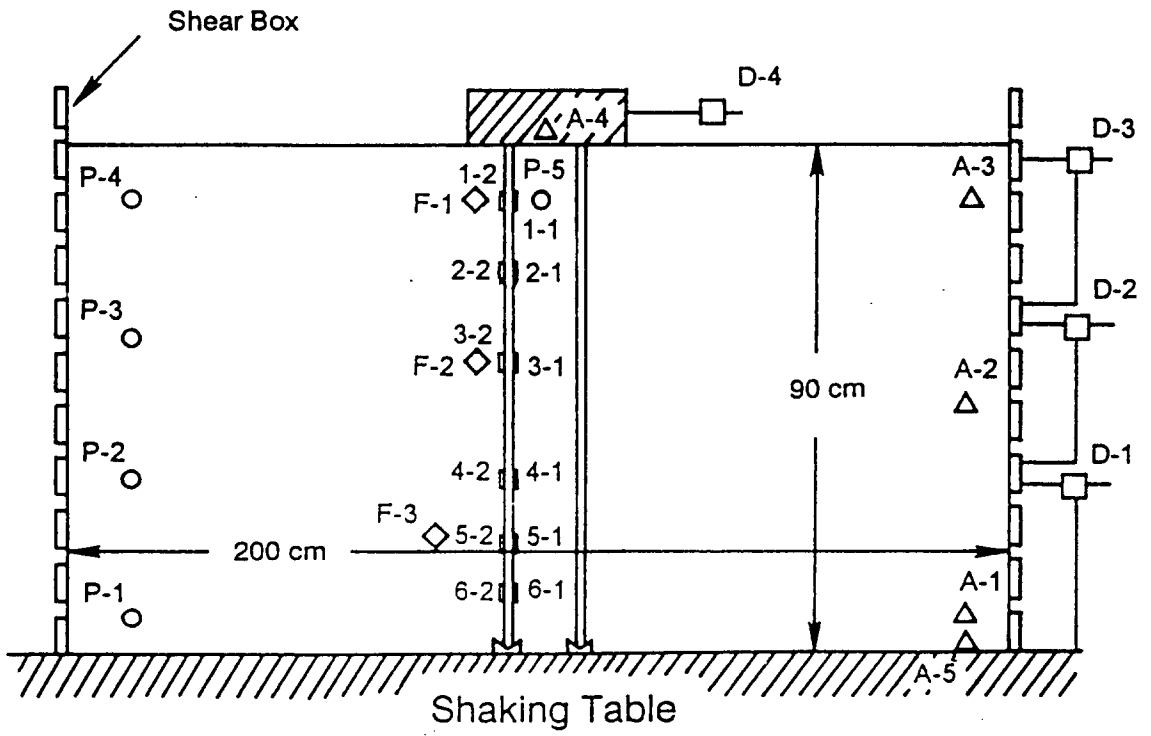

A-1 ~ A-5 ... Accelerometers D-1 ~ D-4 .... LVDT P-1 ~ P-5 .... Pressure Transducers

1-1 ~ 6-1 & 1-2 ~ 6-2 .... Strain Gages F-1 ~ F-3 .... Soil Pressure Transducers

Fig. 2 Layout of Instrumentation

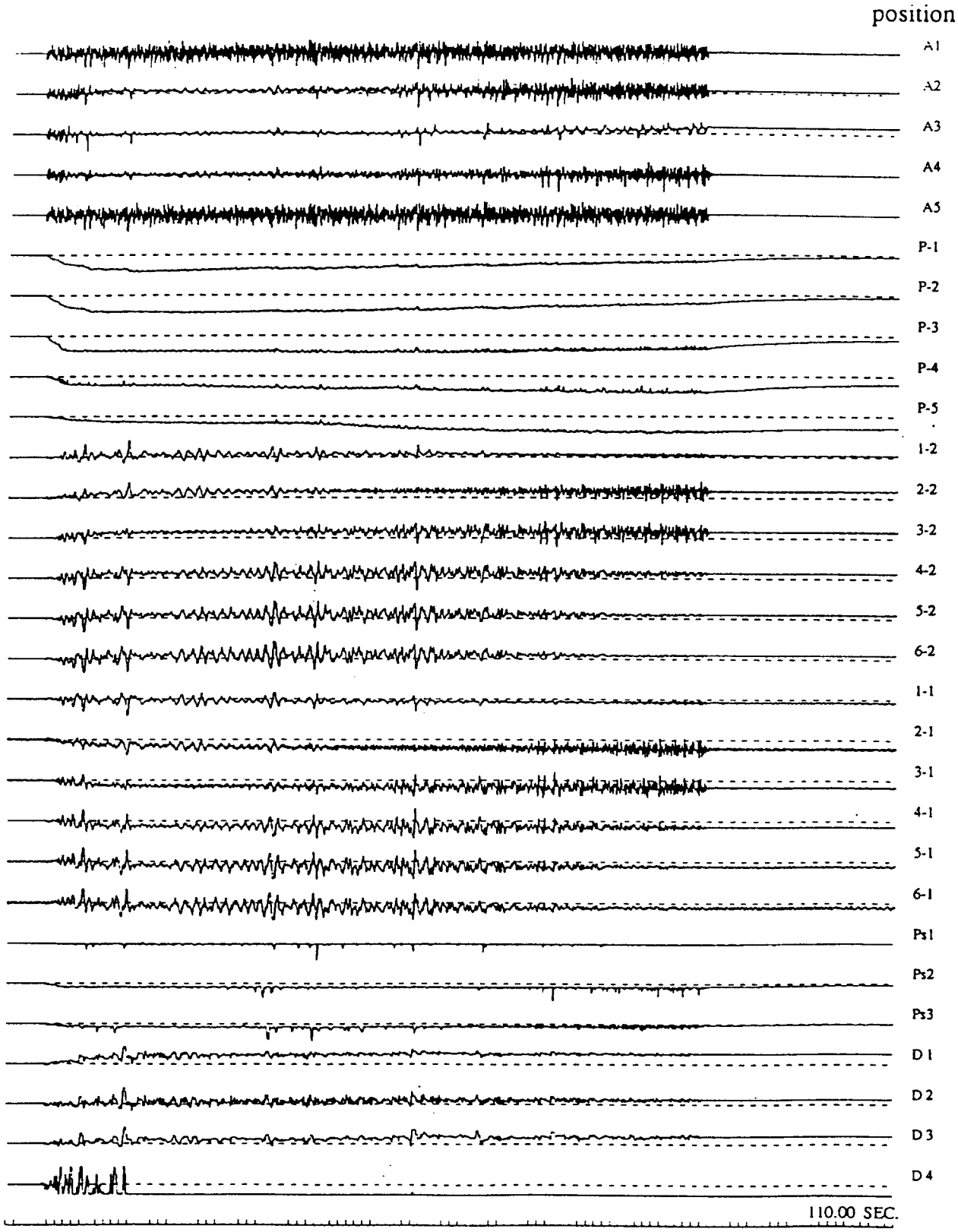

Fig. 3 Time Histories of Measured Responses (Test 3)

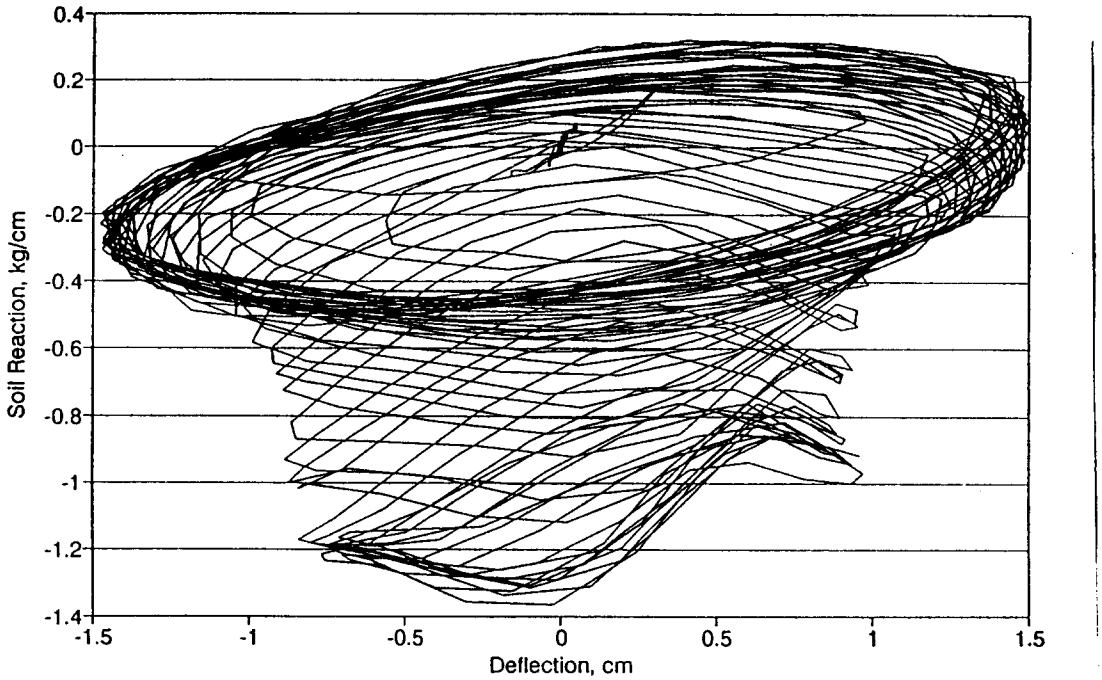

Fig. 4 Soil Reaction versus Pile Deflection Relation of the Model Pile

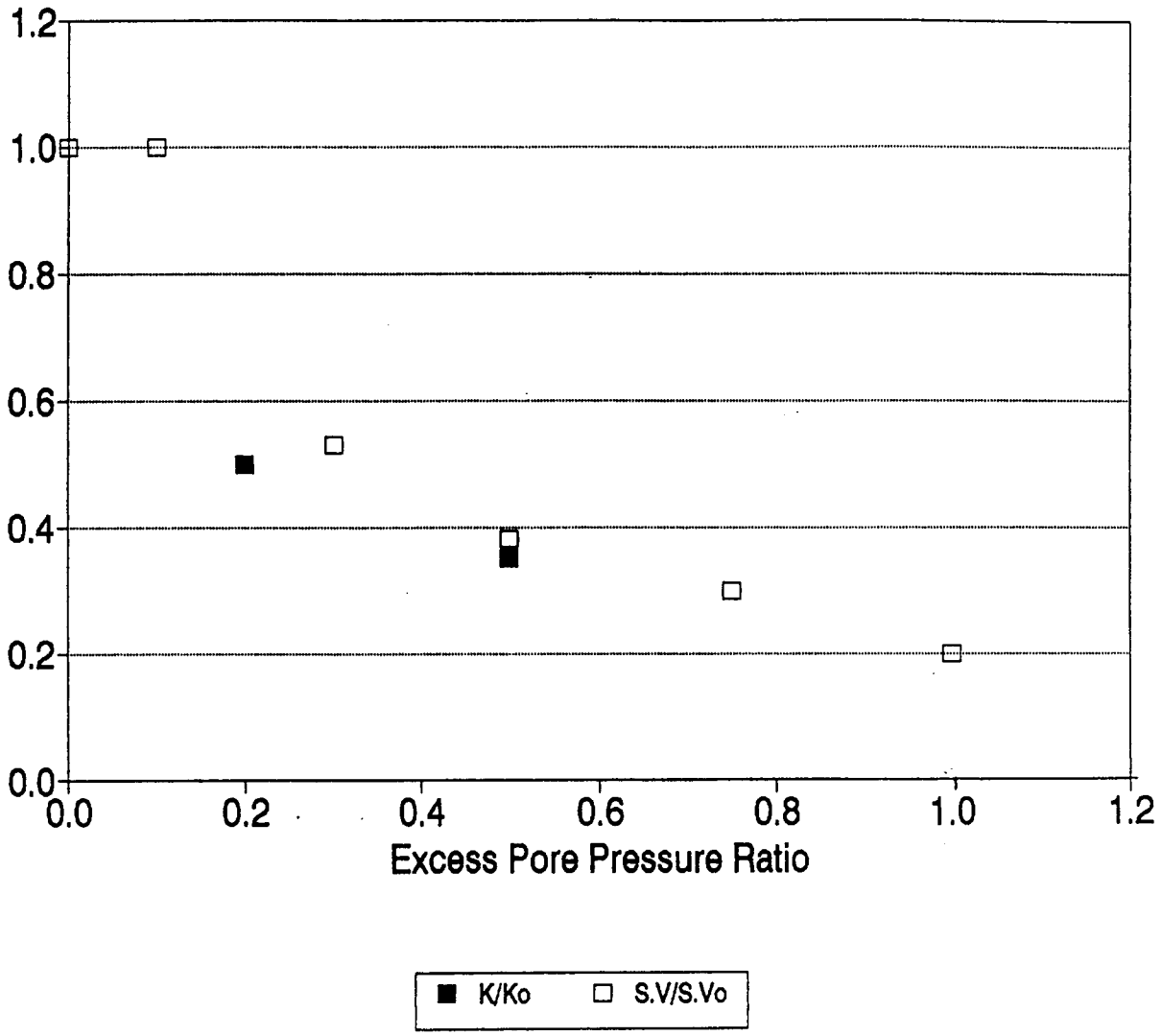

Fig. 5 The change of lateral soil reaction coefficient versus pile and the shear velocity

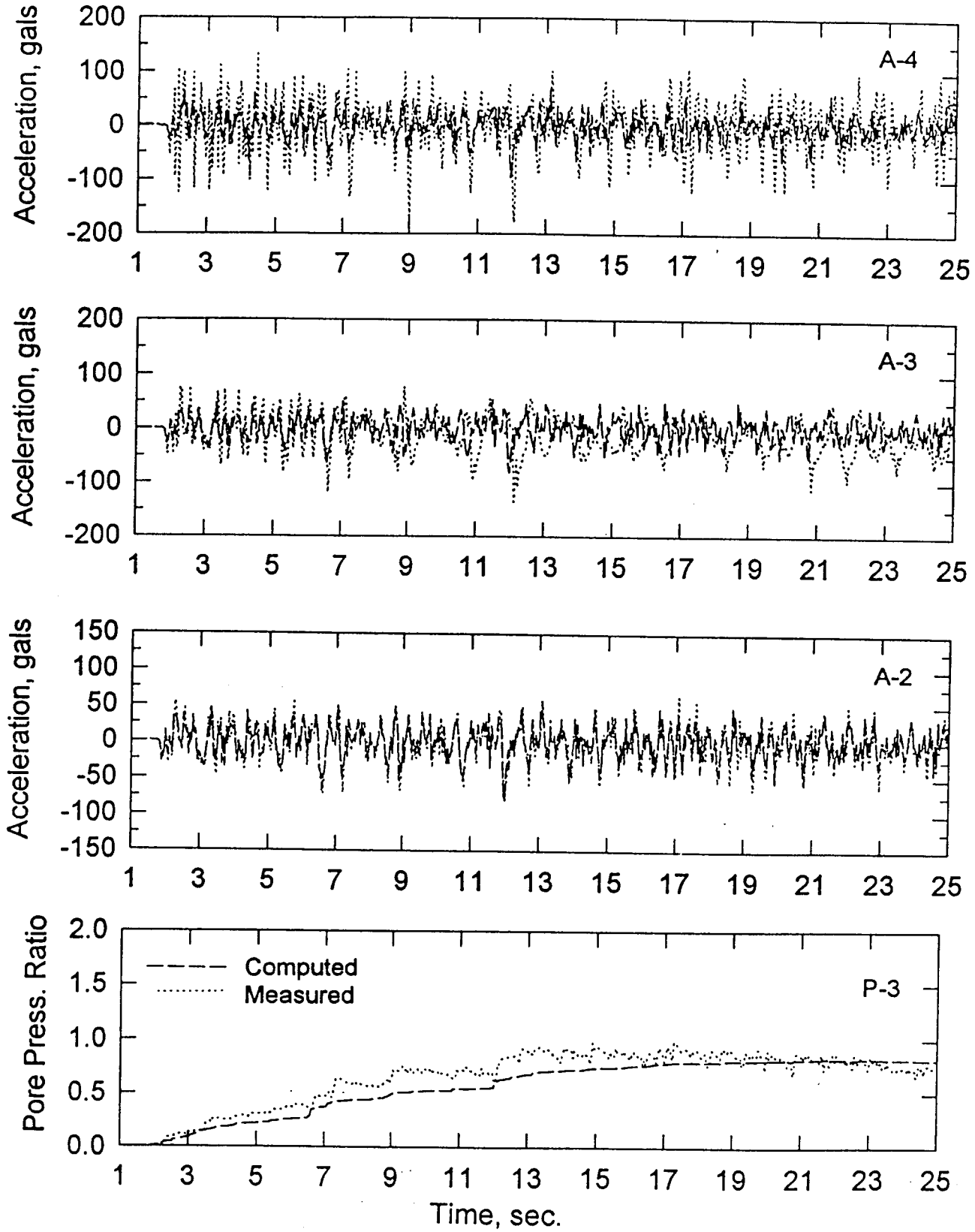

Fig. 6 Comparison between Computed and Measured Soil-Pile-Responses

Table 1. Physical Properties of the Sand Layers for the Shaking-Table Tests.

Physical Properties	Test 2	Test 3	Test 4	Test 5	Test 6
Dry unit wt. bef. shaking (g/cm^3)	1.488	1.495	1.490	1.489	1.492
Dry unit wt. aft. shaking (g/cm^3)	1.495	1.508	1.495	1.498	1.500
Water content bef. shaking (%)	26.4	28.7	27.2	27.8	26.9
Relative density bef. shaking (%)	37.8	40.1	38.5	38.3	39.2
Relative density aft. shaking (%)	39.7	42.2	40.1	40.9	41.2
Shear-wave velocity bef. shaking (m/sec.)	86	118	80	96	92
Shear-wave velocity aft. shaking (m/sec.)	132	132	128	128	135

Table 2. Peak Pore Pressure Ratios within the Sand Layer

Location	Test 2	Test 3	Test 4	Test 5	Test 6
P-5 (bet. Piles)	1.40	1.11	3.86	3.52	3.68
P-4	1.86	2.56	1.82	3.18	1.26
P-3	1.13	1.29	1.27	1.32	1.14
P-2	0.66	1.05	1.03	1.00	1.03
P-1	0.49	0.98	0.94	0.93	0.91

Table 3. Peak Accelerations (in gals) within the Sand Layer - Model Pile System

Location	Test 2	Test 3	Test 4	Test 5	Test 6
Structural Mass	376	413	398	368	442
A-3	329	294	175	450	363
A-2	102	215	667	318	333
A-1	100	149	154	164	172
Shaking Table	98	143	143	156	165

Suitability of SASW Method in Complex Geosystems

by

D. W. Sykora*, J. M. Roesset**, and K. H. Stokoe II**

ABSTRACT

Surface wave methods were developed as a non-intrusive and non-destructive means to determine the variation of elastic moduli with depth. These methods have been widely applied to soil, rock, and pavement systems. Initial simplifying assumptions included that the ground is level, the sub-surface layers are horizontal and extend laterally to infinity, and the effective sampling depth can be related to some fraction of the wavelength. Recent modifications and the findings of field and analytical studies indicate that surface wave methods, specifically the Spectral-Analysis-of-Surface-Waves (SASW) method, can be useful for conditions that do not meet these assumptions.

This paper addresses the application of the SASW method to complex systems of soil and rock (geosystems). The results of numerical analyses and field measurements are used to show that the SASW method can reliably and accurately determine the variation of elastic moduli in sloping ground or a system where discontinuous layers exists. The SASW method has also been used successfully to:

1) profile tunnel and shaft walls;
2) locate significant fractures within structural beams or behind tunnel liners; and
3) detect cavities or other irregularities at shallow depths below an exposed surface

which are also briefly described.

The SASW method may someday be used to characterize material properties in even more complex systems such as zoned, earth-fill embankments. The SASW method has been found to not work well to detect and locate cavities or tunnels at significant depths below the ground surface.

KEYWORDS: cavities; elastic moduli; rock; seismic methods; site characterization; soil; surface waves.

1. INTRODUCTION

The analysis of surface waves has been used for several decades to obtain the variation of soil stiffness with depth. The steady-state surface wave technique was developed in the late 1950's (Heukelom 1958; Jones 1958; Heukelom and Foster 1960) for the analysis of pavement systems. This technology was adapted by the U.S. Army Engineer Waterways Experiment Station (WES) to be an exploration tool at soil sites (Fry 1963; Ballard 1964). This technique involved interactively determining the wavelength at several frequencies of excitation by measuring the distances from the source to successive standing wave (displacement) peaks. The Rayleigh wave velocity, V_R, is calculated knowing the wavelength, λ, and frequency of excitation, f:

$$V_R = f \lambda \qquad (1)$$

and was assumed to correspond to an average depth between $\lambda/3$ and $\lambda/2$. The SASW method was established to obtain a more accurate variation of elastic moduli with depth.

The SASW method was developed nearly two decades later (Heisey 1982; Heisey, Stokoe, and Meyer 1982; Nazarian 1984; and Nazarian and Stokoe 1985a, 1985b) at the University of Texas at Austin (UT). Since that time, research, development, and application activities have continued at UT (e.g., Coll-Calderon 1985; Nogueira 1986; Sanchez-Salinero 1987; Sheu 1987; Rix 1988; Lopez 1989; Gauer 1990; Kang 1990; Madianos 1991; Sedighi-Manesh 1991; Bowen

* Woodward-Clyde Consultants, Santa Ana, California, 92705; formerly, Geotechnical Lab., U.S. Army WES, Vicksburg, Mississippi 39180
** Dept. Civil Engr., University of Texas, Austin, Texas 78712

1992; Sykora 1993; Kalinski 1994; Luke 1994), at the University of Michigan (e.g., Hiltunen 1988; and Gucunski 1991), at WES (Alexander 1992; Sykora, Alexander, and Roesset 1994), as well as at other universities and laboratories.

2. SASW METHOD

The determination of stiffness profile using the SASW method consists of three phases: data measurement, signal analysis, and forward modeling/inversion, each of which is described briefly below.

2.1 Data measurement

The SASW method involves measuring seismic signals at the ground surface (thus it is non-intrusive) produced by some type of vertical excitation, shown as either harmonic or impulsive in Figures 1 and 2, respectively. Signals typically are recorded with two receivers and stored digitally. The receivers may be velocity or acceleration transducers; acceleration transducers are normally reserved for cases when a significant amount of high frequency energy is being recorded.

2.2 Signal analysis

Signal analysis is normally performed using a spectral analyzer. If an impulsive source is used, a time window with the full length of the transient response is usually collected. The cross-power spectrum phase difference and coherence between the two receivers is calculated, averaged with a number of other responses using the same configuration and source, and stored. Data for harmonic sources are averaged and converted to cross power phase and coherence. Then the data are analyzed to determine the variation of signal phase as a function of source frequency and develop a dispersion curve (variation of phase velocity versus wavelength).

The phase velocity and wavelength are calculated directly from the real and imaginary parts of the dynamic displacements (Nazarian and Stokoe 1985a). At a given frequency, f, the travel time, t, between two receivers is:

$$t = \frac{\phi_2 - \phi_1}{360\, f} \qquad (2)$$

where ϕ_1 and ϕ_2 are the phases at points 1 and 2 (the location of the receivers) in degrees. Then, the phase velocity, C_ϕ, is:

$$C_\phi = \frac{(d_2 - d_1)}{t} = 360\, f\, \frac{(d_2 - d_1)}{(\phi_2 - \phi_1)} \qquad (3)$$

where the wavelength, λ, is:

$$\lambda = \frac{C_\phi}{f} \qquad (4)$$

2.3 Forward Modeling/Inversion

This phase is an iterative process of forward modeling which is independent of whether the data were collected using an impulsive or a harmonic source. The site is assumed to be ideally layered (horizontal and extending to infinity). Different algorithms allow for the evaluation of plane waves or cylindrical-front surface waves. Typically an initial profile of layer thicknesses and moduli is selected and the dispersion curve calculated using matrix solutions (Haskell 1953 and Thompson 1950), comparing the measured and matrix-calculated dispersion curves, modifying the profile if necessary, then repeating the process until a close match exists. Automatic matrix inversion using least squares is also used at UT and elsewhere (Nazarian and Desai 1993) and neural networks (Rix and Leipski 1991) have been proposed as an alternative to matrix inversion. The inverse problem does not necessarily produce a unique solution, however.

2.4 Validation

Numerous validation studies of the SASW method have occurred over the years, mainly through comparisons with in-situ shear wave velocity profiles determined by independent seismic measurements. The independent measurements have generally been performed using either the crosshole or downhole method. Typical comparisons of this type are shown in Figures 3 through 5 for some of the geotechnical settings where the SASW is especially well suited.

The results of tests performed on liquefiable gravelly soils are shown in Figure 3. These gravels are difficult to sample because of their looseness as well as their large aggregate size. Figure 4 shows a comparison of shear wave

velocities measured at the site of an asphaltic (AC) pavement. This site represents a difficult site for testing by non-intrusive techniques because of the very stiff layer (asphaltic concrete) overlying the much softer base and subgrade layers. Finally, the results of a recent application offshore are shown in Figure 5. In this case, the cost effectiveness of the SASW make its application offshore very desirable.

In the examples shown in Figures 3 through 5, a good comparison between the shear wave velocity profiles determined by the SASW and conventional intrusive methods is seen. This close comparison has occurred because of the lateral uniformity which existed in the test areas. Hence, these comparisons could be used to validate the SASW method. However, it must be kept in mind that intrusive techniques, like the downhole and crosshole tests, result in measurements over short travel paths. Therefore, when lateral variability exists, one should expect to see differences in the shear wave velocity profiles determined by the test methods because of the different materials sample by each test method.

3. DISCONTINUOUS LAYER

3.1 Numerical formulation and implementation

The computer code *vib3* is a research tool used to evaluate the effects of complex geosystems on surface wave propagation (Sykora and Roesset 1992; Sykora 1993). This semi-analytical computer code was created using principles of the Finite Element Method (FEM) and validated with closed-form solutions for axi-symmetric problems (Kausel 1981). Parametric analysis have also been conducted to define appropriate ranges for system and problem variables.

The primary assumptions used to develop *vib3* are that the geometry and boundary conditions of the system and the distribution of material properties are planar (2-D) but the loads can be non-planar (3-D). This set of conditions has a broader range of applications than that for plane strain (commonly used in engineering analysis) while circumventing expensive 3-D solution methods. Other assumptions are that all media are isotropic, the hysteretic behavior is represented by complex moduli, and the source produces vertical, steady-state excitation on surface at one discrete frequency.

The formulation involves two primary components: the condensation of 3-D dynamic stiffness matrices to equivalent 2-D matrices and the representation of the distribution of loads in the out-of-plane direction using a Fourier expansion. The condensed 2-D system of equations are first solved in the frequency and wave-number domain; inverse Fourier transforms are then performed to obtain the solution as a function of out-of-plane distance and time, if so desired.

Validation studies were conducted to prove that the formulation and computer implementation are sound for the limited class of problems considered. The general accuracy of calculated displacements in terms of amplitude and phase was evaluated. Validation of *vib3* through comparisons with analytical results was possible only for the simplest class of planar geometry—a horizontally layered system extending to infinity. Green's function solutions formulated for axi-symmetric problems (with disk loads) by Kausel (1989) were used exclusively with point and square loads (in plan). The same total area and a total load of unity were used to adequately equate problems with different load configurations.

Comparisons between the numerical approximations and closed-form solutions at distances from the source between 0.5λ and 5.0λ are excellent for nearly all of the cases considered. The data confirm that the formulation and computer implementation are accurate.

3.2 Results of numerical analysis

The results of computations suggest that surface wave measurements can be used to detect, locate, orient, and characterize discontinuous buried layers (within certain limits). The ability to detect and characterize a buried layer is strongly dependent on the velocity contrast, I, and the thickness-to-depth ratio, t/z_L. It appears unlikely that surface wave methods will work well when the thickness of the layer is less than 20 percent of the depth to the layer.

An example of how a buried layer can be detected is shown in Figure 6. The dispersion curves corresponding to surface waves propagating away from the end of the buried layer (+x direction) and surface waves propagating over the buried

layer (-x direction) when the load is directly over the discontinuity are considerably different.

The orientation (azimuth of the edge) of a discontinuous buried layer can be determined from a point on the edge by making measurements along lines in a number of horizontal directions. The azimuth of the discontinuous edge is 90 degrees from the measurement line that produces the greatest contrast in C_ϕ.

The location of the edge of (point above) a buried layer is more difficult to determine. This process is iterative and would also work from the direction of maximum difference in C_ϕ. Once that direction was determined, dispersion curves would be developed along lines perpendicular to that direction. A significant change in the dispersion curve would mark a transition from a homogeneous system to a buried layer system, or vice versa.

4. SLOPING GROUND

4.1 Results of numerical analysis

The variations of dynamic vertical displacements in the x-direction (direction of maximum topographic gradient) and the y-direction (direction of zero topographic gradient) were calculated and analyzed using the computer code *vib3* described in section 3.1. The variables defining the problem are shown in Figure 7 with the slope angle, α, and the load set-back distance, x_{LC}, being the primary variables. Square loads were used throughout and can be related to circular load areas by equating total loads.

Calculations were made using six common engineering slope ratios (horizontal:vertical)—1:1, 1.5:1, 2:1, 2.5:1, 3:1, and 6:1. The load was placed at the top and base of the slope with these ratios to produce α = 135, 146, 153, 158, 162, 171, 189, 198, 202, 207, 214, and 225 degrees. (An α of 180 degrees corresponds to the level ground conditions.) The center of the load was used as the reference point for distance measurements. Unit-less dimensions are used for convenience. The shear wave velocity was fixed at 1000 with 5 percent damping. The mass density and Poisson's ratio were 4.00 and 0.40, respectively, producing a V_R equal to 940.

The variations of vertical displacement and phase at a slope, ϕ_s, for a slope ratio of 1.5:1 (α = 146 degrees when the load is at the crest of the slope and α = 214 degrees when the load is at the base of the slope) are shown in Figures 8 and 9, respectively. The relative location of the discontinuity along the abscissa is shown as a vertical dashed line. The level-ground solution is also shown for comparison.

The primary effect of the slope discontinuity is a phase shift for waves traveling in the direction of maximum topographic gradient that occurs between the discontinuity and a distance of $3\lambda/4$ beyond (when $x_{LC} = 1.0\,\lambda$). The phase difference becomes essentially constant at greater distances. The phase has a marked lag from the level ground solution at distances beyond the discontinuity when α = 146 degrees and a marked phase lead when α = 214 degrees. The calculated solutions in the y-direction along the crest and base correspond well to the level-ground solution, regardless of α.

The amount of phase shift at these two slope angles was examined by comparing the total (unwrapped) phase with the total phase assuming a uniform increase of 360 degrees per wavelength and passing through the origin, ϕ_{360} (which is used to calculate dispersion curves for the SASW method). The difference in phase is shown in Figure 10. The variation of phase difference after the shift, beyond distances of about $3\lambda/4$ from the discontinuity, is relatively constant when α = 146 degrees. The small fluctuations that exist are similar to those for the solution along the crest. The overall variation of phase in the x-direction when α = 214 degrees is much larger and less consistent. Along the base and crest there is no noticeable phase difference and the magnitude of fluctuations is small.

These data strongly suggest that measurements can be reliably used both down the slope and perpendicular to the slope to determine soil stiffness using the SASW method, especially if the receivers are placed at a distance greater than $3\lambda/4$ beyond the discontinuity to avoid the phase shift. The results for measurements up the slope (α = 214 degrees) are not as consistent. The phase difference appears to vary considerably at surface distances beyond the initial phase shift. The general trend at distances greater than 2.5 λ is for the phase to decrease uniformly (lag) as a

ratio of distance until a sudden shift occurs (e.g., at 3.4 λ).

The variation of phase from a larger perspective indicates that the differences shown in Figures 9 and 10 may not be of importance from a practical standpoint. The variation of unwrapped phase with distance for most slope angles (minor discontinuities not included) are shown in Figures 11 and 12. Also shown in Figure 11 are lines corresponding to a least squares linear fit of data between surface distances of 1.0 and 5.0 λ for each slope angle.

The data in Figure 11 shows that the distribution of unwrapped phase is fairly consistent and unique when $\alpha < 180$ degrees. The best-fit segments at these angles effectively represent a variation of phase between 360 and 350 degrees per wavelength. The increased variation in phase when $\alpha > 180$ degrees is also seen in Figure 11 although the best-fit linear segments are very similar and are close to ϕ_{360}. The error associated with this variation is small and can be minimized by using large spacings. The data in Figure 12 clearly shows the independence of phase change along the crest and base to α and how close the phase is to ϕ_{360} (shown as a line segment in Figure 12).

Although it appears possible to predict the phase shift caused by a surface discontinuity, calculated phase velocities are likely to be more accurate if this phase shift is avoided in the analysis. The difference in phase as a function of α was found to be independent of x_{LC} as long as $x_{LC} > 0.5\,\lambda$.

The combined results suggest that measurements made along the crest or base of a slope can safely be processed using existing SASW inversion schemes to obtain stiffness profiles. Phase velocities representing measurements down a slope can also be reliably obtained from vertical measurements. The best method would be to place receivers beyond $3\lambda/4$ thus avoiding any interpretation. Much more variation is expected for measurements made up a slope. For homogeneous systems, the phase velocity will closely approximate V_R.

4.2 Field measurements

Field measurements of vertical dynamic displacements on level ground and sloping ground were made on the WES Reservation in Vicksburg, Mississippi, during the month of August, 1993. The site consists of a road cut with a maximum height of 25 ft and slope angles between about 155 and 165 degrees and a concrete bridge with a steel support system. Natural soil consists of Pleistocene-age loess indigenous to the Vicksburg area. This loess is uniformly graded and typically has a low unit weight. Groundwater does not exist within the depths tested.

A field testing program was designed to measure dynamic vertical displacements along the crest and down the slope at two locations. A harmonic source was used to produce surface waves. The vibrator was programmed to run a swept-sine test between frequencies of 25 and 325 Hz at increments of 0.375 Hz. Five cross-correlations between the source and each receiver were averaged at each frequency, the coherence calculated, and results stored.

The slope angles were 160.5 and 163 degrees at two sites where measurements were made (Locations A and B). The testing configuration was selected to avoid measuring phase shifts near the discontinuity and allow the use of a wide range of frequencies. Velocity transducers were positioned vertically at locations down the slope and along the crest (toward the other array location) at 1-ft spacings between distances of 10 and 21 ft from the center of the source platen.

The measured displacements were examined at a number of discrete frequencies between 50 and 200 Hz although aliasing of phase relationships typically began to occur at wavelengths less than 3 ft (frequencies greater than about 125 Hz). Typical results of slope measurements are shown in Figure 13. The real and imaginary parts of displacement are shown along with the wrapped and unwrapped phase for waves propagating down the slope and along the crest.

Very little difference exists between the change in phase with distance for wave traveling down the slope as compared to waves traveling along the crest as shown in Figure 14. This finding is consistent with the results of numerical approximations at distances greater than $3\lambda/4$ beyond the discontinuity.

5. TUNNELS AND SHAFTS

The SASW method has been used successfully underground to evaluate conditions around unlined and lined openings (Lopez 1989; Nelson et al. 1989; Madianos 1991; Olson et al. 1993). For underlined openings in rock, in-situ evaluation of rock mass stiffness and changes associated with the excavation and stress redistribution processes have been studies. A typical profile of shear wave velocity determined at the Waste Isolation Pilot Project (WIPP) is shown in Figure 15. In this case, testing was performed along the exposed rock wall of one of the underground rooms. Very little change in the rock mass occurred due to the excavation and stress redistribution processes as shown by the nearly uniform velocity with depth behind the exposed wall.

Lined openings of tunnels and shafts have also been tested with the SASW method. Testing has been successfully used for purposes such as:

1) evaluation of liner integrity,
2) determination of liner thickness,
3) detection of voids immediately behind the liner, and
4) evaluation of the rock stiffness behind the liner.

A typical result for an intact concrete liner with sound, but softer rock behind the liner, is shown in Figure 16.

6. CAVITY AND TUNNEL DETECTION

6.1 Numerical formulation and implementation

Computer codes were created at UT to solve the problem of a harmonic line load imposed on the surface of a half space containing a void. Coll-Calderon (1985) used a horizontal line load and Nogueira (1986) used a vertical line load. Assumptions of plane strain were used (making the void extend to infinity--a tunnel) and the line load was oriented into the plane. The model was formulated using the Boundary Element Method (BEM) which allowed discretization of only the 2-D cavity outline. The codes also computed the cross power spectrum and displacements at target points along the ground surface.

6.2 Results of numerical analyses

The results of these studies indicated that there should be some clear and distinguishable variations in the dispersion curve if the source and receivers are moved along the surface, as they pass over a cavity. Figure 17 shows the variation of the phase velocity, normalized by the free field value, between closely-spaced points on the surface. The arrows extending from abscissas (x/d) of 0.5 to 1.5 represent the position of a square cavity with side d and its center at a depth also equal to d. Similar variations are obtained for the displacement amplitudes rather than the phases. One must have, however, some idea of the expected size and depth of the cavity to select an appropriate range of frequencies, or wavelengths.

6.3 Prototype testing

Rosenblad et al. (1994) conducted small-scale tests using a prototype model to test the ability of the SASW method to detect near-surface cavities. The model was 1.2 *m* by 3 *m* by 0.5 *m* deep concrete slab which was composed of unreinforced Portland cement concrete with a maximum aggregate size of 10 *mm*. Two square "tunnels" (elongated cavities), each 50 *mm* by 50 *mm*, were cast in the upper portion of the slab. The cavities had crown depths of 25 *mm* and 70 *mm*.

SASW testing of the prototype slab was performed using a "marching" technique such that the source and receivers were moved incrementally along an array line on the slab. The array line was oriented perpendicularly to the longitudinal axis of the cavity. Constant source and receiver spacings were maintained during the marching process. A spacing ratio, d_2/d_1, of 2 was used (see Figure 1), with values of d_1 of 76 *mm* and 152 *mm*. Measurements from each test were performed over a frequency range of 0 to 100 kHz and an exponential window was applied to each record in order to minimize the effects of reflections from the edges of the slab.

The results in terms of dispersion curves from two sets of measurements are shown in Figure 18. A source-receiver spacing of 76 *mm* was used in each measurement set. The dispersion curve for sound concrete was determined well away from the cavity. This curve is shown by the dotted line

and is typical of tests on intact concrete slabs, beams, and columns (Bowen and Stokoe 1992; Kalinski et al. 1994). This dispersion curve exhibits some fluctuations but shows the general trend of a constant velocity with wavelength. The dispersion curve determined when the receivers were centered directly over the shallower cavity is shown by the solid line in Figure 18. For very short wavelengths, wavelengths less than about 25 *mm*, the dispersion curve overlaps the one determined without a cavity. However, for longer wavelengths, the cavity has the effect of significantly reducing wave velocities and can be readily identified by this change. Similar results were also found with the deeper cavity, with the difference being that longer wavelengths were required before the divergence in dispersion curves could be recognized. Bowen and Stokoe (1992) and Kalinski et al. (1994) have shown similar comparisons for the identification of cracked versus sound concrete in beams and columns.

7. SUMMARY

Although the SASW method was developed under the assumptions that the ground surface and subsurface layers are horizontal and extend to infinity, the results of numerical approximations and field measurements show that it is a versatile tool that can be applied to more complex geosystems. Examples of validation studies and the results of numerical approximations and field measurements show that the SASW method can be widely used to accurately determine the variation of stiffness wherever a free surface exists. The primary limitation is the depth sampled which is controlled by the range of frequencies applied.

8. ACKNOWLEDGEMENTS

Research on the application of surface waves to sloping ground, through a discontinous layer, and for tunnel and cavity detection was sponsored by the U.S. Army Engineer Waterways Experiment Station. Permission was granted by the Chief of Engineers to publish this information.

9. REFERENCES

Alexander, D. (1992). "In Situ Material Characterization for Pavement Evaluation by the Spectral-Analysis-of-Surface Waves (SASW) Method," Tech. Rpt. GL-92-10, U.S. Army WES, Vicksburg, MS.

Andrus, R., Stokoe, K., II, Bay, J. and Youd, T. (1992). "In Situ V_s of Gravelly Soils Which Liquefied," Proc., 10th World Conf. Earthq. Engr., Madrid.

Ballard, R., Jr. (1964). "Determination of Soil Shear Moduli at Depth by In-Situ Vibratory Techniques," Misc. Pap. 4-691, U.S. Army WES, Vicksburg, MS.

Bowen, B. (1992). "Damaged Detection in Concrete Elements with Surface Wave Measurements," PhD diss., Univ. Texas, Austin, TX.

Bowen, B. and Stokoe, K., II (1992). "Evalua-tion of Cracked and Repaired Beams and Columns Using Surface Stress Waves," Proc., 10th World Conf. Earthq. Engr., Madrid.

Coll-Calderon, J. (1985). "Cavity Detection by the SASW Method: Preliminary Studies," MS thesis, Univ. Texas, Austin, TX.

Fry, Z. (1963). "Development and Evaluation of Soil Bearing Capacity, Foundations of Structures," U.S. Army WES, Tech. Rpt. 3-362, No. 1, Vicksburg, MS.

Gauer R. (1990). "Experimental Study of Applying the Spectral-Analysis-of-Surface_waves Method Offshore," MS thesis, Univ. Texas, Austin, TX.

Gucunski, N. (1991). "Generation of Low Frequency Rayleigh Waves for the Spectral-Analysis-of-Surface-Waves Method," PhD diss., Univ. Michigan, Ann Arbor, MI.

Haskell, N. A. (1953). "The Dispersion of Surface Waves in Multilayered Media," Bull. Seism. Soc., Vol 43, No. 1, pp 17-34.

Heisey, J. (1982). "Determination of In Situ Shear Wave Velocities from Spectral Analysis of Surface Waves," MS thesis, Univ. Texas, Austin, TX.

Heisey, J., Stokoe, K., II, and Meyer, A. (1982). "Moduli of Pavement Systems from Spectral Analysis of Surface Waves," Trans. Res. Rec. 852, Washington, DC, pp 22-31.

Heukelom, W. (1958). "Investigation Into the Dynamic Mechanical Properties of Some Runways in the U.S.A. Carried Out in 1958,"Rpt. M-35220, Shell Oil Labs, Amsterdam.

Heukelom, W., Foster, C. (1960). "Dynamic Testing of Pavements," J. Soil Mech. and Found. Div., ASCE, Vol 86, No. SM1, pp. 1-28.

Hiltunen, D. (1988). "Experimental Evaluation of Variables Affecting the Testing of Pavements by the Spectral-Analysis-of-Surface-Waves Method," U.S. Army WES, Tech. Rpt. GL-88-12, Vicksburg, MS.

Jones, R. (1958). "In-Situ Measurement of the Dynamic Properties of Soils by Vibration Methods," Geotechnique, Vol 8, pp 1-21.

Kang, Y. (1990). "Effect of Finite Width on Dynamic Deflections of Pavements," PhD diss., Univ. Texas, Austin, TX.

Kalinski, M. (1994). "Non-destructive Testing of Concrete Structural Elements Using the SASW Method," MS thesis, Univ. Texas, Austin, TX.

Kalinski, M., Stokoe, K., II, Jirsa, J. and Roesset, J. (1994). "Nondestructive Identification of Internally Damaged Areas of a Concrete Beam Using the SASW Method," Mtg., Transp. Res. Board, Washington, DC.

Kausel, E. (1981). "Explicit Solution for the Green Functions for Dynamic Loads in Layered Media," MIT Res. Rpt. R81-13, Cambridge, MA.

_____, (1989). "**PUNCH**: Program for the Dynamic Analysis of Layered Soils," ver. 3.0, Massachusetts Inst. Technology, Cambridge, MA.

Lopez, M. (1989). "Investigation of Variations in Rock Stiffness by the SASW Method Following Excavation by Blasting and Mining," MS thesis, Univ. Texas, Austin, TX.

Luke, B. (1994). "In Situ Measurement of Stiffness Profiles in Seafloor Using Spectral-Analysis-of-Surface-Waves Method," PhD diss., Univ. Texas, Austin, TX, (in progress).

Madianos, M. (1991). "Field and Laboratory Investigation of Rock Masses Using Surface Wave Testing (SASW)," MS thesis, Univ. Texas, Austin, TX.

Nazarian, S. (1984). "In Situ Determination of Elastic Moduli of Soil Deposits and Pavement Systems by Spectral-Analysis-of-Surface-Waves Method," PhD diss., Univ. Texas, Austin, TX.

Nazarian, S. and Desai, M. (1993). "Automated Surface Wave Method: Field Testing," J. Geotech. Engr., ASCE, Vol 119, No. 7, pp 1790-1804.

Nazarian, S. and Stokoe, K., II, (1985a). "In Situ Determination of Elastic Moduli of Pavement Systems by Spectral-Analysis-of-Surface-Waves Method (Practical Aspects)," Res. Rpt. No. 368-1F, Cntr. Transp. Res., Austin, TX.

_____, (1985b). "In Situ Determination of Elastic Moduli of Pavement Systems by Spectral-Analysis-of-Surface-Waves Method (Theoretical Aspects)," Res. Rpt. No. 437-1, Cntr. Transp. Res., Austin, TX.

Nelson, P., Lopez, M., Stokoe, K., II, and Roblee, C. (1989). "In Situ Evaluation of Rock Mass Stiffness Variations for Underground Openings Using Surface Waves and Boreholes Seismic Methods," Proc., 7th Workshop, Mines Systems Design and Ground Control, Blacksburg, VA.

Nogueira, E. (1986). "Effects of Cavities on the Propagation of Surface Waves," MS thesis, Univ. Texas, Austin, TX.

Olson, L., Sack, D., Stokoe, K., II, and Buchinski, K. (1993). "Stress Wave NDT of Tunnels/Shafts," Mtg., Transp. Res. Board, Washington, DC.

Rix, G. (1988). "Experimental Study of Factors Affecting the Spectral-Analysis-of-Surface-Waves Method," PhD diss., Univ. Texas, Austin, TX.

Rix, G. and Leipski, E. (1991). "Accuracy and Resolution of Surface Wave Inversion," Recent Advances in Instr., Data Acq. & Test. in Soil Dyn., ASCE, Geot. Pub. No. 29, ed. Bhatia and Blaney, pp 17-32.

Rosenblad, B., Stokoe, K., II, Chiang, C., and Roesset, J. (1994). "Near-Surface Cavity Detection Using the SASW Method," Geot. Engr. Rpt. GR-94-2, Univ. Texas, Austin, TX.

Sanchez-Salinero, I. (1987). "Analytical Investigation of Seismic Methods Used for Engineering Applications," PhD diss., Univ. Texas, Austin, TX.

Sedighi-Manesh, M. (1991). "Theoretical Investigation of Spectral-Analysis-of-Surface-Waves (SASW) Technique for Application Offshore," PhD diss., Univ. Texas, Austin, TX.

Sheu, J. (1987). "Applications and Limitations of the Spectral-Analysis-of-Surface-Waves Method," PhD diss., Univ. Texas, Austin, TX.

Sykora, D. (1993). "Dynamic Vertical Displacements in Planar Geosystems," PhD diss., Univ. Texas, Austin, TX.

Sykora, D., Alexander, D., and Roesset, J. (1994). "Determination of Soil Moduli in Soil-Structure Systems on Highways; Report 1: Surface Waves in Sloping Ground," Tech. Rpt. (in publ.), U.S. Army WES, Vicksburg, MS.

Sykora, D. and Roesset, J. (1992). "2-D Planar Geosystems Subjected to 3-D Dynamic Loads," Tech. Rpt. GL-92-16, U.S. Army WES, Vicksburg, MS.

Thomson, W. (1950). "Transmission of Elastic Waves Through a Stratified Solid Medium," J. Sound Vib., Vol 2, No. 3, pp 210-226.

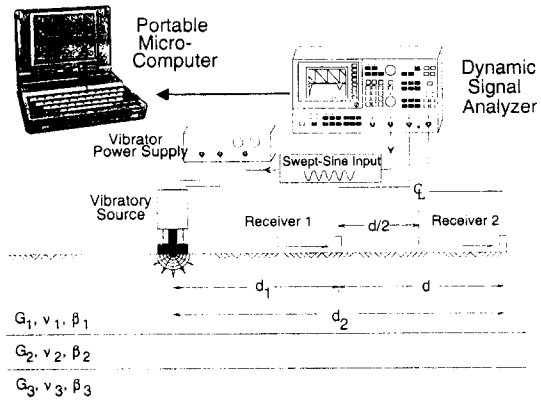

Figure 1. Schematic of SASW method using harmonic source

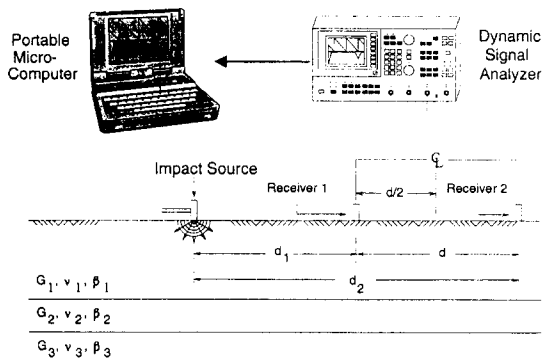

Figure 2. Schematic of SASW method using impulsive source

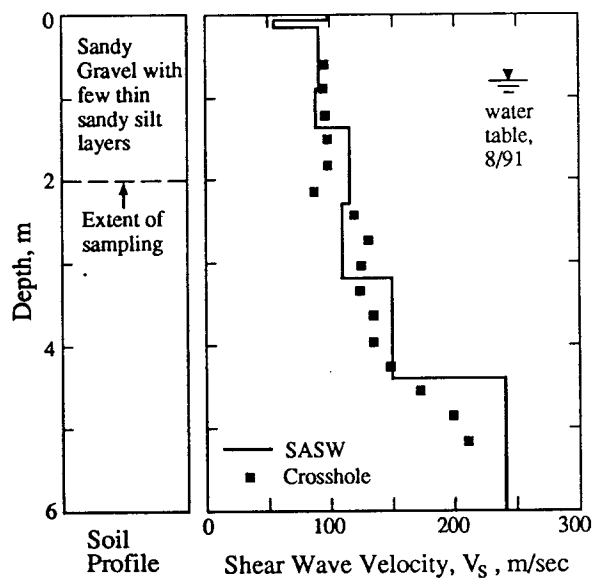

Figure 3. Shear wave velocity profile determined at site where gravelly soils liquefied during the 1983 Borah Peak Earthquake (Andrus et al. 1992)

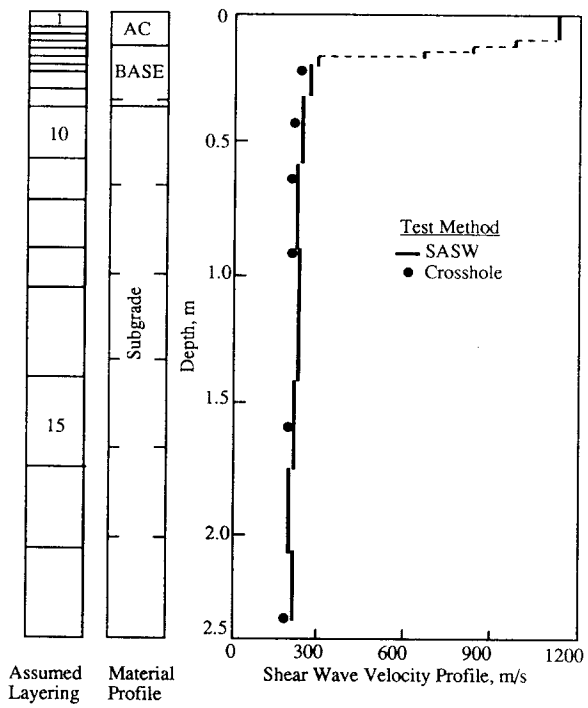

Figure 4. Comparison of shear wave velocity profiles at a pavement site (Nazarian and Stokoe 1985b)

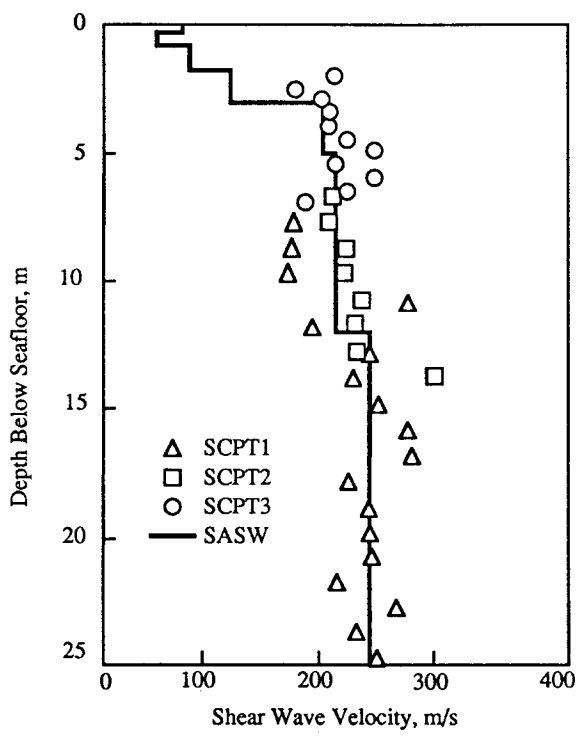

Figure 5. Comparison of shear wave profiles from SASW and seismic cone penetrometer (SCPT) measurements offshore Venice, Italy (Luke 1994)

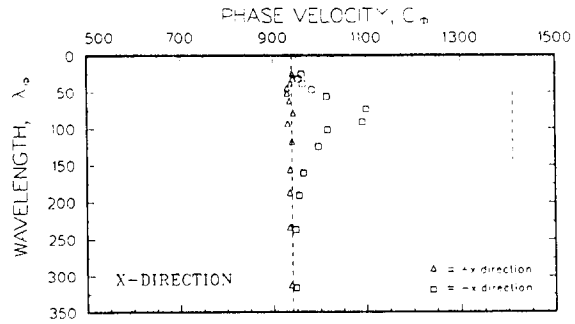

Figure 6. Dispersion curves for surface waves travelling over and away from high-velocity buried layer (Sykora 1993)

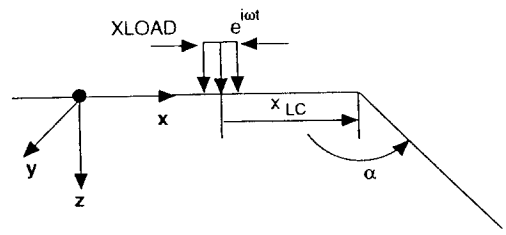

Figure 7. Variables used to define sloping ground problem (Sykora 1993)

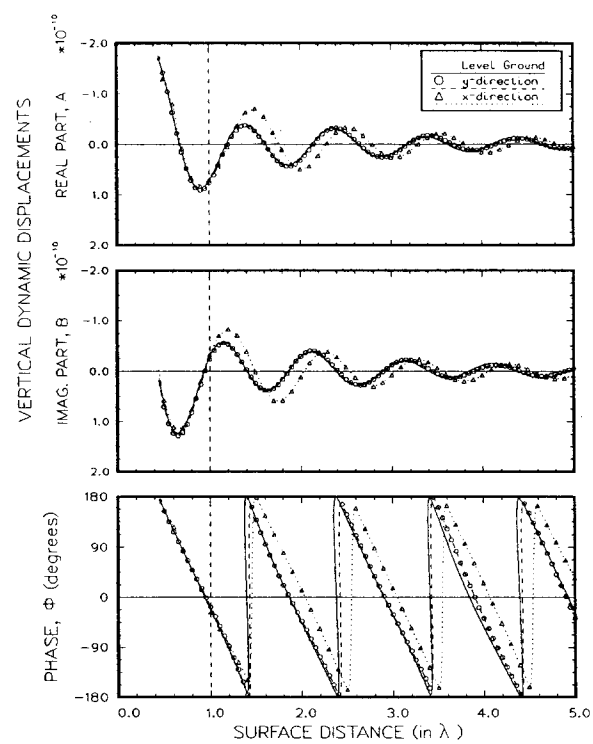

Figure 8. Displacements and phase for α = 146 degrees (Sykora 1993)

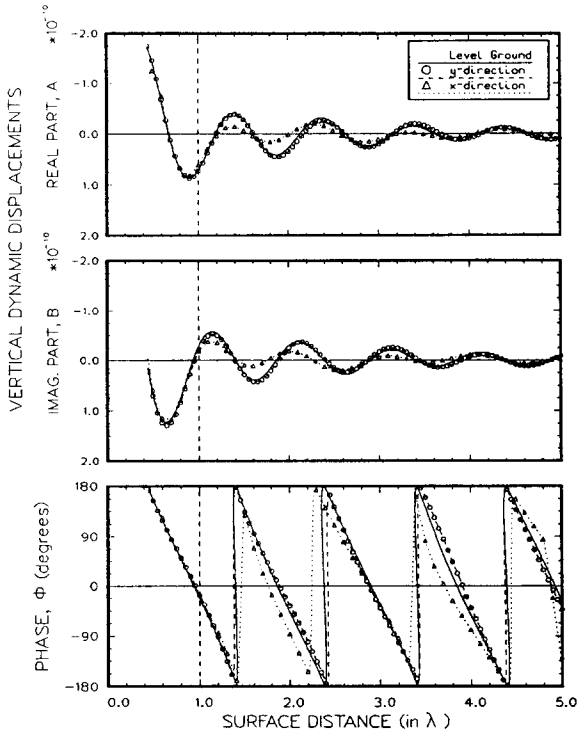

Figure 9. Displacements and phase for α = 214 degrees (Sykora 1993)

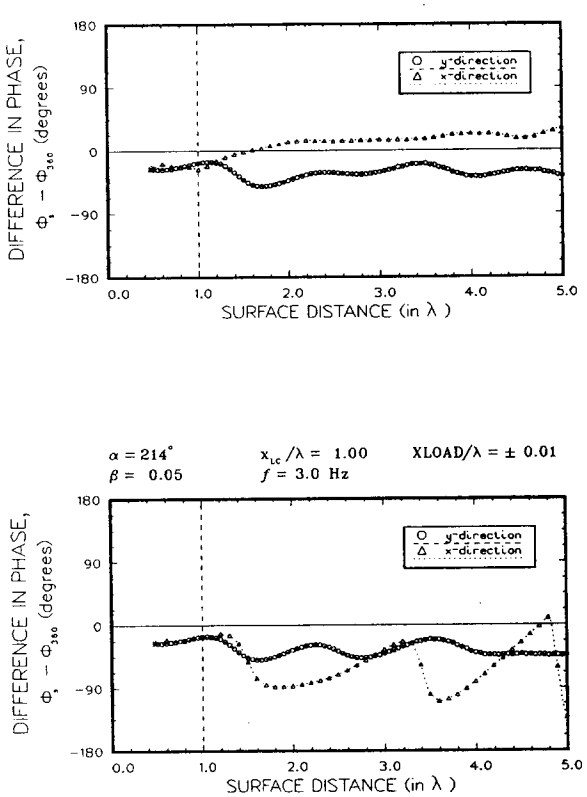

Figure 10. Difference in phase between sloping ground and uniform increase of 360 degrees per wavelength (Sykora 1993)

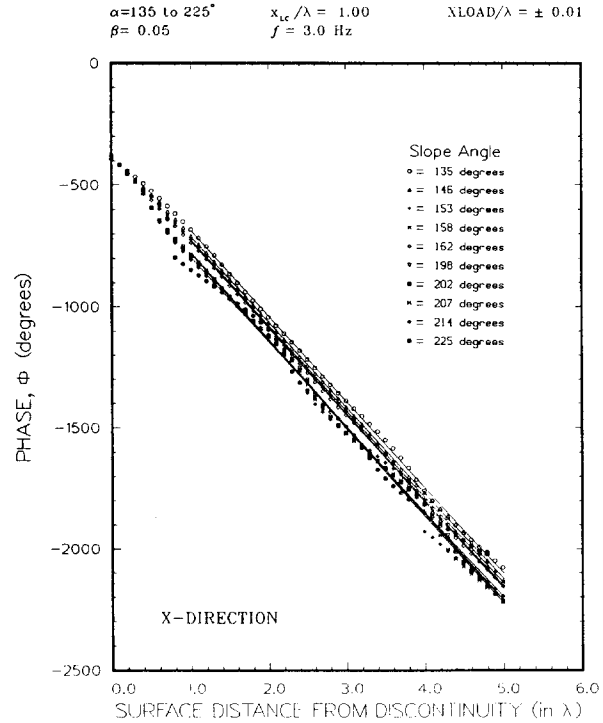

Figure 11. Comparisons among the variations of phase with distance for different slope angles less than 180 degrees (Sykora 1993)

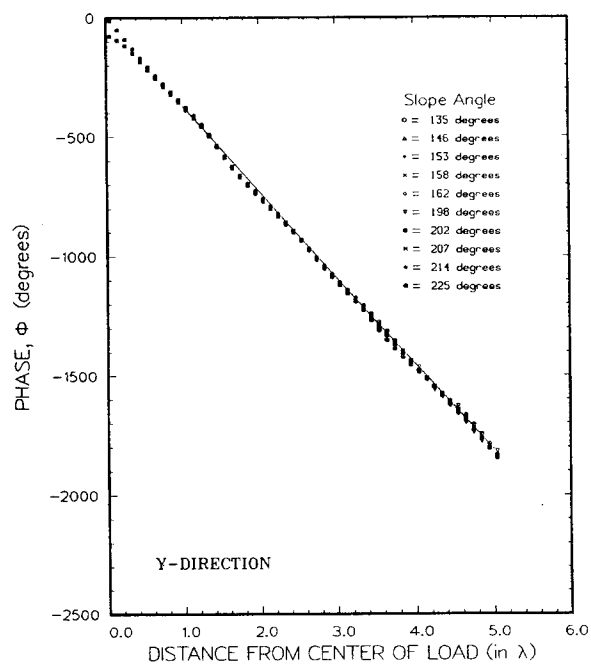

Figure 12. Comparisons among the variations of phase with distance for different slope angles greater than 180 degrees (Sykora 1993)

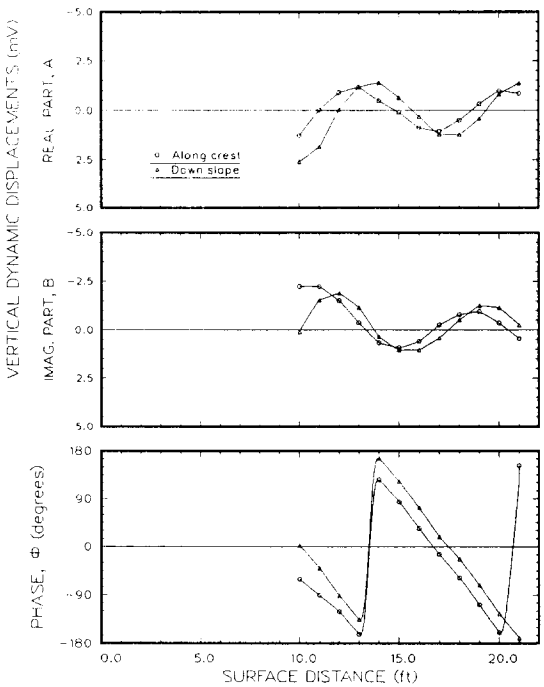

Figure 13. Displacements for measurements down slope (Sykora 1993)

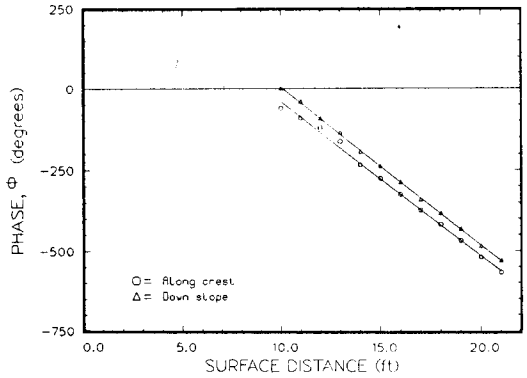

Figure 14. Phases for measurements down slope (Sykora 1993)

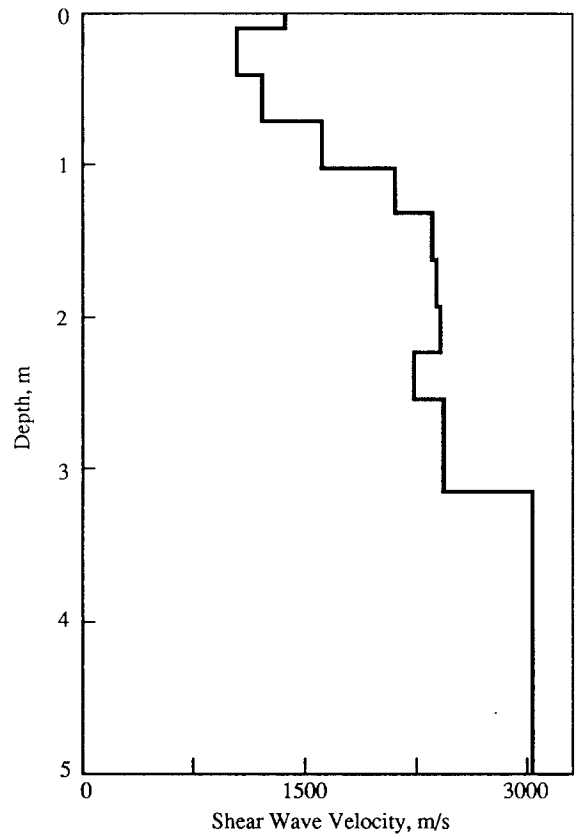

Figure 15. Shear wave velocity profile determined by SASW testing along an exposed rock wall at the underground WIPP facility (Nelson et al. 1989)

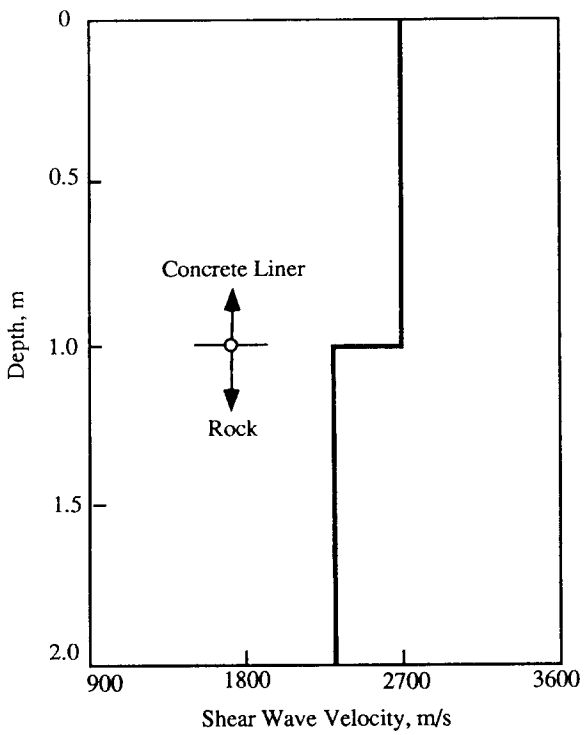

Figure 16. Velocity profile determined from SASW tests performed on a concrete shaft liner (Olson et al. 1993)

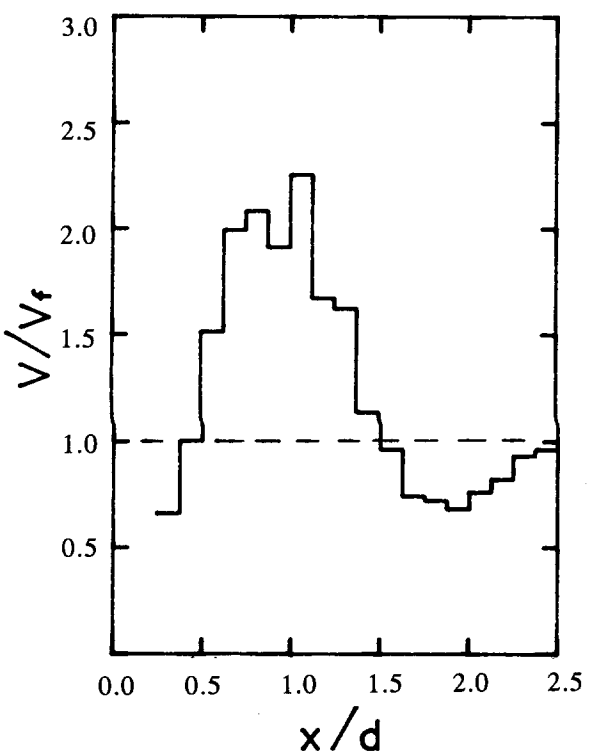

Figure 17. Variation of phase velocity as a function of normalized distance for a half-space with a square cavity of width *d* at a depth *d* (Noguiera 1986)

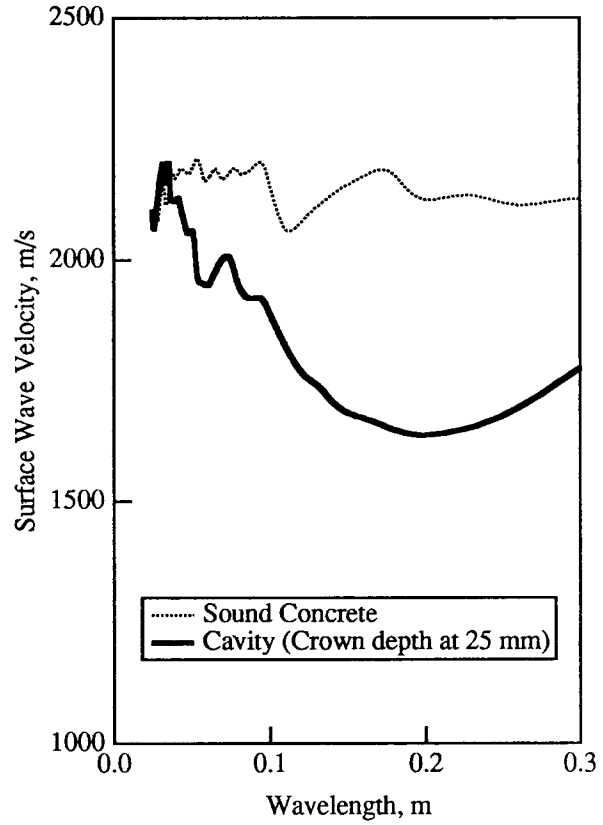

Figure 18. Comparison of experimental dispersion curves determined by SASW testing on sound concrete and over a shallow cavity in concrete (Rosenblad et al. 1994)

Effectiveness of Measures Against Liquefaction Confirmed at a Recent Earthquake—A Case History During 1993 Kushiro-Oki Earthquake

by

S. Iai*, Y. Matsunaga*, T. Morita* and H. Sakurai*

ABSTRACT

During the 1993 Kushiro-Oki Earthquake of magnitude 7.8, Kushiro Port being located at 15 km from the epicenter was shaken with a peak horizontal acceleration of 0.47g. Many of the quay walls at the Kushiro Port suffered damage due to liquefaction of backfill sand. However, the quay walls having backfill sand compacted as measures against liquefaction survived the earthquake without damage. Since the contrast in the performance of those quay walls are of significance in the engineering practice, the present paper is devoted to report the details including the recorded earthquake motions and the ground conditions.

Key words : liquefaction, sand, earthquake, quay walls

INTRODUCTION

In recent Japanese practice, measures against liquefaction have often been put into practice in order to mitigate damage to structures sitting on potentially liquefiable foundations. While laboratory data are abundant to evaluate the effectiveness of those measures against liquefaction, in-situ data during strong earthquake shaking are very scarce.

On January 15, 1993, an earthquake of magnitude 7.8 in the scale of Richter-Japan meteorological Agency (JMA) hit a northern island of Japan called Hokkaido. The epicenter was located 15 km south of Kushiro city as shown in Fig. 1; the earthquake was named the 1993 Kushiro-Oki earthquake. The focal depth was 107 km, being much deeper than the ordinary depth of about 40 km for the earthquakes occurring around Japan.

Kushiro Port was shaken with a peak horizontal acceleration of 0.47g. The earthquake caused liquefaction of untreated backfill sand at the port, resulting in damage to many of the quay walls. The extent of the damage was generally moderate; the displacements of the quay walls were less than about 5 percent of the water depth in front of the quay walls. In contrast, the quay walls having the backfill sand compacted as measures against liquefaction survived the earthquake without damage.

In the present paper, the performance of these quay walls will be reported in detail including the recorded earthquake motions and the ground conditions.

---

* Geotechnical Earthquake Engineering Laboratory, Port and Harbour Research Institute

KUSHIRO PORT

Kushiro Port is developed at the estuary of the Kushiro River as shown in Fig. 2. As understood by the former beach line shown by the broken line in Fig. 2, most of the port area has been reclaimed from the sea by filling the sand dredged from the nearby sea. The port has been constructed step by step from a quay wall located at the eastern most end toward west direction along the former beach line; the quay wall at the western most end, i.e. Pier No.3 in the West Port District, has been just constructed in 1992.

The natural ground along the former beach line is of sand dune origin, being dense with SPT N-values of about 50. The fill above the original ground gradually increases its thickness from none at the former beach line to about ten meters at the southern end of the piers in the West Port District.

Though Kushiro City is located at the latitude 43 degrees north, at about the same as that of Rome in Italy, the average temperature falls below the water freezing point during winter. When the earthquake hit, the ground surface was said to be frozen with a thickness of about 0.5 to 1.0 meters in Kushiro City. However, the port engineers reported that the materials used for the ground surface layer in the port areas were chosen to serve as anti-freezing layer to prevent the damage to the pavement due to the soil freezing. The anti-freezing layer is made of coarse sand, its thickness about 0.8 meters. At present, the authors could not obtain the definite evidence to determine whether the ground surface in the port area was frozen at the time of the earthquake. When the earthquake occurred, the ground at Kushiro City was not covered with snow. It began to snow the next day and the ground was covered with snow with a thickness of about 0.2 meters.

EARTHQUAKE MOTION AT KUSHIRO PORT

Kushiro Port has a strong motion recording station at its central location. This is one of the station deployed under the network of the Port and Harbour Research Institute in cooperation with the Kushiro Port Construction Office, Hokkaido Development Bureau (Kurata and Iai, 1992).

The strong motion recording station is located on the former beach line at the estuary of the Kushiro River as shown in Fig. 2. The ground condition is shown in Fig. 3. In this figure and the figures to follow, all the borings and the Standard Penetration Tests (SPT) were conducted before the earthquake. The ground at this site consists of a fill with a thickness of about three meters, underlain by a medium to dense sand layer of SPT N-values about 20 with a thickness of about seven meters, underlain by a dense sand layer of SPT N-values of about 50.

The instrumentation at this site consists of two accelerographs; one is installed at the ground surface, the other installed at the base of the bore

hole 77 meters below the ground surface. The accelerographs are of force balance servo type, having the flat gain in the frequency range from 0.01 to 30 Hz. The acceleration data are recorded in the digital format in the integrated circuit (IC) cartridge memory with 16 bits/data at the time intervals of 0.01 seconds. The digital recorder is equipped with a pre-event memory to record earthquake motions from ten seconds before triggering.

The recorded earthquake motions during the 1993 Kushiro-Oki Earthquake are shown in Fig. 4. In this figure, main portion of the earthquake motion is plotted out of the original record obtained for a duration of 180 seconds; the origin of the time is ten seconds before the triggering of the recorder. Loci of integrated velocities and displacements computed for the accelerations at the ground surface and the base, shown in Fig. 5, clearly indicate that the predominant motion is in the north-south direction in this earthquake.

By comparing the ground surface motion in the north direction shown in the third row in Fig. 4 with the corresponding base motion at a depth of 77 meters shown in the bottom row, it is easy to notice the sudden change in the response of ground after about 30 seconds; most of the high frequency motions are filtered out; instead, a long period motion with a period of about 1.5 seconds becomes predominant, overlain by a spiky wave form at each peak.

This type of ground response has been often observed in the laboratory (e.g. Lee and Schofield, 1988); it is considered as manifestation of the effect of cyclic mobility of dense sand. The effect of the dilatancy of sand plays a major role when the ground is saturated and shaken with a strong motion as in this earthquake. In in-situ condition during earthquakes, similar spiky acceleration was observed at loose silty sand deposit at the Wildlife site during the 1987 Superstition Hills Earthquake (Holzer et al, 1989). In the dense clean sand deposit, the present record represents the very evidence that the effect of dilatancy of sand plays a significant role in the ground response during strong earthquake shaking.

In the current practice of ground response analysis such as often done with the equivalent linear model, the effect of the dilatancy of sand has been often neglected. The definite evidence presented here cautions us against the current practice of ground response analysis at strong earthquake motions.

DAMAGE TO GRAVITY QUAY WALLS

The most serious damage to the gravity quay walls in Kushiro Port was found at the North Pier in the East Port District. The location is designated in Fig. 2 as the site A. As shown in Fig. 6, displacement toward sea registered 2.0 meters at maximum, settlement 0.4 meters at maximum. The ground conditions shown in Fig. 7 indicates possibility of liquefaction down to an elevation of about -6.0 meters below the water level.

Among the gravity quay walls affected by liquefaction of back fill sand, quay walls designed with a seismic coefficient of 0.2 suffered relatively minor displacement. As an example is shown damage to a quay wall with a water depth of 12 meters located at the south end of the Pier No.2 in the West Port District. The location is shown in Fig. 2 designated as the site B. As understood from the height to width ratio of the caisson being close to unity, the quay wall was designed to resist relatively strong earthquake motions.

The backfill sand at this pier was loosely deposited as shown in Fig. 8 and was of a coarse sand as shown in Fig. 9. It was planned to be compacted as measures against liquefaction; unfortunately the earthquake hit the Kushiro area before the work was actually done. The back fill sand liquefied due to the earthquake. The caisson suffered deformation as shown in Fig. 8 but the displacement toward sea was only about 0.3 meters.

DAMAGE TO A SHEET PILE QUAY WALL

The most serious damage to the sheet pile quay walls in Kushiro Port was found at the Fishery Pier in the East Port District. The location is designated in Fig. 2 as the site C. The structure of this quay wall is of a steel sheet pile type anchored by battered steel piles. The cross section is shown in Fig. 10. As shown in Fig. 11, the ground at this pier consists of a loosely deposited back fill sand with a thickness of about ten meters, underlain by medium to dense sand deposit which forms the original ground.

The original ground level becomes deeper to the level of 11.5 meters at the eastern end of the quay wall so that this part of the quay wall slightly differs from that shown in Fig. 10; the quay wall at the eastern end uses longer sheet piles with an embedment depth of -20.5 meters and longer anchor piles installed to a depth of -14.9 meters on the sea side and -20.6 meters on the land side.

The earthquake caused liquefaction in the back fill sand, resulting in the serious deformation of the sheet pile wall as shown by the solid line in Fig. 10. In accordance with the deformation of the sheet pile wall, the apron exhibited serious settlement between the sheet pile wall and the anchor piles. Detailed investigation of the sheet pile wall by diving in the sea revealed that cracks opened in the steel sheet pile wall at the level of four meters below the water level.

PERFORMANCE OF A SHEET PILE QUAY WALL WITH COMPACTED BACK FILL SAND

In contrast to the damaged sheet pile quay wall described earlier, quay walls with compacted back fill sand survived the earthquake without damage. An example is the quay wall at the south end of the Pier No.1 at the West Port District. The location is designated as the site D in Fig. 2.

The structure of this quay wall

is of a steel pipe pile wall anchored by a steel sheet pile wall as shown in Fig. 12. The water depth of this wall is 12 meters. The ground at this wall had initially consisted of fill sand with a thickness of about ten meters, underlain by the original ground of medium to dense sand. The back fill sand was later treated by a sand compaction pile method as shown in Fig. 12. The SPT N-values of the ground before and after the compaction are shown in Fig. 13. In order to avoid the adverse effect upon the existing steel pipe pile wall during the ground compaction work, gravel drains were installed near the wall as shown in Fig. 12.

Despite the strong shaking of the earthquake, the earthquake caused no effect on this quay wall. The measures against liquefaction as well as the overall design of the quay wall according to the current design practice (Ports and Harbours Bureau, 1991) was proven to be good enough to provide resistance the strong earthquake shaking.

LIQUEFACTION AND DAMAGE TO STRUCTURES

In order to grasp an overall picture of the effects of liquefaction on damage to quay walls at Kushiro Port, Table 1 summarizes the relevant data for quay walls with water depths deeper than 7.5 meters. In this table, "liquefaction" is identified with respect to the soils within "the area of a quay wall cross section," shown in Fig. 14, which includes the back fill area treated as measures against liquefaction. This similarly applies to quay walls without measures against liquefaction, including the back fill area which is supposed to be treated as measures against liquefaction.

As shown in Table 1, the quay walls designed with a seismic coefficient of 0.15 suffered serious sea ward displacement of more than 20% of the water depth. Both the excessive strong shaking and the liquefaction might be the cause for this. In comparison to these quay walls, the quay walls designed with a seismic coefficient of 0.20 suffered sea ward displacement of less than 10% even when liquefaction occurred.

A closer look at the displacements of the quay walls with a seismic coefficient of 0.20 reveals that those without measures against liquefaction suffered displacement ranging from 0.5 to 10% whereas those with measures against liquefaction suffered displacement less than 3%, suggesting the measures against liquefaction reduces displacement of quay walls.

Among these features observed above, the effectiveness of measures against liquefaction to reduce displacement of quay walls is what was expected through laboratory studies; the in-situ evidence observed here is the very confirmation of this fact. The effects of seismic coefficient on displacement of quay walls are also what was expected from the balance of inertial forces and resistance force of quay walls. However, the effects of seismic coefficient also include the resistance against the effects of liquefaction. The larger resis-

tance of gravity body, which is massive and large if designed with seismic coefficient of 0.20, may contribute to resist the increase in earth pressures due to liquefaction as well.

From the point of view of measures against liquefaction, the back fill part of ground consisting of rubble behind a wall shown in Fig. 14 might be regarded as treated area as measures against liquefaction. Though the area of this part is not wide enough to cover whole area of active earth failure zone, this part still contributes to reduce the effects of liquefaction. Indeed, past case histories of performance of quay walls during earthquakes suggests that the effects of rubble can be regarded to reduce liquefaction induced displacement of quay walls (Tsuchida, 1981).

CONCLUSIONS

The present paper was devoted to compile the case history data on the performance of quay walls during the 1993 Kushiro-Oki Earthquake. The analyses are currently underlay and will be reported elsewhere. Implications from the present case history data can be summarized as follows.

(1) The strong motion record with a peak acceleration of 0.47g at Kushiro Port indicates that the effect of dilatancy of sand plays an important role in the ground response during strong shaking.

(2) Performance of the quay walls at Kushiro Port manifest the importance and the effectiveness of the measures against soil liquefaction in the earthquake resistant design of waterfront structures.

REFERENCES

Holzer, T.L., Youd, T.L. and Hanks, T.C. (1989) : "Dynamics of liquefaction during the 1987 Superstition Hills, California Earthquake, Science 244, pp.56

Kurata, E. and Iai, S. (1992) : "Annual report on strong motion earthquake records in Japanese ports (1991)," Technical Note of the Port and Harbour Research Institute, No.727

Lee, F.H. and Schofield, A.N. (1988) : "Centrifuge modelling of sand embankments and islands in earthquakes," Geotechnique, Vol.38, No.1, pp.45-58

Ports and Harbours Bureau (ed.) (1991) : "Technical standards for port and harbour facilities in Japan," Overseas Coastal Area Development Institute of Japan

Tsuchida, H. (1981) : "Damage to quay walls affected by liquefaction," 16th Research Conference of Earthquake Engineering, JSCE, pp.201-204 (in Japanese)

Table 1 Liquefaction and deformation of quaywalls

quaywalls	structure	water depth (m)	seismic coefficient	displacement toward sea (cm)	settlement of apron (cm)	settlement behind apron (cm)	liqueffaction *
Central Wharf East Quaywall	steel sheet pile	-7.5	0.20	0	0～10		◎
Central Wharf East Quaywall	steel frame	-7.5	0.20	0	0～10		◎
Central Wharf East Quaywall	steel sheet pile cell (under renovation)	-7.5	0.15	0	0～10		●
North Wharf East Quaywall	gravity type	-8.1	0.15	20～200	20～40		●
North Wharf South Quaywall	gravity type	-8.0	0.15	50～160	20～100		●
North Wharf West Quaywall	gravity type	-9.0	0.15	100～160	10～30		●
Fishery Wharf South Quaywall	steel sheet pile	-7.5	0.20	0～30	30		●
Wharf No.1 East Quaywall	jointed steel pipe wall	-9.0	0.20	0	0	0	○
Wharf No.1 South Quaywall	jointed steel pipe wall	-12.0	0.20	0	0	0	○
Wharf No.1 West Quaywall	jointed steel pipe wall	-10.0	0.20	-25～0	20～30	0	●
Wharf No.1 West Quaywall	gravity type	-9.0	0.20	5～70	20～30	10～35	●
Wharf No.1 West Quaywall	gravity type	-9.0	0.20	20～75	10～35	10～35	●
Wharf No.2 East Quaywall	gravity type	-7.5	0.20	10	10～35	0～10	●
Wharf No.2 East Quaywall	gravity type	-10.0	0.20	5	25～30	0～10	●
Wharf No.2 South Quaywall	gravity type	-12.0	0.20	20～30	30～45	20～70	●
Wharf No.2 West Quaywall	gravity type	-9.0	0.20	20～30	30～40	10～40	●
Wharf No.2 West Quaywall	gravity type	-7.5	0.20	10～25	10～30	0～30	●
Wharf No.3 East Quaywall	gravity type	-7.5	0.20	0～15	10～15	20～30	◎
Wharf No.3 South Quaywall	gravity type	-12.0	0.20	-7～6	10～20	5～35	◎
Wharf No.3 West Quaywall	gravity type	-12.0	0.20	5～25	10	10～40	◎
Wharf No.3 West Quaywall	gravity type	-10.0	0.20	15～25	10～15	5	◎

* ○ : Non-liquefaction (no need for measures against liquefaction)
◎ : Non-liquefaction (with measures against liquefaction)
● : Liquefaction (without measures against liquefaction)

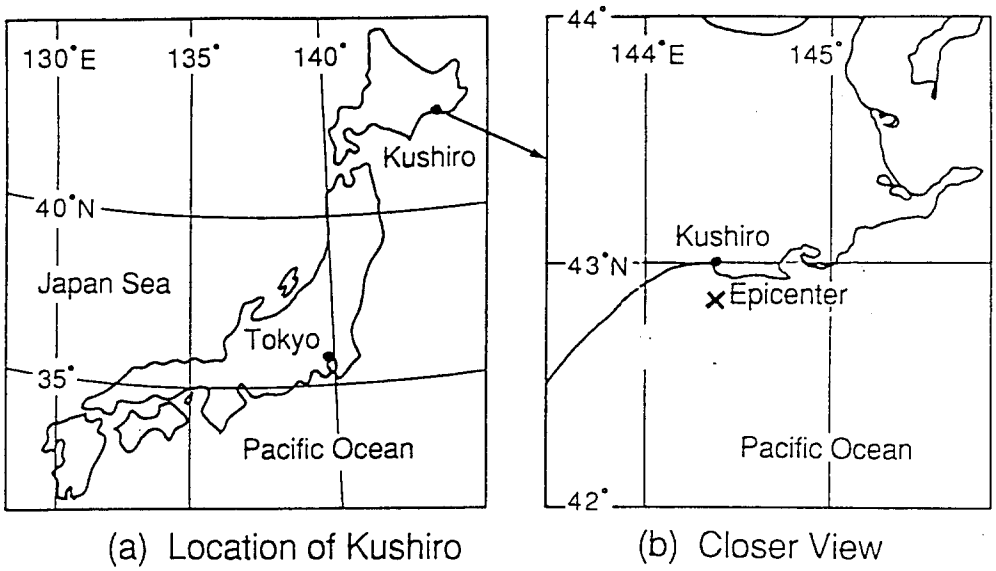

Fig. 1 Location of Kushiro City and the epicenter

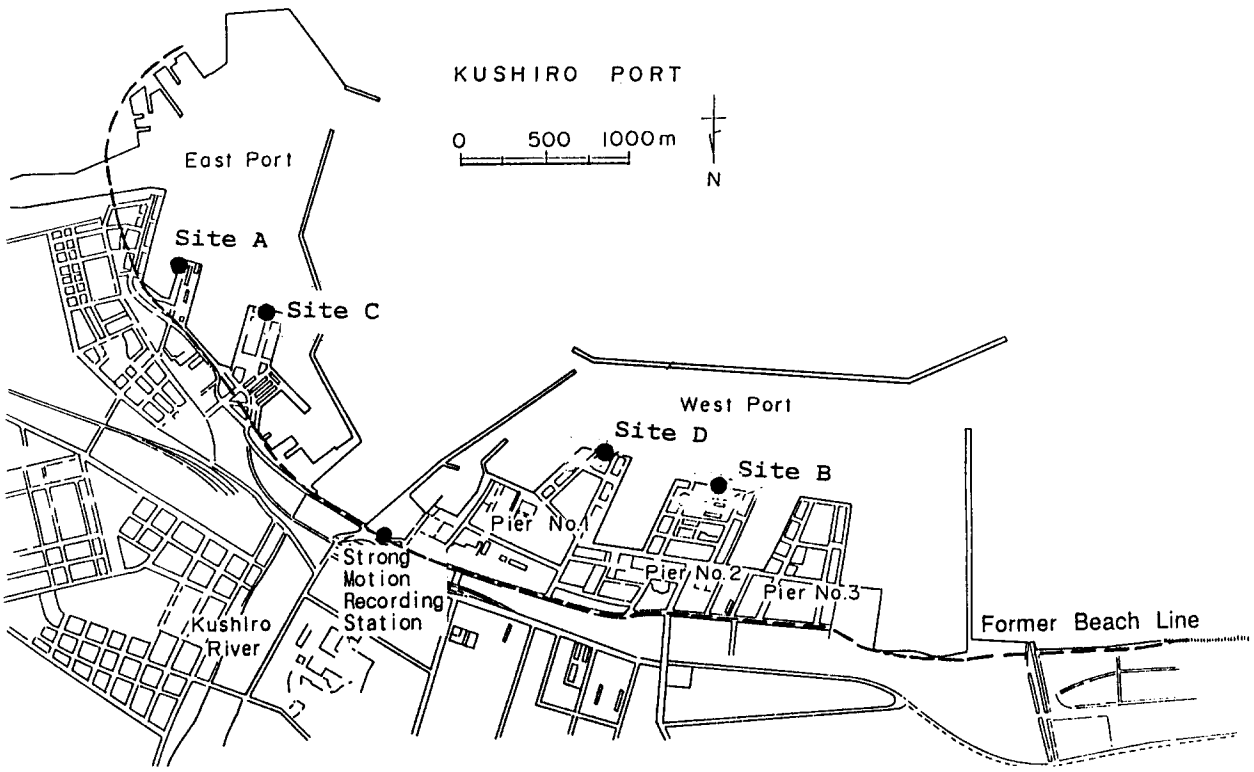

Fig. 2 Plan of Kushiro Port

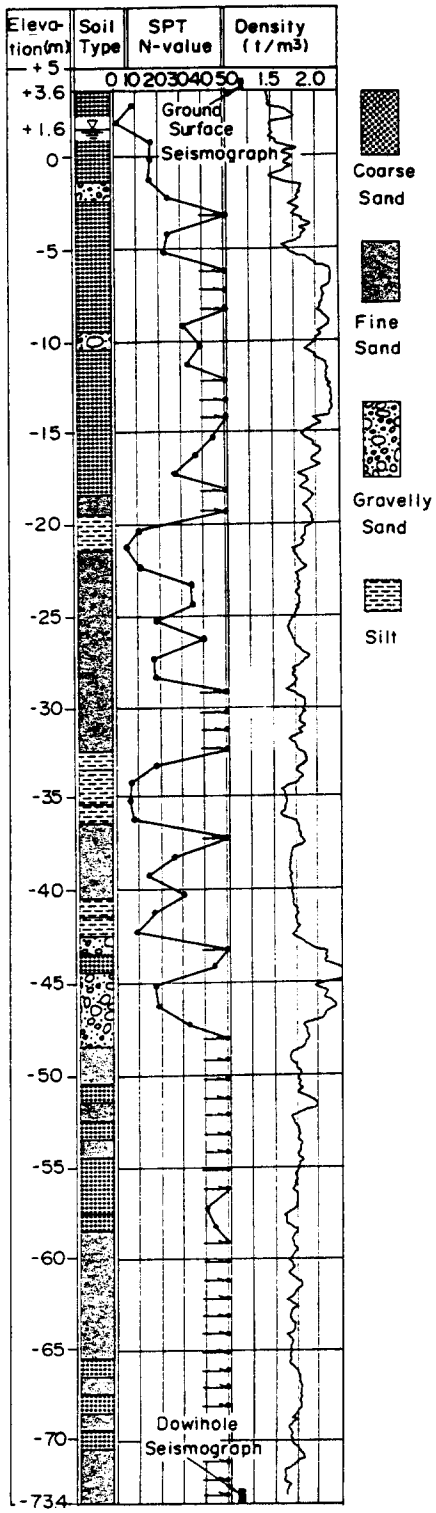

Fig. 3 Ground condition at the strong motion recording station

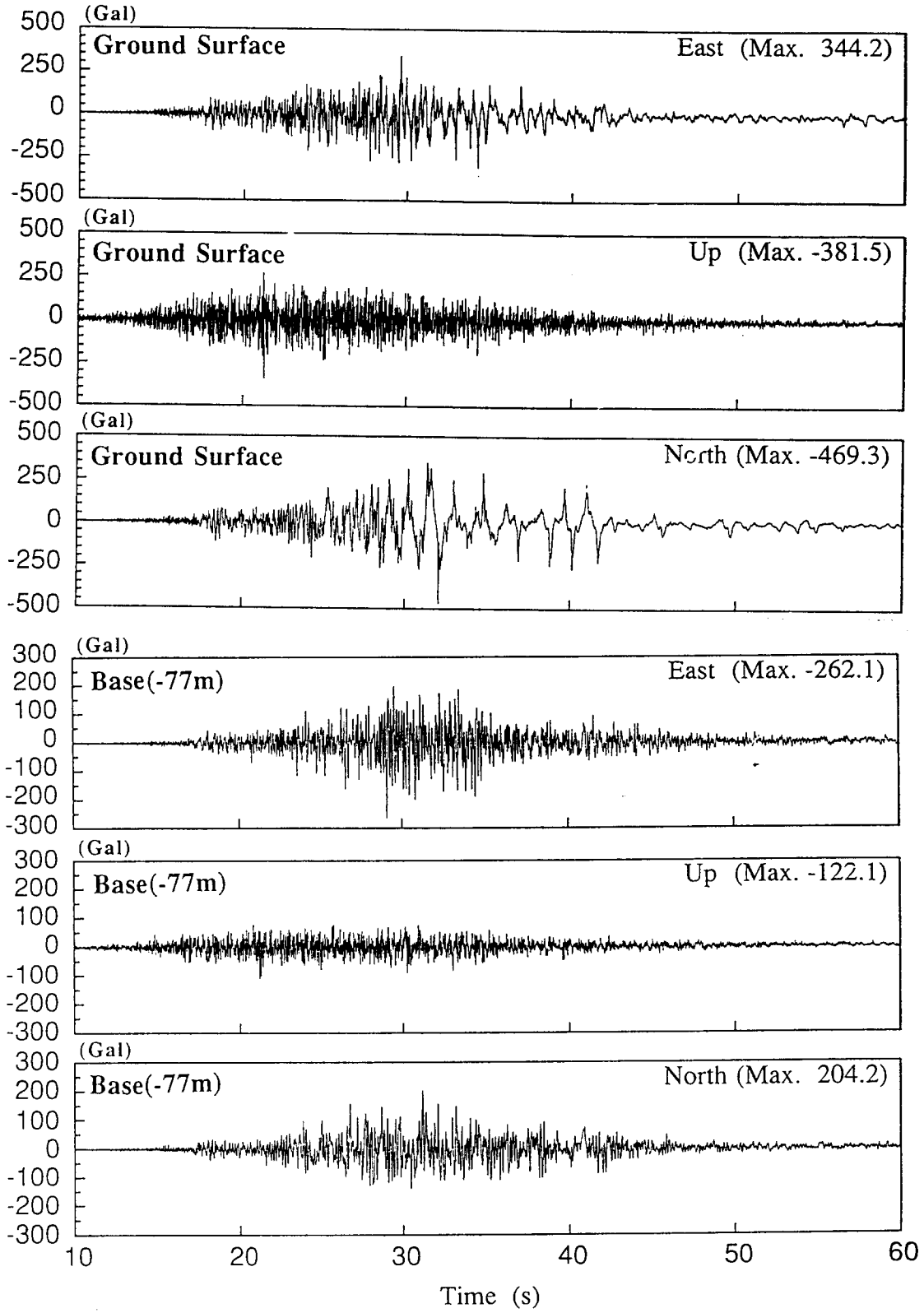

Fig. 4 Strong earthquake motions at Kushiro Port on Jan. 15, 1993

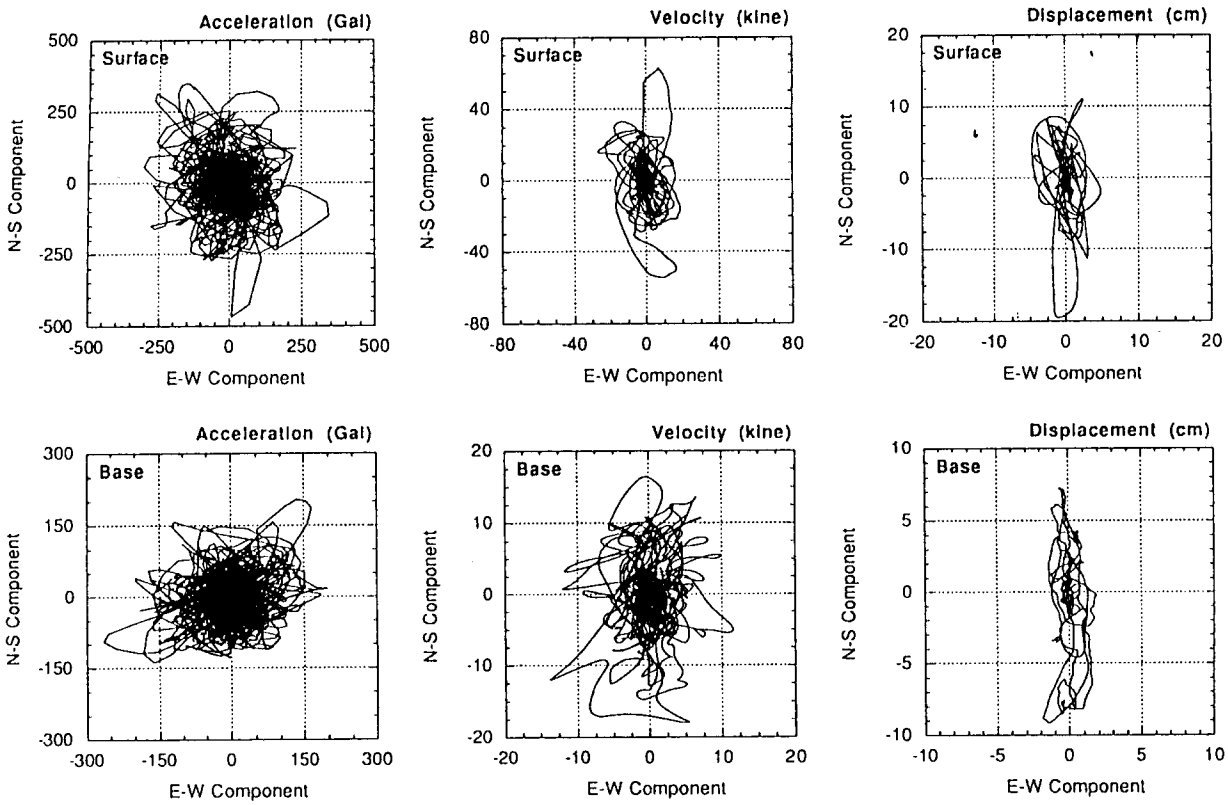

Fig. 5 Loci of accelerations, velocities and displacements

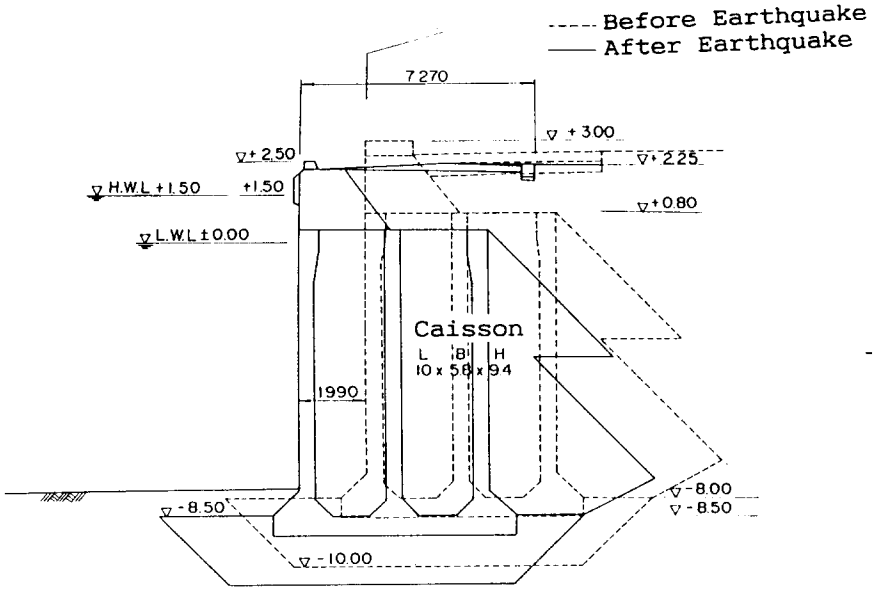

Fig.6 Damage to a quay wall at Site A

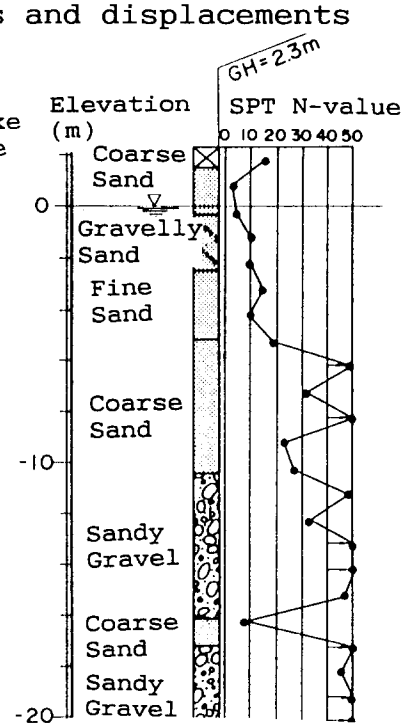

Fig.7 Ground Condition at Site A

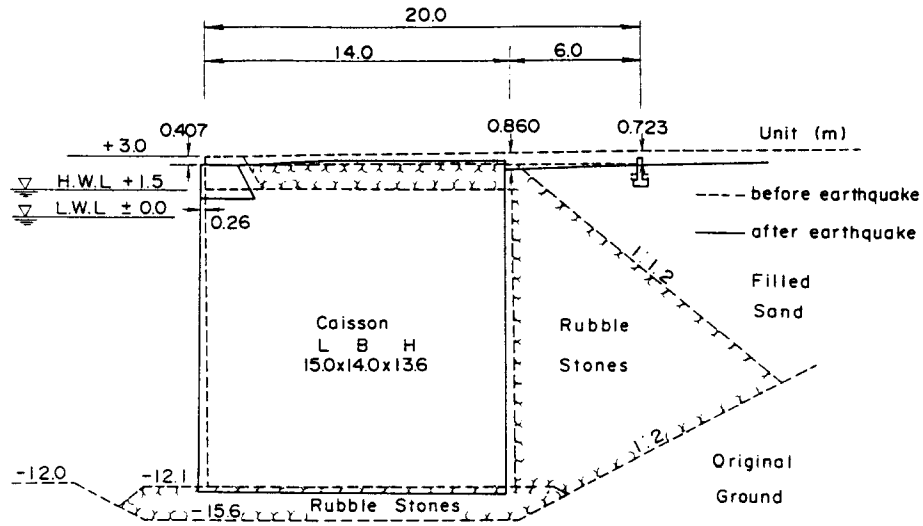

Fig.8 Damage to a quay wall at Site B

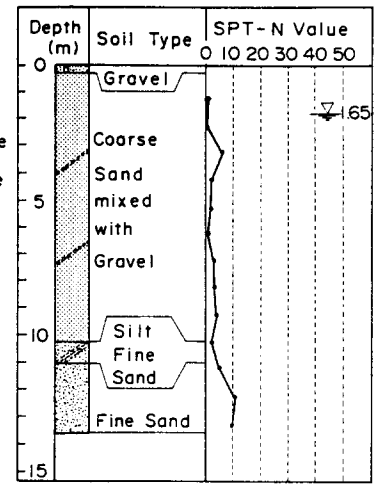

Fig.9 Ground Condition at Site B

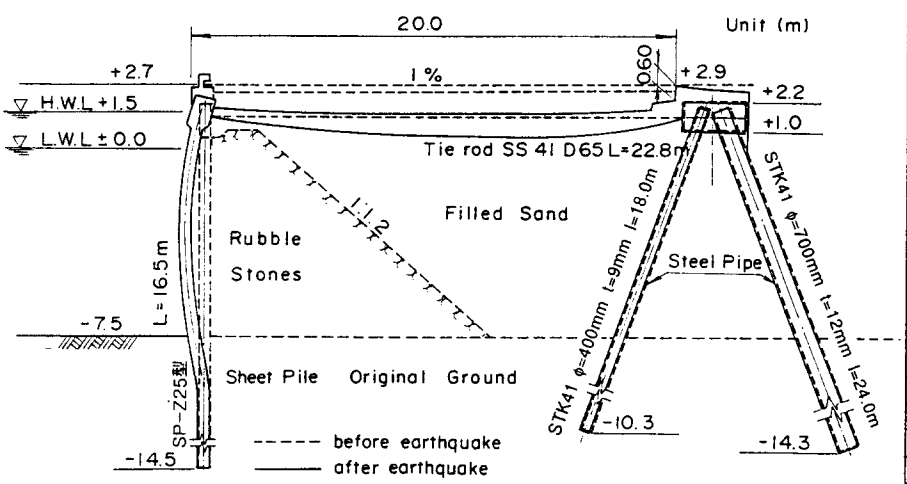

Fig.10 Damage to a quay wall at Site C

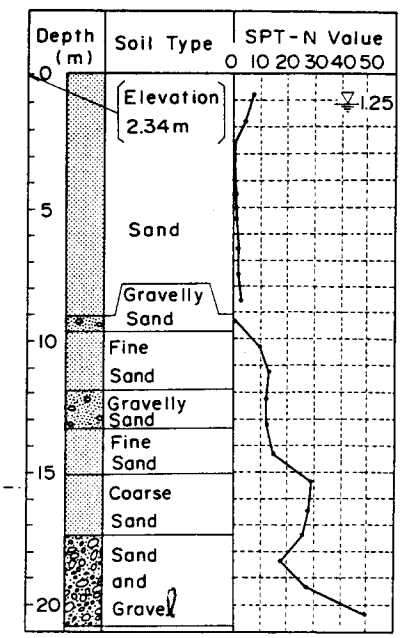

Fig.11 Ground condition at Site C

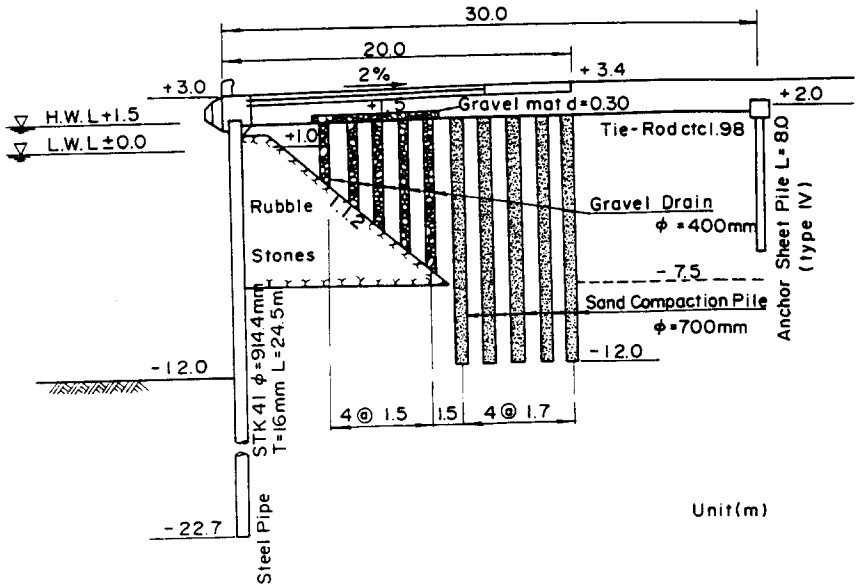

Fig.12 Cross section of a quay wall at Site D

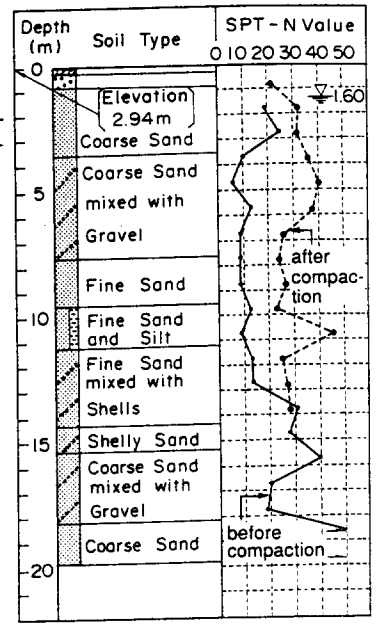

Fig.13 Ground condition at Site D

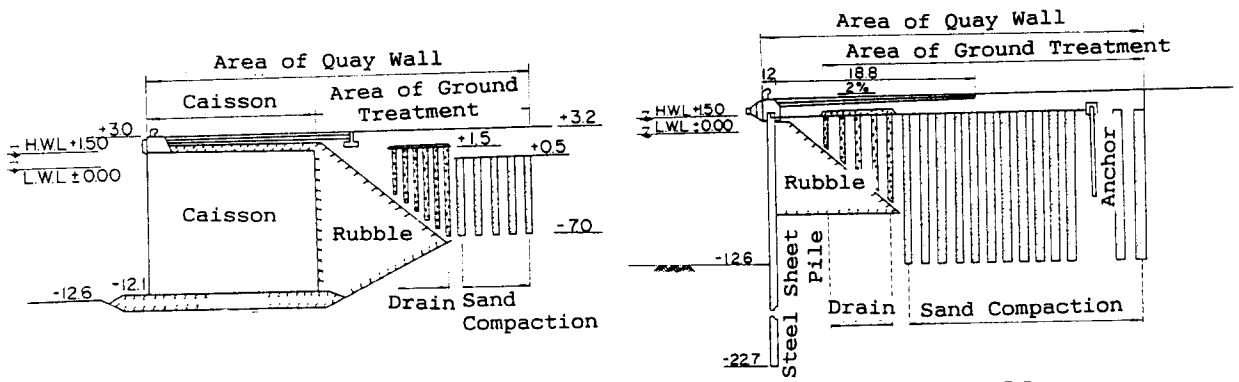

Fig.14 Schematic figures of the area of quay walls

Review of Progress in Dynamic Geotechnical Centrifuge Research

by

Ronald F. Scott

ABSTRACT

A great deal of research has been performed in the last ten years in the area of dynamic geotechnical centrifuge testing. The progress made is reviewed, with particular reference to papers presented at this Symposium, problem areas are identified, and suggestions are made to clarify some of the difficulties.

KEYWORDS: centrifuge; dynamic testing; earthquake; soil.

1. INTRODUCTION

In the past decade, activity in dynamic geotechnical centrifuge research has increased very substantially; new apparatus has been developed, instrumentation and data acquisition has become more complex, input excitation has been tailored to represent more realistic earthquake strong ground motions, and a great variety of model geometries has been explored. This review paper attempts to give a summary of this effort, the progress made, and improvements which, in the author's view, still need to be made.

2. PROGRESS TO DATE

Dynamic centrifuge testing has become virtually routine at a number of research institutions. The progress that has been made may be classified into a number of different areas.

2.1 Input Motions

In the early stages of dynamic centrifuge testing it was only possible to submit model structures in the centrifuge environment to very simple dynamic motions such as impact or shock tests or simple vibratory motion caused by compressing and releasing a spring to shake the specimen container. The frequency and ring-down duration depended on the mass and spring constants involved. There were also a number of investigations of explosion-generated shock waves in the centrifuge for the purpose either of shaking a structure, or to study the explosive tests themselves. In some tests of this character the explosive charge was used to form a crater in the soil medium during centrifuge rotation, for the purpose of studying the crater depth and diameter for different locations and sizes of explosive charge (Schmidt and Holsapple 1980).

The possibility of dynamic testing using electromagnetic means has been examined (Fuji 1991); such equipment had been used in laboratory and centrifuge testing for material other than soil, for example, structures, telemetry systems, or components of missile systems. Electromagnetic shaking has a number of desirable features including high-frequency activation of the shaking table, and the ready control of frequency content and amplitude. However, the equipment is subject to a number of drawbacks such as its substantial mass. This is generally unsuitable for testing soil specimens, which form payloads inherently large in mass. Another system of shaking developed was the so-called "bumpy road" at Cambridge University to subject samples to approximately 10 cycles of a rather noisy sine wave motion. The advantage of the device is its simplicity and in its original form it was eventually intended to include replaceable bumpy road tracks on the wall of the centrifuge containment. With these, different frequency contents could be included in the motion such as, for example, earthquake-like motions, but only two different tracks were ever produced. The disadvantage of the bumpy

* California Institute of Technology
Pasadena, California 91125

road motion is that the developed frequency input depends on the rotation rate of the centrifuge, since the frequency is controlled by a cam riding on a bumpy track of fixed geometry on the wall of the centrifuge. Thus, the faster the centrifuge goes, the higher the frequency that is obtained. However in most seismic centrifuge testing, the desirable frequency is set by the scale of the model and a natural event which is to be simulated. In the centrifuge, the model scale is set by the g-level, which depends on the square of the centrifuge rotation rate whereas, as pointed out above, the excitation frequency of the bumpy road depends on the rotation rate directly. This does not permit the necessary flexibility in the test input.

Finally, an electrohydraulics shaker was developed for the centrifuge (Aboim et al. 1983); these are commonly used for operation of laboratory shake tables of all sizes. The electrohydraulic apparatus had to be adapted for centrifuge tests because of the relatively small duration (0.3 to 0.5 seconds) of earthquakes in centrifuge testing at high g-levels. Thus, the actuating servovalve has to supply a surge of hydraulic fluid at a high flow rate to the hydraulic pistons that actuate the shaking table to get the high frequencies demanded by the compressed acceleration histories required. This is accomplished by mounting hydraulic accumulators on the centrifuge in which hydraulic fluid is stored at a pressure of about 3,000 psi in sufficient quantity to conduct the test without additional flow of hydraulic fluid from outside the centrifuge arm. These accumulators have generally been mounted on the arm, which is probably the most efficient location for them, but in some centrifuges with a lack of space available for arm mounting, the accumulators have been placed on the centrifuge bucket itself; this considerably reduces the space available for the shake table. An advantage of the electrohydraulic apparatus is that the nature of the motion imparted to the specimen is readily controllable. It is possible to supply the shake table with a variety of motions of selectable durations ranging from sine, square or triangular waves, to random excitation, and earthquake-like excitation, which is essentially random motion shaped in terms of amplitude as a function of time. There are difficulties in obtaining suitably high scaled frequencies on the centrifuge to simulate the complete range of earthquake motions. A number of these electrohydraulic shakers are now in operation on various centrifuges.

In addition to this equipment, the shake tables themselves have developed in a variety of types. Some have been suspended by tension members from overhead beams, others are mounted on roller bearings or elastomeric pads which permit greater visibility of a cross section of the specimen if the side of the sample container is made of transparent material.

2.2 Tests Performed

A number of numerical codes has been developed with the object of predicting the pore pressure increases in a saturated fine sand as a result of dynamic or earthquake shaking. These numerical codes have been developed in a virtual absence of measured field data on the behavior of such soils in earthquakes. They are lacking because, of course, the occurrence of earthquakes is essentially random and there have been very few sites at which pore pressure transducers have been installed in ground, which has subsequently been shaken by an earthquake. It was proposed to remedy this deficiency by supplying the necessary data by centrifuge tests in the "VELACS" project (Verification of Earthquake Liquefaction Analyses by Centrifuge Studies) (Arulanandan and Scott 1993). As described by Arulanandan et al (1994), the required experiments have been conducted by eight universities on a variety of centrifuges. The testing arrangement among the universities was to shake saturated soil specimens in models of controlled geometric configuration, arranged so that they would either undergo high pore pressure increases or liquefaction during earthquake-like events. The results from these tests could be used to verify numerical calculations performed with the same input applied to models with the same simulated numerical properties as the material used in the centrifuge tests. During preliminary studies for

the performance of the tests to be carried out, the question arose as to the degree of difference between test results carried out on different centrifuges, of different sizes, by different investigators at the various universities. If substantial differences in test data from "identical" tests were actually discovered, these results would mislead comparisons with numerical investigations. Consequently, it was decided to perform one uniform centrifuge test at all universities and to compare the results from that test to see what sort of differences could be expected. The paper reports the results of that test and compares and contrasts the information received from the different investigators.

There have been a number of tests done to investigate the behavior of soils subjected to explosions, which have been generated on a centrifuge by means of small plastic explosive charges set on the surface or below the surface of the soil specimen Schmidt and Holsapple 1980; Gill and Kuennen, 1991). Some of these tests have been performed in order to examine the stresses generated on structures as a result of the pressure waves generated; these have required strain gauges, load cells, and pressure transducers attached to the structures. The great advantage of the centrifuge apparatus for explosion tests consists in the scaling of energy implicit in the scaling relations. The energy scaling varies as the cube of the ratio of the centrifuge g levels to 1g. In general, for most static testing, this is in the range 50 to 100 so that if, for example, a scale of 100 is chosen, then a 1 gram explosive charge on the centrifuge at 100g represents a 10^6 gram explosive charge or 1 ton of explosive in the prototype. This is a realistic amount for real tests. In practice, however, it would be of considerable advantage to have a centrifuge running at a much higher rotation rate generating, perhaps, 1,000g at the specimen, in which case the magnification of the explosive charge in the centrifuge in terms of energy is a factor of 10^9, so that a few grams of high explosive in the centrifuge can represent an explosion in the prototype at the low kiloton level.

In cratering tests there are some difficulties such as, the possible distortion of the trajectories of the particles emerging from the crater by Coriolis forces compared to those of the prototype. In addition, the limited size of the test bucket means that not all of the material thrown out by the explosion is collected in the centrifuge bucket. Therefore, the pattern of fallback of material that typically occurs around a crater to form some of its rim will not be correctly represented in the centrifuge. It must be borne in mind for these, and other tests where particles are generated that move freely through the space adjacent to the centrifuge bucket, that the centrifuge does not represent an *ng* planet, but is a highly specialized dynamic environment for test purposes. Only when a particle is connected to the centrifuge container is it subjected to *ng* radially. Released into the fluid above or in the container, which follows its prescribed circular path, the particle experiences the one g vertical gravity field of earth as well as, of course, fluid movements (Tan and Scott 1985).

There has been a great increase in the number of structures that have been subjected to dynamic loads and tested in the centrifuge, from early tests on simple structures like single piles, or model footings, to complicated evaluations of earth dams with internal structure and layering, retaining walls, a variety of foundations, embedded structures, and some structures on the surface of the soil. These structures have been subjected to shocks and earthquake-like vibrations in order to generate solutions for comparison with numerical codes, and also to compare with full-size prototype tests on similar geometries of test specimen. Full understanding of model behavior requires comprehensive programs of instrumentation.

2.3 Instrumentation and Data Acquisition

In the past few years there has been a wider use of, and more ambitious programs in, instrumentation for centrifuge testing. It is not uncommon now to have 20 to 30 channels of information returned from a specimen in-flight. The equipment involved includes pressure transducers, accelerometers, strain gauges, and displacement transducers. The signals from these pass

through data acquisition equipment in which various signal conditioners are employed to amplify, filter, or otherwise treat the signal before it is transmitted out of the centrifuge through slip rings. The nature of the equipment has not changed particularly during this period. It is common practice to mount the signal conditioning equipment and, as described above, portions of a computer on the centrifuge arm in order to process the signal and, in some cases, perform the analog to digital conversion before passing it out of the centrifuge to the storage medium, usually in another computer outside the centrifuge. The signal may be stored in a memory device on the arm for downloading later. Some increase in the rate at which signals can be sampled and acquired has taken place, and it is now routine to sample signals from dynamic tests at 10 to several hundred kilohertz sampling rates, with the occasional use of a single channel sampled at 1 megahertz sampling rate for certain specialized tests, such as wave propagation in structures.

2.4 Test Containers

There has been an increasing use of specialized containers particularly for earthquake tests. Formerly, tests were generally done in rigid containers with stiff walls constructed for static testing purposes. Here, the primary consideration was that the walls would not flex and cause lateral strains, or stress reductions in the test specimen, that were not accountable for by the analytical developments. These were replaced in the early 1980's by test containers deliberately built to be flexible so that the motion of the soil in the container was dictated by the soil itself rather than by the container. When a rigid container is used and the box is excited by, for example, an earthquake, then there are unrealistic (in terms of prototype scale) vibrations that pass back and forward between the ends of the box. These reflections interfere with the "natural" seismically-generated motion of a test specimen that might be embedded in or mounted on the soil surface. On occasion an essentially rigid box is used, lined with an energy-absorbing material called "duxseal" applied at the ends perpendicular to the axis of one-dimensional excitation. The "duxseal" is intended to damp out the reflected motions.

Although the study of such tests is still of value and they can be simulated with numerical codes involving the same boundary conditions, these reflection effects are undesirable for tests in which simulation of a specific prototype is required. In consequence, many tests in recent years involving earthquake-like excitation of a container on the centrifuge have employed a device called, variously, a stacked ring or laminar box, (Hushmand et al, 1988) which is designed to permit the soil to deform with minimal interference by the box in one-dimensional shear tests. The device consists of a number of rings of metal, usually in rectangular form and separated from one another by either teflon or by roller bearings to reduce the lateral resistance of the rings to movement. The idea is that an ideal box would be essentially massless and frictionless; the response of the soil to input shaking at its base would be controlled by the soil rather than the box properties. Laminar boxes eliminate many of the end reflections and permit a container full of soil to deflect in the shear beam mode that is expected in a layer of soil of infinite lateral extent during excitation by an earthquake.

The principal criterion with respect to the rings of a laminar box is their mass compared to the overall mass of the soil specimen. If the mass of the confining rings can be made essentially negligible (less than 15%, say) of the total mass of the specimen then the contribution of the rings to the dynamics of the soil motion is very small. Because of the increased ring thickness required to preserve box stiffness these systems are less efficient the larger the container size becomes and therefore, the system works better for smaller centrifuges. In addition, such laminar boxes permit the lateral motion of the soil specimen at all depths to be measured by the use of displacement transducers mounted outside the container and bearing on the ends of the containment rings. When the displacement data are assembled, snapshots can be obtained of the vertical profile of soil at any time during the excitation. The disadvantage of laminar boxes

is that the specimen preparation is rendered more complicated, since the box requires a plastic or rubber liner, and special preparations have to be made in order to apply a vacuum on the box when tests are required on saturated sands.

Since, in all centrifuge shake tables, the input force is applied to the base of the box, well below the center of mass of the box and soil specimen, some test boxes exhibit rocking or pitching motion on being shaken. This generates accelerations or stresses in the vertical direction 180° out-of-phase at each end of the box.

After this brief review of the state-of-the-art in dynamic testing to the present, a discussion follows of improvements or advancements that are needed in order to develop more sophisticated tests and to enhance our knowledge of the behavior of soil under conditions more complex than those which have been attempted in the centrifuge so far. This will be considered in the next section.

3. NEEDED IMPROVEMENTS

3.1 Equipment

3.1.1 Two and Three-Dimensional Shaking

So far in earthquake studies the shaking that has been imparted to the soil model has been primarily one-dimensional, the equivalent of horizontal ground motion in the prototype in one direction only. Although some other components of motion are normally represented in the data (Figure 1), they are accidental byproducts of the dynamics of the centrifuge and shaking system and vary from centrifuge to centrifuge. Depending on the design of the shaking apparatus, vertical motions (referring to the full-scale prototype) of an intensity that depends on the design are usually generated. These can be as high as 30 to 50% of the horizontal peak earthquake accelerations. To a lesser extent, transverse horizontal motions with peak accelerations of the order of 2 or 3% of the primary horizontal input accelerations are also developed. In all cases the basic intention is to eliminate other components of motion to simplify analysis and interpretation of the results. When two different centrifuges are used to study the same scaled event, with the same model and with intentionally similar one-dimensional horizontal earthquake input, it can be the case that differences in the results are obtained due to different intensities of vertical shaking accompanying the same (approximately) horizontal motion (Figure 2). No studies have yet been made of the effect of the additional accidental vertical motion on the phenomena being examined. This would require an apparatus in which the vertical motion was capable of being controlled and could be added to the horizontal motion in any intensity desired.

For this reason and for other investigations, it would be very desirable to place on a centrifuge a shake table with at least two- and preferably three-dimensional capability of shaking the specimen to simulate the major components of measured input earthquake motion. It appears feasible to produce two horizontal components but it may be difficult to obtain controllable vertical earthquake motion by design.

3.1.2 Other Input Requirements

An examination of the spectra such as are shown in Figure 3 reveals that the typical centrifuge motion is limited in the frequencies that can be attained by means of the electrohydraulic devices in current use. Although there are some differences in the spectra from different machines, in general, the frequencies are too low to properly represent the rather broad frequency spectra of real earthquakes. There is therefore, a necessity to improve the characteristic motion represented in centrifuges in order to make the spectra more realistic and more representative of the real earthquake motion. Very little is known at present on the effect of different frequencies on the performance of soils in earthquakes. It seems likely that, in particular, pore pressure increases might be substantially affected by the frequencies developed during the

earthquake, but it is not known whether a given intensity of high frequency will be more or less likely to liquefy soil than the same intensity at a lower frequency. In some centrifuges (see Figure 3) there are very distinct gaps between the peaks on the spectra; these appear to be caused by various harmonics of the system and the apparatus used to generate the earthquake motion. Because of other design constraints it may be difficult to eliminate equipment frequencies in the design range. There are differences in the performance of large and small centrifuges in this respect.

In addition, it is desirable that higher accelerations be achieved. The Northridge, California earthquake of January 17, 1994 developed at one site (Tarzana) sustained peak ground horizontal accelerations of about 1.8g, and it must be possible in centrifuge tests to achieve this level of acceleration so that the behavior of structures in such areas can be adequately followed. It may be noted that, with time, the increasing density of strong motion accelerographs produces greater peak accelerations as earthquake motions are recorded at a greater number of sites. The Northridge earthquake was the most recent to demonstrate this.

Increased accelerations in shake tables appears to be a fairly difficult goal to achieve. Peak accelerations, at the present time, of about 35g are attainable on a few centrifuge shaking apparatuses. If the tests are carried out at 50g this represents about 0.7g peak horizontal acceleration in the prototype; if at 100g then, of course, only 0.35g prototype acceleration is obtained. The peak acceleration generated is a result of the combination of the mass of the shaking table, the size of the servovalve, the accumulator volume and pressure, and the design of the piping and tubing which admits hydraulic fluid to the servovalve. To some extent the peak acceleration achieved is a chance event which depends on the natural frequencies of the equipment as described above, but it should be possible to design systems which would achieve higher acceleration frequencies than those commonly experienced.

3.1.3 Transducers

A variety of instrumentation is employed in the soil in centrifuge testing, including strain gauges, pore pressure transducers, accelerometers and pressure transducers in general. External to the soil mass, other transducers such as displacement transducers (LVDTs are normally used) can be applied to measure settlement or displacements of the soil mass or container. The sensing components that are normally imbedded in the soil have dimensions of the order of 3 to 7 millimeters in diameter and length depending on the manufacturer and the type of instrumentation involved. When employed in centrifuge tests at 50 to 100g range these then represent prototype dimensions of transducers of approximately 0.15 to 0.7 meters in size.

In any normal prototype application, such instruments would be considered to be large; their presence would interfere with the response being measured. It must therefore be assumed that there is a similar uncertainty in the interpretation of the output of these transducers in the centrifuge test where, in addition to their absolute size, they are also relatively large compared to the soil specimen dimensions. It is past time to develop equipment that is substantially smaller than these dimensions for centrifuge testing; advantage should be taken of the great advances in fabrication of micromechanical devices developed for other purposes (Barth et al, 1988; Schlichting et al, 1993). Smaller devices, of the order of a sand grain in size, would give more reliable readings of the variables in soil, and more of them could be placed in or around model structures to determine the stress fields, pore pressures, etc. on a wider basis. Local inhomogeneities in the stress field could be detected by such small devices. Lower practical limits to the size are imposed by the connecting wires, and the packaging of the device.

Not much attention is paid at present to the mass density of transducers; this is an important feature in dynamic tests, where a mismatch in

soil-transducer density will result in spurious signals. The transducer and its attached cable can be viewed as a small structure with mass, stiffness and damping (cable) which are different from those properties in the soil which it is replacing. Consequently, when vibrations pass through the soil, they interact with the transducer and cable, to cause motions in that system which are not the same as those in the causative vibrations.

One difficulty with all such equipment is, of course, the necessity of attaching it to signal conditioning equipment by means of wire, which, with a larger number of sensors, raises questions about the effect of wires on the response of the material. An accompanying issue that needs to be addressed is: If more sensors are to be introduced into the soil then more data channels need to be available in order to process the signals and make them available for subsequent analysis. If 50 to 100 transducers could be installed in a soil profile a corresponding increase in the amount of the signal conditioning equipment would be required. At the moment about 20 to 30 channels are typically used for centrifuge testing at the upper end of the range (frequently, fewer are used), and this already strains most signal conditioning equipment, recording devices, and the slip ring capabilities.

The development of signal conditioning equipment has been leading towards the installation of computers on the centrifuge arm where the data is not only processed, but stored during the centrifuge test without passing through slip rings to outside data storage facilities. If a substantially greater number of channels is envisioned, then this form of data acquisition might be necessary. There are advantages, particularly in noise level suppression, to storing the data on the centrifuge arm, but the disadvantage is that the performance of the test would not be known (without using slip rings) until the centrifuge had been brought down to 1g, and the signals downloaded to a laboratory computer for examination. In the present arrangement of passing signals through the slip rings there is the great advantage in knowing what is happening while the test is in progress. There is then a capability of repeating the test if, in fact, something seems to be wrong that is curable. An expansion in the number of transducers installed also complicates the preparation of the soil model.

3.1.4 Data Acquisition

This subject has already been taken up in the previous section, but there are other considerations with respect to data acquisition which need to be addressed in the next generation of this equipment. One of these is the transmission of the signals within and without the centrifuge. It is desirable to avoid the wiring harnesses, which are now such a common and obvious feature of centrifuges, by introducing alternative photo-optical or infrared transducer devices to transmit the signal. This could lead to a greater compactness of the equipment, and to isolation of the instrumentation in the soil from the signal acquisition equipment mounted on the centrifuge arm, with the consequent elimination of noise which is always picked up by the current wiring arrangements. The further possibility of using radio transmission from transmitters closely associated with the instrumentation to receiving stations outside the centrifuge also needs to be examined. Some preliminary investigations were made on this by the author 15 years ago, but, at that time, the signal transmitters were very expensive and the apparatus was limited in the number of channels that could be handled. With the micro-miniaturization of equipment, it is now possible to include the radio in the package with the transducer. This does not appear to have been done in centrifuge testing as yet.

It would be desirable to try to match instrumentation development, which needs to be done by manufacturers, with such requirements as these. This raises the difficult question that, although the centrifuge business is proliferating, there are still, at a commercial level, rather few centrifuges in the world, and they do not represent a very large market for a manufacturer. How is it possible to get electronic manufacturing companies to design and build

micro-miniature transducers for a market which might only purchase several hundred of these devices a year? The same question applies to the development of new signal transfer devices and, to a lesser extent, to data acquisition. The latter is used in more fields of experiment, and is therefore common to a variety of equipment, including centrifuges. An examination of the advertisements in electronics and physics magazines, for example, will show a wide range of data acquisition equipment made available for general purpose use.

In this subject area there are certain other needs which require to be met. At present the state-of the-art of data acquisition seems to be limited (at a reasonable price) to approximately 1 million sample acquisitions per second (1 megahertz sampling rate), and this can be performed on only one channel. If two channels are used, half the sampling rate is obtained, etc. Such a rate is applicable for tests such as wave transmission in parts of structures embedded in soil such as, for example, in a pile struck by a pile driver. The pile, if it is made of steel (both model and prototype), has a wave speed through the material of approximately 5,000 meters per second; however, in the model the model pile is perhaps only 30 centimeters long, and therefore, the wave makes one trip down the pile and back up again in only 120 microseconds. The total duration of the signal from a strain gauge attached to the model pile surface is only a few milliseconds. The short duration of reverberation at a point on the pile requires a very high sampling rate. However, since in such an experiment there might be 6 to 10 channels of information from strain gauges or accelerometers mounted on the pile as well as from a number of pressure transducers in the adjacent soil, a megahertz sampling rate would need to be available for perhaps 15 or 20 channels instead of 1 channel. At present, this does not seem to be available at a reasonable price. The second aspect of such data acquisition is, of course, the volume of data that will be received from 20 transducers, say, all sending in data at a 1 megahertz or greater rate. This is a very substantial amount of information, coming in at a very rapid rate so that storage needs to be available in the order of 20 or more megabytes per second.

One other problem requires attention. In the past, at Caltech, we have made use of a high speed movie camera, mounted on the centrifuge arm, to record earthquake-induced displacements of the test structure (say a model dam) at speeds of up to 6,000 frames per second. Some of these models were tested at 100g, and, if a conventional movie camera filming the prototype has a framing rate of 20 frames per second, the movie of the model on the centrifuge, to be shown at a normal viewing rate, should be taken at 2,000 frames per second. Since "slow motion" permits a better analysis of the data, we chose to use 6,000 frames per second. Special high speed film is required. Normally, at Caltech we would take the 16mm film to a company in Hollywood for same day processing (a "rush"), view the movie, and decide on the next test to be done. The last time we attempted this the film company said "nobody here processes 16mm film anymore; you have to send it to San Francisco". We did, and received it back 10 days later, which had an impact on our testing operations. Clearly, soon, if not already, no commercial concern at all will process 16mm film, and we will have to do it ourselves. Processing color movie film is not a simple task.

The 16mm film is vanishing because of video cameras and videotape. But their framing rate is only about 30 frames per second, and an increase to 6,000 is not in the foreseeable future. Even were the video camera available, with one frame generating say, 700,000 bytes of data, then at 6,000 frames per second, a storage rate (tape or other) of about 4,200 megabytes per second would be required. Since a model earthquake might last 0.5 seconds, a storage capacity of about 2,000 megabytes is needed. For some tests, such as those involving explosion or impact, much higher framing rates (to 100,000 frames per second) would be desirable. It is possible, with special equipment, to capture a few frames (Gill and Kuennen 1991) with video techniques, but the technology is at an early stage. There seems to be an impossible gap here. What is to be done?

3.2 Physical Problems

3.2.1 Scaling Relations

Geotechnical centrifuge tests were devised so that properly derived scale relations could be applied to scale models involving soil. In a substantial number of static and dynamic situations these, by now familiar, relations are appropriate and have been used. There are, however, conditions for which conflicting scale relations apply, and where the proper construction of models, and interpretation of their test behavior is not clear. Perhaps the best-known of these circumstances is the conflicting time scales encountered when the generation and dissipation of pore pressures occur as a result of dynamic excitation. Time for dynamic effects in the model is n times the prototype time, where n is the ratio of prototype to model lengths, whereas in the diffusion process the model time is n^2 times full-scale time. Thus the rate of pore pressure dissipation in, for example, a seismically excited saturated sand may exceed the rate of generation.

It is possible, if the prototype sand is used in a centrifuge test, that little or no pore pressure increase will be observed during excitation, because of the rapidity of diffusion. The expedients adopted to resolve this dilemma so far have drawbacks. One technique is to use finer soil in the model than prototype, but then the mechanical properties of the material, on which the scaling assumption depends, are no longer the same. The other is to employ a liquid more viscous by the factor n, in the model than the water usually found as the pore fluid in the prototype. Silicone oil, or glycerin/water mixtures are commonly used. In this case a question arises as to the effect of a more viscous fluid on the mechanical behavior of the soil, specifically, in the seismic case, on those properties which affect pore pressure generation.

A *reductio ad absurdum* argument would indicate that in the limiting case of an extremely viscous pore liquid, say asphalt, no grain separation, and thus no pore pressure generation would occur on seismic input to the soil. This would indicate that viscosity has a significant effect, but does a higher viscosity by a factor in the typical centrifuge range of 50 to 100 substantially modify the pore pressure generation, or not? This needs to be investigated, probably for sands of different grain sizes.

The other discrepancy in scaling laws occurs if viscous flow is important in the model during the time of the experiment – that is to say in a quasi-static test. If the soil (model and prototype the same) can be represented as a linearly viscous material, then, since strain is dimensionless, and the shearing stress is the same at homologous points in model and prototype, it follows that the time scale is unity (model and prototype times are the same). A certain amount of strain would take the same time to develop in model and prototype.

Slope creep would be a condition where this consideration holds. Another is volumetric change in a soil over a period of time, where a component of the change during and after primary (diffusion) consolidation, referred to as secondary consolidation, continues as a function of time. A way around the difficulty of modeling this phenomenon has been suggested (Sathialingam and Kutter, 1994).

There are still a substantial number of problems involved if very large structures require modeling on the centrifuge since, in general, the scaling ratio cannot be made high enough with existing machines to bring the model dimensions down to a size suitable for the model test chamber. Under these circumstances, on occasion, individual components rather than the whole of the structure can be tested. It is common to use centrifuge testing as a verification or validation of numerical models, and many of the above considerations become relatively less important if the point of the experiment is simply to test the correct physical phenomena at the correct stress levels in the centrifuge for code verification purposes. If a given model can be simulated correctly by a numerical program, then confidence is given that a

numerical calculation with, say, different geometry or material properties, can handle the real prototype question at issue.

Scaling relations also need to be examined in problems involving liquid density-driven-thermal convection in the centrifuge, although dynamic conditions related to this mechanism have not yet appeared. The relevant dimensionless parameters are the Rayleigh number, where the gravitational acceleration appears, the Prandtl number, which expresses the importance of mechanical to thermal diffusion, and the Taylor number, which brings in the rotation of the centrifuge. For liquid flowing through soil, the kinematic viscosity of the liquid should probably be replaced by the consolidation coefficient of the soil.

3.2.2 System Dynamics

Much of the work that has been done so far on the development of rapid motion-generating systems on centrifuges has been done on a purely *ad hoc* basis. The shaking tables, servovalves, and accumulators which accompany them have been assembled more or less instinctively, based on past experience. It is time for analysis of the performance of such systems to be based on proper numerical models of the entire system structure. It is necessary to form a model (Figure 4) showing the system including centrifuge arm, drive system, shaft, boundary conditions, and so on, and then to insert in this model the desired shaking system performance at the appropriate intermediate position on the swinging bucket, to examine the effect on the system. Only by such studies can an understanding be obtained of the source of the natural frequencies that are observed in the shake table response, and of what can be done in order to make the motion more representative of real-life or other desired input motions. When even the simplified Figure 4 is viewed it can be seen how many inputs come from the mechanical structure of the centrifuge. The results of such numerical studies combined with modal data from tests with shaking machines mounted on the centrifuge will give the necessary system or transfer functions.

One component in particular in this system needs to be described rather precisely and that is the actual hydraulic shaking system. It is suggested that a model of the hydraulic system also needs to be constructed, including the accumulators, piping system, the compliance of the various components, the compressibility of the hydraulic fluid, and the system function of the servovalve that is employed. With a suitable and realistic numerical model of this kind it would be possible, as a separate issue, to examine the effect of increasing the hydraulic flow or changing the design or capacity of the servovalve.

At the same time, the design of the shaking system itself needs to be evaluated more closely than has been the case to date. The motion of the shake table is intimately connected with the mechanics of its design. In particular, for example, an important consideration is the location of the actuating pistons with respect to the center of mass of the soil container being shaken. Such a study might make it possible to construct a better shaking table to eliminate some of the vertical and transverse motions which are observed in most such machines (Figures 1 and 2). An undesirable component observable in some centrifuges is the presence of pitching motions of the centrifuge test box caused by the location of the actuating pistons far below the center of mass, as discussed earlier. This shaking motion (see Figure 5) gives rise to vertical accelerations at the ends of the soil container which are as large as the horizontal values but out-of-phase with respect to one another.

The analysis of the entire centrifuge system and the hydraulic actuators involved should, of course, be carried out under in-flight conditions with payload so that the stresses in the arm are realistic.

3.2.3 Model Construction in Flight

A question which persists in centrifuge model testing and analysis refers to the difference in the stress field in models which are constructed at 1g in the test laboratory before being brought

to 50 or 100g in the centrifuge, and the stress field in the prototype, where everything is constructed or formed at 1g. Ideally all models in the centrifuge should be constructed in flight, including the installation of the appropriate structure. To explain in more detail: the empty container should be brought up to speed in the centrifuge, and the soil placed in it by raining or by centrifugation of the material in water so that consolidation and/or stress-induced settlement takes place as the soil profile is formed under the artificial gravity field of the centrifuge. This ensures that the region to be tested is under the correct stress conditions (depending on the boundary conditions of the specimen). The next stage is to insert, for example, a pile or other required structure into the soil to generate the correct stress conditions appropriate to the prototype. Although it would be easier to insert the pile by pushing it into the soil in flight, this would not represent the conditions which would be generated by a driven prototype pile and thus, model piles ought to be driven by a model hammer. During this operation in flight the stress field caused by the pile or other foundation insertion would be duplicated in the pressure transducers, strain gauges, accelerometers, and so on, installed in the soil.

For this example (pile) the installation of the system, although complicated, is perhaps more simple than many other realistic conditions in practice. For example, there have been studies (Kimura 1984) of the construction of sand embankments on top of clay layers in-flight on the centrifuge by raining or pouring the sand from a hopper. When the embankment reaches a certain height failure may occur, and the observation of a failure mechanism can be made. However, because of Coriolis effects it is very difficult to construct an embankment with proper shape. The sand passing through the air from the hopper to the soil surface follows a curved path, as shown in the paper cited. Tests including buried structures subjected to explosions and/or dynamic shaking are even more difficult to consider. A particular difficulty of course involves installing the necessary structure with attached instrumentation.

It is suggested that it might be necessary to develop much more complicated systems than are presently visualized for the construction of such detailed and correctly-dimensioned models. The process might be facilitated by an excursion into the problem of designing and constructing suitable robots or robotic arms which could deposit soil or pick up and place transducers in a soil while the centrifuge is in flight. Such transducers or other probes could be moved at various times during the experiment in order to examine different aspects of the material behavior. Alternatively, the robotic arms could introduce testing devices into the soil to measure soil properties during flight. A conceptual sketch of such an experiment with suitable robotic arms to extract piles from a quiver and install them in a group is shown in Figure 6. One difficulty in design is that the robot is also required to function at 50g, 100g, or higher.

It is necessary at this stage to make a plea for more full-scale field tests of a variety of problems and boundary conditions with which centrifuge tests can be compared, so that the necessity for conducting more realistic sample preparations can be documented, and those which are necessary, as compared with those which cause only minor differences in the behavior of a sample can be identified.

An additional consideration, which follows the same train of reasoning, is that there is a need for more in-flight studies of the material behavior and material properties. In general, centrifuge test properties are determined largely in the 1g condition of the material. In the case of sands, the material properties are identified from the known stress field and the initial in-place density of the sand. There have been a few tests in which material properties have been determined from in-flight tests by means of miniature cone penetration tests or miniature vane tests (Corté et al, 1991; Stewart and Randolph 1991); these tools have been inserted into the soil in flight. Seismic analysis techniques are useful in this regard. For example, it is possible to place seismic signal generating elements in the walls

of a container, and receiver elements on other walls. Signals are passed through the soil at different depths in order to determine *P* and *S* wave velocities in the material and thus, the profile and properties at least in the elastic range of the soil (Gohl and Finn 1987; Shibata et al, 1991). Care must be taken that the signal does not take a different route through the container walls. This can be done before and after performing a test. It is possible, for example, to perform such measurements while a test is in progress, and, by means of mathematical transform and deconvolution techniques, to examine the change in soil properties graphically as the soil is stressed by static or dynamic loads. Soil profiles have been examined by means of the generation and measurement of Rayleigh waves which have also been adapted for centrifuge experiments. The advantage of the centrifuge over the prototype material is that in all centrifuge tests the soil is *placed* and therefore the experiment carries with it the possibility of including experimental micro-apparatus in the soil profile as it is being constructed. These pieces of equipment could then be actuated subsequently during the actual test.

3.2.4 Test Containers

In all centrifuge tests so far, great use has been made of rigid-walled containers, some with a transparent single wall so that the experiment cross section can be visualized in flight by movie or television camera. For dynamic tests the stacked ring or laminar box equipment has been developed; this has been of value in one-dimensional shaking tests but presents difficulties, of course, in its present form, for multi-dimensional tests. For many dynamic tests it is desirable to design and construct different types of boxes which will allow for two- and three-dimensional motion of the specimen. The majority of centrifuge tests performed to date has consisted of plane strain tests, in which the influence of the side-wall boundaries is always open to question, and a variety of methods of treating these boundaries has been suggested. More work needs to be done on the possibility of substituting various materials, which modify the reaction of the box on the soil or permit wave reflections to be dampened or modified sufficiently so that they are no longer a consideration in the behavior of the model. These new boxes should have built-in drainage conditions at the boundary to permit soils to consolidate more rapidly or to admit the introduction of water into a soil sample to saturate it. The application of a vacuum on the soil specimen in order to facilitate deairing the specimen and to ensure appropriate performance of pore pressure transducers embedded in it is also necessary. A test container manufactured so that pressure and other transducers can be more readily installed in the soil with their leads and terminals plugged into the side of the test box is also useful in the soil testing process.

4. CONCLUSIONS

Up to this point it has been relatively easy to develop new dynamic centrifuge tests, models, inputs, and instrumentation. It will get progressively more difficult as the rigor of experimental proof becomes more demanding. Not enough work has yet been done to demonstrate conclusively that even the most straightforward of static centrifuge model tests exhibit correctly-scaled prototype behavior. It may require the effort and expense of constructing a prototype test to represent, complete with respect to soil, boundary conditions and input, a centrifuge model. In dynamic tests, the problem is more difficult, when different scaling factors, dynamic material properties, and material substitutions are employed. It is not clear that numerical simulations assist in the elucidation of the mechanisms at work.

There are further difficulties, alluded to earlier, in obtaining quantitatively similar data from the same dynamic centrifuge test carried out on different centrifuges at different institutions, even when the same sample preparation procedure is used for all tests. Small differences in soil density persist, the input motion is very difficult to reproduce, especially if it is intended to represent the motion of an earthquake, and there may be differences caused by the centrifuge radius, direction of excitation (circumferentially or axially), and the vibration

field of the rotating centrifuge arm. The consequences of these variables need to be explored in more detail, and their effects minimized, in order to produce uniform test results to provide a basis for extrapolations to prototype scale and for verification of numerical predictions.

Undoubtedly, because of the attractiveness of the method, the centrifuge method will continue to be used, but a pessimistic view indicates, from past experience, that the fundamental question of the validity of the technique will continue to go unexamined to the depth it deserves.

5. REFERENCES

1. Aboim, C. A., R. F. Scott, and W. Roth, "Centrifuge Earth Dam Studies: Earthquake Tests and Analyses," Report to the U.S. National Science Foundation, Grant CEE-7926691, Dames & Moore, Los Angeles, California, 1983.

2. Arulanandan, K., and R. F. Scott, "Project VELACS-Control Test Results," paper accepted for publication in Journal of Geotechnical Engineering, ASCE, 1993.

3. Arulanandan, K., R. Dobry, A. Elgamal, H. Y. Ko, B. L. Kutter, J. Prevost, A. N. Schofield, R. F. Scott, "Interlaboratory Studies to Evaluate the Repeatability of Dynamic Centrifuge Model Tests," Dynamic Geotechnical Testing II, R. J. Ebelhar, V. P. Drnevich, and B. L. Kutter, Eds., ASTM STP 1213, January 1994.

4. Barth, P. W., F. Pourahmadi, R. Mayer, J. Poydock and K. Petersen, "A Monolithic Silicon Accelerometer with Integral Air Damping and Overrange Protection," Proceedings IEEE "Solid-State Sensor and Actuator" Workshop, 35-38, Hilton Head Island, S.C., June 1988.

5. Corté, J.-F., J. Garnier, L. M. Cottineau, and G. Rault, "Determination of Model Soil Properties in the Centrifuge, Centrifuge 91, Balkema Rotterdam, 607-614, 1991.

6. Fuji, N., "Development of an Electromagnetic Centrifuge Earthquake Simulator," in Ko, H. Y., and F. G. McLean, eds., Centrifuge 91, Balkema, Rotterdam 351-354, 1991.

7. Gill, J. J., and S.T. Kuennen, "Half-Space Modeling of Explosively-Formed Craters," in Centrifuge 91, Balkema, Rotterdam, 465-472, 1991.

8. Gohl, W. B., and W. D. L. Finn, Proceedings of Conference on Prediction and Performances in Geotechnical Engineering, 419-426, 1987.

9. Hushmand, B., R. F. Scott, and C. B. Crouse, "Centrifuge Liquefaction Tests in a Laminar Box," Geotechnique, **48** (2) 253-262, 1988.

10. Kimura, T., "Geotechnical Centrifuge Model Tests at the Tokyo Institute of Technology," Proceedings of International Symposium on Geotechnical Centrifuge Model Testing, 59-79, Tokyo, Japan, 1984.

11. Sathialingam, N. and B. L. Kutter, "Scaling Laws for Rate Dependent Shear and Consolidation of Clay," Dynamic Geotechnical Testing II, R. J. Ebelhar, V. P. Drnevich, and B. L. Kutter, Eds., ASTM STP 1213, January 1994.

12. Schlichting, V., G. Pollak-Diener, E. Obermeier, D. Hammer-Schmidt, F. V. Schatz, and B. J. Hosticka, "Digital Programable Pressure Sensor with On-Clip CMOS Signal Processing and Data Storage," Proceedings of the Seventh International Conference on Solid-State Sensors and Actuators, Transducers '93, Digest of Technical Papers, 988-991, Yokohama, Japan, June 1993.

13. Schmidt, R. M., and K. A. Holsapple, "Theory and Experiments on Centrifuge Cratering," Journal of Geophysical Research, **85** (B1), 235-252, 1980.

14. Scott, R. F., "Centrifuge and Modeling Technology: A Survey," Revue Francaise de Geotechnique, **48**, 15-34, 1989 (in French).

15. Shibata, T., K. Kita, S. Kobayashi, and A. Yashimia, "Performance of Shaking Table Tests and Measurement of Shear Wave Velocities in a Centrifuge," in Centrifuge 91, Balkema, Rotterdam, 391-398, 1991.

16. Stewart, D. P., and M. F. Randolph, "A Newsite Investigation Tool for the Centrifuge," in Centrifuge 91, Balkema, Rotterdam, 531-538, 1991.

17. Stokoe, K. H., and S. Nazarian, "In Situ Shear Wave Velocity from Spectral Analysis of Surface Waves," Proceedings of the Eighth World Conference on Earthquake Engineering, 3, 31-38, 1984.

18. Tan, T.-S., and R. F. Scott, "Centrifuge Scaling Considerations for Fluid Particle Systems," Geotechnique **35** (4) 461-470, 1985.

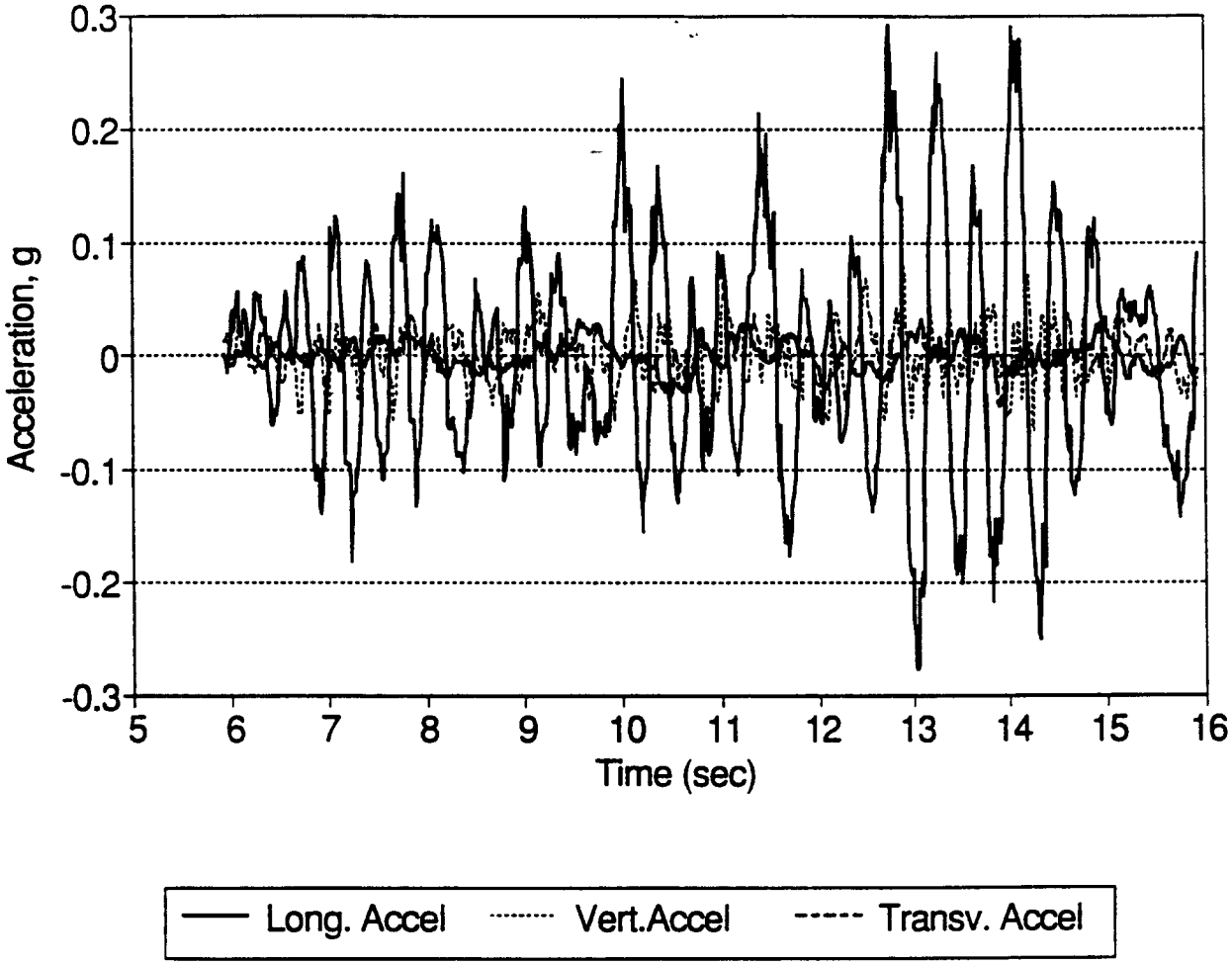

FIG. 1 Accelerations in longitudinal (principal horizontal), vertical and transverse directions on a centrifuge shake table.

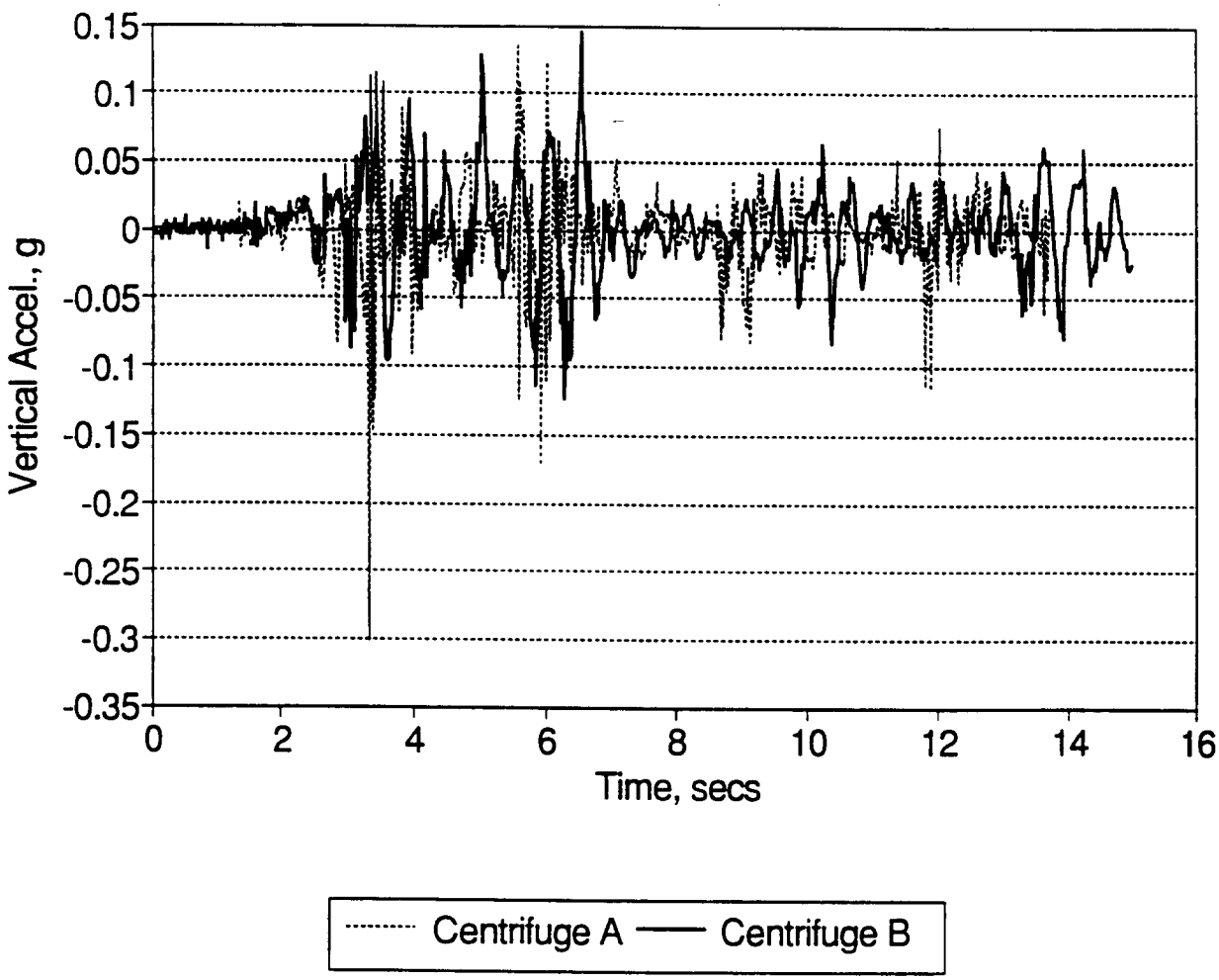

FIG. 2 Vertical acceleration in difference centrifuges for (approximately) same horizontal earthquake motion.

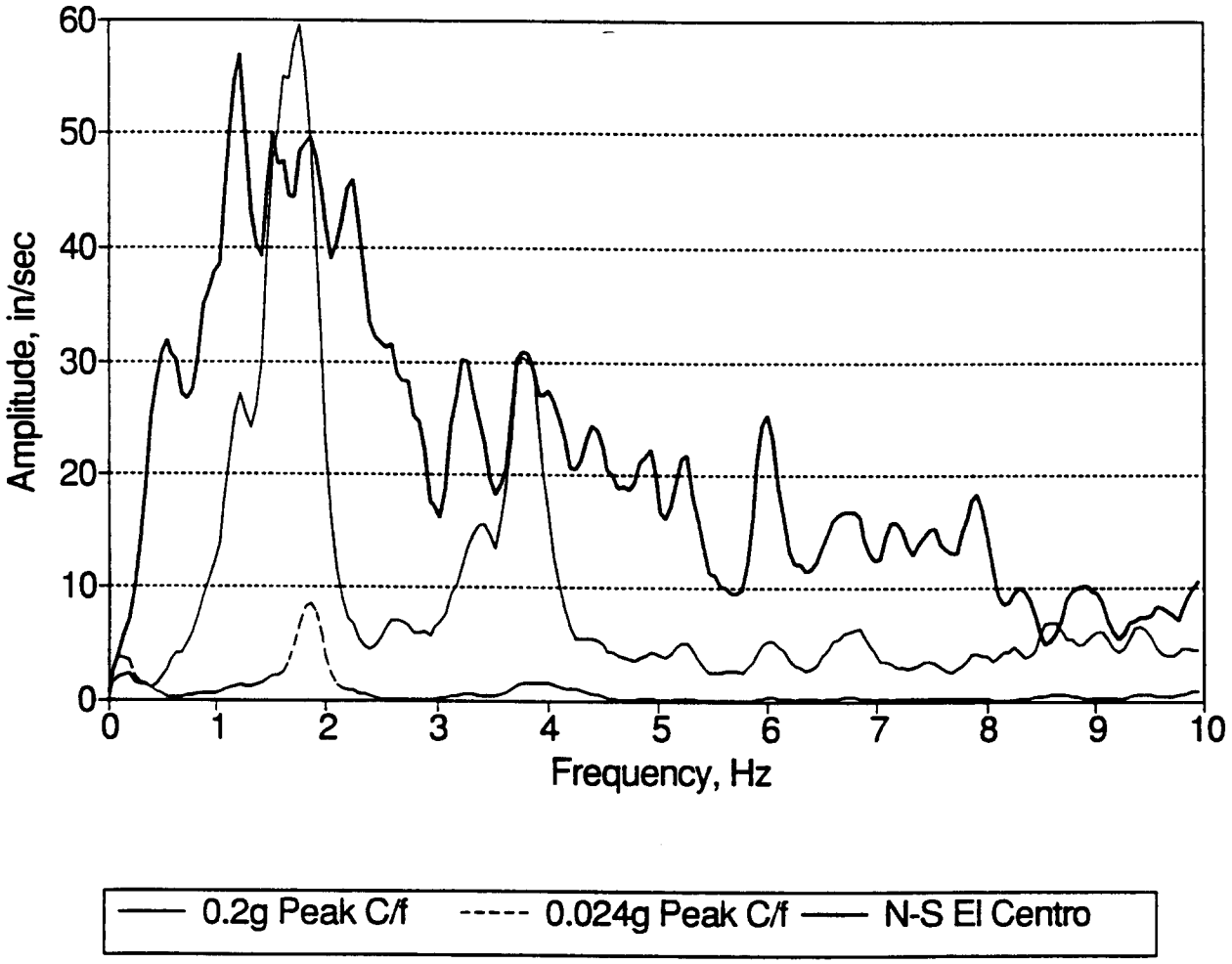

FIG. 3 Fourier Spectra of horizontal input motions on a centrifuge compared to NS El Centro, 1940.

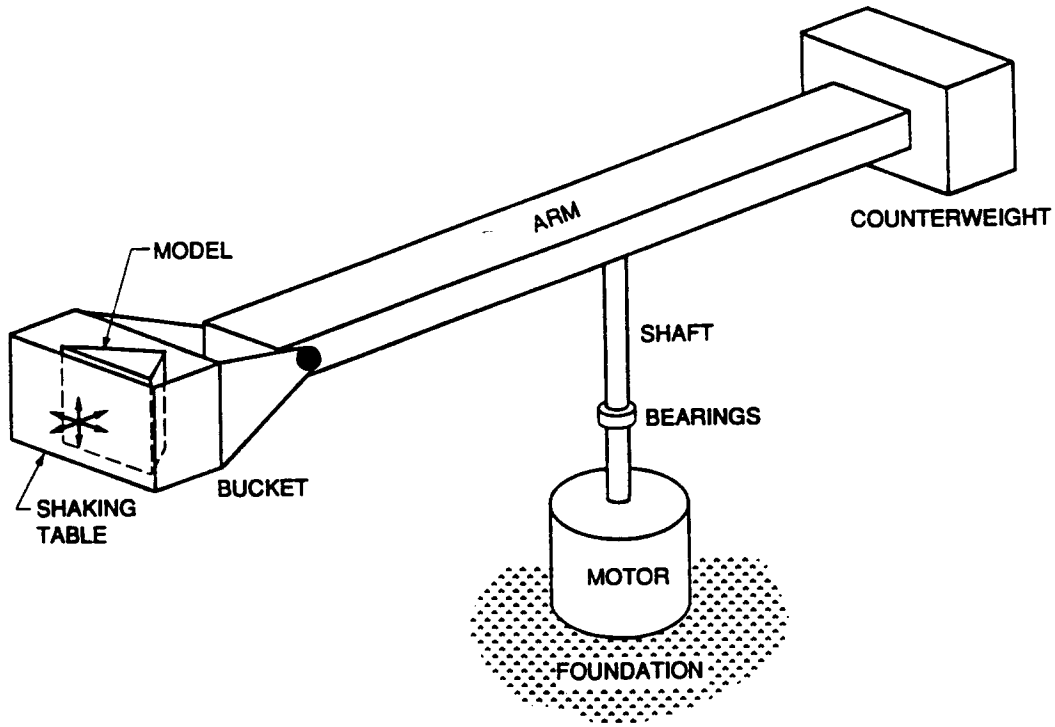

PHYSICAL CONFIGURATION

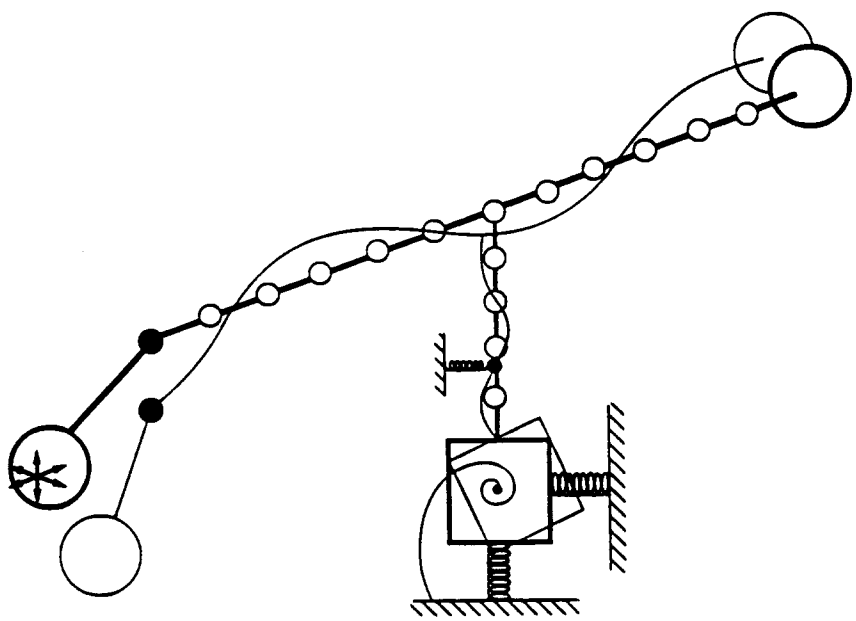

DYNAMIC REPRESENTATION

FIG. 4 Centrifuge and representation for dynamic numerical simulation.

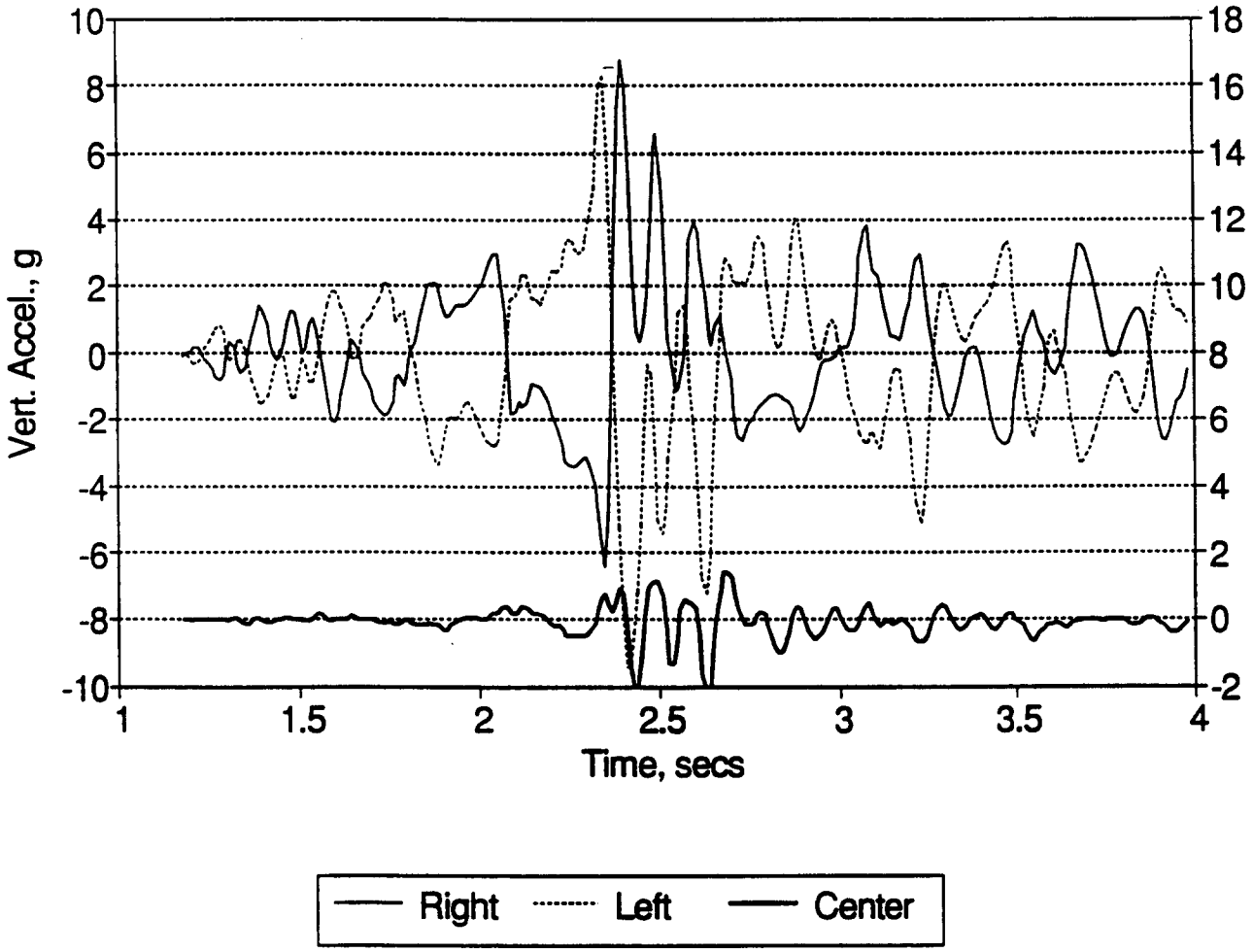

FIG. 5 Pitching motion of centrifuge shaking table, as indicated by out-of-phase vertical accelerations at ends.

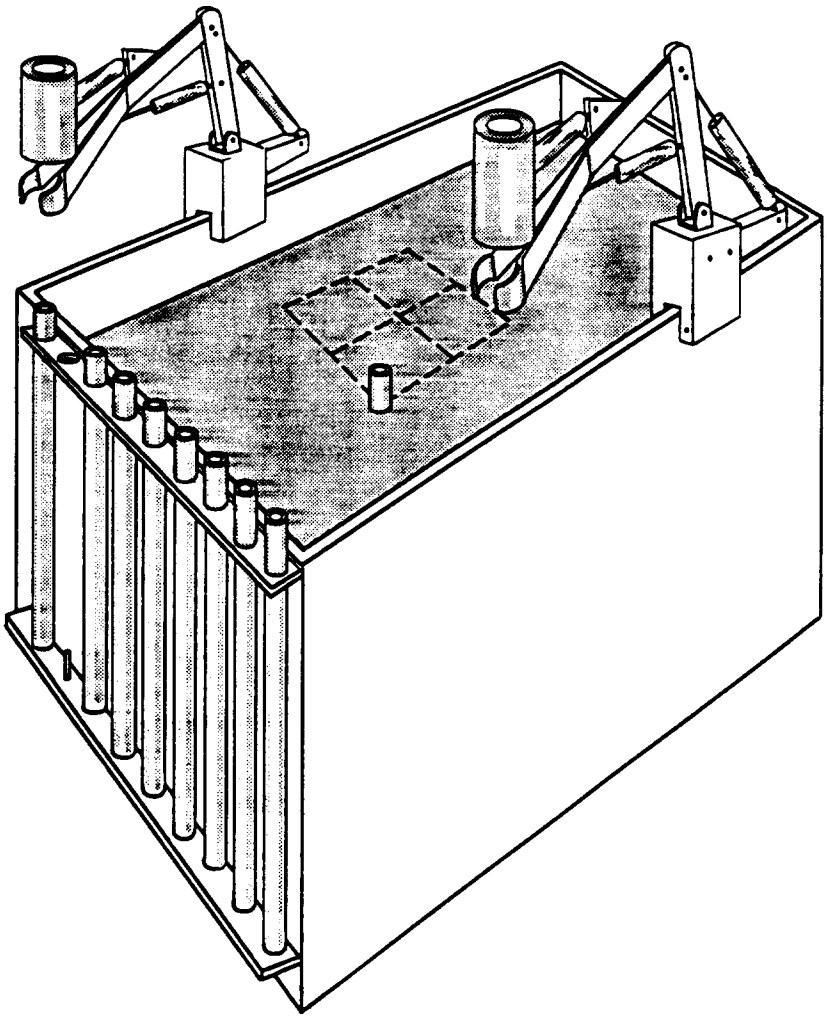

FIG. 6 Possible use of robotic arms to drive piles in flight and assemble with pile cap for centrifuge test.

Shaking Table Failure Tests of Actual Size RC Structures

by

Chikahiro Minowams[1], Keiichi Ohtani[2], Nobuyuki Ogawa[3],
Tadashi Mikoshiba[4], Toshihiro Hayashida[5], Tsuneo Okada[6]

ABSTRACT

We conducted the failure tests for actual size reinforced concrete frame structures (1-story and 3- stories models) by using the large-scale shaking table of the National Research Institute for Earth Science and Disaster Prevention (NIED). 2 specimens of 1- story model were tested for making clear the effects of hoop reinforcement of column. The specimen, which has a dense hoop reinforcement, was shown a ductile behavior, but the other specimen, which has a rough hoop reinforcement, has no ductile behavior. The damping coefficient was increased depend upon the plastic properties. The actual size 3-stories RC moment frame specimen was designed to week beam and strong column properties. The test result was shown the failure mechanism as same as predicted.

Keywords: Reinforced concrete structure, Dynamic failure mechanism, Shaking table test, Effects of hoop reinforcement.

INTRODUCTION

We supposed that the buildings, which were constructed in the recent year, have a good ductile properties and enough aseismic performance, but the buildings, which were constructed until more than ten years ago, did not always have a sufficient aseismicity. The study of the failure mechanism for the old buildings is very important to establish the earthquake countermeasures. And it is to say nothing that the study of the failure procedures of buildings is also important to develop the advanced earthquake resistant design criteria.

The earthquake resistant design criteria was constructed mainly by using the study results of static tests. It was scarce the using of the dynamic test results for the design criteria. We pointed out for this reason that we do not have enough data of shaking table tests and we are difficul to obtain the remarkable fruits. There are few large-scale shaking table, which has a capacity of failure test for the actual size specimen, such as RC frames. The shaking table test has the demerits as follows; (1) the difficulty to obtain the response of specimen, (2) the need of long preparing time and big cost for the 1 minute testing duration. But, the shaking table test has the merit that we can clearly reproduced the actual earthquake response such as a

---

1) Cooperative Research Officer, NIED
2) Director, Disaster Prevention Research Division, NIED
3) Head, Earthquake Engineering Laboratory, NIED
4) Researcher, Earthquake Engineering Laboratory, NIED
5) Head, Vibration Laboratory, Tokyu Co. Ltd.
6) Professor, Institute of Industrial Science, University of Tokyo

dynamic behavior, whcih is more real testing method than that of static test such as pseudo-dynamic testing.

We, National Research Institute for Earth and Science and Disaster Prevention, conducted the failure tests of actual size reinforced concrete frame structures by using the large-scale shaking table of NIED, for the specific joint research program between the government and private sectors under the sponsorship of the Science and Technology Agency. This research program is the 4-year project, which is including the actual size 1-story tests, the actual size 3-stories tests for the reinforced concrete frame. This report describes the test results of the actual size 1-story specimens and the actual size 3-stories specimen.

The research objects for 1-story specimen tests, which those have different hoop intervals, were the realization of mechanism of the column failure during earthquake motion. And, for the 3-stories specimen, we want to conduct a beam failure of the frame by earthquake motion, which was designed a weak-beam and strong-column frame.

ACTUAL SIZE 1-STORY SPECIMENS

1) Specimens

We conducted the test for two specimens. These specimens were constructed 1-story, one bay RC frame with 4 columns. The section and height of columns are 35 cm x 35 cm and 2 m, respectively. The roof slab was made by H shaped steel and steel block for the simulation of dead and live weights. The weight of roof slab is 103 ton, and height of gravity of roof slab is 453 cm from the surface of shaking table. The specimens were arranged to the symmetry for both directions with the center of table. Photo. 1 shows the total view of specimen, which was assembled on the shaking table. The elevation and plan of specimen arrangements are shown in Figs. 1 and 2. The sections of each specimen are shown in Figs. 3 and 4. At the rearrangement of specimen, the part of roof weight was removed. We constructed the steel frames for mitigation of drop shocks at the column failure. The weight of roof was fixed prior day of testing. Until them, the weight was supported by the oil jacks, which was set on the steel frames.

The column of A-type specimen (Fig. 3) was designed the early occurrence of bending yield, which has the shear capacity larger than the bending capacity. The column of B-type specimen (Fig. 4) was designed the early occurrence of shear yield, which has the bending capacity larger than the shear capacity. The main reinforcing bars of each column were same arranged to 8-D22. The reinforcing bars of hoop were used D6 for both specimens. The intervals of hoop were 10 cm for A-type and 40 cm for B-type specimens. The values obtained by the material tests are as follows;

	A-type	B-type
Design Target	Bending failure	Shear failure
Section	35cm x 35cm	ditto
p_w	0.0018	0.0005
N_c	21 kg/cm^2	ditto
${}_cF_c$	358 kg/cm^2	357 kg/cm^2
${}_cF_t$	32.2 kg/cm^2	29.9 kg/cm^2
${}_cE$	249 kg/cm^2	264 kg/cm^2
${}_sF_t$	3730kg/cm^2	ditto
${}_sE$	2.1x10^{6}kg/cm^2	ditto
K_e	30.1 t/cm	31.9 t/cm
P_b	504 t*cm	476 t*cm
D_b	0.117 cm	0.104 cm
P_y	1868 t*cm	1868 t*cm
D_y	2.17 cm	2.11 cm
Q_y	18.7 t	18.7 t

Q_u	20.6 t	17.3 t
Q_y/Q_u	0.91	1.08
Q_B	0.725	0.670

Where p_w : Ratio of shear reinforcement, N_c : Axial stress, ${}_cF_c$: Compressive strength of concrete, ${}_cF_t$: Tensile strength of concrete, ${}_cE$: Young modules of concrete, ${}_sF_t$: Yield strength of steel bar, ${}_sE$: Young modules of steel bar, K_e : Rigidity of elastic range, P_b, D_b : Strength and displacement at bending crack, P_y, D_y : Strength and displacement at bending yield, Q_y : Shearing force at bending yield, Q_u : Ultimate ahear strength, Q_y/Q_u : Ratio between Q_y and Q_u, Q_B : Base shear coefficient.

2) Testing and Measuring Methods

The one dimensional shaking table of NIED was used for this test program. The dimension of shaking table is 14.5 m x 15 m. The maximum velocity and maximum amplitude of table are 75 cm/sec and ± 22 cm, respectively.

In this test program, the shaking table have been dried by the shock wave for measurement of damping properties of specimen (rectangular wave of displacement, period : 20 sec., double amplitude : 0.5 cm) and the strong earthquake motion recorded of E-W component at Hachinohe harbor during 1968 Tokachi-oki earthquake. The shock wave was generated by the synthesizer. The strong motion was generated by the personal computer through the high-pass filter of 0.4 Hz. Fig. 5 shows the time history and velocity response spectra of shaking table response for the A-type specimen.

We used several types of sensor; the strain gauge type accelerometer and the potential type, the inductance type and the laser type displacement sensors. The strains of steel bars were measured by the 2 gauge method. The data from sensors were recorded to the hard disk of the computers by the 1,000 Hz sampling through the 16 bits A/D converter. And we used 8 of Video recorders. The data collection system ad the video recording systems were synchronized by the time controller and wave duplicating system.

3) Test Results

3-1 A-Type Specimen

The specimen was collapsed by the two times excitations of strong motion. The reason of two times excitations was that the specimen was not collapsed by the occurrence of emergency stop of shaking table during the first exception. Therefore, we conducted the second excitation to make a complete collapse of specimen. The maximum displacement, velocity and acceleration of table response at the first excitation were 144 mm, 73 cm/sec and 800 GAL, respectively. The response wave forms of relative displacement and acceleration of roof slab, and the hysteresis loop between acceleration and relative displacement of roof slab are shown in Fig. 6. We conducted the shock motion excitations to make clear the change of rigidity and damping characteristics between before and after the strong motion excitation. The response of free vibrations, which was measured by the shock motion, are shown in Fig. 7. The predominant frequencies and damping coefficients, determined by the AR model analysis for this free vibrations, are follows;

Before the test

4.2 Hz, 1.6%, $c=4\pi$ m x 0.0672

After the test

3.2 Hz, 2.9% $c=4\pi$ m x 0.0928

The two columns faced north side within total 4 columns were collapsed by the second strong motion excitation. The two columns faced south side were not collapsed, but severely cracked. The maximum displace-

ment, velocity and acceleration of table response at the second exception were 165 mm, 68 cm/sec and 730 GAL, respectively. The response wave forms of relative displacement and acceleration of roof slab, and hysteresis loop between acceleration and relative displacement of roof slab are shown in Fig. 8. The predominant frequency was changed from 4.2 Hz to 3.2 Hz during the first exception and to 2 Hz at just before the collapse by the second excitation. The hysteresis loop in Figs. 6 and 8 are recorded at C4 column located in north side. Photos. 2 to 5 show the column collapse procedures of the north side during second excitation. From these photographs, the shear crack was occurred at the top of C3 column, the cracks were progressed after that, and the shear crack was occurred at the bottom of C4 column, which is the main cause of collapse by this excitation. The reason, why the south side columns didn't collapsed, is estimated to the effect of slips of specimen from shaking table. We installed the displacement sensors between the foundation of column and table surface for the purpose of watching the occurrence of slip between them. These records are shown in Fig. 9. We can find the occurrence of slip at the south side columns during both strong motion excitations. The north side columns were occurred little amount of slip during the first excitation, but the bottom of C3 column, which was happened the first shear crack, didn't slipped during the second excitation, we supposed.

3-2 B-Type Specimen

This specimen was failed at once by the strong motion excitation. The maximum displacement, velocity and acceleration of table response were 109 mm, 56 cm/sec and 630 GAL, respectively.

The vibration characteristics of specimen at the initial state are as follows;

4.4 Hz, 1.7% $c=4\pi$ m x 0.0794

The wave forms of relative displacement and acceleration of roof slab, and the hysteresis loop between them are shown in Fig. 10. The running gain spectrum between roof and table was shown in Fig. 11. From this spectrum, we can find the predominant frequency was changed from 4.5 Hz at the initial state to 2.5 Hz at just before the collapse. The hysteresis loop (Fig. 10) is drawn the features of the C4 column at the north side. Photos. 6 to 9 show the procedures of column collapse. From these photographs, the shear cracks at the top of C3 and C4 columns in the north side and the bottom of C1 column in the south side were occurred at the nearly simultaneous timing (within 0.01 second time differences), the bottom of C2 column in the south side was cracked at 1.5 second after the former crack occurring, these cracks were propagated to the upward direction of column, and then the specimen was totally collapsed. The slip between the foundation of column and the table surface didn't occurred by the effects of installation of L-shaped steels between the foundation of column and the steel frames for the mitigation of drop shocks.

4) Consideration for Hysteresis Loop Properties

4-1 A-Type Specimen

The third gradient for both excitations were estimated to the negative slopes as the peak oriented rule for reinforced concrete structures. The maximum strength of this specimen was estimated to 103 ton x 0.9 G = 92.7 ton. The residual displacements were observed at every columns for west direction after the first excitation. The amount of residual displacements of each column were as follows;

Column	D_R	Column	D_R
C1	7.4 mm	C2	7.6 mm

C3 13.1 mm C4 5.4 mm

The second elastic limit displacements were estimated to 1.5 - 2 cm for the first excitation and 2 - 3 cm for the second excitation. These phenomena were corrsponded to the rcord of video tapes sech as the opning of cracks.

4-2 B-Type Specimen

The hysteresis loop between the load and displacement can not estimated, because the specimen was destroyed before the drawing of loop. The maximum strength of this specimen was estimated to 103 ton x 0.8 G = 82.4 ton. From the correspondence of video tape records, the specimen was collapsed by the occurrence of cracks just after the arrival to maximum strength. The second elastic limit was estimated to 1.8 - 2 cm.

4-3 Comparison of Specimens

The both A-type and B-type specimens were recorded to the two different values of the second elastic limit. The both specimens had the third elastic limit and the negative slope after this limit. If they had the third elastic limit, the displacement between the second and third elastic limits was estimated to about 5 mm.

ACTUAL SIZE 3-STORIES SPECIMEN

1) Specimen

This specimen had a plan of 6 m x 6 m with 3 stories and one bay. The section of each column was 45 cm x 45 cm (8-D22, □-D10-@100) for each story. The height of each story was 3 m. The sections of girder were 50 cm x 30 cm (2-D22+1-D19, 2-D16, □-D10-@200) for the second and third floors and 40 cm x 25 cm (2-D22, 2-D16, □-D10-@200) for the roof. The thickness of slabs was 15 cm for each floor. The concrete foundations were 2.6 m x 2.6 m x 0.9 m. The total height of specimen was 10.2 m. This specimen was designed to have a property of weak- beam and strong-column. The beams were assembled to the transverse direction of excitation for each slab, which size was same as girder of each floor (2-D19, 2-D16, □-D10-@200). The reinforcement arrangements of slab were D10-@300 for the excitation direction and D10-@200 for the transverse direction. The 18 of one ton steel block were arranged on the slab for the simulation of live load. Therefore, the total weight of each floor was 30 ton. For the test safety, we were constructed the steel frame. Fig. 12 shows the schematic view of the specimen.

2)Testing Method

The shaking table was driven by the strong motion as same as 1-story test. The strong motion was generated by the personal computer through the 0.4 Hz high pass filter from FFT method. Fig. 13 shows the pre-analytical results of the displacement response for each floor during the strong motion. We conducted this test on March 14 of this year. And now, we are processing the test data and analyzing the test results.

CONCLUSION

During the first excitation for the 1-story A-type specimen (hoop interval : □ -D6-@100), the emergency stop, just after the first peak response, was occurred depend on the safety-control logic system of shaking table. At the second excitation for this specimen, the shear crack was generated at the C3 column after the second peak response, and the specimen was failed by the opening of cracks after the third peak response with 6 cm displacement. The B-type specimen (hoop interval : □-D6-@400) was collapsed just after the occurrence of crack at the first peak with 2 cm displacement. From these facts, we can confirm that the dense reinforcing against

shear force is very effective to maintain the earthquake resistant capacity of building.

We conducted the test for the actual size 3-stories specimen at 2 month ago. The dynamic and failure behaviors of specimen were shown almost same as the pre-analyzed results. We hope that we will present a more detailed report at the next joint meeting.

ACKNOWLEDGMENTS

These test projects were conducted by the specific research program between the government and private sectors under the sponsorship of Science and Technology Agency. For the success of this project, we established the technical coordinating committee (chairman : Prof. Tsuneo Okada), which the committee members are consisted from NIED, University of Tokyo, Tokyu Co., Obayashi Co. and Aoki Co.. The authors acknowledge the assistance of the members of the committee.

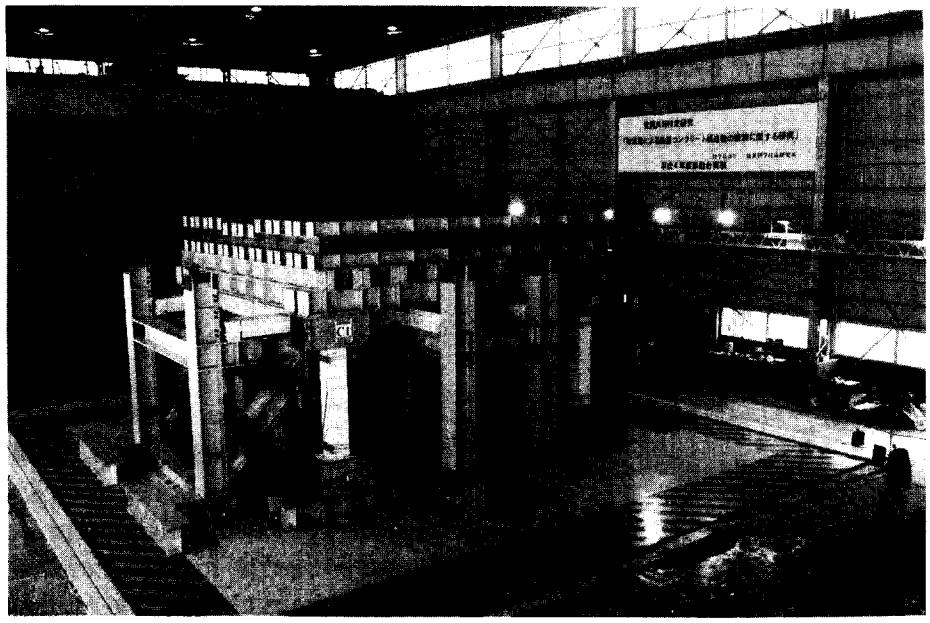

Photo. 1. Actual Size 1-stoty Reinfoced Concrete Specimen

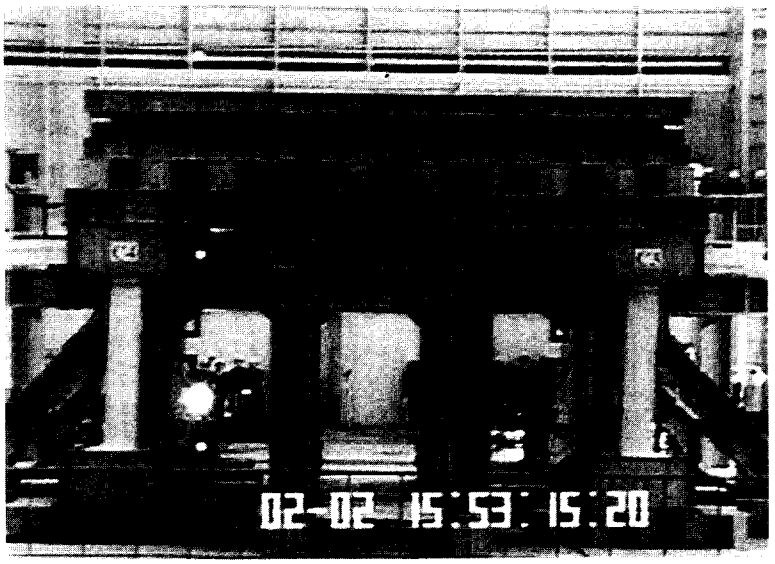

Phpto. 2. Initial Crack at the Top of C3 column (A-TYpe, North Side)

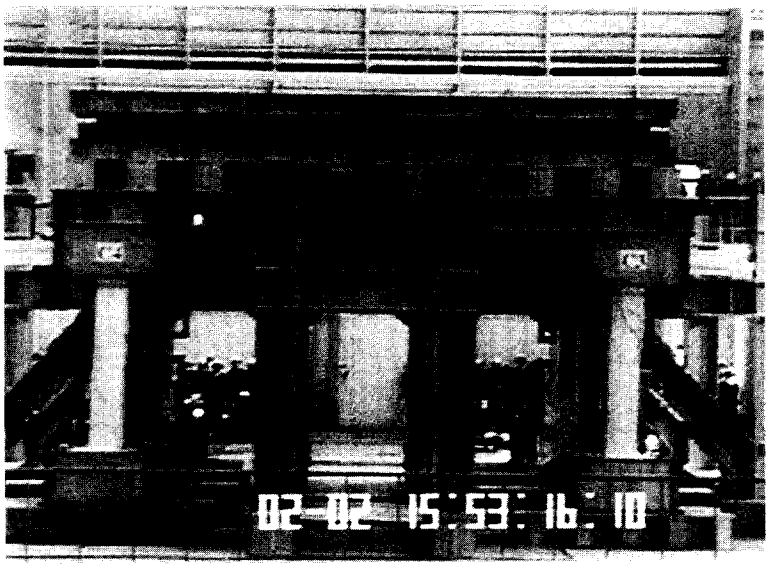

Photo. 3. Crack at the Bottom of C4 Column (A-Type, North Side)

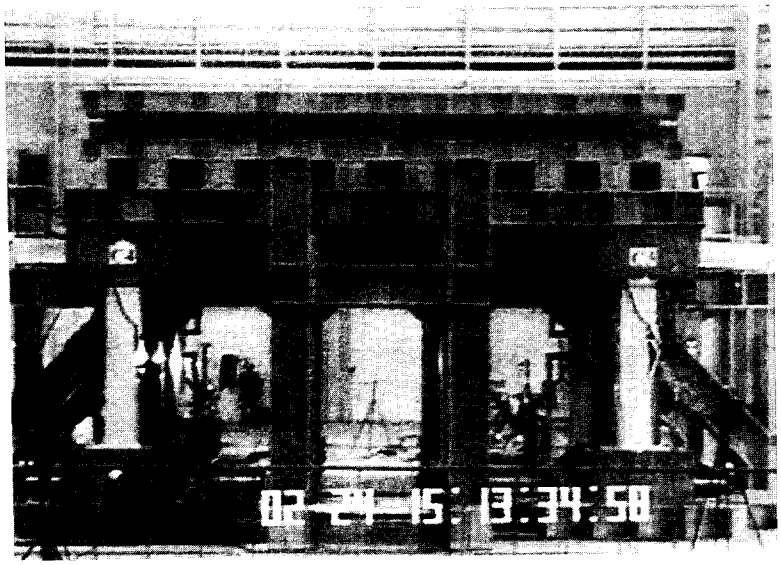

Photo. 6. Shear Cracks at C3 nad C4 Columns (B-Type, North Side)

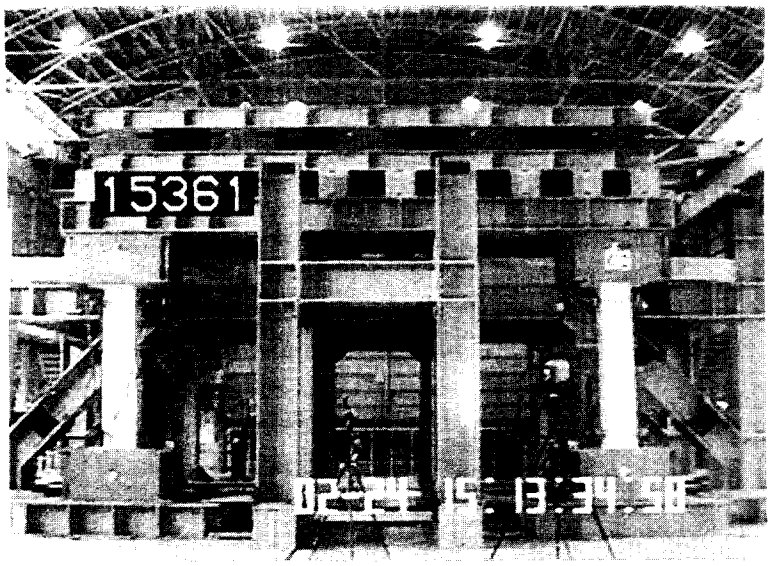

Photo. 7. Cracks at the Bottom of C1 Column (B-Type, South Side)

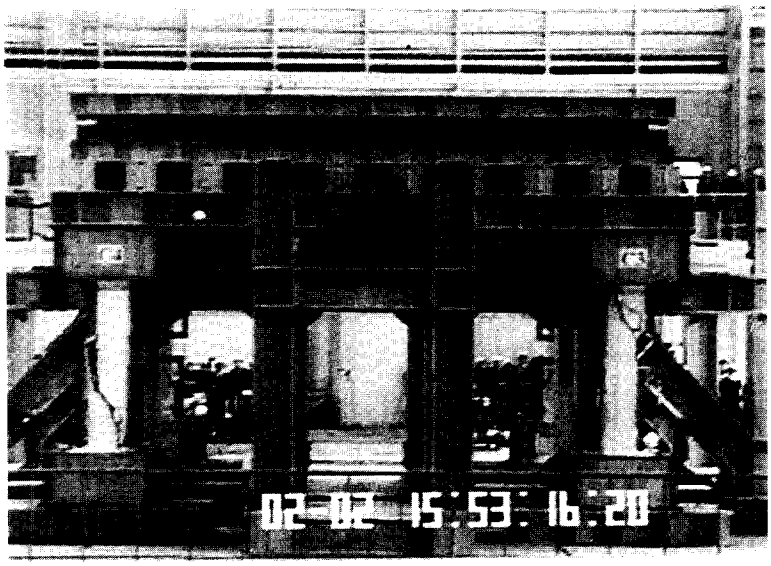

Photo. 4. Crack Opning at C3 and C4 Columns (A-Type, North Side)

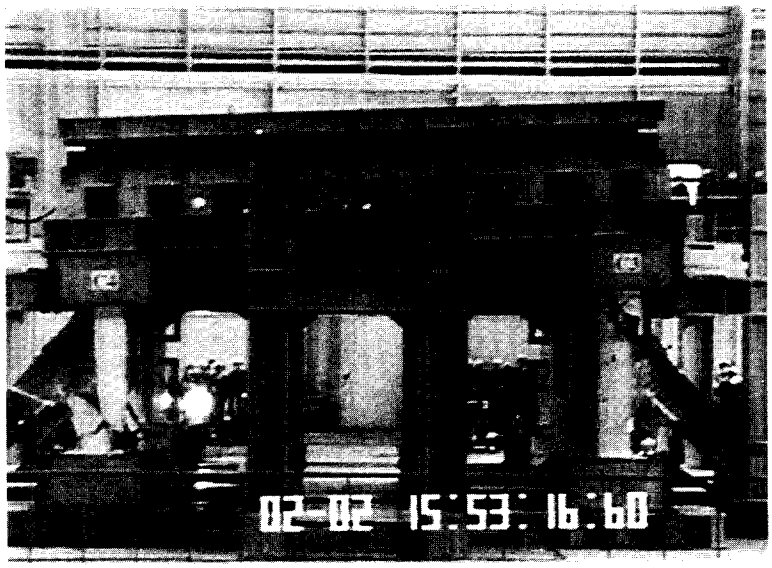

Photo. 5. Damage Process of North Side (A-Type)

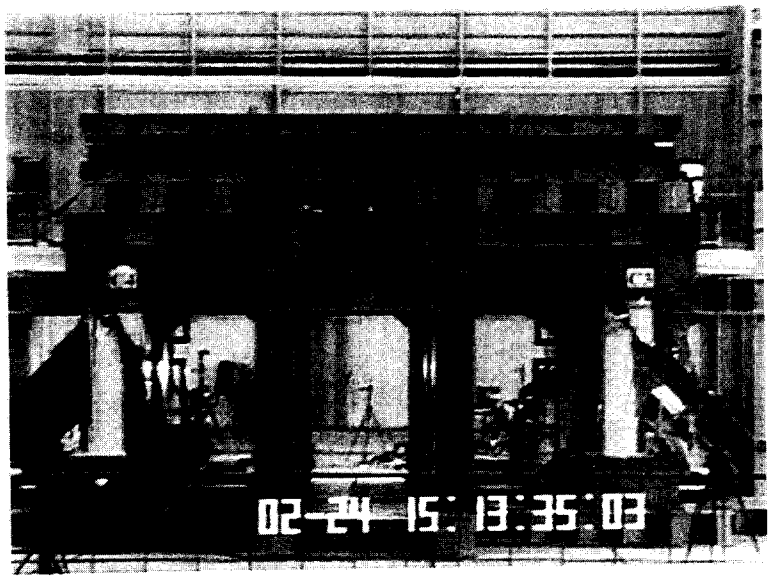

Photo. 8. Separation of the Top of C3 and C4 Columns (B-Type, North Side)

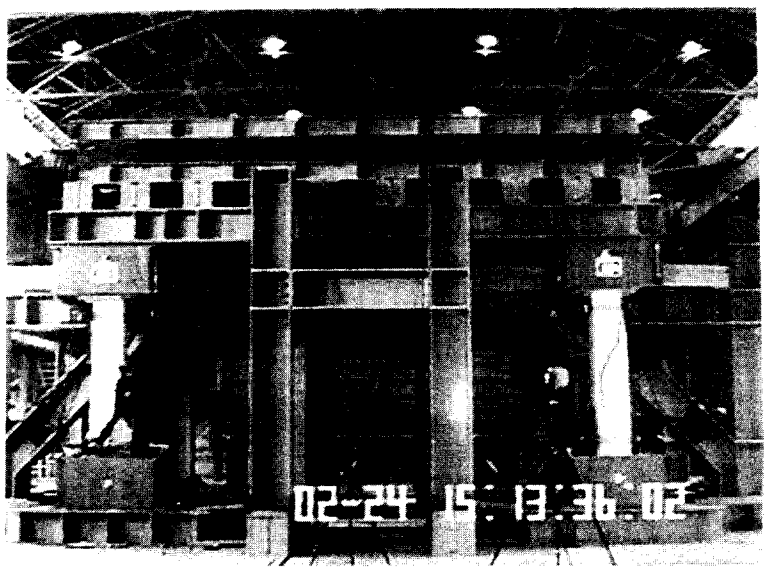

Photo. 9. Damage Process at Soutn Side (B-Type)

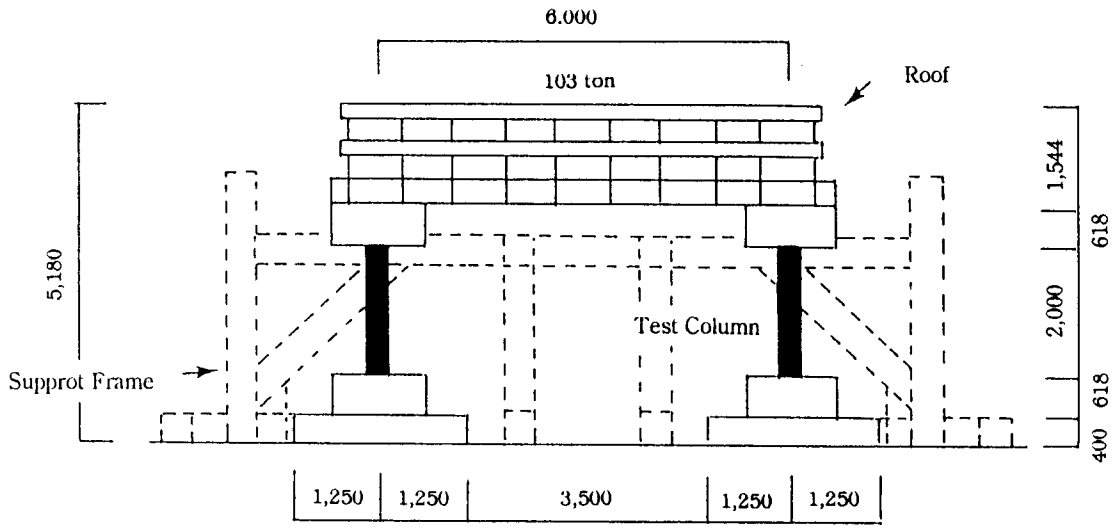

Fig. 1. Setup Elevation of 1-Story Test Specimen

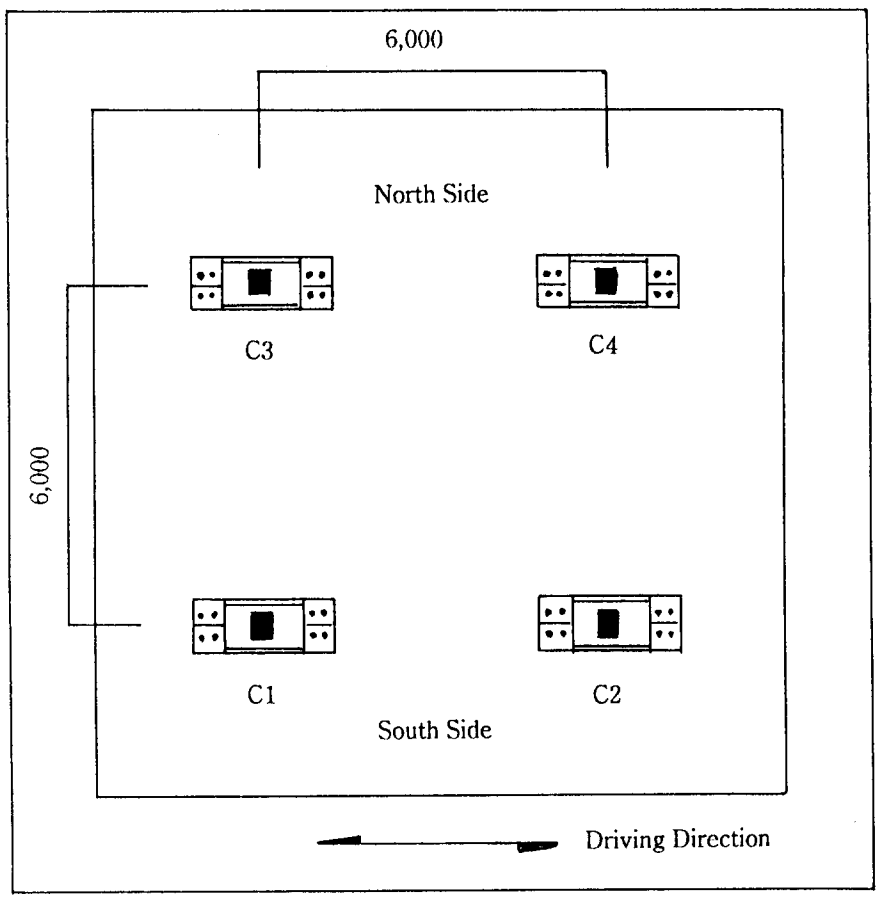

Fig. 2. Plan of 1-Story Test Specimen on Shaking Table

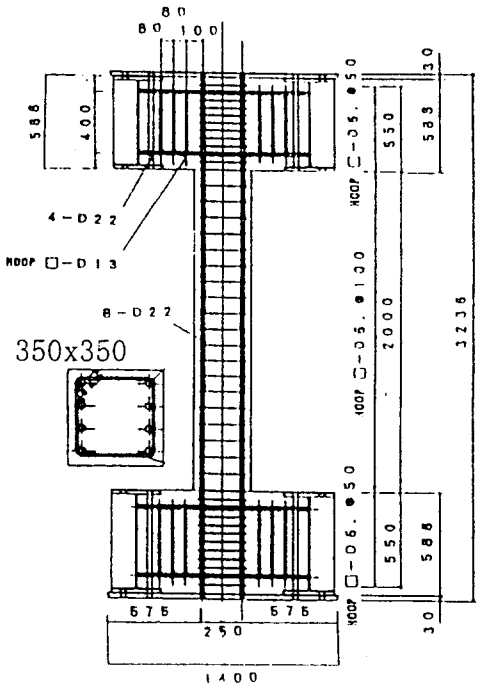

Fig. 3 Column of A-Type Specimen
(Hoop : □-D6-@100)

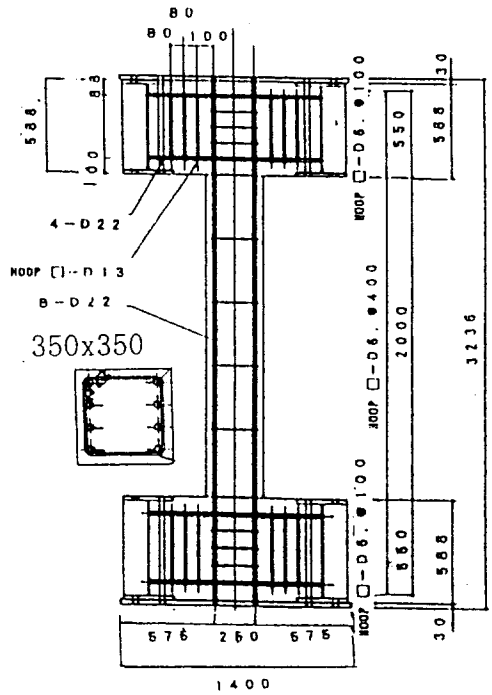

Fig.4. Column of B-Type Specimen
(Hoop : □-D6-@400)

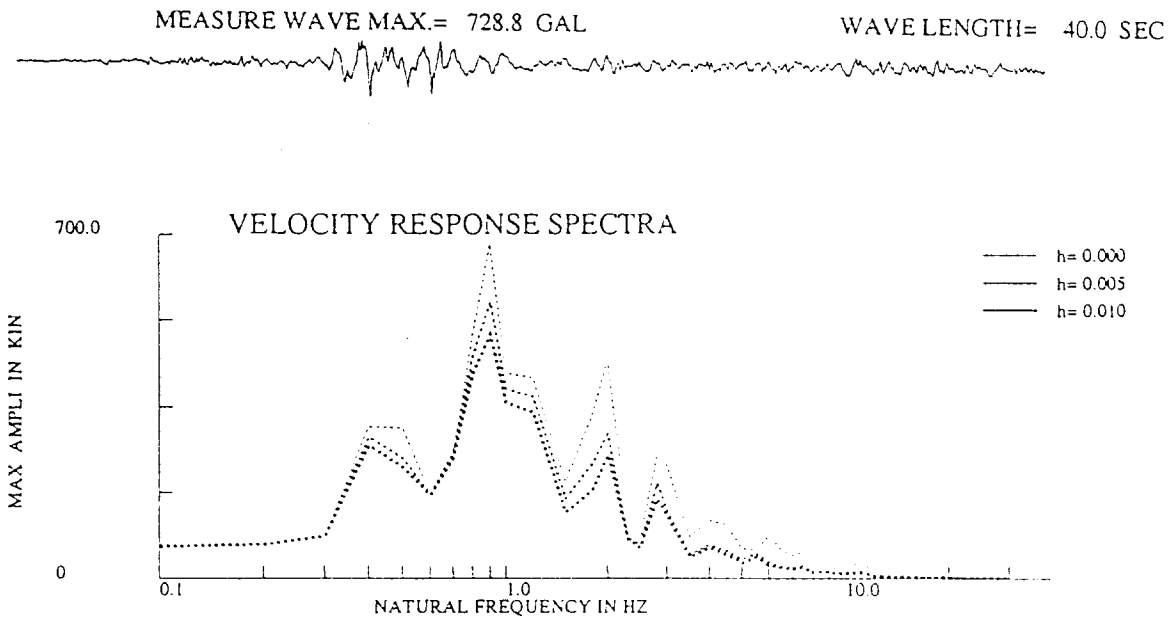

Fig. 5. Velocity Response Spectra of Table Response
(A-Type, Second Excitation)

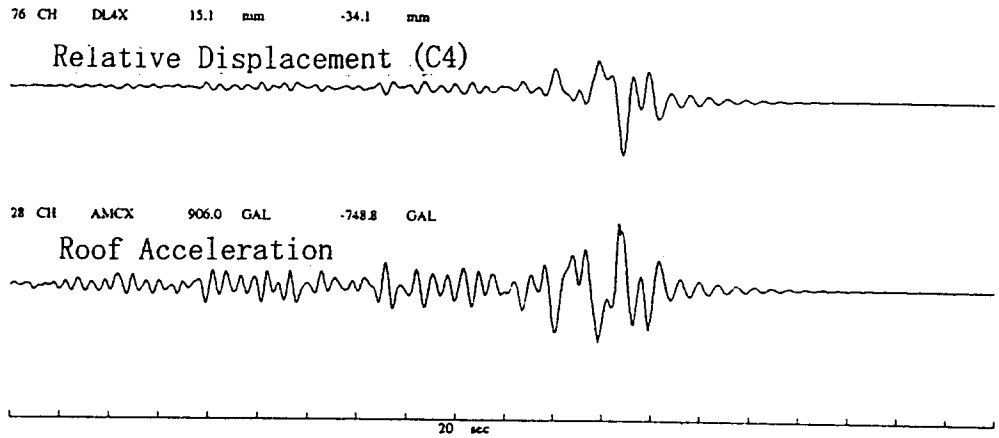

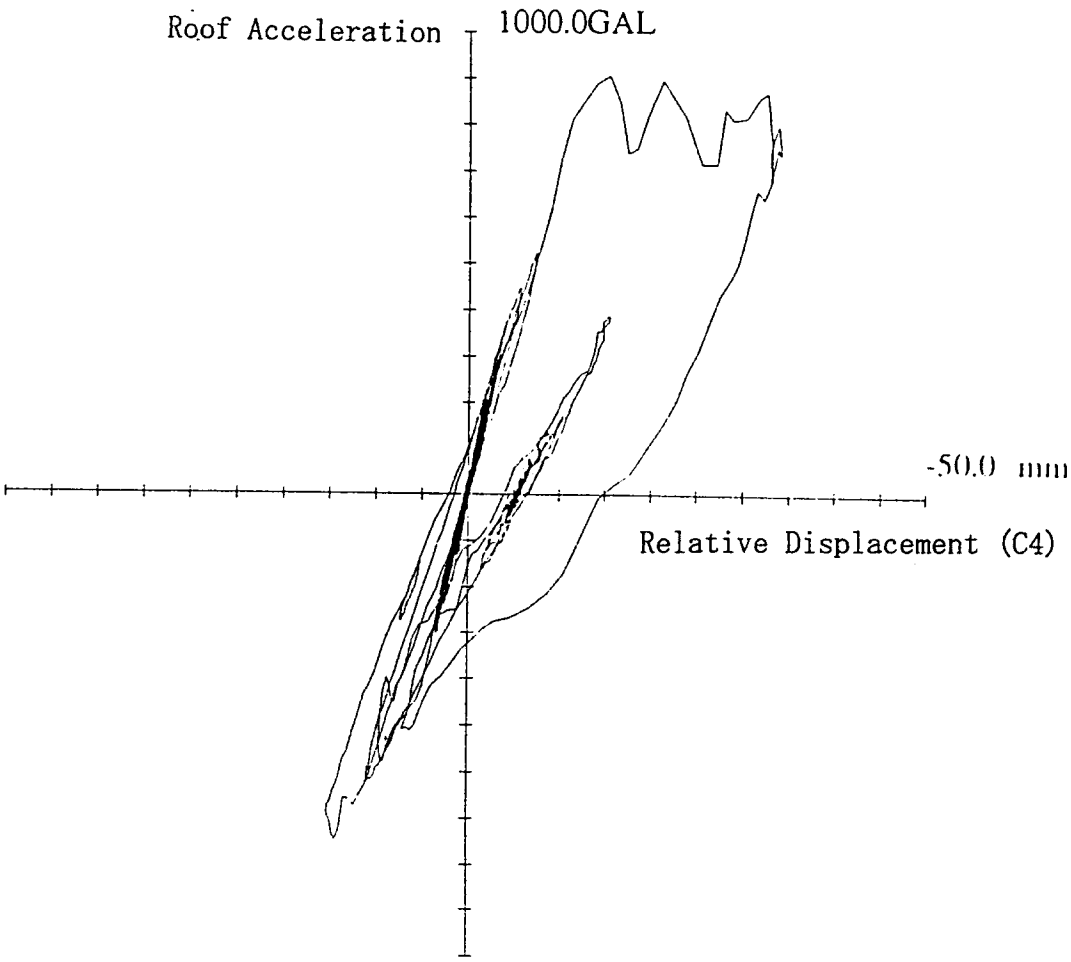

Fig. 6. Hysteresis Loop of A-Type C4 Column at the First Excitation

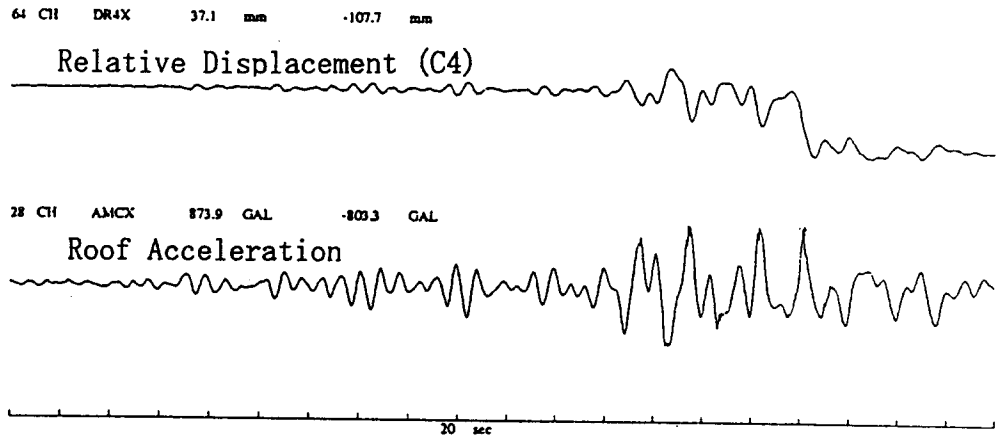

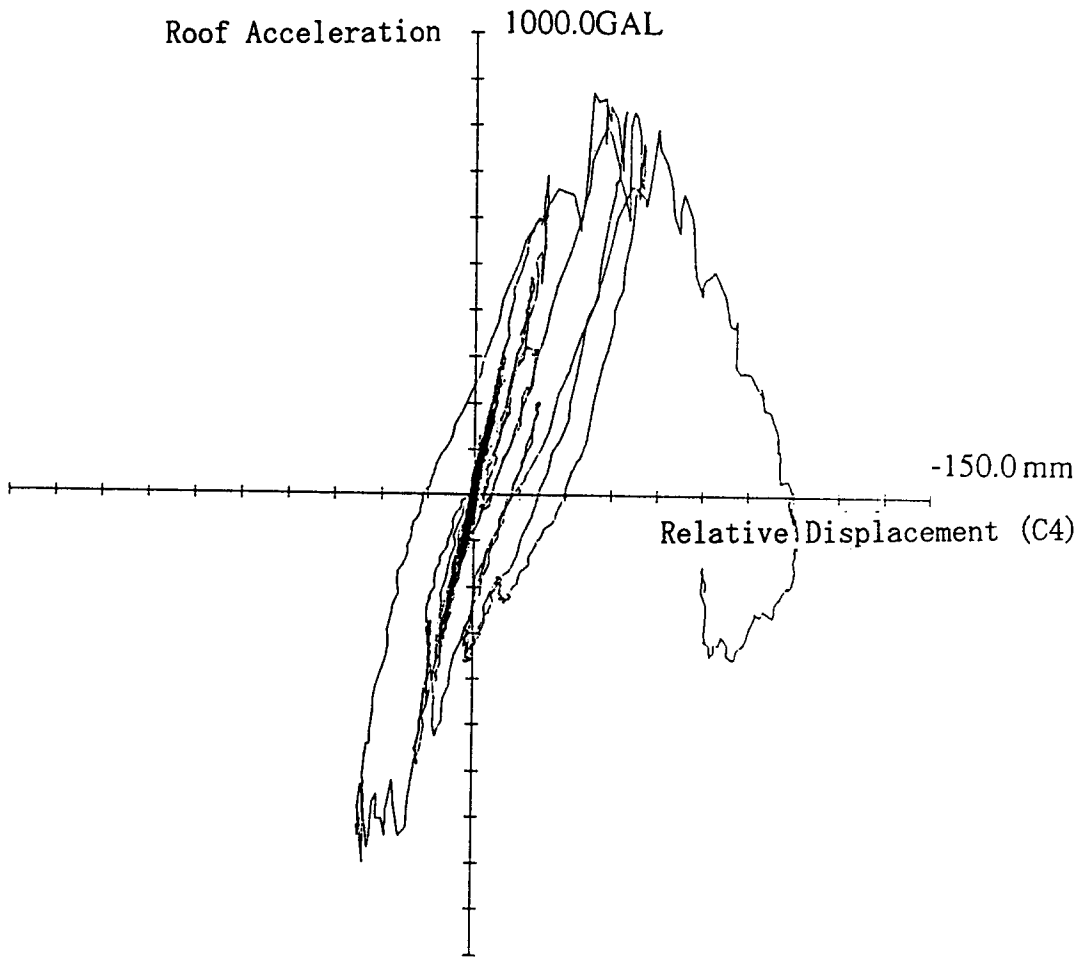

Fig. 8. Hysteresis Loop of B-Type C4 Column at the Second Excitation

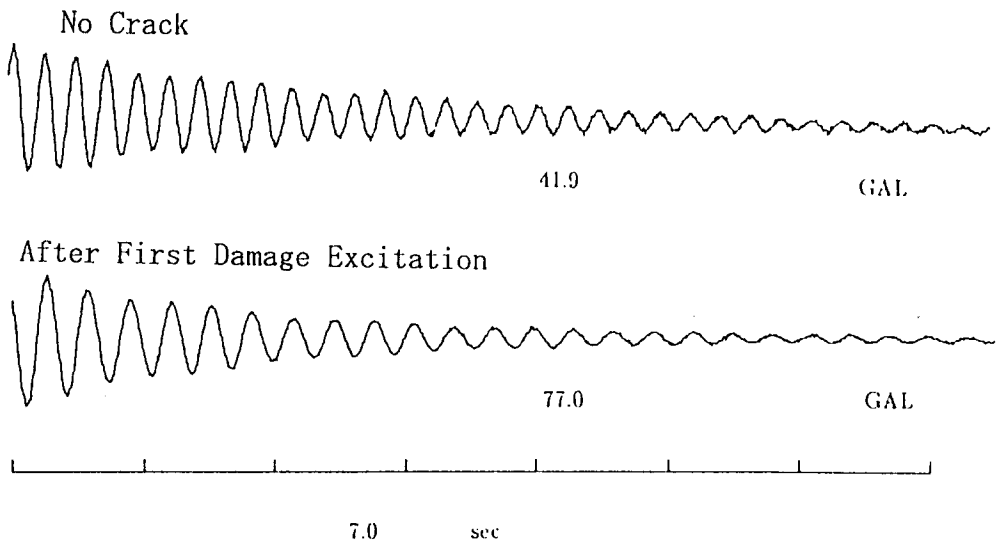

Fig. 7. Free Vibrations of A-Type Specimen

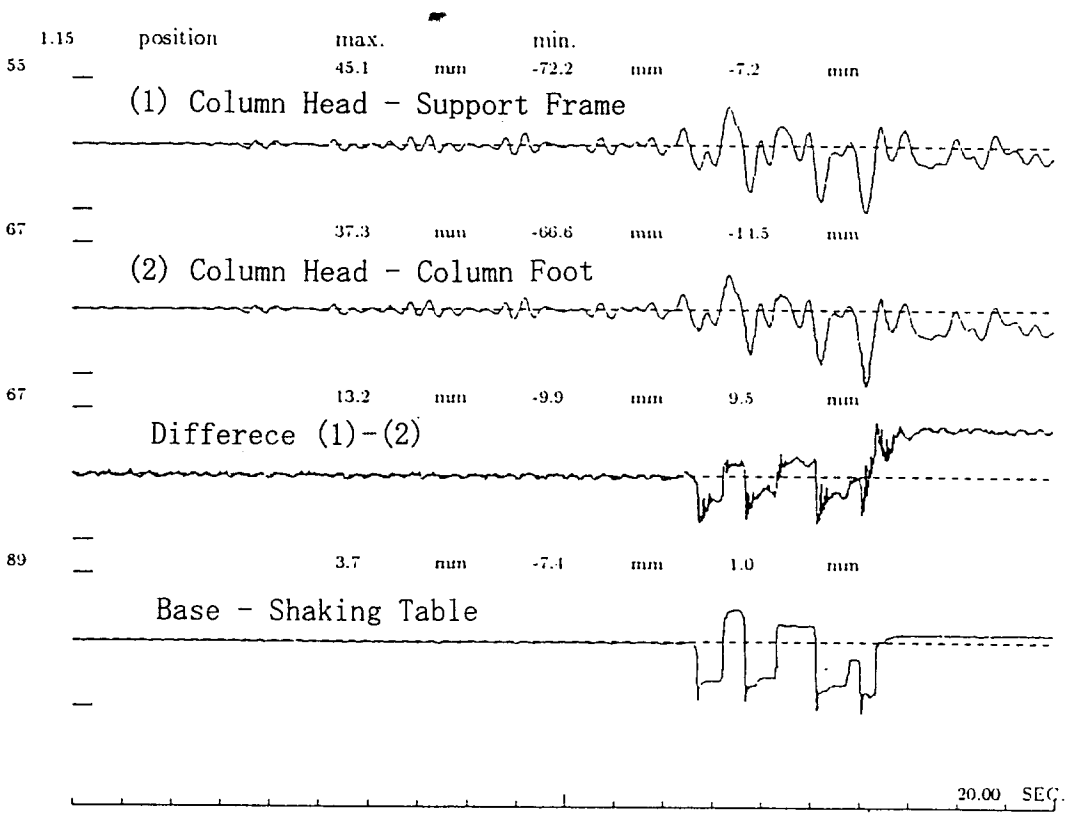

Fig. 9. Slip of Column Base (C1) of A-Type Specimen at Second Excitation

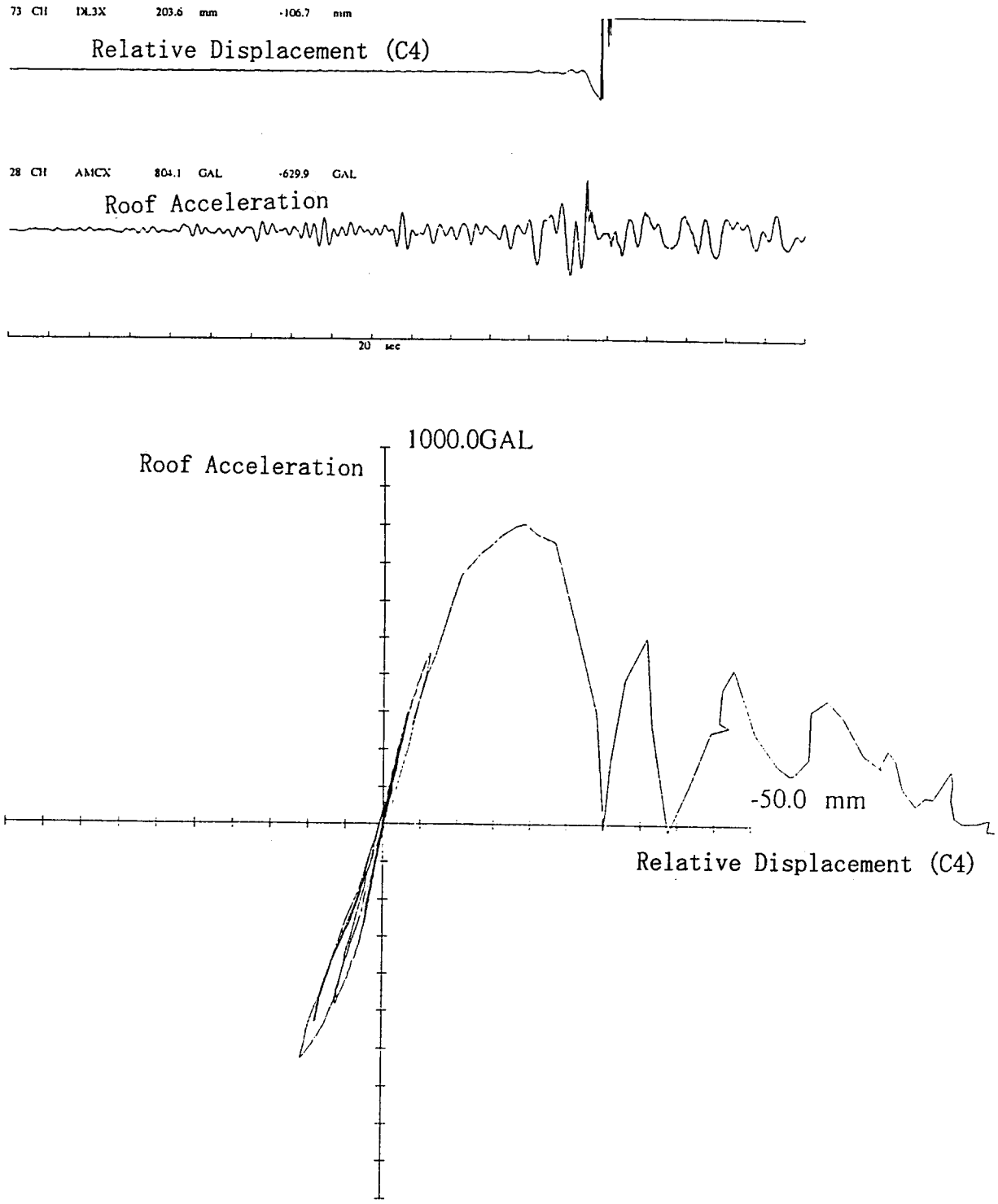

Fig. 10. Hysteresis Loop of B-Type C4 Column

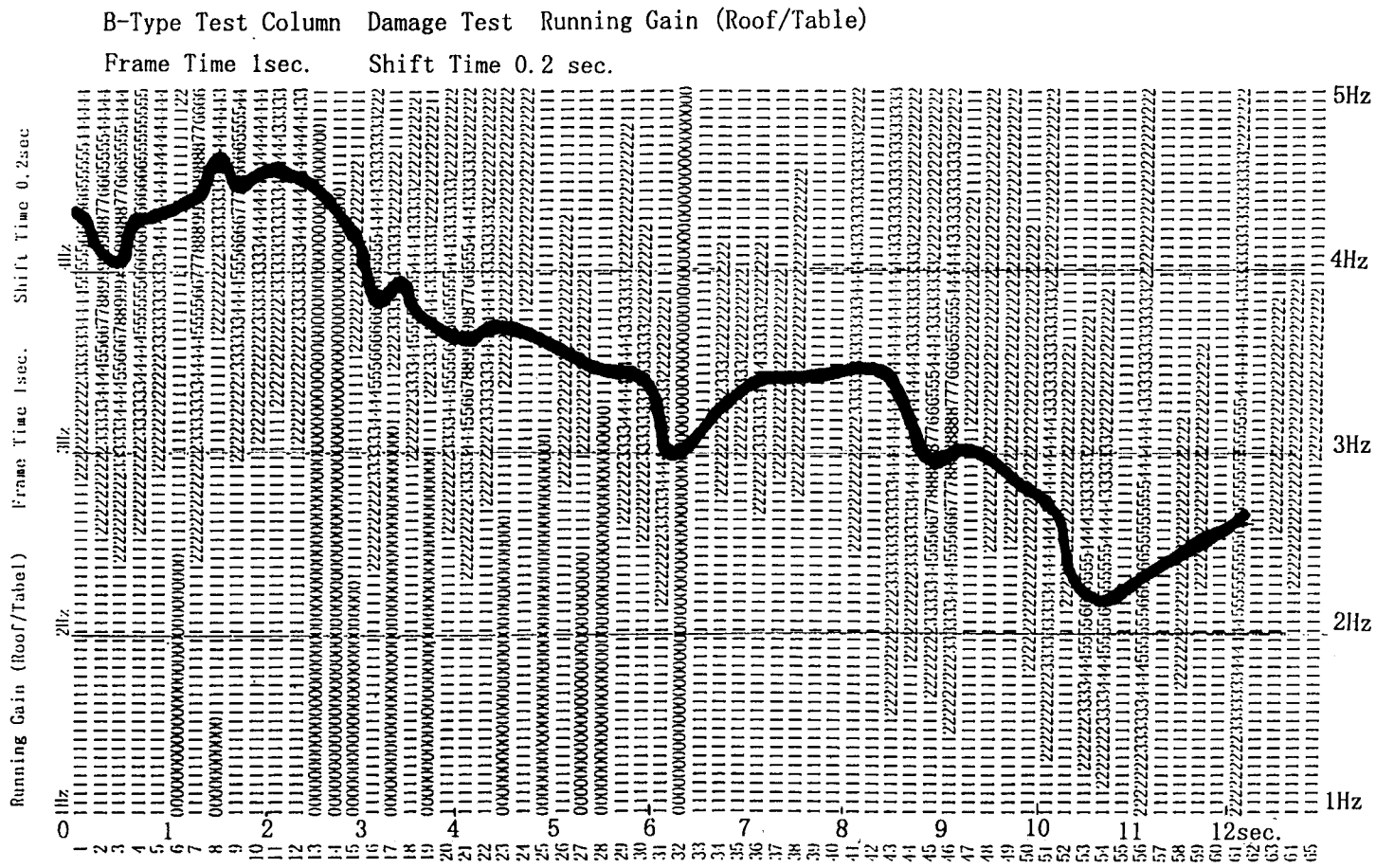

Fig. 11. Running Spectrum of Strong Motion Excitation for B-Type Specimen

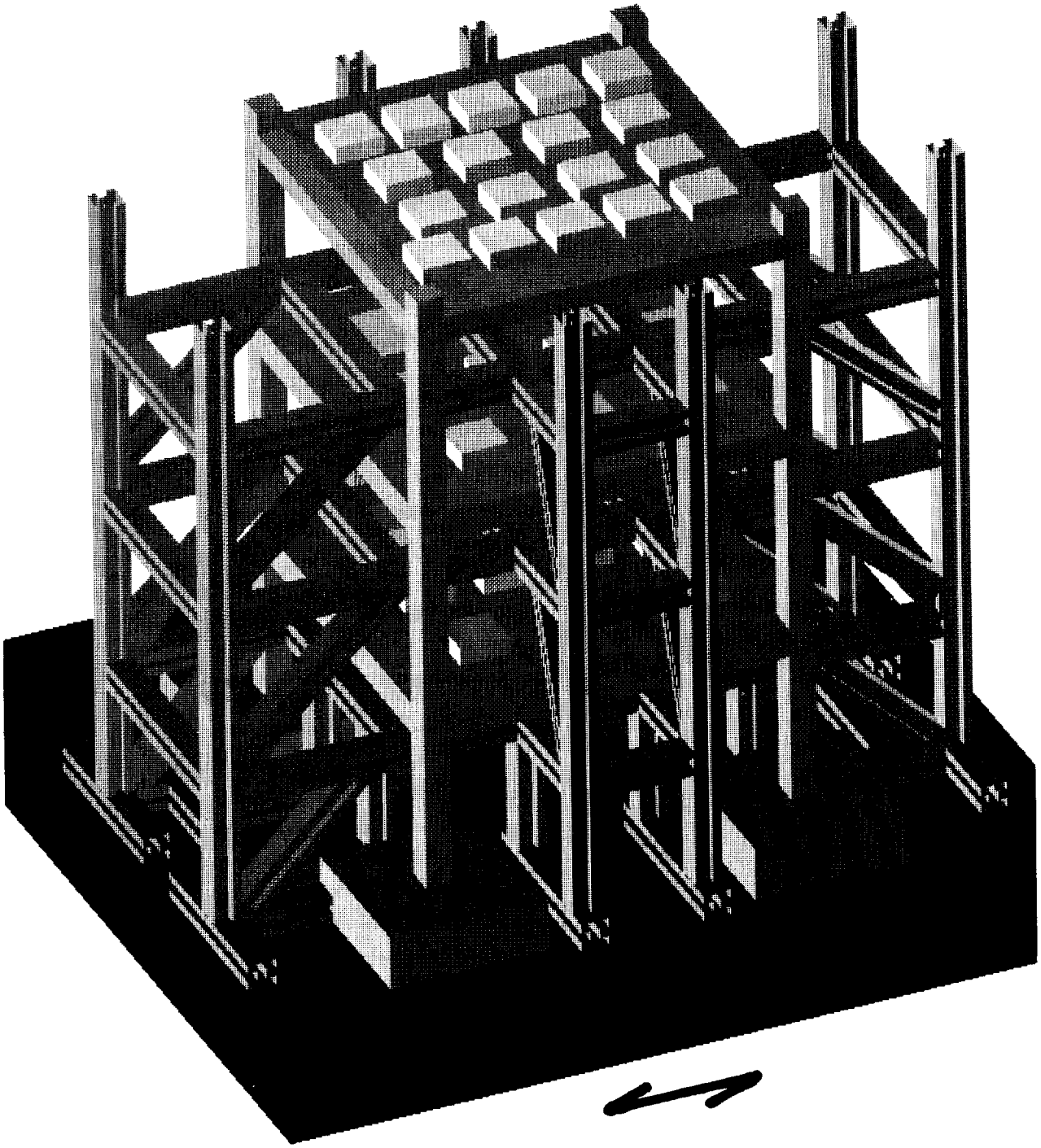

Fig. 12. Schematic View of 3-Stories Test Specimen

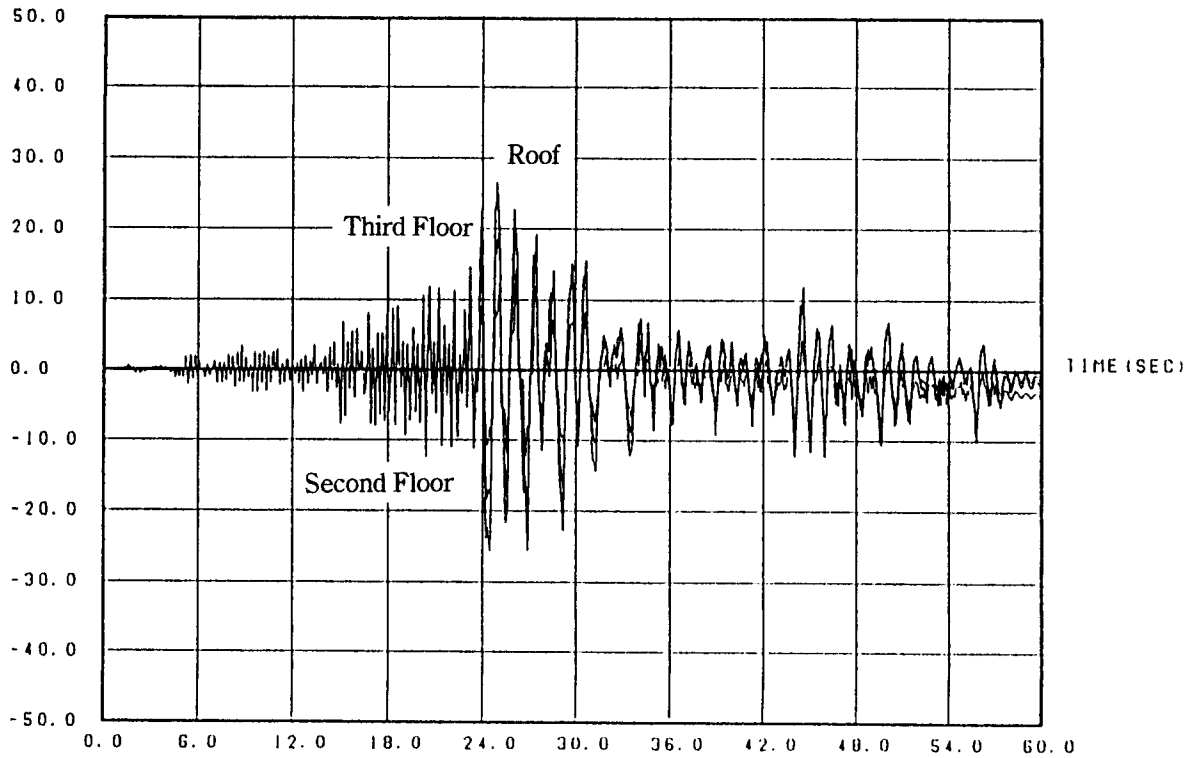

Fig. 13. Predicted Time Histories of Displacement response for 3-Stories Specimen

Response of a Mid-Water Depth Platform Subject to Earthquakes

by

Charles E. Smith*

ABSTRACT

Seismic analyses of offshore platforms may be accomplished using classical finite element techniques with the input forcing function modeled for earthquake loadings. The significant difference between an offshore structure and an onshore structure is that the analysis procedure must be modified to consider the fluid-structure and the soil-pile interaction effects. Current practices use earthquake forcing functions obtained from ground accelerations measured in the vertical and horizontal directions recorded from onshore sites. However, recent research has suggested that the seafloor may not respond in the same manner as onshore sites during an earthquake. This paper will compare the response of a typical mid-water depth offshore platform subject to both onshore and offshore recorded ground motions from the same earthquake. Recommendations are put forth for the type of seismic forcing function to be in the design or requalification of offshore structures, as well as relevant research for the future.

KEYWORDS: Earthquake ground motions, offshore platforms, offshore research, platform seismic response, seismic design criteria.

1. INTRODUCTION

Offshore platforms have several key structural and environmental differences as compared to typical onshore buildings[1]. The differences can be grouped into the following areas: (1) geology and response of subsea soils (soft-saturated soils and lack of offshore seismic data), (2) a water column that provides a source of loading and dampening to the structure (fluid-structure interactions), (3) special structural characteristics (deep pile foundation, large mass, large number of redundant members, larger overturning moments, and the fact that the mass is concentrated at the top of the platform as opposed to being distributed over its height as in most building structures), and (4) the unusual engineering properties of offshore soil deposits (often normally consolidated and extremely soft and compressible near the seafloor). Thus, the dynamic behavior of an offshore structure during an earthquake may be significantly different from its onshore counterpart.

The current (1994) methodology for the design and/or reassessment of offshore structures makes use of data obtained from onshore seismic events. However, based on the vital differences between onshore and offshore structures cited above, a joint program was started in 1976 between the Department of Energy and the Conservation Division of the U.S. Geological Survey (now the Minerals Management Service) to develop advanced instrumentation systems to assist government and the petroleum industry in characterizing environmental and engineering conditions offshore. As part of this program, an instrumentation system was developed and installed offshore southern California to collect strong motion seismic data from remote ocean floor sites[2]. The program was called the Seafloor Earthquake Measurement System Program and was given the name SEMS for brevity.

Sleefe[3] studied data obtained from these units, as well as data obtained from a second series of SEMS instruments installed offshore Long Beach in 1985. Of particular

*Research Program Manager
Technology Assessment and Research Branch
Minerals Management Service
Herndon, Virginia 22070-4817

interest was the data obtained from the North Palm Springs Earthquake (6.0 magnitude, 91 mile epicentral distance) of July 8, 1986. Figure 1 shows a plot of the peak horizontal accelerations from the North Palm Springs Earthquake measured from a number of land-based sites, the SEMS unit, and data recorded at the base of Shell's Platform Eureka as a function of their epicentral distances form the earthquake. Figure 2 shows the relationship between peak vertical accelerations and peak horizontal accelerations for the land-based and SEMS sites. It is obvious from the data that the offshore site exhibited a lower peak vertical acceleration than onshore sites with comparable peak horizontal accelerations. Based on this, as well as similar data from the July 13, 1986, Oceanside Earthquake (5.8 magnitude, 46 mile epicenter distance), Sleefe makes the following observations: "The vertical component of acceleration observed at both the SEMS site (i.e., free-field seafloor motion) and on the platform legs at mud-line level is significantly different than the corresponding vertical components of acceleration observed on-shore. . . . It appears that the peak horizontal components of acceleration observed at the SEMS site and by the platform legs at mud-line level are comparable to the corresponding onshore measurements."

The above considerations have important implications for the design and requalification of offshore structures located in seismic regions. With the marked reduction in the vertical accelerations, as well as any possible changes in the horizontal accelerations, it is clear that the design process using such data would result in a more economical structure. The design of topside production facilities, as well as the analysis of a structure for requalification, would greatly benefit from seismic data obtained from realistic offshore sites.

Therefore, due to the uncertainties which exist concerning the use of onshore seismic data in the analysis of an offshore platform, a study was undertaken to investigate the dynamic response of a typical offshore structure subject to actual seafloor-induced ground motions. The structure will be analyzed using strong motion data obtained from an onshore and an offshore site located at approximately equal epicentral distances from the actual earthquake. The information from these analyses was used to formulate conclusions and recommendations for future guidelines to be used in the design of new platforms or in the requalification of existing structures.

2. PLATFORM SEISMIC RESPONSE ANALYSES

The subject platform is a typical structure used by the oil and gas industry to drill for and produce hydrocarbons in seismic regions of the world. As shown in Figures 3 and 4, the facilities at the top of the structure are quite large to include the drilling, production, and processing operations, the crew quarters with helideck, the drilling derricks, and miscellaneous items associated with working offshore. Also visible from the rendering is the massive steel-jacket structure which supports the topside facilities. The platform was detailed in accordance to current U.S. industry standards[4] for platforms located in seismic areas.

Both onshore and offshore scaled earthquake records (time series of ground accelerations) were used in the platform analyses. The platform foundations were modeled using three different site conditions to include a soft clay, a stiff clay, and a dense sand that are representative of offshore areas as shown in Figure 5. Time histories of data were obtained on deck displacements, on member forces in the steel-jacket, on pile loads, and on the global base shears and overturning moments and used to assess the platform response.

3. GROUND MOTION DATA

The 1981 Santa Barbara Island Earthquake of September 4, 1981, offers the best opportunity to compare the effects of offshore and onshore recordings due to the availability of compatible data sets. As shown in Figure 6, the SBVictor (onshore) and SBHenry (offshore) sites are located in the same general direction from the earthquake

epicenter and are within 10 percent of the same epicentral distance. These recordings were obtained from similar SEMS instruments, both onshore and offshore, thus avoiding another source of uncertainty. Also, additional recordings from other onshore stations (SB38 and SB51) were available for comparison. Another incentive to use this data set was the fact that Anderson[5] completed an extensive study of onshore recordings for the same earthquake (did not include the SBVictor site). An analysis of the recording for SBVictor in terms of peak horizontal and vertical accelerations corresponds to Anderson's data for other onshore sites, thus providing confidence in the SBVictor results.

The SBVictor and SBHenry earthquake were scaled to match the API response spectrum using an effective acceleration of 0.25 g. This resulted in a scaling factor of 18 for SBVictor and 12 for SBHenry. An additional analysis was conducted with a scaling factor of 18 for SBHenry in order to have a direct corresponding earthquake for SBVictor. Table 1 lists the earthquakes and soil profiles used in the analyses. Figures 7-9 show the actual ground motion records used to conduct the platform analyses.

4. PLATFORM RESPONSE ANALYSES

The platform was analyzed using the Seastar and Cap computer codes on a SUN IPC Workstation with 24 megabytes of ram and a 643 megabyte hard disk drive. The SUN operating system, WINDOWS, Seastar and Cap Computer Codes, the platform model, and other general support programs took over half of the available memory space, thus leaving approximately 240 megabytes remaining for computed results. Therefore, due to the limited available memory, only selected node and member responses; i.e., pile load, base shear, overturning moment, and deck node displacements, etc., could be saved. A typical analysis took upwards of 120 hours of run time and created approximately 228 megabytes of data. The data for each run were downloaded onto one quarter inch magnetic tape and were re-recorded as necessary to obtain results.

Considerable attention was given as to what data would be best suited to assess the differences in the response of the platform when subjected to the designated earthquakes. A corner node at the top of the steel jacket was selected to judge the deck responses, and a brace in both the longitudinal (X-axis, stiff) and transverse (Y-axis, soft) directions was selected to assess member forces. Base shears were obtained in the longitudinal and transverse directions, as well as the effective total vertical force exerted by the platform. The base overturning and torsional moments were also calculated, as well as pile capacities for a corner pile in both the longitudinal and transverse faces. Table 2 provides a listing of the time series response plots obtained for each run listed in Table 1.

A frequency response analysis of the platform was conducted for each of the three soil profiles considered; i.e., soft clay, stiff clay, and a dense sand. Table 3 shows a comparison of the platform responses in the first 10 modes for each soil condition.

Table 4 lists the ratios of the results from the platform analyses using onshore and offshore records of earthquakes as forcing functions. The SBVictor (onshore - Runs 1, 2, and 3) and SBHenry (offshore - Runs 4, 5, 6, and 7) earthquake records show a consistent relationship for the soft clay site (Runs 1 and 4), the stiff clay site (Runs 2 and 5), and the dense sand site (Runs 3, 6, and 7) in that the offshore site produced smaller ratios of results comparing offshore to onshore data. The ratios of data for the soft clay site are somewhat smaller than for the stiff clay or dense sand sites as was previously stated. The peak values for the acceleration response spectra for the horizontal directions of the deck Node 56 are of the same magnitude; however, the periods at which the peak values occurred are consistently larger for the offshore records. This could have an impact on the design of deck equipment components depending on their period of response. The periods of the peak values of the response spectra for the vertical direction for Node 56

are consistent for both the onshore and offshore data. This would imply that there is no difference in the response as a result of the frequency content of the offshore and onshore records and that the differences in the vertical component of deflection are due only to the differences in the intensity of the offshore and onshore earthquakes' vertical component of motion.

5. CONCLUSIONS

A total of seven computer runs and three site conditions were used to assess the differences which might exist in analyzing a typical offshore platform using either onshore or offshore earthquake records as the forcing function. Reference 6 presents a more detailed analysis of earthquake ground motions from onshore and offshore sites and contains the results of additional computer runs that support the conclusions stated here.

Additional offshore records are needed from different offshore regions in order to fully generalize the results. However, the data obtained from this investigation are still quite significant for the design or requalification of platforms offshore California.

The following are the main results from the study:

- The type of foundation conditions (soft versus stiff) has a major impact on the periods of vibration of the platform. As the foundation stiffness increases, the periods of vibration decrease (frequencies of vibration increase). The effect is more pronounced for the higher periods of vibration (fundamental modes) than for the lower periods of vibration. The major changes occur in the first six modes of the platform used in this investigation.

- The offshore earthquake recordings produced, for all site conditions, smaller displacements and loads within the platform as compared to compatible onshore earthquake records. The horizontal components of the deck displacement was of the same magnitude; however, there was a marked difference in the vertical component of motion by a factor of 2 to 3; i.e., less than that produced by an onshore recording. The same trend was also present for the base shears and overturning moment with the total.

- The periods of peak horizontal responses of the deck node for the offshore records were greater than the periods of peak horizontal responses for the onshore records. However, the periods of peak vertical responses were equal for both types of earthquake records. With the records (both onshore and offshore) used in the analyses, it appears that there are no differences in the frequency content of the vertical motions of the deck, but there are slight differences in the frequency content of the horizontal motions. The differences are more pronounced for lower periods of motion than for higher periods of motion. The major differences in the vertical components of motion are due to ground motion intensities and not frequency content.

- Additional offshore earthquake records are needed from different regions with varying soil conditions and water depths to study and develop more specific recommendations concerning the relationship between the types of records. A corresponding need exists to determine the influence of the various environmental factors; i.e., soil type, water depth, etc. on the properties of the offshore records.

6. FUTURE RESEARCH NEEDS

The following recommended research needs are not listed in any order of priority but represent the uncertainties identified as part of this paper that would improve the assessment of the seismic response of offshore steel-jacket platforms:

1. A need exists to instrument and create a data base of recorded responses of steel-jacket platforms subject to seismic events. The validity of computer codes and models should be tested and calibrated through the use of field measurements of actual offshore structures subject to strong-motion earthquakes. This could be further enhanced by having an instrumented free-field seafloor site near the platform so that the structure could be analyzed using actual seafloor seismic response as a forcing function. This is extremely important for strong earthquakes that would cause nonlinear behavior in the structure, as well as in the surrounding soils.

2. There is a critical need for more earthquake seafloor motion data, especially in areas of different geology and local soil conditions. There is an abundance of data for onshore sites consisting of soft and firm soils and for rock. However, the data for varying offshore sites are very limited. Before specific recommendations can be put forth for using offshore recordings, as opposed to onshore recordings, for the design of offshore structures, it is important that additional offshore recordings be obtained and analyzed. Seafloor response data for earthquakes, especially strong earthquakes, would be of tremendous assistance to the offshore industry.

3. Additional information should be developed on methodologies for scaling existing earthquake records. Large earthquakes are extremely rare, and the ability to obtain such data is compounded by the small probability of having an instrument in place at the desired site to measure the event. This situation is even more pronounced for offshore sites. Recordings from smaller or more distant events can be obtained rather easily; yet to make them useful, they need to be increased in intensity. Analytical and experimental studies should be conducted to examine the effect of using different scaling techniques on the response of offshore structures.

7. REFERENCES

1. Poulos, H.G. (1988). Marine Geotechnics, Allen & Unwin, Ltd., Wellington, New Zealand.

2. Ryerson, D.E. and Reece, E.W. (178). "The Development of a Seafloor Earthquake Measurement System," Proceedings, Oceans '78 Conference, Washington, D.C.

3. Sleefe, G. E. (1990). "The Long-Term Measurement of Strong-Motion Earthquakes Offshore Southern California," OTC 6336, Proceedings, Offshore Technology Conference, Houston, Texas.

4. Recommended Practice for Planning, Designing, and Constructing Fixed Offshore Platforms, (1993). API P2A, 20th Edition, American Petroleum Institute, Washington, D. C.

5. Anderson, J. G. (1984). "The 4 September 1981 Santa Barbara Island, California, Earthquake: Interpretation of Strong Motion Data," Bulletin of the Seismological Society of America, Volume 74.

6. Smith, C. E. (1994). "Dynamic Response of Offshore Steel-Jacket Platforms Subject to Measured Seafloor Seismic Ground Motions," D.Sc. Dissertation, The George Washington University, Washington, D. C.

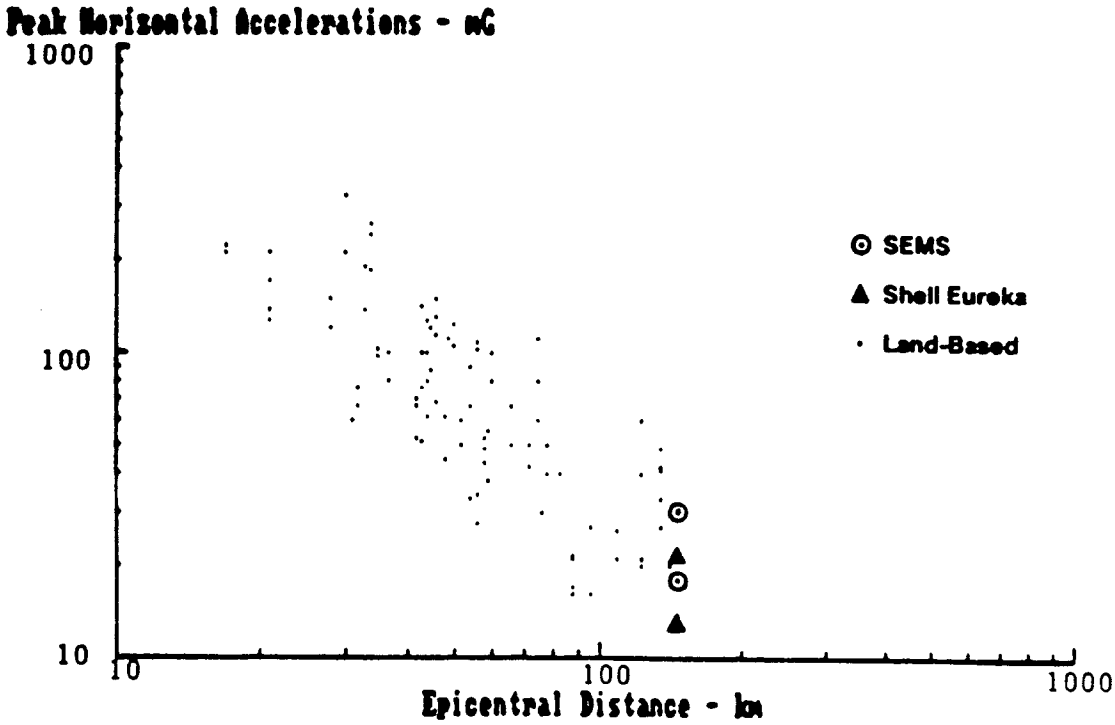

Figure 1. Peak Horizontal Accelerations vs. Epicentral Distances for Onshore and Offshore Sites (North Palm Springs Earthquake of July 8, 1986)

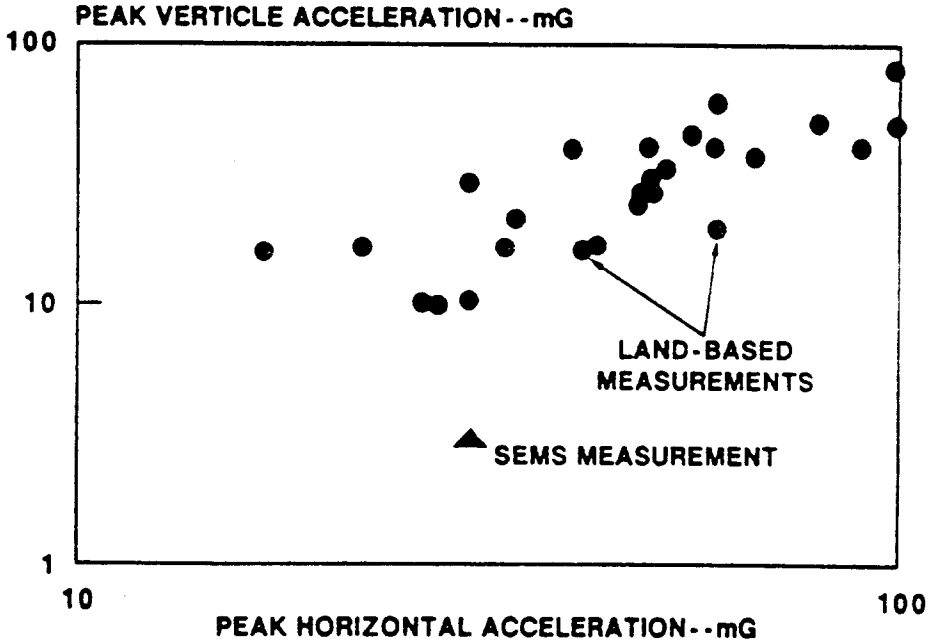

Figure 2. Peak Vertical Accelerations vs. Peak Horizontal Accelerations for Land-Based and SEMS Sites (North Palm Springs Earthquake of July 8, 1986)

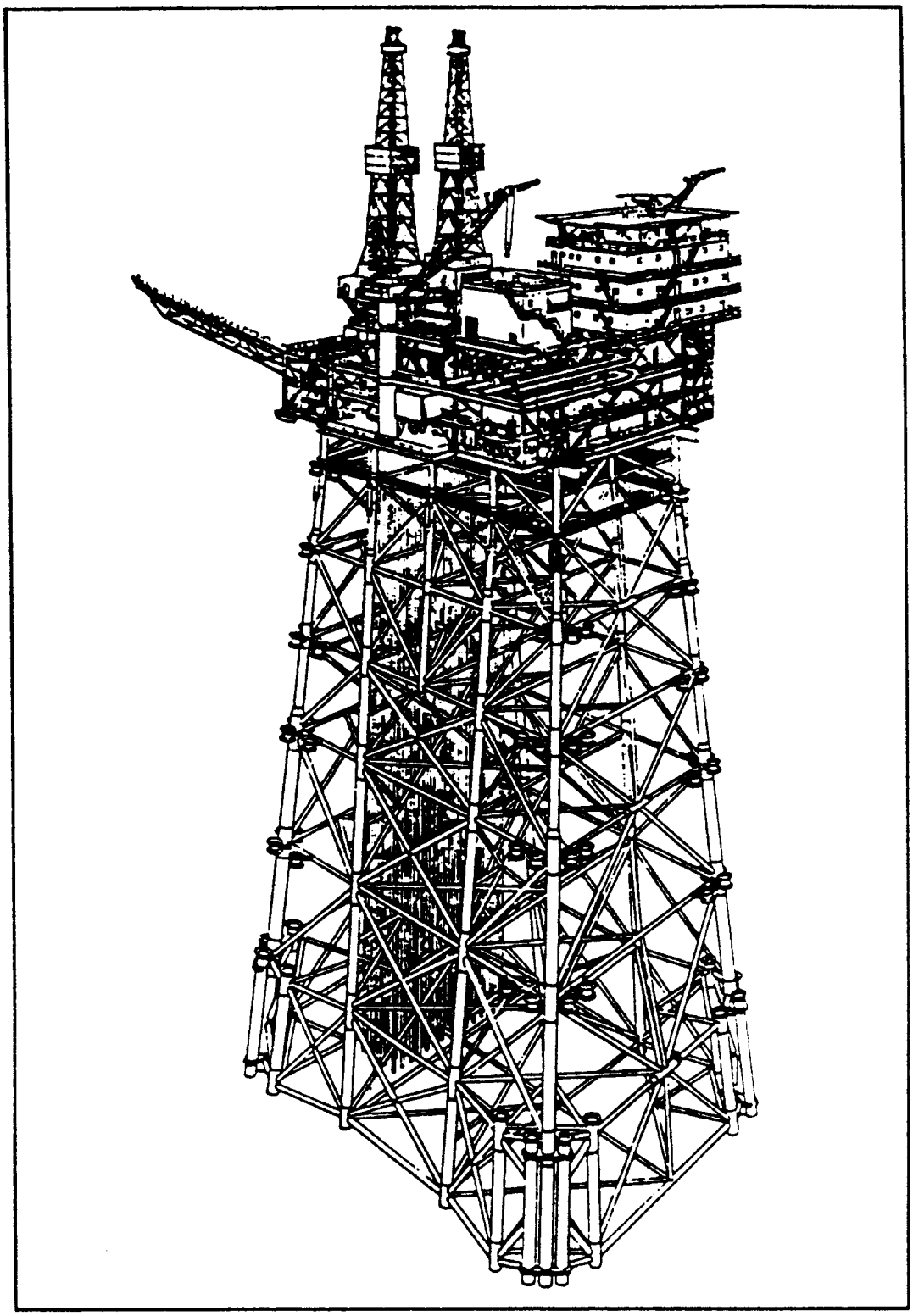

Figure 3. Artist's Rendering of the Offshore Platform Selected for Analysis (Rendering Courtesy of PMB Engineering)

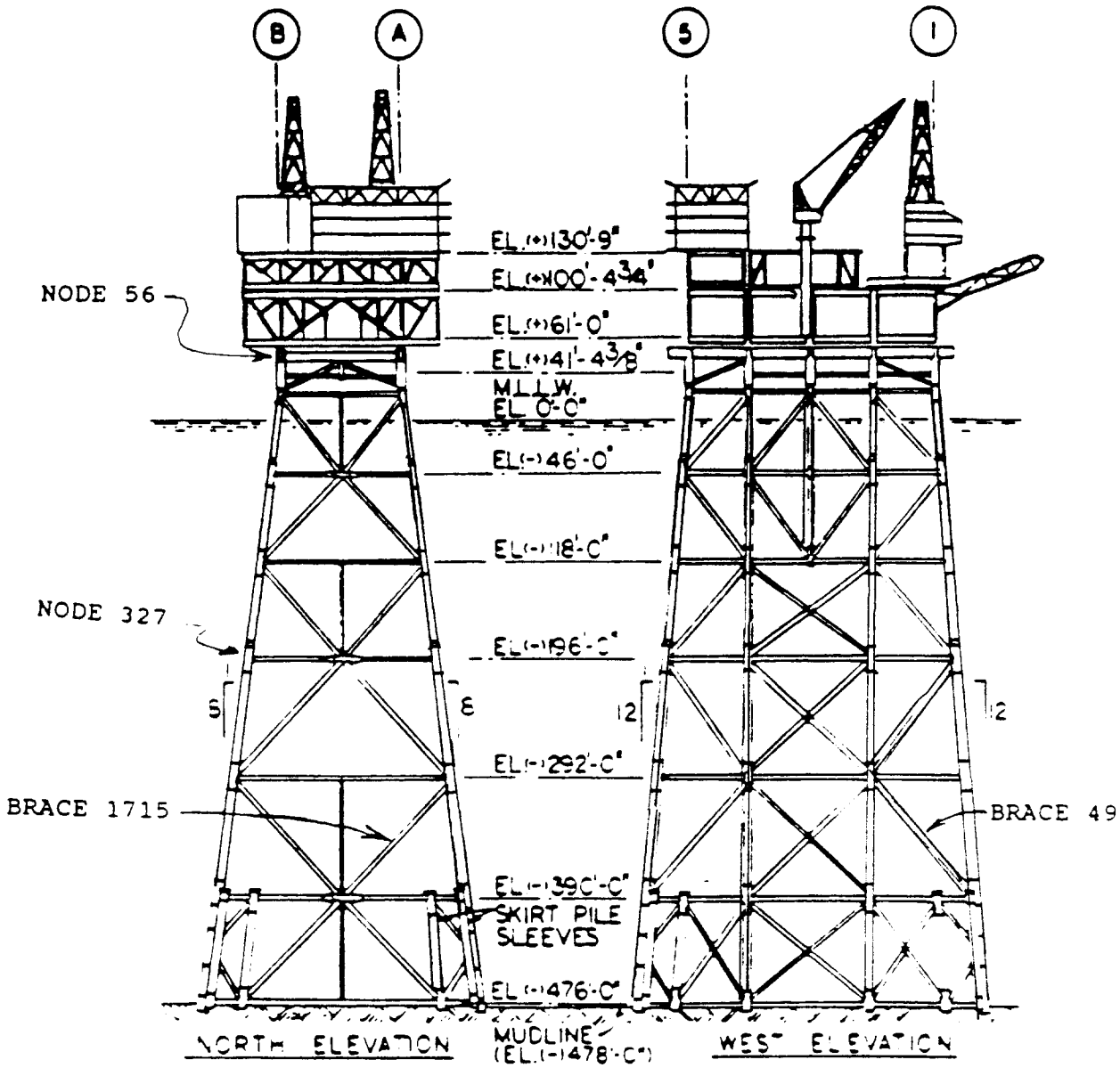

Figure 4. Platform Elevations Showing General Arrangement of Members (Figure Courtesy of PMB Engineering)

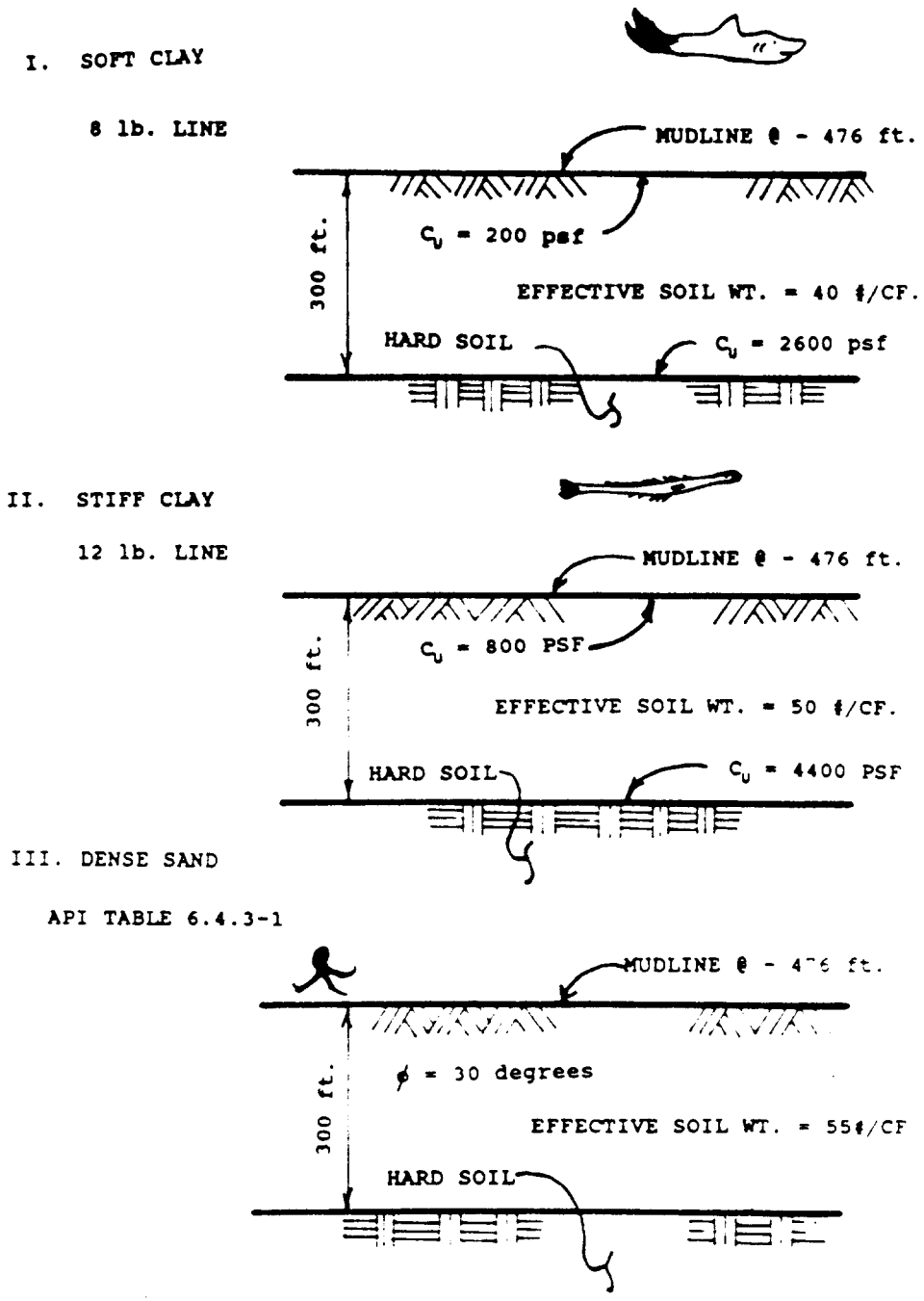

Figure 5. Soil Profiles and Properties

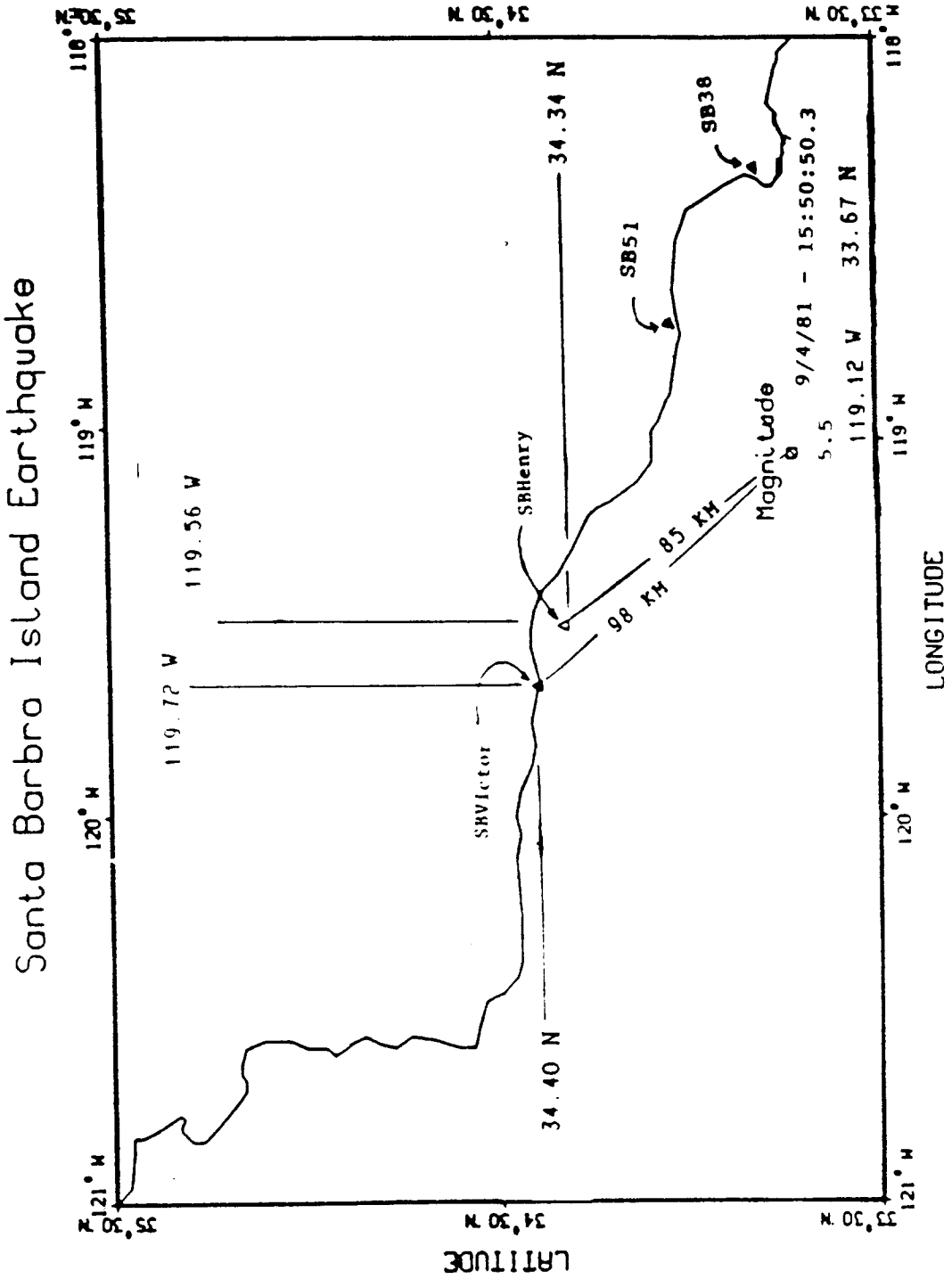

Figure 6. Location of SBHenry (offshore) and SBVictor (onshore) Recording Sites with Respect to the Earthquake Epicenter

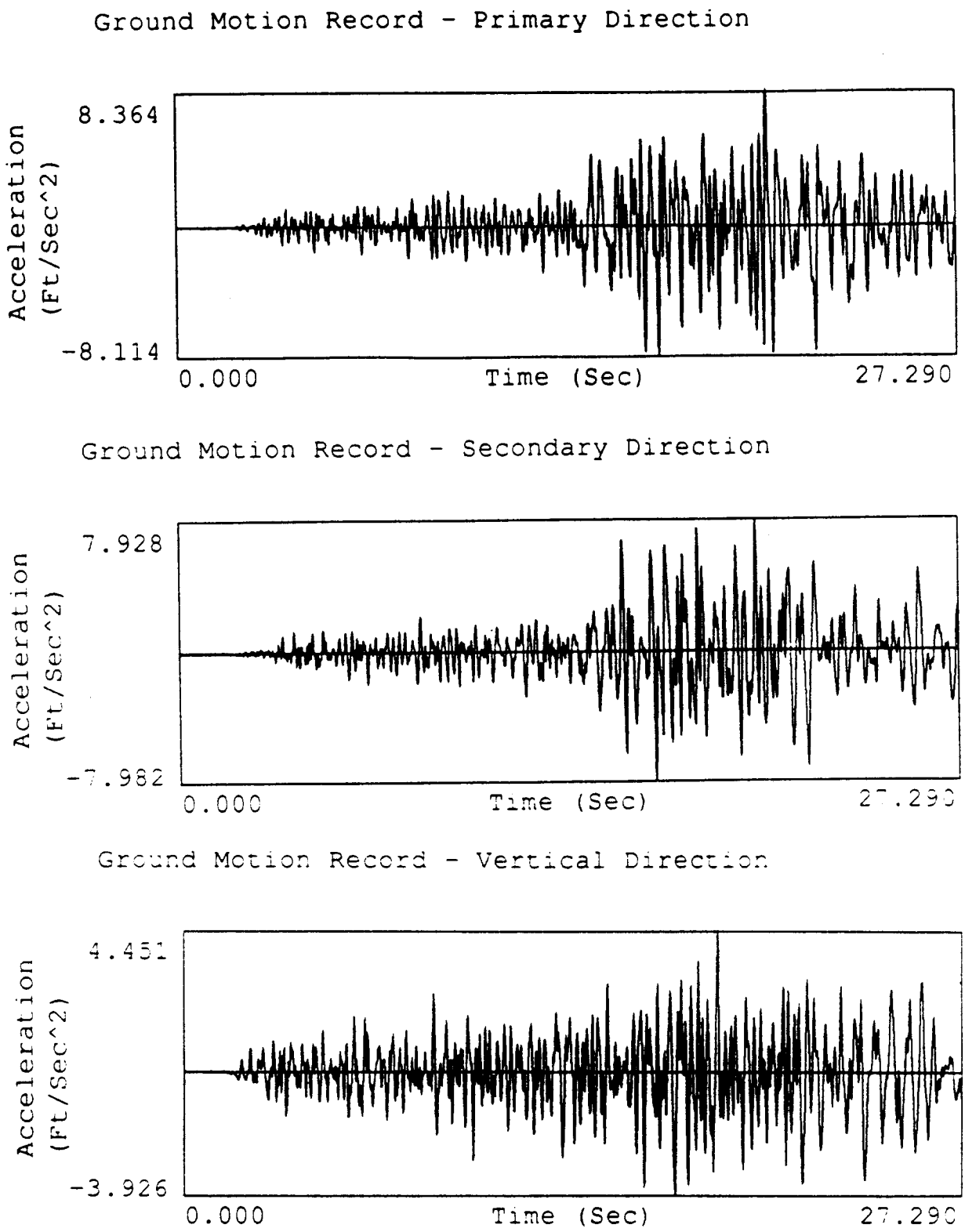

Figure 7. SBVictor; Scaled (x18) Components of Acceleration Time Histories

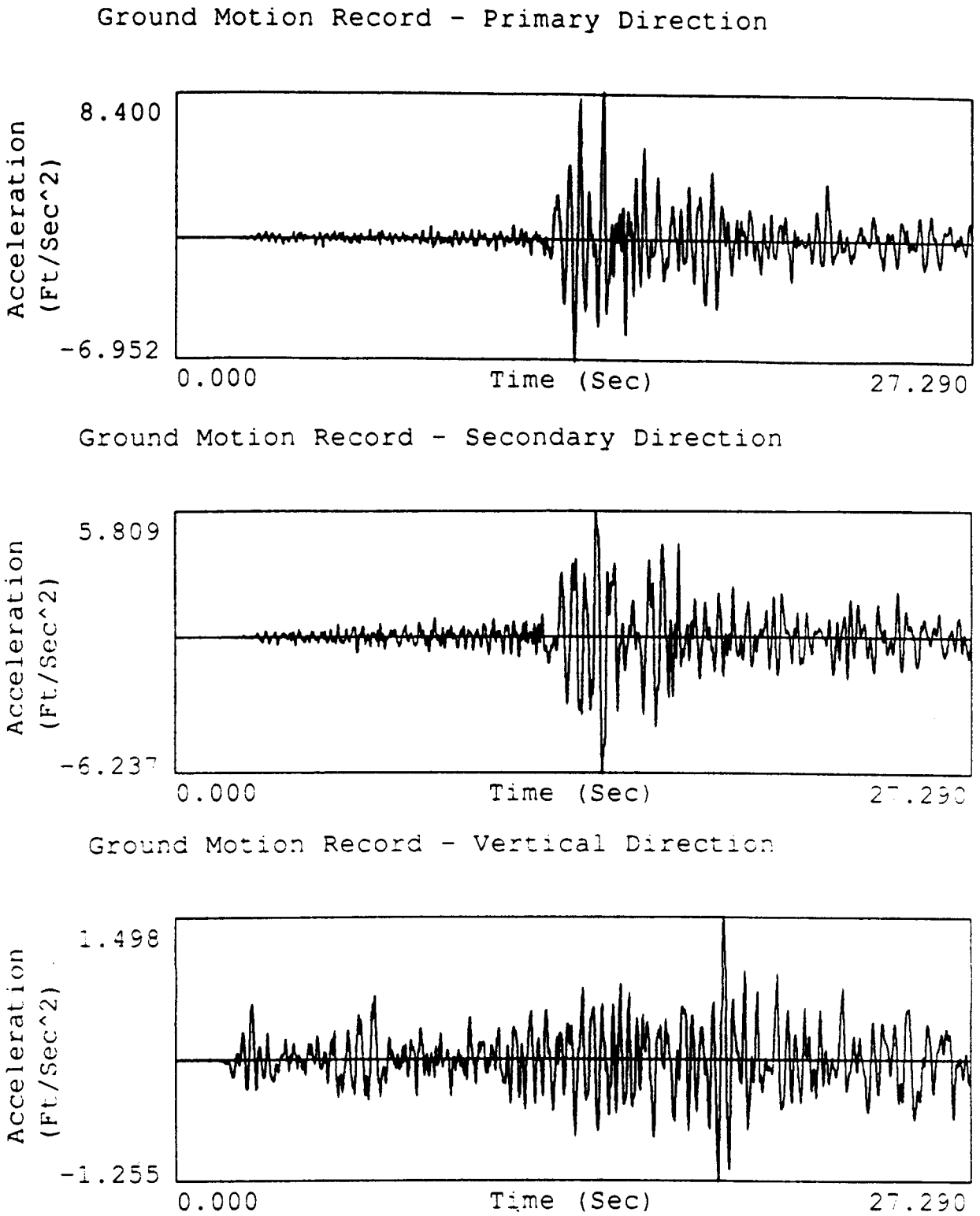

Figure 8. SBHenry; Scaled (x12) Components of Acceleration Time Histories

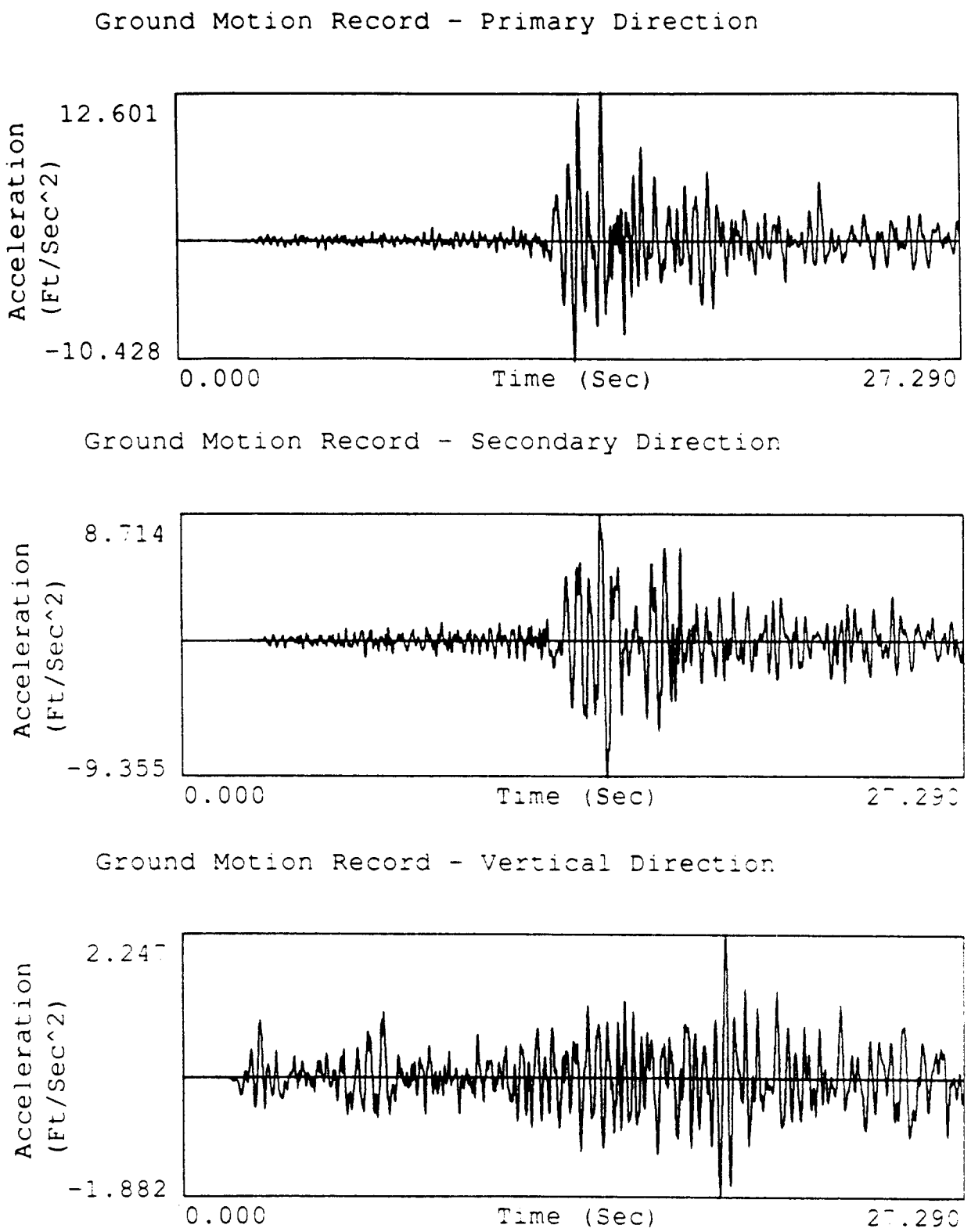

Figure 9. SBHenry; Scaled (x18) Component of Acceleration Time Histories

Table 1 - Earthquake Time Series and Soil Profiles Used in Assessing Platform Responses

Run No.	Earthquake	Structure	Soil Profile
1	SBVictor x18	Linear	Soft Clay
2	SBVictor x18	Linear	Stiff Clay
3	SBVictor x18	Linear	Dense Sand
4	SBHenry x12	Linear	Soft Clay
5	SBHenry x12	Linear	Stiff Clay
6	SBHenry x12	Linear	Dense Sand
7	SBHenry x18	Linear	Dense Sand

*Primary earthquake direction along transverse (Y-Axis) of the platform

Note: Each earthquake includes 3 components (primary, secondary, and vertical directions) applied to the structure simultaneously.

Table 2 - Time History Response Plots Obtained from a Computer Run

Data Plot	Item
*1	Node 56 - Deflection Along X-Axis; dx
*2	Node 56 - Deflection Along Y-Axis; dy
*3	Node 56 - Deflection Along Z-Axis; dz
*4	Node 56 - Acceleration Response Spectrum at 5% Damping; dx
*5	Node 56 - Acceleration Response Spectrum at 5% Damping; dy
*6	Node 56 - Acceleration Response Spectrum at 2% Damping; dz
7	Node 56 - Velocity Response Spectrum at 0% Damping; dx
8	Node 56 - Velocity Response Spectrum at 0% Damping; dz
9	Node 56 - Fourier Response Spectrum; dx
10	Node 56 - Fourier Response Spectrum; dz
*11	Base Shear; Fx
*12	Base Shear; Fy
*13	Total Vertical Load; Fz
*14	Base Overturning Moment; Mx
*15	Base Overturning Moment; My
*16	Base Torsional Moment; Mz
17	Pile Load; Fx (Pile 1071-82, Longitudinal Face)
18	Pile Capacity Chart (Pile 1071-82, Longitudinal Face)
19	Pile Capacity Chart (Pile 1141-93, Transverse Face)
*20	Brace Longitudinal Face (49); Fx
*21	Brace Transverse Face (1715); Fx
22	Node 327 - Deflection Along X-Axis; dx
23	Node 327 - Deflection Along Y-Axis; dy
24	Node 327 - Deflection Along Z-Axis; dz
25	Node 327 - Acceleration Response Spectrum at 5% Damping; dx
26	Node 327 - Acceleration Response Spectrum at 2% Damping; dz

Note: a) Node 56 at Elevation (+) 51 ft.
b) Note 327 at Elevation (-) 196 ft.
c) Base Shear and Moments at Elevation (-) 480 ft.
d) *Indicates Primary Data Set

Table 3 - Platform Frequency Analysis Summary

Mode No.	Soft Clay (period, sec.)	Stiff Clay (period, sec.)	Dense Sand (period, sec.)	Description
1	3.190	2.513	2.546	1st Transverse
2	2.998	2.406	2.420	1st Longitudinal
3	2.028	1.391	1.394	1st Torsional
4	1.560	0.951	0.964	2nd Transverse
5	1.415	0.941	0.935	2nd Longitudinal
6	0.911	0.808	0.808	2nd Torsional
7	0.809	0.771	0.772	1st Vertical
8	0.774	0.765	0.765	3rd Transverse
9	0.766	0.761	0.761	3rd Longitudinal
10	0.762	0.741	0.741	Complex Mode

Note: The Longitudinal, X-Axis, corresponds to the platform North-South Direction (West Elevation); and the Transverse, Y-Axis, corresponds to the platform East-West Direction (North Elevation) as shown in Figure 63.

- o Frequency (Cycles/Sec.) = 1/period
- o Circular Frequency (Rad./Sec.) = 2π x Frequency

Table 4 - Ratios of Primary Data from Platform Analyses Based on Offshore to Onshore Earthquake Records

Data Plot Number	Run 7/Run 3	Run 6/Run 3	Run 4/Run 1	Run 5/Run 2
1. Node 56 - Deflection X-Axis	0.950	0.659	0.554	0.483
2. Node 56 - Deflection Y-Axis	0.676	0.610	0.529	0.593
3. Node 56 - Vertical Deflection	0.611	0.458	0.248	0.315
4. Node 56 - Horizontal Accel. Resp.				
Spectrum at 5% Damp. (dx)	1.207	0.802	0.813	0.969
Period	1.601	1.601	1.149	1.599
5. Node 56 - Horizontal Accel. Resp.				
Spectrum at 5% Damp. (dy)	0.887	0.588	0.726	0.669
Period	1.315	1.315	1.640	1.369
6. Node 56 - Vertical Accel. Resp.				
Spectrum at 2% Damp. (dz)	0.565	0.387	0.329	0.357
Period	1.000	1.000	0.953	1.009
11. Base Shear (Fx)	1.060	0.798	0.412	0.698
12. Base Shear (Fy)	0.568	0.401	0.559	0.690
13. Total Vertical Load (Fz)	0.462	0.323	0.258	0.369
14. Base Overturning Moment (Mx)	0.586	0.401	0.469	0.591
15. Base Overturning Moment (My)	0.877	0.603	0.576	0.442
16. Base Torsional Moment (Mz)	0.718	0.533	0.598	0.916
20. Brace Longitudinal Face (Fx)	0.691	0.461	0.449	0.496
21. Brace Transverse Face (Fy)	0.565	0.419	0.459	0.464

Note: a) Run Numbers correspond to Computer Runs listed in Table 1.
b) Runs 4, 5, 6, and 7 are from offshore recordings, Runs 1, 2, and 3 are from onshore recordings.

Uplift of Sewage Manholes During 1993 Kushiro-Oki Earthquake

by

Osamu Matsuo[1], Hisanori Otsuka[2], Yoshio Ninomiya[3] and Junichi Koseki[4]

ABSTRACT

Boring and cut-off investigations were carried out to survey both the original ground and back-filled soil surrounding sewage manholes damaged by the 1993 Kushiro-oki earthquake. Based on these results, a liquefaction resistance ratio F_L and a safety factor against uplift Fs were estimated, and those factors were compared with the observed uplift displacement of the manholes.

KEYWORDS: Sewage Manhole, Uplift, 1993 Kushiro-oki Earthquake, Liquefaction

1. INTRODUCTION

The Kushiro-oki Earthquake on January 15th, 1993 caused severe damage to roads, railways, port and harbor facilities, lifeline infrastructures and fill-up ground for housing lots[1)2)]. Among these, several wastewater manholes in Kushiro Town along National Highway No.44 suffered uplift amounting up to 1.5m due to liquefaction of surrounding ground. This paper deals with the results of intensive survey which was conducted after the earthquake to reveal the mechanism of uplift.

2. SURVEY METHODS

Location of surveyed manholes is shown in Fig.1. All 18 manholes in the section requiring restoration work were investigated. They consist of 5 manholes on Nichii route, 6 on Ishiguro Homer route and 7 on Satsuru Veneer route. The total length of installed sewer pipes in the investigated section is 723m.

Contents of the survey are summarized in Table 1. Before the restration work, level survey and boring survey in conjunction with standard penetration tests for both the original ground and back-filled soil surrounding the manholes were conducted. During the restoration work, which was executed by open-cut method, the soil profile was observed to find any sign of ground alteration which is suggestive of liquefaction effect. Cyclic triaxial tests were performed using undisturbed tube samples for the original ground and block samples for the back-filled soil.

Based on these results, a liquefaction resistance ratio F_L[3)] and a safety factor against uplift Fs[4)5)] were evaluated as follows.

$$F_L = \frac{R}{L} \quad (1)$$

$$R = R_1 + R_2 + R_3 \quad (2)$$

1) Head, Soil Dynamics Div., Public Works Research Institute, Ministry of Construction, Tsukuba Science City, Japan

2) Head, Earthquake Engineering Div., ditto (formerly head, Ground Vibration Div.)

3) Senior Research Engineer, Ground Vibration Div., ditto

4) Research Engineer, Soil Dynamics Div., ditto

$$L = r_d \cdot k_s \cdot \frac{\sigma_v}{\sigma_v'} \quad (3)$$

where R: dynamic shear strength ratio,
L: shear stress ratio during an earthquake,
R_1: first term of R represented by a function of SPT N-value and effective overburden pressure σ_v',
R_2: second term of R represented by a function of mean grain diameter D_{50},
R_3: third term of R represented by a function of fines content FC,
r_d: reduction coefficient along depth,
k_s: horizontal seismic coefficient on the ground surface defined by $k_s = a_{max}/g$ (a_{max} is the maximum horizontal acceleration on ground surface and g is a gravitational acceleration), and
σ_v: total overburden pressure.

$$Fs = \frac{W + Q}{Us + Ud} \quad (4)$$

$$Ud = A \cdot Lu \cdot \sigma_{vb}' \quad (5)$$

$$Lu = \overline{F_L}^{-p} \text{ (if } \overline{F_L} < 1.0 \text{ then } Lu = 1) \quad (6)$$

where W: weight of manhole,
Q: frictional resistance force between the side wall of manhole and surrounding ground (a section which is shallower than the water level was considered),
Us: buoyancy force due to static hydraulic pressure,
Ud: uplifting force due to excess pore water pressure caused by liquefaction,
A: cross sectional area of manhole on a horizontal plane,
Lu: excess pore water pressure ratio,
σ_{vb}': effective overburden pressure in surrounding ground at the same depth as the bottom of manhole,
$\overline{F_L}$: liquefaction resistance ratio averaged over the depth of interests (refer to 3.4 for layers considered in the calculation), and
p: parameter representing the characteristics of excess pore water pressure generation (in ref.4, it is set to be 7).

3. RESULTS AND DISCUSSIONS

3.1 Ground Profile

The general ground profile is summarized in Table 2. The original surface of the surveyed ground had been peat (denoted as Ap), and it was filled with sand (F) dredged from the Old Kushiro River around 1962. The thickness of alluvial deposit is between 30 to 40m. Its shallower part mainly consists of sandy soil which can be classified into two groups. The upper sandy layers (Acs1, Acs2 and As1) are with mean SPT N-value 3 to 17 and with fines content 20 to 30% approximately. The lower sand layer (As2) is with mean SPT N-value more than 30 and fines content 10% approximately. Alluvial clay (Ac) is occasionally sandwiched between Acs1 and Acs2. The grain size distribution is shown in Fig.2.

The estimated ground profile along each route is shown in Fig.3 as well as SPT N-value for the original ground (denoted as N) and the back-filled soil (B). The boundary between the upper and the lower sand layer is slightly inclined to downstream side along each route. The ground water level is 2m below the ground surface on the whole. The back-filled soil is with mean SPT N-value 3 and with fines content 8% approximately.

3.2 Condition of Manholes

The standard cross section of facilities buried under the road is shown in Fig.4. After excavating the original ground by 1.3 to 1.6m in width and 2 to 5m in depth, the wastewater manholes and sewer pipes were installed and were back-filled by dredged sand and commercial sand brought from mountainous area. They were put into

operation in 1978.

Adjoining manholes for storm-water were not damaged, which had shallower foundation than the uplifted manholes for wastewater. Some part of connecting sewer pipes for storm-water are reported to have been bent slightly.

The composition of the wastewater manholes is shown in Fig.5. The main body is a precast-concrete pipe with a diameter of 1,050mm. Underneath its bottom plate, a latice-shaped wooden foundation was placed with crushed stones.

Observed height of the steel cap from the ground surface after the earthquake (denoted as uplift displacement), estimated settlement of the ground surface due to the earthquake and original depth of the bottom plate of each manhole are shown in Fig.6. The maximum uplift displacement was 1.46m at No.65 on Nichii route, 0.56m at No.92 on Ishiguro Homer route and 1.24m at No.9 on Satsuru Veneer route. Manholes which did not uplift had relatively shallow foundation, and the uplift displacement increased as the settlement of the ground surface developed. However the site at which uplift displacement was the maximum did not coincide with one at which ground settlement was the largest.

3.3 Condition of Surrounding Ground and Connecting Pipes

The cut-off investigation revealed that the manhole bodies were not damaged except some cracks at several sites. Underneath the bottom of the uplifted manholes, a void was not observed and the occupying sand was similar to the back-filled soil. Although sign of ground alteration indicating liquefaction effect such as penetration of liquefied sand into neighboring layer was not observed, the back-filled soil with low SPT N-value as shown in Fig.3 is judged to have liquefied and moved laterally toward the bottom of the manholes.

The latice-shaped wooden foundations were found almost at the original depth. Although this may imply that no ground movement occurred under the foundation, further investigations are required on its effect.

At some manholes where uplift displacement was large, the grain size distribution of the sand underneath the manhole was similar to that of adjoining original ground such as Acs1. This suggests that lateral movement of liquefied soil in the original ground may have occurred at these manholes.

Pipes connecting the uplifted manholes also moved upward without any breakage at the connection with the manholes. At some sections the vertical displacement of the sewer pipes was larger than the uplift displacement of the manholes. This supports the judgement that the back-filled soil was liquefied, which was described in the first paragraph of this section.

3.4 Liquefaction Assessment of Original Ground

The liquefaction resistance ratio $\overline{F_L}$ averaged over the layers Acs1, Acs2 and As1 is shown in Fig.3. The layer As2 was excluded from the assessment, because its SPT N-value was more than 30. When the seismic coefficient k_m is 0.2, $\overline{F_L}$ was not more than 1.0 except at manholes No.63 and No.67. It was less than 1.0 at all manholes when k_m is 0.25.

For reference of k_m, the recorded maximum horizontal acceleration on ground surface was 320gal at the foot of a levee in the Kushiro River which was located at an epicentral distance of 23km. Because the uplifted manholes were located at an epicentral distance

of 19km, actual value of k_s is estimated to be at least 0.25. This implies that liquefaction may have occurred in the original ground surrounding the manholes.

Comparison of the dynamic shear strength ratio R estimated from the results of boring survey and R_{20} from cyclic triaxial tests using undisturbed tube samples of the original ground is shown in Fig.7, where R_{20} is defined as the ratio of cyclic shear stress causing 5% double amplitude axial strain in 20 cycles to initial effective confining pressure. For the layers Acs1 and Acs2, R_{20} was almost equal to or slightly larger than R. For the layer As1, R_{20} was smaller than R. Reduction of R_{20} due to sample disturbance may have affected the results for As1, because it was relatively clean sand with fines content of 13%.

Relationship between uplift displacement of the manholes and the estimated total thickness of liquefied layer in the original ground is shown in Fig.8, where the liquefied portion was defined as a layer with F_L less than 1.0. When k_s is 0.15, the uplift displacement increased as the liquefied layer got thicker. Although k_s may have been larger than 0.25, as mentioned above, the liquefied layer estimated using k_s=0.15 can be regarded as the one which liquefied extensively during the earthquake. This suggests that extensively liquefied layer in the original ground as well as the back-filled soil may have affected the uplift of manholes.

Relationship between settlement of the ground surface and the estimated total thickness of liquefied layer in the original ground is shown in Fig.9. As well as uplift of the manholes, ground settlement increased as the liquefied layer estimated using k_s=0.15 got thicker.

3.5 Stability of Manholes against Uplift

Relationship between uplift displacement of manholes and a safety factor against uplift Fs based on $\overline{F_L}$ in the original ground is shown in Fig.10. The parameter p, which was used in the prediction of excess pore water pressure, was evaluated to be 2.1 on the average by analizing the result of cyclic triaxial tests.

When the seismic coefficient k_s is 0.2, which is lower than the value estimated based on observed strong motion, Fs was less than 1.0 at all manholes irrespective of the uplift displacement. This indicates that the evaluation of the stability against uplift based on Fs may have some safety margin.

However when k_s is reduced to 0.15, Fs was still less than 1.0 at manholes with large uplift displacement. On the contrary, it was more than 1.0 at other manholes except one. This indicates that the uplift displacement agreed with Fs qualitatively by reducing k_s and supports that original ground may have affected uplift of manholes as mentioned in 3.4. Further investigations are needed on the mechanism of uplift of manholes including the wooden foundation in a lattice shape which did not move during the earthquake.

4. SUMMARY AND CONCLUSIONS

Based on the cut-off investigation and SPT N-value, the back-filled soil of the manholes is judged to have liquefied and moved laterally toward the bottom of the uplifted manholes. An analysis of the average liquefaction resistance ratio $\overline{F_L}$, which was evaluated using SPT N-value, grain size distribution and horizontal seismic coefficient k_s, implies that liquefaction may have

occurred in the original ground surrounding the manholes.

Uplift displacement of the manholes and ground settlement increased as the extensively liquefied layer, which was estimated based on F_L, got thicker. The uplift displacement also agreed with the difference of safety factor against uplift Fs qualitatively by reducing k_a.

Further investigations are needed on the mechanism of uplift considering the lattice-shaped wooden foundation which did not move during the earthquake.

ACKNOWLEDGEMENTS

This investigation was carried out by PWRI and Japan Sewage Works Agency in cooperation with Kushiro Town. The authors wish to thank the concerned persons for their thoughtful and helpful assistance.

REFERENCES

1) Iijima, T. et al.: Damage to Infrastructures Caused by the 1993 Kushiro-oki Earthquake, 25th UJNR Joint Meeting on Wind and Seismic Effects, 1993.

2) Murota, T. et al.: Damage to Buildings and Housing Lots Caused by the Kushiro-oki Earthquake, 1993, 25th UJNR Joint Meeting on Wind and Seismic Effects, 1993.

3) Japan Road Association: Specifications for Highway Bridges, Part V: Seismic Design, 1990.

4) Japan Road Association: Design Manual for Common Utility Ducts, 1986 (in Japanese).

5) Koseki J. and Koga, Y.: Uplift of Semi-buried Structures in Liquefiable Sands during Earthquake, Proc. of 8th Japan Earthquake Symposium, pp.933-938, 1990.

Table 1 Contents of Survey

Route	Nichii Route	Ishiguro Homer Route	Satsuru Veneer Route
Level Survey	No.63, 64, 65, 66, 67	No.91, 92, 93, 94, 95, 96	No.7, 8, 9, 10, 11, 12, 13
Boring Survey	No.63, 65, 67	No.91, 92, 94, 95	No.8, 9, 11
Cut-off Investi-gation	No.64, 65, 66	No.91, 92, 93, 94, 95	No.8, 9, 10, 11, 12, 13
Cyclic Triaxial Tests	No.65 (Acs1[1], Acs2), No.66 (B)	No.92 (Acs1, Acs2, B)	No.9 (Acs2, B), No.11 (Acs2, As1, B)

1) Refer to Table 2 for notations.

Table 2 General Ground Profile

Profile		Notation	Major Soil	SPT N-value
Back-filled Sand		B	Fine sand with some silt	0~11 (3)[1]
Original Ground	Filled Sand	F	Fine sand (with some silt)	1~4 (2)
	Peat	Ap	Peat, Organic soil	1~3 (2)
	Upper Sandy Soil	Acs1	Silty fine sand, Medium Sand	1~21 (7)
	Clayey Soil	Ac	Silt, Sandy clay	1~5 (3)
	Lower Sandy Soil	Acs2	Silty fine sand	1~13 (5)
	Upper Sand	As1	Fine sand with some silt	8~38 (17)
	Lower Sand	As2	Fine sand, Medium sand	16~50 (43)

1) Minimum~Maximum (Mean value)

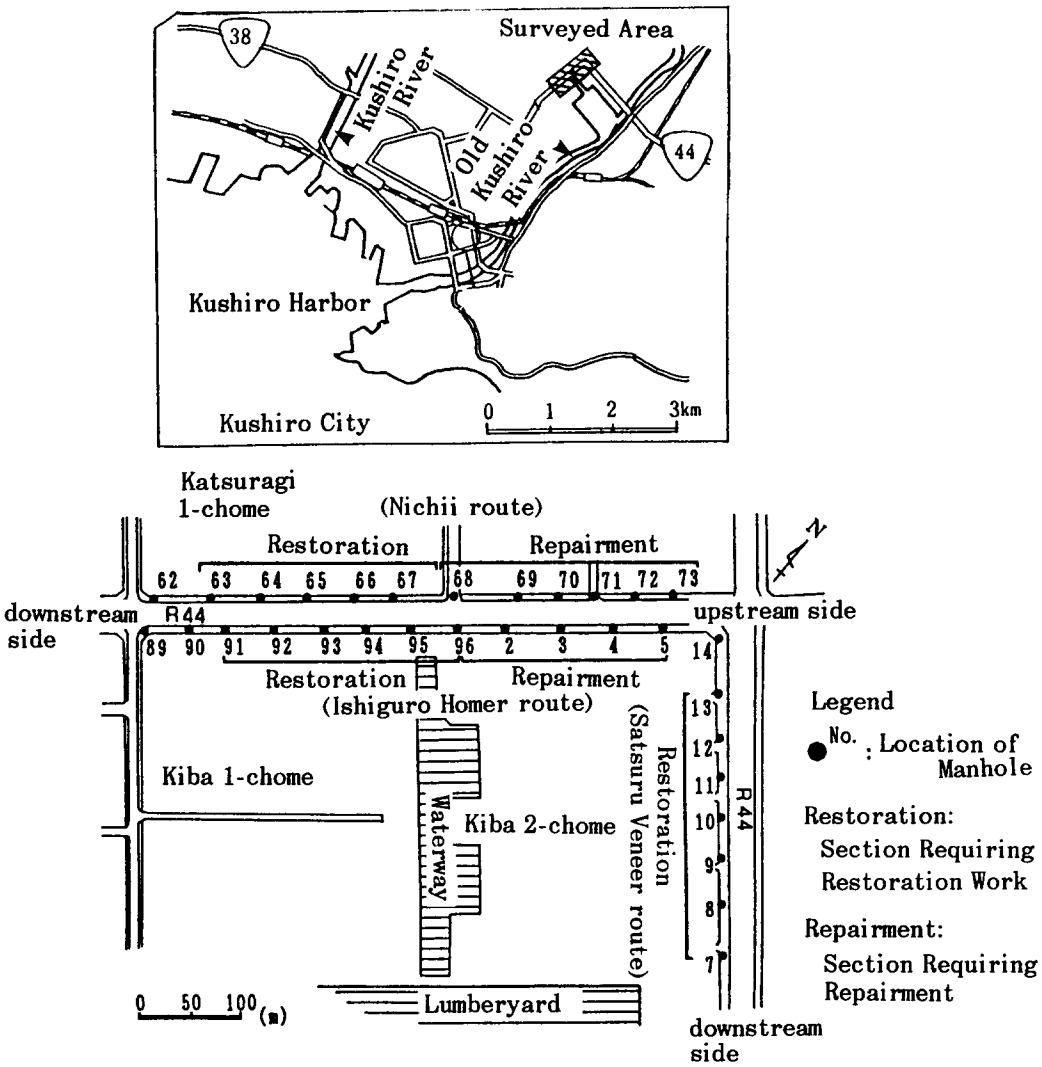

Fig.1 Location of Surveyed Manholes

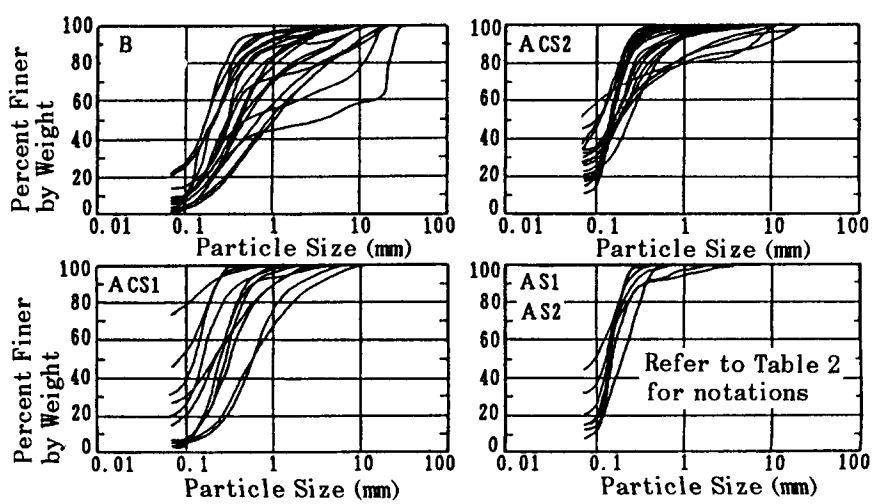

Fig.2 Grain Size Distribution

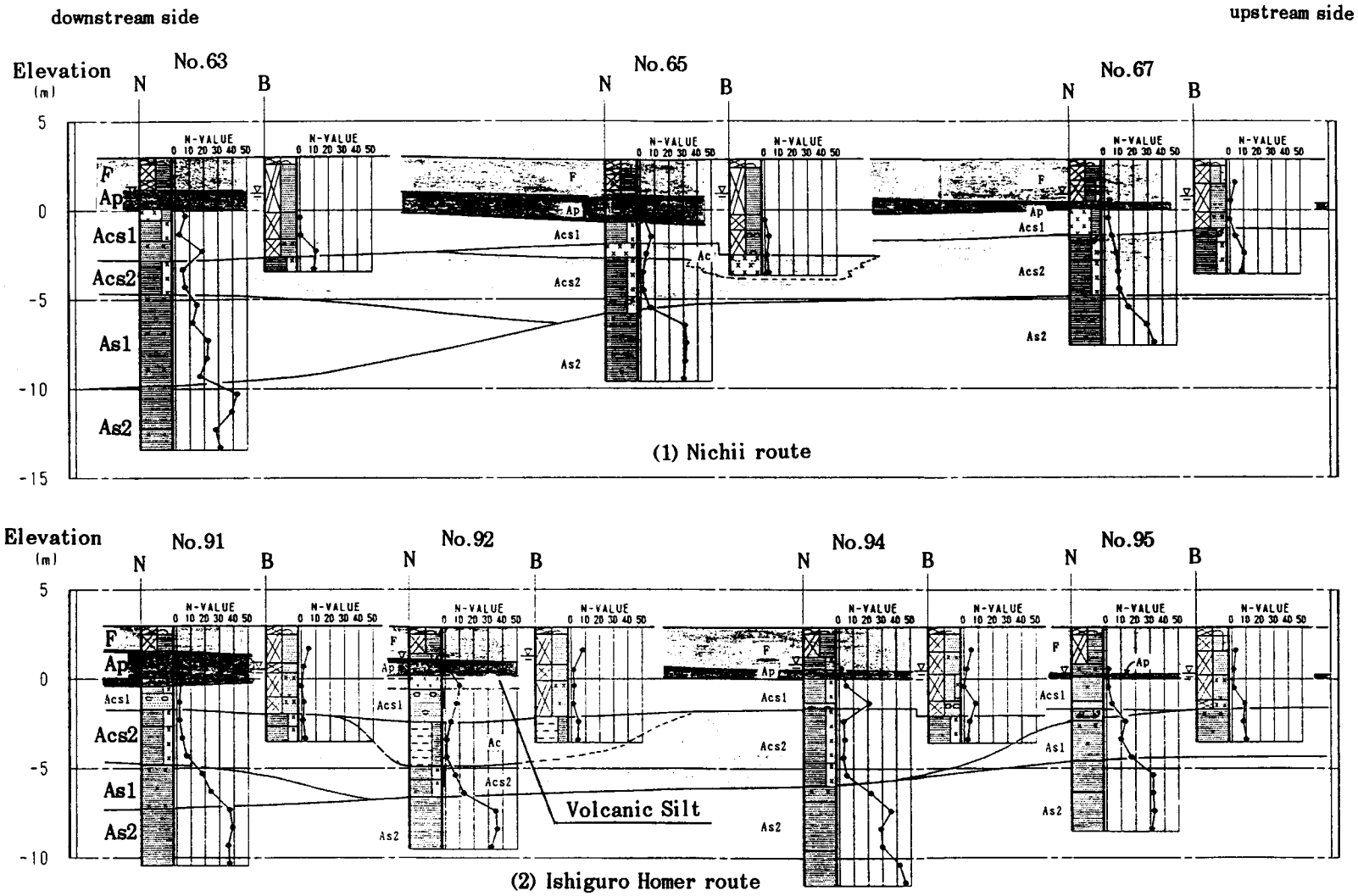

Fig.3 Estimated Ground Profile

B: Back-filled Soil
N: Original Ground
No.: Manhole No.

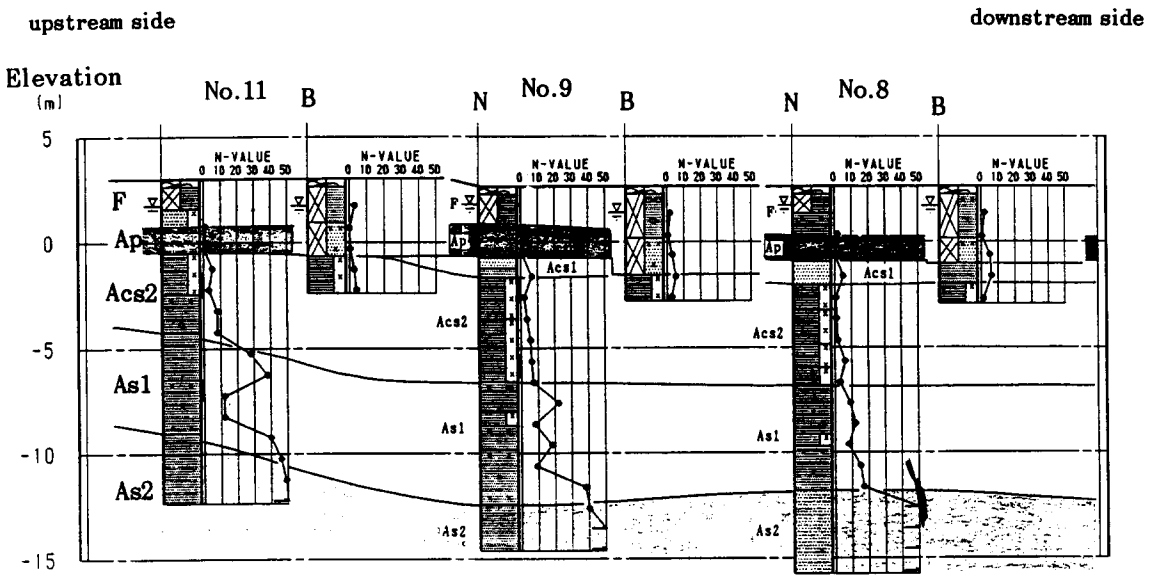

(3) Satsuru Veneer route

Fig.3 Estimated Ground Profile (continued)

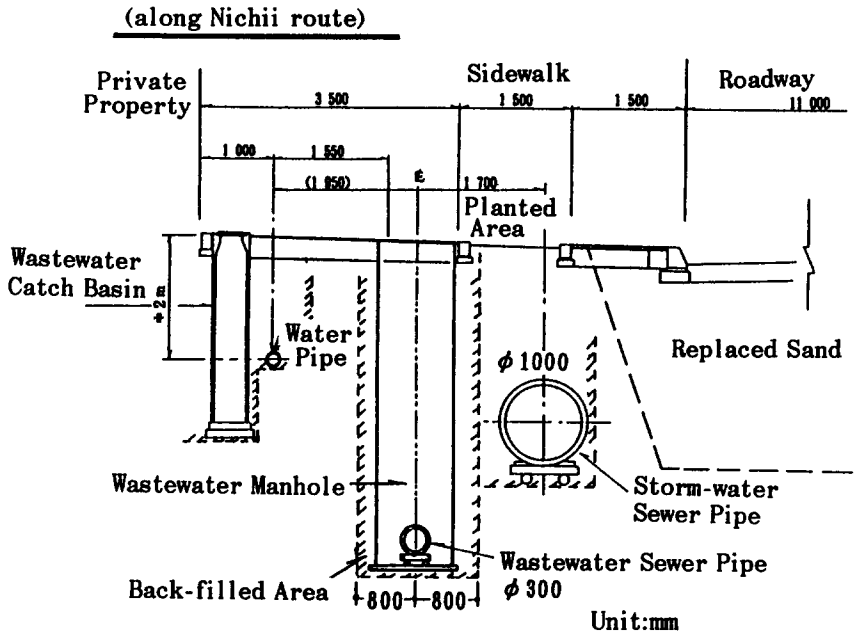

Fig.4 Standard Cross Section of Buried Facilities

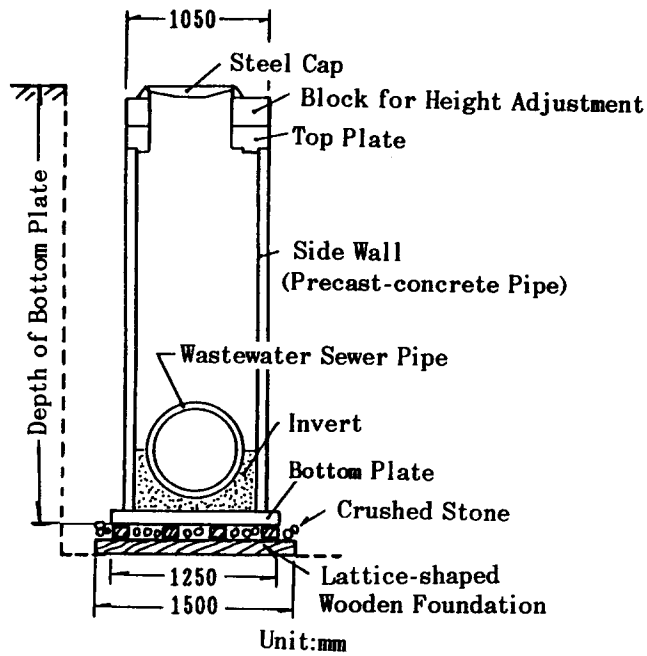

Fig.5 Composition of Wastewater Manhole

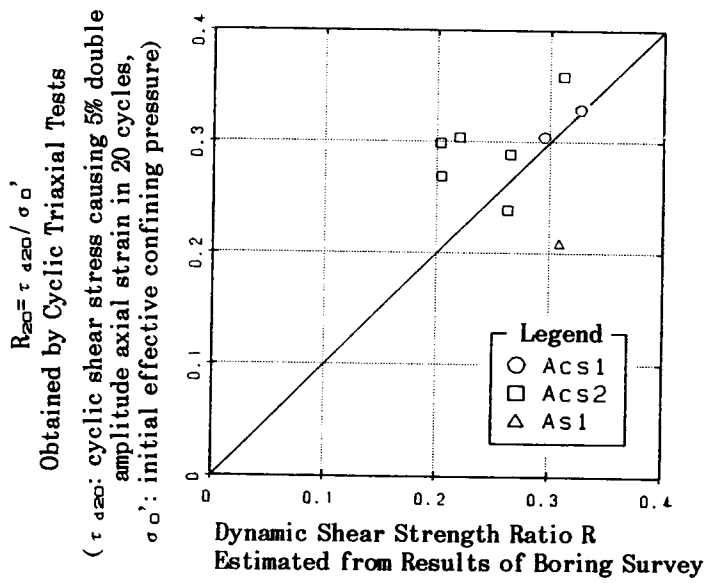

(Grain size distribution was adjusted to that of samples used for cyclic triaxial tests)

Fig.7 Comparison of Dynamic Shear Strength Ratio

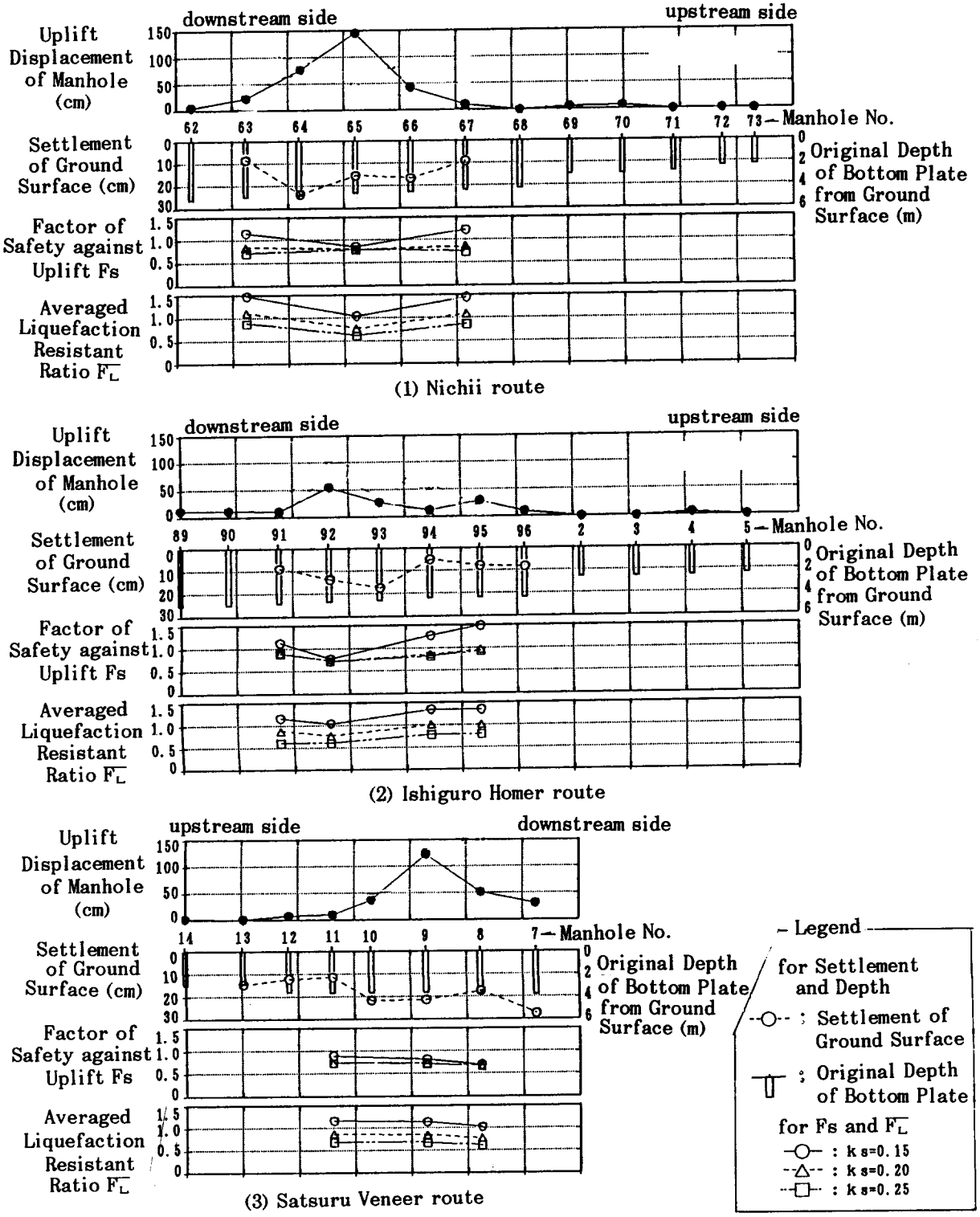

Fig.6 Distribution of Uplift Displacement of Manhole, Ground Settlement, F_L and Fs

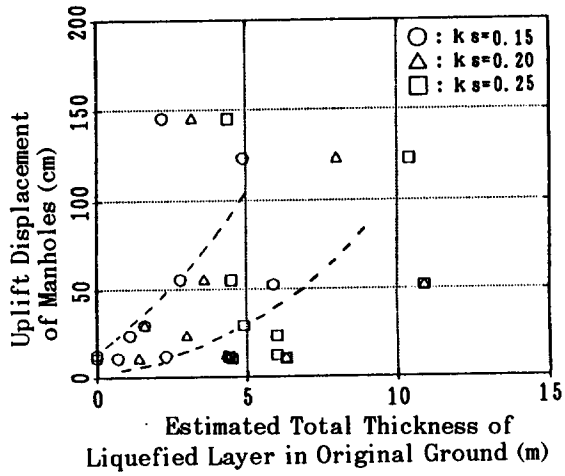

Fig.8 Uplift Displacement of Manholes vs. Estimated Total Thickness of Liquefied Layer

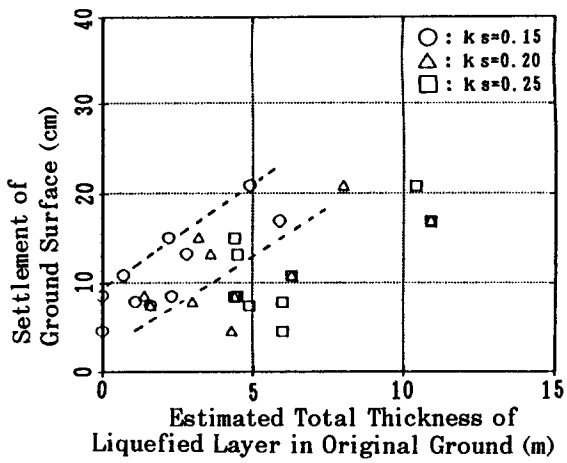

Fig.9 Settlement of Ground Surface vs. Estimated Total Thickness of Liquefied Layer

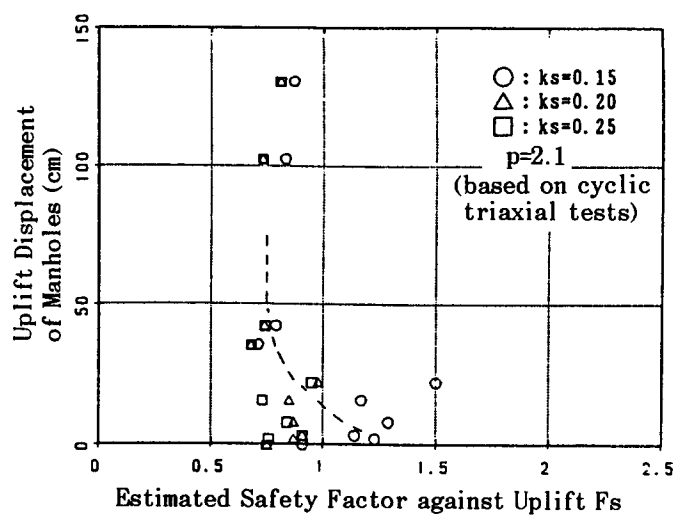

Fig.10 Uplift Displacement of Manholes vs. Esimated Safety Factor against Uplift Fs

Survey of Research in the Area of Seismic Response of Concrete Dams

by

Robert L. Hall, PhD* and
William E. Roper, PhD, PE**

ABSTRACT

The Corps of Engineers (CE) has started an earthquake engineering research and development effort called the Earthquake Engineering Research Program (EERP). The EERP will address needs in the general areas of earthquake ground motions and site characterization, material behavior, and the seismic response of concrete dams. The priorities of the EERP have been established by both structural and geotechnical field review groups consisting of the Corps' premier engineers who are actively designing new structures or the remediation of existing structures. The EERP is closely coordinated with representatives from the Office of the Chief of Engineers in Washington, D.C., who solicited the assistance of the Civil Engineering Research Foundation (CERF), which is part of the American Society of Civil Engineers (ASCE). CERF's role was to ensure that the proposed structural research was a well-developed program which would: (1) develop the state-of-the-art design and analysis tools dealing with all aspects of concrete dams and appurtenant structures, (2) identify any ongoing or planned research which would either duplicate or complement the Corps' planned research, and (3) identify any possible opportunities to develop partnerships with others to meet the objectives of the planned research program. This paper summarizes the findings of CERF's activities.

KEYWORDS: concrete dams; earthquake engineering program; nonlinear response; intake towers.

1. INTRODUCTION

The CE has begun an earthquake engineering research and development effort (Roper, et al, 1992) called the Earthquake Engineering Research Program (EERP). The EERP will address needs in the general areas of earthquake ground motions and site characterization, material behavior, and the seismic response of concrete dams. The Corps has an inventory of 22 concrete dams subject to potentially significant earthquake ground motions. The failure of any of these critical structures would typically result in more damage than that with the 1989 Loma Prieta or 1994 Northridge earthquakes. The concrete portion of the Folsom Dam serves as an example of typical damage which would occur as a result of a dam failure. Studies from about 10 years ago indicate that the damage would exceed $6,000,000,000 and 6,000 lives would be lost.

It is planned that the EERP will coordinate closely with other organizations conducting research pertinent to the seismic response of dams. In the development of these plans, CERF, which is part of the ASCE, was contacted to assist the Corps. CERF's role was to ensure that the proposed structural research was a well-developed program which would: (1) develop the state-of-the-art design and analysis tools dealing with all aspects of concrete dams and appurtenant structures, (2) perform literature searches on recent publications in the area of earthquake engineering related to hydraulic structures, (3) identify any ongoing or planned research in the U.S. and worldwide which would either duplicate or complement the Corps' planned research, and (4) identify any possible opportunities to develop partnerships with the Corps to meet the objectives of the planned

* U.S. Army Engineer Waterways Experiment Station, Vicksburg, MS 39180-6199
** U.S. Army Corps of Engineers, Washington, D.C. 20314-1000

research program. This paper summarizes the findings of these efforts.

2. BACKGROUND

The objective of the EERP will be to develop the necessary validated analytical tools and corresponding guidance to predict the dynamic response of the Corps' critical structures from elastic behavior to the development of failure mechanisms. The understanding of the failure mechanisms will allow the determination of the ultimate capacity of these critical structures during and after structural response induced from earthquake ground motions. The results of past research have recently resulted in the saving of millions of dollars in rehabilitation costs. However, there are no analytical tools or guidance for considering the nonlinear response of these structures. The accomplishment of this objective will be through a program utilizing the expertise in the U.S. and worldwide.

3. EARTHQUAKE ENGINEERING PROGRAM

Details about the EERP have been described in two publications. The first paper (Roper et al, 1992) provides information about the entire program which includes both geotechnical and structural research. The second paper (Hall and Roper, 1993) describes the structural aspects of the program which were reviewed by CERF. The current structural aspects of the EERP are the following areas:

Concrete Dams (Area 1) - Focus on research to determine the dynamic ultimate capacity of concrete gravity, roller-compacted, and concrete arch dams. This research will address the nonlinear behavior and failure mechanisms of the different types of dams as well as component tests, scale-model tests, and tests of existing structures.

Intake Towers (Area 2) - Research to determine dynamic ultimate capacity of intake towers. One major area will be to determine the ductility of existing lightly reinforced structures. Other research will focus on other nonlinear behavior and failure mechanisms including stability of these reinforced concrete structures.

Earthquake Analysis Tools (Area 3) - Develop analytical tools to support the research on concrete dams and intake towers. This research will produce postprocessing tools to aid in the interpretation and understanding of output from time-history and response spectrum analyses.

4. STUDY OVERVIEW

CERF surveyed 90 organizations from government, academia, private industry, and foreign countries for information related to the EERP (CERF, 1993). The survey documentation which was sent to each organization contained a letter explaining the survey, the priorities of the EERP, and a list of the organizations being contacted. Responses were obtained from each organization by responding to the initial mailing or by follow-up telephone calls. All responses are given in Vol 1 of CERF's report.

Thirty of these organizations indicated an interest in partnering with the EERP on at least one of the three structural areas of research and development. CERF considered 14 of these to be excellent candidates for partnering and 6 others as good candidates for partnering. The selections were based on the responses to the survey and the applicability of their R&D to the EERP. Table 1 provides a summary of these organizations and their research and development areas of interest. The following are summaries of the capabilities of the 14 candidates and partnering opportunities.

4.1 National Center for Earthquake Engineering Research, Buffalo, NY

The National Center for Earthquake Engineering Research (NCEER) is a National Science Foundation-funded Research Center. NCEER conducts research in the areas of buildings, non-structural components, lifelines, and highways. The NCEER utilizes a consortium of researchers in universities and private industry throughout the U.S. in performing their research. NCEER does perform research on large hydraulic

structures or large mass concrete structures. They are conducting some research on dams and appurtenant structures in association with their Lifeline Project. Their research on analytical tools for time-history analysis of lightly-reinforced concrete structures, soil structure interaction, and seismic-induced displacements on buried and partially buried structures complements milestones of the EERP.

4.2 Bureau of Reclamation, Denver, CO

The Bureau of Reclamation has designed and constructed over 400 concrete and embankment dams. Since many of these are in high seismic zones, the Bureau has conducted R&D to support their seismic evaluations of their extensive inventory of dams. These seismic evaluations consist of seismotectonic studies, ground motion studies, geotechnical site investigations, and structural analyses. These evaluations are conducted with close coordination to provide confidence in the conclusions of the studies.

The Bureau provided the following five examples of their R&D which are directly applicable to the EERP:

- Modification of ADAP-88 to include the effect of contraction joints and nonlinear behavior of concrete with constitutive modeling.

- Proposed funding of centrifuge modeling of concrete arch dams with contraction joints.

- Capability to perform laboratory vibration experiments to determine dynamic characteristics of concrete.

- Software development of seismic analysis tools.

- Investigation of a combined analytical approach to concrete dams and their foundations, including abutments.

4.3 University of California, Berkeley, CA

Professors Anil K. Chopra and Gregory L. Fenves conduct extensive research in the area of seismic response of concrete dams and appurtenant structures at the University of California, Berkeley. Some of their research accomplishments and ongoing research are :

- Earthquake analysis of concrete dams including soil-rock interaction, reservoir-structure interaction, and reservoir-sediment interaction. The time-history procedure has been implemented in the computer program, EAGD-84.

- A simplified analysis procedure including all the important interaction effects and the fundamental mode of vibration.

- Investigation of the nonlinear structural response in gravity dams from water cavitation and the tensile cracking of the concrete.

- Development of nonlinear analysis procedures to determine the effects of contraction joint openings on arch dams.

- Development of a nonlinear procedure for determining the earthquake sliding stability of concrete gravity dams.

- Development and implementation of a unified constitutive model for mass concrete for determining the earthquake behavior of concrete in dams.

4.4 Ray W. Clough, Sc.D., Structures Consultant, Sunriver, OR

Dr. Clough is a world-renowned expert in the field of earthquake engineering research for concrete dams and appurtenant structures. He has worked closely with the CE on many earthquake-related R&D programs and projects. His contributions in this field are demonstrated by the many research projects successfully completed at the University of California, Berkeley, and the current design guidance within the CE.

4.5 Agbabian Associates, Pasadena, CA

Agbabian Associates is a private consulting firm specializing in earthquake engineering and

structural dynamics. They also perform applied R&D, analysis, and designs related to hydraulic structures. Recent applied R&D (internally and externally funded) projects include:

- Retrofit design for large, complex highway bridges.

- Seismic qualification of components and systems.

- Seismic risk analysis.

- Seismic risk/mitigation development for museum contents.

- Design, installation, and operation of a network of vertical strong-motion instrumentation arrays in California (funded by the Japanese government) for study of soil site response.

- Retrofit design for an intake tower, based upon a new nonlinear analysis technique.

- Geophysical measurements and analyses, some related to seismic analyses of dams.

- Seismic analyses of several concrete dams and field studies including forced-vibration studies to verify analytical models.

4.6 Quest Structures, Emeryville, CA

Quest Structures is a private engineering consulting firm which specializes in earthquake engineering and has been working with the CE on many earthquake engineering projects.

Dr. Yusof Ghanaat, Principal Investigator, states that their research interests in earthquake engineering are primarily focused on the earthquake response prediction of concrete dams validated by field measurements and dynamic response during actual earthquakes. Details were given about experimental studies of dam-water-foundation interaction conducted on the Dongjiang Dam, the highest double-curvature arch dam in China. Quest Structures has assisted with the following CE projects:

- Portuguese Arch Dam, Puerto Rico.

- Seven Oaks Inclined Intake Tower, CA.

- Olmsted Locks and Dam, KY.

- Montgomery Point Dam, AR.

4.7 Professor Xia Songyou, Hohai Unversity, China

Professor Songyou's research efforts have been focused on the seismic response of concrete dams, navigation locks, and electric powerhouses. The following is a brief summary of his past and planned earthquake engineering activities:

- Modeling the seismic response of concrete dams and powerhouses.

- Foundation-structure-reservoir interaction.

- Modeling earthquake-induced water pressure in navigation locks.

- Modeling the seismic response of nuclear power stations.

- Modeling the earthquake-induced excitation for foundation-structure-reservoir interaction effects.

- Modeling the response of the concrete face of rock-filled dams.

4.8 Professor Zhang, Chuhan, Tsinghua University, China

Professor Zhang, Chuhan has been engaged in earthquake engineering research on dams since the Hsinfengjiang concrete dam in China was severely damaged in a 1962 earthquake. A summary of R&D activities at Tsinghua University is:

- Preliminary design of the Laxiwa arch dam (250 m high).

- Feasibility study of the Yunnan Province arch dam (290 m high).

- Numerical modeling of the infinite canyon and dam-foundation-reservoir system.

- Effects of radiation damping and inertial mass of the canyon on arch dam response.

- Effects of nonuniform input and wave propagation on arch dam response.

- Numerical modeling of reservoir sedimentation based on Biot's saturated porous theory and effects on arch dam response.

- Seismic cracking analysis of concrete gravity dams using fracture mechanics.

- Numerical modeling of dynamic behaviors of Roller-Compacted Concrete (RCC) gravity dams including effects of layering.

- Dynamic tests of RCC specimen cut from concrete layer from the field.

- Development of numerical model for static and dynamic stability analyses of RCC.

- Dynamic modeling of arch dam abutments, 3-D discrete element model for evaluation of seismic safety of arch dam abutments.

- Field measurement and numerical simulations of the rocky slope stability using explosive techniques.

4.9 Public Works Research Institute, Ministry of Construction, Japan

The Public Works Research Institute (PWRI) has been active in the areas of earthquake engineering R&D of concrete and steel hydraulic structures. PWRI has been actively involved with the Panel on Wind and Seismic Effects, UJNR, for the exchange of technical information on wind and seismic effects between the U.S. and Japan for the past 24 years. They are presently working with this Panel to organize a new Task Committee for Dam Structures. Some R&D conducted by PWRI includes:

- Seismic design for hydraulic structures.

- Linear and nonlinear dynamic behavior of concrete dams.

- Strong motion observation of dams.

- Dynamic interaction of dams including dam-foundation interaction and dam-reservoir interaction.

- Seismic design of steel gates.

4.10 Swiss Federal Office for Water Economy, Division of Safety of Dams.

The Swiss government performs earthquake engineering R&D through in-house resources and contracts to universities. Their current earthquake engineering R&D in hydraulic structures is summarized:

- Development of a nonlinear analytical method of analysis accounting for effects of interactions between reservoir, foundation, and concrete dams.

- Creation of a strong-motion instrumentation network including a free-field network of 33 accelerographs and a network of 29 accelerographs on four different dams.

4.11 ANATECH Research Corp., Lajolla, CA

ANATECH has been performing earthquake engineering R&D for the Electric Power Research Institute and the California Department of Transportation. The following is a brief list of ANATECH's earthquake engineering R&D:

- Modeling of the earthquake-induced excitation accounting for foundation-structure-reservoir interaction effects.

- Modeling the response of the dam-foundation structure to determine the ultimate capacity of the dam with respect to the concrete and dam-foundation interface strengths and material properties.

- Developing analytical models with field and physical model verification.

- Developing extensive earthquake analysis tools, including pre- and postprocessing design aids.

4.12 University of Texas at Austin, TX

The University of Texas at Austin and the Ferguson Structural Engineering Laboratory have been active in research related to earthquake engineering. Their work has not been directly related to hydraulic structures but they have conducted research for concrete and steel structures which could be applicable to hydraulic structures as well. The following is a summary list of their R&D activities:

- Behavior of slab-beam-column joints under simulated seismic loads.

- Behavior of columns under uni- and bi-directional cyclic loadings.

- Development of technical data for design of rehabilitation work on inadequate existing buildings.

- Behavior and design studies of welded connections in steel systems subject to simulated seismic loading.

- Behavior and design of connections in composite frame systems under monotonic and cyclic loading histories.

- Soil-structure and soil-dynamic studies.

4.13 Applied Technology Council, Redwood City, CA

The Applied Technology Council (ATC) is a nonprofit corporation established in 1971 through the efforts of the Structural Engineers Association of California. The purpose of ATC is to assist the design practitioner in structural engineering and related fields in keeping abreast of and effectively using technological developments. ATC has worked with the CE by giving seminars on post-earthquake building evaluation.

4.14 Southeast Missouri State University, Cape Girardeau, MO

The Center for Earthquake Studies at Southeast Missouri State University has a partnership with the Missouri State Emergency Management Agency for dissemination of earthquake risk and preparedness information to governments, schools, businesses, health-care facilities, and the general public.

5. COMMENTS ON EERP PRIORITIES

The survey indicated that the priorities developed for EERP are important and applicable to current dam safety issues. The Bureau of Reclamation provided the following comment: "We feel the proposed research noted in your memorandum is vital to our industry and applaud your efforts." Dr. Yusof Ghanaat of Quest Structures states, "The research topics identified by the CE include specification of seismic input, modeling of nonlinear response behavior, and verification of analytical procedures with field and model tests. These constitute essential research needed to perform a realistic analysis for seismic safety evaluation of the hydraulic structure."

6. CONCLUSION

The results of CERF's survey have identified ongoing or planned research which will assist the CE in locating partners to conduct the necessary R&D to develop state-of-the-art earthquake design and analysis tools for all aspects of concrete dams and appurtenant structures. This will also result in the elimination of the duplication of any earthquake engineering R&D which is being performed by other organizations. This worldwide review of the EERP's priorities assures the CE of having a well-developed earthquake engineering R&D program.

7. ACKNOWLEDGMENT

We gratefully acknowledge permission from the Chief of Engineers to publish this paper.

8. REFERENCES

1. Roper, W.E., Hynes, M.E., and Davidson, R.F. (1992). "U.S. Army Corps of Engineers Earthquake Engineering Research Program, "Wind and Seismic Effects Proceedings of the 24th Joint Meeting."

2. Hall, R.L., and Roper, W.E. (1993). "Corps of Engineers Research Program on Concrete Dams, "Wind and Seismic Effects Proceedings of the 25th Joint Meeting."

3. CERF (1993). "Civil Works Structural Engineering Seismic Research Study," Vol 1.

Table 1. Organizations and Research Areas of Interest

Organization	Research Areas of Interest			
	Concrete Dams A	Outlet Structures B	Analysis Tools C	Public Information D
National Center for Earthquake Engineering Research	X	X	X	
Bureau of Reclamation	X	X	X	
University of California, Berkeley	X	X	X	
Dr. Ray W. Clough, Structures Consultant	X	X	X	
Agbabian Associates	X	X		
Quest Structures	X	X		
Hohai University, China	X	X		
Tsinghua University, China	X			
Public Works Research Institute, Japan	X	X	X	
Swiss Division of Safety of Dams	X			
University of Texas at Austin			X	
ANATECH Research Corp.	X	X	X	
Applied Technology Council				X
Southeast Missouri State University				X
National Science Foundation	X	X	X	
National Institute of Standards of Technology			X	
Naval Civil Engineering Laboratory			X	
North Carolina State University	X			
Washington University	X	X	X	
Tokyo Electric Power Services, Japan	X		X	

Damage and Behavior of Dams During the 1993 Kushiro Oki Earthquake and the 1993 Hokkaido Nansei Oki Earthquake

by

Akira Nakamura[1], Nario Yasuda[2], and Tomoya Iwashita[3]

ABSTRACT

In 1993, two large earthquakes with a magnitude of 7.8 occurred near Hokkaido in Japan, severely damaging public works facilities in the area. The 1993 Kushiro Oki Earthquake damaged the upstream slope protection and the ground slope of the Mombetsu Dam slightly. The 1993 Hokkaido Nansei Oki Earthquake caused moderate damage to the Niwa-Ikumine Dam. The liquefaction of the lower part of the dam body and the riverbed deposit under the dam caused settlement, cracking, and bulging of the upstream slope of the dam body. Slight damage was caused at the Pirika Dam and the Makomanai Dam. At some other dams, the both earthquakes increased the amount of leakage or the turbidity of the leakage water.

This paper begins by describing the damage and effects on these dams. Next, with the results an analysis of the acceleration records observed at the dams during the earthquakes, we present the relationship between the maximum acceleration or predominant period and the epicentral distance and the acceleration response amplification factor at the crest for each dam type. The results show that, for a certain distance, the attenuation of the maximum rock acceleration conforms closely to the attenuation formula for rock mass proposed after Tamura and Okamoto.

KEYWORDS: Dam; Earthquake Damage; Observed Earthquake Motions;
The 1993 Hokkaido Nansei Oki Earthquake;
The 1993 Kushiro Oki Earthquake

1. INTRODUCTION

Hokkaido in Japan was attacked by two earthquakes in 1993. The first was the 1993 Kushiro Oki Earthquake of January 15, and the second was the 1993 Hokkaido Nansei Oki Earthquake which occurred about 6 months later on July 12. The magnitude of both earthquakes was 7.8. The 5th or 6th degree on the seismic intensity scale was observed close to the epicenters of the two earthquakes by the Japanese Meteorological Agency (J.M.A.). They resulted in severe damage: human casualties, the destruction of dwellings, and damage to public works facilities. The total damage exceeded 50 billion yen and 160 billion yen respectively. Some dams were either damaged or suffered slight effects. This paper describes the dams damaged and effected by the two earthquakes and the behavior of the dams during the earthquakes.

2. OUTLINE OF THE EARTHQUAKES

2.1 The 1993 Kushiro Oki Earthquake

The 1993 Kushiro Oki Earthquake was a magnitude 7.8 earthquake with its hypocenter located at a focal depth of 107 kilometers and over 10 kilometers offshore from the City of Kushiro. The Kushiro Meteorological

1) Head, Fill-type Dam Division, Public Works Research Institute, Ministry of Construction, Tsukuba City, Japan
2) Head, Planning Division, ditto (Former Senior Research Engineer, Fill-type Dam Division)
3) Research Engineer, Fill-type Dam Division, ditto

Observation Station observed it as a violent earthquake with the 6th degree on the J.M.A. seismic intensity scale. A total of 968 persons in Hokkaido suffered from this earthquake, and damage to public works facilities amounted to approximately 21 billion yen.

2.2 The 1993 Hokkaido Nansei Oki Earthquake

The 1993 Hokkaido Nansei Oki Earthquake was a magnitude 7.8 earthquake with its hypocenter at a focal depth of 34 kilometers and about 80 kilometers offshore to the south-west of Shiribeshi-Province Suttsu-cho. Several meteorological observation stations facing the Japan Sea near the epicenter observed it as a strong earthquake with the 5th degree on the J.M.A. seismic intensity scale. Giant tsunami induced by this earthquake caused a total of 552 casualties including 202 fatalities. The damage to public works facilities amounted to about 79 billion yen.

3. DAMAGE AND EFFECTS ON DAMS

3.1 Damage and Effects on Dams Caused by the 1993 Kushiro Oki Earthquake

Emergency inspections of the dams were conducted immediately after the earthquake, but because it was the coldest period of the winter, snow was piled up on the dam bodies and the surrounding ground, so detailed visual inspections were not possible. After the spring thaw, staff from the dam control office conducted an inspection. The inspection revealed that only the Mombetsu Dam suffered slight damage. At the Mombetsu Dam, part of the concrete facing blocks forming the slope protection on the upstream side of the dam body were raised, but no deformation was found which would have any effect on the stability of the dam.

After the earthquake, the amount of leakage water increased at three dams (Kanoko Dam, Tokachi Dam, and Samani Dam), and the turbidity of the leakage water increased at three dams (Samani Dam, Takami Dam, Niikappu Dam), but after a period ranging from a few hours to a few months, the leakage water at the dams returned to its pre-earthquake state. Fig.1 shows the change over time of the amount of leakage water at the Kanoko Dam. Generally, temporary changes in the amount of leakage water at dams after earthquakes have been observed in the past, but it is assumed that this does present particular problems as long as the change is not extremely large and increased leakage does not persist. Fig.2 shows the locations of dams where the above damage and effects occurred.

No dam with a height of 15 meters or more was located within about 100 kilometers of the epicenter. Therefore, damage and effects to dams was small considering the strength of the earthquake. The following describes the damage to the Mombetsu Dam in detail.

3.1.1 Mombetsu Dam

The Mombetsu dam is a homogeneous earthfill dam managed by the Mombetsu Land Improvement District. Fig.3 and 4 are the plane diagram and a typical cross-section of the dam. Concrete facing blocks have been placed on the upstream slope of the dam body to protect the dam from wave action. The geology of the dam site consists of mudstone in a Kasai Formation, the Takigawa Group of the Pliocene Series, the Neogene System, and includes fine sandstone and siltstone. The dam body consists of material excavated from the dam foundation and soil from the weathered mudstone at downstream ground of the left bank. The dam is 180 kilometers from the epicenter.

After the earthquake occurred, the dam staff conducted an inspection, but the reservoir surface was covered with a thick frozen layer, preventing the inspectors from determining the full extent of the damage. In February, they confirmed that there was water leaking from the dam body drain. Soon after the spring thaw in April, they conducted a second inspection

after removing all the water from the reservoir. This confirmed that the upstream slope of the dam body, and the ground slope on the left bank were deformed.

The deformation of the dam body was found at protective facing blocks which overlapped one another and rose up about 10 centimeters along the entire dam axis directly below the elevation where the gradient of the upstream slope changed from 1:2.5 to 1: 2.0 (EL. 87.50 meters and with a reservoir water level of EL 89.0 meters at the time of the earthquake) (Photo.1). It is believed the earthquake caused the top 1/3 of the dam body to settle, applying compressive force in the slope direction on the facing blocks causing them to buckle. When the inspectors removed the deformed facing blocks to check the surface of the earthfill dam, they concluded that there was no deformation in the body, and that the safety of the dam was unaffected. Generally, in a case where the dam body of a fill dam is surfaced with material such as concrete blocks, because their stiffness is different from that of the dam body, this kind of facing cannot follow the deformation of the dam body during an earthquake, with the result that the facing is deformed.

Undulating deformation was seen on the facing blocks close to the intake pipe on the upstream concrete part of the left bank (Photo.2)

3.2 Damage and Effects on Dams Caused by the 1993 Hokkaido Nansei Oki Earthquake

Immediately after the earthquake, staff of dam offices performed emergency inspections of a total 52 dams: 6 dams owned by the Ministry of Construction (M.O.C.), 11 dams subsidized by the M.O.C., and 35 other dams used for water utilization. The inspection revealed that among dams with a height of 15 meters or more, the Niwa-Ikumine Dam suffered moderate damage. Minor damage was discovered at the Pirika Dam and the Makomanai Dam, but it was not severe enough to effect the safety of these dams.

Immediately after the earthquake, increase in leakage water was observed at six dams (Pirika Dam, Jozankei Dam, Okusawa Dam, Sasanagare Dam, Kamiiso Dam, Shimoyu Dam), and the amount of leakage water decreased at 2 dams (Asari Dam, Subari Dam). Fig.5 shows the change over time of the amount of leakage water at the Jozankei Dam. The turbidity of leakage water increased at the Subari Dam. However, these changes in leakage water were not considered to indicate serious problems, because the leakage water returned to its pre-earthquake state within a period ranging from a few days to a few weeks. The surface displacement of the Kamiiso Dam changed a little, while at other dams (Pirika Dam, Shiriuchi Dam) the width of the cross joints was slightly altered, but in all cases the displacement was small, and the deformation does not seem to cause any safety problems. Fig.6 shows the locations of dams where the above damage and effects were discovered.

Furthermore, two small irrigation ponds with dikes less than 15 meters high located only 65 and 70 kilometers from the epicenter in Setana-cho in Hokkaido were destroyed. And along the Japan Sea Coast near the epicenter, some dikes of this kind were damaged by settlement or cracking.

The following is a detailed description of damage and effects suffered by the Pirika Dam, the Niwa-Ikumine Dam, and the Makomanai Dam.

3.2.1 Pirika Dam

The Pirika Dam, which is managed by the Construction Department of the Hokkaido Development Agency, is a combined dam consisting of a concrete gravity dam and a rockfill dam. Fig.7 and 8 are a section diagram of block 39 in the concrete dam section and a downstream surface diagram of the Pirika Dam. This dam is located 89 kilometers from the epicenter.

As Fig.9 and 10 show, in the structure between block 0 of the concrete dam body and the connecting corridor leading to the control office, the floor panel concrete of the connecting corridor was pushed up and spalled over a length of about 1.5 meters due to compression in the axial direction of the dam. The spalling is shown in Photographs 3 and 3.4 and in Fig.11. Slight concrete spalling was also discovered in other cross joints of the connecting corridor. This connecting corridor rides on the rock zone of the core wall connected perpendicularly to the concrete dam body, so it was subjected to severe compression caused by differences in the earthquake response of the dam body and the rock zone. Because the connecting corridor and the concrete dam body are completely separated structurally and there was no deformation of the inspection gallery in block 0, the deformation did not effect the dam body itself.

Above the previously mentioned connecting section, the surface paving of the crest road settled, and a gap was formed on the connection to the upstream railing (Photo.4). And at a nearby location in the park plaza above the connection between block 0 of the concrete dam and the left bank core wall, part of the block surface was lifted (Photo.5). The locations of these deformations are shown in Fig.9 and 10. All these deformations were caused by unequal behavior of the concrete dam body and the backfilled soil above the connecting corridor or the rock zone of the core wall at the left bank. And when the block pavement was restored by removing mortar and base material, a slight unevenness was revealed on surface of the core wall on the left bank. So as a precaution, rolling compaction was performed. This unevenness, however, is considered to be a result of initial execution work instead of an effect of the earthquake.

After the earthquake, water leaked from the intersection of the inspection gallery and the blocked section of the temporary diversion channel inside the dam on the block 28. This section was sealed after leakage was observed from it during the previous test filling, but up till the time of the earthquake, no leakage was observed at the sealing, so it is considered that the earthquake opened a small gap in the sealing, causing another leakage. Fig.12 shows changes over time in the amount of leakage. The amount has been small, only between 80 and 100 milliliters per minute since 10 days after the earthquake, and it was not turbid, so the leakage is not considered to be a serious problem.

The water leakage from both foundations and cross-joints of the two zones of the divided concrete dam body (AW-1: Blocks 1 to 34, AW-2: Blocks 35 to 47) is collected and that from the fill dam section is also collected by a drain pipe installed at the end of the downstream filter. Fig.13 shows changes over time in the amount of water leakage before and after the earthquake. At the time of the earthquake, the amount of water leakage from the concrete dam declined only about 0.8 liters per minute and that from the fill dam body rose by 4.7 liters per minute, but the change was small, and it returned to its normal level after a few days, so it is not a problem.

The width of the joint aperture in the inspection gallery ranged from 0.85 to 0.6 millimeters before and after the earthquake (June 29 - July 13). After the earthquake, many of the joints closed and traces of the ejection of rusty water were found at many joints in the inspection gallery of the concrete dam.

3.2.2 Niwa-Ikumine Dam

The Niwa-Ikumine Dam is a central core type earthfill dam managed by the Kita-Hiyama Land Improvement District. It is an old dam, completed 66 years ago in 1927, and rehabilitated in 1934 and 1961. Fig.14 are a typical section diagram of the dam. This dam was not provided with a seismograph or water leakage observation equipment. However, considering that it is located 70 kilometers from the epicenter, that a maximum

acceleration of 114gal was recorded in the foundation bedrock of the Pirika Dam, which is 89 kilometers from the epicenter, and that the foundation rock of the both dams belongs to the same Setana Formation, the acceleration at the Niwa-Ikumine Dam was likely higher. By substituting a magnitude 7.8 and an epicentral distance of 70 kilometers into the distance attenuation formula of maximum acceleration after Tamura and Okamoto, we obtain the maximum acceleration 188gal, and it is estimated that the rock at the Niwa-Ikumine Dam site quaked at an acceleration of about 200gal.

Photo.6 shows the damage to the dam body three days after the earthquake. And Fig.15 is a plane diagram of the dam body showing an outline of the damage. The earthquake caused bulging and cracking of the dam body at two elevations, and undulating deformation of the upstream slope. The bulging appeared in the middle and close to the toe of the upstream slope (Elevation EL.90.90 meters, or about 50 centimeters below the water level at the time of the earthquake, EL.91.35 meters). The maximum level difference of the bulge at the toe of the slope was about 1 meter over the 40 meter length (Photo.7). As shown in Fig.15, the cracking consisted of five longitudinal cracks at the crest of the dam. The longest crack extended for a total length of approximately 120 meters on the crest at a depth of two meters. It settled on the upstream side, and its maximum level difference was about 1 meter (Photo.8). Fig.16 is a 10-meter interval section diagram of the dam body from where cracks formed at a point 80 meters from the right bank spillway, which corresponds almost exactly to the center of the dam. And a 60-centimeter deep crack was formed at an elevation of about 2 meters above the bulge near the toe of the upstream slope. Also, several cracks were formed with a sand boil extending from the sand stratum in a sedimentary mound at the bottom of the reservoir near the toe of the upstream slope.

The day after the earthquake, the District used an underwater pump to drain the water (water depth at the time of the earthquake was about 4 meters). It was completely drained by the morning of July 21. Believing that there was a degree of partial loosening on the upstream side of the dam body, they faced a safety control problem: if a flood occurred, it would be difficult to release the water to prevent the reservoir water level from rising by using only the inclined and the bottom intake drain pipe (drain capacity of $2.5m^3/s$). Therefore, on July 26, the District began an emergency excavation at the left side of the dam body to open a channel with a bottom width of 2 meters and a section area of 3 square meters, to provide discharge capacity of 10.9 cubic meters per second (About 5,500 cubic meters of the dam body was excavated).

And at the same time, they carried out emergency repair work on the dam body by pouring lime into the cracks on the crest, and roller compacting it with a heavy compactor. This emergency work was completed on August 6. The water channel that they excavated is shown in Photographs 9. It was difficult to visually confirm the sliding surface on the excavated slope surface.

As a result of later consultation with the river authorities, the dam body embankment would be removed, and new headworks would be installed.

At a point shown in Fig.15, boring inspections and Swedish sounding tests carried out. The dam body is an embankment on the riverbed deposit between 4 and 5 meters thick, and a Setana Formation composed of sandstone with a low degree of consolidation is found under that. The dam body consists of core zones of clay mixed with pebbles and silt-and-sand-zones mixed with pebbles, and core zones separate into two zones of center core and upstream slope core. Silt-and-sand-zone is extremely loose with N value between 2 and 4 and compaction degree of a 81%. The riverbed deposit consist of loose sand or sand mixed with pebbles with N value between 3 and 8 and gravel with N value about

20.

It is believed that the earthquake caused the silty sand zone of the upstream side part of the dam embankment to occur liquefaction and the dam body to settle, because the zone consists of loose sand and is saturated with water owing to the location between two core zones.

3.2.3 Makomanai Dam

The Makomanai Dam is a central core type rockfill dam with a height of 34 meters managed by the Agricultural and Fisheries Department of the Hokkaido Development Agency. It was completed in 1987, and located 66 kilometers from the epicenter. This dam was not provided with seismographs.

The earthquake caused settlement of the dam body and bulge of the lower part of the body. So, the concrete frame of the upstream slope had been deformed ,and the joints of it had been slightly broken. Several cracks had been caused at the sprayed concrete in front of the overflowing wall of the spillway. The facing concrete blocks on the right bank had undergone undulating deformation. None of these damages presented any particular problems related to the safety of the dam body.

4. EARTHQUAKE MOTIONS OBSERVED AT DAM SITES

Records of acceleration in the dam bodies and at the dam sites were obtained at 15 dams in Hokkaido and at 26 dams in the Tohoku region during the 1993 Kushiro Oki Earthquake, and at 10 dams in Hokkaido and 19 dams in the Tohoku region during the 1993 Hokkaido Nansei Oki Earthquake. The locations of these dams are shown in Fig.2 and 6.

The attenuation of the maximum accelerations at dam site rock with epicentral distance during the two earthquakes, are shown in Fig.17 and 18 respectively. Where dam site rock includes the dam foundation rock or the rock in the ground of both banks, and in the case of a fill dam, because an inspection gallery is excavated in the foundation bedrock, the filldam inspection gallery is included. Within the figures, a broken line represents a magnitude 7.8 earthquake for the attenuation of the maximum accelerations formula after Tamura and Okamoto(1979). This attenuation formula was based on seismic records observed at underground rock within an epicentral distance of 280 kilometers, but records of the 1993 Kushiro Oki Earthquake provide values that tend to be smaller than those of the attenuation formula at dams less than 300 kilometers from the epicenter and larger at dams further than 300 kilometers from the epicenter. In the case of the 1993 Hokkaido Nansei Oki Earthquake, up to an epicentral distance of about 400 kilometers, the attenuation is extremely close to that provided by the attenuation formula after Tamura and Okamoto.

Fig.19 and 20 show the relationship between the predominant period of the seismic vibration in the dam site rock and the epicentral distance for both earthquakes. And within the figures, a dotted line shows the assessable line of a predominant period after Seed *et al.*(1968) with a magnitude of 7.8.

The maximum acceleration at the dam foundation (the foundation or the inspection gallery) and the ratio of the maximum acceleration at a crest to that at a foundation, in other words its relationship with the acceleration response amplification ratio for both earthquakes are shown in Fig.21 for fill dams, and in Fig.22 for concrete gravity dams and concrete arch dams. Within the figures, cases of other earthquakes are also shown. In the case of any earthquakes, the response amplification ratio ranged from 2 to 8 for filldams and from 1 to 9 for concrete gravity dams. The response amplification ratio was larger in the case of concrete arch dams, ranging from 6 to 13, and in some cases, as high as 18. Overall, the response amplification ratio for the upstream–downstream component

tended to be larger than that for the dam axial component.

5. EARTHQUAKE ACCELERATION RECORDS OF TYPICAL DAMS

5.1 Acceleration Records During The 1993 Kushiro Oki Earthquake

The following is a report on the results of analyses of acceleration records from three typical dams where the maximum acceleration observed at the crest exceeded 60gal.

5.1.1 Kanoko Dam

The Kanoko Dam is a concrete gravity dam with a height of 55.5 meters, located 116 kilometers from the epicenter. Seismographs were installed at three locations, a low elevation in the dam body (A1), a middle elevation in the dam body (A2), and the crest (A3). These locations are shown on Fig.23 and 24: a typical section diagram and a downstream surface diagram of the dam. The geology of the dam foundation rock consists of pyroxene andesite in the Pliocene Series, the Neogene System. The maximum accelerations recorded in the up-downstream direction were 23.1gal at A1 and 64.9gal at A3. The predominant frequency of the power spectrum of the acceleration was in the low frequency zone of 2Hz or less for A1, while for A3, the frequency was close to 6Hz, except for the dam axial direction. Fig.25 shows the Fourier spectrum ratio or frequency response function (The Parzen Window with a band width of 0.4Hz was executed.) of the up-downstream direction component of A1 and A3. From this figure, the fundamental natural frequency is 6.4Hz, a value smaller than 8.2Hz of the natural frequency theoretically obtained from a bending vibration of a cantilever element under storing in the reservoir.

5.1.2 Tokachi Dam

The Tokachi Dam is a rockfill dam with a height of 84.3 meters, and located 125 kilometers from the epicenter. Seismographs were installed at four locations, in the inspection gallery (A1), inside the core (A2), on the crest (A3), and in the left-bank ground (A4). These locations are shown on Fig.26 and 27: a typical section diagram and a longitudinal section diagram. The geology of the dam foundation rock consists of slate, sandstone, and diabase in the Upper Cretaceous System, and while on the right bank, includes keratophyre. The maximum accelerations recorded in the axial direction of the dam were 34.9gal at A1 and 120gal at A3. The power spectrum of the up-downstream and dam axial direction component accelerations at A3 peaked sharply near 2Hz. Fig.28 shows the frequency response function of the up-downstream direction component. From this figure, the fundamental natural frequency is 2.0Hz, and this is in the range of 1.8 ~ 3.4Hz obtained from the empirical formula of natural frequency for rockfill dams as the result of earthquake observations and vibration tests after Okamoto(1984).

5.1.3 Takami Dam

The Takami Dam is a rockfill dam with a height of 120 meters, and located 149 kilometers from the epicenter. Seismographs were installed at four locations, in the inspection gallery (A1), inside the core (A2), on the crest (A3), and at the toe of the slope of the downstream left-bank (A4). These locations are shown on Fig.29 and 30: a typical section diagram and a longitudinal section diagram. The geology of the dam foundation rock consists of schalstein, diabase schist, and chert in the Iwashimizu Formation of the Hidaka Group. The maximum accelerations recorded in the up-downstream direction were 38.5gal at A1 and 230.6gal at A3. The power spectrum of A3 includes almost no high

frequency constituent of 5Hz or higher, and it peaked sharply. Fig.31 shows the frequency response function of the up-downstream direction. From this figure, the fundamental natural frequency is 1.9Hz, and this is in the range of 1.3 ~ 2.4Hz obtained from the empirical formula of natural frequency for rockfill dams as the result of earthquake observations and vibration tests after Okamoto(1984).

5.2 Acceleration Records During the 1993 Hokkaido Nansei Oki Earthquake

The following is a report on the results of analyses of acceleration records from three typical dams where the maximum acceleration observed at the crest exceeded 60gal.

5.2.1 Pirika Dam

The Pirika Dam is located closer to the epicenter (89 kilometers) than any of the other dams where the time history of the acceleration was recorded. This Dam is a combined dam with a height of 40 meters. At the dam, 3 seismographs were installed: in the inspection gallery, (A1), at the crest (A2) in block 39 of the concrete dam body section, and at the foundation rock under block 14 (A3). These locations are shown in Fig.7 and 8: a section diagram of block 39 in the concrete section and a diagram of the downstream surface of the dam. The maximum accelerations recorded in the up-downstream at A1 and A2 were 122.8gal and 142.2gal respectively. The principal motion began about 12 seconds after the initial motion, and continued for about 60 seconds. The maximum acceleration of the horizontal direction component appeared about 43 seconds after the initial motion. The predominant frequency of the power spectrum of the horizontal direction component ranged between 1.2 and 1.8Hz at all points. Fig.32 shows the frequency response function of A2 to A1 of the up-downstream direction component. In this figure, the frequency response function is lined without a peak that indicates the natural frequency, within the range of 12Hz or less. The response was not amplified at the crest of the Pirika Dam because, not only is this dam low, the ratio of the elastic modulus of the foundation rock to that of the dam body concrete (Ed), Ef/Ed, is small at approximately 1/40, and as Fig.8 shows, the alternative beds of mudstone and shale (Shm) that form the foundation rock for a concrete gravity dam have an elastic modulus (Ef) of 700MPa, and as foundation rock for a concrete gravity dam, is comparatively soft rock.

5.2.2 Asari Dam

The Asari Dam is a concrete gravity dam with a height of 73.9 meters, and is located 155 kilometers from the epicenter. Seismographs were installed at two locations: on the inspection gallery (A1), and on the crest (A2). These locations are shown on Fig.33: a diagram of the downstream surface of the dam. The maximum accelerations recorded in the up-downstream direction were 15.1gal at A1 and 68.9gal at A2. The predominant frequency of the power spectrum of the acceleration was, in the horizontal component of A1, in the low frequency range of 1Hz or lower, but was 6Hz in the up-downstream direction component of A2. Fig.34 shows the frequency response function in the up-downstream direction component. From this figure, the fundamental natural frequency is 6.5Hz, and this approximates the value of 6.2Hz theoretically obtained from a bending vibration of a cantilever element under storing in the reservoir.

5.2.3 Hoheikyo Dam

The Hoheikyo Dam is a concrete arch dam with a height of 102.5 meters, and is located 160 kilometers from the epicenter. Seismographs were installed at three locations: in the lower inspection gallery (A1), in the middle inspection gallery (A2), and on the crest

(A3). These locations are shown on Fig.35 and 36: a typical section diagram and a diagram of the downstream surface of the dam. The dam foundation rock consists of andesite. The maximum accelerations recorded in the up-downstream direction were 9.5gal at A1 and 119.6gal at A3. The power spectrum of the acceleration at A1 peaked in the low frequency zone of 1Hz or lower, but at A3, it peaked sharply at about 3.6Hz. Fig.37 shows the frequency response function of the up-downstream direction component. From this figure, the fundamental natural frequency is 3.8Hz, and this approximates the value of 3.3Hz obtained from the empirical formula of natural frequency for rockfill dams as the result of earthquake observations and vibration tests after Okamoto(1984). Additionally, the acceleration response amplification ratio at the natural frequency was large at approximately 40, the same as the 1993 Kushiro Oki Earthquake. This indicates that a thin-walled structure such as an arch dam considerably amplifies the response.

6. CONCLUSIONS

The study confirms that, aside from old dams and irrigation pond dikes constructed using experience-based construction technology, those dams constructed on rock foundations using modern design and execution technology survived these powerful earthquakes without any adverse effects to maintain their safety, and that they are still in sound condition. The behavior of the dams found by analyzing acceleration records coincided with the findings of empirical formulae.

ACKNOWLEDGEMENTS

The authors wish to express sincere thanks to all those persons from the Tohoku Regional Construction Bureau, the Hokkaido Development Bureau, the Tohoku Regional Agricultural Administration Office, Hokkaido Prefecture, Aomori Prefecture, Akita Prefecture, Iwate Prefecture, Miyagi Prefecture, various dam operation offices, land improvement district offices who provided them with valuable materials and cooperated fully with them during the conduct of this study.

REFERENCES

Okamoto,S. (1984): Introduction to Earthquake Engineering, pp.403-523, University of Tokyo Press.

Seed, H.B., Idriss, I.M. and Kiefer, F.W. (1968): Characteristics of Rock Motions during Earthquakes, p.8, EERC 68-5, U.C. Berkeley.

Tamura,C., Okamoto, S. and Kato, K. (1979): Maximum Rock Accelerations of Earthquake Motions , Proceedings of the 13th JSCE on Earthquake Engineering Symposium, Japan Society of Civil Engineers, pp.181-184. (In Japanese)

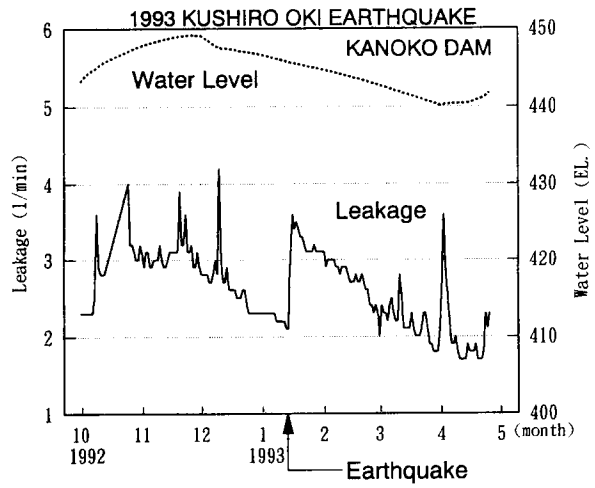

Fig.1 Change Over Time in Amount of Leakage at Kanoko Dam

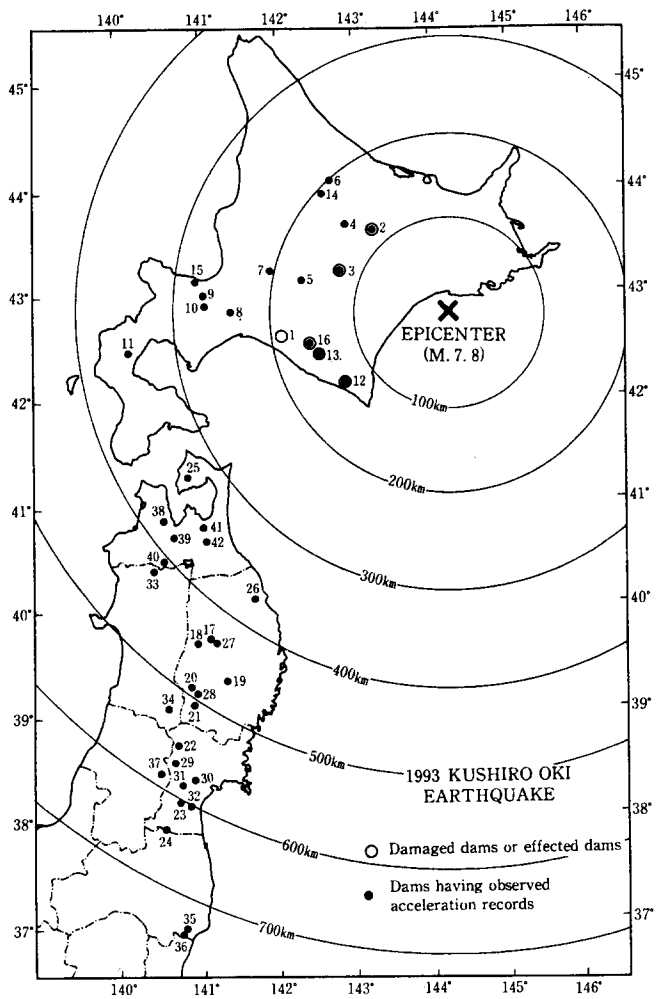

No	DAM NAME
1	Mombetsu Dam
2	Kanoko Dam
3	Tokachi Dam
4	Taisetsu Dam
5	Kanayama Dam
6	Iwaonai Dam
7	Katsurazawa Dam
8	Izarigawa Dam
9	Jozankei Dam
10	Hoheikyo Dam
11	Pirika Dam
12	Samani Dam
13	Takami Dam
14	Aibetsu Dam
15	Asari Dam
16	Niikappu Dam
17	Shijyushida Dam
18	Gosho Dam
19	Tase Dam
20	Yuda Dam
21	Ishibuchi Dam
22	Narugo Dam
23	Kamafusa Dam
24	Shichigasyuku Dam
25	Kawauchi Dam
26	Taki Dam
27	Tsunatori Dam
28	Irihata Dam
29	Urushizawa Dam
30	Minamikawa Dam
31	Nanakita Dam
32	Tarumizu Dam
33	Yamase Dam
34	Minase Dam
35	Takashiba Dam
36	Shitoki Dam
37	Shiramizugawa Dam
38	Odagawa Dam
39	Namioka Dam
40	Hayaseno Dam
41	Shimizume Dam
42	Wada Dam

Fig.2 Location of Damaged or Effected Dams and Dams where Acceleration Records Were Observed from The 1993 Kushiro Oki Earthquake

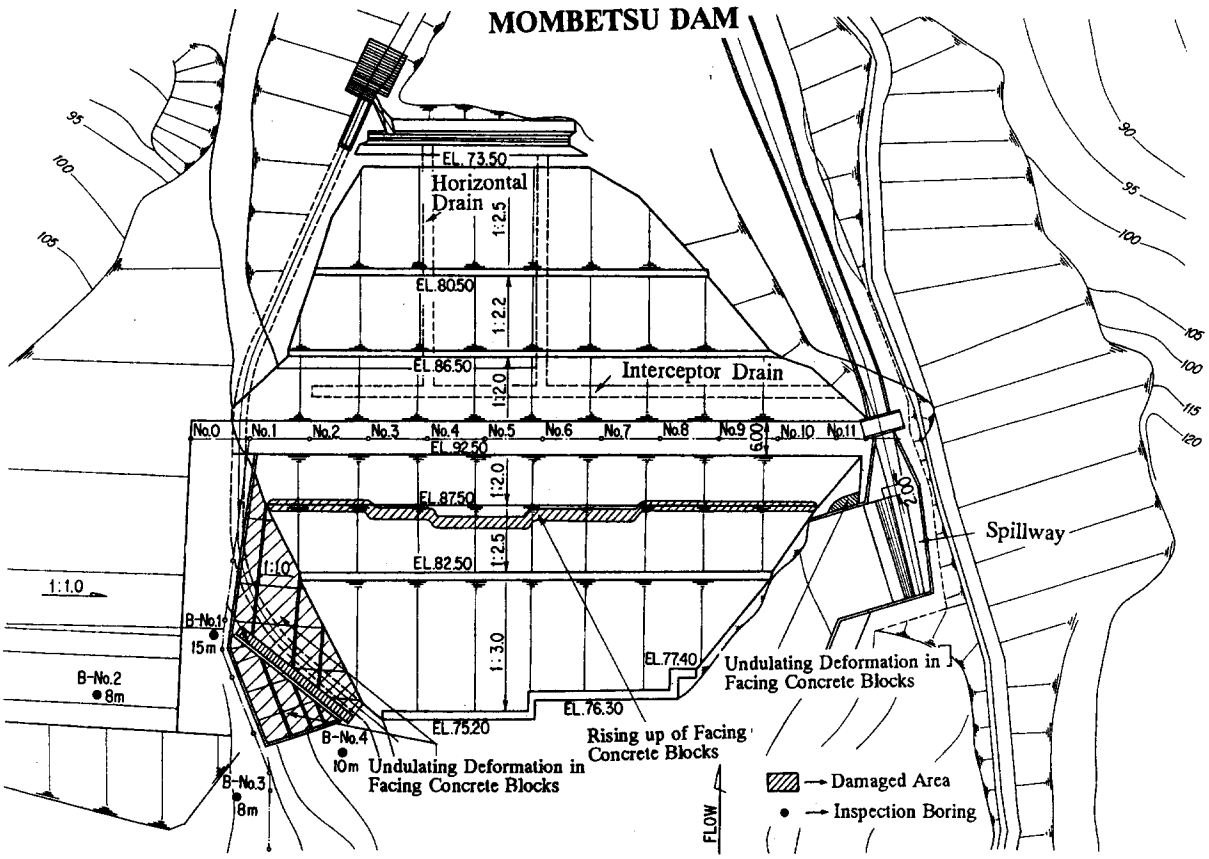

Fig.3 Plane Diagram of Damage Conditions at Mombetsu Dam

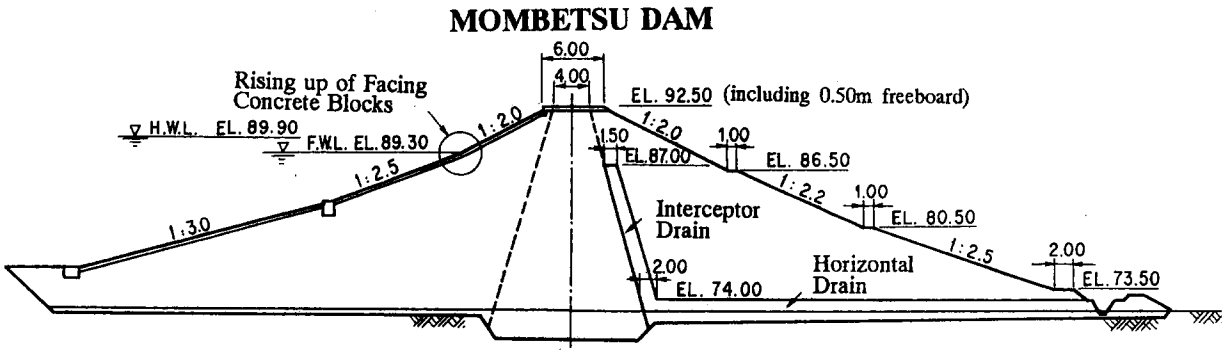

Fig.4 Typical Section Diagram of Damage Conditions at Mombetsu Dam

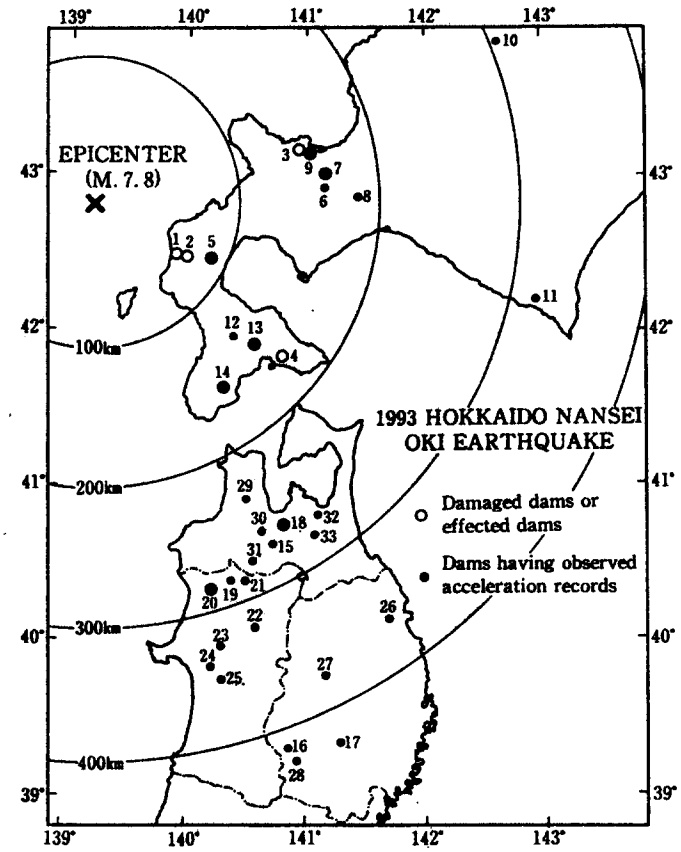

No	DAM NAME
1	Makomanai Dam
2	Niwa-Ikumine Dam
3	Okusawa Dam
4	Sasanagare Dam
5	Pirika Dam
6	Hoheikyo Dam
7	Jozankei Dam
8	Izarigawa Dam
9	Asari Dam
10	Aibetsu Dam
11	Samani Dam
12	Uzura Dam
13	Kamiiso Dam
14	Shiriuchi Dam
15	Aseishigawa Dam
16	Yuda Dam
17	Tase Dam
18	Shimoyu Dam
19	Hayakuchi Dam
20	Subari Dam
21	Yamase Dam
22	Moriyoshi Dam
23	Haginari Dam
24	Asahikawa Dam
25	Iwami Dam
26	Taki Dam
27	Tsunatori Dam
28	Irihata Dam
29	Odagawa Dam
30	Namioka Dam
31	Hayaseno Dam
32	Shimizume Dam
33	Wada Dam

Fig.6 Location of Damaged or Effected Dams and Dams where Acceleration Records Were Observed from The 1993 Hokkaido Nansei Oki Earthquake

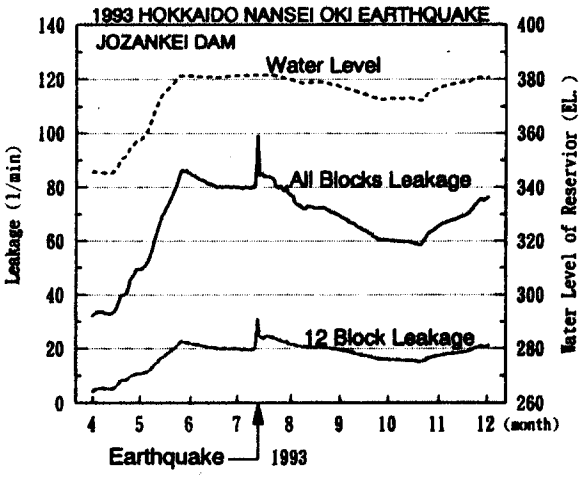

Fig.5 Change Over Time in Amount of Leakage at Jozankei Dam

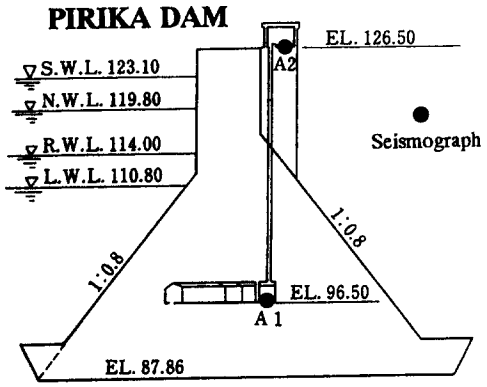

Fig.7 Section Diagram of Block 39 of the Parika Dam Concrete Body

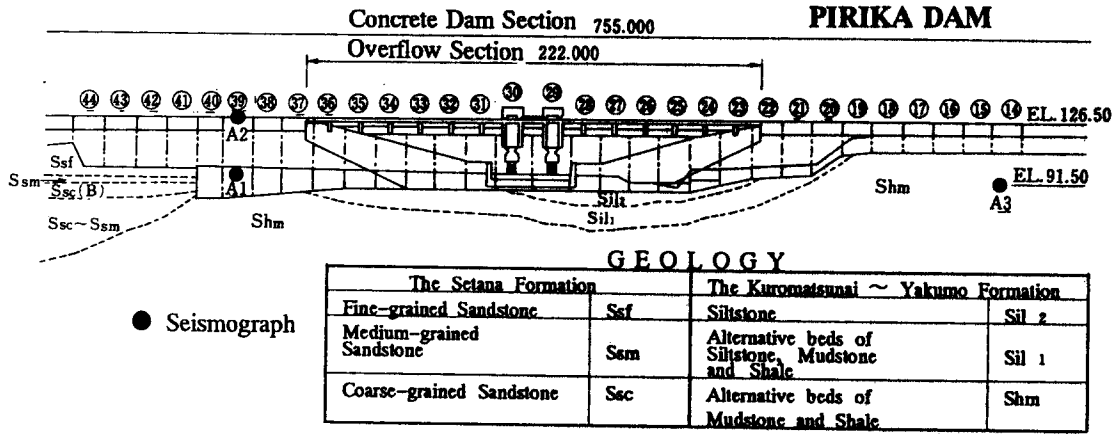

The Setana Formation		The Kuromatsunai ~ Yakumo Formation	
Fine-grained Sandstone	Ssf	Siltstone	Sil 2
Medium-grained Sandstone	Ssm	Alternative beds of Siltstone, Mudstone and Shale	Sil 1
Coarse-grained Sandstone	Ssc	Alternative beds of Mudstone and Shale	Shm

Fig.8 Downstream Section Diagram of the Parika Dam Concrete Body

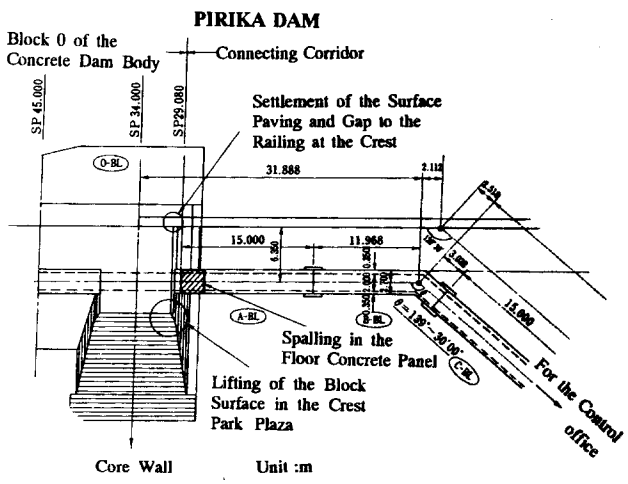

Fig.9 Plane Diagram of Deformed Locations Between Block 0 and the Connecting Corridor at Parika Dam

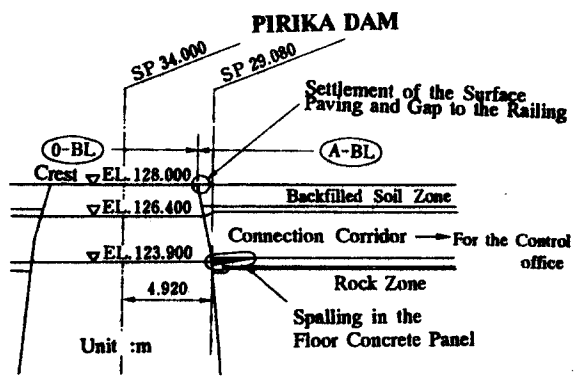

Fig.10 Longitudinal Section of Deformed Locations Between Block 0 and the Connecting Corridor at Parika Dam

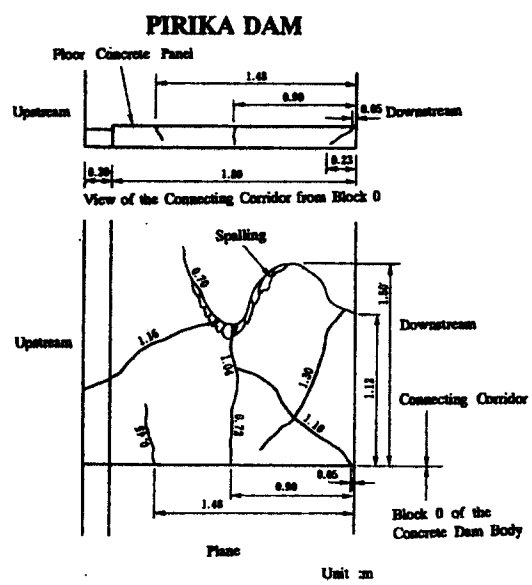

Fig.11 Spalled Cracks of the Floor Concrete in the Connecting Corridor (Parika Dam)

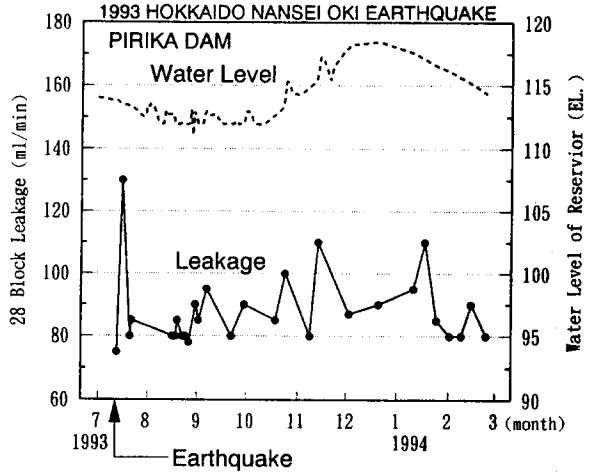

Fig.12 Change Over Time in the Amount of Leakage in the Inspection Gallery at Block 28 of Parika Dam

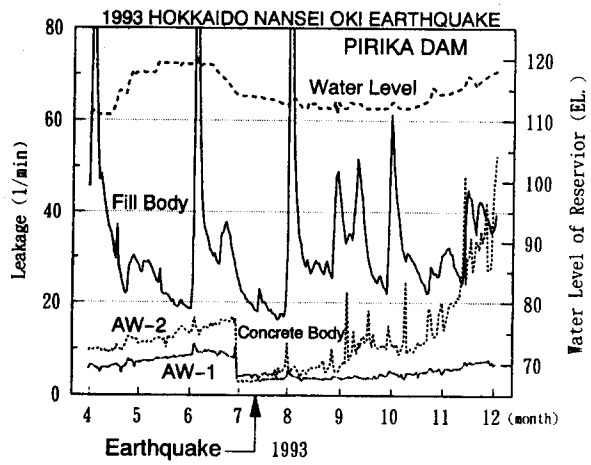

Fig.13 Change Over Time in Amount of Leakage at Pirika Dam

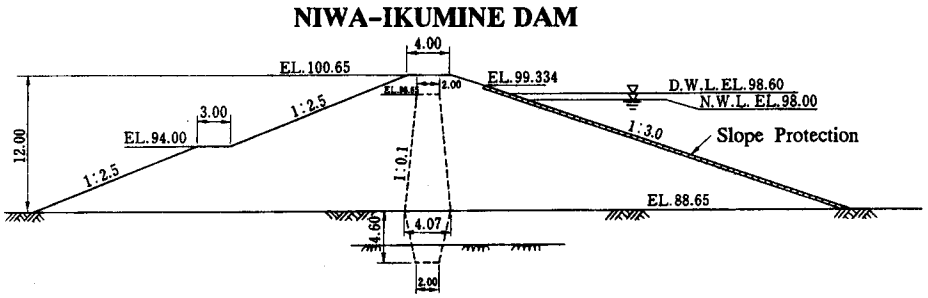

Fig.14 Typical Section Diagram of Niwa-Ikumine Dam

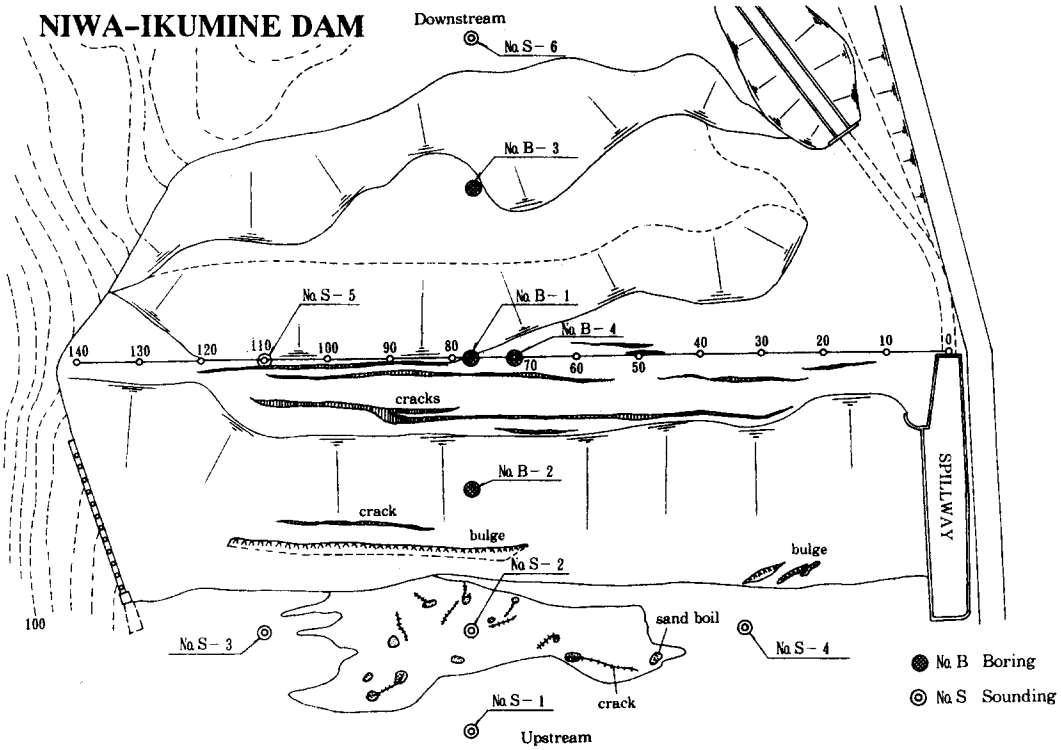

Fig.15 Plane Diagram of Damaged Niwa-Ikumine Dam Body

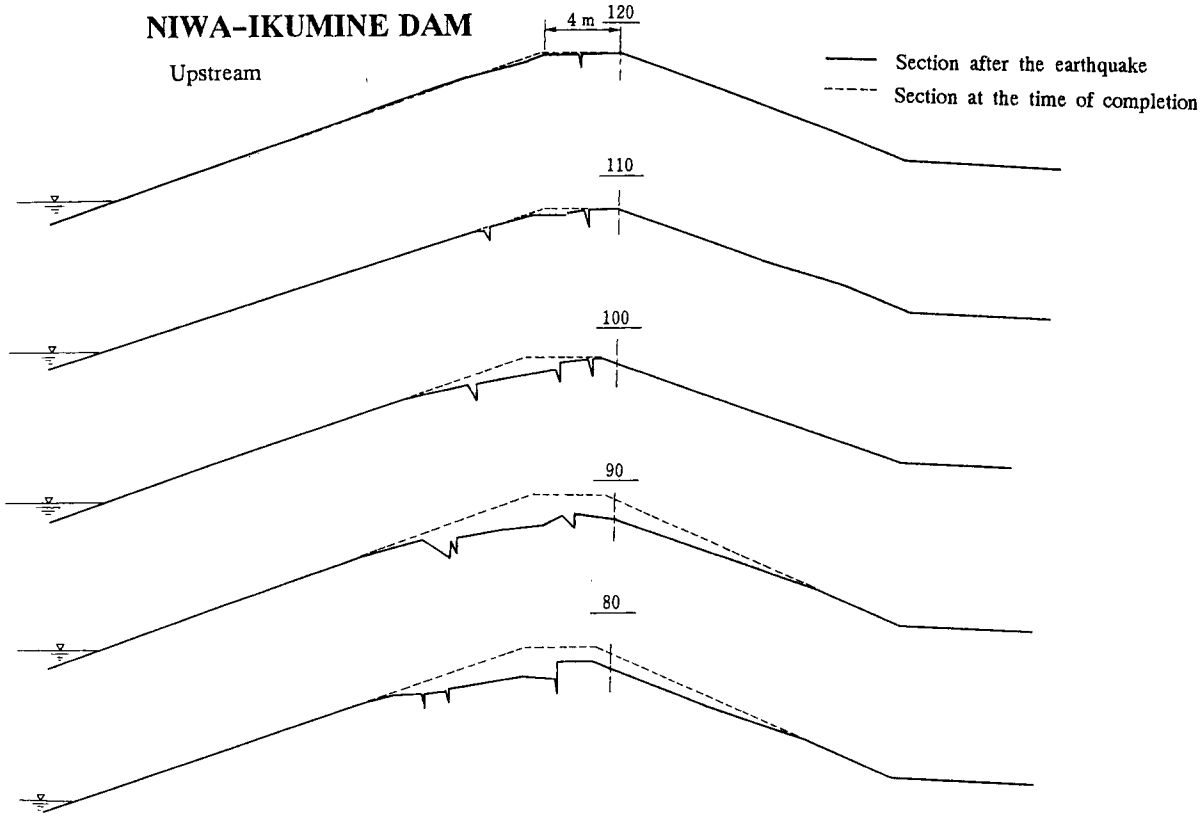

Fig.16 Cross Section Diagrams of the Cracked Niwa-Ikumine Dam Body

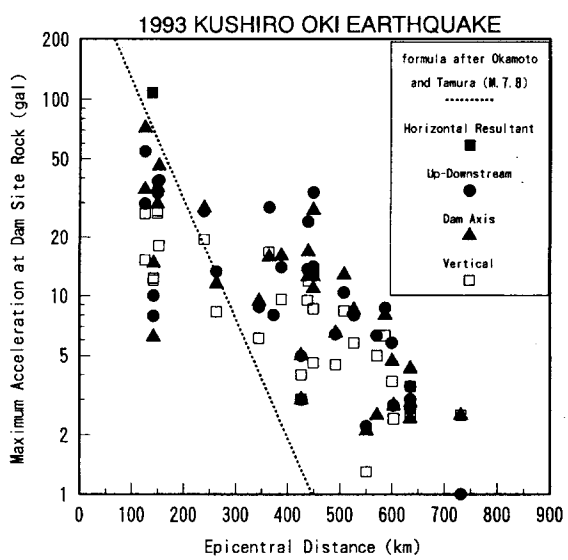

Fig.17 Attenuation of the Maximum Dam Site Rock Acceleration with Epicentral Distance from The 1993 Kushiro Oki Earthquake

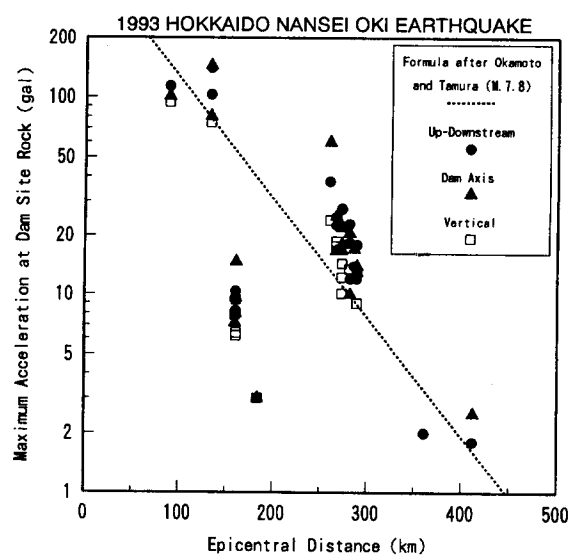

Fig.18 Attenuation of the Maximum Dam Site Rock Acceleration with Epicentral Distance from The 1993 Hokkaido Nansei Oki Earthquake

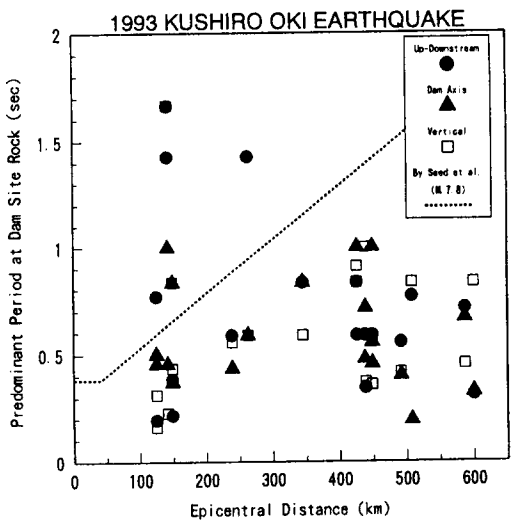

Fig.19 Relationship Between the Predominant Period of Earthquake Motion at Dam Site Rock and Epicentral Distance from The 1993 Kushiro Oki Earthquake

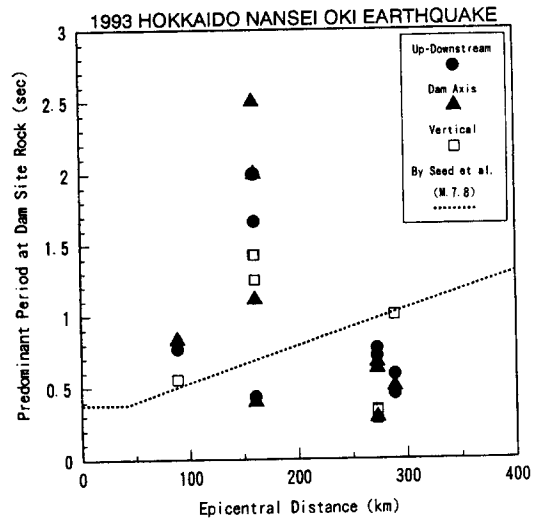

Fig.20 Relationship Between the Predominant Period of Earthquake Motion at Dam Site Rock and Epicentral Distance from The 1993 Hokkaido Nansei Oki Earthquake

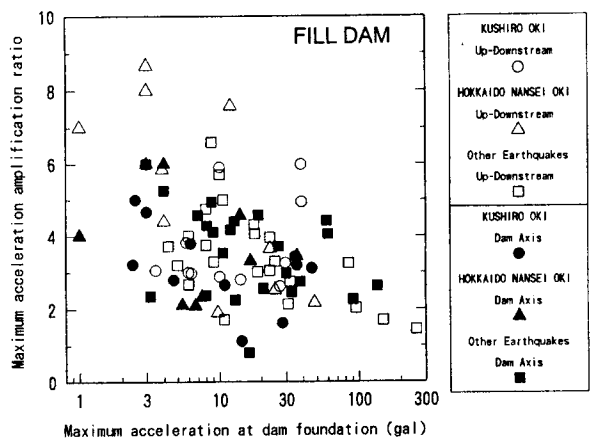

Fig.21 Relationship Between the Maximum Acceleration at the Dam Foundation and the Acceleration Response Amplification Ratio at the Crest (Fill Dam)

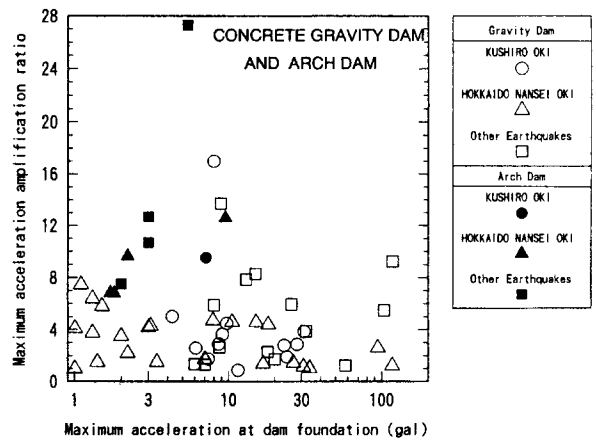

Fig.22 Relationship Between the Maximum Acceleration at the Dam Foundation and the Acceleration Response Amplification Ratio at the Crest (Concrete Gravity Dam and Arch Dam)

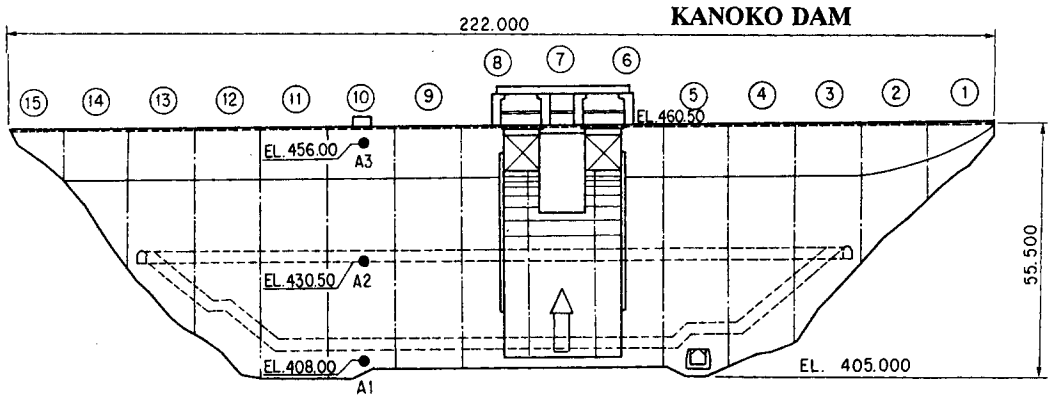

Fig.24 Dam Downstream Surface Diagram of Kanoko Dam

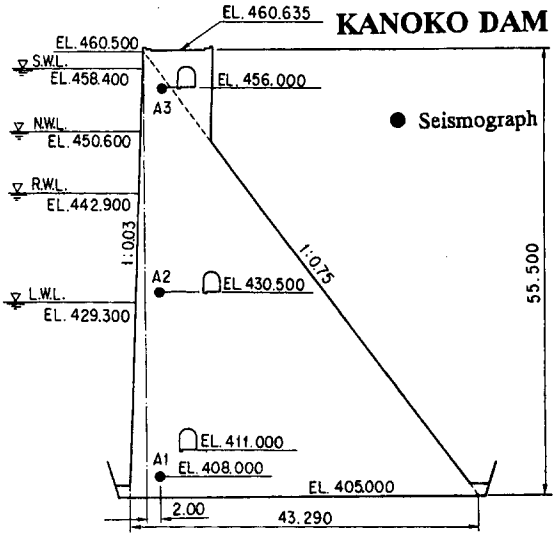

Fig.23 Typical Section Diagram of Kanoko Dam

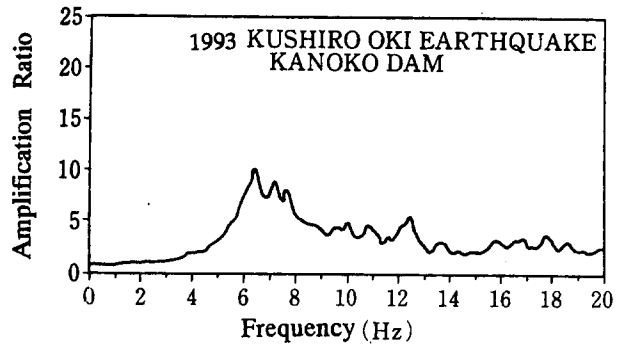

Fig.25 Frequency Response Function at Kanoko Dam

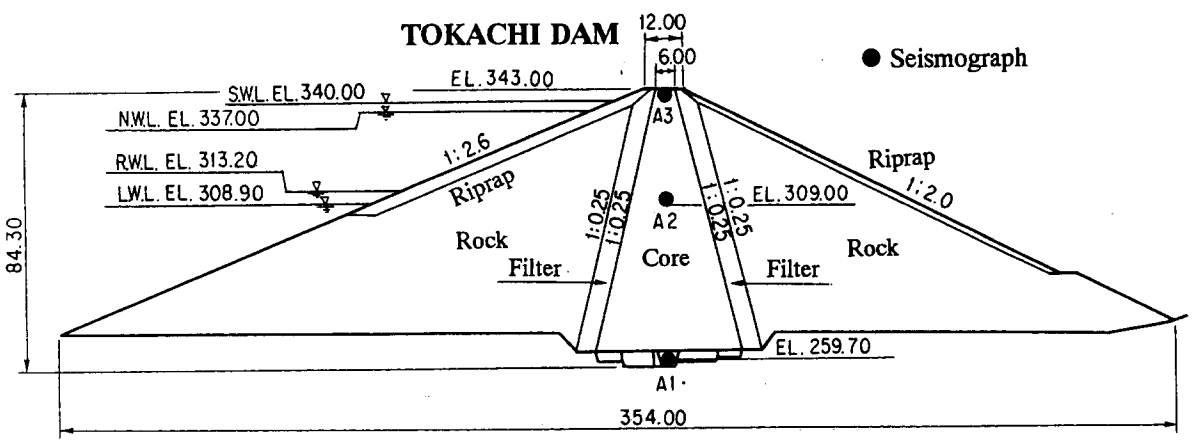

Fig.26 Typical Section Diagram of Tokachi Dam

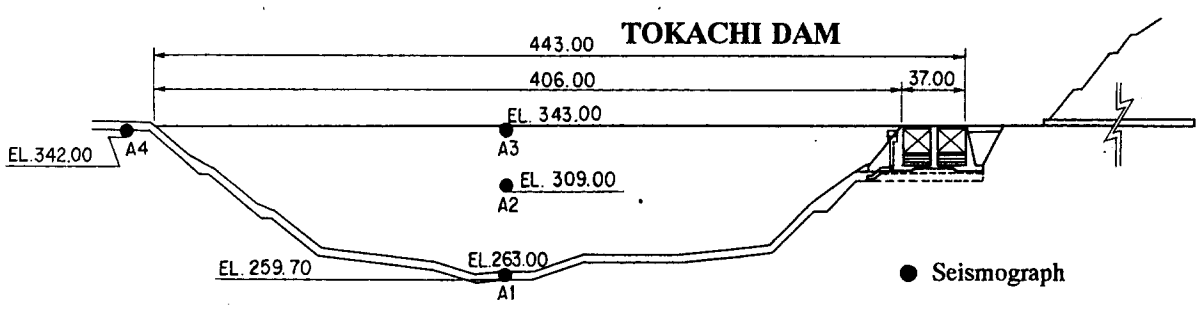

Fig.27 Longitudinal Section Diagram of Tokachi Dam

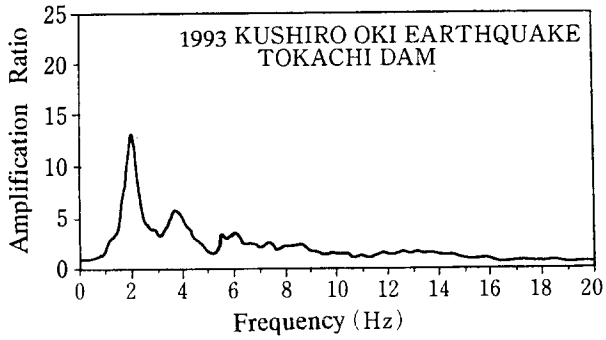

Fig.28 Frequency Response Function at Tokachi Dam

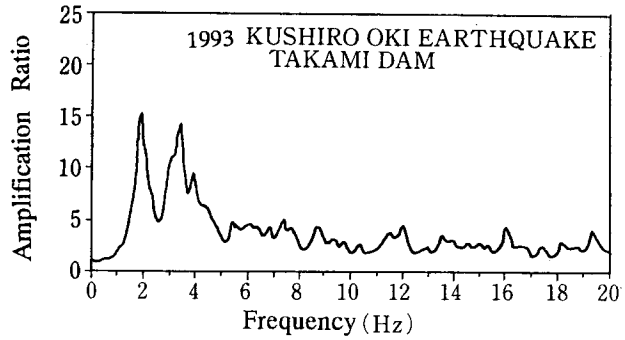

Fig.31 Frequency Response Function at Takami Dam

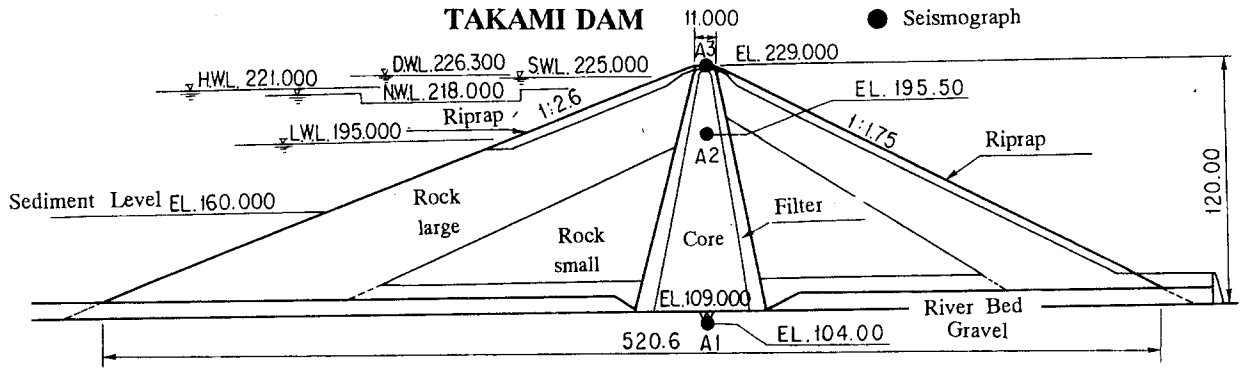

Fig.29 Typical Section Diagram of Takami Dam

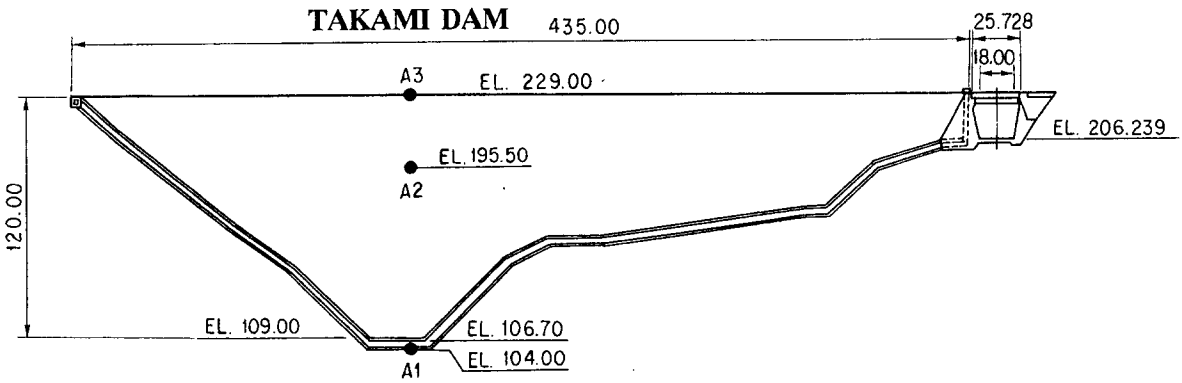

Fig.30 Longitudinal Section Diagram of Takami Dam

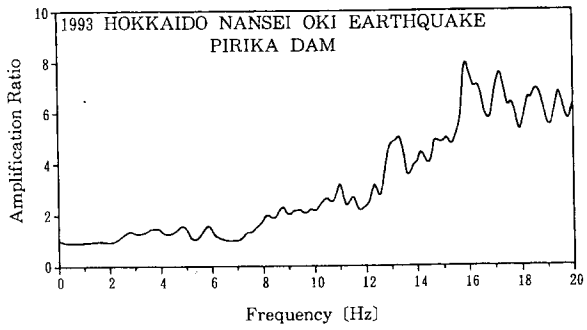

Fig.32 Frequency Response Function at Pirika Dam

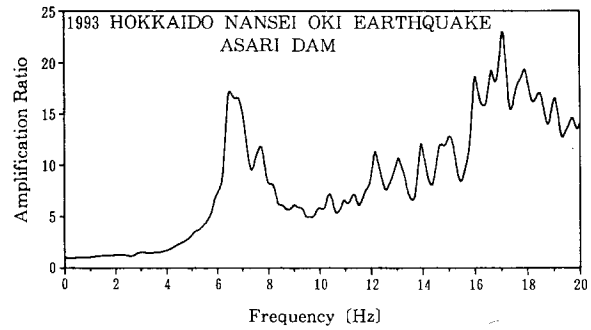

Fig.34 Frequency Response Function at Asari Dam

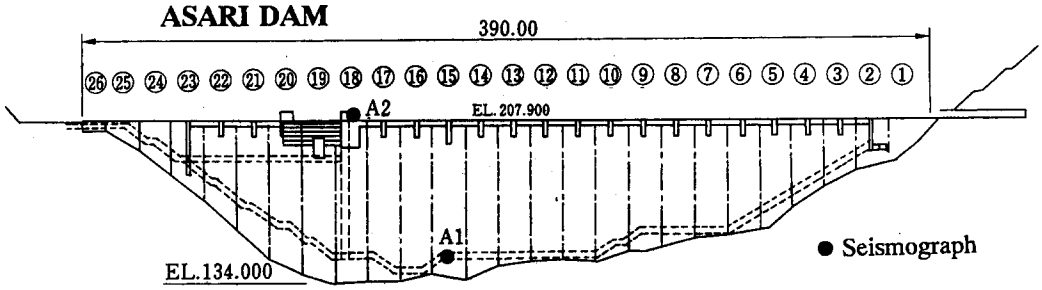

Fig.33 Dam Downstream Surface Diagram of Asari Dam

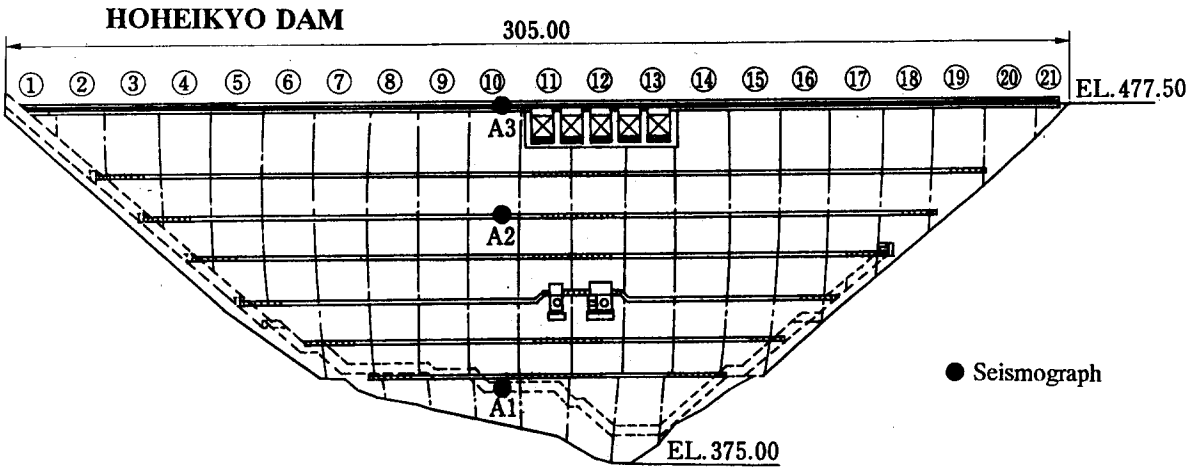

Fig.36 Dam Downstream Surface Diagram of Hoheikyo Dam

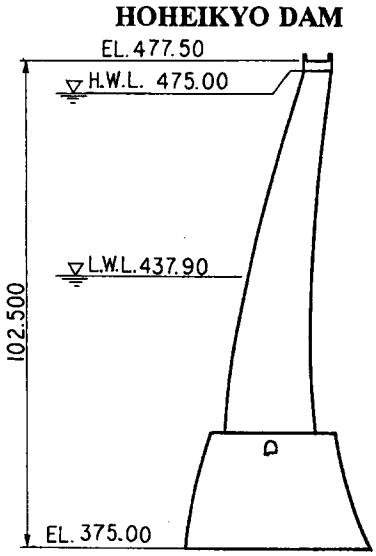

Fig.35 Typical Section Diagram of Hoheikyo Dam

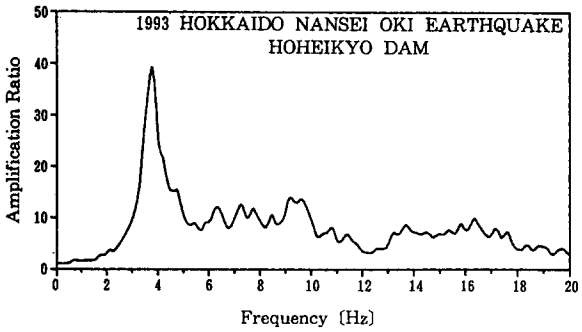

Fig.37 Frequency Response Function at Hoheikyo Dam

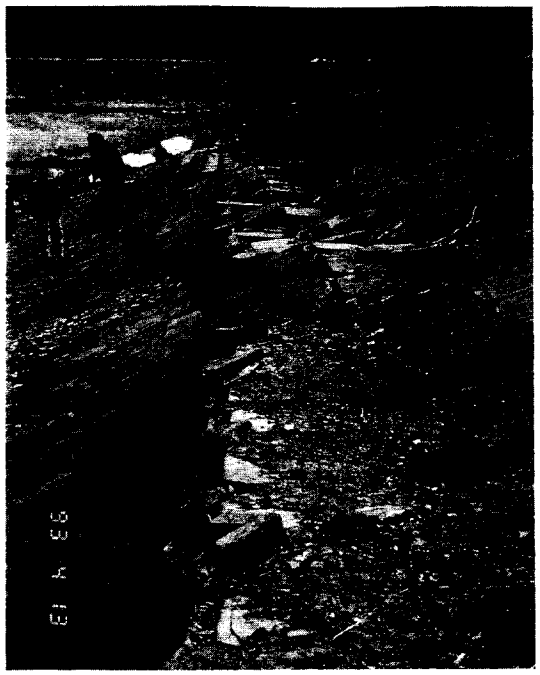

Photo.1 Raised Facing Concrete Blocks on the Upstream Slope Protection of Mombetsu Dam

Photo.2 Undulating Deformation of Facing Concrete Blocks on the Upstream Ground Slope of the Mombetsu Dam Left Bank

Photo.3 Floor Concrete Spalled Cracks in the Structure between Block 0 and the Connecting Corridor at Pirika Dam (Photograph in the Block 0 Direction from the Connecting Corridor)

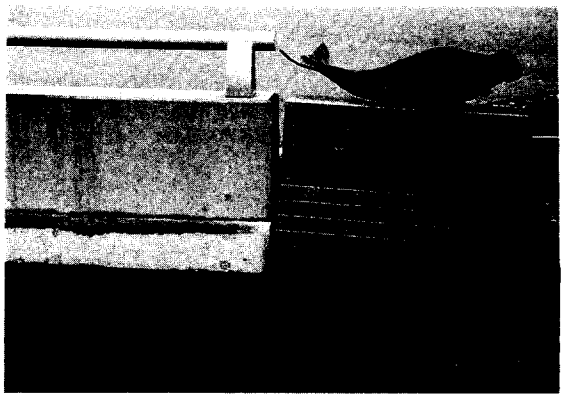

Photo.4 Settlement of Asphalt Paving and Gap of the Railing at the Crest around the Connection with Block 0 at Pirika Dam

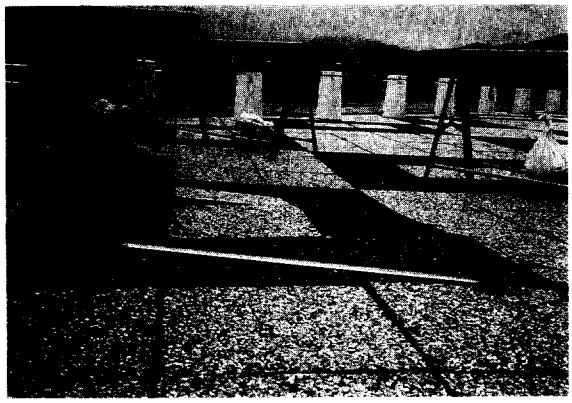

Photo.5 Rising of the Surface Blocks in the Park Plaza above the Connection Between Block 0 and the Core Wall at Pirika Dam

Photo.6 Damage to Niwa-Ikumine Dam (Photographed from the spillway on the left bank on July 15, By the Courtesy of the Kita-Hiyama Land Improvement District)

Photo.7 Bulging on the Upstream Slope of the Niwa-Ikumine Dam (Photographed on July 22)

Photo.8 Level Difference on the Crest Caused by the Settlement of the Upstream Side of the Niwa-Ikumine Dam (Photographed on July 15, By the Courtesy of the Kita-Hiyama Land Improvement District)

Photo.9 Channel Excavated as Emergency Work on the Niwa-Ikumine Dam (Photographed from the Reservoir Side on August 7, and by the Courtesy of the Kita-Hiyama Land Improvement District)

STORM SURGE AND TSUNAMIS

Evaluation of Seismic and Flood Hazards Potential for a Large Earth-Filled Dam

by

N. Simon, M. Reich, P. C. Wang, R. Khanbilvardi* and T. McSpadden**

ABSTRACT

The impacts of seismic and flood events on the PAR Pond Dam were evaluated by Brookhaven National Laboratory (BNL) for the Department of Energy.

The seismic evaluation involved several steps, each of which addressed a specific aspect of dam stability. Results of these various steps are linked and assessments of stability are made. Specifically, the analysis includes: (a) the determination of the basic physical parameters (density, shear modulus, etc.) from available or extrapolated field data (such as standard penetration tests results and soil permeability), (b) the evaluation of the steady state stress conditions corresponding to soil dead weight and reservoir water, (c) the calculation of the seepage forces and consequently the initial effective stresses, (d) the evaluation of the potential for slope sliding failure for static conditions and for static conditions amplified to simulate a seismic input using a simplified method to estimate slope stability, (e) the calculation of the dynamic response of the dam and its foundation to earthquake excitations and, (f) the evaluation of the failure potential based on the calculated dynamic and steady-state results.

The flood evaluation used deterministic and probabalistic models together with stochastic and actual rainfall data to investigate the probability of a flood overtopping the dam. The Probable Maximum Flood (PMF) was determined using rainfall data consistent with the Probable Maximum Precipitation (PMP). This is compared to a flood frequency analysis that uses probabilistic methods and actual rainfall data for the Savannah River site and region.

KEYWORDS: dams; earthquake; flood; liquefaction; probabilistic; rainfall.

1. INTRODUCTION

The PAR Pond Dam is an earthen dam constructed in 1958-1959 across the Lower Three Runs Creek located on the U.S. Department of Energy's (DOE) Savannah River Site in South Carolina. The dam has a 30 foot-wide crest at a design elevation of about 211 feet above mean sea level (MSL). It has a height of 66 feet and a length of 4500 feet. At the spillway elevation (200.00 feet MSL) the reservoir has a surface area of 2700 acres and an impoundment of approximately 54000 acre-feet.

The embankment cross section is essentially homogeneous consisting of silty and clayey sands with relatively low permeability, flanked on the downstream side by a pervious zone of silty sand with a width about one-fourth of the total embankment width. The foundation is relatively pervious. A reinforced concrete outlet conduit, with internal sectional dimensions of 8 feet by 8 feet, was constructed at the base of the dam near its maximum section to serve as a sluiceway and spillway.

In 1991 a depression in the vicinity of the outlet conduit was discovered, together with flow from beneath the conduit and associated downstream wet areas. Because of the adverse conditions, DOE contractors performed comprehensive geotechnical and hydraulic investigations in 1991 and 1992. A series of soil tests conducted for both the embankment and the foundation layers indicated that a layer of loose sand exists deep in the foundation of the dam which had not been accounted for in the original design of the dam.

Further studies to determine the capacity of the dam to withstand flooding and earthquake events were performed in 1992 and early 1993. This paper is a summary of the seismic and flood hazards safety evaluations performed by BNL for DOE.

2. SEISMIC EVALUATION

Due to the complexity of the physical problem and uncertainties in the true values of key parameters (such as soil damping, soil relative density, etc.), assessments of the failure potential of the dam were made through parametric evaluations to provide estimates of the susceptibility to failure due to either liquefaction or slope sliding.

The dynamic response is evaluated by treating the saturated soil as a two-phase medium. This approach involves the determination of both the intergranular stresses and the pore pressures in the medium for the entire duration of the earthquake. Even though the formulation is a linear description of the constitutive response of the soil-water medium, important conclusions can drawn concerning the dam stability.

The failure potential of the dam for a Charleston-like earthquake with a peak ground acceleration of 0.11g, considered to be representative of the site, is estimated. The analysis indicated that, (1) for competent soil property assumptions the safety factor against slope failure remains above 1.0 and, (2) for the same dynamic event and under extremely conservative assumptions of soil damping and strength, liquefaction failure can be triggered at the bottom of the weak layer.

In further analyses the benefits of a berm placed downstream of the dam were evaluated. The presence of the berm reduced the potential for liquefaction and shifted the critical zone downstream. Additional studies to assess the behavior of the weak sand under the increased effective stress field produced by the berm must be performed to confirm the positive effect.

Lastly, based on analysis results, stronger ground motions combined with the conservative estimates of the key soil properties, reduce the safety factors for both modes of failure below tolerable limits.

2.1 Technical Analysis

The analysis consists of a series of steps each of which addresses a specific aspect of dam integrity.

---

* Brookhaven National Laboratory, Upton, NY 11973
** US Department of Energy, Washington, DC 20585

Specifically, the following important parameters were assessed:

- Seepage forces generated by the flow of water through the dam and its foundation.
- Present soil conditions within the embankment that dictate both the amount of seepage as well as the inherent strength of the structure.
- Driving forces along potential failure surfaces that determine the level of safety against slope sliding and failure during an earthquake.
- The influence of critical soil parameters and their impact on the dynamic response and structural integrity of the dam.
- The profile and the condition of the soil constituting the foundation of the dam and its potential to liquify.

This complete matrix of critical system parameters is addressed with emphasis given to the coupling between them. Subsequently, on the basis of the computed dam response the potential for failure is estimated. The slope failure potential in the embankment is assessed in terms of a safety factor against sliding along a failure surface while the liquefaction potential is measured against the ability of the soil in the embankment and the foundation to withstand an anticipated level of shear stress during a seismic event. It should be emphasized that while basic procedures exist in assessing such failure potential, they fail to (a) represent the soil as a two-phase medium, and (b) implement seismic inputs in the form of acceleration time histories.

Initial conservative estimates of safety are obtained by utilizing the slope stability program REAME. This program is based on the quasi-static analysis of slopes and treats the soil as a single-phase medium. Subsequent analyses are performed using the POROSLAM 2-D finite element program which allows two-phase soil representation and accepts a time history variation of the ground acceleration.

The stability of the dam and its susceptibility to failure was evaluated taking proper consideration of the important coupling exists between the various steps. It is important to note that results from one phase of the evaluation provide important information for the next phase. A profile of these analysis steps in their proper order is provided below:

2.1.1 Screening

Screening of the susceptibility of the dam to slope failure is first performed using the REAME (Rotational Equilibrium Analysis of Multilayered Embankments) program. The code provides conservative first estimates of the safety margins regarding slope stability of the dam. Important parameters that impact on the safety criteria are the soil frictional angle and cohesion. Safety factors against sliding along assumed failure surfaces through the embankment and the foundation layers are evaluated for a range of soil parameters that seem reasonable. The analysis considers both the steady-state (static) and a pseudo-static (to account for seismic effects through a seismic coefficient) loadings. Based on the results, the impact of each parameter is assessed.

2.1.2 Seepage Forces

Seepage forces are evaluated by considering the flow of water through the dam. The steady state pore water pressure field is evaluated through a finite element seepage analysis using the ANSYS general purpose program. The pore pressure field is an important input in the determination of the steady state stress distribution. The pore water supports a fraction of the static stresses reducing the intergranular soil stresses. The analysis also provides the location of the phreatic surface.

2.1.3 Steady state stress

The steady state stress condition in the embankment and the foundation layers is evaluated. This in-situ stress field, resulting from the action of the reservoir water and the soil overburden, is key to the definition of stability of the dam. With elastic soil properties extrapolated from test data for the site and using finite element analysis, the stress field in the embankment and the foundation caused by the reservoir load and the overburden is evaluated. The effective stress field that exists prior to a dynamic event is evaluated by incorporating the calculated pore pressure field. Effective stress is the difference between the soil overburden stress and the pore water pressure. Through the same analysis the steady state shear stresses are also evaluated. Each of these stress calculations is performed using the ANSYS code.

2.1.4 Dynamic response

The dynamic response of the embankment/foundation system to earthquake loadings is evaluated next. This seismic analysis provides the stress time histories throughout the structure caused by the design earthquake. This stress history combined with the steady state effective stress field become the basis of the safety assessment for both slope stability and liquefaction. The design seismic input is a Charleston-like earthquake with a ZPA of 0.11g. The dynamic response is evaluated using the POROSLAM code which is a linear analysis program that treats the soil as a two-phase medium.

2.2 Failure Potential Evaluation

Based on the in-situ stress conditions and its dynamic response, the margins of safety against failure in the following modes are evaluated to assess the capacity of the dame to withstand the design earthquake.

2.2.1 Slope Stability

Along various surfaces where sliding can occur, the dynamic factors of safety are computed and the most critical or potential failure surfaces are identified. This process is performed using extrapolated values of soil cohesion and frictional angle. Since there are uncertainties in the exact values of these two parameters, the safety factors are calculated considering a parametric variation of them.

2.2.2 Liquefaction

This mode of failure occurs when the embankment and the foundation liquify during a dynamic event. The driving force in the liquefaction process is the dynamic (cyclic) shear stress generated in the soil layers. The resisting force is the shearing strength of the soil. This strength can be addressed by bore hole testing and correlation with laboratory test results. The dynamic shear stress is provided by the POROSLAM analysis while the standard penetration test results along with predicted initial (steady state) effective stress provide the shear strength of the entire cross section of the embankment and the foundation layers.

2.2.3 Slope Failure/Liquefaction Connection

The possibility that a localized liquefaction condition can trigger a slope failure is also examined. It is possible that in the lower foundation layers where dynamic shear stresses are at a maximum, portions of the weak layer will liquify. Localized liquefaction does not necessarily mean loss of strength in the entire layer, but it could mean a reduction of the safety factor over a potential failure surface transversing the liquified spot. Such a reduction could precipitate sliding failure. In order to evaluate the coupling of the two failure modes, the safety factor against slope failure is re-evaluated taking into account the change in cohesion and frictional angle that occurs within the liquified zone.

2.3 Results and Conclusions

2.3.1 Significant Seismic Results

Slope failure and liquefaction were identified as the mechanisms that could lead to failure during a seismic event. The potential for failure in these two modes taken separately and coupled was evaluated to assess the safety of the dam. The results and the conclusions from the analysis are summarized below:

- The strength of the in-situ soil from which the susceptibility of the section is judged is related to the friction angle ϕ and cohesion c. The values of these soil parameters are estimated from the available penetration resistance test results performed at the site.

- Screening analyses that are based on the stability program (REAME, based on pseudo-static assumption), with the assumption of a uniformly weak soil layer (critical zone) in the lower foundation of the dam, indicated that there was a high potential for slope failure even under the action of the existing static loads. Since the dam is able to support its static loads in spite of the apparent weak zone, the REAME Code results are interpreted as very conservative. It is more probable that the assumption that the weak zone is uniformly weak is incorrect.

- A more sophisticated finite element analysis indicated that unless the critical layer is uniform and very weak (very low frictional angle ϕ), the dam is able to withstand an earthquake of intensity of 0.11g without exhibiting slope failure. An earthquake of this level is considered appropriate for the Savannah River site. Further, based on the limited measurements taken at the site the critical layer is not uniformly weak, and hence, the potential for slope failure is even less. Assuming the soil strengths chosen for the analysis are correct, the 0.11g mentioned above is considered an appropriate assessment of the dam capacity.

- With conservative assumptions of soil properties, (i.e., assumed low values of hysteretic soil damping), the potential for liquefaction in the critical zone is high. The liquefaction, however, is expected to occur at the bottom of the critical zone directly under the downstream toe. This zone is susceptible to liquefaction because of its relatively high induced shear stresses and smaller confining stresses. However, since the location of the liquefiable soil is about 100 feet below the ground surface, is old geologically, and is a small zone, it should not lead to liquefaction induced failure of the dam.

- Localized liquefaction alone does not lead to failure. Re-evaluation accounting for slope failure coupled with localized liquefaction effects was made. Even for this case, the safety factor was found not to fall below acceptable levels. This result is based on a model incorporating stiff and weak subzones in the critical layer. Use of weak and stiff subzone modeling is consistent with the standard penetration resistance test results and is therefore more indicative of actual site conditions.

- With a value of 2% for the hysteretic soil damping assigned to the material in the critical zone (instead of the very conservative value of 0.5% used in the analysis), the susceptibility for liquefaction is eliminated for an earthquake with a peak level of 0.11g. Based on the computed effective strains of 0.13% obtained for the 0.5% damping case, it is anticipated that the actual hysteretic damping for the soils will be significantly higher than 2%.

- Results show that when the most conservative assumptions for soil properties are used with the most conservative evaluation procedures, liquefaction is possible under the upstream pool. However, since the confining pressure is higher upstream, the safety factor remains above 1.0 and liquefaction induced failure of the dam is not indicated.

- An analysis that incorporates both vertical and horizontal earthquake inputs, correlated in time, indicates significant increases in the embankment shear stresses

which reduce the safety factor against slope sliding, but does not drive it below 1.0. Moreover, this combined earthquake activity does not amplify the liquefaction potential in the critical zone. It should be noted that horizontal and vertical earthquake inputs correlated in time is not considered to be realistic. It will usually be uncorrelated in time. This case can, however, be considered as an upper bound load case.

- When a seismic input of 0.2g is considered (instead of the 0.11g), the potential for both slope failure and liquefaction increase to unsafe levels.

2.3.2 Remedial Benefits of a Berm

The analyses have shown the structure to have sufficient structural integrity to survive a credible seismic event. However, that conclusion is strongly dependent on the soil properties assigned to the critical zone. If the critical zone is assigned the most conservative (poorest) definition for soil properties, the dam seismic integrity was found to be marginal. Given the uncertainties in the properties of the soil in the critical zone, a limited study of the placement of a berm on the downstream surface of the dam, as a possible remedial action, was undertaken.

A berm improves the seismic integrity of the dam by increasing the effective static stresses in the dam/foundation system. The berm induces greater static effective stresses which reduce the likelihood of liquefaction, shifts the zone susceptible to liquefaction downstream, and increases slope stability. As berm size increases, the susceptible zone shifts further downstream.

The predicted benefits of the berm are based on the assumption that the soil can support the additional load without excessive consolidation. If consolidation is great, the dam foundation system may not exhibit an effective stress increase in the critical locations and the benefits of the berm will not be realized. Needless to say, if the placement of a berm is seriously considered the competency of the soil to support its additional load must first be determined.

2.3.3 Results Requiring Further Definition and/or Clarification

Although the POROSLAM code analysis is substantially advanced from those of the REAME Code and other analytical techniques used in the industry, there are still areas of the safety evaluation, especially those pertaining to the development of a High Confidence of Low Probability of Failure, that need further definition and/or clarification as listed below:

- As has been stressed, the seismic integrity of the dam is strongly dependent on the properties of the soil and the extent of the weak or critical foundation layer. Recently, extensive additional soil testing of the dam/foundation system were performed. This information should be made available for review and correlation. Using this new material information a comprehensive properties matrix for the dam/foundation system will be developed. A detailed finite element model will be created consistent with the soil properties matrix to correctly characterize the dam/foundation system.

- Following an accurate definition of soil properties another important element affecting dam seismic integrity is the exact character of the site seismic excitation. To correctly account for this, develop a design earthquake incorporating site specific properties appropriate to PAR Pond. Use this as input for the new finite element model and perform dynamic analyses considering simultaneous horizontal and vertical inputs. Assess dam/foundation safety margins. Investigate the sensitivity of the safety margins to different families of earthquake inputs and evaluate the sensitivity of results to the rigid base assumptions.

- Although the onset of failure is adequately predicted with linear analysis methods, only the application of non-linear methods will allow a realistic simulation of dam response in a failure mode and an assessment of the corresponding consequences of the failure. In order to address this deficiency, incorporate the capability to account for non-linear soil behavior into the POROSLAM code. Use the updated code to obtain more realistic estimates of dam response, including pore pressure buildup and possible large deformations in the embankment, that would result from liquefaction and slope sliding.

3. HYDRAULIC AND HYDROLOGIC EVALUATION

To investigate the probability of a flood overtopping the dam, BNL conducted a hydrological and hydraulic study using deterministic and stochastic models. The study was first carried out using rainfall data consistent with the Probable Maximum Precipitation (PMP). Using standard procedures the 72-hour PMP, a "catastrophic" storm, was found to be 47.8 inches for the Savannah River Site. This is the maximum amount of precipitation expected in any period of 72 hours, based on a symmetrical "center-peaking" distribution for the precipitation intensity during the period of the storm. The PMP distribution used throughout the study was developed for a representative watershed area of 31.7 square miles. The resulting Probable Maximum Flood (PMF) was computed using the PMP as input to the HEC-1 program.

The HEC-1 estimate of the PMF corresponding to the PMP indicated that the level of water would be 3.56 feet above the top of the dam. The concept of the PMP and the resulting PMF are often considered to be rather low probability and arbitrary criteria that cannot be substantiated for some applications. The PAR Pond Dam is considered to be one such application.

Historical rainfall data have been collected at the Savannah River Site (11 rain gages) and in the regional area of the site (two raingage stations).

These data sets are available for periods of 30 to 46 years. This rainfall data is clearly helpful in the rainfall analyses for this site. A flood frequency analysis based on these 13 raingage stations collecting data for 30 to 46 years is more useful than the PMP value obtained from the National Weather Service's HMR-51 and HMR-52. The PMP is a concept which is developed to simulate the ultimate "catastrophic" precipitation event that could ever be created under the most unfavorable combination of the specific meteorological conditions of a region involving parameters such as temperature, wind, and humidity. Although the impact of the 72-hour PMP was evaluated in this study, BNL contends that a 72-hour rainfall event with a probability of occurrence of 10^{-5} developed from actual site/region rainfall data is more meaningful and appropriate. The 13 raingage stations with 30 to 46 years of data produce a very specific rain distribution for the Savannah River Site. Applying probabilistic methods and using this data, the 72-hour 100,000-year storm was found to be approximately 1/2 of the PMP. DOE Standard 1020 permits use of a 100,000 year flood to evaluate structures with the potential for high consequences.

The HEC-1 evaluation for this 72-hour rainfall estimate indicated that the dam would not be overtopped by a 100,000-year storm. That is, a rainfall event with a probability of occurrence of 10^{-5} would not cause the PAR Pond Dam to be overtopped. However, this result is based on selected values of parameters related to the watershed characteristics for the site. The importance of accurately estimating the Curve Number, soil losses from sub-basins, and sedimentation potentials in the reservoir behind the dam are discussed in the BNL report.

4. REFERENCES

4.1 Simos, N., and Reich, M., (1994). "Seismic Analysis of the PAR Pond Dam." Brookhaven National Laboratory, Upton, New York.

4.2 Reich, M., et. al. (1993). "Hydraulic and Hydrologic Evaluation of PAR Pond Dam." BNL-49681, Brookhaven National Laboratory, Upton, New York.

4.3 Natural Phenomena Hazards Design and Evaluation Criteria, DOE-STD-1020.

Tsunami Runup Distribution Generated by the July 12, 1993, Hokkaido-Nansei-Oki Earthquake

by

E. N. Bernard and F. I. González*

ABSTRACT

The Hokkaido-Nansei-Oki earthquake produced one of the largest tsunamis in Japan's history. Tsunami vertical runup measurements varied between 15 and 30 m over a 20-km portion of the southern part of Okushiri Island with several 10-m values on the northern portion of the Island. Along the west coast of Hokkaido, no survey values exceeded 10 m, but damage was extensive at several coastal towns. Given the sudden onset of the tsunami and its high energy, it is amazing that more people were not killed. We also observed that the seawall at Aonae was effective in reducing runup amplitudes.

KEY WORDS: Sea of Japan; TSUNAMI RUNUP; TSUNAMI SURVEY

1. INTRODUCTION AND BACKGROUND

On July 12, 1993, at 2217 local time (1317 UTC), an M_s-7.8 earthquake rocked the west coast of Hokkaido and the small, offshore island of Okushiri in the Sea of Japan (Figure 1). A major tsunami was generated and, within 2 to 5 min, extremely large waves engulfed the Okushiri coastline and the central west coast of Hokkaido. As of July 21, 185 fatalities were confirmed, with 120 attributed to the tsunami; this death toll is expected to rise, as missing persons are included among the fatalities (Hokkaido Police Headquarters). Property losses have been estimated at $600 million, due principally to tsunami damage.

The Japanese immediately dispatched damage assessment and survey teams. Most of these Japanese teams were mobilized and began surveying tsunami runup by July 13; on July 18, three U.S. scientists, under the auspices of the January 31, 1994, U.S.-Japan Cooperative Program in Natural Resources (UJNR), joined Japanese scientists to complement the tsunami survey. The 1993 Hokkaido Tsunami Survey Group included the following teams and members:

Tohoku University team: N. Shuto (leader), H. Matsutomi
University of Tokyo team: Y. Tsuji (leader)
Public Works Research Institute, Ministry of Construction, team: H. Ito (leader), K. Yamamoto, Y. Iwasaki, K. Sasaki, A. Hattori
Port and Harbour Research Institute, Ministry of Transportation, team: Y. Suzuki (leader), S. Takahashi, C. Goto, N. Hashimoto, T. Hosoyamada, T. Nagao
Civil Engineering Research Institute, Hokkaido Development Bureau, team: Y. Mizuno (leader), K. Yano
United States-Japan Natural Resources team: E. Bernard (leader), F. González, D. Sigrist, H. Tsuruya, K. Kato
Japan Meteorological Agency team: O. Nagaoka (leader), S. Honda, H. Tatehata

2. FIELD MEASUREMENTS

The primary measurements in the field surveys were the tsunami vertical and/or horizontal runup values, which are the maximum vertical height and/or horizontal extent of flooding. In this report, only vertical runup estimates are presented. Traces left by the tsunami include water marks on buildings, debris lines along the coast, or vegetation that is damaged or killed by salt water. Measurements of vertical height above sea level of the tsunami trace are obtained

*National Oceanic and Atmospheric Administration, Seattle, Washington 98115

by a series of measurements down to the shoreline, using a surveyor's staff and level. The effects of tides are normally removed from such measurements, but during the period of the survey, the predicted tidal range in the study area was only 2–30 cm, referred to mean sea level. Since this range is a relatively small fraction of the observed runup, the data presented in this report are not corrected for tides. This report is a collaborative effort that pools 281 measurements acquired by seven of the survey teams—188 around the island of Okushiri and 93 along the western coast of Hokkaido. These measurements included 110 by Tohoku University, 48 by the Public Works Research Institute (PWRI), 44 through the combined efforts of the Port and Harbour Research Institute (PHRI) and the Civil Engineering Research Institute (CERI), 36 by the Japan Meteorological Agency (JMA), 28 by UJNR, and 15 by the University of Tokyo. Some sites were visited by more than one team as shown in Figures 2 and 3, which summarize the data.

Another very important source of information is the approximate time of tsunami arrival, as inferred by the time at which clocks have stopped due to saltwater flooding. The UJNR team conducted an active search for such clocks in the tsunami debris and in the surrounding area of each of the 28 sites visited. Eight clocks were found in various locations—on the beach, in wrecked automobiles, and in homes and other buildings—which are taken to be a rough indication of tsunami arrival times.

3. DESCRIPTION OF THE EARTHQUAKE/ TSUNAMI

Figure 1 provides an overview of the region, including the aftershock zone (courtesy Japan Meteorological Agency) for a 40-hour period, and its location relative to Hokkaido and Okushiri Island. Note that this zone, frequently taken as an indicator of the area of crustal deformation, includes the island of Okushiri. The seismic moment of 5.6×10^{27} dyne/cm (corresponding to $M_w = 7.8$) with a (fixed) centroid depth (a point source representative of the overall faulting) of 15 km was estimated by Harvard University. Assuming a fault length of about 150 km and a fault width of 50 km based on aftershock data and a shear modulus of 3×10^{11} dyne/cm^2, this moment and fault geometry suggests an average slip of 2.5 m on the fault plane. The focal mechanism estimated by Harvard has one nodal plane dipping eastward at 24° from the horizontal. This fault plane orientation is comparable with the aftershock distribution and is consistent with subduction of the floor of the Japan Sea beneath northern Japan.

The tsunami was probably generated within the deformation area as defined by the aftershock pattern shown in Figure 1. Eye-witness accounts collected by Y. Tsuji (University of Tokyo) and F. Imamura (Tohoku University) indicate that the tsunami hit the west coast of Okushiri Island almost immediately after the main shock. The UJNR tsunami survey team found the electrical clock at an electrical power station had stopped at 2223, which was 6 min after the start of the earthquake. Along the west coast, the tsunami runup measurements were the highest from north of Monai (see Figure 2). The village of Monai was totally destroyed (10 persons killed and all 12 houses destroyed). Runup measurements around the village were 20 m, and in a small valley north of Monai, the runup was measured at 31 m. South of Monai, tsunami runups between 15 and 20 m were measured all along the coast. Vegetation was stripped off the hillside, and large boulders (up to 1 m in diameter) were deposited where the vegetation was flooded. These data are consistent with the initial tsunami arriving from the west of Okushiri Island very near the generation area.

The tsunami was refracted by the shoaling bathymetry at both ends of the Island. Hardest hit was the town of Aonae (population 1,600), where the first tsunami wave flooded the southern tip of the Island and the entire first row of houses in the harbor area within 4–5 min after the main shock (see cover photos). Tsuji reported (based on eye-witness interviews) that the tsunami arrived from the northeast, with flooding of 3–7 m throughout the town. About 7 min after the first wave, a second, larger wave

hit from the east carrying boats into the main town. The second wave completely flooded the first three rows of houses, and runup was measured around 5–10 m throughout the town. The UJNR survey team found battery-operated clocks in this area that had stopped at 2237 and 2238. Fires ignited at 2240, and the combination of a strong, northeast wind and an ample supply of propane and kerosene (used for heating) spread the fire quickly, which burned through the night and destroyed 340 homes. Autopsies revealed that only 2 of the 114 deaths in Aonae were caused by fire. This section of Aonae was the hardest-hit developed area in spite of the fact that a massive, 4.5-m breakwater and 10-m high sand dunes were very effective in reducing the runup to 5–10 m along the southeastern tip of the peninsula (Figure 2). In this regard, note that runup values rise rapidly again to the 10–20-m level a short distance northeast of the peninsula (Figure 2); this is probably due to the absence of breakwaters or sand dunes along this part of exposed coast.

The extent of damage to Aonae is illustrated in figures 3 and 4. The breakwater in the foreground of photograph 1 is 4.5 m. The houses in the central part of the photograph were flooded by tsunami waves that ran up to a height of 5 m. To the right of these houses, one can see the smoking remains of over 200 houses. The area in the left portion of the photograph was a residential section before the tsunami. This area was completely stripped of all houses as seen in photograph 2, a view of the area from the south. The tsunami destroyed a portion of the seawall as seen in the lower right-hand portion of photograph 2. Notice that the seawall was destroyed by wave forces pushing it seaward. Also note the scattered fishing boats in the center of the photograph. In both photographs, the remnants of the wooden structures are seen as the brown debris, completely covering the harbor area and outsidethe breakwater. These two photographs were taken by Y. Tsuji from a helicopter the morning after the earthquake.

A similar refraction of the tsunami took place on the northern point of Okushiri Island at Inaho where 13 persons were killed and all houses were destroyed by waves that ran up over 10 m. The eastern side of Okushiri Island was less affected where the tsunami runup was measured between 2 and 5 m. Subsidence was observed by Tsuji at Aonae, Okushiri, and Monai, while uplift was observed at Inaho Point. These data again suggest that Okushiri Island was part of the deformation area, which is consistent with the aftershock data.

The tsunami also hit the island of Hokkaido (Figure 5), arriving at Ota Bay within 5 min of the main shock and destroying five homes. Runup in this area was 9 m. Damage was also observed at Setana due to 6-m runup waves. The coastline from Suttsu to south of Ota Bay was hardest hit with runup values of 5–9 m. Outside this area, the tsunami intensity tapered off rapidly, and runup values fall below 5 m. The closest tide gauge to the earthquake was Esashi, which recorded a 2-m wave approximately 10 min after the main shock. Those data suggest that the eastern portion of the source was between Okushiri Island and Hokkaido.

The tsunami propagated to Russia within 30 min, where 1–4-m tsunami runups were reported by Valentin Fedorey (Hydromet). Damage estimates were over $6 million, with $4 million in damage at Kamenka. After 90 min, the tsunami struck the coast of South Korea, where B.H. Choi of Sung Kyun Kwan University measured tsunami runup of 1–2 m.

4. SUMMARY

In summary, the Hokkaido-Nansei-Oki earthquake produced one of the largest tsunamis in Japan's history. Tsunami vertical runup measurements varied between 15 and 30 m over a 20-km portion of the southern part of Okushiri Island with several 10-m values on the northern portion of the Island. Along the west coast of Hokkaido, no survey values exceeded 10 m, but damage was extensive at several coastal towns. Given the sudden onset of the tsunami and its high energy, it is amazing that more people were not killed. We also observed the seawall at Aonae was effective in reducing runup amplitudes.

Figure Captions

Figure 1. Locator map of study area. Also shown in the inset is the survey area and the aftershock zone for a 40-h period.

Figure 2. Distribution of vertical tsunami runup for Okushiri Island. The legend indicates data source, and runup values are projected onto offshore scales. A projection from a data point onto the coastline will identify the geographical position of the measurement.

Figure 3. A view of the tsunami damage from the east of Aonae, a small town on the island of Okushiri, which is in the Sea of Japan east of Hokkaido. Photo by Y. Tsuji.

Figure 4. A view of the tsunami damage from the south of Aonae. Photo by Y. Tsuji.

Figure 5. Distribution of vertical tsunami runup for the west coast of Hokkaido. Legend and data presentations are the same as in Figure 2.

Hokkaido Nansei Tsunami
12 July 1993

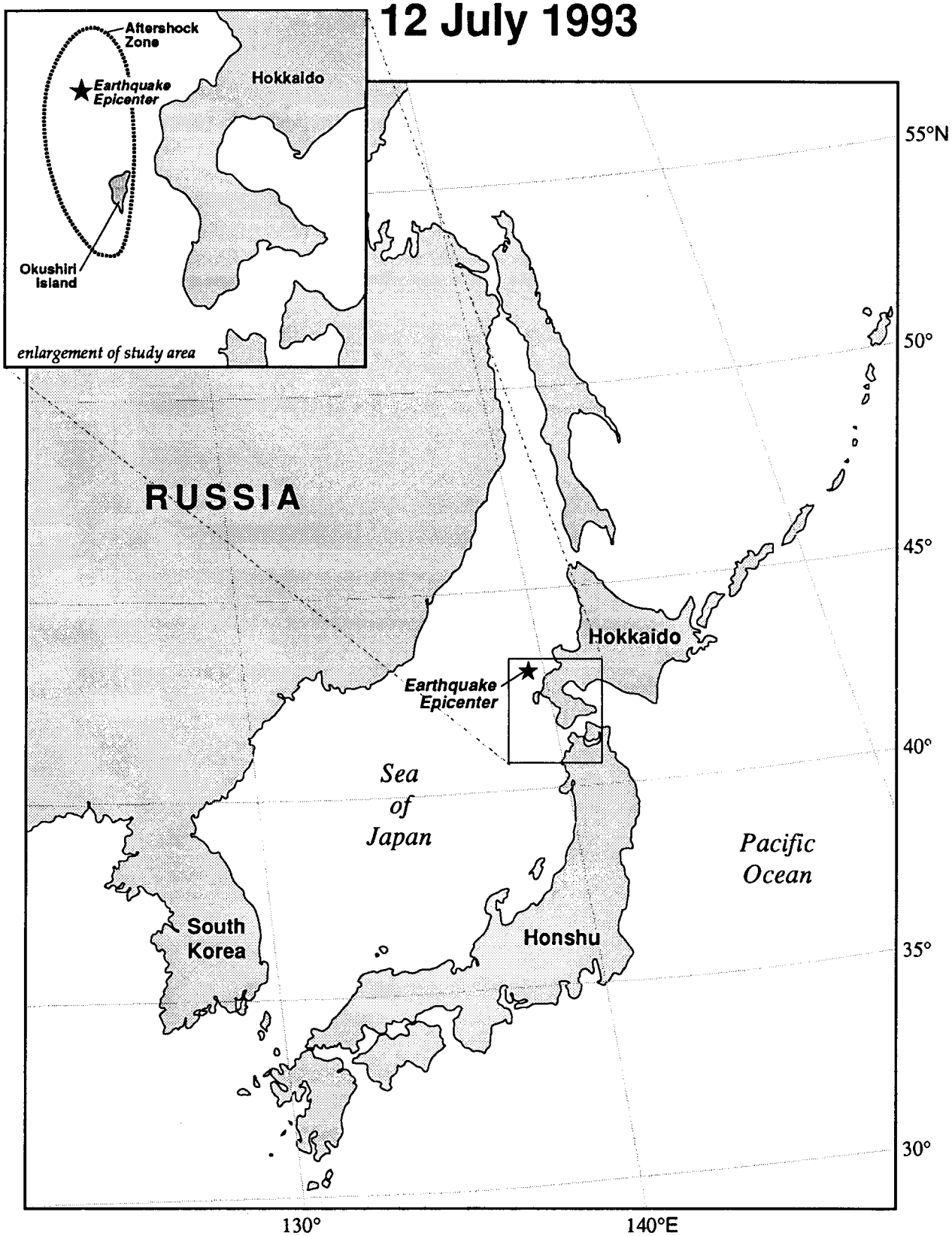

Hokkaido Nansei Tsunami
12 July 1993

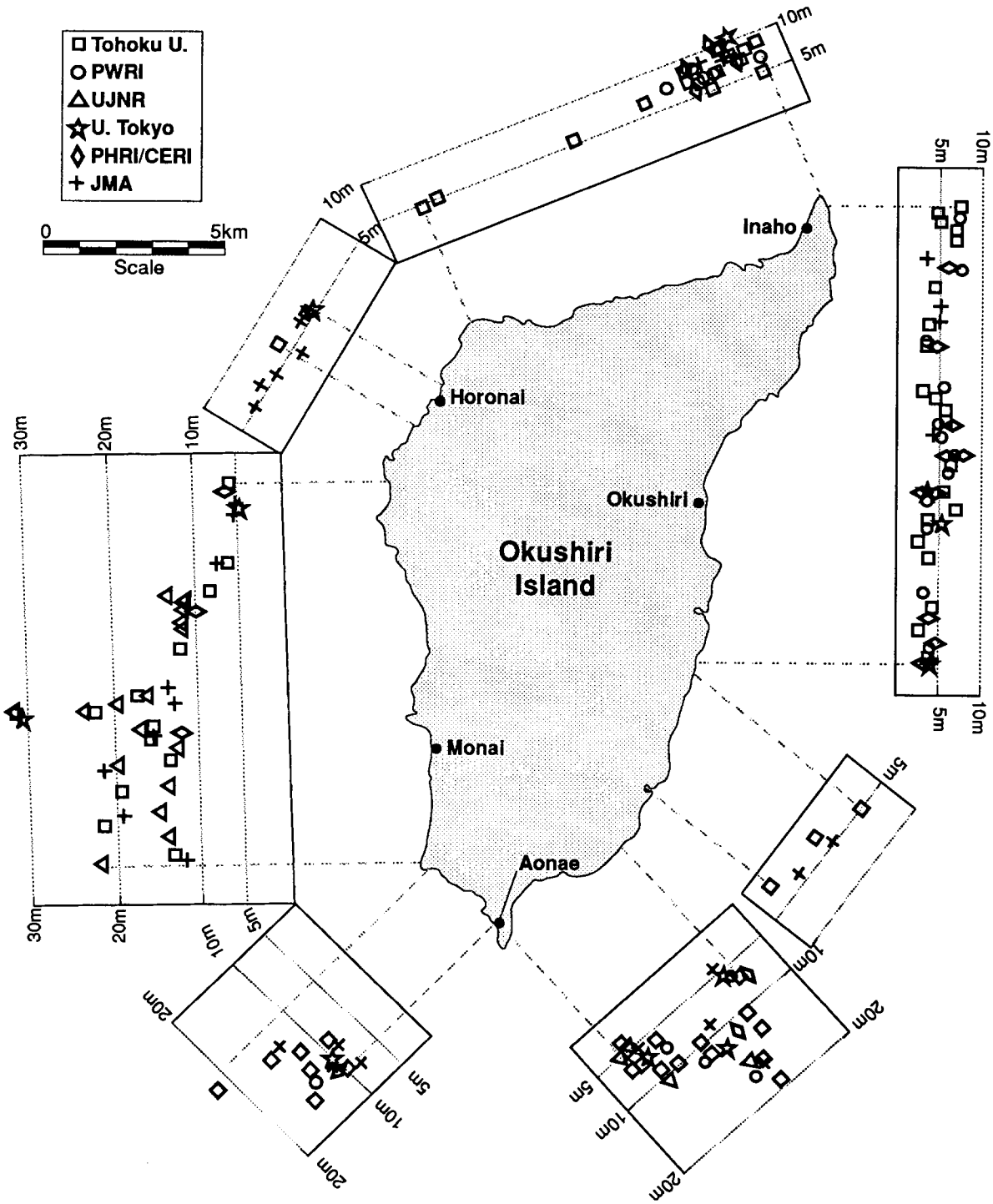

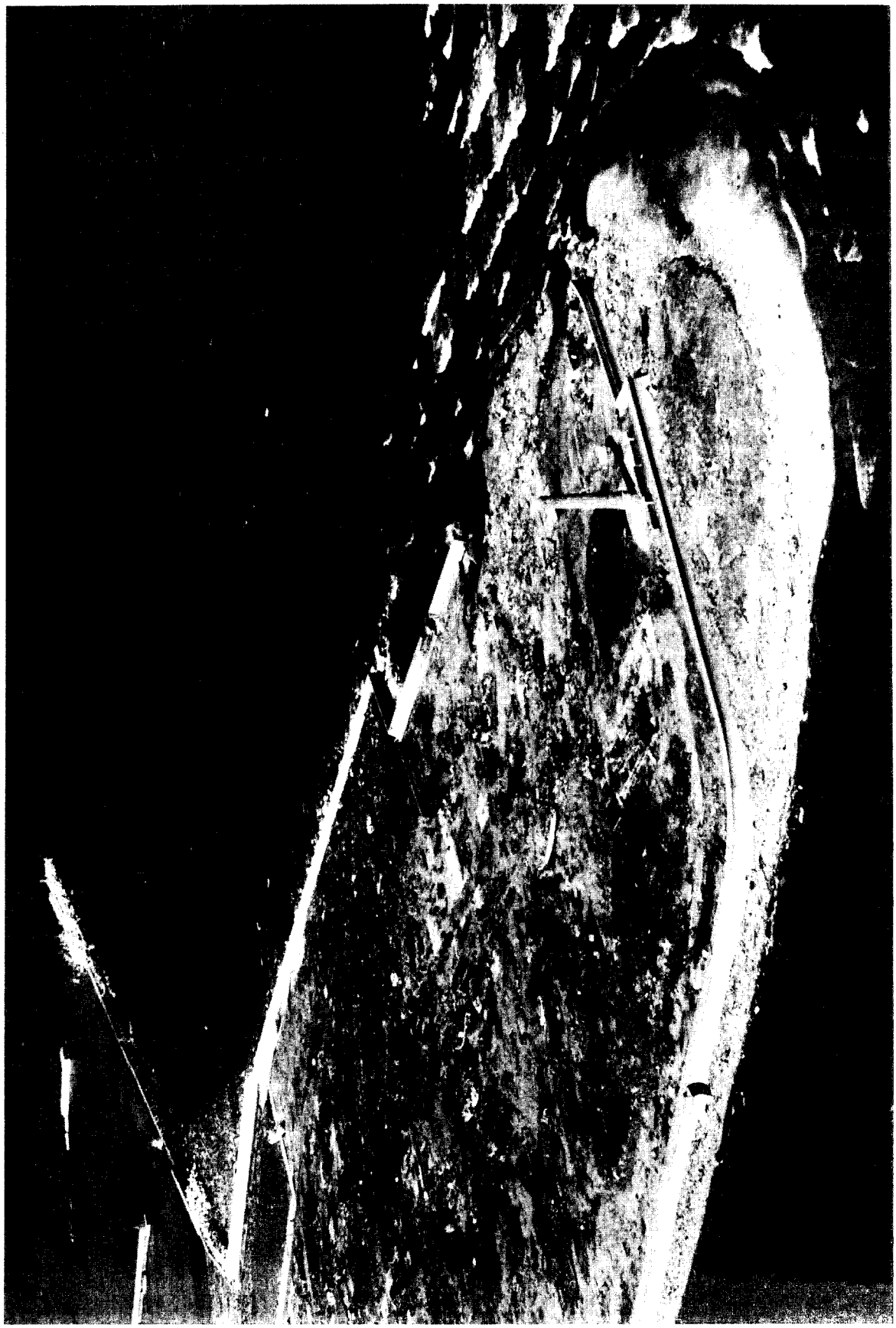

Hokkaido Nansei Tsunami
12 July 1993

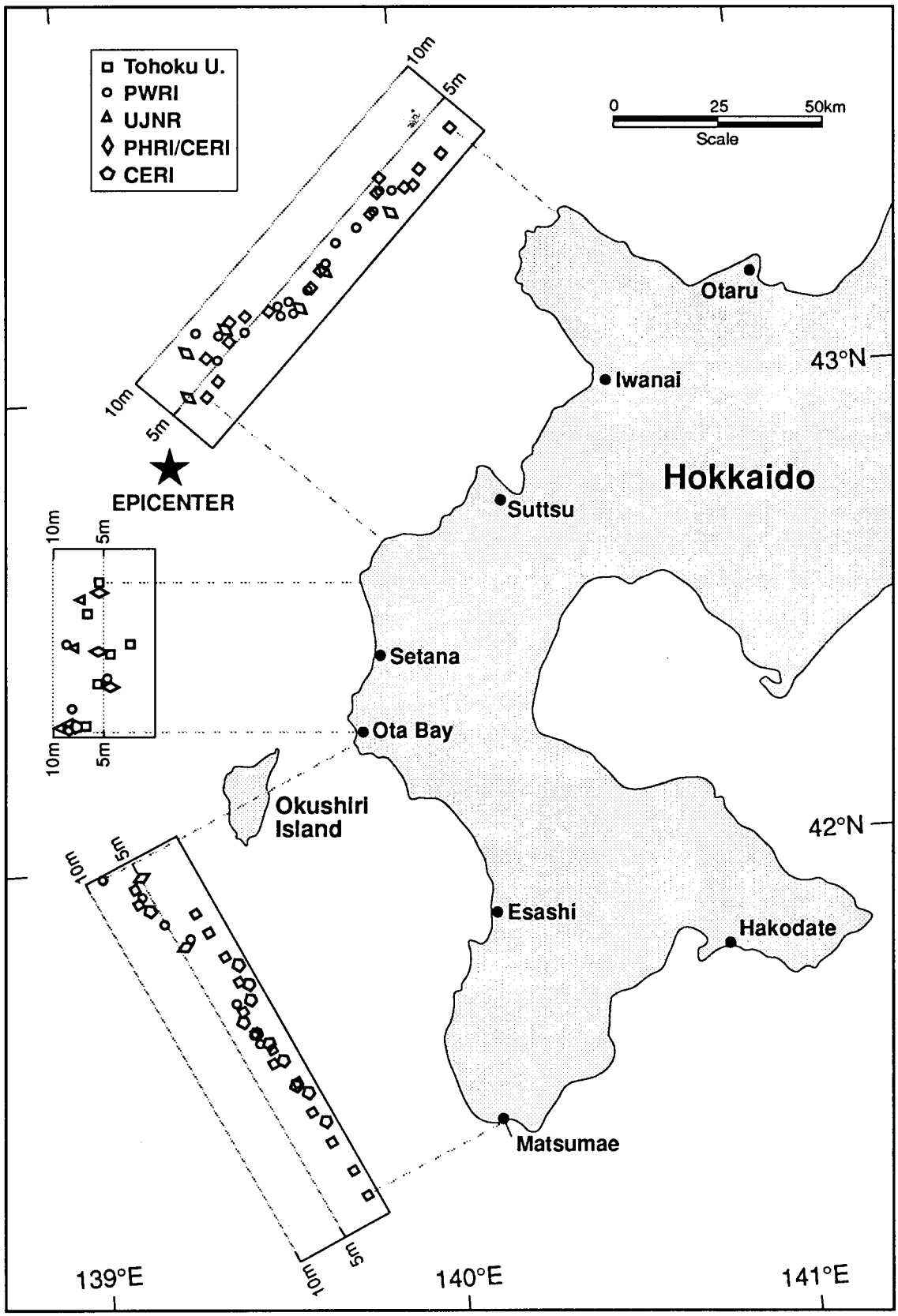

Propagation of Hokkaido-Nansei-Oki Earthquake Tsunami Around Cape Aonae

by

Shigenobu Tanaka[1], Shinji Sato[2] and Kenji Noguchi[3]

ABSTRACT

Hokkaido-Nansei-Oki earthquake rocked the west coast of Hokkaido on July 12, 1993. It caused devastating tsunami which quickly hit Okushiri Island and the west coast of Hokkaido. Because the tsunami source was in the west of the island, the tsunami runup was generally large on the west coast but small on the east coast of the island. However, it was pointed out that the runup height at Hamatsumae was extraordinarily larger than that near around. The location is on the southeast edge of the island, but it was sheltered from the tsunami source area. So, it has been remained as a problem what mechanism had occurred during the tsunami propagation. This paper shows in what way the tsunami propagates in shallow water around Cape Aonae and attacks Hamatsumae based on a large scale hydraulic model test.

KEYWORDS

Hokkaido-Nansei-Oki earthquake; tsunami runup; hydraulic model test; soliton wave; non-linear effect on tsunami propagation

INTRODUCTION

Hokkaido-Nansei-Oki earthquake of magnitude 7.8 rocked the west coast of Hokkaido at 22:17 on July 12, 1993. The earthquake caused devastating tsunami which quickly hit Okushiri Island and the west coast of Hokkaido. The tsunami also attacked whole edge of the Japan Sea. The death toll was 202, 29 were still missing, and the property losses were 145 billion yen within Japan.

---

1)Head of Coastal Engineering Division, River Department, Public Works Research Institute, Ministry of Construction

2)Dr.,Senior Researcher, ditto

3)Researcher, ditto

Public Works Research Institute, Ministry of Construction (PWRI), surveyed vertical tsunami runup heights along the southwest coast of Hokkaido and Okushiri Island's coast. Also, many survey teams measured vertical runup heights. The highest runup 31.7m, which is the highest record in this century in Japan, was found at Monai, west coast of Okushiri Island. The runup heights along west coast were about 5 to 22m except for Monai, and those around south tip, Aonae Cape, and north tip, Inaho Cape, were about 10m. Those for the east side of the island were about 3 to 8m except for around Hamatsumae. The highest runup in Hamatsumae was about 20m. Among the researchers, it was pointed out that the runup height at Hamatsumae was extraordinarily larger than that near around. The location is on the southeast edge of the island, but it was sheltered from the tsunami source area. So, it has been remained to be investigated what mechanism had occurred during the tsunami propagation.

In order to study this phenomenon, PWRI carried out a large scale hydraulic model test. The result reveals the tsunami propagation mechanism clearly. A refracting wave and a diffracting wave generated by the offshore shoal attack together in a big synthetic wave against Hamatsumae coast. In the nearshore, furthermore, the second soliton catches up to the first one and then runup onto the shore.

FIELD SURVEY

PWRI sent a survey team to survey the damage due to the tsunami on July 14. They selected local maximum runup points and measured vertical height above the sea level of each point using a handlevel and staffs. They also wrote down the time of each measurement and modified the vertical height referring to the tide table of Esashi Port. Figure 1 shows vertical runup heights for the southwest coast of Hokkaido. The runup heights are higher in Shimamaki, Setana, Kitahiyama and Taisei. Figure 2 shows the runup height distribution for Okushiri Island. PWRI survey team could not survey some west part of the island. PWRI's highest runup 19.8 m was found at Cape Kuki and the second one 15.9 m was at Hamatsumae.

Figure 3 shows distribution of vertical tsunami runup for Okushiri Island compiled by Bernard and Gonzalez(1993). It can be seen that the

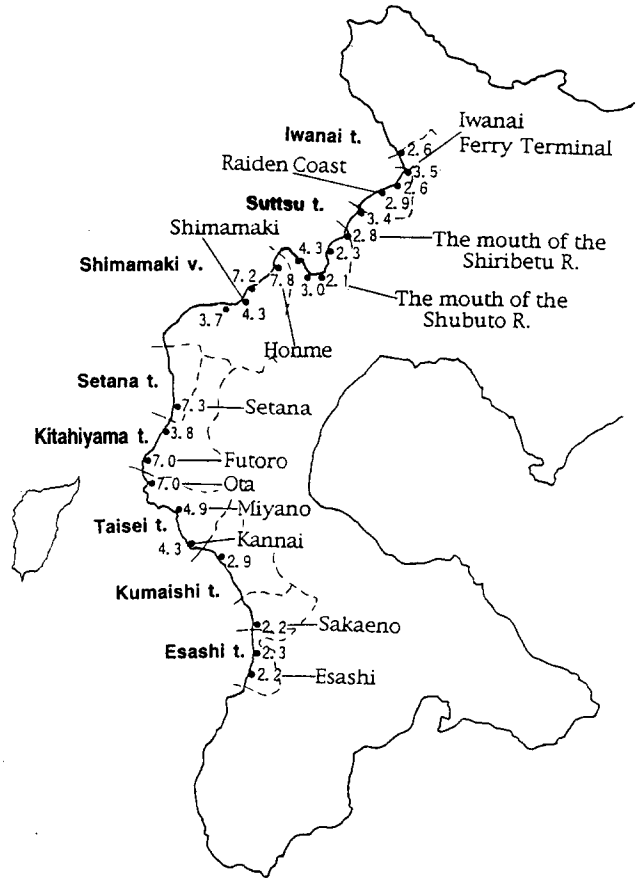

Fig. 1 Distribution of vertical runup for the southwest coast of Hokkaido

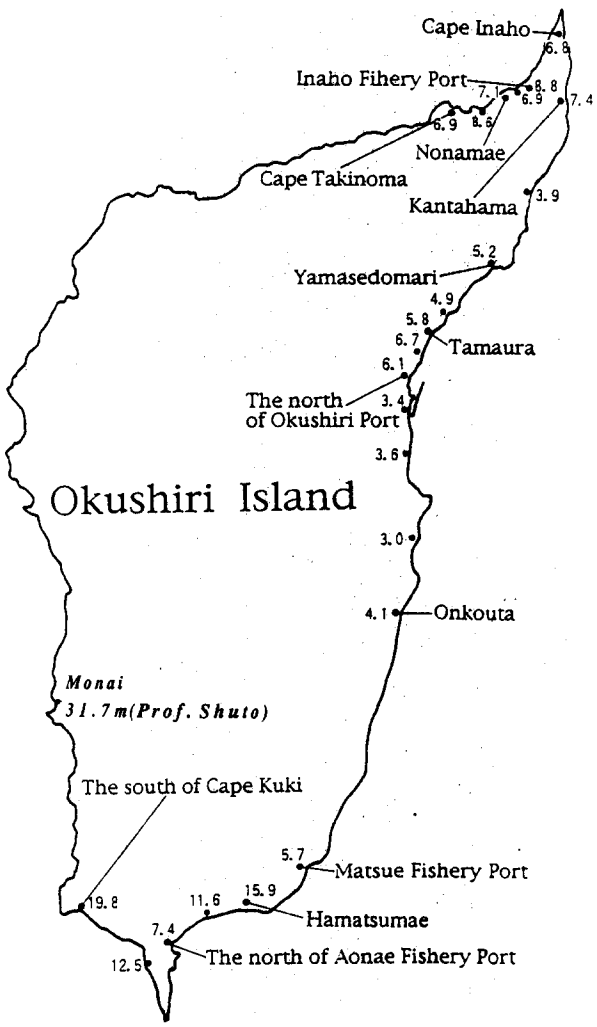

Fig. 2 Distribution of vertical runup for Okushiri Island

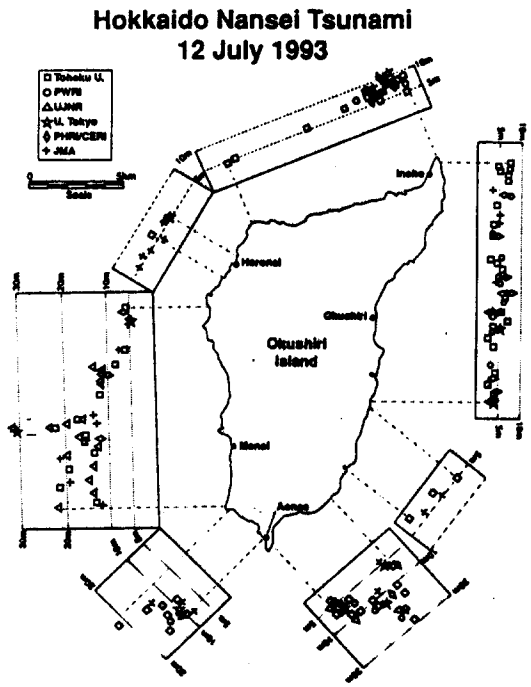

(after Bernard et. al.)

Fig. 3 Distribution of vertical runup for Okushiri Island(after E. Bernard et al.)

highest runup more than 30m was measured at Monai on the west coast. On the east coast, however, because it is sheltered from the tsunami source, runup height was generally small except for the southeast edge, Hamatsumae, where runup was as high as about 20m. It remains to be investigated why so high tsunami runup took place at Hamatsumae only.

EXPERIMENT ON TSUNAMI PROPAGATION

PWRI carried out a hydraulic model experiment in order to find out the above phenomenon because it was pointed out that numerical simulations could not give good explanation to the phenomenon.

(1)Model and Tsunami Generator

Figure 4 shows seabed topography around Cape Aonae. It can be seen that there is a very shallow region stretching to the south from the cape and there is Murotu Shoal about 4 km offshore. The water depth between Cape Aonae and Murotu Shoal is less than 20m. Figure 5 shows tsunami travel time and refraction diagram around Cape Aonae by numerical simulation. It can be seen that tsunami source is very close to Okushiri Island and tsunami of wide area refracts through the shallow region and gathers Aonae and Hamatsumae.

As the purpose of our experiment was focused on finding out the mechanism which caused the high tsunami runup at Hamatsumae, we made an extensive model to include all composition in the source affecting Hamatsumae. The scale of the model is 1:1100 without distorsion. Figure 6 shows a plan view of our model. Figure 7 shows sectional profile of pneumatic type tsunami generator. It can generate a tsunami by sucking water

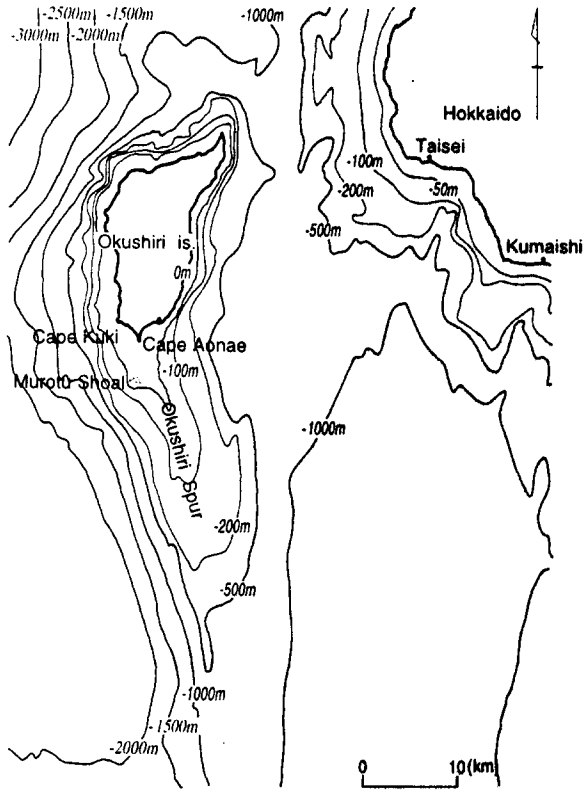

Fig. 4 Seabed topography around Cape Aonae

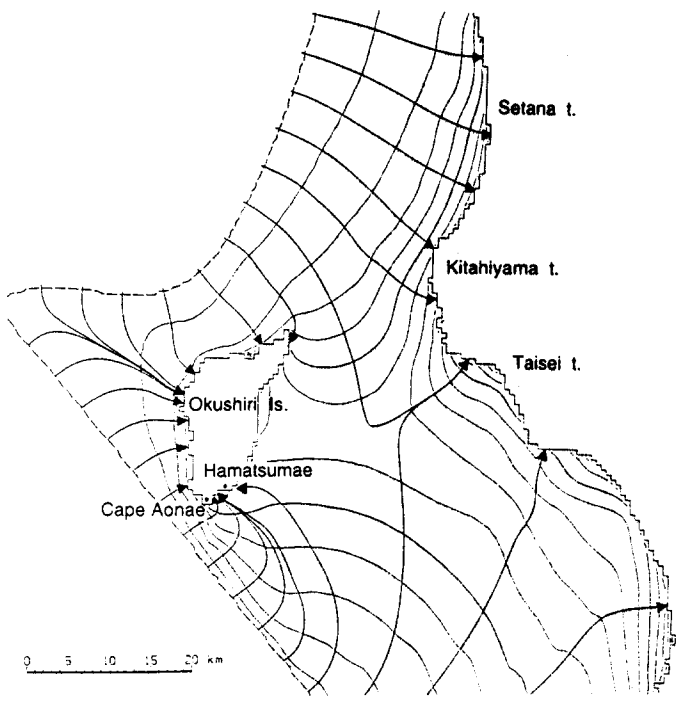

Fig. 5 Tsunami travel time and refraction diagram

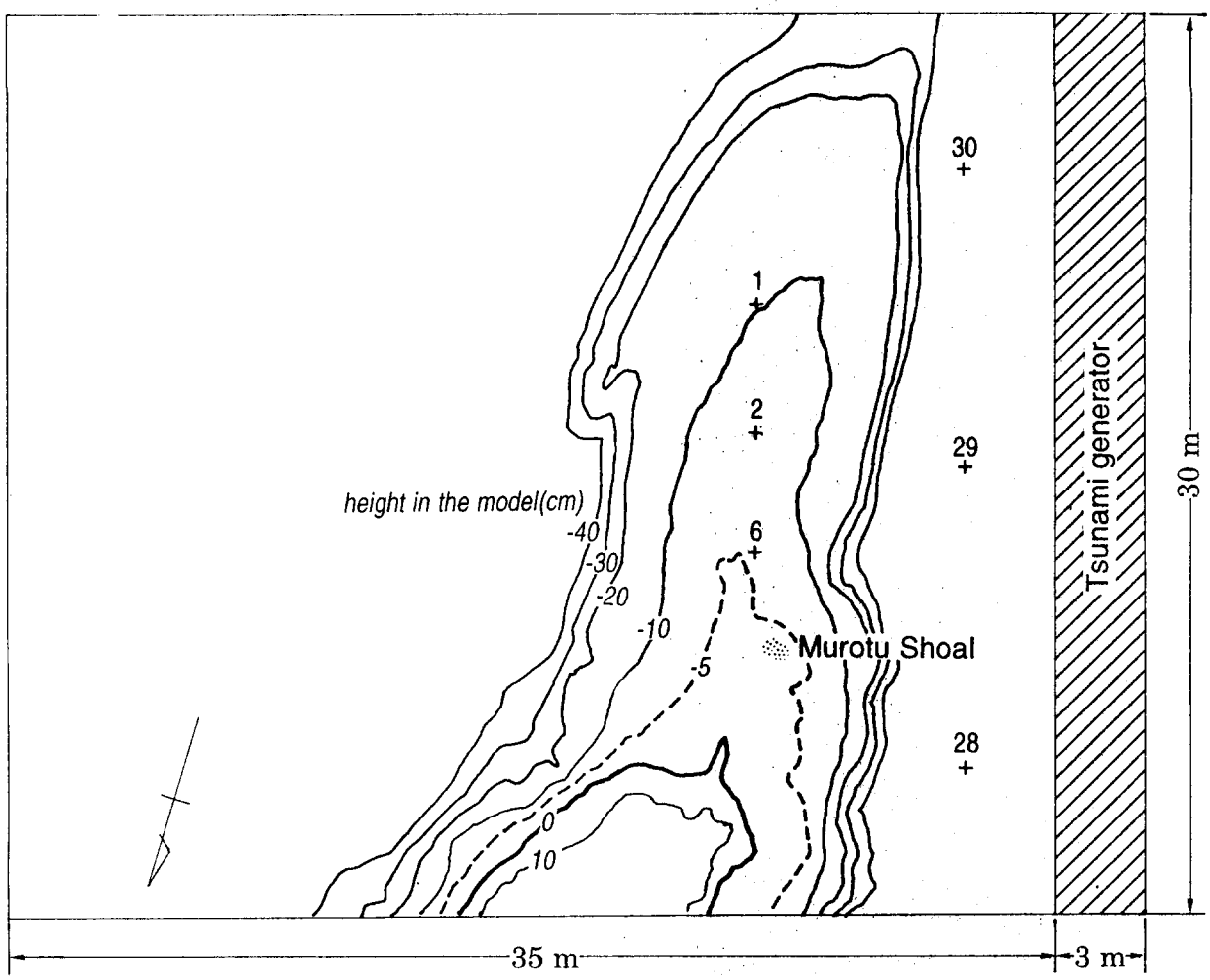

Fig. 6 Plan view of experimental model

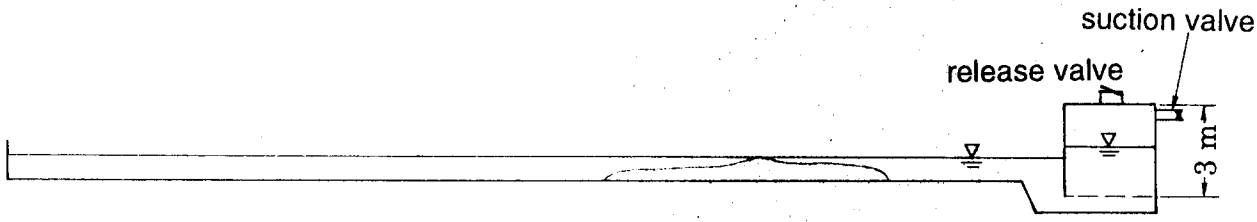

Fig. 7 Sectional profile of tsunami generator

into the air chamber and releasing it suddenly. Any reflected waves by the wall of tank do not affect the first tsunami attacking Hamatsumae in this model.

(2)Measurement

Tsunami profile was measured with capacitance-type wave gages at 30 points shown in Fig. 6 and 8. Water level after the suction was set to the mean water level. Because the scale of the model is very big, we do not strictly stick to the similarity of the wave height but we focused on the ratio of wave height at each point to the incident wave height. In order to catch the movement of crest line, we record wave with a VCR.

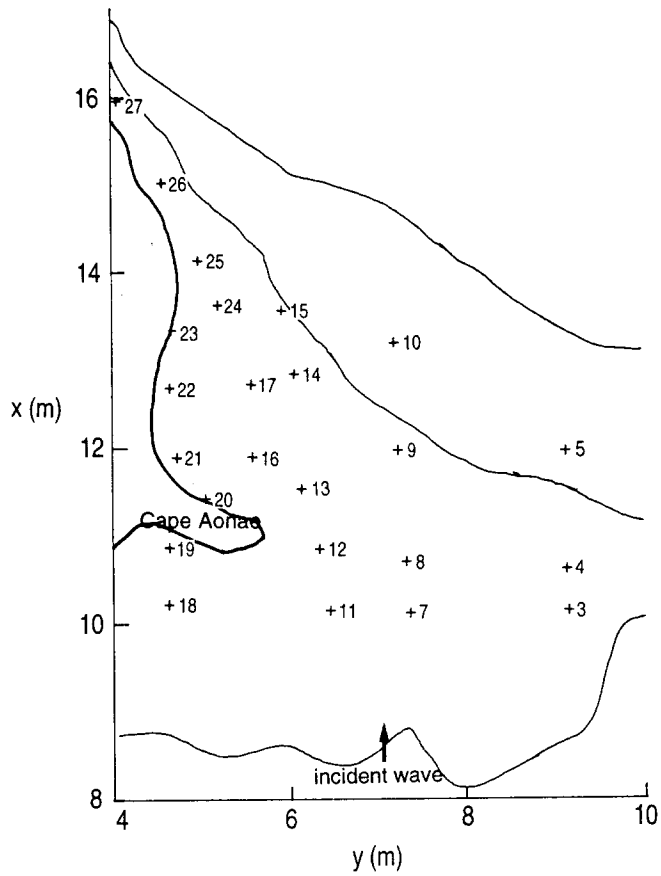

Fig. 8 Arrangement of wave gages

(3)Results

Figure 9 shows wave profiles with incident wave height of 4mm. As to the first wave, soliton fission was observed in the east side of the ridge of the spur. Especially, a very clear soliton fission was observed at pt. 10. But at pts. 25, 26 and 27, near Hamatsumae, soliton fission was not so clear and wave profile was sharp and peculiar. On the other hand, at points near around Cape Aonae and on the ridge or in the west side of the ridge of the spur, no soliton fission was observed in the first wave. The first soliton at pt. 10 had a longer period than the successive ones and the one at another point.

Concerning wave height, the magnifi-cation ratio against the incident wave height was about two at pts. 14, 15, 17, 24 and 25. The ratio was about three at pts. 10, 26 and 27. In this way, wave height was magnified near around Hamatsumae. The occurence of the

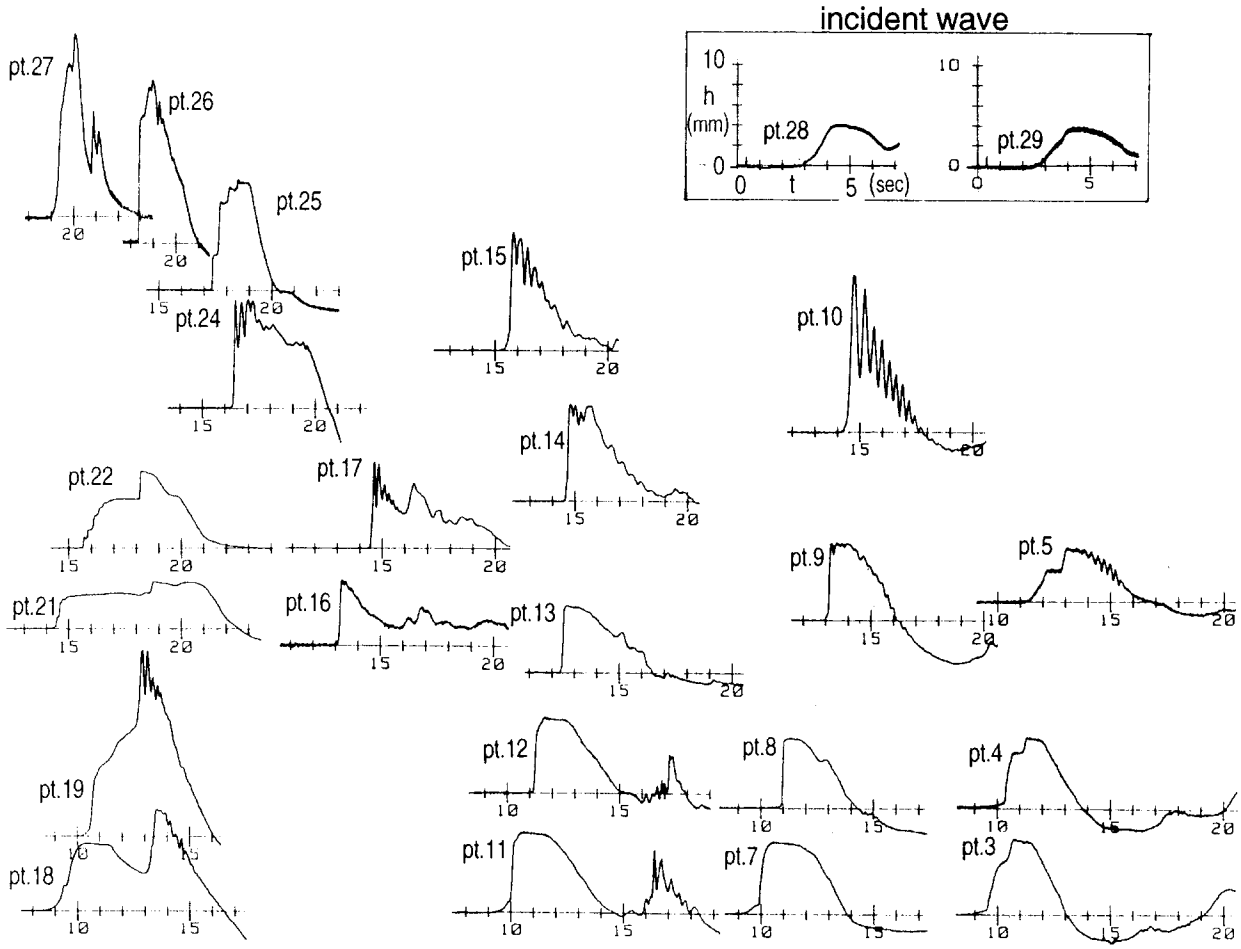

Fig. 9 Tsunami profiles measured with wave gages (incident wave height : 4mm)

large wave in this area agrees well with the field survey, although the maximum wave height in the experiment was attained at a little northern point.

It was also observed that a reflected wave due to Cape Kuki propagated to the south along the coast and diffracted at Cape Aonae. This situation appeared as the second wave in the record at pts. 11, 12, 18 in Fig. 9. At the nearest point to Cape Kuki, pt. 19, the reflected wave arrived at 13sec after wave generation with a clear soliton fission and it passed pt. 18 and then pts. 11, 12. Point 19 is located near the west foot of Cape Aonae. At this point, the reflected wave was superimposed to the incident first wave, resulting a rather big wave height. The magnification ratio at pt. 19 against the incident wave height was about

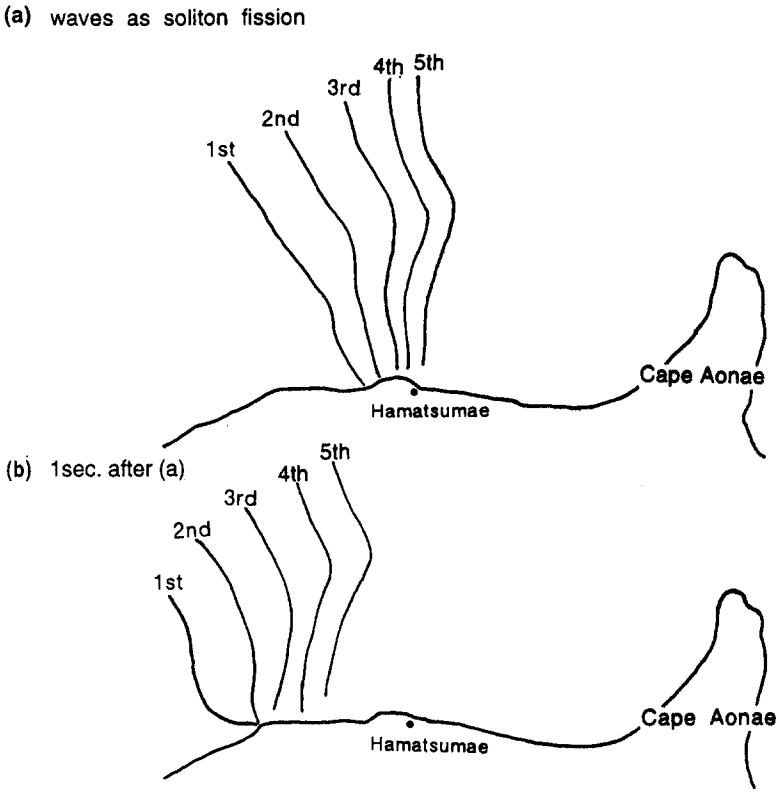

Fig. 10 Snapshots of wave crest line

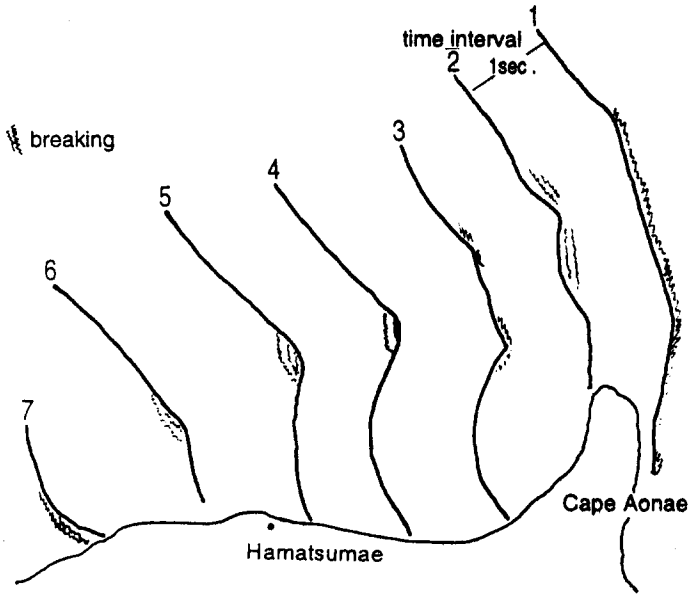

Fig. 11 Sketch of the propagation of the wave front

three. This value is almost same as that near Hamatsumae. Furthermore, it agrees well with the distribution of runup height shown in Fig. 3.

In order to study the mechanism of the occurrence of the large wave around Hamatsumae, the propagation of wave crest lines was investigated in detail through video frame analysis.

Figure 10 illustrates snapshots of wave crest line in the vicinity of the southeastern edge of the Okushiri Island. As was explained in Fig. 9, the tsunami was split into several solitons. Since the area in the vicinity of the shoreline is shallower than the offshore area, the direction of the propagation of each soliton is changed through refraction so that the crest lines become parallel to the shoreline. The celerity of the soliton is also affected by the bottom topography so that the celerity in the vicinity of the shoreline is smaller than that in the offshore. The celerity of the second soliton is larger than the first one since the second soliton propagates on a relatively high water level as seen in Fig. 9. The bottom topography in Fig. 6 indicates that the first soliton lost its speed in the vicinity of the shoreline and the crest line of the first soliton was strongly curved at around pt. 27. It is also noticed that the second soliton catched up to the first soliton at this location. It is therefore considered that the wave height at pt. 27 becomes large due to the combined effects of the refraction and the merge of two solitons.

Figure 11 illustrates a sketch of the propagation of the wave crest line of the first soliton. As is noticed in Fig. 6, there is a shallow shoal at the upperright edge of this figure. In the behind of this shoal, two crest lines were formed owing to the wave diffraction. The two crest lines intersect with a thin angle, forming a new crest with large amplitude through the nonlinear interaction. Since the newly created wave propagates with large celerity because of its large amplitude, another nonlinear interaction occurs at the both sides of the newly created wave crest. Figure 11 indicates that the large wave crest, which was formed through repeated nonlinear interaction, may hit the area of pts. 26 and 27.

CONCLUSIONS

Laboratory experiments were performed in order to study the mechanism of the occurence of large waves along Okushiri Island observed in the field survey of the Hokkaido-Nansei-Oki Earthquake

Tsunami. The propagation and the transformation of the tsunami were measured in detail with wave gages and a VCR. It is concluded that the two mechanisms are the reason for the occurrence of the large wave. The one is the combined effects of the wave refraction and the merge of the solitons which was split due to the effect of wave dispersion. The other is the nonlinear interaction of two waves intersecting with a thin angle.

ACKNOWLEDGEMENTS

The authors wish to express their appreciation to Professor N. Shuto, Tohoku University, for his helpful suggestions on the design of the hydraulic model test.

REFERENCES

E. Bernard and F. I. Gonzalez: Tsunami Devastates Japanese Coastal Region, Eos, Transactions, American Geophysical Union, Vol. 74, No. 37, pp.417-432, September, 1993.

Numerical Modeling Tsunamis

by

Philip L.-F. Liu*

ABSTRACT

A brief review of different aspects of numerical modeling of tsunami generation, propagation and inundation is given. Several difficulties are identified. They include the accurate description of the initial conditions from the seismic data, the appropriate modeling of wave breaking in the inundation model.

KEYWORDS: tsunami; inundation; propagation; numerical modeling.

1. INTRODUCTION

Tsunamis are impulsively generated ocean waves. They may be caused by an earthquake, landslide or volcanic eruption. In this paper we shall focus our discussions on earthquake-generated tsunamis. In an open ocean tsunamis are best described as long waves: the characteristic wavelength of tsunamis is usually one to two order of magnitude larger than the typical water depth. In the Pacific Ocean, tsunamis move at speeds of over 500 miles an hour, but their wave heights are usually low, perhaps only a foot. As tsunamis move into the continental shelf, they are refracted to conform to the shape of the bathymetry. At the same time, the shoaling water causes wave heights to increase greatly. As the tsunami rushes landward, the maximum run-up could reach as high as 30 m.

Historically, many tsunamis have caused severe damages in Japan, U.S. and other countries around the Pacific rim. Researchers and engineers have been working toward a goal which can not only predict the arrival time of a tsunami, but also calculate the detailed inundation map. Various degrees of success have been achieved towards this ambitious goal. In this paper, we will review briefly different elements of the tsunami modeling. We shall stress particularly the difficulties and unresolved issues.

2. SOURCE REGIONS

To model the propagation of a tsunami across an ocean, one must first calculate the initial water surface displacement, which depends on the characteristics of the earthquake. Most of large tsunamis have been generated near plate boundaries where an oceanic plate and a continental plate meet. The oceanic plate is subducted under the continental plate, while each plate moves slowly against each other. Although the movement is slow, roughly 2 to 10 cm/hr, a significant amount of stress and stain is accumulated along the interplate boundary. When the strain reaches the failure strain, a portion of the subduction boundary breaks and causes the rebound of the continental plate. Hence the earthquake. For an ordinary earthquake, the size of the source region is much greater than the water depth and the rupture velocity is usually very short in comparison with the tsunami propagation velocity. Therefore, the initial water surface displacement is almost exactly the same as the vertical displacement of the seafloor.

---

*School of Civil and Environmental Engineering, Cornell University, Ithaca, NY 14853

Using the elastic dislocation theory, Mansinha and Smylie (1971) obtained analytical expressions for the seafloor displacement due to inclined finite, strike-slip and dip-slip faults. To utilize Mansinha and Smylie's model, the following parameters are required: the length of the fault area (L), the width of the fault area (W), orientation of the fault area with respect to the North (θ) the dip angle (δ), the slip angle (λ), the dislocation on the fault (D), and the focal depth (d). All these parameters can be estimated from the seismological data. However, the accuracy of these parameters is often not certain. For instance, the dip angle, the slip angle, the orientation of the fault, and the seismic moment (M_o) can be obtained by inverting the spectra of both Rayleigh and Love waves over a specified period (e.g. Kanamori and Given, 1981). The fault area is determined approximately from the distribution of aftershocks. The dislocation on the fault, D, can be approximated as

$$D = \frac{M_o}{\mu LW} \qquad (1)$$

where μ is the rigidity of the earth at the source region. Therefore, this simple model ignores the heterogeneous fault motion, which could become important in some tsunamis (e.g. Satake and Kanamori, 1991).

In some subduction zones, a layer of subducted soft sediments could be sandwiches between the oceanic and continental plates. The rupture velocity becomes smaller, and the high-frequency part of the seismic spectrum is greatly reduced for the same seismic moment M_o. Therefore, a small earthquake measured in terms of seismic waves of high frequencies could produce a large tsunami as long as the rupture velocity is still much smaller than the tsunami propagation velocity. This kind of earthquake is called tsunami earthquake (Kanamori, 1972). Further complication could exist when an accretionary prism appears near an oceanic trench. Because of the large amount of soft sediments in the accretionary prism, seismic slip cannot reach the seafloor. Thus these earthquakes do not excite tsunamis very efficiently. As the deformation in the accretionary prism proceeds as a result of repeated occurrence of these events, sediment instability may eventually develop and finally a large-scale slumping occurs. This slumping may be the cause of a large tsunami.

While the elastic dislocation theory (Mansinha and Smylie, 1971) has been used widely to calculate the initial water surface displacement, numerical simulations of three recent tsunamis indicate that the theory under-estimates the resulting runup heights (Imamura et al., 1992). The causes for the discrepancies are not clear. Furthermore, the theory for determining the size and the shape of slumping and the corresponding water surface displacement has not been developed.

3. TRANSOCEANIC TSUNAMI PROPAGATION

To calculate the propagation of a tsunami over an open ocean, one needs to select appropriate governing equations. In the vicinity of the source region, the wavelength of the leading wave is roughly the same as the length of the source region, L, which is usually much greater than the water depth. Furthermore, the initial free surface displacement is also small in comparison with the depth. For instance, in the source region of the 1960 Chilean tsunami, the initial free surface displacement has a wave height about 8 m and a wavelength of 600 km, while the averaged water depth in the Pacific Ocean

is 5 km. Therefore, the wave slope is $0(10^{-5})$ and the depth to wavelength ratio is $0(10^{-2})$. It is obvious that the linear long wave theory is quite adequate for describing the transformation of the initial surface profile in the neighborhood of the source region.

As the tsunami propagates into an open ocean, the wave amplitude decreases because of the two-dimensional spreading. The wavelength increases due to the dispersive effects. Away from the continental shelf, the transoceanic tsunami propagation can be suitably described by the long-wave approximation. Although Boussinesq equations are the most uniformly valid, solving simpler equations is more preferable, if appropriate. Kajiura (1963) suggested that within the following traveling distance

$$R = \frac{6}{64} h \left(\frac{L}{h}\right)^3 \qquad (2)$$

the linear and nondispersive shallow-water theory is adequate. Kajiura's analysis was based on a two dimensional theory. More recently, Hammack and Segur (1978) re-examined the one-dimensional waves and reached the similar conclusion that the dispersion effects become important only if the leading wave of the tsunami has traveled a distance much greater than $6h\,(L/h)^3$. Using (2) as a guide, we can estimate the region within which the linear and nondispersive theory is valid for the 1960 Chilean tsunami, i.e. $R = (6/64)(5)(10^2)^3 \cong 10^6$ km, which is much larger than the dimension of the Pacific Ocean. Therefore, as far as the modeling of the leading wave of the 1960 Chilean tsunami is concerned, the linear, nondispersive wave theory is appropriate. On the other hand, for a small size earthquake such as the 1983 Hokkaido earthquake in the Japan Sea, the length of the source region is L = 20 km and the averaged depth is h = 2 km. As the result R = 200 km, while the length of the Japan Sea is about 900 km. Therefore, if one needs to obtain the tsunami information along the Korean coastal region, the dispersive effects must be included in the propagation model.

The Coriolis parameter of the earth is roughly 10^{-4} rad/s. For a transoceanic tsunami across the Pacific Ocean the Coriolis force becomes important because the traveling time is about 23 hours or 8.28×10^4 sec. Similarly, for the tsunamis in the Japan Sea, the traveling time from the Japanese west coast to the Korean east coast is approximately 9 hours or 3.24×10^4 sec. Therefore, the Coriolis force needs to be included in the computations if such a long duration is desirable.

In summary, to model the tsunami propagation over a long distance, the linear Boussinesq equations with the Coriolis force is the most adequate governing equations:

$$\frac{\partial \eta}{\partial t} + \nabla \cdot \vec{M} = 0 \qquad (3)$$

$$\frac{\partial \vec{M}}{\partial t} + gh\,\nabla\eta + 2\vec{\Omega} \times \vec{M} = \nabla\left[\frac{h^3}{3}\frac{\partial}{\partial t}\nabla\cdot\left(\frac{\vec{M}}{h}\right)\right] \qquad (4)$$

where η is the free surface displacement, $\vec{M}$ the depth-averaged volume flux, h the depth and $\vec{\Omega}$ the Earth's angular velocity. Equation (3) is the exact expression of the conservation of mass, while equation (4) represents the approximate equation for the conservation of momentum averaged over the depth. The right-hand side term of equation (4) is the contribution from the vertical acceler-

ation. Note that if this term is ignored, equations (3) and (4) become the linear shallow-water equations with the Coriolis force.

Equations (3) and (4) can be rewritten in a scalar component form. The spherical coordinate system coinciding with the longitude and the latitude of the Earth should be employed if the computational domain is large, such as the entire Pacific Ocean. On the other hand, for a smaller region such as the Japan Sea, the local Cartesian coordinate system can be used. Many numerical schemes are available for solving the Boussinesq equations. Because the modeling of transoceanic tsunami propagation involves a large computational domain and a long simulation time, both accuracy and efficiency are essential. In this paper we present and discuss an explicit, leap-frog, finite difference scheme, which has been used in many applications (Liu, et al. 1994).

For the ease of presentation, we only demonstrate the case where the Coriolis force is ignored and the depth is constant. The linear Boussinesq equations, (3) and (4), can be written in the following component forms:

$$\frac{\partial \eta}{\partial t} + \frac{\partial P}{\partial x} + \frac{\partial Q}{\partial y} = 0 \qquad (5)$$

$$\frac{\partial P}{\partial x} + gh\frac{\partial \eta}{\partial x} = \frac{h^2}{3}\left[\frac{\partial^3 P}{\partial t \partial x^2} + \frac{\partial^3 Q}{\partial x \partial y \partial t}\right] \qquad (6)$$

$$\frac{\partial Q}{\partial t} + gh\frac{\partial \eta}{\partial y} = \frac{h^2}{3}\left[\frac{\partial^3 P}{\partial x \partial y \partial t} + \frac{\partial^3 Q}{\partial t \partial y^2}\right] \qquad (7)$$

where P and Q are the volume fluxes in the x- and y-direction, respectively. By eliminating P and Q from (5), (6) and (7), we obtain

$$\frac{\partial^2 \eta}{\partial t^2} - gh\left(\frac{\partial^2 \eta}{\partial x^2} + \frac{\partial^2 \eta}{\partial y^2}\right) = \frac{gh^3}{3}\left(\frac{\partial^4 \eta}{\partial x^4} + 2\frac{\partial^2 \eta}{\partial x^2 \partial y^2} + \frac{\partial^4 \eta}{\partial y^4}\right) \qquad (8)$$

Liu, et al. (1994) show that the following explicit, leap-frog, finite-difference scheme satisfies (8) up to the third order of the grid size and time step size. Thus,

$$\frac{\eta_{i,j}^{n+1/2} - \eta_{i,j}^{n-1/2}}{\Delta t} + \frac{P_{i+1/2,j}^{n} - P_{i-1/2,j}^{n}}{\Delta x} + \frac{Q_{i,j+1/2}^{n} - Q_{i,j-1/2}^{n}}{\Delta y} = 0 \qquad (9)$$

$$\frac{P_{i+1/2,j}^{n+1} - P_{i+1/2,j}^{n}}{\Delta t} + gh\frac{\eta_{i+1,j}^{n+1/2} - \eta_{i,j}^{n+1/2}}{\Delta x} + \frac{gh}{12\Delta x}\left[\left(\eta_{i+1,j+1}^{n+1/2} - 2\eta_{i+1,j}^{n+1/2} + \eta_{i+1,j-1}^{n+1/2}\right)\right]\left[\left(\eta_{i,j+1}^{n+1/2} - 2\eta_{i,j}^{n+1/2} + \eta_{i,j-1}^{n+1/2}\right)\right] = 0 \qquad (10)$$

$$\frac{Q_{i,j+1/2}^{n+1} - Q_{i,j+1/2}^{n}}{\Delta t} + gh\frac{\eta_{i,j+1}^{n+1/2} - \eta_{i,j}^{n+1/2}}{\Delta y} + \frac{gh}{12\Delta y}\left[\left(\eta_{i+1,j+1}^{n+1/2} - 2\eta_{i,j+1}^{n+1/2} + \eta_{i-1,j+1}^{n+1/2}\right)\right] - \left[\left(\eta_{i+1,j}^{n+1/2} - 2\eta_{i,j}^{n+1/2} + \eta_{i-1,j}^{n+1/2}\right)\right] = 0 \qquad (11)$$

in which indices (i,j) denote spatial nodes and η the time level, Δx and Δy represent the grid sizes in the x- and y-direction, respectively, and Δt the time step size. The dispersion effects, represented by the right-hand side terms in the Boussinesq equation (8), are fully simulated by the finite-difference scheme (9), (10), and (11), up to the third order if the following condition is satisfied

$$(\Delta x)^2 = 4h^2 + gh\,(\Delta t)^2 \qquad (12)$$

The leap-frog scheme is stable if the Courant number, $C_r = \sqrt{gh}\ \Delta t/\Delta x$, is less than or equal to 0.866.

In practical applications, water depths vary and equation (12) cannot be satisfied everywhere. The computational domain is usually divided into several subdomains according to the objectives of the simulation. Within each subdomain an averaged water depth is used in (12) to determine the appropriate Δt and Δx. In general, in the region where h is smaller, a finer grid system with a smaller time step is necessary. A numerical algorithm has been developed for exchanging information between two regions of different grid sizes (Liu, et al. 1994).

4. INUNDATION MODEL

As the tsunami propagates over the continental shelf and enters the coastal zone, the amplitude grows and the wavelength shrinks. The nonlinearity gradually becomes important. During the final flooding stage, a tsunami might break and the energy dissipation features significantly. Even if the tsunami does not break the bottom frictional effects are definitely important because of the shallowness of water.

In terms of numerical modeling, the nonlinear shallow-water equations with dissipation terms are the appropriate governing equations. However, our knowledge on modeling wave breaking is still in its infancy. At the present, only the bottom frictional terms are included in the governing equations.

$$\frac{\partial \eta}{\partial t} + \frac{\partial P}{\partial x} + \frac{\partial Q}{\partial y} = 0 \qquad (13)$$

$$\frac{\partial P}{\partial t} + \frac{\partial}{\partial x}\left(\frac{P^2}{H}\right) + \frac{\partial}{\partial y}\left(\frac{PQ}{H}\right) + gH\frac{\partial \eta}{\partial x} + \tau_x H = 0 \qquad (14)$$

$$\frac{\partial Q}{\partial t} + \frac{\partial}{\partial x}\left(\frac{PQ}{H}\right) + \frac{\partial}{\partial y}\left(\frac{Q^2}{H}\right) + gH\frac{\partial \eta}{\partial y} + \tau_y H = 0 \qquad (15)$$

where $H = \eta + h$ is the total depth and τ_x and τ_y are the x- and y-component of bottom frictional force, respectively. Notice that the nonlinear convective forces are included in the momentum equations, (14) and (15). The frictional force is expressed in terms of either the Manning's n or the Chezy's coefficient c_f. Both Manning's and Chezy's formula are empirical formulas for steady state flows. The direct application of these formulas to a transient flow problem such as the tsunami inundation is not obvious. Moreover, during the run-up phase of the leading wave of a tsunami, a mass of water moves onto a dry land. The bottom friction caused by a dry land is different from that by a wet surface.

Equations (13), (14) and (15) can be integrated numerically by using the similar leap-frog scheme presented in (9), (10) and (11). The nonlinear terms are linearized by a upwind scheme. As a result, the accuracy of the numerical scheme is reduced to the first order in Δx and Δt. Therefore, a fine grid mesh is usually required to calculate the tsunami inundation heights. A moving boundary algorithm is also necessary for computing the movement of the shoreline. Liu et al. (1994) presented a simple scheme, which satisfies both conservation of mass and momentum.

Many issues concerning the inundation zone are to be resolved. For instance, the

interaction of tsunami and large obstacles, such as buildings and coastal facilities, needs to be examined. On the other hand, in an open coast, tsunami might cause significant sediment transport, which might be a good indicator for the maximum run-up heights.

5. CONCLUDING REMARKS

The computing technology has been improved significantly in the last decade. This trend will continue in future. Therefore, the accuracy and the capability of the tsunami modeling have also been increased. The weakest link of the tsunami modeling is the accurate description of the initial conditions from the seismic data. Because the fault parameters are obtained from the seismic waves, it might be useful to examine the source region problem by using the tsunami data directly. In the inundating zone, the physics of the dissipative mechanism, such as wave breaking, need to be understood. Forces acting on the coastal structures and buildings and tsunami induced sediment movements should also be examined in the future.

6. ACKNOWLEDGMENTS

This research was, in part, supported by a grant from the National Science Foundation to Cornell University (BCS9024965).

7. REFERENCES

1. Hammack, J.L. and Segur, H. 1978 "Modeling criteria for long water waves", J. Fluid Mech., 84:359-373.

2. Imamura, F., S. Ide, Y. Yoshida, K. Abe, and N. Shuto, 1992 "Estimate of the Tsunami Source of the 1992 Nicaraguan Earthquake from Tsunami Data", Geophys. Res. Let.

3. Kanamori, H. 1972 "Mechanism of tsunami earthquakes", Phys. Earth Planet Inter. 6:346-359.

4. Kanamori, H. and Given, J.W. 1981 "Use of long-period surface waves for fast determination of earthquake source parameters" Phys. Earth and Planet.

5. Lewis, C.H. and Adams, W.M. 1983 "Development of a tsunami-flooding model having versatile formulation of moving boundary conditions", Monograph series, The Tsunami Society.

6. Liu, P.L.-F, Cho. Y.-S., Seo, S.N. and Yoon, S.B. 1994, "Numerical Simulation of Tsunami Propagation and Inundation with Application to Hilo, Hawaii", Res. Rep. School of Civil and Environmental Engineering, Cornell University.

7. Mansinha, L. and Smylie, D.E. 1971 "The Displacement of the Earthquake Fault Model", Bull. Seismol. Soc. Amer. 61:1400-1433.

8. Mei, C.C. 1989 " The Applied Dynamics of Ocean Surface Waves" World Scientific Publishing.

9. Satake, K. and Kanamori, H. 1991 "Use of tsunami waveforms for earthquake source study", Natural Hazards, 4:193-208.

10. Shuto, N. 1991 "Numerical Simulation of Tsunamis - Its Present and Near Future", Natural Hazards, 4:171-191.

SUMMARY OF JOINT COOPERATIVE RESEARCH PROGRAMS

The Status of the U.S. Precast Seismic Structural Systems (PRESSS) Program

by

M. J. N. Priestly[1] and H. S. Lew[2]

ABSTRACT

The paper provides a brief overview of the recently completed Phase I U.S. PRESSS program, and the current Phase II program, which emphasizes theoretical and experimental studies of ductile connection systems for precast frame and panel structures

KEYWORDS:

buildings; concrete; earthquake; precast; research; seismic; structures

1. INTRODUCTION

The U.S. PRESSS coordinated research program on Precast Seismic Structural Systems has now been underway for four years. The aims of the program are to develop new economically and technically viable precast systems for seismic zones, and to develop design recommendations to enable these to be used in practice.

A preliminary feasibility phase (Phase I) of research was completed last year. This phase concentrated on analytical and design studies to investigate feasible design concepts, and to provide frameworks for design recommendations and for future analytical parameter studies needed to calibrate and quantify the design recommendations.

A second phase of research, involving analytical and experimental studies was initiated prior to completion of Phase I feasibility studies.

It is anticipated that several new programs will be funded, with particular emphasis on panel structures, analytical studies and cladding/frame interaction. Applications have been submitted to the National Science Foundation for research relative to the performance of precast structures in the January 17, 1994 Northridge earthquake. As a consequence of the post-earthquake activities the scope and extent of the U.S. PRESSS program is expected to expand significantly in the near future. The following notes briefly summarize the Phase I and II programs.

2. PHASE I RESULTS

As mentioned above, Phase 1 research is complete, and the following final reports are in preparation.

2.1 PRESSS Concept Development [1]

The report summarizes analyses and design studies carried out to identify and investigate feasibility of different structural concepts for precast frame and panel structures.

2.2 PRESSS Connection Classification [2]

Different possible connection systems between precast elements are collated and reviewed for technical merit, constructability and versatility, using a standardized review format.

2.3 PRESSS Analytical Platform [3]

The report consists of a user manual for a modified version of the well known DRAIN 2D

---

[1] University of California, San Diego, La Jolla, California 92093

[2] National Institute of Standards and Technology, Gaithersburg, MD 20899

inelastic time-history analysis program. Three new programs have been developed. Two of these are three-dimensional programs (DRAIN-3D and DRAIN-BUILDING), one with simplified input and the ability to simply constrain floor nodes in accordance with rigid diaphragm behavior, and the other, an enhanced version of DRAIN-2D, with features and hysteretic models appropriate for precast structures.

2.4 PRESSS Design Recommendations [4]

The principal effort described in the final report on this project was an investigation of the advantages of use of reliability theory to seismic design of ductile precast concrete structures. In addition, a framework of options for seismic design recommendations, using existing and novel code formulations has been prepared [5].

3. PRESSS PHASE II PROJECTS

The following projects are currently funded in Phase II of the U.S. PRESSS effort.

3.1 Ductile Connections for Precast Concrete Frame Systems [6]

Research is being jointly carried out at the University of Minnesota and the University of Texas at Austin, to provide rational design recommendations for seismic design of precast frame systems using ductile connections, based on experimented testing of a number of options representing the four categories of connectors being considered in the PRESSS Phase II research program. The categories are:

1. Nonlinear elastic connections
2. Connections relying on axial tension and compression yield of connecting elements
3. Connections involving shear yield
4. Connections involving added damping.

To date, tests have been carried out on the first two categories.

3.2 Ductile Connections for Precast Concrete Panel Systems [7]

Parallel to the above mentioned frame program, a study being jointly carried out at the National Institute of Standards and Technology (NIST), and the University of Nebraska-Lincoln is investigating ductile connections for panel structures, and seismic systems for low-to medium-rise buildings in regions of moderate seismicity.

Current testing is focusing on vertical connections between panel units, where the connectors are designed to be weaker than the panels, and to exhibit some energy dissipating characteristics.

3.3 Precast Frames with Unbonded Tendons [8]

At the University of California, San Diego, the use of continuous prestressing with unbonded tendons is being investigated. The focus of the research is to structurally simplify the precast elements as much as possible, and to minimize the amount of mild steel reinforcement. Particular emphasis is being placed on the force transfer mechanism within the beam-column joint region. Preliminary testing has been carried out on one exterior and one interior beam/column units, and six more are planned. Results indicate much lower levels of damage for a given drift level than for equivalent monolithic joints of similar dimensions and strength.

3.4 High Performance Fiber-Reinforced-Concrete (FRC) Energy Absorbing Joints for Precast Concrete Frames [9]

Building on previous research at the University of Michigan, Ann Arbor, experimental research is being carried out to provide design criteria for FRC plastic hinge regions forming the connections between precast elements. The specific objectives are (i) to determine the bond-stress/slip relationship between FRC and rebar in the plastic hinge region, (ii) to determine the shear strength of FRC under

monolithic and cyclic shear loading, and (iii) to develop a model for the joint to describe its hysteretic moment-rotation response.

3.5 Seismic Response Evaluation of Precast Structural Systems for Various Seismic Zones and Site Characteristics [9]

This analytical project is being carried out at Lehigh University. The aims are to carry out dynamic inelastic analyses of specific precast frame and panel buildings with connection characteristics appropriate for the four basic connection categories described earlier. Based on the results of these analyses, appropriate simplified design rules will be generated. Of particular importance is the quantification of dynamic amplification effects for shear and moment in columns, beams, and panels, so that required strength of precast elements can be determined based on appropriate capacity design principles.

3.6 Development of Seismic Design Recommendations for PRESSS

The continued refinement of design recommendation, begun in Phase 1 of the U.S. PRESSS project, is being continued in Phase II. This will be a joint effort with input from the University of Illinois, the University of California, Los Angeles, and the University of California, San Diego. Current efforts are well advanced to provide prescriptive requirements for 'strong-connection' precast frames [9].

3.7 Dynamic Scale Model Tests

A program of small scale dynamic shake table model testing of precast frames using different connector types is currently being planned at the University of Illinois, Champaign, Urbana. These tests will enable comparisons to be made between predicted results from time history analyses, and experimental results on complete structural systems.

4. CONCLUSIONS

The above represents a very brief summary of the U.S. PRESSS program. It is expected that further projects will be added to the program in the near future. A final stage (Phase III) is currently planned involving full-scale subassemblage testing of one or more five-story precast structures to test the final design concepts and analytical models developed in the program. These will be accompanied by rigorous analytical studies, and comparison of theoretical predictions and experimental results.

5. REFERENCES

[1] Dow Nakaki, Suzanne, and R. Englekirk, "PRESSS Concept Development, Project 1.1 - Final Report," Report No. PRESSS 94/03 (In Press).

[2] Stanton, J., "PRESSS Connection Classification, Project 1.2 - Final Report," Report No. PRESSS 94/04 (In Press).

[3] Powell, G.H. and F. Filippou, "PRESSS Analytical Platform, Project 1.4 - Final Report," PRESSS Report 94/06 (In Press).

[4] Hart, G., "PRESSS Design Recommendations, Project 1.6 - Final Report", Report No. PRESSS 94/06 (In Press).

[5] Priestley, M.J.N. and G. Hart, "A Framework of Options for PRESSS Seismic Design," Proceedings from the "Fourth Meeting of the U.S.-Japan Joint Technical Coordinating Committee on Precast Seismic Structural Systems," Tsukuba, Japan, May 1994.

[6] French, C. and M. Kreger, "PRESSS Phase II: Ductile Connections for Precast Concrete Frame Systems,"

Proceedings from the "Fourth Meeting of the U.S.-Japan Joint Technical Coordinating Committee on Precast Seismic Structural Systems," Tsukuba, Japan, May 1994.

[7] Schultz, A., M. Tadros and R. Magana, "Ductile Connections for Precast Panel Structures - Concepts and Experiments," Proceedings from the "Fourth Meeting of the U.S.-Japan Joint Technical Coordinating Committee on Precast Seismic Structural Systems," Tsukuba, Japan, May 1994.

[8] Priestley, M.J.N. and G. MacRae, "Testing of Two Precast Post-Tensioned Beam/Column Joint Subassemblages with Unbonded Tendons," Proceedings from the "Fourth Meeting of the U.S.-Japan Joint Technical Coordinating Committee on Precast Seismic Structural Systems," Tsukuba, Japan, May 1994.

[9] Priestley, M.J.N., Editor, "Report on the Fourth U.S. PRESSS Coordinating Meeting," Report No. PRESSS 94/02, March 1994, 173 pp.

[10] Englekirk, R., "Damage to Ductile Steel Frames in the Northridge Earthquake," Proceedings from the "Fourth Meeting of the U.S.-Japan Joint Technical Coordinating Committee on Precast Seismic Structural Systems," Tsukuba, Japan, May 1994.

[11] Cheok, G. and J. Stanton, "Beam-to-Column Connections for Precast Concrete Moment-Resisting Frames," Proceedings from the "Fourth Meeting of the U.S.-Japan Joint Technical Coordinating Committee on Precast Seismic Structural Systems," Tsukuba, Japan, May 1994.

The Present and Future of the United States-Japan Cooperative Earthquake Research Program Utilizing Large-Scale Testing Facilities

by

Hiroyuki Yamanouchi*

ABSTRACT

First, this paper reviews briefly the history and significance of the U.S.-Japan Cooperative Earthquake Research Program Utilizing Large Scale Testing Facilities. Then, some proposals regarding a new stage of future cooperation are presented.

KEYWORDS:
U.S.-Japan Cooperative Research Program, future cooperation, framework

INTRODUCTION

The U.S.-Japan Cooperative Research Program on Earthquake Engineering Utilizing Large Scale Test Facilities under the auspices of the U.S.-Japan Natural Resources Panel on Wind and Seismic Effects (UJNR) was initiated in 1979 by an agreement between the U.S. National Science Foundation (NSF), and the Japanese Ministry of Construction (MOC) and the Science and Technology Agency (STA). The agreement was based on the recommendations as outlined in the final report of the U.S.-Japan Planning Group for the program (Ref.1). The Cooperative Research Program focused on the following four building structure phases up to 1993, on the line of the Planning Group report:

The first phase: reinforced concrete structure (1979-1981)
The second phase: steel structure (1981-1984)
The third phase: masonry structure (1984-1989)
The fourth phase: precast concrete structure (1989-1993)

Also, in the Planning Group report, research on Mixed Steel/Reinforced Concrete Structures was identified as an important phase of the Program. After the recommendations, it has become widely recognized that innovative uses of two or more different materials in a structure leads to more efficient system for resisting seismic forces. In particular, during the past ten years the use of composite and hybrid structures has gradually increased both in the U.S. and Japan. In spite of some research and development work by Japanese construction companies, not enough is known at present regarding their seismic behavior and performance. Design procedures and codes for use in typical design offices are, thus, currently non-existent.

Looking at the importance of developing design guidelines (a unified code development) for typical composite and hybrid structures that are used in current practice, and of developing new and innovative composite structural elements and hybrid systems using advanced new materials and/or devices, a five-year research program on Composite and Hybrid Structures was proposed by the Building Research Institute (BRI) and the U.S. interested professors in 1991 as the fifth Phase of the U.S.-Japan Cooperative Earthquake Research Program. Then, new recommendations on the new Phase were made on the basis of a number of technical meetings of the U.S. and Japan Planning Groups and a Joint Planning Group Workshop held in Berkeley on September 10-12, 1992 (Ref.2). On the basis of the Workshop, the first Joint Technical Coordinating Committee (JTCC) on the Composite/Hybrid Phase was held on 8-9 November 1993 at BRI, to discuss more detailed research plans and summarize up-to-date recommendations.

Further, considering the prospect of the U.S./Japan Cooperative Research Program, not only limited to seismic and wind effects, some critical situations and needs raised both in the U.S. and Japan should be taken into

---

* Director of Structural Engineering Department, Building Research Institute (BRI), Ministry of Construction (MOC), Tatehara-1, Tsukuba, Ibaraki 305, Japan.

account in planning the future cooperation. Thus, in this paper, some thought and proposals are given in this regard.

REVIEW OF THE PAST PHASES

A lot of technical knowledge and practical information was obtained from the past cooperative research phases. While elsewhere we can refer to various papers and reports for each research result and technical information, the essence of significance and achievements of the past Phases can be described as follows:

(1) Through the first and second Phases, the "Pseudo Dynamic Testing Method" applicable to full-scale building structures completed. After this success, the testing method become one of major earthquake-resistance test methods; many research institutes of Japanese construction companies, several U.S. universities and a few of developing countries have introduced the pseudo dynamic testing facilities.

(2) Since a full-scale test structure was designed, tested and analyzed jointly by the U.S. and Japanese sides in the first and second Phases respectively, mutual understanding on the difference between the U.S. and Japan in the design codes, practice and also even in the way of thinking was improved.

(3) On the other hand, in the third and also in the fourth Phases, a common full-scale test structure between both sides was not reached, because the discrepancy in the design codes and practice between the two countries was so much large for determining a unified test building. However, from the viewpoint of design and practice on each side, new guidelines for design and construction have been or are being developed, though the practical results of the first two Phases were referred to just modifying the then design codes.

(4) In each Phase, active exchange of personnels with short and long terms was performed between both the countries. As the effect of this activity, mutual understanding on research and construction circumstances in both the countries was expanded and deepened. Also through these exchanged-people, associated man to man channels have dramatically increased.

TOWARD A NEW STAGE

In one word, the past four Phases dealt with examination and modification of existing structural systems with conventional materials such as ordinary steel and concrete. Also in these Phases, the technical validity of current codes and design practice was examined by experimental and analytical manners, and particularly in the latter two Phases, new guidelines on design and construction technology were proposed on each side. Now, as previously mentioned, the current Phase, Composite and Hybrid Structures, has aspects somewhat different from the past Phases. That is, the Phase will deal with new structural members and systems by mixing two or more different materials, and some research topics will involve new materials and devices. This slight but significant change of basic characters of research contents means a transition to a new stage of the cooperation.

Then, questions on the next step of the cooperation would be raised as follows:

Based on the past and current achievements, and experiences, what direction should the future cooperation face to? And, what target should the future program deal with? Furthermore, what framework of cooperation should we create for more efficient and beneficial research and development? To answer these questions, we should think about the following items.

(1) <u>Interactive Research between Structural Engineering and Other Research Fields</u>

The research on existing conventional structural systems and materials, generally speaking, has nowadays been less attractive as new topics of the future U.S.-Japan Cooperative Research Program, since such the research has almost reached to a "critical point" where it becomes hard to attain significant findings and innovative knowledge. This means, in other words, that most significant and principal problems have been solved. Also, looking at various performance recently required to building structures, such as durability, fire-resistance, human comfort, life

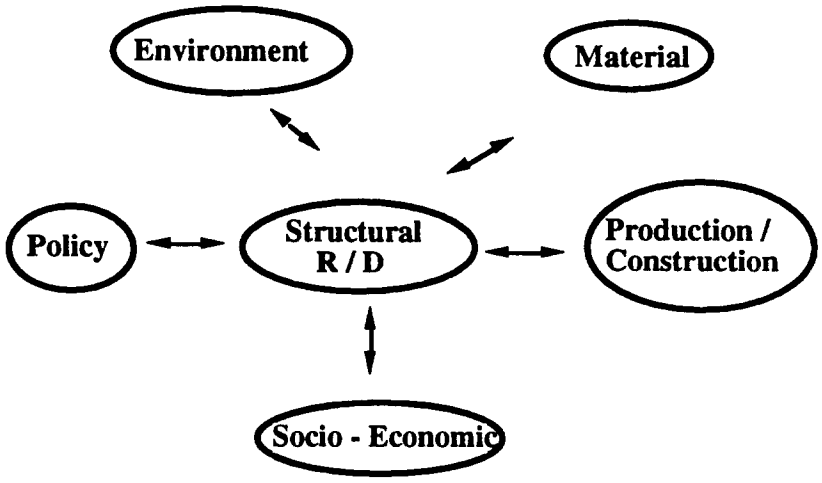

Fig. 1 Interactive Cooperation with Other Research Fields

cycle cost and so on, existing structural systems and materials cannot add function with something new, or cannot give birth to high performance based on today's diverse needs. From this point of view, research on building structures should be expanded into cooperative research with other research fields (Fig. 1). In this regard, the interactive research with the field of material science and technology would have the highest priority to stimulate and improve structural engineering research.

(2) Increasing Roles of Private Firms

At least in Japan, during the past two decades private companies have come to establish and foster their own research laboratories or institutes. Then, their ability of research and development has much increased, and in many areas, in particular related to construction or production, their ability and achievements become superior to those of universities and governmental research institutes. According to this circumstances, efficient research and development can be done in cooperation with private firms on equal terms.

In the Composite and Hybrid Phase, the above thing is considerably taken into account, that is, research work and necessary funds are adequately shared among private sectors and BRI. This type of cooperation will be much more needed in a future new stage, not only in Japan but also in the U.S..

(3) Framework of Cooperation in Pursuit of Mutual Benefits

The past Phases were performed under the auspices of the UJNR Panel on Wind and Seismic Effects . This is the formal framework of the U.S.-Japan Cooperative Earthquake Research Program; the UJNR Panel has been useful and will continue to implement the cooperative work. And, the Composite and Hybrid Phase will be carried out also within this framework. However, this framework is inflexible so far to incorporate private companies and academic people into the Panel, on terms of equality. As previously mentioned, considering the increasing importance of roles of private sectors, a new and expanded framework seems necessary to promote effectively the future new stage cooperation where private firms can actively participate on equal terms.

Regarding the framework, there is another topic, that is, the U.S.-Japan Framework for A New Economic Partnership / Positive Cooperation in Global Perspective. The two round-table talks at sub-cabinet level were held in September and December 1993 to set up Action Plans for the cooperation. In the broad items for positive cooperation, "Construction Technology" is included. To arrange Common Agenda, BRI/MOC and NSF are working together as the action offices. Here, our

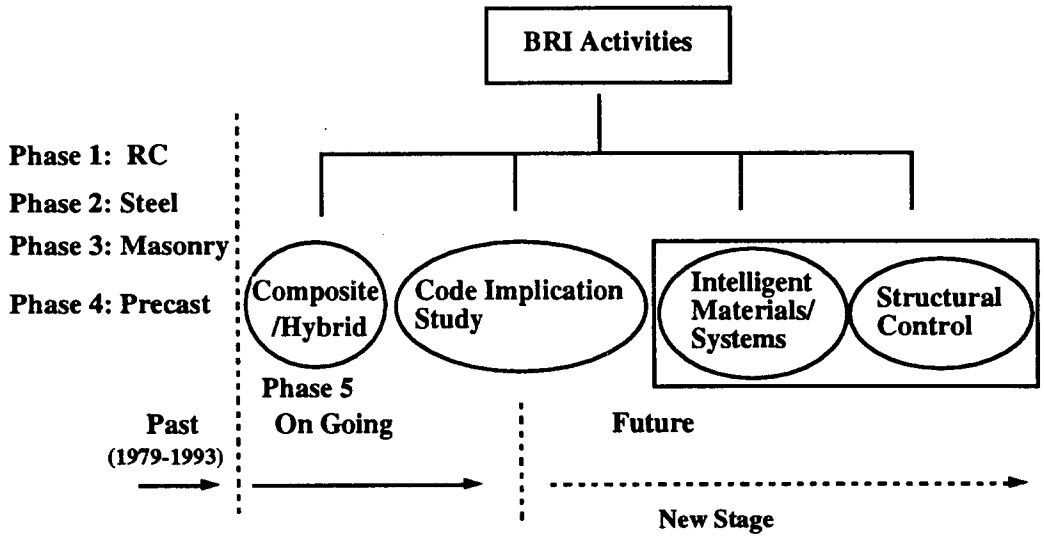

Fig. 2 BRI Activities in US/Japan Cooperation

general agreement is that the cooperation could be modeled after the UJNR except that it should be more broad-based under the new cooperation program, minimizing any duplication with the UJNR efforts.

BRI ACTIVITIES

Now, considering the above situations and NSF initiatives on recent programs, BRI will move to the second stage of the U.S.-Japan cooperation, with strong willingness, in the future (Fig. 2). In this cooperation, the contributions of BRI will be as follows:

(1) To fill the role as the host institution on Japanese side in the field of building-related technology,

(2) To propose the evaluation system of innovative technology, and

(3) To develop new comprehensive design/ evaluation methodology and system based on performance, which should be able to deal with innovative systems as well.

SUMMARY

The significance of the U.S.-Japan Earthquake Research Program from 1979 to today was briefly reviewed. Also, some recent change of circumstances around research and development on building structures were discussed. By these discussions, some proposals were presented for the future new stage of cooperation.

REFERENCES

1. "Recommendations for a U.S. -Japan Cooperative Research Program utilizing Large-Scale Testing Facilities," Report No. UCB/EERC 79-26, September 1979.
2. "Recommendation for U.S.-Japan Cooperative Research Program -Phase 5 Composite and Hybrid Structures," Report No. UMCEE 92-29, November 1992.

NORTHRIDGE SOUTHERN CALIFORNIA AND HOKKAIDO NANSEI-OKI EARTHQUAKES

The January 17, 1994, Northridge Earthquake, California

by

H. S. Lew[1], Jim Cooper[2], Sam Hacopian[3], Walter Hays[4], and Mike Mahoney[5]

ABSTRACT

The magnitude 6.8 earthquake occurred during the pre-dawn hours of January 17, 1994 provided a crucial test for assessing our progress in earthquake resistant design and construction over the past two decades, following a similar magnitude event, the San Fernando earthquake in 1971.

A reconnaissance team was organized by NIST through the auspices of the National Earthquake Hazards Reduction Program and the Interagency Committee on Seismic Safety in Construction, to observe the damage, assess the performance of various types of engineering structures, and document the effects of the earthquake on the built environment: buildings, bridges, and lifeline systems. This paper summarizes what we learned from the reconnaissance effort. More detailed documentation has been presented in an NIST Special Publication, 862, "1994 Northridge Earthquake: Performance of Structures, Lifelines, and Fire Protection Systems."

1. INTRODUCTION

A strong earthquake of magnitude 6.8 centered under the community of Northridge in the San Fernando Valley in California shook the entire Los Angles area at 4:31 a.m. local time on Monday, January 17, 1994. January 17 was a federal holiday honoring Dr. Martin Luther King's birthday and, because of this and also the early morning hour, most non-residential buildings were empty and traffic was extremely light. These fortuitous circumstances greatly helped limit the number of deaths and injuries.

As of February 14, there were a total of 58 deaths attributed to the earthquake. About 1,500 people were admitted to hospitals with major injuries, another 16,000 or so were treated an released.

Estimates of the number of people temporarily or permanently displaced because of damage to their houses or apartments ranged from 80,000 to 125,000. Total loss from this earthquake was estimated to reach $30 billion, the costliest earthquake in U.S. history.

Although the earthquake caused unprecedented damage and disruption, it also created an unprecedented opportunity to learn about earthquake mechanisms and effects. The earthquake triggered a historically high number of strong ground motion recordings. These recordings, coupled with wide-reaching damage surveys and analyses of specific structures, can provide a wealth of new insight into and understanding of earthquakes and their effects.

2. SEISMOLOGY AND GEOTECHNICAL EFFECTS

2.1 Seismology

The epicenter of the earthquake was located at 34°12'N, 118°32'W, about 30 km west-northwest of Los Angeles in Northridge (Figure 1). The focal depth was estimated at about 15-20 km (USGS 1994

1. National Institute of Standards and Technology
2. Federal Highway Administration
3. Department of Housing & Urban Development
4. U.S. Geological Survey
5. Federal Emergency Management Agency

and EERI 1994). The strong shaking lasted about 15 seconds in the epicenter area. The earthquake occurred on an unidentified fault. The fault had no distinct surface rupture.

Records from the main shock and aftershocks indicate that the rupture had a thrust focal mechanism, striking 10o north of west and dipping 30° to 45° south (Hauksson 1994, EERC 1994, and EERI 1994). Thousands of aftershocks were recorded in the following months; there were seven of them having a magnitude 5 or greater as of March 20.

Over one hundred strong-motion instruments were triggered by the event. In the epicenter area, peak horizontal ground accelerations approached or exceeded 1g in several locations (USGS 1994). Figure 2 shows the locations of selected peak horizontal and vertical ground acceleration recorded by the USGS's National Strong Motion Program. The Los Angeles Building Code specifies a design acceleration of 0.4g. An accelerograph recorded on the grounds of the Veterans Affairs Hospital in Sepulveda is shown in Figure 3. Note that the transient peak accelerations shown were each one-time events and not typical of the body of the shaking.

The high vertical accelerations recorded in numerous locations have induced discussions among the engineering community over the need to consider vertical accelerations in design. Currently, the model codes only require consideration of vertical accelerations in the design of cantilevered elements and post-tensioned horizontal elements, and those only in regions of high seismicity. In this event, a free-field vertical acceleration of 1.18g was recorded at Tarzana, about 6 km south of the epicenter, and maximums of about 0.6g occurred at several other locations.

2.2 Geotechnical Effects

The fracture of the thrust fault apparently did not reach the surface. No major surface faulting had been identified as of late March. Landslides, rock slides and slope failures were the most visible geotechnical effect caused by the earthquake. Soil liquefaction was widely reported, but apparently caused little structural or agricultural damage. Sand boils were reported along the Pacific coast from Mugu Lagoon to the north to the Port of Los Angeles to the south, and inland in the epicentral area, near the junctions of interstate highways 5 and 210 and 5 and 405, and in areas around Simi Valley northwest of the epicenter (EERI 1994 and EERC 1994).

Liquefaction-related surface cracking and vertical offsets were reported at all sites where sand boils were observed. At other sites, such as the Jensen Filtration Plant in Sylmar and the nearby San Fernando Juvenile Hall, no sand boils were reported but lateral spreading and ground settlement indicate that liquefaction occurred. Minor breaks in water, sewer, and other pipe systems were widespread in areas of lateral spread and liquefaction.

3. BUILDINGS

The earthquake provided the first full scale "test" of modern (post 1970's) seismic building codes in this country. For the first time, a large and varied population of buildings was subjected to ground shaking equal to or exceeding that recognized in modern codes for design. The epicenter of the earthquake was located in a heavily populated urban-suburban area, the San Fernando Valley northwest of Los Angeles. In the epicentral region, most buildings experienced ground accelerations equal to or greater than that upon which the code design values are based.

The building damage caused by the 1971 magnitude 6.6 San Fernando earthquake in 1971 prompted significant revisions to earthquake design requirements. As a result, the 1976 Uniform Building Code (UBC) is often specified as a "benchmark" code that ushered in "modern" seismic design methods (FEMA 154, 1988). Comparisons of building response in the 1971 and 1994 quakes give some insight into the efficacy of earthquake mitigation practices that have been undertaken in the Los Angeles area in the intervening years.

The intent of building codes is to specify the minimum requirements needed for a structure to provide acceptable life-safety. Viewed in this light, the earthquake demonstrated the success of modern building codes. Of the 58 deaths attributed to the earthquake, 22 were caused by structural failures of buildings. The population of the three affected counties (Los Angeles, Ventura, and Orange) totals about nine million people. However, 80,000 to

125,000 people were made temporarily or permanently homeless because of damage to their homes and apartments. Schools, hospitals, offices, stores, and other commercial and industrial enterprises were forced to close due to damage, much of it nonstructural. Viewed in this light, the earthquake demonstrated the limitation of modern building codes. Because they do not include postearthquake serviceability requirements for most buildings, they do not ensure preservation of normal building function after an earthquake. Because they area not intended to prevent property damage in a large earthquake, economic losses can be high.

Building codes cover only new construction or changes to existing construction. The City of Los Angeles established a requirement that all unreinforced masonry buildings (URMs) larger than a specified size that were constructed prior to 1934 be assessed for seismic adequacy and, if necessary, be rehabilitated. This requirement, called "Division 88" led to the rehabilitation of all the older URMs, certainly helped reduce the life loss from this earthquake.

Buildings of all ages and types were damaged in the quake. However, it also should be noted that many buildings of all ages and types performed well. In the epicentral area, from the California State University, Northridge campus, to the Northridge Fashion Center mall, serious damage occurred. Several pockets of severe damage occurred at widely separated locations, such as downtown Santa Monica, along Ventura Boulevard in Sherman Oaks, downtown Glendale, and Hollywood Boulevard in Hollywood (Figure 4). The following sections present a few of the most spectacular damages resulted from the earthquake.

3.1 Northridge Meadows Apartment Complex

Collapse in a single apartment complex caused sixteen of the twenty-two deaths related to building failures. The Northridge Meadows complex, constructed in 1972, consisted of several three-story wood-frame buildings. About half of the units had open spaces for parking on the street level, typically around the perimeter of the complex. Most of the interior courtyard facing units had living space at the ground level rather than parking. About half of the buildings in the complex collapsed. The first story gave way while the second and third stories remained largely intact. The sixteen people killed were in the first story apartments. All the buildings in the complex suffered some damage (Figure 5).

The apartment buildings were predominantly wood-frame,with wire mesh and stucco walls. Rows of steel pipe columns supported the upper stories along the building perimeter between parking bays (Figure 6). Transverse walls were typically spaced about every three parking bays. Longitudinal walls separated the parking areas from first story living spaces. The wire mesh and stucco coating on these walls provided insufficient resistance to the lateral earthquake forces generated by this earthquake.

The upper stories of the collapsed buildings were displaced laterally and in some cases came to rest offset by as much as three meters from their original locations. The steel pipe columns, which hinged at their bases, apparently controlled the distance of the offset as they bent to the ground (Figure 7). The Northridge Meadows building configuration, two stories of living space in a long, narrow building above one level of parking, is common in the San Fernando Valley. Many buildings of this type sustained serious damage, and some collapsed. These buildings were also built in the late 1960's or early 1970's, when use of stucco for seismic resistance in low-rise buildings was common. Current codes have essentially ban the use of this material.

3.2 Champagne Towers

Champagne Towers on Ocean Avenue in Santa Monica, a 16-story concrete apartment building, suffered serious damage. The condition of this building illustrates two classic examples of earthquake damage: damaged coupling beams between linked shear walls and shear failure of unintentionally short columns.

The transverse end walls are pierced by a single vertical row of window openings. The wall segments between the windows act as coupling beams linking the wall segments on either side. These beams suffered serious diagonal cracking (Figure 8). In the longitudinal direction, the lateral-force resistance is provided by concrete moment frames. The front of the building shows

no sign of damage. At the back, the columns and transverse wall ends are diagonally cracked (Figure 9). The solid infill railings which rise to about mid-height of the columns create an unintentional "short-column" effect, causing the columns to fail in shear. At the front of the building, metal pipe railings are provided at the balconies rather than solid infill, as at the back. This may partially explain why there is no apparent damage at the front of the building.

3.3 Hospitals

The original hospitals of Holy Cross and Olive View were badly damaged in the 1971 San Fernando earthquake. They were rebuilt following the requirements of the Hospital Act introduced by the State of California after the 1971 quake. The structural systems of these two hospitals performed well in the Northridge earthquake. However, damage to the sprinkler and chilled water systems at Olive View rendered the building temporarily unusable. At Holy Cross, damage to the air handling system forced closure of the hospital. However, St. John's Hospital in Santa Monica was closed due to structural damage. The 7-story northwest wing, which was built in 1952, had severe diagonal cracks in the piers between windows (Figure 10).

3.4 Bullock's Department Store

The collapse of large portions of the roof and floors of the 3-story concrete Bullock's department store at the Northridge Fashion Center could have caused more deaths than any other single building failure in this earthquake. Many multi-story columns were left intact as the concrete slab floors and roof fell on top of each to the basement, presumably due to punching shear failure of the slabs. The remaining-standing columns showed no evidence that slab reinforcement had been continuous through the columns (Figure 11).

3.5 Unreinforced Masonry Buildings

Reinforced masonry construction was introduced in 1934 after the 1933 Long Beach earthquake. Yet many pre-1934 unreinforced masonry buildings still exist today and all of them in the City of Los Angeles have been retrofitted with through-bolts and face plates to connect the masonry walls to the wood floor and wood diaphragms, as required by the so called "Division 88 requirement (Figure 12). The City of Santa Monica doesn't have the same rehabilitation requirements, nevertheless, most, if not all URMs have been retrofitted with above-mentioned techniques.

Despite rehabilitation, many URMs in Santa Monica and in Hollywood were badly damaged. As a life-safety measure, rehabilitation was somewhat successful in this earthquake. However, rehabilitation was not successful at preventing damage; portions of buildings disintegrated, top stories and corners were particularly vulnerable (Figure 13). Such damages could present a real and serious threat to the safety of persons outside the affected building.

3.6 Kaiser Permanente Office Building and Barrington Building

The Kaiser Permanente office building on Balboa Boulevard in Northridge was badly damaged. The second story columns disintegrated, causing the upper stories to collapse onto the first story, which remained intact (Figure 14). The bare frame exposed by the damage suggests that the buildings had a strong-beam/weak-column configuration (Figure 15). The damage appears to have initiated at the joints.

The L-shaped concrete frame Barrington Building in West Los Angeles also had damage concentrated in the second story columns (Figure 16). The horizontal architectural panels stiffened the lower half of the columns at each story, creating a short-column effect.

3.7 The American Savings Bank Building

A steel-frame office building on the west side of Topanga Canyon Boulevard in Canoga Park, housing the American Savings Bank, experienced significant movement in its first story columns (Figure 17). A nearly identical building on the same site, oriented at right angles to the first, had only minor damage to glass at the first story. The first story column heights of the two buildings differed significantly: the ones in the undamaged building were considerably shorter than the ones in the damaged structure.

In the weeks following the earthquake, reports surfaced about a surprisingly large number of

damaged steel-frame buildings, which, as a class, have been viewed relatively earthquake-resistant. Failure modes reported include brittle fractures of column flanges, base plates, and welds at connections; and buckling of diagonal tube bracing (Los Angles Times, 2/27/94 and EERI 1994).

3.8 Parking Structures

Eight major public parking structures suffered collapse or severe damage. Many other parking structures suffered less spectacular, but nevertheless serious, damage. The damaged parking structures were scattered throughout the affected area. A few key damaged structures are described herein.

California State University at Northridge Campus The four-level garage was built in 1991 of precast concrete with cast-in-place concrete slabs. The lateral resisting system was an exterior perimeter frame constructed of precast "Trees" (columns with half-length beams cast as one piece) connected in the field to form a moment frame. The collapse apparently started at the interior of the building and the exterior perimeter frame was pulled over towards the center of the structure (Figure 18), suggesting that interior beams had lost their vertical support, causing the floor plates to collapse and pull the exterior walls in with them.

Kaiser Permanente Medical Complex on Cadillac Avenue The five-level parking garage in West Los Angeles experienced a similar collapse. All four facades were pulled inward, suggesting that interior damage precipitated the failure (Figure 19). The garage was a post-tensioned, cast-in-place concrete structure with shear walls providing the lateral-force resisting system at the east and west ends, and moment frames at the north and south perimeter. The shear walls were cracked horizontally throughout their height due to the out-of-plane bending (Figure 20).

Trans World Bank Parking Structure The two-level concrete parking structure adjacent to the Trans World Bank in Sherman Oaks had been seismically strengthened after suffering serious damage in the 1971 San Fernando quake. Flared extensions were cast next to the interior columns along their north-south axes (Figure 21), creating short wing walls supporting the precast beams. The unrehabilitated exterior columns were badly damaged in the Northridge earthquake (Figure 22).

4. BRIDGES

4.1 Overview

The vast majority of bridges in the Los Angeles metropolitan area performed well in the Northridge earthquake. However, the quake caused the collapses of six major highway bridges and heavy damage to 157 other high bridges. The estimated cost to replace or repair these bridges is $1.5B. Figure 23 shows the locations of the bridges inspected by the reconnaissance team. This section provides a brief description of field observations of several major bridge damages or collapses.

4.2 Interstate 5 (the Golden State Freeway) at Gavin Canyon Undercrossing

This bridge was designed in 1964 and constructed in 1967. It carries Interstate 5 over Gavin Canyon, about 3 km north of the intersection of Interstate 5 and State Route 14. An aerial photograph of the damaged bridge, after demolition had begun, is shown in Figure 24, and a ground level view is shown in Figure 25. The structure consists of two parallel bridges, with about a 66 degree skew alignment. Each bridge is composed of five spans. Each bridge has four two-pier bents, and there is a structural hinge near each of the two center bents. The superstructure consists of reinforced concrete box girders, and the central portion (between hinges) is post-tensioned. The bridge survived the 1971 San Fernando earthquake with virtually no damage. In 1974, the hinges were retrofitted with cable restrainers. The seat length at the hinges is 200 mm, which by current design standards would be considered inadequate, especially for a structure of this size and flexibility.

Despite the presence of cable restrainers at the hinges, failure of three of the four end spans of the bridge was apparently initiated by the spans falling off the hinge seats. The fourth end span, at the far western corner of the bridge, partially came off its hinge seat but did not collapse. After support was lost at the hinges, a triangular portion of three of the end spans collapsed. It is likely that the skewed alignment of the bridge was an important contributing factor in this failure. The skewed alignment

permitted rotation of the superstructure in a counter-clockwise direction, when viewed from above. The tall, flexible piers of the two center bents would have offered relatively little resistance to rotation in a horizontal plane. Rotation of the superstructure would have resulted in differential displacements at the hinges, and eventually unseating of the end spans at the hinges.

4.3 State Route 14 (The Antelope Valley Freeway) Interchange with Interstate 5 (the Golden State Freeway)

Two bridges partially collapsed at this interchange: the Route 14/5 Separation and Overhead Ramp C, which is the ramp linking westbound SR14 to southbound I5; and the North Connector Overcrossing Ramp M, which is the ramp linking westbound SR14 to northbound I5. In addition to the two collapsed ramps, there was evidence of pounding between spans at several hinges, and permanent differential offsets (both horizontal and vertical) were observed between the ends of the spans, as shown in Figure 26. The cable restrainers installed at hinges in this interchange during the early 1970's may have been responsible for preventing further collapses during the Northridge earthquake.

This interchange was designed in 1968 and was under construction in 1971 when portions were damaged by the San Fernando earthquake. At that time, one of the completed ramps in the interchange collapsed, and two ramps which were under construction were damaged. The portion which collapsed in 1971 was the South Connector Overcrossing, connecting southbound I5 with eastbound SR14. A photograph of the collapsed ramp, taken in 1971, is shown in Figure 27. This ramp was later rebuilt, with improved pier reinforcement, and it suffered no significant damage in the Northridge earthquake. The damaged portions of the other two ramps under construction in 1971 were repaired in place, but not strengthened; the portions not yet constructed were completed with limited seismic upgrading. Both of the ramps which partially collapsed in the Northridge earthquake were under construction at the time of the 1971 earthquake.

4.3.1 Route 14/5 Separation and Overhead Ramp C

This ramp was designed in 1968 and constructed in 1971. The structure consists of multiple-cell concrete box girders, most of which are post-tensioned, supported on single pier bents with flared tops. The portion of the ramp which collapsed was between Abutment 1 and the hinge located near Pier 4. A ground-level view of the collapsed span is shown in Figure 28, and a view of damaged Pier 3 is shown in Figure 29. The mode of failure of this ramp has not yet conclusively been determined, but the following scenario appears likely. Because Pier 2 was the shortest and stiffest pier in the structure, it probably attracted a large share of the horizontal seismic forces. The reinforcing details of the pier indicate that the pier contained quantities of lateral reinforcement which would be considered inadequate by current standards. Thus it is likely that Pier 2 was damaged and collapsed, pulling the superstructure off the seat at Abutment 1. It was reported that Pier 2 had completely disintegrated in the collapse. This observation is consistent with the conjecture that the pier was initially severely damaged in shear, and was then so badly weakened that it was crushed in compression. Following the collapse of Pier 2, a failure of the superstructure was initiated by excessive shear and negative bending moment at Pier 3. The superstructure sheared off on either side of Pier 3, leaving the pier standing nearly intact, as shown in Figure 29. The span between Piers 3 and 4 then collapsed, pulling the superstructure off the hinge seat near Pier 4.

4.3.2 North Connector Overcrossing Ramp M

This ramp was designed in 1968 and constructed in 1971. Photographs of the collapsed portion of the ramp are shown in Figures 30 and 31. The portion of the ramp which collapsed was located between Abutment 1 and Pier 3. This ramp was under construction in 1971 and was nearly completed when the San Fernando earthquake occurred, with only the portion from the hinge near Pier 8 to Abutment 11 remaining to be constructed. The portion of the ramp which collapsed in the Northridge earthquake, between Abutment 1 and Pier 3, was already constructed when the San Fernando earthquake occurred. Only minor damage to this ramp was reported following the 1971 earthquake (State of California, 1971). This damage consisted of permanent offsets at the hinges near Piers 4 and 6.

The collapse in the Northridge earthquake appears to have been initiated by the failure of Pier 2. After Pier 2 failed, the simply supported span between Abutment 1 and the hinge near Pier 2 collapsed, and, as shown in Figure 31, the superstructure failed in bending near Pier 3 due to a large negative moment. Pier 2 completely disintegrated, as shown in Figure 32. This is the shortest pier in the structure, so it is likely that it attracted a high level of lateral force, was damaged in shear, and finally collapsed in compression. Pier 10 is similar in height to Pier 1, but the quantities of lateral reinforcement in Pier 10 are greater than those in Pier 1. This is because Pier 2 had already been completed, but Pier 10 had not yet been constructed, when the 1971 earthquake occurred. Following the 1971 earthquake the plans for Pier 10 were revised to provide increased lateral reinforcement.

4.4 State Route 118 (The Simi Valley Freeway)

SR118 is the major east-west transportation route for northern Los Angeles County. The route passes just north of the epicentral region of the quake. A number of bridges along SR118 received minor, repairable damage, but two bridges were damaged severely: portions of a bridge collapsed at the intersection of San Fernando Mission Boulevard and Gothic Avenue; and nearby there was severe pier damage and a near collapse of the bridge at Bull Creek Canyon Channel. The performance of these two bridges is described below.

4.4.1 State Route 118 (Simi Valley Freeway) at San Fernando-Mission Blvd. and Gothic Ave

Because the Mission-Gothic Undercrossing was designed in 1972, after the San Fernando earthquake, the bridge contains seismic details which are improved over the details used in designs of the 1960's and earlier. Most notably, the spiral hoops in the bridge piers are spaced closely together. Nonetheless, the piers of the Mission-Gothic Undercrossing suffered severe damage in this quake, and one of the two parallel spans partially collapsed. Damage to piers at Mission-Gothic is shown in Figures 33 and 34. In addition to pier damage, there was also severe damage to the abutments, including cracked wing walls, settlement of soil behind the abutments, and apparent shifting of the abutments.

The likely failure mode of the bridge was that the piers initially suffered severe shear damage, followed by crushing of a number of piers in compression. The structure may also have shifted to the southwest, as constrained by the geometry of the abutments. Although unseating at Abutment 5 did occur, this was probably a secondary effect, as the seat lengths were generous by current standards. Rather, failure was probably initiated by damage to the piers. In this case the failure of piers has important theoretical implication, as the piers of this bridge contained quantities of lateral reinforcement similar to those required by current seismic design standards. Therefore, further research will be required to determine why the pier reinforcement was inadequate in this case.

4.4.2 State Route 118 (The Simi Valley Freeway) at Bull Creek Canyon Channel.

The bridge did not collapse completely, but many of the piers were severely damaged, as shown in Figures 35 and 36. In addition to pier damage, there was significant damage to the abutments, including cracked wing walls, settlement of soil behind the abutments, and possible shifting of the abutments.

This bridge was designed just after the 1971 San Fernando earthquake, so it contains some seismic detailing which is improved over earlier bridge designs. However, since it was not until several years after the San Fernando earthquake that seismic design codes for bridges were significantly changed, the design of this bridge would be considered substandard by current design codes.

All ten of the piers in Bent 3 failed in combined shear and compression near their bases, as shown by Figures 35 and 36. In Bent 2, Piers on the south side of the span failed near their top end, and the damage became progressively less for piers to the north in Bent 2. The farthest north piers in Bent 2 showed relatively little damage - only diagonal shear cracks near the base, with no spalled concrete. This uneven distribution of damage to piers was probably caused by the asymmetric plan geometry of the bridge.

The confining reinforcement in the piers is inadequate by current standards. All pier failures occurred in

the zone of wide spiral spacing. Another factor contributing to pier failure was that the effective lengths of the piers were much shorter than the distance between the footings and the girder soffit. The lengths of piers varied between roughly 6000 and 9100 mm. In Bent 2, the effective pier lengths were decreased roughly one-third by compacted backfill soil above the pier footings. In Bent 3, the pier lengths were also decreased roughly one-third, but by a reinforced concrete channel liner wall, which was cast abutting the piers. The shortened effective pier length resulted in stiffer piers, which were more susceptible to shear-dominated failure than bending-dominated failure.

4.5 Interstate 10

Interstate 10 is a major east-west artery running between Santa Monica and downtown Los Angeles. The freeway was constructed in 1966. Major bridge collapses occurred at two locations: the La Cienega Blvd.-Venice Blvd. Separation and the Fairfax Ave.-Washington Blvd. Undercrossing.

4.5.1 Interstate 10 La Cienega Blvd./Venice Blvd. Separation

Figure 37 is a ground-level view of the portion of the westbound lane that collapsed to the ground at the hinge located between Bents 7 and 6. The pier in the foreground is the northernmost pier of Bent 7. It is seen that there was extensive column shortening due to the failure of the lateral reinforcement to provide adequate confinement of the core concrete. Fractured lateral reinforcement can be seen to the right of the failed portion of the pier. Figure 38 shows the other two piers of Bent 7 which supported the westbound lane. Extensive failure and column shortening is evident. The concrete block wall behind the piers is part of a storage building that was constructed beneath the bridge structure. The storage building extended from Venice Blvd. to La Cienega Blvd. The piers of Bent 7 which supported the eastbound lane suffered relatively minor damage, and the roadway to the east of Bent 7 remained largely at its original elevation.

Figure 39 shows the northernmost pier of Bent 6, located just to the west of the hinge. This pier totally disintegrated, but the storage building prevented the roadway from collapsing to the ground. Figure 40 shows the southernmost pier supporting the eastbound lane at Bent 3. The top of the pier is severely damaged and it is likely that the storage building prevented the total collapse of the roadway.

In summary, the bridge structure spanning La Cienega Blvd. and Venice Blvd. was extensively damaged. The failure is attributed to the small amount of lateral pier reinforcement. As the piers cracked due to the lateral loading, the lack of adequate confinement resulted in a reduction of the vertical load capacity because of core concrete loss and buckling of the longitudinal bars. Had it not been for the storage building located beneath the bridge, it is likely that more spans would have collapsed to the ground.

4.5.2 Interstate 10 Fairfax Ave.-Washington Blvd. Under Crossing

The earthquake caused partial collapse of two spans of the eastbound and westbound lanes on either side of Bent 3. The piers in Bent 3 had failed and caused the girders to sag at this location. However, cable restrainers at the hinge west of Bent 4 prevented the girders from falling off of the hinge seats (Figure 41). Figure 42 shows the westbound lane of I10 over Fairfax Ave. It can be seen that the piers in Bent 3 shortened and caused the girder to sag. It can also be seen that the span to the west of Pier 2 lifted off of the abutment. Figure 43 is a close up view of one of the piers in Bent 3. The failure mode is similar to that observed at Venice Blvd. and La Cienega Blvd. When the piers were subjected to lateral ground motions, the lateral reinforcement was not able to adequately confine the core concrete. As a result of lateral load damage, there was a loss of axial load capacity and the piers shortened under the action of the vertical loads. As mentioned, the piers at Bent 4 had considerably more longitudinal reinforcement than the other piers. Examination of the piers in Bent 4 revealed varying degrees of diagonal cracking and spalling of the concrete cover. At the time of the site visit, these piers were surrounded with wooden shoring as a precautionary measure during the demolition of the collapsed spans.

5. LIFELINE SYSTEMS

5.1 Introduction

Lifelines include water, sewer, gas, fuel, electric power, telecommunications, and transportation

systems. These systems are critical to the vitality of the built environment and the functioning of modern society. They provide services to the community to maintain its safety, health, financial transactions, and to stimulate economic activities. Damaged lifelines can impede emergency response following an earthquake, and can hinder postearthquake recovery. Disruption of regional lifeline systems due to a major natural disaster such as an earthquake can have a profound effect on the entire nation because of the economic interdependence of lifeline systems and the functions they support.

This section offers a brief overview of the performance of lifeline systems, including observations made by many investigators, but with particular emphasis on the sites that the team visited personally.

5.2 Water Supply Systems

In addition to limited sources from the region's local groundwater basins, the main water supply is from Northern California and the Colorado River. January 17, 1994 was the first time in history that an earthquake resulted in the breakage of all four pipelines that feed water to the region's three water treatment facilities.

Compared with the extensive damage caused by the 1971 San Fernando earthquake to the Jensen treatment plant in Sylmar (under construction at the time), the 1994 earthquake caused only minor damage. The 1994 damage included lateral spreading of the ground or soil settlement around the facilities, leaks in pipelines, and leaks at construction joints.

While water supply to these facilities was available once the major pipelines were repaired, the system nevertheless failed to provide water to customers because of the failure of the water supply distribution network, especially the network serving areas near the epicenter. Thousands of main line leaks were reported and the repairs were very time-consuming.

Among the numerous situations that contributed to the disruption of the water supply system was damage to one of the four damaged pipelines, Los Angeles Aqueduct No. 2 at Terminal Hill. Aqueduct No. 2 is made of 2.1-m diameter steel pipes. Terminal Hill is located about 20 km north-northeast of the epicenter, southeast of the intersection of I-5 and SR14. There is no strong motion record available for the site. However, two stations maintained by the California Division of Mines and Geology (CDMG) and the U.S. Geological Survey (USGS) about 5 km south of the site showed peak ground accelerations over 0.9g.

A steel pipe brings water up from the canyon below (Figure 44). The pipe is supported on concrete saddles built along the mountain slope. In a few places, the pipe separated from the saddles creating 50 to 80 mm gaps. In at least one location, the pipe crashed into the saddle. In two other locations, the pipe sections bulged 80 mm and 150 mm respectively. However, no rupture or leakage was noticed. The ruptured section of the 2.1-m pipe is located near top of the hill. The two sections where the rupture occurred were connected together using a mechanical coupling system (Figure 45). To restrain the relative movement between the two pipe sections during strong shaking, the sections were connected by eight pairs of restrainer rods 35 mm in diameter and 2.2 m long. The rods were attached to brackets, which were welded to the pipes. These welds broke due to strong shaking and resulted in the separation of the two pipe sections.

Repair of the pipe sections began immediately after the earthquake. The repair work was completed in the evening of January 19 and the aqueduct started operation at 2:00 a.m. January 20. However, leakage was found shortly thereafter which caused the operation to shut down again. Excavation was required to repair two other sections. The pipeline was back in operation on January 21.

There were numerous breaks of water lines during this earthquake. Two water mains were ruptured at a site along Balboa Boulevard adjacent to the rupture of a 0.6-m gas main. A major fire resulted, which is described later in this section.

5.3 Gas and Liquid Fuels

Natural gas systems consist of transmission, distribution, and service lines. In the earthquake-affected area, transmission lines are steel pipes with diameters ranging from 0.3 to 0.8 m. Most of the failed lines were of pre-1971 construction. The distribution lines are either steel or plastic pipes. Compared with the effects of the 1971 San Fernando earthquake, this earthquake resulted in more ruptures in the distribution lines than in the

transmission lines. Most of the breaks occurred to old steel pipes. Plastic pipes used in the distribution system seemed to perform well.

As happened in earlier earthquakes such as the 1987 Whittier Narrows earthquake and the 1989 Loma Prieta earthquake, tens to hundreds of thousands of gas supply outages occurred. Most outages were the result of customers shutting off gas valves because of fear of gas explosions or fires. While immediate safety is the intent of this action, it can result in a long delay before service is restored because gas company technicians must test each system before turning the valve back on.

The rupture of a 0.6-m gas main occurred along Balboa Boulevard between Rinaldi Street to the south and Lorillard Street to the north, about 0.5 km north of the intersection of Balboa Boulevard and SR118 (Figure 46). Along this stretch, compressional ground failures occurred between Rinaldi Street and Halsey Street, and extensional ground failures occurred between Bircher Street and Halsey Street.

Three pipelines ruptured as the result of ground contraction; a 150-mm gas distribution line, the 1.8-m Rinaldi trunk water line, and a 0.6-m gas main (Figure 47). The Rinaldi trunk line was of post-1971 construction and the gas main was of 1930 vintage. These pipes showed a shortening of 125 to 150 mm.

About one block north, the ground extension caused rupture of the same 0.6-m gas main and a 1.2-m water main (Figure 48). The rupture of the gas main caused a major fire at the site that destroyed five houses (Figure 49). The loss of both water mains at this location and the difficult access to the site due to the fire and flooding in the street made fire fighting difficult.

An excavated section just north of the fire site revealed some additional underground lines (Figure 50). The 460-mm crude oil line in the middle of the photo performed well. The 150-mm gas distribution line shown is a replaced section.

In addition to the above damage in the epicentral area, the strong shaking from the earthquake cracked welds at several locations along a 250-mm pipeline transporting crude oil to refineries from the San Joaquin Valley. As a result there was an oil spill along the Santa Clara River.

5.4 Electric Power

Power was lost to most of the Los Angeles basin area after the earthquake. Nearly 2 million customers were out of service immediately after the quake. About half of them had power restored within one day and over 95 percent had power restored by midnight Tuesday, January 18. All power was restored within ten days after the earthquake.

Some transmission towers suffered significant damage, many as the result of foundation failure. Damage to several high voltage substations near the epicenter, such as Sylmar, Pardee, and Rinaldi, led to the widespread power outage in the Los Angeles basin, as well as the isolated outages throughout seven western states (Figure 51). As happened during the 1971 San Fernando earthquake, porcelain elements of equipment of 230 kV and 500 kV classification suffered the most damage (Figure 52). This highlights the urgent need for developing new materials that would be more earthquake resistant to replace porcelain, which is very brittle. Furthermore, most of the 230 kV circuit switchers, similar to those in the forefront of Figure 53, at the Sylmar substation, were damaged. However, none were damaged during the 1971 earthquake, a possible indication of much stronger ground shaking by the Northridge earthquake. Most of the capacitor banks, similar to those in the background in Figure 53, performed well in this earthquake, whereas most collapsed during the 1971 quake. Better performance of the capacitor banks is the result of higher seismic requirements in equipment qualification and in installation practices.

The level and types of damage to electrical systems experienced in the Northridge earthquake demonstrate that many valuable lessons have been learned since the 1971 earthquake. Many improvements have been made in areas such as requirements for equipment qualification and installation practices.

5.5 Transportation

All airports in the region survived the earthquake with no major problems. The airports were shut down immediately after the quake as a precautionary move to allow for the inspection of runways and taxiways. All airports were re-opened for operation once the inspections had been completed. No structural damage was observed in airport facilities.

However, they did suffer some typical types of non-structural damage, such as fallen ceiling tiles and leakage of water pipes.

There was a freight train derailment in Northridge during the earthquake (Figure 54). The 64-car freight train belonged to Southern Pacific and was on its way from Houston to Sacramento. Twenty-five cars derailed, sixteen of which carried sulfuric acid or diesel fuel. The derailment resulted in the spill of 30,000 liters of sulfuric acid and 7,500 liters of diesel fuel. There were no casualties in this incident. About 200 m of railroad tracks were replaced immediately following the earthquake and rail service was restored at 2:00 a.m., January 19. Removal of damaged cars and cleanup of debris were completed on January 21.

Strong ground shaking and lateral movement of subgrade materials resulted in numerous ruptures of asphalt pavement and concrete sidewalks in the epicentral area (Figure 55). In some instances, local traffic was interrupted temporarily waiting for the repair of these cracks. In most cases, the damage was minor and local traffic was not interrupted. The south approach of Balboa Boulevard at SR118 caved in from loss of abutment fill due to a water main break. This bridge was closed for traffic due to some structural damage to the piers and the loss of the south abutment fill.

6. POSTEARTHQUAKE FIRES

6.1 Introduction

The Northridge earthquake resulted in fires which challenged the resources of the fire service due to the number of fires, disruption of the water supply, and damage to fire protection systems within buildings. The majority of the estimated 30 to 50 significant fires were located in the San Fernando Valley and confined to the building of fire origin either by separation or by fire department action. Fortunately there was no loss of life from fire. A principal cause of the fires involved natural gas leaks. A small number of fires were caused by hazardous chemical interactions. The only major instances of building-to-building fire spread occurred in three manufactured housing developments (mobile home parks). Fire incidents occurred at a greater than normal rate in the days following the earthquake with the cause of some of the fires directly attributable to the restoration of power and gas to buildings shaken in the initial earthquake and aftershocks. Fire sprinkler systems sustained damage in some buildings although the number and extent of damage is not known at this time.

Fire protection in the municipal environment is derived from private and public systems including building construction, building fire protection systems, land use, public and private water supplies, public and private fire departments, and communication and utility systems. In the aftermath of a major earthquake the normal interactions between these systems is disrupted. Even though emergency operational plans exist, the interaction between these systems in reducing the loss from fire is complex since it involves decisions on the part of a great many people.

The loss of life and property caused by fire occurs in a different time frame than the structural and property damage caused directly by the earthquake. While most of the loss caused by shaking occurs during the time of ground movement, there is basically no fire loss during that time. Fire loss directly attributable to the earthquake begins immediately following the earthquake and can continue for days after the ground movement has stopped.

This section examines the factors contributing to the cause, spread of and loss from fire in selected buildings affected by the earthquake.

6.2 Fire Events Following the Earthquake

Immediately following the earthquake the Los Angeles City Fire Department initiated the Earthquake Operational Mode which included placing emergency equipment on patrol throughout the city and dispatching fewer pieces of equipment to each incident in order to accommodate the increased number of incidents. Earthquake damage was wide spread but occurred mostly within the City of Los Angles and most of the fire incidents were within the San Fernando Valley. Immediately following the earthquake electrical power was lost and telephone service disrupted throughout the city. At 0545 hours Mayor Riordan declared a state of emergency and by 0645 as many as 50 structure fires had been reported and over 100 incidents were being handled by the fire department. By 0945 all fires were under control.

Although the earthquake was centered within the City of Los Angeles, there was damage in surrounding counties and emergency resources throughout the region were utilized. In addition to responding to fire incidents, the fire department provided emergency medical, hazardous materials, and urban search and rescue services. The Los Angles City Fire Department responds to over 900 fire, medical, and other emergences on a typical day. This number increased to over 2200 on the day of the earthquake and remained at twice the normal level in the following days. The continued high number of incidents was due in part to fires associated with the restoration of utilities.

Water available for fire fighting was generally adequate in the San Fernando Valley area during the day following the Earthquake. The exceptions were in areas near the boundaries of the system and in areas at higher elevation. In the hours following the earthquake pressure in the water system dropped due to disruptions in supply and more than 3000 leaks. By the day after the earthquake, water tankers had been deployed throughout the San Fernando Valley to assist in fire fighting operations. On January 20th fire department pumpers were used to pump water from areas of adequate pressure within the system to areas with low pressure.

6.3 Fire Causes

The 30 to 50 fires reported initially following the earthquake occurred in a variety of residential and commercial occupancies. The majority of buildings in the San Fernando Valley are four stories or less in height and therefore the fires occurred primarily in these types of buildings. Figures 56 to 59 show some examples of buildings involved in postearthquake fires. The fire in the rear of the apartment complex shown in Figure 59 was the only fire observed in completely collapsed portion of a structure.

Preliminary indications are that a significant number of fires were associated with natural gas leaks. Natural gas is not in itself a source of ignition but it is relatively easy to ignite especially in confined spaces. Natural gas is the predominant fuel used for space and water heating in the Los Angeles area. Although electrical power was lost throughout the area immediately after the earthquake, the most likely source of ignition was a combination of electrical sources and flames in the gas appliances themselves. Gas leaks occurred both inside and outside of buildings. The fire resulting from a leak in a gas main under a street destroyed several nearby houses. Figure 60 shows a gas meter in a manufactured housing development (mobile home park) in which there were at least six individual ignitions. Although there was not a leak in the gas service shown, it demonstrates how the movement of the manufactured homes following the earthquake damaged the gas service resulting in leaks which were ignited by unknown sources. There were no postearthquake fires in the newest section of the development where an improved gas service design was used. As in past California earthquakes, water heaters appear to be a source of gas leaks (Mohammadi, et al, 1992). Inadequately secured water heaters are the gas appliance most likely to tip over during an earthquake. The fire which destroyed the multi-family housing unit shown in Figure 61 was reported to have started as the result of damage to a water heater. An undamaged housing unit similar to the one which was destroyed can be seen in the background. Even though natural gas leaks may have played a role in a significant number of the 30 to 50 reported fires, this number is very small when compared to the total number of buildings exposed to significant shaking as a result of the earthquake. Since residents of this area are aware of the dangers of gas leaks following an earthquake many fires may have been averted by individuals shutting off the gas to buildings or appliances.

The rapid failure of the electrical power distribution system probably resulted in fewer fires than might have been expected. As electrical and gas service was restored in the days following the earthquake a significant number of fires were reported. Some of these fires were a result of earthquake damage to electrical and gas equipment which went unnoticed or unattended. Electrical and gas service was not disconnected in all red tagged buildings which were identified by authorities as unsafe to enter. These and additional fires may have all occurred immediately following the earthquake if electrical service had been maintained.

As in past California earthquakes, a small number of fires appear to have been caused by flammable liquid or chemical spills. Figure 62 shows a science building at the California State University at Northridge in which the fire was reported to have

been the result of a chemical spill. No fires were known to have occurred at service stations. Since the earthquake occurred when most people were asleep, fire causes such as overturned candles and barbecue grills and fires associated with industrial processes appear to be nearly nonexistent.

A small number of wildland fires were attributed to earthquake related causes, most likely arcing in overhead power lines. Since the wind was light and the vegetation was not excessively dry, these fires were easily extinguished.

6.4 Performance of Fire Protection Systems

Some damage to fire sprinkler systems has been reported but the full extent is not known. Damage to these systems is frequently the most visible of the fire protection systems since it may result in water leaks. Interviews with persons who have entered buildings in the earthquake area indicate that many sprinkler systems remained intact particularly those installed in accordance with latest seismic standards. Typical damage to fire sprinkler systems included broken pipes due to differential building movement or the sway generated in long pipe runs without adequate bracing. Sprinklers installed in the downward or pendent position from piping above ceilings were in some cases sheared off.

In other cases pendent sprinklers installed in drop ceilings were pulled through the ceiling by the upward movement of the pipes and punched new holes in the ceilings during the downward movement. While the punching may not have resulted in leaks, it damaged the sprinkler deflectors which generate the desired spray pattern.

Damaged deflectors usually result in a significant decrease in sprinkler performance requiring the sprinklers to be replaced.

Sprinkler systems normally have one or more check valves which prevent water from flowing from the sprinkler system into the water supply system. In the most common wet pipe system, the pressure in the sprinkler system piping will be the highest pressure attained in the water supply system over time. In the days following the earthquake, as the fire department pumped water from one part of the municipal water supply system to another, there were significant local increases in pressure. These higher pressures were then "trapped" in the sprinkler systems. Although it is probably not a major problem and can easily be remedied by bleeding off the pressure, these higher pressures could lead to premature failure of the system and reduced effectiveness at the time of activation until the system returns to the design pressure.

Damage to fire alarm, detection, smoke control, other extinguishing systems, and passive building fire protection systems such as fire and smoke barriers has not been reported at this time. The disruption of land based communication systems is reported to have affected the ability of systems to dispatch alarms.

7. CONCLUSIONS

7.1 Introduction

The Northridge earthquake caused severe damage to a wide range of structural types because the epicenter was located in a populated urban area. Damaged structures revealed a number of deficiencies in current construction practices and areas needing improvements in code provisions. Implementing lessons learned about structural performance and postearthquake fires will reduce seismic hazards throughout the United States.

7.2 General

- The Northridge earthquake claimed 58 lives and caused over 1500 serious injuries. However, fewer than half of the deaths were attributed directly to structural failures. Because it occurred at 4:31 a.m., on a holiday, life loss was limited to a small number. Had the earthquake occurred during business hours, the collapse of parking structures alone could have caused a large number of deaths.

- Although a number of fires started immediately following the earthquake, calm winds limited spreading of fires in residential and commercial districts. At mobile home parks, fires spread from unit to unit. In most instances, fires were caused by natural gas leaks.

- Damage to multi-family dwellings contributed significantly to the over 25,000 dwelling units that became unhabitable. Providing adequate shelter for displaced persons is a major task after an earthquake. Special attention should be paid to improving the seismic performance of existing dwelling stock.

- At many locations, peak ground acceleration exceeded 0.4g, the maximum design value in building codes. However, most buildings met code expectations for performance. Because many strong motion records and response measurements are available from this earthquake, valuable opportunities exist for in-depth studies of building performance to assess the adequacy of design values for earthquake forces and provisions for seismic resistance.

7.3 Building Performance

- In many cases, buildings designed and constructed in accordance with modern (mid-1970's or later) seismic requirements performed well structurally. This clearly shows the value of incorporating modern seismic design and construction requirements into building codes. However, failures of structures characterized as "Undefined Structural Systems" (UBC 2333(i)2), such as the parking garage at California State University at Northridge, indicate that the performance of such structural systems needs to be evaluated carefully to update code provisions.

- Damage to unreinforced masonry (URM) buildings was widespread. In most cases, those URM buildings rehabilitated with parapet braces and floor-wall ties, as those rehabilitated in response to the Los Angeles division 88 ordinance, escaped total collapse. However, walls sustained severe cracking and, in many cases, pieces fell onto sidewalks. This posed life-threatening hazards to pedestrians.

- Nonstructural damage caused hospitals, schools, businesses, and industrial facilities to be inoperative even though structural damage was minimal or non-existent. An in-depth review of current code requirements and standards for nonstructural elements is needed to improve their seismic performance.

- Damage to steel structures was not readily visible from the exterior of buildings because most steel members are hidden behind architectural finishes and fire proofing. Removal of such coverings revealed brittle failures of welds and connections in many steel frame structures. Because owners of damaged structures often wish to keep damage reports confidential, damage information is not forthcoming. Detailed failure analyses of available data should be performed to understand the underlying causes of these failures.

7.4 Bridge Performance

- In general, bridges designed using standards developed after the mid-1970's performed well. Several bridges near the epicentral region, which were designed and constructed in the 1960's and early 1970's, sustained severe damage. Of the seven major bridges which sustained severe damage, six failed due to inadequate lateral reinforcement of the bridge piers.

- Most older bridges which had been seismically retrofitted (with cable restrainers, pier jacketing or foundation strengthening) performed well in the Northridge earthquake. However, because this earthquake was relatively moderate in magnitude, it should not necessarily be concluded that all seismic retrofit methods for bridges have been adequately proof tested by this event. Design criteria for cable restrainers may need to be reviewed. Even though jacketed bridge piers apparently performed well in this earthquake, it would be valuable to study the intensity of ground motions experienced at the specific bridge sites where jacketed piers have been employed, so that the performance of jacketed piers in larger events can be estimated.

- It is likely that some bridge piers were damaged because their effective lengths had been reduced. Several factors reduced the effective lengths: architectural flares at the tops of piers; backfill soil over a portion of the pier height; and concrete walls cast integrally with, or directly abutting, piers. Such constraints need to be minimized, or the effects of the constraints must be considered carefully in the design of piers.

- In bridges with piers of varying heights, the shortest piers tended to sustain the most damage. This is apparently because short piers have high lateral stiffnesses, and therefore attract a large share of the seismic loads. A better understanding of the role of short piers in overall bridge performance, is needed.

- Bridge spans which had skewed alignments or irregular plan configurations often sustained severe damage. Special attention should be paid to the potential for problems with bridges having skewed alignments or irregular plans.

- Older bridge bearings, of the steel rocker type, are highly susceptible to damage during strong ground shaking. Loss of rocker bearing support can lead to a broad range of bridge damage, including cracked girders, loss of roadway elevation alignment, and complete collapse of the superstructure.

7.5 Performance of Lifelines

- Damage to older trunk lines and main lines for water distribution caused serious disruptions in water supply in the epicentral region. About 50,000 Los Angeles Department of Water and Power customers were without water on the first day after the earthquake. About 10,000 customers were still without water one week after the earthquake.

- Buried pipelines which carry natural gas and oil fractured at many locations due to ground motion. Over 1300 breaks and leaks in the gas piping system were reported.

- As in the past earthquakes, brittle ceramic elements, which are often the weak links in circuit breaker assembles, were damaged.

7.6 Fire

- The occurrence of the earthquake before the start of morning traffic on a federal holiday allowed the fire department to respond to fires promptly without delays.

- Damage to natural gas pipelines and appliances resulting in leaks contributed significantly to postearthquake fires.

- In many cases, electric power was restored to buildings which were identified as unsafe for entry. The desire to restore utility service as quickly as possible is at odds with the desire not to cause fires.

- In general, fire sprinkler systems designed and installed in accordance with the latest seismic standards withstood the earthquake with little damage. However, in some instances, sprinkler pipes ruptured where sprinkler systems interacted with suspended ceilings.

8. References

1. EERC (1994), Jack P. Moehle, editor. Preliminary Report on the Seismological and Engineering Aspects of the January 17, 1994 Northridge Earthquake, Earthquake Engineering Research Center Report No. UCB/EERC-94/01, University of California, Berkeley, CA.

2. EERI (1994), John F. Hall, editor. Northridge Earthquake January 17, 1994, Preliminary Reconnaissance Report, Earthquake Engineering Research Institute, 94-01, Oakland, CA.

3. FEMA (1988). Rapid Visual Screening of Buildings for Potential Seismic Hazards: A Handbook, FEMA 154, Federal Emergency Management Agency, Washington, D. C.

4. Hauksson, E., Jones, L., Mori, J., Heaton,

T., and Hutton, K. (1994). Aftershocks of the Magnitude 6.6 Northridge, California Earthquake of January 17, 1994, Southern California Seismographic Network, California Institute of Technology, Pasadena, CA.

5. LA Times, February 27, 1994

6. Mohammadi, J., Alyasin, S., Bak, D.N., Investigation of Cause and Effects of Fires Following the Loma Prieta Earthquake, Illinois Institute of Technology, IIT-CE-92-01, May, 1992, 181 pages.

7. State of California (1971), "The San Fernando Earthquake: Field Investigation of Bridge Damage," State of California, Business and Transportation Agency, Department of Public Works, Division of Highways, Bridge Department, 209 pages.

8. USGS (1994), Porcella, R.L., Etheredge, E.C., Maley, R.P., and Acosta, A.V., authors. Accelerograms Recorded at USGS National Strong-Motion Network Stations During the M_s=6.6 Northridge, California Earthquake of January 17, 1994, U.S. Geological Survey Open File Report 94-141.

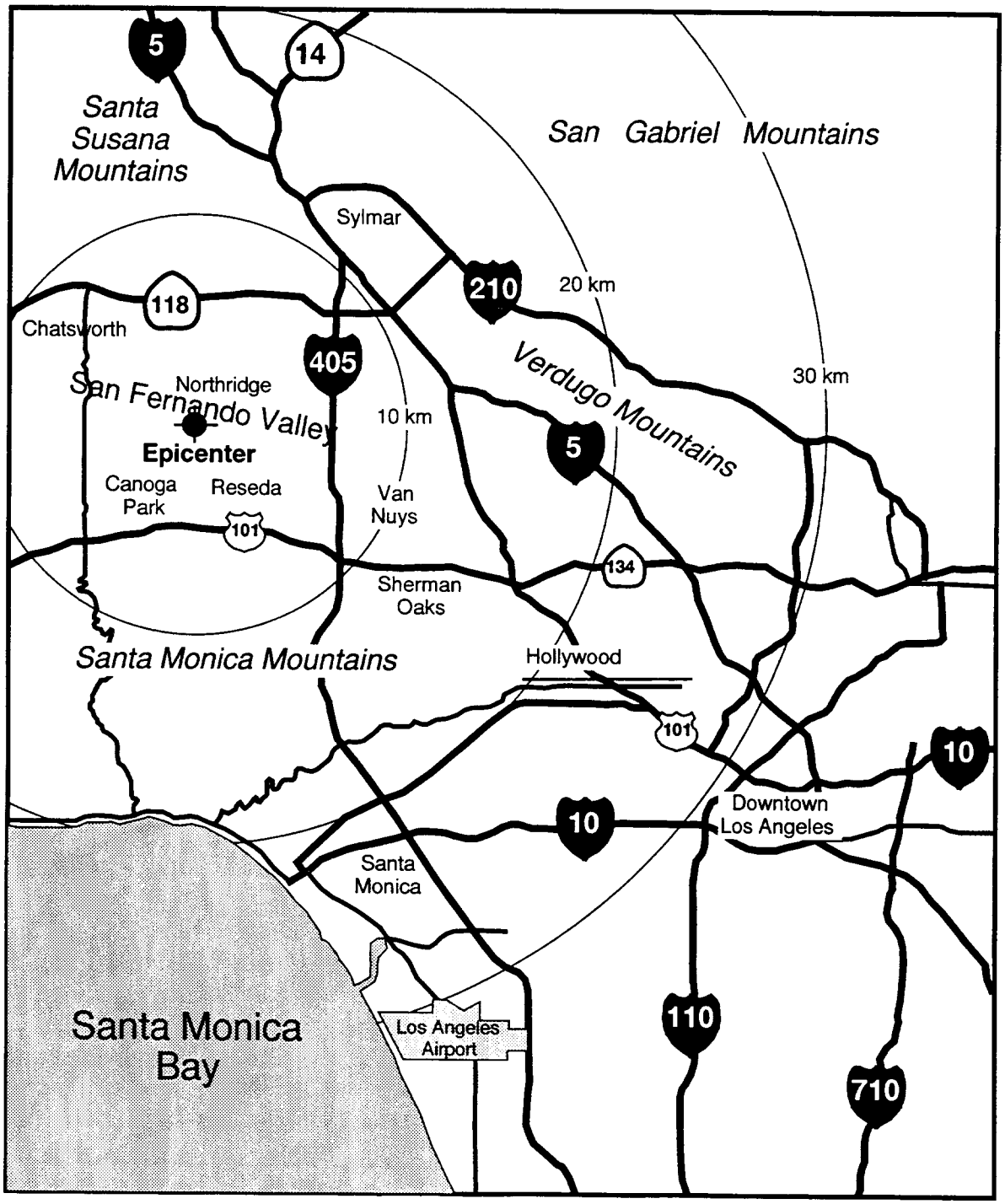

Figure 1 The epicenter of the January 17, 1994 Northridge earthquake was centered about 30 km northwest of Los Angeles in the San Fernando Valley.

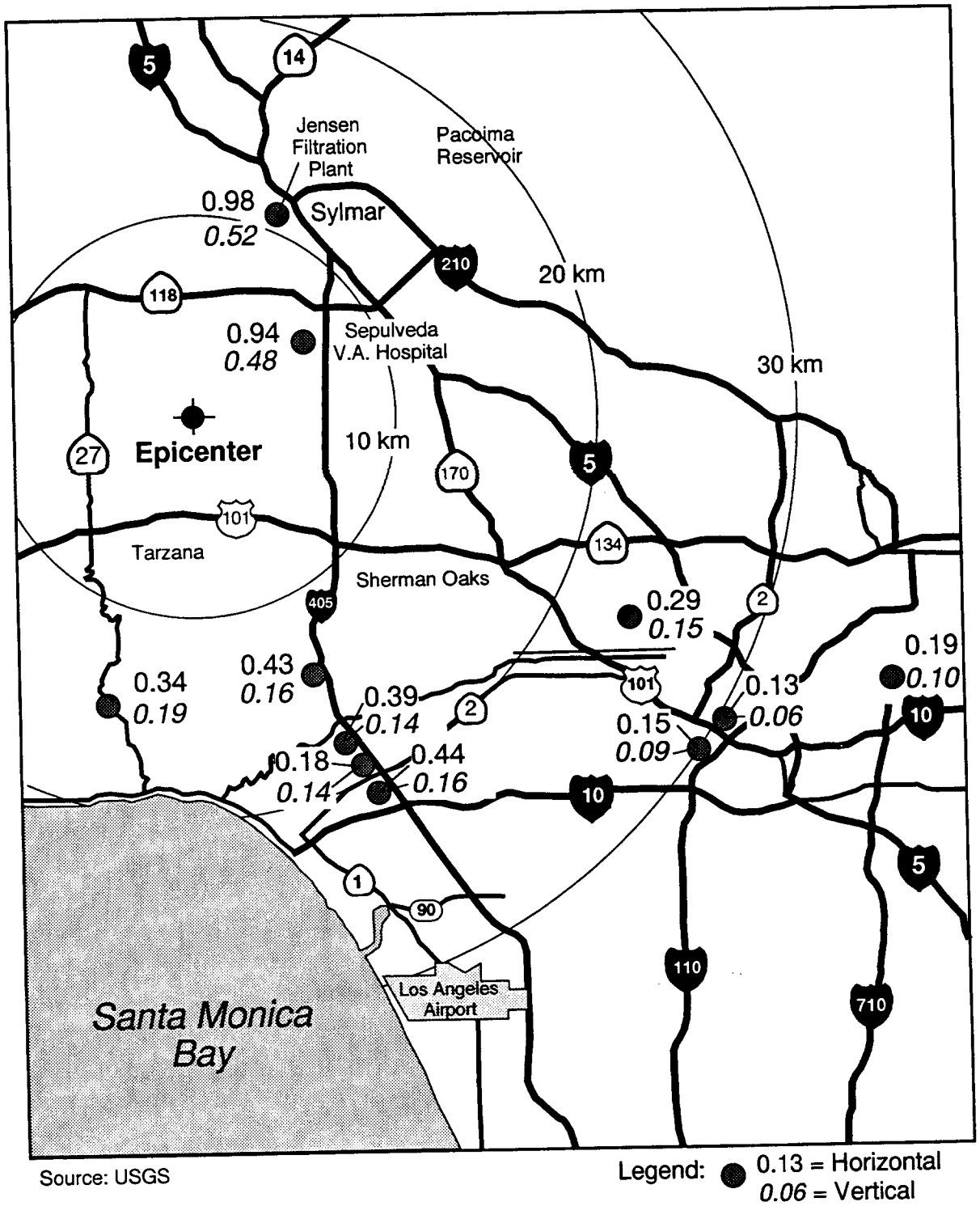

Source: USGS

Figure 2 Peak horizontal and vertical ground accelerations recorded at some of the instruments in the affected area operated by the USGS's National Strong Motion Program.

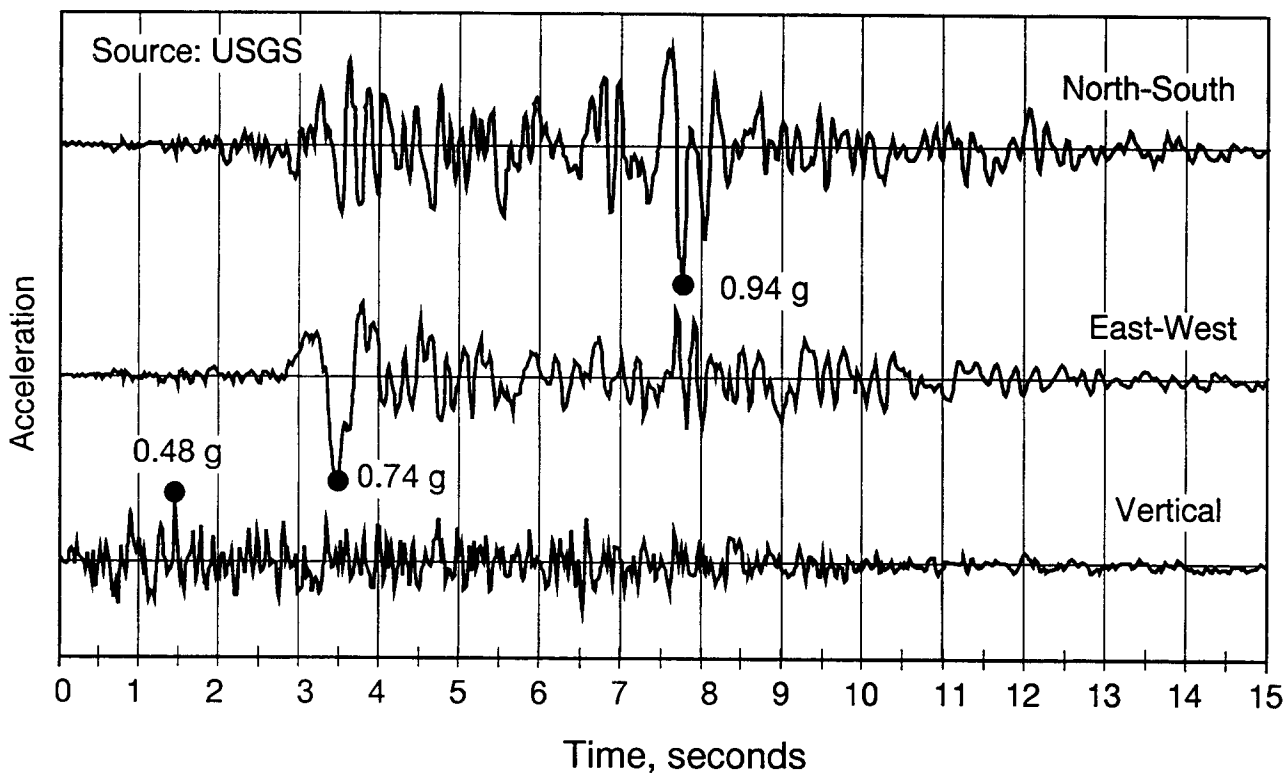

Figure 3 Accelerograph record from the grounds of the Sepulveda Veterans Affairs Hospital, 7 km from the epicenter.

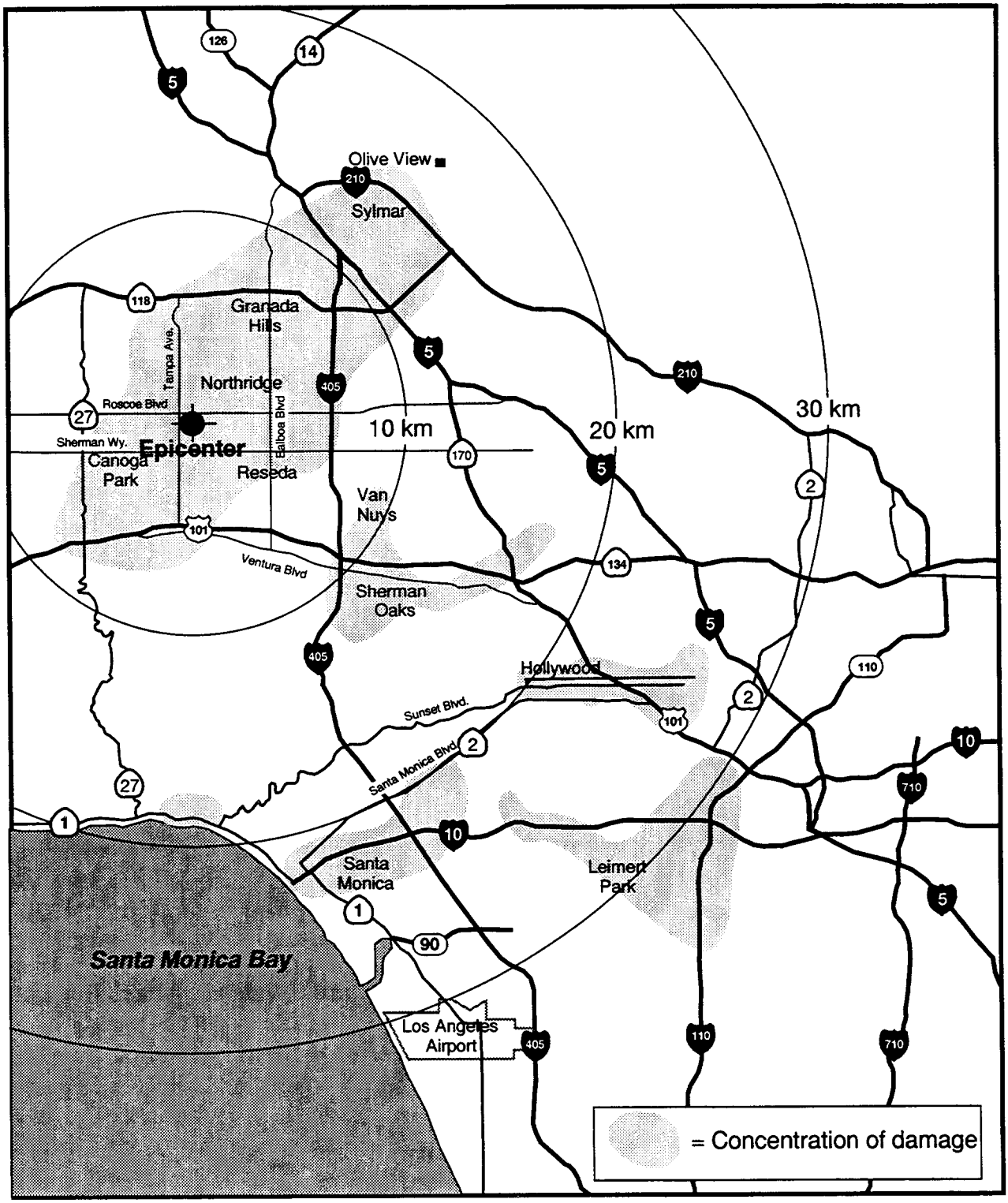

Figure 4 Serious damage to buildings caused by the magnitude 6.8 Northridge earthquake was widespread, but, outside of the epicentral area, seriously damaged buildings tended to occur in pockets.

Figure 5 At the Northridge Meadows apartment complex near the epicenter the first story in several of the buildings collapsed, killing sixteen people. The second and third stories remained essentially intact. Large portions of the first story in these buildings were open space for parking. This type of collapse occurred in a significant number of similar apartment buildings throughout the affected area.

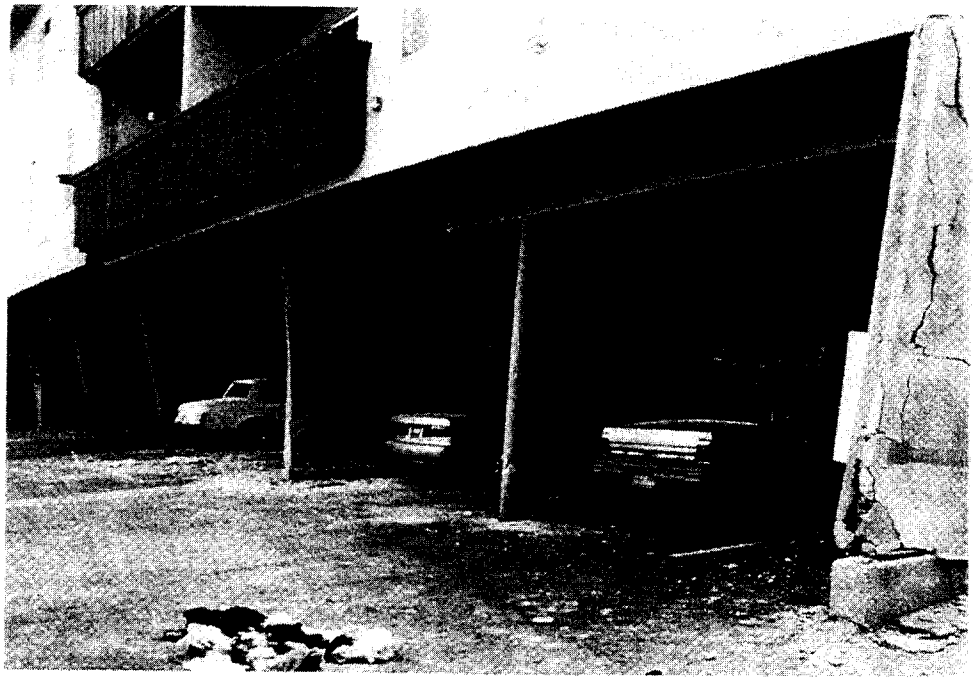

Figure 6 Steel pipe columns between parking bays supported the upper stories of the Northridge Meadows apartment buildings. Few of the buildings in the north half of the complex collapsed, but all were damaged.

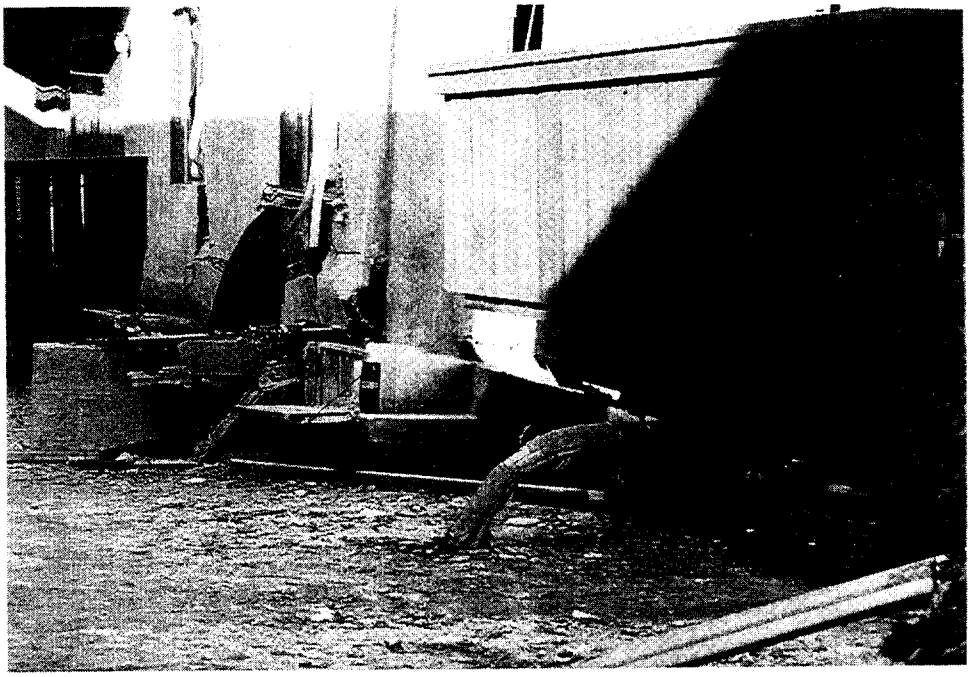

Figure 7 At Northridge Meadows, the first story steel pipe columns generally hinged near their bases but retained their length, controlling the displacement of the upper stories.

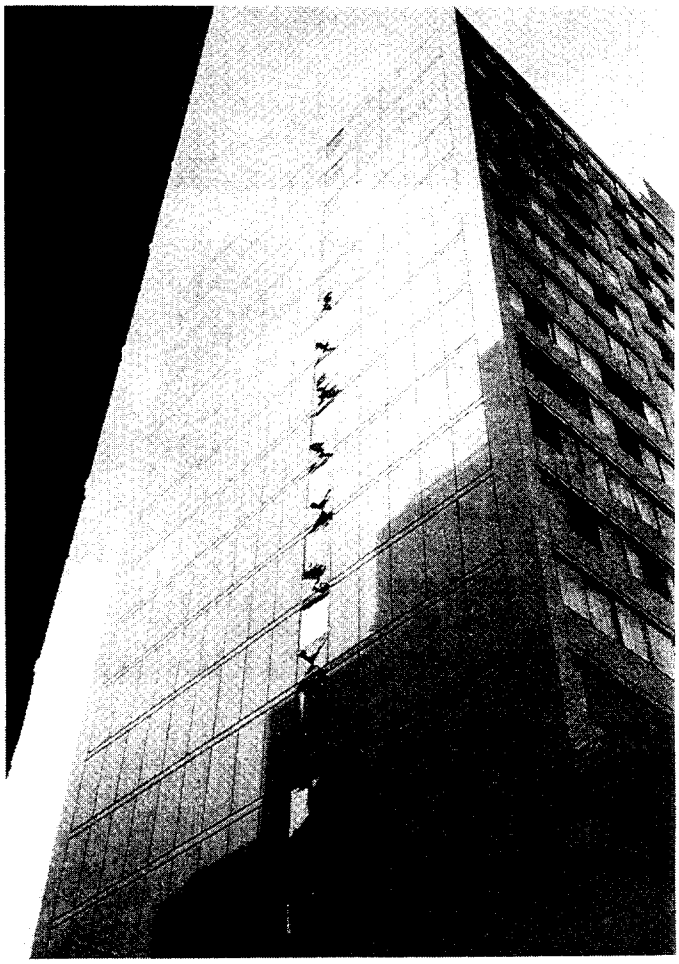

Figure 8 Champagne Towers apartment building in Santa Monica suffered a classic form of earthquake damage: shear failure of the coupling beams between linked shear walls at the transverse end of the building.

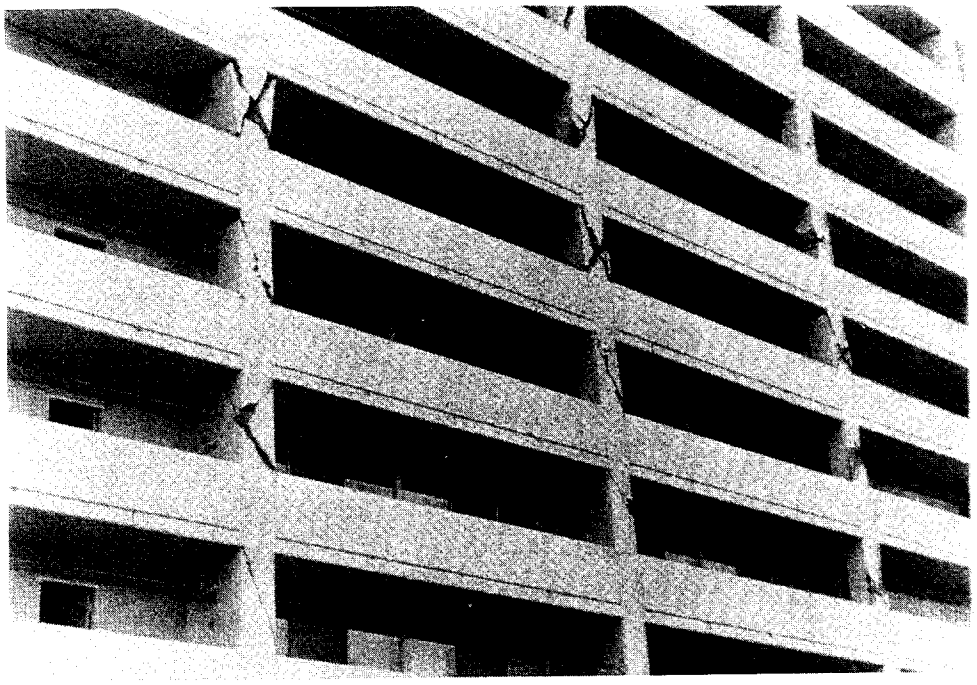

Figure 9 The back of the Champagne Towers building was badly damaged. The railings here are solid infill, which effectively stiffen the lower half of the columns. The shortened upper half of the columns were forced to accommodate all the displacement, and they failed in shear.

Figure 10 The seven-story northwest wing of St. John's hospital in Santa Monica experienced severe X-cracking in the piers between the second story windows.

Figure 11 A portion of the concrete waffle slab roof and the interior floor slabs at the Bullock's department store at the Northridge Fashion Center mall fell to the basement, leaving many of the columns standing. No reinforcing steel can be seen in the remaining columns that would have connected the columns to the floor slabs.

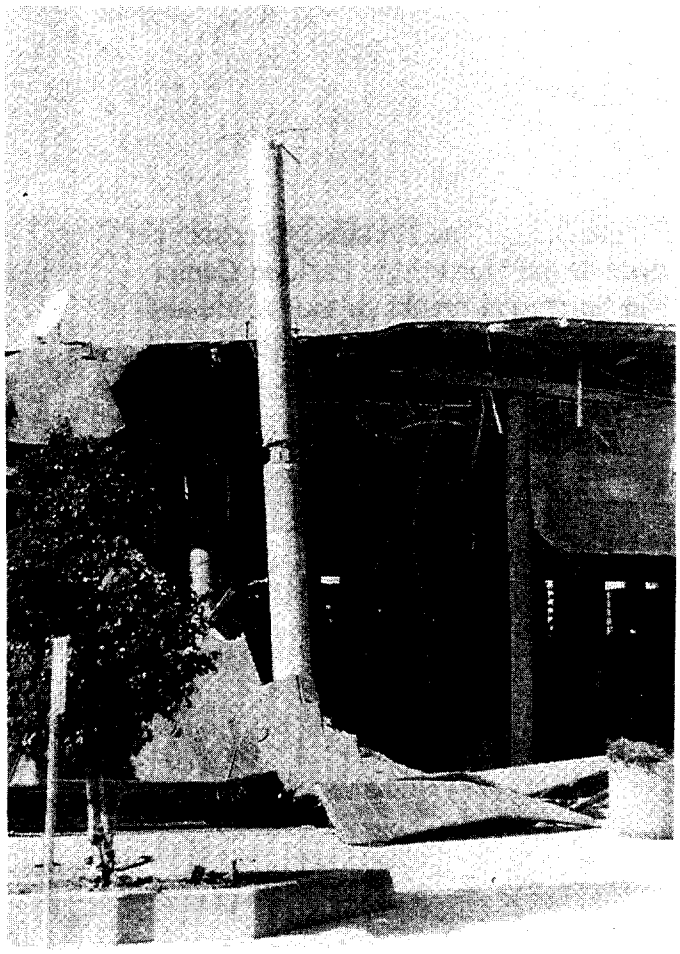

Figure 12 Damage to unreinforced masonry buildings, even those that had been rehabilitated, was common. Upper stories and corners were particularly vulnerable to damage. The rows of light-colored diamonds on the face of this building are the end plates of through-bolts used to connect the wall to the floor joists, a typical rehabilitation technique. The remains of parapet braces can be seen on the roof.

Figure 13 The corner of this rehabilitated unreinforced masonry apartment building in East Hollywood crumbled on all four stories.

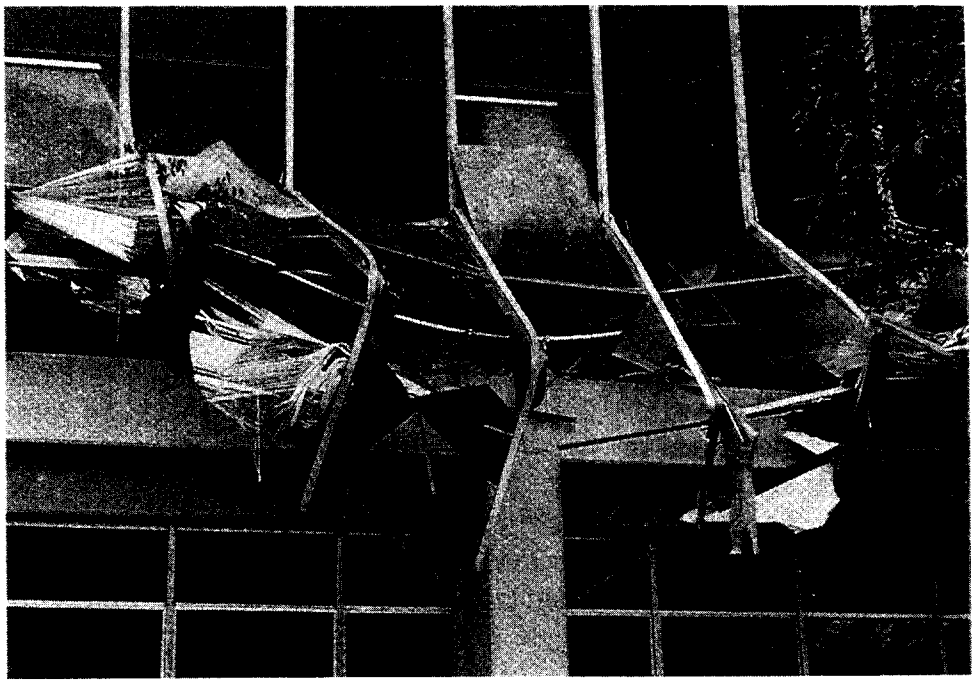

Figure 14 The second story of the concrete frame Kaiser Permanente office building on Balboa Avenue in Northridge completely collapsed. The first story was relatively undamaged, suggesting it was far stiffer than the story above.

Figure 15 The exposed concrete frame of the Kaiser Permanente building, revealing deep beams, suggests that the building had a strong-beam, weak-column configuration. Except for the second story columns, the columns and beams remained intact while the joints disintegrated.

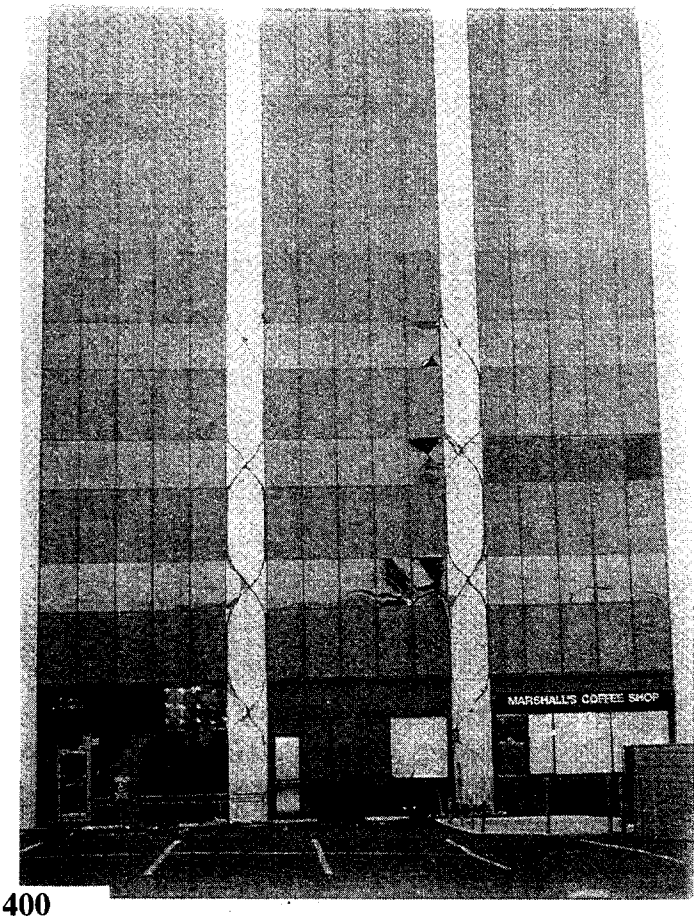

Figure 16 The stiff infill panels of the Barrington Building effectively shortened the concrete columns, forcing all the displacement into the column sections bounded by windows. Diagonal X-cracking decreased in severity towards the top of the building.

Figure 17 The first-story columns of the steel-framed building housing the American Savings Bank on Topanga Canyon Road in Canoga Park flexed during the quake and ended up slightly displaced from their original positions.

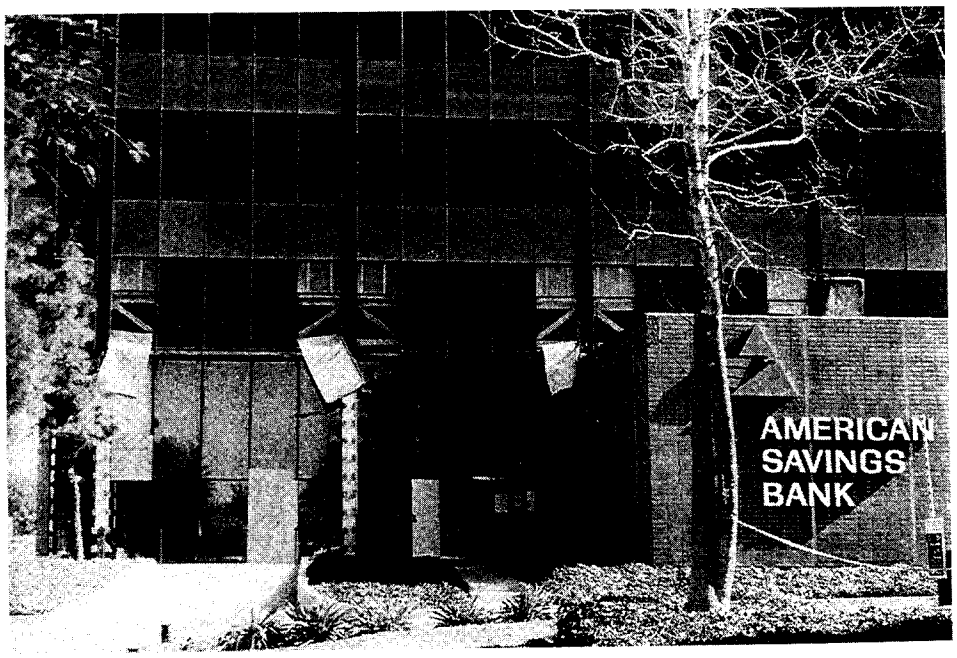

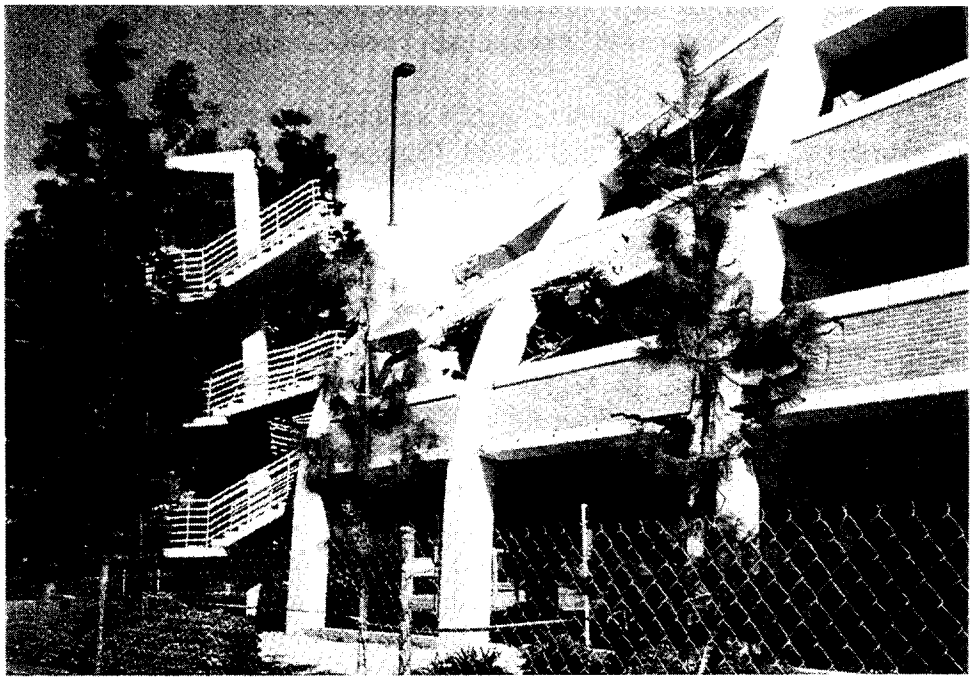

Figure 18 The three-year old four-level parking garage at the Northridge campus of California State University partially collapsed in the earthquake. The collapse apparently started at the interior, causing the exterior walls to be pulled in to the middle of the structure. Precast concrete "trees" were connected to form a moment-resisting frame at the exterior of the structure.

Figure 19 The cast-in-place concrete parking garage at the Kaiser Permanente Hospital complex in West Los Angeles collapsed in on itself. The moment frame that provided lateral resistance on the south face of the structure could not resist the out-of-plane forces apparently caused by the collapse of interior elements.

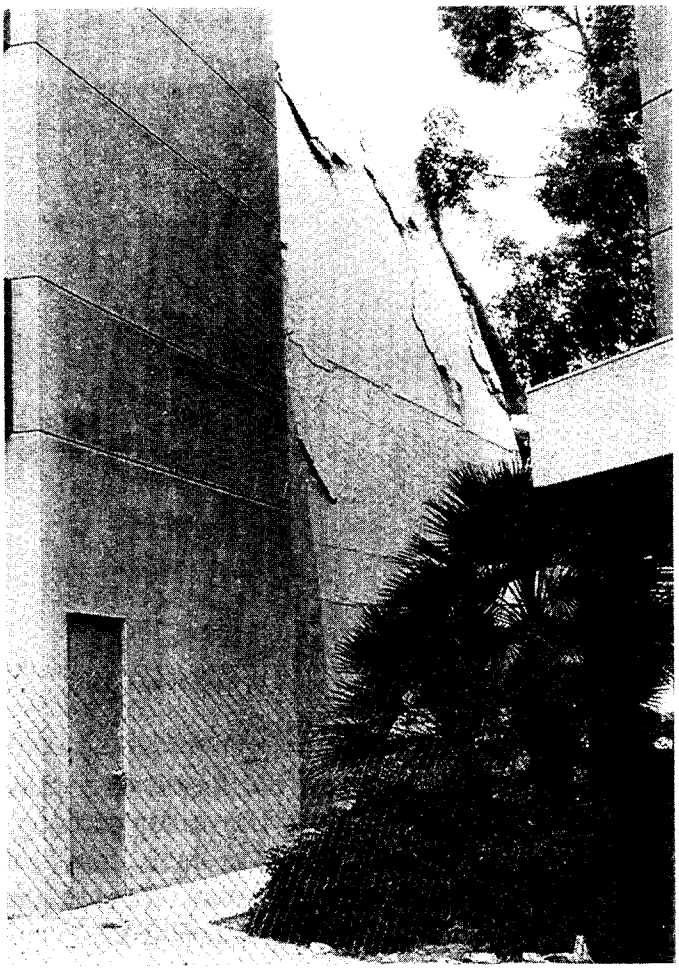

Figure 20 - At the east and west faces of the Kaiser Permanente Hospital parking garage, shear walls made up the lateral force resisting system. Both walls had horizontal cracks caused by the out-of-plane bending when the walls were pulled inward. Neither wall had major diagonal cracking, suggesting that the lateral load was never fully delivered to the walls. The stair towers remained erect. The east wall and stair tower are shown here.

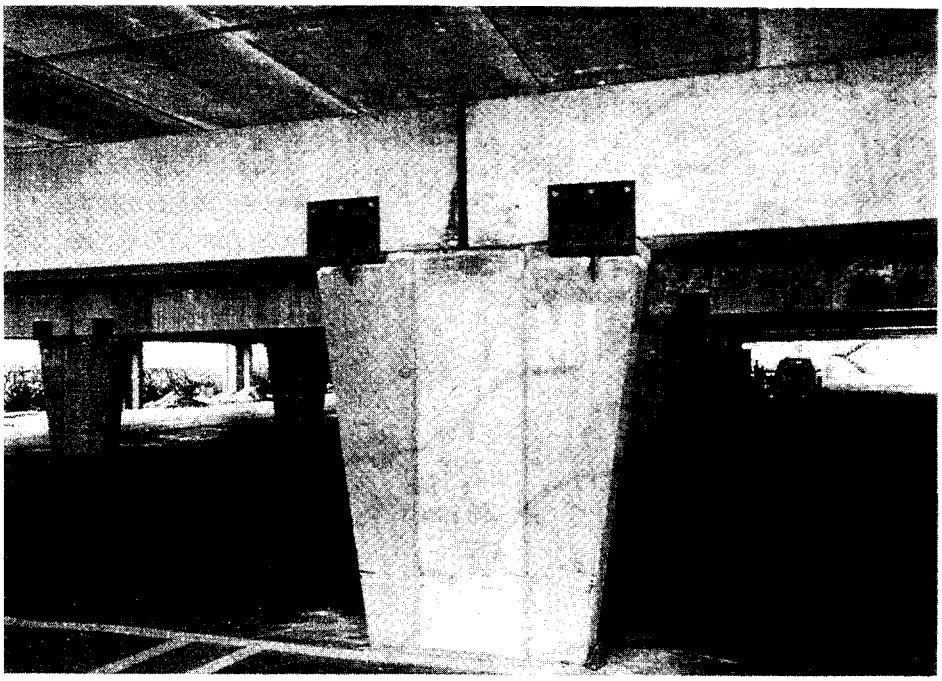

Figure 21 The interior columns of the two-level parking garage at the Trans World Bank in Sherman Oaks had been seismically strengthened after it suffered damage in the 1971 San Fernando quake. The interior columns fared well in the 1994 Northridge quake.

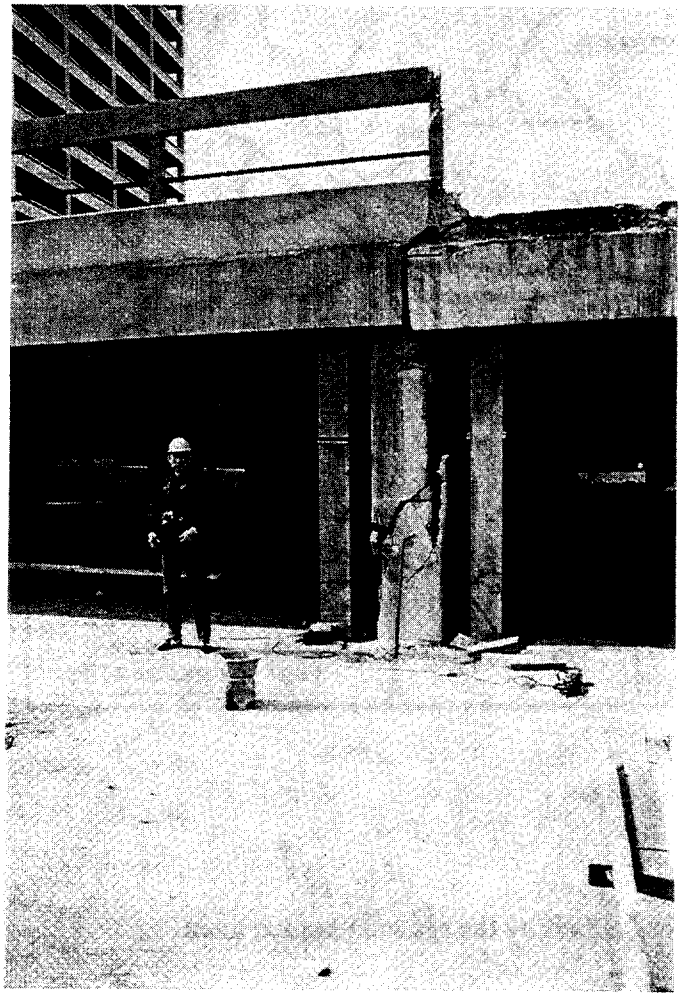

Figure 22 The exterior columns of the Trans World Bank parking garage, which had not been strengthened, were badly damaged.

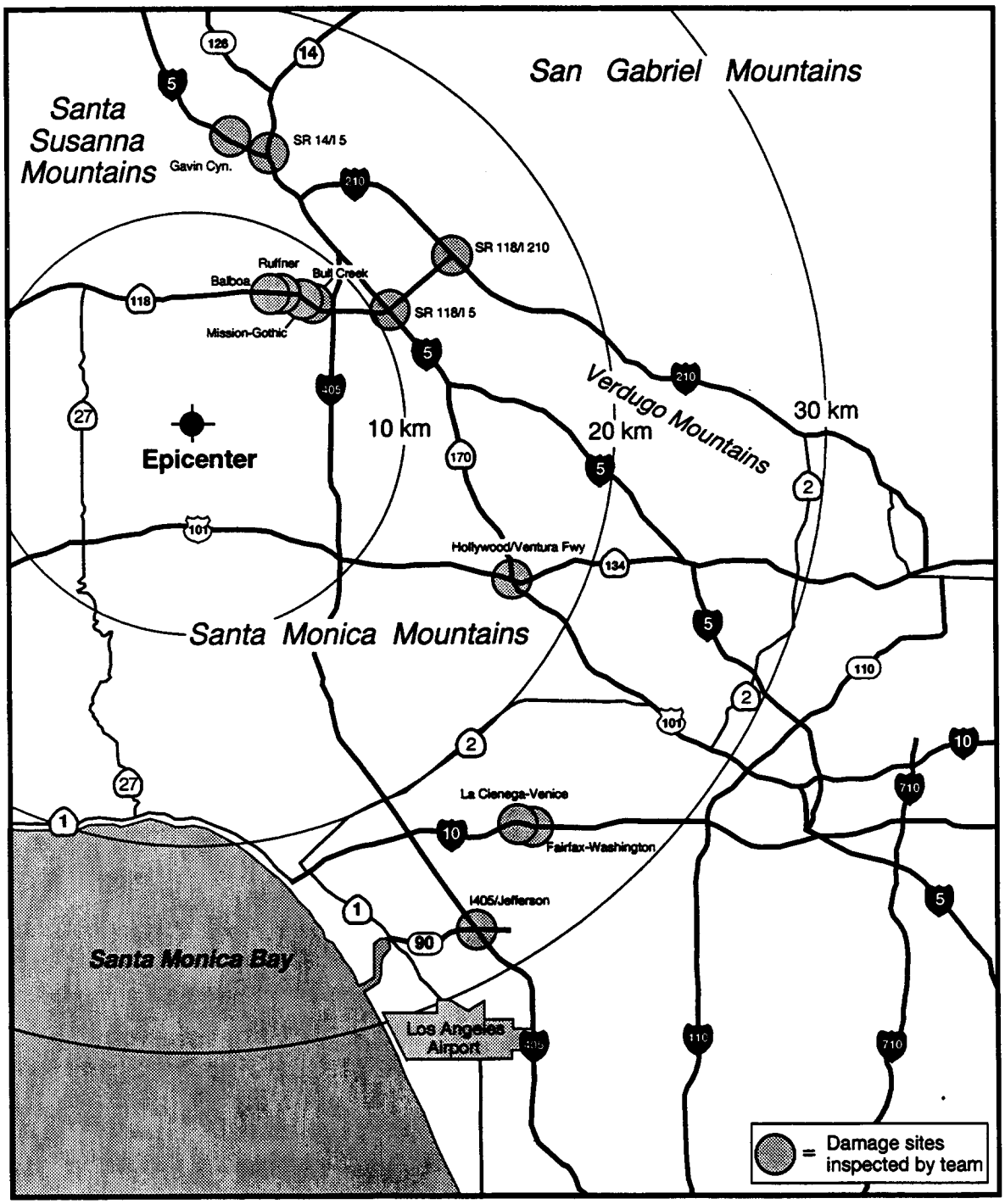

Figure 23 Bridge damage sites studied by the reconnaissance team

Figure 24 Aerial view of the bridge at Gavin Canyon, looking to the east, showing appearance of the four end spans shortly after demolition had begun

Figure 25 Ground level view of the southbound bridge at Gavin Canyon, looking to the northwest, showing the hinge bearing seat near Bent 3.

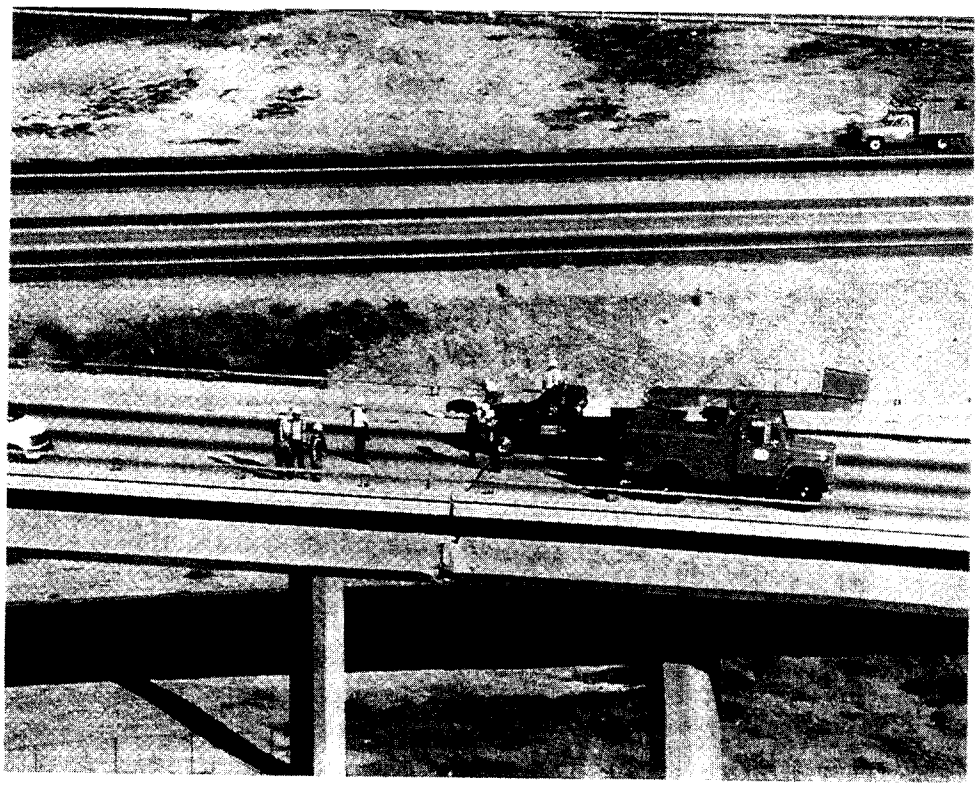

Figure 26 Example of pounding and offset at a hinge in the SR14/I5 interchange

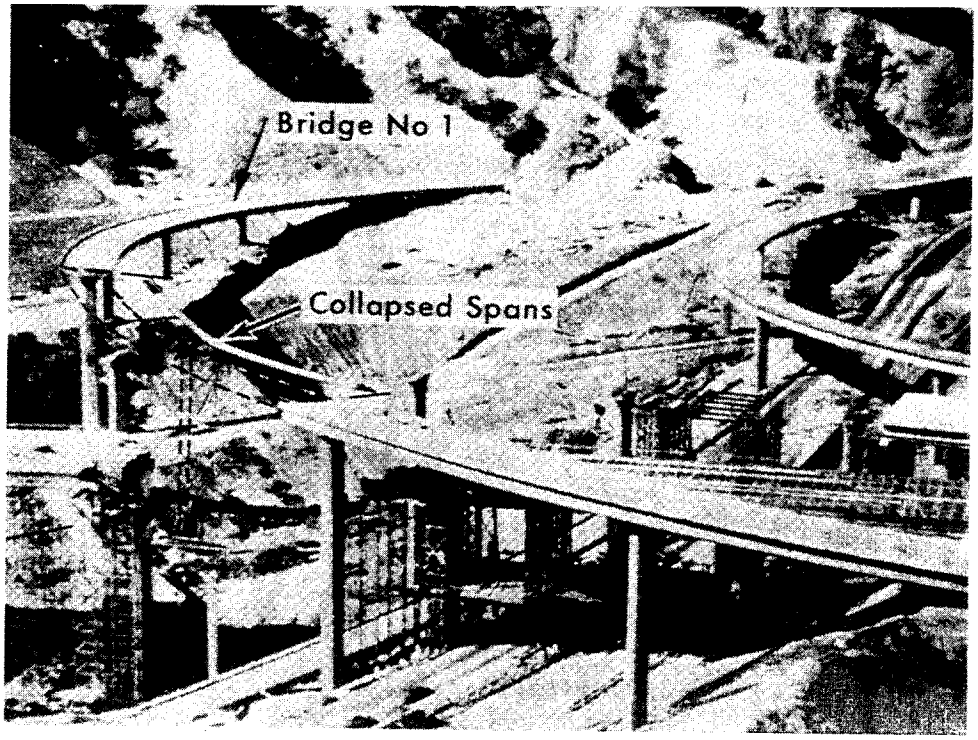

Figure 27 SR14/I5 interchange after the 1971 San Fernando earthquake. View looking to the west, showing collapsed South Connector Overcrossing

Figure 28 Overview of the collapse of the SR14/I5 Separation and Overhead, Ramp C, looking to the south at Abutment 1. Pier 3 can be seen at the right of the photograph (Courtesy of EERC)

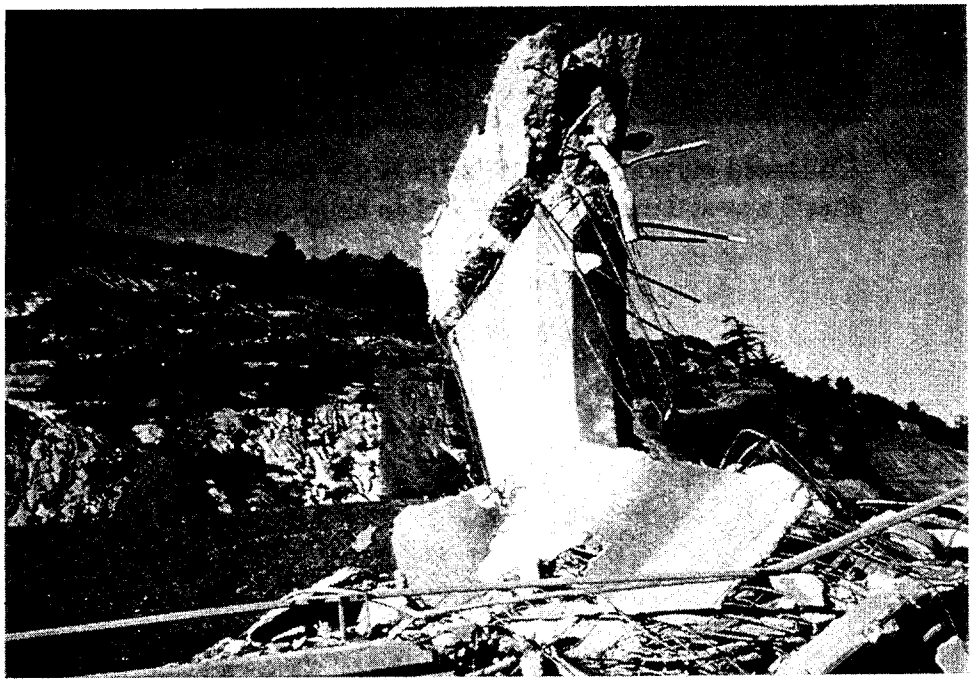

Figure 29 Damage at Pier 3 of the SR14/I5 Separation and Overhead, Ramp C, looking to the west (Courtesy of EERC)

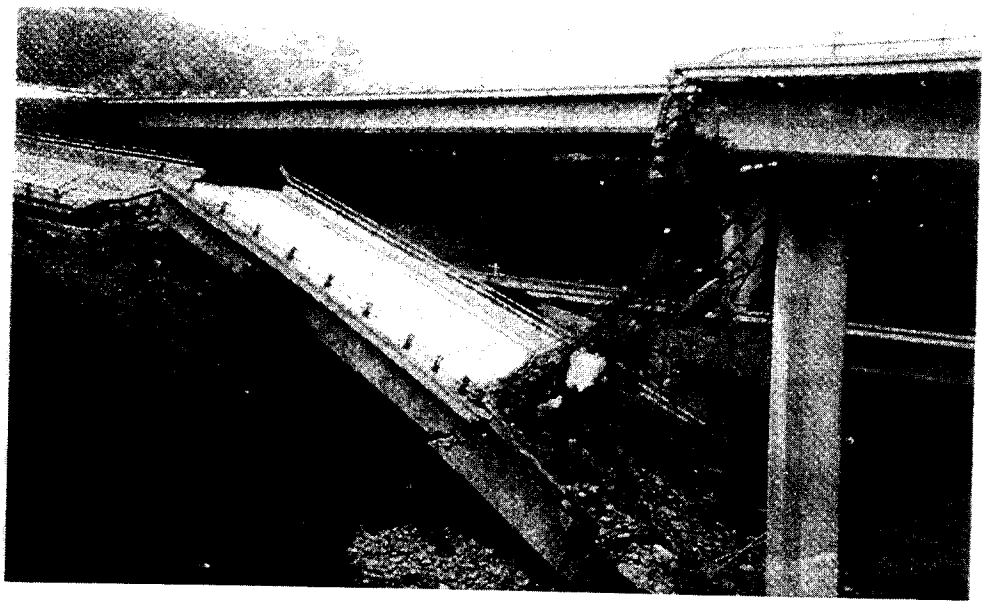

Figure 30 Collapsed portion of the SR14/I5 North Connector Overcrossing, looking east.. Pier 2 was at the left, near the broken hinge on the ground (Courtesy of EERC)

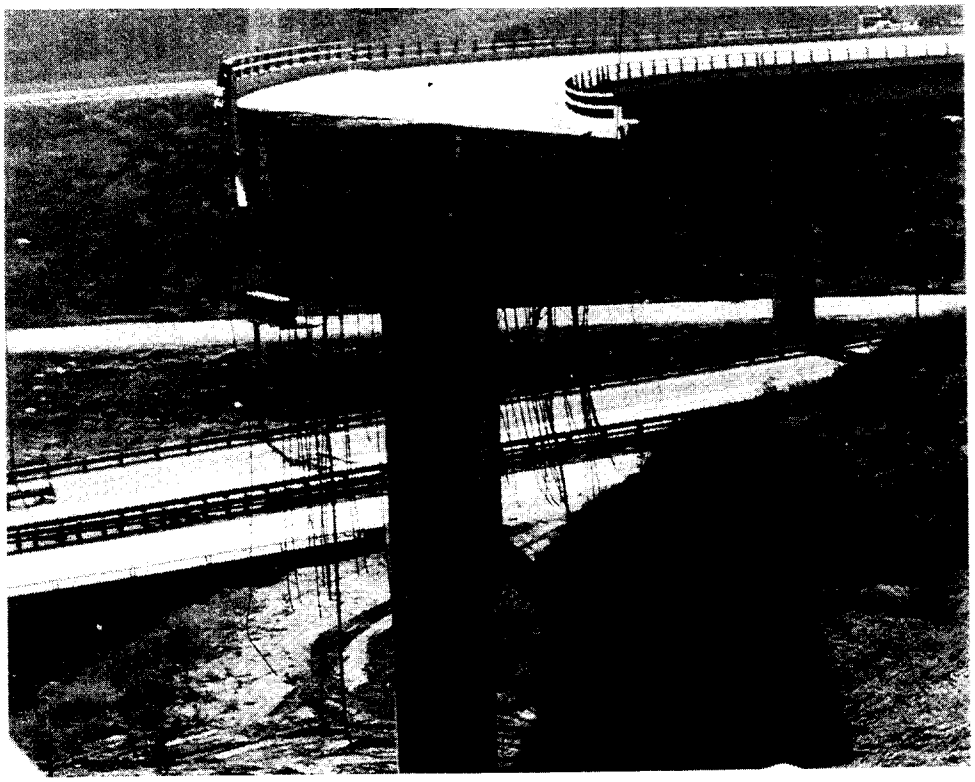

Figure 31 View of the flexural failure at Pier 3 of the SR14/I5 North Connector Overcrossing, looking to the south

Figure 32 View of crushed Pier 2 and the hinge near Pier 2 (Courtesy EERC)

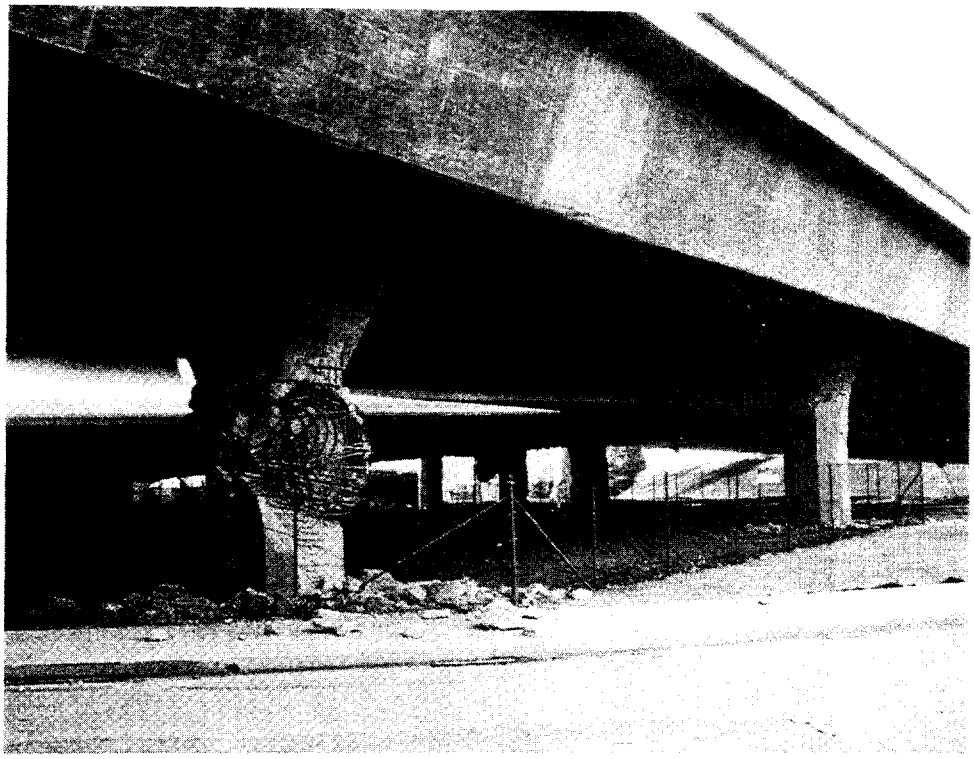

Figure 33 Damage to piers of the SR118 Mission-Gothic Undercrossing, looking to the northwest at the north face of the westbound bridge, Bents 3 (foreground) and 2.

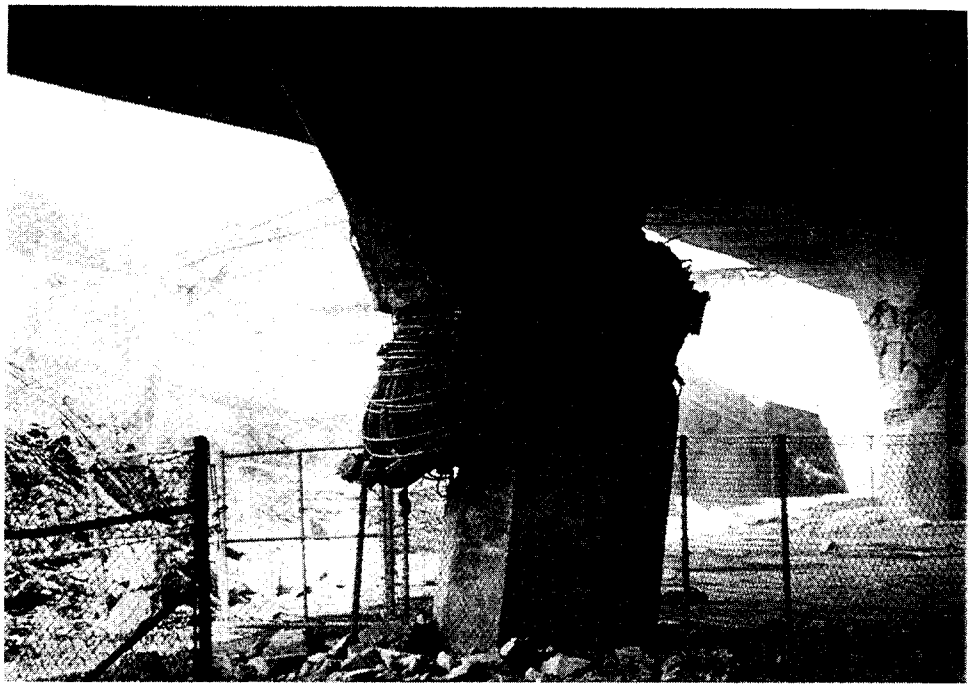

Figure 34 Damage to a pier of the SR118 Mission-Gothic Undercrossing, looking to the northwest at the southernmost pier of Bent 3 of the westbound bridge.

Figure 35 Damage to pier 3S-1 of State Route 118 at Bull Creek Canyon Channel, looking to the northwest

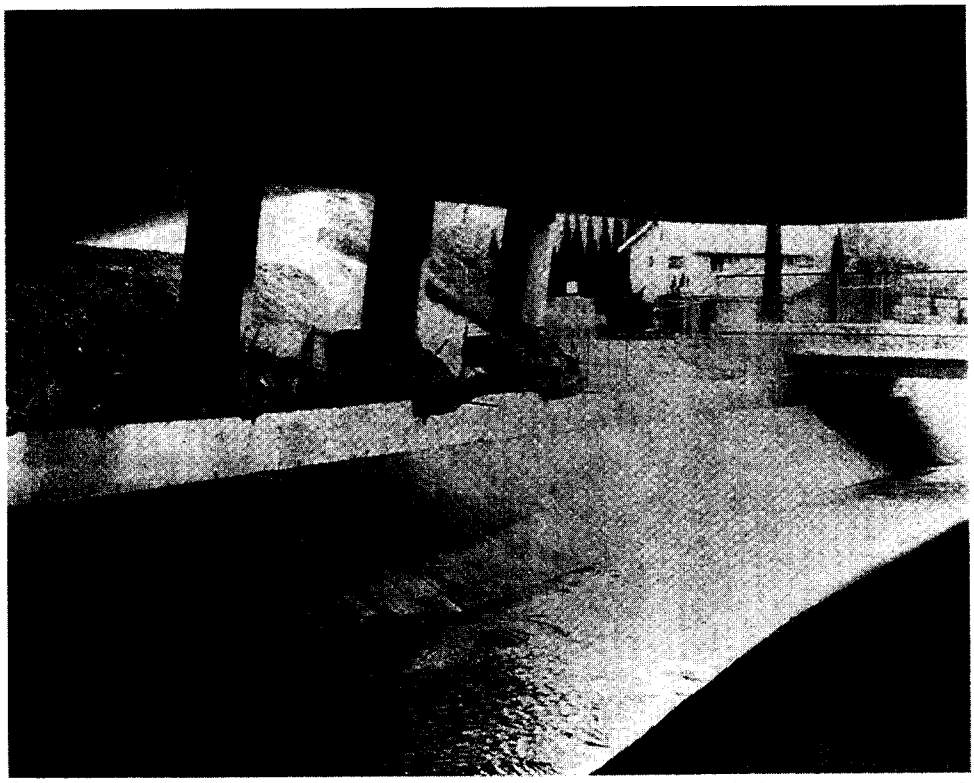

Figure 36 Damage to piers of Bent 3S of State Route 118 at Bull Creek Canyon Channel, looking to the southeast.

Figure 37 Collapsed westbound lane of I10 at Venice Blvd.; pier of Bent 7 in foreground

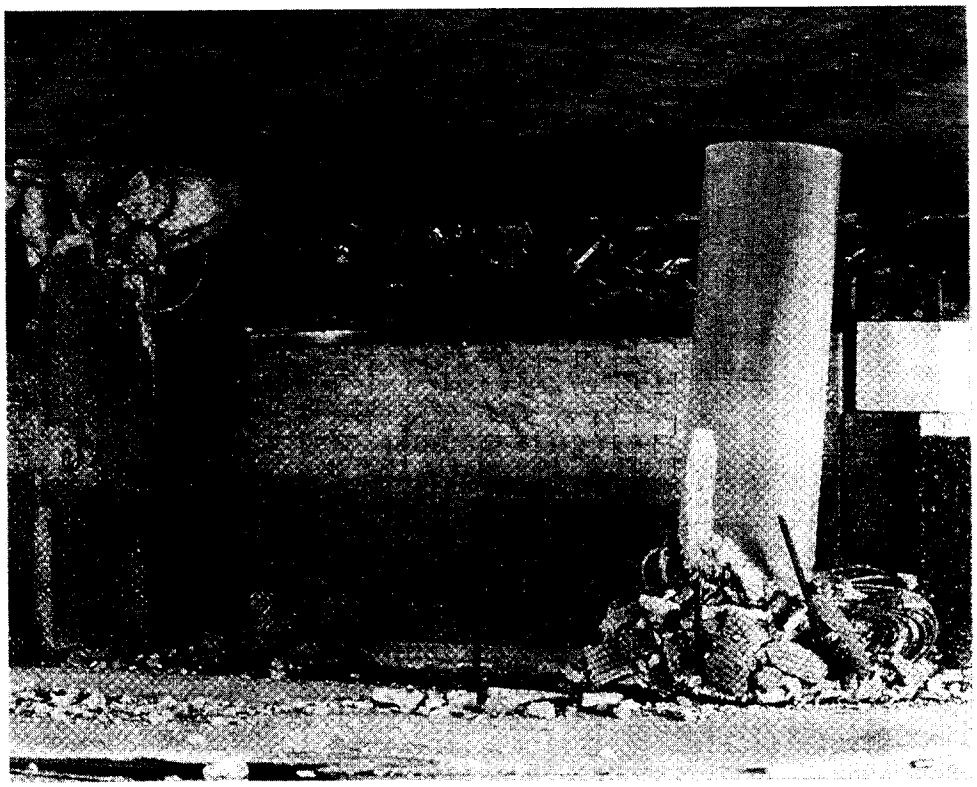

Figure 38 Failed piers in Bent 7 supporting westbound lane of I10 at Venice Blvd.

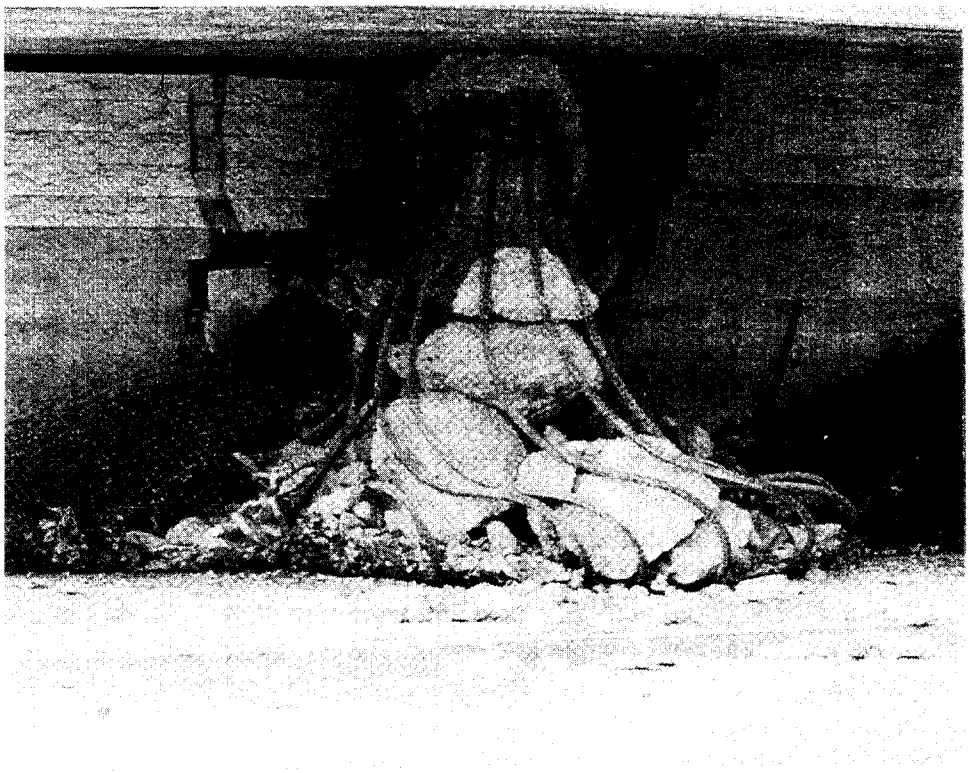

Figure 39 Northernmost pier of Bent 6 supporting westbound lane of I10 (west of Venice Blvd.)

Figure 40 Piers of Bent 3 supporting eastbound lane of I10 at La Cienega Blvd.

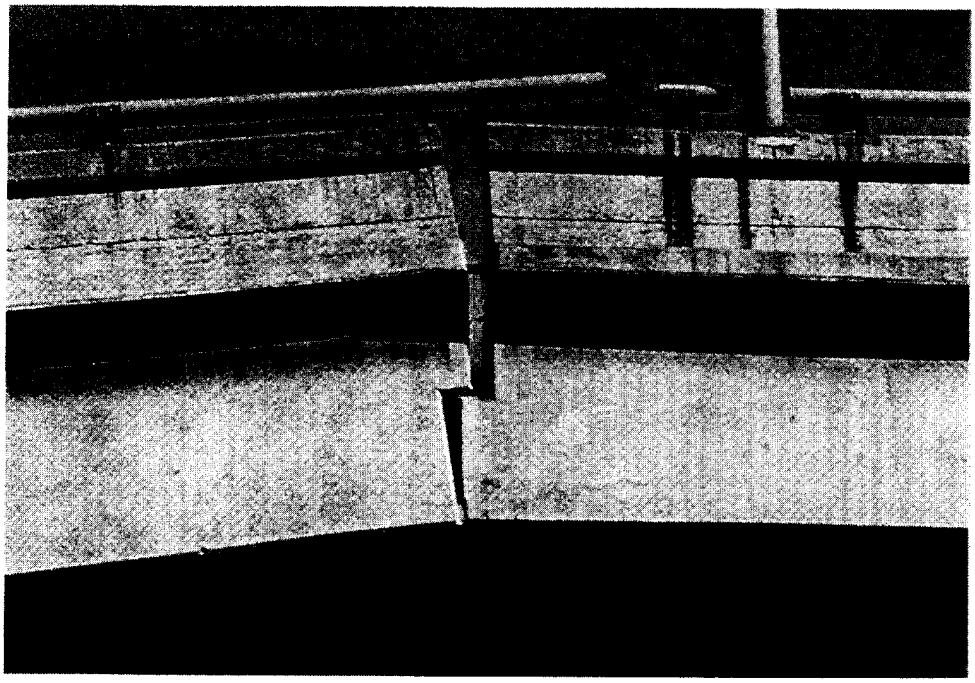

Figure 41 Hinge adjacent to Bent 4 of I 10 at Fairfax Ave.; cable restrainers prevented loss of support (Courtesy of EERC)

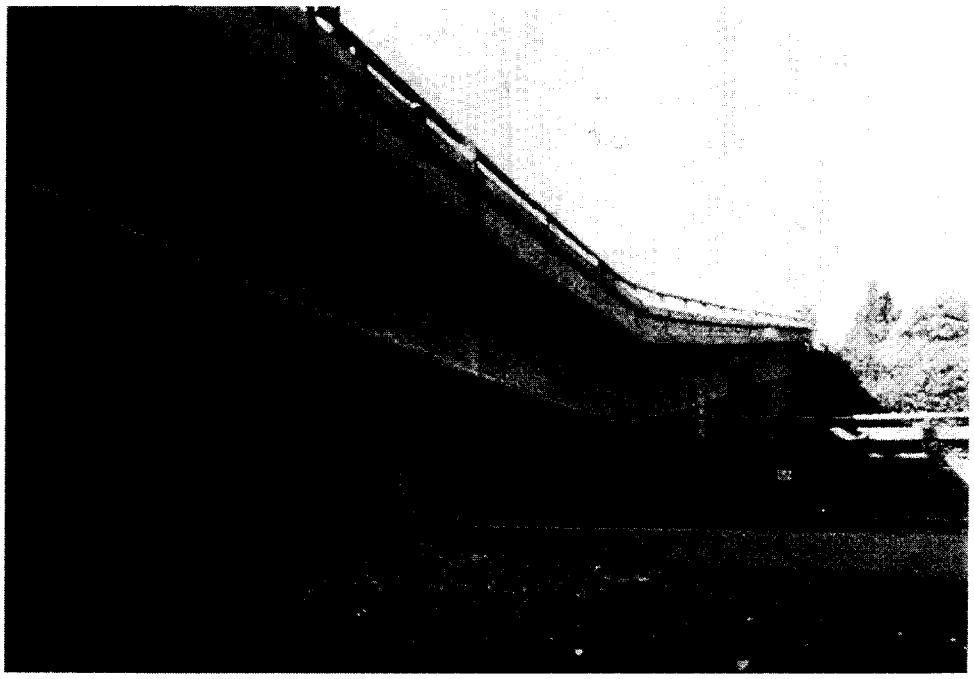

Figure 42 View of collapsed span of I10 over Fairfax Ave.; note rotation of girder over Pier 2 (Courtesy of EERC)

Figure 43. Failed column in Bent 3 of I10 at Fairfax Ave. (Courtesy of EERC)

Figure 44 The steel pipeline at Terminal Hill separated from its supporting saddle at several places and pipe sections bulged at other locations along the alignment.

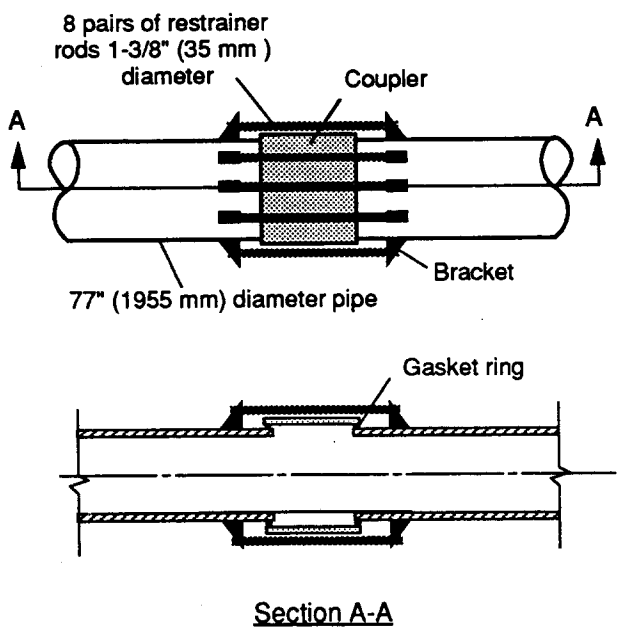

Figure 45 Schematic drawing of connection of the two steel pipe sections which were pulled apart during the earthquake.

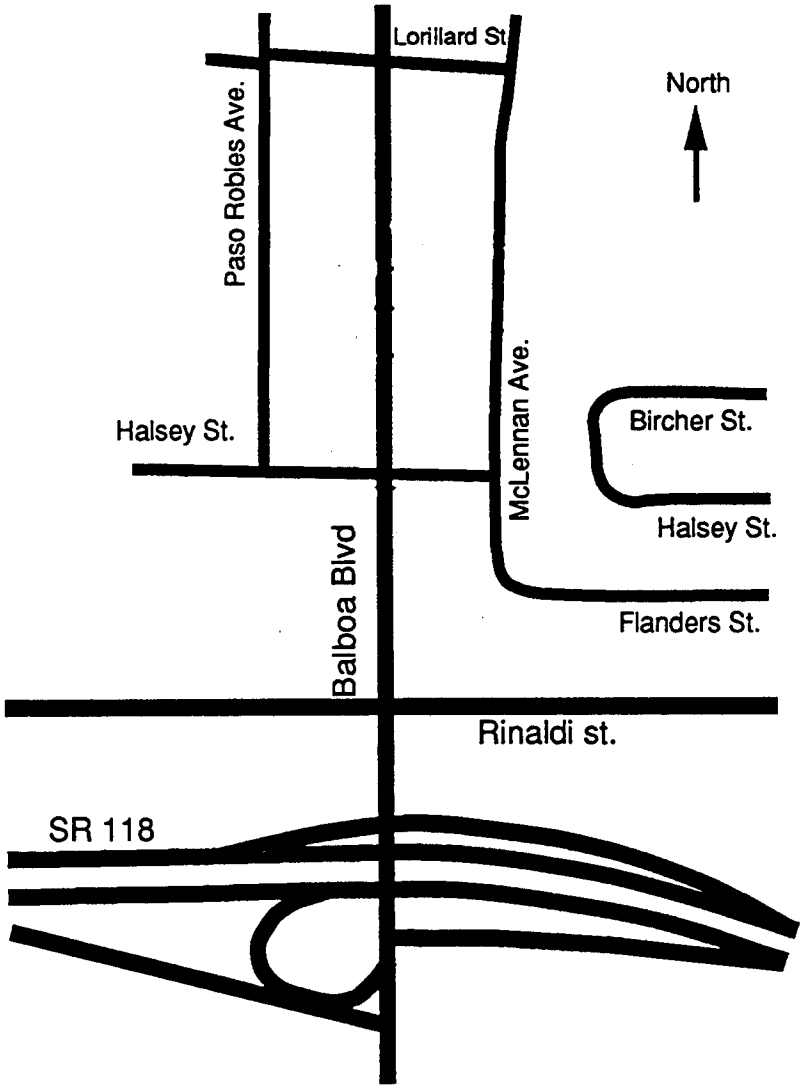

Figure 46 Location of the 0.6-m gas main rupture on Balboa Boulevard.

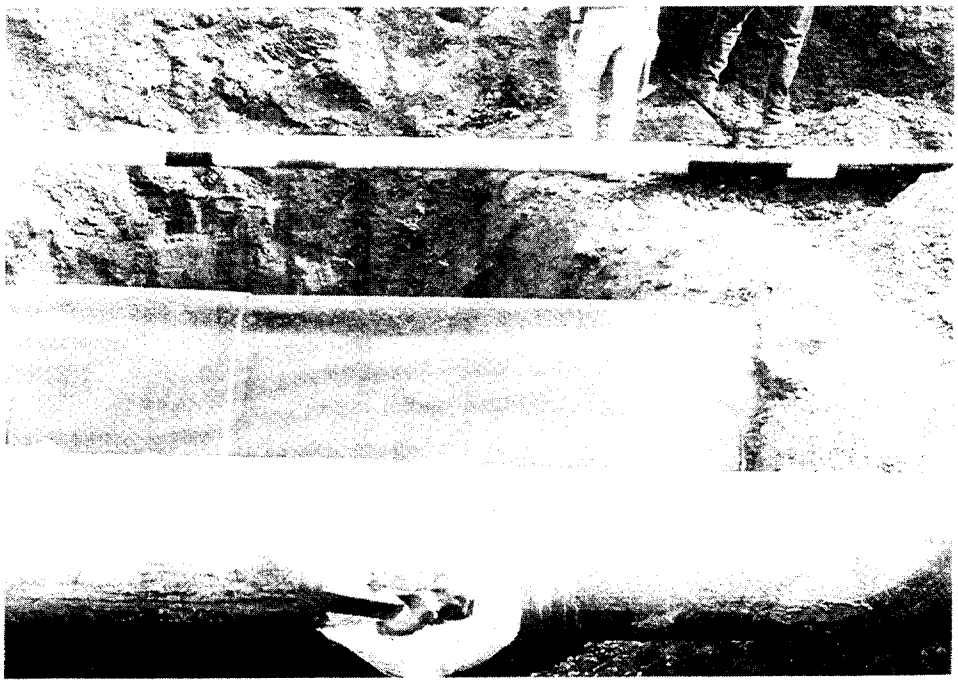

Figure 47 Ground contraction along Balboa Boulevard caused the rupture of a gas distribution line, the Rinaldi trunk water main, and a gas main.

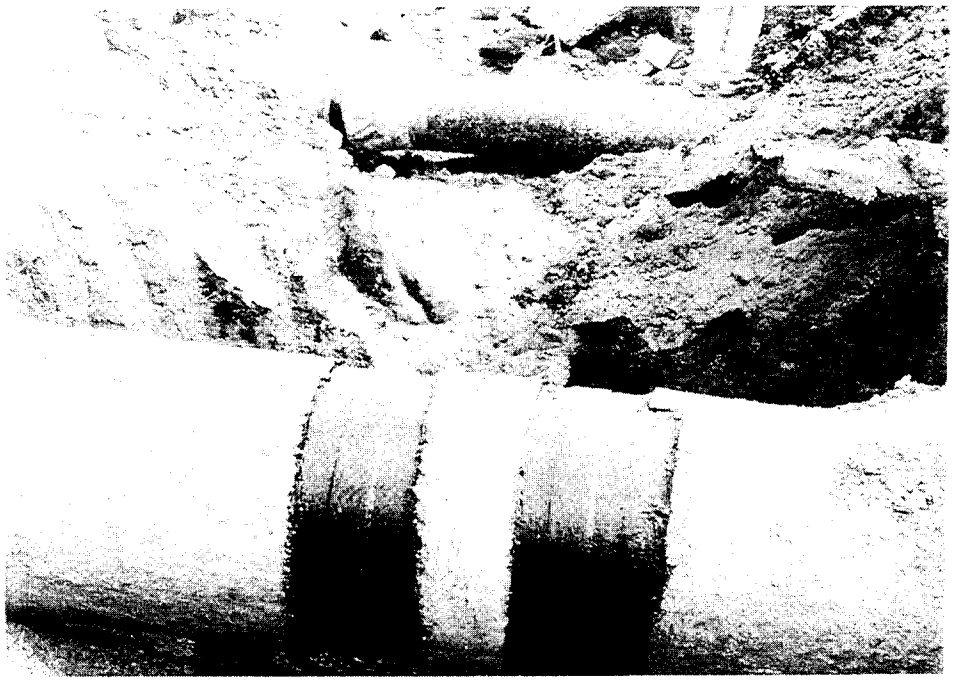

Figure 48 Ground extension along Balboa Boulevard resulted in the rupture of the same gas main and water main shown in Figure 47. The rupture of the gas main here caused a major fire that engulfed five houses.

Figure 49 Houses destroyed by a fire resulting from the rupture of the 0.6-m gas main along Balboa Boulevard.

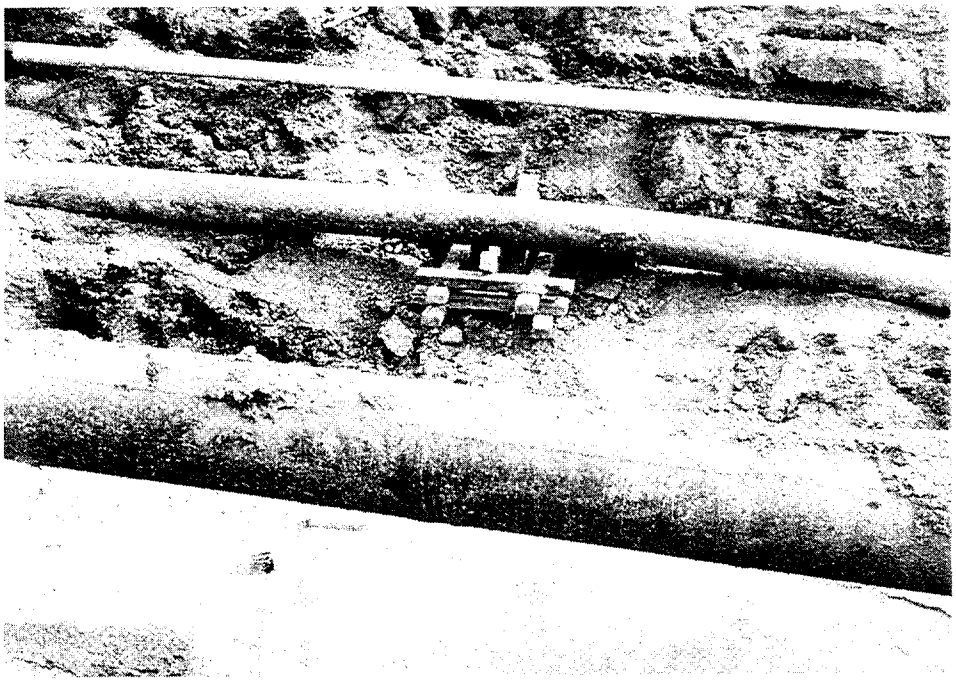

Figure 50 Some of the buried pipelines located near the intersection of Balboa Boulevard and Bircher Street--the potential hazard of co-location of lifeline systems. At this site are three water lines (two of them main lines); three gas lines; two sewers; one crude oil line; overhead power, telephone, and cable TV lines; the street lighting system; and the street itself.

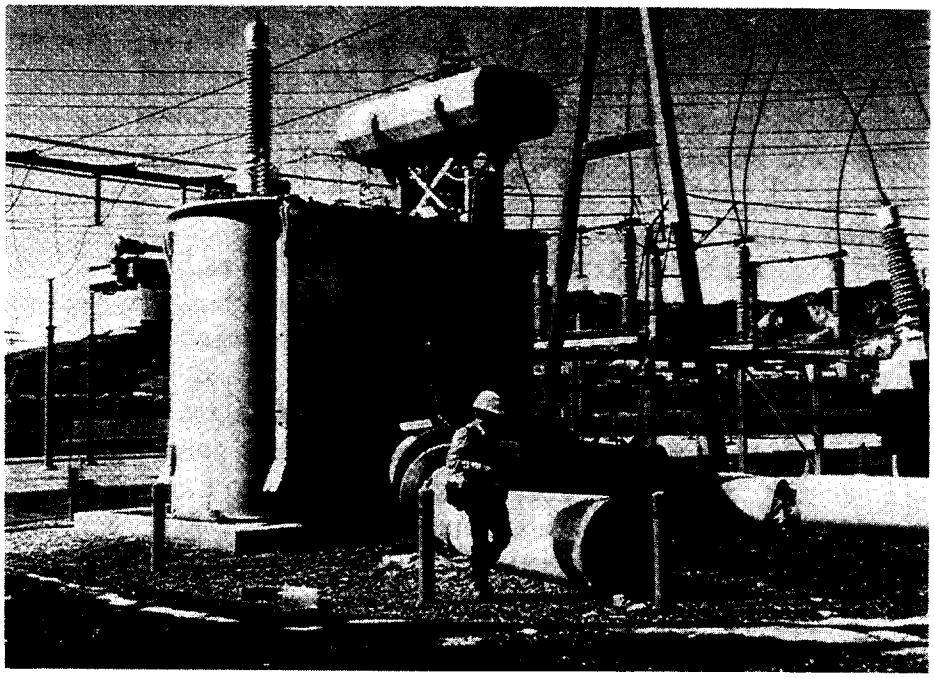

Figure 51 Damage to DC equipment at several high voltage substations, such as this one at Sylmar, led to widespread power outages in the Los Angeles area as well as isolated outages throughout seven western states. (Photo courtesy of Edward Matsuda, Pacific Gas and Electric Company.)

Figure 52 Porcelain is an integral part of high voltage electrical equipment due to insulation requirements and is also the most vulnerable to damage during strong earthquake shaking. (Photo courtesy of Edward Matsuda, Pacific Gas and Electric Company.)

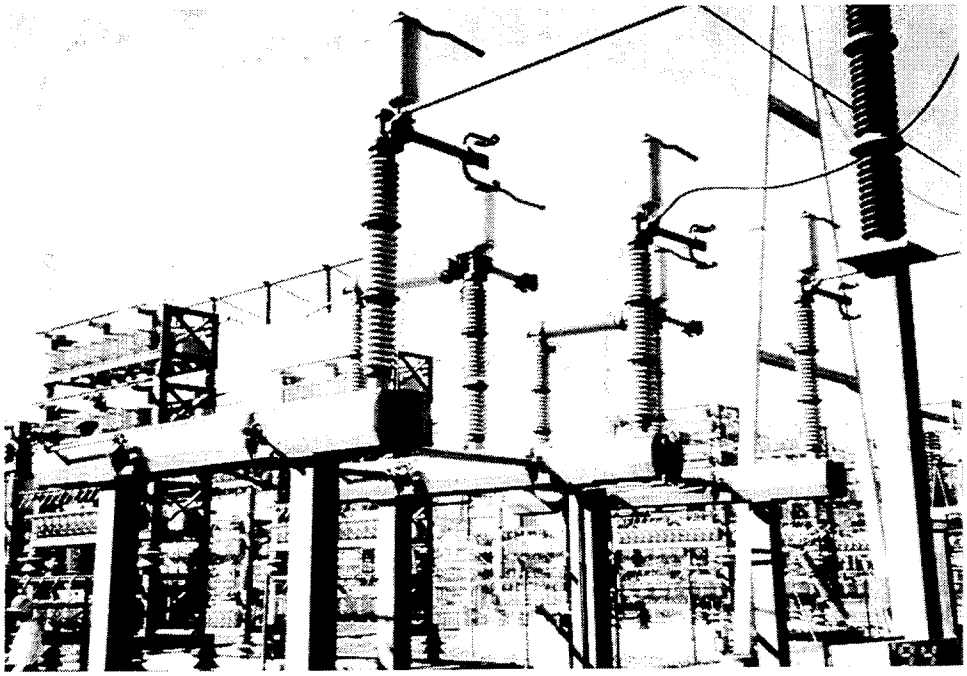

Figure 53 Most of the 230 kV circuit switchers (in the forefront) at the Sylmar substation were damaged. Most of the capacitor banks (in the background) performed well in this earthquake, whereas most collapsed during the 1971 quake. (Photo courtesy to Edward Matsuda of Pacific Gas and Electric Company.)

Figure 54 Derailment of a 64-car freight train in Northridge. The incident resulted in the spill of 30,000 liters of sulfuric acid and 7,500 liters of diesel fuel.

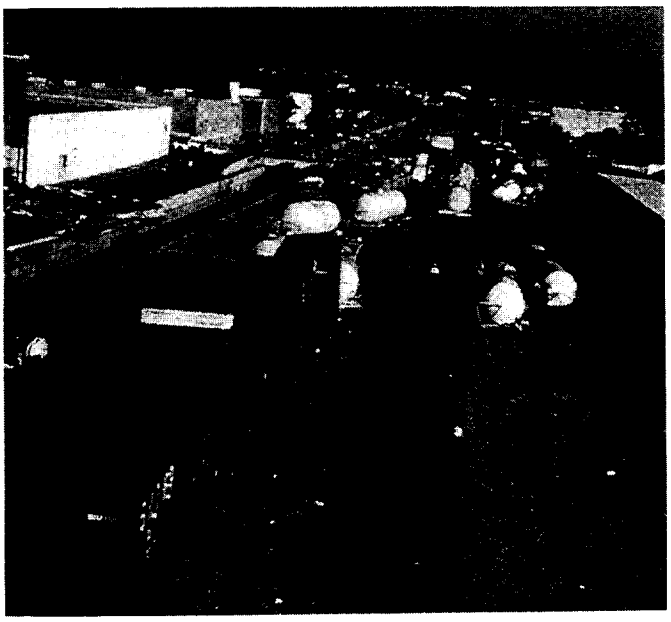

Figure 55
Transverse cracks in pavement along Balboa Boulevard in Northridge area.

Figure 56 Fire damage in a single story commercial building.

Figure 57 Fire damage in a two story commercial building.

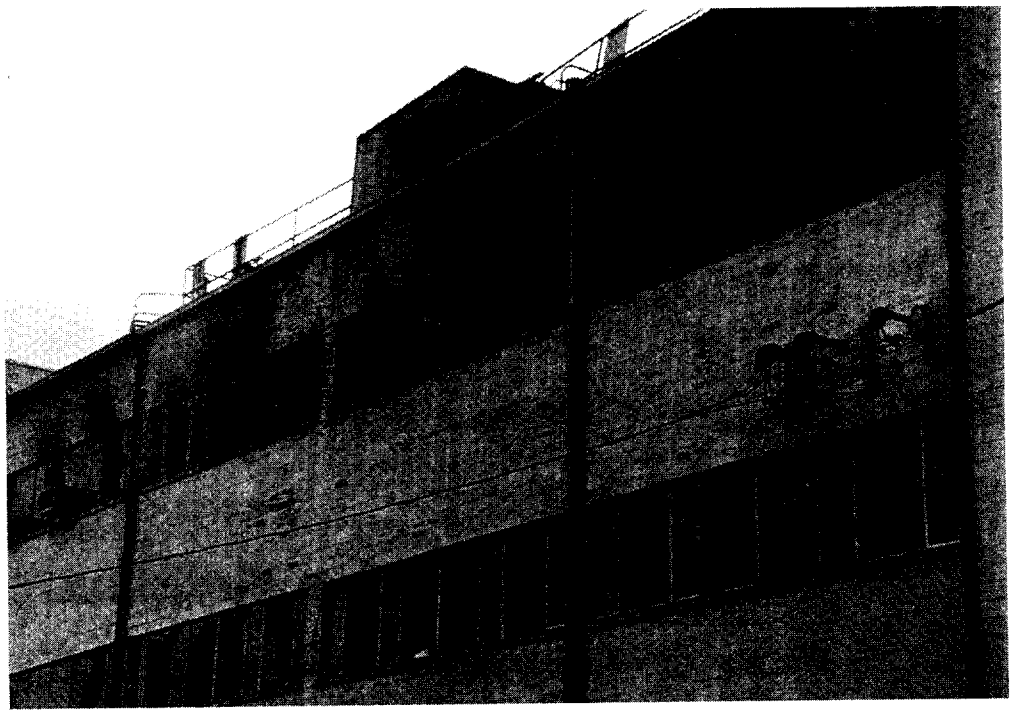

Figure 58 Fire damage in a three story commercial building.

Figure 59 Partially collapsed apartment building with fire damage in the rear.

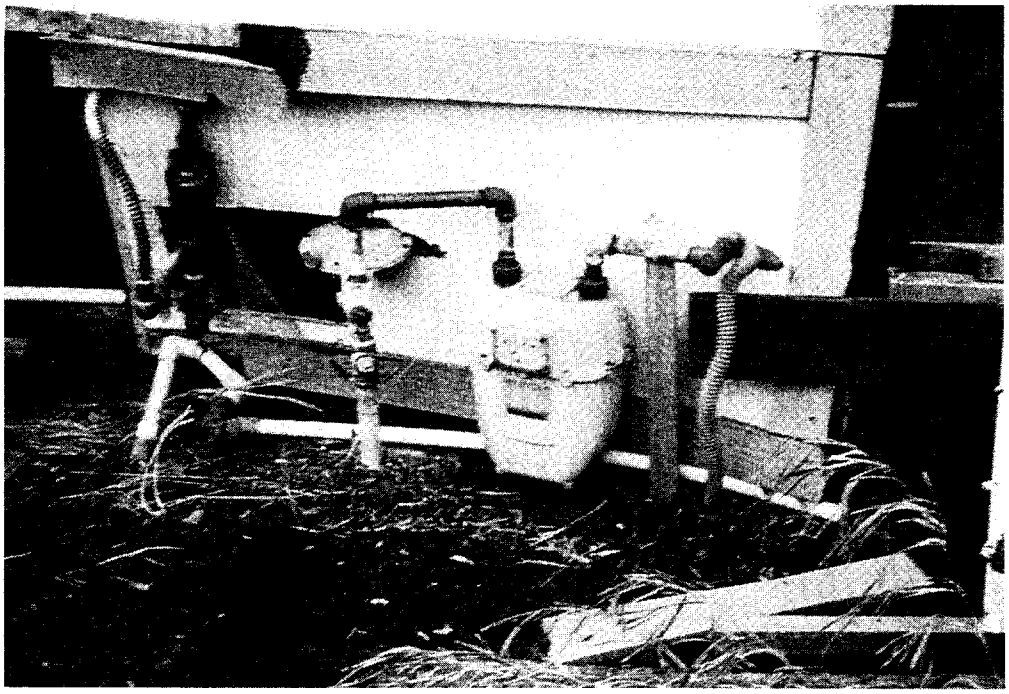

Figure 60 Damaged gas service in a manufactured housing development.

Figure 61 Multi-family residential building destroyed by fire.

Figure 62 University science building damaged by fire.

Summary Report on the Northridge, South California, U.S.A., Earthquake of January, 1994

by

Yukihiko Sumiyoshi[1], Tomomitsu Fujii[2], Kazuhiko Kawashima[3], Tatsuo Uwabe[4], Kouichi Koshiumi[5], Eiichi Itoigawa[6], Yoshiaki Nakamura[7], Kimihiko Izumi[8] and Hideki Sugita[9]

ABSTRACT

The Northridge, California, U.S.A., Earthquake occurred at 4:31 on January 17, 1994. Destructive damage was developed in the epicenter region. This paper describes a summary of the damage investigation by the Japanese Government Study Team for the Northridge Earthquake.

Key Words :Northridge Earthquake, Damage Investigation, Urban Disasters, Earthquake Disaster Countermeasures

1. INTRODUCTION

Destructive damage was developed due to the Northridge earthquake which occurred at north/west of Los Angeles at 4:31 on January 17, 1994. Because the earthquake occurred close to a major urban area, the urban-type earthquake damage such as collapse of freeway bridges and buildings, damage of lifeline facilities were developed.

The Japanese government sent a study team consisting of 21 experts of the ministries, agencies and institutions concerned to contribute to the development of earthquake disaster prevention measures not only for Japan but for world-wide countries where the occurrence of earthquakes is a great threat. Two experts from Railway Technical Research Institute and Tokyo Gas Company and six experts for fire office of local governments accompanied to the study team. Mr. Yukihiko Sumiyoshi, former Director-General of the Public Works Research Institute, Ministry of Construction and Tomomitsu Fujii, Director of Earthquake Disaster Countermeasures Division, National Land Agency served as the leader and sub-leader of the study team.

The investigation in the epicentral region was made from March 1 to 12, 1994 with a great assistance and support of many organizations concerned including U.S. Federal organizations, county and city governments, private companies and individuals. The main objectives of the study team were to investigate 1) damage and restoration of civil infrastructure and buildings, 2) damage and restoration of lifeline facilities, 3) fire, and 4) emergency treatment and support for damaged peoples.

The investigation by the study team was

1) Former Director-General, Public Works Research Institute, Ministry of Construction
2) Director, Earthquake Disaster Countermeasures Division, Disaster Prevention Bureau, National Land Agency
3) Research Coordinator for Underground Development, Public Works research Institute, Ministry of Construction
4) Chief, Earthquake Disaster Prevention Laboratory, Structures Division, Port and Harbor Research Institute, Ministry of Transport
5) Assistant Director, Building Guidance Division, Housing Bureau, Ministry of Construction
6) Senior Researcher, Urban Disaster Prevention Division, Urban Planning Department, Building Research Institute, Ministry of Construction
7) Chief, Traffic Management Section, Traffic Operation Department, Japan Highway Public Corporation
8) Chief, Design Division, 3rd Construction Department, Metropolitan Expressway Public Corporation
9) Research Engineer, Earthquake Engineering Division, Earthquake Disaster Prevention Department, Public Works Research Institute, Ministry of Construction

successfully completed with great supports by Dr. R. N. Wright, U.S. Chairman of the Panel on Wind and Seismic Effects, UJNR, Mr. Noel J. Raufaste, Secretary General of the Panel, Dr. H. S. Lew, Mr. James D. Cooper, Dr. S. C. Liu, and Mr. James H. Gates (Panel members).

The original full report is being prepared with the contents as[1]:

Preface
1. General
2. Natural and Social Condition
3. Systems of Earthquake Prediction and Precursors of the Northridge Earthquake
4. Outline of the Event, Crustal Movement and Strong Motion Observation
5. Soil Liquefaction and Slope Failure
6. Damage and Restoration of Roads and Bridges
7. Damage and Restoration of Buildings
8. Damage and Restoration of Lifeline Facilities
9. Break out of Fires and Countermeasures
10. Emergency Response
11. Administrations for Disaster Prevention
12. Concluding Remarks

This paper presents a summary of the report with an emphasis on the damage of roads, bridges, buildings and lifeline facilities, and fires.

2. OUTLINE OF DAMAGE

Based on the information from OEM of City of Los Angeles, FEMA and OES of State of California, the major damage of the earthquake was as:

(1) death:	57
(2) injured:	9,348
(3) families affected:	about 18,000
(4) source of fire:	about 100
(5) loss:	about 15–30 billion dollars

In addition to the death of 57, there were several persons who died due to indirect effect of the earthquake such as heart attack. The families affected means those whose houses were so badly damaged that they could not stay there. The source of fire represents the fire which broke out in one hour after the earthquake in Los Angeles City. Besides those fires, there were several fires outside Los Angeles City.

3. GROUND MOTION

Many strong motion records with high accelerations were obtained by CDMG, USGS and LADWP.

Fig. 3.1 shows the records at Tarzana Cedar Nursery where a very high acceleration over 1.8 g was measured. It was measured on a hill by a SMA–1 strong motion accelerograph installed in a plastic case as shown in Photo 3.1. Because the SMA–1 is to measure an acceleration up to 1 g, the acceleration over scaled from the recording film space as shown in Photo 3.2. The peak acceleration with 1.8 g was recorded beyond a driving hole at a side of the film. It is expected that the recording accuracy for over 1.8 g acceleration is verified by a shake table test of the SMA–1 accelerograph.

It is interesting in the Tarzana records to note that the duration of high acceleration is about 8 seconds, and that this is quite different with other near field records which have much shorter duration. This would suggest the large amplification by the surface soils. But the shear wave velocity measured at 250 m west of the Tarzana recording site is 278 m/sec from the surface to 5 m below the surface, and 409 m/sec from 5 m to 30 m from the surface. It is noted that the ground impedance is not so high.

Fig. 3.2 shows the Arleta record. This was recorded at Arleta Fire Station at Nordhoff Avenue. The vertical peak acceleration was 0.59 g and was lager than the horizontal components of 0.35 g and 0.29g. It should be noted that this is not the free field record but was recorded on a concrete floor of the fire station as shown in Photo 3.3.

Fig. 3.3 shows the response accelerations of the records at Arleta, Newhall, Pacoima and

Sylmar. Although the soil boring data are not available for those sites, it is interesting to know that the response acceleration at longer natural period such as the value at 1 second is quite large at Newhall and Sylmar. The highest response acceleration at 0.3 second is close to 0.3 g at Sylmar. It is a very important task to investigate why damage was not developed for most of structures although they were subjected to such large ground motions. Few number of inelastic excursion developed in structural members associated with short duration of ground motion may be a possible reason for this.

4. DAMAGE OF ROAD FACILITIES

4.1 Outline of Damage

Destructive damage was developed to road facilities. Fig. 4.1 shows the locations of major road damage. Among various types of road damage, such as cracks and buckling of pavements, damage of bridge was significant. Failure of gas and petroleum pipelines embedded under ground suffered damage and this suspended the roads. Overturning of masonry and concrete block fence occurred. Because there are enough space in roads and because the earthquake occurred early in the morning, this did not cause serious damage.

Seven bridges suffered significant damage as:

1) I-10 Fairfax/Washington Undercrossing
2) I-10 La Cienega/Venice Blvd. Undercrossing
3) S-118 Mission/Gothic Undercrossing
4) S-118 Bull Creek Channel Bridge
5) I-5/S-14 Interchange, South Connector
6) I-5/S-14 Interchange, North Connector
7) Gavin Canyon Undercrossing

The damage was developed due to insufficient lateral force and inadequate design details considered in the pre-1971 seismic design practice.

Among those bridges, two typical damages are presented in the followings.

4.2 Damage of S-118 Mission/Gothic Undercrossing

The bridge is of 3 span continuous prestressed concrete box girder with 152 m long (west bound) and 4 span continuous prestressed concrete box girder with 170 m long (east bound) as shown in Fig. 4.2. It was designed in 1973 and the construction was completed in 1976. Although the design was completed after 1971, the original design concept depends on the pre-1971 design practice. Only some design detailing such as spiral was updated according to the current design method.

The sectional area of concrete was small as shown in Fig. 4.3. The columns had a hexagonal shape with diameter of 1.8 m. They had flare at the top. The main reinforcements and spiral were of 45 deformed bars with diameter of 39 mm and round bars with diameter of 15 mm at 8.75 cm interval.

Two spans of the east bound bridge collapsed as shown in Photo 4.1. Although the west bound bridge suffered significant damage to reinforced concrete columns, it did not collapsed.

There were various columns which suffered different level of damage. By comparing the damage degree of those columns, it can be seen that how damage progressed. When the column was subjected to a seismic lateral force, flexural cracks were firstly developed as shown in Photo 4.2. It is supposed that the main reinforcements and the spirals already yielded at this stage.

As the lateral force increases, the shear failure was initiated from the flexural cracking as shown in Photo 4.3. Because the sectional area of concrete was small and because the lateral confinement was not enough, the shear strength was low. The core concrete was initiated to be crushed and moved outward direction. The main reinforcements bucked in outward direction. The spirals were initiated to be ruptured.

As the columns were subjected to the

alternative lateral force, the lateral resistance of the columns was lost, and the columns were dislodged as shown in Photo 4.4. Finally, the columns lost the bearing capacity for supporting the weight of superstructure, and failed as shown in Photos 4.5 and 4.6.

The similar damage was developed at Bull Creek Channel Bridge on State Freeway 118 as shown in Photo 4.7, Fairfax/Washington Undercrossing (I-10) and La Cienega/Venice Undercrossing (I-10) as shown in Photo 4.8.

4.3 Damage of I-5/S-14 Interchange

Various destructive damage was developed at this interchange. The S-14/I-5 Separation and Overhead which connects southbound S-14 to southbound I-5 collapsed as shown in Photo 4.9. It was of five frames with 475 m long as shown in Fig. 4.4. Three spans from the abutment 1 (A1) collapsed. The collapsed section was of a prestressed concrete box girder, and the both ends were supported by A1 and the gerver hinge near P4. The pier 2 collapsed and the pier 3 stranded as shown in Photo 4.10 with the deck being felt down.

The dimension of piers supporting the collapsed section may be as shown in Fig. 4.5. They were reinforced by deformed bars with diameter of 57 mm and the tie reinforcements with diameter of 15 mm placed at 30 cm interval.

The failure may be initiated by the shear failure of P2. Because of higher stiffness of P2 associated with shorter pier height, the seismic lateral force induced in the deck concentrated at P2. Failure of the cable restrainers as shown in Photo 4.11 at the joint near P4 may be developed as the a result of the collapse of deck.

Although the failure is attributed to the insufficient design lateral force and the detail considered in design, it shows the importance of taking a total structural response into account in design. Lateral force distribution of a bridge supported by piers with different height depends on the stiffness of piers as well as the stiffness of soils.

The North Connector Overcrossing also failed as shown in Photo 4.12. The deck consisting of the second frame from A1 collapsed at P3. This may be caused by the shear failure of P2. Similar mechanism with the S-14/I-5 Separation and Overhead contributed to the failure of P2.

Separation of the two adjacent decks occurred at many hinges. Photos 4.13 and 4.14 show two examples of such large separations. Cable restrainers ruptured at some hinges as shown in Photo 4.15. Nevertheless the effectiveness of the cable restrainers was apparent. More collapse might be developed unless the cable restrainers.

4.4 Effectiveness of Seismic Strengthening

There are many bridges which were strengthened against an earthquake. As shown above, the effectiveness of cable restrainers was apparent for reducing the damage. No seismic damage was observed at columns which were strengthened by steel jacketing. Photo 4.16 shows an example of such columns.

4.5 Prompt Repair and Restoration

It was remarkable to know that every efforts were made to prompt recovery of the damage. Demolish of the major bridge damage was initiated from the day following the earthquake. Explosive material was used at some bridges as shown in Photo 4.17 to reduce the time required to demolish the damaged bridges. A special contract among about 5 construction companies was made for reducing the time required for usual open bids. A penalty/bonus system was used for reconstructions. Seven days per week and 24 hours per day reconstruction is being made.

Well considered countermeasures were/are being adopted for mitigating the traffic congestion due to close and damage of roads. Detours were designated promptly after the earthquake. High priority was given to high occupancy vehicles. Time interval of traffic signals was adjusted so that the smooth traffic flow could be made. Many well prepared traffic signs were provided at various locations. Thus

serious traffic congestion was avoided.

It should be noted that this could be made because the U.S. highway system is much better than that of Japanese system from various points such as traffic volume, number of lanes and network systems. For example, I-5/S-14 Interchange was one of the bottle necks in Los Angeles Area, because they cross the narrow canyon. But number of lanes at this section including interstate freeway, freeway and other roads is 22. Although this reduced to 6 lanes soon after the earthquake, it was soon increased to 13 by detours. Even normal streets and boulevards in residential zone have 4 lanes. If the similar type of bridge damage occurs in urban areas in Japan, unexpected damage and effect might be developed. It is therefore obvious from such evident that further earthquake disaster prevention measures are inevitably required in Japan for reducing the critical effects of earthquakes.

5. DAMAGE OF BUILDINGS

5.1 Locations of Building Damage

According to the map showing unsafe buildings (Red tagged) and limited entry buildings (Yellow tagged) in Los Angeles city, there are several areas where damage concentrated because of difference of ground shaking intensity. Within about 7 to 8 km from the epicenter, damage of buildings distributed almost uniformly, and in the outside area from the epicenter beyond the Santa Monica Mountain there were some areas where damage concentrated such as Sherman Oaks, Hollywood and Adams. It seems to be related with the soil condition. This requires more study.

5.2 Building Damage and Social System

At Sherman Oaks area, many multi-story apartment and condominium buildings were significantly affected by the earthquake. Most of these building were constructed before 1974 at that time the structure code was revised. According to the zoning code for city planning, the area is designated as R3 (Multiple Dwelling Zone). The code requests 1 to 2 parking spaces for each dwelling unit and 90 to 130 dwelling units per one hectare. Therefore parking space is provided at first floor or basement floor as "pilotis type". This structure type seems to have increased the damage level of building during the earthquake as shown in Photos 5.1, 5.2 and 5.3. Because it is required to provide parking space in dwelling buildings in urban areas, a city planning control system which matches with the building planning and structure design may be required.

In case of complete collapse of precast concrete parking garage at California State University at Northridge as shown in Photo 5.4, the damage seems to be developed due to an insufficient connection between elements of the structure and lack of ability to support the vertical loads while undergoing to large lateral deformation. It is interesting to note that compared with Japanese buildings, more freedom seems to be accepted in U.S. in designing buildings. For example, structural engineers can adopt more free use of frame under the condition that they can verify the safety of buildings against the seismic loading by dynamic response analyses. In such case, it is required for structural engineers to conduct overall and comprehensive engineering judgment besides the requirements by the building code.

5.3 Quick Administrative Response

It can be highly evaluated that California State and Los Angeles city made a prompt administrative response for the damage. For example State Governor of California directed the SSC to coordinate a study of the specific policy implications arising from the earthquake, with particular attention to implications for seismic structural safety and land-use planning. And the structural codes of chimney and block fence were revised. It is important to take necessary measures to safety taking account of seriousness of social influence based on building damage in case of large scale earthquake.

5.4 Retrofit Program

Most of the retrofitted unreinforced masonry building (URM) clearly performed better than the unretrofitted ones as shown in Photo 5.5. Only some retrofitted URM suffered minor damage as shown in Photo 5.6. On the other hand, retrofitted program has not yet been initiated for RC buildings, tilt-up buildings, steel constructions, and wooden buildings. They suffered damage as shown in Photos 5.7 and 5.8.

5.5 Post Earthquake Safety Evaluation of Buildings

The procedures taken for post earthquake safety evaluation of buildings seem considerably effective to prevent secondary disaster by the aftershocks. This activity exhibited a very good style of social contribution of the engineers including the volunteers. Also these results were effectively provided to other organizations such as FEMA and OES, and used to support the application and repair/ reinforcement consultation of damaged buildings at DAC and ESC. The most important point evaluated was to collect information for safety evaluation of buildings and to release the data to appropriate organizations.

6. DAMAGE OF RAILWAY AND PORT

6.1 Railway

Twenty nine trains of a 64 car freight train traveling through Northridge district derailed by the earthquake. Twenty tank cars carrying sulfuric acid derailed, and 2,000 gallons of acid spilled from one of these cars. There was no other damage caused by this spilled acid.

As there was no damage of derailing of traveling train due to an earthquake in Japan, this damage is very impressive and interesting for Japanese railway engineers.

6.2 Port and Harbor

Some damage occurred at the Port of Los Angeles. A piled pier as shown in Fig. 7.1 at the American President Lines container terminal was damaged. Several cracks formed in asphalt pavement in the backland area which was placed hydraulically from dredged materials. Sand boils were present in this backland area. The concrete deck of piled pier moved approximately 4 inches away from the backland. Photo 7.1 shows crack of the rock dike. Cracks also formed on the top of the several prestressed concrete piles.

There was no damage at the Port of Long Beach adjacent to the Port of Los Angeles.

Over a distance of about 300 feet of the north pier at the King Harbor, substantial subsidence occurred to a maximum of about 0.6 m to 0.9 mt, and the concrete bulkhead located on the right side at the north pier moved away from the backland shown in Photo 7.2. The maximum lateral offset in the bulkhead is estimated to be about 3 m. There was no damage at the concrete bulkhead on the left side of the north pier. This damage of large displacement was due to the liquefaction of the reclaimed land.

7. DAMAGE OF LIFELINE FACILITIES

At the Aqueducts Water Plant of the Department of Water and Power, City of Los Angeles, six water pipes suffered damage as shown in Photos 7.1, 7.2 and 7.3. This resulted the suspension of operation for 24 hours. However, because there is enough storage of 10 times daily consumption, serious problem for distribution was not developed. Pipes broke at about 1,200 locations, and it required about 7 days for repair.

Several cracks with 5 cm wide were developed at the crest of Lower San Fernando Dam as shown in Photo 7.4. Because many sand boils as large as 10 m were observed at the floor of the reservoir at upstream side. It seems that the damage was developed due to soil liquefaction. The dam is empty and is served as a flood control basin.

At Joseph Jensen Filtration Plant,

Southern California Water District, one of the two water intake pipes ruptured as shown in Photo 7.5. It took about 60 hours to repair the pipe, and the operation was suspended during the repair.

Electricity in Los Angeles is supplied by the Los Angeles Water and Power and Southern California Edison. Electric facilities suffered damage at conversion stations, power stations, and towers supporting high-voltage transmitting lines. Electricity was suspended to all customers supplied by LADWP (1.4 million homes) and 0.63 million customers supplied by Edison by the seismic damage. Many equipments have been replaced with the the ones with high seismic performance after the San Fernando Earthquake. They performed quite well.

The gas pipes of Southern California Gas Company suffered damage at 37 main transmitting lines, 118 main lines and 79 service lines. Among damage of 37 main transmitting lines, 27 were damaged at oxy-acetylene girth weld. They were constructed before 1932.

At Balboa Street of Granada Hill, a service pipe with 6 inch diameter and a main pipe with 22 inch diameter were ruptured as shown in Photos 7.6 and 7.7, and was ignited the fire. Five single family houses along the street were burned down. A main transmitting line with 30 inch diameter embedded at the same location did not suffer damage. Large lateral movement of pavement and surface soils as large as 30 cm was developed in road axis as shown in Photo 7.8.

A rupture of petroleum pipe was developed at Wolfskill Street, San Fernando. The oil was ignited, and caused a fire at houses along the street.

Further fires due to breaks of gas pipes were developed at several mobile homes (refer to Chapter 8).

The telecommunication systems suffered damage due to structural and nonstructural damage of buildings, rupture of optical fiber associated with a fire and damage of telephone exchanger. Emergency electricity back-up system did not work at some stations. Concentration of telephone traffic caused suspension of traffic. The traffic increased 60 % at AT&T on January 17.

Wasted water treatment facilities suffered damage at pipes. Small TV cameras were effectively used to identify the damage. The damage information of buildings was effectively used to identify the areas where possible damage was developed.

8. STRUCTURAL DAMAGE BY FIRES

8.1 Introduction

Major cities in Japan are quite vulnerable to urban fires because of a great number of combustible buildings. It is anticipated that numerous fires would break out in such big cities, if a large earthquake with magnitude 8 such as the anticipated Great Kanto Earthquake occurs. Fires would spread uncontrollably over a wide area. They would grow into large scale fires called as "Post Earthquake City Fire" in the areas where wooden houses located densely. Over 140,000 people were killed in the 1923 Great Kanto Earthquake because they lost their way to evacuate by fires. Therefore the investigation was conducted with a great interest for the structure fires by the Northridge earthquake.

8.2 Structure Fire Incidents

Many fires broke out after the earthquake and some of them grew into large scale fire in mobile home parks.

The Los Angeles City Fire Department (LAFD) was alerted many times including requests for rescue because of the telephone congestion. The LAFD made quick response according to "Earthquake Emergency Operational Plan".

In mobile home parks, there were many fire breakouts. At Sylmar, LA City, 20 to 60 mobile homes were burnt down in the parks.

It was interesting that except such mobile home parks fires which broke out at built-up areas did not spread widely across streets and

that most of these fires were isolated.

By 9:45 of the day, all fires in LA City were controlled and there were no active major structure fires in progress.

8.3 Number of Breakouts, Scale of Fires and Cause

According to LAFD, there were about 100 structure fire incidents within 1 hour after the earthquake in LA City. Although number of breakouts of each incident has not yet identified at the present time, the fires during the earthquake may be recognized as "simultaneous fire breakouts after an earthquake." About 80% of these fires were in Division 3 which includes San Fernando Valley.

One of the significant incidents was the rupture of a large natural gas main and a water main at the intersection of Balboa and Rinaldi as shown in Photo 8.1. Subsequent to the rupture, the natural gas main ignited, and five single family homes were burnt down.

Also significant loss of property resulted from structure fires at three mobile home parks. According to LAFD, there were 9 fire incidents even in a mobile home park. The structural building codes are not applied to the mobile homes and mobile home parks. Therefore, the supports of mobile homes were weak, and many mobile homes felt down from their supports. Because the natural gas valves were plumped to mobile homes, the natural gas valves and pipes were ruptured as shown in Photos 8.2 and 8.3.

Mobile homes have also no restriction of fire regulation. Therefore the performance of fire prevention of mobile home are generally poor and they are vulnerable to fires as shown in Photos 8.4, 8.5 and 8.6. Distance between adjacent mobile homes are also relatively small as show in Photo 8.7. These made fire spread inside mobile home parks.

Most of fire breakouts following the earthquake were developed due to leak of natural gas. Pilot flame of water heaters ignited the natural gas. Another cause of the fire breakouts in the evening of the day and the next day was ignited by electric sparks after electric power supply was restored.

Fires in wooden buildings in built-up area didn't spread as is afraid in Japan because the distance between buildings is large. The performance of fire prevention of the wooden buildings is not the only one reason for having prevented the fire spread.

9. CONCLUDING REMARKS

The followings are the major findings of the Japanese Governments Study Team for the Northridge Earthquake.

(1) Many strong motion records with high peak accelerations were obtained. It is required to investigate how structures behaved during the earthquake based on the measured accelerations. It is particularly interesting to study why damage was not developed in many structures even though they were subjected to such strong ground shaking.

(2) It was fortunate that the earthquake occurred very early in the morning. If the earthquake had occurred in the daytime, much larger loss of human beings might be developed. This is particular true for the damage of transportation and building facilities and for the effects of structure fires.

(3) The bridges which were designed in accordance with the pre-1971 seismic design practice suffered major damage including collapse. Small lateral force considered and small concrete section with insufficient lateral bars caused extensive shear failure. Small seat length at hinge joints also contributed to the collapse. The bridges which were strengthened by cable restrainers and steel jacketing performed quite well.

(4) The pilotis type wooden houses suffered extensive damage. It should be noted that this structural type was adopted to provide a parking space at the first floor. A precast concrete parking garage collapsed due to insufficient connection of beams and columns.

Most of retrofitted unreinforced masonry buildings performed well. Reinforced concrete buildings, tilt-up buildings and steel constructions which have not yet retrofitted suffered damage.

(5) Many pipes suffered damage, and caused extensive leakage of gas, water and oils. Gas and petroleum were ignited fires and burned down houses along roads.

(6) A railway which was travelling at the earthquake overturned. Because there was no such damage in Japan, it is impressive and important to learn why the overturning was developed.

(7) Many fires simultaneously broke out immediately after the earthquake. But they were controlled in a few hours. No extensive spreading of fires extending streets occurred. The long distance between houses contributed to avoid the spreading. There was no automatic/manual system to cut off the gas flow when the gas leaked immediately after the earthquake.

(8) Response and countermeasures after the earthquake were prompt and appropriate. Every effort was made to minimize and mitigate the loss and effect of damage.

ACKNOWLEDGEMENTS

Valuable supports were provided from both Japan and U.S. governments to the Japanese Government Study Team for the Northridge Earthquake. Special thanks are directed to the Ministry of Foreign Affairs, Consulate-General of Japan in Los Angeles and San Francisco, National Land Agency and Ministry of Construction.

Sincere appreciation is also directed to U.S. Federal government organizations, county and city governments, private companies and individuals concerned. The valuable support through the Panel on Wind and Seismic Effects, UJNR for arranging the visits to various organizations and sites is highly acknowledged and appreciated. Sincere appreciation is directed to Dr. R. N. Wright (U.S. Chairman of the Panel, and Director, Building and Fire Research Laboratory, National Institute of Standards and Technology), Mr. Noel J. Raufaste (Secretary General of the Panel, NIST), Dr. H. S. Lew (member of UJNR Panel, NIST), Mr. James D. Cooper (member of UJNR Panel, Federal Highway Administration), Dr. S. C. Liu (member of UJNR Panel, National Science Foundation), Mr. James H. Gates (member of UJNR Panel, California Department of Transportation), and Mr. LeVal Lund.

REFERENCES

1) Japanese Government Study Team for the Northridge Earthquake : Report on the Damage by the Northridge Earthquake, National Land Agency, in preparation (in Japanese)
2) Kawashima, K., Unjoh, S., Sugita, H., Hoshikuma, J., Iwasaki, T., and Yoshida, Y. : Reconnaissance Report on the Damage by Northridge, California, U.S.A., Earthquake of January 1994, PWRI Technical Note, No. 3272, Public Works Research Institute, February 1994 (in Japanese)
3) CSMIP Strong Motion Records from the Northridge, California Earthquake of January 17, 1994, California Earthquake, Department of Conservation, Division of Mines and Geology, Office of Strong Motion Studies, Report OSMS 94-07, February 1994
4) Processed Strong Motion Records from the Northridge, California Earthquake of January 17, 1994, California Earthquake; Release No. 1 and No. 2, Department of Conservation, Division of Mines and Geology, Office of Strong Motion Studies, Report OSMS 94-06B and 94-08, February 1994
5) Cooper, J. D. and Friedland, I. : 1994 Northridge California Earthquake of January 17, 1994, FHWA News, 1994

6) California Department of Transportation: Post Earthquake Investigation Team Report on the Northridge Earthquake, 1994
7) Preliminary Report on the Seismological and Engineering Aspects of the Northridge Earthquake, EERC, University of California, Berkeley, Report No. UCB/EERC-94/01, January 1994
8) Seismological and Engineering Aspects of the January 17, 1994 Northridge Earthquake, Earthquake Engineering Research Center, University of California, Berkeley, 1994
9) Priestley, M. J., Seible, F. and Uang, C. M. : The Northridge Earthquake of January 17, 1994, Damaged Analysis of Selected Freeway Bridges, Report N. SSRP-94/06, University of California, San Diego, February 1994
10) Kawashima, K. : Seismic Retrofit of Existing Road Bridges in the State of California - Two Years Later after the Loma Prieta Earthquake, Bridges and Foundations, 92-5, May 1992 (in Japanese)
11) EQE: The Northridge, California, Earthquake of January 17, 1994
12) Fumai, T. E., Gibbs, J. F. and Roth, E. F.: In-situ Measurements of Seismic Velocity at 19 Locations in the Los Angeles, California Region, USGS, Open-File Report 81-399, 1981
13) Earthquake Engineering Research Institute: Northridge Earthquake of January 17, 1994, March 1994
14) Persson, V. H. : Assessment of Damage to State Jurisdictional Dams Caused by the Northridge Earthquake on January 17, 1994, Seismic Safety Commission Meeting, Burbank Airport Hilton, March 1994
15) Status Report on Collection System Damage Assessment to Northridge Earthquake, Collection System Engineering Division, Bureau of Engineering, Department of Public Works, City of Los Angeles, March 1994

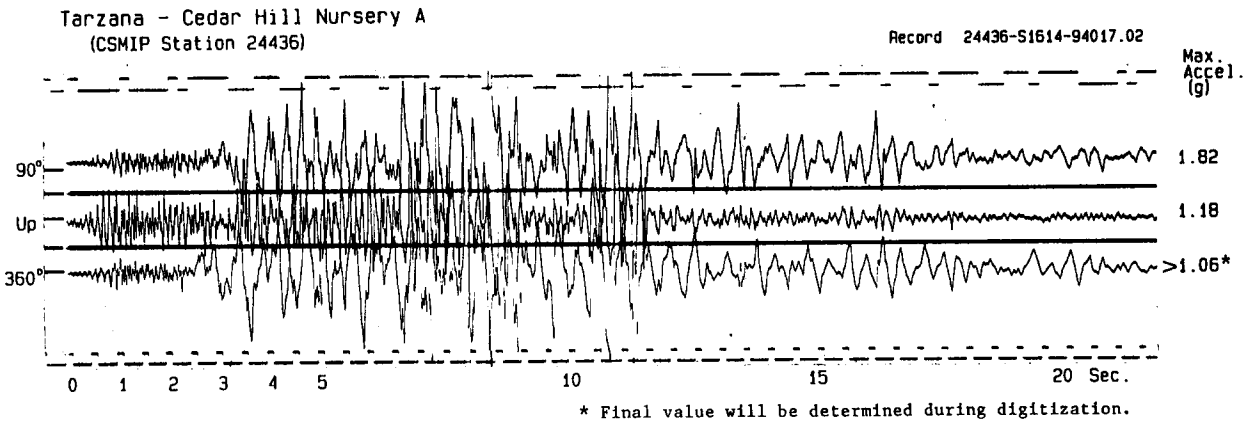

Fig. 3.1 Acceleration Record at Tarzana – Cedar Fill Nursery (from CDMG)

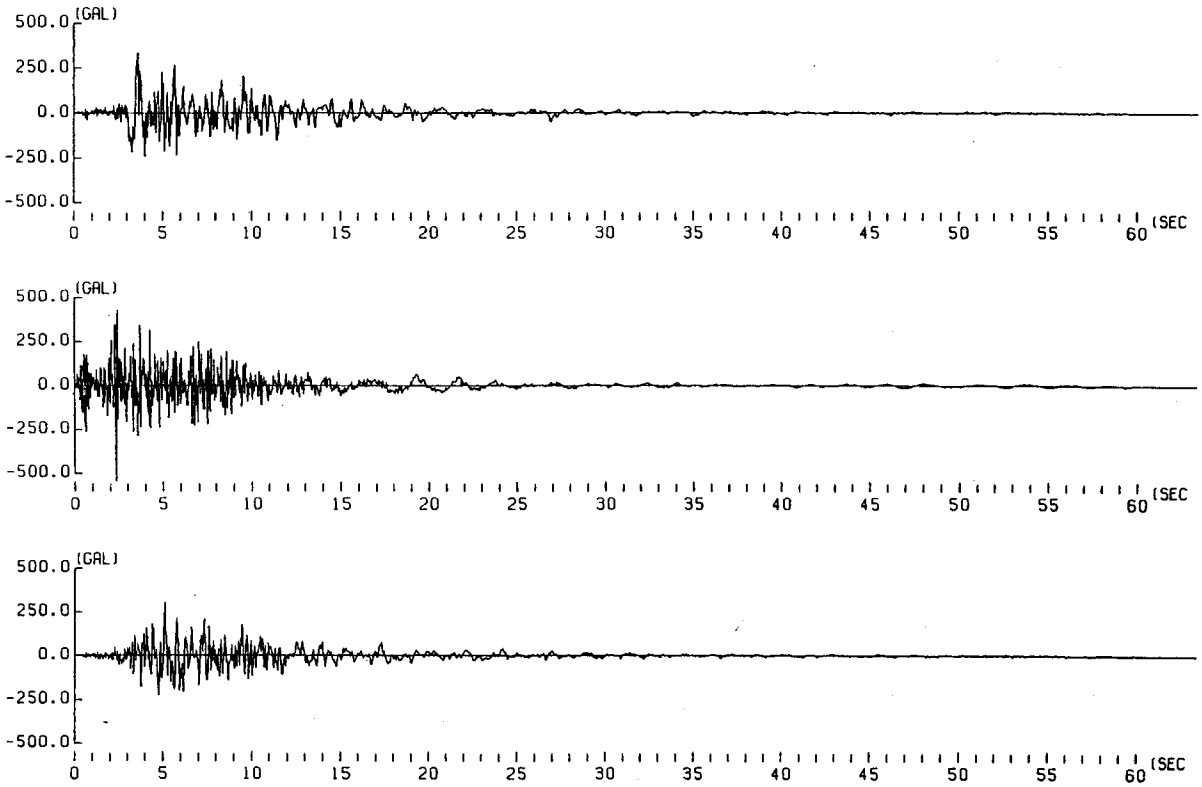

Fig. 3.2 Acceleration Record at Arleta – Nordhoff Avenue Fire Station (from CDMG)

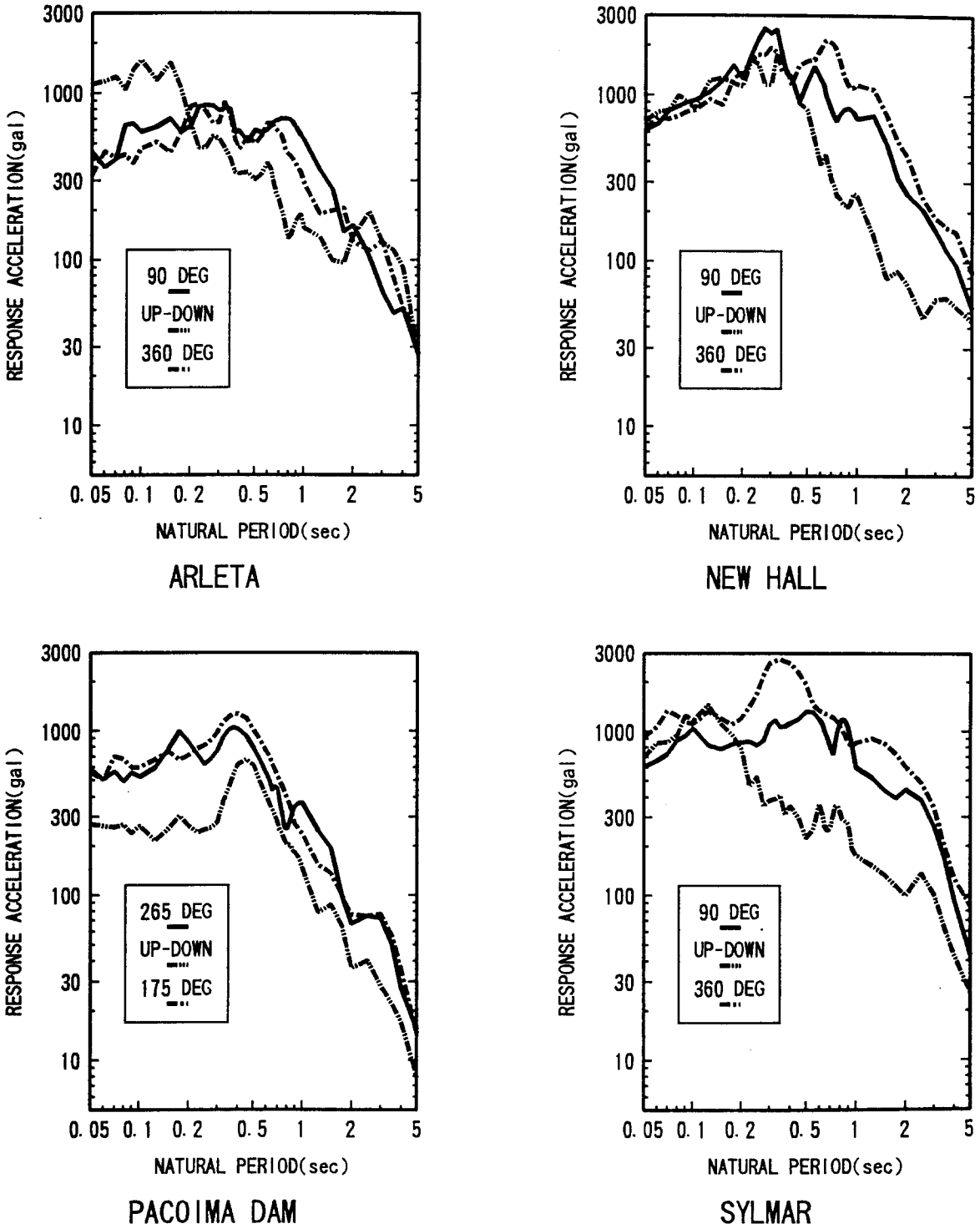

Fig. 3.3 Response Acceleration Spectra with 5% Damping Ratio

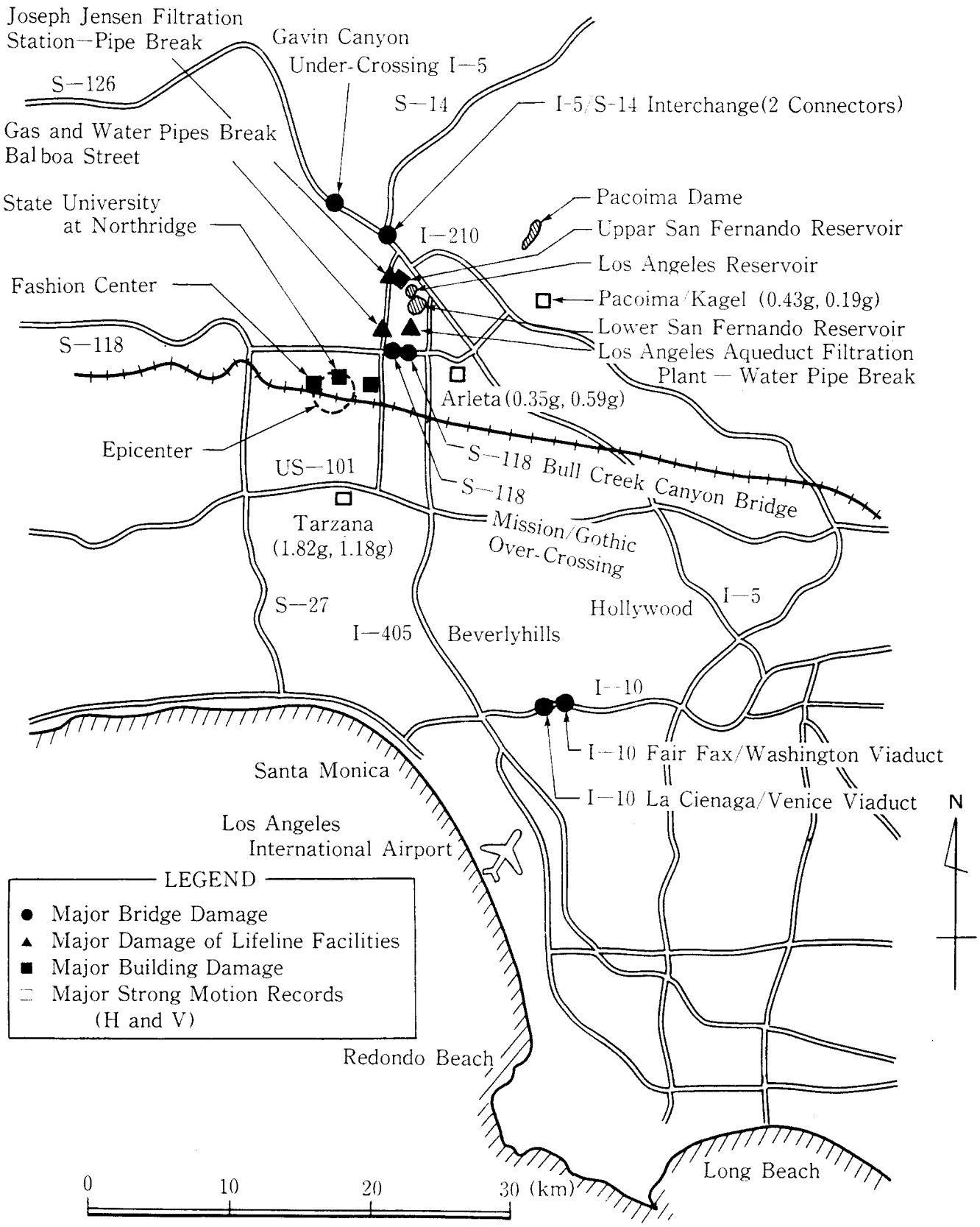

Fig. 4.1 Locations of Major Road Damage

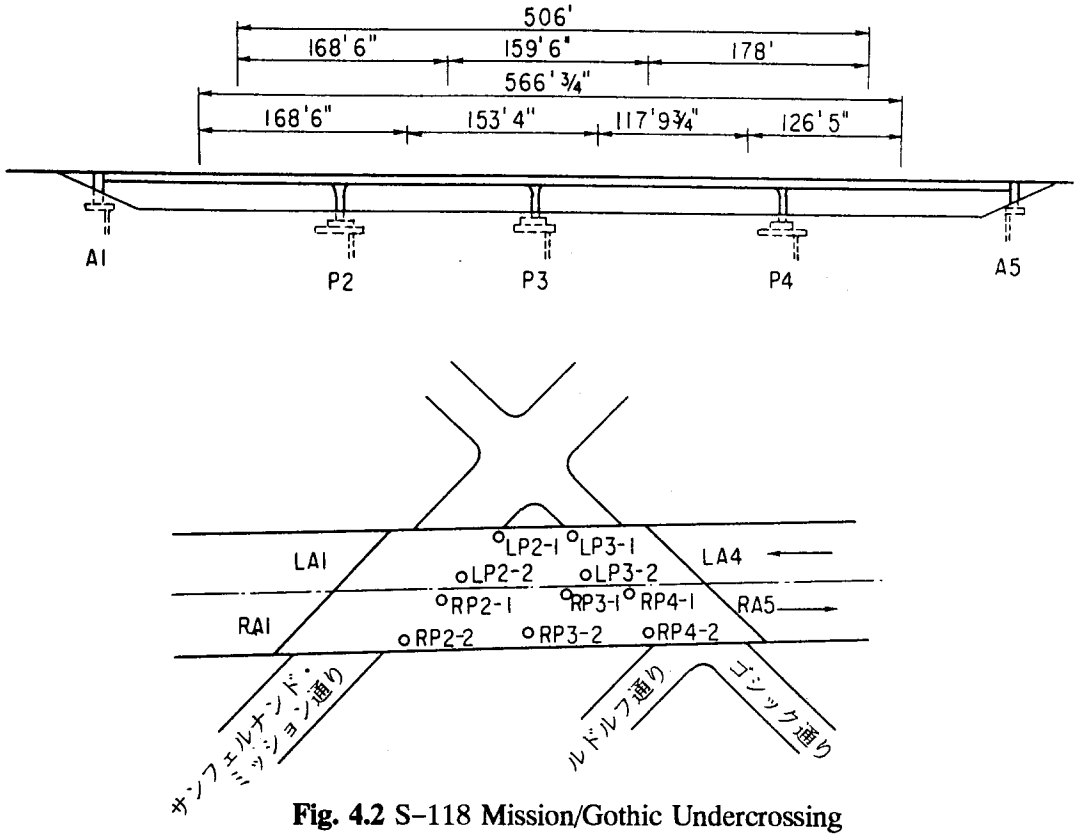

Fig. 4.2 S–118 Mission/Gothic Undercrossing

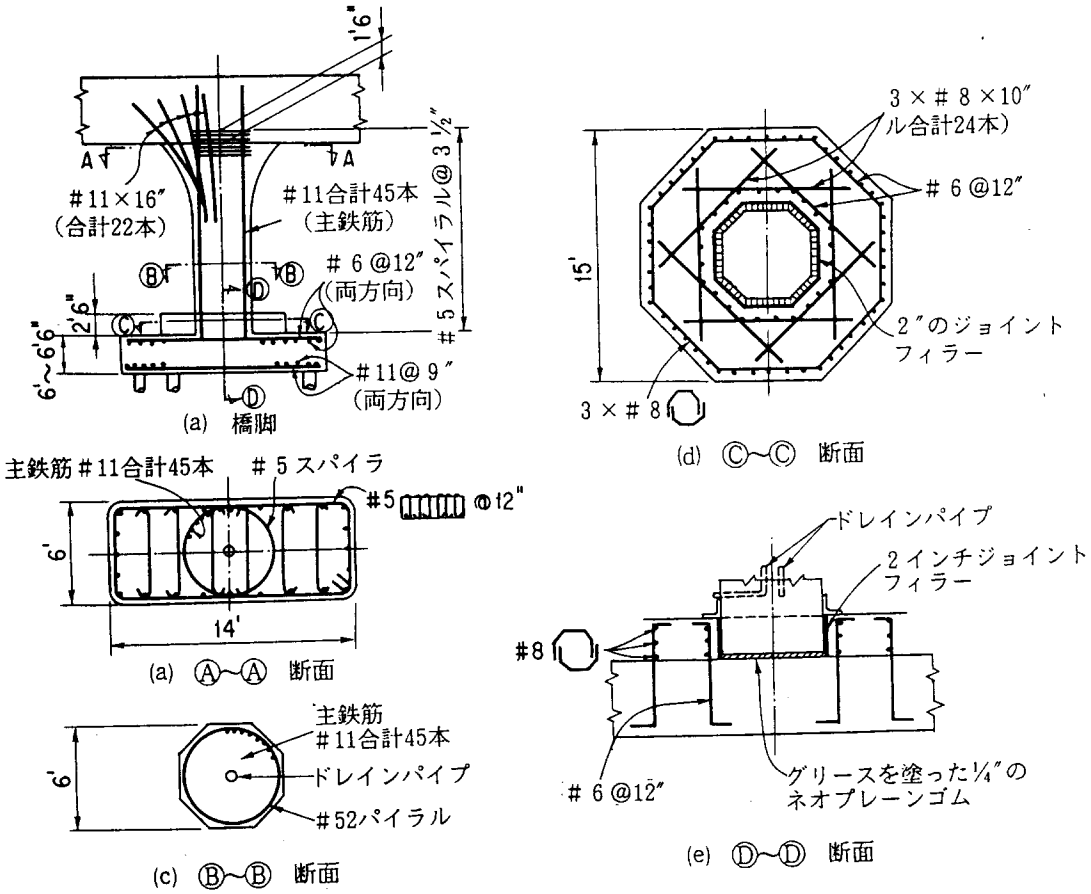

Photo 4.3 Initiation of Shear Failure (S–118 Mission/Gothic Undercrossing)

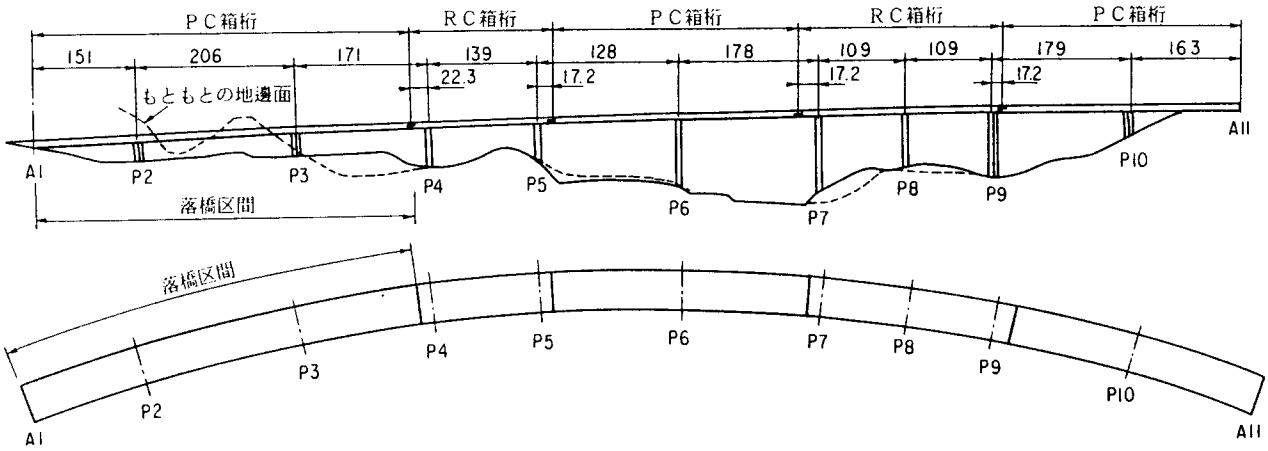

Fig. 4.4 Collapse of S-14/I-5 Separation and Overhead

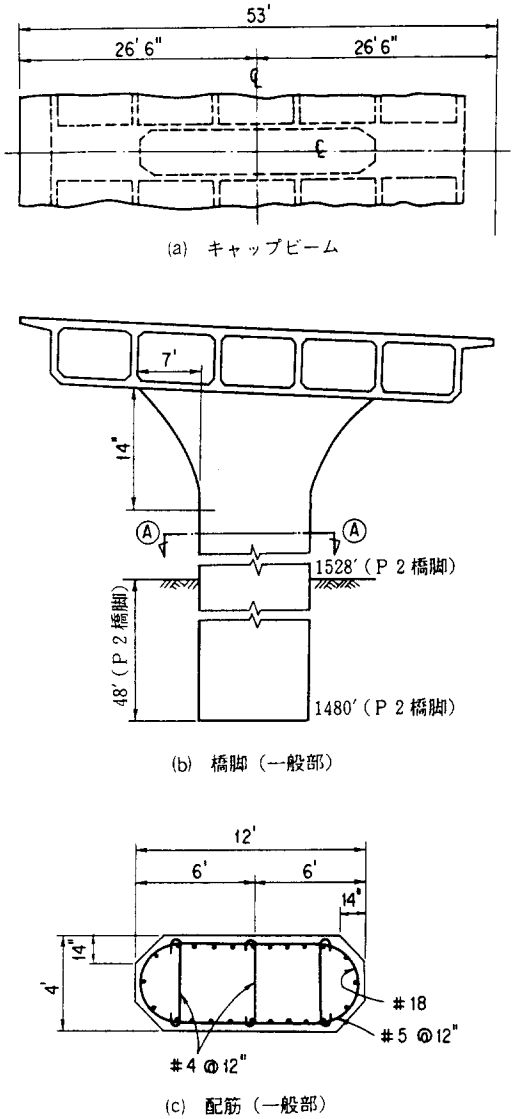

Fig. 4.5 Typical Section of Piers Supporting the Collapsed Part of S-14/I-5 Separation and Overhead

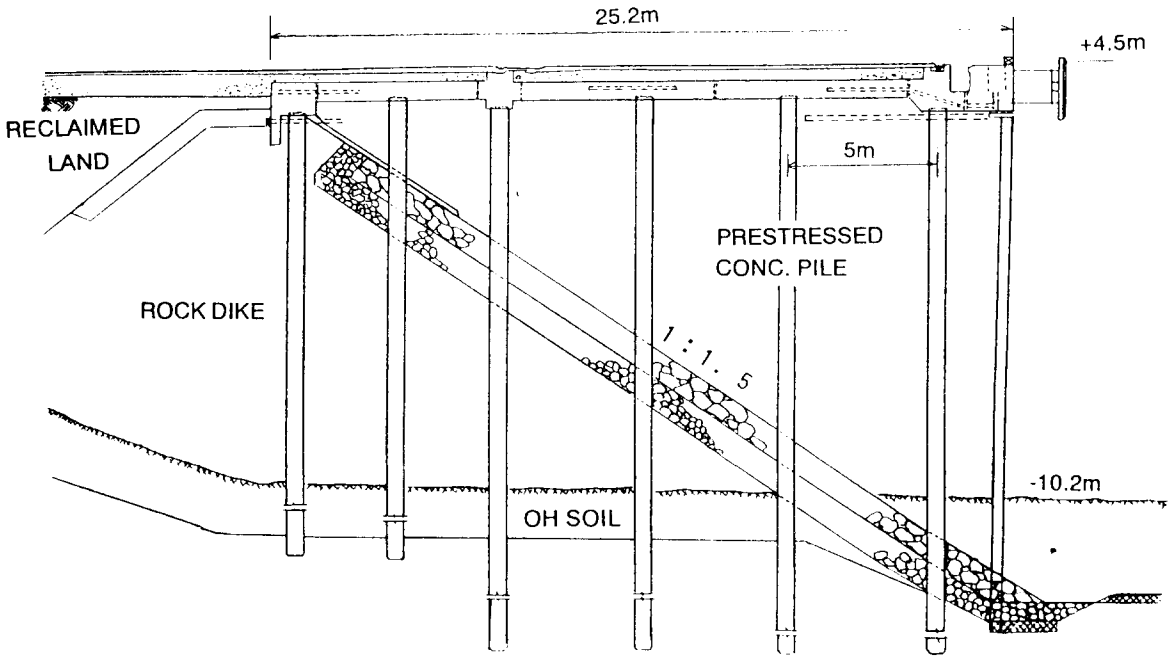

Fig. 6.1 Piled Pier at APL Terminal

Cedar Fill Nursery

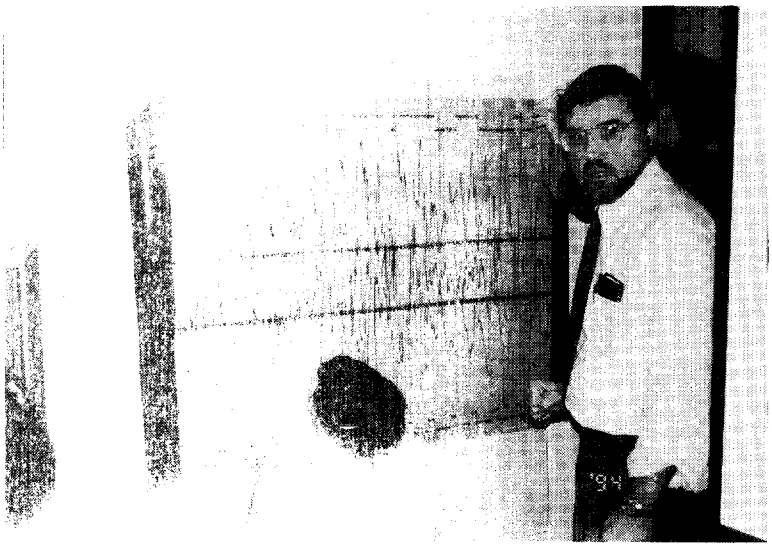

Cedar Fill Nursery

Avenue Fire Station

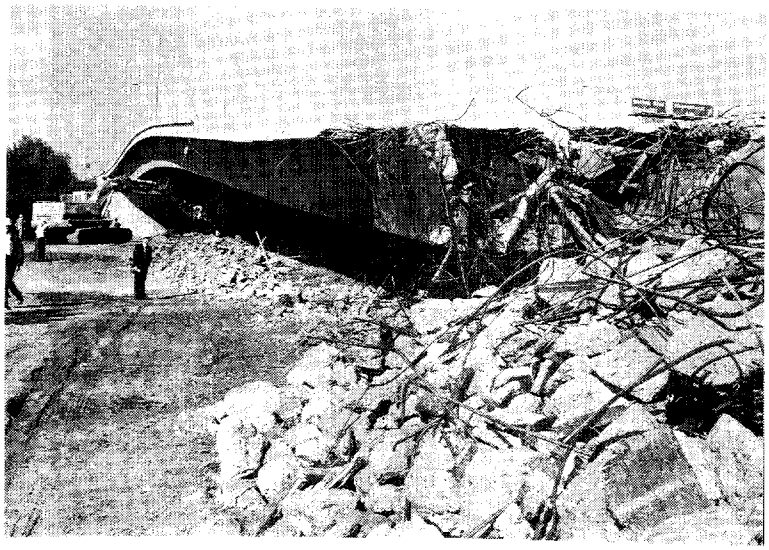

Photo 4.1 Collapse of S–118 Mission/Gothic Undercrossing

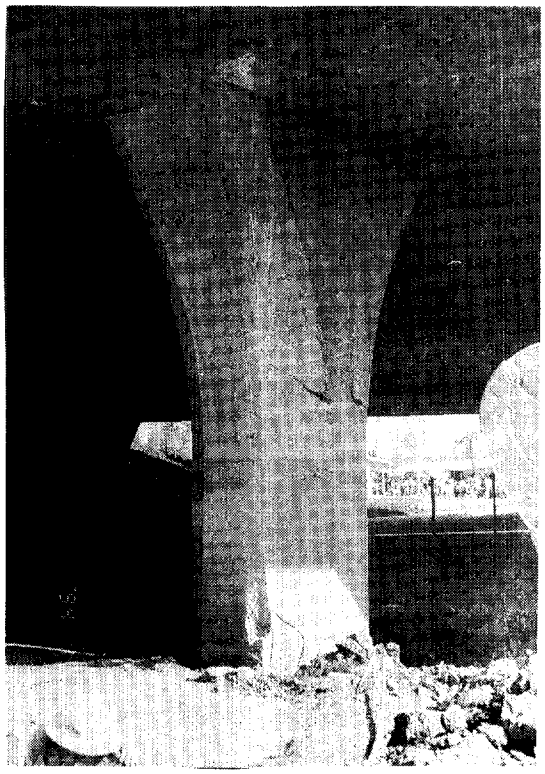

Photo 4.2 Initiation of Flexural Cracks
(S–118 Mission/Gothic Undercrossing)

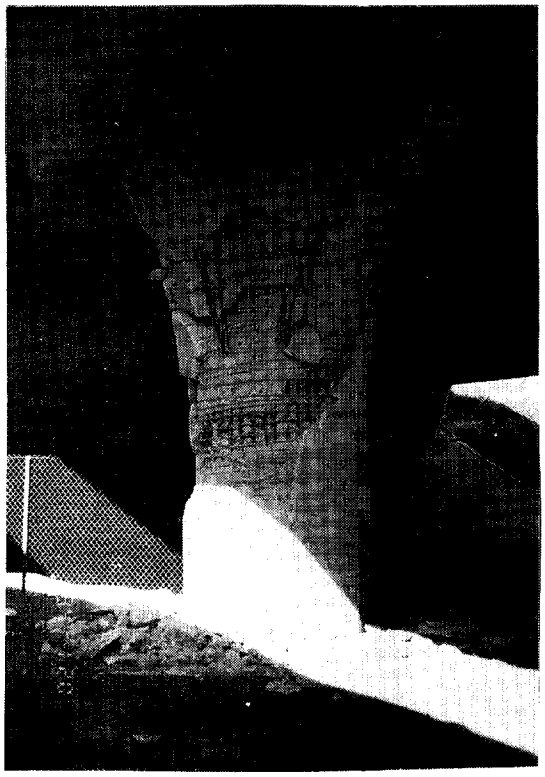

Photo 4.3 Initiation of Shear Failure
(S–118 Mission/Gothic Undercrossing)

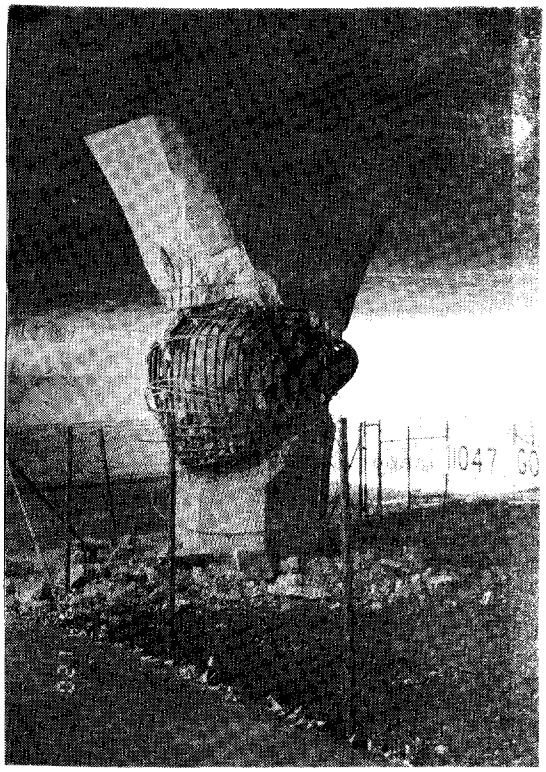

Photo 4.4 Shear Failure and Extensive Outward Deformation of Main Reinforcements (S-118 Mission/Gothic Undercrossing)

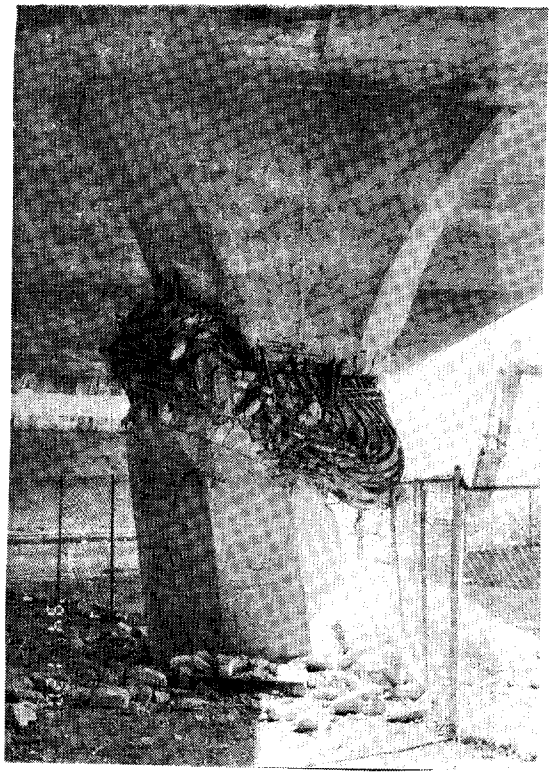

Photo 4.5 Dislodgement of Column Axis due to Shear Failure (S-118 Mission/Gothic Undercrossing)

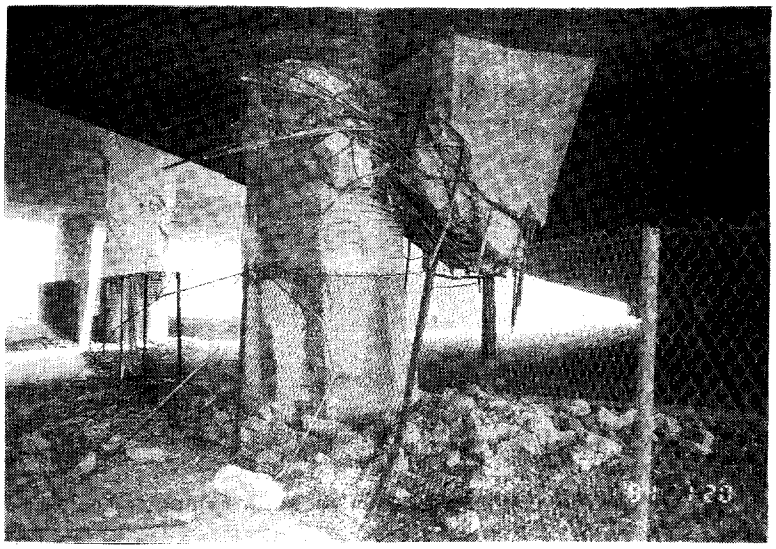

Photo 4.6 Complete Failure (S-118 Mission/Gothic Undercrossing)

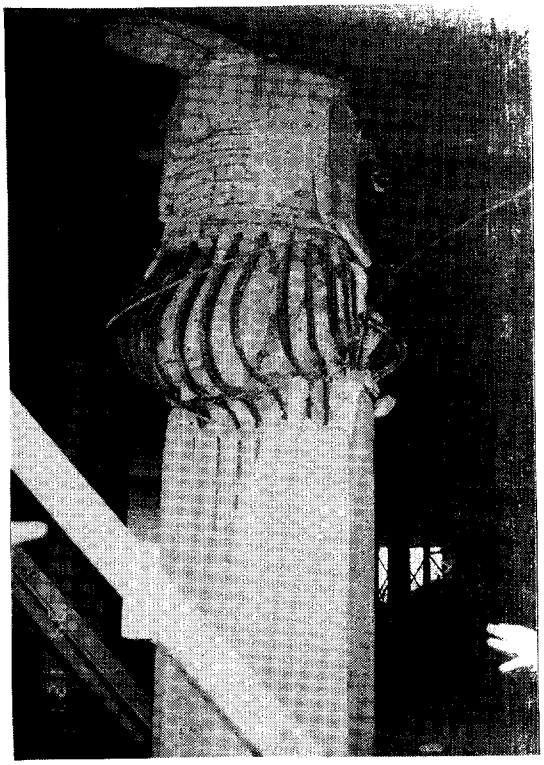

Photo 4.7 Damage of Columns of Bull Creek Channel Bridge

Photo 4.8 [illegible] La Cienega/[illegible]

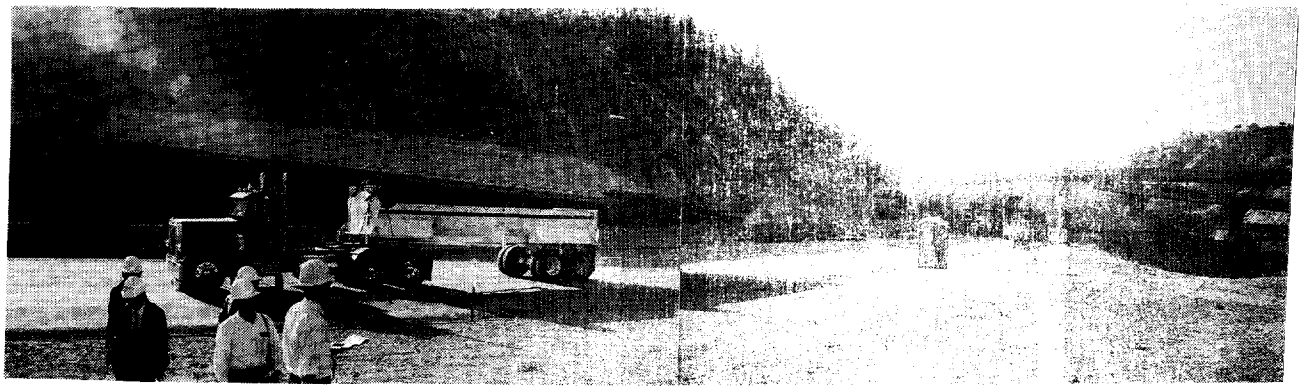

Photo 4.9 Collapse of I5/SR14 South [illegible]

Photo 4.10 Damage of P3 (Courtesy of EERC)

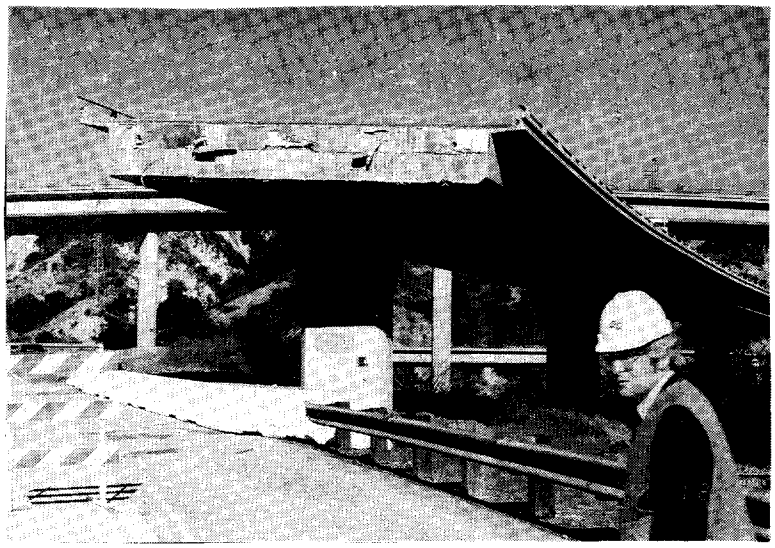

Photo 4.11 Failure of Cable restrainers at a Joint near P4

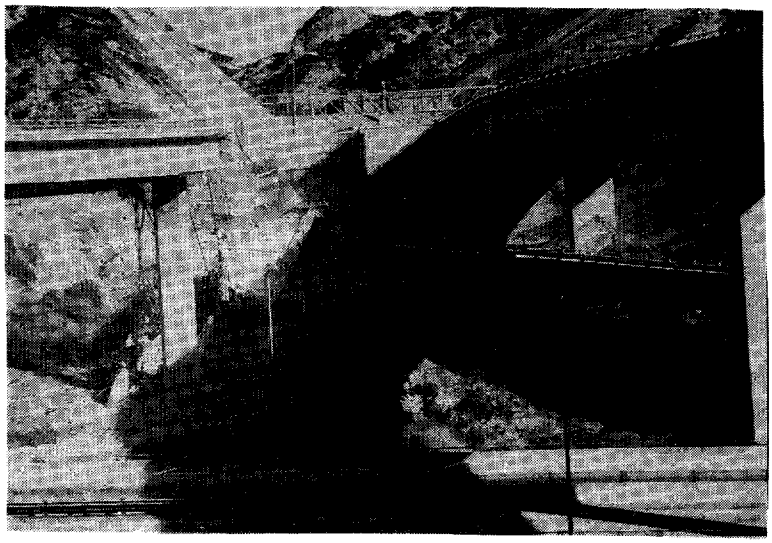

Photo 4.12 Collapse of North Connector Overcrossing
(Courtesy of Patrick K. Hipley, Caltrans)

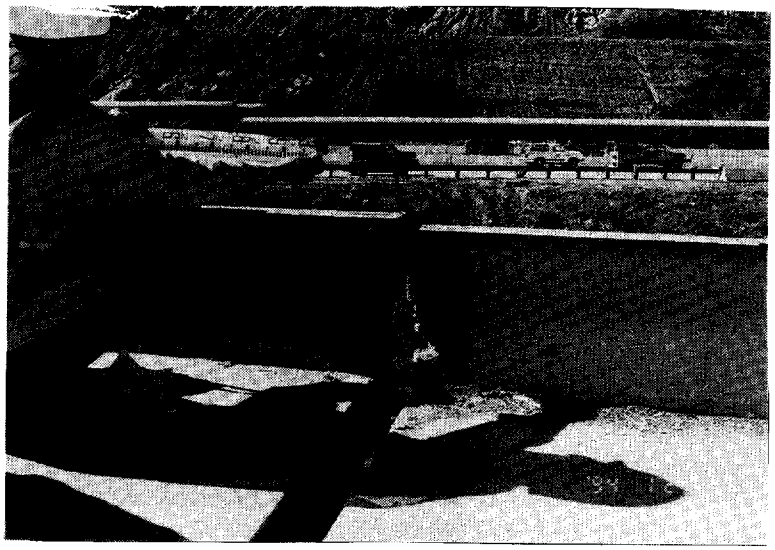

Photo 4.13 Large Separation Developed at Hinge

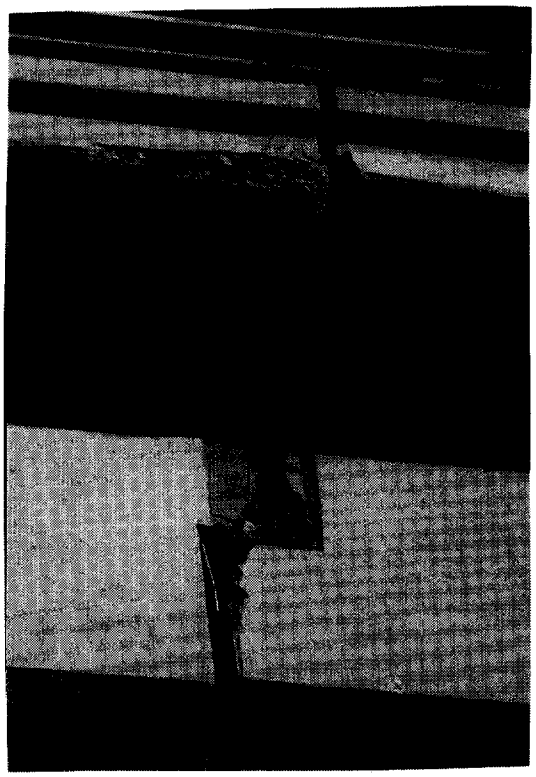

Photo 4.14 Large Separation and Damage of Hinge Seat (Courtesy of Patrick K. Hipley, Caltrans)

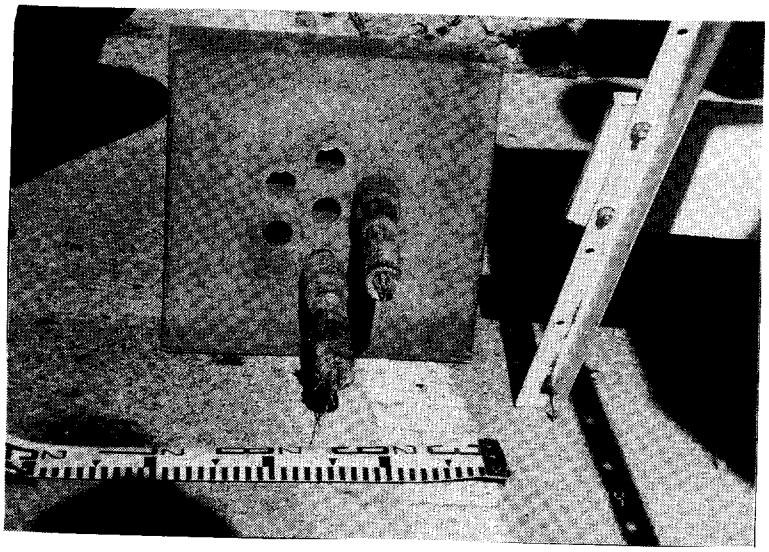

Photo 4.15 Rupture of Cable restrainers

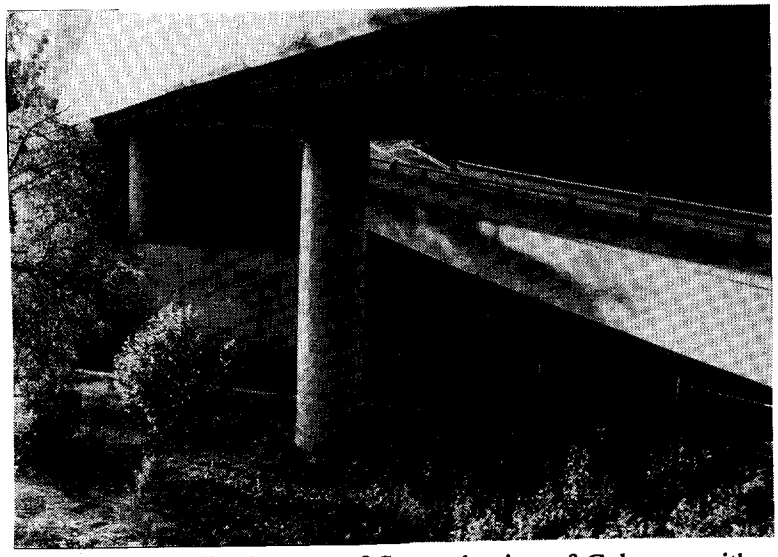

Photo 4.16 Effectiveness of Strengthening of Columns with Steel Jacketing

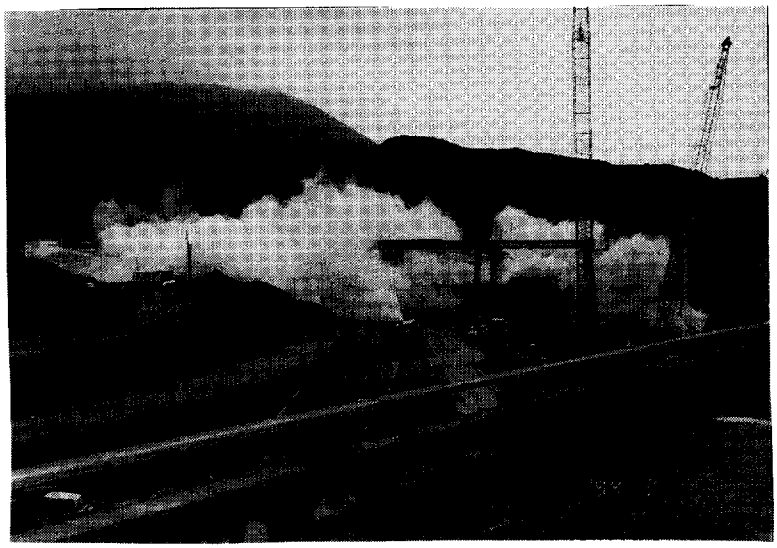

Photo 4.17 Demolish of Damaged I-5/S-14 INterchange by Explosion

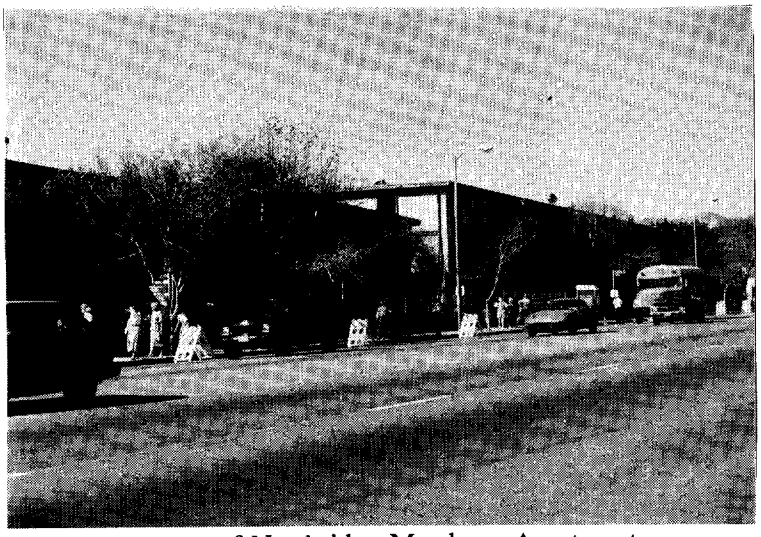

Photo 5.1 Damage of Northridge Meadows Apartment
(First floor of the left side building collapsed completely)

Photo 5.2 Damage of Northridge Meadows Apartment (First floor of the right side building was reinforced using wooden columns. Original posts were slender steel pipes)

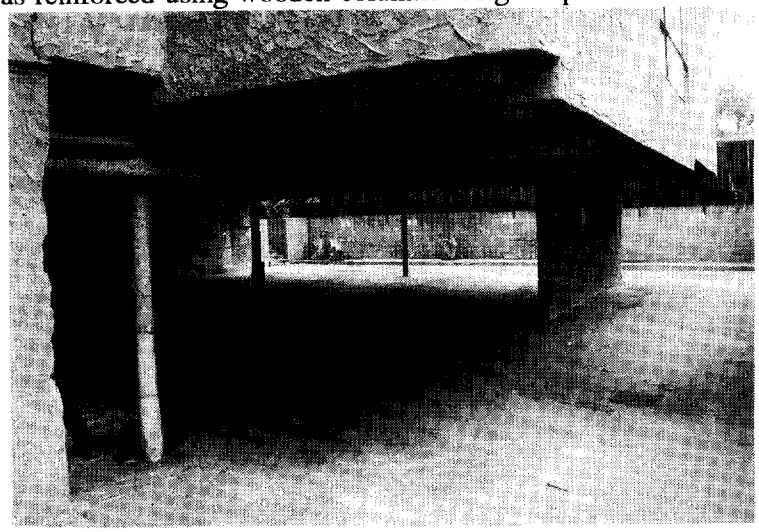

Photo 5.3 Basement Floor of an Apartment in Hollywood (To provide require parking spaces required, number of columns and walls at the basement floor is small)

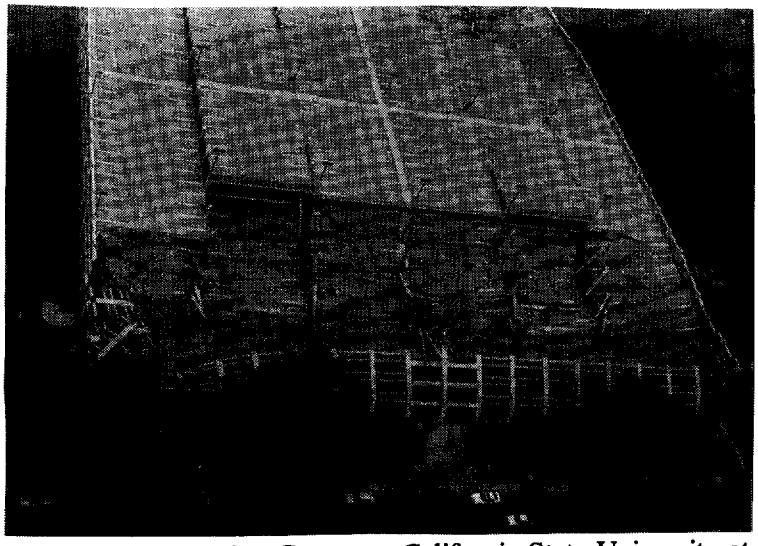

Photo 5.4 Damage of Parking Garage at California State University at Northridge

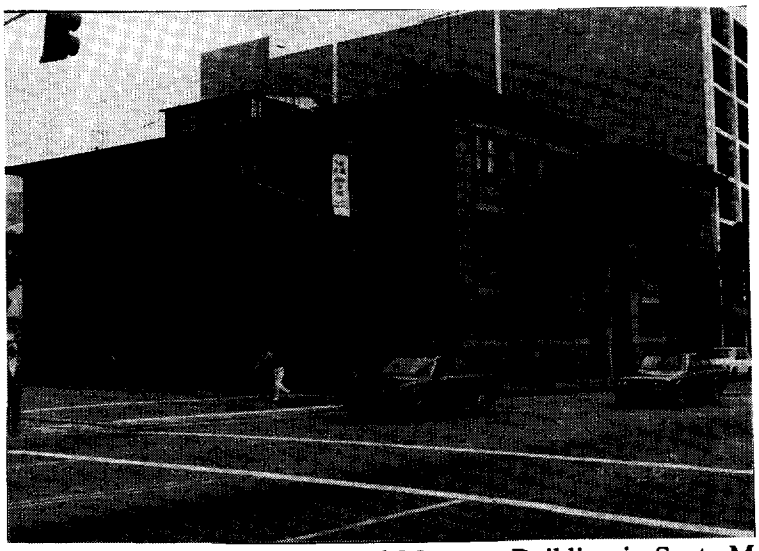

Photo 5.5 A Retrofitted Unreinforced Masonry Building in Santa Monica
(This building suffered no damage)

Photo 5.6 Wall Failure of Retrofitted Unreinforced Masonry Building in Adams.

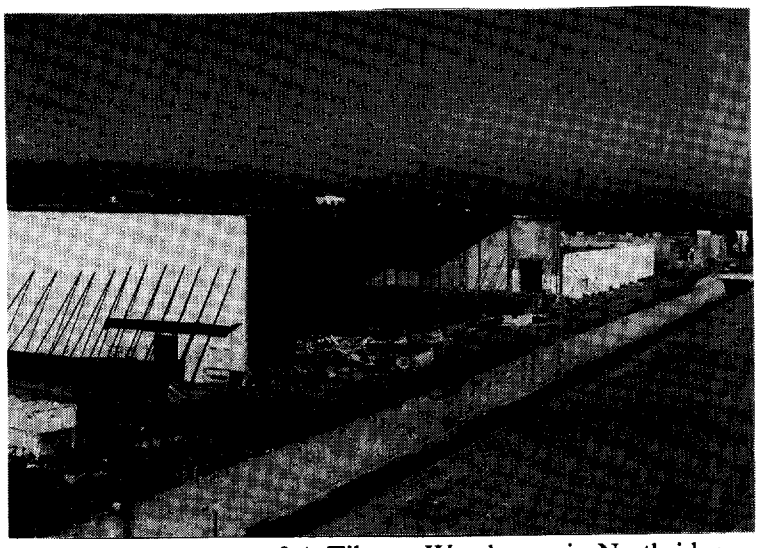

Photo 5.7 Damage of A Tilt-up Wearhouse in Northridge

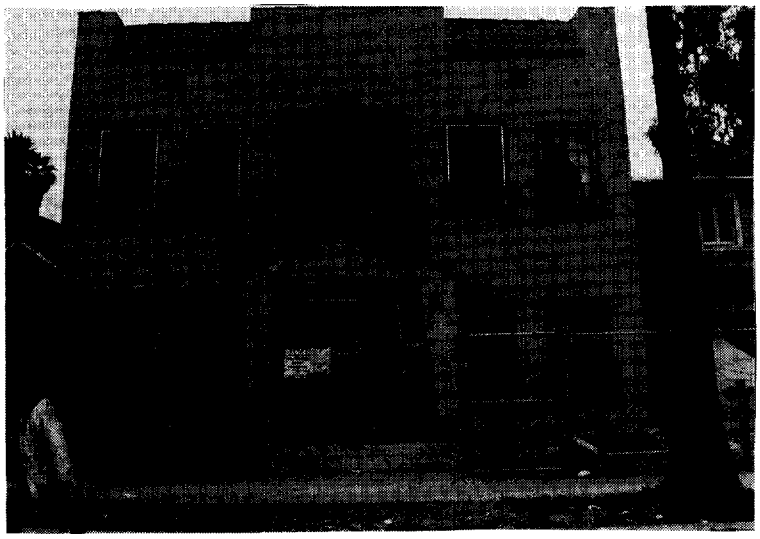

Photo 5.8 Damage of an Old Apartment in Hollywood

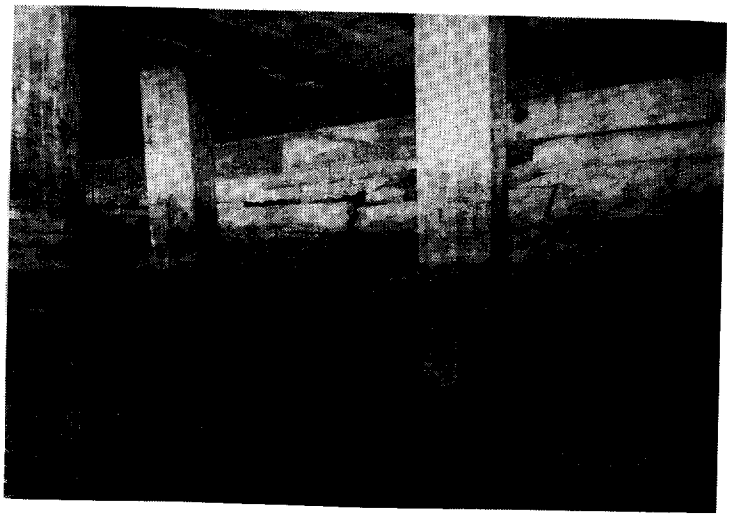

Photo 6.1 Cracks of Rock Dike

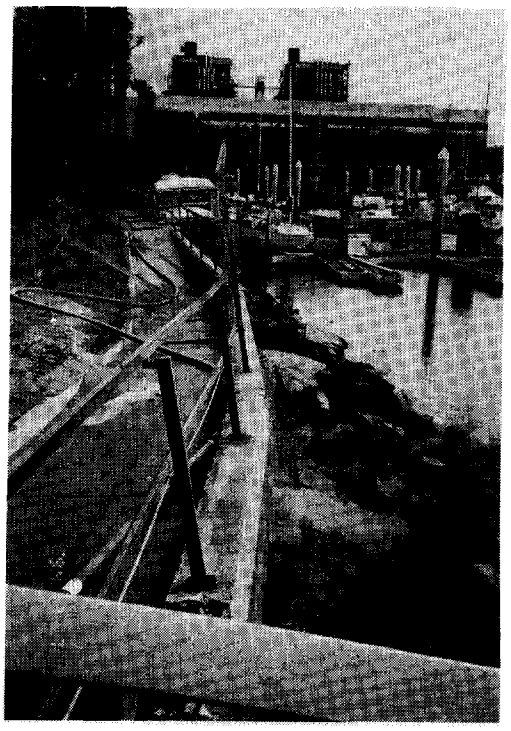

Photo 6.2 Displaced Bulkhead

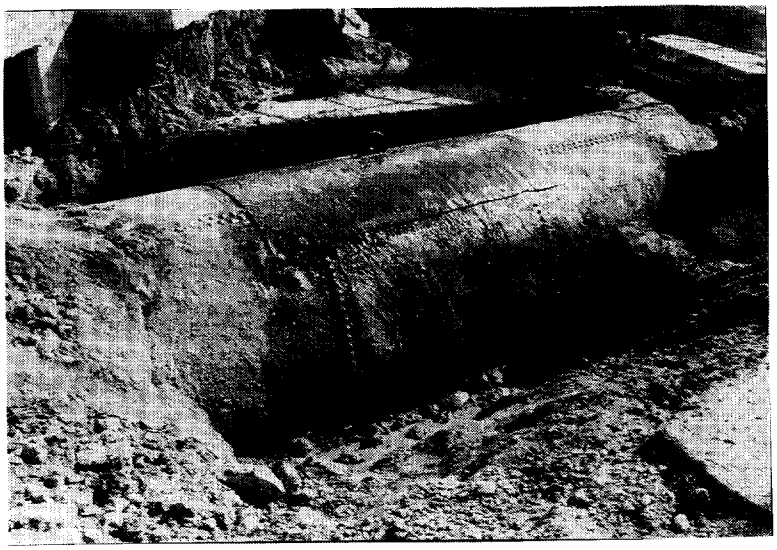

Photo 7.1 Rupture of a Main Water Pipe (Aqueducts Plant, DWP, City of Los Angeles)

Photo 7.2 Damage of a Expansion Joint Water of a Pipe near a Tank on a Hill (Aqueducts Plant, DWP, City of Los Angeles)

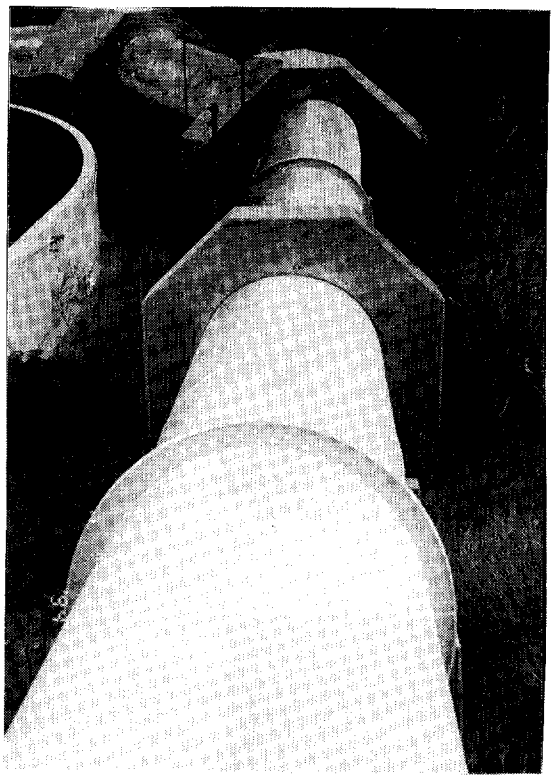

Photo 7.3 Local Buckling of a Water Pipe on Downslope of a Hill (Aqueducts Plant, DWP, City of Los Angeles)

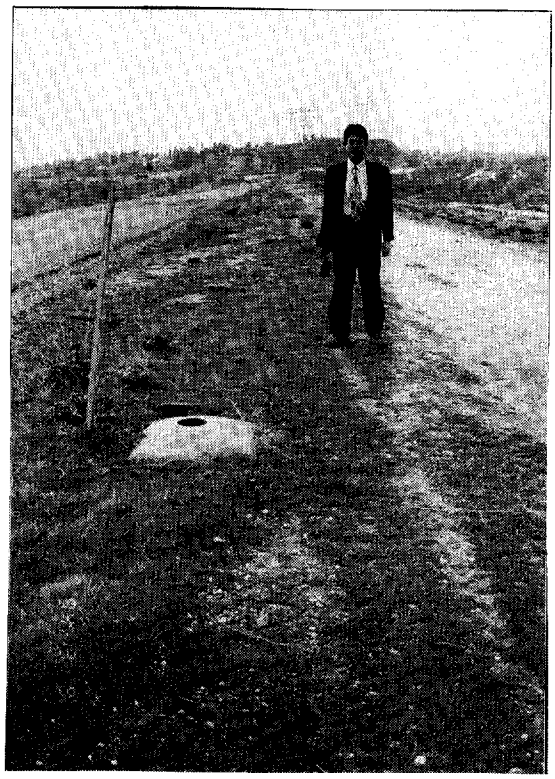

Photo 7.4 Cracks on Crest of Lower San Fernando Dam (Aqueducts Plant, DWP, City of Los Angeles)

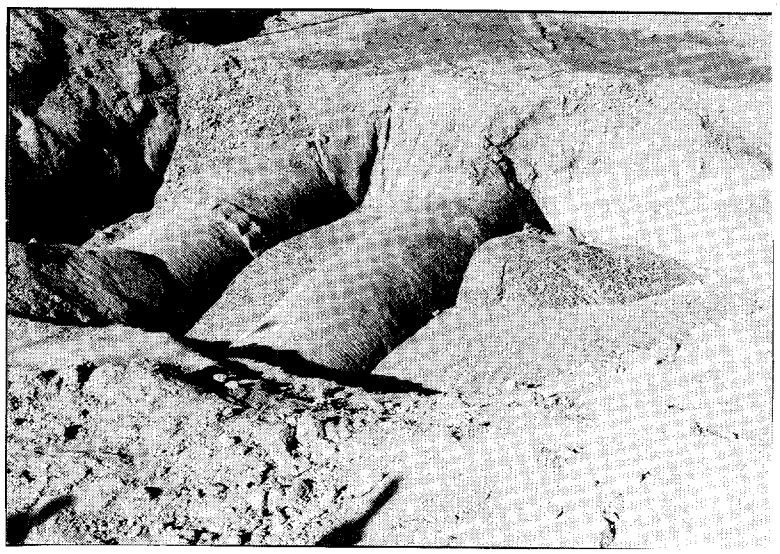

Photo 7.5 Rupture of a Water Pipes (Joseph Jensen Filtration Plant, Southern California Water District)

Photo 7.6 Rupture of Gas and Water Pipes due to Tension
(Balboa Street, Granada Hill)

Photo 7.7 Rupture of Gas and Water Pipes due to Compression
(Balboa Street, Granada Hill)

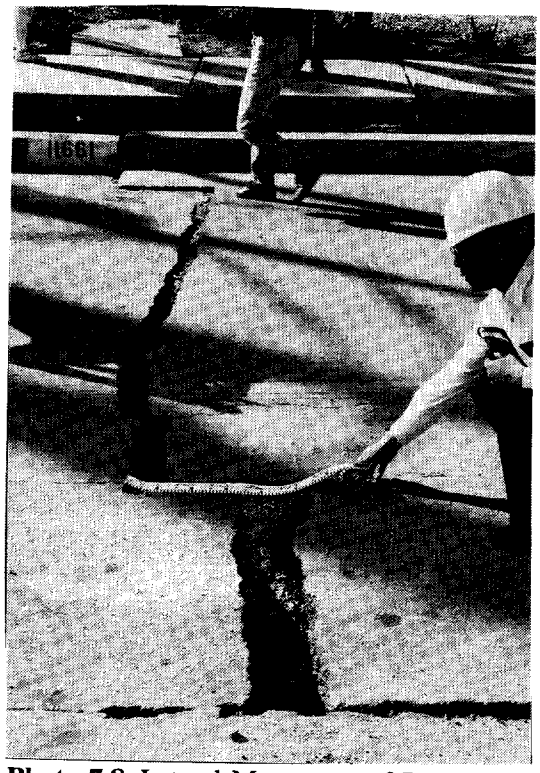

Photo 7.8 Lateral Movement of Pavement and Surface Soils as Large as 30 cm (Balboa Street, Granada Hill)

Photo 8.1 Damage of Five Single Family Homes due to Fire at Intersection of Balboa and Rinaldi

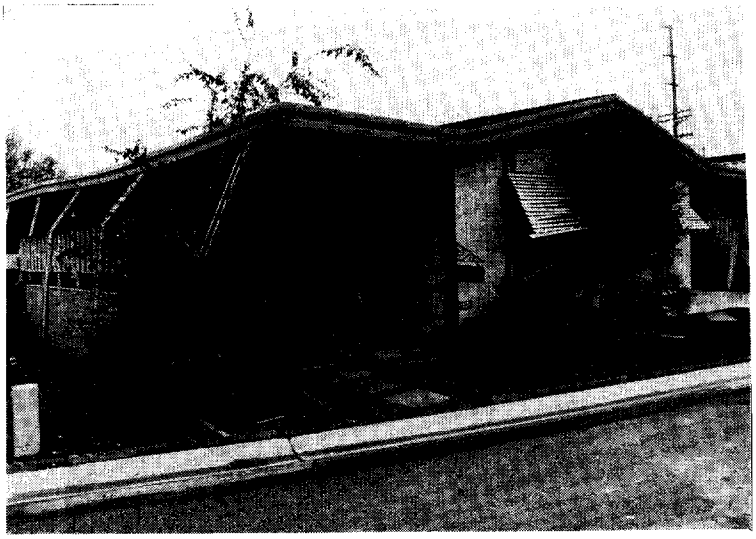

Photo 8.2 Damage of Mobile Homes due to Weak Supports

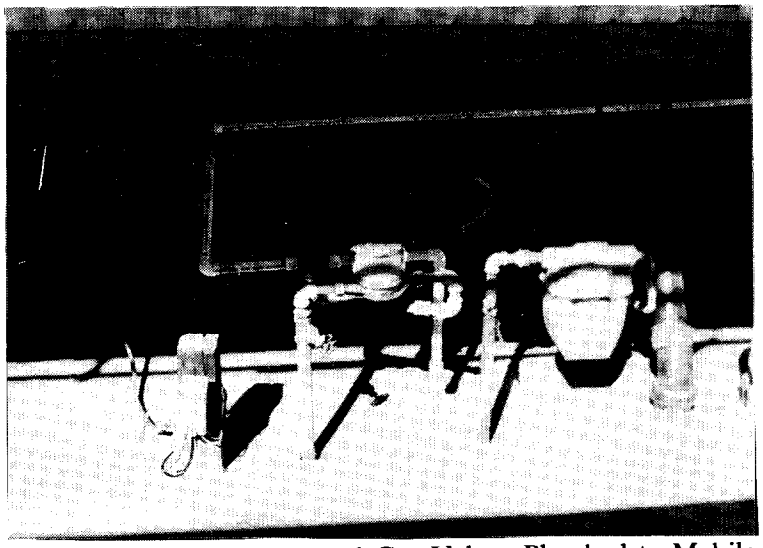

Photo 8.3 Rupture of Natural Gas Valves Plumbed to Mobile Homes Which Fell Down their Supports)

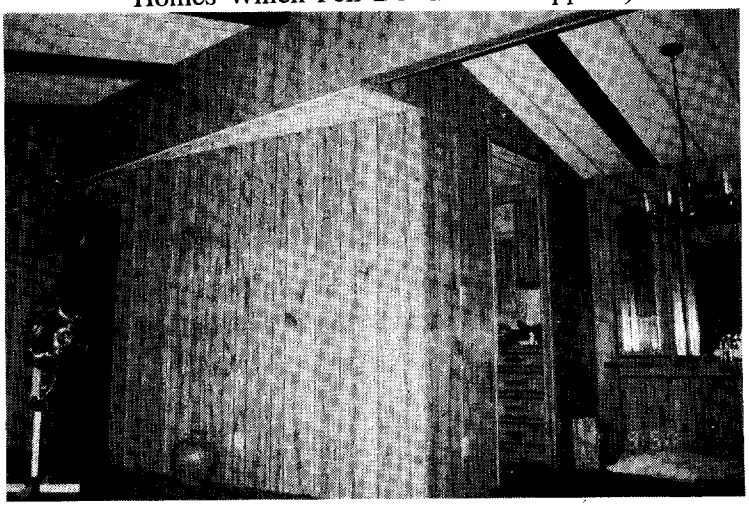

Photo 8.4 Vulnerable Mobile Homes to Fire (Mobile homes have no restriction of fire regulation based on fire code)

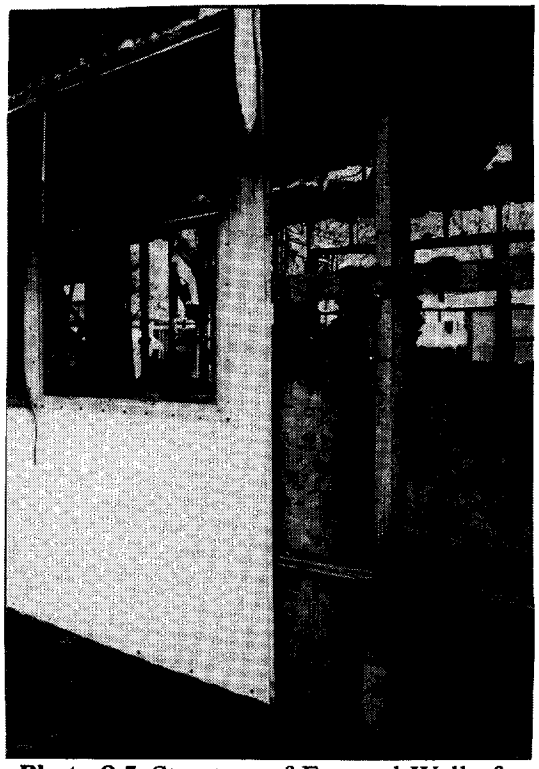

Photo 8.5 Structure of External Wall of a Mobile Home (Frame is of wood and siding is of hard board or aluminum panel)

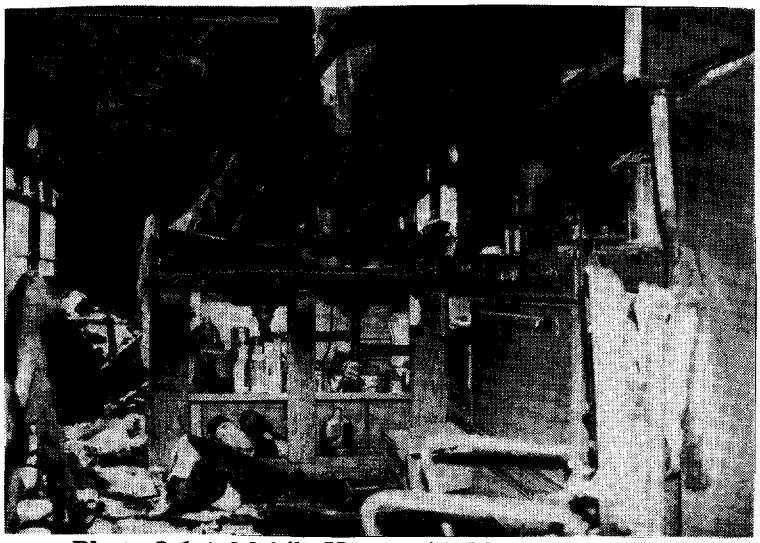

Photo 8.6 A Mobile Home with Plywood Ceiling

Photo 8.7 Road spacing Mobile Homes (Though roads in mobile home parks are relatively wide, distance between mobile homes is small because of terrace)

The M8.1 Guam Earthquake of August 8, 1993

by

A. Gerald Brady[1]

ABSTRACT

Guam's seismicity is controlled by its position in the Mariana Islands at the uplifted eastern edge of the Philippine plate, under which the Pacific plate is subducting. This deep thrust magnitude 8.1 event occurred on the junction between the plates. The source mechanism, geometry, and attenuation factors contributed to significant structural damage to hotels in Tumon Bay, but not to stiff, one- and two-story residential and commercial buildings. Future earthquakes on closer, smaller faults threaten these high-frequency structures. No serious injury or deaths were attributed to the earthquake, and therefor media attention was minimal. The maintenance of three strong-motion instruments had been neglected due to fiscal constraints, and electronic and power failures occurred at the USGS observatory. No records were recovered.

KEYWORDS: earthquake; ground motion; Guam; seismicity; structures.

1. INTRODUCTION

Guam is the southernmost island of the Mariana Islands in the western Pacific Ocean (Figure 1, from Tracey and others, 1964). The islands form a slight arc, convex to the east, and span from 13° 30′ to 20° 30′ N, and 145° to 146° E. The island chain is 770 km (480 miles) long. Guam is 46 km (30 miles) long, averages 11 km (7 miles) wide, and is aligned approximately NE-SW. The island arc outlines the Mariana Ridge at the eastern edge of the Philippine Plate, which is forced to rise in elevation as the Pacific Plate dives below it in a northwesterly direction. At the same time, the descending Pacific Plate, while dragging the eastern edge of the Philippine Plate with it, forms the Mariana Trench where the two plates converge. The Mariana Trench contains the greatest measured depth of the world's oceans, approximately 11.3 km (37,000 feet) located to the southwest of Guam. The trench is arc-shaped like the island chain, and its minimum distance from Guam is 112 km (70 miles) to the southeast, where it is aligned predominantly in the northeast-southwest direction, at right angles to Guam's azimuth (Figure 2). Given this geometry, if a deep thrust earthquake on this fault system were to be close enough to Guam to cause significant structural damage, it would seem that the earthquake would have to be located southeast of Guam, or at least in the southeast quadrant.

2. SEISMOLOGY

The seismicity of Guam can be briefly outlined by the listing of earthquakes from 1825 to 1936 in Table 1 (from Tracey and others, 1964) and by the map showing damaging Guam earthquakes from 1975 to the present (Figure 2, from the USGS/National Earthquake Information Center (NEIC) in Golden, Colorado).

2.1 The 1993 magnitude 8.1 Guam earthquake

Updated information on the 1993 epicenter location was available from NEIC over the first several weeks following the earthquake. At various times, the epicenter was placed at all points of the compass around the island, as different or more recent subsets of data and interpretation were considered. As of 8/26/93, 18 days after the earthquake, the magnitude 8.1 earthquake was located at 12.97° N, 144.74° E at a depth of 61 km (38 miles).

---

[1]USGS, Menlo Park, CA94025

This places the epicenter 60 km (37.5 miles) due south of Agana, the commercial center of the island. It is a few kilometers further to Tumon, where most of the tourist hotels are located. The origin time was 08:34:25.0 on Sunday, August 8, 1993 (GMT), 6:34 pm local time. The depth estimate of 61 km (38 miles) is not dependent on the USGS' World Wide Seismic Station on Guam, so the failure of the instrumentation there, both in the electronics and the power supply, does not affect the accuracy or precision of the estimate.

Guam is a remote island in the western Pacific Ocean, and epicenter and depth calculations cannot be made as confidently as in California. For a 90% confidence level in the epicentral location the error circle has a radius of 660 km (412 miles).

The moment tensor solution for the source mechanism provides two planes on which the first motion might have occurred. With the restrictions placed on the correct mechanism by geologic considerations outlined above, the preferred fault plane strikes at N70E and dips steeply (77°) to the NNW. The first motion has the Pacific Plate moving down dip (to the NNW) and along the strike (to the WSW) in equal amounts.

The aftershocks listed in NEIC's 8/26/93 summary are constrained to have depths of either 60 or 33 km. They are plotted in plan in Figure 2. With this constraint, only the plan view of the portion of the fault ruptured during the main shock can be identified using aftershock epicenters.

A seismicity map received from NEIC with plotted epicenters, (10° to 15° N, 143° to 148° E, M=5.5 and above) shows that there are many earthquakes on faults near Guam. It is not likely that magnitude 8 events will ever be closer than this one. But lesser magnitude events can occur on closer faults, whether such faults are already known, inferable from this plot, or not yet found. These have the potential for much damage, affecting particularly stiff structures such as one- or two-storied houses and buildings.

3. STRONG GROUND MOTION

An estimate can be made of the character of the ground motion from observations on the island. Many people interviewed agreed with the newspaper accounts of the shaking lasting 60 seconds. The aftershock distribution indicates that the mainshock rupture must have been for the most part in one direction, namely to the northeast, and could well have lasted 40 seconds or more. Wave motion arriving from the rupture's start, at the focus, will have been only slightly stronger than the motion arriving from the rupture's end, which is not much further from Guam. If we maintain the assumption that the rupture was travelling to the northeast it will have finished up receding from Guam, and therefore the later arrivals will have been further attenuated in amplitude. We conclude that the strong shaking lasted 30 seconds, and then slowly lessened.

A 61-km depth and 60-km epicentral distance permits geometric three-dimensional spreading to occur for a greater distance and longer duration than would be expected for a shallow high-magnitude California event. We conclude that peak acceleration amplitudes will be low (say 0.25 g), and that high frequencies, greater than 5 Hz, will not be present. Slight damage to small, solidly-built houses and buildings of one and two stories, and flimsy buildings, too, in some cases, also points to a lack of high frequencies. On the other hand, the damage to the tourist hotels of four to twenty stories indicates prominent ground motion components having periods between 0.5 and 2 seconds.

The fault plane is approximately perpendicular to a line to Guam, so few high-amplitude P-waves arrived there. Furthermore, most shear waves generated on the fault arrived at Guam refracted sufficiently to be travelling vertically, thereby supplying minimal vertical accelerations. There were no indications of disturbed soil at hill crests, ex-

cept landslides, and no reports of furniture or equipment moving sideways while airborne. We conclude that vertical accelerations certainly did not exceed 1 g, and probably offered a negligible contribution to damage, considerably less than was provided by the horizontal accelerations.

3.1 Ground motion at damage sites.

The 61-km focal depth ensured that the attenuation of ground motion amplitudes was not rapid from the southern to northern extremities of the island. All firm foundation soils or rock in the Agana business district and the Tumon hotel district probably received shaking of the same character. Accelerations are unknown at potentially liquefiable sand layers overlain by fill, that failed and spread during the earthquake.

3.2 Tsunami

A tsunami was generated, but passed by Guam without fanfare. A parked pick-up truck on a beach on the east coast was partially swamped. Much more common typhoons provide ample experiences of high ocean waves. Tide gauges recorded maximum wave heights of 98 cm at Japan and 19 cm at Hawaii.

4. US NAVY INSTRUMENTATION

The US Navy over a period of years ending in 1988 maintained three instruments in Guam as part of their network of strong-motion accelerographs. No records were recovered from the instruments, which had remained in place.

A network of strong motion accelerograph instrumentation does not generate support, either personnel or financial, by its very nature of patiently waiting for an earthquake event. A network needs an associated research team of earthquake scientists or engineers to provide incentives for good recordings, and to provide successful appeals for long-term maintenance funding.

Some preliminary conversations have been held between representatives of the Department of Public Works and the US Geological Survey's Guam Observatory, with respect to the installation and maintenance of a small network of strong-motion instruments. Cooperation with the USGS in Menlo Park for processing records and analyzing ground motion is a possible future goal.

4.1 The 1983 magnitude 6.3 earthquake record.

The U.S. Navy strong-motion earthquake instrumentation on Guam included one Kinemetrics SMA-1 accelerograph installed in 1979 in Building 372, the Transportation Equipment Maintenance Shop. This instrument produced a record from the magnitude 6.3 1983 earthquake (Brady and Mork, 1993) with an epicenter 30 miles (48 km) northeast of Agana, the business center of the island, and 31 miles (50 km) from the instrumented site. It was the first such record from Guam, and the architect/engineer contractors working on building analysis on Guam requested response spectra. Through an arrangement between Stan Takahashi (retired, Navy Civil Engineering Laboratory (NCEL), Port Hueneme, California), IOM Towill (at the time, a digitizing company in Santa Clara, California), and the USGS, Menlo Park, California, the record was digitized and processed, and the data was sent to NCEL.

5. NOTES ON THE STRUCTURAL DAMAGE

The Royal Palm Resort Hotel consisted of two closely-spaced 12-story, reinforced concrete, matching towers, with a structural connection. Several second-story columns near the southwest corner of one of the towers failed, shortening by the height of the window opening. The tower came to rest leaning against its twin. The connecting arm suffered major structural damage as it attempted to reconcile the displacements of the two towers. Both towers have been demolished.

The Grand Hotel was a 4-story reinforced concrete building, L-shaped in plan. The non-symmetrical plan and the glass-fronted commercial first story contributed to the fail-

ure of the first story columns and resulting horizontal offset of 8 inches (0.2 m) in the building's final position. The top three stories remained in a relatively undamaged state. The hotel has been demolished.

The Guam Reef Hotel had a very heavily constructed canopy over the entrance to its twin structures. The canopy was supported on four circular columns which failed catastrophically, allowing the canopy to fall to the ground, with almost no lateral offset. Two taxis were caught.

Gas station shelters, built to shield the pumps and customers from vertical sun and rain, suffered severe structural damage at the top and bottom of the supporting columns.

6. WIND AND SEISMIC EFFECTS

Damage to one class of structure, characterized by the canopy and the gas station shelters in the section above, and by the umbrella-shaped bus-stop shelters, is an interesting consequence of a design philosophy that is dominated by the typhoons that threaten Guam every year. The design wind speed is 155 mph (240 km/hr) which produces a horizontal force that is not excessively high on roof cross-sections, and a vertical uplift force that is relatively high. These wind loads are resisted satisfactorily with heavy roofs, and do not require great ductility in column members. But the inertial loads at roof level during strong earthquake excitation are high, and require great ductility in support columns. The typhoon design philosophy does not address this requirement, and the structures are damaged during earthquakes.

7. LIQUEFACTION

Parts of the Navy port area, the commercial port area, and the electric power generation plant site to the southwest of Agana, are built on filled land. As is usually the case where sufficient precautions against ground failure, ground spreading and liquefaction are not taken, these areas suffered to various extents. Cracks in the ground surface on the piers reached down to the water table and beyond, the cranes were ordered stopped while insurance questions were addressed, and the docksides were no longer straight but bulged out toward the water.

8. CONCLUSIONS AND LESSONS TO BE LEARNED.

No earthquake as large as this, magnitude 8.1, is ever likely to be closer to Guam, so this earthquake provided representative shaking for the big event. The shaking had predominant periods in the range of 0.3 to 3 seconds, coinciding with the natural resonant periods of the seriously damaged high-rise structures. Causes of the damage, once the ground motion is given, are typical: architectural layout of the structures, lack of ductility details, an understanding of the structural dynamics, material quality and construction techniques. Smaller earthquakes have occurred on closer faults, and will do so again, with a greater content of high frequency ground motion. These will affect the stiffer low-rise residential structures.

The island absorbed the tourism industry very rapidly, and may have occasionally outstripped its ability to provide quality assurance during all stages of a hotel project.

Filled land, and other bad ground (for example, soft, amplifiable, and liquefiable), must be identified, rectified, or must not be built upon.

Strong ground motion records in the regions of strong shaking and structural damage are imperative for accurate assessment of a damaged building's performance. The effort required to design, fund, and install a network, no matter how small, should be followed with successful efforts for maintenance for the expected instrumentation life.

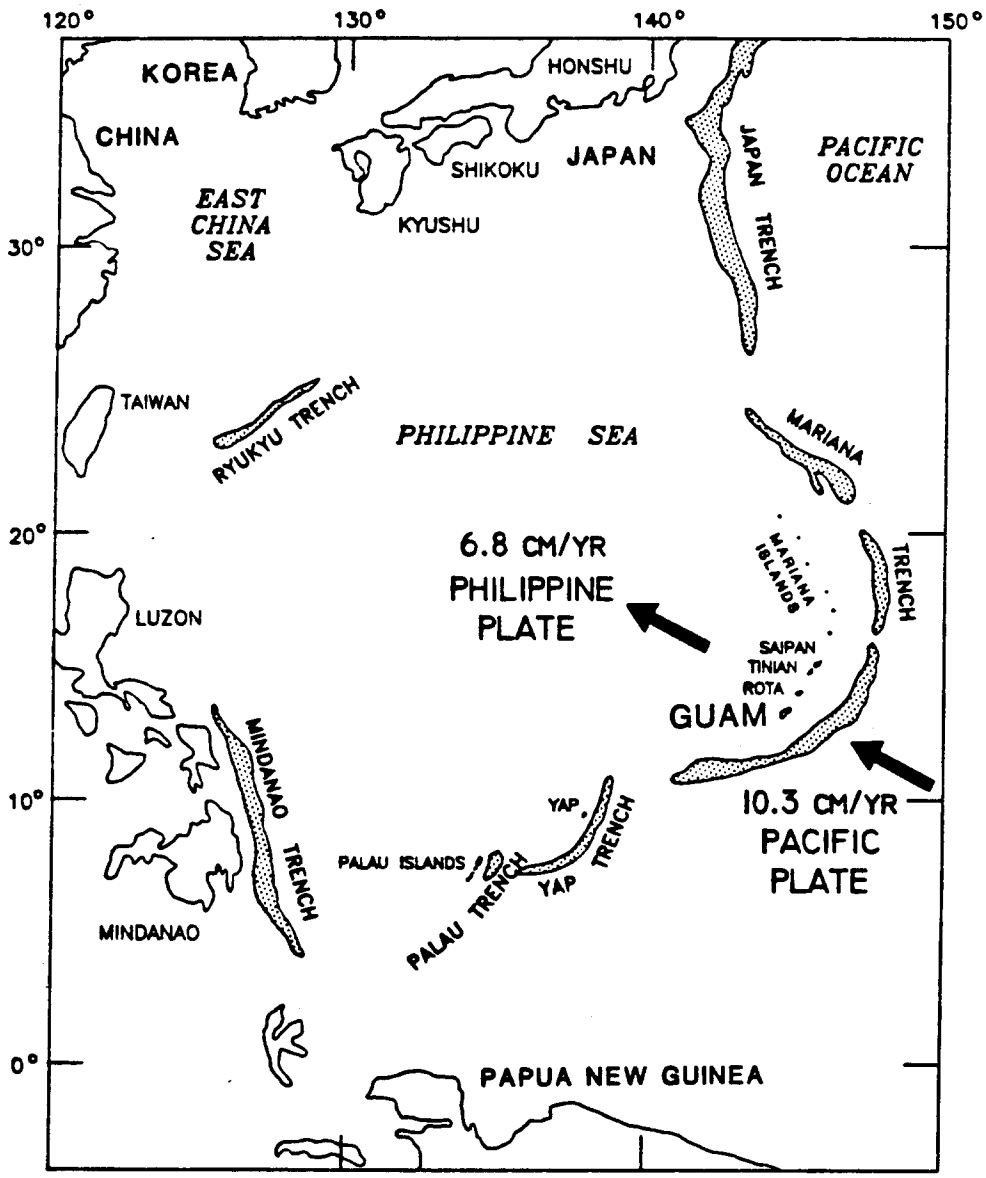

Figure 1. Plate tectonics in the western north Pacific Ocean

9. ACKNOWLEDGEMENTS

The author was on the Earthquake Engineering Research Institute reconnaissance team that visited the island for a week shortly after the earthquake. A complete report is in preparation for *Earthquake Spectra*. This paper includes some of the views of other members of the team. Paul Hattori, of the USGS Guam Observatory, was a great help with transportation and local knowledge. Personnel from Dames and Moore, with an office on Guam, and from H.J. Degenkolb Associates, contributed to the author's understanding of the earthquake's effects.

10. REFERENCES

1. Brady, A.G. and Mork, P.N. (1993). "Processing of the US Navy strong-motion record from the February 13, 1983 magnitude mb 6.3 Guam earthquake." USGS Open File Report in press.

2. EERI (1993). "The Guam earthquake of August 8, 1993." EERI Newsletter, v 27, n 10, 12p.

3. Tracey, J.I., S.O. Schlanger, J.T. Stark, D.B. Doan, and H.G. May (1964). "General geology of Guam." Geological Survey Professional Paper 403-A, 105 p.

TABLE 1.
GUAM EARTHQUAKES, 1825-1936.

Date	Max MMI
April, 1825	7-8
May, 1834	7-8
Jan 25, 1849	8-9
Jul 1, 1862	6
Dec 7, 1863	5-6
Jun 24, 1866	5-6
May 13, 1870	5-6
May 16, 1892	7-8
Sep 22, 1902	8-9
Dec 24, 1902	5-6
Feb 10, 1903	6
Dec 10, 1909	7-8
Oct 26, 1912	5-6
May 10, 1917	5-6
Nov 24, 1917	5-6
Jun 12, 1932	5-6
Oct 30, 1936	7-8
Nov 12, 1936	5-6
Dec 14, 1936	6

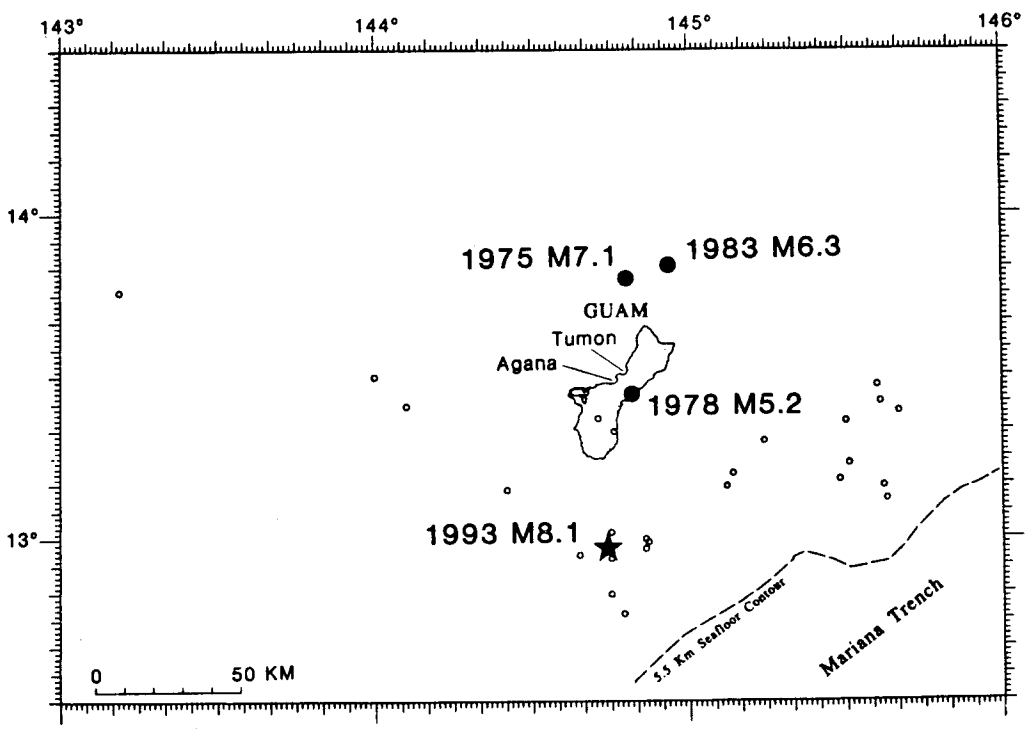

Figure 2. Earthquakes damaging Guam since 1975, and 1993 aftershocks

Infrastructure Damage by 1993 Hokkaido-Nansei-Oki Earthquake

by

Takashi Iijima[1], Yutaka Iida[2], Kazuhiko Kawashima[3],
Hisanori Otsuka[4], Osamu Matsuo[5], Shigenobu Tanaka[6],
Akira Nakamura[7], Masanori Nakano[8], and Ryosuke Tsunaki[9]

ABSTRACT

Seismic damage caused by the Hokkaido-nansei-oki, Japan, Earthquake of July 12, 1993 is described. Description is given to the damage of road, road bridges, river hydraulic facilities, dams and sewage facilities, and effect of tsunami, slope failure and soil liquefaction.

Key Words: Earthquake Damage, Hokkaido-nansei-oki Earthquake, Road, Bridge, Lifeline Facilities, Dam, Tsunami, Slope Failure, Soil Liquefaction

1. INTRODUCTION

The Hokkaido-nansei-oki earthquake occurred at 22:17 on July 12, 1993 at sea bottom of the south west Hokkaido Island. The magnitude was 7.8 on Richter scale. Extensive damage was developed by tsunami, fire, slope failure and soil liquefaction at the south-west Hokkaido. In particular, damage was destructive at Okushiri Island where tsunami attacked soon after the earthquake.

This paper summarizes the damage caused by the Hokkaido-nansei-oki earthquake (Ref. 1). Emphasis is given to the damage of roads, road bridges, river hydraulic facilities, dams, sewage facilities, and effect of tsunami, slope failure and soil liquefaction.

2. THE EARTHQUAKE AND EARTHQUAKE GROUND MOTIONS

Magnitude of the earthquake was 7.8 according to the Japan Meteorological Agency. The epicenter was about 80 km from the west coast of Hokkaido Island, and the focal depth was about 34 km. The aftershock area extended 220 km in north/south and 70 km in east/west.

Fig. 2.1 shows the distribution of JMA Seismic Intensity. It was V at Otaru, Suttsu, Esashi and Fukaura, and IV at Kutchan, Tomakomai, Muroran, Hakodate, Mutsu and Aomori.

A number of strong motion records were obtained as shown in Fig. 2.2. The peak horizontal ground acceleration was 496 gal at Kuromatsunai and 386 gal at a free field near the Shichiho Bridge. It should be noted that the Kuromatsunai record is not a free field ground motion. It was recorded on a concrete floor of a first story JR station.

Fig. 2.3 shows the strong motion accelerations measured at Shichiho Bridge site. The duration is quite long. The bracketed duration (Ref. 2) with the acceleration larger than 50 % of the peak acceleration is about 10 seconds. Response accelerations of the records for 0.05 damping ratio are presented in Fig. 2.4. A high response acceleration of 1,652 gal was developed at a natural period of 0.15

1) Director-General, Public Works Research Institute, Ministry of Construction
2) Director, Technical Department, Trans-Tokyo Bay Highway Corporation (Former Director, Earthquake Disaster Prevention Department, PWRI)
3) Research Coordinator for Underground Development, PWRI
4) Head, Earthquake Engineering Division, PWRI
5) Head, Soil Dynamics Division, PWRI
6) Head, Coastal Engineering Division, PWRI
7) Head, Fill-type Dam Division, PWRI
8) Head, Foundation Engineering Division, PWRI
9) Head, Slope Failure Division, PWRI

second. The ground where the records were obtained is classified as the Group I (stiff, Ref. 3).

Fig. 2.5 shows the attenuation of peak ground accelerations. Attenuation by an empirical equation by Eq. (2–1) (Ref. 4) is also presented in Fig. 2.5 for comparison.

$$a_{max} = \begin{cases} 987.4 \times 10^{0.216M} \times (\Delta+30)^{-1.213} & \text{(stiff)} \\ 232.5 \times 10^{0.313M} \times (\Delta+30)^{-1.213} & \text{(moderate)} \\ 403.8 \times 10^{0.265M} \times (\Delta+30)^{-1.213} & \text{(soft)} \end{cases} \quad (2\text{–}1)$$

where, a_{max} : peak ground acceleration (gal), M : earthquake magnitude, and $\triangle$: epicentral distance (km). It is seen in Fig. 2.5 that the acceleration at Kuromatsunai is extremely higher than the empirical evaluation, and that the attenuation of the measured records in terms of distance was lager than Eq. (2–1).

3. OUTLINE OF DAMAGE

Table 3.1 shows the human loss and damage developed in Hokkaido Island. Although some more damage was developed in the Main Island along the Japan Sea, most of damage occurred in Hokkaido Island. The total damage was about 100 billion yen.

The earthquake caused 201 deaths (200 in Hokkaido Island), 33 missings and 236 seriously or slightly injured. Among the 201 deaths, 171 were killed at Okushiri Island by Tsunami. This corresponds to 3.6 % of the total residents (4,719) in the Island.

The number of houses which were partially damaged or completely destroyed was 3,555 in Hokkaido. Among 567 houses which were completely destroyed, 410 were located in Okushiri Island. A fire broke out soon after the earthquake, and it burned down 192 houses.

The damage to road facilities occurred at 88 locations on 7 National Roads and 291 locations on municipal roads. A serious failure of embankments occurred on National Road 5 at Chirai, Oshamanbe Town. Among rivers with the jurisdiction of Hokkaido Development Bureau, shore protections in Okushiribetsu River and Shiribetsu River were damaged at 43 locations, and other damage was developed at 143 locations in the rivers with the jurisdiction of Hokkaido government. The damage to civil engineering facilities was about 32 billion yen, which is 32% of the total loss.

Water and gas supply was out of service at 16,000 and 15,000 houses, respectively. The facilities were recovered by July 25. The electric power supply was suspended to about 33,000 houses, and the recovery was completed by July 16. The railway service was restored on July 18, and the ferry boat and the air flight service were recovered on July 17.

4. DAMAGE TO ROADS

Damage of roads occurred at the south–west Hokkaido including the Okushiri Island. The damage included land slides, surface submergence by tsunami, failure of embankments, collapse of road shoulders, settlement/uplift of road surfaces. Fig. 4.1 and Table 4.1 show the location of major road damage.

One of the major damage was developed at a road embankment at Chirai in Oshamanbe–cho on National Road 5 as shown in Photo 4.1. A 9.5m–wide road embankment collapsed to a depth of 7.5m along 100m. The volume of collapsed soil amounted to 5,000m^3. Fig. 4.2 shows the cross section of the embankment before and after the earthquake. The embankment was filled on the soft ground consisting of peat layer. A temporary road for the emergency restoration was constructed on harder ground near the collapsed embankment and was put into operation after 12 days following the earthquake (July 24).

Permanent undulating deformation as shown in Photo 4.2 was developed at a road section between Oshamanbe and Yakumo on National Road 5 along Uchiura Bay. Nakanosawa Elementary School located along the Road 5 suffered shear failure at the top of

piles supporting a new wooden frame building. Extensive sand boils, cracks, vertical discontinuities and lateral flow in the yard occurred. Uplift of manholes installed in the pedestrian way along the Road 5 also occurred. In this area, iron sand had been produced, and the holes were re-filled with loose sand. This caused extensive soil liquefaction.

On a bypass of National Road 5 at Oshamanbe, an embankment and retaining walls, which were under construction along a sea shoreline, moved laterally toward the sea by a distance of several tens centimeter. Manholes installed in the embankment for surface water drainage and sewage also uplifted.

On the National Road 228 at Arikawa, Kamiiso-cho located at west of Hakodate City, cracks were developed at edges of a concrete pavement slab with length of 10m and width of 7m both in the longitudinal and transverse directions. The slab moved by about 10 cm in longitudinal direction. The pavement crashed and uplifted as shown in Photo 4.3. On the new road under construction along the damaged existing Road 228, boiling holes and circular subsidence holes were developed and diagonal cracks to the longitudinal axis were developed. The curb moved and slope of the embankment collapsed with width of about 1.5 m. Cracks were developed at manholes and concrete pipes installed in the pedestrian way.

A PC arch-type snow-shelter collapsed as shown in Photo 4.4 on a regional road in Okushiri Island. The structure was just completed but was not yet in service. The shelter collapsed due to the overturning of the foundation toward outside. Since two arch members were connected only at the arch crown and the other sides were supported by the foundations with rubber pads, the shelter was statically determinant.

5. DAMAGE TO ROAD BRIDGES

Twenty four bridges were damaged by the earthquake. Among them, 7 bridges were of the jurisdiction by the Hokkaido Development Bureau, 12 bridges by Hokkaido Government and 5 bridges by municipal governments.

Table 5.1 shows the major bridges damaged. Damage occurred at reinforced concrete piers, wings and parapets of abutments, and mortar and anchor bolts of bearing supports. Major causes of the damage were as follows (Ref. 5):

(1) Damage to reinforced concrete piers with termination of main reinforcement without enough anchoring length

Significant damage was developed at the reinforced concrete piers of Motoe Bridge on a municipal road. The bridge was of 7-span simply supported plate girder with a deck length of 165.7m. The deck was supported by the T-type reinforced concrete piers with circular section of 1.8 m. The bridge was constructed in early 1970s. Medium to heavy damage was developed at 3 piers among 6 piers.

The most significant damage was developed at Pier 3 as shown in Photo 5.1. Crack and spalling-off of cover concrete, and outward buckling of longitudinal reinforcement were developed at the section where the part of longitudinal reinforcements were terminated. The requirements for anchoring length of the reinforcements described in the pre-1980 Design Specifications (Ref. 6) was not sufficient. This is a typical damage developed in the bridges designed in accordance with the pre-1980 Design Specifications (Ref. 5).

In accordance with the Guide Specifications for Post Earthquake Countermeasures (Ref.7), this damage corresponds to the "Substantial Damage" which requires to close the bridge for traffic.

The similar type of damage was developed at two more bridges as shown in Photos 5.2 and 5.3.

Fig. 5.1 shows the evaluation of seismic vulnerability for 14 bridges which suffered/did not suffered this type of damage at reinforced concrete piers during this earthquake and the Kushiro-oki Earthquake of January 1993 (Ref.

8). A method proposed to evaluate seismic vulnerability of such type of reinforced concrete piers in terms of the Failure Mode Factor S and Safety Factor F_y^T (Ref. 9) was applied after the earthquakes to show the accuracy of the proposed method. It is obvious that the proposed method provides a reasonable prediction for the damage.

(2) Damage caused by soil liquefaction

Oshamanbe Bridge at Oshamanbe on the National Road 37 was damaged by the effect of soil liquefaction. It is of 5-span simply supported post-tension T-shaped girder bridge with deck length of 150.1 m. The foundations were of a caisson type. The bridge was constructed in 1960, and the pedestrian bridge was added at the upper stream side in 1976.

The bridge piers inclined in the upper stream direction as shown in Photo 5.4 resulting in the residual lateral displacement of the deck of 42 cm. The inclination was 1-2 degree in angle. This caused some damage to the deck slab and the expansion joints.

Fig. 5.2 shows the soil boring data at the site. It is considered that the sandy layer at depth of 3.5 - 7 m caused liquefaction resulting loss of bearing capacity. The Seismic Design Specifications of Road Bridges (Ref. 10) in which the first requirement for soil liquefaction was included was issued in 1971. Because this bridge was designed before the Seismic Design Specifications was issued, the consideration against the soil liquefaction was not adequate.

The bridge piers have an antisymmetric shape due to the added pedestrian deck, and this caused tilting of the foundation only in one direction.

6. DAMAGE TO RIVER DIKES

Flood control earth-fill river dikes suffered strict failure. Damage occurred at 224 sites with a total length of 29 km. The repair cost including other river works amounted to about 3.9 billion yen.

The damage of river dikes consisted of cracking, settlement, lateral spreading and slumping. In many cases, sand boils were observed at the ground near the toe of dikes. Such dikes are filled on alluvial deposits without exception. It is considered that soil liquefaction triggered the damage.

The most extensive damage occurred at the dikes of Shiribeshi-Toshibetsu River and Shiribeshi River. Typical damage at the rivers are as follows:

(1) Kabutono Dike at Shiribeshi-Toshibetsu River

Kabutono Dike suffered the most serious damage at its right dike at the mouth. Longitudinal and transverse cracking, settlement, slumping and lateral spreading were developed for about 2.2 km. Sand boils were also observed at the sites. Fig. 6.1 shows the cross section. It is 6 m high and 6 m wide at its crest, with side slope of 2 H : 1 V. The cracks developed at the crest extended to as deep as 2.3 m associated with slumping of 2 m and width of 1 m. Occurrence of fissures and sand boils in ground near and away from the dike indicates that the liquefaction took place mostly in material beneath the dike. As shown in Fig. 6.1, the top soil is underlain by fluvial sand deposit of 3 m thick. This layer has a relatively low SPT-N value of 10 or less.

(2) Hatsuta Dike at Shiribetsu River

The right-hand dike of the River suffered damage as shown in Photo 6.1 for 0.89 km long upstream from the 4.8 km-post. The damage included longitudinal cracks at the crest associated with slumping of as deep as 1.5 m, cracks at both slopes, and lateral spreading. Fig. 6.2 show the cross section of the dike as well as soil profile. There is an extremely loose fluvial sand deposit from 7 m below the ground surface. Many fissures and sand boils were observed between the dike and river. It is obvious that the damage was developed due to soil liquefaction.

Fig. 6.3 shows how damage rate of river dikes decreases as the epicentral distance increases. The damage ratio is defined as a ratio

of the length of river dikes damaged and the total length. The damage ratio for other previous earthquakes such as 1964 Niigata Earthquake and 1978 Miyagi-ken-oki Earthquake (Ref. 11) is presented in Fig. 6.3 for comparison. It is seen that the damage ratio for the Hokkaido-nansei-oki earthquake shows the similar attenuation with the previous earthquakes. Such result may be valuable to evaluate the damage degree for a certain combination of an earthquake magnitude and epicentral distance.

Fig. 6.4 shows the damage ratio vs. surface geology relation. The surface geology is represented in terms of the micro-landform classification. It is obvious from Fig. 6.4 that the damage ratio is considerably high at the former river bed. It is important to note that the river dikes on the river beds tend to cause substantial damage due to an earthquake.

7. DAMAGE TO DAMS

Immediately after the earthquake, an emergency inspection was made for 52 dams: 6 dams are owned by the Ministry of Construction (M.O.C.), 11 dams were subsidized by M.O.C., and 35 other dams are for water utilization. The inspection revealed that among dams with height of 15 meters or more, the Niwa-Ikumine Dam suffered moderate damage. Minor damage was discovered at the Pirika Dam and the Makomanai Dam. But they were not so severe as to affect the safety of the dams (Ref. 12).

(1) Pirika dam

Pirika Dam is a combined dam consisting of a concrete gravity dam and a rockfill dam. The dam was located 89 km from the epicenter.

In the structure between block 0 of the concrete dam body and the connecting corridor leading to the control office, a floor panel concrete of the connecting corridor was pushed up and spalled in the length of about 1.5 meters due to compression in axial direction of the dam. Slight concrete spalling was also discovered in other cross joints of the connecting corridor. This connecting corridor rides on the rock zone of the core wall at the left bank connected perpendicularly to the concrete dam. It was therefore subjected to severe compression caused by differences of the earthquake response between the dam body and the rock zone. Because the connecting corridor and the concrete dam body are completely separated and there was no deformation in the inspection gallery for block 0, the deformation did not effect the dam body itself.

After the earthquake, water leaked from the intersection of the inspection observation gallery and the blocked section of the temporary diversion channel inside the dam on the block 28. This section was sealed after leakage was observed during the previous test filling. Because since then, no leakage was observed at the sealing, it is considered that a small gap opened in the sealing due to the earthquake causing leakage. The leakage was small (between 80 and 100 milli-liters per minute) after 10 days, and it was not turbid. Therefore the leakage is not considered to be a serious problem.

(2) Niwa-Ikumine Dam

Niwa-Ikumine Dam is a central core type earth fill dam. It is an old dam completed in 1927. Fig. 7.1 shows a plane of the dam.

The earthquake caused bulging and cracking of the dam body at two elevations, and undulating deformation of the upstream slope. The bulging appeared in the middle and close to the toe of the upstream slope. The maximum level difference of the bulge at the toe of the slope was about 1 meter over the 40 meter length. The cracking consisted of five longitudinal cracks at the crest. The longest crack extended for a total length of approximately 120 meters on the crest of the dam, with the depth of 2 meters. It settled on the upstream side, and its maximum level difference was about 1 meter. Fig. 7.2 shows the cross sections at 10 m interval measured from the point 80 m apart from the right bank

spillway. This point is almost the center of the dam. It is believed that the earthquake caused the liquefaction of the sandy stratum and the settlement of the upstream side of the dam body. Sand boil was seen on the surface of the sediment on the bottom of the reservoir near the toe of the upstream slope of the dam body. The bottom of the dam body and river-bed sedimentary stratum consist of loose sand with a small N value.

(3) Makomanai Dam

Makomanai Dam is a central core type rockfill dam with a height of 34 meters. It was completed in 1987 and located 66 kilometers from the epicenter.

The dam body damage included deformation of the concrete frame on the upstream slope, and the riprap had shifted. In the ground, the facing concrete blocks on the right bank had undergone undulating deformation, sprayed concrete on the left bank slipped, and the small-scale failure had occurred on the slope of mountain. None of these damages presented any particular problems related to the safety of the dam body.

Immediately after the earthquake, increase in leakage water was observed at six dams, and the amount of leakage water decreased at 2 dams. The turbidity of the leakage water increased at one dam. However, these changes in leakage water were not considered to indicate serious problems, because the leakage water returned to its pre-earthquake state within a period ranging from a few days to a few weeks.

Furthermore two small irrigation ponds with dike of less than 15 meters high located only 65 and 70 kilometers from the epicenter in Setana-cho in Hokkaido were destroyed. And along the Japan Sea Coast near the epicenter, some dikes of this kinds were damaged by settlement or cracking.

8. DAMAGE TO SEWAGE FACILITIES

Damage of sewage facilities was developed at 8 cities and towns at the west south of Hokkaido. About 2/3 of the total damage concentrated at Oshamanbe Town, in which about 10 % of the sewage pipes suffered damage. Hume pipes and polyvinyl chloride pipes are generally used for sewer.

Damage included break and offset of pipes, leakage, damage of side wall of manholes and uplift of manholes (Ref. 13). Only minor damage such as nonstructural damage and break of window was developed at sewage treatment plants. Damage of small diameter pipes was surveyed by small video cameras which either crawled or are pulled into the pipes. Break of pipes and joints, dislodging of pipes, pull-out of pipes at joints and leakage of water could be clearly identified. Photo 8.1 shows the damage detected by such a small video camera.

Table 8.1 shows the type of pipe and joint failures developed at Oshamanbe Town. Permanent settlement of pipes and leakage of water were the most frequently developed damage. The damage of polyvinyl chloride pipes was less than the damage of hume pipes.

Most of uplift of manholes as shown in Photo 8.2 was developed due to soil liquefaction. The uplift of manholes was as high as 50-80 cm. Fig. 8.1 (a) shows the uplift of 10 manholes on a same sewer. For analyzing the uplift, the Liquefaction Resistant Factor F_L (Ref. 14) was evaluated for each manhole, and the safety of uplift was evaluated as (Ref. 15)

$$F_S = \frac{W_M + F}{U_S + U_P} \tag{8.1}$$

in which F_S: safety factor for uplift, W_M: weight of manhole, F: friction between the soils and manhole, U_S: uplift force due to static water pressure, and U_D: uplift force due to pore water pressure. The pore water pressure was evaluated from the Liquefaction Resistance Factor F_L (Ref. 14).

Fig. 8.1 (b) and (c) shows the Liquefaction Resistance Factor F_L and Safety Factor F_S. The safety factor F_S is minimum at

manhole No. 6 where the largest uplift was developed. Thus it is obvious that some correlation is seen in Fig. 8.1. More data are required to verify the accuracy for predicting the uplift.

9. DAMAGE DUE TO TSUNAMI

Okushiri Island suffered the most destructive damage due to tsunami. In particular, the damage concentrated at Aonae district (southern part) and Inaho district (northern part) in the Island.

Photo 9.1 shows a village backyard at Inaho fishery harbor. Even houses located on a hill side of a road were completely destroyed. The tsunami inundation height was as high as 8.9 m at this site.

Aonae district suffered much more destructive damage due to the tsunami. Photo 9.2 shows the north-east of Aonae fishery harbor. Even though this site was sheltered by Aonae Cape from the tsunami source, it suffered such destructive damage. It is considered that tsunami came over the site by refraction and diffraction. Some witnesses who saw that the highest tsunami attacked the Aonae district from the north-east to south-east confirm this. The tsunami inundation height was 7.4 m at this site.

The tsunami inundation height measured by PWRI members is presented in Fig. 9.1 (Ref. 16). It was high at Shimamaki village and the coast from Setana to Taisei town. The tsunami height was as high as 3 m. At Okushiri Island, the survey of tsunami height was made only at east coast, because population is more dense at this side. The highest tsunami inundation height was 19.8 m at Kuki cape. The tsunami inundation height decreased from south to center, because the tsunami attacked from the west. It should be however noted that the maximum tsunami height of 15.9 m was observed at Hamatsumae district even though this district is sheltered by Aonae Cape. It must be also pointed out that the maximum inundation height was 31.7 m at Monai. This is the highest tsunami inundation height ever experienced in this century in Japan.

10. DAMAGE DUE TO SLOPE FAILURE

Slope failures concentrated in Okushiri Island and in the western region of the Oshima Peninsula. This section shows two slope failures at Okushiri Island as shown in Fig. 10.1.

(1) Failures in the Okushiri District

Most of death in the Okushiri District in Okushiri Island was developed by landslides. A slope collapsed as shown in Photo 10.1 at the terrace behind Okushiri Harbor. The failure was 200 m wide and 120 m high. Downslope of about 100,000 m^3 of debris destroyed the Hotel Yoyo-so.

The geological structure of the collapsed slope consisted of surface soil, sediments, tuff breccia, tuff sandstone and tuff of the Neogene lacustrine epoch and Pliocene Hotokesawa layer from the surface. The average inclination of the slope after failure was 40 degree. The debris moved a maximum 70 to 80 meters toward the sea. A considerable amount of earth and rock mass which was observed in the middle and bottom parts of the slope, retained its original shape, and is estimated to have fallen along the shear plane. A flat plane, which nearly corresponds to the terrace plane before the earthquake, remains intact and is wooded at the uppermost part of the remaining earth mass. Rock masses of maximum diameter of 5 to 7 meters are included in the earth mass.

Such slope failures have led to speculation that the earth mass did not move at once, instead, a certain range of the lower slope section probably collapsed first, then the unstable upper part slipped down.

(2) Failures in the Monai District

Numerous slope failures and falling rocks were observed along roads in the Monai District as shown in Fig. 10.1. A considerable number of rocks fell, especially near the Hoyaishi District, from steep cliffs and slopes of tuff breccia, greatly damaging retaining walls

and roads. Earth movement similar to landslides, and fluctuation of colluvial deposits of considerable range and thickness, which were believed to include weathered rock layers, were also recognized.

(3) Influence of knick lines on failure risk

Investigation on slope failures caused by earthquakes confirmed that slopes with knick lines easily collapse by earthquakes. Topographic analysis was conducted for the slopes near the Horonai River, where most slope failures were observed. The influence on failure risk by projecting forms on slopes formed by knick lines was investigated.

The central region of Okushiri Island was subjected to analysis. The number of slope failures within this range was 44. They have the slope height ranging from 30 to 120m. Although the slope height is one of the most controlling factors for damage vulnerability, a precise evaluation for the effect of slope height was not made in this analysis. This requires further analysis.

Fig. 10.2 shows the results of the analysis. Here it is seen that the steeper the slope, the higher the risk if the degree of knicking is the same. It is also seen that the vulnerability slope failure increases as the degrees of knicking increases if the slope inclination is the same.

11. CONCLUDING REMARKS

The preceding pages presented a summary of the damage caused by the Hokkaido-nansei-oki Earthquake of July 1993. The feature of the earthquake damage may be summarized as:

(1) The tsunami caused destructive damage and loss of many human lives. The highest tsunami inundation height ever experienced in Japan in this century was recorded. It is important to take the refraction and diffraction into account for tsunami countermeasures.

(2) Bridges suffered at the reinforced concrete piers with termination of main reinforcement without enough anchoring length. The piers which suffered damage can be predicted with sufficient accuracy by a vulnerability evaluation method proposed at PWRI. Seismic strengthening of such type of piers is required.

(3) Most of soil structures such as road embankments and river dikes suffered damage due to soil liquefaction under and around the embankments. It is required to develop appropriate and cheap measures to decrease the damage.

(4) Aside from old dams and dikes of irrigation pond constructed with experience-based construction technology, those dams constructed on rock foundations with modern design and execution technology survived this powerful earthquake without any adverse effects to maintain their safety, and that they are still in sound condition.

(5) Extensive slope failure was developed at Okushiri Island. It was confirmed that the steeper the slope, the higher the risk if the degree of knicking is uniform. It was also confirmed that slopes tend to collapse more easily at higher degrees of knicking if slope inclination is uniform.

(6) Sewage damage concentrated at pipes and manholes. Small TV cameras were effectively used to identify the damage. Uplift of manholes was as high as 50-80 cm, and they were developed due to soil liquefaction.

ACKNOWLEDGEMENTS

For conducting the post earthquake damage investigation, invaluable supports were provided by Hokkaido Developing Bureau, Hokkaido Government, and other local governments. The authors express their sincere appreciation for the warm supports of the organizations and personels concerned. A post earthquake damage survey was jointly made on July 20-23, 1993 with the U.S. Damage Study Team headed by Dr. Riley Chung, Building and

Fire Research Laboratory, National Institute of Standards and Technology as one of the technical cooperation through the Panel on Wind and Seismic Effects, UJNR. Various discussions with the U.S. Damage Study Team members were extremely valuable for the Japan-side. A great appreciation is directed to Dr. Richard N. Wright, U.S. Chairman of the Panel and Mr. Noel J. Raufaste, Secretary of the Panel for their cooperation.

REFERENCES

1) Public Works Research Institute: Report on the Hokkaido-nansei-oki Earthquake, PWRI report, in preparation (in Japanese)
2) Kawashima, K. and Aizawa, K. : Bracketed and Normalized Duration of Earthquake Ground Acceleration, Earthquake Engineering and Structural Dynamics, Vol. 18, 1989
3) Japan Road Association : Part V Seismic Design, Design Specifications of Road Bridges, 1990
4) Kawashima, K. and Aizawa, K.: Attenuation of Peak Ground Acceleration, Velocity and Displacement Based on Multiple Regression Analysis of Japanese Strong Motion Records, Earthquake Engineering and Structural Dynamics, Vol. 14, 1986
5) Kawashima, K., Unjoh, S. Hoshikuma, J. and Nakajima, T. : Damage of Road Bridges by Hokkaido-nansei-oki Earthquake of July, 1993,Bridges and Foundation, Vol. 94-3, March 1993 (in Japanese)
6) Japan Road Association : Part IV Substructures, Design Specifications of Road Bridges, 1980 (in Japanese)
7) Japan Road Association : Guide Specifications for Earthquake Disaster Prevention Measures of Road Facilities (Post Earthquake), 1988 (in Japanese)
8) Kawashima, K., Hoshikuma, J. and Unjoh, S. : Damage Analysis of Reinforced Concrete Bridge Piers by the Kushiro-oki Earthquake of January 1993 and the Hokkaido-nansei-oki Earthquake of July 1993, "nd U.S.-Japan Workshop on Seismic Strengthening of Bridges, Berkeley, California, U.S.A., January 1994
9) Kawashima, K., Unjoh, S. and Iida, H. : Seismic Inspection and Seismic Strengthening of Reinforced Concrete Bridge Piers at Mid-height where Main Reinforcements are terminated with In Adequate Anchoring Length, Report of PWRI, Vol. 189, Public Works Research Institute, September 1993 (in Japanese)
10) Japan Road Association : Seismic Design Specifications of Road Bridges, 1971(in Japanese)
11) For example, Hashimoto, H. et al: Chapter 8 Damage to River Facilities, Report on the Disaster by the Nihon-kai-chubu Earthquake, Report of PWRI, No. 165, Public Works Research Institute, 1985 (in Japanese)
12) Nakamura, A., Yasuda, N. and Iwashita, T. : Damage and Analysis of Dams during 1993 Kushiro-oki Earthquake and 1993 Hokkaido-nansei-oki Earthquake, 26th Joint Meeting, UJNR Panel on Wind and Seismic Effects, Gaithersburg, MD, U.S.A., May 1994
13) Ninomiya, Y., Otsuka, H. and Azuma, T. : Damage of Sewage Facilities due to 1993 Hokkaido-nansei-oki Earthquake, 29th Japan National Conference on Soil Mechanics and Foundation Engineering, Morioka, June 24027, 1994 (in Japanese)
14) Japan Road Association : Design Specifications of Common Utility Ducts, March 1986 (in Japanese)
15) Matsuo, O., Otsuka, H., Ninomiya, Y. and Koseki, J. : Uplift of Sewage Manholes during the 1993 Kushiro-oki Earthquake, 26th Joint Meeting, UJNR Panel on Wind and Seismic Effects, Gaithersburg, MD, U.S.A., May 1994
16) Tanaka, S., Sato, S. and Noguchi, K. : Propagation of Hokkaido-Nansei-Oki Earthquake Tsunami around Cape Aonae,

26th Joint Meeting, UJNR Panel on Wind and Seismic Effects, Gaithersburg, MD, U.S.A., May 1994

17) For example, Yasue, T., Iwasaki, T., Kawashima, K. and Nakano, M. : Seismic Response of Slopes, Civil Engineering Journal, Vol. 23, No. 4, 1981 (in Japanese)

Table 3.1 Damage and Loss in Hokkaido Island

Category		Hokkaido (Unit)
Death		200 (Person)
Missing		33 (Person)
Serious Injured		39 (Person)
Slight Injured		197 (Person)
Number Residental HousesDamaged		3,913 (Houses)
Number Non-residental HousesDamaged		736 (Houses)
Loss	Agricultural Products	11,909,918 (Thousand Yen)
	Public Works	31,422,824 (Thousand Yen)
	Fishery	13,229,326 (Thousand Yen)
	Forestry	21,629,977 (Thousand Yen)
	Sanitation	989,701 (Thousand Yen)
	Commerce and Industry	9,763,154 (Thousand Yen)
	Education	2,523,941 (Thousand Yen)
	Social Education Facilities	468,461 (Thousand Yen)
	Welfare Facilities	472,530 (Thousand Yen)
	Others	721,881 (Thousand Yen)
Total		100,702,194 (Thousand Yen)

Table 4.1 Major Damage to Road Facilities

No.	Damage Type	Site
1	Failure of Embankments	Chirai in Osyamanbe Town on National Road 5
2		Echizen in Esashi Town on Municipal Road
3		Higashihama in Hakodate City on National Road 228
4		Section between Osyamanbe and Yakumo on National Road 5
5		Osyamanbe Bypass on National Road 5
6	Damage to Bridges	Kamiiso-shin Bridge on National Road 228
7		Shin-arikawa Bridge on National Road 228
8		Motoe Bridge in Esashi Town on Municipal Road
9		Yanagisaki Bridge on National Road 229
10		Shin-ei Bridge on National Road 229
11		Osyamanbe Bridge on National Road 37
12		Sakkaishi Bridge on National Road 229
13		Aonae Bridge in Okushiri Island
14		Motouriya Bridge in Kikonai Town on Municipal Road
15		Shin-shiriuchi Bridge in Shiriuchi Town on Municipal Road
16	Settlement of Road Surfaces	Utashima in Shimamaki Town on National Road 229
17		Mena in Imakane Town on National Road 230
18		Kunnui in Osyamanbe Town on National Road 230
19		Yamazaki in Yakumo Town on National Road 277
20		Nodaoi in Yakumo Town on National Road 5
21		Akaigawa in Mori Town on National Road 5
22		Sakkaishi in Kitahiyama Town on National Road 229
23	Uplift of Road Surfaces	Kamiiso in Kamiiso Town on National Road 228
24	Land Slides	No.2 Shiraito Tunnel on National Road 229
25		Section Facing Okushiri Port in Okushiri Island
26		Hutamata in Taisei Town on National Road 229
27	Surface Submergence by Tsunami	Setana Town on National Road 229
28		Miyano in Taisei Town on National Road 229
29		Esashi Town on National Road 227
30	Damage to Snow Shelters	Senjouzaka in Okushiri Island

(Note) Refer to Fig.4.1 for location.

Table 5.1 Major Damage of Road Bridges

Damage Type / Bridge	Route	Bridge Length (m)	Bridge Type		Damage to Superstructure					Damage to Abutment				Damage to Pier		Damage to Bearing Support	
			Superstructure	Foundation	A	B	C	D	E	F	G	H	I	J	K	L	M
Shin−Arikawa	National Road 228	98.5	3 span simply supported steel plate girder	Pile	○		○			○			○			○	
Kamiiso	National Road 228	53.1	4 span simply supported steel plate girder	Direct		○	○		○	○	○		○			○	○
Aonae	Regional Road Okushiri	60.0	2 span simply supported PC girder	Pile						○	○	○	○			○	○
Motoe	Manicipal Road Motoebashi	165.7	7 span simply supported steel plate girder	Pile										○			○
Yanagisaki	National Road 229	181.1	5 span simply supported steel plate girder	Direct		○		○	○		○		○			○	○
Oshamanbe	National Road 37	150.1	5 span simply supported steel plate girder	Caisson	○		○								○	○	○
Motouriya	Manicipal Road Uriya 2	63.0	2 span simply supported PC girder	Pile										○			
Shin−Shiriuchi	Manicipal Road Motomachi 1	148.0	7 span simply supported PC girder	Caisson										○			

Note) Damage to Superstructure : A:Slab, B:Girder, C:Expansion Joint, D:Falling−off Prevention Device, E: Handrail
Damage to Abutment : F:Parapet, G:Wing, H:Inclination, I:Subsidence of Embankment
Damage to Pier : J:Pier, K:Inclination
Damage to Bearing Support : L:Stopper. M:Shoe Mortar

Table 8.1 Damage of Pipes and Joints at Oshamanbe Town

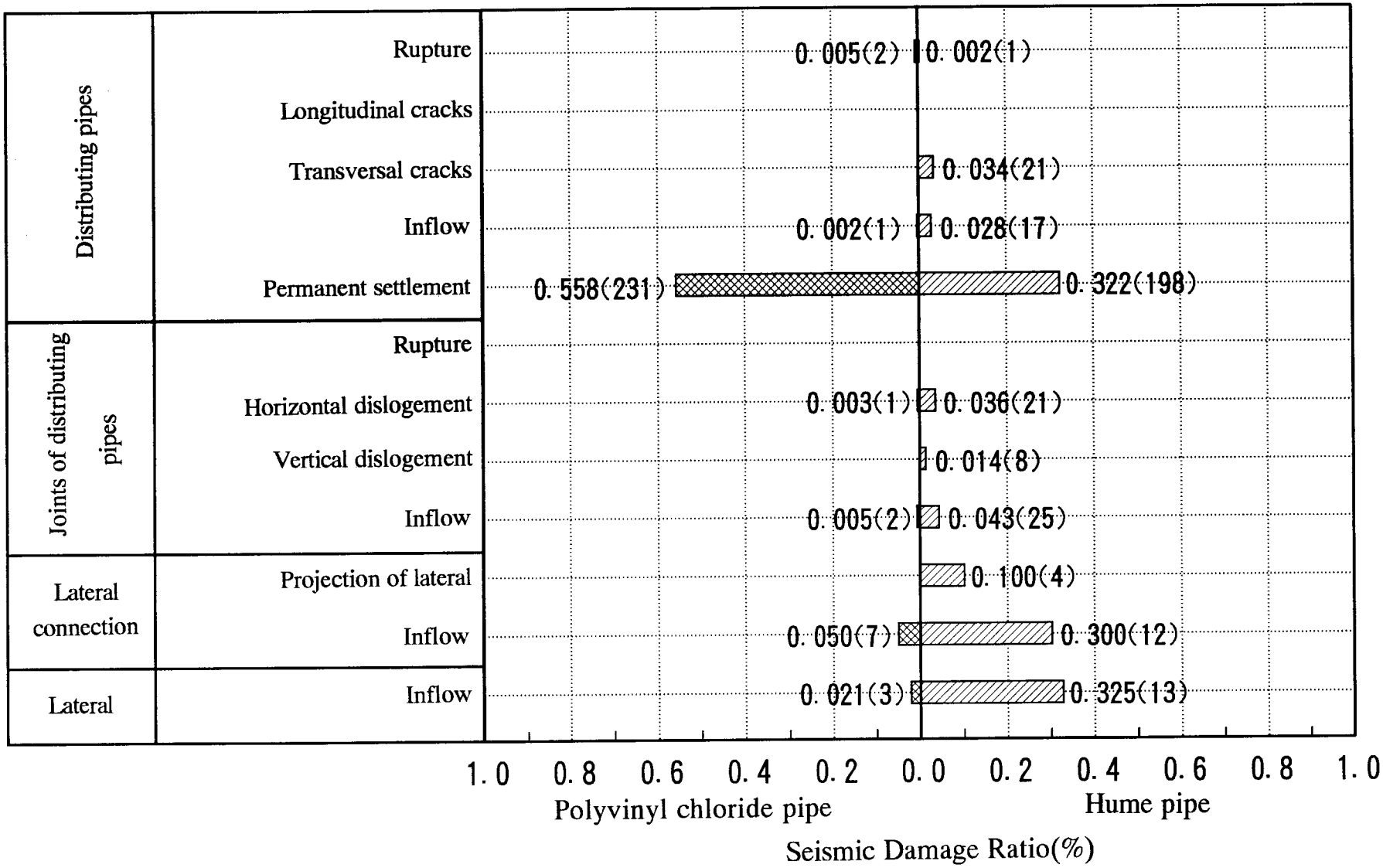

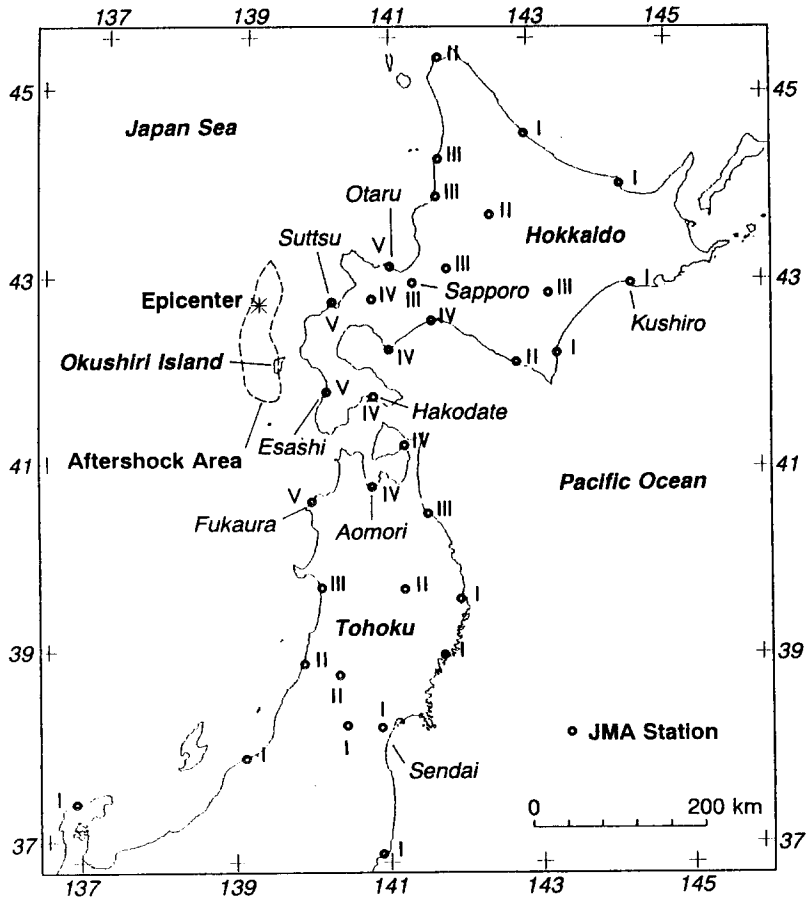

Fig. 2.1 JMA Seismic Intensity

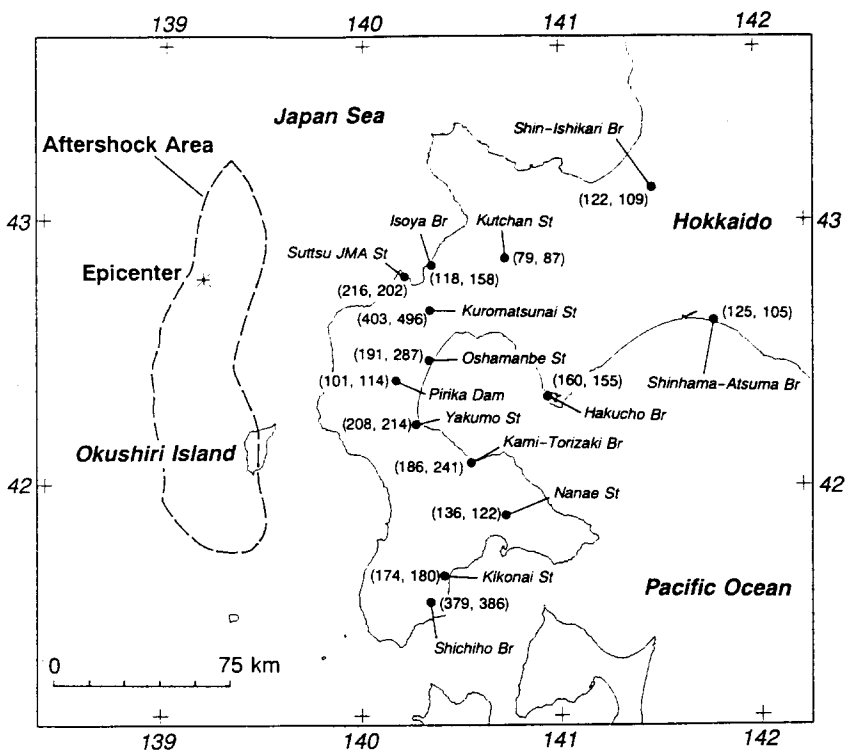

Fig. 2.2 Peak Ground Accelerations (Two Horizontal Components)

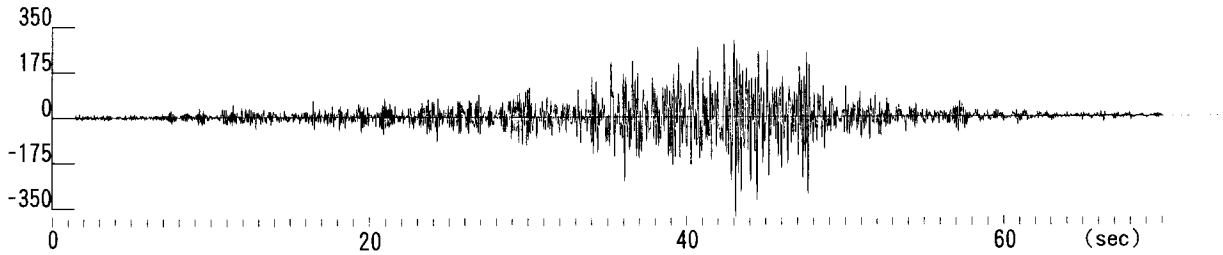

(a) Transverse Component (a_{max} = 386 gal)

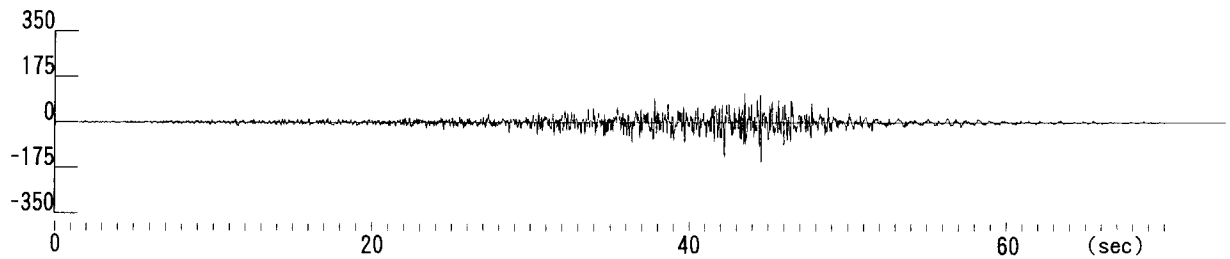

(b) Vertical Component (a_{max} = 153 gal)

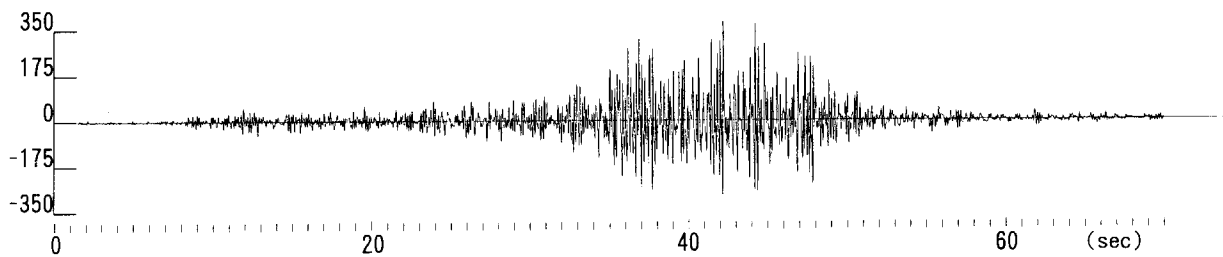

(c) Longitudinal Component (a_{max} = 379 gal)

Fig. 2.3 Ground Accelerations at Shichiho Bridge Site

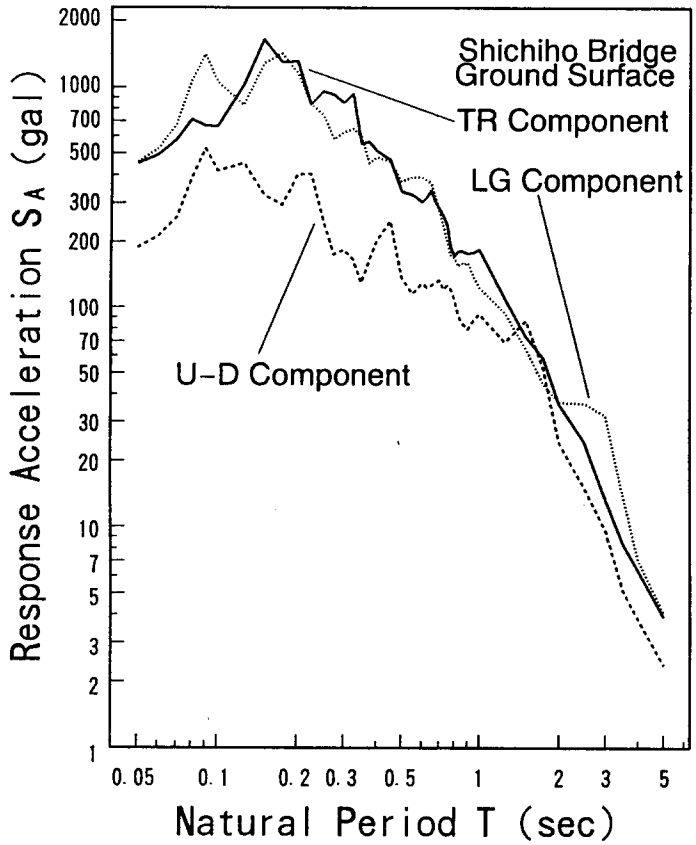

Fig. 2.4 Acceleration Response Spectra for the Records at Shichiho Bridge Site

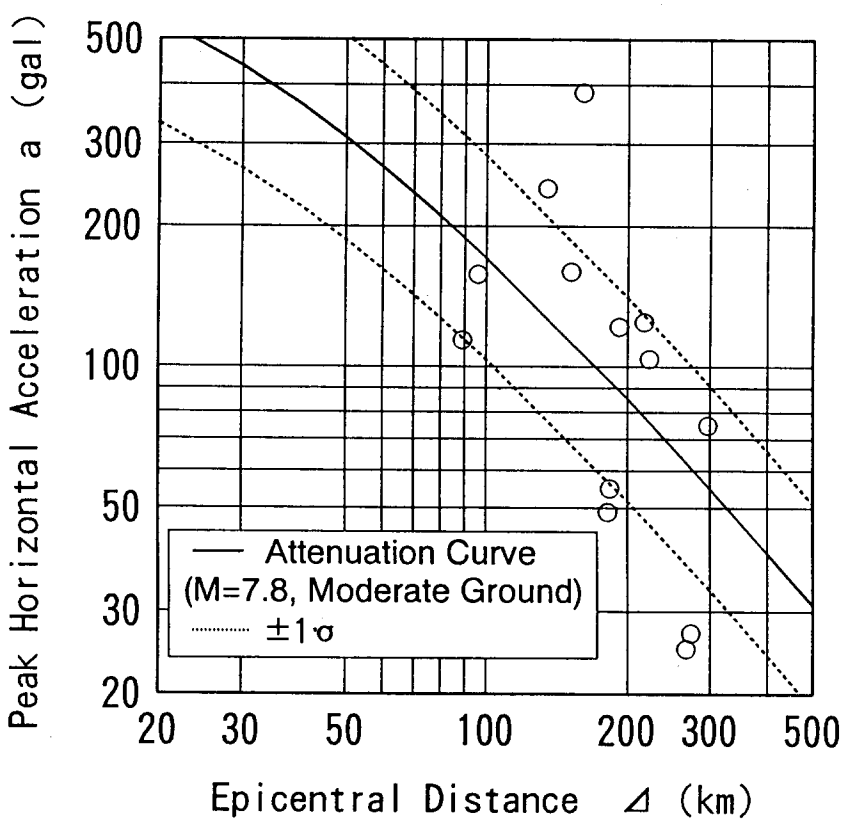

Fig. 2.5 Attenuation of Peak Ground Acceleration

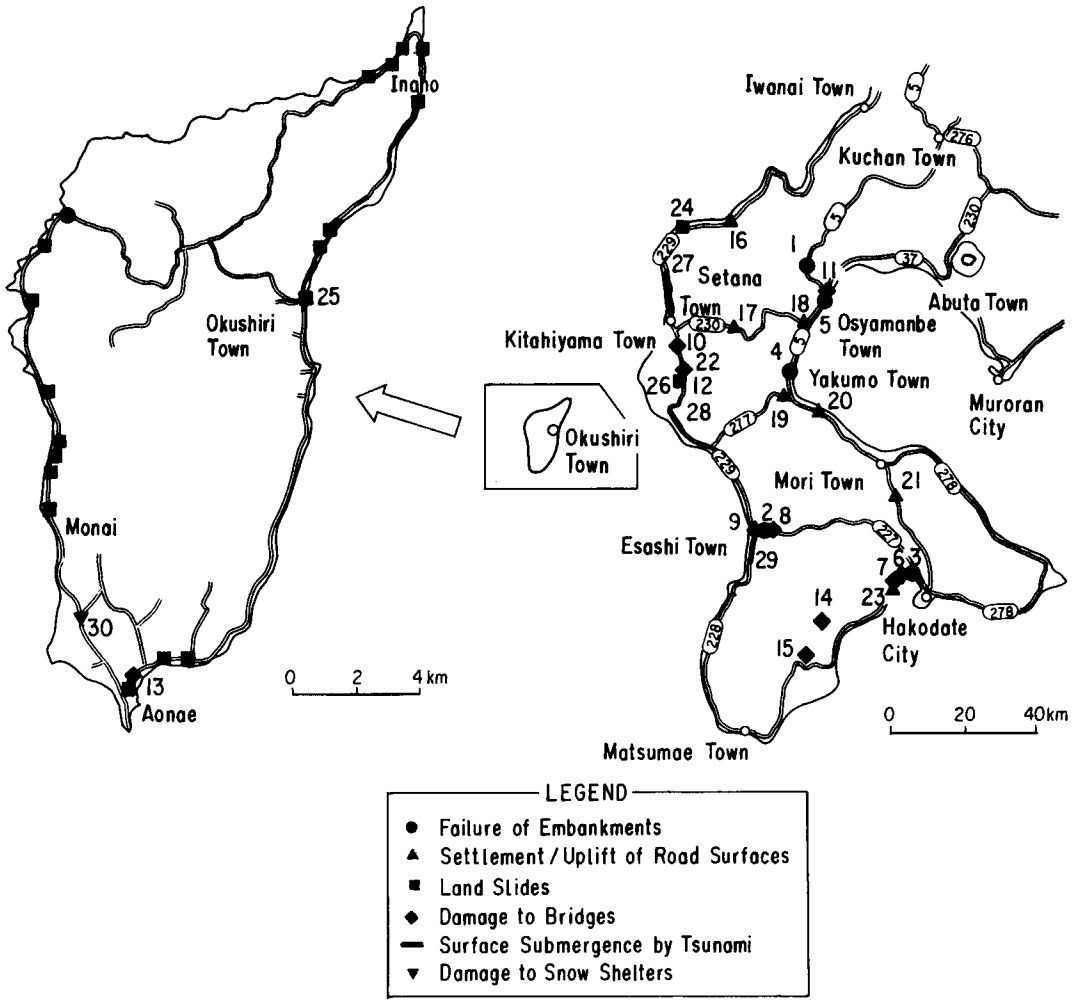

Fig. 4.1 Locations of Road Damage

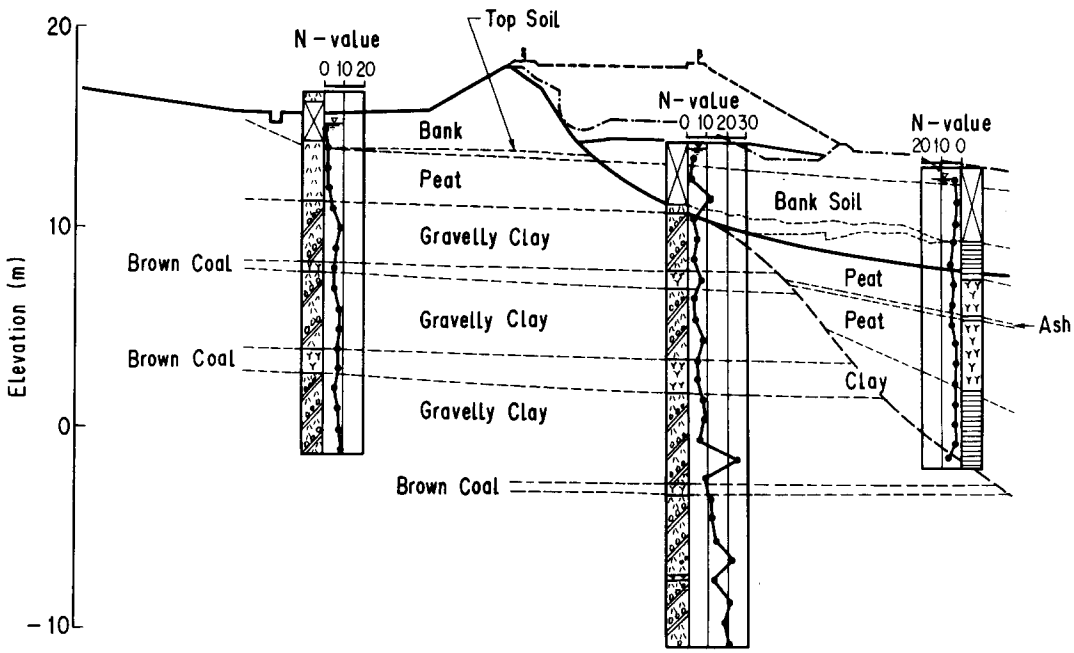

Fig. 4.2 Cross Section of Collapsed Embankment on National Road 5 at Chirai, Oshamanbe

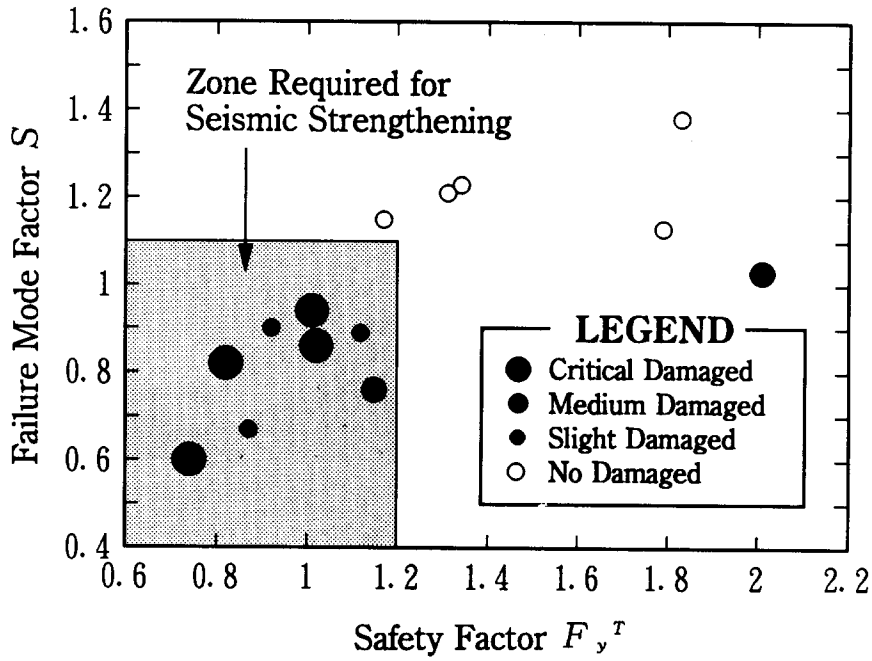

Fig. 5.1 Evaluation of Seismic Vulnerability of Reinforced Concrete Piers without Enough Anchoring Length at Termination Section of Main Reinforcements

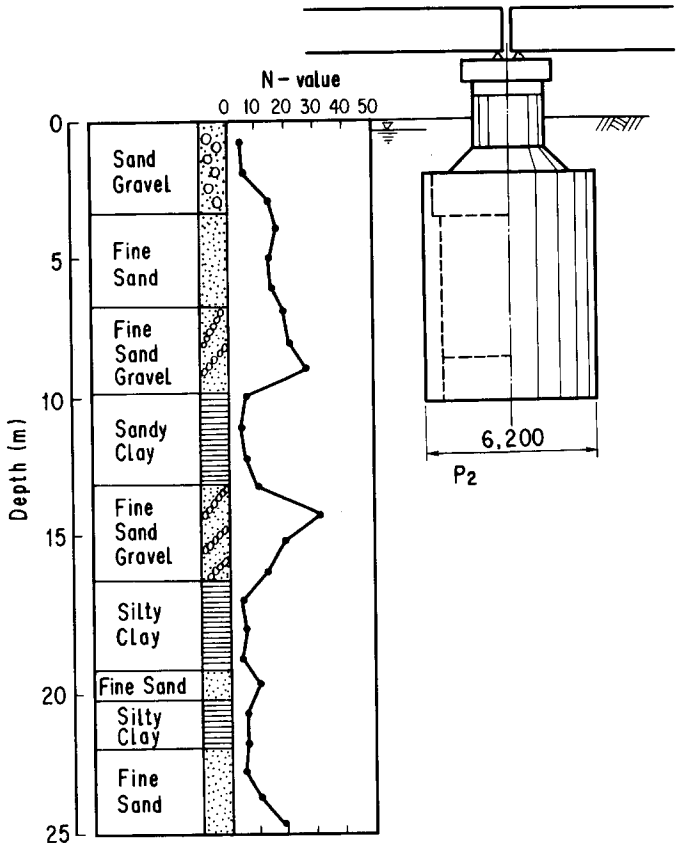

Fig. 5.2 Soil Boring Data at Oshamanbe Bridge

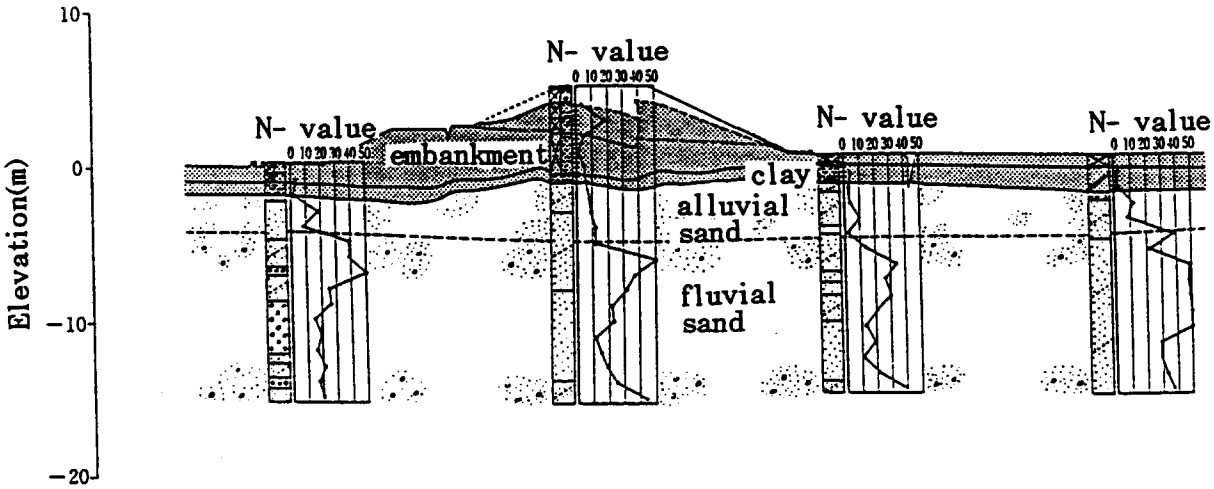

Fig. 6.1 Cross Section of Kabutono Dike (Shiribeshi–Toshibetsu River, Left–Side Dike)

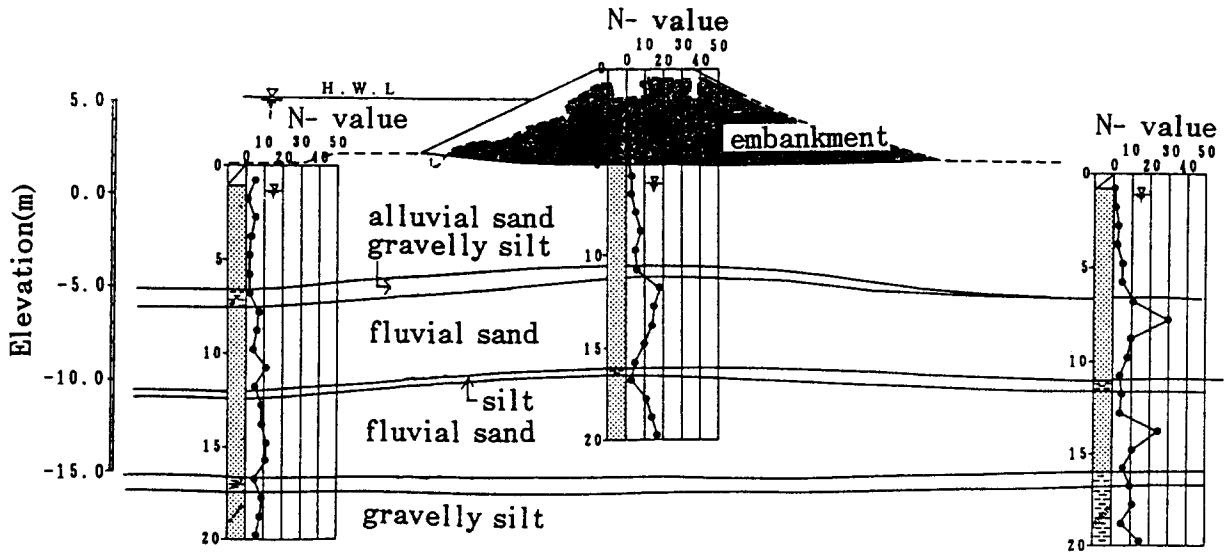

Fig. 6.2 Cross Section of Hatsuta Dike (Shiribetsu River, Right-Side Dike)

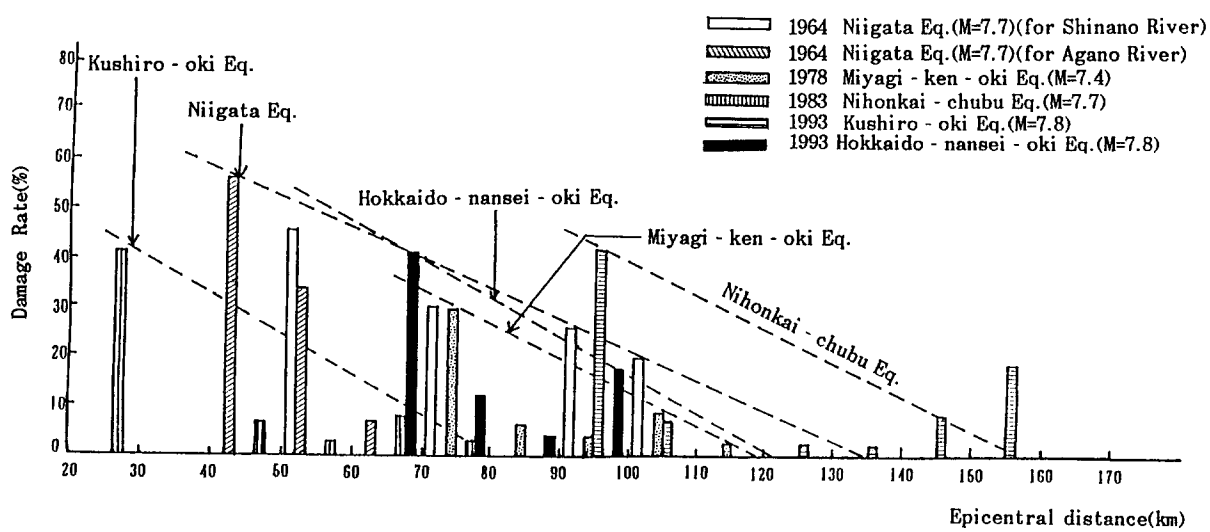

Fig. 6.3 Epicentral Distance vs. Damage Rate of River Dikes

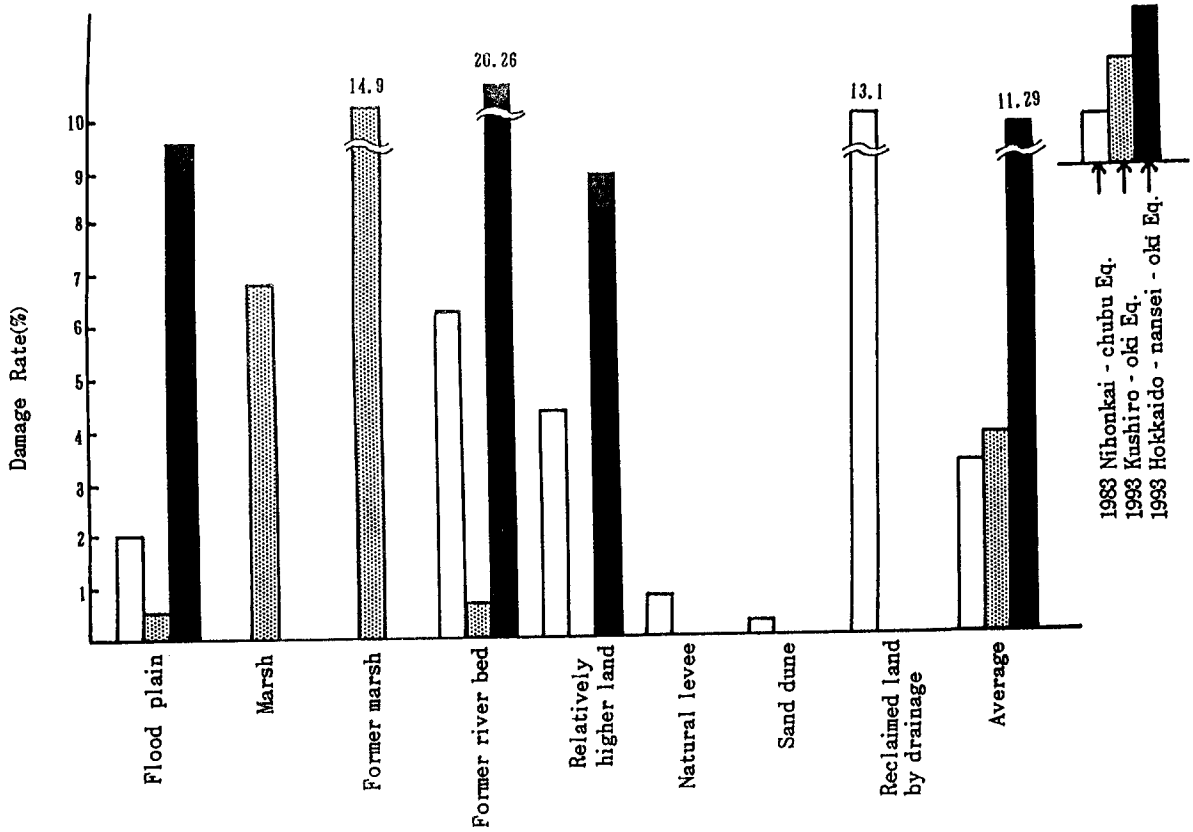

Fig. 6.4 Micro Land Form vs. Damage Rate of River Dikes

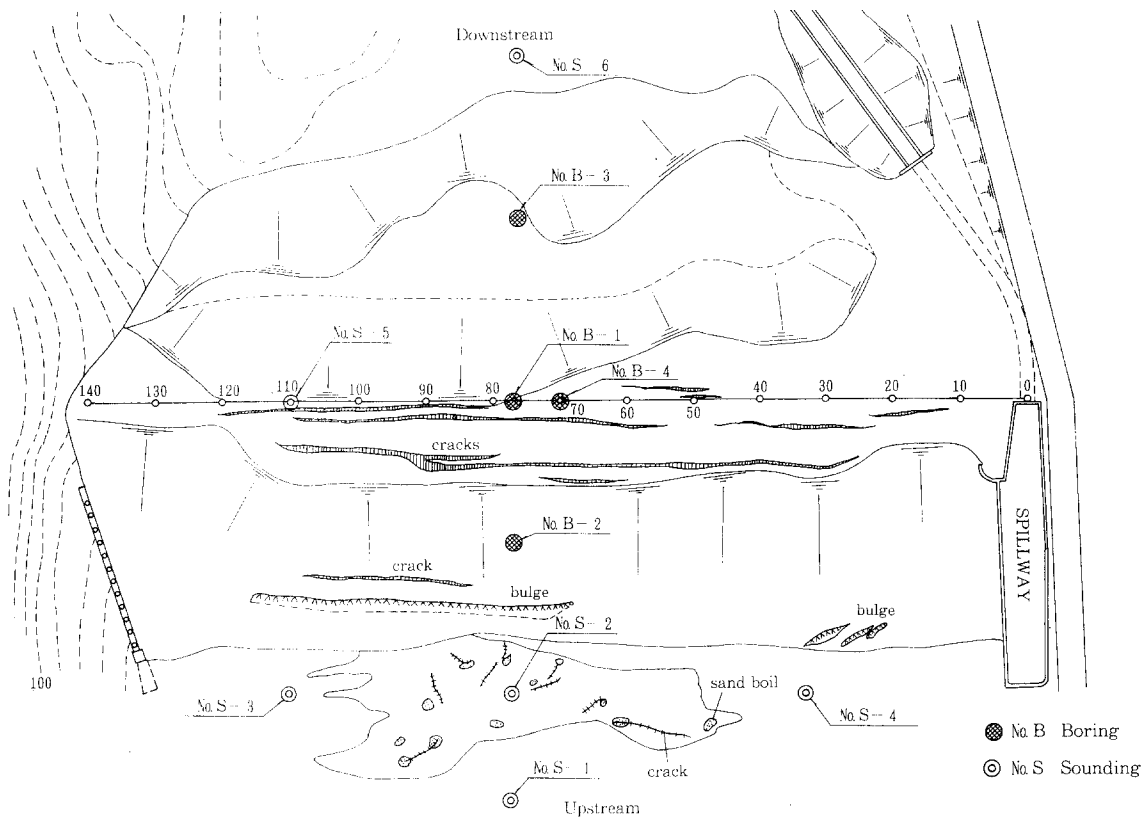

Fig. 7.1 Niwa–Ikumine Dam

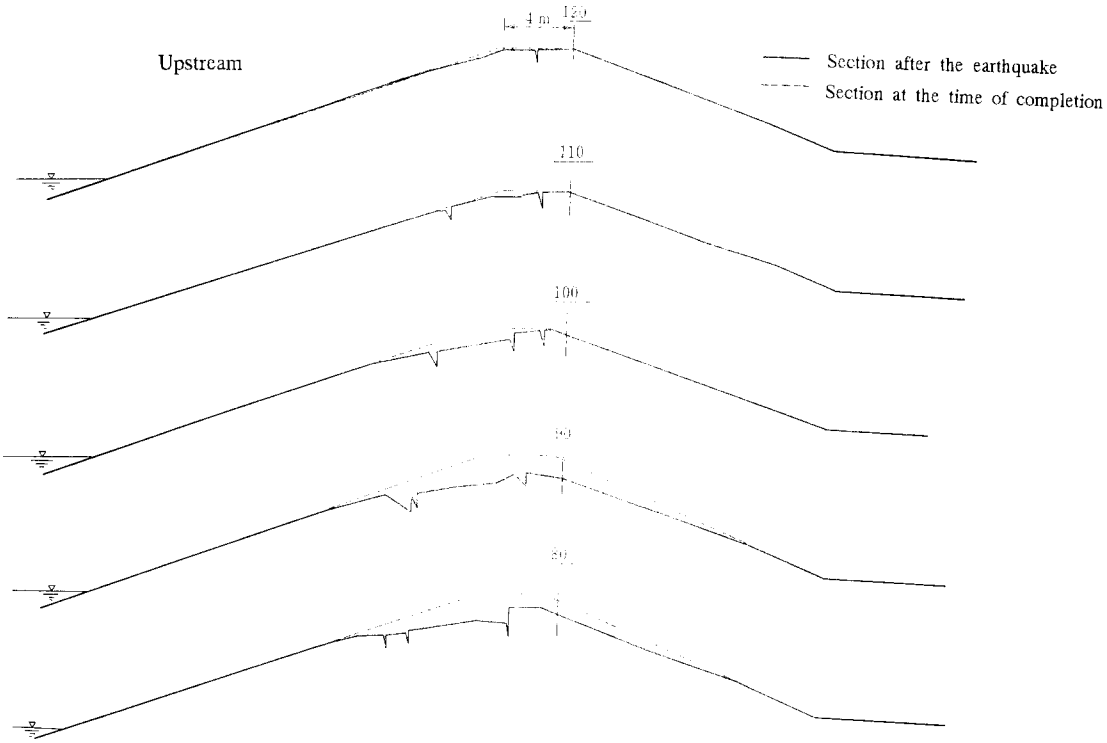

Fig. 7.2 Cross Sections of Niwa–Ikumine Dam

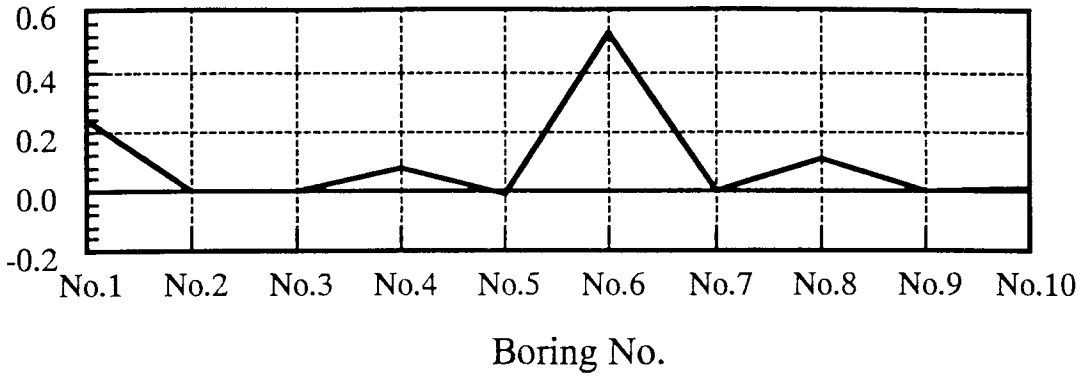

(a) Uplift of Manholes

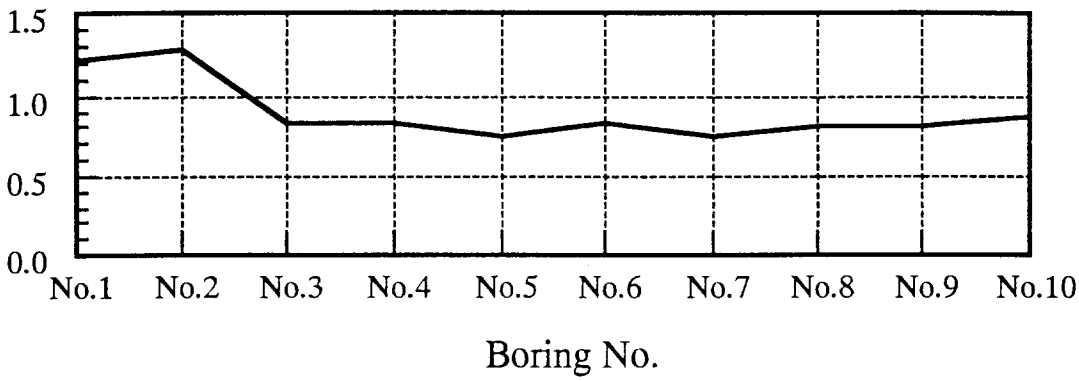

(b) Liquefaction Resistance Factor F_L

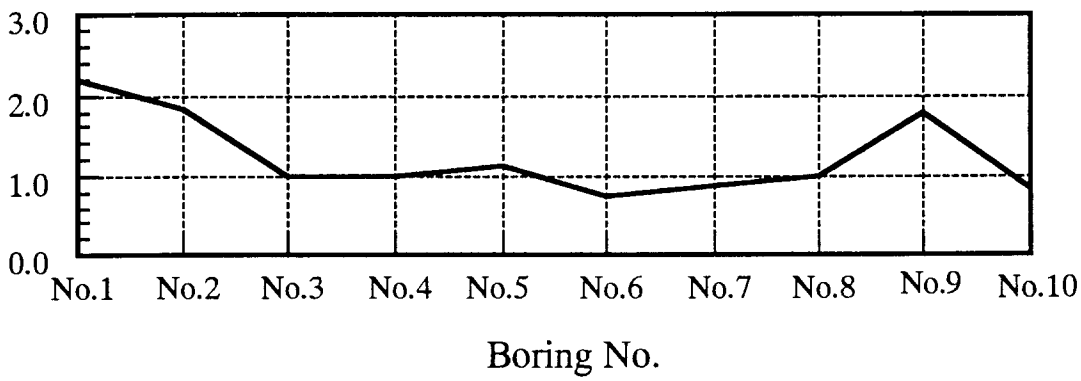

(c) Safety Factor F_S by Eq. (8.1)

Fig. 8.1 Dependence of Uplift of Manhole on Liquefaction Resistance Factor F_L and Safety Factor F_S by Eq. (8.1)

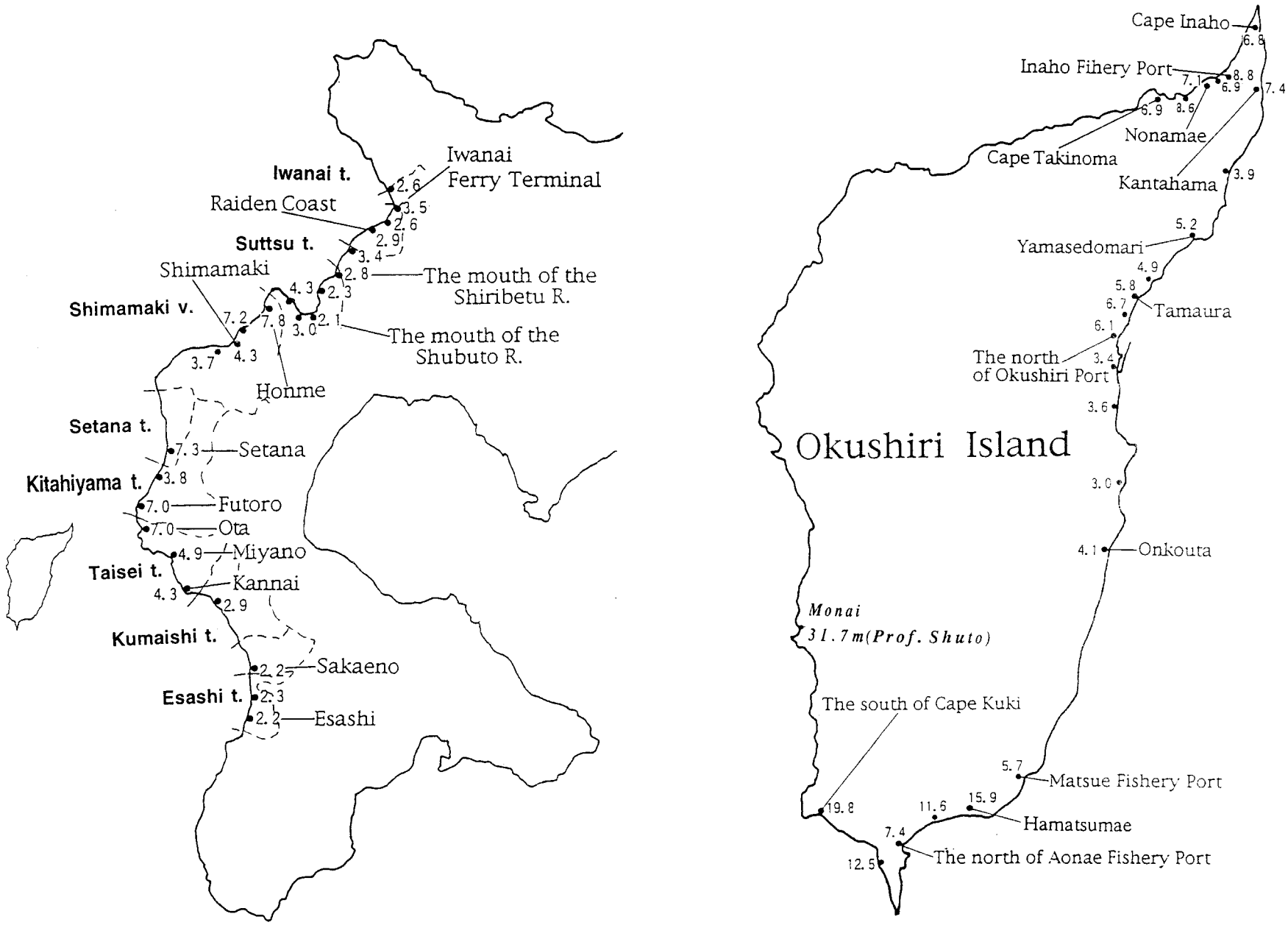

(a) West Cost of Hokkaido

(b) Okushiri Island

Fig. 9.1 Tsunami Inundation Height

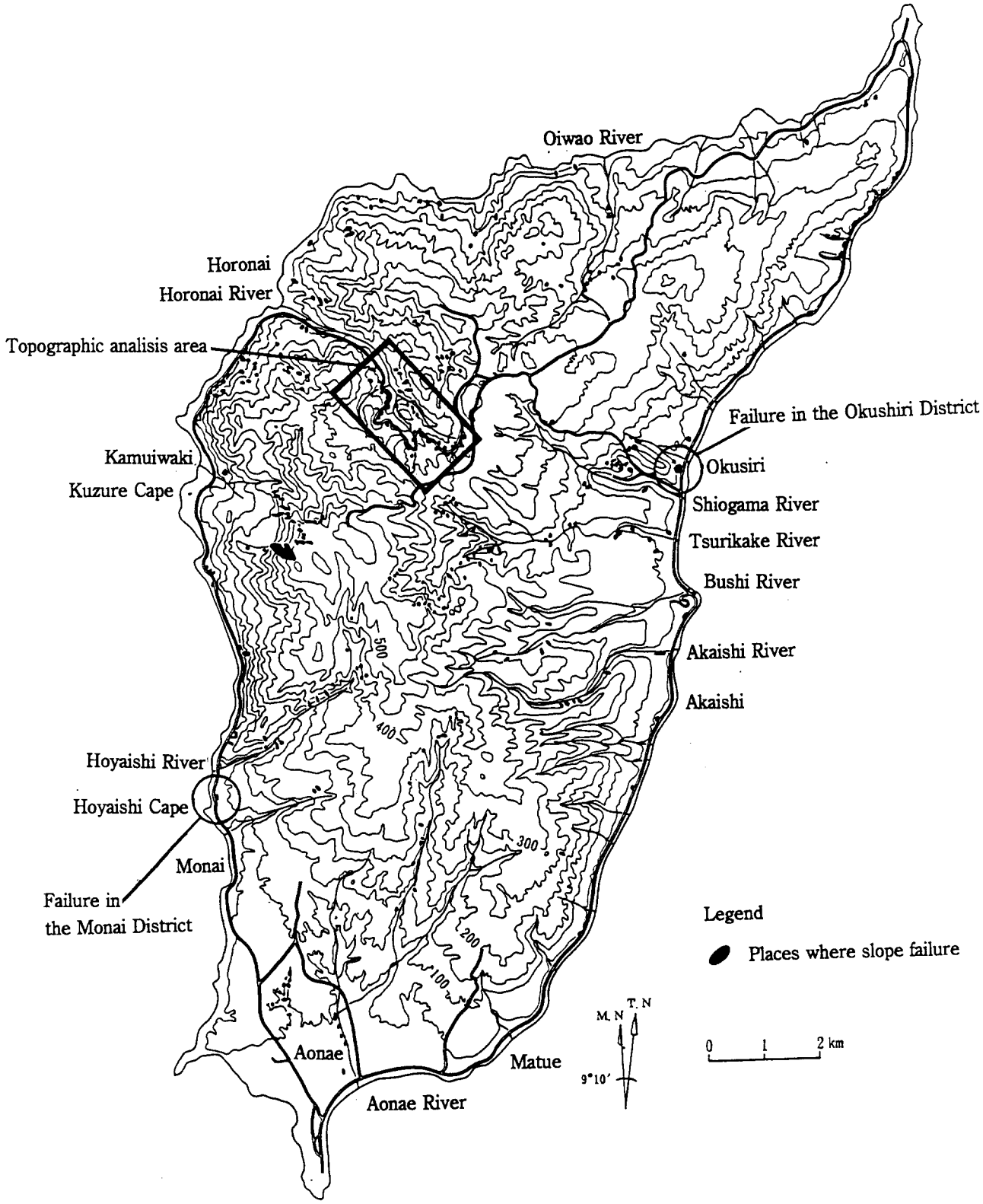

Fig. 10.1 Locations of Slope Failures

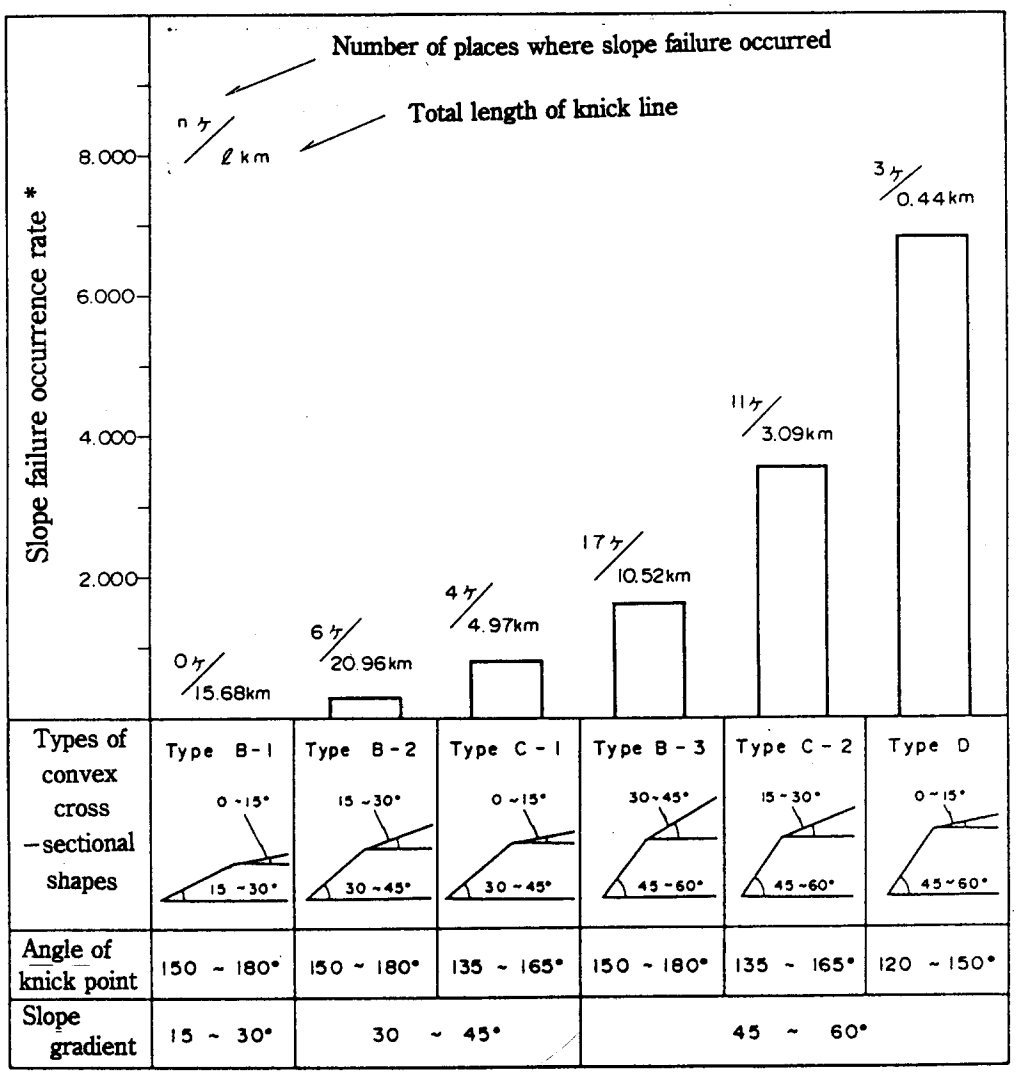

* Number of places where slope failure occurred per 1km of knick line

Fig. 10.2 Dependence of Slope Failure Occurrence Rate on Type of Convex Cross-Sectional Shape

Photo 4.1 Collapse of An Embankment (National Road 5)

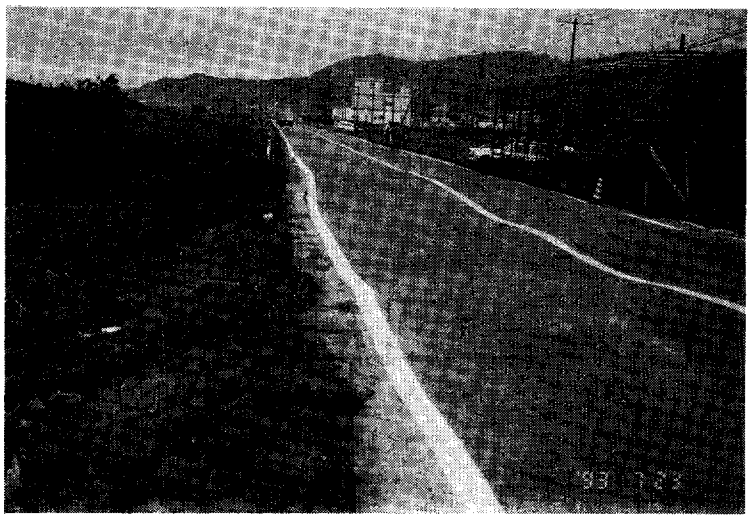

Photo 4.2 Permanent Undulating Deformation of Road Surface (National Road 5)

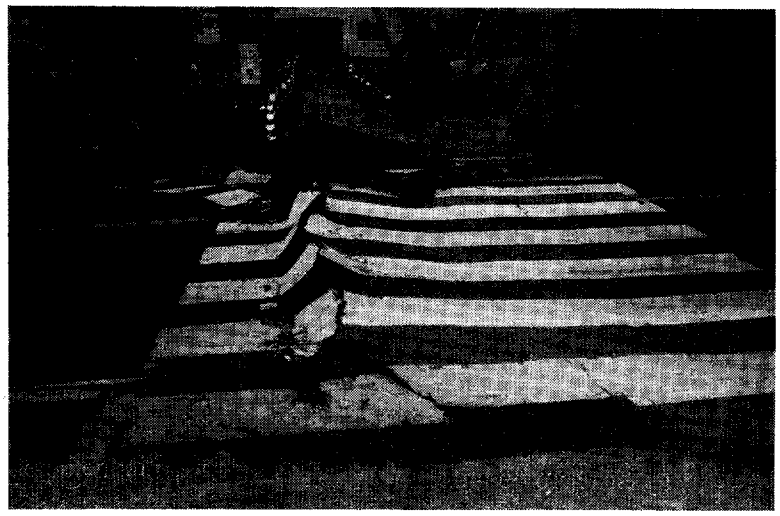

Photo 4.3 Crash and Uplift of Pavement (National Road 228)

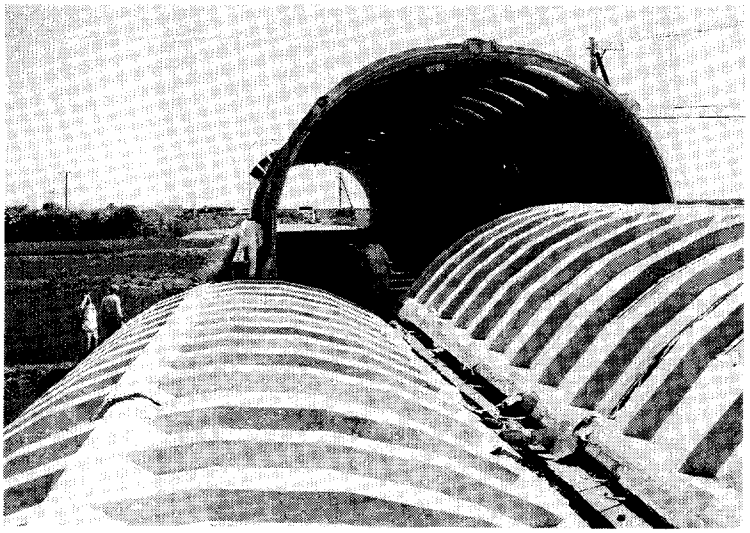

Photo 4.4 Collapse of A Snow Shelter (Okushiri Island)

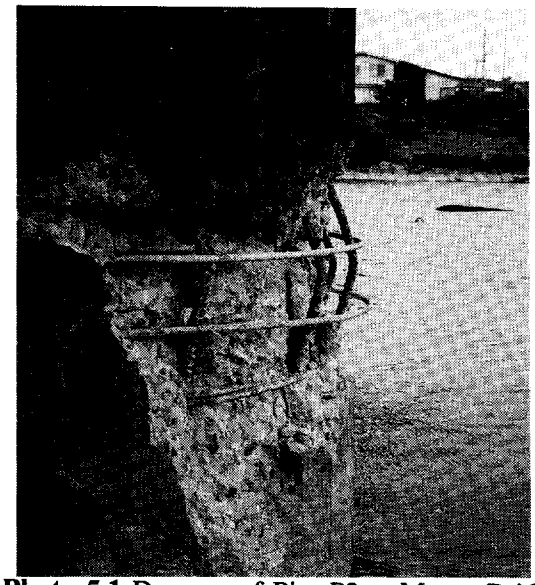

Photo 5.1 Damage of Pier P3 at Motoe Bridge

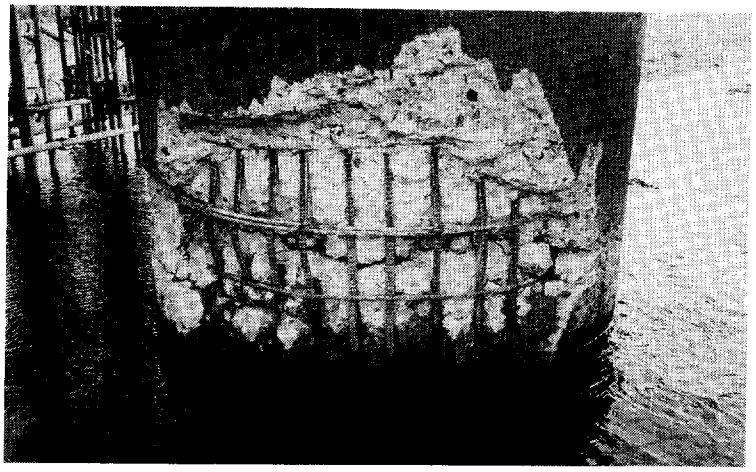

Photo 5.2 Damage of Pier P3 at Shin-shiriuchi Bridge

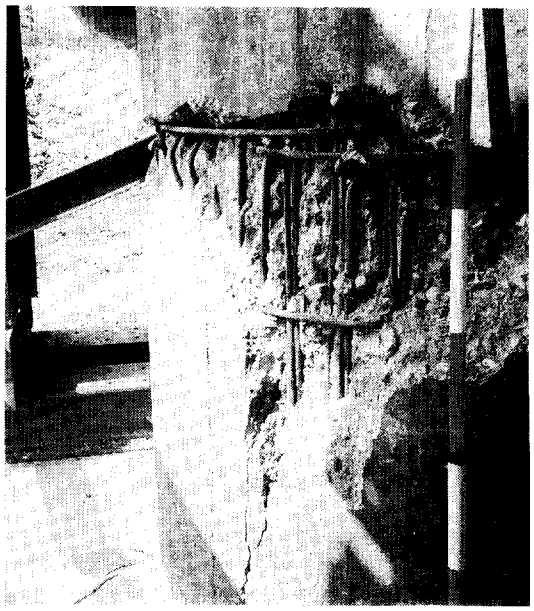

Photo 5.3 Damage of Pier P1 at Motouriya Bridge

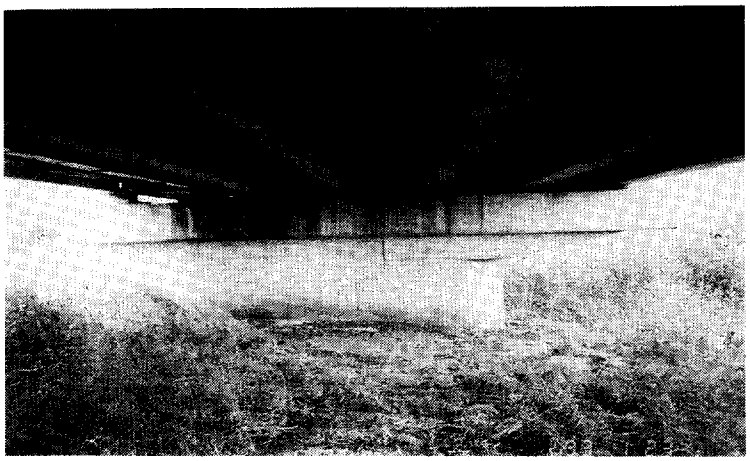

Photo 5.4 Inclination of Piers and soil Liquefaction (Oshamanbe Bridge, Pier P2)

Photo 6.1 Damage to Hatsuta Dike (Shiribetsu River, Right–Side Dike)

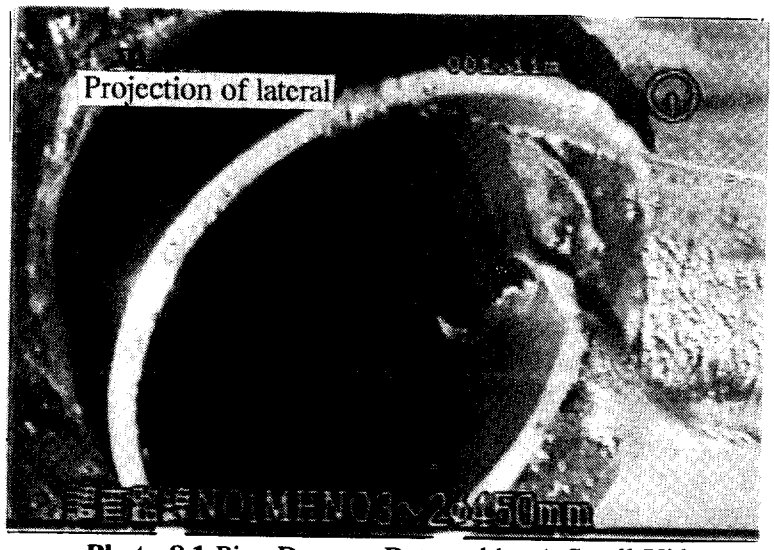

Photo 8.1 Pipe Damage Detected by A Small Video

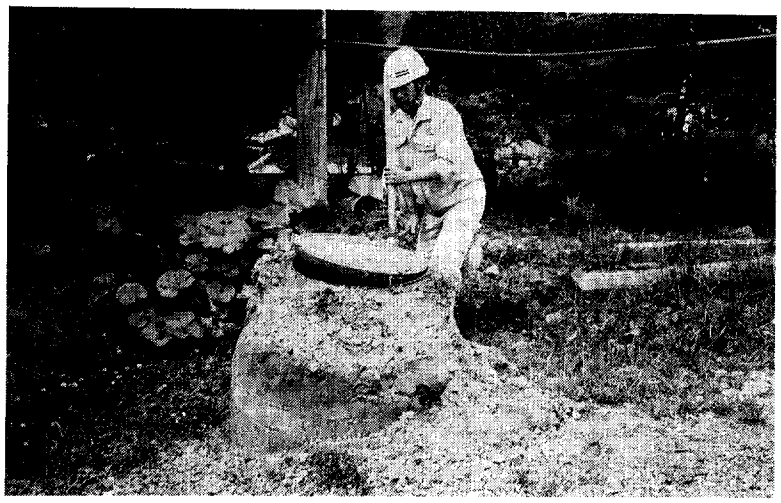

Photo 8.2 Uplift of Manholes

Photo 9.1 Tsunami Damage at A Village Backyard of Inaho Fishery Harbour

Photo 9.2 Tsunami Damage at Aonae Fishery Harbour

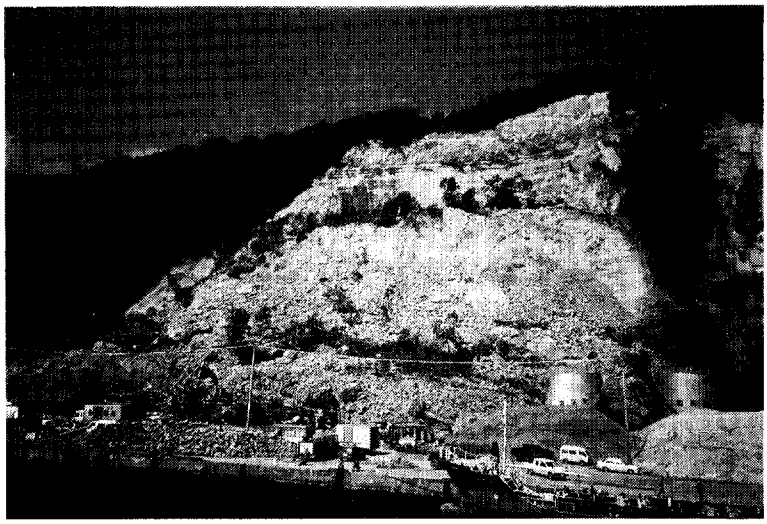

Photo 10.1 Slope Failure at Okushiri District

12 July 1993 Hokkaido-Nansei-Oki Earthquake

by

Riley M. Chung[1]

ABSTRACT

An earthquake measuring 7.8 on the Richter scale struck northern Japan at 9:17 a.m., EDT, Monday, July 12, 1993. The quake, with epicenter about 80km west of Hokkaido Island, was the largest Japanese earthquake in the past 15 years. Total life loss has reached 231, most of them from the tsunamis and fires. Total dollar loss was estimated at $1B.

Immediately after the earthquake and under the auspices of the U.S.-Japan Panel on Wind and Seismic Effects, the U.S. dispatched a team to jointly investigate the impact of this earthquake to the built environment. The earthquake provided an opportunity to study the performance of wood-framed buildings, the causes of and response to fires, the effect of tsunami, and the performance of lifelines and other infrastructure systems.

Damage to the built environment was primarily caused by tsunamis, fires, landslides, and ground failures, i.e., liquefaction, sand boils, and lateral spread. Okushiri, a small island off the coast of Hokkaido and 48km south of the epicenter, was devastated by the fires, tsunamis, and landslides. Buildings and houses performed well, with minor damages noticed in a some instances. Most bridges suffered no damage. Those with damage experienced failure at the interface of the bridge deck and their abutments. Lifeline systems, especially those in Hokkaido, performed well. Those that had been damaged were restored quickly after the quake. Tsunami warnings were issued promptly by Japanese authority. However, they were still not quick enough to reduce the casualties in coastal villages of Okushiri Island and a few others along the west coast of Hokkaido. Experience from the 1983 Nihonkai-Chubu tsunami helped the villagers' prompt evacuation.

INTRODUCTION

The powerful earthquake measuring 7.8 on the Richter scale struck northern Japan at 9:17 a.m., EDT, Monday, July 12 (or 10:17 p.m., local time). The quake, with epicenter about 80 km west of Hokkaido Island, was the largest Japanese earthquake in the past 15 years (Figure 1). The earthquake provided U.S. and Japanese researchers and practitioners an opportunity to study the performance of the built environment against earthquake forces. Immediately after the quake, under the auspices of the U.S.-Japan Panel on Wind and Seismic Effects, United States. dispatched a team to visit the disaster sites. The team stayed in the field for about one week, teaming up with a Japanese team led by the Public Works Research Institute, to conduct postearthquake investigations.

Okushiri, a small island southwest of Hokkaido and 48 km south of the epicenter, was devastated by the quake, resulting from tsunamis, fires, and landslides (Figure 2). Less damage to buildings, roads, railroads, tunnels, bridges, and other lifelines were observed on Hokkaido. As of September 1993, the final count of life loss was at 231, most of them tsunamis, and the total dollar loss was placed at around $1B.

The teams were to collect perishable data and observe and assess the performance of various structures against seismic loading. Key observations and conclusions from each of the studied areas are given in this paper.

---

1. National Institute of Standards and Technology

EARTHQUAKE MECHANISM AND STRONG GROUND MOTION

The subduction plate boundary along the Japan Sea coast of northern Honshu and Hokkaido has only been recognized recently. It is estimated that subduction may have begun about one million years ago at a rate of 1 cm/yr, which would have resulted in only 10 km of subduction to date. The earthquake struck on July 12 at 22:17 p.m. local time at latitude 42°47' North, longitude 139°12' East. The aftershocks define a zone about 150 km long (north-south) and 30 km wide (east-west) having a predominant depth range of one to 20km (Figure 3).

The earthquake was not preceded by any anomalous geophysical measurements. The currently available data appear to be mostly consistent with a rupture model in which the northern part of the earthquake involved westward subduction and the southern (and predominant) part of the earthquake involved eastward subduction. However, the interpretation is preliminary, and a conclusive interpretation will evolve only after a considerable period of data analysis and interpretation.

Strong ground motions were recorded on a variety of instrument types by numerous agencies. There were no strong motion recordings from Okushiri Island or the immediately adjacent southwest coast of Hokkaido between Taisei and Motsutanosaki. At a cemetery on Okushiri, 80 percent of the tombstones were overturned, suggesting peak accelerations in the ranges of 0.4 to 0.5g. On the immediately adjacent mainland of Hokkaido, there was no major structural damage to buildings, and few gravestones were overturned, suggesting that the ground motions were not unusually high.

The duration of strong ground motion was approximately one minute at most locations within about 100 km from the rupture surface, which is compatible with the source duration of about one minute inferred from teleseismic seismograms, and is expected from an earthquake of this magnitude. Comparing the attenuation relationships for subduction earthquakes for soil sites currently used in the United States, the peak accelerations recorded during this earthquake are generally larger for distances ranging from 70 to 150 km and attenuate more rapidly than the attenuation relations (Figure 4). This rapid attenuation is interpreted as being due to higher anelastic absorption as the result of the thermal effects of volcanism.

TSUNAMIS

The earthquake produced one of the largest tsunamis in Japan's history. Within 2 to 5 minutes, extremely large waves engulfed the Okushiri coastline and the central west coast of Hokkaido (Figure 5). At Okushiri, the tsunami was refracted by the shoaling bathymetry at both ends of the island. Extensive damage occurred at both southern and northern tips of Okushiri, particularly in the south at the town of Aonae. Tsunami vertical runup measurements varied between 15 to 30 m over a 20-km portion of the southern part of Okushiri Island, with several 10-m values on the northern portion of the island (Figure 6). Along the west coast of Hokkaido, no survey values exceeded 10m, but damage was extensive at several coastal towns. Given the sudden onset of the tsunami and its high energy, it is amazing that the life losses were comparatively low.

CONFLAGRATION

The town of Aonae, a fishing village of about 1,600 population, experienced the only known fire ignitions as a result of the earthquake. The fires eventually consumed 190 houses and buildings over an 11 hour period. Buildings (or houses) are typically one- and two-story post and beam (heavy timber) construction, although some steel and concrete (commercial) structures were also present. Exterior coverings are generally non-combustible cement board cladding over wood, with corrugated metal roofing. Typically each home has a 490 L kerosene tank for heating which sat on a steel rack on cement blocks, and were not anchored down; and also a pair of propane tanks for cooking, typically 20 kg. The propane tanks are normally not secured.

Two fires broke out after the earthquake. The first fire began in a structure above the area directly affected by the tsunami. Fire department officials thought the fire began from an overturned kerosene

tank; the ignition source is unclear since power was knocked out by the quake. Villagers told of the quake overturning all their furniture, so numerous ignition sources such as cooking and heating appliances are possible.

The fire spread was relatively slow because of low wind velocity. The fire fighters had been battling the fire for about 2 hours when a second fire broke out to their rear near the shore in an area which had been devastated by the tsunami. Finding themselves between two fires, the firefighters took up a new position to the south of the second fire and continued to fight the fire. After 5-1/2 hours, they ran out of water in the last accessible cistern and decided to draft sea water but access to the sea was blocked by debris. Eventually the fire fighters had to knock down houses on the fire side of a road to widen the fire break and as a result, saved the remainder of the town.

The principal mechanisms of building-to-building fire spread involved ignition of exterior wood trim, radiant ignition of combustible contents through windows, spread along scrap wood between buildings, and the burning of kerosene and propane tanks.

LANDSLIDES

Landslides were triggered throughout Okushiri Island and throughout much of the southern peninsula of Hokkaido. The slides consisted mainly of rock falls and rock slides on steep (>50°) natural slopes and engineered cut slopes. Volumes ranged from several cubic meters to the 800,000 m^3 rockslide that buried the Yo Yo Hotel at Okushiri Port (Figure 7). As of July 24, 1993, there were 10 confirmed casualties and 10 still missing at the hotel site. The scarp of this major rock slide is a planar to slightly concave outward surface that is highly weathered. This suggests that the scarp is a pre-earthquake fracture that provided a structural discontinuity or surface of weakness along which failure took place.

Numerous rock falls and slides took place along the coast of the island where extremely steep slopes of volcanic breccia, basalt, and tuffaceous sandstone shed rock debris that was shaken apart along highly weathered fractures.

The occurrence of rock falls and rock slides triggered by the earthquake on the southern Hokkaido Peninsula was similar to that on Okushiri Island. These types of failures appeared to be most numerous on the western coast of the peninsula where the steepest slopes exist. About 15 km north of Setana on Highway 229, one of the sections of a talus shed, made from concrete ducts, collapsed when debris from a rock fall struck the concrete duct work (Figure 8). Total volume of the rock fall was several hundred cubic meters and originated from a near vertical cliff about 60 m above the highway.

The distribution and types of landslides triggered by the earthquake on Okushiri Island and the southern Hokkaido Peninsula were characterized by the absence of small rockfalls and rock slides from both natural and cut slopes. This absence was, in part, due to the wide fracture spacing within the andesitic volcanic breccia that is predominant along the coasts of these geographical locations. The frequency content of strong shaking during the earthquake may also be another factor influencing the size of failures and fragment size. Preliminary strong motion recordings indicate that the accelerations were somewhat low for a magnitude 7.8 earthquake and that frequencies of 5 Hz and greater are lacking. The long duration of about one minute and relatively low frequencies of shaking would thus favor displacement of larger blocks of rock and individual boulders of one meter diameter and larger.

GEOTECHNICAL EFFECTS

The earthquake caused widespread liquefaction in the southwestern part of Hokkaido and at one location near Aonae on Okushiri Island. The areas affected included alluvial river valleys on the west coast of Hokkaido, alluvial plains along the east and south coasts of Hokkaido, and filled ground at several ports. On Okushiri Island, liquefaction developed in an alluvial plain near the Aonae airport. The observed effects included sand boils, fissure, lateral spreads, ground oscillation, loss of bearing strength, ground settlements, and the buoyant rise of manholes and buried tanks. These effects caused damage to

constructed works, but in several notable instances well-built structures survived the occurrence of liquefaction without significant damage.

Most of the ports on southwestern Hokkaido and on Okushiri Island suffered some damage, typically seaward tilt of quay walls accompanied by fissures, ground settlements, and sand boils in filled areas behind the walls. None of the damages was catastrophic, nor were there any major disruptions to port operations as a consequence of liquefaction. The most severe damage occurred at Pier 1 of Hakodate Port (Figure 9). Fortunately, Pier 1 is an older part of the port which was used primarily for the docking of unused ships. Its severe damage therefore did not affect the port operation. At Pier 1, large ground fissures and settlements disrupted an asphalt-paved apron behind the quay wall, and the wall displaced or tilted seaward by as much as 3 m. The fissures were as wide as 1 m and generally paralleled the wall. Ground settlements in the filled area were as great as 0.5 m.

Several storage tanks were damaged during the quake. At Pier 16 of Hakodate Port, a cement storage tank, 20 m high and 8 m diameter, tipped due to loss of bearing strength as a result of liquefaction of surrounding soils (Figure 10). The tank tipped about 2.5° southward during the quake. The most spectacular failure of a tank was the buoyant rise of a buried oil storage tank at an industrial facility southwest of the Highway 229 bridge over the Assabu river, about 6km north of Esashi. The tank was 7.2 m long with a diameter of 1.8 m, and was about one-third full of oil at the time of the earthquake (Figure 11). It was shallowly buried with a cover slab and few tenths of a meter of soil above the tank.

Liquefaction and consequent ground failure also contributed to the outages of many lifeline systems, which were reported after the quake. Japanese utility personnel responded quickly, and most of the damage was repaired and service was resumed by the time the study team arrived at the sites one week after the quake.

The study team also observed many buildings that were constructed in areas where minor to rather severe liquefaction effects occurred. Most of the buildings performed well, some exceptionally well; but a few suffered rather severe damage. The most spectacular damage was at the Oshamanbe Nakonosawa Elementary School, located west of Highway 5 in Oshamanbe. The school consists of two main structures, a wood-frame classroom building with glue-laminated beams and a steel-frame gymnasium (Figure 12). They were surrounded by grassy open areas and playing fields. The area beneath and surrounding the buildings had been filled. Liquefaction occurred in sediments beneath the site generating widespread sand boils, ground fissures, and ground displacements. Despite these ground disturbances, other than fractured piles and minor cracks in foundation walls, the buildings were undamaged. An overwhelming majority of houses and small buildings performed well in areas of minor liquefaction-induced ground disturbance examined by the study team. One reason for the excellent performance of these structures may have been the strength of their foundations, which consist of a gridwork of well reinforced and interconnected wall footings.

Several bridges suffered minor damage as a consequence of liquefaction-induced ground displacements. The most common disruption of bridge sites was settlement of the approach fill due to compaction of the embankment materials. These settlements produced vertical separations as great as a few tenths of a meter between the approach pavements and the bridge decks. The most common bridge damage associated with liquefaction was generated by the lateral displacement of abutments toward river channels (Figure 13). These displacements were most likely caused by lateral spread of floodplain sediments toward river channels, but may also have been caused by inward rotation of abutment walls due to compaction-induced increases in lateral forces. The abutment displacements crowded walls into bridge stringers and compressed railings and other linear features spanning the bridges.

The flow of traffic was disrupted at more than 350 locations in the highway system. Many of those disruptions were caused by the settlement of bridge-approach fills, or by landslides or tsunami debris.

Another major source of such disruption was liquefaction. In several areas where highways crossed terrain underlain by liquefiable soils, the highway fills settled differentially, deforming the roadway into long vertical waves with troughs as deep as 0.6 m. And the roadway took on the appearance of a low roller coaster.

Kilometers of flood-control dikes along rivers in southwestern Hokkaido were damaged due to liquefaction of subsurface sediments (Figure 14). The dikes usually split longitudinally, approximately down the centerline of the crest, and subsided. Liquefaction of sediments beneath the dike allowed the core to penetrate downward into the liquefied layer. The downward penetration apparently produced a type of bearing capacity failure that thrust the flanks of the dikes outward and upward, generating fissures with dike-facing scarps along the outer margins of the flanks. Simultaneously, the dike split into two approximately symmetrical segments, each penetrating into the liquefied soil, but each being carried outward by the displaced soil.

STRUCTURAL ASPECTS

In general, shaking damage to buildings on Hokkaido and even on Okushiri Island was light to non-existent, while tsunami damage on Okushiri Island varied from total loss for wood buildings severely inundated, to moderate for concrete or steel buildings well anchored to their foundations. For concrete or steel buildings, tsunami inundation resulted in partial or total loss of contents of cladding on the first story, stripping the building to its bare structure, while leaving the building above the inundation line almost undamaged.

A lighthouse at Aonae on Okushiri Island, a one-story reinforced concrete building with a reinforced concrete tower approximately 8 m high, was severely damaged by the earthquake (Figure 15). The tower failed at its base, rotating en masse onto the one-story building and coming to rest at approximately a 45° angle. Inspection indicated an apparent bond failure of plain "J" anchorage bars, approximately 24 mm in diameter. Perhaps the building most sustaining the most damage was a three story school in the northern part of Aonae. Significant diagonal shear cracking occurred in columns, spandrels, and walls.

LIFELINE EFFECTS

Highways performed well with most damage to pavements resulting from general ground settlement, and settlement at approaches to bridge abutments. Few bridges exist on Okushiri Island. In Hokkaido, bridge performance was generally very good, with few bridges sustaining more than minor damage. The most heavily damaged bridge observed was a six span two lane 1970 vintage steel plate girder highway bridge over the Assabu river, at Assabu-Cho (Figure 16). Lateral spreading was observed on the south bank of the bridge, which did not appear to affect the superstructure. Significant cracking was observed just above the water line at the 1.8 m diameter reinforced concrete bridge piers founded in the river; significant spalling and broken hoop reinforcement were noted.

Just north of Aonae a recently constructed snow shed collapsed as the result of rotational failure of perimeter footings (Figure 17). The most heavily damaged tunnel in Hokkaido was the Shiroito tunnel north of Setana on Highway 229, as described earlier in the landslide section.

Electric power does not appear to have been significantly impacted. However, significant number of distribution poles in the tsunami inundation areas, particularly on Okushiri Island, were swept away by the wave runups. Water supply to Aonae was not affected and structural performance of the Aonae Sewage Treatment Plant did well during the earthquake. However, the sewage treatment plant was shut down following the quake as the result of contamination by seawater of pumps, motors, electrical equipment etc, located in a pump room below grade.

The Okushiri-Cho remote control switches system performed well during the earthquake (Figure 18). It is located in a two story reinforced concrete building and built on firm soils. Atop of the building is a 40 m free-standing steel truss microwave tower. No damage was reported. Telecom equipment in the building was well-braced in both directions, to floor and ceiling. Backup diesel generators functioned well.

SOCIETAL ISSUES

The tsunami warning system worked well in this earthquake. Five minutes after the earthquake, the Japan Meteorological Agency (JMA) issued a warning that a major tsunami had been generated. JMA transmitted the warning via seven television and radio stations to local jurisdictions in the affected areas. In addition, Nippon TV issued a notice 1.5 minutes after the earthquake about a possible tsunami.

The importance of prior public awareness in areas potentially vulnerable to a tsunami was clearly demonstrated by this event. The first tsunami waves arrived on the east side of Okushiri Island and were observed during the quake. On the other part of the island, the first waves arrived approximately 2 to 5 minutes after the shaking. A second and larger waves arrived after the first waves. People reported that they began to run immediately for higher ground. In Aonae, people vividly remember the 1983 Nihonkai-Chubu tsunami, and knew that they had to run very quickly to higher ground when they felt the strong shaking. Many of the fatalities were children who had been sleeping and mothers who tried to wake them up and carry them to safety. Many of the men were out fishing. In Taisei, tsunami warning sirens were not activated because of power failure, again demonstrating the importance of backup emergency power supply.

Adequate shelters were provided immediately after the quake for both displaced residents and for rescue workers and responders. In Okushiri Island, approximately 90 percent of displacees initially took advantage of temporary shelter in two schools and community meeting houses. The ratio dropped to approximately 2 percent by the end of the week. In Taisei, damage was concentrated in three coastal districts where approximately 60 percent of displacees took shelter.

RESTORATION AND RECONSTRUCTION

The frequent occurrence of earthquakes requires that the Japanese government and its people to be well prepared to cope with their damaging effects. Emergency headquarters were established at all levels of government within an hour after the quake to coordinate damage assessment and emergency response including search and rescue efforts. Such early efforts were continued through the fall of 1993 to restore the services of all lifeline systems. In October 1993, the restoration program had progressed to the phase of construction and repair of permanent facilities. On Okushiri Island, multi-story buildings were being erected of pre-fabricated components on higher ground for resettlement.

CONCLUSIONS

The study team members were impressed by what they had learned during the post-event investigations of this earthquake. In all respect, the event demonstrated the well-prepared nature and resilience of the Japanese community, from preparedness, emergency response, sheltering, repair, to restoration and reconstruction. All of these elements were carefully planned and orderly executed. It also demonstrated their insight in engineering design and construction practices, particularly of their in-depth understanding of the effects of liquefaction to superstructures.

While it is understood that the earthquake struck a region which is far from heavily populated with only low rise buildings and less complex lifeline systems, and the potential impact of an earthquake of such magnitude to a populated region in Japan is remain to be seen. The general attitude of Japanese toward the impact of earthquakes nevertheless still can set an excellent example for us to follow in the United States.

Can major fires and tsunami damages happen here in the States? Actually, major fires have already happened; but we have been fortunate enough in recent earthquakes that none of them had spread out to become conflagrations. For instance, in 1989 Loma Prieta earthquake in California, 22 ignitions occurred in San Francisco alone. Water supply in the densely built Marina District was completely lost, and a large fire developed could not be extinguished until a fireboat supplied water from the Bay through a special large diameter hose system developed by the fire department for just such a purpose. The 1993

Cape Mendocino earthquake in Northern California resulted in a fire that destroyed most of the business district of the small town of Scotia. The most recent 1994 Northridge earthquake in Los Angeles area further put us on notice that major fires or conflagrations are indeed possible. They can devastate a major metropolitan area like Los Angeles if less favorable conditions, such dry weather, strong winds, and inadequate preparation in fire fighting, prevail during future earthquakes. It is important that these factors be carefully examined in all jurisdictions to develop comprehensive plans of attack to avoid conflagrations in future earthquakes.

Fortunately, we have not had to face the devastation of a tsunami in any of our recent earthquake events. Nevertheless, a subduction similar to that in Japan runs through Seattle and into Puget Sound. If an earthquake of magnitude 7.8 struck there, major tsunami damage could be expected. On Okushiri Island, the residents ran for high ground as soon as they felt the shaking, expecting the arrival of a tsunami. In contrast, when a tsunami warning was issued for the northwest coast following the 1964 Alaska earthquake, people drove to the shore to watch the wave come in. Will we now have a different attitude toward such event thirty years later?

The Hokkaido-Nansei-Oki earthquake provided a number of successful stories in the performance of buildings and bridges. Joint effort should be established to bring together experts from both countries to examine such performance in detail so that better and improved engineering design and construction practices in both countries can be achieved.

ACKNOWLEDGMENT

The author would like to thank all U.S. team members and members of the Japanese team for the opportunity to work together in their field investigations immediately after the earthquake. U.S. team members are: Les Youd, Richard Barnes, Eddie Bernard, Richard Bukowski, Frank Gonzales, Edwin L. Harp, Jane Preuss, Charles Scawthorn, Dennis Sigrist, Paul Somerville, David Tyree, Peter Yanev, and Robert Lo.

Particularly thanks will go to Messrs. Iida, Kawashima, Unjoh, and Nakajima, and colleagues at the Hokkaido Development Bureau, for their technical and logistical support to make the investigation effort a success one. The author also would like to express our appreciation to a number of organizations who supported this reconnaissance effort. These organizations are the National Institute of Standards and Technology, Earthquake Engineering Research Institute (EERI), National Center for Earthquake Engineering Research (NCEER), National Science Foundation who funded the postearthquake investigation activities of EERI and NCEER, National Oceanic and Atmospheric Administration (NOAA), U.S. Gelogical Survey and the U.S. Forest Product Laboratory.

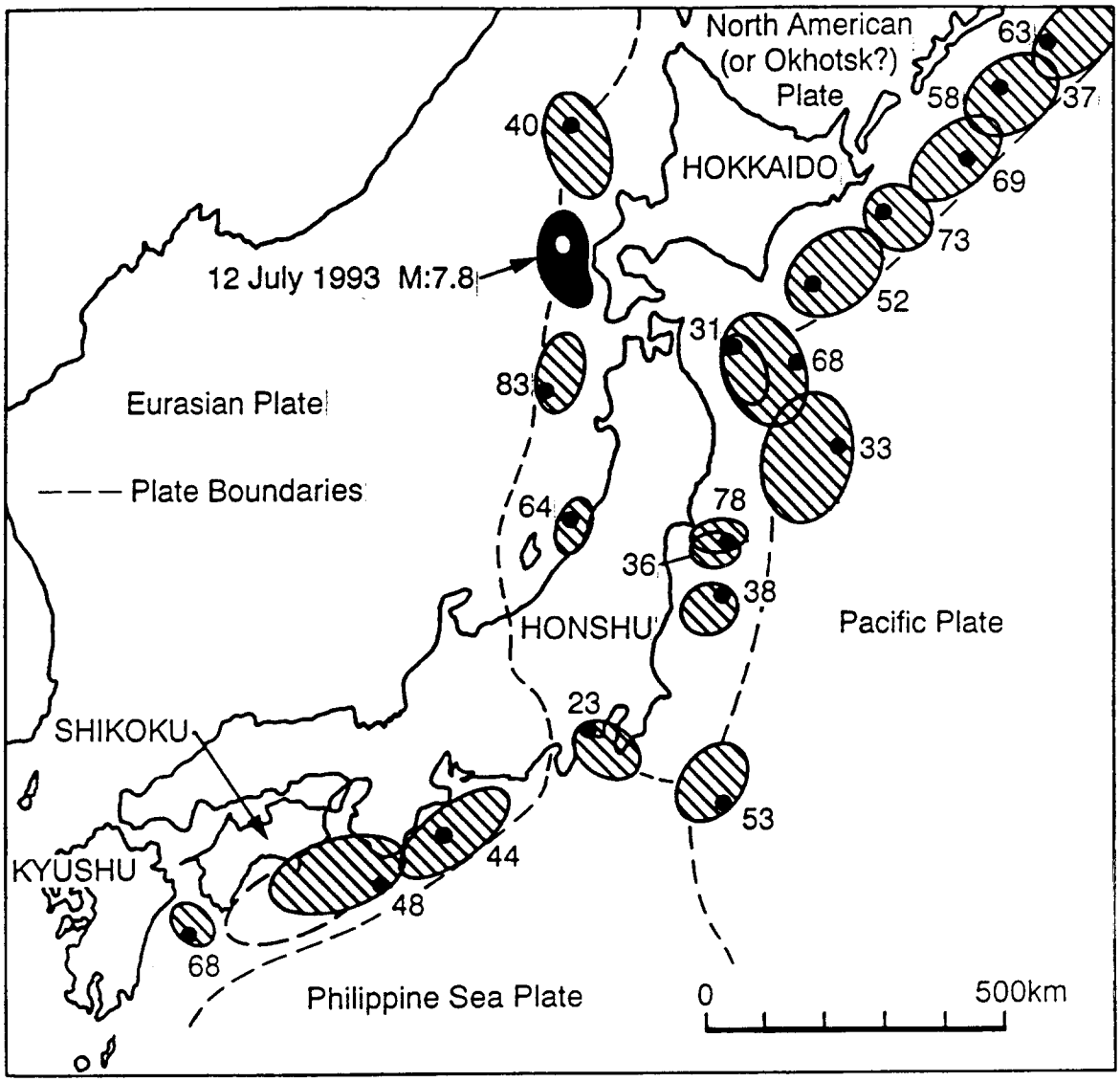

Figure 1 Rupture zones of offshore earthquakes in Japan larger than magnitude 7.4 since 1923, with plate boundaries shown on dashed lines. Source: Modified from Japan Meteorological Agency

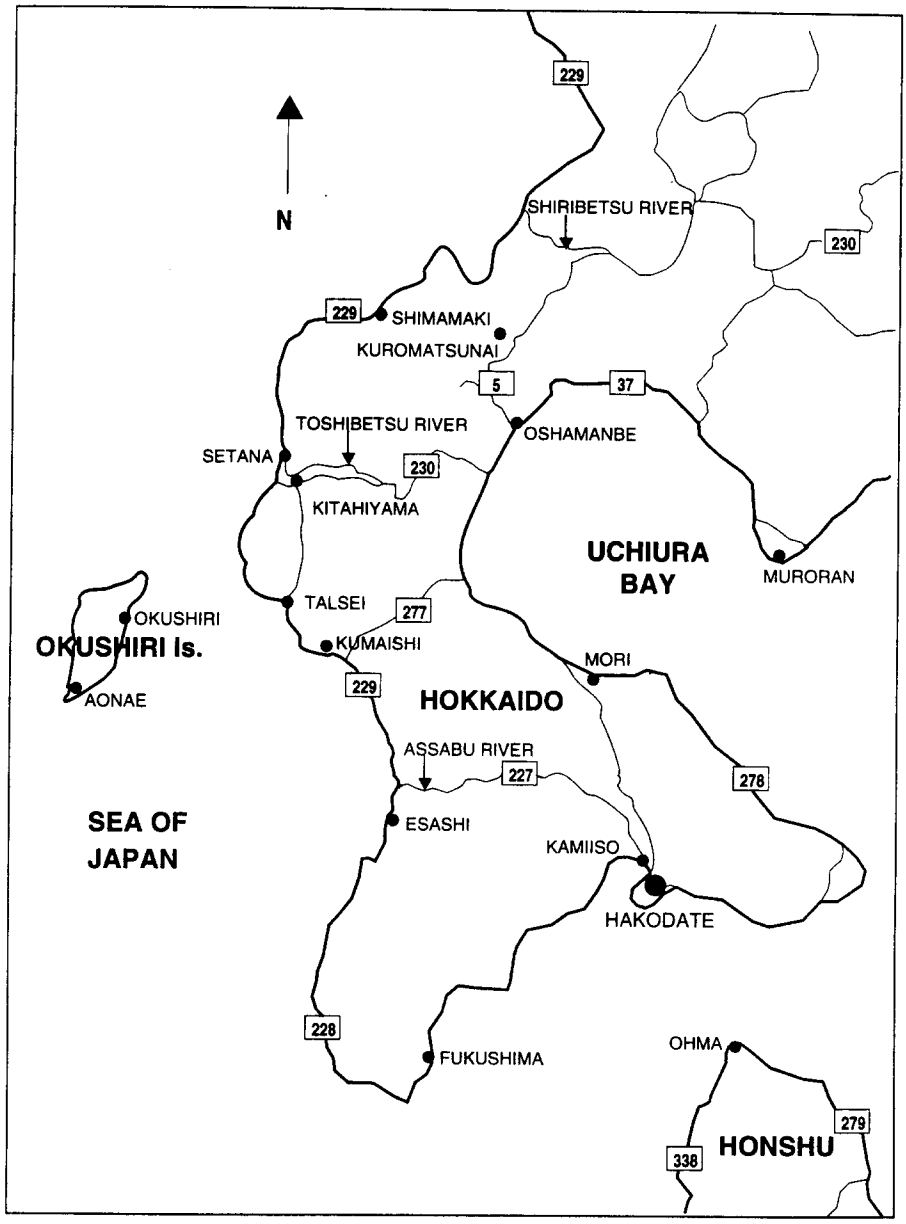

Figure 2 Map of southwestern Hokkaido and Okushiri Island showing principal localities referred to in this report

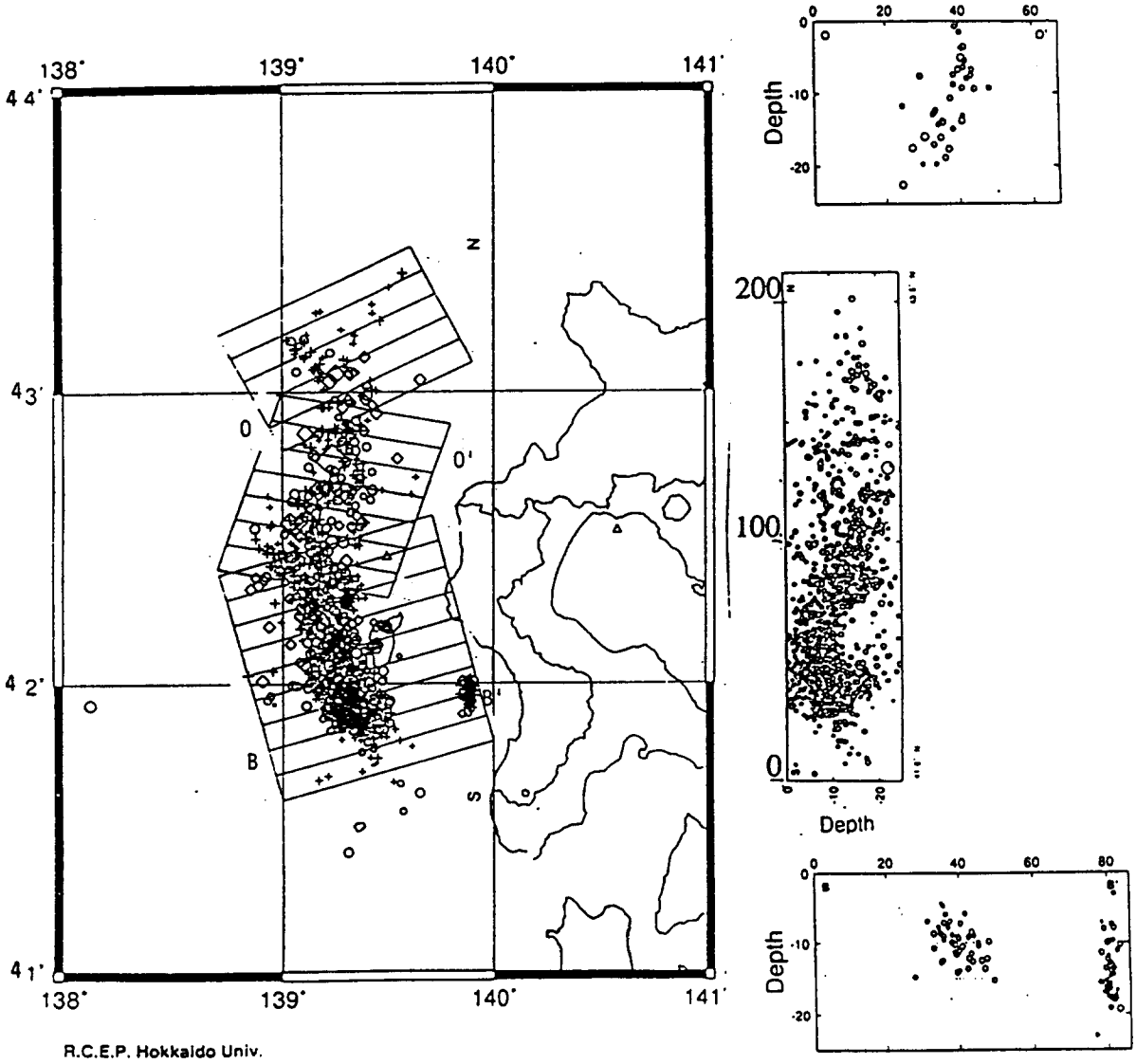

Figure 3 Mainshock and aftershock hypocenters, July 17 through 18, 1993. Depth cross sections O-O', S-N, and B-B' are shown on the right with vertical exaggeration of a factor of 2. Source: Research Center for Earthquake Prediction, Hokkaido University

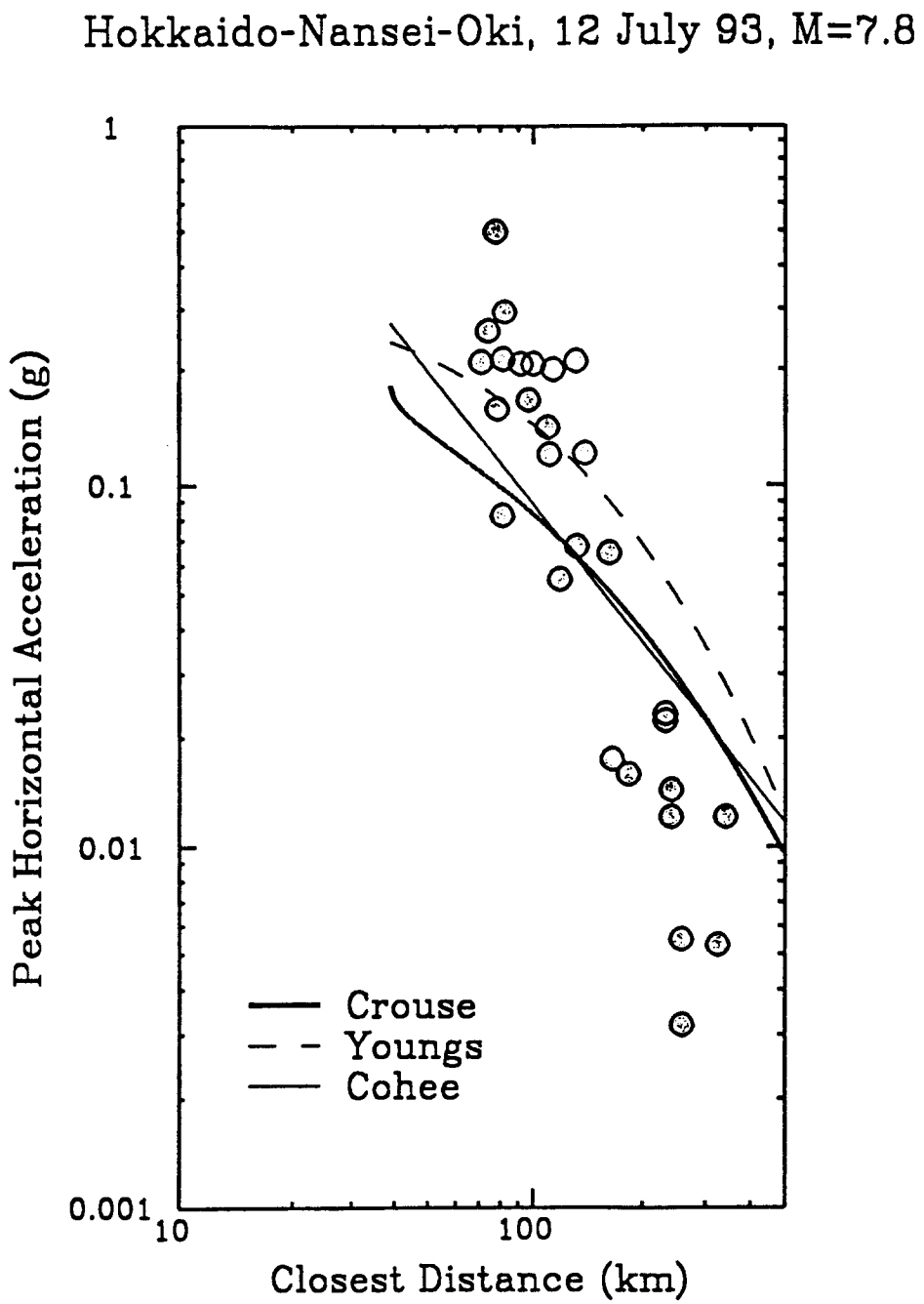

Figure 4 Very preliminary uncorrected peak horizontal acceleration plotted against closest distance to the rupture surface, compared with attenuation relations for subduction earthquakes used in the United States. Source: Hokkaido Development Agency, Japan Meteorological Agency, Japan Rail, Ministry of Construction's Port and Harbor Research Institute

Figure 5 A view of tsunami damage from the south of Aonae. Source: Y. Tsuji, 1993

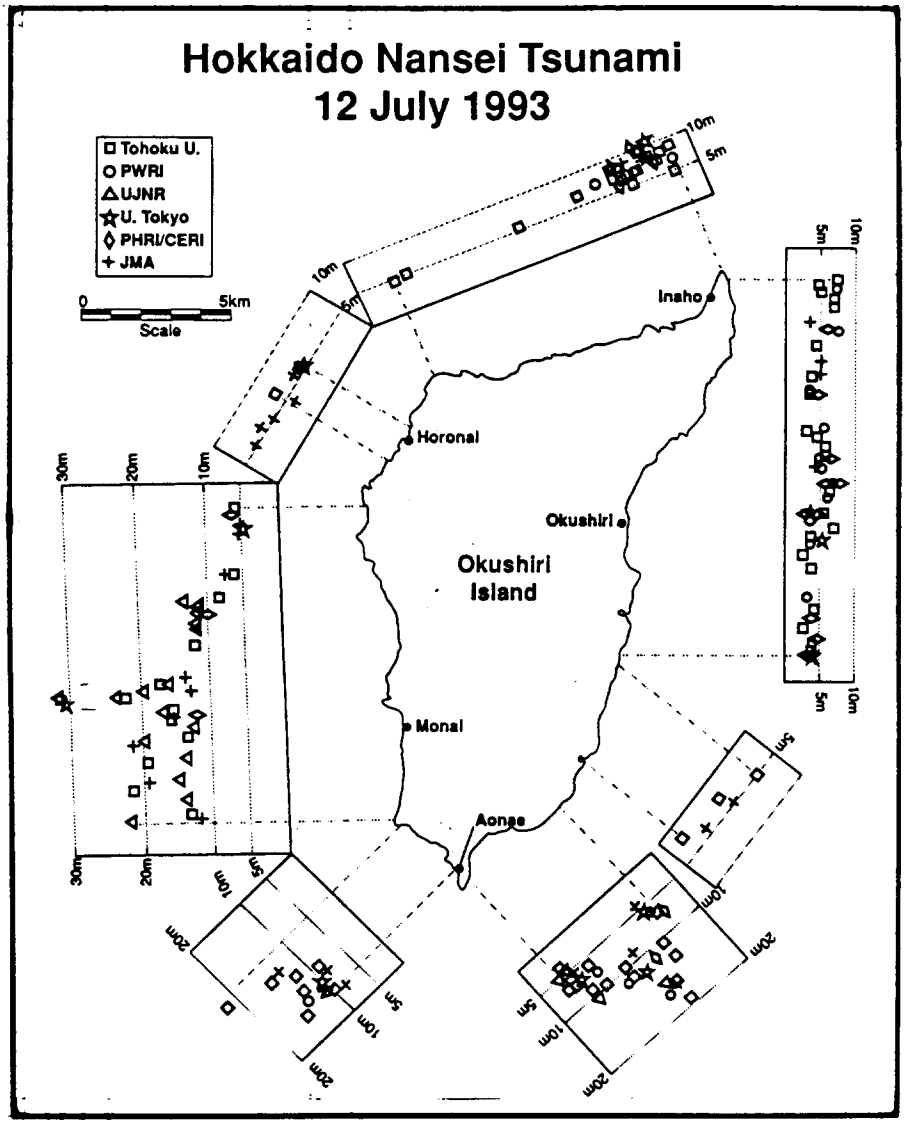

Figure 6 Distribution of vertical tsunami runup for Okushiri Island. The legend indicates data source, and runup values are projected onto offshore scales. A projection from a data point onto the coastline will identify the geographical position of the measurement

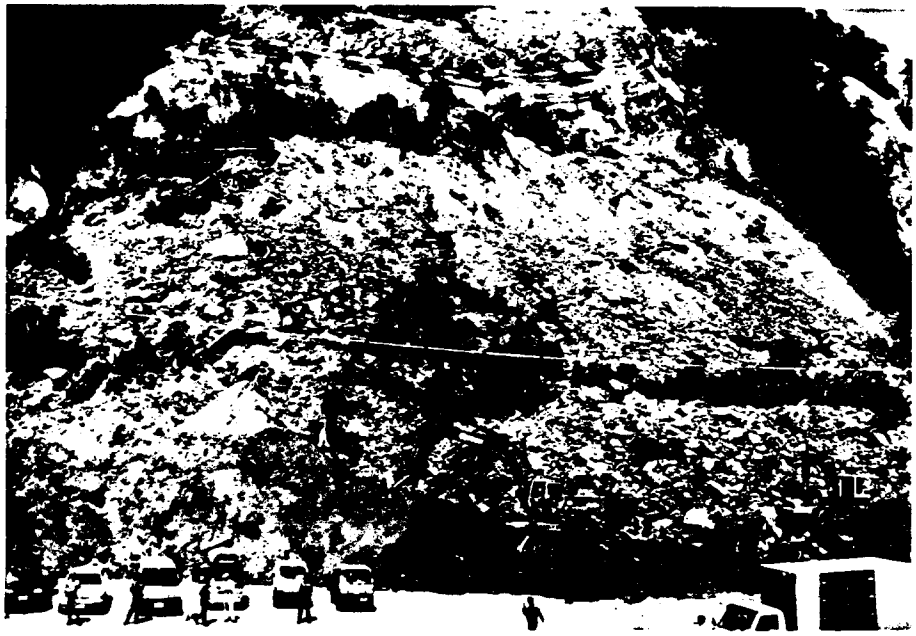

Figure 7 Rock slide near the ferry terminal in Okushiri Port that buried the Yo Yo So (Hotel). The slide is comprised of Pliocene tuff, tuffaceous sandstone, and conglomerate and is approximately 800,000m^3 in volume.

Figure 8 Concrete talus shed collapsed by rock fall along highway 229 north of Setana.

Figure 9 Pier 1 at the Port of Hakodate was the most severely damaged port facility we visited. (A) View southward of quay wall that tilted or shifted seaward by as much as 3m. (The warehouse in background is further illustrated in Figure 19.) (B) View northward of paved area that was disrupted by settlements as great as 0.5m and fissures with separations as great as 1m. Source: T.L. Youd

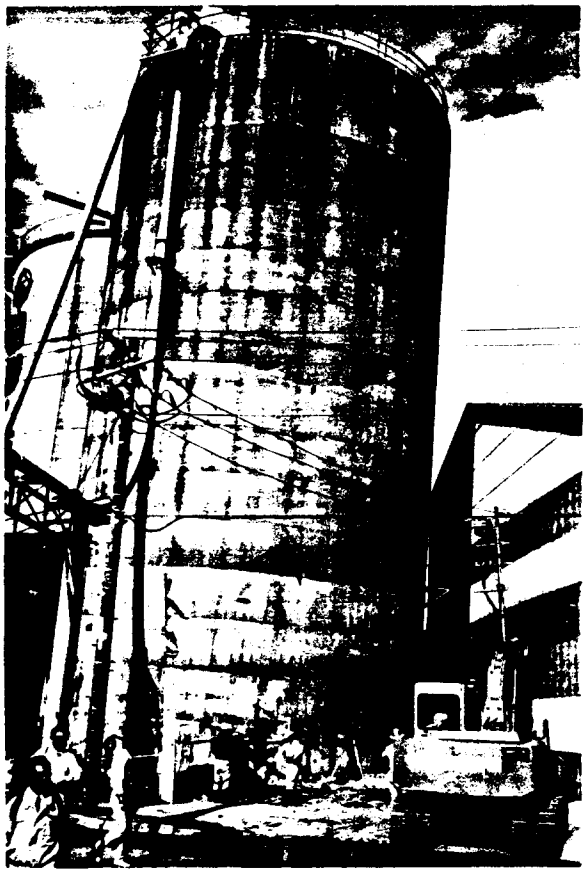

Figure 10 Cement storage tank near Pier 16 at the Port of Hakodate. The tank tipped about 2.5 degrees southward due to transient loss of bearing strength. Source: T.L. Youd

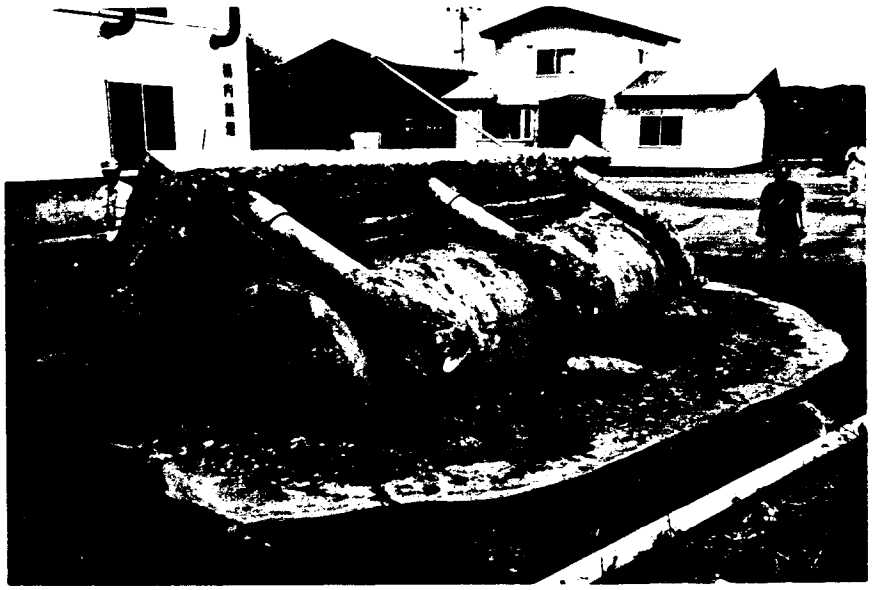

Figure 11 Buried storage tank that floated out of the ground at an industrial facility about 6km north of Esashi. The tank was about one third full of oil at the time of the earthquake. Source: T.L. Youd

A

Figure 12 (A) Southward view across campus of Oshamanbe Nakonosawa Elementary School showing classroom building (center) and gymnasium (right). The playing fields in foreground were disrupted by ground fissures and ground settlement. (B) Disrupted pavement in roadway near gymnasium; overlapped pavement indicates compressional impacts due to ground oscillation. Source: T.L. Youd

Figure 13 View of rotated bridge bearing and a girder that penetrated into abutment wall at west end of Kamiiso-shin bridge. This damage was caused by displacement or tilting of the abutment toward the river. Source: T.L. Youd

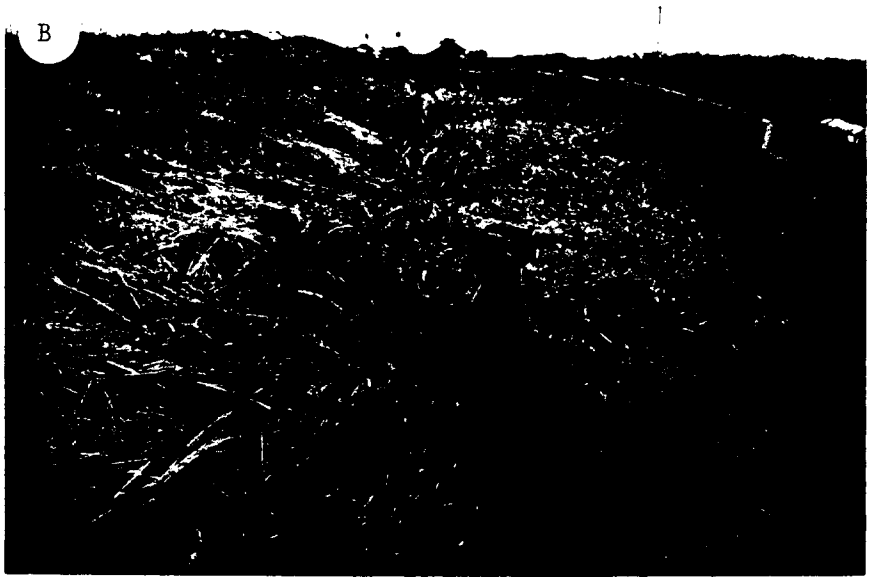

Figure 14 Views of dike along the north bank of the Assabu River, illustrating the deformations diagrammed in Figure 6-39. (A) View westward showing longitudinal fissure along the center line of dike crest. (B) View along north flank of dike showing fissure with southward (toward dike) facing scarp, indicating flank had risen relative to dike.

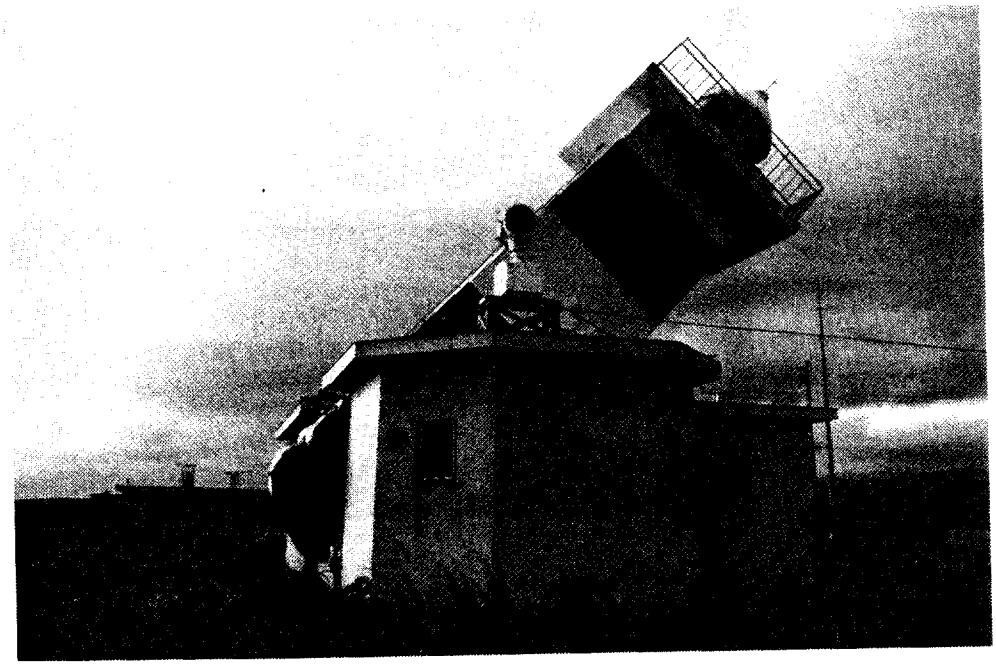

Figure 15A Aonae Lighthouse--the structure failed because of the pull-out of inadequate ties (dowels) between the foundation and the superstructure. The dowels were 24mm (1 inch) in diameter.

Figure 15B Aonae Lighthouse--detail of reinforcing anchorage failure.

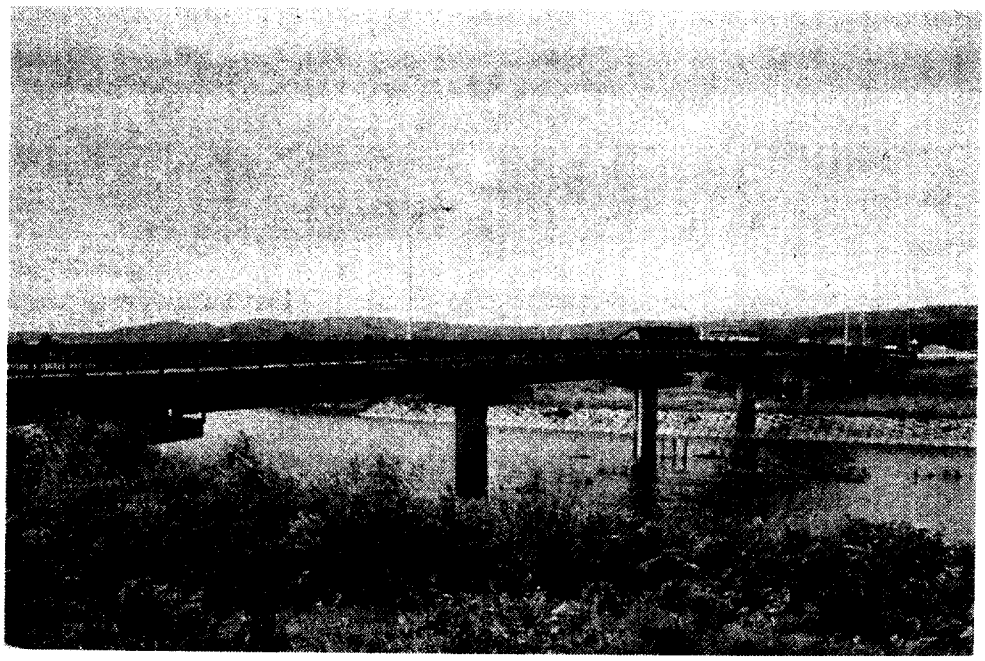

Figure 16A A six span, two-lane, 156m long, 1970 vintage steel plate girder bridge at Assabu on Highway 227. Severe shear damage to all visible columns which are about 2m (6 ft) in diameter. The bridge is located about 80km (50 miles) from the epicenter. No significant damage was observed to the superstructure.

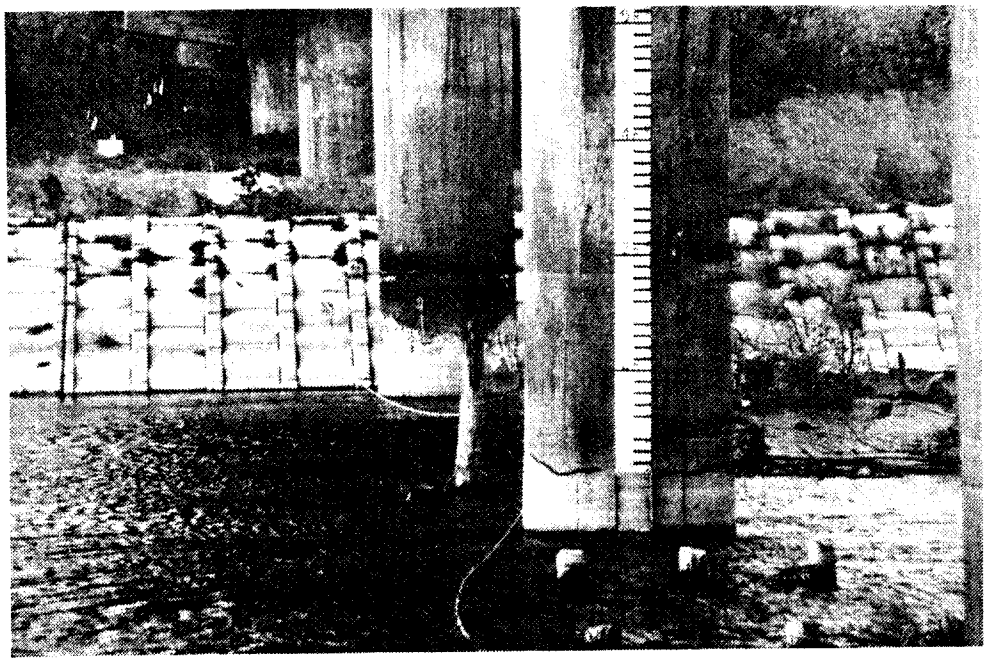

Figure 16B View of Assabu bridge piers--note cracking near waterline.

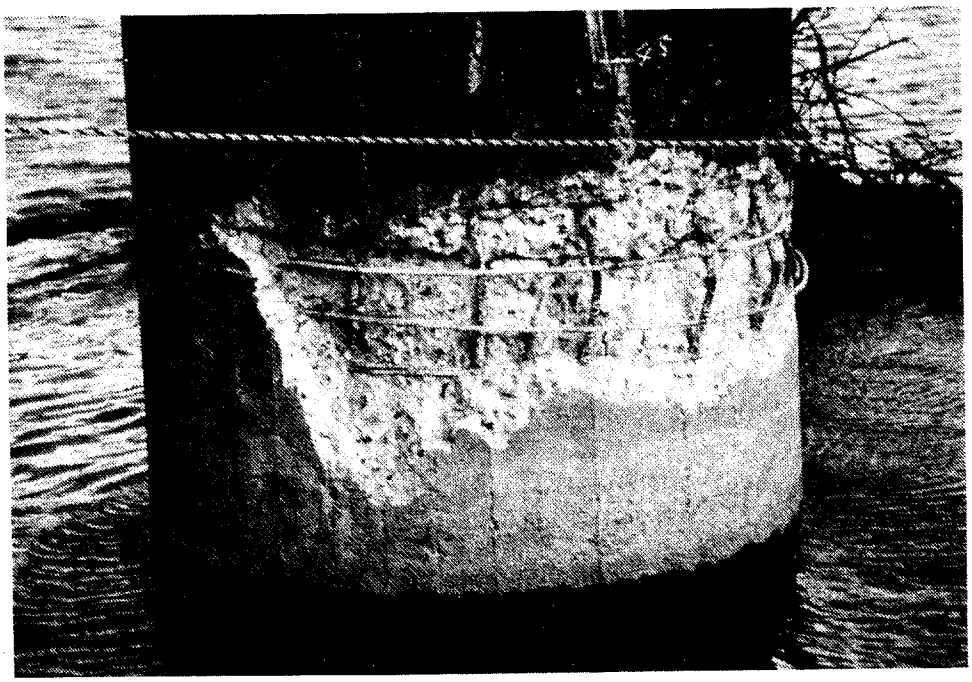

Figure 16C Detail of a damaged column of the bridge over the Assabu River. Note the buckling of the vertical reinforcing steel and the wide spacing of shear (horizontal) reinforcement. The estimated damage is 25 to 50% of the value of the bridge.

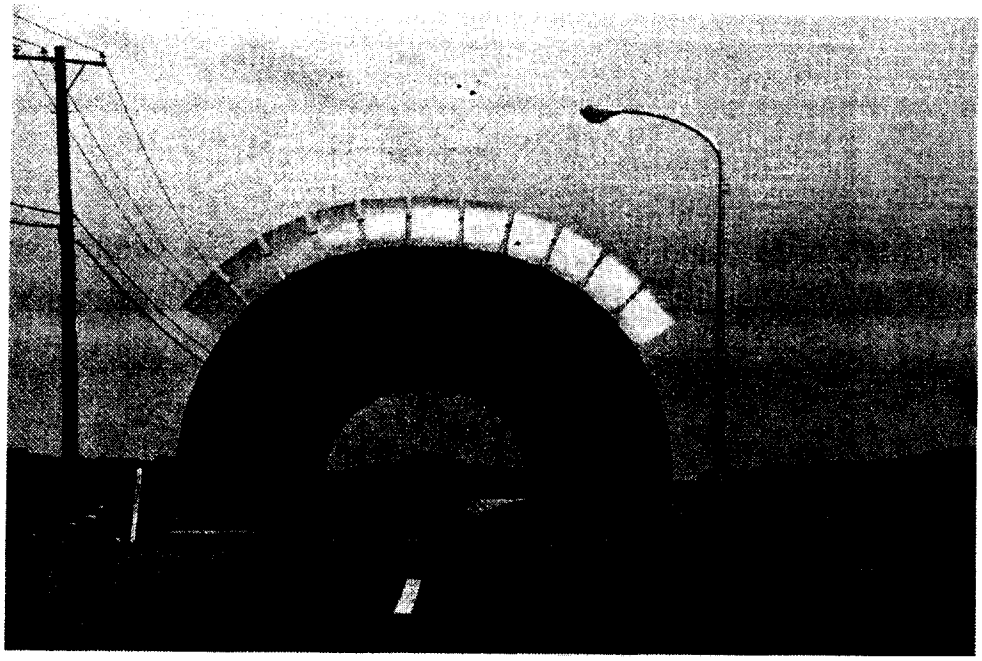

Figure 17A A collapsed snow shed (tunnel) just north of Aonae. The just completed structures is on fill in rice paddies. About 1/3 of the three-hinged arch structure has collapsed. The rest is severely damaged. The approximately 2m (6 ft) wide quarter circle panels are precast concrete and are bolted to the footings and to each other at the top.

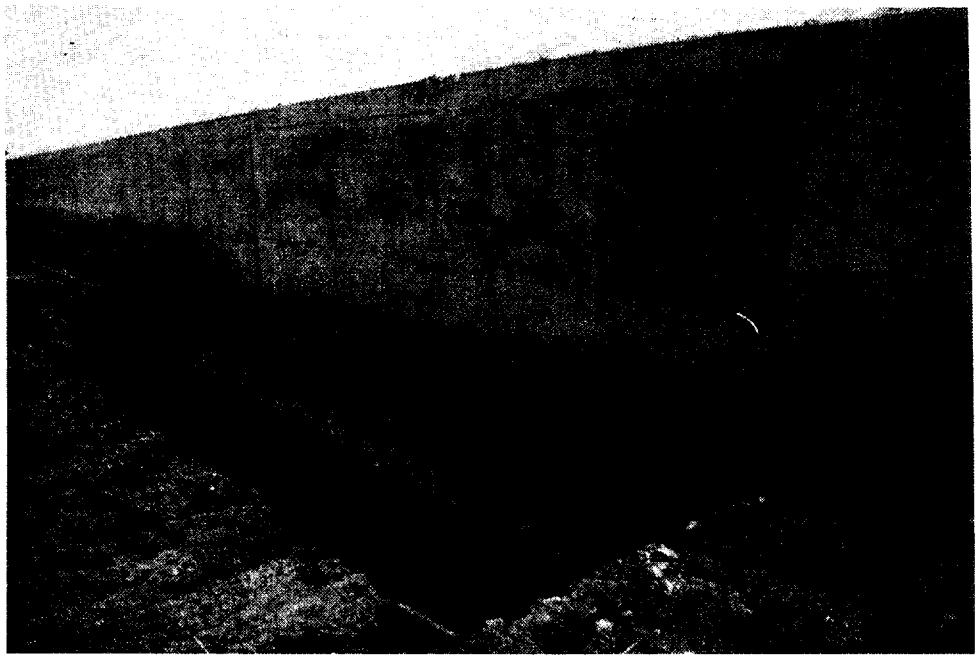

Figure 17B Exposed footing and stem wall of snow shed (west side - undamaged).

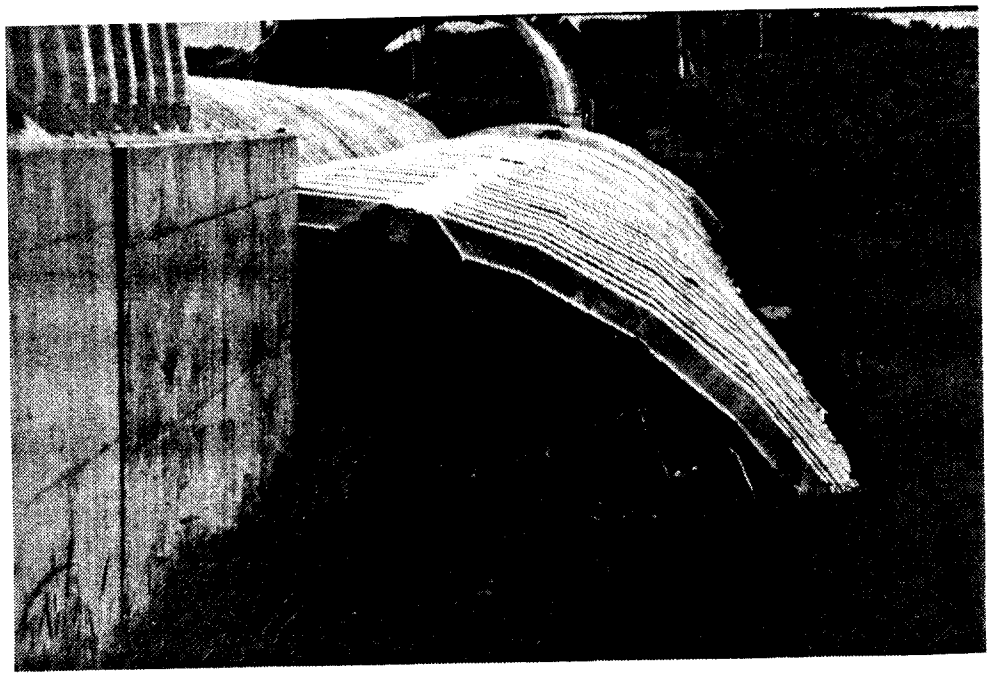

Figure 17 C Failed east side of snow shed--lateral spreading of the fill and/or liquefaction caused spreading, rotation, and failure of the footings.

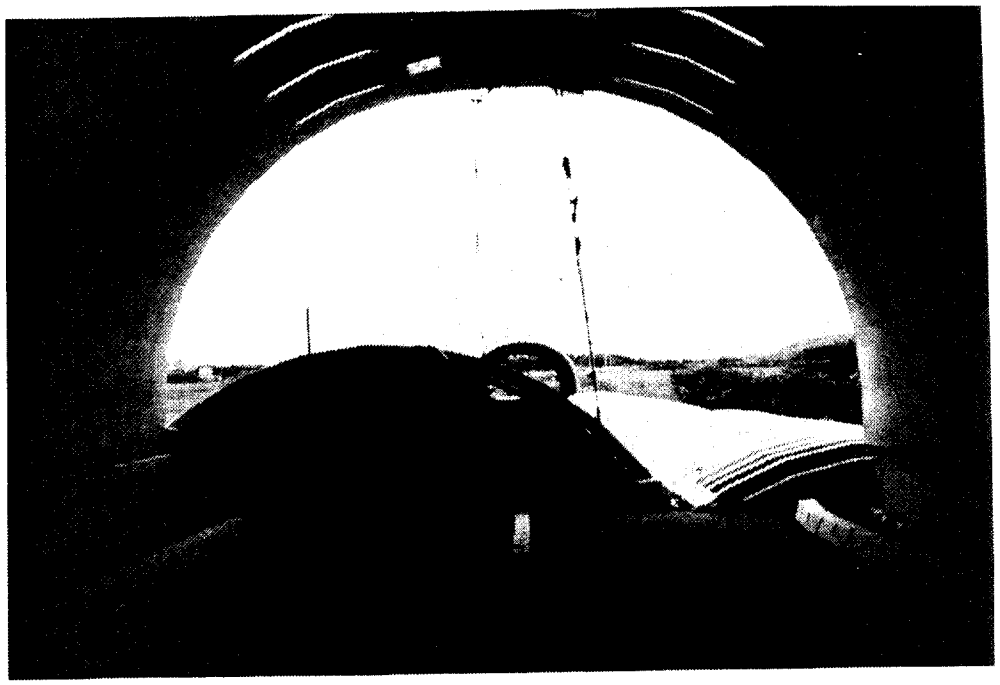

Figure 17 D Note that, although the arch has collapsed and dropped the precast planks onto the pavement, the planks area relatively undamaged, testifying to the general quality of construction.

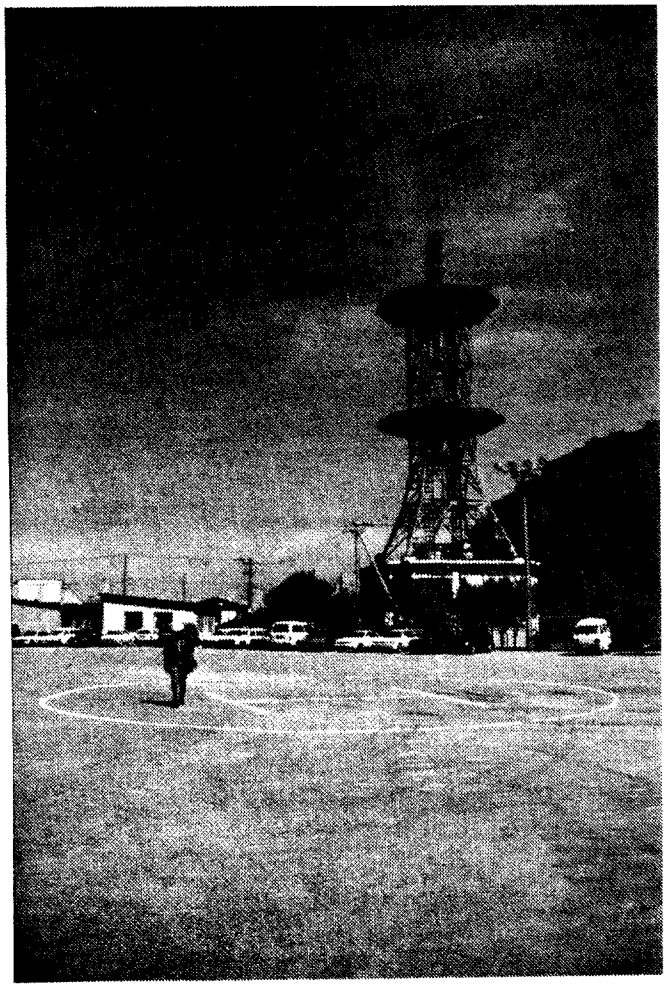

Figure 18 Okushiri-Cho Remote Control Switch--it is a concrete shear wall building. Atop the building is an approximately 40m (130 ft) free-standing steel truss microwave tower.

MANUSCRIPTS AUTHORED FOR PANEL MEETING BUT NOT PRESENTED ORALLY

Technological Development for Automatic Construction Methods of Caissons

by

Masanori Nakano*, Jiro Fukui** and Shigeru Takagi***

Abstract

In recent years, the construction industry has been facing such problems as skilled labor shortages and an aging work force, while at the same time, foundation structures are becoming wider and deeper. Therefore, it has now become necessary to improve the efficiency of field work for smooth and expeditious construction of foundation structures.

With this in mind, the Ministry of Construction is undertaking a comprehensive development project to automate the construction of caissons. This development project deal with open caissons[1], including the precasting of caisson bodies and development of technologies for automatic excavation, earth removal and press-in settlement, and pneumatic caissons[2], which entail the development of technologies for automatic excavation and earth removal inside a working chamber under high pressure of air.

Key words: foundation, open caissons, pneumatic caissons, precasting, automation, excavation, earth removal, press-in settlement

1. Introduction

In recent years, demands have arisen in the construction industry to improve construction efficiency and working environments to counteract problems such as skilled labor shortages and an aging work force. With this in mind, the Public Works Research Institute (PWRI) initiated a five-year project in 1990 to improve the efficiency of field works and promote the technological development for automating several construction methods presently in use on site.

This paper will introduce the technological development for automating the construction of open caissons and pneumatic caissons.

2. Technological development for automating the construction of open caissons

2.1. Present state of the construction method for open caissons

The open caisson method has been widely used for constructing foundations, shafts of tunnel structures, etc. However, alternative methods, such as the pile foundation method, are gradually replacing it. Figure 1 shows the transition of methods for foundation structures. Caisson foundations accounted for 26 % of the total in 1966; however they decreased to 6 % in 1976, and 4 % in 1985. Open caisson foundations accounted for 4.3 % of all caisson foundations in 1976 (123 out of a total of 2,837 foundations investigated); however, this proportion decreased to 2.4 % in 1985 (90 out of a total of 3,697 foundations investigated). One plausible reason for this may be the failure of the open caisson method to stay competitive with the pile foundation method.

New techniques, such as the enlargement of diameter, were developed for the pile foundations, while integral technologies, such as methods for caisson production and excavation, were not actively developed for the open caisson method. Thus, the open caisson method could not go beyond the confines of convention.

The procedure for constructing open caissons using the conventional method is as follows: a caisson body is constructed using cast-in-place reinforced concrete; the earth inside the caisson is removed with a clamshell bucket or a hammer grab bucket; then the caisson is settled using a press-in device (oil pressure jacks). However, its construction efficiency in terms of the number of workers and the term of construction is not satisfactory, since several construction works must be done in situ, such as assembly of reinforcing bars and molds, concrete placement, and curing. In addition, problems such as reduced precision or failure of caisson settlement occur when the caisson is constructed deep underground, since the ground under the cutting edge cannot be precisely excavated during excavation and settlement. As a technique to solve these problems, the PC well caisson method[3] has already been put to practical use. With this method, the caisson body is constructed by assembling ring-shaped precast blocks at the point of settlement, to which tension is applied by PC steel bars.

---

*)Chief, Foundation Engineering Division, Structure & Bridge Department, PWRI, MOC
**)Senior Researcher, ditto.
***)Researcher, ditto.

However, this method is applicable only to caisson foundations with small diameters of 4.0 m or less due to the limitations imposed by conveyance of precast blocks. In addition, the construction is imprecise, since the settlement using a press-in jack heavily relies on the experience and observations of workers.

2.2. Objectives of the technological development and outlines of construction methods

To improve the open caisson method, the PWRI is proceeding with the development of construction technologies[1][3]. The purpose of this development is to sharply reduce both labor and construction terms in field works, expand the applicable domain of open caissons and ensure high construction precision by introducing precast caisson bodies and automating the excavation and press-in works.
This development comprises the following three systems. The major advantages of each system are summarized in Table 1. Any combination of these systems can be used depending on the conditions at each work site (see Figure 2).

(1) Development of a precast body system
This system is designed to assemble precasted materials in situ, the scantling of which is smaller than that of the PC well caisson method. This system enables the construction of a caisson body of high quality with less labor during a shorter period of time than a caisson body constructed using cast-in-place concrete.

(2) Development of an automatic excavation and earth removal system
With this system, the ground under the cutting edge of caisson body can be accurately excavated, allowing for deep, highly efficient underground construction. Thus, the range of applications for open caisson construction can be expanded.

(3) Development of an automatic settlement control system
This system automatically controls the press-in settlement and the position of caissons, processing data measured by various sensors. With this system, press-in settlement can be conducted with high precision.

2.3. Precast caisson body system

2.3.1. Structure of a caisson body
The structure of a caisson body using precast blocks is similar to that of shield segments; a caisson body is constructed by connecting precast blocks using horizontal and vertical joints. The horizontal joints are connected by applying tension to PC steel bars, as is the case with the PC well caisson method, while the vertical joints are connected by wedge connecting joints.
As shown in Figure 3, external forces act on the vertical joints. Wedge connecting joints are resistant against bending force by wedge metals, out-plane shearing force by square steel pipe keys (see Figure 4), and in-plane shearing force by the confining force of upper and lower blocks. With regard to the structure of a wedge metal, blocks are connected to each other by inserting an H-shaped wedge metal into a C-shaped metal planted in a body in advance; resistance against bending is provided by the tensile force of the H-shaped metal (see Plate 1).
When the automatic excavation and earth removal system and the automatic settlement control system are used for constructing a caisson, guide rails and various sensors, such as an earth pressure gauge, a hydraulic pressure gauge and an inclinometer, are installed on the caisson body.

2.3.2. Design method of a caisson body
The precast caisson body system differs from the conventional method in that a caisson body is constructed by connecting precast blocks in situ using joints. The performance of the joint sections, such as stiffness and strength, affects greatly the deformation and the sectional force of the entire caisson body due to external forces such as the bending moment and horizontal force. In accordance with the Design Specification[4] for Caissons presently in effect, a caisson must be a monolithic body constructed with cast-in-place concrete. Therefore, in order for the precast caisson body system to meet the specification, the stiffness and strength of joint sections must be made equal to those of monolithic materials.
In order to confirm the performance of the various types of joints mentioned above, the Public Works Research Institute conducted a loading tests using models with thickness identical to that of the side wall of actual-size caissons.
As shown in Figure 5, the test results proved that the vertical joint possessed stiffness and strength roughly equal to those of a monolithic concrete body that uses no joints, at the level of allowable stress in the present design method.
A loading test was also conducted for horizontal joints in order to understand the features of deformation and the strength of joint sections (see Plate 2). This test elucidated the reduction of stiffness that occurred locally to horizontal joint sections and the progress of bending and shear failure due to the yield of PC steel bars.
In addition to these loading tests, the influence of joint sections on deformation and sectional force was examined by conducting an analysis based on the finite element method. Figure 6 shows the model for analysis and an example of

the results. In this model, the stiffness against the tensile force in the joint sections of members was neglected. However, the test results proved that no region of tensile stress appeared on the caisson body and that the influence of the joint sections on deformation and sectional force was almost negligible.

2.3.3. Production of precast blocks of a caisson body

Precise work is required for the production of precast blocks, since any deficiency is likely to affect the performance of joint sections; an aperture or projection on a joint surface may cause cracks when the blocks are prestressed by applying tension to the PC steel bars. In the precast caisson body system, blocks are produced by the match-cast method in order to eliminate irregularity on joint surfaces. This method is to utilize the surface of a block made by casting concrete as the mold of an adjacent block. Specifically, the two block surfaces become concavo-convex, the irregularity on the surface of the first block being offset by the second block. Thus, there exists no aperture on the joint surface. This production method is also used for the joint surfaces of precast block girders of bridge superstructures, and its reliability is high. The problem, however, is that breaks caused by joints exist on the joint surfaces. Therefore, the production precision and the assembly method must be kept under close watch.

The construction procedures of a caisson body are as follows: PC steel bars are set up prior to the installation of blocks; an adhesive agent is applied on the horizontal joints; blocks are installed; tension is applied to PC steel bars; then, vertical joints are installed.

2.4. Automatic excavation and earth removal system

This system comprises a back hoe-type automatic underwater excavator, which travels along guide rails, and a portal crane-type automatic earth lifter coupled to the excavator that removes earth. The automatic underwater excavator excavates the earth inside a caisson including the earth under the cutting edge, traveling along the guide rails installed on the lower end inside the caisson body (see Plate 3). Several excavation patterns to meet various soil conditions and inclination of the caisson body are programmed in the excavator; the excavator automatically conducts excavation, selecting the most appropriate excavation pattern (see Figure 7). The portal crane-type automatic earth lifter detects its own location so that it does not touch the arm of the excavator. It travels along the circumference of the caisson in a link motion with the circular travel of the excavator, and removes the earth with its clamshell bucket (see Plate 4).

With this system, the above operation is commenced automatically upon designation of an excavation depth, which is repeated until the caisson reaches that depth.

2.5. Automatic settlement control system

The automatic settlement control system is an improved version of the conventional press-in open caisson method. This is to control the settlement and the position of a caisson by controlling the press-in force based on the data measured by various sensors installed on the caisson body. This system consists of measurement and control systems.

By the measurement system, data collection and processing, display of calculated data and figures, and issuance of warnings are all done automatically. The measurement factors are the settlement, inclination, eccentricity, the reaction force of the cutting edge, skin friction, and earth and hydraulic pressures.

Using the data obtained by the measurement system, the control system calculates the most appropriate press-in force and press-in moment for controlling the settlement and the position of the caisson. The press-in force of each jack is adjusted to the most appropriate one in real time.

2.6. Trial construction test

In order to confirm the applicability of this proposed method, tests using an actual-size caisson model have been conducted in 1993. In these tests, to confirm their performance and applicability, the automatic excavation and earth removal system and the automatic settlement control system in the test are introduced at the stage where a caisson body is constructed using precast blocks. For the purpose of examining the applicability of the systems to different types of soil, the ground conditions are modeled after sandy, clayey and mudstone layers. Major confirmation items in the test are shown in Table 2. The test results concerning the precision of caisson construction, automatic excavation, and automatic press-in settlement are discussed below:

(1) Construction of a caisson body

The construction precision and applicability of a caisson body using wedge connection joints and concrete connection joints were examined. The precision of the construction of a caisson body proved that the errors are invariably less than 6 mm by the test.

(2) Excavation precision

Figure 11 shows the cross sections of both sandy and mudstone layers to illustrate the excavation precision; excavation patterns instructed by the control system and the outcomes of the actual excavation are compared. Although the curves of the actual excavation differ conspicuously from the targetted excavation curves around the point where the excavator turns upward under the cutting edge, the excavation errors were within a few centimeters across the board, almost negligible for practical use.

(3) Settlement precision

Figures 8 and 9 show, respectively, the inclination angle and the eccentricity in terms of the precision of the position control. When going through the sandy and mudstone layers, which is equivalent to the initial stage of actual caisson settlement, the caisson showed slight and transient inclination; however it immediately assumed the proper position automatically. When each lot had settled, the caisson was built with its eccentricity and inclination angle within the standard control values (allowable limit).

3. Technological development for automating the construction of pneumatic caissons

3.1. Present situation of the pneumatic caisson method

The pneumatic caisson method is designed to settle a body to a designated depth by iterating the procedures of caisson building and settlement; when the base ground is excavated, compressed air is sent to the airtight working chamber installed underneath a caisson in order to prevent the groundwater from flowing into the work yard. The construction reliability of this method is high, since, for example, the bearing capacity of the bottom of a caisson can be confirmed directly. Therefore, this method is widely used for shafts, and foundations of bridges and other underground structures.

However, with the present method, construction work depends heavily on manual labor; skilled workers are sent down to the working chamber to excavate the ground using electric excavators and exchange a earth bucket to carry out the excavated earth. The working environment worsens as the construction depth increases. Since the air pressure inside the working chamber increases, the workers are susceptible to "caisson disease," and the allowable terms to work in the working chamber is decreased for the health control. Therefor, to protect the safety and health of workers, the maximum construction depth must be limited.

In order to solve these problems, private sector corporations have been conducting research on labor saving and automation of the pneumatic caisson method since 1980. Presently, the focus of the research is the remote operation of an excavator inside a working chamber. The technology for the remote operation of the excavator from an operation panel installed either inside a pressure-resistant capsule or on the ground is shortly put to practical use; some automatically-controlled excavators are already in use (see Plate 5). Nevertheless, the earth removal works have not yet been automated, and workers are still sent to the high-pressure caisson box for exchanging buckets. In addition, a worker (lock attendant) must be assigned for opening and closing the air lock in the upper part of the material shaft; this worker is also vulnerable to accidents such as falls, since his work post is elevated, as the depth of caisson construction increases.

The excavator is also used for loading the excavated earth in the buckets, during which the excavation work is suspended. For improving the work efficiency, the earth loading and removal must be kept separate from the excavation work. Problems still unresolved concerning the construction of pneumatic caissons are as follows:

(1) Earth removal work inside the working chamber and the lock switching operation should be automated.

(2) To maintain excavation efficiency during the earth removal work, the earth removal system must be separated from the excavation system.

3.2. Goal of the development and the outline of the construction method

PWRI is developing an automatic conveyance system for excavated earth, which does not require either workers stationed inside a caisson box for earth removal or a lock attendant[2]. The goal of this development is to completely automate the works inside a pneumatic caisson, by combining this system with the automatic excavator being developed in the private sector. Figure 10 shows a schematic diagram of the automatic conveyance system for excavated earth devised and examined by the institute.

The pre-conditions for this system are reasonable production costs and the feasibility of switching to the conventional method without suspending the construction work when problems such as breakdown of the machines occur.

With this system, the excavated earth is automatically removed using the following procedure:

(1) The residual earth excavated by the automatic excavator in the working chamber is collected on the bottom of caisson center;

(2) The accumulated earth is lifted out of the

working chamber by a telescopic clamshell bucket;
(3) The earth receiving board is closed, and the earth is led to the shoot;
(4) The slide gate is opened, and the earth is fed into the bucket; and
(5) Using the automatic-control skater, the bucket is rolled up, the shaft is lifted, and the earth is dumped into the earth hopper.
Here, operations such as the collection of excavated earth, the switching of the earth receiving board, the slide gate, and the lock, the raising and lowering of the bucket, and the dumping of earth into the earth hopper, are all conducted automatically.
When system trouble occurs, the construction continues, being switched to the conventional method; the bucket is put into the working chamber which is being loaded with earth by the excavator.

3.3. Element test

A test using an actual-size model of the earth removal system was conducted in order to confirm in detail the performance and durability of each element of this system. In the test, emphasis was placed on the earth flow in the shoot, the durability of the slide gate, and the precision and durability of various sensors for the automatic control (see Plate 6).

4. Conclusion

As mentioned earlier, PWRI has been developing technology for automating the construction of open and pneumatic caissons. The results of tests using actual-size models, all of which had been completed by last year, are now being used to prepare design and construction manuals for putting the methods to practical use.
Road construction in Japan is expected to become increasingly difficult in the future, since it will be required in mountainous areas and congested urban areas. Therefore, construction terms and on-site works must be reduced. Moreover, the number of deep underground construction works is expected to increase. The technological development for automating construction works introduced in this paper will be helpful for saving labor and meeting such social needs.

Notions:
(1) Open caisson method
Method to cause a caisson to settle into a desired bearing layer by using a clamshell or grab bucket to excavate and remove earth within the caisson interior.
(2) Pneumatic caisson method
Method to install a working room at a bottom of a caisson to which compressed air is supplied for discharging water and to cause the caisson to settle onto a desired bearing layer by using human labor or machines to excavate and remove earth within the caisson interior.
(3) PC well caisson method
PC well caisson method is same to open caisson methods for excavation and settlement. The difference of this method is using precast concrete blocks for the main body, and using PC steel bars to conect the each blocks. The height of black is 2.0-2.5m and its diameter is 1.6-4.0m.

References
1) Ministry of Construction, et al.; Research on the Technological Development for Automating the Construction of Bridge Foundations (Open Caissons), 1992 Joint Research Report, 1993.3 (In Japanese)
2) Ministry of Construction, et al.; Research on the Technological Development for Automating the Construction of Bridge Foundations (Pneumatic Caissons), 1992 Joint Research Report, 1993.3 (In Japanese)
3) Nakano, et al.; Technological Development for Automating the Construction of Open Caissons, Civil Engineering Journal, 1994.1 (In Japanese)
4) Japan Road Association; Specifications for Highway Bridges, Part IV. Substructures, 1994.2 (In Japanese)

Table - 1. Advantages of the development

Developments items	Safety improvement	Quality improvement	Reduction of the number of workers	Reduction of construction terms	Scale-down of work yard	Practicability for large-scale foundations
Precasting of bodies	○	○	○	○	○	○
Development of an automatic excavation and earth removal system			○	○	○	○
Development of an automatic-control press-in settlement system		○	○			○

Table - 2. Verifications items in the trial construction test

	Purposes of the test	Check items in the test
General	Understanding the overall applicability and work efficiency of the construction	Applicability and work efficiency
		Construction control data
Body assembly works	Understanding the applicability and work efficiency concerning the assembly of precasted materials	Efficiency in the transportation of precasted materials
		Change in the stress of the joint sections and the precision of the body assembly
		Volume of consumable materials used, such as mortar and adhesive agents
		Safety and Feasibility
	Understanding the practicability of the connection between the precasted materials and cast-in-place sections	Construction efficiency and installation precision of PC steel bars
		Volume of consumable materials used
Excavation and earth uplift works	Understanding the performance of machines(the excavator, the earth lifter and the press-in equipment)	Applicability of disassembly and assembly
		Performance of the automatic control during operation
		Operational feasibility, safety, and maintenance feasibility
	Understanding the excavation efficiency	Excavation efficiency in each layer
	Understanding the linkage between the excavator and the earth lifter	Linked operation of the excavator and the earth lifter
		Operational feasibility, safety, and maintenance feasibility
	Understanding the linkage between the earth lifter and the press-in equipment	Linked operation of the machines and the systems
		Safety and maintenance feasibility
Settlement control works	Understanding the performance of the press-in position control	Performance of the press-in settlement and the precision of settlement
		Operational feasibility, safety, and maintenance feasibility of the press-in equipment and measurement instruments
		Behavior of the caisson and the evaluation of the settlement resistance
	Understanding the affect on the surroundings	Deformation of the surrounding ground

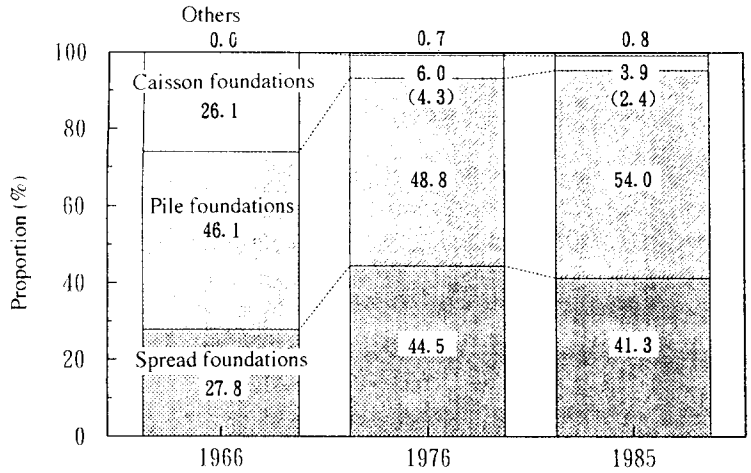

* Figures in parentheses indicate the proportion of open caissons

Figure - 1. Transition of foundation usage

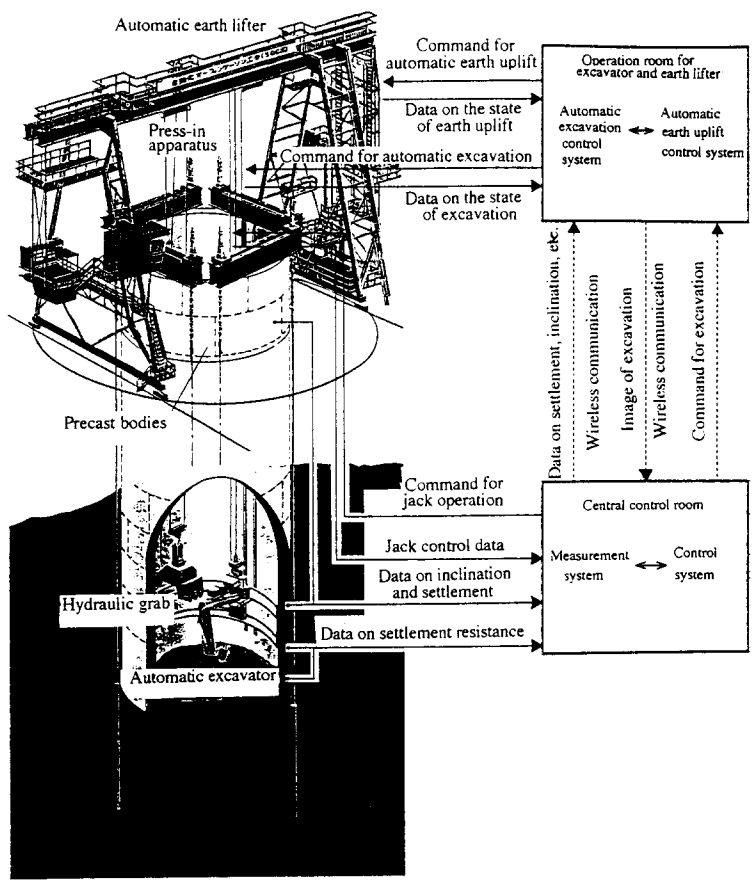

Figure - 2. Overview of the systems

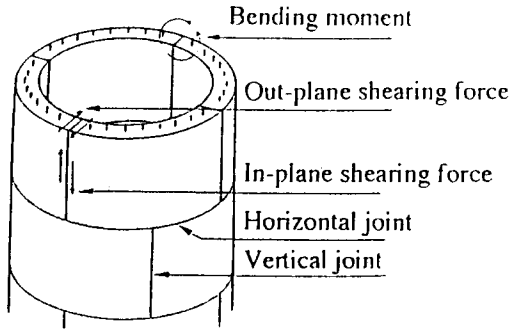

Figure - 3. The precast body using horizontal & vertical joints

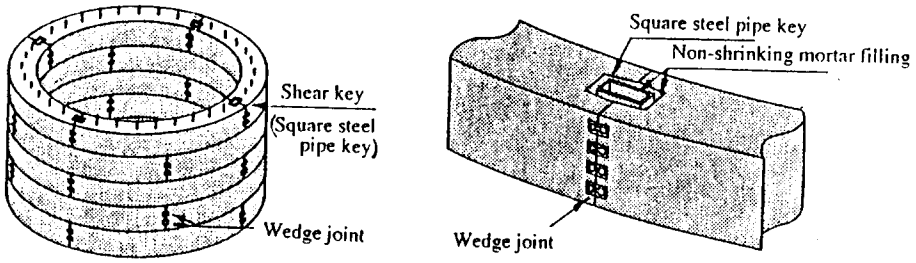

Figure - 4. Structure of wedge connection joint

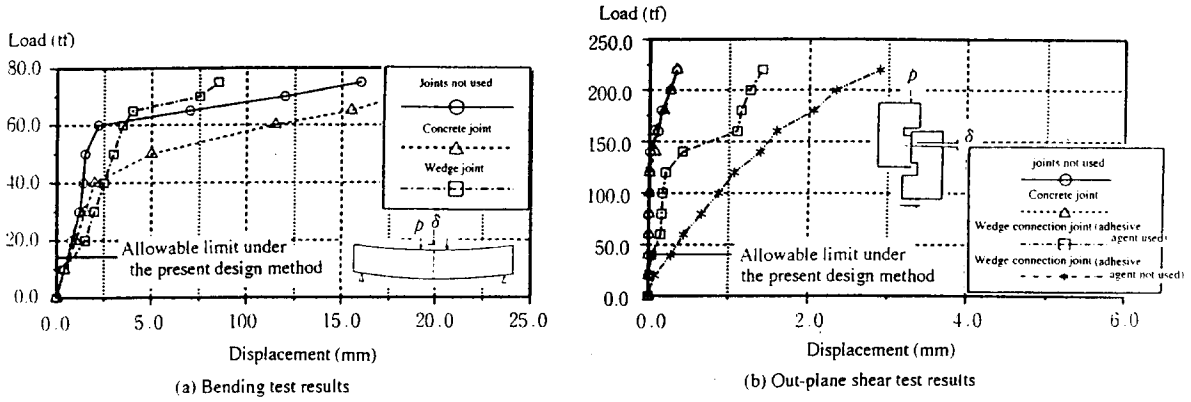

Figure - 5. Results of the loading tests on a vertical joint

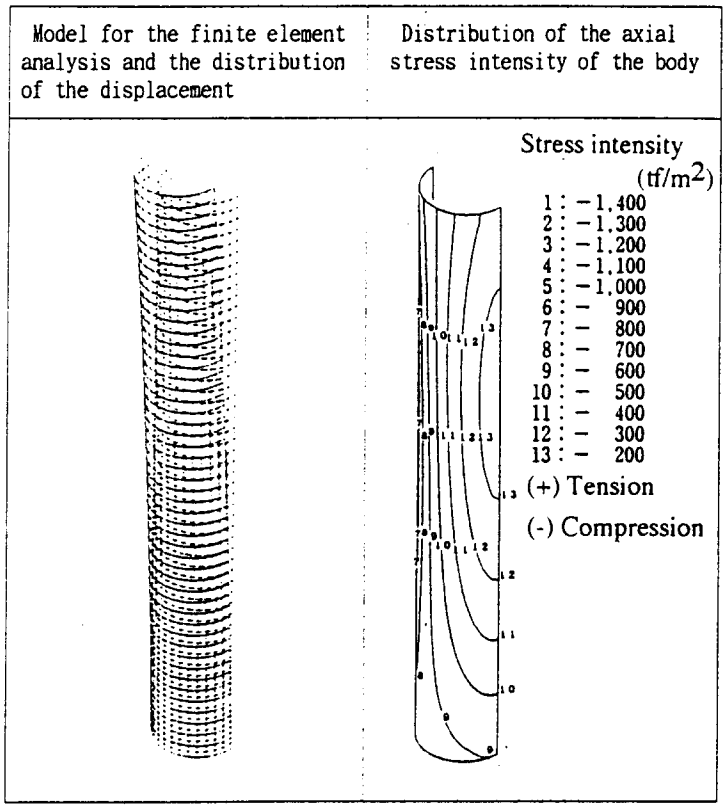

Figure - 6. Sample results of the finite element analysis

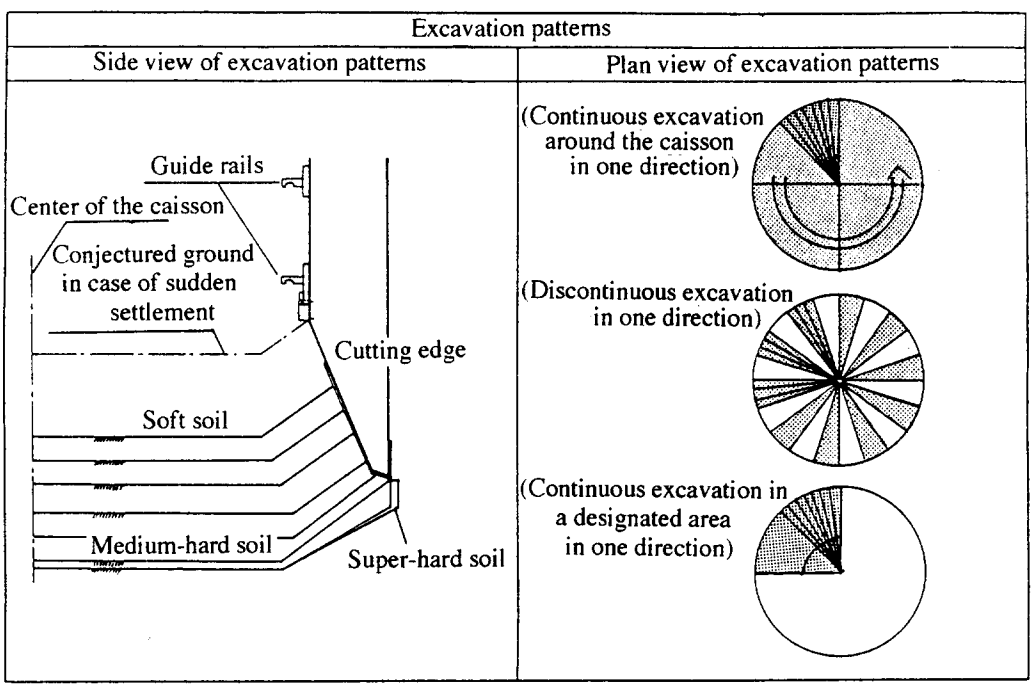

Figure - 7. Automatic control excavation patterns

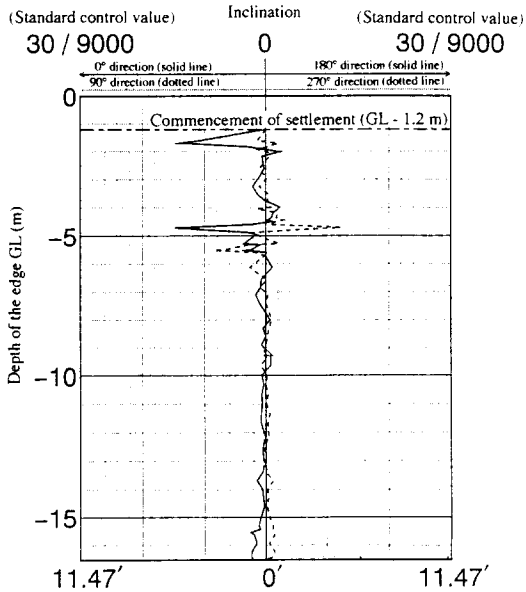

Figure - 8. Caisson inclination

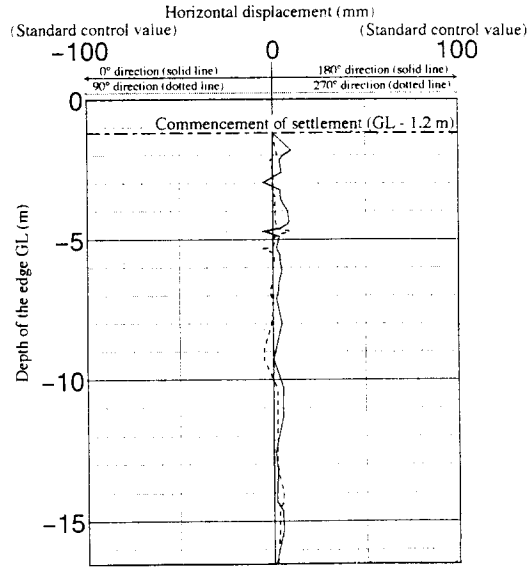

Figure - 9. Eccentricity on the top of the caisson

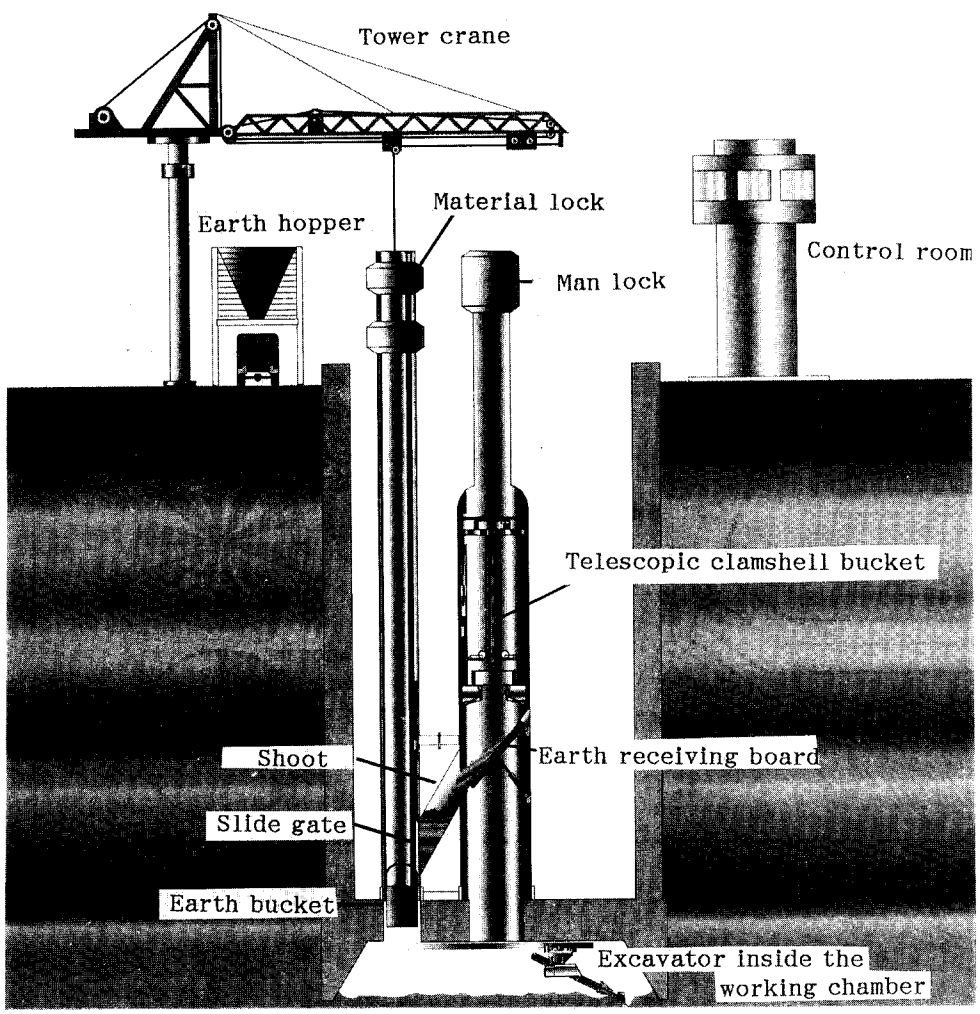

Figure - 10. Schematic diagram of the automatic earth removal system

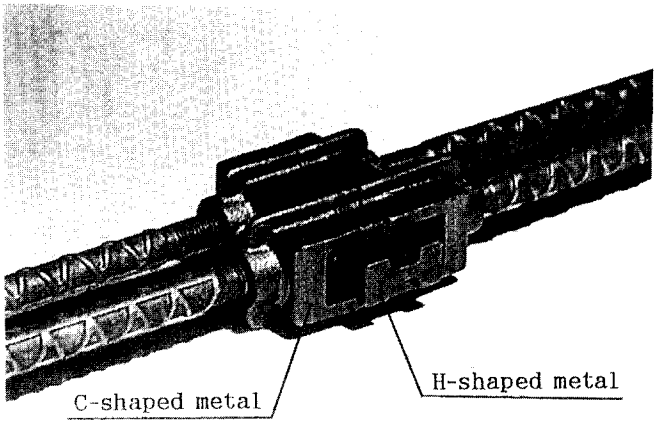

Plate - 1. Wedge metal

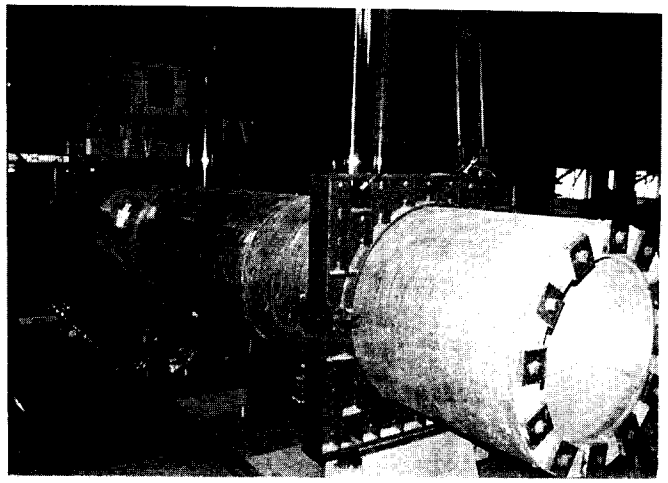

Plate - 2. Loading tests on the horizontal joints

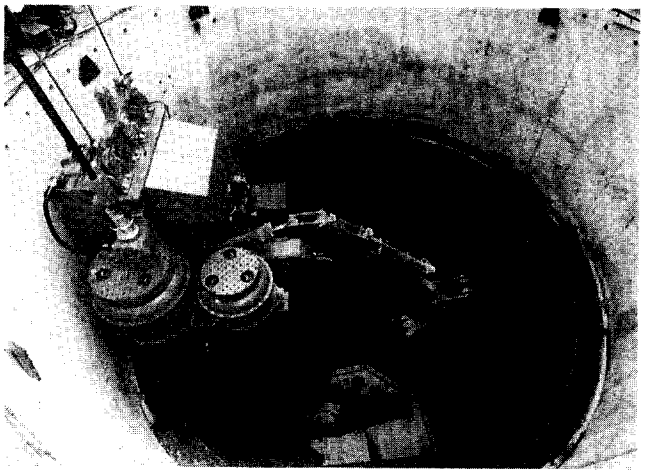

Plate - 3. The automatic excavators on the guide-rails

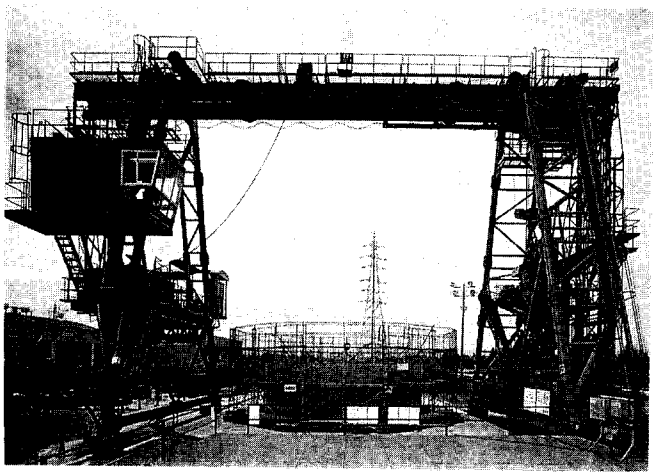

Plate - 4. The automatic earth removal device

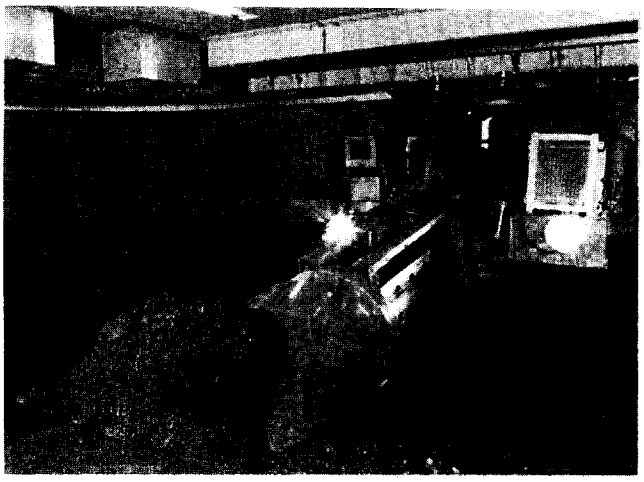

Plate - 5. The automatic excavator for Pneumatic caisson

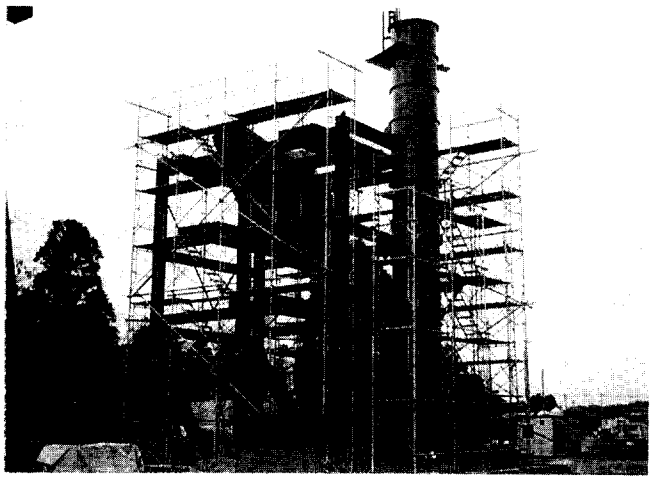

Plate - 6. Overview of the element test equipment

Strong-Motion Records on the Hokkaido-Nansei-Oki Earthquake in 1993

by

Masashi Satoh[1], Yuji Ono[2], Toshio Yamauchi[3], and Hiroaki Nishi[4]

ABSTRACT

On July 12, 1993, an earthquake occurred whose epicenter was off the southwest coast of Hokkaido. Large-scale tidal waves (tsunami) struck immediately following the earthquake and fires broke out, killing many people on Okushiri Island. Road embankments, bridges, river embankments, and harbor facilities particularly those on the Oshima Peninsula were seriously damaged.

The road division of the Hokkaido Development Bureau has installed strong-motion seismographs at 28 bridges in Hokkaido to observe strong motion. In the July 1993 earthquake, strong-motion records were obtained from 12 of these seismographs.

Various spectrum analyses and polarization analyses were conducted on typical strong-motion records of these 12, and the following facts were found: no predominant frequency was found, and there were many strong-motion records with short-periodic components.

KEYWORDS: The 1993 Hokkaido Nansei-oki Earthquake, strong-motion records, polarization analysis

1. Introduction

A large earthquake occurred in the southwest region of Hokkaido at 22:17, June 12, 1993. In this earthquake, strong seismic motions of the V degree on the seismic intensity scale of the JMA (Japan Meteorological Agency) were recorded in Otaru City and Suttsu and Esashi towns, while tremors were felt in a wide range of areas from throughout Hokkaido to the Tohoku district. The epicenter was approximately 100 km off the southwest coast of Hokkaido, at 42° 7' N. lat. and 139° 2' E. long., at a depth of 34 km. The quake measured 7.8 on the Richter scale of magnitude. This earthquake occurred in a region where few earthquakes had occurred before. It was the first earthquake along the shore of the Sea of Japan since the Central Sea of Japan Earthquakes (Richter magnitude 7.7) of 1983, and the scale of the Nansei-oki Earthquake was the same as of the 1993 Off Kushiro Earthquake. The Hokkaido Nansei-oki Earthquake was the nation's 5th largest earthquake since the Great Kanto Earthquake of 1923 as shown in Table 1. After the July 1993 earthquake, many aftershocks occurred, including over 150 tremors, and strong seismic motions of V degree on the seismic intensity scale were recorded again on Okushiri Island on August 8.

As of 1994, the Structures Section, the Civil Engineering Research Institute of the Hokkaido Development Bureau, had installed strong-motion seismographs at 28 bridges on national highways from 1966 when a strong-motion seismograph was installed at Chiyoda Bridge in the Tokachi district of Hokkaido. In the 1993 Hokkaido Nansei-oki Earthquake,

1) Head, Structures Section, Civil Engineering Research Institute
2) Research Engineer, Structures Section, Civil Engineering Research Institute
3) Deputy Head, Structures Section, Civil Engineering Research Institute
4) Research Engineer, Structures Section, Civil Engineering Research Institute

strong-motion records were obtained from 12 of these seismographs, and strong-motion records of over 100 gal were obtained at 5 strong-motion seismic stations. The largest acceleration was 249 gal, recorded at the Shichiho Bridge 155 km away from the epicenter. This paper reports on response acceleration spectra, running spectra and polarization analysis performed on these major records.

2. Outline and Damage of the Earthquake

In the 1993 Hokkaido Nansei-oki Earthquake, which was not as big as the Off Kushiro Earthquake of January 1993 when compared on the JMA seismic intensity scale of 1-7, strong seismic motions of V degree on the seismic intensity scale were recorded at 3 JMA observation stations. When measured on the Richter scale, however, it was equivalent to the Great Kanto Earthquake of 1923, the Tokachi Offshore Earthquake of 1968, and the Kushiro Offshore Earthquake of January 1993. The depth of its epicenter was 34 km, which was almost the same as depths of previous earthquakes, while that of the Off Kushiro Earthquake was very deep.

A large-scale tsunami warning was given in the area along the Sea of Japan of Hokkaido and of the Tohoku district immediately after the occurrence of the earthquake. In fact, a tsunami struck the coastal area of the Sea of Japan, and - especially on Okushiri Island - the tsunami and subsequent fires caused great harm to human life.

It also damaged public infrastructure including 711 roads, 14 bridges and 124 railway facilities. In road traffic networks, 16 sections of 5 public roads were closed, and it took 3 months to reconstruct some roads that had suffered collapses and landslides. The damage to traffic networks was so serious that some towns and villages near the epicenter remained isolated temporarily from the outside world. This speaks of the enormity of the earthquake. The major damage to bridges included the subsidence of embankments at the bases of bridges, and the breakage of bearing support mortar, of bridge anti-collapse devices, and of T-shaped columnar bridge piers (which also had been damaged in the Off Kushiro Earthquake). Table 2 shows the damage conditions.

3. Observation Stations and Strong-motion Records

Figure 1 shows strong-motion observation networks of the road division of the Hokkaido Development Bureau. Figure 2 indicates that, in this earthquake, records were obtained from 12 out of 28 observation stations. Circles in the figure show that the seismic wave records at the observation stations were digitized. Table 3 shows the names of bridges with digitized records, the ground classifications of the stations under the specification of road bridges, the types of strong-motion seismographs installed, and distances from the epicenter. Records are recorded on stylus paper for SMAC-B2 or on scratch film for SMAC-Q and D except at the Hakucho Bridge. However, since the frequency characteristics of records differ depending on machine types, records are corrected, after digitization, in relation to main axis, circular arc, and frequency characteristics.

Table 4 shows the maximum acceleration of the following 3 components with corrected records at each bridge: the bridge axis direction (Longitude: LG), the right angle direction of the main axis (Transverse: TR) and the up-down direction (UD). The maximum acceleration measured in this earthquake was

249 gal at the Shichiho Bridge (ground classification Class-I by the specification of road bridges), which was 155 km away from the epicenter. Compared with the Off Kushiro Earthquake of 1993, no acceleration of over 300 gal was recorded, probably because bridges were far away from the epicenter.

Strong-motion records at the Kamitorisaki Bridge and the Shichiho Bridge, which are comparatively near the epicenter, are shown in Fig. 3-(a),(b). As indicated by these strong-motion records, the P-wave recorded at both the Kamitorisaki Bridge and the Shichiho Bridge (both Class-I ground, roughly equidistant from the epicenter) was equal and was 30 seconds. However, comparing the S-waves, that of the former was 50 seconds, of the latter 25, respectively; in other words, the length of principal shock differed greatly. No common term was found for original waveform characteristics.

4. Running Spectra and Acceleration Response Spectra

Running spectra were obtained to conduct waveform analysis, including dynamic characteristics of the ground. The analysis was made by obtaining the power spectrum for 9 seconds waveform in time axis, by moving step width by 5 seconds. A Lag window of 0.25 Hz was used to smoothen spectrum. Figure 4-(a) shows the results for the Kamitorisaki Bridge of Class-I and the Hakucho Bridge of Class-III, by the ground classification. The dotted lines in the figure show characteristic value (T_G) of the ground calculated from the specification of road bridges. Concerning frequency characteristics at the Kamitorisaki Bridge, the frequency predominated at 1.5 Hz near second 50 of the principal shock, but it shifted to 3 Hz, which is almost the same as T_G of the ground, near second 70. Figure 4-(b) shows running spectra at the Hakucho Bridge which stands on Class-III ground. The frequency characteristics at the Hakucho Bridge had no typical predominant period, but it was found that the bigger acceleration amplitude of principal shock, the more the low-frequency component tended to be amplified. This is thought to have been due to a non-linear tendency of the ground which became remarkably apparent along with acceleration of amplitude.

Figure 5-(a),(b) shows acceleration response spectra (damping constant of 5%) at a right angle to the bridge axis at the Kamitorisaki Bridge and the Shichiho Bridge, while Fig. 6-(a),(b) shows that at the Hakucho Bridge and the Sapporo IC viaduct. The response spectrum tended to decrease gradually with the lengthening of natural period.

5. Polarization Analysis

For back azimuth estimates, a time-domain non-linear polarization filter analysis originally proposed by Flinn has been used. In this study, "Rectilinear Motion Director Filter Analysis" was adopted, which is widely used to emphasize the phase difference in a direction of seismic waves. The characteristics of this analytical method are expressed by the dual parameters of the rectilinearity of the elliptic, particle orbital motion in a three dimensional space and in the direction of polarization.

A data set was built from the analysis of three-component recordings from the seismic station at the Kamitorisaki Bridge. This technique, however, was used for calculating an accelerogram in a given direction.

Figure 7 shows the results of the analysis. In the figure, sigma indicates power in the ma-

jor axis direction of time width at a given time, theta indicates azimuth from due north in the direction of the major axis, and phi indicates angles between major axis and vertical axis. Figure 8 shows component waves calculated from polarization analysis. They are, from top to bottom, the up-down direction component wave, the east-west direction component wave, the south-north direction component wave, the horizontal component wave in the maximum major axis direction at the peak power, the horizontal component wave at a right angle to the maximum major axis at the peak power, the P-wave, and the SV-wave. Consequently, horizontal seismic motion dominated at the Kamitorisaki Bridge. As indicated in Table 5, the tendency of horizontal seismic motions was also obtained from the other records.

6. Conclusion

The characteristics of the 1993 Hokkaido Nansei-oki Earthquake are:

1) On the Richter scale, it was the 5th largest earthquake in Japan since 1923.

2) On the seismic intensity scale of the Japan Meteorological Agency, the earthquake was smaller than the 1993 Off Kushiro Earthquake, but it caused serious harm to human life.

3) Even though ground classifications and the distances from the epicenter were the same, the lengths of principal shock differed.

4) According to various spectrum analyses, no predominant frequency was recognized.

5) Except at the Sapporo IC viaduct, the seismic wave had waveform characteristics containing high-frequency component waves.

6) According to the polarization analysis of seismic motion, horizontal motion dominated.

References

1) "Control System of Strong-motion Records"; Civil Engineering Institute Monthly Reports No100

2) Flinn, E.A.: Signal Analysis using Rectilinearity and Direction of Particle Motion

3) "Outline of Strong-motion Records on the Off Kushiro Earthquake of 1993" 25th joint UJNR

table-1 Details of Recent Major Earthquake

Date	Name	Mj	Focal Depth
September 01, 1923	Great Kanto Earthquake	7.9	-
December 21, 1946	Nankai Earthquake	8.0	20km
March 04, 1952	Off Tokachi Earthquake	8.2	0
August 12, 1961	Off Kushiro Earthquake	7.2	80
June 16, 1964	Niigata Earthquake	7.5	40
May 16, 1968	Off Tokachi Earthquake	7.9	0
June 17, 1973	Off Nemuro Peninsula Earthquake	7.4	40
June 12, 1978	Off Miyagi Peninsula Earthquake	7.4	40
March 21, 1982	Off Urakawa Earthquake	7.1	40
May 26, 1983	Off Akita Prefecture Earthquake	7.7	14
January 15, 1993	Off Kushiro Earthquake	7.8	107
July 12, 1993	SW Off Hokkaido Earthquake	7.8	34

table-2 Outline of the 1993 Hokkaido nansei-oki earthquake

Date	July 12, 1993
Time	22:17
Magnitude on the JMA scale	7.8
Hypocenter	Long.139°12'E, Lat.42°47'E
Depth of focus	34km
Killed	202persons
Wounded	305persons
Missing	29persons
Damage to buildings (half to full)	805 houses
Damage to buildings (less than half)	2,193 houses
Damage to public utilities	445 houses
Damage to roads	711
Damage to bridges	14
Damage to railroads	124
Damage to harbor facilities	11
Damage to fishingports	58
Damage to ships	1,748
Damage to river facilities	326
Damage to agriculture facilities	2,953
Damage to commerce and industry facilities	2,264
Damage to life lines	38
landslips	14

As of September 15, 1993

table-3 Ground and Other details of Seismic Stations

Bridge Name	Ground Classfication	Type	Distance
Isoya	3rd class	SMAC-D	96
Kamitorisaki	1st class	SMAC-Q	140
Hakucho	3rd class	AJE-306	152
Shichiho	1st class	SMAC-B2	155
Ishikari-Kako	3rd class	SMAC-B2	182
Sapporo IC	3rd class	SMAC-Q	184
Shin-Ishikari	3rd class	SMAC-B2	193

table-4 Maximum Accelerations

Bridge Name	Latitude	Longitude	Acceleration (gal)		
			LG	TR	UD
Isoya	42.87°	140.37°	118	148	53
Kamitorisaki	42.10°	140.57°	181	231	77
Hakucho	42.35°	140.95°	151	170	81
Shichiho	41.59°	140.31°	235	249	97
Ishikari-Kako	43.22°	141.35°	31	36	12
Sapporo IC	43.07°	141.43°	41	57	27
Shin-Ishikari	43.14°	141.52°	107	98	28

LG : Longitude Direction
TR : Transversal Direction
UD : Up and Down

table-5 Direction of Major Axis & Angle between this Axis and Epicenter

Bridge Name	Incident Angle			
Kamitorisaki	84°	50°	106°	95°
Hakucho	82°	-23°	48°	31°
Shichiho	90°	-53°	22°	13°
Ishikari-Kako	90°			
Shin-Ishikari	82°	46°	148°	91°

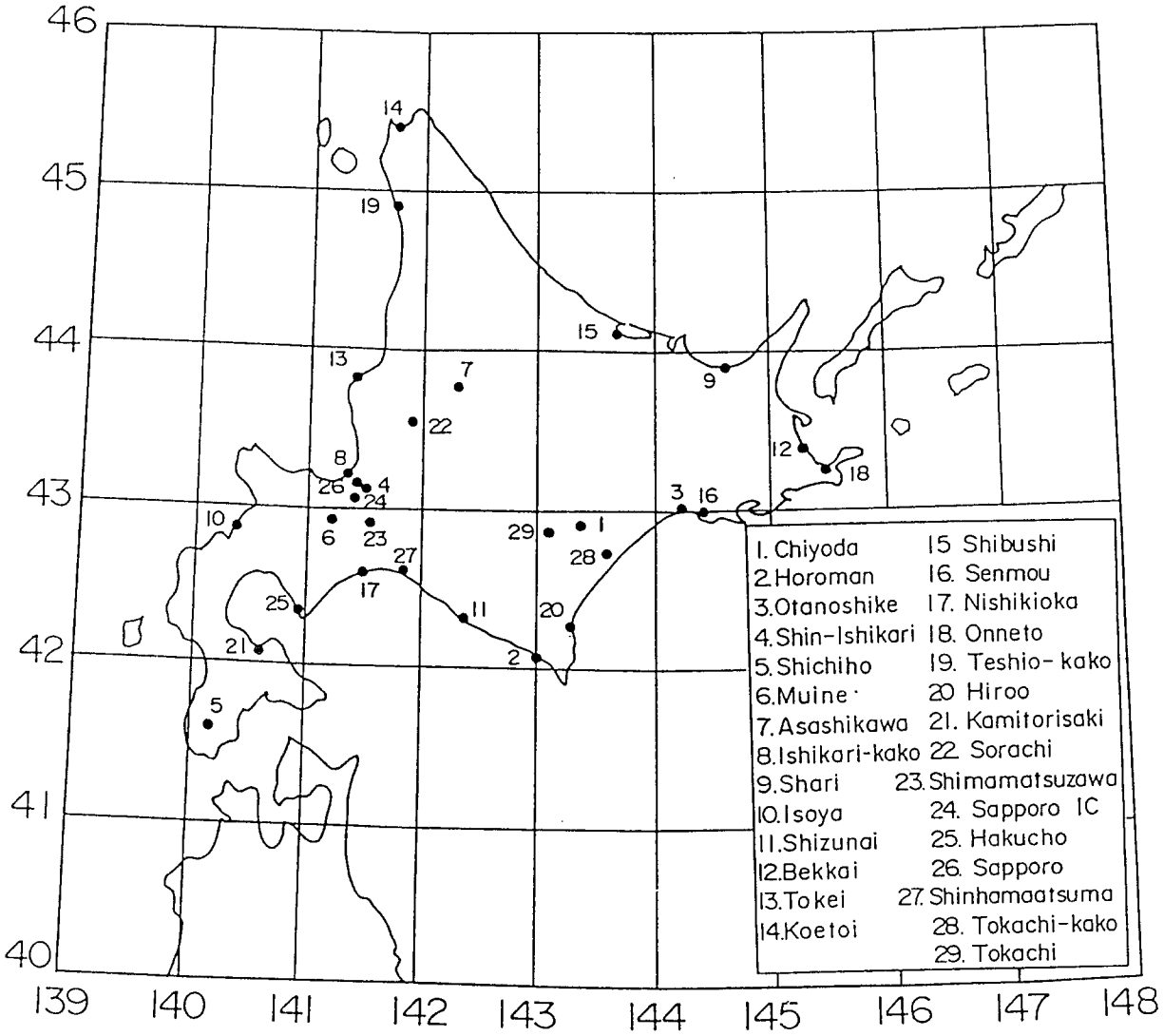

Figure - 1 Location of seismic stations of the Stractures Section.

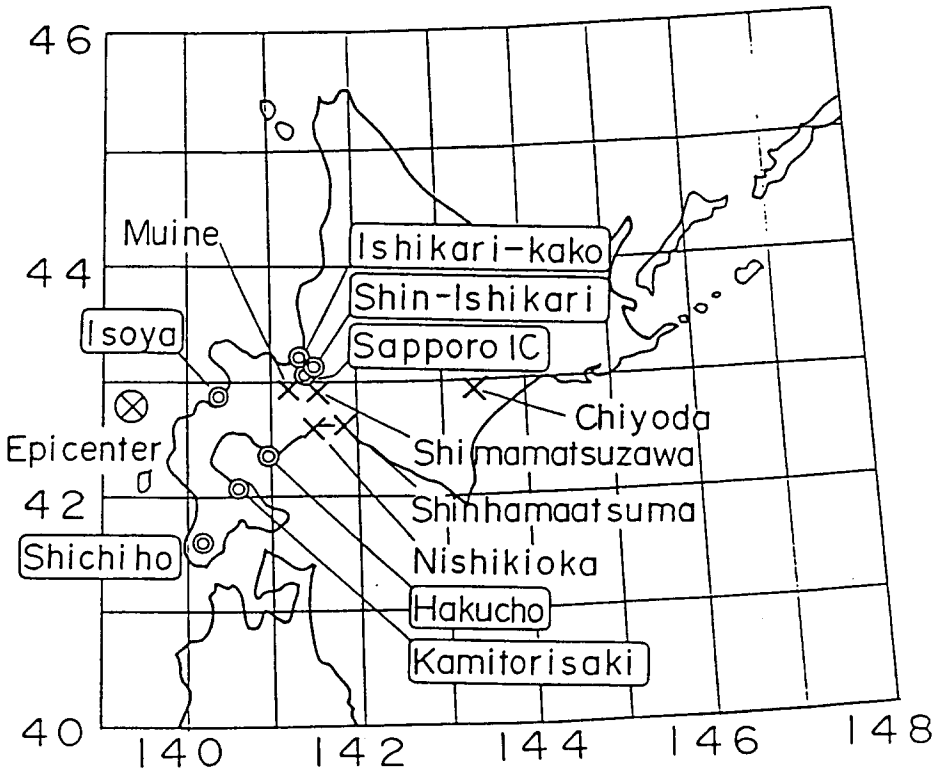

Figure - 2 Epicenter and location of seismic stations investigated in this study

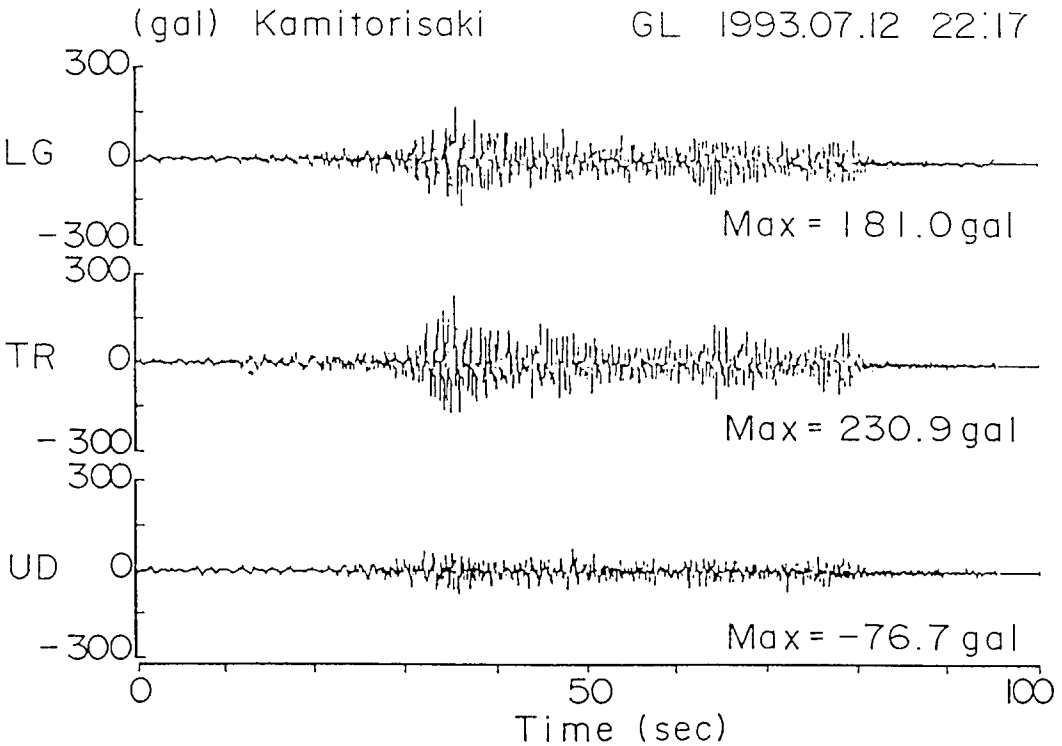

Figure-3(a) Storong motion record at the kamitorisaki Bridge. (Grand)

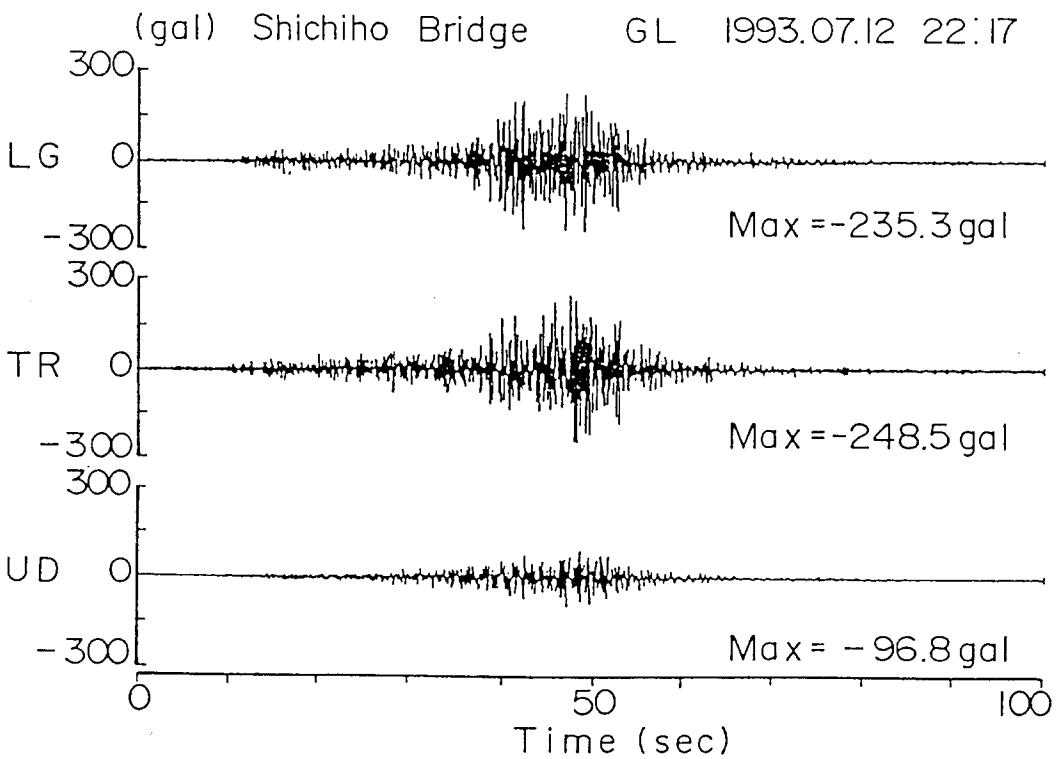

Figure-3(b) Storong motion record at the shichiho Bridge. (Grand)

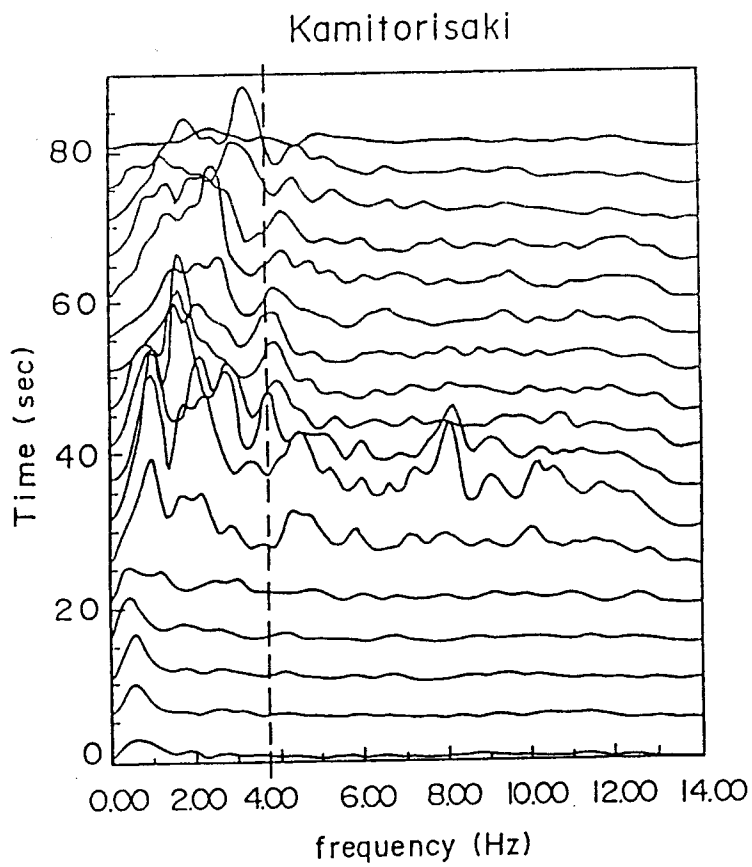

Figure-4(a) Running spectrum of storong motion record at the Kamitorisaki Bridge.

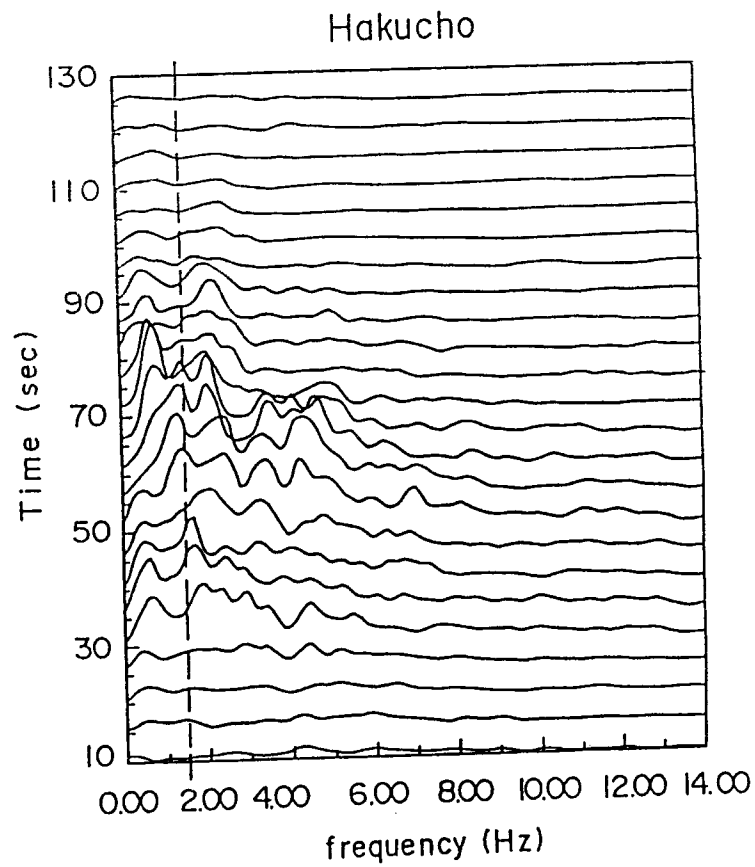

Figure-4(b) Running spectrum of storong motion record at the Hakucho Bridge.

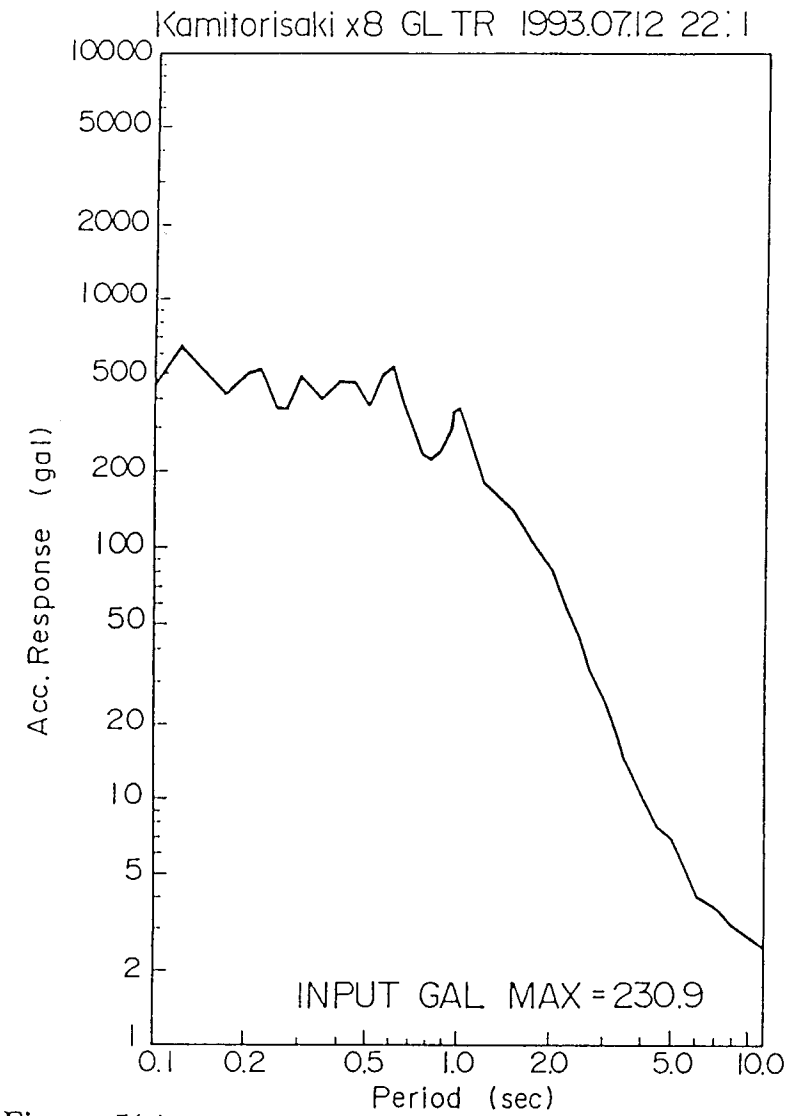

Figure-5(a) Accelerate resporse spectrum of Storong motion record at the Kamitorisaki Bridge. (Damping constant ; 5%)

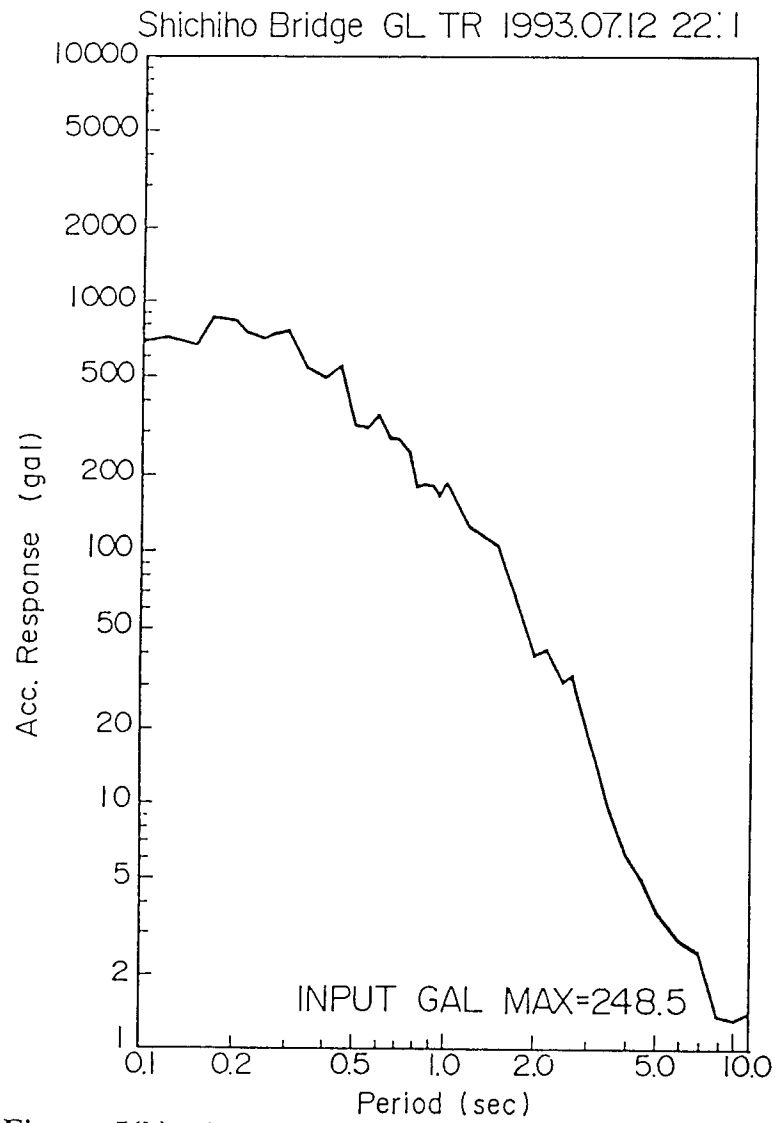

Figure-5(b) Accelerate resporse spectrum of Storong motion record at the Shichiho Bridge (Damping constant ; 5%)

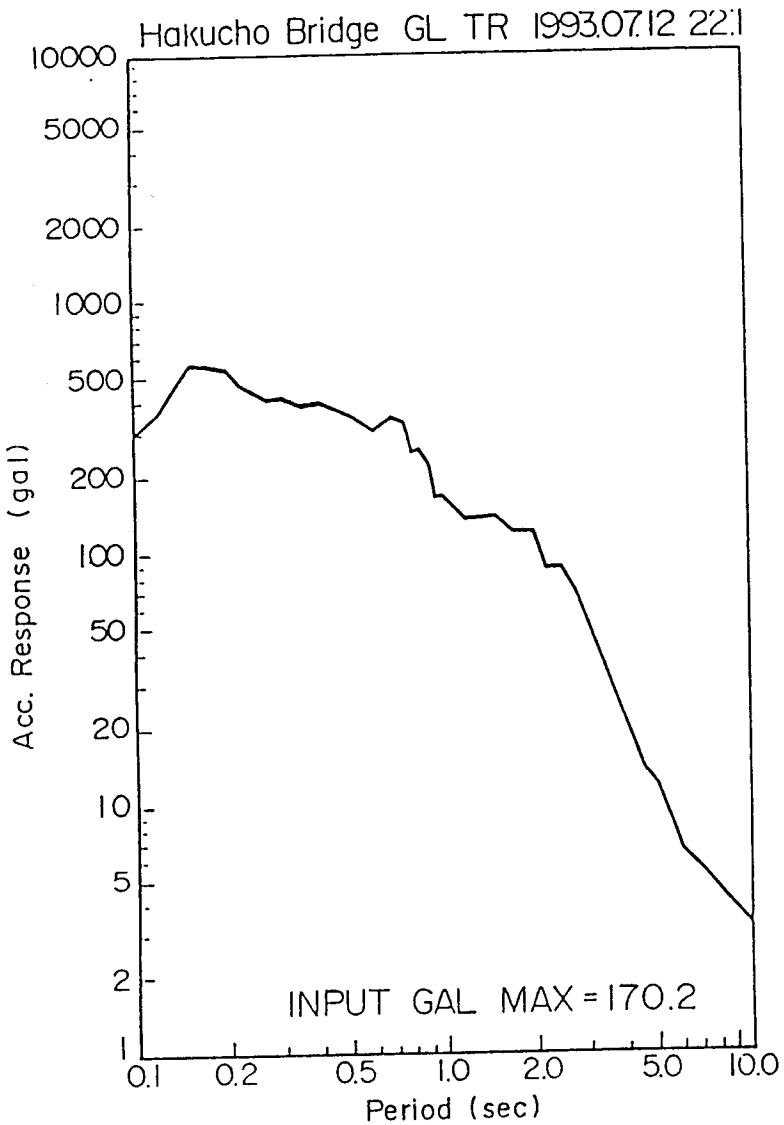

Figure-6(a) Accelerate resporse spectrum of Storong motion record at the Hakucho Bridge. (Damping constant ; 5%)

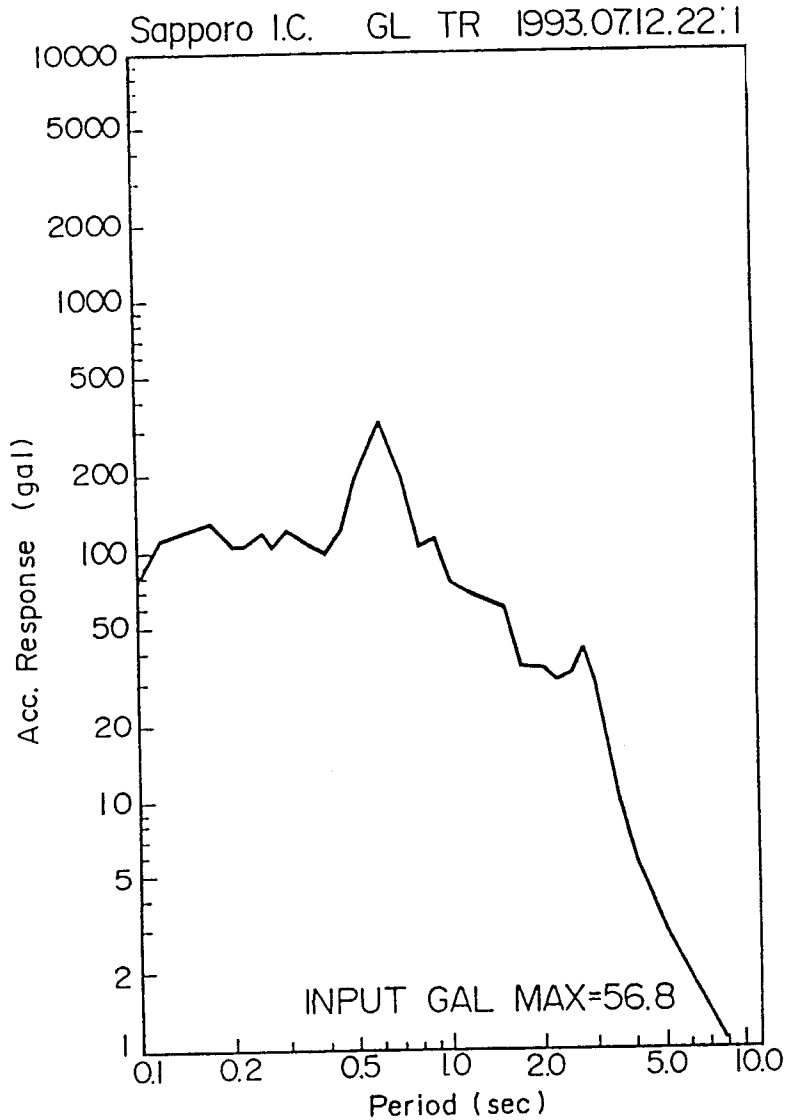

Figure-6(b) Accelerate resporse spectrum of Storong motion record at the Sapporo I.C Bridge. (Damping constant ; 5%)

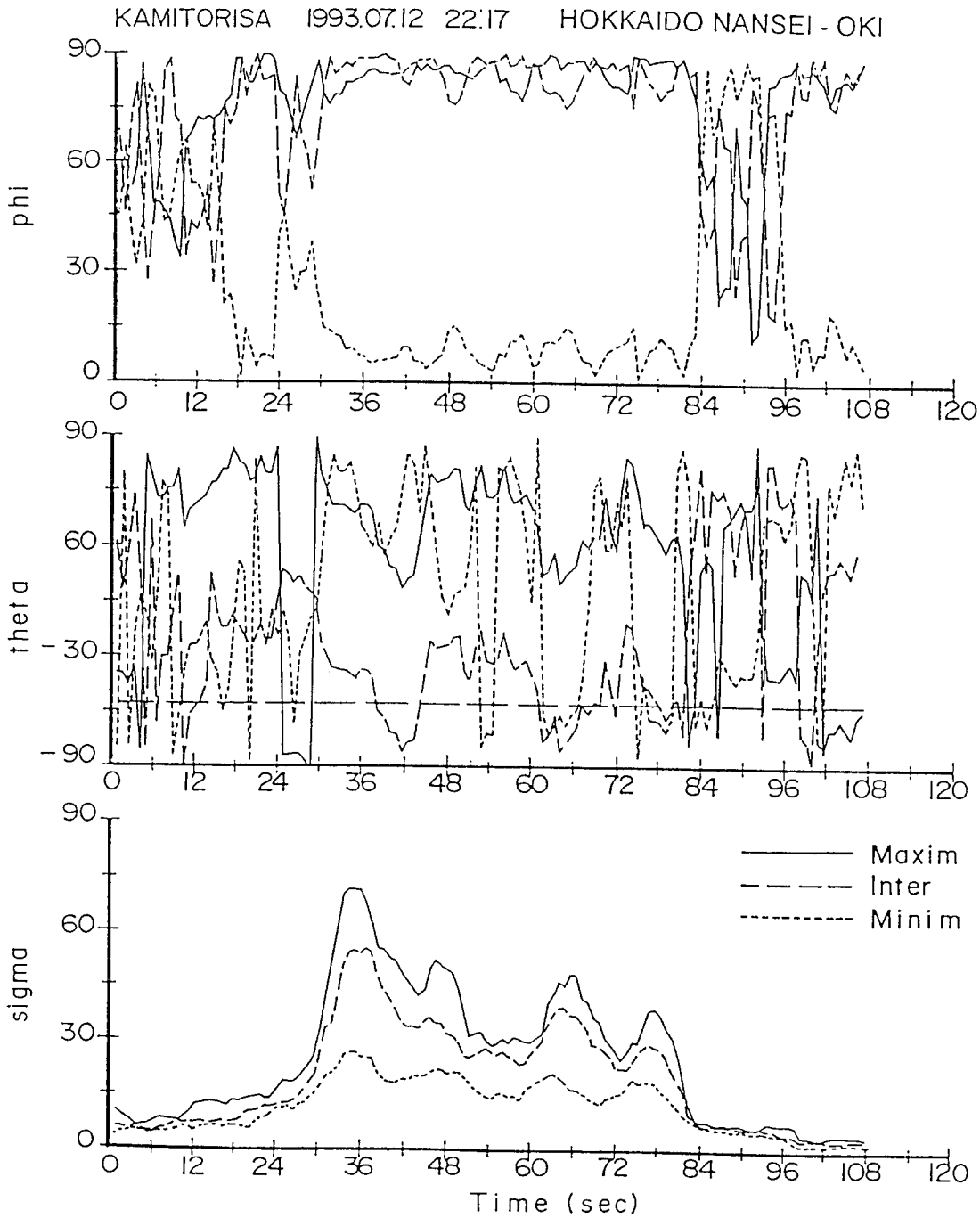

Figure - 7 Power spectrum of Storong motion record at the kamitorisaki Bridge.

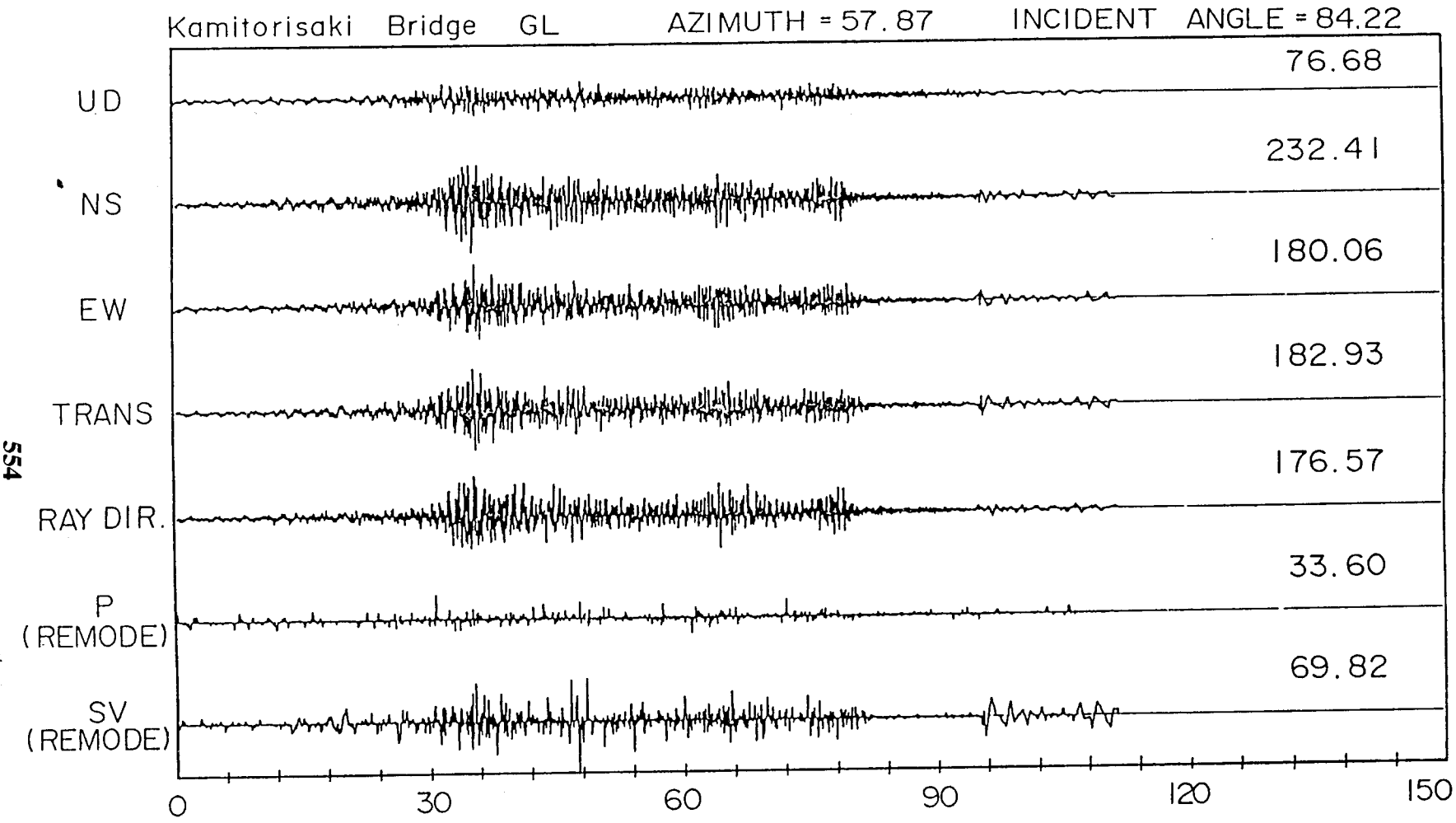

Figure - 8 Principal Axis Analysis the Kamitorisaki Bridge (Grand)

Development of Integrated Numerical Research System for Prevention and Estimation of Coastal Disaster

by

Tomotsuka Takayama[1], Chiaki Goto[2], Hidenori Shibaki[2], and Toshio Aono[2]

ABSTRACT

This paper presented an outline of the design and applications of the Integrated Numerical Research System for Prevention and Estimation of Coastal disasTers (INSPECT)system. This system was developed to efficiently perform studies for preventing disasters on Japanese coasts due to wave, tsunami, and storm surge.

INTRODUCTION

Japan is located in an area with a severe natural environment. Typhoons and earthquakes hit frequently, and strong, northwest seasonal winds blow in the winter. For this reason, the coastal area shave often been heavily damaged by natural sea disasters. Typical of such disasters were the Ise-Wan Typhoon storm surge disaster in 1959 and the Chilean Tsunami disaster in 1960.

By experiment of these two disasters, research on the prediction andprevention of disasters has attracted considerable attention, and the construction of facilities to prevent disasters has been active. In 1994, the Hokkaido-Nansei Earthquake Tsunami hit Okushiri Island and caused severe damage. At that time, the island had disaster prevention facilities that were designed using external forces based on the Nihonkai-Chubu Earthquake Tsunami, which had occurred 10 years before. Nevertheless, a tsunami exceeding this level hit the island. This disaster provided the precious lesson that it is almost impossible to build facilities that can fully prevent damage from natural disasters, and that the development of disaster prevention measures based on previous disaster conditions is limited.

At the same time, we strongly believed in the necessity to develop systematic analytical techniques for preventing coastal disasters that can respond quickly to unexpected events and that can be applied to the wide range of Japanese coastal conditions.

To analyze coastal disasters, we must first study the phenomena causing the disasters. The use of numerical simulation experiments to scientifically reproduce these phenomena and predict the irreoccurrence in the future is believed to be well suited for the study of disaster phenomena. The development and wide-spread use of computers, in addition to the dramatic expansion of their capabilities, have made simulation practical. However, the analysis of phenomena using numerical simulation requires advanced, special techniques. To solve this problem, we developed the Integrated Numerical Research System for

1) Director of Hydraulic Engineering Division, Port and Harbour Research Institute, Ministry of Transport, Yokosuka City, Japan

2) Former Member of Ocean Energy Utilization Laboratory, Hydraulic Engineering Division, Port and Harbour Research Institute, Ministry of Transport

Prevention and Estimation of Coastal disasTers (INSPECT) system, which effectively combines past studies and numerical analysis for disaster prevention and systematizes the analysis process.

The INSPECT system is designed to be used for the Japanese coasts and is intended to be effective for processing follow-up calculations (hindcasting) of previous disasters, as well as for predicting future disasters. Compared to conventional analysis methods that require high-level knowledge, this system semi-automatically performs a series of processing steps, from the preparation of data to numerical simulation and the evaluation of results.

DESIGN OF THE INSPECT SYSTEM

1. Equipment configuration

The INSPECT system is an expert system for using numerical analysis to prevent disasters. This system has been developed to perform numerical simulations and a series of analyses for wave, tsunami, and storm surge extreme sea conditions through simple operations. Therefore, the system was designed to quickly output the same level of results as that of specialists, without requiring difficult analysis or high-level knowledge. The analysis is basically performed in an interactive mode, and consideration was given to the ability to perform processing using only simple data input.

The system is composed of engineering workstations (EWS), personal computers (PC), and peripheral equipment, as shown in Fig. 1. The EWS performs numerical simulations of wave, storm surge, and tsunami. The PC prepares the input data necessary for calculation, analyzes the observed or estimated values, and outputs the calculation results on a screen or paper. The EWS and the PC are connected on a network that transmits input and output information between them. Peripheral equipment for the system include externalhard disks for the EWS and the PC, and a laser printer, optical disk unit, and digitizer connected to the PC. The (1GB) hard disk for the EWS temporarily stores estimation results, while the (300MB) hard disk for the PC stores the observed value database. The laser printer provides paper output, the optical disk unit stores large-volumedata, such as computed values, weather charts, and the water depth charts database, and the digitizer converts analog information such as weather charts and water depth charts into digital data. The system also has video editing and playback equipment and a special-purpose EWS to perform dynamic picture processing of computation results.

2. System configuration and analysis

The wave climate statistical analysis system has two subsystems: wave statistical analysis, which can statistically process observed wave data at all places in Japan, and probable wave analysis, which determines the design wave (50-year probable wave) to be used for designing harbors.

The wave estimation system has four subsystems: wave hindcasting on Japanese coasts from a plane output type spectrum method model, wave hindcasting in inner bays (short fetch sea areas) using a plane output type parameter method model, wave prediction during a typhoon by a single point output type spectrum method model, and wave prediction on Japanese coasts by a physical factor multiple regression model. An output system for estimation results is also provided.

The tsunami calculation system has a

near-field tsunami calculation subsystem, which is used for tsunamis originating in the nearby sea area of Japan, a far-field tsunami calculation subsystem, which is used for tsunamis propagated across the ocean from a remote source, and an output system for the results.

The storm surge calculation system has an inner bay sea wind calculation subsystem, which uses a hybrid wind hindcasting model that combines an empirical formula with the MASCON model, a storm surge calculation subsystem, which uses a multi-layer model, and the results output system.

The support system is used for the preparation of input data for wave, tsunami, and storm surge calculations. The weather chart processing system digitizes the analog atmospheric pressure information plotted on a weather chart and generates a digitized database. This atmospheric pressure information is used for estimating wind, which is an external force for developing waves and storm surge. The water depth chart processing system digitizes the analog information on commercially available sea bottom topographical charts, marine charts, ground topographical charts, sea bottom sounding charts, and similar sources into a database. This digital, water depth and elevation information is used as basic data for preparing the calculation grid and the grid point water depth data that are used for calculating wave, tsunami, and storm surge characteristics.

In shallow water deformation calculations, wave deformation is calculated for shallow sea waves of various directions and periods. The resulting refraction and shallow water coefficient table (collectively called the coast coefficient) for a wave of a given direction and period at a given point is entered into a database. By using the coast coefficient, the time series information for offshore waves (which is calculated by wave hindcasting) is converted into shallow water information. The dynamic picture processing system processes the computations for wave, tsunami, and storm surge into dynamic pictures. These pictures make dynamic evaluation of the phenomenon possible.

Six databases are available for supporting these subsystems: the observed value database for observed waves, tsunami mark height, storm surge deviations, etc., the weather chart database, the water depth database, the coast coefficient database, the input value database for numerical simulation such as typhoons, fault parameters, calculation grid, grid point water depth, and the estimated value database for wave, tsunami, and storm surge. The use of these databases enables processing such as the preparation of input data for numerical simulation to be done rapidly and provides comparisons of observed and estimated values.

ANALYSIS THEORY OF THE SYSTEM

1. Wave analysis

(1) Wind estimation

The sea wind, which provides the external force for developing waves, is estimated using atmospheric pressure information. The first step in the sea wind estimation is to estimate the wind in a free atmosphereusing a hybrid model that combines a gradient wind model with a typhoon model. The next step is to convert the results into a sea wind using a boundary layer model[1].

(2) Spectrum method wave prediction

One method for handling irregular

waves is to assume that the wave is composed of component waves, each with a different height, period, and direction, and to represent the waves by their wave energy spectrum. Wave estimation by the spectrum method is based on the energy equilibrium equation and follows the time series change of direction spectrum, which represents frequency and wave direction. The MRI method of Isozaki and Uji[2] is used in this system. This model has been used in many applications, such as for wave predictions performed by the Meteorological Agencyand for calculations of the design wave for harbor facilities.

(3) Parameter method wave estimation

The parameter method[3] traces the change in non-dimensional wave energy and is used for wave hindcasting in short fetch sea areas such as inside of a bay. The fundamental wave development equation is formulated by the relationship between non-dimensional fetch and non-dimensional energy and by the 3/2-power relationship between non-dimensional wave height and - non-dimensional-wave period.

(3) Wave deformation calculation

In shallow sea areas, effects become important that otherwise need not be considered in the offshore wave calculation, such as shallow water effects, refraction, diffraction, reflection, and wave breaking. In this system, evaluation is performed by wave deformation calculations using the energy equilibrium equation only for the propagation term.

(4) Wave prediction

In addition to design wave analysis using a plane output type wave hindcasting model, the prediction of coastal waves is also important for preventing disasters. Offshore wave prediction is performed using a physical factor multiple regression model[4]. In this model, prediction is performed using a linear algebraicequation for the development, propagation, and decay of waves, while the wind-driven wave energy and swell energy are used as descriptive variables. Two models are available: model 1, which uses only the estimated wave energy, and model 2, which uses both the observed and estimated wave energies.

When high wave prediction is performed only where a typhoon is going to attack, a calculation method is used that traces the wave spectrum along the wave direction lines. The spectrum method is used for the wave development and propagation equation, and the output is for a single prediction point. Therefore, this method is named the single point output type spectrum method[5].

2. Tsunami analysis

(1) Numerical calculation of near-field tsunami

When the initial wave is formed, it propagates as a surface wave by the water pressure differential between that point and the surroundings. The tsunami is expressed by the long-wave theory equation since a long-wave approximation is possible. Numerical simulation quantitatively traces the water level and flow velocity of the tsunami, which is deformed in the process of propagation by the effects of shallow water, concentration, and resonance that are caused by the changing water depth and coastal topography. In this system, one of two fundamental equations is used (linear or nonlinear long wave), depending on the minimum water depth of the subject area.

(2) Numerical calculation of far-field tsunami

Spherical coordinates must be used for assessing phenomena propagating over distances greater than 10,000km, such as with the Chilean Tsunami. The scale is so large that the wave number dispersion property cannot be neglected. Therefore, linear dispersed wave theory considering the Coriolis force is used as a governing equation. In far-field tsunami calculations, as in near-field tsunami calculations, the initial waveform is calculated from fault parameters.

3. Storm surge analysis

(1) Inner bay sea wind prediction

The sea wind in an inner bay surrounded by land is different from that of an offshore sea wind because it is subject to the effects of land topography. This topographical effect greatly influences the accuracy ofinner bay wave and storm surge estimations. In this system, a hybrid wind model is used that combines an empirical formula with the MASCON model.

(2) Multi-layer storm surge model

Among the storm surge phenomena, the rise in waterlevel due to drift is caused by concentration of the drift current driven by the strong typhoon wind in the coastal area. The drift current has a vertically distributed flow velocity. The flow velocity is at its maximum at the sea surface and decreases with water depth. Therefore, if the drift current is approximated by a single-layer model, the vertically distributed flow velocity is incorrectly replaced by an average velocity that is uniform throughout the water depth. The flow rate can then be approximated, although the upper-layer flow velocity is underestimated, and the lower-layer flow velocity is overestimated. In the storm surge calculation, therefore, a multi-layer model is used to enhance the accuracy of the drift current estimate.

APPLICATION TO THE ANALYSIS

1. Wave climate analysis

(1) Analysis of design wave

The major reason for the development of design wave analysis is to identify the causes of wave disasters and to determine the probable magnitude of waves. In calculating design offshore waves, the extraction of weather turbulence, preparation of weather chart data, wave estimation in weather turbulence, calculation of the coast coefficient, verification of the estimated value, statistical analysis of extreme values, assumption of model weather turbulence, wave estimationin model weather turbulence, and study of the design offshore wave are performed in that order. The related analysis systems are the wave condition statistical analysis system and the wave estimation system. Subsystems for weather chart processing and shallow water wave calculations are used as support systems.

To extract weather turbulence, weath er conditions that caused high waves at t he point of interest over a long period of time are determined. During processing, a list of high waves by year, the maximum significant wave distribution during the period, and other parameters are generated by the wave statistical analysis subsystem. Such information is used as the basis for extracting the weather conditions corresponding to the

yearly maximum and extreme waves.

Wave prediction is performed after the weather data is prepared. Calculations are made on the time series changes of the significant wave height, significant wave period, and wave direction at the point of interest when the high wave occurs. In the wave hindcasting system, when the area and period of time are specified, the EWS automatically performs gridpoint interpolation of the atmospheric pressure, wind estimation, and wave estimation in that order. The gridpoint pressure is calculated using the spline plane interpolation method converted into latitude-longitude coordinates. As described in the theory of wave analysis, wind estimation is performed by using the gradient wind/typhoon hybrid model and the atmosphere boundary layer model. In wave estimation, either the plane output spectrum method or the parameter method isselected depending on the sea area.

For wave hindcasting using the plane output spectrum method, the latitude-longitude coordinates are used. For main harbors on Japanese coasts, the wide area where wind-driven waves develop is approximated by a 1/2 degre grid. As it approaches the harbor, the area is approximated by a 1/8 degree grid and then by 1/24 degree grids to accurately represent the shielding effect of the land. The hindcastings are summarized as alist of maximum significant wave height and significant wave period by direction at all grid points for each turbulence. This list is stored as the wave estimated value database. The design wave at the point concerned is calculated by using this database and the probable wave analysis system.

The probable wave analysis system performs the various processing tasks that are required for calculating the probable offshore wave. Such calculations include the extraction of estimated data at the point of interest, correlation analyses of the estimated and observed values, and statistical analysesof extreme values. The time series change of the maximum significant wave and the extreme wave by direction for each year are obtained from the estimated wave value database over a long period of time, as shown in Fig. 2. This is used as basic data for calculating the design wave at the point concerned. Because of the calculation errors in wave estimation, the correlation between the estimated and observed values is analyzed to improve the empirical formula and produce estimations closer to the observed value. To perform this correlation automatically, observed values for the same weather turbulence as the one being estimated are searched and extracted from the observed wave database.

However, when the observed value is in shallow water, a table of coast coefficients for the observation point should be prepared by wave direction and wave period using the wave deformation calculation subsystem. The estimated value must be converted into a shallow water value before comparison to the observed value. To perform the wave deformation calculation, the calculation grid and the grid point water depth are needed as input data. This data is automatically prepared for the point concerned by using the coastline and water depth information that is stored in the water depth database.

Statistical analysis of the extreme wave value is performed using the estimated value corrected by the observed value. Fig. 3 shows the distribution of wave height of a 50-year probable wave calculated for each direction.

(2) Coastal wave prediction[4]

The object variables for wave prediction using thephysical factor multiple regression model are the estimated wave energy at the time to be predicted, the estimated and observed wave energy at the present time (when the prediction is performed). Therefore, estimates of the wind at the present and at the time tobe predicted are required. The wind at the present can be calculated from the wind estimation model by converting the flash weather chart into digital information using the weather chart processing subsystem. The predicted wind can be calculated by digitizing the predicted weather chart. Figure 4 shows an example of a 12-hour wave prediction at Hitachi Naka Harborin February, 1983, obtained using model 2.

Wave prediction is shown in two components, wind wave and swell. Shown from the top to the bottom in the figure are the predicted wave direction of the composite wave for the wind wave and swell, the time series change between the predicted and observed significant wave height, the time series change between the predicted and observed significant wave period, the component wave direction for the wind wave and swell, and the time series change in equivalent significant wave height and equivalent significant wave period for the wind wave and swell. The prediction results are satisfactory for both low- and high-wave periods. During wave development, the direction of the composite wave coincides with the direction of the wind wave, while during wave decay, the composite wave direction agrees with the swell direction. Regardng the wind wave and swell components of significant wave height, the wind wave component was predominant on February 17 when the maximum height wave developed, while the swell component was predominant from the 20th to the 21st, when the wave was decaying. During wave development, the period of the wind wave componentis almost equal to that of the composite wave.

Thus, the wave prediction model can predict not only the significant wave height, but also the significant wave period and its direction. It also can separate the wind wave component from the swell component. Moreover, the predicted offshore wave can beconverted into shallow water wave information by providing the coast coefficient database at multiple points (e.g., at the front of a breakwater) in the shallow water area.

The single point output type wave prediction modelis intended for wave prediction when a typhoon hits. Fig. 5[5] shows the wave predictions for Typhoon No. 8213 off Kochi, as output on the PC screen. The time series change of the typhoon path, the typhoon scale, and the observed wave state are displayed on the screen. The estimated and observed values of significant wave height, period, and direction are also displayed during the progress of calculation. Prediction of the maximum wave for the typhoon is performed on the PC by simple input of the typhoon information, including the predicted path and scale, using a mouse or keyboard. The time required for prediction of the maximum wave is about one minute for a five-day wave prediction.

3. Tsunami and storm surge analysis

(1) Analysis of tsunami and storm surge

Numerical calculations of tsunami and storm surge are often used to investigate the effect of disaster prevention structures. First, calculations for reproducing previous great tsunami and storm surge events are performed to determine the tsunami wave source and the storm surge weather

turbulence. Predictions are then calculated for the planned location. Tsunami waves and storm surge are numerically computed by sequentially combining zones with different grid intervals from the offshore sea area, where the wave or weather turbulence source is located, to the coastal or harbor area concerned. This is to keep the discrete and cancellation errors small. Normally, a grid interval of 1/20 to 1/30 or finer of the tsunami or storm surge wave length is used.

A feature of the system is that the calculation program and input data can be prepared automatically simply by editing control data for the specified mode. Control data is edited interactively. One piece of control data connects the calculation grid and grid point water depth data for tsunami/storm surge calculations with input data such as the calculation range, grid interval, time in terval, fault parameter and typhoon constant, and completes the calculation preparations. The calculation grid and the grid point water depth can be prepared using any calculation rangeand grid interval for any coastal area in Japan, whether off-shore or on-shore, by using the water depthchart processing system and the water depth chart database. When detailed topographical approximation of a harbor and coast isquired, the plan view of the planned structure and the harbor bottom sounding chart are entered into a database, and the calculation is performed in the same manner. In the tsunami/storm surge calculation system, the Japanese coast is separated into distinctive sea areas, and each sea area is independently systematized. The database for the harbor is added to the corresponding sea area system if necessary.

Input data is provided for previous tsunamis from the fault parameter database by selecting the tsunami number. Likewise, input data for a previous storm surge is provided from the typhoon database by selecting the typhoon number.

The prediction results are output on the screen or paper. Information about the maximum tsunami/storm surge water level and other parameters for each grid point is stored in the tsunami/storm surge estimated value database. The estimated value is correlated with the tsunami mark height data or the storm surge deviation data to verify the calculation accuracy.

(2) Sanriku coast tsunami analysis[6]

The Sanriku coast is divided into 33 zones for calculation. Each calculation zone has six grid interval stages from A to F. The deep sea area (zone A) has a grid interval of 5,400m and ranges from off of the Nemuro Peninsula in Hokkaido to the coastal area in Miyagi Prefecture. This covers the sea area where near-field tsunamis develop that hit Sanriku. The coastal area is composed of zones with grid intervals from 1,800m (two zones of B1 and B2) to 50m (four zonesof F1 to F4). Four harbors are included (Ohfunato Bay, Kamaishi Bay, Kuji Bay, and Hachinohe Bay).

Regarding previous Sanriku tsunamis, the Meiji Sanriku Tsunami, Showa Sanriku Tsunami, Tokachi-Oki Earthquake Tsunami, and Chilean Earthquake Tsunami can be specified from the fault parameter database. For theChilean Earthquake Tsunami, the calculated results of propagation from the Pacific Ocean onto the Sanriku coast is extracted from the tsunami estimation databaseand is used. The topographies of the harbors at the time of the previous tsunamis (e.g., the Meiji, Showa Sanriku and Chilean Earthquake tsunamis) were prepared from old topographical charts and various tsunami records at each location and were

put into the database.

Figure 6 is a propagation chart for the Chilean Earthquake Tsunami obtained by numerical calculation. The numerals represent the elapsed time from the start of the tsunami. The Pacific Ocean propagation calculation for the Chilean Earthquake Tsunami covers the area from 60 degre South to 60 degree North and from 120 degree East to 70 degree West (i.e., the whole Pacific Ocean surrounded by Far East Asia, Australia, North America, and South America), as shown in the figure. The calculation grid interval is 10 minute in both latitude and longitude (about 18.5km distance at the equator), and the total number of calculation points is about 730,000.

The upper side in Fig. 7 shows the output of the maximum water level distribution in Ohfunato Bay on the Sanriku coast for the Chilean Tsunami. This result wasobtained by connecting the ocean propagation and near-field tsunami calculations, the latter using a finer grid in the sea area near the Sanriku coast. The figure indicates the contour lines for the maximum water leveland the tsunami water level at points where the tsunamimarks are apparent. The numerals in the figure are based on T.P.(m), and the numerals in the parentheses indicate tsunami height marks. The shaded area denotes the flooded land area. The water level for the Chilean Earthquake Tsunami in Ohfunato Bay was about 1.8m at the mouth of the bay and about 4.5m at the innermost point of the bay, gradually increasing from the bay mouth to its inner most point. This indicates resonance with the natural vibration of the bay with the mouth being a node and the inner most point being a loop. Flooding from the tsunami reached the urban area, suggesting that the damage caused by the tsunami was heavy.

The lower side in Fig. 7 shows the results of numerical calculations for the imaginary maximum water level distribution from the Chilean Earthquake Tsunami, assuming a bay mouth breakwater is installed and using the same fault parameters as those in the verification calculation. The calculated water level from the tsunami is about 1.2m at the mouth of the bay and 1.9m at the inner most point of the bay. This indicates that the water level is halved by the addition of a bay mouth breakwater. Flooding is limited to narrow area, where a tidal embankment is not installed and the ground elevation is low.

(3) Ise-Wan storm surge analysis

In the storm surge calculation system, wind estimated by the typhoon model is added to that from the tsunami calculation. Storm surge is very different from a tsunami in that the external storm surge forces are from atmospheric pressure and the typhoon wind, which changes constantly, while the external force in atsunami is the initial water level determined from the fault parameters. In general, the water level rises remarkably when a typhoon approaches. However, even when a typhoon is distant, the water level may rise in a bay if the free waves developed in the typhoon zone propagate through the ocean and enter the bay. It is also assumed that the drift current developed in the ocean is blown to the coast, affecting the rise in water level not only at the mouth of a bay, but also in the entire bay. Therefore, the region used for storm surge calculations should be a wide ocean region including the continental shelf and the sea area where the typhoon passes.

Along the coast, grid intervals of about 100m or narrower are necessary to evaluate the effect of delicate topography such as harbor structures on

storm surge. In an inner bay with shallow water, the effect of astronomical tide cannot be neglected, particularly when the amount of land flooding due to a storm surge is calculated, so a highly accurate calculation of astronomical tide is necessary. However, using current tech nology, it is difficult to simultaneously perform atide calculation for the ocean and an accurate tide calculation for an inner bay, because the information on boundary conditions is insufficient. For this reason, the storm surge calculation is performed by separating the area into ocean and inner bay regions. Fig. 8 shows the distribution of maximum storm surge deviations in the ocean region during the Ise-Wan Typhoon. The ocean region is subdivided into six zones, from the ocean to Ise Bay to perform the calculation efficiently. In each zone, the topography is approximated by grid intervals that decrease gradually at a rate of 1/2 or 1/3 as the bay is approached.

Fig. 9 shows the flow velocity distribution that was estimated by using a two-layer model for Ise and Mikawa bays during the Ise-Wan Typhoon. Water depth in the open sea is several thousand meters, and the sea area in front of the mouth of Ise Bay has a depth of several hundred meters or more with a steep sea bottom slope. Under such topographical conditions, the drift current generated by the storm surge develops mainly in the upper layer. If a single layer model is used for the open sea, the transfer of sea water due to the drift current is approximated as being uniform throughout the layer. This results in part of the water layer being reflected back to the open sea at the steepsea bottom slope, so that it does not enter the bay. For this reason, multi-layer modeling is used.

CONCLUSIONS

This paper presented an outline of the design and typical on-site applications of the Integrated Numerical Research System for Prevention and Estimationof Coastal disasTers (INSPECT) system. This system was developed to efficiently perform studies for preventing disasters on Japanese coasts due to wave, tsunami, and storm surge. The main conclusions follow.

(1) The system was developed to systematize the numerical analysis of wave, tsunami, and storm surge and to efficiently perform a series of processing steps, from the summarization of observed information and the preparation of input data for numerical simulation, through numerical calculation, to the analysis and evaluation of results, by a simple operation. The design premise is to permit an engineer to quickly output the results by a simple operation without difficult analyses or high-level special knowledge.

(2) The equipment used in this system consists of engineering workstations, personal computers, and theirperipheral devices, which provide a general-purpose configuration. Processing is performed in teractively, and the results can be output on screen or paper.

(3) The system is composed of five analysis systems (wave statistical analysis, wave estimation, tsunami calculation, storm surge calculation, and calculation support), and six support databases (observed value, weather chart, water depth chart, coast coefficient, numerical simulation input value, and estimated value). Each analysis system has multiple subsystems. Analyses are performed by using combinations of the subsystems and databases.

(4) Numerical simulation is the basis of this model andis performed by advanced numerical calculation techniques. The models used include a spectrum method wave estimation model, a physical factor multiple regression wave prediction model, a near- and far-fieldtsunami calculation model, and a storm surge multi-layer model.

(5) Design wave analyses for Japanese coasts, wave predictions for the Hitachi Naka Harbor, tsunami calculations for the Sanriku coast, and storm surge calculations for the Ise Bay were presented as typical applications of this system. The analysis procedure, the inter relations between the analysis systems, and output examples were described for these applications.

REFERENCES

1) Goto, C. and H. Shibaki : A hindcast of maritime surface wind including effects of land topography, Report of PHRI, Vol.32, No.3, 1993.

2) Isozaki, I. and T. Uji : Numerical model of marine surface winds and its application to the prediction of ocean wind waves, Papers in Met. and Geo., Vol.25, No.3, 1974.

3) Goto, C., K. Suetsugu and T. Nagai : Wave hindcast model for short fetch sea, Report of PHRI, Vol.29, No.3, 1990.

4) Goto, C., H. Shibaki and T. Aono : Multiple regression wave forecast model described in physical parameters, Report of PHRI, Vol.31, No.5, 1993.

5) Goto, C. and T. Aono : A spectral wave prediction system for a single point, Report of PHRI, Vol.31, No.2, 1992.

6) Goto, C. and K. Sato : Development of tsunami numerical simulation system for Sanriku Coast in Japan, Report of PHRI, Vol.32, No.2, 1993.

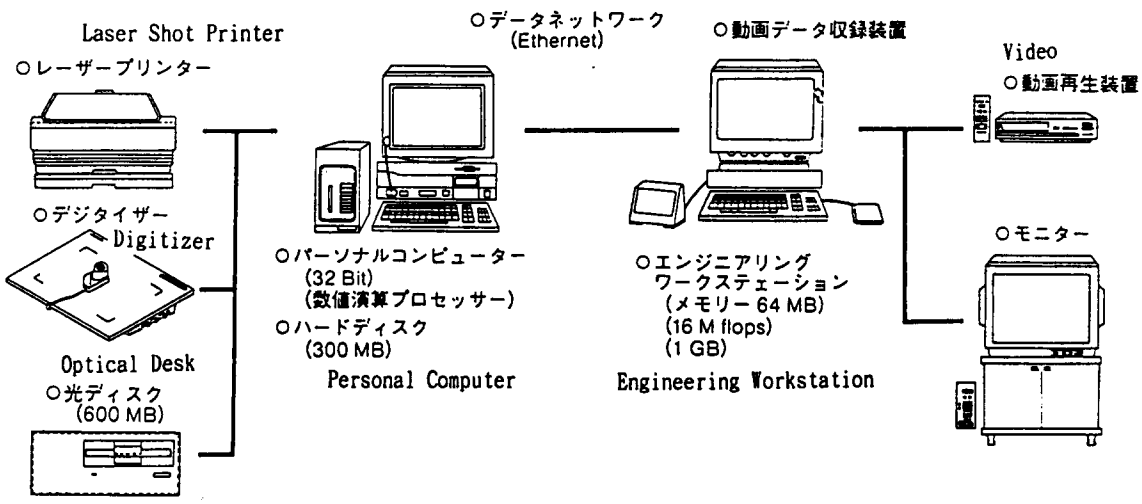

Fig. 1 INSPECT system equipment configuration

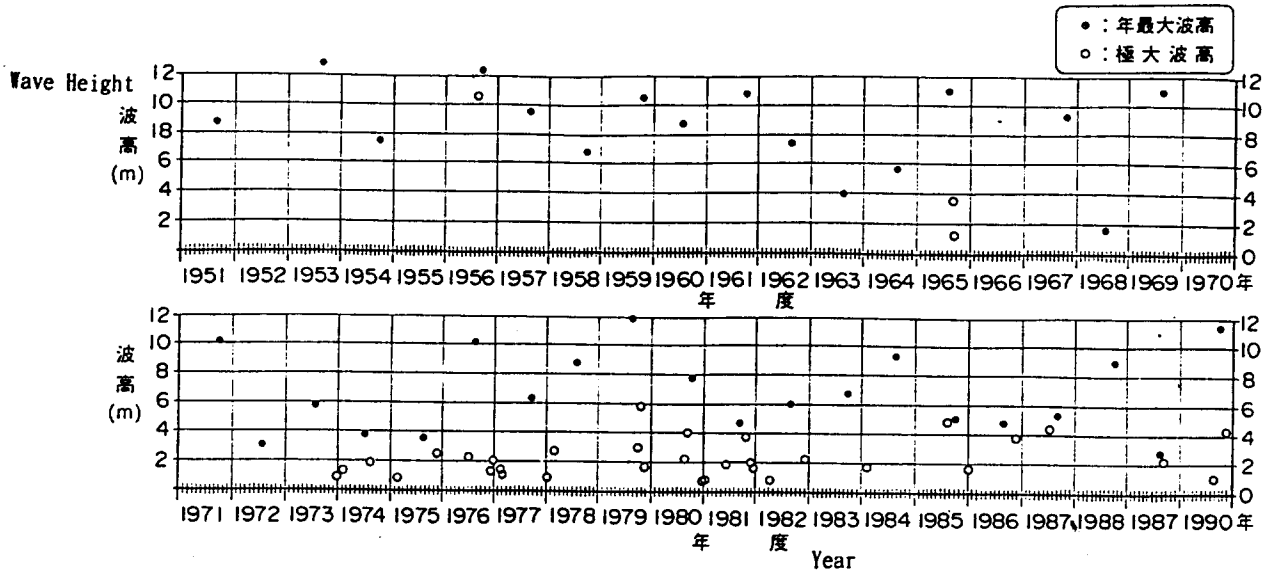

Fig. 2 Time series distribution of yearly maximum and extreme waves for the statistical period

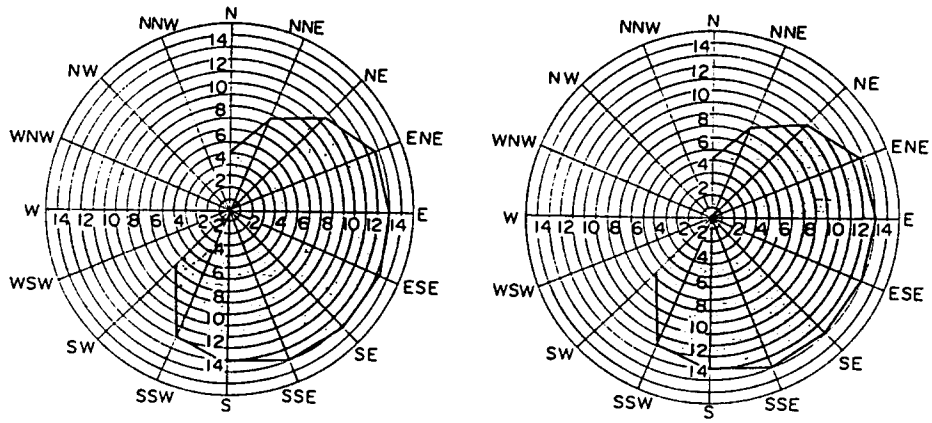

Fig. 3 Directional distribution of the probable wave and wave period corresponding to probable wave height

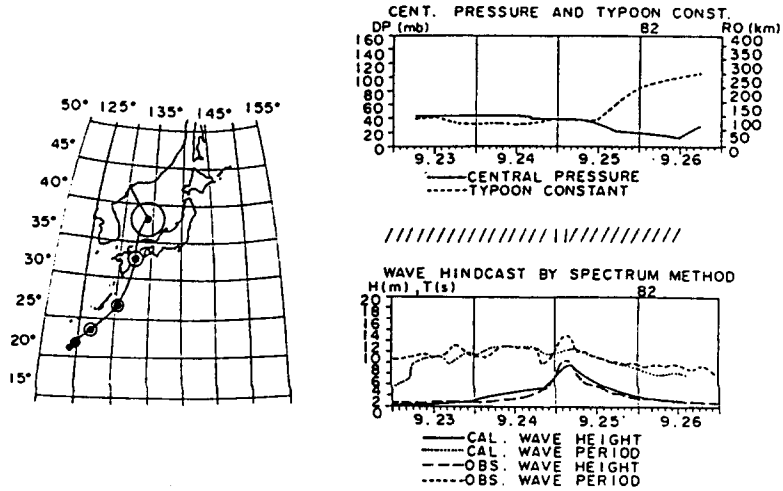

Fig. 5 Screen output for high wave prediction during a typhoon using the single point output type wave hindcasting model

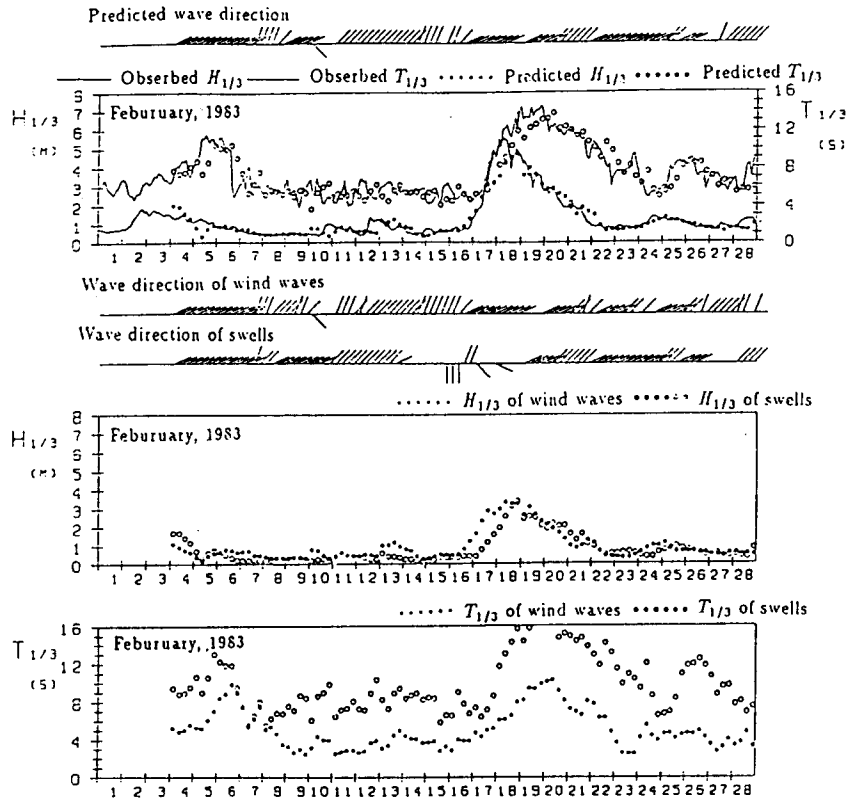

Fig. 4 12-hour wave prediction and wind-driven wave/swell separation at Hitachi Naka Harbor using the physical factor, multiple regression wave prediction model

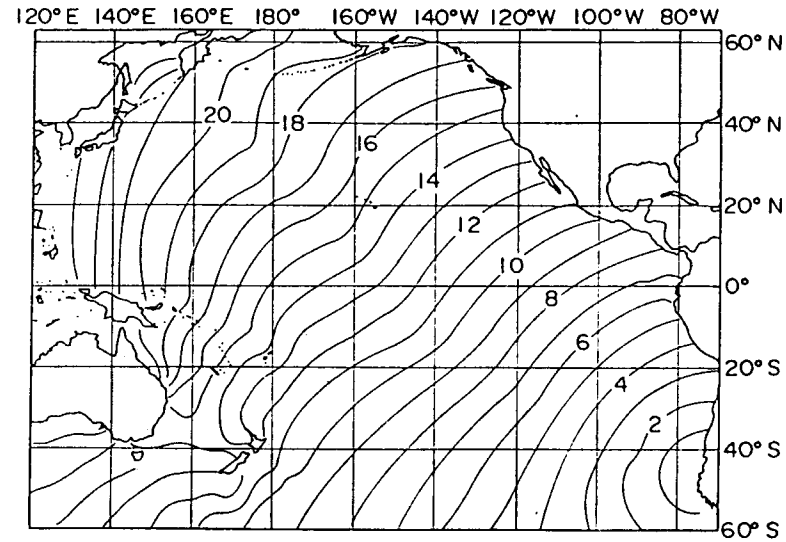

Fig. 6 Pacific Ocean propagation calculation zones and propagation chart for Chilean Tsunami

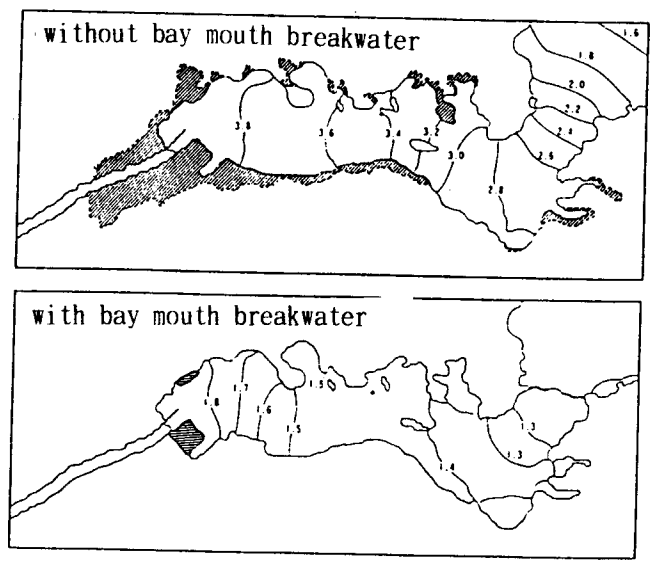

Fig. 7 Maximum water level distribution at Ohfunato Bay for Chilean Earthquake Tsunami (hindcast calculations and prediction calculations with a bay mouth breakwater)

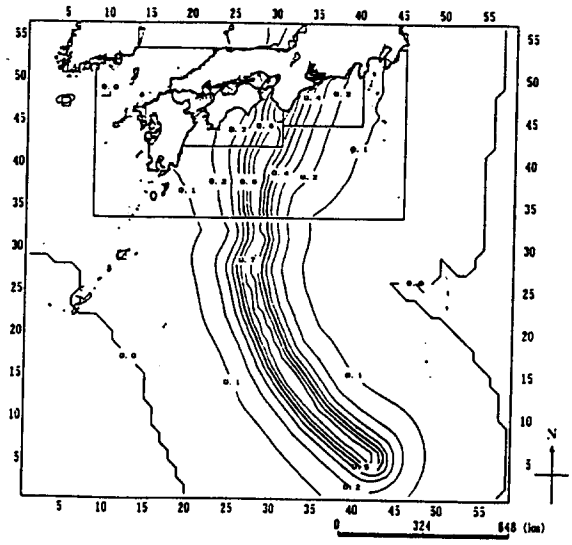

Fig. 8 Open sea calculation zones for storm surge estimation and distribution of maximum storm surge deviations during Ise-Wan Typhoon

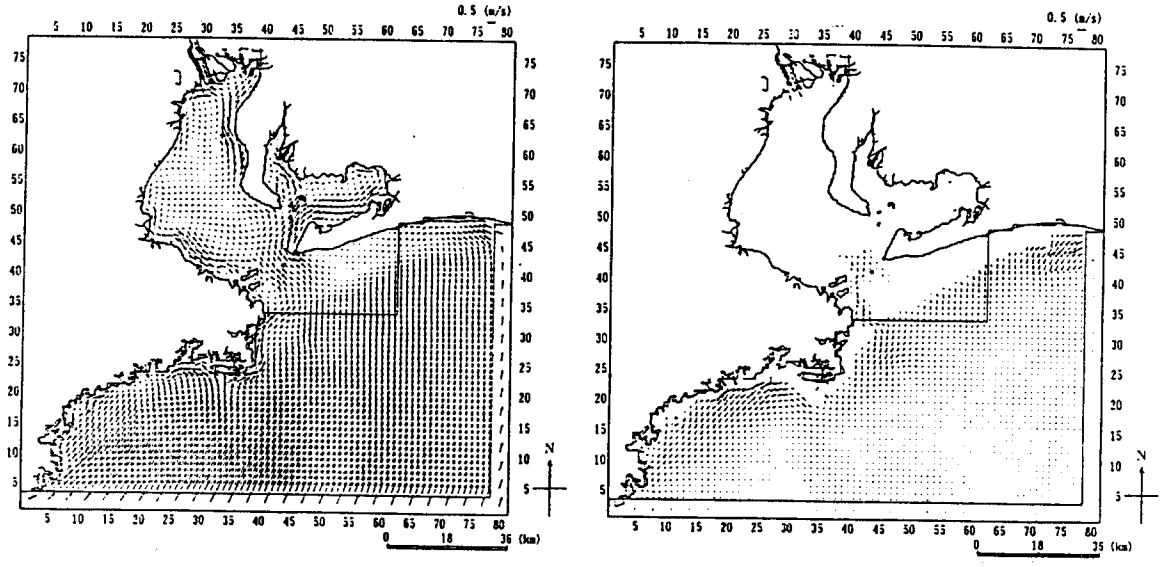

Fig. 9 Flow velocity distribution in Ise Bay and Mikawa Bay estimated by 2-layer model

Structural Testing of Confined Masonry for the Third World Housing

by

Hatsukazu Mizuno[1], Tetsuro Goto[2], Masanori Iiba[3], Hiroto Kato[4] and Yutaka Yamazaki[5]

ABSTRACT

This paper presents structural testing of confined masonry structure, which is selected as an appropriate candidate of apartment house building in urban areas of the Third World countries. It also includes a background description of housing construction conditions of the Third World. In static loading tests, about half-scale specimen of confined masonry wall was used. Main experimental parameters are cross section size of reinforced concrete columns, axial reinforcement and shear reinforcement of reinforced concrete columns, and lateral reinforcements in brick wall horizontal joints. Confinement effects of reinforced concrete frame on brick wall, lateral reinforcement effects in horizontal joints and axial stress are examined.

KEY WORDS : the Third World, Housing, Economic Aspects of Construction, Confined Masonry Structure, Structural Testing

1. INTRODUCTION

Urban areas of the third world countries are subjected to excessive population concentration due to some social and economic conditions, and lack of healthy housing. Development of economic and earthquake-resistant apartment house is required to supply massive housing in urban areas.

Japanese Government has been and is carrying some technical cooperation programs, especially a few research center projects with some of the Third World countries. A few earthquake reconnaissance and technical consulting in repair and retrofit of damaged buildings were also done in a few earthquakes. Through those experiences, We found something in common as well as some differences in structural engineering and construction technology between them and us. Our understanding on housing construction technology motivated us to develop structural design method of appropriate masonry-based construction method in urban areas of the Third World countries.

2. PROBLEM DESCRIPTION

We surveyed earthquake damage, conventional housing structures, prices of industrialized basic construction in materials, e.g. steel bar, cement and masonry units in the third world countries, as a preliminary study. Our understandings are as follows[1];

(1) Earthquake Damage

Damage patterns of masonry structure types are summarized as follows;

Adobe houses frequently suffered from severe damage, especially total collapse due to heavy mud roof, and a lot of human lives were lost, such as the Iran Manjil Earthquake of June 21, 1990. Unreinforced masonry also had severe damage. Damage patterns of these two types are overturning of walls in the out-of-plane direction and shear diagonal failure of walls.

Almost the same damage to brick masonry buildings is found in the 1891 Mino-Owari earthquake in Japan. Japan transplanted brick masonry buildings in the second half of the

---

1) Program Director of International Codes and Standards, Building Research Institute, 2)Senior Research Engineer, Housing Construction Division, BRI, 3) Senior Research Engineer, BRI, 4) Research Engineer, Full-Scale Structural Testing Division, BRI, 5) Director of Research Planning Department, BRI

nineteenth century from Europe as a token of modernization or industrialization. In the 1923 Kwanto earthquake, similar damage is reported.

Floors of these two types of masonry structure are usually wood floor slab, concrete joist slabs etc. In-plane stiffness of these slabs, and box effects of floors and walls are smaller than those of reinforced concrete slab.

Damage to confined masonry is found in the 1985 Chilean earthquake[2]. Confined masonry is composed of confining reinforced frame and confined walls. After masonry walls are setup, reinforced concrete frame is constructed in confined masonry structure. Typical damage patterns are 1) shear diagonal failure of walls, 2) shear and bending failure of heads and feet of reinforced concrete columns and 3) separation between brick walls and columns. The damage to confined masonry, however, is not severe, compared with adobe houses and unreinforced masonry.

Damage to masonry-infilled wall structure is reported in the 1985 Mexican earthquake etc. After concrete frame is constructed, masonry units like bricks are infilled as walls in the structure.

We have no data of damage to reinforced masonry, in which hollow bricks or concrete blocks are used as permanent forms for reinforced concrete casting.

(2) Construction and Economic Aspects

1. Masonry structures prevail in many earthquake-prone countries of the third world.

2. From building cost and dissemination viewpoints, however, masonry-based apartment buildings are most appropriate to supply housing to the urban people, because masonry units like bricks are comparatively cheaper than industrialized materials. Steel bars and cement have a tendency to be international trade goods as well as crude oil, and the prices of these are expensive for people of lower GNP per capita.

3. We selected confined masonry structure, which is composed of confined masonry walls and confining reinforced concrete frame (sometimes steel frame), as an appropriate apartment building on the basis of above-mentioned building cost.

4. Confined masonry structure has been studied and is already used in some countries. But, more studies, especially experimental and analytical ones are needed to improve structural design of the structure, because structural design data are not much accumulated.

3. RESEARCH OBJECTIVES

Building Research Institute has begun a research project of housing construction technology transfer including this study since 1989 fiscal year. The objectives of the study are to analyze damage patterns of masonry structures, to examine improvement methods for minimizing earthquake damage, and to prepare guideline of structural design with special emphasis to common aspects of confined masonry. Modification of the guideline to each country is supposed to be carried out in other research projects, because level of structural performance should be decided by each country, and local conditions, especially social economic conditions much differ.

4. STRUCTURAL TESTING

Static cyclic loading tests are intended for clarifying basic structural performance of confined masonry structures.

Figure 1 shows an example of Chilean confined masonry apartment house. That seems a little stiff, compared with other countries ones. We considered a wall in Fig. 1, as a reference model of the tests. Materials of specimens are domestic (Japanese). Scale ratio of length in specimens is about half. Specimen brick walls composed of full-scale bricks and cement mortal joints, are considered to be properly scaled on the basis of "spatially integrated effects".

We carried out the following two series of static cyclic loading tests of confined masonry wall units to clarify basic structural performance of confined masonry, and to find most effective reinforcement arrangements of confined masonry structures on the above-mentioned basis; No.1 series of the tests were executed to clarify

confinement effects of reinforced concrete frame (column) on brick wall, which is one of the key factors of confined masonry structure. No.2 series of the tests were done to clarify to lateral reinforcement effects in brick wall horizontal joints, which is one of possible measures of improving structural performance of confined masonry, and also to clarify effects of axial stress on structural performance of walls due to overburden of the upper story of apartment house. A set up of the tests is shown in Fig. 2.

(1) Confinement Effects of Reinforced Concrete Columns

Figure 3 presents specimens of No. 1 series of the tests. Table 1 summarizes nine specimens of the series, and experimental parameters and conditions. Main experimental parameters are cross size of reinforced concrete column, axial reinforcement and shear reinforcement of reinforced concrete column. Figure 4 depicts range of axial reinforcement and shear reinforcement of columns, which is determined making reference to Peruvian, Chilean and Mexican design codes.

Figure 5 shows envelope curves of relation between shear stress and deflection angle of the specimens. Shear stress of the figure is defined as stress derived from dividing shear force by total cross section area of brick wall and columns.

Figure 6 shows rapture sketches at final loading stage of specimen CR–A, the strongest one, and specimen CR–I. The specimen CR–A behaved stably and sudden rapture did not occur during the test, though reinforced concrete columns were cracked due to bending moments, and four corners of brick wall were cracked due to shear. On the other hand, in the specimen CR–I, shear cracks occurred at the right and lower corner of the brick wall at about 0.0014 radian of deflection angle propagated into the upper part of left reinforced concrete column, and then loading capacity deteriorated. All specimens except for CR–A were subjected to shear diagonal cracks at deflection angles less than 0.0025 radian, and loading capacity deteriorated. Shear diagonal cracks penetrated into reinforced concrete columns at final loading stages of the specimens.

Figure 7 presents relationship between maximum shear strength values of the specimens, and axial reinforcement and shear reinforcement of reinforced concrete columns. Maximum shear strength tends to increase with axial reinforcement of reinforced concrete columns. But maximum shear strength is not found to be related with shear reinforcement of reinforced concrete columns. Table 2 summarizes tested values and calculated values of maximum strength of the nine specimens. In the specimen CR–B, a loading capacity value at the first large shear diagonal crack is defined as maximum strength, though the CR–B recovered somewhat loading capacity due to compressive struts of brick wall in cyclic loading process, after loading capacity deterioration by the first large diagonal crack.

In Table 2, proposed evaluation equation Q1 of maximum strength in confined masonry structure is derived from adding crack strength evaluation of brick wall to maximum strength evaluation equation of reinforced concrete columns. The derivation procedure is as follows;

$Q_{cr} = {}_wQ_{cr} + \Sigma_c Q_{cr}$,

where

${}_wQ_{cr}$; Shear Crack Strength of Brick Wall (Principal Stress Evaluation Formula),

${}_cQ_{cr}$; Shear Crack Strength of Column (Ohno–Arakawa Evaluation Formula)

Explicit expression of ${}_wQ_{cr}$ is;

${}_wQ_{cr} = 0.5(\sigma p)^{0.5} tL/K$

$Q1 = {}_wQ_{cr} + \Sigma_c Q_{su}$,

where

${}_cQ_{su}$: Max. Shear Strength of Column (Ohno–Arakawa Mean Formula).

Explicit expression of ${}_cQ_{su}$ is;

$${}_cQ_{su} = \{0.0679\ p_t^{0.23}(180+\sigma_B)/(M/Qd+0.12) + 2.7(p_w\ \sigma_{wy})^{0.5} + 0.1\ \sigma_o\}\ bj$$

where

p_t : Ratio of Tensile Axial Reinforecement Area and Cross Section area of Column ($p_g/2$)

j : 7d/8. where d: effective height of cross section

σ_B : Compressive Strength of Column Concrete
M/Qd: Shear Span Ratio of Confined Masonry
p_w : Ratio of Shear Reinforecement in Reinforced Concrete Column
σ_{wy} : Yielding Strength of Shear Reinforecement Bar in Reinforced Concrete Column
σ_o : Axial Stress of Confined Masonry Wall
σ_p : Prism Compressive Strength of Brick Wall
t : Thickness of Brick Wall
L : Length of Brick Wall
K : Shape Factor (1.0)

The equations were modified from shear crack evaluation equation and maximum strength evaluation equation of reinforced concrete members used in Japan.

Figure 8 shows relationship between ratio of tested value exQ_u and calculated value Q1, exQ_u/Q1 and axial reinforcement of reinforced concrete columns.

Another evaluation equation Q2 of maximum strength is used for reinforced concrete block structure in Japan[6], as shown in Table 2.

Figure 9 compares tested values of maximum strength $_{ex}Q_u$ with proposed equation Q1 and another equation Q2. Proposed maximum strength evaluation equation Q1 agreed with the tested values. Evaluation equation Q2 overestimates the tested values.

(2) Effects of Lateral Reinforcement in Brick Wall Joints and Axial Stress

Table 3 summarizes nine specimens of No.2 series of the tests. Figure 10 shows the specimens and experimental parameters, namely lateral reinforcement arrangement in horizontal joints of brick walls, and axial stress due to overburden of the upper story of apartment house. Figure 11 demonstrates envelope curves of relationship between loading force and horizontal deflection.

Specimens I, P and Q without lateral reinforcement in horizontal joints of brick wall was damaged in separation between brick wall and reinforced concrete columns at stages of small deflection. And then shear diagonal cracks occurred and lost bearing capacity of vertical loads. Figures 12 demonstrates loading force versus deflection relationship of specimen M, compared with that of specimen I without lateral reinforcement. From the figure, lateral reinforcement improves behavior, especially ductility.

Specimens M, N and O with column-to-column lateral reinforcement showed ductile behavior up to large deflection, namely up to deflection angle 0.0020 radian.

Specimens J, K and L with partial reinforcement showed shear failure at stages of deflection angle 0.0020 radian, after axial reinforcement yielding of reinforced columns. Partial reinforcement means to improve ductility, compared with specimens I without lateral reinforcement. Improvement by partial reinforcement is less than that of specimens M, N and O with column-to-column lateral reinforcement.

Figure 13 demonstrates effects of axial stress due to overburden by comparing specimen Q of axial stress 14kgf/cm^2 with specimen I of axial stress 4kgf/cm^2. High axial stress makes maximum strength large, but sudden deterioration of loading capacity is remarkable.

Figure 14 shows sketches of final stage rapture of specimens Q and M.

Maximum Shear strength is improved 1.2 – 1.3 times by adding lateral reinforcement. Specimen Q with high axial stress, 14 kgf/cm^2 maximum shear strength is about 1.5 times as large as specimen I with low axial stress.

From construction cost viewpoint, partial reinforcement at four corners of brick wall is recommended, because specimen K with the smallest lateral reinforcement showed good behavior, compared with the other lateral reinforcement.

5. CONCLUDING REMARKS

Basic structural performance of confined masonry structure is revealed as follows;

1. Axial reinforcement of reinforced concrete columns increases maximum strength of confined masonry structure from semi-quantitative

viewpoint.

2. Lateral reinforcement in horizontal joints of brick wall and shear reinforcement of reinforced concrete columns both improves ductility of confined masonry structure. The former effects is more remarkable than the latter.

ACKNOWLEDGMENT

No.2 series of the tests was carried out as cooperative research project with "Structure Subcommittee" (Convener: Ex-Director of Structural Department, BRI, Now, Team leader of CENAPRED, Mexico) under the auspice of "Committee on International Asesmic Network of Buildings and Housing" (Chairman: Professor T. Okada, Tokyo University). The fund of the cooperative research was supported by Japan International Cooperation Agency. The authors would like to express their thanks to whom concerned.

REFERENCES

1. Mizuno, H. et al., "Some basic considerations on appropriate housing construction technology in the Third World countries," Kenchiku Kenkyu shiryo, No. 68, Building Research Institute, Mar. 1990 (in Japanese)

2. Cruz, E. et al., "Lecciones del sismo del 3 de Marzo de 1985," Instituto Chileno del Cement y del Hormigon, 1988 (in Spanish)

3. Ishibasi, K. et al., "Aseismic structural testing of confined masonry in Mexico (Part 1) & (part 2)," Proceedings of A.I.J. Convention, pp1969-1972, 1992, (in Jpanese)

4. Katsumata, H. et al, "Nonlinear analysis of confined masonry walls (Part 1) & (Part 2)," Proceedings of A.I.J. Convention, pp325-328, 1993, (in Japanese)

5. Kato, H., Goto T., Mizuno H. and Iiba, M. "Cyclic loading tests of confined masonry wall elements for structural design development apartment houses in the Third World," Proceedings of the tenth World Conference on Earthquake Engineering, Balkema, vol.6, pp3539-3544, 1992

6. Architectural Institute of Japan, "Ultimate strength and deformation capacity of buildings in seismic design," 1990, (in Japanese)

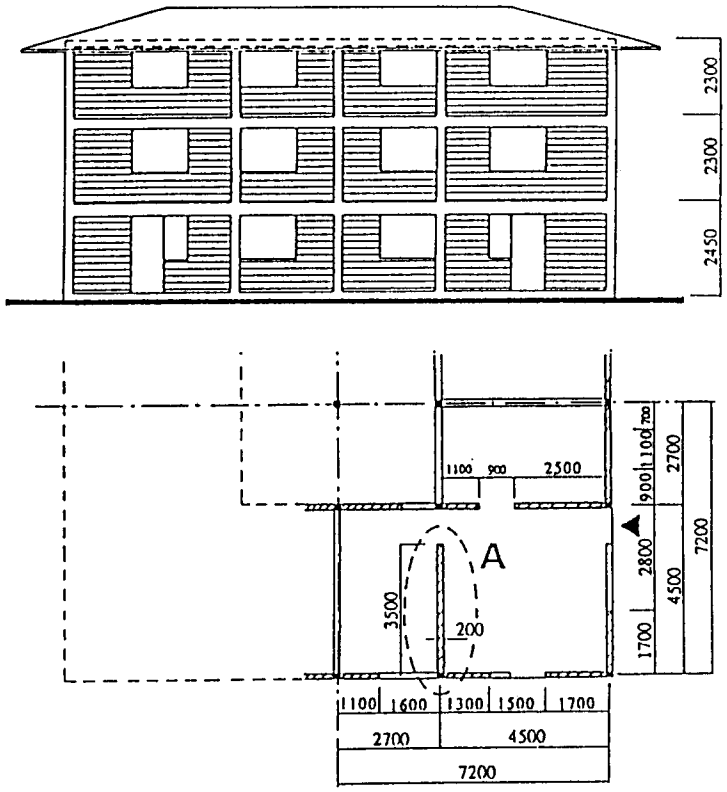

Fig.1 Apartment House damaged in 1985
Chilean Earthquake (Plan & Elevation Views)

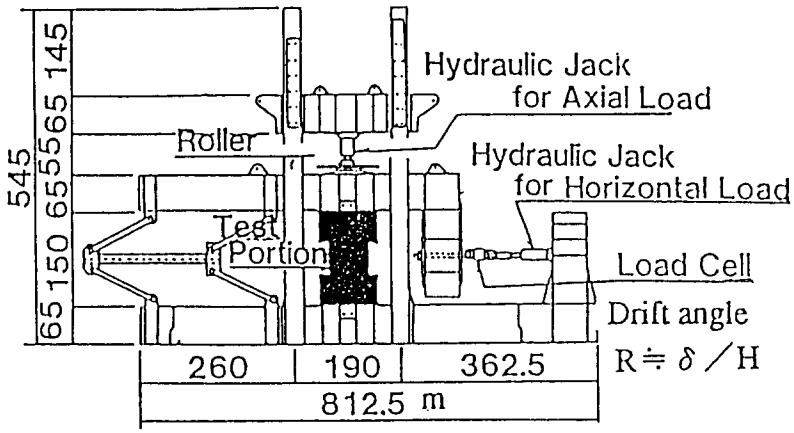

Fig.2 Setup of Static Loading Test

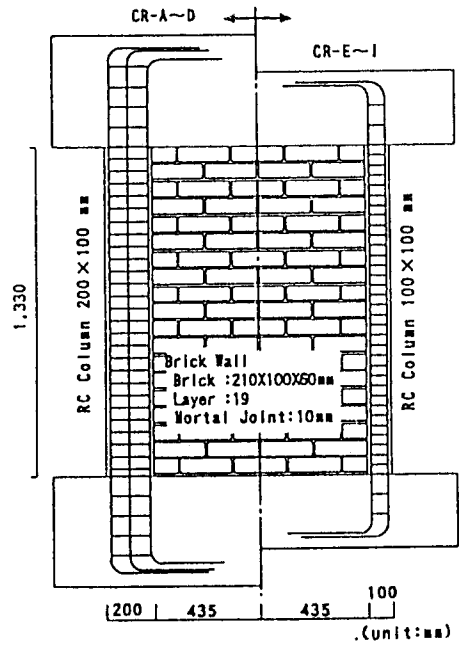

Fig.3 Specimens & Reinforcement
Arrangement (Confinement Effects)

Table 1 WALL SPECIMENS OF STATIC TESTING (No.1 Series)
(CONFINEMENT EFFECTS OF R.C. FRAME)

Specimen	Size	Axial Reinf. of RC Column	Shear Reinf. of RC Column	Strength of Brick Prism σ_p	Strength of Concrete σ_B	Yield Strength of Steel f_y
CR-A	Wall : 870x100 mm Col. : 200x100 mm	6-D13	D6-@50	411.1 kgf/cm²	207.2 kgf/cm²	D13 : 3544.2 D8 : 4145.4 D6 : 3778.0 kgf/cm²
CR-B			D6-@220			
CR-C		4-D8	D6-@50			
CR-D			D6-@220			
CR-E	Wall : 870x100 mm Col. : 100x100 mm	4-D8	D6-@50	320.9 kgf/cm²	258.0 kgf/cm²	D8 : 4208.4 D6 : 4694.4 D4 : 3369.5 D3 : 3805.6 kgf/cm²
CR-F			D4-@80			
CR-G		4-D6	D4-@40			
CR-H		4-D4	D3-@45			
CR-I		4-D8	D4-@40			

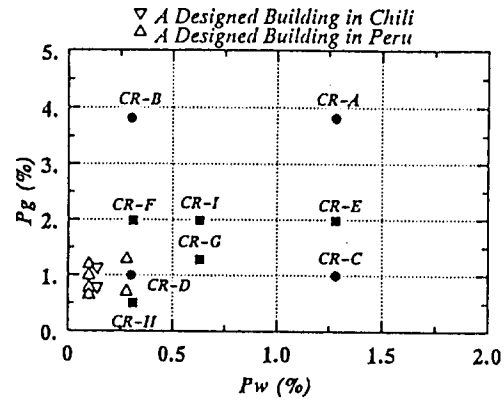

Fig.4 Experimental Parameters (Axial Reinf. of RC Columns versus Shear Reinf. of Columns)

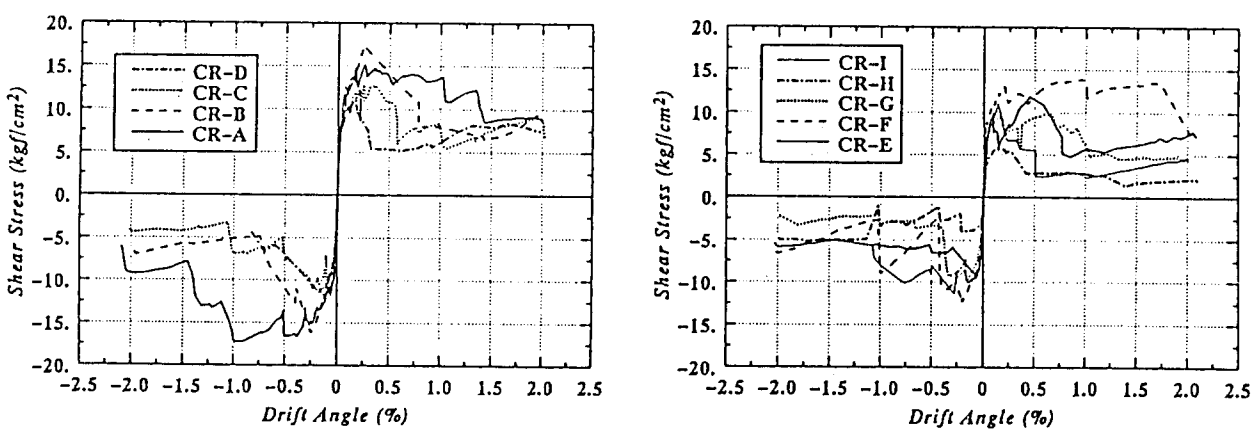

Fig.5 Envelopes of Shear Stress - Deflection Angle Relation

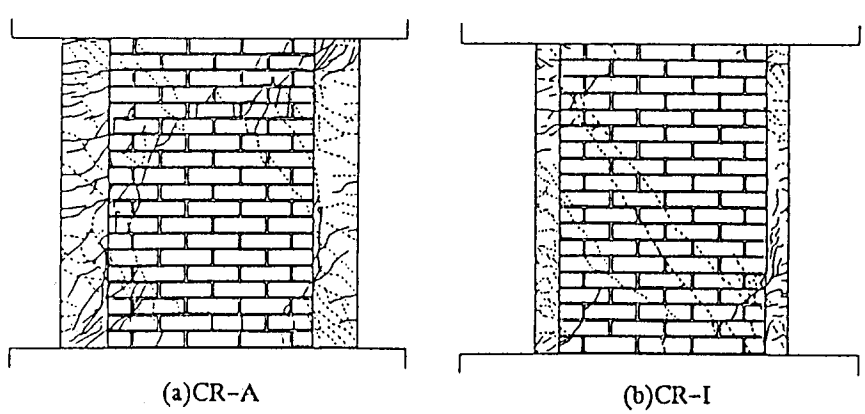

Fig.6 Sketch of Rapture (Final Loading Stage)

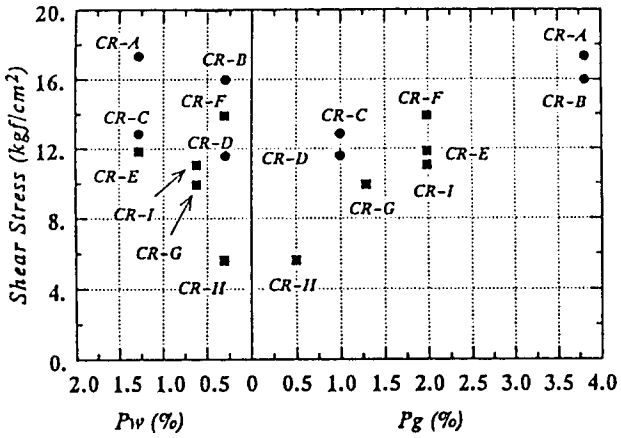

Fig.7 Max. Strength versus Experimental Parameters (Axial Reinf. of RC Columns, Shear Reinf. of RC Columns)

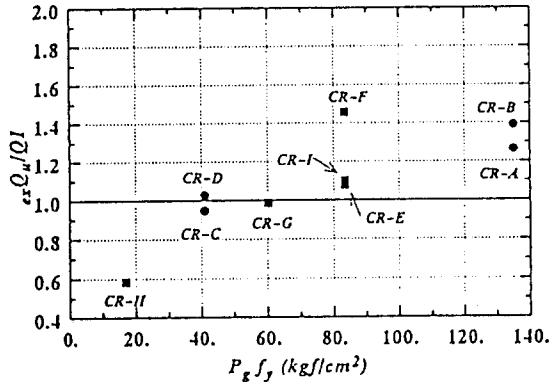

Fig.8 $_{ex}Q_u/Q_1$ Versus Axial Reinf. of RC Columns

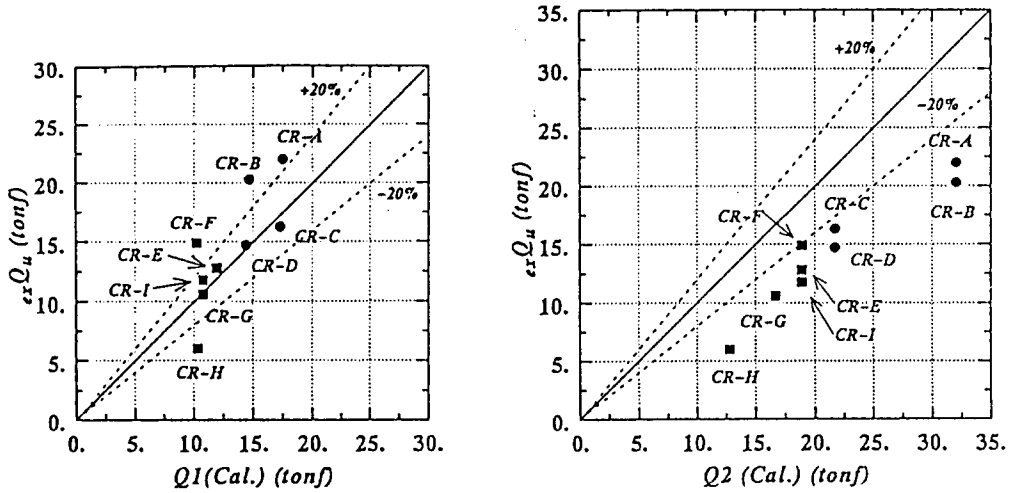

(a)Q1 との比較　　(b)Q2 との比較

Fig.9 Comparison of Tested & Calculated Max. Strength

Table 2 COMPARISON OF TESTED AND CALCULATED MAXIMUM STRENGTHS (tonf)

Specimen	Tested Max. Streng. exQ_u	Cal. Shear Crack Streng. Q_{cr}	Calculated Maximum Shear Strength		Ratio of Tested and Cal. Max. Strengths	
			Q1	Q2	$exQ_u/Q1$	$exQ_u/Q2$
CR-A	22.0	12.43	17.43	32.07	1.26	0.69
CR-B	20.3	12.43	14.59	32.07	1.39	0.63
CR-C	16.3	12.43	17.22	21.68	0.95	0.75
CR-D	14.7	12.43	14.43	21.68	1.03	0.68
CR-E	12.8	10.89	11.89	18.89	1.08	0.68
CR-F	14.9	10.89	10.22	18.89	1.46	0.79
CR-G	10.6	10.89	10.75	16.66	0.98	0.64
CR-H	6.0	10.89	10.29	12.74	0.58	0.47
CR-I	11.8	10.89	10.75	18.89	1.10	0.62

LEGEND

$Q_{cr} = {}_wQ_{cr} + \Sigma_cQ_{cr}$, where ${}_wQ_{cr}$: Shear Crack Strength of Wall (Principal Stress Formula), ${}_cQ_{cr}$: Shear Crack Strength of Column (Ohno-Arakawa Formula)

$Q1 = {}_wQ_{cr} + \Sigma_cQ_{su}$, where ${}_cQ_{su}$: Max. Shear Strength of Column (Ohno-Arakawa Mean Formula),

$$Q2=(K_u \cdot K_p(\frac{2.42}{h/D+0.7}+0.04)\sqrt{\sigma_p}+0.108\sqrt{P_{h'h}\sigma_y \cdot \sigma_p}+0.2\sigma_o)\, t \cdot j$$

Table 3 WALL SPECIMENS OF STATIC TESTING (No.2 Series)
(EFFECTS OF LATERAL REINFORECEMENT & AXIAL FORCE)

SPEC IMEN	COMMON EXPERIMENTAL PARAMETERS	BRICK TYPE (Grooves)	LATERAL REINFORCEMENT IN HORIZONTAL JOINT OF BRICK WALL	REMARKS
No.I	•a/D : 0.62 •Column Size 10cm × 10cm •Ax.Reinf.of Column : 4-D8 (P_g = 1.98%) •ShearReinf. of Column □D4-@40 (P_v = 0.64%) •Brick with & without Groove Size : 100 x 210 x 60mm, No. J - N : 1 Groove, No. Q : 2 Grooves •Concrete Strength 210kgf/cm² •Axial Stress(σ_o) ≒ 4kgf/cm²	No Groove (0)	No Reinf.	The same specimen as No. P & No. Q
J		Groove (1)	D4 : Single Through Upper Five Layers	Five Joints ≒ H/4
K			D4 : Single Partially Reinf. at Four Corners of Wall (Up. & Low. 5 J.)	Anchor:1.5 times of brick length
L			D4 : Single Through Each Two Joints	The same reinf. as No. J
M			D4 : Single Through Each Joint	
N			D8 : Single Through Each Joint	The richest reinf.
O		Groove (2)	D4 : Double Through Each Joint	The 2nd richest reinf.
P	The same parameters as those of No. I - O except for AXIAL STRESS	No Groove (0)	No Reinf. AXIAL STRESS (Normal stress due to Axial Force) : 7kgf/cm²	Axial Stress of No. I : 4kgf/cm²
Q			No Reinf. AXIAL STRESS (Normal Stress due to Axial Force) : 14kgf/cm²	

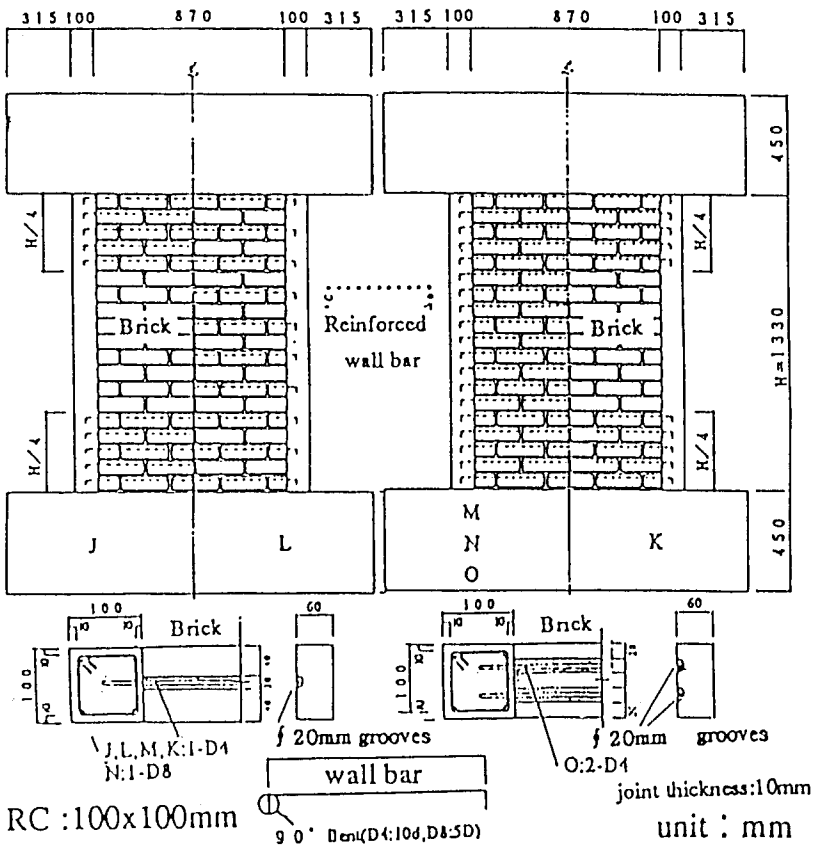

Fig.10 Specimens & Reinforcement Arrangement (Effects of Lateral Reinf. of Wall & Axial Stress)

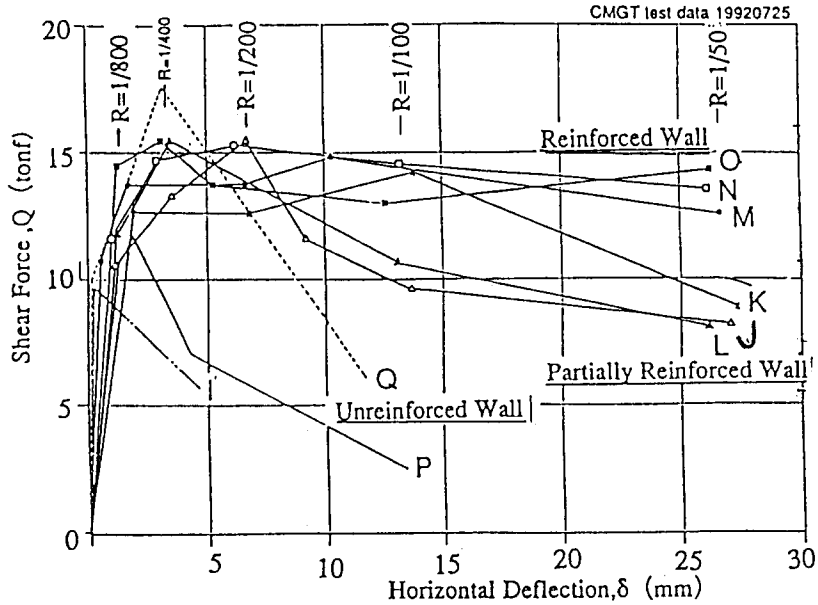

Fig.11 Envelopes of Loading Force Versus Hor. Deflection

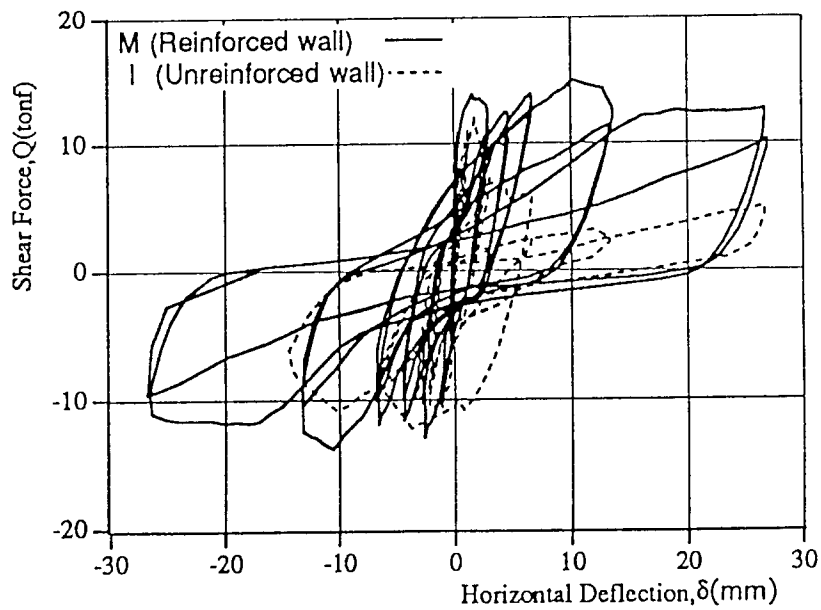

Fig.12 Loading Force Versus Hor. Deflection of Specimen M

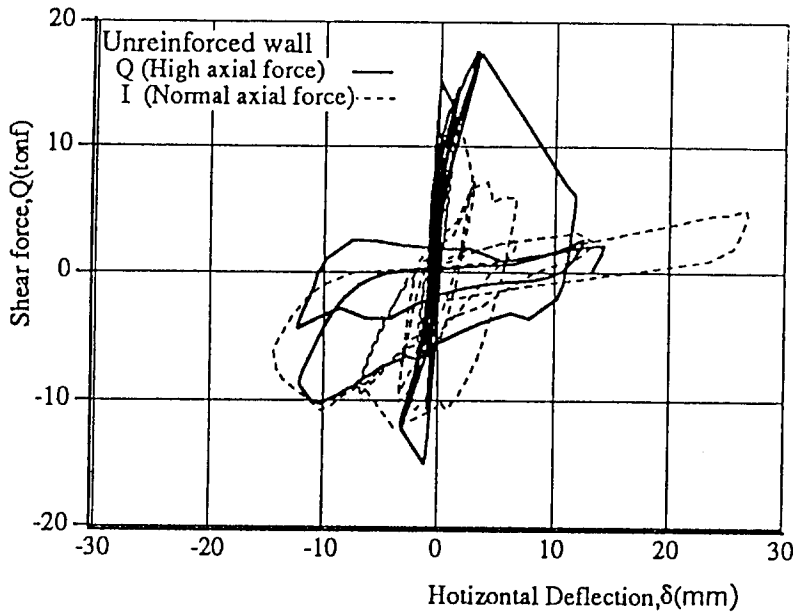

Fig.13 Loading Force Versus Hor. Deflection of Specimen Q

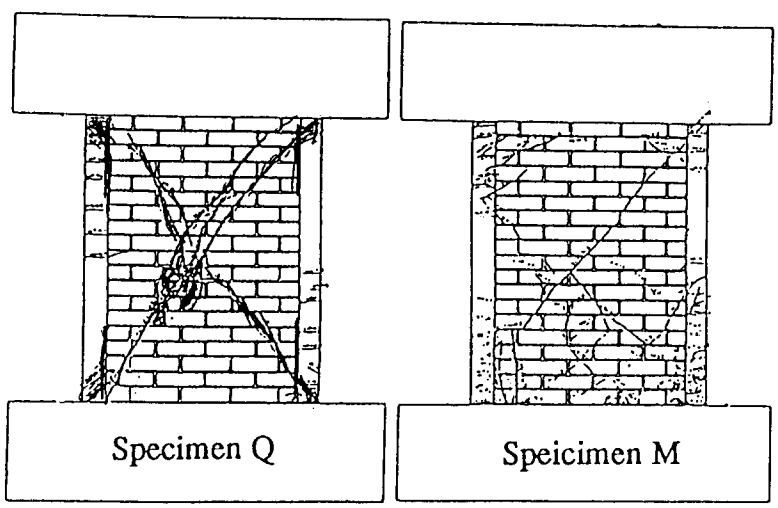

Classified (Shear Type :I,P,Q,) , Flexure and Shear Type :K,J,L)

Failure Mode: (Flexure Type :M,N,O)

Fig.14 Sketches of Final Stage Rapture of Specimens Q & M

Guideline for Safety Evaluation of Structural Response-Control Building (Tentative)

by

Kitagawa Yoshikazu [1], Midorikawa Mitsumasa [2],
Iiba Masanori [3], Fujitani Hideo [3] and Kashima Toshihide [4]

ABSTRACT

At present, structural response-control technology for practical use in buildings is developed mainly by private companies aiming to improve the living comfort against strong winds or moderate earthquakes. A general social consensus of this type of new building is not yet to be reached. Therefore, it is desirable that safety evaluation procedures of structural response-control buildings are established to not interfere with but encourage free development of the state-of-the-art. The Building Research Institute promoted the project of the government/private sector join research & development titled "Research & Development to Achieve Active Structural Response-control of Building Structures" from 1990 to 1993. The part of the results was reported as the "Guideline and Commentary for Safety Evaluation of Structural Response-control Buildings (Tentative)". This guideline mainly consists of three chapters; "General", "Safety Evaluation of Structures", "Safety Evaluation of Response-control Devices". Presented is the Tentative Guideline in this report.

Key words: Safety evaluation, Structural response-control, Building, Earthquake, Wind

INTRODUCTION

Structural response-control technology for practical use in buildings is presently developed mainly by private companies aiming to improve the living comfort against strong winds or moderate earthquakes. Structural engineers, however, have not yet reached a consensus on the design philosophy and safety of structural response-control buildings, and a general social consensus of this type of new building is not yet to be developed. Under this situation, it is desirable that safety evaluation procedures of structural response-control buildings are established to not restrict but promote the development of this new technology. The Structural Response-control Research Committee was established for this purpose in the Building Center of Japan in 1990 as part of the project, partly sponsored by the Ministry of Construction, of the government/private sector join research & development titled "Research & Development to Achieve Active Structural Response-control of Building Structures". This committee was in charge of developing the safety evaluation guideline for structural response-control buildings, and was chaired by Professor INOUE Yutaka of the University of Osaka. The work of the committee was reported as the "Guideline and Commentary for Safety Evaluation of Structural Response-control Buildings (Tentative)" in 1993[1] on which this report is based. This guideline mainly consists of three chapters; "General", "Safety Evaluation of Structures", "Safety Evaluation of Response-control Devices". In this report, we present the Tentative Guideline.

CONTENTS

1. General
   1.1 Scope
   1.2 Definitions
   1.3 Classification of structural response-control buildings in safety evaluation
   1.4 Safety evaluation of structural response-control buildings

1) Director, International Institute of Seismology and Earthquake Engineering, Building Research Institute, Ministry of Construction, 1 Tatehara, Tsukuba, Ibaraki, 305 Japan.
2) Head, Structure Division, Structural Engineering Dept., BRI, MOC.
3) Senior Research Engineer, Structural Engineering Dept., BRI, MOC.
4) Research Engineer, IISEE, BRI, MOC.

2. Safety Evaluation of Structures
   2.1 Outline of buildings and ground conditions
   2.2 Design principles and safety evaluation contents
   2.3 Setting of design conditions
   2.4 Design of structures
   2.5 Detail design at response-control device location
   2.6 Earthquake and wind response analysis of structural response-control buildings
   2.7 Effects to structures in unusual condition of active control devices
3. Safety Evaluation of Response-control Devices
   3.1 Composition and specifications of response-control devices
   3.2 Control design of active control devices
   3.3 Operation program of active control devices
   3.4 Performance validation and durability of response-control devices
   3.5 Maintenance inspection of response-control devices
   3.6 Environmental safety
4. Others
   4.1 Construction

GUIDELINE

1. GENERAL

1.1 Scope

This guideline is applied to the safety evaluation of a structural response-control building which has an active control device. The items that are not shown in this guideline shall be followed by the Building Standard Law of Japan and the related specifications and recommendations.

1.2 Definitions

The definitions of the following apply to this guideline.

Structural response-control building: A building that has an active or hybrid control device receiving the supply of external energy to carry out the response control of the building for earthquake ground motions or wind loading.

Response-control device: A device carrying out the response control of a building for earthquake ground motions or wind loading.

Active control device: A response-control device receiving the supply of external energy to carry out the response control of a building for earthquake ground motions or wind loading, which is composed of the sensing system, the control system, and the drive system.

Passive control device: A response-control device that needs no external energy to carry out the response control of a building for earthquake ground motions or wind loading.

Hybrid control device: A response-control device composed of an active and passive control devices that are arranged in a series or in parallel to carry out the response control of a building for earthquake ground motions or wind loading.

Level 0 earthquake ground motion: An earthquake ground motion that has a smaller level than level 1 earthquake ground motion.

Level 1 earthquake ground motion: The largest earthquake ground motion expected to occur at a building site once or more during the life time of a building.

Level 2 earthquake ground motion: The largest earthquake ground motion believed to have occurred, and that considered to possibly occur in the future, at a building site.

Level 0 wind loading: The wind loading that has a smaller level than level 1 wind loading.

Level 1 wind loading: The largest wind loading at the wind velocity expected to occur at a building site once or more during the life time of a building.

Level 2 wind loading: The largest wind loading at the wind velocity believed to have occurred, and that considered to possibly occur in the future, at a building site.

Relaxation of design conditions: Setting the relaxed design conditions, based on the judgment of a designer, such as design loads and structural specifications that correspond to the response reduction or the structural characteristics of a structural response-control building.

Operation limit of active control devices: A level of upper limit of earthquake ground motions or wind loading at which an active control device operates effectively.

Criteria for earthquake and wind resistance: The criteria that structural response-control buildings should satisfy in order that structural response-control buildings shall possess the seismic and wind safety equivalent to or more than that of ordinary buildings for earthquake ground motions and wind loading.

Target performance: A target value of the response-control effect that is set by the

designer or the client regardless of the seismic and wind safety of a structural response-control building.
Safety margin: The degree of safety allowance that a structural response-control building holds for the design conditions.
Block diagram: A summary figure that shows the connection and composition of various kinds of elements of an active control device.
Backup system: A system that substitutes the function and that secures the safety when a response-control device is in unusual conditions.
Quantity of state: The information that expresses the motion of structure and response-control device, and the control state of response-control system.
Sensing system: A system sensing the motion of structure and response-control device, and the condition of transmitted signals.
Control system: A system generating the control signal to drive the drive system, based on the quantity of state sensed, in order that the response-control system may show the response-control effect.
Drive system: A system that receives the control signal and drives the response-control device.
Signal processing: Applying operations on the signal indicating the quantity of state sensed.
Control theory: A theory used to make the control signal that is sent to the drive system based on the quantity of state.
In unusual condition of active control devices: In unusual condition that is impossible to prevent and is unpredictable in the control design, maintenance, and restoration design of an active control device.
At power failure: In condition that the all electricity supply to an active control device is cut off from some unpredictable causes.
In excitation: Shifting from the normal control state to the state exciting for a building from some unpredictable causes.
Performance monitoring: Monitoring the sound performance of an active control device.
Environmental safety: Safety in relation between the response-control device and its surroundings.

1.3 Classification of Structural Response-control Buildings

Structural response-control buildings are classified based on the relaxation of design conditions of structure and the operation limit of active control device as shown in Table 1.1. (Refer to Fig. 1.1)

1.4 Safety Evaluation of Structural Response-control Buildings

Safety of a structural response-control building is evaluated for the structure and the response-control device. Necessary evaluation items are determined according to the classification of structural response-control buildings in Table 1.1. (Refer to Table 1.2)

2. SAFETY EVALUATION OF STRUCTURES

2.1 Outline of Buildings and Ground Conditions

The use, scale, shape, structure, dynamic characteristics of a building, and the site/subsoil conditions and circumstances of the construction site shall be made clear.

2.2 Design Principles and Safety Evaluation Contents

In the safety evaluation of a structural response-control building, the design principles and evaluation contents shall be confirmed according to the following. Necessary evaluation items are determined according to the classification of structural response-control buildings in Section 1.3.
1) Design principles such as the goal of structural response-control building, the criteria for earthquake and wind resistance of structural response-control building, the operation limit of active control device, and the relaxation of design conditions.
2) The structural design and the response analysis results for earthquake ground motions and wind loading that satisfy the criteria for earthquake and wind resistance.
3) Safety margin.

2.3 Setting of Design Conditions

The design conditions such as external disturbances on a structure, design loads acting on a structure, and others shall be determined taking into account the site, subsoil, and structural conditions of structural response-control building.

2.4 Design of Structures

2.4.1 Design for Permanent Loads

Structural members shall be investigated for dead and live loads, and snow load where applicable, so as not to exceed the

permanent allowable stress as specified in the Enforcement Order of the Building Standard Law, in addition to an appropriate check for serviceability.

2.4.2 Design for Design Seismic and Wind Loads

Structural members shall be appropriately investigated for the design seismic and wind loads considering the dynamic characteristics of structural response-control building and the site conditions.

2.4.3 Ultimate Limit State of Structures

The ultimate limit state of structure shall be investigated corresponding to the structural characteristics.

2.5 Detail Design at Response-control Device Location

The details at the location of response-control device shall be designed appropriately considering the aspects of architectural planning and design, building equipment, and structural details.

2.6 Earthquake and Wind Response Analysis of Structural Response-control Buildings

2.6.1 Response for Earthquake Ground Motions

(1) Criteria for Earthquake Resistance

In general, a structural response-control building must be shown to respond to two levels of earthquake ground motions as follows.

1) Under level 1 earthquake ground motion, the structure remains in elastic range, and the response-control device maintains the function.

2) Under level 2 earthquake ground motion, the structure remains within general yield of stories (or within permissible ductility factor), and the response-control device maintains the function.

(2) Input Earthquake Ground Motions

Earthquake ground motions used as input in the response analysis of structural response-control building shall be determined appropriately reflecting the locality of the construction site. The intensity of earthquake ground motions must be the two levels as follows.

1) Level 1 earthquake ground motion: The largest earthquake ground motion expected to occur at the building site once or more during the life time of the building.

2) Level 2 earthquake ground motion: The largest earthquake ground motion believed to have occurred, and that considered to possibly occur in the future, at the building site.

(3) Analytical Method and Mathematical Model

An analytical method shall be adequate for the calculation of the significant features of its dynamic response. A mathematical model of the physical response-control building shall be used which adequately represents the dynamic characteristics of structure and response-control device within the expected response.

(4) Evaluation of Seismic Safety

Criteria for earthquake resistance in two levels must be shown to be satisfied by earthquake response analysis.

2.6.2 Response for Wind Loading

(1) Criteria for Wind Resistance

In general, a structural response-control building must be shown to respond to two levels of wind loading as follows.

1) Under level 1 wind loading, a building suffers no loss of serviceability and function caused by the structural deformation without damage, and the response-control device maintains the function.

2) Under level 2 wind loading, the structure remains in elastic range, and the response-control device maintains the function.

(2) Wind Loading

Wind loading used as input in the response analysis of structural response-control building shall be determined reflecting the wind environment of the building and the construction site. The intensity of wind loading must be two levels in terms of reference wind speed based on mean wind velocity as follows.

1) Level 1 wind loading: The largest wind loading at the wind velocity expected to occur at the building site once or more during the life time of the building.

2) Level 2 wind loading: The largest wind loading at the wind velocity believed to have occurred, and that considered to possibly occur in the future, at the building site.

(3) Analytical Method and Mathematical Model

An analytical method shall be adequate for the calculation of the significant features of its dynamic response. A mathematical model of the physical response-control building shall be used which adequately represents the dynamic characteristics of structure and

response-control device within the expected response.

(4) Evaluation of Wind Safety

Criteria for wind resistance in two levels must be shown to be satisfied by wind response analysis.

2.7 Effect to Structures in Unusual Condition of Active Control Devices

2.7.1 Principles

This section is applied when there is inconsistency in the safety evaluation of response-control devices in Chapter 3, or when there is no reliable guarantee of normal operation of response-control devices.

2.7.2 Unusual Condition

There are two conditions at power failure and in excitation for a building as unusual condition considered.

2.7.3 Safety of Structure in Unusual Condition

Under the unusual condition considered, a structure must be shown to be satisfied by either of the following.

1) Safety of structure taking the unusual condition into consideration.

2) Safety of structure in the state of certain stop of active control device.

3. SAFETY EVALUATION OF RESPONSE-CONTROL DEVICES

3.1 Composition and Specifications of Response-control Devices

The composition and specifications of response-control device shall be determined adequately so as to meet the target performance.

3.2 Control Design of Active Control Devices

The control system of active control device shall be designed adequately corresponding to the target performance.

3.3 Operation Program of Active Control Devices

An active control device shall be adequately operated, within the safety guaranteed range, based on the operation program according to the control design of active control device.

3.4 Performance Validation and Durability of Response-control Devices

3.4.1 Performance Validation Test

The sound performance of response-control device concerning with control shall be validated by the following.

1) The fabrication and product inspection procedures

2) The test program validating the operation and performance of response-control device, and the performance test and evaluation of response-control device according to the test program.

3.4.2 Durability

The contents and time of maintenance inspection shall be determined based on the life time and durability of each component of response-control device.

3.5 Maintenance Inspection of Response-control Devices

3.5.1 Type of Inspection

The maintenance program of response-control device and its vicinities shall be determined adequately. In general, the inspection of this purpose shall consist of three types of inspections; ordinary, periodical, and temporary inspections.

3.5.2 Inspection Contents

Inspection points, inspection items, inspection procedures, criteria, and countermeasures when not meeting the criteria, shall be determined in each of ordinary, periodical, and temporary inspections.

3.5.3 Performance Monitoring of Response-control Devices

The performance monitoring system keeping check the sound operation of response-control device shall be prepared.

3.5.4 Countermeasures of Malfunction

Diagnosis procedures, criteria of malfunction, and countermeasures shall be established in advance against malfunction of response-control device, and the countermeasures shall be taken immediately when malfunction of the device was discovered.

3.5.5 Maintenance Organization

The maintenance organization shall be established which comprises members such as the owner, administrator, designer, constructor, and maintenance administrator of a building.

3.6 Environmental Safety

3.6.1 Active Factors

Countermeasures reducing the effects of the existence and operation of response-control device on existing human beings and things around it shall be adequately taken investigating the factors to be considered and the degree of effects.

3.6.2 Passive Factors

Countermeasures keeping a response-control device in normal condition shall be adequately taken investigating the factors and influence from the condition that is required to keep the device normal by its surroundings, and that possibly affects the device externally.

4. Others

4.1 Construction

A structural response-control building shall be constructed appropriately considering the specifications of building and the safety of construction work.

CONCLUDING REMARKS

The Tentative Guideline for Safety Evaluation of Structural Response-control Buildings is presented that may be needed further to be polished because the development of structural response-control buildings is still in the initial state. The commentary following the guideline will be introduced in another report.

In general the dynamic characteristics of a physical building include the uncertainties caused by the scatter and secular change of structural strength, materials, and construction quality. Therefore the uncertainties of various factors is needed to be investigated when constructing a structural response-control system. Further studies on the reliability, safety margin, and response-control effect index are needed because of insufficient data of uncertain factors.

Reference

1) Report of the Project on Research & Development to Achieve Active Structural Response-control of Building Structures, Ministry of Construction, Government of Japan, March, 1993 (in Japanese).

Table 1.1 Classification of Structural Response-control Buildings

Relaxation of Design Conditions	Operation Limit of Active Devices		
	Level 0 Earthquake Motions or Wind Loading L-0	Level 1 Earthquake Motions or Wind Loading L-1	Level 2 Earthquake Motions or Wind Loading L-2
Not Relaxed R-1	A	B	C
Relaxed R-2	D	E	F

Notes:

1) Relaxation of design conditions means that some design conditions of a structural response-control building are relaxed considering the effects of response-control device in comparison with an ordinary building.

2) Operation limit of active control devices means a level of upper limit of earthquake ground motions or wind loading at which an active control device operates effectively.

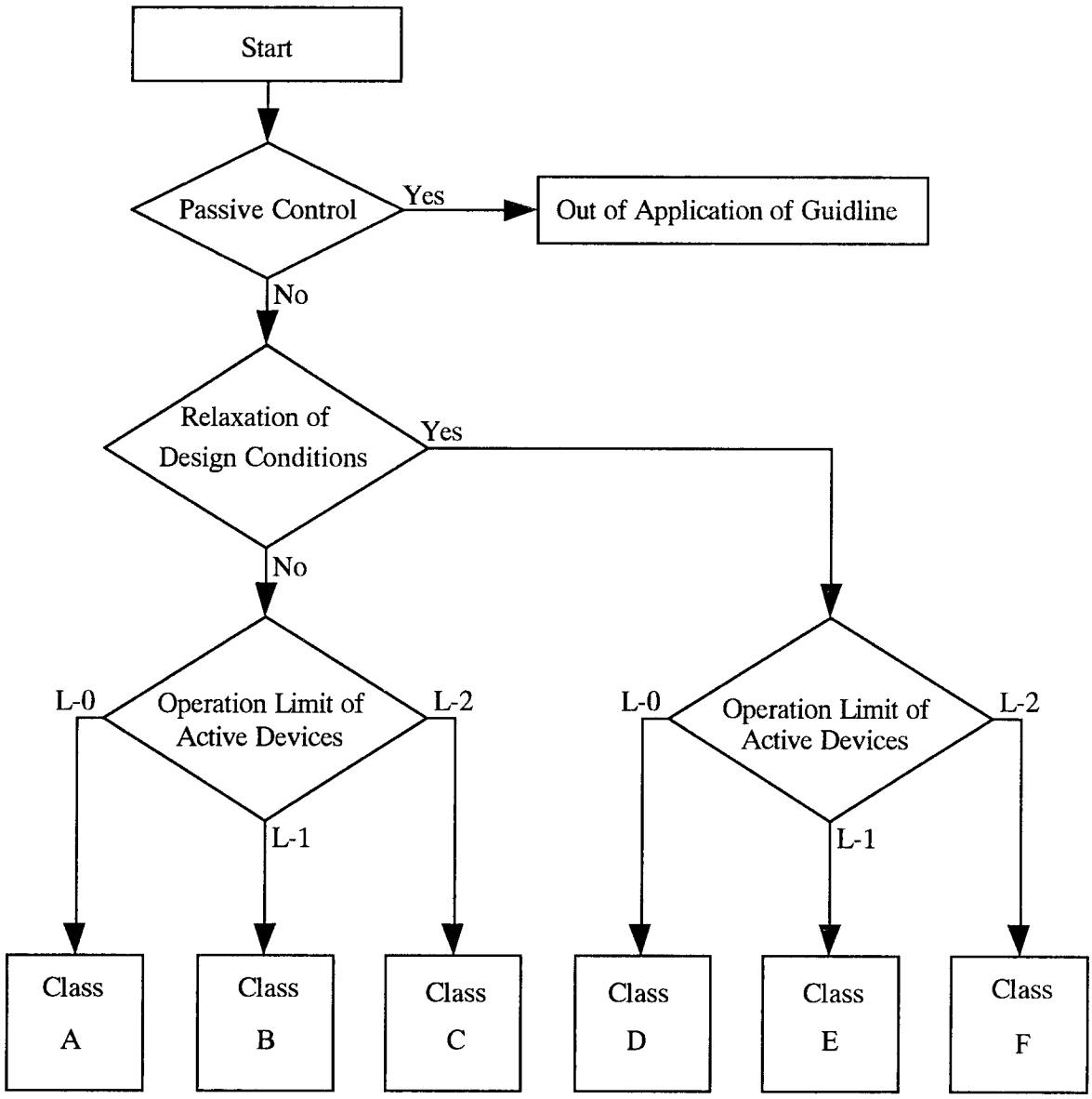

Fig. 1.1 Flow of Classification of Structural Response-control Buildings

Table 1.2 Safety Evaluation Items for Structural Response-control Buildings

Class of Response-control Buildings						Evaluation Items	Remarks
A	B	C	D	E	F		
						(1) Outline of Building to be Evaluated	(To understand outline of a building to be evaluated)
						1. Outline of Ground	
0	0	0	0	0	0	a. Site	
0	0	0	2	2	2	b. Conditions around site (topography, environment)	
0	0	0	2	2	2	c. Subsoil conditions	
						2. Outline of Building	
0	0	0	0	0	0	a. Use	
0	0	0	0	0	0	b. Scale and shape	
0	0	0	2	2	2	c. Structure (structural type, foundation)	
2	2	2	2	2	2	3. Outline of Response-control Device	
						a. Type of system	Active, Hybrid
						b. Size and shape of device	
						c. Setting location	
						4. Design Principles	
2	2	2	2	2	2	a. Goal of response-control	Living comfort, Function, Earthquake and wind resistance
2	2	2	2	2	2	b. Criteria for earthquake and wind resistance	
1	1	1	1	1	1	c. Target performance of earthquake and wind resistance	
2	2	2	3	3	3	d. Operation limit of active control device	
0	0	0	3	3	3	e. Relaxation of design conditions	Relaxed or not, Relaxed contents
						(2) Safety Evaluation of Structure	(To confirm that a structure is designed appropriately considering earthquake and wind response of response-control building)
						5. Design Conditions of Structure	
0	0	0	0	0	0	a. Materials	
0	0	0	3	3	3	b. Design loads (permanent load, seismic load, wind load, others)	
0	0	0	3	3	3	c. Story drift limitation	
0	0	0	3	3	3	d. Structural specifications	
						6. Design of Structure	
0	0	0	0	0	0	a. Design for permanent load	
0	0	0	0	0	0	b. Design for temporary load	
0	1	1	0	3	3	c. Ultimate limit state	
2	2	2	2	2	2	7. Detail Design at Response-control Device Location	Supporting structure, equipment, others

Table 1.2 Safety Evaluation Items for Structural Response-control Buildings (Continued)

Class of Response-control Buildings						Evaluation Items	Remarks
A	B	C	D	E	F		
						8. Response for Earthquake Ground Motions	
0	2	3	2	3	3	a. Input earthquake ground motions	Locality, Level 1, Level 2
0	2	3	2	3	3	b. Analytical method	Time history response analysis
0	2	3	2	3	3	c. Mathematical model	Structure, Response-control device
0	1	2	2	3	3	d. Evaluation of seismic safety	Criteria for earthquake resistance, Safety margin
						9. Response for Wind Loading	
0	2	3	2	3	3	a. Wind loading	Level 1, level 2
0	2	3	2	3	3	b. Analytical method	Time history response analysis, Frequency response analysis
0	2	3	2	3	3	c. Analytical model	Structure, Response-control device
0	1	2	2	3	3	d. Evaluation of wind safety	Criteria for wind resistance, Safety margin
						10. Effect to Structure in Unusual Condition of Active Control Device	
1	2	3	1	3	3	a. Necessity of consideration on unusual condition	Reliability on normal operation, Simultaneous effects of earthquake and wind
1	1	1	1	3	3	b. Safety of structure at power failure	Out of operation, Impulsive force
1	2	3	1	3	3	c. Safety of structure in excitation	Exciting force, Simultaneous effects of earthquake and wind, Operation limit
1	1	1	1	1	1	d. Emergency interruption mechanism	Reliability of emergency interruption mechanism, Effect of sudden stop on structure
						(3)Safety Evaluation of Response-control Device	(To confirm that a response-control device is in normal operation)
2	2	3	2	3	3	11. Composition and Specifications of Response-control Device	
						a. System Composition	Block diagram, Backup system
						b. Components and specifications (Sensing system, Control system, Drive system)	Size, Weight, Input and output, Accuracy, Capacity, Computing performance, Environmental conditions
2	2	3	2	3	3	12. Control Design of Active Control Device	
						a. Sensing of quantity of state	
						b. Signal processing	
						c. Control theory	
						d. Driving program	

Table 1.2 Safety Evaluation Items for Structural Response-control Buildings (Continued)

Class of Response-control Building						Evaluation items	Remarks
A	B	C	D	E	F		
1	2	3	1	3	3	13. Operation Program of Active Control Device	
						a. Period, conditions and method of operation	Program of start and stop
						14. Performance Validation and Durability of Response-control Device	
2	2	3	2	3	3	a. Fabrication and product inspection procedures	Quality and standards of device material
2	2	3	2	3	3	b. Operation test and performance test	Operation of device, Performance of response-control building
1	2	3	2	3	3	c. Durability	Environmental conditions, durable year, and durability of sensor, CPU, driving device, power source, and others
1	2	3	2	3	3	15. Maintenance Inspection of Response-control Device	
						a. Type and contents of inspection	Measuring system, CPU, Control software, Driving device, and Power source
						b. Maintenance organization	
						c. Performance monitoring	Monitoring of response-control system, Diagnosis method, and Restoration design and manual
						d. Countermeasures of malfunction	Control design considering malfunction
						16. Environmental Safety	
2	2	3	2	2	3	a. Active factors	Influence of device on circumstances
2	2	3	2	3	3	b. Passive factors	Influence of circumstances on device
						(4) Others	
1	1	1	1	1	1	17. Others	
						a. Construction	
2	2	2	2	2	2	18. Reference Documents	Materials related to Item 14
						a. Performance validation test data	

Notes:
1) "0" denotes that evaluation equivalent to ordinary building is necessary.
"3" denotes that detailed evaluation as response-control building is necessary.
"2" denotes that evaluation as response-control building is necessary.
"1" denotes that evaluation as response-control building is not necessary except for special cases.
2) Earthquake and wind response analysis is for a structural response-control building including the structure and response-control device. Degree of investigation for each item is different according to a balance between the potential performance of response-control device and the lateral load-carrying capacity of structure.

Tsunami Disaster Caused by Hokkaido-Nansei-Oki Earthquake in 1993

by

Shunji Niwa, Takekazu Akagiri, Masakatsu Horino, Masaharu Tsuzawa

ABSTRACT

The earthquake was accompanied by big tsunamis. Okushiri island, which is in the southwest of Hokkaido, was severely damaged by the tsunamis with a loss of 201 persons. The maximum heights of the traces of the tsunami were measured by using a parallax bar on aerial photographs. The naximum height of the tsunamis is 21m in the west coast of the island.

Key words: Okushiri island, maximum height of the tsumamis, parallax bar, aerial photograph.

1.Introduction

At 22:17 on July 12 in 1993, a big earthquake hit Okushiri Island which is located in the southwest of Hokkaido, off the west coast of the Oshima Peninsula , of which magnitude was 7.8. In Okushiri Island, very strong shock hit the island, and subsequently, about 300 sites of failures were caused mainly along the coastline and in the mountainous area. In Oshima Peninsula, many collapses, liquefaction of soil, subsequent disruptions of roads were caused in many sites.

The earthquake was accompanied by big tsunamis. (Tsunami is very strong and high wave which is caused by a strong earthquake in the sea.) It hit Okushiri Island and other areas and caused intensive damages which included loss of many people and various kinds of damages in the coastal areas in Japan, Korea, Russia and other areas. In the case of Okushiri Island, tsunamis hit the island only several minutes after the earthquake. And subsequently 201 persons were lost and many houses and buildings were destroyed.

Geographical Survey Institute(GSI) took aerial photographs to catch actual conditions of damages in the southwestern coastal zone of Hokkaido main land and Okushiri Island on July 13 and 14, and worked in the field from 15 to 20 of July and from 3 to 5 of August. Based on the interpretation of these aerial photographs with fieldcheck, the authors clarified actual conditions of tsunamis using traces of tsunamis, mainly on the areal distribution of drowned area and the height of the tsunami. (Fig.2)

In this report, we will report the general conceptions of the damage and heights of tsunamis.

2.Outline of the Hokkaido Nansei-oki Earthquake

According to the Meteorological Agency, the hypocenter of the earthquake is 34km deep, 42° 47'N, 139° 12'E. It is located at about 70km off to the northwest of Okushiri Island. According to the distribution of hypocenter of the aftershocks, it is assumed that the fault plane is tilted westside down. Okushiri Island subsided about 20 cm to 80 cm by the earthquake. We clarified

Geographical Survey Institute, Ministry of Construction, Kitasato 1, Tsukuba-shi,Ibaraki-ken, 305 Japan

the quantitative value of subsidence using change of landscapes, which are subsidence of rocks along the coastline, change of shore protection, the change of the vertical distribution of small life in tidal zones in comparison with before and after the earthquake based on photointerpretation, photo-grametric way and fieldcheck.

The source area of the tsunami is distributed in the area about 150 km from north to south in the area of south-west off of Hokkaido. Based on the initial motion, this earthquake caused the submergence in the east, and the upheaval in the west. Several models of the fault with two faults planes were proposed and mostly that the fault planes are westside down.

3.Outline of Okushiri Island

Okushiri Island is an island which is 22km from north to south, 13km from west to east. In the island, the highest peak is Mt.Kamui with 585m above the sea level and various terraces can be seen from the coast to the top of the mountainous area. Terraces develop in the southern part, east coast and north edge of the island. but few in the west coast. The central area of the island is remarkably dissected. The terraces, which had been formed about one hundred and twenty thousand years ago, have heights of 70m to 80m in the south, 120m to 130m in the north. The island repeatedly raised up by tectonic upheaval by earthquakes and the island has been being formed. But this time, the island subsided. Villages are distributed only along the east coast and both north and south ends of the island, but very few along the west coast and in the mountainous area.

4.Damage Caused by Tsunami

As of 11 of August, there were loss of life:200 persons, missing:34. Among them, 169 loss, 32 missing at Okushiri Island. Most of them were by tsunami. As for damage of houses: complete destruction 558, partial destruction 247, drown, inundation and slight destruction 3,348 (as of 27 of July). Most of houses were destroyed or washed away by tsunami at Aonae, Hatsumatsumae in the south of the island and Inaho in the north end.

Fire was caused after the hit of tsunami and subsequently a few hundreds of houses burned down at Aonae. The fire started in a few sites, but it spread to the broad area because of a few promoting factors: 1)anxiety about following tsunami waves, 2)accumulation of destroyed houses, damaged cars and logs and wastes from the sea by tsunami waves were seen on town roads. These reasons interrupted fire service team to enter and work in the area. Subsequently fire spread to the broad area. Tsunami waves also caused damage of port facilities, destruction of ships, washed ashore ships and many other things were burned and washed ashore or washed away to the open sea.

5.Drowned Area by Tsunami Waves and the Distribution of Maximum Flooded Level (Flood Mark)

It is clearly and easily found to distinguish the drowned area and the maximum flooded level of tsunami waves based on color change of grass-covered area, washing away and destruction of houses, various kinds of wastes, driftwood and others. Vegetation color in the drowned area was changed from green to brown and the boundary was very clear. Salt in sea water which overflowed let grass dry and changed color. And the distribution of driftwood and

other kinds of wastes were seen in the same zone. This boundary was seen clearly in the southwest and north end of the island, but it was not so clear in the northwest and east coasts, because the heights of tsunami waves were not so high and very few area is covered by vegetation in the low area along the coast line, and sometimes, such area consists of rock.

6.Measurement of Tsunami Waves using Aerial Photographs

We used a parallax bar on the aerial photographs to measure heights of tsunami. And we checked the value at several sites in the field. The method using a parallax bar is to get relative height between two points and a parallax bar is a tool to measure parallax of the same point on two leaves of aerial photographs. Using this tool, it is possible to measure parallax between two points. Based on the parallax difference, it is possible to calculate relative heights between two points. The heights of tsunami waves must be calculated from the sea level, for the reason, it is possible to measure maximum heights of tsunami waves easily based on the relative heights of maximum flood mark on aerial photographs. Thus, we could get the distribution map of tsunami heights which went upstream in the land area(Fig.2).

The maximum value is 21m in the west coast, but 3-7m in the east coast. Tsunami damage was intensive at villages at low sites in the areas of north and south ends.

In aerial photographs, traces of tsunami waves were recorded very clearly on the aerial photographs taken on July 13 and 14. The record includes drowned area and heights which tsunami reached upstream in the land area. And we measured the heights of tsunami waves using aerial photographs as a part of urgent survey in a very short period and officially announced on August 2 as a part of "The urgent report of the Hokkaido nansei oki earthquake".

The method to measure relative heights is never special one, rather very fundamental method of photogrammetry, but we have not seen an example to have measured the area and heights of tsunami waves, then, here we will report the result.

7.Interpretation of Aerial Photographs

Information of aerial photographs consist of 1)location, 2)tone, 3)pattern, 4)texture, 5)color, 6)form. This time, we could use color aerial photographs. Then, it was possible to use color information enough for interpretation. Naturally, various information of actual conditions of damage was very important, that is, destruction of houses, erosion, accumulation of wastes change of landscapes along the coastline. Especially, color change of grass-cover land. Based on the preliminary interpretation and measured map, the survey team made sure whether or not the map was correct. In most cases, the result was very good with very few exceptions.

Aerial photographs used are as follows: 1) the whole area of Okushiri Island., taken by GSI, flight height is 2,600m, color, 2) the coastal zone. taken by Kokusai-kogyo Co. flight height is 1,275m. color.

8. Method

Procedure is shown in the followings: 1)Interpretation of damaged area using aerial photographs stereoscopically. The boundary of damaged area is marked on the photographs. At this stage, every site, one stereo pair of photo-

graphs was prepared. 2)using each pair of aerial photographs on which the interpretation was marked, and the relative heights (area and maximum heights of tsunami waves) were calculated based on parallax differences which were measured using a parallax bar. The values were not the same and values above 40 sites were measured using aerial photographs and were made sure in the field. The result of interpretation and measurement was almost the same as the values which were measured in the field. The result is shown in the Table 1.

9.Procedure

1)Preparation of two leaves of aerial photographs on which drowned area is shown. Plotting principal point of each photo.

2)Transferring principal point to each other and to measure the air base length between principal point and transferred principal point on each photo.

3)Set the stereo pair of photos. Two principal points and two transferred principal points must be set in straight to be able to get stereoscopically using a mirror stereo scope.

4)On the pair of photos, using a parallax bar, measure value of the same point A (coast line) by adjusting, measureing mark of the parallax bar. Adjusting point B and measure value. If the values of A and B are the same, A and B are the same heights. If A and B are not the same, the ground height of A and B are different. This difference is parallax difference. Based on this value, the relative height is calculated.

5)The relative heights (maximum height of tsunami) is calculated as follows:

$$dh=H \times \frac{dp}{b+dp}$$

dh : relative height
H :flight height
b :base length
dp:parallax difference

6)Repeat measurement of parallax differences at least several times. And average the result except maximum and minimum to decrease error. This time, because the parallax difference is relatively small to base length, the parallax difference in the denominator of the formula can be neglected.

This method can be available to get uniform quality of the result in a short period. If it is impossible to visit the sites, the result using aerial photographs is almost the same as the result from fieldcheck.

It is possible to distinguish distance by eyes when intersection angle is above 20" (Kimoto:1971). This shows that 1.3m is the minimum resolution when the intersection angle above 20" is 0.09mm in the case of 25cm in clear vision of the photos which were taken at 1,275m in flight height. For the reason, the measured values were counted fractions of 5 and as a unit and cut away the rest.

Objectives to research using photos must be shown in the photos. It is pretty difficult to interpret and measure the sites which are in shadow, in the deep valley bottoms, in a deep transparent sea.

To get better results, surveyors must use the center of the photos as possible as they can. And also to get better results of measurement, aerial photographs should be taken along the

coast line. It means that decision of flight courses is pretty important.

10. Conclusion

As of the maximum height of tsunami waves, some researchers reported that the maximum value was over 30m, but based on our research, the maximum value was 21m. Usually it is pretty difficult to measure in the shadow, in valley deep floor, but the difference was too large.

It is possible to clarify the distribution of tsunami waves using aerial photographs with parallax bar. This method is very fundamental method in photogrammetry. Such a fundamental method is available to catch actual conditions of tsunami waves.

11.Acknowledgment

The authors are full of gratitude to Mr.Haruo Fujimaki, Mr.Minoru Hoshino, Mr.Yohta Kumaki and other members of the team for the urgent research on the Hokkaido Nansei-oki Earthquake.

12.Reference

Ujihisa KIMOTO(1971):*Practical photogrammetry.* Sankaido, Tokyo, p267, in Japanese.

The Emergent Research Group for the Hokkaido Nansei-oki Earthquake Hazard(1993):The emergent survey report of the geomorphological hazard induced by the Hokkaido Nansei-oki Earthquake of 1993. *Kokudochiriin jihou*, GSI, 20-27, in Japanese.

Table 1. Calculation of the height that tsunami reached

No.	b	p_s	p_t	dp	dh	Airphotos
1	83	35.28	35.57	0.29	6.9	GSI*
2	82	32.33	32.63	0.3	7.2	
3	82	32.99	33.27	0.28	6.8	
4	83	31.19	31.47	0.28	6.7	
5	78	34.92	35.02	0.10	2.5	
6	80	33.3	33.46	0.16	3.9	
7	82	34.39	34.59	0.2	4.8	
8	87	29.56	29.78	0.22	5.0	
9	79	28.75	28.98	0.23	5.8	
10	87	29.35	29.74	0.39	8.9	
11	86	31.46	31.89	0.43	9.9	
12	77	33.31	33.65	0.34	8.7	
13	88	31.82	32.31	0.49	11.0	
14	88	31.05	31.41	0.36	8.1	
15	98	21.55	21.77	0.22	4.4	
16	82	14.40	14.61	0.21	5.1	
17	98	21.22	21.63	0.41	8.3	
18	99	20.89	21.14	0.25	5.0	
19	86	25.91	26.27	0.36	8.3	
20	84	16.70	18.01	1.31	19.9	Kokusai Kogyo Co. Ltd.**
21	84	3.99	5.36	1.37	20.8	
22	84	13.30	14.30	1.00	15.2	
23	84	16.57	17.88	0.84	10.5	
24	88	15.90	16.92	1.02	14.8	
25	88	3.63	4.42	0.79	11.4	
26	89	8.12	8.83	0.71	10.2	

No.:Locality numbers. b:The length of baselines.(mm) p_s:Parallax at the sea level.(mm) p_t:Parallax at the highest level that tsunami reached.(mm) dp:Parallax difference.(mm) dh:The highest level that tsunami reached.(m) Airphotos:Airphotos used for measurement.

* Geographical Survey Institute, July 14 1993, 1:13,000

** July 13 1993, 1:8,000

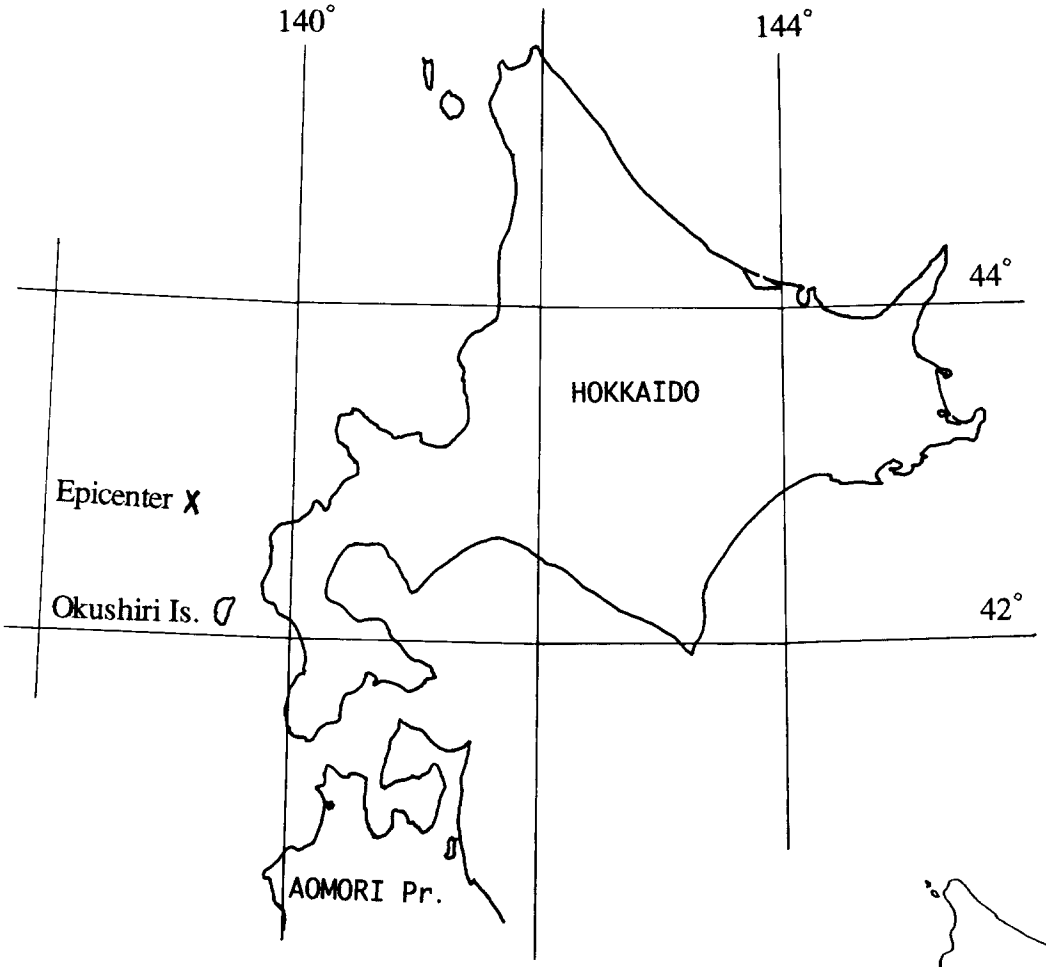

Fig. 1 Location of the epicenter of the earthquake and the Okushiri island

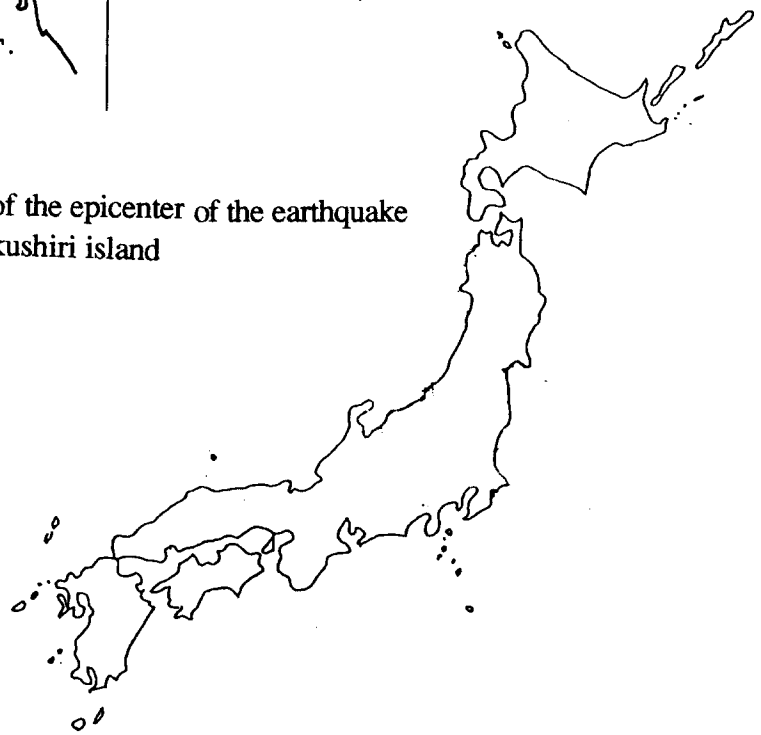

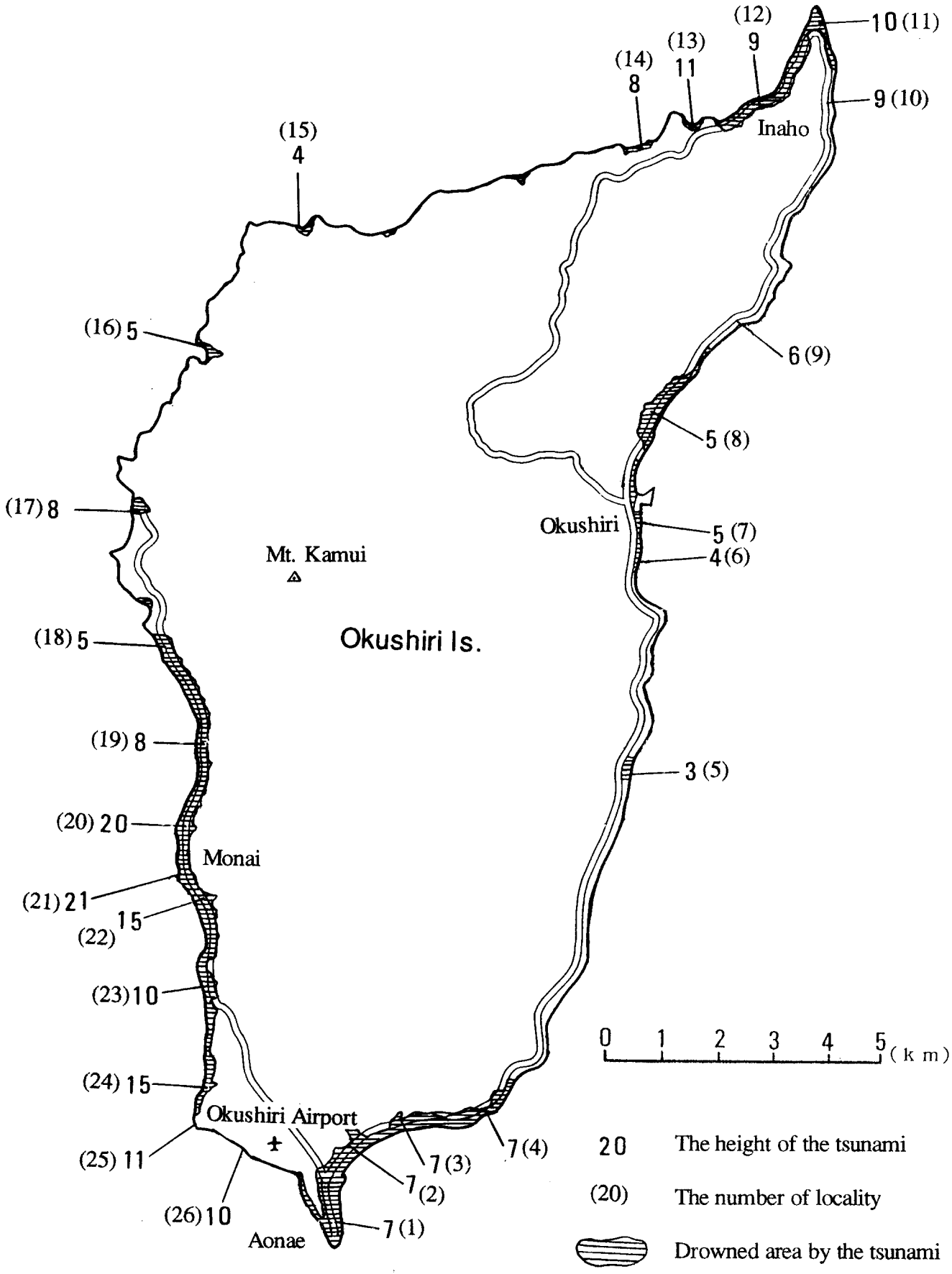

Fig. 2 Distribution of the height of the tsunami

Photo 1. Destroyed area (foreground) by the tsunami (Aonae)

Photo 2. Boundary of drowned area (arrows)

The Dam Safety Program

by

William S. Bivins* and Harold W. Andress*

ABSTRACT

The United States does not have a legislated National Dam Safety Program. Devastating dam failures in the 1970's raised public concern but surprisingly did not produce legislation to mitigate the loss of lives and property. In 1980, the Federal Emergency Management Agency (FEMA) initiated a program to pull together concerned professionals. It was an attempt to substitute a concensus-building process for the missing legislation (with the attendant funding). The process produced The Partnership, a term defined as the intertwining of individual interests in the dam safety community to enhance the safety of dams. The Partnership in turn produced the leadership, technical assistance, and public awareness to mitigate the risks from the nation's dams.

KEYWORDS: concensus-building, dams, dam safety, guidelines, inventory, training.

1. INTRODUCTION

Currently there is no National Dam Safety Program. There is a need for one and the need will continue. In November, 1982, the National Research Council undertook a study for the Federal Emergency Management Agency (FEMA) and published a report titled, *Safety of Nonfederal Dams - A Review of the Federal Role*. One of the conclusions of that study was "[b]ecause of inadequate state supervision and the magnitude of the consequences of widespread dam failures, a National perspective on dam safety is needed. The problems will not be solved entirely without a Nationwide perspective or the impetus that a broad-based group can offer."

However, no legislation to create such a National perspective has been forthcoming. Each federal agency had autonomous dam safety programs. Some states also had programs but they varied widely.

In 1980, the Federal Emergency Management Agency (FEMA) began a process to substitute consensus building for legislative mandate. This paper describes the evolution of The Partnership — an intertwining of the interests of the dam safety communities of the federal government, of states, and of the private sector. While legislation is still needed, the FEMA initiative has resulted in the partial mitigation of risks from the nations dams.

2. BACKGROUND

The Federal dam safety program had its beginning in disasters of the 1970's. It was after the failure of Buffalo Creek, Teton, and Kelly Barnes dams that Federal efforts in dam safety began in earnest.

2.1 Buffalo Creek

Saturday morning, February, 1972, a mine tailings dam failed at Buffalo Creek, West Virginia, killing 125 people. The Buffalo Creek Dam was neither designed nor built to accepted engineering standards. Nor was it operated, maintained, inspected or regulated in accordance with sound practices of dam safety. This disaster created public concern about the safety of the Nation's dams which in turn stimulated Congress to pass the *National Dam Inspection Act* (Public Law 92-367). The Act authorized an inventory and an inspection of the Nation's dams. The inventory began, but the inspection had to await another disaster.

2.2 Teton

The Teton Dam, near Newdale, Idaho, failed June 5, 1976, killing 14 people. This induced the federal government to take a hard look at existing dam safety programs, to assess what they accomplished and to define what they needed to be. The assessment led to the development of the *Federal Guidelines for Dam Safety*.

2.3 Kelly Barnes

It was a rainy night in Toccoa Falls, Georgia, November 6, 1977, when the Kelly Barnes Dam failed without warning; killing 39 people, mostly

* Federal Emergency Management Agency
Washington, DC 20472

Bible college students. This disaster provided the impetus to fund the inspection portion of P.L. 92-367. The U.S. Army Corps of Engineers began a program to inspect 8818 high hazard potential non-federal dams. The inspection revealed that 2925 dams were unsafe.

In October 1979, President Carter directed the agencies to implement the *Federal Guidelines for Dam Safety* and report to the newly created Federal Emergency Management Agency (FEMA). The Federal program for dam safety was born.

3. THE PROGRAM

The goal of the dam safety program is to identify and mitigate the risk of dams to protect the lives and property of the public. This is accomplished by establishing and enforcing acceptable design, construction, operation and maintenance standards for dams. The goal is further elaborated upon in the FEMA dam safety doctrine:

"Dams must be designed, built, operated and maintained safe. Ensuring the safety of dams is not a passive activity. The responsibility for protecting lives and property never ends. New approaches and policies must be developed, implemented and evaluated. New players must be continually recruited and drawn into the group of involved participants. New programs must be promoted; weak programs must be revitalized. Leadership, awareness, dedication and action must be advocated and repeatedly fostered. Opportunities must not be overlooked."

The dam safety program objectives are to improve federal dam safety through implementation of the *Federal Guidelines for Dam Safety* and to foster non-federal dam safety by assisting States, local governments and the private sector in developing and implementing effective programs. The objectives are expressed in the following vision statement:

"FEMA will accomplish its operational objectives for national dam safety through the creation of quality policies, procedures and products to enhance personal safety, protect property and benefit the dam safety community. By becoming pacesetters as resource stewards and leadership providers, through commitment to high quality, reliable service and effective management, FEMA will achieve results beyond the dam safety community and public's expectations."

4. FEMA'S ROLE

FEMA's role in National dam safety is unique. FEMA neither owns dams nor has regulatory responsibility for dams; but, FEMA coordinates hazard mitigation dam safety activities. FEMA's role includes activities in the federal and non-federal sectors.

4.1 Federal:

The federal role embodies all the activities undertaken by federal agencies to safety build, operate and maintain dams. FEMA coordinates the activities of the federal agencies to implement the *Federal Guidelines for Dam Safety* through the Interagency Committee on Dam Safety (ICODS). FEMA is the chair for ICODS and its administrator.

4.2 Non-Federal:

Non-federal program activities involve the practices undertaken by State and local governments and the private sector to design, build, operate and maintain safely the dams they own and/or regulate. FEMA coordinates non-federal program activities primarily with the Association of State Dam Safety Officials (ASDSO). FEMA's role in this sector is to foster state efforts to establish effective dam safety programs patterned after the *Model State Dam Safety Program* and to provide technical assistance and public awareness support.

4.3 Partnership

National dam safety goals and objectives are pursued in partnership with Federal, non-Federal and private sector participants. This consortium embodies the power of partnership:

Partnership is essential to National dam safety; partners enhance capability, minimize duplication and maximize efficient use of resources. Success is directly related to success of the Federal and non-Federal partnership. Federal agencies working together form one element of the partnership while State and local governments and the private sector working together form the other. The Federal and non-Federal elements working together form the 'ultimate' partnership. Together these partners make the National Dam Safety Program truly National.

4.3.1 Federal Partners

4.3.1.1 Interagency Committee on Dam Safety

ICODS exemplifies the Federal partnership. ICODS is a potent force. It is the only Federal forum where Federal agencies initiate cooperative efforts and offerings of talent and resources to meet National dam safety needs.

FEMA chairs ICODS which consists of representatives from; the Departments of Agriculture, Defense, Energy, Interior, Labor and State (International Boundary and Water Commission), the Federal Energy Regulatory Commission, Nuclear Regulatory Commission and the Tennessee Valley Authority.

ICODS was established in 1980 and one of its function is to assist FEMA in fulfilling its National dam safety responsibilities. It continues to excel in its role of providing an arena where Federal dam safety issues are identified, discussed and resolved, and where progress and contributions are made in cooperative efforts to resolve non-Federal dam safety issues.

4.3.2 Non-Federal Partners:

The year 1993 marked the completion of a successful decade of partnership between the Federal and non-Federal dam safety communities; between ICODS, ASDSO and the United States Committee on Large Dams (USCOLD).

4.3.2.1 Association of State Dam Safety Officials

ASDSO brings together the partnership of the States and the private sector. It provides the non-Federal voice to address National dam safety issues. ASDSO, organized in 1984, continues to carry out far reaching projects for which it has become known and which have made it one of the leading organizations dealing with dam safety issues, nationally and internationally. ASDSO produces products which benefit the entire dam safety community while maintaining its primary focus of supporting State dam safety programs and maintaining intergovernmental relations.

ASDSO continues to prosper as the word of its good work continues to spread. Membership from other countries has steadily increased. Countries represented include; Australia, Brazil, Canada, India, Iran, Italy, Japan, South Africa, South Korea, and Turkey. Total ASDSO membership should reach 1000 in 1994, up from 379 in 1988.

4.3.2.2 United States Committee on Large Dams

USCOLD is the United States member of the International Commission on Large Dams (ICOLD), an international organization composed of nearly 80 countries. USCOLD is a nation-wide professional organization dedicated to advancing the technology of dam design, construction, operation and maintenance, and to promoting awareness of the role of dams in the beneficial development of the nation's water resources.

USCOLD members come from many professional disciplines, including Civil, Mechanical, and Electrical Engineering; Environmental Sciences, Social Sciences; Finance; Economics and Law. They are contractors; consulting engineers; representatives of local, State and Federal government agencies; academicians; managers and owners of water resource projects.

FEMA is represented on USCOLD's Committee on Public Relations. The role of the committee is to communicate about dams to the public and is closely aligned with FEMA public awareness activities in dam safety. USCOLD adds the third leg to the triad - the partnership of Federal sector, non-Federal public sector, and private sector - which broadens the base of support for national dam safety.

4.3.2.3 "Ultimate" Partnership

Federal and non-Federal partners working together form the "ultimate" partnership by consolidating their efforts to meet the goals and objectives of National dam safety. FEMA coordinates these efforts.

5. FEMA ACTIVITIES

FEMA conducts its dam safety activities primarily in three areas:

5.1 Leadership

FEMA provides strong National leadership by chairing ICODS and coordinating Federal actions in non-Federal dam safety.

An important leadership project in dam safety today is maintaining a current National Inventory of Dams (NID). In 1986 FEMA funded ASDSO to determine the feasibility of updating the NID. The update was

feasible and the states agreed to participate. However, the states did not have adequate funding for update. In November 1986, Congress passed the *Water Resources Act of 1986* which authorized U.S. Army Corps of Engineers to update the inventory. Funds were appropriated in fiscal year 1988. On March 16, 1989 FEMA and the U.S. Army Corps of Engineers signed an agreement whereby FEMA assumed responsibility for a program using the appropriated funds. The update program was completed in 1992. The inventory, available in CD ROM form, is updated annually.

As previously mentioned, FEMA chairs ICODS which meets quarterly to further dam safety goals. Workshops and meetings are sponsored to review, discuss, and debate current issues relative to national dam safety. An example is the 1990 Probable Maximum Precipitation/Probable Maximum Flood (PMP/PMF) workshop held to discuss the formulation of PMP/PMF guidelines. PMP and PMF estimates have taken on greater importance in liability and dam construction and modification costs. Since no uniform standards existed for estimating the PMP and PMF, differences of opinion concerning these estimates had caused considerable confusion. Uniform standards allay this confusion and allow practitioners to develop estimates that are both widely acceptable and reproducible.

5.2 Technical Assistance

Technical assistance is delivered through the exchange of dam safety knowledge, skills, experiences and resources between the Federal and non-Federal sectors.

One of the most successful technical assistance programs is the Training Aids for Dam Safety (TADS). TADS was developed as an ICODS project, with non-Federal participation and adept lead agency management by the Bureau of Reclamation.

TADS consists of 21 training modules, text and video, grouped in three components: 1) The Inspection component, designed to teach regulators how to conduct a dam safety inspection; 2) The Awareness component which emphasized dam safety mitigation; and 3) The Analysis component, which provides evaluation techniques for dam safety program managers, owners/operators and experienced engineers. FEMA distributed TADS materials to the States free of charge. They in turn can train their own engineers and regulators in dam safety.

Despite the efforts to minimize the risk, dams occasionally fail. When this happens it is very important that dam owners and operators have a plan to deal with the emergency. For this reason a State requirement for an emergency action plan for each high hazard dam is one of the eight essential elements of an effective dam safety program. The plan is absolutely essential for dams which have a high hazard potential for failure and highly recommended for dams having a significant hazard potential. The Federal Energy Regulatory Commission (FERC) developed a training program to teach hydroelectric licensees how to develop and exercise emergency action plans. FEMA is cooperating with FERC to adapt this course for all dam owners/operators.

5.3 Public Awareness

This activity includes proactive and aggressive public awareness enterprises to bring the dam safety message to the general public, emergency management officials, Federal, State and local officials, and the private sector dam safety community.

Most people know very little about dams, even if they live or work near one. Therefore, knowledge about how dams operate and what to do in the event of an emergency is important for everyone. It is through public awareness that we raise the level of consciousness of dam safety in both the Federal and non-Federal sectors.

Public awareness takes many forms. It can be as straightforward as a State Dam Safety Public Awareness Workshops or the biennial National Dam Safety Program Progress Report to the President.

FEMA publishes many materials emphasizing dam safety; most written with the assistance of other agencies. These publications are designed for diverse audiences such as dam owners/operators, State and local officials, and the general public.

FEMA also disseminates other types of information to the public and Federal agencies. For example, several years ago dam owners in the Great Lakes region became aware of a new crustacean which clogged water intake valves, bred prolifically, and was extremely difficult to eradicate. This crustacean, the Zebra mussel, found its way to the United States from the Caspian Sea via shipping in the St. Lawrence Seaway. The mussels are now spreading throughout the waterways of the Midwest, East and Southern United States. FEMA, through ICODS, has

created a clearinghouse for information on the Zebra mussel so dam owners can keep abreast of new developments on how to eradicate these creatures or impair their ability to attach themselves to critical structures and associated equipment.

All of FEMA's public awareness programs have the proactive goal of disseminating information to the widest possible audience in order to save lives, mitigate property damage and conserve resources.

6. CONCLUSIONS

The concensus-building process, tentatively embarked upon in 1980, worked. A *de facto* National Dam Safety Program does exist. It has produced phenomenal results.

The National Inventory of Dams, the Training Aids for Dam Safety, the development of numerous guidelines and the enhancement of public awareness, all evolved from the development of The Partnership. Legislation, with adequate funding would have been desirable. The results produced in 14 years would have been available sooner. Loss of lives and property damage may have been avoided. However, funding was not available.

The Partnership of literally thousands of dedicated dam safety professionals from federal and state governments and the private sector proved an acceptable substitute.

6. REFERENCES

6.1 *Safety of Nonfederal Dams - A Review of the Federal Role*, National Research Council for FEMA, 1982.

6.2 *Federal Guidelines for Dam Safety*, Federal Coordinating Council for Science, Engineering and Technology, (FEMA-93) 1979.

6.3 *Model State Dam Safety Program*, Association of State Dam Safety Officials for FEMA, 1987.

6.4 *Proceedings of Probable Maximum Precipitation and Probable Maximum Flood Workshop*, FEMA, 1990.

6.5 *Emergency Action Planning Guidelines for Dams*, Emergency Action Planning Subcommittee, ICODS, (FEMA 64) 1985.

6.6 *Federal Guidelines for Earthquake Analyses and Design of Dams*, Design Earthquake Task Group, ICODS (FEMA-65) 1985.

6.7 *Federal Guidelines for Selecting and Accommodating Inflow Design Floods for Dams*, Inflow Design Floods Working Group, ICODS, (FEMA-94) 1986.

Multi-Hazard Mitigation for Non-Engineered Structures

by

Michael Mahoney*

ABSTRACT

The Federal Emergency Management Agency (FEMA) is the Federal agency responsible for coordinating all of the Federal government's activities relating to disasters. One of this agency's primary goals is to reduce, or mitigate, the nation's losses that result from natural hazards, such as earthquake, high winds, flooding and fire. In order to accomplish this goal, FEMA is committed to encouraging building practices that address these different hazards and minimize the damage that can result. To accomplish this, FEMA has worked with the design and engineering communities and the nation's three model code organizations to encourage the use of loss reduction design standards. While this has generally been effective in their own way, there are two reasons why they could be more successful.

One reason is that each approach only dealt with its own hazard. The development of design criteria has historically only examined the impact on the hazard being addressed, and did not examine what the impact was on other hazards. There is a growing awareness that mitigation must look at all hazards; that coordination is needed to avoid conflicts where action taken to reduce the threat of damage by one hazard may increase the threat of damage from another.

A second reason is the building codes themselves and how they are used. Model building codes usually work well with an engineered building, where the engineer can translate the performance requirements into construction requirements, or plans. The problem is with marginally- or non-engineered buildings, where that interpretation is usually left up to the builder or contractor. The success of that building in resisting the forces generated by the different natural hazards then becomes dependent upon their level of expertise and attention to detail. As shown by several recent disasters, such as the Northridge earthquake and Hurricane Andrew, this is where the process often breaks down.

To address the need for technical guidance for non-engineered buildings, and to do so using a multi-hazard approach, FEMA has recently undertaken two projects that will be of significant benefit. However, the coordination of efforts between the different hazards may require an independent, non-governmental body that is capable of coordinating the present standards writing organizations as well as the various outside interests, such as the architects, engineers, materials interests, contractors and other similar groups.

1. INTRODUCTION

The Federal Emergency Management Agency (FEMA) is the Federal agency responsible for coordinating all of the Federal government's activities relating to disasters. One of this agency's primary goals is to reduce, or mitigate, the nation's losses that result from natural hazards, such as earthquake, high winds, flooding and fire. In order to accomplish this goal, FEMA is committed to encouraging building practices that address these different hazards and minimize the damage that can result.

To help encourage building practices that can reduce the threat presented by different natural hazards, FEMA has worked with the design and engineering communities and the nation's three model code organizations to encourage the use of loss reduction design standards. This effort has taken several forms.

---

* Federal Emergency Management Agency
Washington, DC 20472

To address the seismic hazard, the National Earthquake Hazards Reduction Program (NEHRP), which is made up of four Federal agencies (FEMA, National Institute of Standards and Technology, National Science Foundation, and the U.S. Geological Survey) worked with an outside organization, the Building Seismic safety Council (BSSC) to develop a resource document for use by all regulatory organizations. This document, the *NEHRP Recommended Provisions for the Development of Seismic Regulations for New Buildings*, was developed using a consensus procedure, and has now been either adopted or utilized by all three of the model code organizations.

To address the flood hazard, FEMA, which is responsible for administering the National Flood Insurance Program (NFIP), started with design criteria based on the legislation that authorized the program. We then funded the development and publication of technical guidance materials based on the design criteria, and then worked directly with the model code organizations to have this material incorporated into the nation's model building codes.

With regard to the wind and fire hazards, there are currently no specific government mitigation program that addresses these hazards. This is primarily because these hazards have generally been addressed by non-governmental concerns, such as the American Society of Civil Engineers and their ASCE 7 standard for wind and the National Fire Protection Association for fire. Most government agencies accept and use the current model code requirements for these hazards.

While all of these approaches have generally been effective in their own way, there are several reasons why they could be more successful.

2. MULTI-HAZARD APPROACH

One of the reasons why the mitigation of different natural hazards has not been completely effective is that, until now, each approach only dealt with its own hazard. The development of design criteria, from initial research up to actual code language, has historically only examined the impact on the hazard being addressed, and did not examine what the impact was on other hazards. There is a growing awareness that mitigation must look at all hazards; that coordination is needed to avoid conflicts where action taken to reduce the threat of damage by one hazard may increase the threat of damage from another.

One example of a potential conflict between hazards is whether seismic loads acting on a structure that has been built on an raised foundation to elevate the building above flood levels would result in increased damage. Seismic loads could cause an elevated foundation to act as a moment arm, and greatly increase the shaking of the building. However, if such a structure and its elevated foundation were properly constructed and reinforced to resist coastal wind forces, the additional steps needed to provide adequate seismic resistance may well only consist of a strengthened pile to beam connection or the addition of knee bracing, both of which are already common coastal construction techniques.

A second example is the issue of whether protecting a structure against flooding by elevating it above flood levels increases its potential of wind damage. In this case, elevating a structure does reduce the shielding effects of vegetation and other buildings. However, the ANSI Standard and the building codes all treat wind loadings as the same up to a height of 30 feet, so a building properly constructed to withstand wind forces should generally do so whether it is on the ground or elevated above flood levels.

The model codes address this coordination issue every year during their annual code change process, when staff members review every change to avoid such conflicts. However, this is not the most effective way to address this problem, since each code may ultimately solve the problem in a different manner. It would be more effective to address this problem during the development of these individual standards.

FEMA has also attempted to deal with this issue in two ways. With regard to the *NEHRP Recommended Provisions*, this was avoided by using a consensus process, which incorporates such a review. Since the flood design standards of the NFIP are not consensus-backed, FEMA recently had a "Code Compatibility Report" prepared. This review also looked at other natural hazards as they relate to flood, and resulted in a series of recommendations that now need to be resolved.

3. CODES AND NON-ENGINEERED BUILDINGS

A second reason why the mitigation of natural hazards on the built environment has not been completely effective is the building codes themselves and how they are used. Model building codes usually need to be general enough to be relevant to all types of construction. It is for this reason that they are normally performance-based in nature, meaning that they specify how a building should perform as opposed to how they should be built. This generally works well with an engineered building, where the engineer can translate the performance requirements into construction requirements, or plans. The problem is with marginally- or non-engineered buildings, where that interpretation is usually left up to the builder or contractor. The success of that building in resisting the forces generated by the different natural hazards then becomes dependent upon their level of expertise and attention to detail. As shown by several recent disasters, such as the Northridge earthquake and Hurricane Andrew, this is where the process often breaks down.

It is for this reason that several reports prepared after Hurricanes Hugo and Andrew recommended that the local building code examine the possibility of including prescriptive design details within their code where possible. For example, this was particularly relevant after Hurricane Andrew with regard to the design of residential gable roof systems, where it was recommended that the South Florida Building Code require the use of blocking and/or bracing so that the roof trusses would be capable of withstanding horizontal wind loads independent of roof sheathing.

It is this need for prescriptive language that various standards groups are trying to address with what have been referred to as "deemed to comply" standards. One example of such a standard is the "Standard for Hurricane Resistant Residential Construction" (SSTD 10-93), developed by the Southern Building Code Congress International.

The biggest percentage of non-engineered buildings are residential structures, and it is this class of building that has been responsible for a disproportionate amount of the losses FEMA has had to handle in the most recent natural disasters. It is for this reason that FEMA has begun to target residential dwellings and the home building industry. This problem was never more apparent than in Hurricane Andrew, where virtually every home in the 300 square mile impacted area suffered some degree of damage. However, even in events where conditions have been well below the design criteria, this class of building has often still suffered significant amounts of damage, especially when construction techniques have been shown to be less than adequate. What is particularly important from FEMA's point of view is that, given the sheer numbers of this type of building, even minor damage represents a significant loss potential that needs to be addressed by all levels of government if we are going to even begin to control the cost of disasters.

However, FEMA has also observed that this does not have to be the case. In every natural disaster we have investigated, there have been examples of residential structures that have successfully resisted design conditions with little significant damage. The residents of these buildings suffered little loss to their homes or possessions, and they were able to quickly reoccupy their dwellings. The difference was that in these cases, the builder not only properly followed the local code, but also took the steps needed to ensure that the critical connections

worked to allow the home to withstand these loads.

While it is important that home construction remain affordable, it is equally important that it follow the current codes and be capable of surviving a moderate hurricane or earthquake. It seems to us that the home building industry would rather have homes that are still standing shown on the evening news as opposed to what we all saw after Hurricane Andrew.

4. GUIDANCE FOR NON-ENGINEERED BUILDINGS

To address the need for technical guidance for non-engineered buildings, and to do so using a multi-hazard approach, FEMA has recently undertaken two projects that will be of significant benefit.

The first project addresses residential structures that are exposed to both flood and earthquake hazards. As described above, to mitigate against flood hazards, FEMA has developed a series of flood resistant design criteria, one of which requires that all new construction as well as all existing structures that have been substantially damaged or improved, be elevated above anticipated flood levels. In a seismic area, such an elevating foundation can increase seismic loads on the entire structure.

To resolve the problem of how to elevate a flood-prone building in a manner that still complies with current seismic building codes, FEMA has contracted for the development of a guidance document that will present basic designs for a series of sample building foundations that can be used to elevate a building above flood levels while being capable of resisting seismic and wind loads. This effort is being performed under FEMA's National Earthquake Technical Assistance Contract (NETAC).

The sample foundation designs provided in this publication will be in compliance with the *NEHRP Recommended Provisions* as well as the seismic requirements of all three of the model building codes. The designs will be for areas of both moderate and high seismicity and will be applicable for different flood conditions. The designs used will be representative of foundations used throughout the country. The publication will introduce the problem of designing for both flood and earthquake resistance and present the foundation designs and supporting background information will be in a manner understandable by the non-engineer, since the target audience is the homeowner and their contractor.

The second project is the development of a series of publications designed to present construction guidance in a manner that can be used by home builders and other non-engineers to mitigate the effects of specific natural hazards for one and two family dwellings. The documents will also include prescriptive building plans based on the state-of-the-art in design that could assist home builders and others in building a non-engineered residential structure that complies with the model codes and is resistant to damage from natural hazards. While each volume will address a specific hazard, related material on other hazards will also be provided.

To date, FEMA has contracted for the development of two documents. The first volume will be the "Home Builder's Guide to Seismic Resistant Construction" and will address earthquake hazards. This volume will supersede the one FEMA manual that already targets the home builder; the "Home Builder's Guide to Earthquake Design" (FEMA-232). That manual was originally published by the Department of Housing and Urban Development (HUD) in 1980 based on data from the San Fernando earthquake and is out of date.

The second volume will be the "Home Builder's Guide to Wind Resistant Construction" and will address high wind hazards. Since high wind areas are normally associated with coastal areas, this second document will also address coastal flood hazards.

The development process of both documents will include a peer review is to ensure that the final

publication contains material that is technically correct and complete. Possible reviewers will include home builders, contractors, engineers, architects, building code officials, materials interest groups, and knowledgeable homeowners. Such an outside review will serve as a "reality check" for the final product.

Both documents will make it very clear that they are not a substitute for using the local building code or working with the local code enforcement office, but instead are meant to be a resource to provide several techniques by which the home builder can meet the local building code in an manner that addresses the risk presented by that particular hazard.

FEMA is very excited about these projects, and believes that they will be of real benefit to both the home builder community and the emergency management community.

5. MULTI-HAZARD COORDINATION

The coordination of efforts between the different hazards will require more than a few guidance documents that take a coordinated look at several different hazards. What is needed is an independent, non-governmental body that is capable of coordinating the present standards writing organizations as well as the various outside interests, such as the architects, engineers, materials interests, contractors and other similar groups.

Such a body must recognize and utilize the existence of existing consensus bodies that now address specific hazards. Examples of these groups include BSSC for seismic, NFPA for fire, and the Wind Engineering Research Council for wind. Such a body would not replace these established groups, but would instead act as a coordinating body. A possible model for this body would be ASCE, which now brings together these various groups in the periodic update of its loads standard, ASCE 7.

In addition to coordinating the efforts of existing consensus bodies, such a body may need to be capable of developing its own material if necessary. If this body is to be capable of developing or revising these standards, then it must itself be a recognized consensus body.

The role of the Federal government in such an undertaking may be to initially fund a study to develop a plan of action. One goal of such a plan would be to identify a coordinating body that could oversee all of these diverse efforts. Once such a body has been identified, the Federal government could then fund the operation of this body to examine and coordinate the improvement of existing building standards, technical resource materials and model code language that address wind, flood and seismic hazards.

6. CONCLUSION

If this country is going to reduce the cost of natural disasters, we will need to improve the way we build our structures, particularly those that do not presently have the benefit of engineering design. Just as there are different hazards that must be addressed when designing a building anywhere in the country, there are different mitigation techniques that can be employed to reduce losses. The key to reducing losses is knowing how, and where, to properly build.

If building practices as they now exist are going to be revised to take into account the different hazards that may be present, this nation will need to coordinate the activities of the existing groups that address these hazards. This will allow us to resolve any incompatibilities and fill in the gaps that exist in the current standards and codes.

Use of Structural Response Data from Small Earthquakes and Aftershocks

by

Erdal Şafak*

ABSTRACT

With some simplifying but reasonable assumptions, the seismic response of a structure to different sized earthquakes can analytically be correlated with the physical parameters of the earthquakes. This correlation allows prediction of the structural response to future earthquakes by scaling the recorded responses from past earthquakes. In this paper, three methods are introduced to predict structural response to large earthquakes by using recorded responses from smaller earthquakes and aftershocks. The accuracy of the methods are tested by applying them to the data from a highway overpass.

KEYWORDS: Earthquakes, vibrations, structural dynamics, seismic response, seismic scaling.

1. INTRODUCTION

Studying the correlation of ground motions from co-located large and small earthquakes has been a popular research subject in seismology. Methods to simulate large earthquakes by summing smaller earthquakes have been developed (e.g., Hartzell, 1978; Mueller, 1985; Wennerberg, 1990). The limitations of such simulations and the constraints of the summation are discussed in Joyner and Boore (1986). Similar simulation techniques can also be developed for structural response. The problem is somewhat simpler for structures, because the structure acts as a narrow-band filter, thereby eliminating the need for matching the entire frequency band in the simulation.

This paper introduces three methods to predict structural response to large earthquakes from the recordings of smaller earthquakes. Although the basic philosophy is the same, the methods are less elaborate than those suggested by the seismologists, so that they can be adopted for practical applications. The first method is the simplest, and uses only the magnitudes of the earthquakes to scale the recorded peak amplitudes from the small earthquakes, whereas the second method uses both magnitudes and the corner frequency of the small earthquakes for scaling. The third method treats small earthquakes as impulsive point sources, and simulates the entire time history of the response for the large earthquake.

The methods are applied to data from a highway overpass in Rio Dell, California (Shakal et al., 1992). The data consist of two sets of recordings from two co-located earthquakes. The first set is from the Cape Mendocino earthquake of magnitude 5.1 occurring on 21 November 1986, and the second set is from the Petrolia earthquake of magnitude 6.4 occurring on 25 April 1992. The epicentral distances

* *Research Structural Engineer, U.S. Geological Survey, 922 National Center, Reston, VA 22029, USA.*

and the depths are 26 km and 18 km, respectively, for the smaller earthquake, and 24 km and 15 km for the larger earthquake. The highway overpass is a two-span, cast-in-place concrete bridge, and is instrumented with 20 acceleration sensors. A schematic of the bridge and the instrumentation, taken from Shakal et al. (1992), is given in Fig. 1.

2. SCALING BY MAGNITUDES

We can write the FAS (Fourier amplitude spectrum) of the response recorded by a sensor in an instrumented structure as a product of a series of filters:

$$A_y(f) = C \cdot A_x(f) \cdot H_p(f) \cdot H_l(f) \cdot H_s(f) \tag{1}$$

where $A_y(f)$ is the FAS of the recorded response component $y(t)$, and $A_x(f)$ is the FAS of the accelerations in the source region, known as the source spectrum. $H_p(f), H_l(f)$, and $H_s(f)$ are the filters representing the effects of the propagation path, local geology, and the structure on the recorded motion, respectively, and C is a constant. The response $y(t)$ can be made to represent displacements, velocities, or accelerations by selecting the filter $H_s(f)$ accordingly. For a specified response component, and linear wave propagation and structural response, the filters $H_p(f)$, $H_l(f)$, $H_s(f)$, and the constant C can all be assumed to be identical for all co-located (i.e., same source zone) earthquakes. Therefore, we can write the following equation for the ratio of the FAS of structural responses from two co-located earthquakes:

$$\frac{A_{yl}(f)}{A_{ys}(f)} = \frac{A_{xl}(f)}{A_{xs}(f)} \tag{2}$$

where the second subscripts l and s denote the larger and the smaller earthquakes, respectively. Equation 2 shows that the ratio of the FAS of the responses from two earthquakes is equal to the ratio of their source spectra. A simple model for the source spectra for accelerations is given by the following equations (Brune, 1970):

$$A_x(f) = M_0 \cdot \frac{(2\pi f)^2}{1 + \left(\frac{f}{f_c}\right)^2} \tag{3}$$

with

$$f_c = 4.9 \times 10^6 \beta_0 \left(\frac{\Delta\sigma}{M_0}\right)^{1/3} \tag{4}$$

where M_0 is the seismic moment (in dyne-cm), f_c is the corner frequency (in Hz), β_0 is the wave velocity in the source region (in km/s), and $\Delta\sigma$ is the average stress drop (in bars) during the rupture. It can be shown from Eq. 2 that for $f > f_c$:

$$A_x(f) \approx (2\pi f_c)^2 M_0 \tag{5}$$

From random vibration theory (e.g., Lin, 1976), the mean-square value σ_y^2 of the response $y(t)$ is equal to the area under the power spectral density, which can be expressed as the square of FAS divided by the effective duration; that is:

$$\sigma_y^2 = \frac{1}{T} \int_0^\infty A_y^2(f)\, df \tag{6}$$

where T denotes the effective duration. The effective duration can be approximated as the inverse of the corner frequency, i.e., $T = 1/f_c$. Using this in Eq. 6, and also Eq. 5 in Eq. 2, we can derive the following equation for the ratio of the large to small earthquake RMS (root-mean-square) response:

$$\frac{\sigma_{yl}}{\sigma_{ys}} = \frac{M_{0l}}{M_{0s}} \cdot \left(\frac{f_{cl}}{f_{cs}}\right)^{2.5} \tag{7}$$

where the second subscripts l and s again denote the larger and the smaller earthquakes, respectively. If we assume that the average stress drops, $\Delta\sigma$, in both earthquakes are approximately equal, we can write from Eq. 4 that

$$\frac{f_{cl}}{f_{cs}} = \left(\frac{M_{0l}}{M_{0s}}\right)^{-1/3} \tag{8}$$

Using this in Eq. 7 gives:

$$\frac{\sigma_{yl}}{\sigma_{ys}} = \left(\frac{M_{0l}}{M_{0s}}\right)^{1/6} \tag{9}$$

Instead of seismic moments, Eq. 9 can be expressed in terms of moment magnitudes, M, by using the definition of Hanks and Kanamori (1979):

$$M \equiv \frac{2}{3}\log_{10} M_0 - 10.7 \tag{10}$$

which gives

$$\frac{M_{0l}}{M_{0s}} = 10^{1.5(M_l - M_s)} \tag{11}$$

Using Eq. 11 in Eq. 9 results in the following equation for the ratio of RMS responses:

$$\frac{\sigma_{yl}}{\sigma_{ys}} = 10^{(M_l - M_s)/4} \tag{12}$$

where M_l and M_s are the moment magnitudes of the large and small earthquakes, respectively. Random vibration theory shows that the peak response can be obtained by multiplying the RMS response with the peak factor, which is calculated from the moments of the power spectral density function of the response (Lin, 1976). For typical structures (e.g., with dominant first mode and first mode frequencies varying from 0.8 to 2.5 Hz) and earthquakes (e.g., with effective durations varying from two to ten seconds) the peak factors do not vary significantly (Şafak, 1988). Considering all the other uncertainties involved, we can assume for practical purposes that the ratio given by Eq. 12 also represents the ratio of peak responses.

To test the accuracy of the scaling relationship, Eq. 12 is applied to the large and small earthquake data from the US101/ Painter Street overpass. It is assumed that the difference of moment magnitudes is equal to the difference of local magnitudes (i.e., $M_l - M_s = 6.4 - 5.1 = 1.3$). Figure 2 shows the comparison of recorded and predicted large earthquake peak accelerations and displacements for the 20 sensors. The match is good for accelerations but not for displacements. The reason for this is that the scaling factor is valid for frequencies above the corner frequency of the smaller earthquake. The displacement response is influenced by the frequencies from zero to the resonant frequency of the structure, whereas the acceleration response is influenced only by the frequencies near the resonant frequency. Therefore, this model is appropriate to estimate peak acceleration response, but not the displacement response, and applicable only to structures whose dominant frequency is above the corner frequency of the smaller earthquake.

3. RECURSIVE FILTERING

The simple method given above cannot be used to scale the whole frequency band. To account for the entire frequency band, we use Eq. 3, rather than Eq. 5, for $A_x(f)$. Using Eq. 3, Eq. 2 becomes:

$$\frac{A_{yl}(f)}{A_{ys}(f)} = \frac{M_{0l}}{M_{0s}} \cdot \frac{1+(f/f_{cs})^2}{1+(f/f_{cl})^2} = R(f) \tag{13}$$

where $R(f)$ is the frequency-domain filter relating the FAS of responses from large and small earthquakes. The shape of $R(f)$ is similar to that of a low-pass filter and can be converted into a discrete-time filter, $R(q)$, of the following form (Şafak, 1994):

$$R(q) = \frac{\beta_0 + \beta_1 q^{-1}}{1 - \alpha q^{-1}} \tag{14}$$

where q^{-1} is the backward time-shift operator, defined as $q^{-j}y(t) = y(t-j\Delta)$ with Δ denoting the sampling interval. The discrete-time filter given by Eq. 14 leads to a recursive equation to calculate the response time histories of the large earthquake:

$$y_l(t) = \alpha y_l(t-\Delta) + \beta_0 y_s(t) + \beta_1 y_s(t-\Delta) \tag{15}$$

The parameters β_0, β_1, and α are calculated from the following equations:

$$\beta_0 = R_M - \alpha(R_M - R_M^{1/3}) \tag{16}$$

$$\beta_1 = -\alpha R_M^{1/3} \tag{17}$$

$$\alpha = 2 - \cos(2\pi f_p \Delta) - \sqrt{[3-\cos(2\pi f_p\Delta)][1-\cos(f_p\Delta)]} \tag{18}$$

$$f_p = \sqrt{2}\frac{R_M^{1/3}}{R_M - R_M^{1/3}}(f_{cs}^2 - f_{cl}^2) - f_{cl}^2 \tag{19}$$

and

$$R_M = \frac{M_{0l}}{M_{0s}} \tag{20}$$

The derivations of Eqs. 14-20 can be found in Şafak (1994). As the above equations show, the filter relating the large and small earthquakes depends on the ratio of seismic moments, the same as in the previous method, but not on the ratio of the corner frequencies. The filter requires the specific values of the corner frequencies because of Eq. 19. Since data from the small earthquake are available, we can easily calculate f_{cs}. Again by assuming an identical average stress drop for large and small earthquakes, we can calculate f_{cl} from Eq. 8, and also use moment magnitudes instead of seismic moments by utilizing Eq. 11. Thus, by knowing the moment magnitude and the corner frequency of the small earthquake, and specifying the moment magnitude of the large earthquake, we can determine the filter to predict the response for the large earthquake.

To give an example, the acceleration and displacement time histories for each sensor in the US101/Painter Street overpass are simulated for the magnitude 6.4 earthquake from the records of the magnitude 5.1 earthquake by using Eq. 15. The corner frequency of the small earthquake used in the calculations is $f_{cs} = 0.5$ Hz. Figure 3 gives the comparison of the peak values of the simulated and recorded accelerations and displacements. The comparison is good, particularly for the peak displacements.

A key element of this and the previous method is the assumption that the large and small earthquakes have identical average stress drop. When this assumption is removed, one needs to specify not only the magnitude, but also the corner frequency of the large earthquake in order to make

a prediction of the resulting structural response.

4. ORTHONORMAL EXPANSION

A more accurate simulation of large earthquake motions can be done by using the small earthquake motions as Green's functions. The rupture process for the large earthquakes can be assumed as the sum of smaller ruptures, each of which generates a scaled version of the smaller earthquake. With this assumption, we can write a record from the large earthquake as the sum of scaled and time-shifted finite number of records, each of which is identical to the record from the small earthquake. That is:

$$y_l(t) = \sum_{k=0}^{p-1} r_k y_s(t - \tau_k) \qquad (21)$$

where r_k is the constant scaling factor and τ_k is the delay time (where $\tau_0 = 0$) for the kth small earthquake in the sum, and p is the number of small earthquakes required to match the large earthquake. Since r_k, τ_k, and p are initially unknown, we can use a more generalized form of Eq. 21 and assume that:

$$y_l(t) = \sum_{i=0}^{m} a_i y_s(t - i\Delta) \qquad (22)$$

where m is a large number such that $m\Delta >> \tau_{p-1}$. If Eq. 21 is valid, we would then find in Eq. 22 that $a_i = 0$ for all $i \neq \tau_k/\Delta$, and $a_i = r_k$ for all $i = \tau_k/\Delta$. The sequence a_i is called the impulse-response or the source function. By taking the Fourier transform of Eq. 22, we find that

$$F_{y_l}(f) = F_a(f) \cdot F_{y_s}(f) \qquad (23)$$

where F denotes the complex Fourier transform. If both the large and small earthquake records are available, we first determine $F_a(f)$ from Eq. 23 by taking the ratio of the Fourier transforms of the records, and then determine a_i by taking the inverse Fourier transform of $F_a(f)$. For discrete-time data, the maximum number of a_i coefficients would be determined by the length of the records.

The Fourier transform method of calculating a_i coefficients involves taking the ratio of the Fourier transforms of two noisy records, and therefore is not very robust. When signal to noise ratio is low, this approach can lead to erroneous estimation of a_i coefficients. An alternative would be to use the time domain MA (Moving-Average) time series methods. However, these methods are also not appropriate because the number of a_i terms required to have a good match is usually too large (e.g., $i > 100$). For such high orders, the MA methods do not work because of the accumulation of numerical round-off errors.

A more robust method of obtaining the a_i's can be developed by generating a set of m orthonormal time series $\phi_i(t)$ from $y_s(t)$ by using the following transformation (Şafak, 1994):

$$\phi_i(t) = \sum_{j=0}^{m-1} b_{ij} y_s(t - j\Delta) \qquad (24)$$

where b_{ij} is the $m \times m$ transformation matrix. The transformation matrix is determined from the condition that the $\phi_i(t)$'s form an orthonormal set; that is:

$$\sum_{t=1}^{n_s+m-1} \phi_i(t)\phi_j(t) = \delta_{ij} \qquad (25)$$

where $i, j = 0, \cdots, (m-1)$; $t = 1, \cdots, (n_s + m - 1)$; n_s is the number of points in y_s; and δ_{ij} is the Kronecker delta. The coefficients b_{ij} can be calculated from Eq. 25 by utilizing the singular value decomposition technique, and the orthonormal series $\phi_i(t)$ are calculated from Eq. 24. Once $\phi_i(t)$ are determined, the series $y_l(t)$ can easily be expanded into its orthonormal components by using the equation

$$y_l(t) = \sum_{j=0}^{m-1} c_j \phi_j(t) \qquad (26)$$

where the coefficients c_j are calculated from

$$c_j = \sum_{t=1}^{n_s+m-1} \phi_j(t) y_s(t) \qquad (27)$$

The sequence $c_j \phi_j(t)$ in Eq. 26 represents the contribution to the large earthquake from the jth orthonormal mode. It can be shown by using Eqs. 22 and 26 that the coefficients a_i are related to the coefficients b_{ij} and c_j by the following equation (Şafak, 1994):

$$a_i = \sum_{j=0}^{m-1} b_{ji} c_j \qquad (28)$$

To give an example, we consider the displacements recorded by the three orthogonal sensors (channels 12, 13, and 14) at the free field site near the east abutment of the overpass during the two earthquakes. For each orthogonal direction, $m = 100$ orthonormal displacement time series from the displacements of the small earthquake are generated by utilizing the singular value decomposition technique. The displacements of the large earthquake and the impulse-response coefficients (source functions, a_i) are calculated from Eqs. 26, 27, and 28. Contributions from the three most significant orthonormal modes to the free field displacements are given in Fig. 4 for the longitudinal, transverse, and vertical directions. The source functions for the same directions are given in Fig. 5.

For linear wave propagation and structural response, the source functions for a specified response direction should be similar for all sensors in that direction, irrespective of their location. This suggests that if the source function for a reference location is known, it can then be used to predict the response in another location where we only have the small earthquake record. To test this, we use the displacements from the small earthquake and the source functions calculated from the free-field site, to calculate the displacement response to the large earthquake for three sensors, namely: (1) the longitudinal sensor at the deck at the east abutment (channel 11), (2) the transverse sensor at the girder of the center bent (channel 7), and (3) the vertical sensor at the deck at the center of the west span (channel 6). The comparison of the calculated and the recorded displacements are shown in Fig. 6. The comparison gives a good match.

A practical application of this method would be to predict the response of a structure to the mainshock by recording its response (using portable instruments) during aftershocks. The same aftershocks should also be recorded at the nearby permanent ground stations which recorded the mainshock. To estimate the structure's response to the main shock, we first calculate the source function by using the mainshock and the aftershock data from

the ground station, then convolve it with the aftershock recordings from the structure.

4. CONCLUSIONS

Recordings of structural response from small earthquakes and aftershocks can be used to predict the response to larger earthquakes of the future. Simple scaling laws for the structural response can be developed by using the analytical models of the seismic source spectrum, and assuming constant stress drop and linear behavior. Two such methods introduced here give satisfactory results when applied to recorded data. The records from a large earthquake can be expanded into orthonormal series that are generated by transforming the records from a smaller earthquake. This expansion permits the prediction of the response to the large earthquake (or the mainshock) by using recordings from the small earthquake (or the aftershocks).

5. REFERENCES

1. Brune, J.N. (1970). Tectonic stress and the spectra of seismic shear waves from earthquakes, *J. Geophys. Res.*, 75, 4997-5009.
2. Joyner, W.J. and D.M. Boore (1986). On simulating large earthquakes by Green's-function addition of smaller earthquakes, *Earthquake Source Mechanics*, Geophysical Monograph 37 (Das, et al., Eds.), American Geophysical Union, Washington, D.C., 269-274.
3. Hanks, T.C. and H. Kanamori (1979). A moment magnitude scale, *J. Geophys. Res.*, 84, 2348-2350.
4. Hartzel, S.N. (1978). Earthquake aftershocks as Green's functions, *Geophys. Res. Letters*, 5, 1-4.
5. Lin, Y.K. (1976). *Probabilistic Theory of Structural Dynamics*, Robert E. Krieger Pub. Co., Huntington, New York.
6. Mueller, C.S. (1985). Source pulse enhancement by deconvolution of an empirical Green's function, *Geophys. Res. Letters*, 12, 33-36.
7. Şafak, E. (1988). Analytical approach to calculation of response spectra from seismological models of ground motion, *Earthq. Eng. & Struc. Dyn.*, 16, 121-134.
8. Şafak, E. (1994). Scaling of seismic structural response, *Journal of Structural Engineering*, ASCE, submitted for publication.
9. Shakal, A. et al. (1992). CSMIP strong-motion records from the Petrolia, California earthquakes of April 25-26, 1992, *Report No. OSMS 92-05*, California Department of Conservation, Division of Mines and Geology, Sacramento, California.
10. Wennerberg, L. (1990). Stochastic summation of empirical Green's functions, *Bull. Seism. Soc. Am.*, 80, 1418-1432.

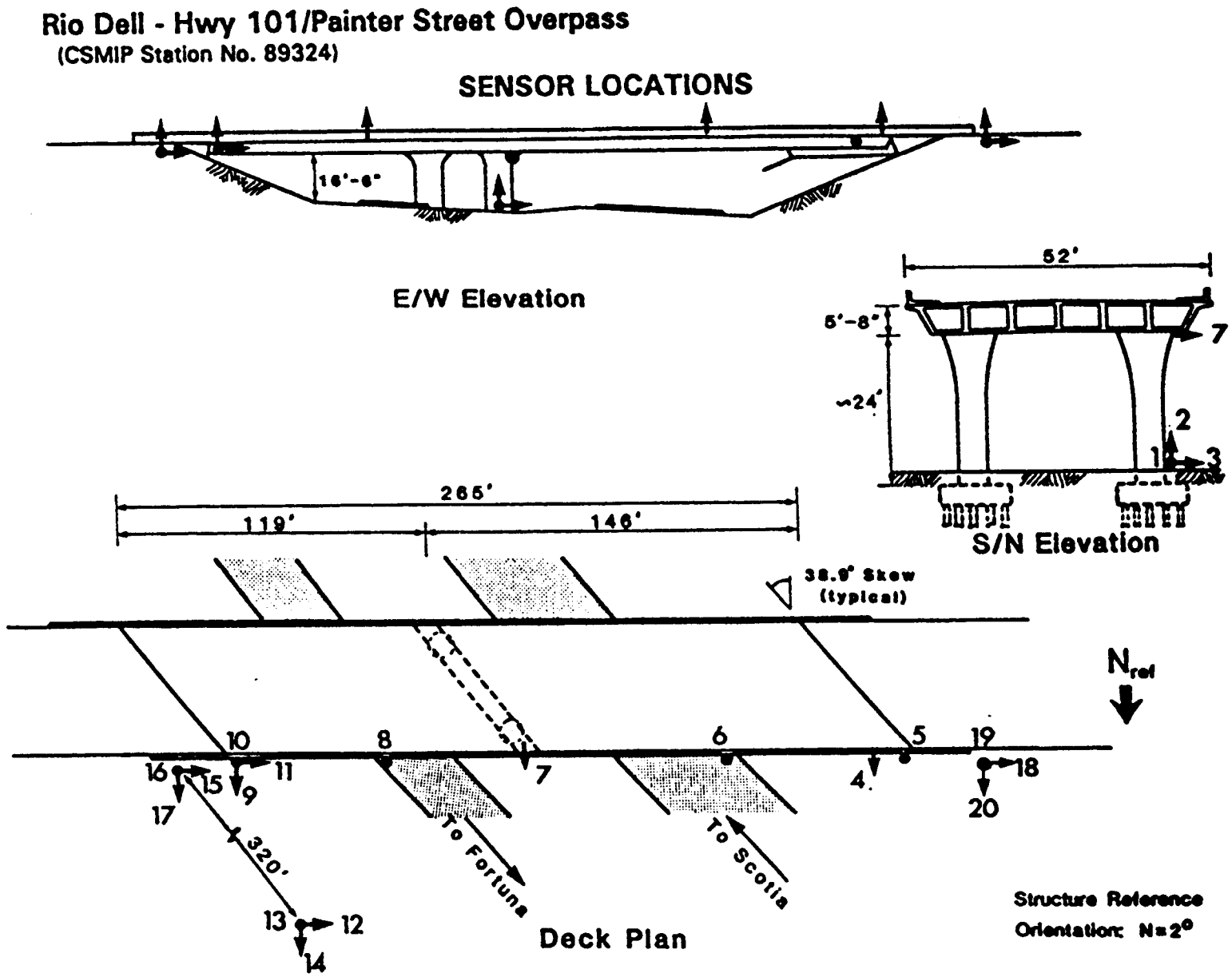

Figure 1. Elevation and plan views, and the instrumentation of the highway overpass in Rio Dell, California (from Shakal et al., 1992).

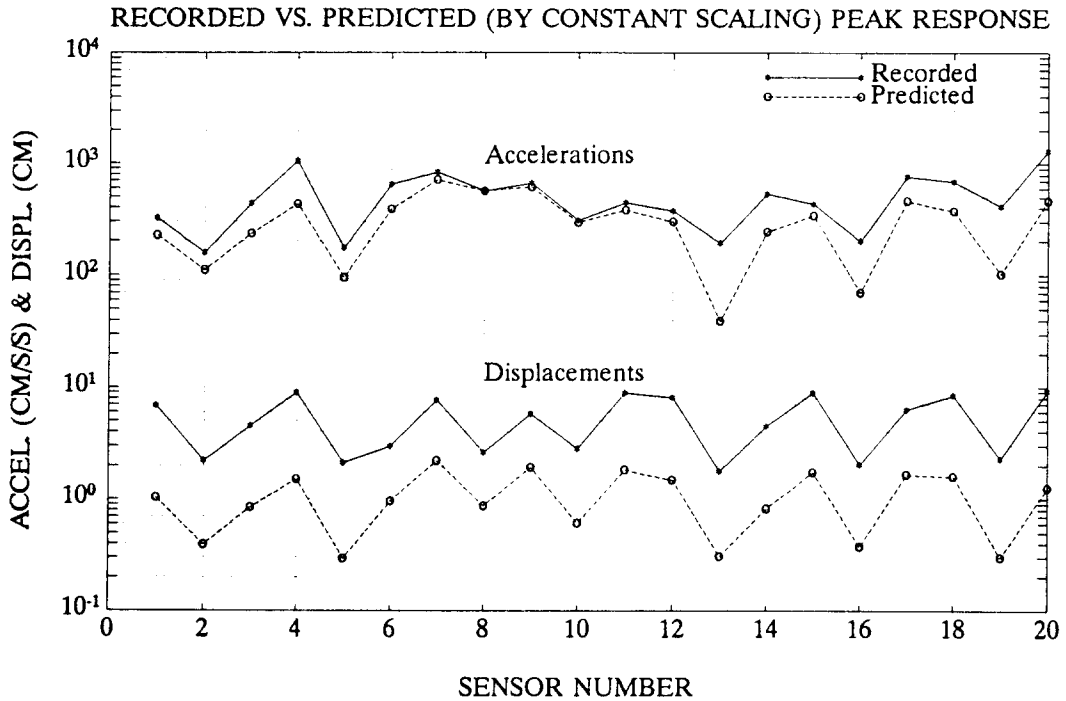

Figure 2. Comparison of recorded and predicted (by using constant scaling) peak accelerations and displacements for all channels.

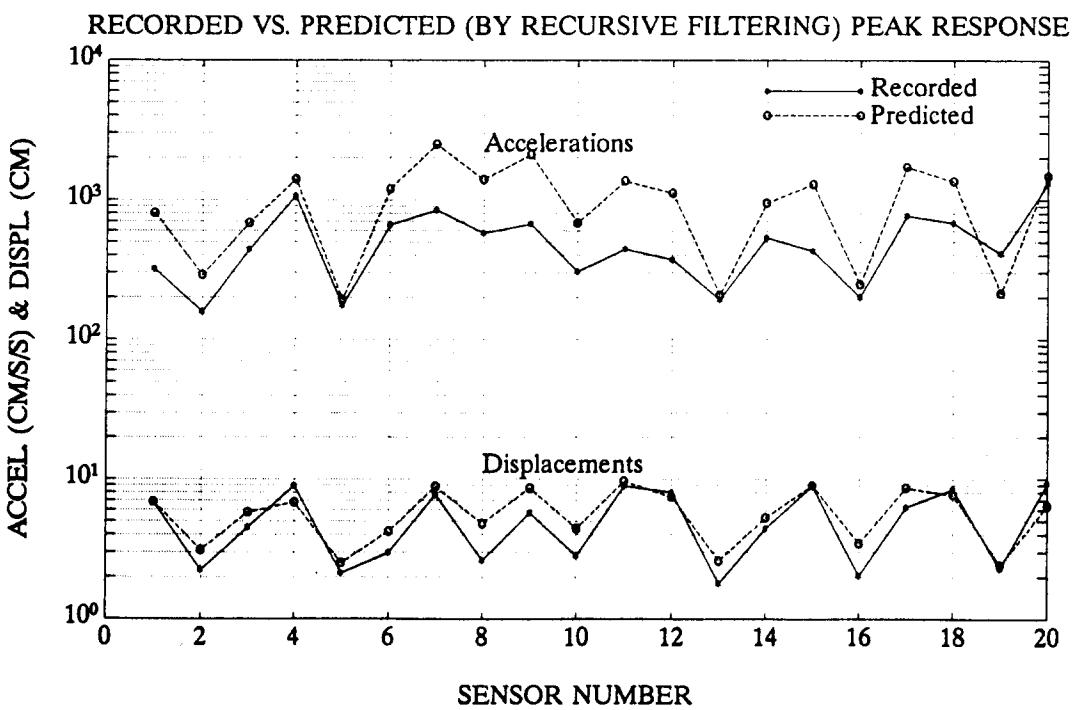

Figure 3. Comparison of recorded and predicted (by using recursive filtering) peak accelerations and displacements for all channels.

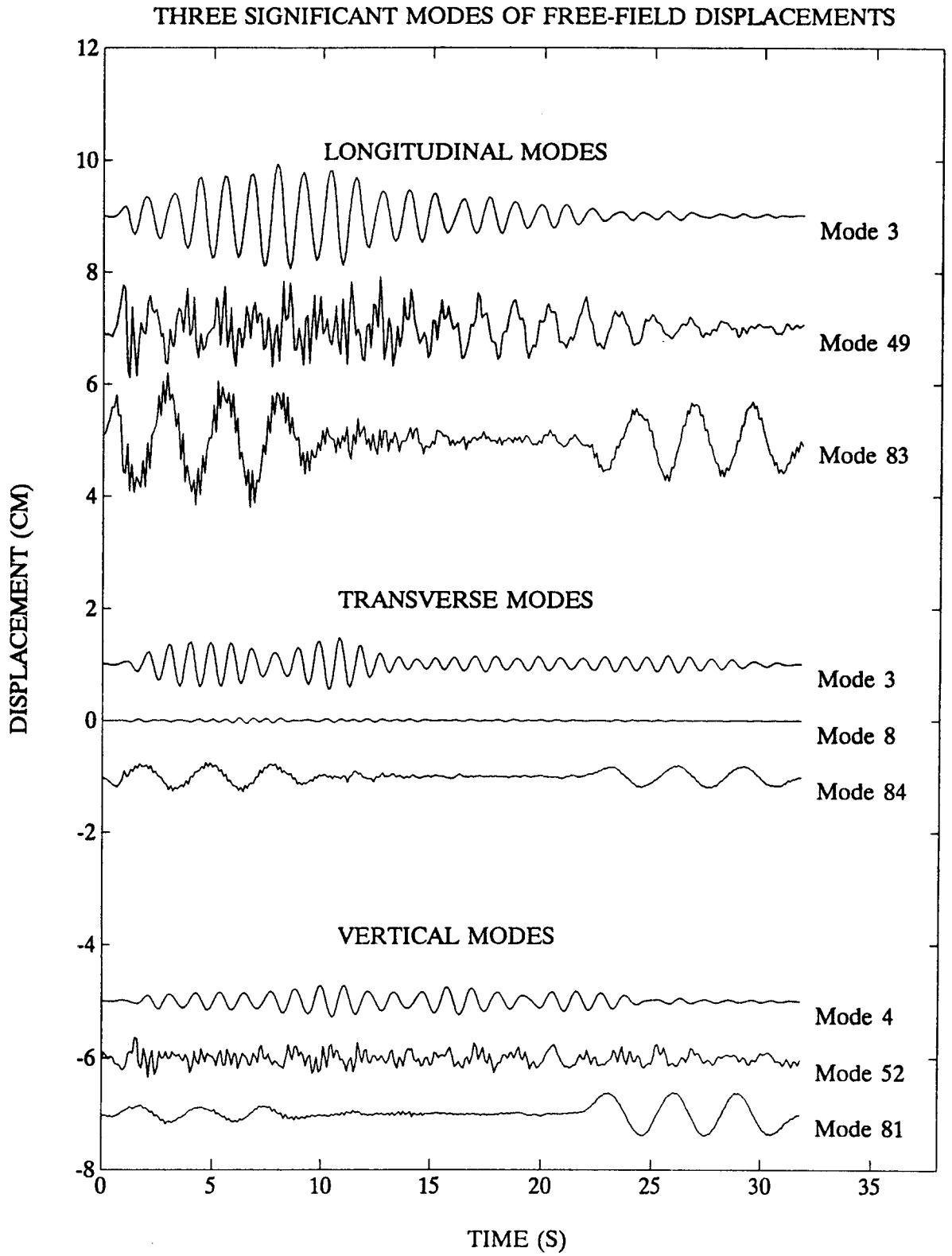

Figure 4. Contributions from the three most significant orthonormal modes to the free field displacements in the longitudinal, transverse, and vertical directions.

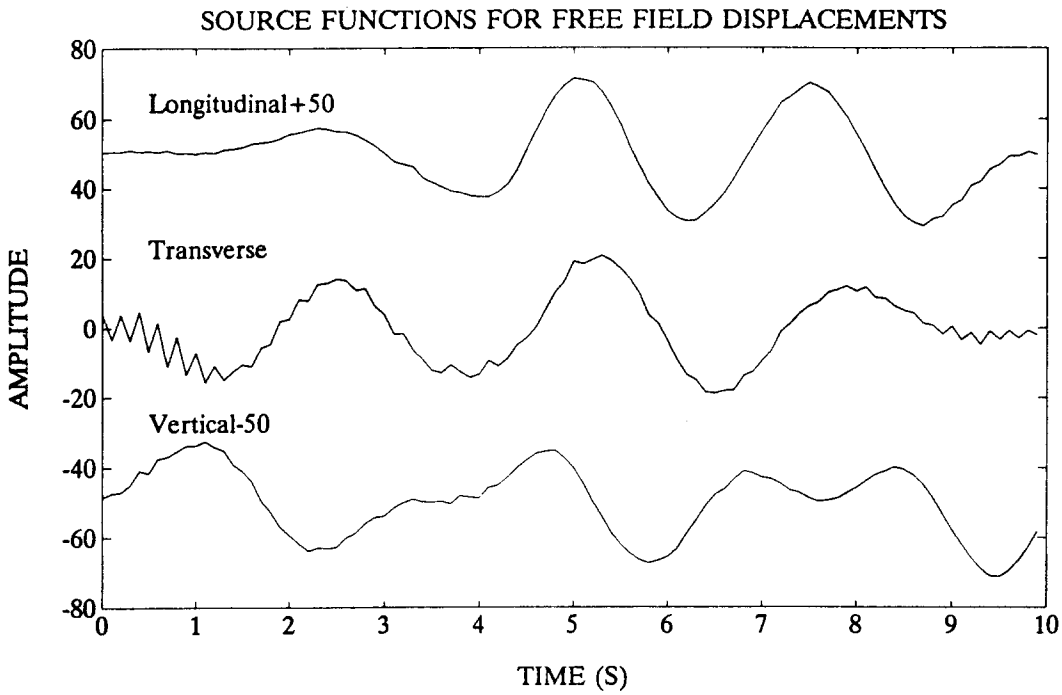

Figure 5. Source functions for the free-field displacements in the longitudinal, transverse, and vertical directions.

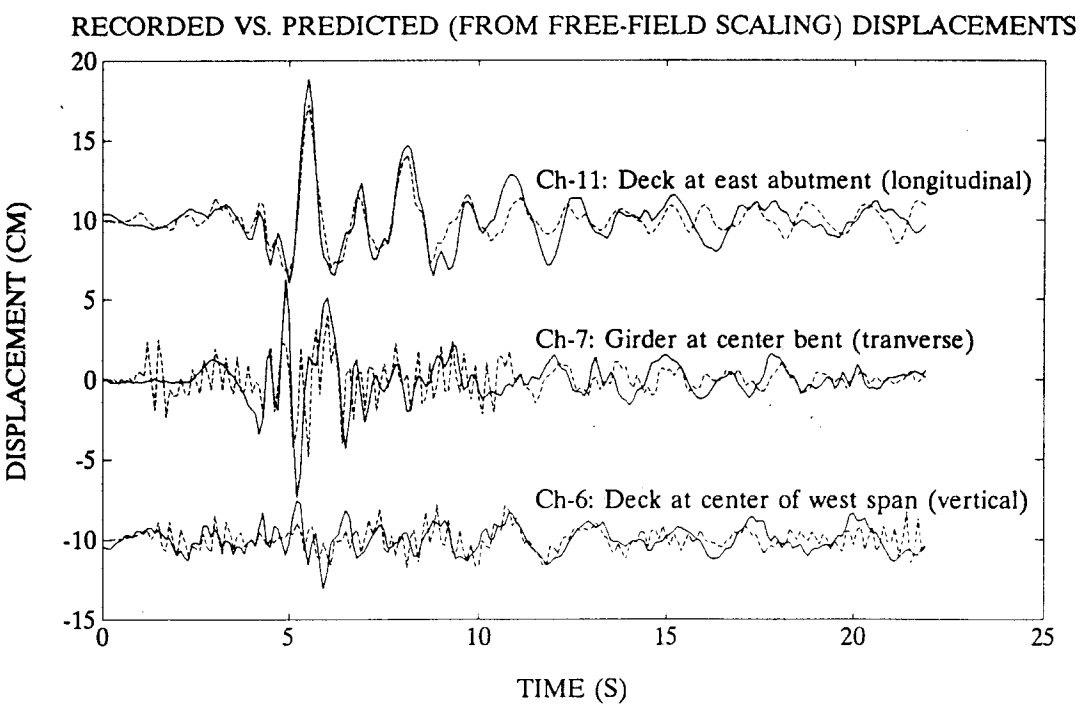

Figure 6. Comparison of recorded and predicted displacements at three sensors in the structure.

Three Recent Tsunamis—Warning System Response

by

Michael E. Blackford*

ABSTRACT

Three recent earthquakes, located in the Pacific basin, that generated tsunamis are selected to represent the response of the United States tsunami warning systems. The earthquakes selected are the northern California earthquake of April 25, 1992, the Nicaraguan earthquake of September 2, 1992, and the Guam earthquake of August 8, 1993. The Nicaraguan earthquake is the only earthquake of the three that resulted in significant destruction and loss of life. All three earthquakes, however, did generate tsunamis that were recorded in Hawaii, remote from the sources. Two of the earthquakes occurred during regular office hours of the warning systems and one was reported to a warning center by phone within six minutes of initial shock. Timing of message dissemination from the warning centers was controlled mainly by earthquake magnitude determination. This delay can become quite long for source areas at some distance from the warning centers, rendering them ineffective as regional warning centers. Additional warning centers are needed in many areas of the Pacific, especially for the coastal areas of Central America and the islands of the western Pacific.

KEY WORDS: body wave magnitude; directed tsunami wave; surface wave magnitude; tsunami warning response

1. INTRODUCTION

Three earthquakes that occurred within the last few years in the Pacific basin are selected as examples of the response of the United States tsunami warning centers to situations that have the potential of generating destructive tsunamis. Only one of the three, the earthquake in Nicaragua, actually resulted in loss of life and significant property damage as a result of a tsunami. Other recent earthquakes such as Indonesian earthquake of December, 1992 and the Japan Sea earthquake of July, 1993, although causing considerable loss of life and property damage, occurred in marginal basins of the Pacific or Indian Oceans and did not generate tsunamis that traversed a significant portion of the main Pacific basin. This paper shall take the reader through a time history of the actions taken by the centers from the onset of the earthquake through the termination of their activities related to the event.

There are two warning centers in the United States. The Pacific Tsunami Warning Center, located in Hawaii, acts as a regional warning center for the Hawaiian Islands and as the operational center for the Tsunami Warning Center for the Pacific. The Alaska Tsunami Warning Center, located in Palmer, Alaska, acts as a regional warning center for the northeastern Pacific from the western end of the Aleutian Islands to the border between the United States and Mexico.

One of the earthquakes selected occurred within the Alaska Tsunami Warning Center's region. The other two earthquakes occurred in areas without regional warning centers.

2. EARTHQUAKE OF APRIL 25,1992 IN NORTHERN CALIFORNIA

At 8:06 A.M. Hawaii Standard Time (HST) (18:06:04.2Z) an earthquake (MS 7.1) occurred off the coast near Cape Mendocino in northern California. About one minute later the seismic waves reached Arnold Ranch seismic station near San Francisco and about eighty seconds

*NWS/Pacific Tsunami Warning Center, Ewa Beach, Hawaii 96706

after that the waves reached the seismic station at Palomar Observatory in southern California. The signals from these stations, which are relayed to the Pacific Tsunami Warning Center (PTWC), through the National Earthquake Information Center (NEIC) in real time, were noticed by the geophysicists. They began to take readings of the P-wave arrival times at these stations and at other United States mainland and Alaska seismic stations that are relayed to PTWC. At about 8:13 A.M. a final reading was taken from the local instrument at PTWC.

The P-wave arrival times were entered into the computer and an initial location for the earthquake was determined. The estimated arrival times for data to determine the magnitude of the earthquake were 8:19 A.M. for the S-wave data used to determine the body wave magnitude, mb, and 8:22 A.M. for the Rayleigh wave data used to determine the surface wave magnitude, Ms. The initial solution had a relatively large r.m.s. time error indicating a potential reading error. The arrival time at the Newport, Washington seismic station had indeed been misread and, when it was corrected, the solution time residual fell to an acceptable level. The final location of the epicenter was 40.4N and 124.1W. This compares favorably with the NEIC solution of 40.4N and 124.3W, however the NEIC solution is much closer to the coastline.

At 8:16 A.M. the Alaska Tsunami Warning Center (ATWC), regional warning center for this area, issued an information message for the earthquake, giving it a magnitude of 7.0 based on the P-wave amplitudes. ATWC did not issue a warning, however it did indicate that some local tsunami wave action may occur.

The body wave magnitude was determined to be 6.8 shortly after the S-wave was recorded at PTWC. A few minutes later, at 8:26, a surface wave magnitude of 7.0 was determined. Twenty minutes had elapsed since the earthquake occurred. PTWC issued an information message indicating that no Pacific-wide tsunami was expected and reported its surface wave magnitude.

Indeed local tsunami action did occur with a maximum peak to trough amplitude of 110 centimeters being recorded at Crescent City, California. Amplitudes of twenty centimeters or less were reported at other sites in northern California and southern Oregon. The tsunami was recorded at two sites in Hawaii, with fifteen centimeters reported for Kahului, Maui and ten centimeters for Hilo. There was no reported loss of life and no property damage specifically attributed to the tsunami was reported.

3. EARTHQUAKE OF SEPTEMBER 2, 1992 OFF THE COAST OF NICARAGUA

At 2:16 P.M. HST, September 1 (00:16:01.6Z, September 2) an earthquake was initiated about eighty kilometers off the Pacific coast of Nicaragua. Five minutes later P-waves from the earthquake reached the seismic stations at French Village, Missouri and Blacksburg, Virginia. A little over a minute later the seismic waves had passed the stations at Golden, colorado and Palomar, California. This activity was noted by the PTWC geophysicists and they went into action determining arrival times and locating the earthquake. Initial efforts indicated the earthquake was centered in Honduras, well inland from the Pacific coast. A body wave magnitude of 7.5 and a surface wave magnitude of 6.8 were determined from seismic waves that arrived at PTWC at twenty minutes and thirty-four minutes after the origin time of the earthquake, respectively. Because of a relatively large time residual error for the solution, the location was redetermined and found to be about 250 kilometers south of the original location, placing the earthquake well into the Pacific. Since procedures are based on the surface wave magnitude, however, no further action was taken other than to determine expected tsunami travel times from the new epicenter.

The closest water level station was Baltra in the Galapagos Islands. Travel time to this station was about two hours and twenty minutes. The time to the first transmission after this arrival time was about two hours and forty minutes.

While waiting for this data, reports came from NEIC and from other sources that a significant tsunami had struck the coast of Nicaragua. Concern over whether or not this tsunami would be destructive Pacific-wide were heightened when data from Baltra indicated a peak-to-trough height of 111 centimeters. This concern was lessened somewhat when data arrived from La Libertad, Ecuador a short while later showing only an eighteen centimeter tsunami wave height. The concern was lessened further when data from the Soccoro station was only twenty-eight centimeters peak-to-trough and other, later arriving data indicated smaller amplitudes. Valparaiso, for example, had a maximum amplitude of only ten centimeters. Easter Island, located along the path of the directed tsunami wave that passed by Baltra, had a peak-to-trough amplitude of eighty-three centimeters. The great circle path of this directed wave did not pass near any large population centers so the threat of a destructive Pacific-wide tsunami was essentially eliminated. With regard to Nicaragua, by the time the location and magnitude of the earthquake had been determined, the destructive wave was already on shore. No action by PTWC could have affected the outcome of this event in Nicaragua.

4. EARTHQUAKE OF AUGUST 8, 1993 NEAR GUAM

At 10:40 P.M., August 7 (08:40Z, August 8) the primary watchstander at PTWC received a telephone call from the observer at the U.S. Geological Survey Seismic Observatory in Guam. He reported the occurrence of a severe earthquake that had caused the loss electrical power at the observatory. He did manage to obtain a P-wave time before power was lost. He passed this on to the watchstander who immediately went over to the PTWC office at 10:42 P.M. to begin processing the earthquake.

A check of the NEIC automatic processor showed that the event had not completed enough of its transit across the national seismic network to generate a preliminary solution. The alarm sounded at 10:44 P.M., nearly ten minutes after the origin time of the earthquake. Over the next six or seven minutes data was read from the seismograms and an initial location at 15.0N and 145.3E was determined. Additional data from seismic stations in Asia and the western Aleutians moved the epicenter closer to the north end of the island of Guam. The final location published by NEIC gave the location as 13.0N and 144.8E, about thirty kilometers south, southeast of the southern tip of Guam. The arrival times for the seismic waves that could be used to determine the body wave and surface wave magnitudes were 10:51 P.M. and 11:00 P.M. respectively.

At 10:54 P.M. HST a body wave magnitude of 7.8 was determined from the S-waves recorded on the horizontal long period seismometers. Six minutes later, at 11:00 P.M. HST, a surface wave magnitude of 8.0 was determined from the vertical long period seismometer. Preparations were made to issue a regional warning/watch message because of the size of the earthquake. By this time, however, had there been a destructive local tsunami, it would have already struck. The expected arrival time for Agana, Guam was 08:41Z, nineteen minutes before the magnitude determination.

At 11:08 P.M. HST a regional warning/watch message was issued. Areas within three hours tsunami travel time were placed in warning status and areas within six hours tsunami travel time beyond the warning area were placed in a watch status.

Efforts now turned to determining whether or not a Pacific-wide destructive tsunami had indeed been generated. This earthquake was the largest earthquake ever to have occurred in the Marianas Islands historically. Therefore there was no previous history of tsunamis in this area for earthquakes of this size. A calculation of tsunami travel times indicated that arrival times would 08:41Z at Guam, 09:47Z at Yap, and 09:56Z at Chuuk. Data was not initially available via satellite telemetry from Guam, however, data at Yap and Chuuk indicated maximum peak-to-trough amplitudes of less than fifteen centimeters. These stations are located along a nodal direction with respect to the

azimuth of a directed tsunami wave so additional data from stations more in line with the azimuth of a directed tsunami were sought. The tsunami arrived at Wake Island at 11:30Z and had a maximum amplitude of fifteen centimeters. While awaiting the Wake data, data from the Agana tide gauge was obtained from a secondary source. The maximum amplitude at Agana was eighteen centimeters peak-to-trough. This information was sufficient to cancel the warning/watch at 01:45 A.M. HST (11:45Z), two hours and thirty-seven minutes after the warning/watch was initiated.

Following the cancellation, reports of tsunami amplitudes of up to ninety-eight centimeters were reported for sites in central Japan and in the Bonin Islands. Since there was typhoon activity in the northwestern Pacific, it is not clear whether these wave heights are totally attributed to the tsunami or are a combination of the tsunami and storm surge associated with the typhoons. The tsunami was recorded on several tide gauges in the Hawaiian Islands with a maximum amplitude of nineteen centimeters being observed on the gauge at Port Allen on Kauai Island.

5. CONCLUSIONS

The response time of the United States warning centers is barely adequate for regional events and is inadequate for events in more remote areas of the Pacific where regional warning centers do not exist. The centers can effectively track the progress of tsunamis across the Pacific and can provide satisfactory warning of tsunami hazard to areas beyond a few hours tsunami travel time from the source. Areas within an hour tsunami travel time require a regional system for warning. Ongoing education of coastal inhabitants of areas subject to tsunami hazard on procedures to take at the time of large local earthquakes is an important adjunct to a regional warning system.

Hurricane Storm Surge Analysis for the Coast of Delaware

by

David J. Mark[1], Norman W. Scheffner[2] and Keith D. Watson[3]

Abstract

Coastal structures are designed to provide protection against various forces of nature acting in the coastal zone. Structures such as seawalls are expected to provide onshore protection from the effects of storm surge. However, the degree of protection is usually limited by the economics of constructing for a specified storm surge elevation. This elevation is determined from a frequency-of-occurrence analysis of historical events. When adequate storm surge data are not available, statistical methods are used in generating reliable stage-frequency relationships. This paper describes the development of a database of storm surge elevations and the application of the Empirical Simulation Technique used in developing stage-frequency relationships for the coast of Delaware.

Keywords: Delaware; empirical simulation technique; hurricane; numerical model; stage-frequency; storm surge.

1. INTRODUCTION

The U.S. Army Engineer District, Philadelphia is presently developing a storm damage reduction and shoreline protection program for the open coast of Delaware (Figure 1). Accurate stage-frequency relationships and storm surge time-histories are required for estimating long-term shoreline erosion. Because of the infrequent occurrence of hurricanes at a given site, and therefore lack of historical data, a standard ranking method could not be used in a stage-frequency analysis; thus, statistical procedures were applied in this analysis.

Traditionally, a joint probability method (JPM) is employed in synthesizing storm events subsequently used in hurricane stage-frequency analyses. However, the JPM usually assumes that all hurricane parameters, such as central pressure deficit and maximum wind speed, are independent, ignoring the interdependence of storm parameters. Consequently, unrealistic hurricanes are created by arbitrarily combining parameter values. For example, one parameter can be assigned a value typical of a weak storm, whereas a second is assigned a value representative of an intense storm. Thus, a level of uncertainty is incorporated into the stage-frequency computations.

An alternative approach to the JPM is the empirical simulation technique (EST) which preserves the interdependence of hurricane parameters. The EST is a statistical resampling procedure which uses historical data to develop joint probability relationships among the various measured storm parameters. The resampling scheme generates large populations of data which are statically similar to a much smaller database of historical events. Using this expanded data set, the EST generates a database of peak storm surge elevations by simulating multiple year periods (e.g., 200-yr periods) of storm activity a multiple number of times (e.g., 100 simulations). Stage-frequency relationships are then generated using the database of peak storm surge elevations.

---

[1]Research Hydraulic Engineer, [2]Senior Research Hydraulic Engineer, US Army Engineer Waterways Experiment Station, 3909 Halls Ferry Road, Vicksburg, MS 39180-6199; [3]Hydraulic Engineer, US Army Engineer District, Philadelphia, Wanamaker Bldg., 100 Penn Square East, Philadelphia, PA 19107-3390.

This technique does not rely on assumed parametric relationships but uses the joint probability relationships inherent in a database of storm parameters. In this approach, probabilities are site specific, do not depend on fixed parametric relationships, and do not assume parameter independence. Thus, the EST is "distribution free" and nonparametric. The only assumption made is that future events will be statistically similar in magnitude and frequency to past events.

This paper describes the process used in developing the hurricane-induced stage-frequency analysis for the coast of Delaware. Their development consists of three interrelated tasks, each employing a numerical model. In the first task, historical hurricanes impacting the study area were analyzed to determine storm statistics and correlations. From these data, a reduced set of hurricanes, representative of all storms impacting the area, were chosen and subsequently simulated with a tropical wind field model to generate wind and atmospheric pressure fields.

In the second task, storm surge events developed with the wind model output were simulated using a long-wave, finite element-based hydrodynamic model to obtain peak storm surge elevations. With the hurricane parameters serving as input to the wind field model together with the corresponding storm surge elevations predicted by the storm surge model, the EST is employed in developing frequency-of-occurrence relationships in the third task. A description of the EST and the methodology used in performing these tasks is presented in the following sections.

2. Description of Empirical Simulation Technique

The EST is a statistical resampling technique which uses historical data to develop joint probability relationships among the various measured storm parameters. For this study, the EST was developed to generate numerous multi-year intervals of possible future hurricane events for the coast of Delaware. The ensemble of modeled or simulated events are consistent with the statistics and correlations of past storm activity at a site. Furthermore, the EST permits random deviations in storm behavior (when compared to historic events) that could occur in the future. For example, simulated hurricanes are permitted to make landfall at locations other than those made by the historical storms. These random deviations can also result in more intense storms than the historical events themselves, allowing for the possibility of a future hurricane being the storm of record.

The simulation approach requires specifying a set of parameters which describe the dynamics of some physical system, such as hurricanes. These parameters must be descriptive of both the process being modeled and the effects of that process. In the case of tropical storms, pertinent input vectors include: 1) the central pressure deficit; 2) the radius to maximum winds; 3) maximum wind speeds; 4) minimum distance from the eye of the storm to the location of interest; 5) forward speed of the eye; and 6) tidal phase during the event. These values are defined for each specific location corresponding to each particular historical or hypothetical event of the total set of storm events used in the study.

The second class of vectors involve some selected response resulting from the input-vector parameterized storm. For this study, the maximum total water surface elevation, reflecting the combined tide plus storm surge, is the response vector of interest. Although response vectors are related to input vectors, the interrelationship is highly nonlinear and involves correlation relationships which can not be directly defined, i.e., a non-parametric relationship. For example, in addition to the storm input parameters, storm surge is a function of local bathymetry, shoreline slope and exposure, ocean currents, temperature, etc. as well as their spatial and temporal gradients. It is assumed, however, that these combined effects are reflected by the response vector.

From the entire set of storms, a subset of storms is selected which is representative of all storms that have impacted a particular location. This subset is referred to as the

training set. This set is used as input for appropriate numerical models, such as the hydrodynamic model, for computing the desired response vector(s). The training set usually includes historical events but may include historical storms with slight perturbations. For example, a historical storm with a slightly altered path.

The training set of storms can be augmented with additional storms contained in the historical data set. Storm events augmenting the training set are referred to as the "statistical set" of storms. Whereas numerical models are used for generating response vectors for events residing in the training set, response vectors for the statistical set of storms are interpolated using the training set response vectors. Thus, stage-frequency relationships can be generated using the entire historical data set without need of simulating all storms in that data set.

With the augmented storm data set (i.e., training and statistical storm sets), the EST produces N simulations of a T-year sequence of events (hurricanes), each with their associated input vectors and response vectors. Because there are N-repetitions of a T-year sequence of events, an error analysis of the results can be performed with respect to median, worst, least, standard deviations, etc.

The simulation of realistic events is accounted for in the nearest-neighbor interpolation, bootstrap, resampling technique developed by Borgman (Borgman, et al 1992). The basic technique can be described in two dimensions as follows. Let X_1, X_2, X_3, ..., X_n be n independent, identically distributed random vectors (storm events), each having two responses $[\mathbf{X}_i = \{\underline{x}_i(1), \underline{x}_i(2)\};\ i=1,n]$.

Each event X_i has a probability p_i as 1/n, therefore, a cumulative probability relationship can be developed in which each storm event is assigned a segment of the total probability of 0.0 to 1.0. If each event has an equal probability, then each event is assigned a segment s_j such that $s_j \rightarrow X_j$.

A random number is selected to identify a storm event from the total storm population or augmented storm set. (The procedure is equivalent to drawing and replacing random samples from the total storm event population.)

Using this storm event, the model performs a random walk from the event X_i with x_1 and x_2 response vectors to its nearest neighbor vectors. The walk is based on independent uniform random numbers and has the effect of simulating responses which are not identical to the historical events but are similar to those events which have historically occurred. Thus, the EST is not simply a resampling of historical events technique, but rather an approach intended to simulate the vector distribution contained in the augmented set of storms.

Because the simulated events correspond to a specific location, the criteria that the total number of storm events selected in a T-year simulation must be statistically representative of the number of historical events impacting that location must be satisfied. For this study, 33 hurricane events were identified which impacted the coast of Delaware during the 104 year period extending from 1886 through 1986 (Jarvinen, et al 1988). Given the mean frequency of storm events for a particular region, a Poisson distribution is used to determine the average number of expected events in a given year. For example, the Poisson distribution can be written in the following form:

$$Pr(s;\lambda) = \frac{\lambda^s e^{-\lambda}}{s!} \qquad (1)$$

for s=0,1,2,3,... The probability $Pr(s;\lambda)$ defines the probability of having s events per year where λ is a measure of the historically-based number of events per year. For this study, λ is computed as 0.32 (33/104).

A 10,000 element array is initialized to the above Poisson distribution. The number corresponding to s=0storms per year is 0.7261, thus if a random number selection is less than or equal to 0.7261 on an interval of 0.0 to 1.0, then no hurricanes would occur during that year of simulation. If the random number is

between 0.7261 and 0.7261 +P[N=1] =0.7261 +0.2324 =0.9585, one event is selected. Two events for 0.9585 +0.0372 =0.9957, etc. When one or more storms are indicated for a given year, they are randomly selected using the nearest neighbor interpolation technique described above.

Output of the EST program is N repetitions of T-years of simulated storm event responses. It is from these responses that frequency-of-occurrence relationships are computed. The computational procedure followed is based on generating a probability distribution function (pdf) that corresponds to each of the T-year sequence of simulated data.

Estimates of frequency-of-occurrence begin with the calculation of a pdf for the response vector of interest (e.g., peak storm surge elevation). Let X_1, X_2, X_3, ..., X_n be n independent, identically distributed, random response variables with a cumulative pdf

$$F_X(x) = Pr[X \leq x] \qquad (2)$$

where Pr[ ] represents the probability that the random variable X is less than or equal to some value x and $F_X(x)$ is the cumulative probability density function ranging from 0.0 to 1.0. The problem is to estimate the value of F_X without introducing some parametric relationship for probability. The following procedure is adopted because it makes use of the probability laws defined by the data and does not incorporate any prior assumptions concerning the probability relationship.

Assume that we have a set of n observations of data. The n values of x are first ranked in order of increasing size such that

$$x_{(1)} \leq x_{(2)} \leq x_{(3)} \leq \ldots \leq x_{(n)} \qquad (3)$$

where the parentheses surrounding the subscript indicates that the data have been rank-ordered. The value $x_{(1)}$ is the smallest in the series and $x_{(n)}$ represents the largest. Let r denote the rank of the value $x_{(r)}$ such that rank 1 is the smallest and rank r =n is the largest.

An empirical estimate of $F_X(x_{(r)})$, denoted by $\hat{F}_X(x_{(r)})$, is given by Gumbel (1954) (see also Borgman and Scheffner, 1991 or Scheffner and Borgman 1992).

$$\hat{F}_x(x_{(r)}) = \frac{r}{(n+1)} \qquad (4)$$

for $\{x_{(r)}, r = 1, 2, 3, \ldots, n\}$. This form of estimate allows for future values of x to be less than the smallest observation $x_{(1)}$ with probability of 1/(n+1), and to be larger than the largest value $x_{(n)}$ also with probability 1/(n+1).

This form of the cumulative distribution function allows for values of x to be greater than the maximum or less than the minimum observed values in the historical data base. In implementing the EST, tail functions (Borgman and Scheffner 1991) are used to define the pdf for events larger than the largest or smaller than the smallest observed event so that there is no discontinuity in the pdf.

The cumulative pdf as defined by Equation 4 is used to develop stage-frequency relation-ships in the following manner. Consider that the cumulative probability for an n-year return period storm can be written as:

$$F(n) = 1 - \frac{1}{n} \qquad (5)$$

where F(n) is the cumulative probability of occurrence for an event with a return period of n-years. Frequency-of occurrence relation-ships are obtained by linearly interpolating a stage from Equation 5.

3. Description of Wind and Atmospheric Pressure Field Model

The Planetary Boundary Layer (PBL) wind field numerical model (Cardone et al. 1979) was selected for simulating hurricane-generated wind and atmospheric pressure fields. The model employs the vertically-averaged primitive equations of motion for

predicting wind velocities experienced within a hurricane. The model includes parameterization of the momentum, heat and moisture fluxes together with the surface drag and roughness formulations.

The model requires a series of "snapshots" for input consisting of a set of meteorological parameters defining the storm at various stages in its development or at particular times during its life. These parameters include: latitude and longitude of the storm's eye; track direction and forward speed measured at the eye; radius to maximum winds; central and peripheral atmospheric pressures; and an estimate of the geostrophic wind speed and direction.

Some meteorological storm parameters were obtained from the HURricane DATabase (HURDAT) developed by the National Oceanic and Atmospheric Administration (NOAA) National Hurricane Center (NHC) (Jarvinen, Neumann and Davis 1988). This database summarizes all hurricanes and tropical storms that occurred in the North Atlantic Ocean over the 104-yr period from 1886 through 1989. Information contained in this database includes latitude and longitude of the storm, central pressure, and maximum wind speed.

Radius to maximum winds is approximated using a function that incorporates the maximum wind speed and the atmospheric pressure anomaly (Jelesnianski and Taylor, 1973). Track directions and forward speeds required by the PBL model are approximated hourly, using a cubic spline interpolation technique, from the storm's 6-hr latitudinal and longitudinal positions provided in the HURDAT database. Peripheral atmospheric pressures were assumed equal to 1013 mb. Geostrophic wind speeds were specified as 6 knots, typical conditions within the Gulf of Mexico (Thompson 1993), and have the same direction as the storm track.

Whereas some models employ a fixed grid system to simulate a hurricane (i.e., stationary grid with a moving storm), the PBL model simulates the hurricane as a stationary storm with a moving grid. A hurricane's translational or forward motion is incorporated into model calculations by adding the forward and rotational velocity vector components. Wind velocities and atmospheric pressures are computed at each node in the translating uniform grid.

The model uses a nested gridding technique, composed of five layers or subgrids, for computing the wind fields. Each subgrid measures 21 by 21 nodes in the x- and y-directions, respectively, and the centers of all subgrids are defined at the eye of the hurricane. Although the number of nodes composing each subgrid is the same, the area of coverage and spatial resolution differs for each grid. For this study, the subgrid with the finest resolution had an incremental distance of 5 km between nodes. Incremental distances for the remaining subgrids were 10, 20, 40, and 80 km.

For each snapshot, the equations of motion are first solved using the grid covering the greatest area, which is the grid having an incremental distance of 80 km between nodes. Computed wind velocities are then used as boundary conditions on the second largest grid, and the equations of motion are solved again. This same procedure is followed for the remaining grids where wind fields are computed using sequentially smaller grids together with wind velocities computed with the next larger grid serving as boundary conditions.

After wind and pressure fields have been computed for each 6-hr snapshot, hourly wind and atmospheric pressure fields are interpolated using a non-linear blending algorithm which produces a smooth transition from one snapshot to the next. Hourly wind and pressure fields are then interpolated from the PBL grid onto the hydrodynamic grid and subsequently stored for use by the hydrodynamic model.

4. Description of Storm Surge Model

The ADvanced CIRCulation (ADCIRC) numerical model (Westerink et al. 1992) was

chosen for simulating the long-wave hydrodynamic processes in the study area. This program employs a two-dimensional, depth-integrated finite element solution of the Generalized Wave-Continuity Equation (GWCE). The fundamental components of the GWCE equation are the depth-integrated continuity and Navier-Stokes equations for conservation of mass and momentum. The time-differentiated form of the conservation of mass equation is combined with space-differentiated form of the conservation of momentum equation to develop the GWCE equation.

The GWCE-based solution scheme eliminates several problems associated with finite element programs which solve the primitive forms of the Navier-Stokes equations, including spurious modes of oscillation and artificial damping of the tidal signal. Forcing functions contained in this code include time-varying water surface elevations, wind shear stresses, atmospheric pressure gradients and the Coriolis effect.

The storm surge model was adapted from the East, Gulf and Caribbean Sea hydrodynamic model developed in the USAE Dredging Research Program (DRP). The numerical grid, specified in spherical coordinates, was developed by increasing the resolution of the DRP East Coast grid in the study and surrounding areas. The grid consists of 11,829 nodes and 21,917 elements. Figure 2 presents the numerical grid used in this study and Figure 3 provides a "zoomed-in" picture of the grid along the study area.

Using a grid which incorporates the entire Eastern seaboard provides several benefits. First, extending the seaward boundary beyond the continental shelf enables a linear tidal signal to be specified at the mid-Atlantic open boundary; overtides, generated in shallow water, are implicitly included in the model computations.

Second, the non-linear effects described above must also be addressed for the lateral open-water boundaries, which extend from shore to the ocean's abyssal plain. Typically, lateral boundaries are placed sufficiently far from the study area so that errors in the time-series do not corrupt model-generated results within the area of interest. With the grid extending from Nova Scotia, Canada to Venezuela, this problem is minimized.

Third, the majority of hurricanes affecting the coast of Delaware approach the mainland from the southeast, then veer away to the northeast. As the hurricane enters the model area, the tidal signal along the lateral open-water boundary can be significantly altered by a storm's atmospheric pressure anomaly. Thus, the flow field can be corrupted in much the same manner as described above. As before, this problem can be alleviated by modeling the entire eastern seaboard.

Bathymetry was supplied from the National Center for Atmospheric Research's ETOPO5 data base. These data are stored at a resolution of 5 min latitude by 5 min longitude and depths have the units of meters. Bathymetry in estuarine and nearshore areas were obtained from NOAA nautical charts.

Time-series of astronomical tidal elevations specified at the open water boundary were computed from tidal amplitudes and phases obtained from Schwiderski and Szeto (1981). Modeled constituents include M_2, S_2, N_2, O_1, P_1, K_2, K_1 and Q_1. Constituent data are provided at one degree increments in latitude and longitude. A bilinear interpolation algorithm was used for estimating tidal amplitudes and phases at the 61 grid nodes composing the open water boundary.

5. Tidal Calibration of Hydrodynamic Model

The hydrodynamic model was calibrated by adjusting local bottom friction coefficients so that model-generated water surface level time-series compare favorably to those reconstructed from tidal constituents. Locations at which comparisons were made include: Cape May, NJ; Reedy Point, DE; Lewes, DE; Indian River Bay Inlet, DE; and, Ocean City, MD. Calibration simulations were conducted over a 30-day period beginning at

0:00 Eastern Standard Time on 1 September 1985. A 30-sec time-step was used in these simulations. Comparison of computed and constituent-generated water surface levels for the Lewes gage is presented in Figure 4.

Of the five stations, the greatest difference between computed and constituent-generated water elevation extrema was experienced at Reedy Point where the model overpredicted tidal amplitudes by 11 percent. Differences in extrema for the remaining stations were less than 4 percent. The discrepancy at Reedy Point is attributed to the station's close proximity to the grid boundary; placed downstream of the head-of-tides, the boundary acts as a dam preventing tides propagating upstream/downstream of the station and, consequently, increases tidal amplitudes at the station.

Phase differences between the computed and constituent-generated tidal oscillations ranged from 0.18 to 0.54 hours. Computed tidal oscillations at the Cape May, Lewes, and Reedy Point stations led the constituent-generated oscillations, whereas at Indian River Inlet and Ocean City, the computed tidal oscillations occurred later than the constituent-generated phases. The difference in phases at the Indian River Inlet and Ocean City stations is attributed to the lack of grid resolution defining these areas.

6. Storm Surge Validation of Hydrodynamic Model

Model validation was achieved by performing a storm surge simulation of Hurricane Gloria which impacted the study area in September 1985. The hindcast began on 1 September 1985 at 0000 Greenwich mean time (GMT) and ended on 1 October at 0000 GMT. A 30-sec time-step was used in the simulation and tidal forcing was specified at the open water boundary.

From the beginning of the hindcast simulation to 16 September at 1200 GMT, no wind or atmospheric pressure gradients were specified in the model. This 16-day period provides sufficient simulation time to develop an accurate tidal current field and to dampen any start-up errors. Thereafter, from 16 September at 1200 through the end of the hindcast at 0000 GMT on 1 October, wind and atmospheric pressure fields were supplied to the model at hourly increments. Furthermore, nodal wind and pressure values were linearly interpolated at time-steps falling between whole hours.

Figure 5 presents a comparison of model-generated and measured water surface elevations recorded at Lewes, DE for the period of 25 September at 0000 GMT to 0000 GMT on 30 September. The model predicted a peak water surface elevation of approximately 6.21 ft mean sea level (MSL), whereas the Lewes gaging station measured a peak elevation of 5.99 ft MSL. Thus, the model overpredicted the peak water level by 0.2 ft.

As shown in the figure, the hydrodynamic model predicted the peak storm surge elevation approximately 1 hr later than its measured occurrence. This lag is attributed to the assumption that the hurricane's forward speed was constant during the 6-hr period between "snapshots" or entries contained in the NHC database.

Whereas the model accurately predicted the peak storm surge elevation, model-generated water surface elevations underpredicted the measured data by as much as 1 ft during the 36-hr period prior to the storm's passage. This discrepancy is believed to be due to differences between PBL-generated wind directions and those experienced during the storm; it is believed that the westerly component of the computed winds were greater than those experienced during the storm, forcing greater water volumes into the upper reaches of Delaware Bay while lowering water levels along the lower bay's southwest shoreline (which is where the Lewes gaging station is located).

7. Selection of Hurricanes

Because stage-frequency relationships are

based on a statistical analysis of storm surge elevations resulting from historical storm events, a thorough analysis was performed to define those storms which impacted the study area. As a first step in selecting hurricanes, track positions of all hurricanes in the NHC database were processed to determine those storms which affected the Mid-Atlantic states. Thus, any hurricane that did not track through the "box" extending from latitude 36 00'00" N. longitude 77 00'00" W. to latitude 41 00'00" N. longitude 68 00'00" W. was eliminated from consideration.

Of the 875 hurricanes in the NHC database, only 66 hurricanes passed through this box. After reviewing these 66 hurricanes, an additional 36 hurricanes were eliminated from the storm ensemble. Reasons for eliminating these hurricanes include: some storms only "clipped" the edges of the box and did not come into close proximity with the study area; a few hurricanes were downgraded to severe storm status before entering the box and were thus ignored in the storm surge analysis; and, some storms tracked along the western edge of the box and did not impact the coast of Delaware.

With this set of 30 hurricanes, a set of 15 storms (referred to as the "training set") was selected and simulated using the storm surge model. Hurricanes composing the training set were selected such that the set is representative of the entire set of 30 storms which impacted the study area.

Storm surge elevations generated using these storms can be considered as approximations of the historical events. Although the frequencies associated with their maximum surge may be considered accurate, the value of peak surge may not correspond to historically observed surge elevations. Differences in peak surge are attributed to estimates of the hurricane parameters which are only approximate; all data necessary to simulate each event are not known and have not been calibrated. Therefore, the hydrographs should not be considered as hindcasts of the historical events.

8. Application of Storm Surge Model

All 15 storms in the training set together with an additional 5 hurricanes were simulated with the storm surge model. These extra hurricanes were added to the training set to ensure the accuracy of the response vector population for input to the EST model. Each storm surge simulation was performed independently of tidal action, eliminating the task of extracting surge levels from a time-series of combined tide- and surge-induced water surface levels. A 30-sec time-step was used in each simulation. Time-series of water surface elevations were recorded, at 15-min intervals, at 40 stations in the study area. Model-generated and measured peak storm surge levels for Lewes are summarized in Table 1.

Differences between computed and measured surge levels ranged from 0.2 ft to 0.9 ft. As with the model validation exercise, these differences are attributed, in part, to discrepancies between the PBL-generated wind directions and those produced by the storms. Winds generated with the PBL model were computed independently of adjacent weather systems; without the adjacent systems, the PBL model is unable to precisely hindcast wind directions necessary for reproducing the measured surge levels. Because the Lewes gage is partially sheltered by Cape Henlopen, small discrepancies in computed wind directions can have an appreciable impact on the hydrodynamic model's ability to predict surge levels.

9. Application of EST Model

Input to the EST model consists of hurricane parameters, or input vectors, describing each storm in the training set together with their associated peak total water surface elevations (or response vectors). This data set is referred to as the training set of storms. Furthermore, the training set was augmented with those storms that occurred in the study area but were omitted from the training set. This second set of storms is referred to as the statistical set. The combined storm set consisting of the training and statistical sets is referred to as the augmented storm set. No response vectors are

specified with the statistical set of storms because the EST model computes these vectors internally. Tables 2 and 3 present the training and the statistical set input vectors for the Lewes gaging station.

Hurricane parameters used as input vectors in the EST model are: maximum wind speed; radius to maximum winds; atmospheric pressure anomaly; translational or forward speed; track direction; and the minimum distance between the study area and the eye of the hurricane. Parameter values are selected at the time a hurricane makes its closest approach to the study area.

The NHC database was processed to determine the necessary parameter values. Data contained in this database, however, are provided at 6-hr increments. Therefore, for each storm in the augmented storm set, a cubic spline interpolation or curve-fitting procedure was followed to compute hurricane positions at hourly intervals. Using the interpolated hurricane positions, the minimum distance between the hurricane's track and the study area was determined. The required hurricane parameters were then interpolated from NHC's 6-hr incremental data.

In developing response vectors, peak storm surge elevations were extracted from the storm surge time-histories created by simulating the storms in the training set. Each surge elevation was then combined with four tidal elevations. The basis for this procedure is that a storm surge event, and therefore its contribution to the peak total water surface elevation, is independent of the tidal cycle. In other words, peak storm surge levels can occur at any time during the tidal cycle. Thus, surge levels must be combined with a range of tidal elevations in order to accurately represent the temporal phasing of surge and tide.

Four tidal elevations were specified for each storm event in order to represent the tidal water level component of the total water surface elevations. One elevation represented high tide elevations whereas a second depicted low tide levels. The two additional elevations equaled zero; thus, the combination of four elevations represent one tidal cycle. Furthermore, the EST model randomly chooses the tide elevation, based on the four elevations, in the simulation procedure. For this study, it was assumed that the maximum and minimum tidal elevations were equal to the summation of the M_2 S_2, N_2, O_1, P_1, K_2, K_1 and Q_1 constituent amplitudes, which represents the average spring tide elevation.

With four tidal elevations being specified with each set of input/response vectors, the total number of storms in the training set were effectively increased from 20 to 80 events. Four identical sets of input vectors or hurricanes were added to the statistical storm set, increasing the number of storms in this set from 25 to 100 storms. Thus, the augmented storm set contained 180 storms. (Adding the additional input vectors to the augmented storm set avoids biasing the training set's input vectors in the stage-frequency computations.)

With the EST model, 100 simulations each having a 200-yr duration were performed for each of the 40 stations. Because the computation is repeated 100 times, 100 individual pdf's and 100 stage-frequency relationships are computed. This family of curves is averaged and the standard deviation computed, resulting in the generation of a stage-frequency relationship containing a measure of variability of data spread about the mean value. Figure 6 shows the plot of the computed mean value as well as all 100 frequency relationships for the Cape May, NJ station.

This figure demonstrates a reasonable degree of variability in the 100 simulations which should be expected from a stochastic process involving a large number of events. Because elevation data are computed continuously, the full population of data are subsequently reduced to a plot of mean value bracketed by plus-and-minus one standard deviation. This presentation of data provides a mean frequency estimate for design as well as an error, or confidence, band which can be incorporated into a risk analysis.

The EST-generated stage-frequency

relationships were compared to those computed using the JPM for the Ocean City and Rehoboth Beach stations (Po, et al 1976). These comparisons are shown in Figures 7 and 8 for the Ocean City and Rehoboth Beach station, respectively. As shown, the EST-generated frequency relationships agree closely with the relationships developed with the JPM. Generally, stages produced with the JPM are within 0.25 ft and also one standard deviation of those stages generated with the EST. Furthermore, the EST required 20 model simulations as opposed to the 468 simulations needed for the JPM.

10. Summary

This paper describes an application of a stochastic modeling procedure for generating frequency-of-occurrence relationships for hurricane-induced surges for the coast of Delaware. Three models were employed in this analysis, including: a wind and atmospheric pressure field model; a hydrodynamic long wave model; and, an empirical simulation model. This paper provides an overview of each model together with description of the procedures taken in generating the frequency-of-occurrence relationships.

The approach uses an expanded data set of historical storms to develop joint probability relationships among the various descriptive storm parameters and responses such that multiple repetitions of multiple years of storm activity are generated. Each simulation reflects the joint probability inherent in the original database of historic events and does not rely on assumed parametric relationships. Therefore, computed probabilities are site specific, do not depend on fixed parametric relationships, and do not assume parameter independence.

The accuracy of the statistical procedures described herein is demonstrated for two stations located along the open coast. Because the approach defines not only the mean frequency-of-occurrence but also a measure of the error, the described procedures show great promise for defining risk-based frequency relationships for any coastal location.

11. Acknowledgments

The technical contributions of Drs. Leon E. Borgman and Joannes J. Westerink to the modeling study described herein are acknowledged. This study was funded by the U.S. Army Engineer District, Philadelphia. Permission was granted by the Chief of Engineers to publish this paper.

12. References

1. Borgman, L., Miller, M., Butler, L., and Reinhard, R. 1992. "Empirical Simulation of Future Hurricane Storm Histories as a Tool in Engineering and Economic Analysis," *Fifth International Conference on Civil Engineering in the Oceans*, ASCE, College Station, TX, 2-5 November 1992.

2. Borgman, L.E. and Scheffner N.W., 1991, "The Simulation of Time Sequences of Wave Height, Period, and Direction," U.S. Army Engineer Waterways Experiment Station, Vicksburg, MS, Technical Report DRP-91-2.

3. Gumbel, E.J., 1954, "Statistical Theory of Extreme Value and Some Practical Application," National Bureau of Standards Applied Math. Series 33, U.S. Gov. Publ., Washington, DC.

4. Jarvinen, B. R., Neumann, C. J., and Davis, M. A. 1988. "A Tropical Cyclone Data Tape for the North Atlantic Basin, 1886-1983: Contents, Limitations, and Uses," NOAA Technical Memorandum NWS NHC 22, National Hurricane Center, Miami, FL.

5. Jelesnianski, C. P. and Taylor, A. D. 1973. "A Preliminary View of Storm Surges Before and After Storm Modifications," NOAA Technical Memorandum ERL WMPO-3, Weather Modification Program Office, Boulder, CO.

6. Po, F.P., Tracey, R.J., Myers, V.A., and Foat, N.S., August 1976, " Storm Tide Frequency Analysis for the Open Coast of Virginia, Maryland, and Delaware," NOAA Technical Memorandum NWS HYDRO-32.

7. Scheffner, N. W. and Borgman, L. E. 1992. "Stochastic Time-Series Representation of Wave Data," Journal of Waterway, Port, Coastal and Ocean Engineering, ASCE, Vol. 118, No. 4, pp. 337-351.

8. Schwiderski, E. W. and Szeto, L. T. 1981. "The NSWC Global Ocean Tide Data Tape, Its Features and Application, Random-Point Tide Program," Technical Report NSWC 81-254, Naval Surface Weapons Center, Dahlgren, VA.

9. Thompson, E. F. 1993. Personal communication. U.S. Army Waterways Experiment Station, Vicksburg, MS.

10. Westerink, J. J., Luettich, A. M., Baptista, A. M., Scheffner, N. W., and Farrar, P. 1992. "Tide and Storm Surge Predictions using Finite Element Model," Journal of Hydraulic Engineering, ASCE, Vol. 118, No. 10. pp. 1373-1390.

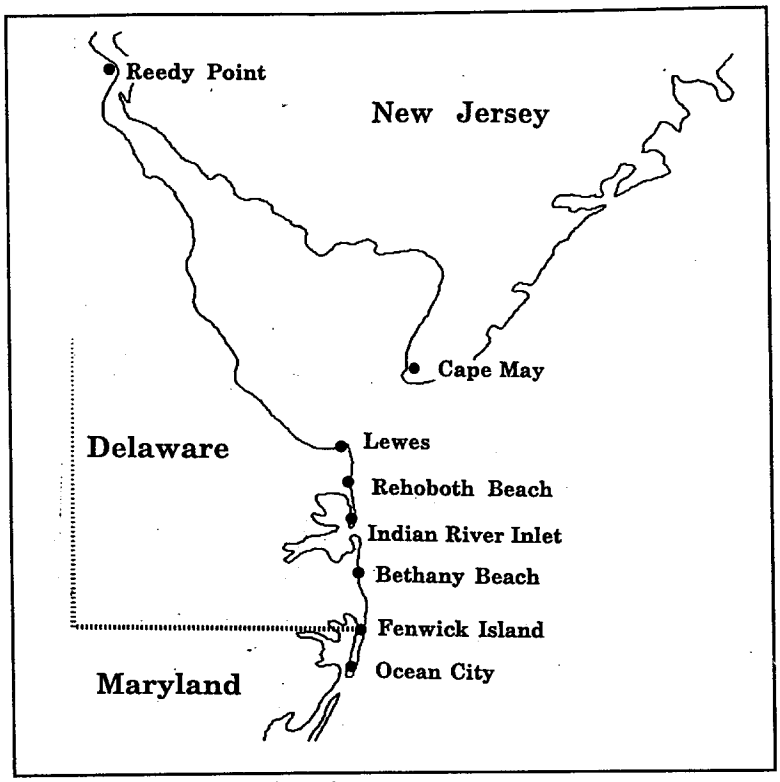

Figure 1 Location of study area.

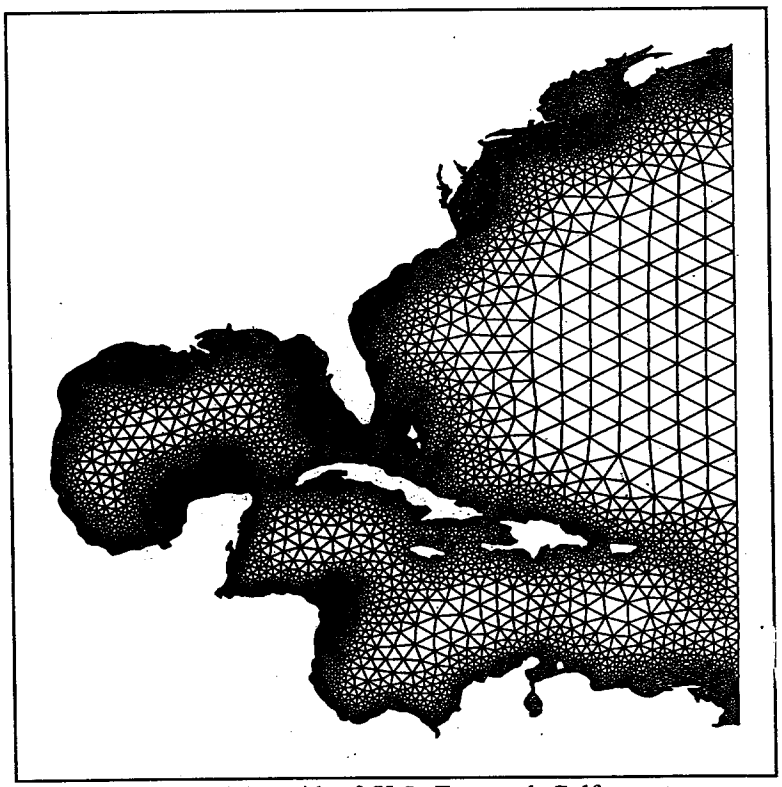

Figure 2 Numercial grid of U.S. East and Gulf coasts.

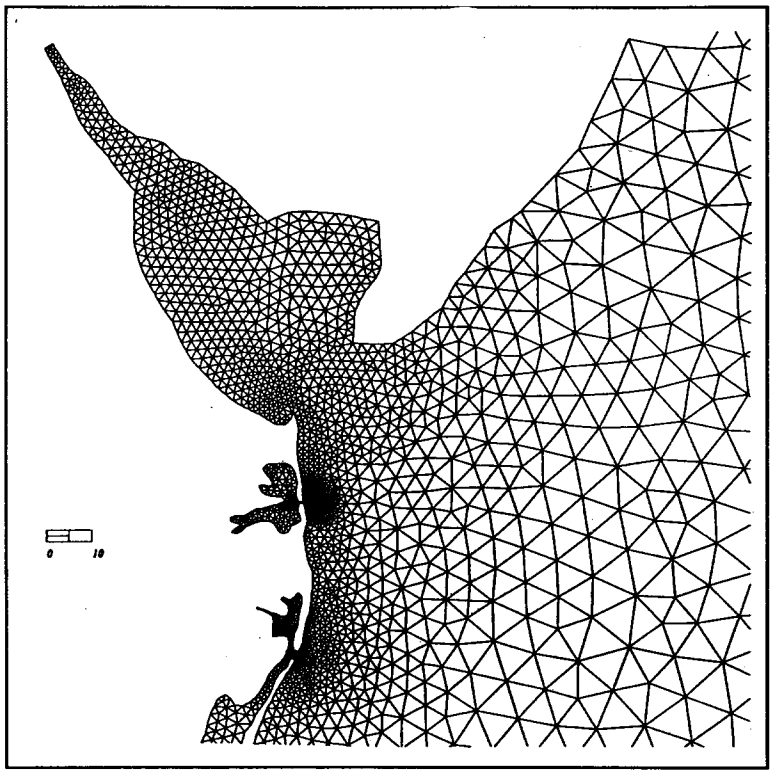

Figure 3 Numerical grid in vicinity of study area.

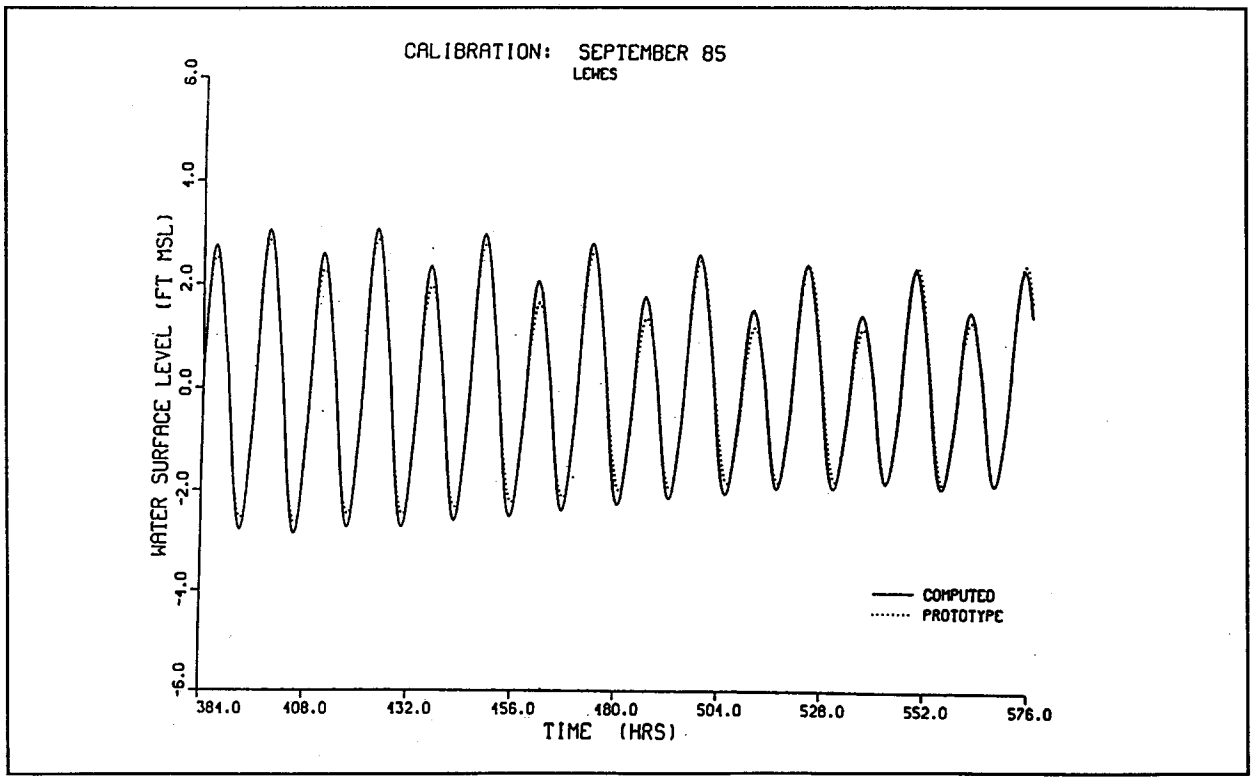

Figure 4 Comparison of water levels at Lewes Station

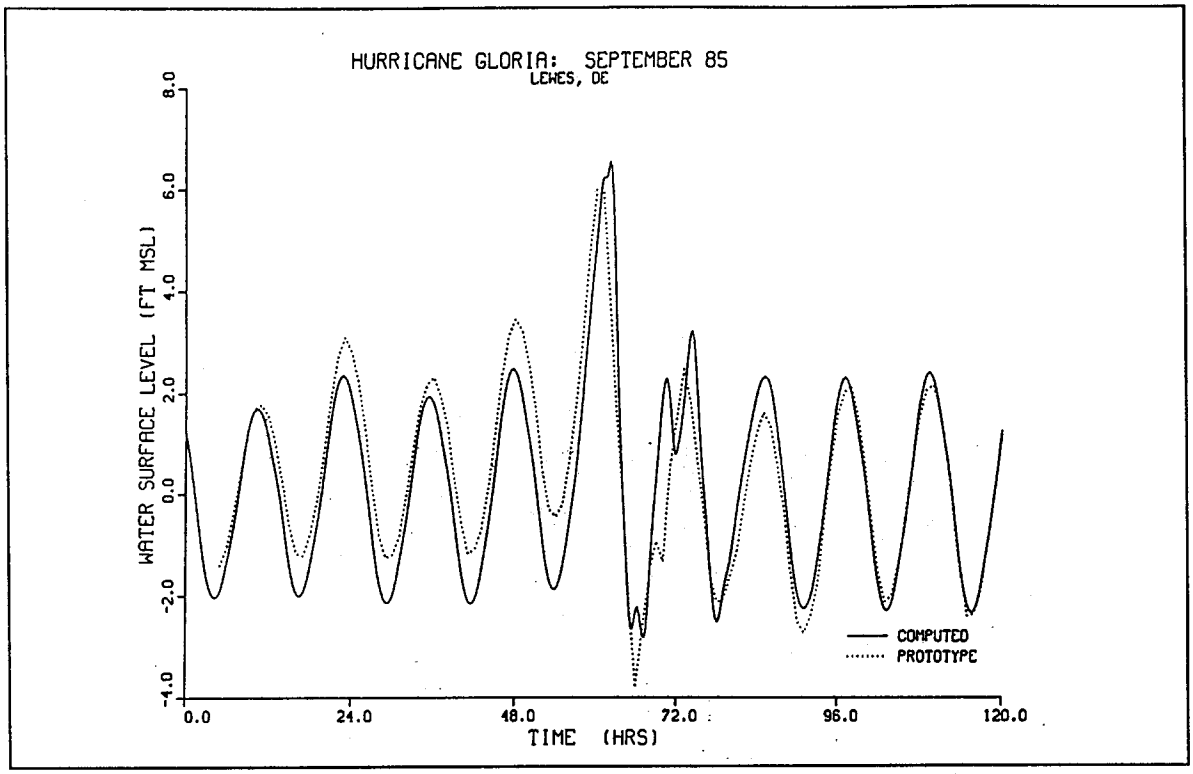

Figure 5 Comparison of computed and measured water levels at Lewes Station

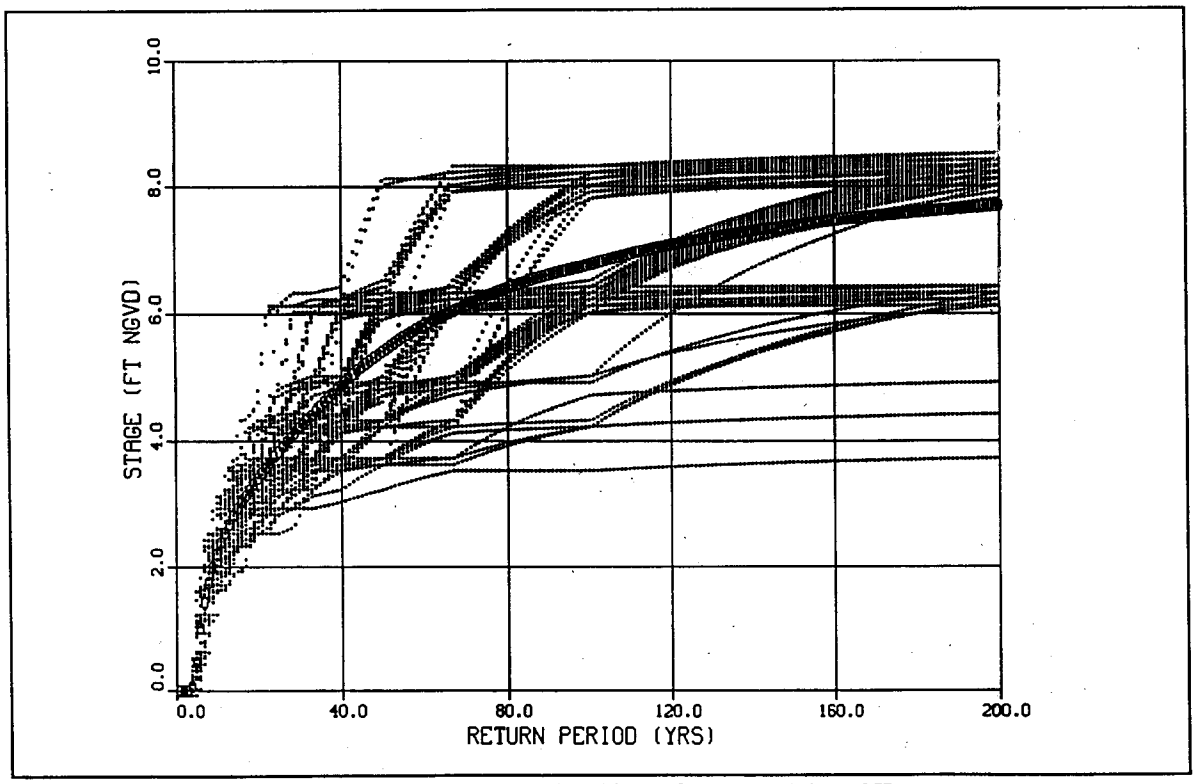

Figure 6 Full population of frequency relationships for Cape May, NJ

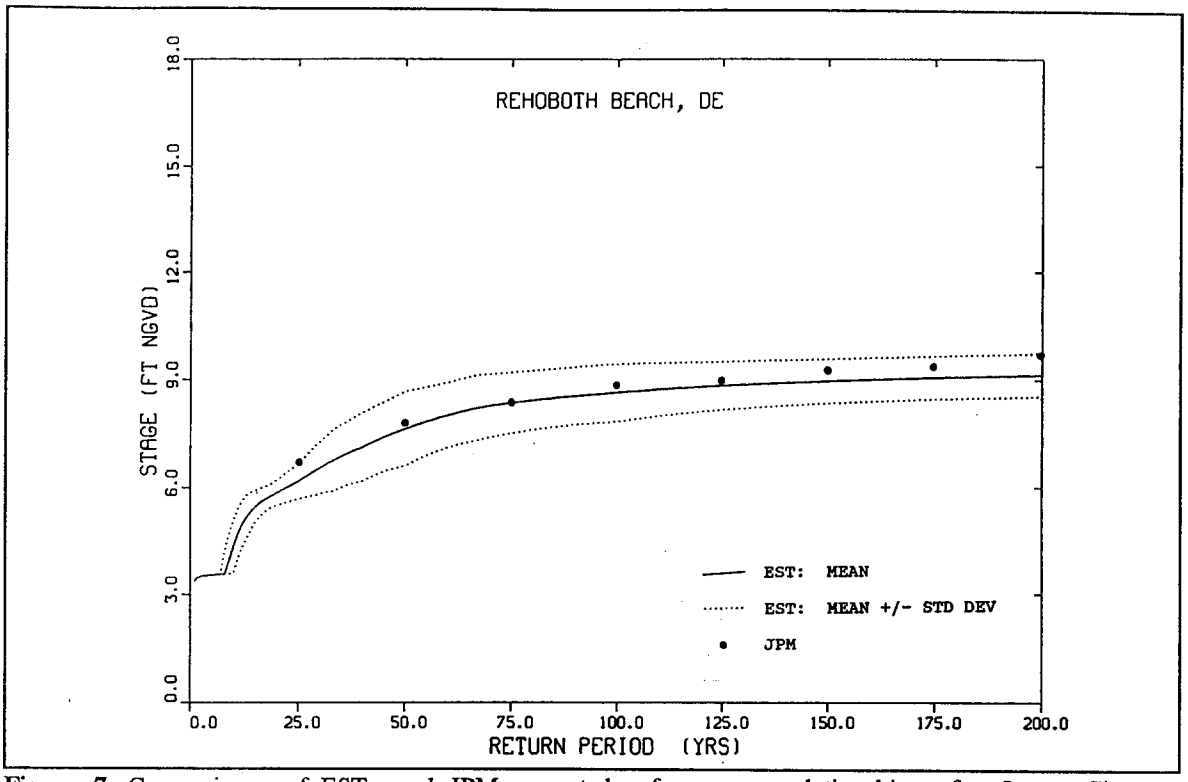

Figure 7 Comparison of EST- and JPM-generated frequency relationships for Ocean City

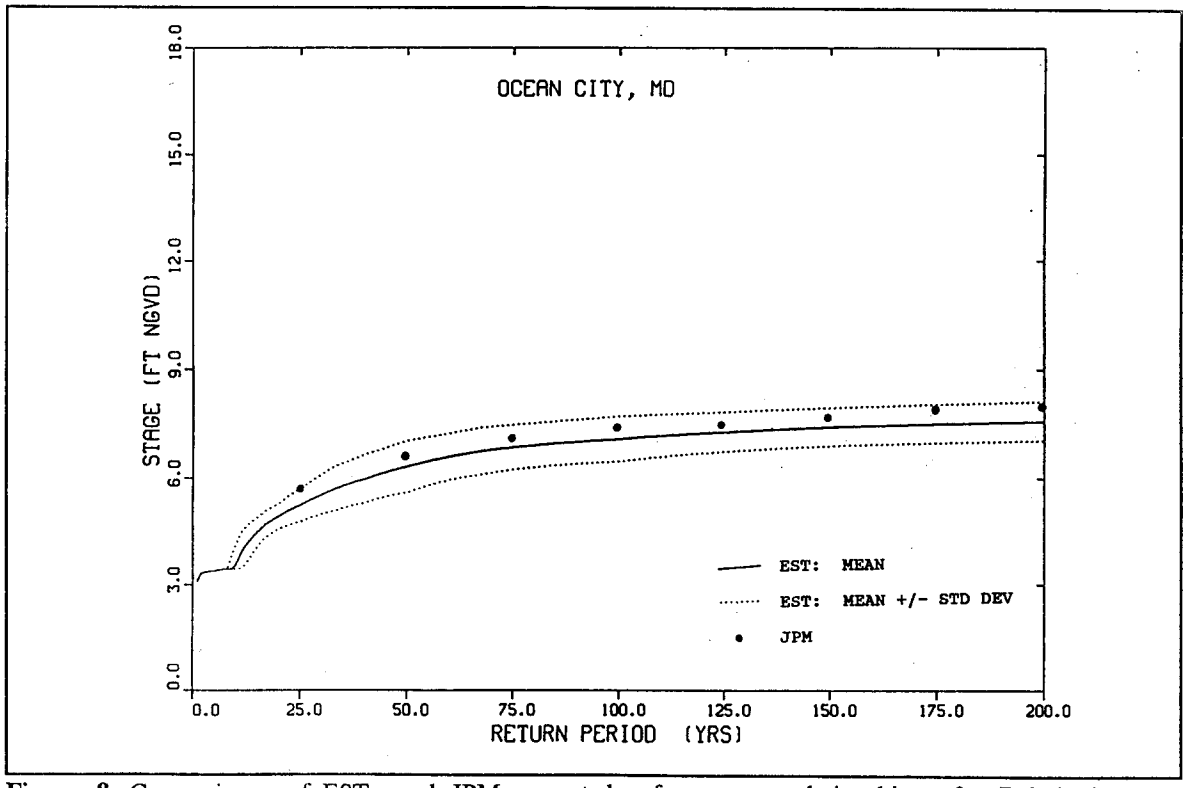

Figure 8 Comparison of EST- and JPM-generated frequency relationships for Rehoboth Beach

Table 1. Comparison of Predicted and Measured Peak Storm Surge Elevations at Lewes, DE.

Hurricane			Peak Surge Elevation	
Name	Number	Date	Predicted (ft)	Measured (ft)
unnamed	327	Aug 1933	2.1	na
unnamed	332	Sep 1933	2.5	1.7
unnamed	370	Sep 1936	2.2	na
unnamed	386	Sep 1938	1.7	na
unnamed	436	Sep 1944	4.7	4.5
unnamed	440	Oct 1944	1.0	na
unnamed	476	Aug 1949	0.5	na
Carol	535	Aug 1954	0.5	na
Connie	545	Aug 1955	3.0	2.3
Daisey	575	Aug 1958	0.3	1.2
Donna	597	Aug 1960	1.1	na
Doria	657	Sep 1967	2.5	3.2
Belle	748	Aug 1976	0.8	na
Gloria	835	Sep 1985	4.5	4.3
Charley	842	Aug 1986	0.1	na

na - not available

Table 2. Summary of Hurricanes and Parameters Composing Training Set

Hurricane Name	Number	Distance Approach (mi)	Track Angle (deg)	Central Pressure (mb)	Maximum Velocity (knots)	Forward Speed (knots)	Radius to Winds (n.m.)
unnamed	327	105.8	352.5	975.5	45.0	16.8	43.4
unnamed	332	108.0	38.5	961.4	74.4	11.0	43.4
unnamed	370	57.9	33.4	970.0	85.5	17.0	16.9
unnamed	386	115.5	357.4	940.0	85.0	44.0	43.4
unnamed	436	64.5	22.5	963.0	79.8	31.0	42.1
unnamed	440	40.6	46.3	996.9	41.0	16.7	39.7
unnamed	476	197.1	57.6	979.5	90.9	19.3	8.6
Carol	535	84.4	20.7	977.8	85.5	32.1	8.6
Connie	545	53.7	344.3	977.0	47.5	13.1	43.4
Daisey	575	131.0	31.1	968.8	110.0	21.5	8.6
Donna	597	67.6	26.0	967.7	94.3	29.6	8.6
Doria	657	82.3	253.2	988.2	58.8	7.8	20.7
Belle	748	71.8	8.8	977.0	80.0	22.7	10.4
Gloria	835	43.8	16.6	951.0	85.0	33.0	20.0
Charley	842	66.9	50.5	991.7	60.3	12.5	10.2
unnamed[1]	370	37.9	33.4	970.0	85.0	17.0	16.9
unnamed[1]	436	44.5	22.5	963.0	79.8	31.0	42.1
Donna[1]	597	67.6	26.0	967.7	94.3	29.6	20.0
Gloria[1]	835	23.8	16.6	951.0	85.0	33.0	20.0
Gloria[1]	835	43.8	16.6	951.0	85.0	33.0	43.4

superscript denotes hypothetical hurricane

Table 3. Summary of Hurricanes and Parameters Composing Statistical Storm Set

Hurricane Name	Number	Distance Approach (mi)	Track Angle (deg)	Central Pressure (mb)	Maximum Velocity (knots)	Forward Speed (knots)	Radius to Winds (n.m.)
unnamed	112	123.7	54.3	974.6	70.6	6.8	31.1
unnamed	299	219.0	49.5	978.7	76.1	10.1	13.2
Barbara	520	85.5	43.3	990.7	68.9	15.0	8.6
Esther	604	156.9	18.8	969.2	114.0	15.3	8.6
Alma	611	151.2	38.0	990.7	76.8	23.9	8.6
Dora	630	164.5	51.0	998.7	50.0	17.0	24.7
Gladys	633	234.9	36.4	979.8	73.9	14.0	14.3
Alma	643	119.0	35.5	1002.0	44.9	6.7	33.2
Gladys	669	198.4	53.0	981.5	70.6	26.2	15.9
Gerda	676	168.9	35.3	984.5	107.0	30.6	8.6
Doria	702	9.4	25.1	993.6	48.9	27.4	26.6
Agnes	712	113.1	1.0	976.5	59.9	19.8	43.4
Carrie	714	215.0	6.9	1000.0	48.5	9.6	27.2
unnamed	805	208.8	24.5	978.4	59.9	7.7	40.9
unnamed	807	164.7	50.6	992.0	60.0	31.7	10.3
unnamed[1]	370	72.9	33.4	970.0	85.5	17.0	16.9
unnamed[1]	370	42.9	33.4	970.0	85.5	17.0	16.9
unnamed[1]	436	79.5	22.5	963.0	79.8	31.0	42.1
unnamed[1]	436	49.5	22.5	963.0	79.8	31.0	42.1
unnamed[1]	440	55.6	46.3	996.9	41.0	16.7	39.7
unnamed[1]	440	25.6	46.3	996.9	41.0	16.7	39.7
Doria[1]	657	97.3	253.2	988.2	58.8	7.8	20.7
Doria[1]	657	67.3	253.2	988.2	58.8	7.8	20.7
Gloria[1]	835	58.8	16.6	951.0	85.0	33.0	20.0
Gloria[1]	835	28.8	16.6	951.0	85.0	33.0	20.0

superscript denotes hypothetical hurricane

APPENDIX: TASK COMMITTEE REPORTS

Report of Task Committee on

(A) Strong-Motion Data and Applications

Date: May 17, 1994

Place: National Institute of Standards and Technology
Gaithersburg, MD

Attendees:

U.S. Side -	G. Brady (Chairman)	(USGS)
	H. Meyers	(NOAA)
	J. Hill	(DOE)
Japan Side -	S. Iai (Acting Chairman)	(PHRI)
	K. Ohtani	(NIED)
	T. Iijima	(PWRI)

1. OBJECTIVE AND SCOPE OF WORK

The objectives of the Task Committee are (1) to coordinate and promote sharing of strong motion earthquake data among researchers and practicing engineers, and (2) to develop techniques and exchange information for evaluating the destructive effects of earthquake motion.

The scope of work includes:

(1) instrumentation,
(2) recording, processing and analyzing strong-motion data,
(3) engineering characterization of ground motion,
(4) design applications, and
(5) seismic zonation.

The activities of the Task Committee include:

(1) regular exchange of data and publications,
(2) creating procedures for the dissemination of significant strong-motion digital data with regard for the rights and expectations of (a) owner, (b) the users of data and (c) the earthquake engineering community,
(3) planning and conducting T/C workshops and meetings, and
(4) coordinating relevant research activities.

2. ACCOMPLISHMENTS

(1) Exchange of Data

From U.S. Side:

- Catalogs of Earthquakes in the U.S.
- Three sets of slides for the M6.7 1994 Northridge earthquake: epicentral area, far-field, and a comparison with the M6.6 1971 San Fernando earthquake, produced by the World Data Center A and NGDC/NOAA, provided by H. Meyers.
- A set of 2 CD's of digital slides on Geologic Hazards, (volcanoes, tsunamis, and earthquakes), produced by NGDC/NOAA from slides from various sources, provided by H. Meyers.

From Japan Side:

- Catalogs of Earthquakes in Japan
- Floppy disk containing accelerograms from the 1993 Off-Kushiro earthquake, recorded by the Building Research Institute, M.O.C., and provided by Y. Kitagawa and T. Kashima.

(2) International Workshop

Conducted a successful International Workshop on Strong Motion Data, December 1993, Menlo Park, California. The workshop dealt with the current state of strong motion recording in the U.S., Japan, and the rest of the world, and compared attenuation relations for peak ground accelerations and response spectra. It was hosted by PHRI and USGS, and sponsored by the Science and Technology Agency, the International Science and Technology Exchange Center, and PHRI, Japan. The published Proceedings contain 36 contributions from US, Japanese and other researchers (from New Zealand, France, and Chile).

(3) Recordings of the Northridge Earthquake

The constant promotion of high-quality strong motion recording networks throughout the world has assisted in the production of useful sets of data from the Northridge Earthquake (on the order of 200 from California's state program (CDMG/SMIP), 100 from USGS, and 60 from the University of Southern California).

3. FUTURE PLANS

An international workshop on strong-motion data concentrating on local site effects is planned for early 1996 in Japan. Momentum from the December 1993 workshop and the large amount of Northridge data will be well-used. Topic detail includes regional geology, topography, local site geology, amplification, non linearity, and liquefaction. Invited attendance of 30-50 is planned, including participants from countries other than the U.S. and Japan. Financial support from international and U.S. sources, and the Japanese Government, will be sought.

Report of Task Committee on

(B) Testing and Evaluation Procedures for Building Systems

Date: May 18, 1994

Place: National Institute of Standards and Technology
Gaithersburg, MD

Attendees:			
	U.S. Side -	H. Lew (Chairman)	(NIST)
		S. Mahin	(UCB)
	Japan Side -	K. Ohtani (Chairman)	(NIED)
		H. Okada	(BRI)
		H. Shiohara	(BRI)

1. OBJECTIVE AND SCOPE OF WORK

The objective of the Task Committee is to develop rational test procedures and to collect performance data of dynamic response of structures through laboratory testing of prototype structures and field testing of structures in situ.

The scope of work includes:

(1) Plans and conducts workshops and joint meetings to identify research topics and develops joint research programs.

(2) Coordinates research projects carried out by various laboratories in the U.S. and Japan. Facilitates publication of research results and implementation of findings in codes and standards.

(3) Facilitates exchange of research personnel, technical information and available testing facilities.

(4) Develops uniform testing procedures including test loading history for case of comparison of results of tests carried out by various researchers, and for establishment of data base.

(5) Develops guidelines for interpretation of test results in consideration for design of structures.

(6) Develops methodology for evaluation and interpretation of physical test results.

2. ACCOMPLISHMENTS

(1) Conducted the fourth U.S. -Japan Joint Technical Coordinating Committee (TCC) meeting on Precast Seismic Structural Systems Program (PRESSS), May 1994, Tsukuba, Japan.

(2) Published seismic design and construction guidelines and design manuals for precast reinforced concrete buildings by Building Center of Japan, July 1993.

(3) Initiated the Japan research program on Composite and Hybrid Structures (CHS), 1993. The Japan TCC meetings were held during the past year.

(4) The Panel endorsed the implementation of the joint research program on CHS during the 25th Joint Panel Meeting in May 1993.

(5) Conducted the first U.S.-Japan Joint TCC meeting on CHS in November 1993, Tsukuba, Japan.

3. FUTURE PLANS

(1) The third phase of the U.S. PRESSS has been planned to be initiated during 1994-1995. The fourth U.S. meeting will be held in October 1994.

(2) The second U.S.-Japan joint TCC meeting on CHS will be held in July 1994 in Chicago, Illinois during the occasion of the 5th U.S. National Conference on Earthquake Engineering.

(3) The joint research program on CHS will be formally initiated in the U.S. in 1994. The first U.S. TCC meeting will be held in the fall of 1994.

(4) In support of the International Decade for Natural Disaster Reduction (IDNDR) Program, techniques will be explored to disseminate finding of the Joint Research Projects carried out under the auspices of T/C "B" to countries with high seismic risks.

(5) To maximize the usefulness of experimental data, it is desirable to develop standards for storage, documentation and retrieval of test data. Researchers and members of the user community from the U.S. and Japan should be encouraged to convene for the purpose of establishing such standards. Efforts should be made to utilize available resources and expertise in Japan and the U.S.

Report of Task Committee on

(C) Design Evaluation and Improvement of Structures

Date: May 18, 1994

Place: National Institute of Standards and Technology
Gaithersburg, MD

Attendees:

U.S. Side -	K. Chong (Chairman)	(NSF)
	C. Anderson	(USBR)
	R. Fuller	(HUD)
	J. Hill	(DOE)
	L. Hultengren	(DOS/FBO)
	J. Scalzi	(NSF)
	A. Taylor	(NIST)
	J. Wilcoski	(COE)
Japan Side -	H. Okada (Acting Chairman)	(BRI)
	M. Kanda	(PWRI)
	S. Kobayashi	(PWRC)
	M. Koga	(CRS)
	K. Nishikawa	(PWRI)
	H. Shiohara	(BRI)
	K. Yokoyama	(PWRI)

1. OBJECTIVE AND SCOPE OF WORK

The objective of the Task Committee is to develop disaster mitigation policies and programs which will improve the performance of new structures and the capacity of existing structures in resisting wind and seismic forces. In order to establish adequate evaluation of performance, each country will coordinate development of condition assessment, screening, and structural analysis and design methodologies. Enhance performance can be obtained by the intelligent renewal, repair and retrofit of existing buildings and other structures. Structures will be analyzed and instrumented, and then evaluated after disasters. Also, effective utilization of new advanced materials and structural systems, associated with appropriate design methods, will provide excellent structural performance in the life cycle.

The scope of work includes:

(1) Exchanging information, planning, and hosting workshops on new design technologies, evaluation technologies, and repair and retrofit techniques.

(2) Developing a uniform system for screening and analyzing wind and seismic resistance capacity of structures in each country.

(3) Developing sensor technology, instrumentation, and "expert" systems to provide reliable condition assessment of existing structures.

(4) Evaluating masonry, precast concrete and composite/hybrid building structures; and providing documentation for post-disaster evaluation of performance.

(5) Studying new materials and methods for repairing and retrofitting existing structures and for new construction.

(6) Coordinating research projects in the U.S. and Japan to minimize duplication and maximize benefits.

2. ACCOMPLISHMENTS

(1) T/C "C" and "G" co-sponsored a workshop on Structural Control and Intelligent Material Systems in May, 1993 in Japan. Proceedings of this workshop will be available soon.

(2) A member of Task Committee C participated in the EERI Reconnaissance Team (Dr. A.G. Brady) which investigated the Guam Earthquake of August 8, 1993.

(3) After the January 1994 Northridge Earthquake, several U.S. agencies conducted cooperative damage assessment studies to determine the necessity to improve building codes and to develop repair and strengthening requirements for existing buildings. (HUD, USGS, NIST, FEMA, NSF)

(4) BRI has sent to the U.S. side the proceedings of the second U.S.-Japan Study Group Workshop on New Design Methodology for Building, which was published by BRI. Although the workshop consisted of the U.S. and Japan Ad Hoc Committees, the activities will lead to an official U.S./Japan joint study group that is recommended in the item (3) of "Future Plans."

3. FUTURE PLANS

The following planning was performed on Design, Evaluation and Improvement of Structures.

(1) Develop a uniform system for screening and analyzing wind and seismic resistant capacity, and improve sensor/inspection technology, instrumentation and expert systems to provide condition assessment of existing structures.

(2) Compile a database of advanced materials/systems that have potential for improving structural performance of new construction, as well as for use in rehabilitating and strengthening existing buildings.

(3) Investigate new design methodologies based on required structural performance, which also will address advanced materials and systems. In order to effectively take this new approach, it is recommended that each country should make an effort to establish a U.S./Japan joint study group of members of appropriate institutions in each country.

(4) Develop design guidelines for applying advanced structural and materials systems to be used for composite and hybrid structures under the joint U.S./Japan Cooperative Research Program.

(5) Participate in activities of the International Decade for Natural Disaster Reduction (IDNDR), including the "World Conference on Natural Disaster Reduction," held in Yokohama, Japan during May 23-27, 1994.

(6) Continue to encourage participation by private industry, consulting engineers, universities, State and local government agencies, and other Federal agencies involved in instrumentation, evaluation, condition assessment, and retrofit and strengthening of existing buildings for seismic and wind resistance.

(7) The second workshop on "Structural Control and Intelligent Material Systems" is scheduled in the U.S. during 1995, in coordination with T/C "G".

4. OTHER ACTIVITIES

(1) MOC delegates visited NSF in September and December 1993. An agreement was reached to promote research programs on "Building Safety and Related Infrastructure Improvements" under the framework of the "New Economic Partnership between the U.S. and Japan".

(2) A workshop on Composites for Construction will be held at NSF - July 8, 9, 10, 1994, to plan a 5-year research program on the basic research topics required for the use of composites in general construction.

(3) A U.S.-Japan Workshop on "Development and Future Directions in Structural Testing" co-chaired by T. Okada and S. Mahin, held in Honolulu, Hawaii in June 1993.

(4) Continued U.S. research sponsored by NSF has developed reports on seismic rehabilitation and retrofit strategies, including innovative techniques for strengthening existing buildings and bridges.

(5) NSF completed panel review of the 3rd year "Repair and Rehabilitation for Earthquake Resistance" proposals and will announce awards in the near future.

(6) A new and improved Seismic Safety Guide is to be published by the Department of Energy in 1994, Donald Eagling, Editor. The "Guide" provides information for engineers and building managers for developing practical and cost-effective seismic mitigation programs for application at sites with several buildings.

(7) Benefits versus costs for retrofitting existing buildings has been studied at the Lawrence Berkeley Laboratory in California. A paper to be completed soon shows benefit/cost ratios saving from 25 to 1 to 100 to 1.

(8) "Second International Conference on Intelligent Materials" co-funded by NSF and other U.S. agencies, will be held June 1994 in Williamsburg, VA.

(9) Continue development of NSF's Civil Infrastructure Systems Research Program, including strong emphasis on evaluation and improvement of structures.

Report of Task Committee on

(D) Earthquake Engineering for Dams

Date: May 18, 1994

Place: National Institute of Standards and Technology
Gaithersburg, MD

Attendees:

U.S. Side -	W. Roper (Co-Chairman)	(COE)
	R. Hall	(WES)
	L. Guthrie	(COE)
	F. McLean	(USBR)
	A. Franklin	(WES)
	J. Wilcoski	(CERL)
Japan Side -	K. Nishikawa (Acting Chairman)	(PWRI)

1. OBJECTIVE AND SCOPE OF WORK

The objective of the Task Committee is to develop technical insights into better understanding of the response of dams to seismic effects. The T/C will plan, promote, and develop research initiatives to assist in assuring seismic safety and economical protective countermeasure against earthquake loading of these structures. The scope of work includes:

(1) Methods of analysis for seismic design of dams. Compare U.S. and Japan design methods. Perform investigations using dynamic analysis methods as tools (modeling, calculation codes).

(2) Dynamic characteristics of dam construction materials. Identify strength and deformation characteristics during an earthquake (concrete, soil and rock).

(3) Analysis of observed behavior of dams during an earthquake. Investigate the mechanism of damages to earthquake loading. Analyze the observed behavior during an earthquake to the earthquake-resistant design.

2. ACCOMPLISHMENTS

Mr. Nario Yasuda, senior research engineer of Fill-Type Dam Division, PWRI, visited Research and Development Directorate, Headquarters U.S. Army Corps of Engineers on January 28, 1994, to discuss future possible activities of T/C (D), feasibility of cooperative research, exchange of technical information and so on.

Dr. Dean Norman, Senior Research Structure Engineer of the Structures Laboratory,

WES, visited the Earthquake Engineering Division, PWRI during February and March 1994. He conducted cooperative studies on retrofit techniques for bridges and other concrete structures, and concrete constitutive models for dynamic finite element applications. During his stay he attended the International Workshop on Construction and Management Technology for Dams, and Enhancement of the Dam Lake Basin Environment for the Next Generation in Tsukuba.

3. FUTURE PLANS

(1) Exchange results of research/investigation and technical information about dam earthquake engineering is encouraged, and feasibility of joint research and investigation is in continuous consideration.

(2) Exchange visits to the institutes concerned, of scientists and engineers between U.S. and Japan, to enhance effective communication.

(3) In accordance with the progress of activities (1) and (2), T/C (D) will coordinate a Workshop on Earthquake Engineering for Dams and the development of a joint publication on the current status of research in this area.

Report of Task Committee on

(F) Disaster Prevention Methods for Lifeline Systems

Date: May 18, 1994

Place: National Institute of Standards and Technology
Gaithersburg, Maryland

Attendees: U.S. Side - R. Chung (Chairman) (NIST)
S. Mahin (UCB)

Japan Side - K. Kawashima (Acting Chairman) (PWRI)
C. Minowa (NRIESDP)
H. Sugita (PWRI)

1. OBJECTIVE AND SCOPE OF WORK

The objectives of the Task Committee are to improve: 1) the performance of lifeline systems during earthquakes and 2) engineering and other seismic countermeasures including the capability in damage estimation techniques and inspection procedures. The scope of work includes:

(1) Planning and conducting workshops on lifeline systems

(2) Facilitating exchange of technical information

(3) Promoting development of design guidelines and standards for lifeline systems

2. ACCOMPLISHMENTS

(1) Published the proceedings of the 5th Joint Workshop on Earthquake Disaster Prevention for Lifeline Systems, which was held in October 1992 in Tsukuba, Japan. The proceedings were distributed to members of the UJNR panel and others in the lifeline earthquake engineering community.

(2) Organized a joint post-earthquake reconnaissance effort for the July 1993 Hokkaido-Nansei-Oki earthquake. The U.S. team members collaborated closely with the Japanese team members in their field investigations.

Results of their joint studies, especially those related to the performance of Lifeline systems, have been presented in a number of meetings, workshops, and conferences.

(3) Assisted in the arrangement of the Japanese Government Study Team's visits to Los Angeles area in January and March, 1994 after the January 17, 1994 Northridge earthquake. The Japanese team has visited a number of sites where critical lifeline systems, such as aqueducts, substations, to receive briefings and assess their performance.

3. FUTURE PLANS

(1) Encourage current efforts in both countries to establish seismic design guidelines and standards for lifeline systems. Existing UJNR channels should be fully utilized to facilitate the exchange of relevant information concerning standards development. Possible collaboration of joint development of guidelines and standards for lifeline systems should be pursued.

(2) Encourage collaborative researchers and development in the following areas:
- planning for urban disaster prevention
- systems approach to lifeline performance
- soil-structure interaction
- performance of underground pipelines and cables
- fire protection/prevention
- geographic information systems (GIS)
- cost-effective ground improvement techniques
- development and operation (including restarting) of safety shut-down systems

(3) Hold the 6th Joint Workshop on Earthquake Disaster Prevention for Lifeline Systems, December 1994, Los Angeles, CA. The Workshop focus will be on soil-structure interactions, performance of underground pipelines and cables, and cost-effective ground improvement techniques.

Report of Task Committee on

(G) Structural Control and Intelligent Material Systems

Date: May 17, 1994

Place: National Institute of Standards and Technology
Gaithersburg, MD

Attendees:

U.S. Side -	K. Chong (Acting Chairman)	(NSF)
	C. Anderson	(USBR)
	R. Fuller	(HUD)
	J. Hill	(DOE)
	L. Hultengren	(DOS/FBO)
	J. Scalzi	(NSF)
	A. Taylor	(NIST)
	J. Wilcoski	(COE)
Japan Side -	H. Shiohara (Acting Chairman)	(BRI)
	M. Kanda	(PWRI)
	S. Kobayashi	(PWRC)
	M. Koga	(CRS)
	K. Nishikawa	(PWRI)
	H. Okada	(BRI)
	K. Yokoyama	(PWRI)

1. OBJECTIVE AND SCOPE OF WORK

The objectives of the Task Committee are to: (1) develop research plans in control of equipment and structures and in high performance structural and material systems; (2) implement control techniques for motion reduction or modification; (3) implement use of advanced materials in actual design and construction of buildings and other infrastructure systems under seismic or wind environments; (4) promote U.S.-Japan cooperation in structural control and intelligent material systems research; (5) bring together governmental, academic, and industrial participants in joint pursuit of these efforts; and (6) contribute to IDNDR by organizing joint research and other technical activities in structural control and intelligent material systems research on the basis of international cooperation.

The UJNR T/C "G" works closely with other organization to provide the leadership in this emerging research by facilitating the exchange of technical data and information through UJNR mechanisms. The scope of work includes:

(1) Providing technical assistance, consultation and coordination to UJNR affiliated research organizations in the initiation, development, and execution of their programs in research areas.

(2) Promoting joint government-university-industry collaborative efforts to facilitate technology transfer and practical implementation.

(3) Sponsoring and conducting inter-disciplinary workshops and meetings to identify key areas of research and opportunities for cooperation, and to exchange new knowledge and experience in practice.

(4) Developing promotional and demonstrative activities to stimulate public awareness and interest in this field of research.

(5) Providing information useful for the establishment of performance standards, design specification, guidelines and code recommendations for application in new construction as well as retrofit/rehabilitation of existing structures.

(6) Initiating research in intelligent material systems, sensors, actuators, optimal control system design, and encourage laboratory and field experiments of prototype and full-scale structures.

2. ACCOMPLISHMENTS

(1) Conducted the "3rd U.S Japan Workshop on Earthquake Protective Systems of Bridges" at Berkeley, California during January 24 and 25, 1994 under the joint auspices of T/C "G" and "J". A study tour to visit base-isolated bridges in the San Francisco area was conducted by participants prior to the Workshop. Proceedings of the Workshop was published by NCEER in March 1994. The workshop was attended by 45 U.S., 32 Japanese researchers, and experts from Taiwan and New Zealand.

(2) To pursue the technical objectives of the T/C "G" and T/C "C", a U.S. domestic workshop was held in Williamsburg, Virginia, on November 17 and 18, 1993 to further define the objectives and research value and needs in intelligent materials/systems. Published the workshop proceedings, "Rebuilding and Enhancing the Nation's Infrastructure: A Role for Intelligent Material Systems and Structures;" it was distributed by the Workshop organizer.

(3) Joint Research Program for Hybrid Control of Bridges is being performed through T/C "G" and "J" by PWRI, NSF, FHWA, NIST, NCEER, and UC Irvine. Under this program, experimental studies have been conducted at PWRI and NCEER (SUNY at Buffalo). The experimental studies at PWRI tested and confirmed the effectiveness of the sliding base-isolation systems developed at NCEER.

(4) International Workshop on Structural Control was held in Honolulu, Hawaii on August 4-5, 1993, with major participation by Japan and U.S. Panel Members. Proceedings was published by the University of Southern California in December 1993.

(5) NIST developed standard test procedures for seismic isolation systems were presented at the 26th UJNR Joint Meeting.

(6) At BRI, research programs on structural control of buildings have been developed and implemented. Collaborative research programs involving possible organizations and private companies were developed. The final report was published by BRI in 1993.

3. FUTURE PLANS

(1) Planning efforts for U.S.-Japan cooperative research projects on seismic response control involving PWRI, BRI, NSF and industries from both sides are continuing. Research cooperation between the U.S. and Japan will be actively pursued using forums such as the UJNR and other inter-governmental mechanisms.

(2) Joint research projects on active and hybrid control of structures, such as bridges and buildings, will be continued and developed by PWRI, BRI, NCEER, CUREe, and others.

(3) In cooperation with T/C "J", the 4th US-Japan Workshop on Earthquake Protective Systems for Bridges is being scheduled in 2 years in Japan. Topics are expected to include: (1) innovative protective systems; (2) design methods for seismic isolated/menshin bridges; (3) full-scale verification of performance; and (4) comparative design examples.

(4) Under the Joint Research Program for Hybrid control of Bridges through T/C "G", the experiment to confirm the effectiveness of variable damper systems developed at PWRI will be performed at NCEER.

(5) A Workshop on "Structural Control and Intelligent Material Systems" is planned for 1995 in cooperation with T/C "C" of the Panel on Wind and Seismic Effects.

4. OTHER ACTIVITIES

(1) The NSF Research on Structural Control will hold a coordination meeting in Pasadena, on August 6-7, 1994.

(2) The First World Conference on Structural Control will be held in Pasadena, California on August 3-5, 1994.

(3) "Second International Conference on Intelligent Materials" co-funded by NSF and other U.S. agencies, will be held in June 1994 in Williamsburg, VA.

(4) The U.S. Panel on Structural Control Research worked closely with one of its counterpart "Japanese Panel on Structural Response Control" in exchanging technical information and developing joint research plans.

Report of Task Committee on

(H) Soil Behavior and Stability During Earthquakes

Date: May 17, 1994

Place: National Institute of Standards and Technology
Gaithersburg, Maryland

Attendees:			
	U.S. Side -	A. Franklin (Chairman)	(WES)
		F. McLean	(USBR)
	Japan Side -	K. Kawashima (Acting Chairman)	(PWRI)
		S. Iai	(PHRI)
		T. Iijima	(PWRI)
		T. Kagawa	(WSU)
		C. Minowa	(NIED)
		H. Sugita	(PWRI)

1. OBJECTIVE AND SCOPE OF WORK

Government agencies responsible for public works must assure seismic safety and provide economical protection against earthquake hazards.

The objective of the Task Committee is to assist in meeting these needs by enhancing the available technology for predicting the dynamic behavior of soils, analyzing dynamic soil-structure interaction, and modifying the earthquake behavior of foundations and earth structures to assure their safe performance during earthquakes.

In accordance with the objective, the scope of work includes:

(1) Present technical papers at annual joint panel meetings on technological developments and on state-of-the-art and practice related to soil behavior and stability during earthquakes.

(2) Exchange information and technical data relating to field performance, research, and methods of practice.

(3) Plan and conduct programs of cooperative research and/or workshops in coordination with the proposed or ongoing programs.

(4) Make other needed efforts including exchange of researchers between U.S. and Japanese research institutions, publication of research results and recommended practice.

2. ACCOMPLISHMENTS

(1) The Japan-side provided to the U.S.-side the "Handbook on Remedial Measures for Reclaimed Land Soil Liquefaction," published in Japanese by the Ministry of Transport. The Waterways Experiment Station (WES) has translated the document into English and has provided a copy of the manuscript to the Japan side for review prior to publication.

(2) The National Research Institute for Earth Science and Disaster Prevention (NIED), the Building Research Institute (BRI), and Wayne State University (WSU), have conducted a cooperative research program on "Research on Earthquake Pile Resistance in Liquefied Soils" (1992-1993) under the auspices of UJNR Panel on Wind and Seismic Effects and have reported results at the 26th Joint meeting. Dr. C. Minowa and Dr. N. Ogawa, NIED, visited WSU, and Professor T. Kagawa visited NIED in connection with this cooperative research.

3. FUTURE PLANS

(1) T/C (H) will hold its 4th U.S.-Japan Workshop on Remedial Treatment of Potentially Liquefiable Soils at the Public Works Research Institute (PWRI) in Tsukuba, 4-8 July 1994.

(2) The Port and Harbour Research Institute (PHRI) and WES will publish the English version of the "Handbook on Remedial Measures for Reclaimed Land Soil Liquefaction" and deliver it to the panel members and participating organizations in 1995.

(3) NIED and WSU will perform a cooperative research program "Physical and Numerical Simulation of Structural Damages Due to Liquefaction and Development of Countermeasure Techniques" (1994-1998) under the auspices of UJNR Panel on Wind and Seismic Effects.

(4) T/C (H) tentatively plans to hold a workshop on Earthquake Simulation in Centrifuges during 1996.

Report of Task Committee on

(I) Storm Surges and Tsunami

Date: May 18, 1994

Place: National Institute of Standards and Technology
Gaithersburg, MD

Attendees:			
	U.S. Side -	H. Meyers (Chairman)	(NOAA)
		M. Blackford	(NOAA)
		W. Roper	(COE)
		J. Wilcoski	(COE)
	Japan Side:	H. Sato (Acting Chairman)	(PWRI)
		S. Iai	(PHRI)

1. OBJECTIVE AND SCOPE OF WORK

The objective of the Task Committee is to mitigate damages from storm surges and tsunamis through shared technologies, research, information sharing, and cooperative work. Storm surges are caused by hurricanes and typhoons. Tsunamis are caused by underwater earthquakes, volcanic activities and landslides. Both hazards may cause serious disasters along coastal region.

The scope of work includes:

(1) Exchange results of research on storm surge and tsunami occurrence, generation, propagation, and coastal effects. This includes observations on historical, current, and theoretical tsunamis. Of particular interest is the effort by U.S. and Japan to acquire deep ocean tsunami measurements.

(2) Exchange results and status of countermeasures against storm surge and tsunami activities including analysis of the problem, planning, warning, and engineering approaches.

(3) Exchange information on development of technologies such as computer programs to predict travel times, land-fall locations, run-up heights, and wave characteristics, improved instrumentation, and use of satellite communications for detection and warning.

(4) Facilitate dissemination of scientific and technical information through exchanges of literature, technical reports at joint meetings, special workshops, joint projects, and direct interaction among participants.

2. ACCOMPLISHMENTS

(1) A joint field investigation was performed during 17-24 July 1993 on the damage caused by the 12 July 1993 M7.8 Hokkaido Nansei-oki Earthquake/Tsunami.

(2) Findings from the investigations on the Tsunami caused by the 12 July 1993 Hokkaido Nansei-oki Earthquake were reported in the 26th Joint Panel Meeting by U.S. and the Japan-side members.

(3) Conducted the Third Tsunami Workshop in Osaka, Japan on 28 August 1993.

(4) In the continuing exchange of publications the U.S.-side provided the Japan-side with a copy of *Tsunamis Affecting the U.S. West Coast 1806-1992* and a set of slides of tsunami damage resulting from the recent tsunamis in Nicaragua, Indonesia, and Japan.

3. FUTURE PLANS

(1) Planning is proceeding to conduct a joint T/C "I and K" Workshop on Wind and Earthquake Engineering for Offshore and Coastal Areas during January 1995 in the United States.

(2) Continue exchanging data and information on tsunami measurements including deep ocean measurements.

(3) 1996 will be the centennial anniversary of the great Sanriku earthquake and tsunami in Japan and the 50th anniversary of the April 1, 1946 Aleutian earthquake and tsunami. These events led to the establishment of warning system and an increased awareness of the damages wrought from these events. The Task Committee agreed to plan a Fourth Workshop to be held in Hawaii in 1996 in observance of these natural disasters.

(4) Publish the proceedings of the 3rd Tsunami Workshop.

4. OTHER ACTIVITIES

(1) The storm surge research community is less well organized and lacks the specialty societies, journals, and international organizations to define and stimulate work in the field. The Task Committee's "I" mission and interests can help fill this gap.

(2) The tsunami problem is less severe in the U.S. than in Japan which leads to a smaller community of researchers. There are few U.S. researchers focusing on tsunamis at any specific location; thus highlighting the importance of tsunamis at T/C "I" meetings and workshop are important to transfer information.

Report of Task Committee on

(J) Wind and Earthquake Engineering for Transportation Systems

Date: May 19, 1994

Place: National Institute of Standards and Technology
Gaithersburg, MD

Attendees:

U.S. Side -	J. Cooper (Chairman)	(FHWA)
	A. Franklin	(COE)
	A. Taylor	(NIST)
	J. Scalzi	(NSF)
	P. Yen	(FHWA)
Japan side -	K. Yokoyama (Chairman)	(PWRI)
	K. Nishikawa	(PWRI)
	K. Kawashima	(PWRI)
	M. Kanda	(PWRI)

1. OBJECTIVE AND SCOPE OF WORK

The objectives of the Task Committee are to: (1) plan, promote, and foster research on the behavior of highway bridges when subjected to wind and seismic forces and (2) disseminate research results and provide specifications and guidelines based on the Task Committee's findings. Surface transportation systems play a vital role in the movement of goods and people. Highway bridges are especially influenced by the forces of wind and earthquakes because of their open exposure to those forces.

The scope of work includes:

(1) Focus research on highway bridges without limitation on their size and function.

(2) Investigate existing and new bridge designs and the behavior of whole bridge systems and/or single components of a bridge.

2. ACCOMPLISHMENTS

(1) Held the Tenth U.S.-Japan Bridge Workshop in Lake Tahoe, Nevada, May 10-11, 1994. Fifty-eight participants representing government, academia, industry, and private practice presented 39 papers in 8 technical sessions. Technical site visits followed to gain knowledge about testing facilities at the University of Nevada, Reno; and to study ongoing bridge construction, and seismic retrofitting at bridge sites in the Seattle, Washington and the San

Francisco Bay Area.

(2) Held the Second U.S.-Japan Workshop on Seismic Retrofit of Bridges at Berkeley, California, January 20-21, 1994. Technical site visits after the workshop included bridge construction, retrofit, and base isolated bridges in the San Francisco Bay Area. The site visits were held in conjunction with the third U.S.-Japan workshop on Earthquake Protective Systems for Bridges. (NOTE: Special trips were made to Los Angeles to document bridge damage from the January 17, 1994, Northridge Earthquake.)

(3) Conducted, in cooperation with Task Committee (G), the third U.S.-Japan workshop on Earthquake Protective Systems for Bridges at Berkeley, California, January 24-25, 1994. Technical site visits to bridge construction, retrofit and base isolated bridges in the San Francisco Bay Area preceded the workshop.

3. FUTURE PLANS

(1) Conduct the 11th U.S-Japan Bridge Engineering Workshop in Tsukuba, Japan, in conjunction with the 27th Joint Panel meeting in May 1995.

(2) Initiate plans to conduct the Third U.S.-Japan Workshop on Seismic Retrofit of Bridges in 1996 in Japan. The workshop will focus on practical seismic retrofit measures.

(3) In cooperation with Task Committee (G), initiate plans to conduct the Fourth U.S.-Japan Workshop on Earthquake Protective Systems for Bridges in Japan. The workshop will focus on research and application including: innovative protective systems; design methods; full-scale verification of performance; and comparative design examples.

(4) Continue to investigate and exchange technical information on improved seismic retrofit and strengthening procedures for highway bridges based on experimental, analytical, and field studies. This exchange should include information on maintenance of existing bridges.

(5) Continue experimental research on the seismic performance of bridge piers and columns, and encourage research on base isolation and hybrid control of bridges in cooperation with Task Committee (G).

(6) Develop a coordinated research study on seismic, aeroelastic, and aerodynamic response of cable-supported bridges with emphasis on behavior of composite materials, cable inspection, vibration control, and corrosion protection.

(7) Continue the coordinated research study to compare the seismic design criteria for bridges in Japan and the U.S. and discuss the method and analysis procedures for bridge column design. Continue information exchange on the

application of the limit state design method.

(8) Encourage a coordinated research study on seismic response and control, system identification techniques, nondestructive evaluation of bridge structures, use and performance of structural materials including new materials, and performance of jointless bridges.

Report of Task Committee on

(K) Wind and Earthquake Engineering for Offshore and Coastal Facilities

Date: May 18, 1994

Place: National Institute of Standards and Technology
Gaithersburg, Maryland

Attendees:			
	U.S. Side -	W. Roper (Acting Chairman)	(COE)
		J. Wilcoski	(COE)
	Japan Side -	S. Iai (Acting Chairman)	(PHRI)
		M. Kanda	(PWRI)
		H. Sato	(PWRI)

1. OBJECTIVE AND SCOPE OF WORK

Criteria for the design of offshore and coastal facilities may differ greatly from their onshore counterparts. These differences can arise due to: unique design of mass distribution; fluid/structure or wind/structure interaction; placement of foundation elements in or on soft fully saturated soils that can be subject to large hydrodynamic pressures; and lack of specific environmental data or the engineering experience that has been developed for most onshore sites.

The objective of the Task Committee is to develop technical insights necessary to mitigate damage to offshore and coastal facilities due to extreme wind and seismic effects. The Task Committee will plan, promote and develop research initiatives to meet this objective, and will disseminate the results of their research for incorporation into future specification or design guidelines.

The scope of work includes:

(1) Sponsoring and conducting workshops and meetings to identify key area research, opportunities for cooperation, and the exchange of knowledge.

(2) Predicting strong ground motions for offshore and coastal sites including assessing the effects of basin geometry, linear, and nonlinear local geological effects using actual seafloor response measurements.

(3) Determining the dynamic response and the interaction of structure/foundation/soil systems to seabed motions and/or extreme wind forces.

(4) Assessing the dynamic response and behavior of various operational facilities mounted on offshore and coastal structures.

(5) Developing assessment methodologies for seismicity and other characteristics of potential seismic sources (e.g. faults) for offshore and coastal sites in regards to how these conditions relate to structural design criteria.

(6) Promoting the implementation of new research results into current design and construction process.

(7) Developing research efforts to include laboratory and field programs to obtain data on the response of offshore and coastal facilities to extreme wind and seismic forces.

(8) Creating performance standards, design specifications, guidelines , and code recommendations for application to new construction as well as remedial action for existing facilities.

2. ACCOMPLISHMENTS

(1) Conducted the 1st U.S.-Japan Workshop on Wind and Earthquake Engineering for Offshore and Coastal Facilities at the PHRI, Yokosuka, Japan during May 12 and 13, 1993.

3. FUTURE PLANS

(1) Hold the 2nd U.S.-Japan Workshop on Wind and Earthquake Engineering for Offshore and Coastal Areas in the U.S. in January 1995. This will be a joint workshop with Task Committee (I) Storm Surges and Tsunami.

(2) Develop workshop agenda and finalize list of speakers from the U.S. and Japan Side.

(3) Publish the Proceedings of the first Workshop; it will be distributed by NIST.

(4) Coordinate, where possible, on-going research on wind and earthquake engineering for offshore and coastal facilities of interest to the members of the Task Committee.

☆ U.S. GOVERNMENT PRINTING OFFICE: 1994 — 386-627/22782